NASA TECHNICAL MEMORANDUM

NASA TM X-2893

NASA TM X-2893

NASTRAN: USERS' EXPERIENCES

Third Colloquium held at
Langley Research Center
Hampton, Virginia
September 11-12, 1973

NATIONAL AERONAUTICS AND SPACE ADMINISTRATION • WASHINGTON, D. C. • SEPTEMBER 1973

NASTRAN: USERS' EXPERIENCES

Compendium of papers prepared for the Third NASTRAN Users' Colloquium

September 11-12, 1973

NASA Langley Research Center

FOREWORD

NASTRAN (NASA STRUCTURAL ANALYSIS) has been available to the public since late in 1970. As a large, comprehensive, nonproprietary, general purpose, finite element computer system for structural analysis, NASTRAN is finding widespread acceptance within NASA, other government agencies, and industry.

NASTRAN is available to the public at a cost of $1,790, which covers reproducing and supplying the necessary system tapes. Furthermore, NASA has provided for the continuing maintenance and improvement of NASTRAN through the establishment of a NASTRAN Systems Management Office located at the Langley Research Center. At present, NASTRAN is in use at over 240 locations, including NASA centers, other government agencies, industry, and commercial computer data centers.

Because of the widespread interest in NASTRAN and because of a desire to better serve the community of NASTRAN users, the NASTRAN System Management Office organized the Third NASTRAN Users' Colloquium at the Langley Research Center, September 11-12, 1973. (Compendiums of papers from previous Colloquiums, 1971 and 1972, were published as NASA TM X-2378 and NASA TM X-2637, respectively.) The colloquium was planned to provide to everyone concerned an opportunity to participate in a comprehensive review of the current status of NASTRAN use, unique applications, operational problems, most desired modifications including new capability, and substructuring.

Individuals actively engaged in the use of NASTRAN were invited to prepare papers for presentation at the colloquium. These papers are included in this volume. Only a limited editorial review was provided to achieve reasonably consistent format and content. The opinions and data presented are the responsibility of the authors and their respective organizations.

Deene J. Weidman, Conference Chairman
NASTRAN Systems Management Office
Langley Research Center
Hampton, Va. 23665
September 1973

PRECEDING PAGE BLANK NOT FILMED

CONTENTS

III. SUBSTRUCTURING

IV. NEW CAPABILITY

V. USERS' EXPERIENCES

VI. SYSTEM EXPERIENCES

N74-14587

FUTURE NSMO PLANS FOR MAINTENANCE OF NASTRAN

By Deene J. Weidman
NASA Langley Research Center

INTRODUCTION

The objectives of the NASTRAN computer program system are to provide a general structural analysis capability for NASA centers and major NASA contractors and to allow effective use of NASA structural analysis capability in other agencies and industries throughout the nation. In addition, the importance of the Space Shuttle project to the nation's space program makes it imperative to provide timely improvements to NASTRAN to support analysis and design of the Shuttle vehicle. Shuttle improvements are expected to have general application.

Use of NASTRAN has increased steadily since the second NASTRAN Users' Colloquium September 11-12, 1972 (ref. 1). The total number of individual users is now estimated to be 2200, an increase of about 50 percent in the past year. NASTRAN is known to be installed at 240 computer sites in the United States and abroad as identified in the following list:

- 9 NASA centers
- 10 Department of Defense sites
- 18 Aerospace company users
- 22 Small aircraft company users
- 181 Nonaerospace users including -
    - 34 Computer company sites
    - 9 Automotive company sites
    - 17 Universities
    - 121 Other users

These estimates are based on the NSMO Newsletter mailing list and are, therefore, believed to be somewhat conservative.

PLANNED DEVELOPMENTS

The overall development plan for NASTRAN is shown in figure 1. The four items on the left of figure 1 are ongoing developments this fiscal year. The design and coding for Level 16 is nearly complete. Because substantial changes have been incorporated into Level 16, extensive debugging, checkout, and thorough exercising of this code are planned which will lead to general public release about the end of calendar year 1974. Automated substructuring, diagnostics and DMAP improvements, and other shuttle improvements are all funded by the Space Shuttle project and will not be introduced into the standard NASTRAN system until after release of Level 16. A subsonic flutter package has been developed for NASTRAN and is operational in-house. Plans call for its installation into the standard NASTRAN system also after the release of Level 16. A long-range study of the impact of fourth-generation computers on NASTRAN is being initiated in-house and may become a contract activity later.

Following fiscal year 1974, new capability development will be principally focused on fundamental improvements such as an improved graphics package, expansion of NASTRAN's nonlinear elastic and plasticity capabilities, and incorporation of some new finite elements. New capabilities will be introduced at less frequent intervals than in the past and release of future levels of NASTRAN will correspondingly occur at a reduced rate. Further into the future, it is envisioned that there may be a complete overhaul of NASTRAN (NASTRAN II(?)) to incorporate advanced finite-element technology, to allow for potential fourth-generation computer usage, and to take advantage of advanced techniques for program organization and data management. A steady incorporation of efficiency improvements and error correction is also necessary to keep a program system of the size and complexity as NASTRAN viable.

CAPABILITY IMPROVEMENTS IN LEVEL 16 OVER LEVEL 15

NASTRAN Level 16 will contain three kinds of improvements compared with Level 15: (1) new capabilities developed by others and installed under contract by NSMO, (2) improvements to existing capabilities in response to aerospace industry requests, and (3) addition of some higher quality finite elements. The first kind of improvement includes a feature which can drastically reduce input, storage, and run times for structures which have cyclic geometric symmetries, a module which resizes once all elements in a structure using a specified allowable stress and a simple stress-ratio resizing algorithm, and complete heat-transfer capability including conduction, convection, and radiation. The second kind of improvement includes an improved differential stiffness capability allowing iteration, the ability to output shear-force information in terms of shear flows, the sorting of stress results from various load cases by element, and an automation of the partitioning vector generation required for substructuring. The third kind of improvement includes isoparametric solid finite elements, rigid elements, improved ring and plate elements, and two improved quadrilateral membrane elements.

EFFICIENCY IMPROVEMENTS IN LEVEL 16 OVER LEVEL 15

A large amount of basic NASTRAN code will be redone in Level 16 to provide major improvements in efficiency - reduced run-time and storage requirements. Probably the most extensive change will be incorporation of a new technique for assembling stiffness and mass matrices. Improvements in symmetric matrix decomposition, the forward and backward substitution, and multiply-add matrices will be included, and the multipoint constraint and dynamic data recovery features will be improved. Single- and double-precision options will be included for IBM, CDC, and UNIVAC computers. Improvements in input/output routines will include string notation for data, nontransmit read, and random- and direct-access features. Detailed discussion of these future efficiency improvements is contained in reference 2.

NEW ERROR CORRECTION PROCEDURE

An overview of the NASTRAN error correction procedure is shown in figure 2. In all cases of receipt of a user report, an action is taken, and a reply letter is sent to the user. For each user-reported inconsistency, NSMO determines into which of three categories the report falls. Those reports that do not appear to be user misunderstandings are assigned an SPR (Software Problem Report) number and priority and then delivered to the maintenance contractor for evaluation and correction. A substantial number of SPR's are not "errors" but in reality represent a need for improvement in the system.

The lower half of figure 2 shows the activities of the maintenance contractor for each SPR he receives. The maintenance contractor screens out any user errors and previously reported bugs (PRB). For valid SPR's, a run using the user-submitted deck is always performed and the contractor determines the cause of the error and the needed correction. At this point, figure 2 shows a proposed departure from current practice. An "ALTER" form would be generated by the maintenance contractor which specifies all code corrections needed to resolve each SPR along with information to aid in installing the corrections in users' decks. Responsibility for making the corrections would be the users! ALTER forms might be released at frequent intervals to the user community via the NASTRAN Newsletter. Evaluation of this and other avenues to quicker error correction response to users is currently underway; of course, error corrections will be incorporated in each new archive level as issued. The final maintenance contractor tasks for each SPR are a validation run of the corrected code on the user's problem and any required documentation updates. Then NSMO verifies the successful completion of the contractor's tasks for each SPR.

CONCLUDING REMARKS

NASTRAN provides a general structural analysis capability for NASA, NASA contractors, and other agencies and industries. In particular it is expected to support structural analysis and design of the Space Shuttle vehicle. A steady growth in the general use of NASTRAN is evident with an estimated 50-percent increase in the number of individual users in the past year. Development plans call for less frequent addition of new capability and corresponding release of future levels at a reduced rate. Near term focus in NSMO will be to implement new error correction procedures to improve communication with users and speed up the error correction process.

REFERENCES

1. Anon.: NASTRAN: Users' Experiences. NASA TM X-2637, 1972.

2. McCormick, Caleb W.: Review of NASTRAN Development Relative to Efficiency of Execution. NASTRAN: Users' Experiences, NASA TM X-2893, 1973, pp. 7-28. (Paper no. 2 of this compilation.)

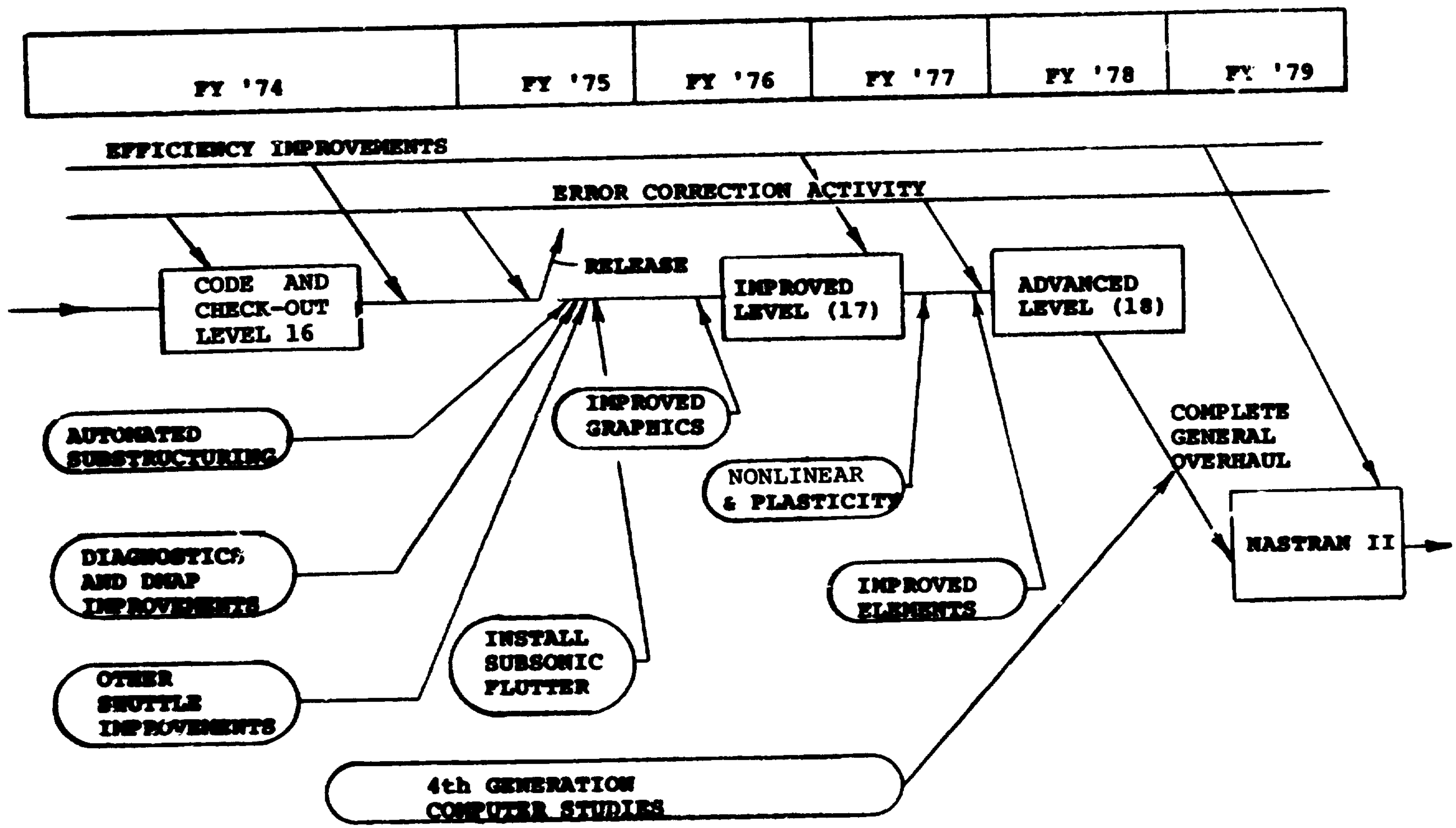

Figure 1.- Planned NASTRAN developments.

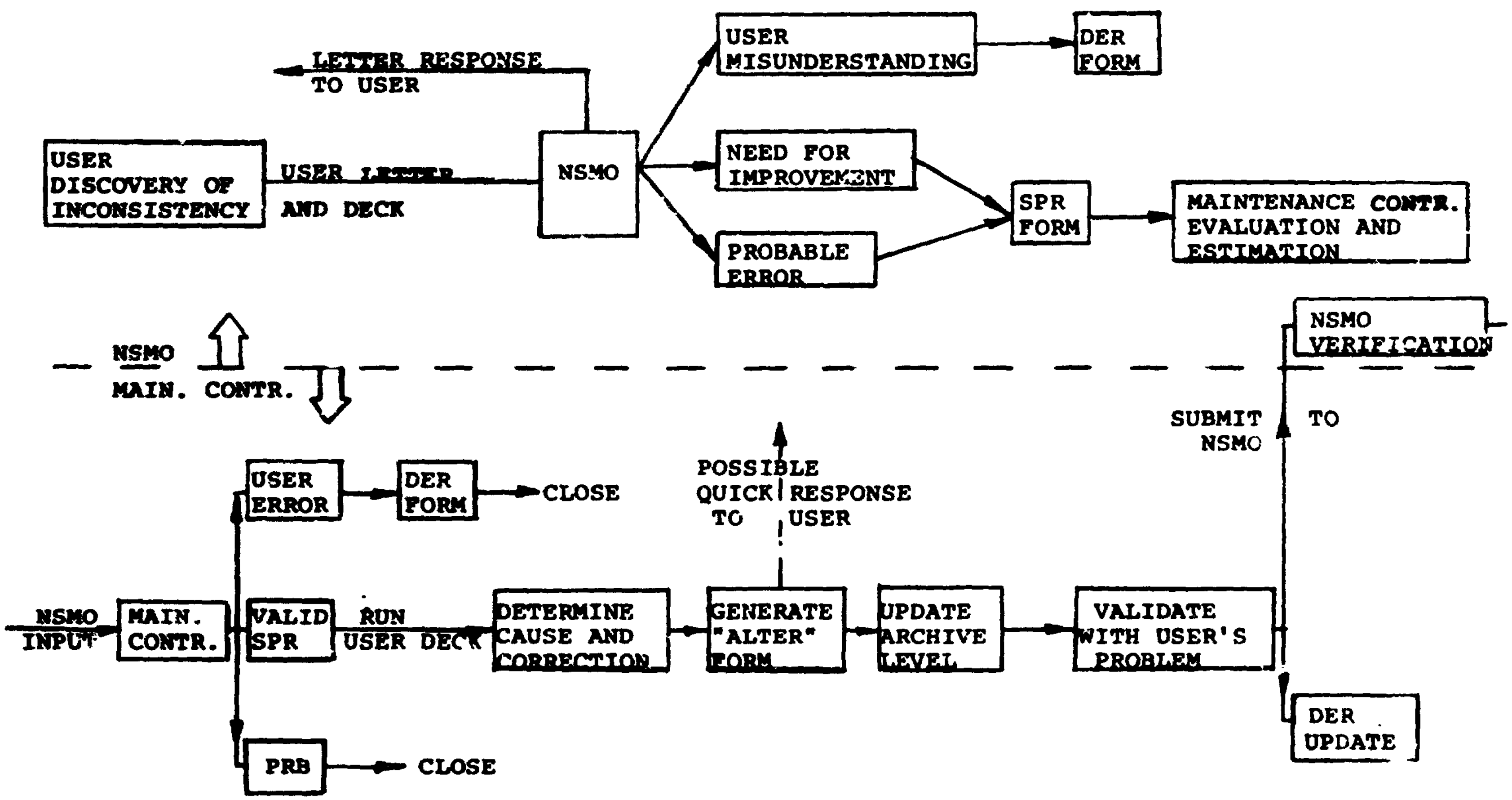

Figure 2.- NASTRAN error correction activity.

N74-14588

REVIEW OF NASTRAN DEVELOPMENT RELATIVE TO EFFICIENCY OF EXECUTION

By Caleb W. McCormick
Director of Engineering Analysis
The MacNeal-Schwendler Corporation
Los Angeles, California

SUMMARY

This paper reviews the development of NASTRAN relative to the efficiency of execution, with particular emphasis on those items which have changed significantly since the original release of NASTRAN. Features discussed include main and secondary storage utilization, matrix packing, matrix assembly, matrix multiplication, matrix decomposition and equation solution. Also a brief look into the future discusses the questions of faster arithmetic units and more effective storage utilization. In some cases the improvements in NASTRAN efficiency have resulted from taking advantage of hardware developments, while in other cases increased efficiency has resulted from improvements in the state of the art for data processing or matrix operations. The modular design of NASTRAN has made it possible to improve the efficiency in many parts of NASTRAN without changing the basic design of the program.

INTRODUCTION

The main goal in the original design specifications for NASTRAN was the solution of large problems in both statics and dynamics. Although efficiency has always been an important consideration, the primary emphasis in the beginning was on the wide range of problem types of large size. However, it was recognized that in order to solve large problems, it would be mandatory to take advantage of sparse matrix techniques. Consequently, all of the original matrix operations were designed to utilize sparse matrix techniques. Since the original release of NASTRAN, a number of improvements have been made in the efficiency of the matrix routines by taking advantage of hardware developments and improvements in the state of the art for data processing and matrix operations.

Hardware and software limitations required that the early versions of NASTRAN use only sequential secondary storage. The current versions of NASTRAN use direct access devices for secondary storage. Level 16 will include the use of random access coding in the matrix assembly and equation solution operations. The use of multiple types of secondary storage devices will be an important development for future releases of NASTRAN.

Most of the original code for NASTRAN was written in FØRTRAN IV in order to reduce both the development costs and maintenance costs. Machine language was used only in those placed where it was necessary to interface with the resident operating systems. However, efforts were made to improve the efficiency of the compiled code by care in the use of FØRTRAN. For example, in the case of nested DØ loops it was found that, for some compilers, the speed of the inner loops for multiply-add operations could be improved by a factor of two by simply writing the inner loop as a separate subroutine. Substantial improvements have been made in Level 15 and Level 16 through the use of machine language in many of the more important matrix operations. Even so, except for the transfer of information between main storage and secondary storage and the matrix packing routines, the use of machine language has been restricted to the inner loops of the matrix operations.

The original emphasis on the solution of large problems has caused NASTRAN to be relatively inefficient for small- and medium-size problems. Many of the Level 16 improvements will substantially improve the efficiency of NASTRAN for the smaller problems. The main improvements in this area are associated with the more effective use of main storage and additional options for the matrix packing routines.

MAIN STORAGE UTILIZATION

The original design of NASTRAN recognized the importance of preserving as much as possible of the main storage for matrix operations. The overlay structure was carefully designed to minimize the amount of code that had to be resident in main storage, particularly during the operation of important matrix routines. Also, in order to preserve the maximum amount of main storage for each matrix operation, all results were transferred to secondary storage prior to the start of a new major operation. This transfer of information to and from secondary storage placed a heavy burden on the matrix packing routines and the associated read and write routines. These routines have contributed heavily to the relative inefficiency of NASTRAN.

The original design of the overlay structure for NASTRAN is still in use and there appears to be no need for major changes in this area. The inefficiencies resulting from the transfer of information between main and secondary storage has been a source of some concern and has received extensive revision in both Level 15 and Level 16.

In order to reduce the requirement for transfers between main storage and secondary storage, Level 16 will provide an option to use a portion of main storage for the retention of data which would otherwise be transferred to secondary storage. This option is under the control of the individual functional modules and has been implemented by allowing the use of multiple buffers in main memory by the I/Ø routines. This option will be particularly effective when relatively small amounts of frequently used information can be retained in main memory and thereby avoid excessive transfers from secondary storage. A strong candidate for using this option is the numerical integration in transient response problems, where currently the triangular factors of the dynamic matrix must be read from secondary storage at each time step. If the problem is not too large, it may be convenient to allocate sufficient main memory to hold the triangular factors in main storage. This option should also be useful for nonlinear problems where the problem sizes tend to be small and repetitive operations form an important part of the total solution time.

SECONDARY STORAGE UTILIZATION

All of the transfers of information between secondary storage and main storage in the early releases of NASTRAN used sequential access methods. Much of the original code was also written in FØRTRAN, which further contributed to the inefficiencies. The original dynamic use of files as supervised by the NASTRAN Executive System has stood the test of time and remains today essentially as in the original design.

Sequential procedures are still used for all write operations. However, read operations may be performed either by the use of sequential procedures or random procedures. Two important uses of the random access procedures in Level 16 are for matrix assembly and the back substitution part of the equation solution routines.

MATRIX PACKING

Efficient operation with large sparse matrices requires an effective packing scheme in order to minimize main memory requirements and the time required to transfer the nonzero elements from secondary storage devices to the working space in main memory. The current matrix packing logic is similar to that used in the original design of NASTRAN. However, substantial improvements in the efficiency were made in Level 15, including the use of machine language on the IBM versions. Level 16 will include further improvements in efficiency, including the use of assembly language on the Univac version. The Level 16 matrix packing routines will use machine language on all machines and will be 1-1/2 to 2 times faster than Level 15.

The matrices in NASTRAN are stored by columns, and each column constitutes a logical record. The first nonzero term in the column is described by an integer indicating its row position and the floating point number describing its value. If the following term is also nonzero, only its value is stored, and in general the position of only the first term in the series of nonzero terms is stored. In order to improve the efficiency when working with strings of nonzero terms, the number of nonzero terms in the string is stored along with the row number of the first nonzero term in the string. An option is also provided to include the row number of the last nonzero term in the string along with the number of nonzero terms in the string. This option makes it possible to perform the backward substitution operation for equation solution in a more efficient manner.

An important addition to the packing routines in Level 16 is a new non-transmit option. In the case of a read operation, each call for this option results in the return of the row number of the first nonzero term in the next string and the number of terms in the string. In the case of a write operation, each call returns the location of the next available space in the NASTRAN I/Ø buffer and the number of spaces remaining in the current buffer. The using routines can then operate directly in the I/Ø buffers, and only the time associated with the initial call for each string is required for the packing operation. The time to access a term or store a term can be absorbed in the using routine, as this operation is required, even when operating outside the buffer.

For strings of reasonable length, the time per term for the nontransmit operation is very small and may well be ten or twenty times less than the transmitting pack options. This option is particularly effective when each term in the buffer is used for a single operation, such as for direct transient response or eigenvalue extraction using the inverse power method, where the running times are dominated by equation solutions with single right hand sides. If the transmitting pack options are used in these cases, the running time is dominated by the packing times, which in turn may be several times the associated arithmetic times. If the nontransmit option is used, the inner loops will run at arithmetic speed, and the speed of operation with single right hand sides will be several times faster.

MATRIX ASSEMBLY

The comparison of the matrix assembly times for various assembly procedures is indicated in Figure 1. The initial straight portion of the solid line indicates a linear growth of matrix assembly time with problem size when the complete stiffness matrix can be held in main memory. The curved portion of the solid line indicates a rapid growth in matrix assembly time with problem size when the stiffness matrix is assembled from element stiffness matrices that are stored on a sequential secondary storage device. The rapid growth in matrix assembly time for large problems was unacceptable for NASTRAN.

Since the large matrices in NASTRAN require the use of secondary storage for assembly, and since only sequential access procedures were available during the initial development period, the regeneration procedure indicated by the long-dash--short-dash line in Figure 1 was used. In this procedure the required partitions of the element stiffness matrices are regenerated at each grid point as needed. Consequently, the slope of this line is proportional to the number of grid points connected to each finite element. As indicated in Figure 1, this procedure will be superior to the storage of element matrices on sequential access devices for large problems. The location of the cross-over point will depend on the ratio of the time to generate an element stiffness matrix to the time required to retrieve the same information from a sequential storage device. A further degradation in running time occurs if all of the element generation routines cannot be held in main memory at the same time. This latter problem was not severe in the earlier releases of NASTRAN because the element library was small and consisted of relatively simple elements.

The dashed line in Figure 1 indicates a linear growth in matrix assembly time when the element stiffness matrices are retrieved from a direct access secondary storage device. The slope of this line is proportional to the time to generate the stiffness matrix for a single element plus the time required to retrieve the element stiffness from a random access device. A new matrix assembly module has been completed for Level 16 in which the element matrices are generated for each type of element and stored on a random access device. The complete matrix is generated by assembling as many columns of the matrix as possible in packed form in main memory, using random access methods to retrieve the element matrices as needed. Since only a single element routine is needed in main memory during the formation of the element matrices, there is no penalty for having a large finite element library.

The new matrix assembly module also provides for taking advantage of identical finite elements in the model. In the case of identical elements, the element generation routine generates only one matrix for each group of identical elements. With random access assembly procedures, it is a routine operation to point to the single element matrix each time it is required for matrix assembly. This procedure substantially reduces the matrix generation time when there are large numbers of identical elements.

Test runs indicate that the central processor time for the actual matrix assembly is about the same in Level 16 as in Level 15, even though the element matrices are retrieved from a secondary storage device in Level 16. In other words, the overhead for the matrix assembly operations in Level 16 is very small. The removal of the requirement to regenerate the element matrices at each connection will reduce the matrix generation time in proportion to the number of connected grid points. The new matrix assembler is particularly important for the new, higher order elements where the number of connections are often greater, and the generation times for the element matrices are substantially greater than for the elements in Level 15.

MATRIX MULTIPLY-ADD

The use of sparse matrix multiply-add routines was part of the original design of NASTRAN. Major improvements in efficiency were made in Level 15 with the use of machine language inner loops and improved logic for Method 2. Level 16 includes a new Method 3 and improved logic for the transfer of the packed matrix terms directly into the working area for Method 2. The details of the multiply-add operations are given in the NASTRAN Theoretical Manual.

The summary of multiply-add operations in Table 1 presents the overall picture of multiply-add efficiency in NASTRAN. Various combinations of densities of the [A] and [B] matrices are presented for both the nontranspose and the transpose multiply-add options. In each case the most efficient multiply-add method is given for the particular combination of densities. The efficiency of the inner loop for multiply-add is always proportional to the length of the strings of the second operand. The total arithmetic time is always proportional to the density of the matrix containing the first operand, except for the nontranspose option of Method2, for which the arithmetic time is proportional to the product of the densities of the two matrices. Although the matrix packing operations contribute to the total execution time, these packing times are not of primary consideration in the relative efficiency of the multiply-add methods.

For either the transpose or the nontranspose multiply-add, the summary in Table 1 indicates that, when [B] is dense, Method 1 will be selected regardless of the density of [A]. In these cases, the arithmetic times are proportional to the density of [A]. Since [B] is assumed full in Method 1, the multiply-add loop operates at maximum efficiency. However, unless [B] is very dense, a large number of unnecessary zero operations will be performed.

If [B] is sparse, Method 2 will always be selected in the nontranspose case, regardless of the density of [A]. In this case the arithmetic time will be proportional to the product of the densities of the [A] and [B] matrices. The efficiency of the multiply-add loop will be proportional to the lengths of the strings of the [A] matrix. The internal selection procedures assume that the average length of the strings in the [A] matrix is proportional to the density of the [A] matrix.

For the transpose case with [B] sparse and [A] sparse, Method 2 will usually be selected. Alt ough the efficiency of the multiply-add loop will be low due to the short strings (low density) in [A], the number of operations will be proportional to the density of [A], and the total arithmetic time will be relatively short. If there is sufficient main memory to perform Method 1 in a single pass, the total time will be less than for Method 2 because of the higher efficiency of the multiply-add loop. In neither case is any advantage taken of the sparsity of the [B] matrix.

For the transpose case with [B] sparse and [A] dense, a new Method 3 is the most efficient. In this method the [A] matrix is assumed full and the multiply-add loop operates at maximum efficiency. However, unless [A] is very dense, a large number of zero operations will be performed. The execution time for Method 3 is proportional to the density of the [B] matrix, with no advantage being taken of the density of the [A] matrix. A nontranspose option is not provided for Method 3, as Method 2 handles all cases of interest more efficiently.

MATRIX DECOMPOSITION

The storage and indexing procedures used in NASTRAN for the new symmetric decomposition routine will be discussed with reference to the matrix in Figure 2. Initial nonzero terms are indicated by X's with the O's indicating nonzero terms created as the decomposition proceeds. The shaded terms indicate the relative locations for nonzero contributions to the upper triangular factor when the first row of the matrix is the pivotal row. If there is sufficient main storage to hold all of the shaded terms, the decomposition may proceed without the need for writing intermediate results on secondary storage. The shaded terms in Figure 3 indicate the relative locations for nonzero contributions to the upper triangular factor when the second row is the pivotal row. In this case not only are there more active columns, and therefore more main storage is required, but one of the new active columns (column 8) is inserted in an intermediate location.

The management of the working storage for triangular decomposition is indicated in Figure 4. The pivotal row and the associated active column vector are stored in a separate space. The active column vector contains the column number for each nonzero term in the pivotal row. The lower portion of the main working storage is always used and the amount is proportional to the number of active columns at each stage of the decomposition. The amount of storage required for each of the first six pivotal rows for the matrix shown in Figures 2 and 3 is indicated on Figure 4. The shaded area indicates the storage space required for pivotal rows 1, 5 and 6, all of which have six active columns. At any particular stage of the decomposition, the previous contributions are accessed according to the number of active columns immediatly preceding the pivotal row, and the results of the current calculations are stored according to the number of active columns in the pivotal row.

As the decomposition proceeds, the number of active columns can increase by any number up to the number of rows remaining in the matrix. However, if it is assumed that the number of active columns will never decrease by more than one for each new pivotal row, it is possible to store the current calculations dynamically in the same array with previous calculations without interference. This is equivalent to assuming that once a column becomes active it remains active until the column intersects the diagonal (column number = pivotal row number). This assumption will not cause errors in the calculations but will result in the performance of a number of zero operations and will require additional working space in main storage.

The shaded part of Figure 5 indicates the nonzero terms in the upper triangular factor of a matrix where the original nonzero terms are indicated with X's. It can be seen that columns 7, 9 and 13 are terminated at row 3, and columns 11 and 14 are terminated at row 6. The new matrix decomposition routine in Level 16 provides for the termination of active columns by changing their status from active to passive. Columns may also change their status from passive to active as indicated in Figure 5 by column 9 at row 7, or column 11 at row 10. The provision for passive columns reduces the number of active columns when row 4 is pivotal from 6 to 3, with an associated reduction in main storage requirements and the number of arithmetic operations. The complete details of the decomposition procedure will be given in the Level 16 NASTRAN Manuals.

The storage management indicated in Figure 4 applies only when there is sufficient working storage for all of the terms generated by the pivotal row. When the number of active columns exceeds the capacity of working storage space, an automatic spill logic is provided. The overhead for the new spill logic is substantially less than provided in the original matrix decomposition routine. Both the CPU cost and the number of secondary storage transfers have been substantially reduced. It should be possible to economically run large problems with about half as much main storage in Level 16.

In order to improve the efficiency of sparse matrix operation in NASTRAN, the inner loops are usually written in assembly language. In general the use of assembly language will reduce the number of instructions and will allow for more effective use of the high speed registers. In the case of the new decomposition routine, three separate inner loops are provided. The differences in the inner loops are associated with the need to combine the previously completed results in the working storage space. Special provision is made when no previously calculated results need to be combined. This applies to the first row of the matrix and for all rows immediately following the creation of passive columns. Special provision is also made for the case of consecutive active columns. This option improves the efficiency of indexing for band matrices and when there are large numbers of active columns adjacent to the diagonal. The third loop provides for the general case in which a test must be made inside the loop for the existence of previously calculated terms.

The aim in the NASTRAN decomposition routine has been to provide a general purpose routine which will operate efficiently for different orderings of nonzero terms, including the cases of band matrices and partitioning or substructuring types of matrix ordering. The NASTRAN decomposition routine has been designed to take advantage of different sequences of nonzero terms along with the use of an ordinary step-by-step elimination procedure. Test runs with square frameworks of 2600 order have given improvements in running time by factors of 2 to 4. It is easy to design problems which will show substantially greater improvements in efficiency, particularly if the new spill logic is used with reduced main memory requirements or unusual sequences for matrices are employed.

The familiar ordering for a band matrix of a square array is shown in Figure 6. Figure 7 indicates the ordering of the same problem with partitioning. In this case, the square array has been divided into four partitions with each of the partitions numbered first and the boundary points numbered last. Figure 8 indicates the locations of the nonzero terms in the triangular factor when the square array is ordered for partitioning. The X's indicate the original nonzero terms and the 0's indicate nonzero terms created during the decomposition operation. In the case of the band matrix, the number of nonzero terms in the triangular factor is 129, whereas Figure 8 contains only 102 nonzero terms. Since the time for the forward/backward substitution operation is directly proportional to the number of nonzero terms in the triangular factor, the time for the forward/backward substitution operation when the square array is ordered for partitioning is only about 80% of that when the array is ordered for a band. The number of multiplications for the decomposition when ordered for a band is 294, whereas the number indicated in Figure 8 is only 177. This indicates that the time for the decomposition when ordered for partitioning is only about 60% of that when ordered for a band. This example indicates the kinds of savings that are possible in decomposition and equation solution, when the decomposition routine can locate the nonzero terms in a triangular factor in a routine fashion. Even greater savings are possible when the partitions are not strongly connected.

EQUATION SOLUTION

The forward/backward substitution operation for the new equation solution routine in Level 16 is performed by holding as many columns of the right hand side in main memory as possible. The forward and backward substitution operations are performed by reading the triangular factors from secondary storage and performing the indicated arithmetic operations. These operations are performed in place, and at the conclusion of the backward substitution operation the solution vectors are stored in the same locations as the original right hand sides. The nonzero terms of the triangular factors are located directly in the I/Ø buffers in strings, using the new nontransmit option of the matrix packing routines.

The general procedure for the forward pass in equation solution is indicated in Figure 9. The operation for each column begins by locating the first nonzero string in the lower triangular factor. The nonzero terms of the current column of the lower triangular factor are indicated by the letter L in Figure 9. Next, the associated term in the first column of the right hand side is tested for zero. If the right hand side term is nonzero, the multiply-add operations are performed for the string, and the results are stored in the first column in the locations indicated by the number 1 in Figure 9. Similar operations are performed for all columns on the right hand side having nonzero entries in the row associated with the current column of the lower triangular factor. The X's on Figure 9 indicate nonzero operations exist in columns 1, 2 and 5. The results for the second string of the current column in Figure 9 are stored in the locations indicated by the number 2. The forward pass is completed by performing similar operations for all columns in the lower triangular factor.

The back substitution operation is performed by reading the strings of the triangular factor in reverse order. The general procedure for the backward solution is indicated in Figure 10. The operation for each row of the upper factor begins by locating the last nonzero string in the current row, indicated by the letter U in Figure 10. The dot product of the string is made for each column on the right hand side in turn, without testing for zero. The location of the second operand is indicated by the number 1 in Figure 10. The partial solutions are accumulated in the current row of the right hand side, as indicated by the X's in Figure 10. The backward pass continues by performing similar operations for all nonzero strings in the current row of the upper triangular factor. The locations of the second operand for the next nonzero string of the upper triangular factor are indicated by the number 2 in Figure 10. When all of the dot products have been performed for the current row of the upper triangular factor, the solution will be located in the positions indicated by the X's. The backward solution is completed by performing the same operations for each row of the upper triangular factor. The final solution is then transferred to secondary storage. If additional right hand sides exist, the next group of columns can be transferred to main storage and a new forward pass started.

It can be seen that the forward/backward substitution operation in Level 16 takes full advantage of the sparsity of the triangular factors. Also, all terms in the triangular factors are located directly in the buffers, so full advantage is taken of the string notation and the nontransmit packing option. Full advantage is also taken of the sparsity of the right hand side in the forward pass. Test runs with the new equation solution routine show improvements in running time by a factor of 10 over those used in Level 15.

FUTURE DEVELOPMENTS

One of the more important future hardware developments will be the availability of much faster arithmetic units. The improvements in speed will come from the use of parallel processors and the use of vector processors. The modular design of NASTRAN should make it possible to take advantage of these new hardware developments by changing only the matrix operation routines. In some cases, it may only be necessary to change the inner loops in the matrix operation routines. In any event, the basic packing routines and the string notation should be useful with these new types of arithmetic units.

Another important hardware development will be the use of high capacity, high speed, secondary storage devices. These high speed storage devices will consist of such things as extended core storage devices and fixed head drums, as well as high speed, high density disc storage devices. The organization of the NASTRAN packing and I/Ø routines lends itself to easy modification for use with different types of secondary storage devices. A modification has already been made for Level 16 to include the use of extended core storage devices on CDC machines.

The organization of the NASTRAN I/Ø routines and the use of working storage and main memory adapt well to the use of paging devices, such as are used with buffer memories and virtual memory machines. The NASTRAN matrix routines tend to access blocks of information in main memory in a sequential manner. The net result is, that even for large problems, only a small amount of working space needs to be resident in main memory at any one time. Furthermore, particularly with the new Level 16 matrix routines, the number of transfers between main storage and secondary storage have been substantially reduced, with a resulting reduction in the work load for paging devices.

CONCLUSIONS

The following conclusions are drawn relative to improvements in NASTRAN efficiency:

1. Most problems will run at least twice as fast on Level 16 as Level 15 due to improvements in times for matrix assembly, equation solution, decomposition, and matrix packing.

2. The use of multiple I/Ø buffers in main memory along with the nontransmit read and write options can make an individual functional module competitive

with core held programs, because no transfers to secondary storage are made and indexing is done directly into the working arrays.

3. The modular design of NASTRAN has made modification easy and should continue to make it relatively easy to adapt NASTRAN to new hardware and improvements in the state of the art for matrix operations and data processing.

Table 1. Summary of MPYAD Operations

$$[A][B] + [C] = [D]$$

Matrix Density		MPYAD Method	Arithmetic Time	
[A]	[B]		Strings	Density
Sparse	Dense	1	[B]	[A]
Dense	Sparse	2	[A]	[A] & [B]
Sparse	Sparse	2	[A]	[A] & [B]
Dense	Dense	1	[B]	[A]

$$[A]^T[B] + [C] = [D]$$

Matrix Density		MPYAD Method	Arithmetic Time	
[A]	[B]		Strings	Density
Sparse	Dense	1	[B]	[A]
Dense	Sparse	3	[A]	[B]
Sparse	Sparse	2	[A]	[A]
Dense	Dense	1	[B]	[A]

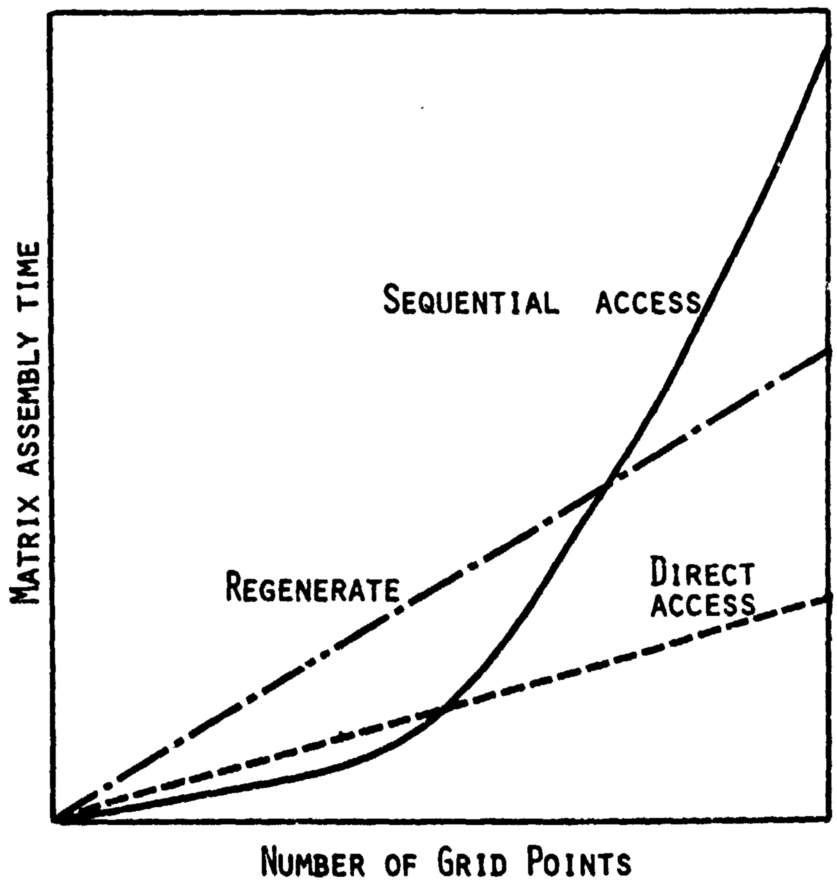

Figure 1.- Comparison of matrix assembly procedures.

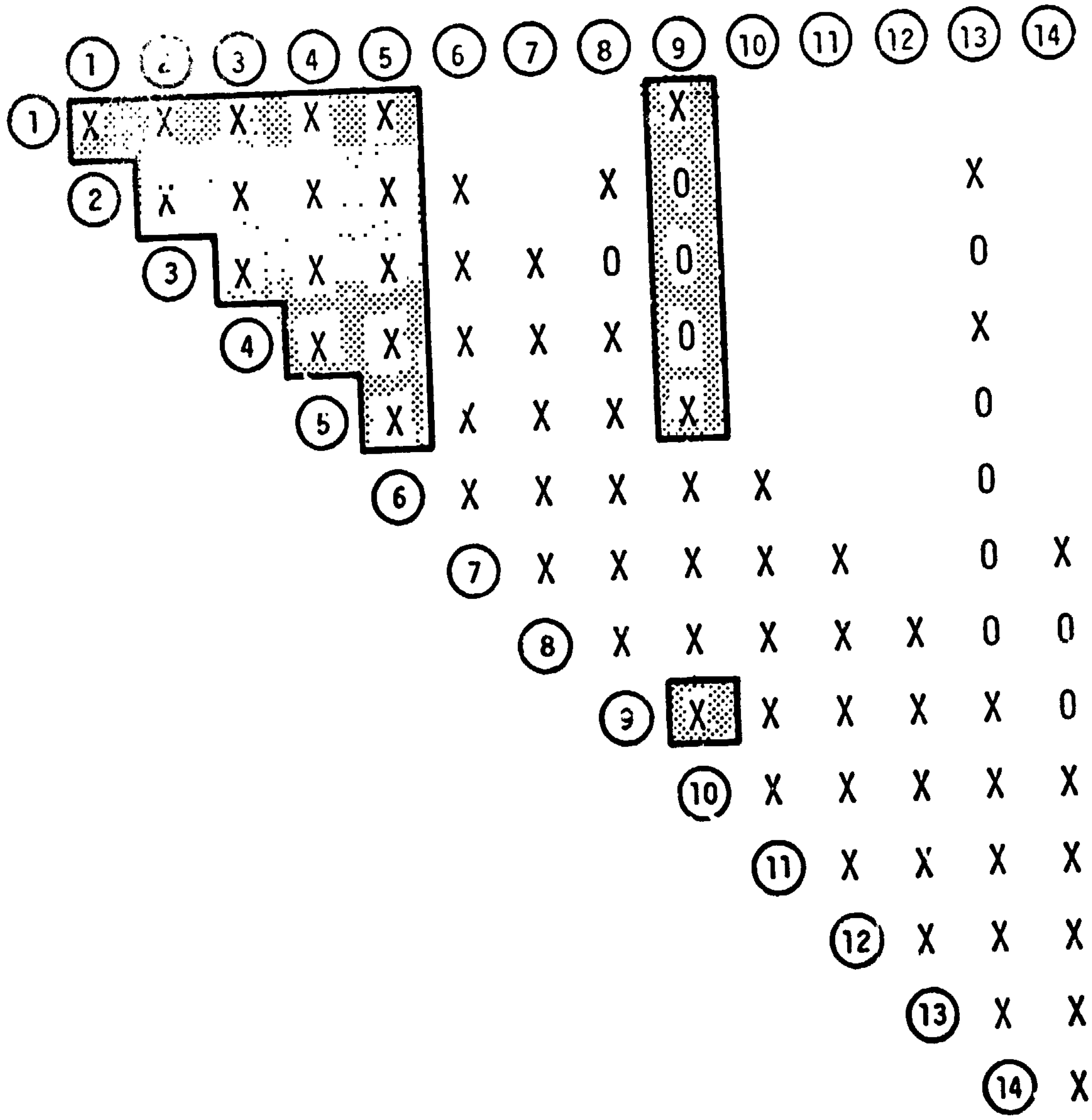

Figure 2.- Decomposition with first row as pivotal row.

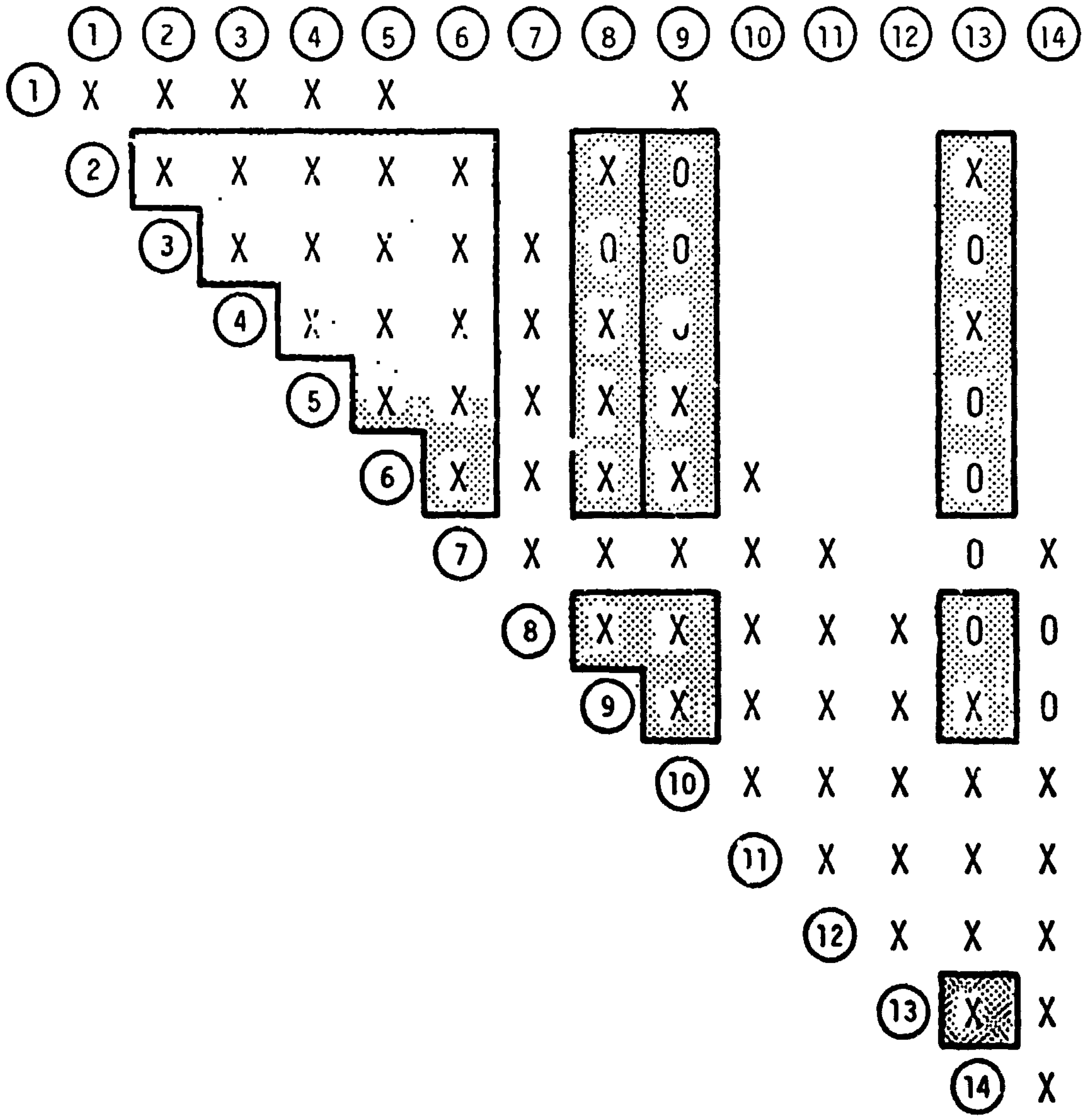

Figure 3.- Decomposition with second row as pivotal row.

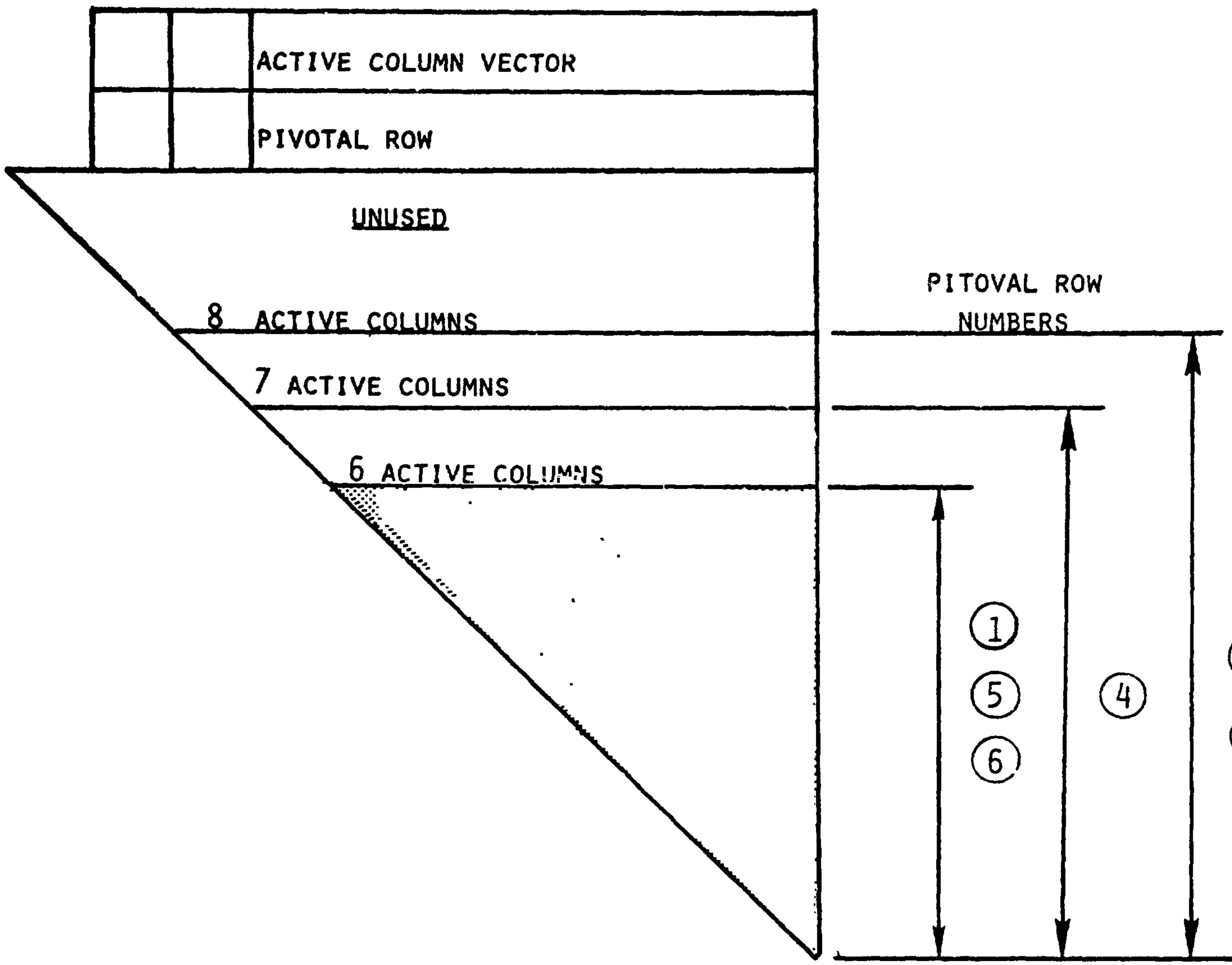

Figure 4.- Compact working storage for triangular decomposition.

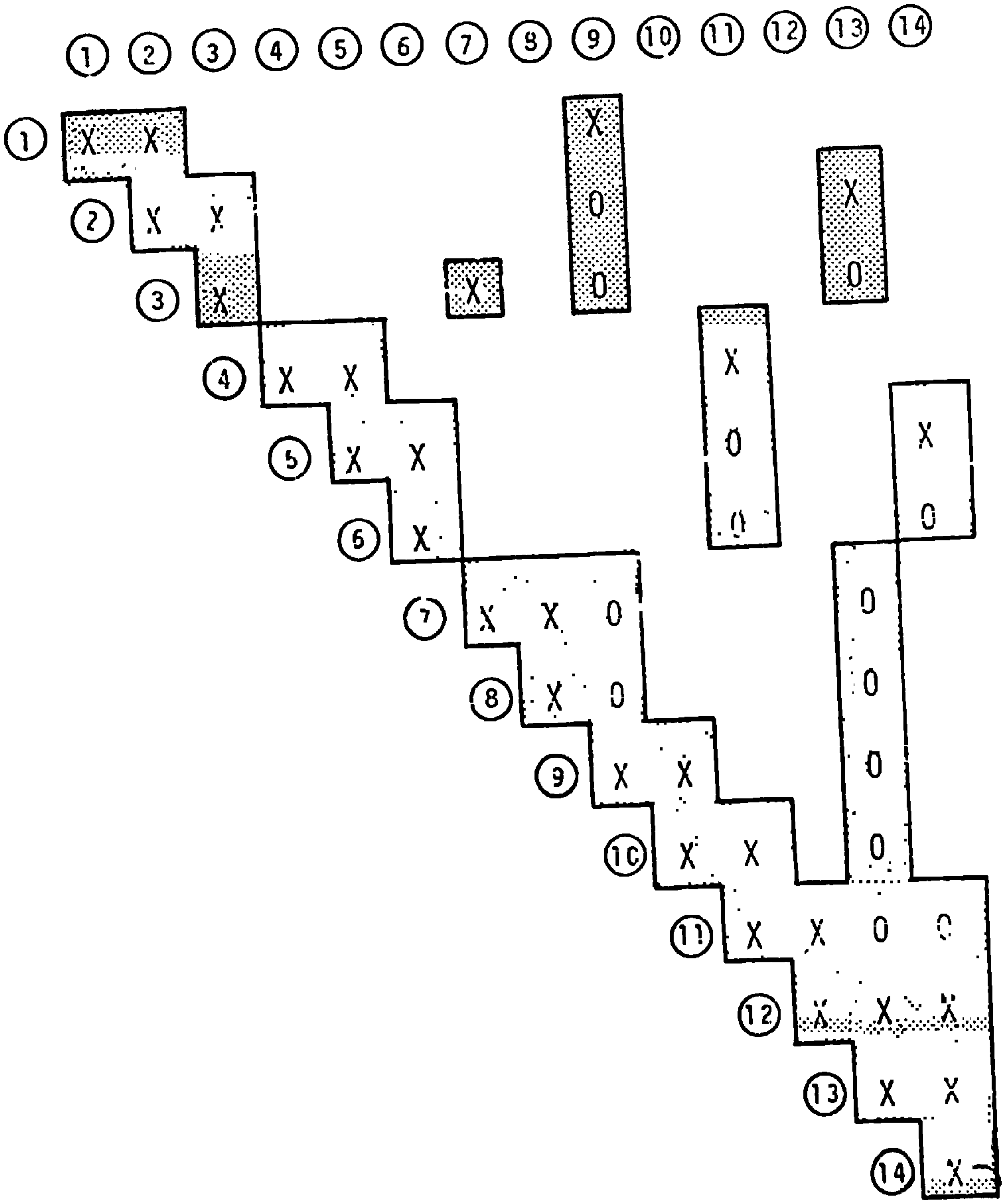

Figure 5.- Decomposition with termination of active columns.

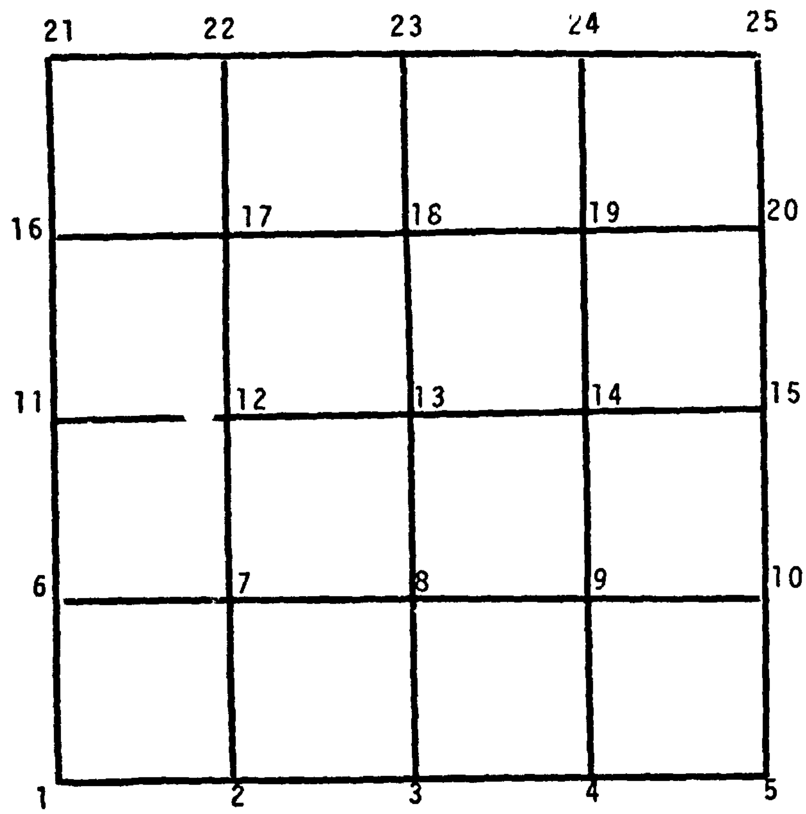

Figure 6.- Ordering for band matrix.

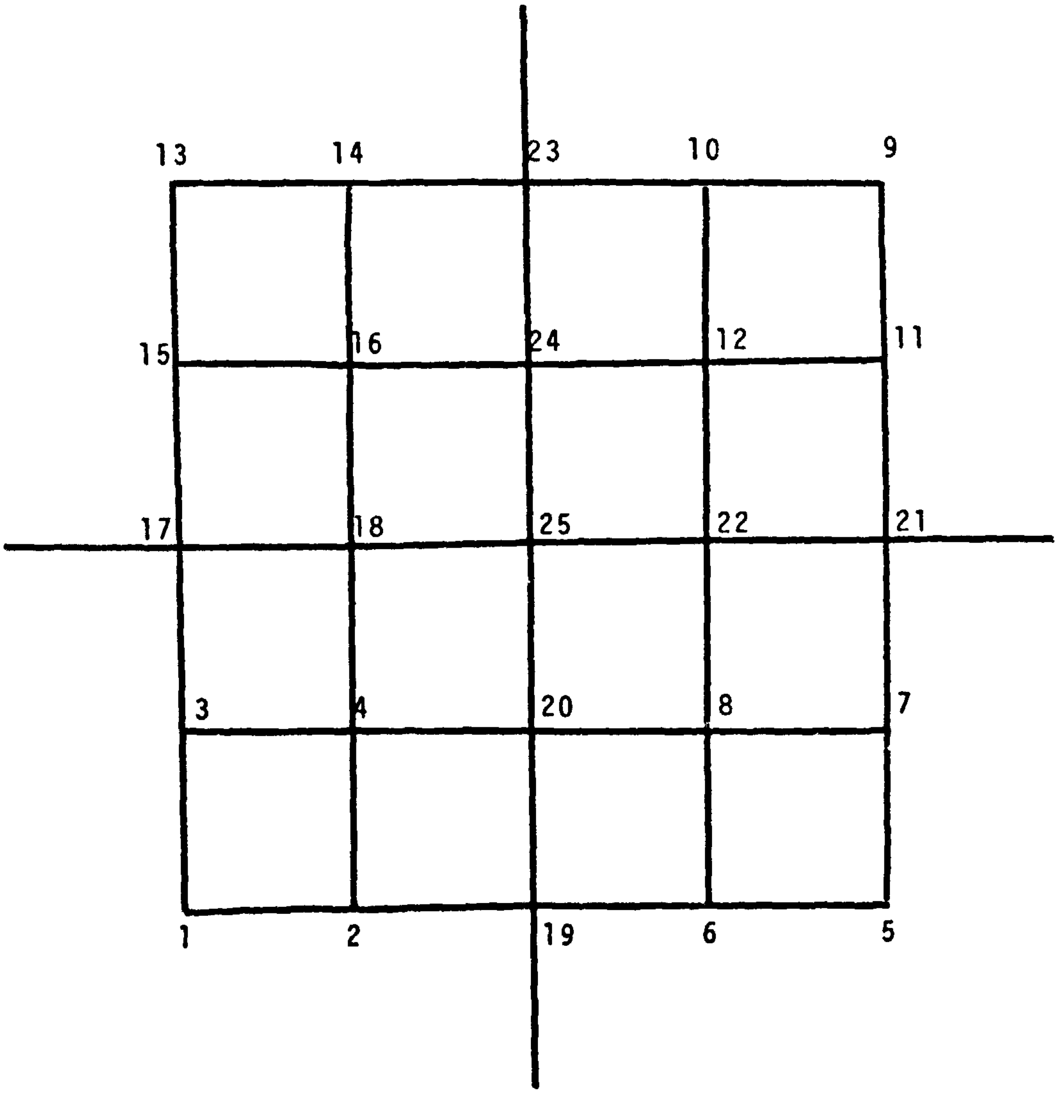

Figure 7.- Ordering for partitioning.

X	X	X																						
	X	0	X															X						
		X	X													X		0						
			X													0	X	0	X					
				X	X	X																		
					X	0	X											X						
						X	X											0		X				
							X											0	X	0	X			
								X	X	X														
									X	0	X											X		
										X	X									X		0		
											X									0	X	0	X	
												X	X	X										
													X	0	X							X		
						SYM.								X	X	X						0		
															X	0	X					0	X	
																X	X	0	0					
																	X	0	0			0	0	X
																		X	X	0	0	0	0	0
																			X	0	0	0	0	X
																				X	X	0	0	0
																					X	0	0	X
																						X	X	0
																							X	X
																								X

Figure 8.- Nonzero terms in triangular factor when ordered for partitioning.

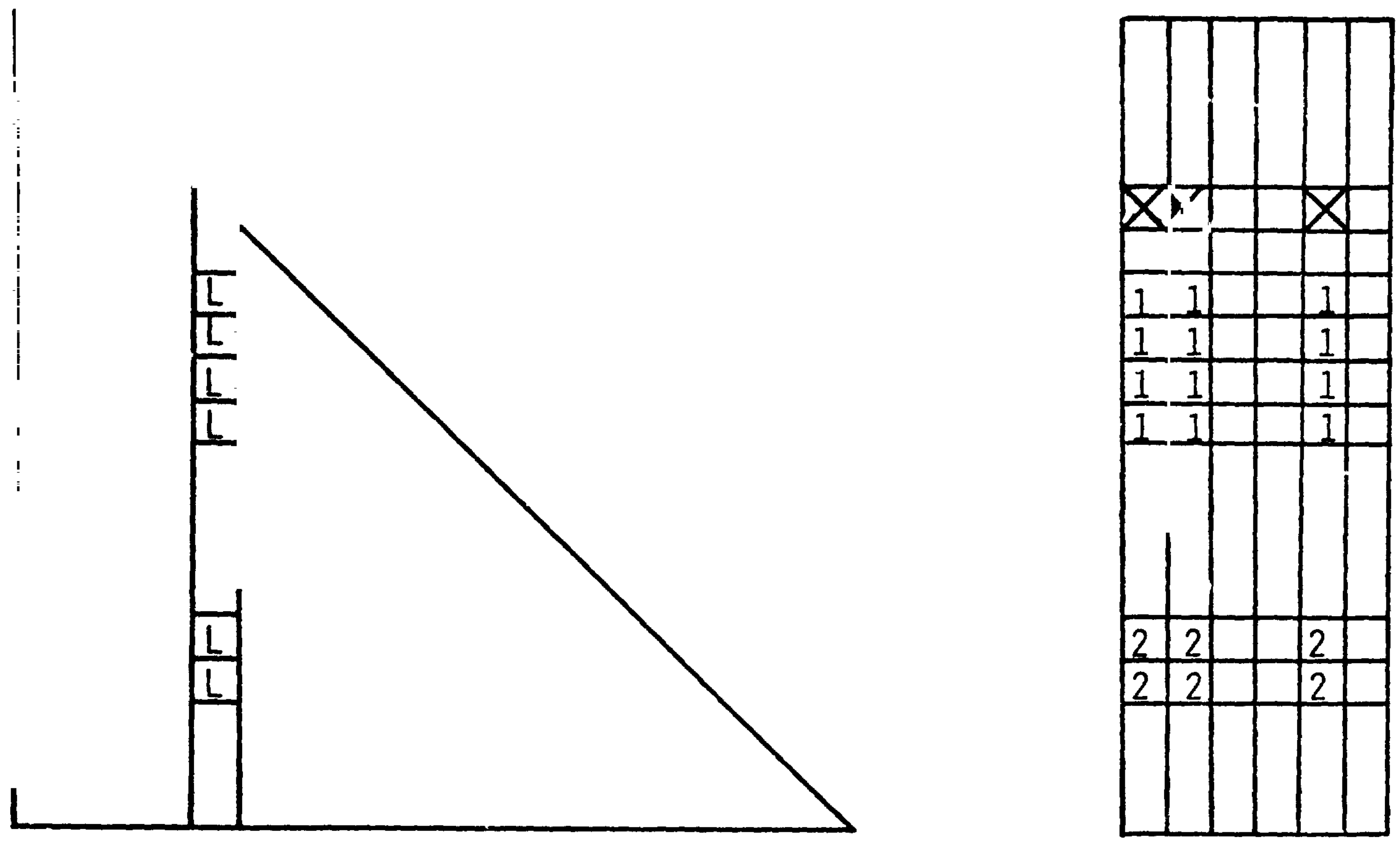

Figure 9.- Forward pass for equation solution.

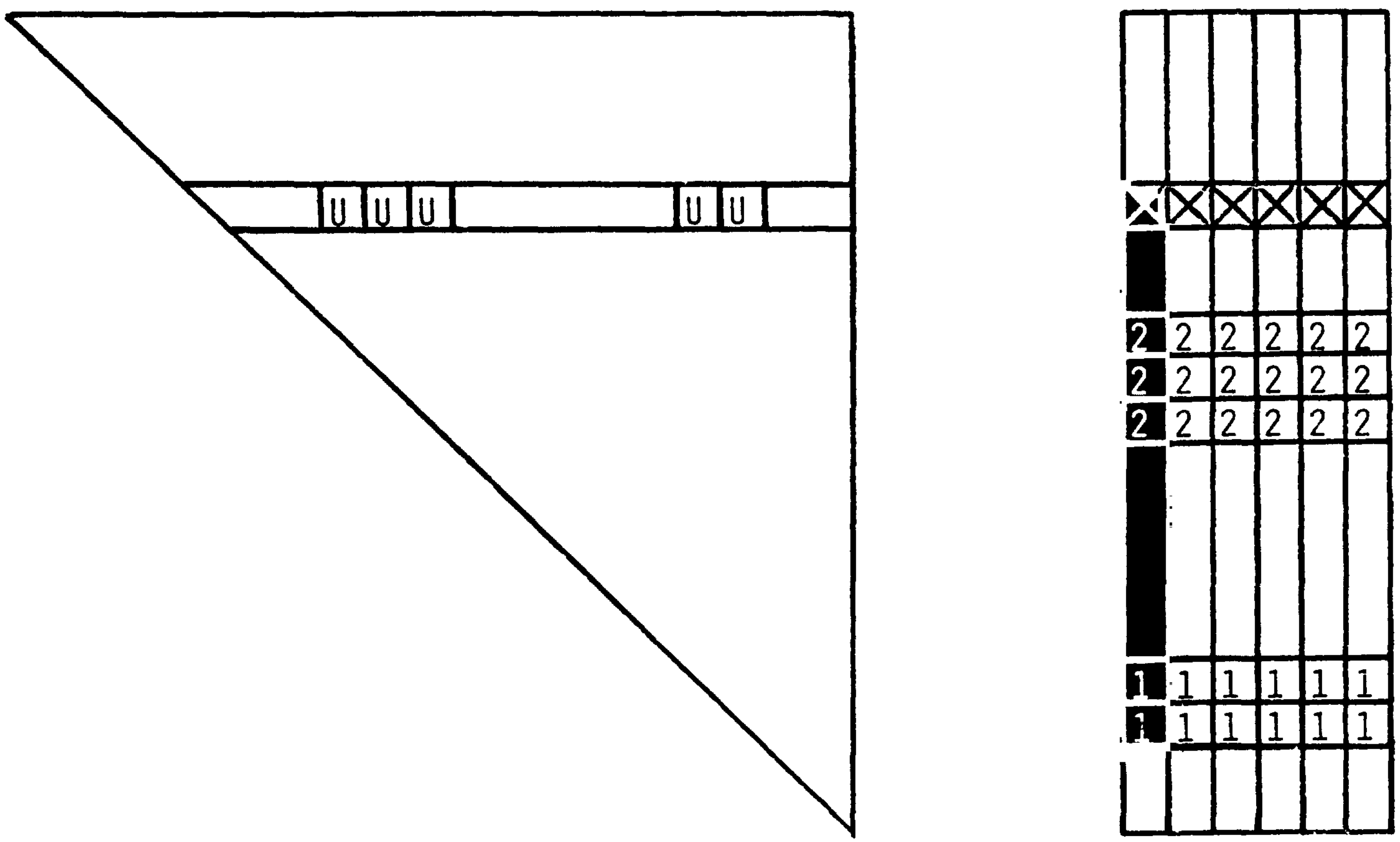

Figure 10.- Backward pass for equation solution.

N74-14589

NASTRAN BUCKLING STUDY OF A LINEAR INDUCTION MOTOR REACTION RAIL

By Jerry G. Williams

NASA Langley Research Center
Hampton, Virginia

ABSTRACT

NASTRAN was used to study problems associated with the installation of a linear induction motor reaction rail test track at the Department of Transportation High-Speed Ground Test Center near Pueblo, Colorado. Specific problems studied include determination of the critical axial compressive buckling stress and establishment of the lateral stiffness of the reaction rail under combined loads. NASTRAN results were compared with experimentally obtained values and satisfactory agreement was obtained. The reaction rail was found to buckle at an axial compressive stress of 78.6 MN/m^2 (11 400 lb/in^2). The results of this investigation were used to select procedures for installation of the reaction rail at the Pueblo test site.

INTRODUCTION

Linear induction motor propulsion systems for high-speed ground transportation vehicles are being tested by the U.S. Department of Transportation at its High-Speed Ground Test Center near Pueblo, Colorado. One of these vehicles, the Linear Induction Motor Research Vehicle (LIMRV) (see fig. 1), has a linear induction motor approximately 3 m (10 feet) long which exerts axial force against a vertical aluminum reaction rail supported by conventional crossties of a railroad track (ref. 1). The reaction rail is a thin plate-like member which is fusion welded into a continuous strip before clamping it to the crossties. It experiences thermal loads because of ambient temperature variations and localized axial loads which react the thrust of the linear induction motor. The axial loads are small in comparison to the thermal loads and are not considered in this study. In addition, lateral loads are imposed on the reaction rail by the guide wheels of the linear induction motor. A drawing showing the rail cross section and its attachment hardware is presented in figure 2.

The expected reaction rail temperature extremes at the test center range from 239 K (-30° F) to 333 K (140° F). Since there are no expansion joints in the reaction rail, normal atmospheric temperature variations cause the rail stresses to change as a function of the ambient temperature. For example, if the rail is installed at 333 K, compressive stresses will not be developed but the tensile stresses will be high at low temperatures. A stress-free installation temperature T_o between 239 K and 333 K subjects the rail to compressive stress when the rail temperature exceeds T_o and tensile stress when the temperature is lower than T_o.

Potential problems associated with compressive loading of the reaction rail, including buckling and reduced lateral stiffness, have been studied by using NASTRAN and by laboratory experiments. A detailed description of experimental procedures and results is presented in reference 2. A special-purpose finite-difference solution to the classical plate equations with appropriate boundary conditions was also formulated and these results are presented and compared with selected NASTRAN results in reference 3. The current paper presents additional results, provides details of the NASTRAN model, and makes comparisons between NASTRAN and experimental results for the critical buckling stress and the lateral displacement response of the rail under combined axial and compressive loads. Suggestions are also proposed for an improved reaction rail geometry.

NASTRAN MODEL

A drawing of the NASTRAN model used to represent the reaction rail is presented in figure 3. A rail length of 5.56 m (219 inch) was selected for study based on preliminary NASTRAN calculations which showed the critical buckling stress for this length rail to be nearly independent of the boundary conditions imposed on the rail ends. This insensitivity to end boundary conditions is important since it implies that it is unnecessary to define the exact boundary conditions imposed on the ends of a typical section selected from the continuous long-length test track. Geometric symmetry about the specimen midlength permitted the problem to be represented analytically by a model which included only half of the specimen length. A rectangular network of isotropic bending plus membrane quadrilateral plate elements (CQUAD2) was used to represent both the vertical web and base flange components.

At any given axial station, the rail vertical web was represented by seven plate elements and the base flange by four plate elements. Axially, the half-rail was represented by 34 plate elements. The center two base flange elements had cross-sectional dimensions of 4.53 cm (1.785 in.) wide and 1.0 cm (0.40 in.) thick while the two outer-base flange elements had cross-sectional dimensions of 1.82 cm (0.715 in.) wide and 0.79 cm (0.312 in.) thick. The vertical web voids were accounted for in the analysis by giving the isotropic quadrilateral plate elements an equivalent bending stiffness of 20.6 kN m (182 600 in-lb) which was calculated by treating the web as a sandwich plate and neglecting the separators between voids. This stiffness representation was verified by comparing NASTRAN and experimental results for the lateral displacement response of a 2.54 cm (1 in.) long section of rail loaded by a 445-N (100-lb) lateral force located at a height of 34.3 cm (13.5 in.) measured from the rail base flange. NASTRAN results compared favorably with experimental measurements as can be seen in figure 4.

Clamped boundary conditions were imposed at the rail end while both symmetry and antisymmetry conditions were considered at the rail midlength to insure that the lowest buckling solution was obtained. The restraint to displacement imposed by clamps mounted to wooden crossties every 0.483 m (19 in.) along the rail base flange was modeled analytically by a set of horizontal and vertical springs discretely located along the free edge of base flange elements. Mathematical ill-conditioning was experienced under certain conditions when the spring constants were specified by a CELS1 data card. This problem was overcome by representing the spring constants by CROD data cards in which a unit area rod had the required axial stiffness and zero torsional stiffness. The horizontal and vertical spring constant magnitudes were determined experimentally for the laboratory setup to be 12.6 and 75.3 MN/m per clamp (72 000 and 430 000 lb/in. per clamp), respectively. Details of the technique used to measure these properties are reported in reference 2. For comparison, calculations were also made assuming the clamps to be fully restrained.

Axial stress was thermally introduced into the NASTRAN model as a result of restraining the rail ends against axial displacement and introducing a near isothermal temperature increase. Lateral loading was introduced by applying a concentrated load at the model midlength and 15.2 cm (6 in.) below the top edge of the rail. Calculations were made with NASTRAN level 15 version. Buckling solutions were obtained by use of the inverse power method of eigenvalue extraction (rigid format 5) and lateral stiffness calculations were made by use of the differential stiffness capability (rigid format 4).

As a check on modeling and problem formulation, the axially loaded classical plate-buckling problem in which the two vertical ends and the lower edge are clamped and the upper edge is free was solved using NASTRAN. The plate size and model characteristics, except for the difference in lower edge boundary and absence of the base flange, were identical to those for the rail problem. The NASTRAN finite-element solution showed almost exact agreement with the known solution (ref. 4). This agreement gave confidence that the model was well formulated and that grid-point spacing was sufficiently refined.

Typical Langley Research Center costs to compute the critical buckling stress for the reaction rail model which had approximately 2000 degrees of freedom using a CDC 6600 computer was $325. This cost included approximately 1700 CPU seconds and 28000 O/S calls and was run at a field length of $155\ 000_8$. Lateral stiffness calculations cost approximately $220 and included approximately 1250 CPU seconds and 18000 O/S calls.

EXPERIMENT

The laboratory test setup involved clamping a 5.56-m (219-in.) length of reaction rail to the center line of wooden crossties spaced every 0.483 m (19 in.) in a fashion representative of the field installation method. This length included a 13-cm (5-in.) section at each end of the rail between the last base flange clamp and the end fixture. Clamped boundary conditions were imposed at the rail ends. Rail crossties and clamp hardware were taken from stock used in the Pueblo field installation. Axial compressive stress in the rail was developed by restraining the ends against axial displacement and heating the rail in a near isothermal manner using radiant heater panels.

Thermocouples were used to measure the rail temperature, strain gages were used to determine stresses, and linear voltage differential transducers (LVDT) were used to measure lateral displacements. The electronic output was recorded automatically and stored on magnetic tape for later reduction. A detailed description of the test technique is reported in reference 2 and a photograph of the laboratory setup is presented in figure 5.

Buckling and lateral stiffness experiments were conducted on each of two reaction rail specimens. Prior to each test, the rail was surveyed and, when necessary, shims were used to obtain the desired conditions of straightness. A brief description of these two experiments is presented below.

Buckling of a "Well-Alined" Rail

In this test the specimen was heated to induce axial compressive stress until large lateral deformations were observed. The term "well-alined" indicates a specimen which was installed as nearly straight on the test bed as was practical. Typically, the upper edge and base flange were laterally alined within ±0.38 mm (±0.015 in.) and ±0.13 mm (±0.005 in.), respectively, of a straight line drawn through the end points of the rail. This arrangement is considerably better than that normally achieved in the field. The purpose of this experiment was to define the rail buckling stress and mode shape and to determine whether large lateral deformations are elastic.

Lateral Stiffness Test

This test involved applying a lateral point load at the rail midlength and 15.2 cm (6 in.) below the top edge in combination with selected magnitudes of axial stress. The purpose of this experiment was to determine the lateral stiffness of the rail as a function of the applied axial compressive stress. Lateral stiffness as used in this report is defined as the ratio of the lateral point load to the lateral displacement at the point of application of the load.

RESULTS

Buckling

Theoretical and experimental buckling results for a "well-alined" rail are presented in table I. Two NASTRAN solutions are presented, one in which the base flange clamps were spring supported and the other in which the base flange clamps were fully restrained (displacements and rotations set equal to zero). The critical buckling stress for the case in which the flange clamps were spring supported is 86.2 MN/m^2 (12 5000 lb/in^2) which is approximately 7 percent lower than the solution in which the base flange clamps were fully restrained. In both cases the lowest buckling stress was obtained with symmetry boundary conditions imposed at the specimen midlength.

The experimentally obtained critical buckling stress was 78.6 MN/m^2 (11 400 lb/in^2) which is 9 percent lower than the NASTRAN spring-supported clamp solution. The experimental value corresponds to a rail temperature rise of 49.1 K (88.4° F) from a stress-free state.

The classical buckling solution of a rectangular plate with properties identical to the rail vertical web which is clamped on the ends and free on the top edge is 37.0 MN/m^2 (5400 lb/in^2) for the lower edge continuously simply supported and 111.4 MN/m^2 (16 200 lb/in^2) for the lower edge continuously clamped (ref. 2). These two extremes in boundary conditions bracket the base flange support conditions and the reaction-rail base flange/clamp-support system results fall approximately midway between the results for the continuous simple support and clamped conditions.

A comparison of NASTRAN and experimental results for the buckling lateral displacement of a line 2.54 cm (1 in.) below the rail upper edge is presented in figure 6. The axial distance from the center line is normalized by the rail height (0.533 m (21 in.)) and lateral displacements are normalized by the maximum displacement magnitude (which occurs at the top edge and center of the rail). The experimental mode shape is not symmetric about the center line, but is biased to the right. This irregularity may have been caused by variations in base flange support conditions. Both NASTRAN and experimental results exhibit a buckling mode shape of five half-waves for the 5.56 m (219-in.) long specimen. The midspan half-wave length given by both NASTRAN and the experiment was approximately 1 m (39.4 in.). A photograph of the buckled rail is presented in figure 7.

Lateral Stiffness

The normal operating clearance between the linear induction motor and the reaction rail is only 2.22 cm (0.875 in.) which sets an upper limit on the permissible peak-to-peak amplitude of lateral displacements. The lateral stiffness of the reaction rail is important not only to static load consideration but also to the dynamic performance of the LIMRV. Although this study addresses only the static behavior of the reaction rail, rail properties necessary for conducting a dynamic analysis were obtained. As indicated earlier, lateral stiffness is defined as the ratio of the lateral point load to the lateral deflection produced at the point of application of the load. The point lateral load in this study was located at the center of the specimen and 15.2 cm (6 in.) below the rail upper edge. The vertical location was selected to coincide with a position half-way between the upper and lower guidance wheels at one end of the linear induction motor. Experimentally, loads of up to 7560 newtons (1700 lb) were applied and lateral displacements as great as 1.9 cm (0.75 in.) were experienced. In all cases the rail elastically reacted the loads and returned to its original configuration upon release of the load.

The variation in lateral spring constant with axial compressive stress is presented in figure 8. The experimental results show a lateral spring constant of 820 kN/m (4680 lb/in.) at zero stress which decreases nearly linearly to a value of 350 kN/m (2000 lb/in.) at an axial compressive stress of 74.5 MN/m^2 (10 800 lb/in^2). The NASTRAN solution in which the base flange clamps were fully restrained is only slightly lower than the experimental result (e.g., by only 5 percent for zero axial stress). The effect of representing the clamps by horizontal and vertical springs is to reduce the lateral stiffness by approximately 6 percent over the fully restrained condition.

The lateral displacement of the vertical portion of the rail corresponding to 35.6 MN/m^2 (5160 lb/in^2) axial stress and a lateral load of 4448 N (1000 lb) obtained using NASTRAN is presented in the displacement contour plot of figure 9. Displacements have been normalized with respect to the maximum amplitude which has been scaled to a value of 100. The maximum amplitude is approximately 1.14 cm (0.45 in.) and occurs at the midlength and upper edge of the rail. In this NASTRAN solution, the clamps were modeled as horizontal and vertical springs.

In addition to reducing the rail lateral stiffness, axial compressive stress also affects the lateral displacement field of a laterally loaded rail. This effect is shown in figure 10 in which the lateral displacements of a line located 2.54 cm (1 in.) below the upper edge are plotted for three magnitudes of axial stress in combination with a lateral load of 4447 N (1000 lb). An increase in the applied axial stress causes an increase in the maximum displacement amplitude and a decrease in the midspan effective wave length. As the axial compressive stress approaches the buckling stress, the combined load results in a distorted five half-wave buckled mode shape biased in the direction of the applied lateral load. NASTRAN and experimental results are in good agreement for an axial stress of zero and 35.6 MN/m^2 (5160 lb/in^2). Experimental results are not available for an axial stress of 71.2 MN/m^2 (10 300 lb/in^2) since 4448 N (1000 lb) lateral load in combination with this axial load would have resulted in unacceptably large lateral displacements. Lower magnitudes of lateral load for this axial stress, however, did establish the distorted five half-wave pattern indicated by the NASTRAN solution.

Improved Rail Design

A parametric study was made to determine the increase in the critical buckling stress resulting from an increase in the bending stiffness of the lower portion of the rail vertical web. The portion considered was the lower one-seventh of the vertical web (7.62 cm (3 in.) measured from the vertical web/base flange intersection). Results of this study are presented in figure 11 where the reference bending stiffness and the reference critical buckling stress are those of the previously described model.

A 25-percent increase in the critical buckling stress is obtained by increasing the bending stiffness by a factor of 8. This increase can be accomplished for the subject rail by taking the same cross-sectional area and increasing the total thickness of the lower portion of the vertical web to a dimension of approximately 5.5 cm (2.2 in.). This approach may have merit in the geometric design of future reaction rails which react to compressive loading subject, of course, to geometric constraints imposed by the linear induction motor.

CONCLUDING REMARKS

Satisfactory agreement was achieved between NASTRAN and experimental results for the buckling load, buckling mode shape, lateral displacement response to a point lateral load, and lateral stiffness of the reaction rail as a function of axial load. Parametric studies of the stiffness of the lower portion of the reaction rail indicate substantial improvements can be obtained in the critical buckling stress by increasing the lower portion bending stiffness.

The results of this investigation show that substantial axial compressive loads can be carried by the LIMRV reaction rail without buckling. Furthermore, lateral deformations up to 1.9 cm (0.75 in.) are elastic and disappear upon release of the imposed loads. The latter result means that even if the reaction rail is installed at a stress-free temperature which is later exceeded by sufficient magnitude to cause buckling, the event is not catastrophic if test operations are suspended for this interim period.

Based on these results, the recommendation was given the Department of Transportation that the LIMRV reaction rail test track be installed at a stress-free temperature of around 297 K (75° F). The predicted buckling temperature, based on a 78.6-MN/m^2 (11 400-lb/in^2) buckling stress, would then be 346 K (163° F) which is higher than the rail can experience through solar heating at the test center. This recommendation was adopted by the Department of Transportation in the fall of 1972 in the installation of the Pueblo test track. Successful operation of the LIMRV has been in progress since that time with no problems encountered with the reaction rail.

REFERENCES

1. Anon.: Linear Induction Motor Research. Vol. I, Rep. 71-7094, AiResearch Manufacturing Co., Oct. 1971. (Available as NTIS PB 212-041.)

2. Haight, E. C.; Hutchens, W. A.; and Williams, J. G.: Experimental Determination of the Compressive Behavior of a Linear Induction Motor Reaction Rail. MTP-374, The Mitre Corp., Nov. 1, 1972. (Available as NTIS PB 214-506.)

3. Williams, Jerry G.; Haight, Edward C.; and Hutchens, Walter A.: Compressive Behavior of a Linear Induction Motor Rail. Paper to be presented at Intersociety Transportation Conference (Denver, Colorado), September 24-27, 1973.

4. Lundquist, Eugene E.; and Stowell, Elbridge Z.: Critical Compressive Stress for Outstanding Flanges. NACA Rep. 734, 1942.

TABLE I. COMPARISON OF THEORETICAL AND EXPERIMENTAL

BUCKLING RESULTS FOR A WELL-ALINED RAIL

	Buckling stress, MN/m^2 (lb/in^2)	Temperature rise to buckle, K (°F)	Buckling half-wave length,[1] m (in.)
NASTRAN Base flange clamps spring supported[2]	86.2 (12 500)	53.8 (96.9)	1.03 (40.5)
NASTRAN Base flange clamps fully restrained	92.4 (13 400)	57.7 (103.9)	1.00 (39.4)
Experiment	78.6 (11 400)	49.1 (88.4)	0.97 (38.2)

[1]Half-wave length measured at center of specimen or model.

[2]Clamp horizontal and vertical spring constants equal 12.6 and 75.3 MN/m per clamp (72 000 and 430 000 lb/in. per clamp), respectively.

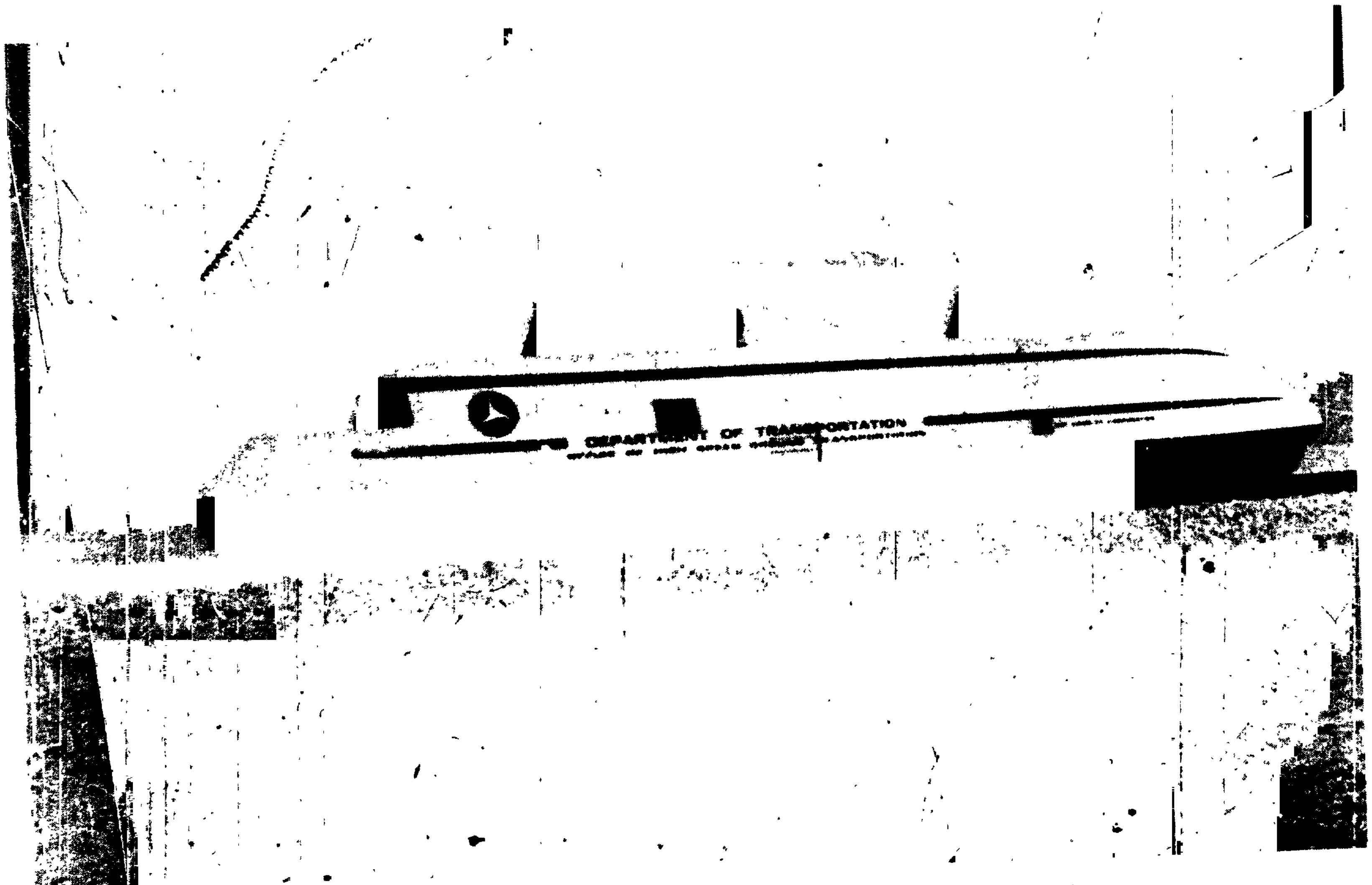

Figure 1. Linear Induction Motor Research Vehicle (LIMRV).

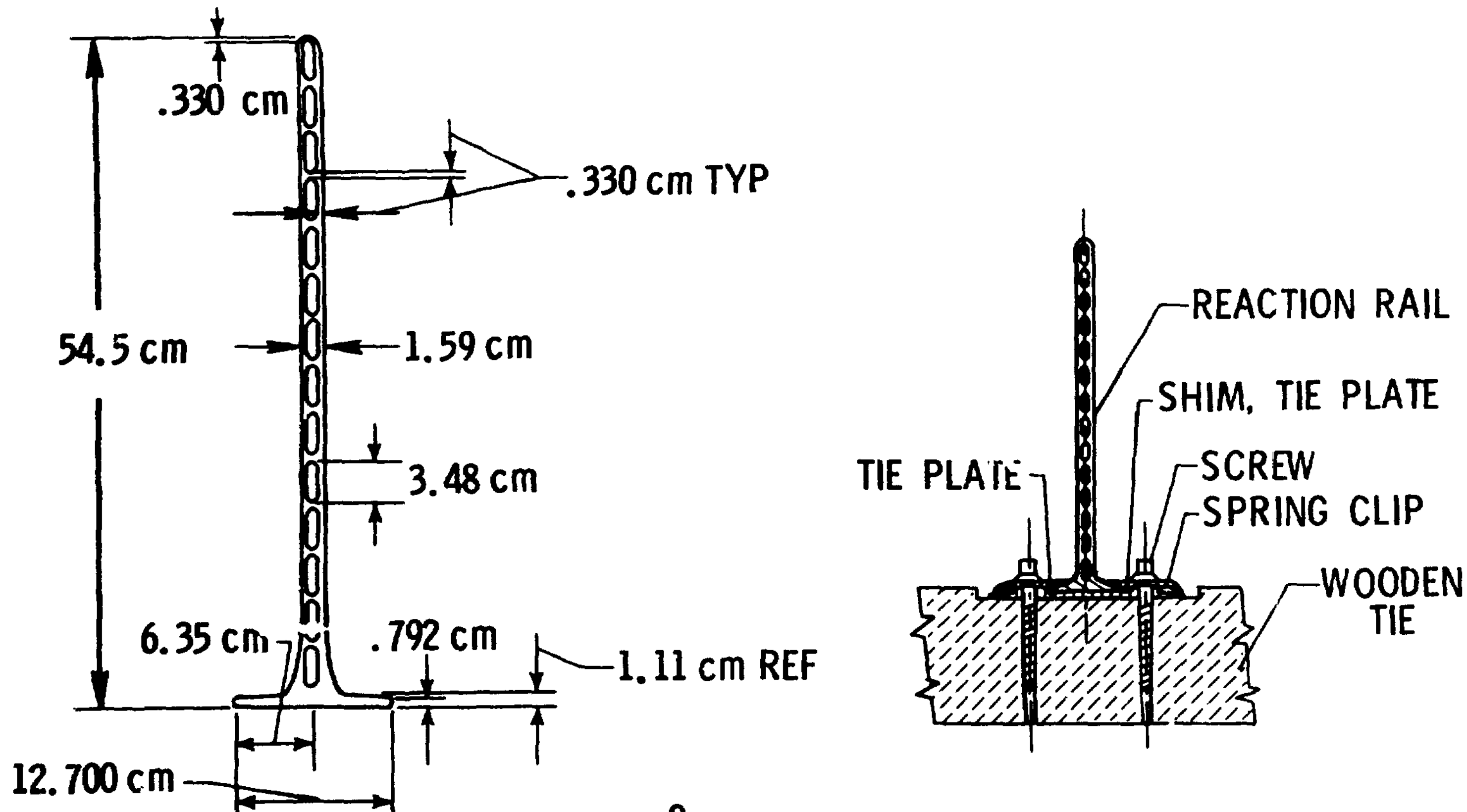

MODULUS OF ELASTICITY = 69.0 GN/m^2
POISSON'S RATIO = 0.3
CROSS-SECTIONAL AREA = 55.94 cm^2
COEFFICIENT OF LINEAR EXPANSION = 2.32×10^{-5} m/m/K
MASS PER UNIT LENGTH = 15.5 kg/m

Figure 2. Reaction rail dimensions and attachment hardware.

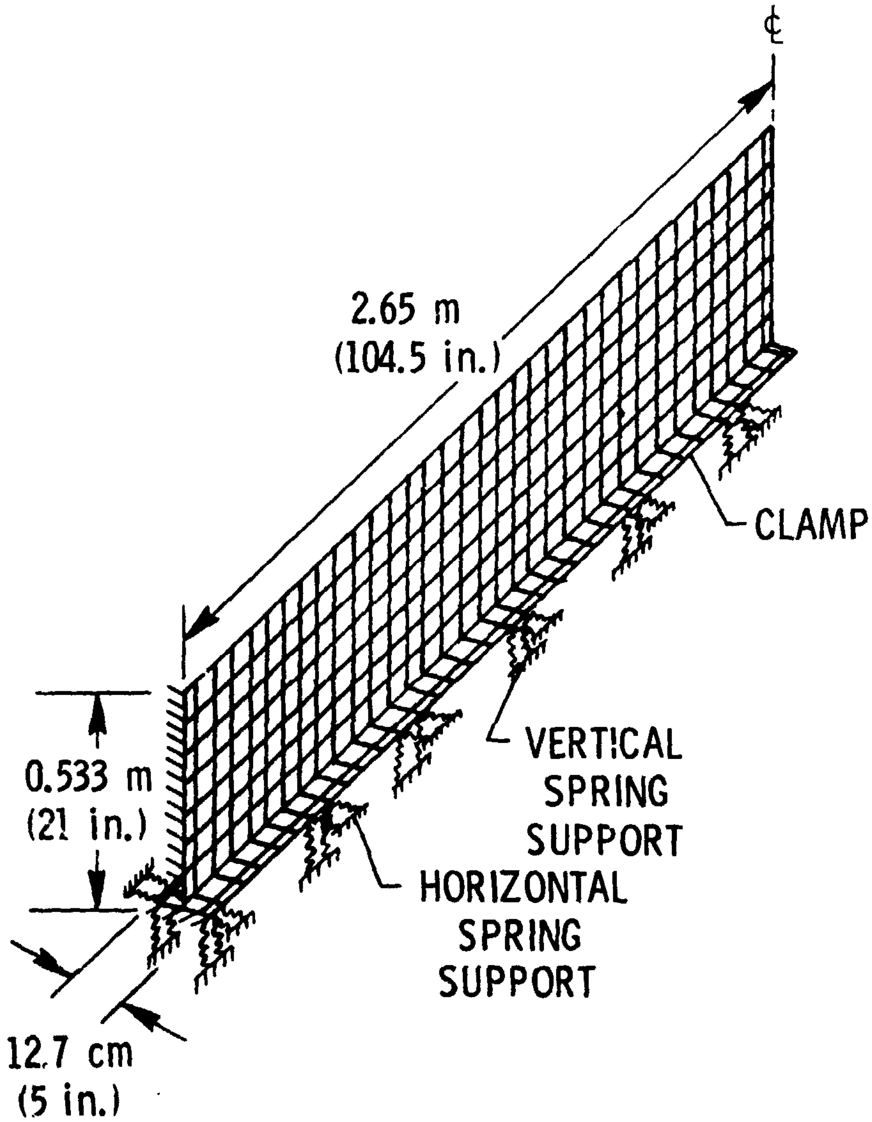

Figure 3. NASTRAN model.

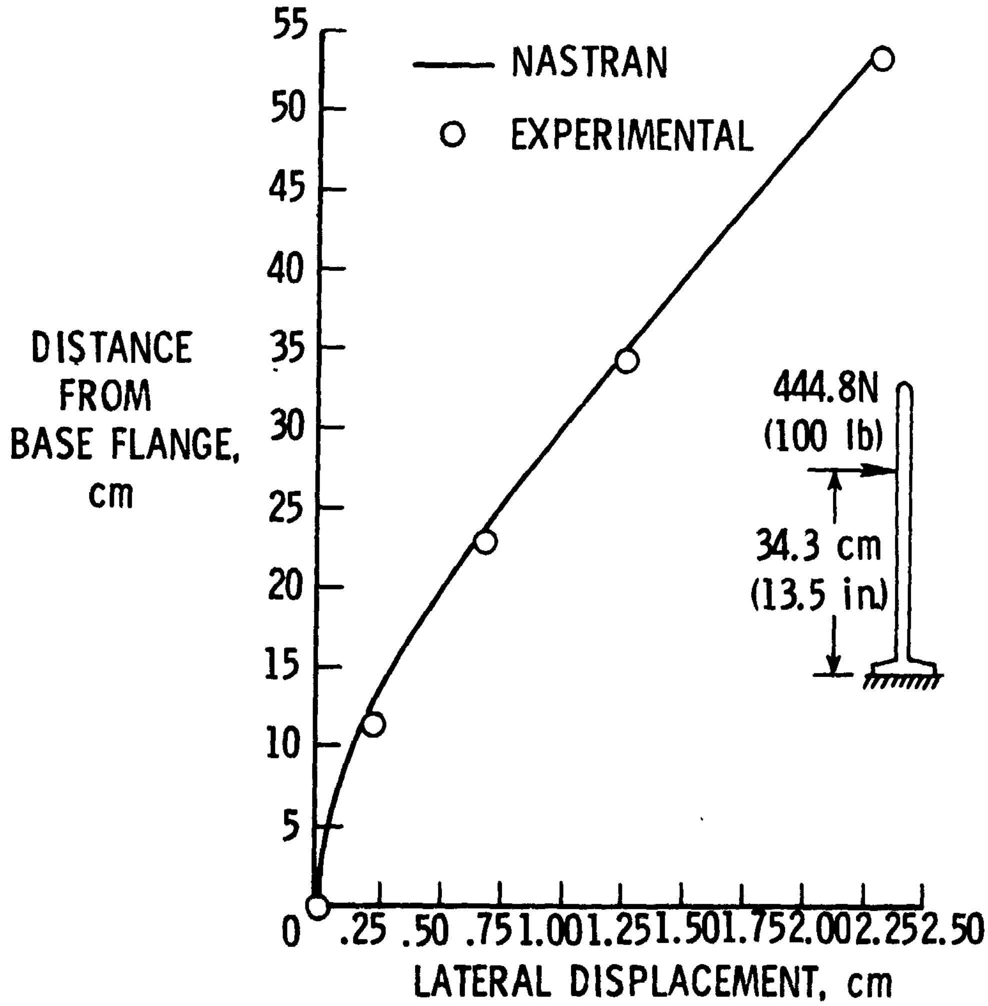

Figure 4. Lateral displacement of 2.54 cm (1 in.) long rail section due to 444.8N (100 lb) lateral load applied 34.3 cm (13.5 in.) above the base flange.

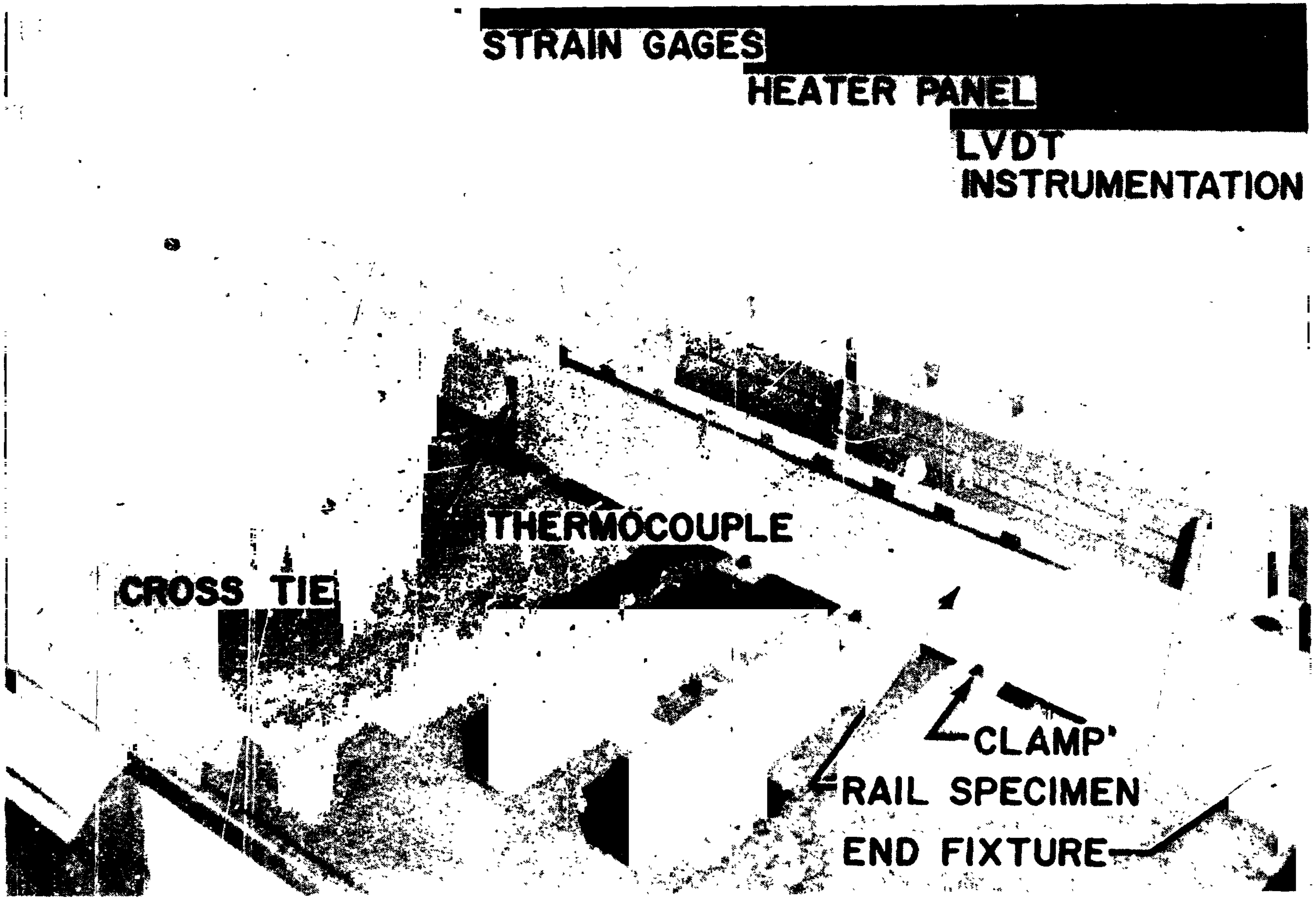

Figure 5. Experimental test setup.

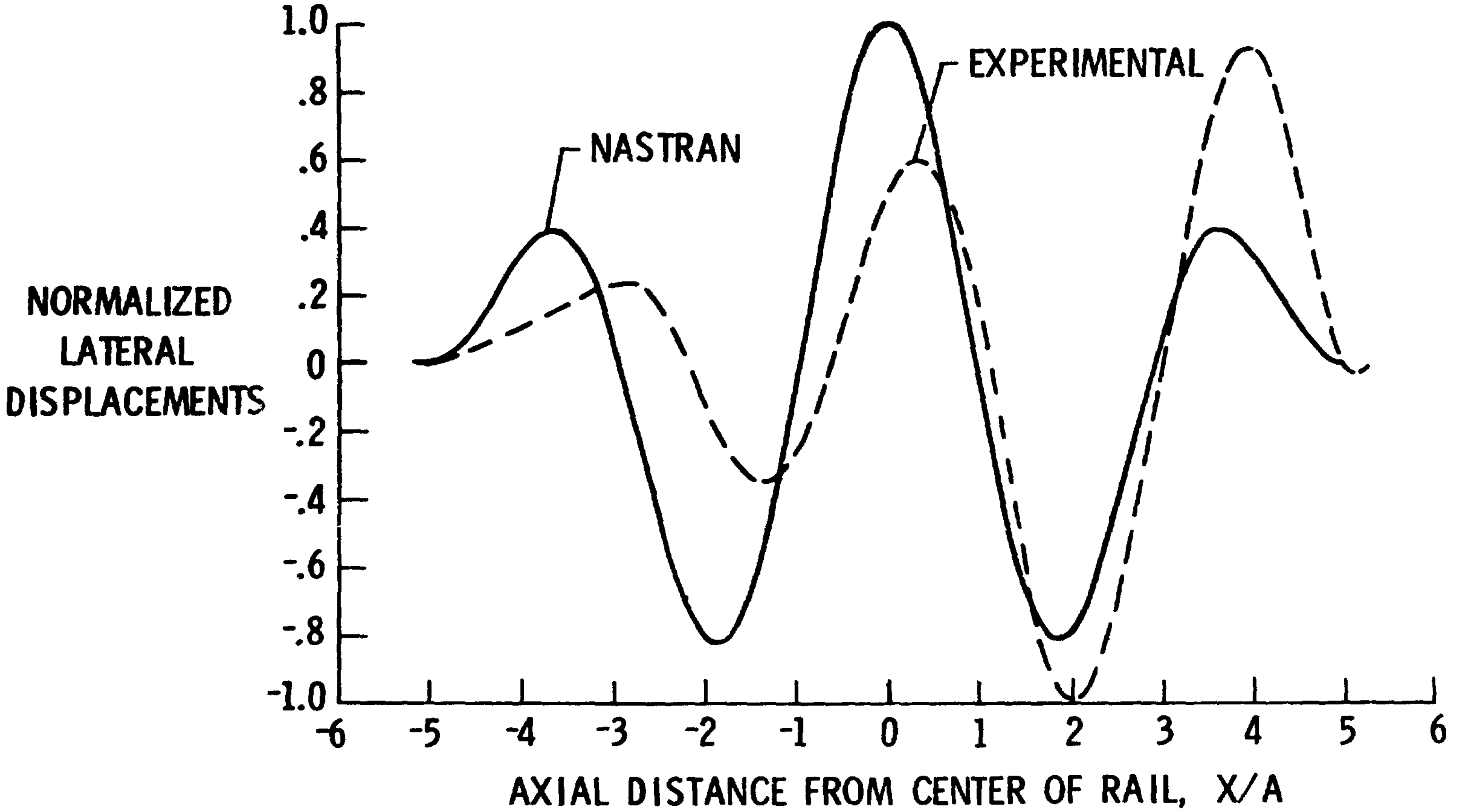

Figure 6. Buckled mode, theoretical and experimental deflections of line 2.54 cm (1 in.) from rail top edge. A is the rail height equal to 0.533 m (21 in.).

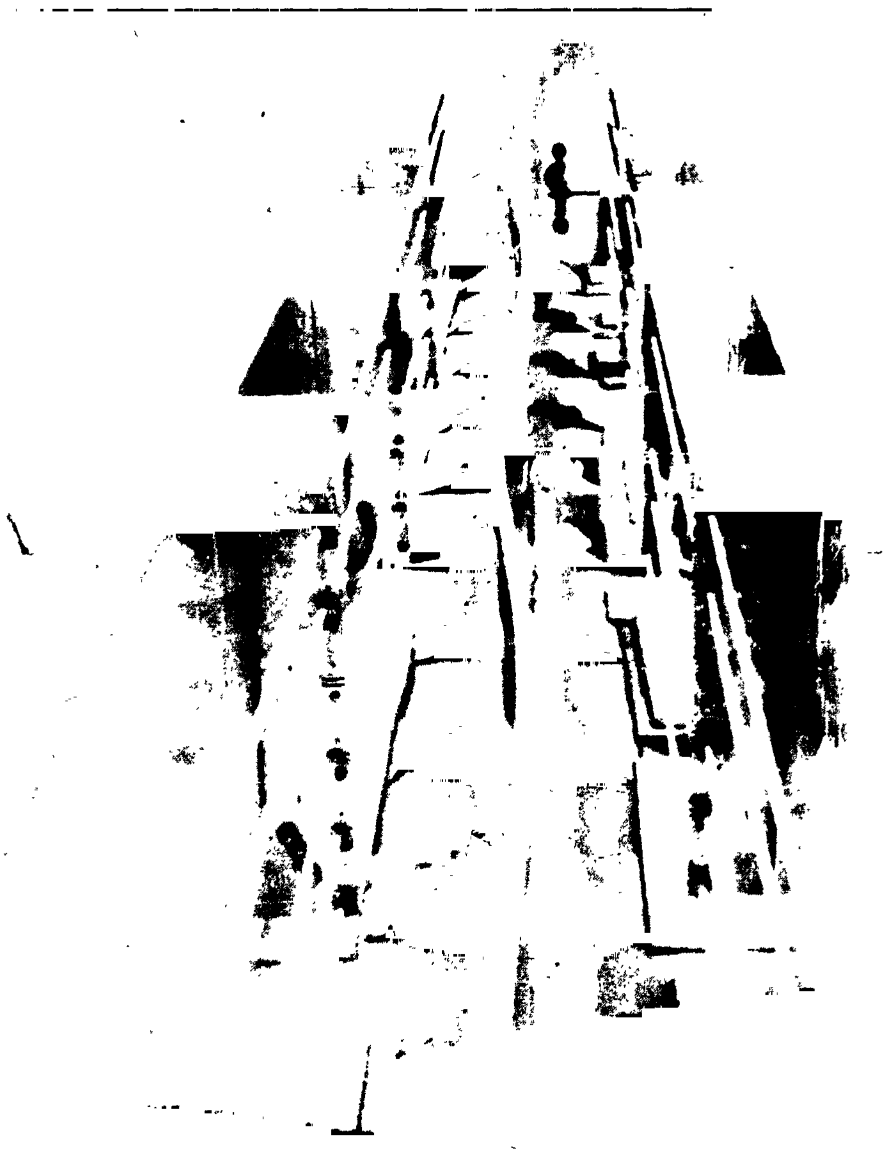

Figure 7. Buckled rail.

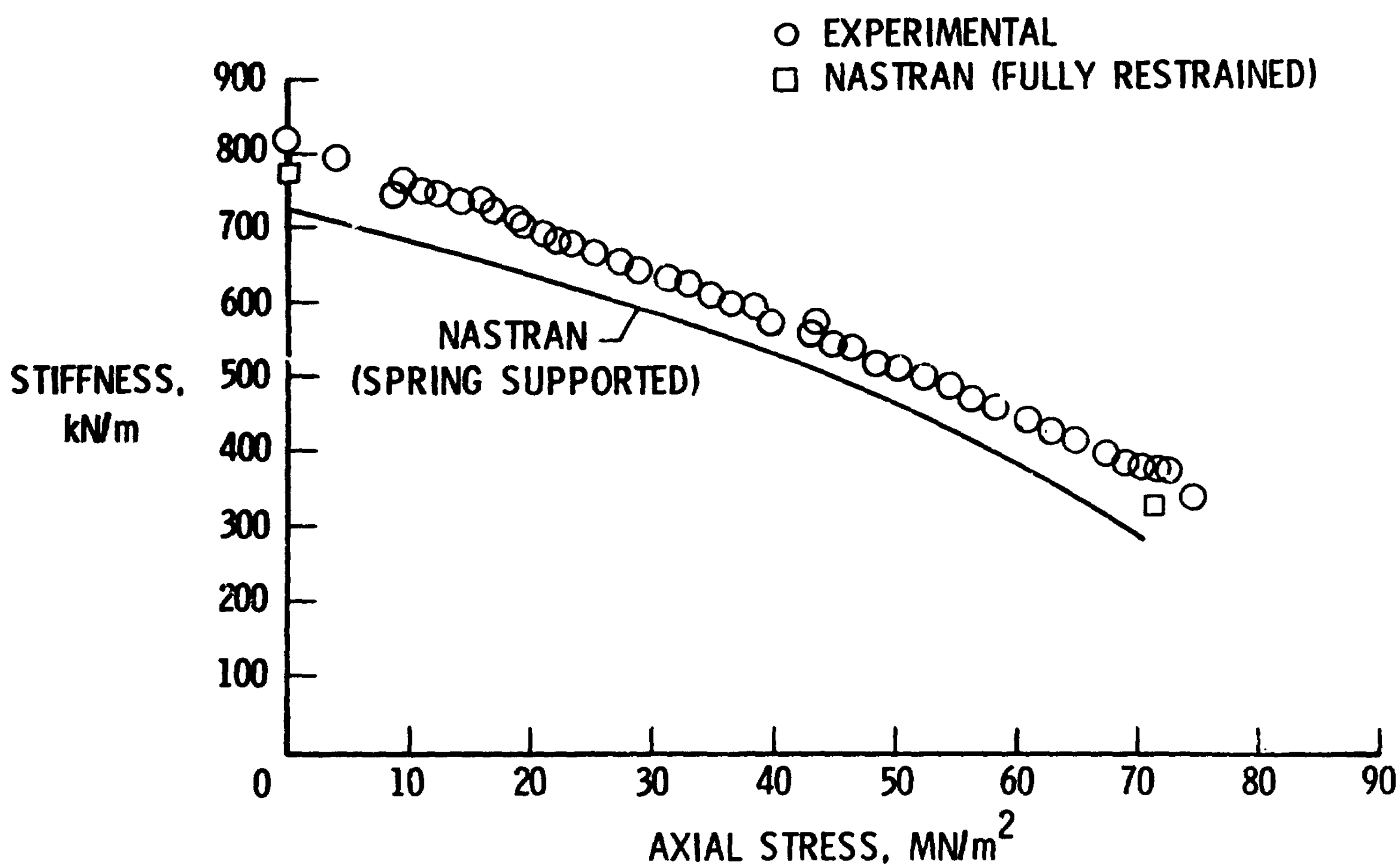

Figure 8. Variation of rail lateral stiffness with axial stress.

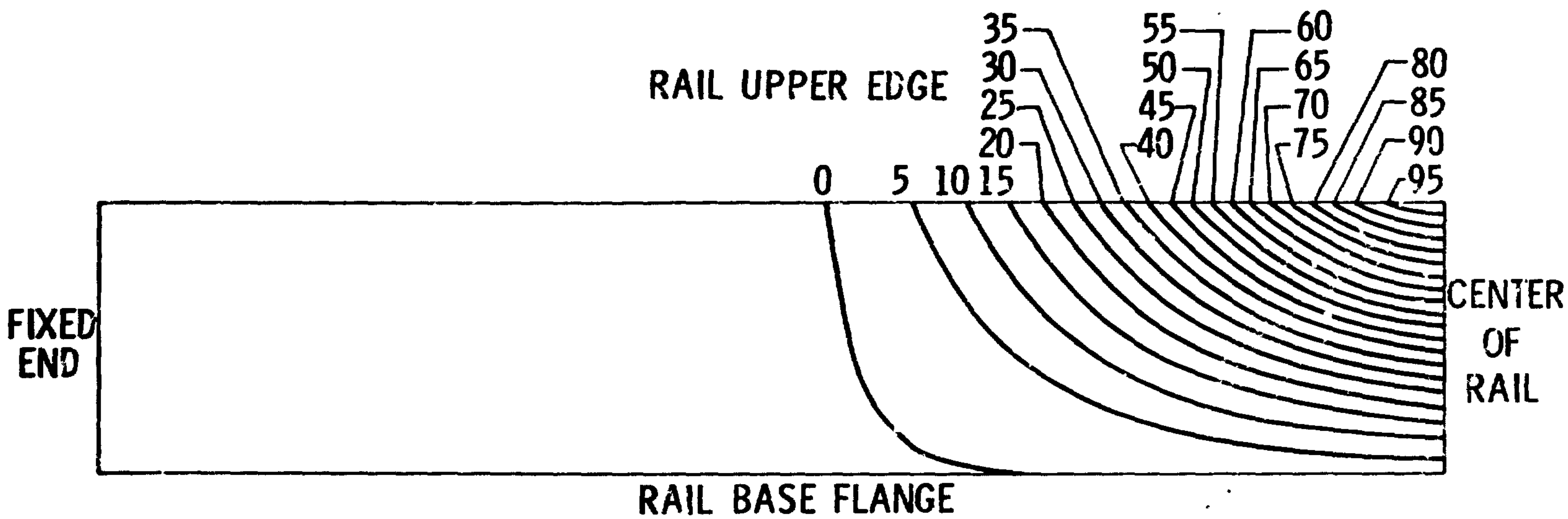

Figure 9. Normalized contour plot for displacements of vertical web under combined axial stress (35.6 MN/m^2 (5160 $lb/in.^2$)) and 4448 N (1000 lb) lateral load. Maximum amplitude equal 1.14 cm (0.45 in.).

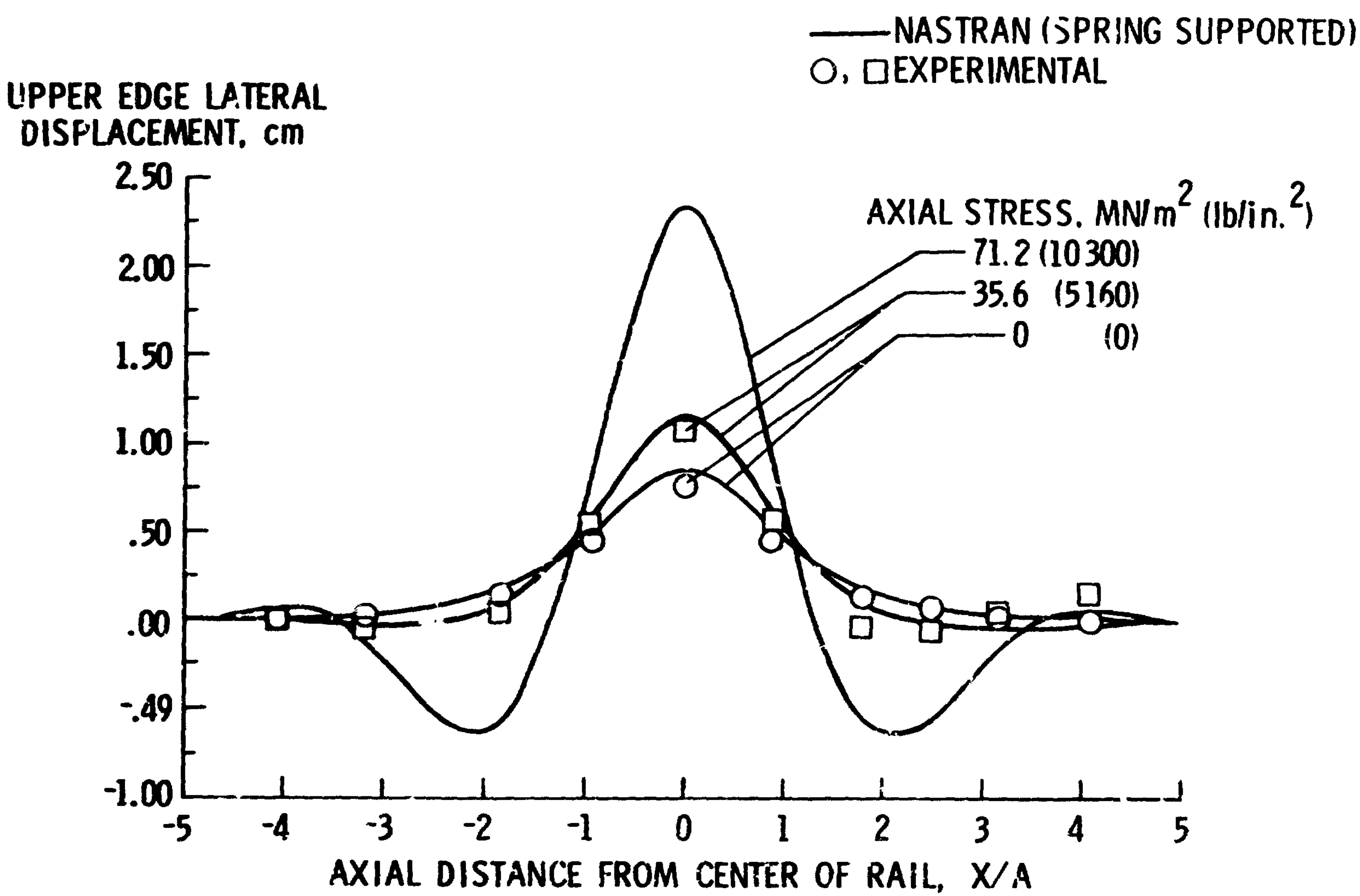

Figure 10. Lateral deflections of line 2.54 cm from rail top edge, 4448 N (1000 lb) lateral load and selected magnitudes of axial stress. A is the rail height equal to 0.533 m (21 in.).

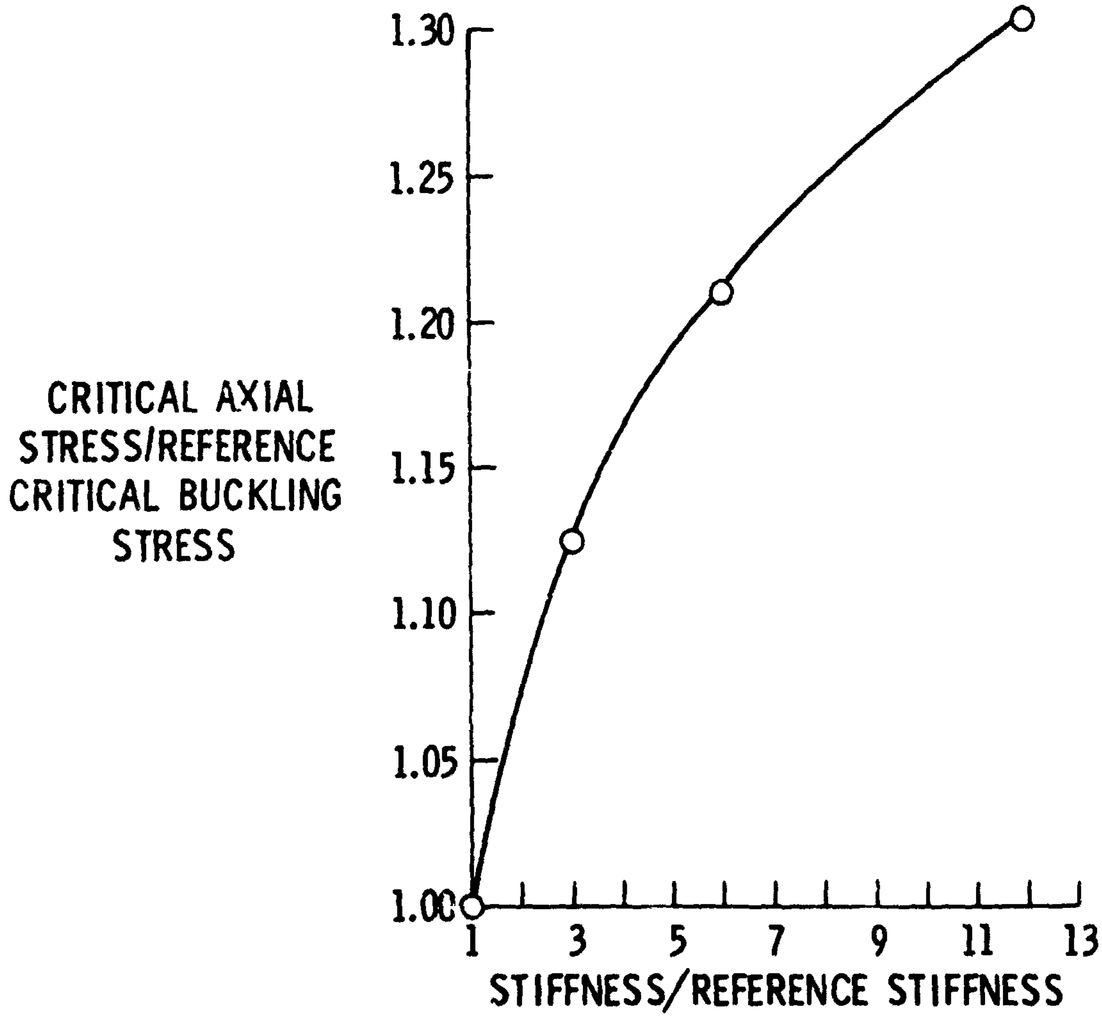

Figure 11. Variation of increase in critical buckling stress with increased bending stiffness of lower 7.62 cm (3 in.) of rail vertical web.

N74-14590

FINITE ELEMENT STRESS ANALYSIS OF POLYMERS AT HIGH STRAINS

by Michel Durand and Etienne Jankovich

KLEBER COLOMBES, Theoretical Tire Engineering,
COLOMBES, France

SUMMARY

A numerical analysis is presented for the problem of a flat rectangular rubber membrane with a circular rigid inclusion undergoing high strains due to the action of an axial load. The neo-hookean constitutive equations are introduced into the general purpose TITUS program by means of equivalent hookean constants and initial strains. The convergence is achieved after a few iterations. The method is not limited to any specific program. The results are in good agreement with those of a Company sponsored photoelastic stress analysis The theoretical and experimental deformed shapes also agree very closely with one another. For high strains it is demonstrated that using the conventional HOOKE law the stress concentration factor obtained is unreliable in the case of rubberlike material.

INTRODUCTION

The structure of a radial motor vehicle tire is made up of two types of components namely the reinforcing cords and the rubber. The most immediate problem in tire stress analysis is that of the large displacements in the inflated tire described in a previous paper (Reference 1). It appears that the more important components are the reinforcing cords allowing the tire to take a stable inflated shape. This particular problem can now be considered as solved.

However, in order to solve the complete problem, the rubber's behavior must also be adequatly analyzed by means of an as economical as possible modification of existing programs. Up until now, this very challenging problem of non linear material behavior and incompressibility has only been solved in a few special cases (Reference 2).

The aim of the present work is to stress analyze the rubber parts of the tire by using NASTRAN and TITUS. A test specimen encompassing a rigid inclusion is calculated in uniaxial extension and the results are compared with those of photoelasticity. The experimental evidence shows the limits of validity of these methods now available to the designer.

SYMBOLS

(k)	Stiffness matrix, Nm
(B)	Matrix relating strain to nodal displacements, mm/mm
Δ	Surface of the membrane element, m^2
(D)	Constitutive law in matrix form, Nm^{-2}
σ	Stress, Nm^{-2}
ε	Strain, mm/mm
ε_o	Initial strain, mm/mm
ν	POISSON's ratio, (no units)
W	Elastic potential per unit volume of the unstrained body, Nm^{-2}
C_1 and C_2	Constants of MOONEY, Nm^{-2}
I_i	Strain invariants, i = 1,2 and 3, (no units)
(E)	Neo-hookean constitutive law of a membrane in matrix form, Nm^{-2}
σ_o	Initial hydrostatic stress of a rubber membrane, Nm^{-2}
u	Displacement, m
σ_1 and σ_2	Principal stresses in the middle plane of the membrane, Nm^{-2}
ρ	Radius of curvature of the transverse isostatic, m
s	Curvilinear abscissa, m
σ_θ	Normal stress tangent to the edge of the disc, Nm^{-2}
C	Photoelastic material constant, $N^{-1}m^2$
a	Radius of the disc, m

Subscripts:

T	transposed
t	true
x	coordinate perpendicular to the load axis centered in the middle of the inclusion
y	coordinate along the load axis centered in the middle of the inclusion

GENERAL APPROACH

HOOKE'S LAW

The elementary tests carried out show that for the material under consideration HOOKE's law applies in relating true stress * to strain even in the 35 % mm/mm range. Thus, it may be assumed tentatively that the non linearity of the rubber's constitutive law is only the result of the large displacements experienced by the rubber.

Stiffness matrix

The stiffness matrix of the membrane plate element used can be written (Reference 3) :

$$(k) = (B^T) \times (D) \times (B) \times \Delta \times d$$

d Thickness, m

Δ Surface of the membrane element, m^2

(B) Matrix relating strain to displacement, mm/mm

(D) Constitutive law, Nm^{-2}

As a result of the incompressibility condition $\Delta\, d$ = const. The accuracy of the forces and the displacements depends on the accuracy of the terms B and D.

Definition of D

$$\left\{\sigma\right\} = [D]\left(\left\{\begin{matrix}\varepsilon_x\\ \varepsilon_y\\ \varepsilon_{xy}\end{matrix}\right\} - \left\{\varepsilon_0\right\}\right)$$

Experimentally the uniaxial law is

$$\sigma_t = E\,\varepsilon \qquad \text{where E is YOUNG's modulus}$$

As a result σ must be replaced by σ_t in the equations. The only remaining term that has to be calculated in the course of the extension of the specimen is B. Thus, this problem would seem to be identical to that of the large displacement problem.

---

* The true stress is computed per unit section area of the deformed body whereas the conventional stress is computed per unit section area of the undeformed body.

In the case of rubber, however, it is well known that there is an additional, pressure type, term "p" in the constitutive equation. To eliminate "p", represented by $-$ (D) $\{\varepsilon_o\}$ above, an additional equation in terms of displacements must be written for each element. NASTRAN with its scalar element can handle such an equation. The resulting data input problem is however very cumbersome. Thus, this solution may be uneconomical for every day use.

In order to demonstrate the existence of "p" a large displacement calculation was carried out with $\varepsilon_o =$ 0 and $\nu = .5$. The largest transverse displacement along the x-axis passing through the middle of the inclusion was 13 % in error relative to the experimental values. This error was much larger than the one obtained by means of the theory developed below.

MOONEY-RIVLIN CONSTITUTIVE LAW

The most common type of rubber material behavior equation is that of Mooney-Rivlin (Reference 4). Considering that W is the elastic potential measured per unit volume of the unstrained body the postulated function is

$$W = C_1 \, (I_1 - 3) + C_2 \, (I_2 - 3)$$

I_i are the strain invariants (i = 1,2)

C_1, C_2 are the constants postulated by Mooney.

The theory of plane stress of very thin membranes applies to the rubber specimen considered here. The deformations are symmetric about the middle plane of the body and are essentially uniform throughout the thickness. The pressure type component "p" is eliminated because in the present problem the normal stress perpendicular to the specimen's surface is zero. Large displacement equations are used in the B matrix.

The equations obtained are: $\{\sigma\} = (E) \, \{\varepsilon\} + \{\sigma_o\}$

σ are defined at points in the deformed body, but are measured per unit area of the undeformed body.
The E and σ_o are functions of not only C_1 and C_2 but also of ε_{xx}, ε_{yy} and ε_{xy}.
The matrix E is positive definite in the strain range considered.

In uniaxial extension the above equations in terms of true stresses must be identical to the well known equation (Reference 5) :

$$\sigma_t^{11} = 2 \left(C_1 + \frac{C_2}{\lambda_{11}}\right) \left(\lambda_{11} - \frac{1}{\lambda_{11}^2}\right) \frac{1}{1-\nu^2} \qquad \text{where } \nu = .5$$

and $\lambda_{11} = 1 + \varepsilon_{11}$

This happens only if C_2 is zero and the de[illegible]mations are limited in size. Such a material is called neo-hookean. The constant C_1 is determined by means of the latter equations in an uniaxial elementary extension test. C_1=.71 MN m^{-2}.

The solution of the equations is carried out by using an equivalent secant modulus method. The full load is applied in this trial and error approach. The first solution is obtained by the hookean constitutive law where σ_0 is set at zero.

NASTRAN AND TITUS ANALYSIS

The program of J.T.Oden, OK1, (Reference 6), is designed for analyzing rubberlike material. Thus it came under consideration first, but it can only analyze plane strain plates whereas our problem is a plane stress problem * .

The solutions obtained by the TITUS and NASTRAN programs have been compared at the first iteration. TITUS uses isoparametric quadrilateral membrane elements while NASTRAN has constant stress CQDMEM elements. The stresses differ only by 2 %. However the difference between the displacements of NASTRAN as compared to those of TITUS was 4 %. The results of NASTRAN were much further away from the experimental ones than those of TITUS. In this particular case the CPU computation time was 50 s for TITUS and 84 s for NASTRAN using UNIVAC 1108 (EXEC 8).

MODIFICATION OF TITUS

The TITUS program was developed in France by CITRA now called SPIEBATIGNOLLES Inc. Because of the proximity of the development team it was easy to modify the program. By means of a minor modification it is possible to calculate the modulus E and σ_0 internally elementwise at each iteration with the help of C_1 and the strains.

The test of convergence was carried out by comparing the arithmetic mean of the displacements obtained at each iteration. At lower loads (9.8 - 19.6 N) the convergence was achieved after about six iterations whereas at 29.4 N ten iterations were needed. In the first case the computation time was 84 s CPU on UNIVAC 1108 (Exec 8).

MODELING OF THE PLATE

The finite element idealization of the membrane encompasses 107 nodal points and 84 quadrilateral elements. In order that the theoretical solution and experimental results could be satisfactorily compared, the three loading

---

* In linear elasticity plane strain and plane stress problems are conjugate. This is not the case, however, for rubberlike materials.

conditions were given in terms of displacements at the end of the specimen. The modeling of the membrane is shown in Fig. 1.

Boundary conditions

	Case 1	Case 2	Case 3
Upper line	$u_y = 3.45$ mm $u_x = 0$	$u_y = 6.613$ mm $u_x = 0$	$u_y = 11.79$ mm $u_x = 0$
Around inclusion	$u_y = 0$ $u_x = 0$	$u_y = 0$ $u_x = 0$	$u_y = 0$ $u_x = 0$
Along Y-Axis	$u_x = 0$	$u_x = 0$	$u_x = 0$
Along X-Axis	$u_y = 0$	$u_y = 0$	$u_y = 0$

Since the loading and the deformations are assumed to be symmetrical, only one-quarter of the plate needed to be considered.

EXPERIMENTAL WORK

TEST SPECIMEN

The model test specimen is a rectangular coupon cut out of a polyurethane plate furnished by PHOTOLASTIC Inc. The coupon is transparent and isotropic when not loaded. A circular hole is cut out of its center and is filled in with araldite which is reinforced with glass beads at a ratio of 100 . The stresses due to the contraction of the disc during polymerisation have been observed by means of crossed polarisors and have been eliminated by an applied compression load in order to keep the neutral state of stress in the specimen. The disc is much stiffer than the rest of the coupon and there is perfect adhesion between them. The grips are glued on to the ends of the rectangle. The only load applied is a vertical load along the specimen's axis and it is measured by means of strain gages. Viscoelastic effects are suppressed by loading up gradually.

The dimensions of the specimen are 117 mm x 42 mm x 1.02 mm and the diameter of the disc is 14 mm.

Using a transmission polariscope, the isoclines are determined with the help of in-plane polarized white light and the isochromes with the help of monochromatic circularly polarized light (D_{Na} = 5890 Å).

The isostatics are obtained from the isoclines using graphical means.

PHOTOELASTIC STRESS ANALYSIS

In rubber the lightwave path difference is proportional to the difference of the principal stresses $\sigma_1 - \sigma_2$ and also proportional to the instantaneous thickness of the specimen (Reference 7)

$$\delta = C\, e\, (\sigma_1 - \sigma_2)$$

The material constant C is determined by a uniaxial elementary tension test. The value obtained is

$$C = 3.21 \pm 0.03 \text{ m}^2 \text{ daN}^{-1}$$

The principal stresses along the vertical and horizontal symmetry axes are determined by integrating graphically the equation of Lamé and Maxwell (Reference 8)

$$\frac{\sigma_1 - \sigma_2}{\rho_1} + \frac{\partial \sigma_1}{\partial s_1} = 0$$

$$\frac{\sigma_1 - \sigma_2}{\rho_2} + \frac{\partial \sigma_2}{\partial s_2} = 0$$

where ρ is the radius of curvature of the transverse isostatic and s is the curvilinear abscissa at a given point. The subscripts 1 and 2 refer to the two families of isostatics.

The starting point of the integration along the x-axis is taken at the edge of the specimen where the stress σ_2 is zero.

For the integration along the vertical axis the poin of reference for the integration is taken in the region of uniform stress betwe.n the grips and the disc where σ_2 is zero. Along the edge of the disc the stresses σ_1 and σ_2 are obtained using the normal stress σ_θ tangent to the disc and they vary as follows:

$$\frac{\partial \sigma_\theta}{\partial \theta} = - \frac{\partial \sigma_{r\theta}}{\partial r}$$

and $$\sigma_1 = \sigma_\theta + (\sigma_1 - \sigma_2) \sin^2 \alpha$$

where α is the angle between the direction of θ and the isostatic σ_1.

The value of σ_θ is a function of the accuracy of the measurement of the isoclines. As the experimental determination of the latter is relatively inaccurate, in particular at the top of the disc, the accumulated errors may be quite large. For this reason, starting from the horizontal axis, the values of σ_1 and σ_2 at the top are 15 % greater than the ones obtained starting form the other axis.

DISCUSSION OF THE EXPERIMENTAL AND THEORETICAL RESULTS

DEFORMED SHAPE

The theoretical and experimental results obtained for the deformed shape are in excellent agreement as shown (Figs. 2-4). By different experimental methods the overall transverse displacements at the horizontal symmetry line have been determined as follows:

LOADING	EXPERIMENT u_x (mm)	TITUS u_x (mm)
6 %	- 0.4 ± 0.05	- 0.434
11.5 %	- 0.75 ± 0.05	- 0.806
20.5 %	- 1.4 ± 0.05	- 1.44

ISOSTATICS

The theoretical and experimental results showing the distribution of the isostatics over the surface of the rubber coupon are plotted in Fig.5. On the left side are shown the calculated principal stresses and on the right side the envelopes of the corresponding experimental principal stresses. Taking into account the fact that the theoretical results are relative to the undeformed surface of the specimen, the agreement is again excellent. The following table shows the values of the applied longitudinal force.

LOADING	EXPERIMENT Force (N)	TITUS Force (N)
6 %	9.8 ± 0.2	10.6
11.5 %	19.6 ± 0.4	18.4
20.5 %	29.4 ± 0.6	28.2

The mesh used in modeling the ends of the specimen was very coarse, the principal aim being to demonstrate the behavior of an inclusion imbedded in a rubbe matrix. Thus, the error obtained is accordingly larger in this region.

ISOCHROMES

The experimental stress distribution over the surface of the specimens has been established by means of the isochromes. No quantitative comparison is shown here as the numerical results are relative to the undeformed shape and are in terms of the conventional stresses, (Fig. 6-8). The automatic plotting of the required true stress isochromes is being developed at the present time.

However, the shape of the isochromes shown agrees qualitatively with the experimental ones. As demonstrated below the numerically obtained longitudinal true stress concentration factor is very accurate. Thus it can be conjectured that the agreement must be also quantitative.

PRINCIPAL MEMBRANE STRESSES

In Fig. 9 the true principal membrane stresses together with the experimental ones are shown. The shape of the two families of curves obtained are identical. However there is a vertical shift of the theoretical ones relative to the experimental ones. The difference is quite small and remains within the limits of the accuracy of the experiment. It must be noted that at the top of the inclusion, on the y-axis, the experimental results differ according to whether the point is approached from the right or the left. The mean of the two values is located very near to the theoretical point.

At the intersection of the x-axis with the contour of the inclusion two nearly identical compression stresses are obtained experimentally. This result agrees with those obtained by theoretical consideration in reference 9. The numerical calculation gives two stresses of opposite sign, however. This is explained by the fact that the stresses are calculated at the center of gravity of the element. In this region C of Fig. 10, the stress gradient is very large. Thus, even though the σ_1 stress is positive at $\frac{x}{a} = 1.07$, the calculation point, it is negative at $\frac{x}{a} = 1$. that is at the experimental recording point. Taking these facts into account the agreement between the finite element results and those of the experiment is very good.

STRESS CONCENTRATION FACTOR

The stress concentration of the longitudinal principal stress along the y-axis is plotted in Fig. 10. The maximum stress concentration factors are

Experiment	1.28
Finite element results	1.31
Linear classical elasticity	1.54

The agreement between the experiment and the numerical results is excellent. It can be concluded further that the linrar elasticity gives unreliable stress values in the case of rubber for strains reaching 18 % or more.

CONCLUSION

The close agreement obtained between theoretical and experimental results demonstrates the validity of the large displacement equations, and of the neo-hookean constitutive law used in the modified TITUS program. However, the use of the derived method is not limited to any specific program. After some minor modifications any geometrically nonlinear finite element program may be applied to the analysis of rubber at relatively high strain.

The importance of using the proposed theory instead of the conventional HOOKE type formulation to design rubber parts is made evident by the fact that, using the conventional theory, the stress concentration factor of the inclusion obtained has an error of about 20 %.

ACKNOWLEDGEMENTS

The authors wish to thank MM. J.LÉVÊQUE and J.P.NOTTIN, Kléber-Colombes, Centre d'Etudes et de Recherches, Bezons, for carrying out the experimental verification and M. Christian VOUILLON, TITUS program manager, SPIEBATIGNOLLES Inc., Paris and M. Ngoc Khai PHAN, STAD Inc., Paris, for their collaboration in using TITUS and NASTRAN.

REFERENCES

1. Durand, Michel, and Jankovich, Etienne: Nonapplicability of Linear Finite Element Programs to the Stress Analysis of Tires. NASTRAN: Users' Experiences, NASA TM X-2637, September 11-12, 1972.

2. Oden, J.T.: Finite Elements of Nonlinear Continua. Mc GRAW-HILL BOOK COMPANY, 1972.

3. Zienkiewicz, O.C.: The Finite Element Method in Engineering Science. Mc GRAW-HILL LONDON, 1971.

4. Mooney, M.: A Theory of Large Elastic Deformation. J.Appl.Phys., vol.11, 1940, pp.582-592.

5. Alexander, H.: A Constitutive Relation for Rubber-Like Materials. Int.J. Engng Sci., vol.6, 1968, pp. 549-563.

6. Key, J.E.: User's Manual for Digital Computer Program OK1, Numerical Analysis of Finite Axisymmetric Deformations of Incompressible Elastic Solids of Revolution. University of Alabama, Huntsville, Research Institute - UARI Research Report N° 121.

7. Treloar, L.R.G.: The Physics of Rubber Elasticity. Oxford University Press, 1958, pp. 197-234.

8. Le Boiteux, H. and Broussard, R.: Elasticité et Photoelasticimétrie. Herman, Paris, 1940.

9. Rehner, John Jr.: Theory of Filler Reinforcement in Natural and Synthetic Rubber. The Stresses In and About the Particles. Rubber Chemistry and Technology, vol. 17, 1944, pp. 865-874.

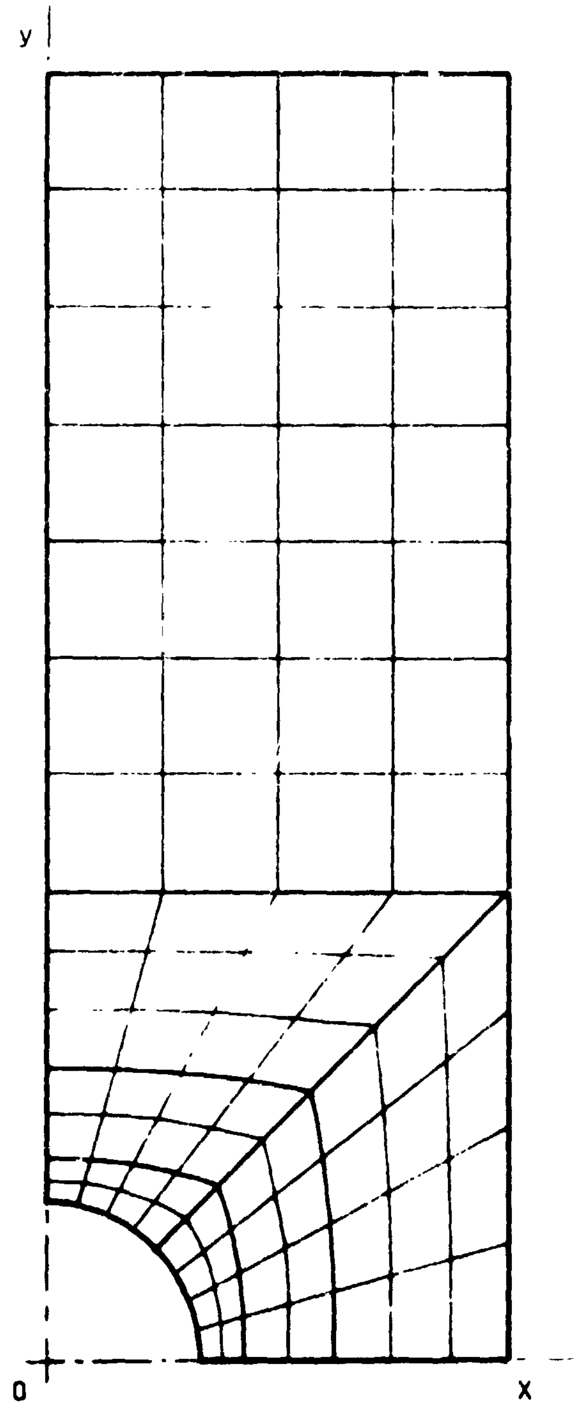

Figure 1. - Super-Elements and Automatically Generated Mesh by TITUS.

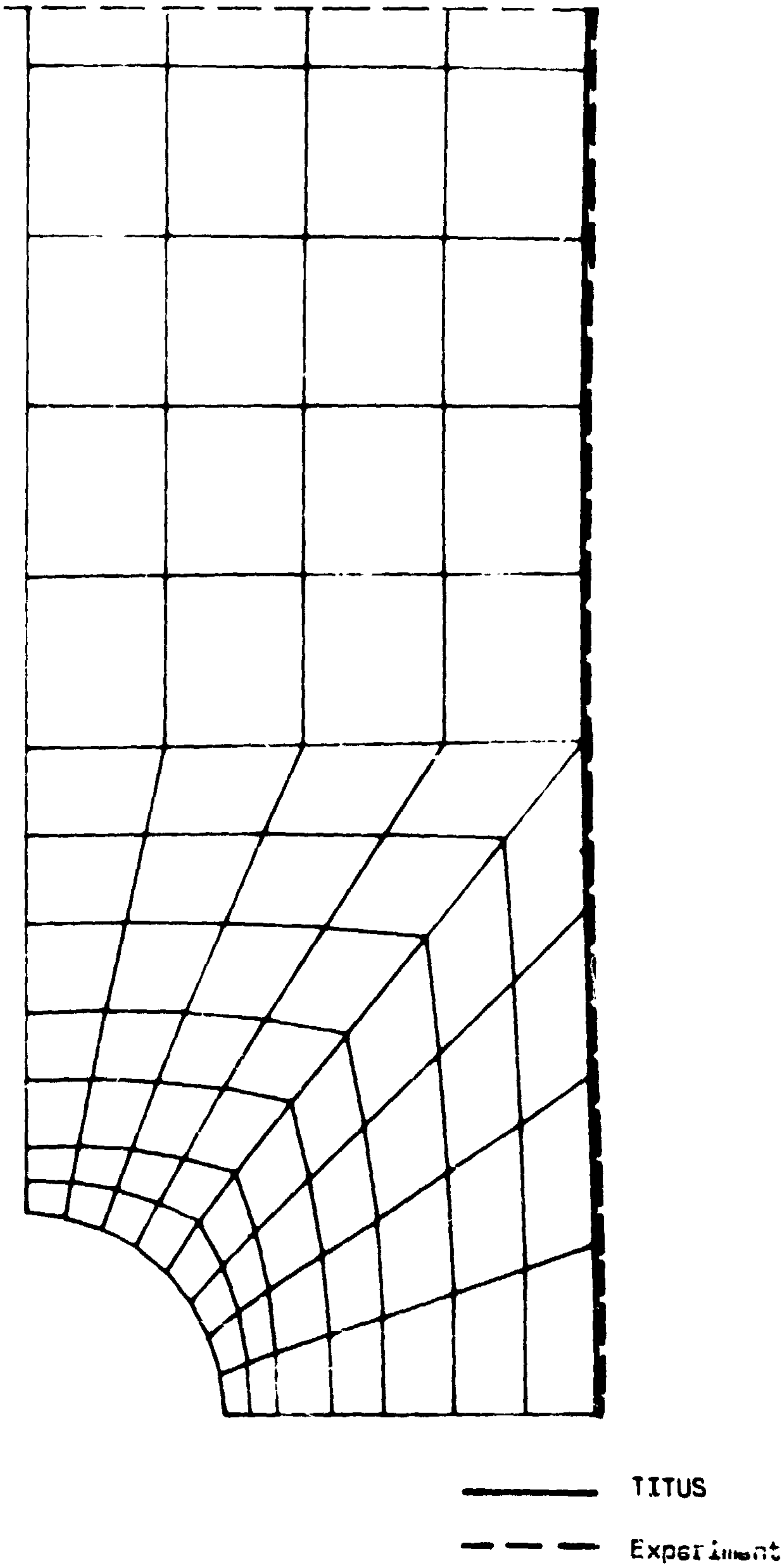

Figure 2. - Finite Element Solution and Experimental Deformed Shape
Load = 19.6 Newtons.

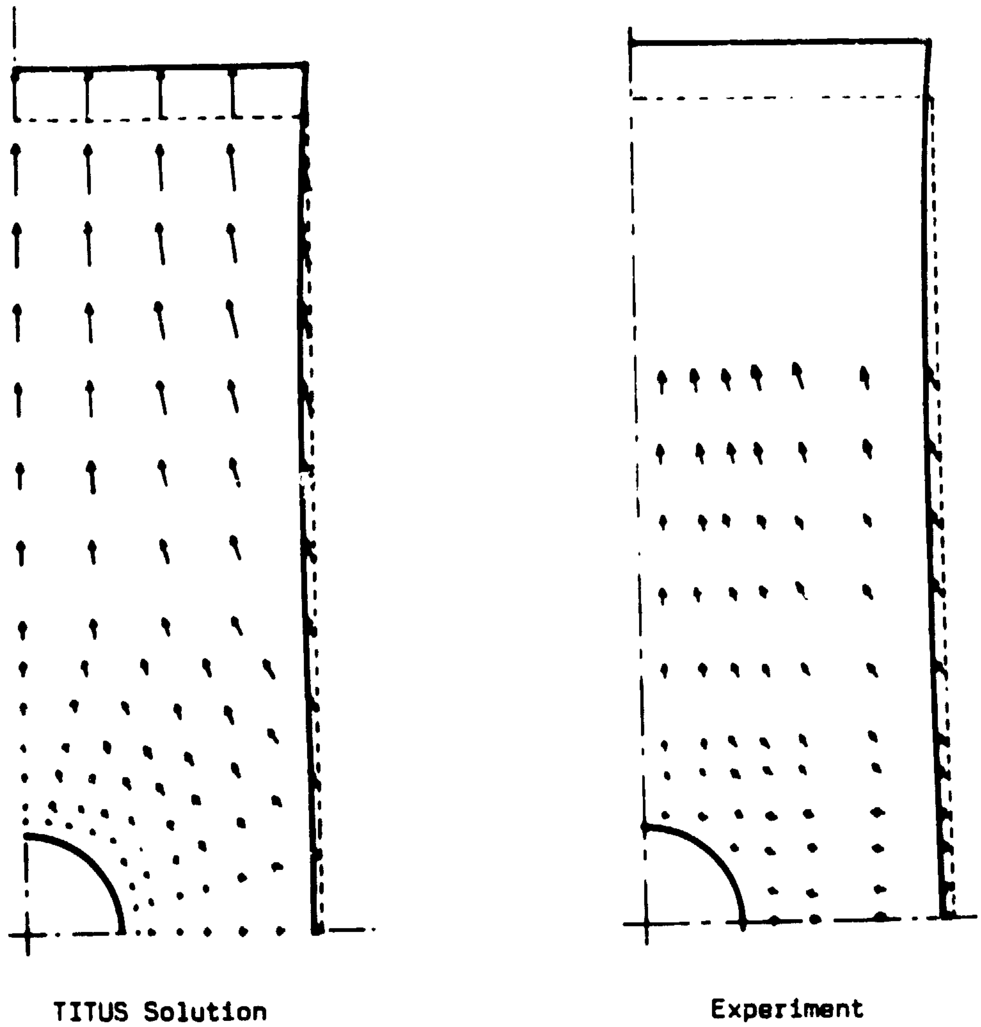

Figure 3. - Displacement Vectors. Load = 9.81 Newtons.

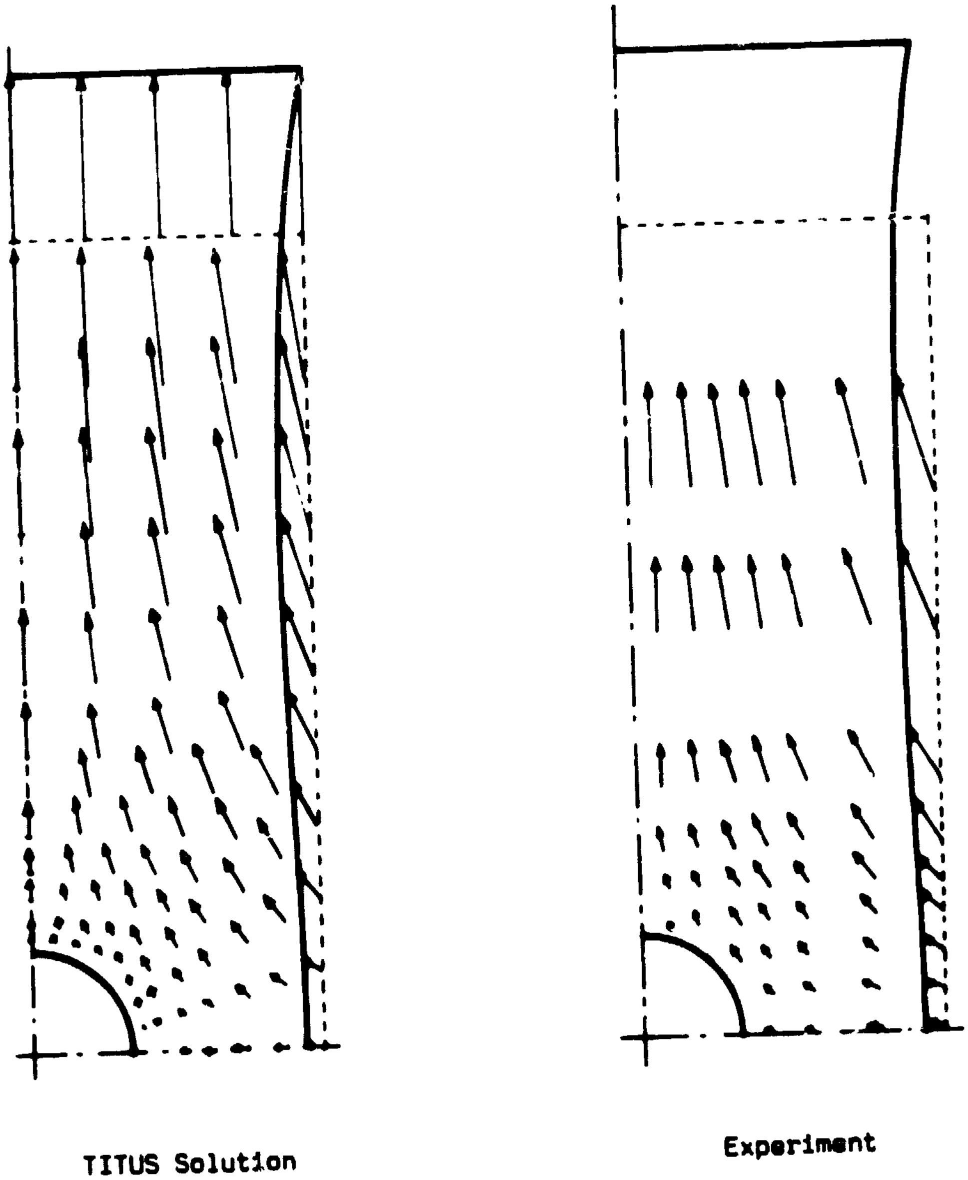

Figure 4. - Displacement Vectors. Load = 29.4 Newtons.

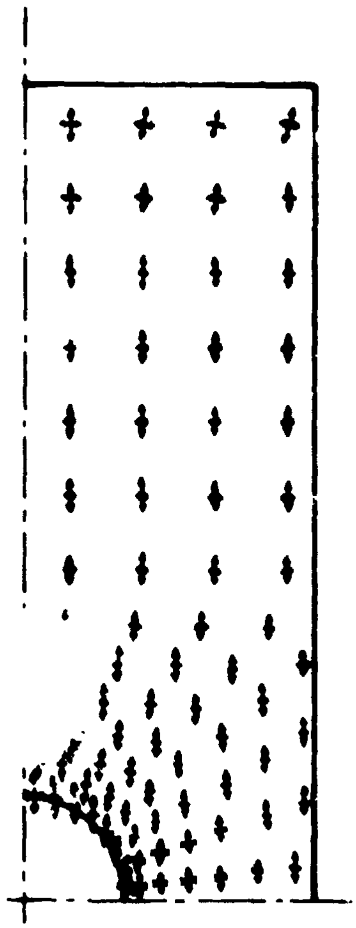

Conventional Principal Stresses
on the Undeformed Shape
(TITUS)

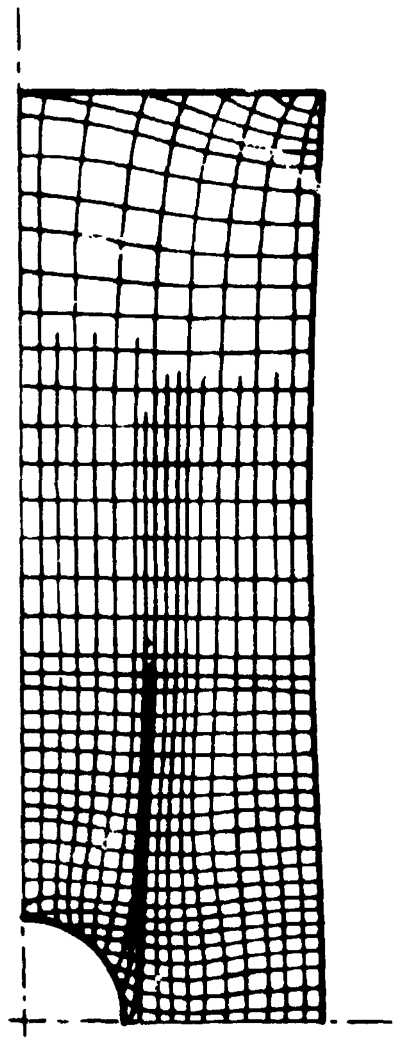

Experimental Isostatics
- Principal True Stress Envelopes -
on the Deformed Shape

Figure 5. - Conventional Principal Stresses and Experimental Isostatics.
Load = 19.6 Newtons.

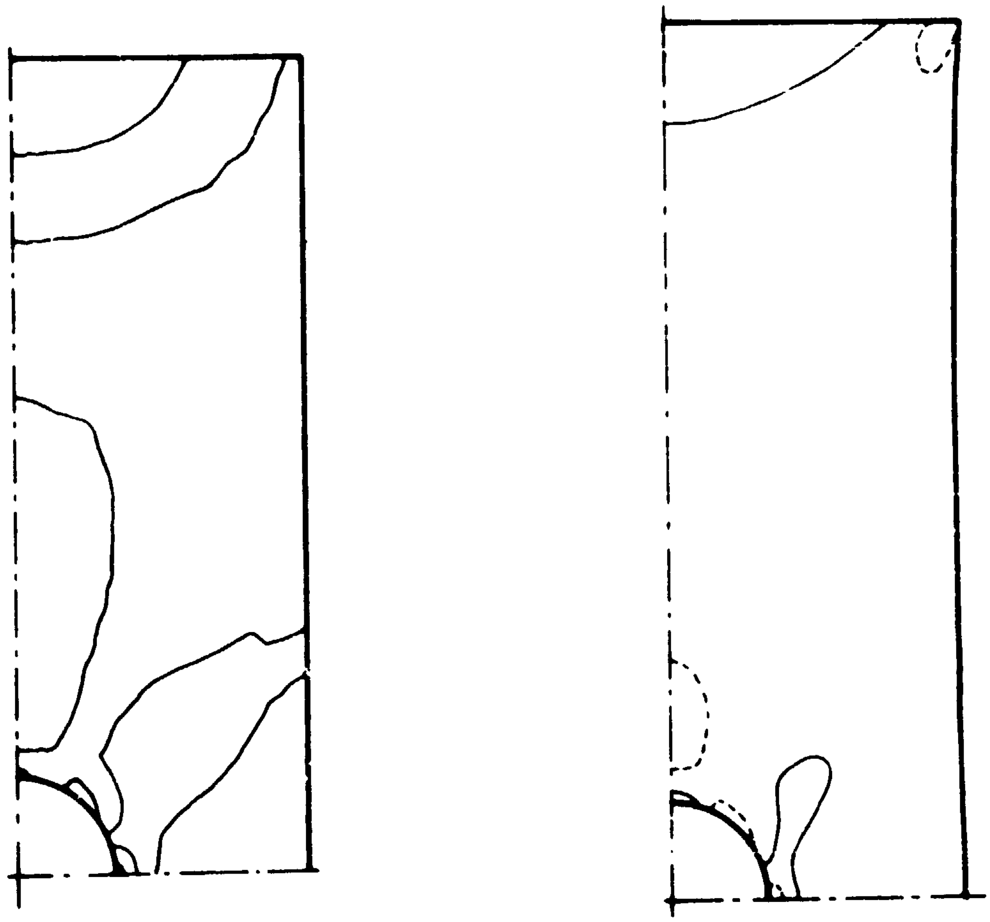

TITUS Solution

Difference of the
Conventional Principal
Membrane Stresses
in the Undeformed Body

Experiment

Isochromes - Difference of the
True Principal
Membrane Stresses
in the Deformed Body

Figure 6. - Isochromes - Numerical Results and Experiment.
Load = 3.61 Newtons.

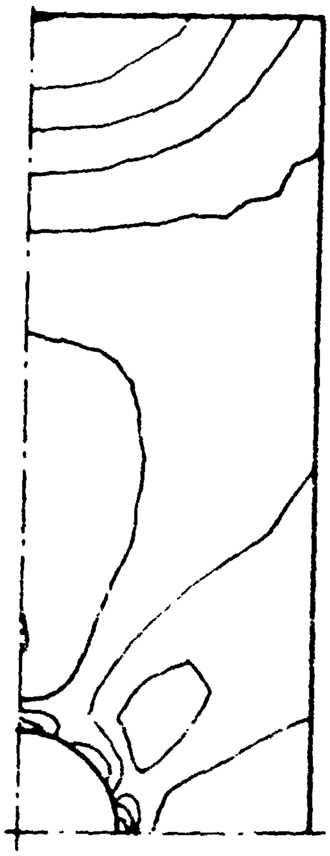

TITUS Solution

Difference of the
Conventional Principal
Membrane Stresses
in the Undeformed Body

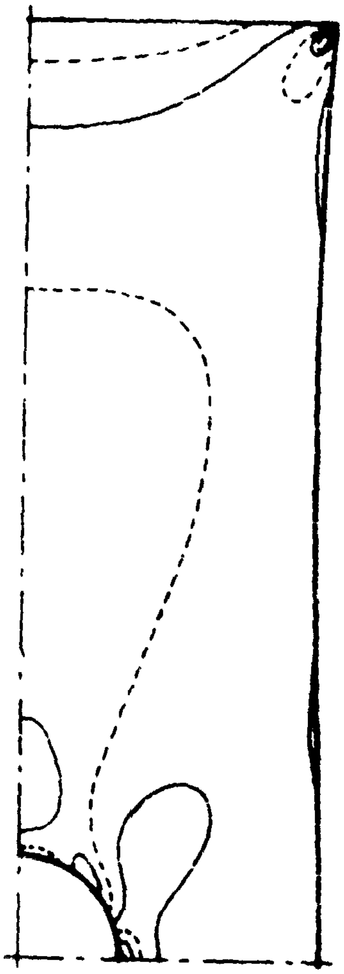

Experiment

Isochromes - Difference of the
True Principal
Membrane Stresses
in the Deformed Body

Figure 7. - Isochromes - Numerical Results and Experiment.
Load = 19.6 Newtons.

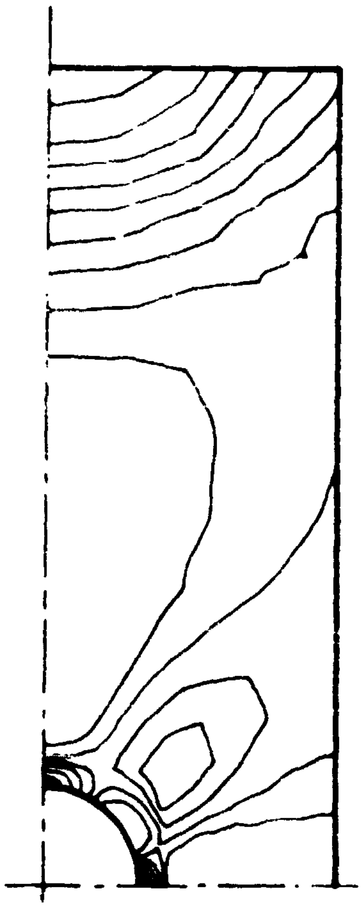

TITUS Solution

Difference of the
Conventional Principal
Membrane Stresses
in the Undeformed Body

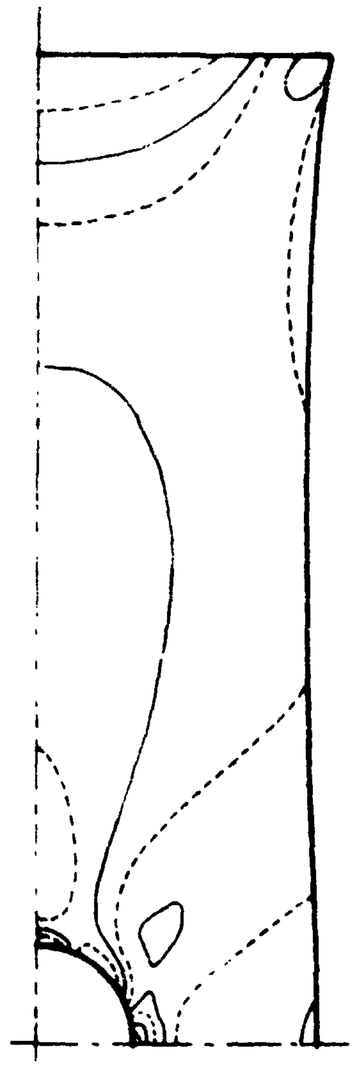

Experiment

Isochromes - Difference of the
True Principal
Membrane Stresses
in the Deformed Body

Figure 8. - Isochromes - Numerical Results and Experiment.
Load = 29.4 Newtons.

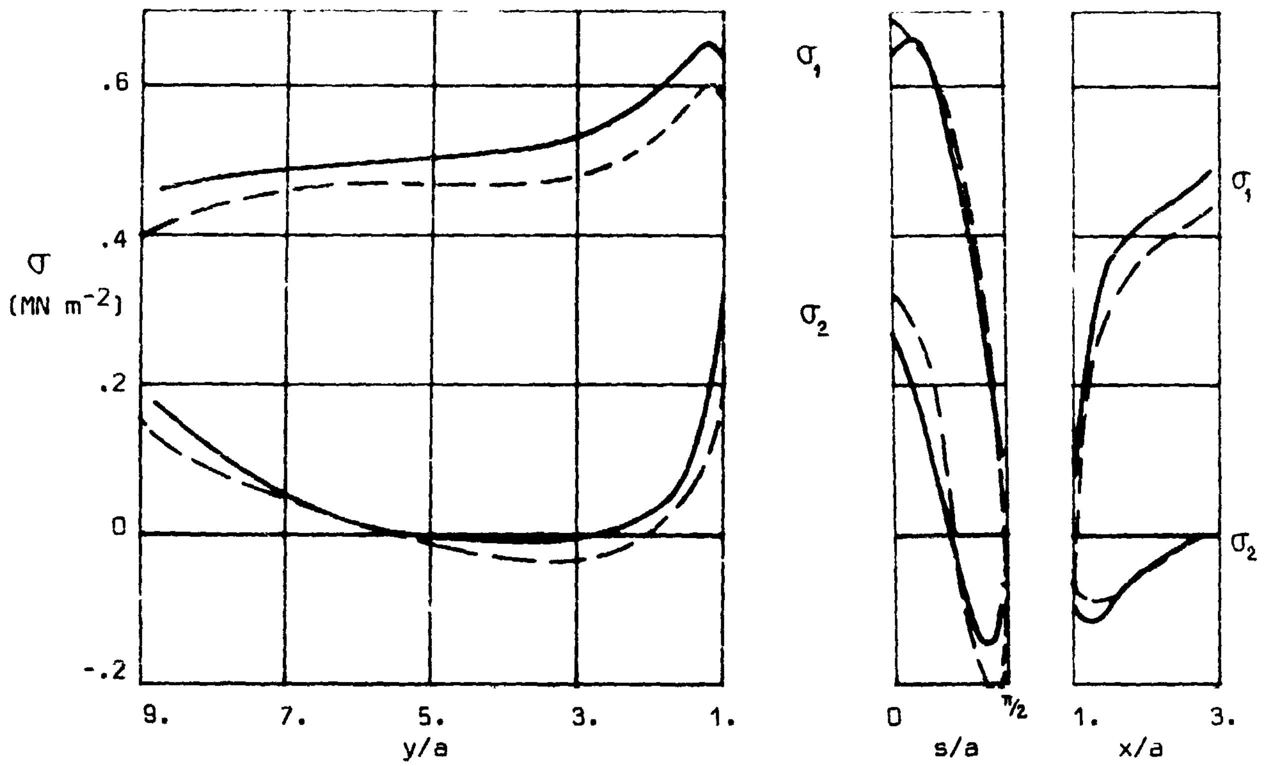

(a) y-Axis. (b) Inclusion Boundary. (c) x-Axis.

Figure 9. - True Principal Stresses at a Load = 19.6 Newtons.

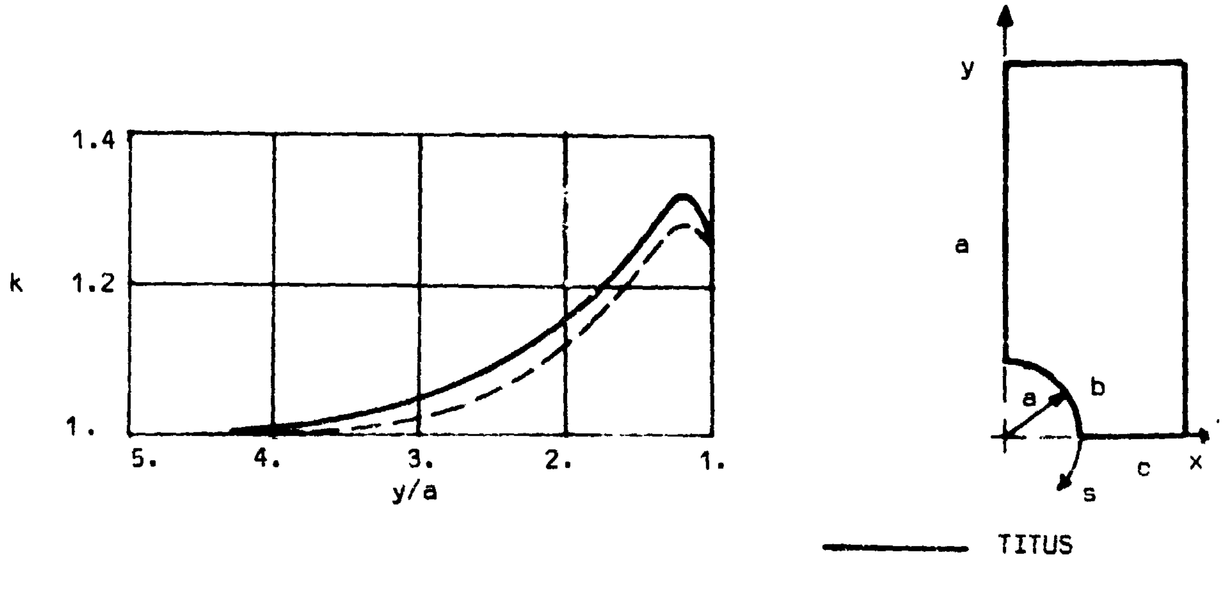

Figure 10. - Longitudinal True Stress Concentration Factor vs. y-Axis. Load = 19.6 Newtons.

N74-14591

NASTRAN STATIC AND BUCKLING ANALYSIS – COMPARISON WITH OTHER LARGE-CAPACITY PROGRAMS

by Lalit C. Shah
Rockwell International
B-1 Division
Los Angeles, California

SUMMARY

A square plate with clamped edges under a concentrated load was modeled using NASTRAN (reference 1) and ASKA (reference 2) finite element computer programs. Deflections were computed for various width-to-thickness ratios (b/t) of the plate element, and were compared against the classical theory to determine the b/t limitations.

A cylinder with simply supported ends was modeled using NASTRAN and STAGS (reference 3) computer programs for buckling analysis. The models were subjected to a uniform radial pressure loading. Several parameters were changed, and the effects of those variations are presented. Utilizing these data, a model which will produce results comparable to published empirical data can be constructed and processed for a minimized cost.

STATIC ANALYSIS

The user of finite element computer programs has numerous limitations to be considered when constructing a mathematical model of the structure to be analyzed. Although considerable information is available concerning the plate element aspect ratio (a/b) (i.e., length-to-width ratio), the effect of varying the width-to-thickness ratio (b/t) has not previously been presented. The effect of varying the plate element b/t ratio was investigated for the NASTRAN and ASKA finite element computer programs.

This investigation utilized a square plate with clamped edges. Two elements, CTRIA2 and CQUAD2, available in NASTRAN, were used in two separate models. One triangle-plate element, TRIB3, available in ASKA, was used in the third model. These models, shown in Figure 1, were 152.4 cm (60 inches) square plates with varied thickness to achieve the b/t ratio desired. The basic model mesh size was selected based upon previous experience. One model with mesh size reduced by a factor of 2 was processed, and the results were compared to verify that the basic model mesh size was valid.

One loading, which consisted of a concentrated load applied in the geometric center normal to the plate, was selected due to its ideal checks for the bending characteristics of any plate element. This loading was applied to each model processed.

The results of the two NASTRAN models and the ASKA model are summarized in table I. The resulting computed deflections for the three models are tabulated for the various b/t ratios investigated. Included in this table are the theoretical deflections based upon classical equations (reference 4). These deflection data are presented graphically in figures 2 through 4. The plot of the percentage difference between computed deflection and theoretical deflection is shown in figure 5 for the three models investigated. The two NASTRAN plate elements, CTRIA2 and CQUAD2, break down in regions of b/t less than five. The ASKA element, TRIB3, is quite consistent, even for extremely low values of b/t. It is apparent that a limitation on the value of b/t exists for the NASTRAN plate elements. This limitation should be considered along with the aspect ratio (a/b) limitations when constructing a model for the NASTRAN computer program.

BUCKLING ANALYSIS

Buckling analysis is an eigenvalue problem which may result in very high computer processing costs to achieve a valid solution. This report presents an investigation into the various modeling parameters that affect the solution and the computer cost. The results of this study reveal an approach to achieving a valid solution for minimized computer cost.

This investigation considered a cylinder under uniform radial pressure loading. According to Donnell's equation, under uniform radial pressure, the buckling stress of the cylinder is:

$$\sigma_{cr} = \frac{K_y \pi^2 E}{12(1-\nu^2)} \left(\frac{t}{L}\right)^2$$

For moderately long cylinders, this equation gives quite good correlation with test data (reference 5). For this investigation, a data point was selected where the test result and the preceding equation value practically coincide. This cylinder model is shown in figure 6. The cylinder was modeled for

NASTRAN, a finite element computer program, and for STAGS, a finite difference computer program. Essentially, the same parameters were varied for both models in determining effects upon the solution validity and the computer costs.

The results of the NASTRAN and STAGS models are presented in tables II and III, respectively. These data are presented in figures 7 through 9. Appendix A contains the mode shapes for all the models studied in this investigation.

A significant parameter in modeling for either NASTRAN or STAGS is the circumferential spacing of grid points which determine the number of elements per half wave-length. As indicated in figure 7, an extremely narrow range of circumferential spacing may be considered in modeling in order for NASTRAN buckling analysis to achieve valid results. The NASTRAN model that is very fine is equally as erroneous as a model that is very coarse. These models that are outside this narrow band of acceptable circumferential spacing produced results that deviated from the theoretical value by up to 70 percent. The improper selection of the circumferential spacing for the STAGS program can result in extremely high errors, over 3,000 percent, as shown in figure 7. The results from the STAGS models indicate that the error percentage is directly related to the coarseness of the model, and as the circumferential spacing is reduced, the computed value approaches the theoretical solution. For this particular cylinder model to achieve a valid solution, the STAGS model required a 3-degree circumferential spacing, whereas the NASTRAN model required a 10-degree spacing.

The aspect ratio of the plate elements was considered as an important parameter in this investigation. Although most of the models utilized a constant number of uniformly spaced longitudinal cuts, a few were processed using nonuniformly spaced longitudinal cuts to determine the effects of varying the aspect ratio. It was a surprise to learn that the results did not change appreciably. Apparently the aspect ratio of the plate elements is not a critical parameter for NASTRAN buckling analysis. The data presented in figure 8 for extremely low and extremely high aspect ratios are related to the very coarse and the very fine circumferential spacing models, respectively. Therefore, the most probable reason for the results is due to the circumferential spacing.

The NASTRAN models were processed on IBM 370/165, and the STAGS models were processed on CDC 6600 computer system. The resulting machine time data are presented in tables IV and V. This information is converted to machine cost in dollars and presented in figure 9. Even the very fine model used in STAGS to achieve a valid solution resulted in less computer cost than any of the NASTRAN models processed. This may be partly attributed to the two computer systems used in the investigation. Although figure 9 presents the computer cost, a significant part of the total cost for buckling analysis is the man-hours required to construct the model and prepare the data. Also, the

NASTRAN program provides a lot more flexibility in modeling as compared to the STAGS program. The total cost data for this investigation are not available, but it is estimated that for a typical problem, the total cost would be nearly equal for these two programs.

CONCLUSIONS

In the static analysis investigation, it was determined that the NASTRAN plate element has a width-to-thickness ratio (b/t) limitation, as well as an aspect ratio limitation. These are both important parameters to be considered in modeling thick plate structures. Extra care should be exercised to avoid large aspect ratios and/or small (less than five) width-to-thickness ratios. The investigation did indicate that ASKA element TRIB3 is consistently valid for extremely low values of b/t. For those structures whose configuration requires modeling to b/t values less than five, it is recommended that they get processed using the ASKA program or use solid elements available in NASTRAN.

The buckling analysis investigation revealed that modeling requirements are quite different from static analysis. The conventional rules for static analysis modeling are neither sufficient nor applicable for buckling analysis. Although the effect of varying aspect ratio is negligible, the effect of varying the number of elements per half wavelength is very critical to both a valid solution and the computer cost. The cost of performing a valid buckling analysis is very high measured by static analysis standards. Although STAGS computer cost is quite low, the man-hour cost is quite high, compared to NASTRAN costs. The evaluation of the buckling analysis performed in this investigation has revealed that it is very difficult to separate a reasonable solution from an erroneous solution. The NASTRAN models indicate an extremely narrow band of circumferential spacing (number of elements per half wavelength) may be selected for a valid solution, whereas the STAGS models indicate the finer models produced an acceptable solution.

ACKNOWLEDGEMENT

The author expresses his gratitude to Mr. W. D. Mock and Mr. Y. N. Tsou for the assistance in carrying out this work.

SYMBOLS

θ	Circumferential spacing
ℓ	Length of cylinder element
a	Length of plate
b	Width of plate
t	Thickness of plate or cylinder
R	Cylinder radius
P_{cr}	Critical buckling load – program output
P	Critical buckling load – theoretical value
σ_{cr}	Critical buckling stress – theoretical value

REFERENCES

1. The NASTRAN User's Manual (Level 15), NASA SP-222(01), June 1972.

2. ASKA User's Reference Manual, ISD Report No. 73, Institute for Statics and Dynamics, University of Stuttgart, 1971.

3. Almroth, B. O., Brogan, F. A., Meller, E., and Zele, F., User's Manual for STAGS Computer Code, LMSC-D266611A, Lockheed Missiles & Space Co., Inc., April 1972.

4. Timoshenko, S.; and Woinowsky-Krieger, S.: Theory of Plates and Shells. Second ed., McGraw-Hill Book Co., Inc., 1959.

5. Gerrad, George, and Becker, Herbert, Handbook of Structural Stability, Part III, NACA TN 3783, August 1957.

Table I

STATIC ANALYSIS - DEFLECTION DATA

Plate Thickness t (cm)	b/t	NASTRAN CQUAD2	NASTRAN CTRIA2	ASKA TRIB3	Theoretical (Ref 4)
1.27	20.0	15.00×10^{-1}	13.64×10^{-1}	13.39×10^{-1}	14.91×10^{-1}
5.08	5.0	24.0×10^{-3}	22.07×10^{-3}	20.9×10^{-3}	23.37×10^{-3}
10.16	2.5	3.2×10^{-3}	2.97×10^{-3}	2.62×10^{-3}	2.92×10^{-3}
15.24	1.67	10.39×10^{-4}	9.73×10^{-4}	7.82×10^{-4}	8.61×10^{-4}
20.32	1.25	4.93×10^{-4}	4.65×10^{-4}	NA	3.63×10^{-4}
25.4	1.00	2.87×10^{-4}	2.72×10^{-4}	16.74×10^{-5}	18.54×10^{-5}

Table II

BUCKLING ANALYSIS - EIGENVALUE DATA NASTRAN MODEL

Shell	Mesh Size θ, deg	Mesh Size ℓ, cm	P_{cr}/P	Degree of Freedom*
90	2	25.4	1.6434	T_1
90	5	25.4	1.5409	T_1
90	9	25.4	1.3614	R_2
90	10	25.4	1.0390	R_2
90	11	25.4	.7844	R_2
180	20	25.4	.5568	R_3
180	30	25.4	.3079	R_3

*Eigenvectors are normalized with respect to this degree of freedom.

Table III

BUCKLING ANALYSIS - EIGENVALUE DATA STAGS MODEL

Shell	Mesh Size θ, deg	Mesh Size ℓ, cm	P_{cr}/P	Degree of Freedom*
90	3.1	4.24	1.08	T_1
90	3.1	9.53	1.09	T_1
90	3.1	19.05	1.11	T_1
90	3.1	38.1	.37	T_1
90	5.3	4.24	1.27	T_1
90	11.25	12.7	2.78	T_1
90	22.5	12.7	29.9	T_1

*Eigenvectors are normalized with respect to this degree of freedom.

Table IV

BUCKLING ANALYSIS - MACHINE TIME DATA NASTRAN MODEL IBM 370/165

Number of Grid Points	CPU Time (sec)	Channel Time (sec)	Billing Units
184	222.432	114.732	28.9015
76	80.208	93.438	12.9706
44	57.732	91.212	10.4553
40	63.23	102 72	12.1796
40	54.63	93.75	10.8106
36	58.398	104.118	11.5798
28	43.662	95.358	9.6276

Table V

BUCKLING ANALYSIS - MACHINE TIME DATA STAGS MODEL CDC 6600

Number of Grid Points	CPU Time (sec)	I/O Time (sec)	System Sec
300	46.228	105.800	72.678
180	18.469	40.9	28.694
150	19.176	48.626	31.332
90	11.312	33.816	19.766
60	7.858	30.624	15.514
36	3.227	21.162	8.517
20	2.036	23.259	7.85

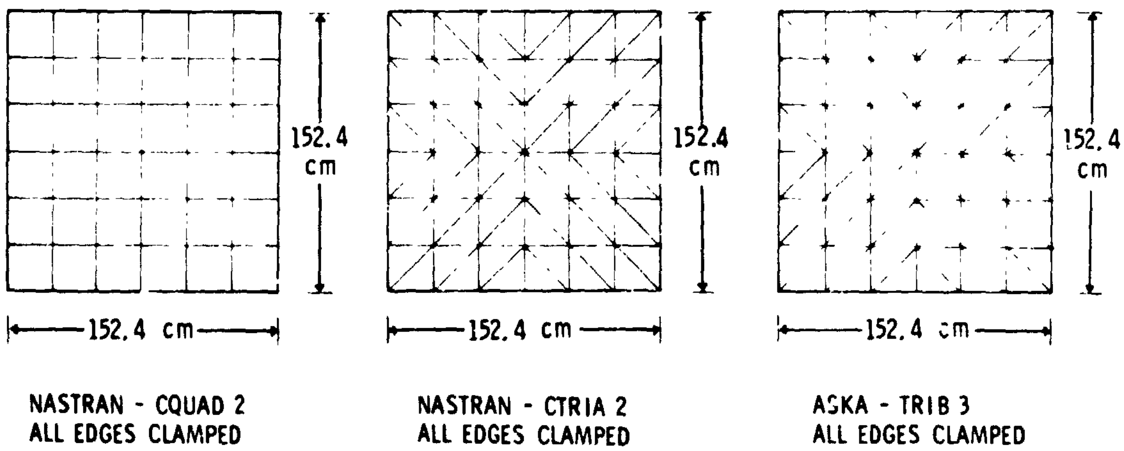

Figure 1. Static analysis - basic model geometry.

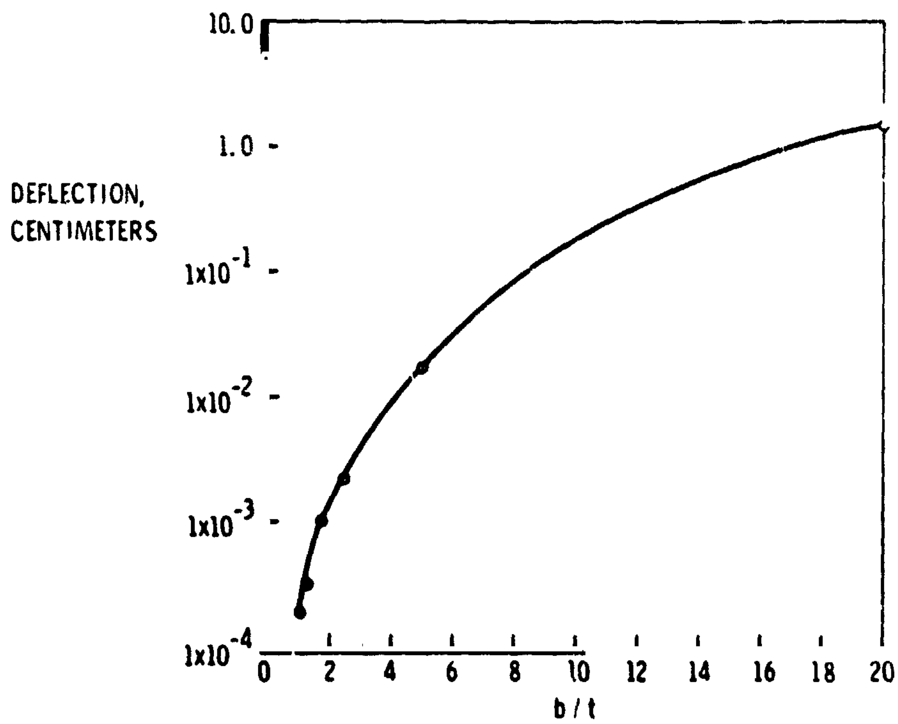

Figure 2. Deflection vs thickness ratio, NASTRAN - CQUAD2.

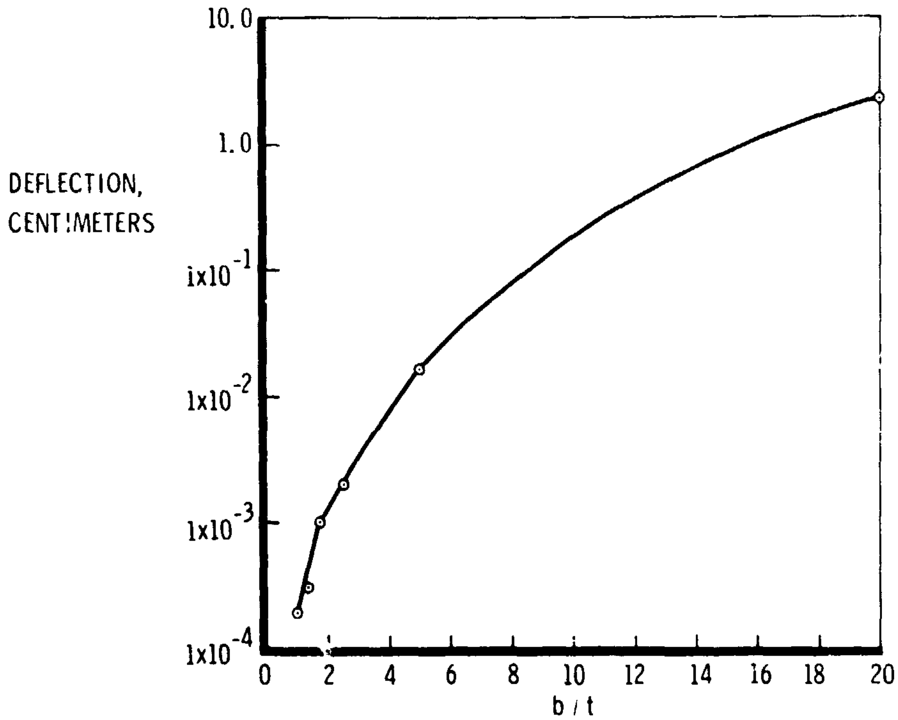

Figure 3. Deflection vs thickness ratio, NASTRAN - CTRIA2.

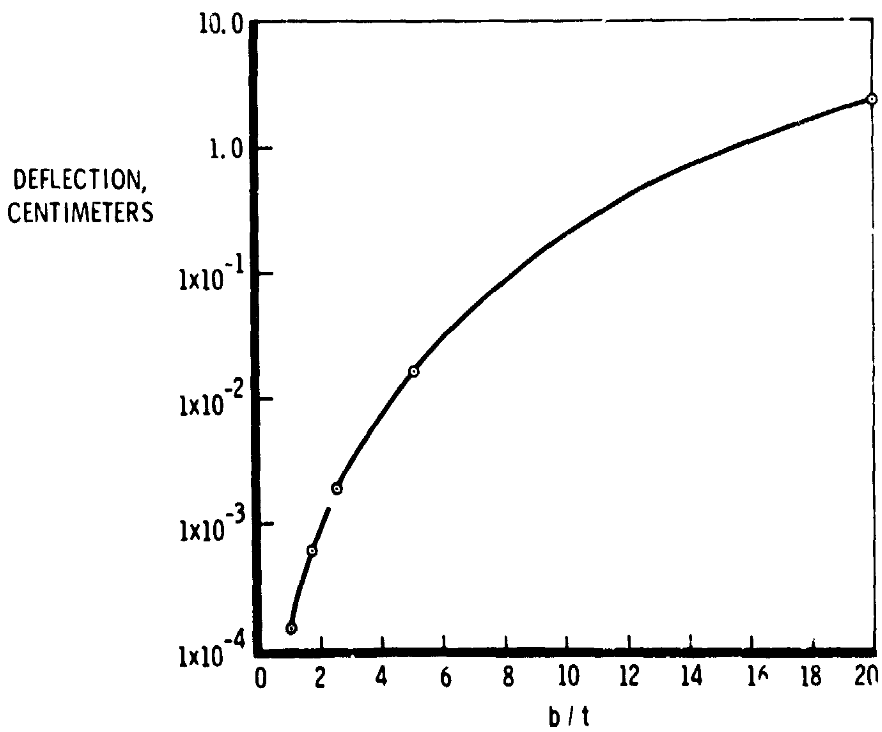

Figure 4. Deflection vs thickness ratio, ASKA - TRIB3.

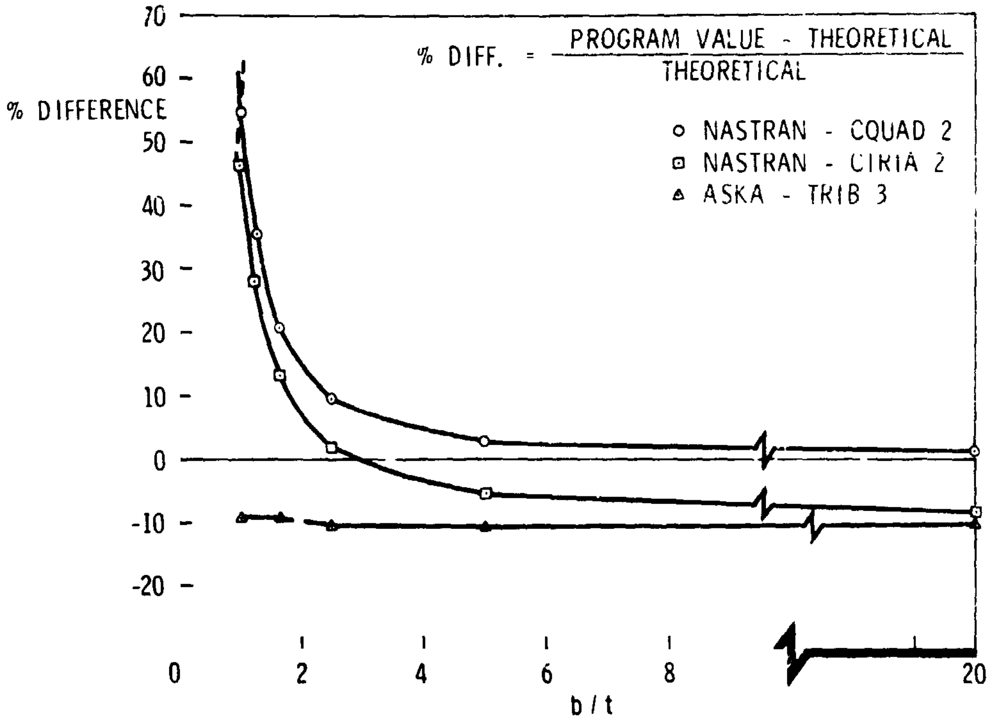

Figure 5. % difference vs thickness ratio.

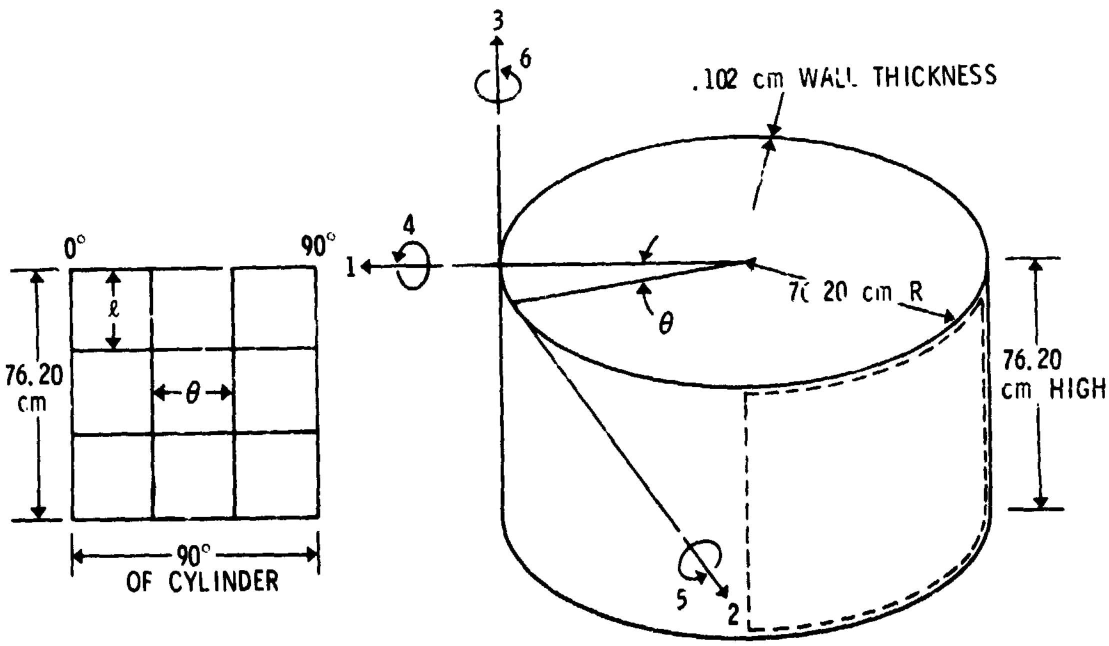

Figure 6. Buckling analysis - basic model geometry.

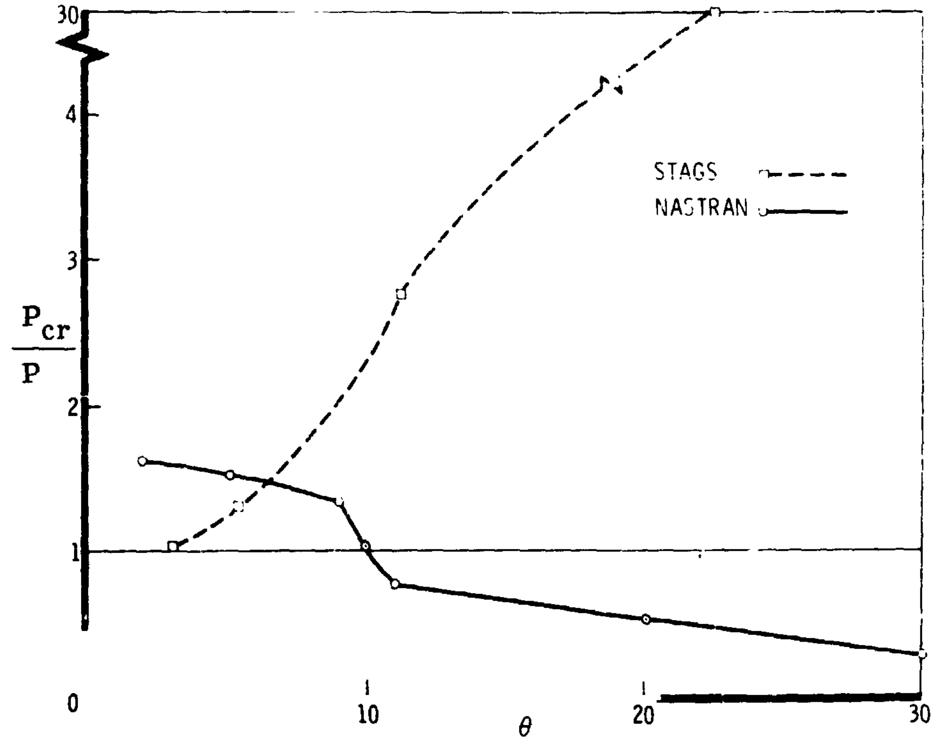

Figure 7. Effect of varying circumferential spacing.

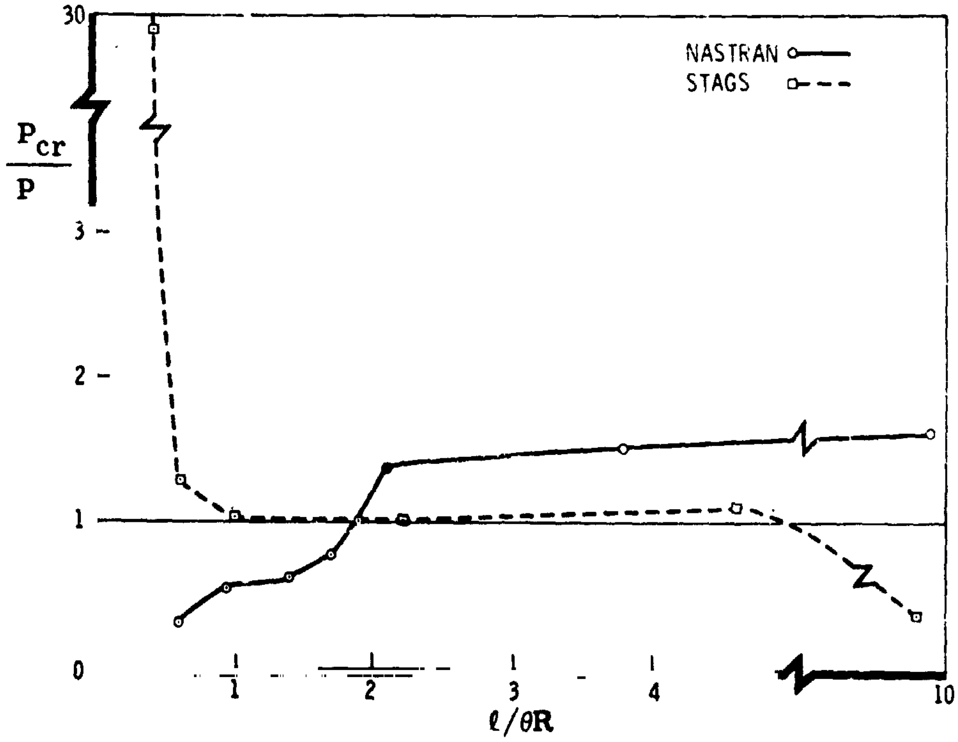

Figure 8. Effect of varying aspect ratio.

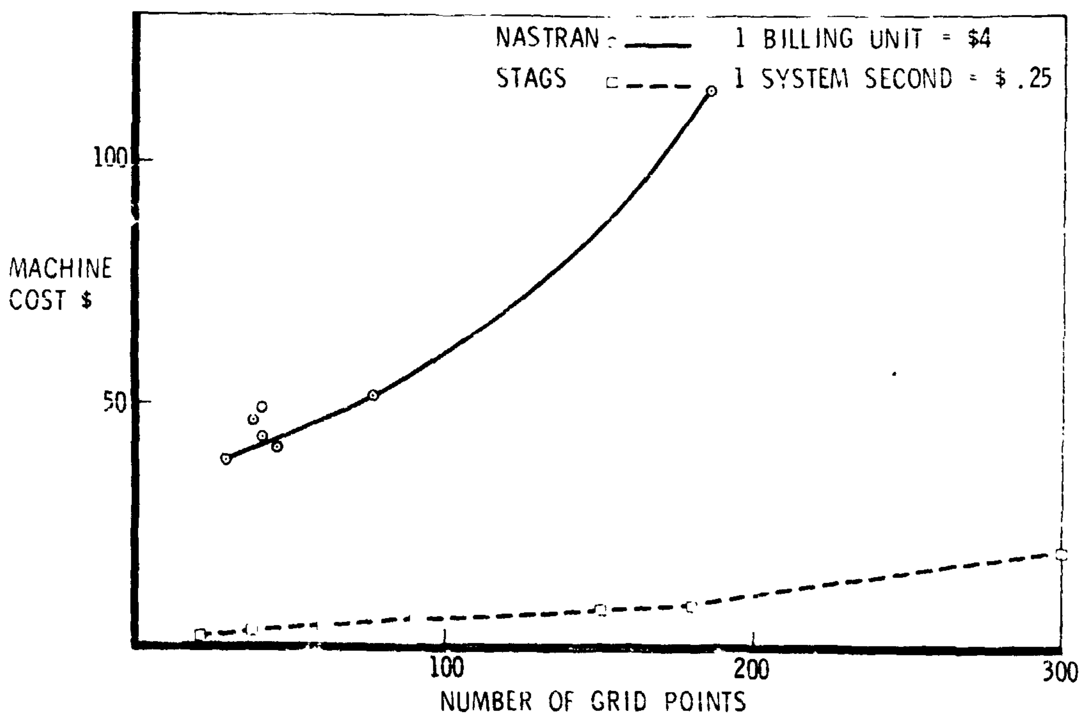

Figure 9. Cost comparison between NASTRAN and STAGS.

$P_{cr}/P = 1.6434$; $\ell = 25.4$ cm; $\theta = 2^{o}$

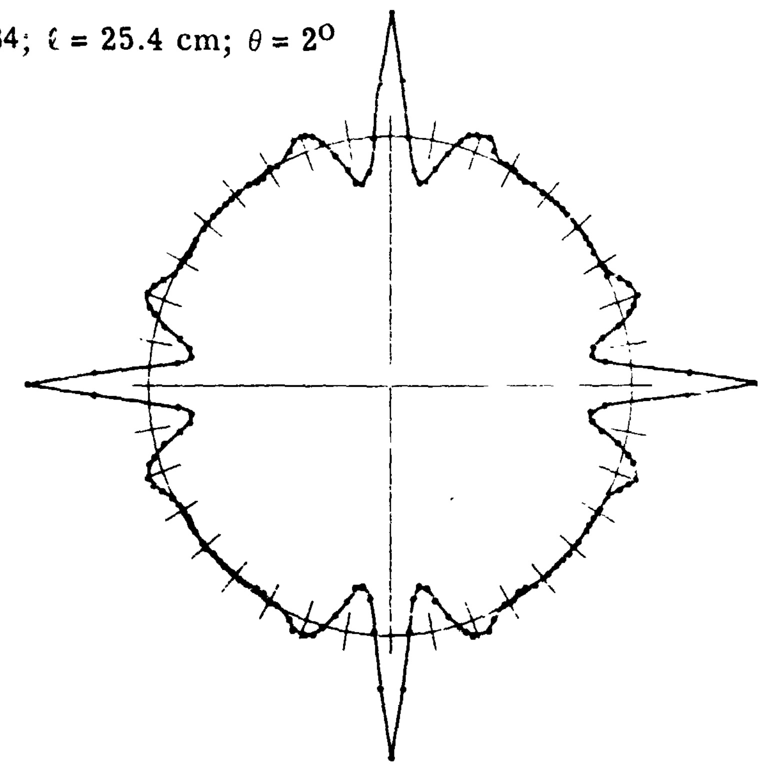

Figure A-1. Mode shape - NASTRAN model.

$P_{cr}/P = 1.5409$; $\ell = 25.4$ cm; $\theta = 5^{o}$

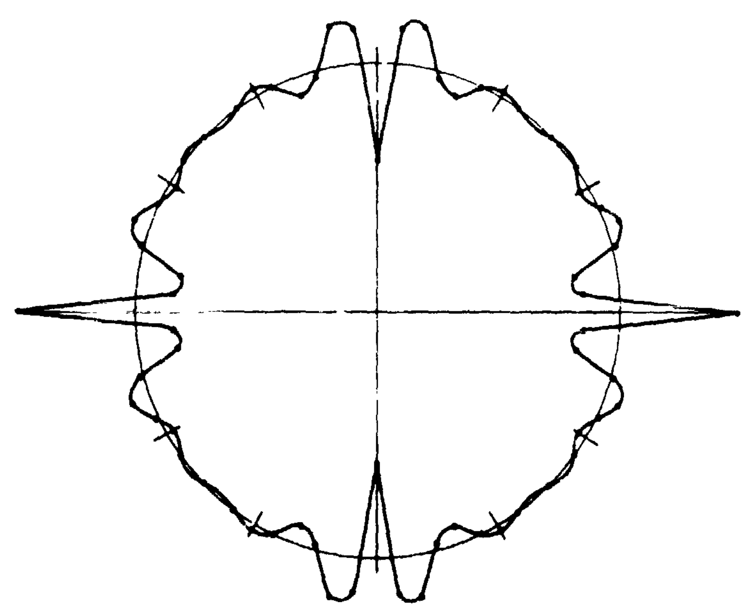

Figure A-2. Mode shape - NASTRAN model.

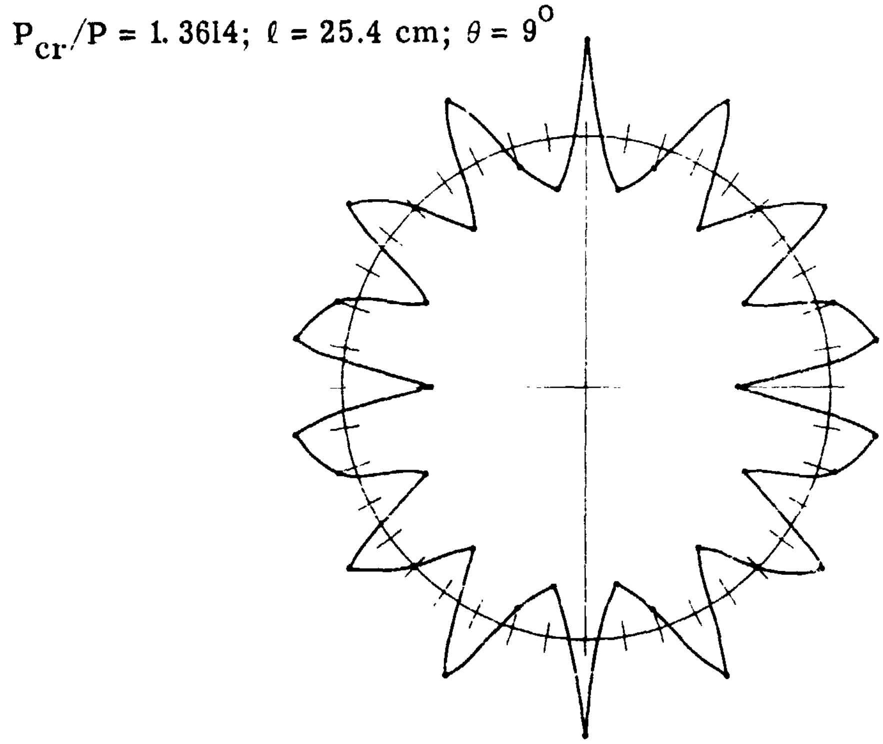

Figure A-3. Mode shape - NASTRAN model.

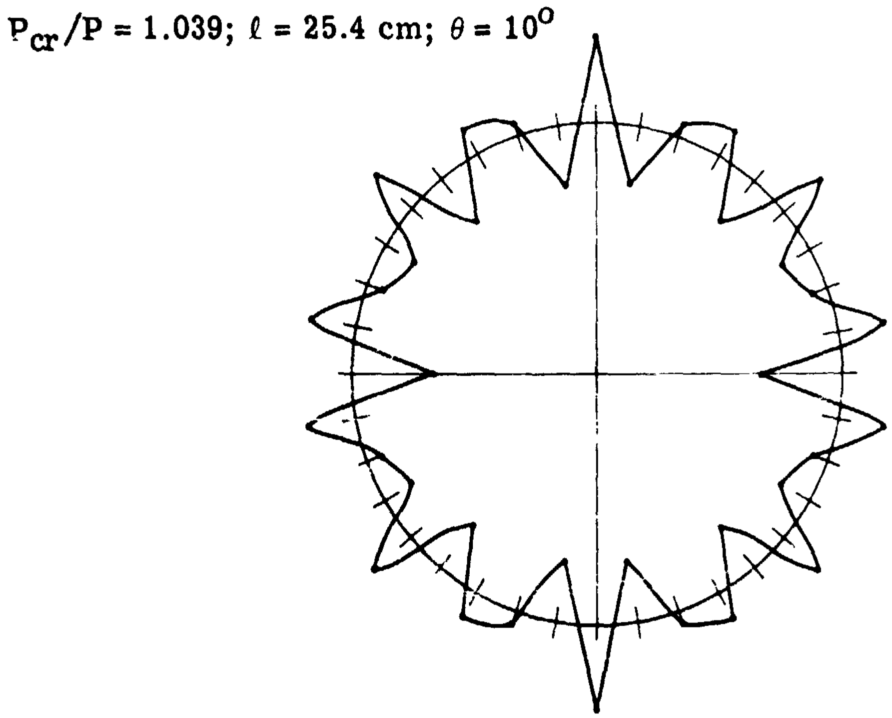

Figure A-4. Mode shape - NASTRAN model.

$P_{cr}/P = 0.7844$; $\ell = 25.4$ cm; $\theta = 11^{o}$

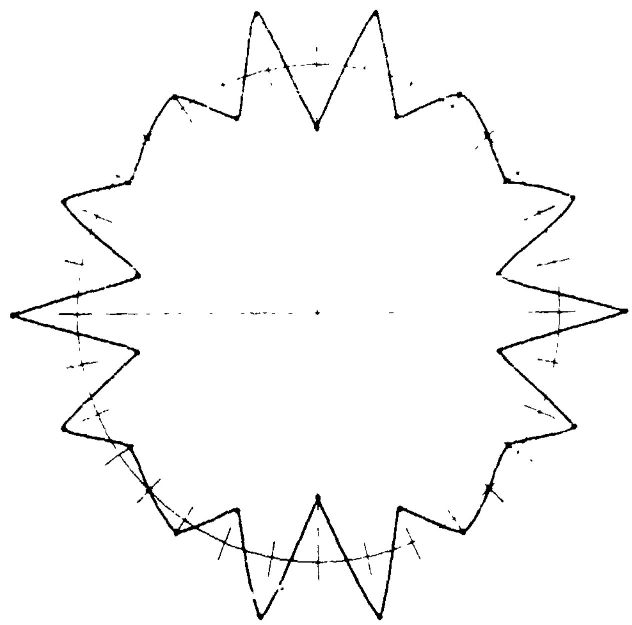

Figure A-5. Mode shape - NASTRAN model.

$P_{cr}/P = 0.5568$; $\ell = 25.4$ cm; $\theta = 20^{o}$

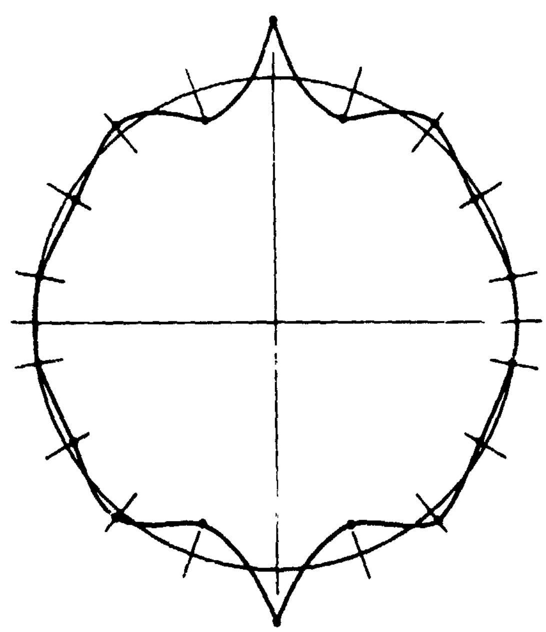

Figure A-6. Mode shape - NASTRAN model.

$P_{cr}/P = 0.3079$; $\ell = 25.4$ cm; $\theta = 30^{o}$

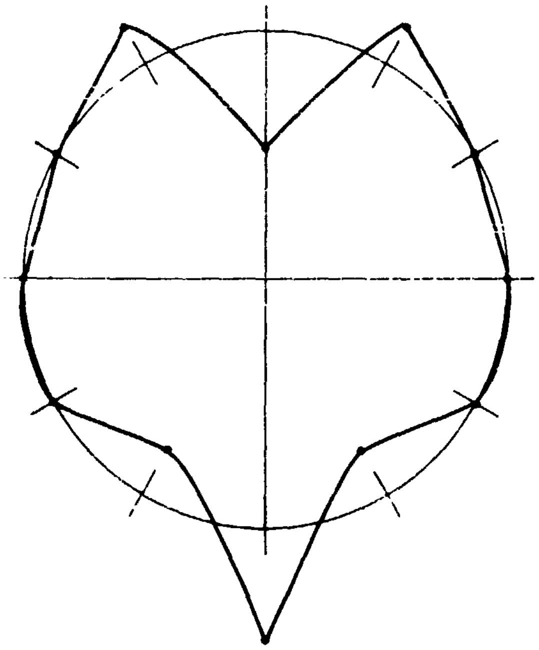

Figure A-7. Mode shape - NASTRAN model.

$P_{cr}/P = 1.08$; $\ell = 4.24$ cm; $\theta = 3.1^{o}$

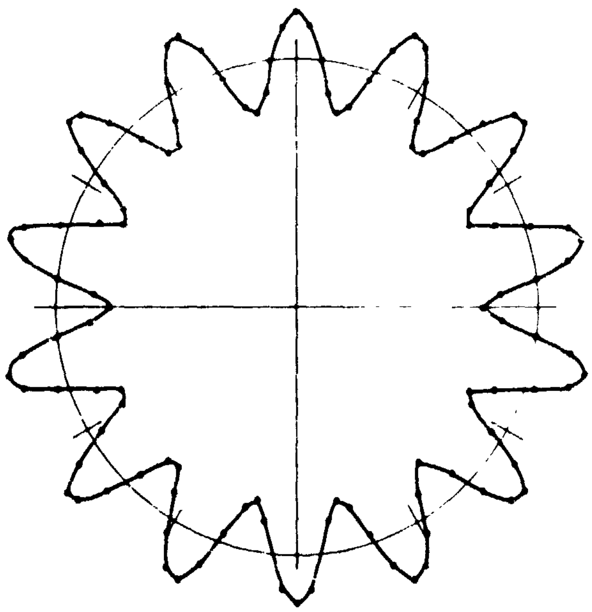

Figure A-8. Mode shape - STAGS model.

$P_{cr}/P = 1.09$; $\ell = 9.53$ cm; $\theta = 3.1^{\circ}$

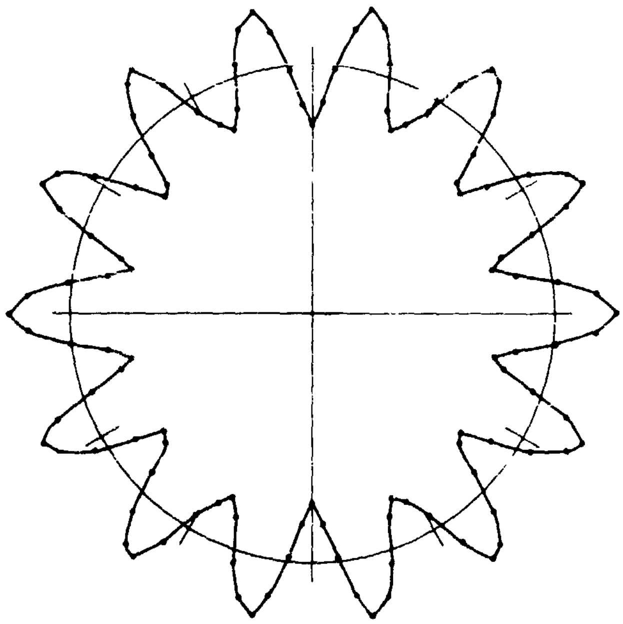

Figure A-9. Mode shape - STAGS model.

$P_{cr}/P = 1.11$; $\ell = 19.05$ cm; $\theta = 3.1^{\circ}$

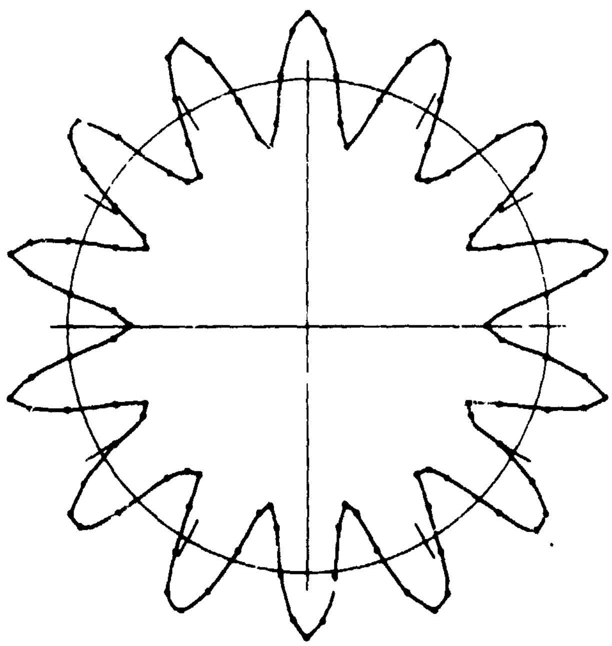

Figure A-10. Mode shape - STAGS model.

$P_{cr}/P = 0.37$; $\ell = 38.1$ cm; $\theta = 3.1^{o}$

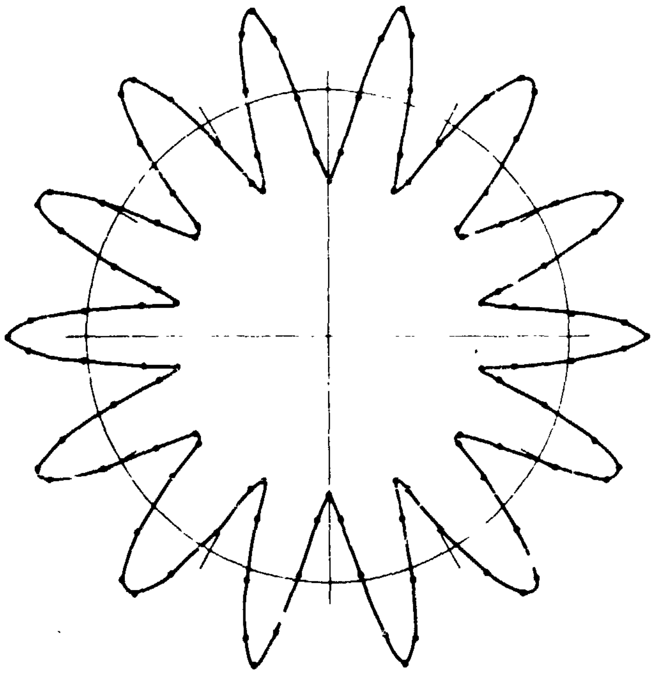

Figure A-11. Mode shape - STAGS model.

$P_{cr}/P = 1.27$; $\ell = 4.24$ cm; $\theta = 5.3^{o}$

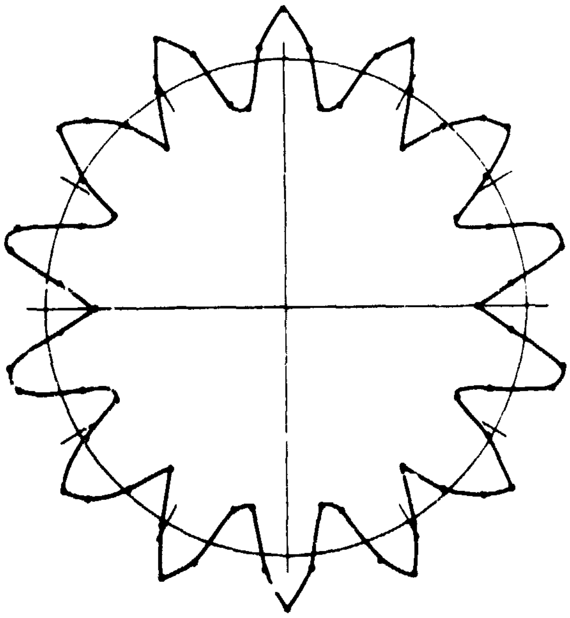

Figure A-12. Mode shape - STAGS model.

$P_{cr}/P = 2.78$; $\ell = 12.7$ cm; $\theta = 11.25^{o}$

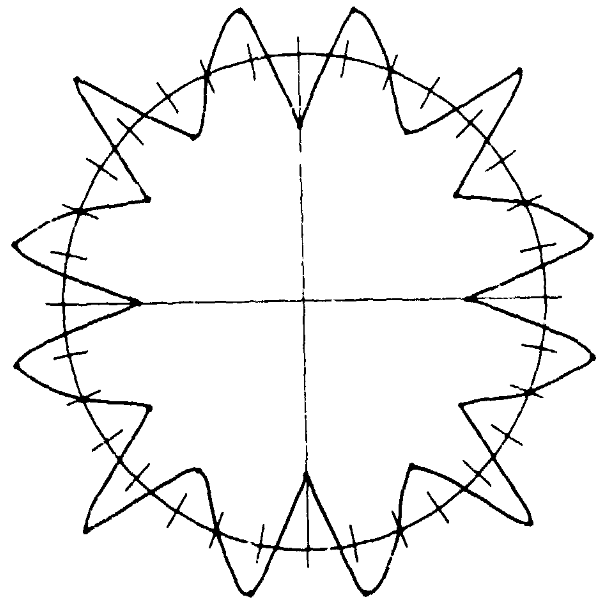

Figure A-13. Mode shape - STAGS model.

$P_{cr}/P = 29.9$; $\ell = 12.7$ cm; $\theta = 22.5^{o}$

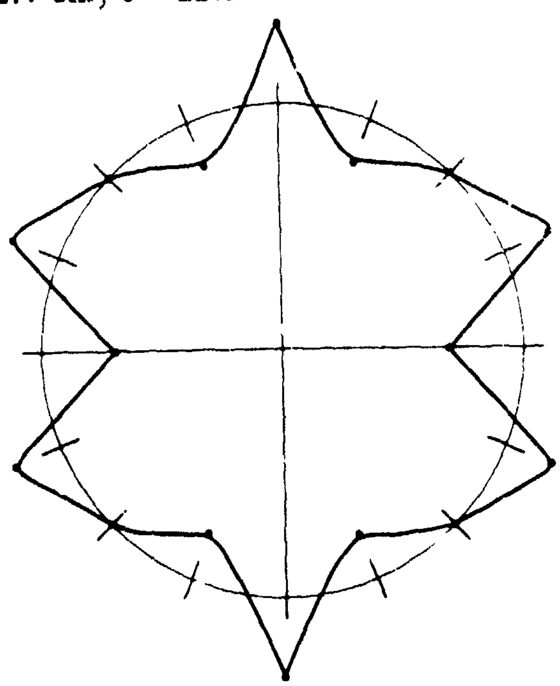

Figure A-14. Mode shape - STACS model.

N74-14593

NASTRAN ANALYSIS OF AN AIR STORAGE PIPING SYSTEM

By Clarence P. Young, Jr., A Harper Cerringer, and Richard W. Faison
NASA Langley Research Center

SUMMARY

This paper summarizes the first Langley Research Center application of NASTRAN to a complex piping design evaluation problem. Emphasis is placed on structural modeling aspects, problems encountered in modeling and analyzing curved pipe sections, principal results, and relative merits of using NASTRAN as a piping analysis and design tool. In addition, the piping and manifolding system was analyzed with SNAP (Structural Network Analysis Program) developed by Lockheed Missiles and Space Company. The parallel SNAP study provides a basis for limited comparisons between NASTRAN and SNAP as to solution agreement and computer execution time and costs.

INTRODUCTION

The new Langley Research Center (LaRC) 4.137 MN/m^2 (600 psia) air storage facility is being constructed to effect repairs to the system that was damaged in the Langley 9- by 6-foot thermal structures tunnel manifold failure in September 1971. Because of the increased concern and emphasis at LaRC on safety in facility design, a rigorous static analysis of the piping and manifolding system design was performed within the Systems Engineering Division (SED). Since NASTRAN had been used extensively within SED for analyzing aerospace-type structures, it was decided that the piping application would provide the desired degree of rigor and at the same time exercise the applicability of NASTRAN as a piping analysis tool.

The purpose of this paper is to document the results and experience gained in applying NASTRAN to a complex pressurized piping system. Although NASTRAN was not developed as a piping analysis tool, it can be used to simulate the extensional and bending behavior of pipes which can be characterized as beams. (See, e.g., ref. 1.) The basic approach is that of a stress analysis of the given design for various static loading conditions. The calculated stresses are then compared with allowable values as obtained from references 1 to 3. These comparisons serve as a basis for evaluating structural adequacy.

SYMBOLS

A cross-sectional area of pipe, m^2 (in^2)

c	distance to outermost fiber measured from bend axis, m (in.)
F_i(PA)	static pressure loading
h	bend characteristic (defined by eq. (1))
I	area moment of inertia of pipe cross section, m^4 (in^4)
IPS	internal pipe size
i_n	stress intensification factor
M	bending moment
P	internal pipe pressure, N/m^2 (lbf/in^2)
R	radius of pipe bend, m (in.)
r_m	mean radius of pipe, m (in.)
T	temperature, °K (°F)
t	pipe wall thickness, m (in.)
V_w	wind velocity, m/s (mph)
x,y,z	element coordinate system
α	angle measured from bend axis of pipe to point of peak stress (see fig. 5), deg
σ_B	stress predicted by elementary beam theory, N/m^2 (lbf/in^2)

Subscripts:

y	bending about Y-axis
z	bending about Z-axis

ANALYSIS

Facility Description

The new air storage facility is depicted in figure 1. Basically, the system consists of 167 air storage bottles connected by manifolding to the main header 0.61-m-diameter (24 in.) supply line. The new main header is tied to an existing overhead line which is illustrated in the photograph of figure 2. In order to assess the total interaction loading effects between the existing line and the new lines, the existing line was modeled as well.

NASTRAN Model Characteristics

The NASTRAN model of the piping and manifolding system is illustrated in the perspective plot of figure 3. The model includes the existing overhead 0.61-m (24 in.) supply line, the new 0.61-m (24 in.) line, the new 0.20-m (8 in.) and 0.25-m (10 in.) lines, 0.15-m (6 in.) manifolds, and 0.038-m (1½ in.) distribution (gooseneck) connections to storage bottles. Anchor points for the piping system are as shown in figure 3 with the gooseneck lines being fixed at the air storage bottle flanges.

Bar elements are used throughout to characterize the pipe elongation, twist, and bending behavior. In total 754 bar elements were used with the reduced problem (constraints and boundary conditions imposed) being characterized by approximately 3500 degrees of freedom.

Curved Pipe Considerations

One of the more interesting aspects of the analysis concerns the structural modeling and prediction of stresses in curved pipe sections. It is known that curved pipe sections behave quite differently compared with straight sections when subjected to bending loads. When bending loads are imposed on a curved pipe, the cross section tends to ovalize or flatten on one side, which results in increased flexibility and a stress redistribution. (See, e.g., ref. 1.)

<u>Structural modeling and flexibility effects</u>.- Since there are no curved bar elements within NASTRAN, the pipe elbows were modeled as a series of straight bar elements as illustrated in figure 4. For the 90° elbows in the 0.61-m (24 in.) line, three bar elements of equal length were used to complete the turn. Additionally, the pressure loadings F_i(PA) shown acting in the figure were developed to satisfy equilibrium around the bend. It should be noted that the number of elements used to represent the curved pipe sections varied, depending on pipe size and turn angle. For example, the 90° bend on the 0.038-m (1½ in.) pipes was modeled using one bar element connecting the pipe center-line points of tangency.

In order to characterize the increased flexibility in the curved regions, the bending modulus of each element was reduced by a flexibility factor defined as the ratio of the resulting increased deflection of a curved pipe to that predicted by beam theory. Theoretical flexibility factor data were obtained from reference 1, which gives the flexibility factor as a function of the bend characteristic h defined as

$$h = \frac{tR}{r_m^2} \qquad (1)$$

<u>Stress intensification</u>.- Elementary beam theory cannot account for the actual stress distributions in curved pipe as illustrated by the comparative distributions given in figure 5. Whereas beam theory would predict the maximum stress to occur at the outermost point from the bend axis, curved pipe theory shows that the peak stress shifts toward the neutral axis (corresponds

to $\alpha = 0$ in fig. 5) and also becomes intensified. The ratio of the maximum stress in a curved pipe to that predicted for a straight pipe is defined as the stress intensification factor i_n. Also, not only do the longitudinal stresses become amplified, but high circumferential stresses are predicted as well.

In figure 5, the orientation of the predicted points of maximum stress for both in-plane and out-of-plane bending of the elbow is seen to be 26° measured from the bend axes. In-plane bending is defined as a bending moment about an axis normal to the plane of bend (Z-axis in fig. 5) while out-of-plane bending corresponds to a moment about an axis in the plane of bend (Y-axis in fig. 5). The i_n values for the elbow of figure 5 as predicted by data given in references 1 and 2 are as follows:

	Reference 1	Reference 2
i_1 (circumferential)	6.6	3.5
i_2 (longitudinal).	5.0	3.5
i_3 (longitudinal).	4.3	3.5
i_4 (circumferential)	7.0	3.5

Note that values given in reference 2 are about one-half the theoretical values given in reference 1 and are constant for both in-plane and out-of-plane bending. The lower values are based largely on experimental results and appear to be more realistic for design.

It is apparent that the actual stress distributions in the curved regions become quite complex for the situation where both in-plane and out-of-plane bending loads are present. Time did not permit research into the area of stress determination around the pipe for combined bending loads; therefore, predicted maximum stresses were added in the most adverse manner as a conservative approach.

Applied Loads

The static loads used for the analysis included the total pressure, thermal loadings for a temperature rise and fall of 288° K (60° F), gravity loads, and steady wind loads at 44.7 m/s (100 mph). Solutions were obtained for the independent loading conditions as well as for the total combined loads. In this manner, the stress contributions for the separate and combined loadings were obtained for comparison with the allowable working stress criteria given in references 2 and 3.

Analysis Procedure

The analysis procedure is depicted in the flow diagram of figure 6. Note from the flow diagram the incorporation of the flexibility and stress intensification factors. As stated previously, the bending flexibility in the elbow regions was accounted for by reducing the section modulus of the bar elements which make up the curved pipe sections.

Since NASTRAN cannot recover the combined stresses for either straight or curved sections of pressurized pipe, it became necessary to write a separate stress calculations program. This program uses the input of element forces and moments and generates the combined pressurized pipe stresses (e.g., hoop stresses are accounted for along with torsional stresses) and also applies stress intensification factors in the elbow regions. Once the combined stresses are calculated for the highest loaded elements, these values are then compared with the allowables and guideline values of references 1 to 3.

DISCUSSION OF RESULTS

The results of the NASTRAN analysis proved to be quite beneficial not only for verifying the adequacy of design but also for identifying potential problem areas and for efficient selection of anchor point locations and pipe bend radii. For example, one early finding in the analysis identified an overstressed situation for the gooseneck at the last row of air storage bottles nearest the main header. In this instance, an error in the design calculations had resulted in a pipe length selection that was too short. Had the NASTRAN analysis not been performed the error probably would have gone unnoticed with failure likely.

General Stress Results

In general the calculated stresses throughout the system were within the required working allowables of references 1 to 3 and in only a few isolated areas equaled or slightly exceeded the conservative combined loading stress guidelines given in reference 1. (The calculated stress values are not presented or discussed in detail for reasons of brevity and lack of significance within the framework of the present paper.) Based on the NASTRAN calculations, the design was acceptable; however, the design was also examined in view of obtaining stress reductions in particular areas of concern. As it turned out, the stress condition of the greatest concern occurs in the last goosenecks nearest the 0.61-m (24 in.) main header. The higher stresses occur in these goosenecks as a result of thermal and pressure expansion in the main header pipe. Two options considered for reducing these stresses were (1) to relocate the anchor point and (2) to select a more desirable bend radius for the goosenecks. These options are examined in the following subsection.

Analysis of Potential Stress Reductions

Two selected studies on stress reduction in the gooseneck pipes are discussed in this section. Other studies were made which proved to be useful for identifying local problem areas but are beyond the scope of the present paper.

<u>Anchor point location</u>.- The main header line and manifolding to the air storage bottles are illustrated in the schematic of figure 7. The point of fixity is located at x = 17.07 m (672 in.) (support tower) with guide locations as indicated. It should be noted that a guide support is designed to allow the pipe to slide (longitudinally) while providing constraint in all other directions.

The basic behavior which leads to the previously mentioned high stresses in the last row of distribution lines (goosenecks) is thermal and pressure expansion of the main header. The local deformation behavior of a row of goosenecks due to the main header expansion is illustrated in figure 8. The fixity at $x = 17.07$ m (672 in.) leads to pipe expansions both toward the origin $x < 17.07$ (672 in.) (negative) and toward the air storage bottle field $x > 17.07$ m (672 in.) (positive). These expansions significantly influence stresses in the gooseneck lines and in the main header elbow located at the origin. Therefore, a logical way to reduce the gooseneck stresses, at the expense of increasing the elbow stresses, would be to relocate the anchor point.

In order to examine the main header expansion behavior, the point of fixity was removed which yields the deflections along the header for pressure and temperature expansion as shown in the graph of figure 7. Note from the curves of figure 7 that a node point ($\Delta x = 0$) exists at $x = 27.94$ m (1100 in.). The node point is ideal for anchor location for the statics load problems as it would be equivalent to the no-fixity case.

In order to explore the stress situation at the particular points of concern, the anchor point locations were varied which gave the stress plots in figure 9. By combining stresses due to thermal plus temperature expansion, it can be seen that a significant stress reduction is obtained by moving the anchor point toward the bottle field. At the same time the stresses are observed to rise in the main header elbow. For example, the combined stresses in the 0.038-m ($1\frac{1}{2}$ in.) pipe can be reduced by 50 percent by locating the anchor at $x = 31.09$ m (1224 in.) (extrapolated point) at the expense of a 33-percent increase in the elbow. The need to have a complete fixity in view of dynamic blowdown effects and at the same time give a much reduced static stress situation would suggest locating the anchor at $x = 31.09$ m (1224 in.).

Bend radius selection for gooseneck geometry.- Another example of stress reduction via NASTRAN analysis is shown in figure 10. The 0.038-m ($1\frac{1}{2}$ in.) gooseneck between the 0.15-m (6 in.) manifold pipe and bottle (assumed as the point of fixity) was initially designated with a length of 0.53 m (21 in.) from manifold to bottle instead of 1.52 m (5 ft). As previously mentioned, the preliminary NASTRAN analysis resulted in unacceptably large stresses, which ultimately led to a parametric study to determine the best design. A space limitation imposed a maximum of 1.52 m (5 ft) available for the length from manifold to bottles, whereas the bottle spacing imposed a maximum radius of bend of 0.46 m (18 in.) for the 0.038-m ($1\frac{1}{2}$ in.) gooseneck. Intuitively, one might think that the maximum radius of bend would provide the lesser stress; however, the stresses are seen to result primarily from the displacement of the main header as previously described. This displacement imposes a large moment at the bottle connection (fixed point in fig. 10), and thus the longer the moment arm, or rather the length from manifold to bottle, the smaller the stress. Figure 10 shows the calculated stresses in the goosenecks as a function of the radius of bend for the given 1.52 m (5 ft) length from manifold to bottle. The input for the study was the displacement of the gooseneck at the manifold end for a selected bend radius of 0.20 m (8 in.). This displacement, associated with the maximum combined for both the temperature and pressure expansion, of the main header was assumed constant and independent of bend radius. Although the data are not depicted in figure 10, the stress increases in the bend and straight section as the 1.52 m (5 ft) length from header to bottle is decreased. Also, the standard minimum radius of bend for a 0.038-m ($1\frac{1}{2}$ in.) pipe as specified in reference 2 is 0.19 m ($7\frac{1}{2}$ in.); thus, the selected gooseneck design was for a 0.19-m ($7\frac{1}{2}$ in.) radius of bend and a length of 1.52 m (5 ft) from manifold to bottle.

COMPARISON OF NASTRAN WITH SNAP

The parallel SNAP analysis was performed for a number of reasons. Chief among these was the need to gain further experience to provide further check-out of the SNAP "statics" program (ref. 4). Also, the SNAP analysis served as a backup solution for NASTRAN and gave a basis for comparing and/or verifying numerical results.

The NASTRAN and SNAP structural models were developed by Gerringer and Faison, respectively, so that the analyses were independent; however, the basic element representations were used for both models. It should be noted that the SNAP model did not include the new 0.20-m (8 in.) and 0.25-m (10 in.) lines shown in figure 1; however, for comparison solutions the aforementioned lines were removed from the NASTRAN model.

The parallel analysis proved to be quite useful for uncovering modeling and loads input errors. Also, the numerical results agreement was very good as one would expect.

From a computer cost point of view, SNAP was found to be much more economical for the study. Typical comparative execution times and cost per run for a combined loads case on the Control Data 6600 computer system are as follows:

	NASTRAN	SNAP
Execution time, sec.	550	120
Cost per run, dollars.	107	15

These comparisons show the NASTRAN execution time is greater by a factor of about 4.5 and costs about seven times as much as the SNAP run. These comparisons should, of course, be recognized as that for a particular static problem solution rather than a general observation. SNAP apparently attains its low execution costs through the use of a direct elimination procedure (see ref. 5) which affords substantial savings when compared with constant or variable-width band matrix, active column, or partitioning solution methods. Information distributed by the author of reference 5 points out that in run-time comparison studies no other program was found to execute as fast as SNAP; in very large problems, very substantial differences in run time (e.g., factors of 10 or more) have often been observed.

CONCULDING REMARKS

The NASTRAN application to the new LaRC piping and manifolding system supports the adequacy of design in view of applied stress criteria. The analysis defined the static behavior of a complex piping system and significantly impacted the design in several areas.

Based on the experience gained in this application, it is believed that NASTRAN can be used as a powerful tool for design evaluation of complex piping systems. However, major additional needs for NASTRAN to be used as an efficient piping analysis tool are identified as (1) development and inclusion of curved beam elements and (2) stress recovery subroutines for pressurized pipes and curved pipe sections subjected to combined bending loads.

The parallel analysis using the SNAP program gave very good agreement in numerical results. However, SNAP proved to be much more economical for this particular problem application.

REFERENCES

1. Design of Piping Systems. M. W. Kellogg Company, John Wiley and Sons, Inc., Second Edition, 1956.

2. Petroleum Refining Piping (American Standard Code for Pressure Piping), ASA B31.3-1966. The American Society of Mechanical Engineers, 1966.

3. Nuclear Power Plant Components, ASME Boiler and Pressure Vessel Code. American Society of Mechanical Engineers, July 1971.

4. Whetstone, W. D.: Structural Network Analysis Program User's Manual, Static Analysis Version V70E. LMSC-HREC D162812, December 1970.

5. Whetstone, W. D.: Computer Analysis of Large Linear Frames. Journal of the Proceedings of the American Society of Engineers, November 1969.

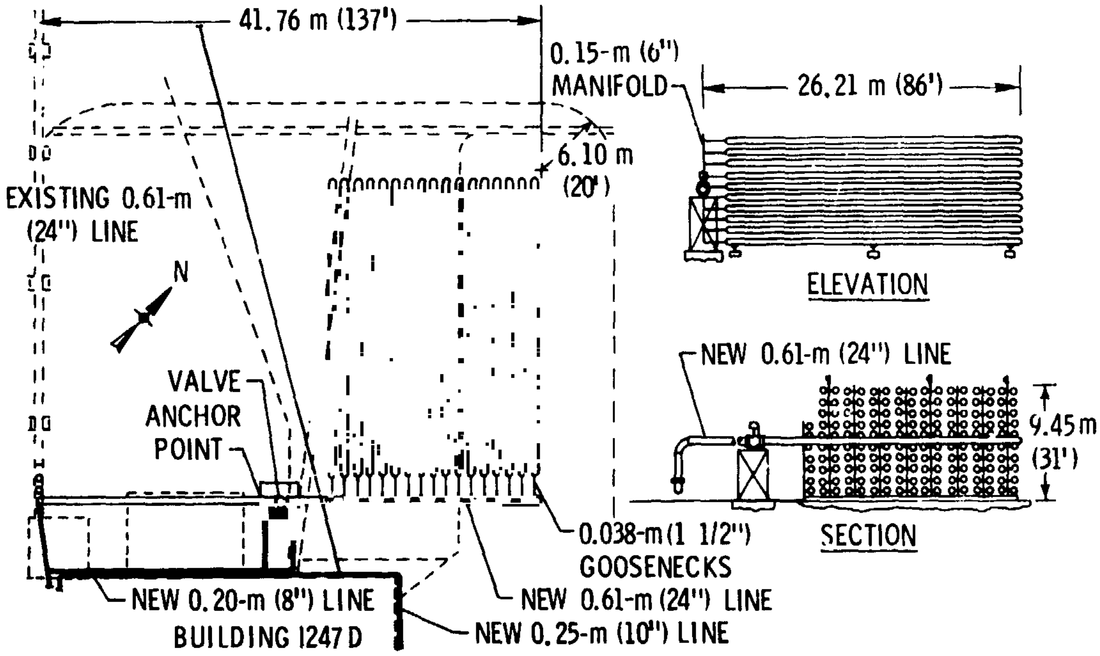

Figure 1.- Air storage facility layout.

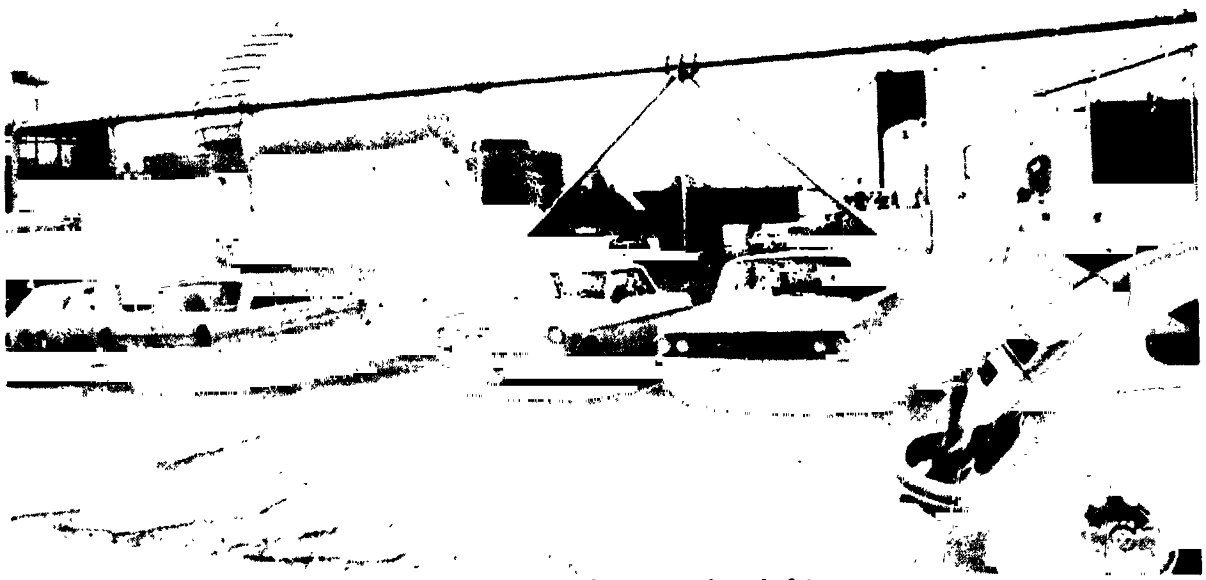

Figure 2.- Existing overhead line.

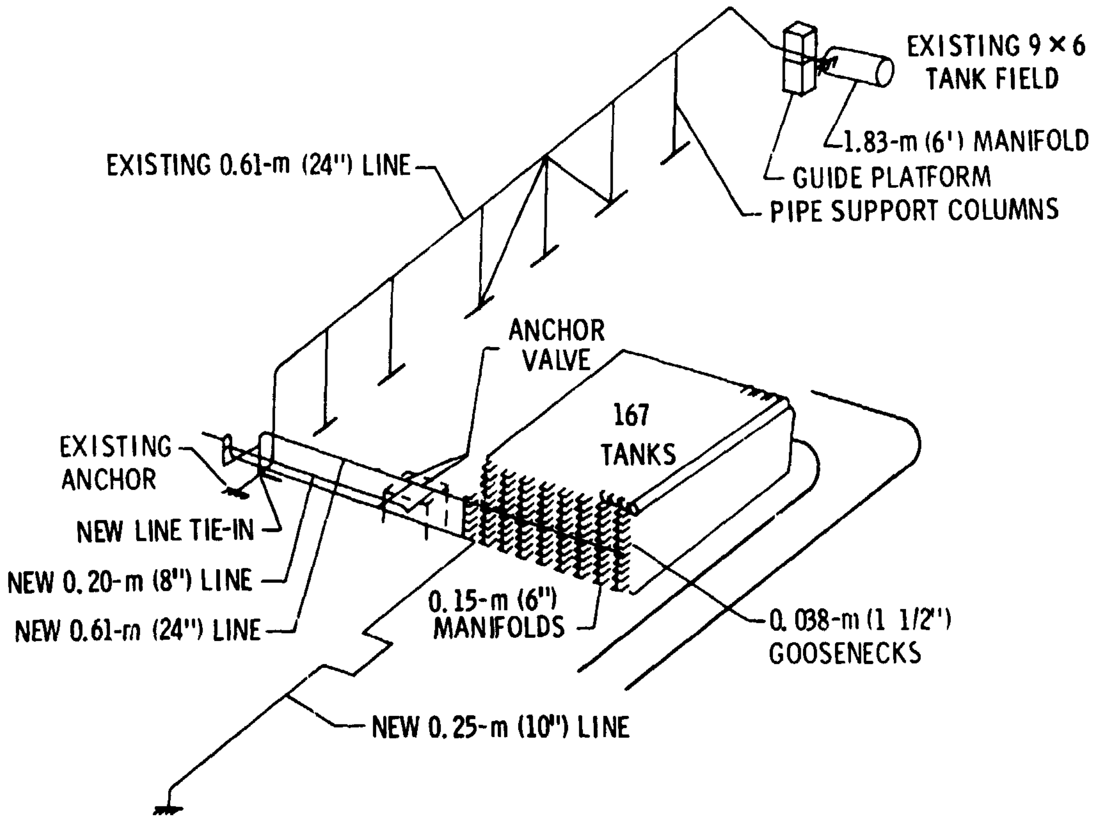

Figure 3.- Perspective of NASTRAN model.

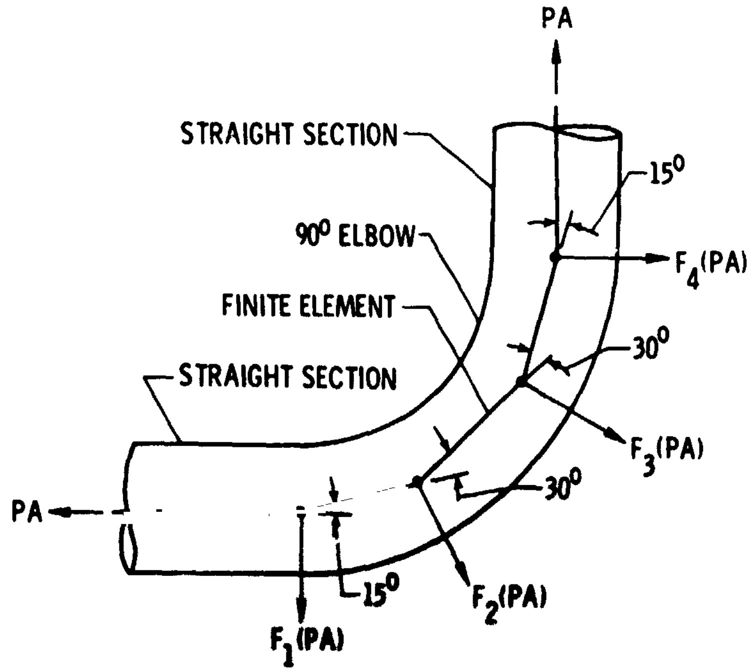

Figure 4.- Modeling of 90° pipe bend.

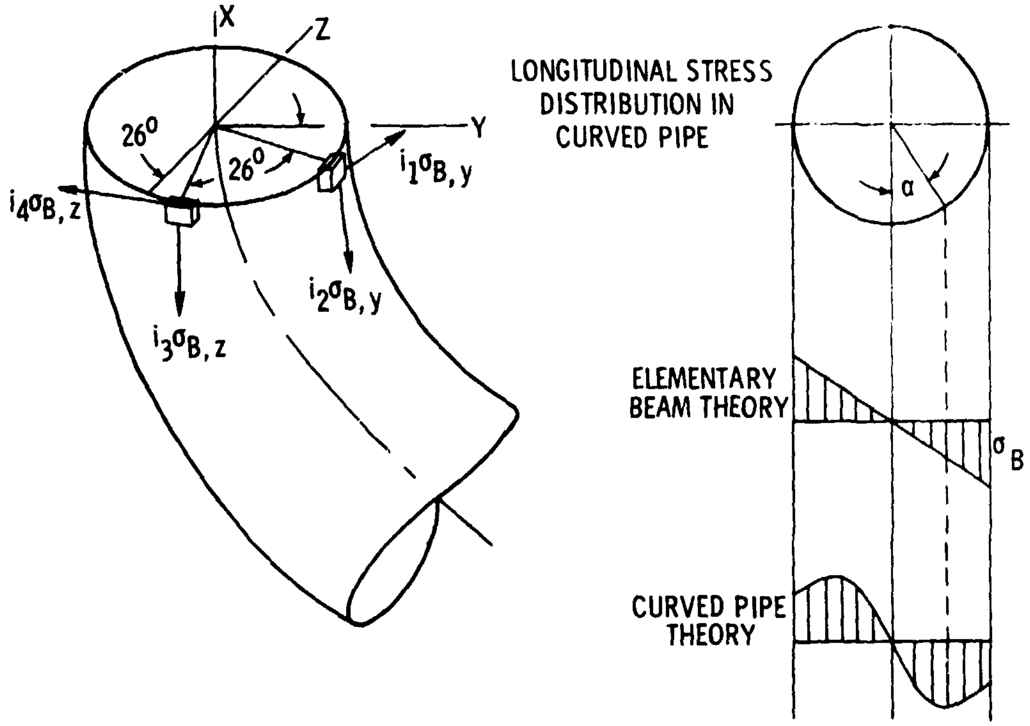

Figure 5.- Stress components for in-plane and out-of-plane bending.

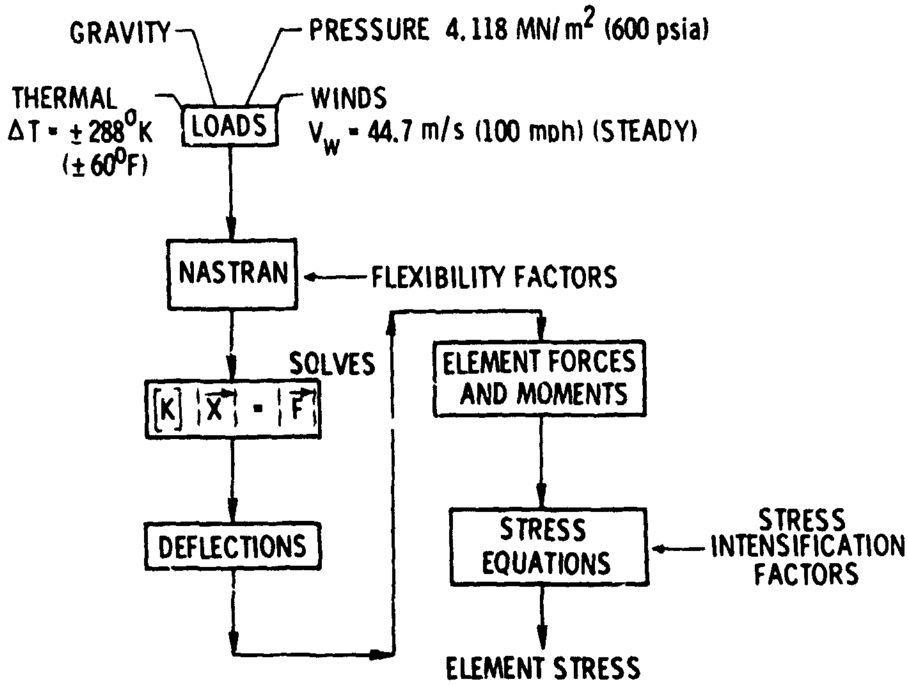

Figure 6.- Analysis procedure format.

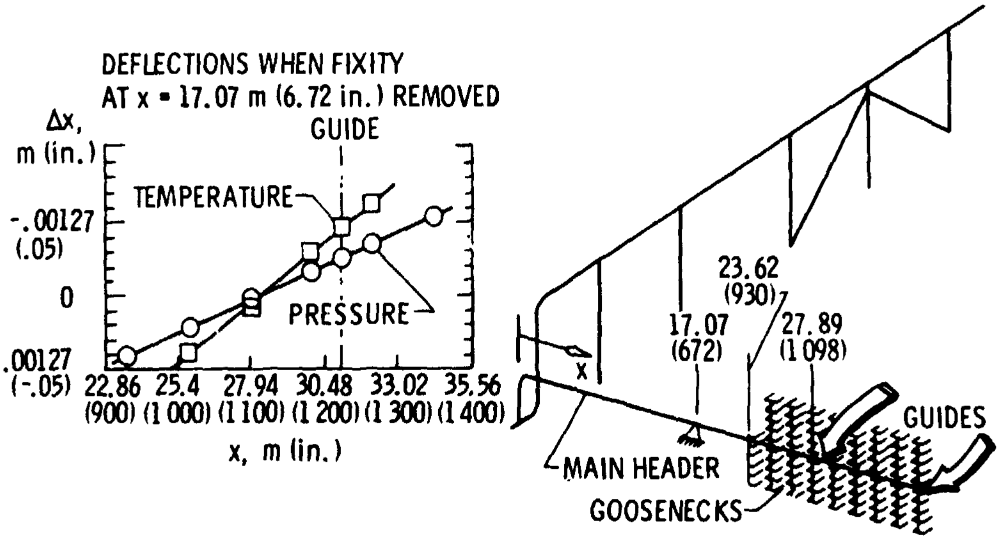

Figure 7.- The 0.61-m (24 in.) header deflections with fixity removed. Dimensions are in m (in.).

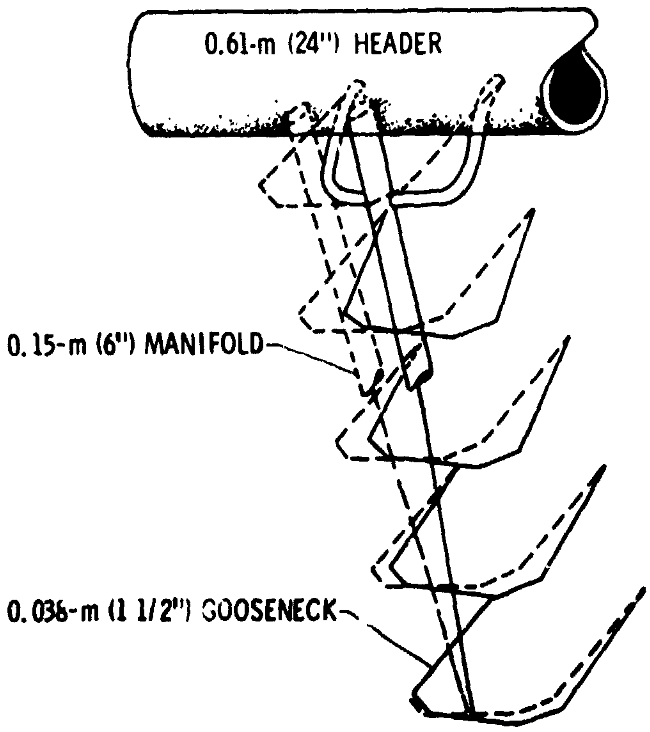

Figure 8.- Deformation behavior of goosenecks due to header movement.

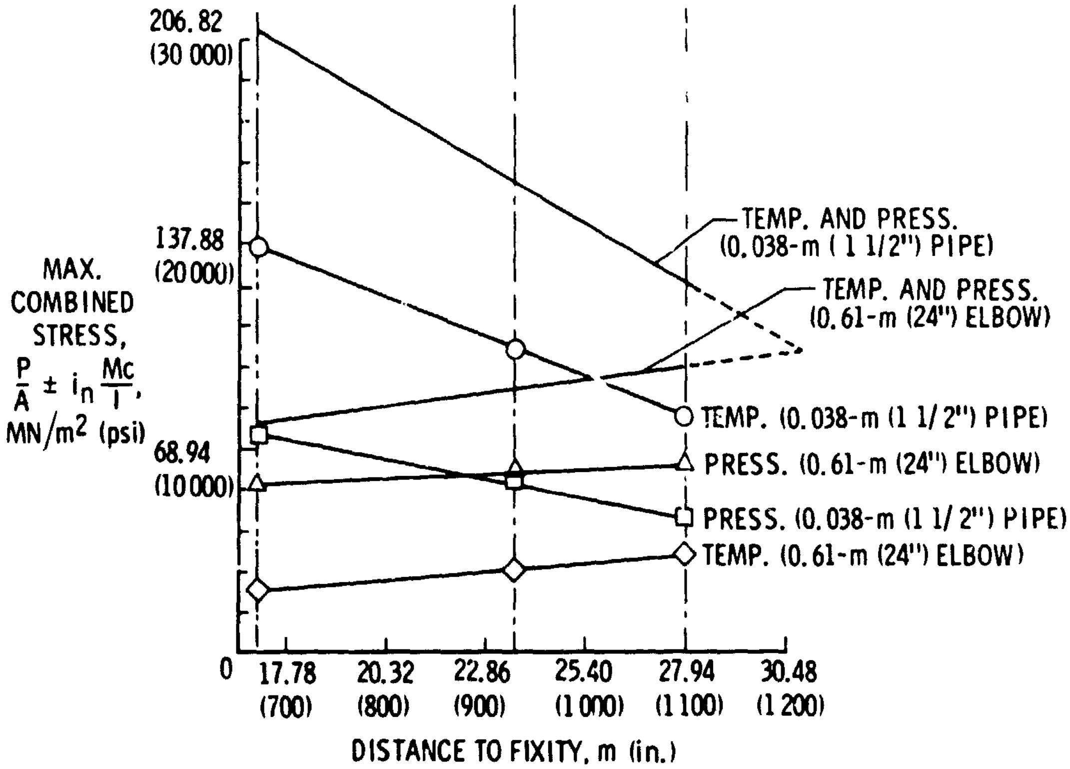

Figure 9.- Stress variations with change in anchor point location.

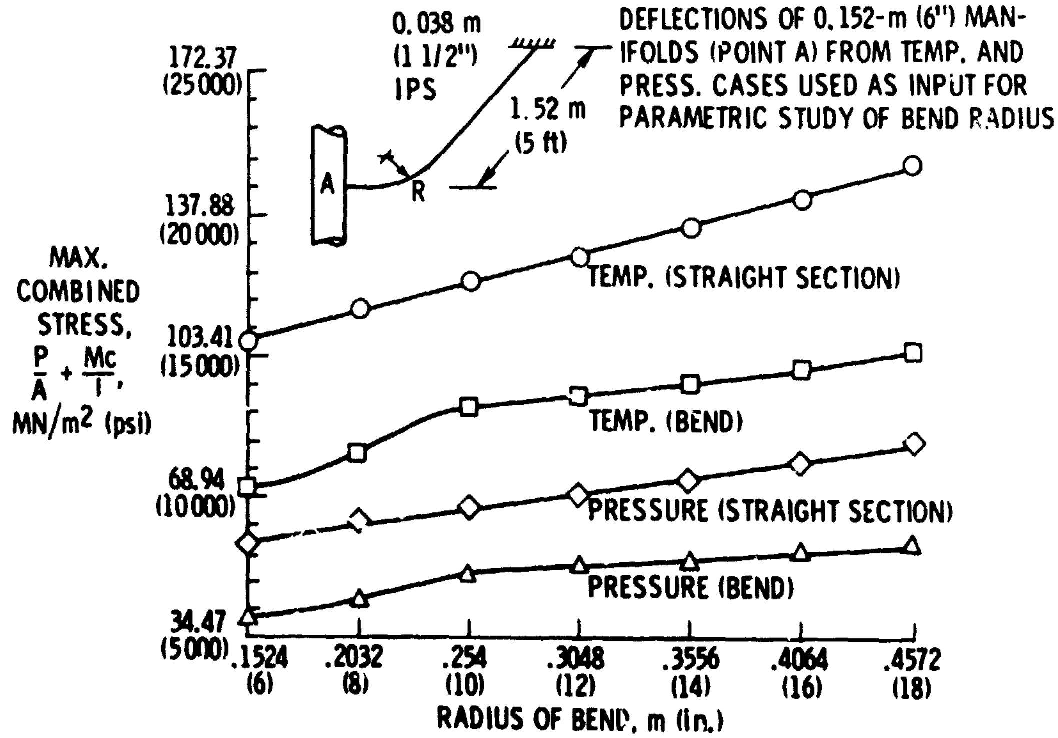

Figure 10.- Stress variations in 0.0381-m (1 1/2 in.) pipe with changes in bend radius.

N74-14593

THERMAL DISTORTION ANALYSIS OF A DEPLOYABLE PARABOLIC REFLECTOR

By Lloyd R. Bruck and George H. Honeycutt

NASA Goddard Space Flight Center

SUMMARY

The Goddard Space Flight Center has performed a thermal distortion analysis of the Advanced Technology Satellite (ATS-F) 9.144m (30 ft.) diameter parabolic reflector using NASTRAN Level 15.1. The same NASTRAN finite element model was used to conduct a 1g static load analysis and a dynamic analysis of the reflector. In addition, a parametric study was made to determine which parameters had the greatest effect on the thermal distortions. This paper describes the method used to model the construction of the reflector and presents the major results of the analyses.

INTRODUCTION

The ATS-F is the latest in a series of spacecraft designated as Advanced Technology Satellites. This 3-axis stabilized synchronous satellite has been designed as a multiple mission system to allow for numerous communications, meteorological and scientific studies.

The ATS-F spacecraft is shown in the launch configuration in Figure 1 and in the orbital configuration in Figure 2. The predominate feature of the spacecraft is a 9.144m (30 ft.) diameter parabolic dish high gain antenna. The success of many of the spacecraft experiments depends on maintaining the design surface contour of the parabolic reflector after deployment. In addition, the spacecraft control system must adhere to stringent pointing and slewing requirements for R-F beam positioning.

The surface contour of the reflector is distorted in orbit by the thermal environment of space. It is necessary to predict what these distortions will be in order to assess the R-F performance of the reflector. As there is no practical or realistic ground test that will provide this data it was necessary to resort to analytical methods. Accordingly, GSFC has performed a thermal distortion analysis of the ATS-F reflector using NASTRAN Level 15.1 for selected thermal load cases that produces the required reflector distortions.

As a partial check on the validity of the NASTRAN model a 1g static deflection analysis was also accomplished. The results were compared with an actual measurement of the 1g deflections to provide some information on the accuracy of the model.

To help determine which parameters were most important in controlling the thermal distortions, a parametric study was made. In this study the effects of the mesh, rib temperature, and rib thermal gradients were varied to determine the relative magnitude of the effects on the thermal distortions.

In addition, the fine pointing and slewing requirements necessitated obtaining the dynamic characteristics of the reflector. With only slight modification to the static NASTRAN model the first natural frequency and mode shape were obtained to provide information for design of the control system.

The prime contractor for the ATS-F spacecraft is Fairchild Space and Electronics Company; the subcontractor for the parabolic reflector is Lockheed Missiles and Space Company. Both of these organizations provided information which made these analyses possible.

REFLECTOR DESCRIPTION

General

The deployed reflector is composed of 48 flexible ribs hinged to the spacecraft hub at 7.5 degree increments as shown in Figure 2. A woven copper coated dacron mesh serves as the reflective surface and is connected between each rib at the top edge of the rib. When stored for launch, the ribs are wrapped around the hub with the mesh carefully folded between the ribs. The packaged reflector is enclosed by a series of doors that are secured by a circumferential restraining cable. When the restraining cable is severed, the elastic energy stored in the ribs is released causing the ribs to unwrap to the deployed position. During deployment the ribs pivot freely about the hinges at the hub; when fully deployed the hinges are locked. The reflector is designed so that there is always a small tension load acting on the mesh keeping it taut during orbit.

Rib Description

An individual reflector rib is shown in Figure 3. The rib tapers in width from its attachment at the hub to the outer edge of the reflector. The cross section of the rib normal to the parabolically curved principal axis is of semi-lenticular shape and also varies along the rib. Each rib is made from a single piece of aluminum sheet with varying diameter holes cut out along its length. The holes are provided to permit the heat input from the sun to pass freely through the rib to prevent excessively severe thermal gradients.

Mesh Description

The R-F reflective mesh is constructed from copper coated dacron yarn bundles overcoated with a thin silicone sealant. The warp yarn running in the longitudinal direction (radially along the rib) is made from double strand dacron, 10 pair/cm while the filling yarn in the transverse direction (circumferential from rib-to-rib) is made from single strand dacron 12.5 strands/cm. This form of construction makes the woven mesh behave nonisotropically and consequently have material properties (modulus of elasticity and the thermal coefficient of expansion) that differ in each principal direction. Tests on the mesh have revealed that Poisson's ratio is essentially zero for this material in both directions indicating that the yarns in either direction behave independently of one another when each is loaded individually.

Hub Description

The aluminum hub, Figure 4, is composed of two ring sections connected every 7.5 degrees by risers located midway between each rib. The reflector is protected in the folded position by a cover as shown in Figure 4. This cover provides no significant load carrying structure to the hub. The rib hinge attachment to the hub is also illustrated.

Attachment of the hub to the spacecraft is provided by the mounting assembly indicated in Figure 5. This assembly, located every 90 degrees, provides for a rigid attachment of the hub to the spacecraft except for the rotation that is allowed to take place at the hinge. The purpose of this method of attachment is to assist in the isolation of the antenna from any structural motion created by the spacecraft.

FINITE ELEMENT MODEL

Rib Model

The finite element model of the rib is shown in Figure 6 where each of the 48 ribs have been represented by 10 bar elements making a total of 480 rib elements. A significant feature of the rib model is that the offset between mesh attachment point and the rib centroidal axes is retained. The effect of this offset is to introduce a twisting moment about the rib longitudinal axis when the rib is loaded in the lateral (circumferential) direction by mesh loads and a bending of the rib about a circumferential axis when loaded in a radial direction by the mesh. This offset is shown in Section A-A of Figure 6.

The shear center of the rib and the rib centroidal axis do not coincide. Prior to the formulation of the 10 element rib model a much more detailed plate element model of a single rib was generated which simulated the shear center offset. Various thermal gradients were applied to this model to determine the resulting twist and warp of the rib. The results of this analysis indicated that the offset shear center causes only slight twist and warp of the free rib. Because the mesh would act to resist the twist of the rib, the restraining force of the mesh would tend to further minimize the effect of twist or warp on the thermal deformations. Therefore, it was concluded the effect of the shear center offset is minimal and can be neglected.

The reflector deflection resulting from thermal or gravitational loads is determined for grid points at the mesh attachment point to the rib.

Hinges are provided at the hub for attachment of the ribs to the hub and to allow the ribs to rotate to their fully deployed configuration. These hinges become fixed at deployment. For this reason the rib hinges were fixed in the model.

Mesh Model

The reflector mesh has been modeled by membrane elements capable of carrying in-plane tension loads. Each mesh section between ribs has been subdivided into 10 trapesoidal membranes that are attached to each corner to the grid points located at the rib edge. The nonisotropic properties of the mesh have been reflected in the model parameters; the mesh thermal coefficients of expansion and modulus of elasticity are given as functions of temperature.

Hub Model

The hub is modeled with bar elements as shown in the hub segment depicted in Figure 7. A centroidal axis offset of the upper and lower hub rings at the hinge has been provided in order to position the hinge elements in their proper location. Four attachment points are provided for securing the hub to the spacecraft. This attachment allows rotation of the hub in the direction of the hinges as in the actual construction by using the pin flag option in NASTRAN.

COMPLETE FINITE ELEMENT MODEL

The complete finite element model, Figure 8, is composed of the hub, mesh, and rib models discussed previously. This figure was obtained by using the plot module of NASTRAN. A total of 1404 elements connected between 728 grid points are used to model the complete reflector. As every grid point is allowed to ave 6 degrees of freedom, with the exception of 4 grid points hat are fixed simulating the spacecraft, there are 4,344 total egrees of freedom.

In the static analysis the decomposition of the stiffness atrix (semi-bandwidth of 15 terms with 87 active columns and 14 ows) consumed the bulk of the computer time. Run time using tandard core on the IBM 360-95 for one static load case was 15 inutes, 10 minutes of which was used decomposing the stiffness atrix.

In the dynamic analysis, using the inverse method eigen-alue extraction routine, obtaining one eigenvalue used about 35 inutes of the total run time of 38 minutes.

1g ANALYSIS

A 1g load in the -Z direction was placed on the reflector n order to check out the finite element model and to provide a omparison with static deployment test results of the actual eflector. Reflector deflection results are presented as plots f the vertical (Z) deflection of the rib tip at 4.572m (180 in.) adius versus rib number. Figure 9 illustrates the rib numbering ystem. The 1g NASTRAN result and actual test results are compared n Figure 10. This comparison indicates good agreement with the ctual test results was achieved.

ORBITAL THERMAL DEFLECTION ANALYSIS

Thermal Load Input

A reference temperature of 294°K (70°F) was assigned to each lement to define the as-assembled temperature. Orbital tempera-ure distribution for the various orbit hours served as the thermal oad input for the finite element model. The temperatures for each ib segment (10 segments per rib) were determined for an upper node T_1) and a lower node (T_2). These temperatures were averaged in he GSFC analysis to define the temperature assigned to the rib lement in the longitudinal direction. The rib gradient across he rib was calculated using $(T_1-T_2)/d$ where d is the distance etween the upper and lower nodes (see Figure 11). Each mesh lement and each grid point was assigned a temperature; for those rid points where nodal temperatures were not defined a linear nterpolation was made.

The effect of the spacecraft attachment to the deployed eflector is presented by a set of initial displacements at the our attach points.

Thermal Deflection Results

Although the deflection results for 12 orbit hours were determined, only those resulting from orbital thermal loads developed during orbit hours 5, 12, and 24 for Beta =0° will be presented as they provide a representative sampling of the total results. Figure 12 presents the satellite orientations for various orbit hours and defines the orbit angle Beta.

- Orbit Hour 12, Figure 13 - The reflector is completely shaded by the earth and is very cold. The shrinkage of the reflector caused the rib tips to deflect to their maximum value.

- Orbit Hour 24, Figure 14 - The reflector sees its least severe thermal load. As a consequence its deflections are a minimum.

- Orbit Hour 5, Figure 15 - One half of the reflector is shaded by the other half. Because of this effect, the thermal gradient developed across the rib is relatively large and takes the shape plotted in Figure 16. Note that the plot of the thermal gradient across the rib corresponds closely to the plot of the deflected shape of the reflector; compare Figures 15 and 16.

PARAMETRIC VARIATION STUDY

In an effort to determine the relative effect of various model parameters on the deflection of the reflector, a parametric variation study was conducted on the finite element model. The temperature distribution present during orbit hour 5, Beta=0 was used for the five cases investigated.

Case 1 - This case determined the reflector deflection with the mesh removed and with the thermal gradient across the width of the rib set equal to zero. The resultant deflection, Figure 17, is caused by the rib temperatures and radial rib gradient only and is relatively small.

Case 2 - The mesh has been removed and only rib temperatures and gradients are present, both radially along the rib axis and across the width of the rib. The results of this variation are shown in Figure 18. Note that the deflections are large and the shape of the plot of the rib deflections again agrees, as expected with the shape of the plot of the average depthwise temperature gradient as shown in Figure 16.

Case 3 - The radial mesh elements have been removed and only circumferential mesh elements are present. The rib temperatures and radial temperature gradient are present along the rib, but the gradient across the width of the rib has been set equal to zero. Deflection results are shown in Figure 19. Although there are major differences in the temperature distribution around the circumference of the reflector ranging from 116°K (-251°F) to 269°K (25°F), the net effect on the mesh is that a uniform tension is created in each circumferential band. This statement is substantiated by the results which indicate a uniform deflection is created at the outer edge of the reflector.

Case 4 - The circumferential mesh elements have been removed and there is no depthwise rib gradient; the radial mesh elements remain, as well as the rib temperatures and radial rib gradients. Figure 20 presents the results. The net effect of the radial mesh can be obtained from subtracting Case 1 results from this case, Case 4. It would appear that the deflections caused by the radial mesh element are insignificant for this case.

Case 5 - The effect of varying the depthwise rib gradient is shown in Figure 21. The results of 3 parametric changes are shown: no gradient, actual gradient, and 3 times the actual gradient. The major impact the rib gradient has on the deflection is evident.

DYNAMIC ANALYSIS

The finite element model was used to determine the first torsional frequency of the deployed reflector. Comparison of the NASTRAN result of 1.18 Hz with a value obtained from a modal survey test of 1.15 Hz indicates good agreement.

A motion picture of the torsional mode was obtained by the proper adjustment of the amplitude in repeated plots of the modal displacements in the plot routine and repeating them sequentially on 16mm film.

CONCLUSION

NASTRAN has proven to be a most valuable tool in conducting the thermal distortion analysis. Because of the capability built into NASTRAN the parametric study was easily accomplished by the alteration or addition of a few input cards The value of the data obtained far outweighed the cost of the additional computer time required. The results of this analysis supplied valuable information on the performance characteristics of the parabolic antenna and provided insight into the structural interactions of the various parts of the reflector.

The results of the lg analysis compared favorably with available test results which provided some confidence that the model was satisfactory. Again with but a few card changes and using a different rigid format the first torsional natural frequency and mode shape were obtained.

The addition of a beam element capable of handling the offset shear center effect would have saved the considerable time and effort expended to prove it had little effect in this problem. It is recommended that this capability be added to NASTRAN.

ACKNOWLEDGEMENT

The authors are pleased to acknowledge Dr. James B. Mason and Mr. Reginald S. Mitchell (NASA/GSFC) for the assistance they provided throughout the analysis tasks.

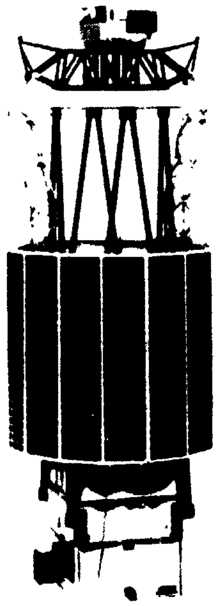

Figure 1. ATS-F Launch Configuration

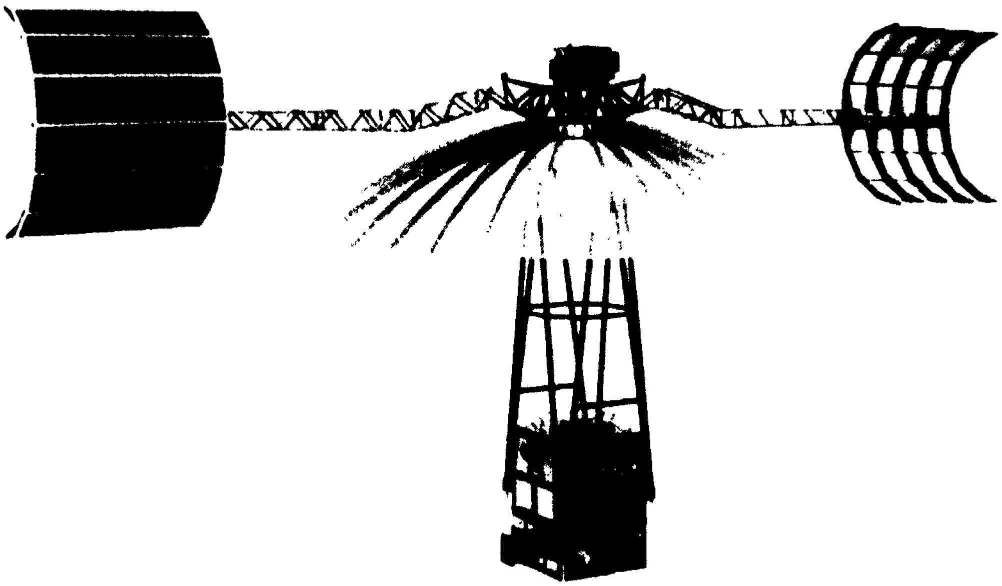

Figure 2. ATS-F Orbital Configuration

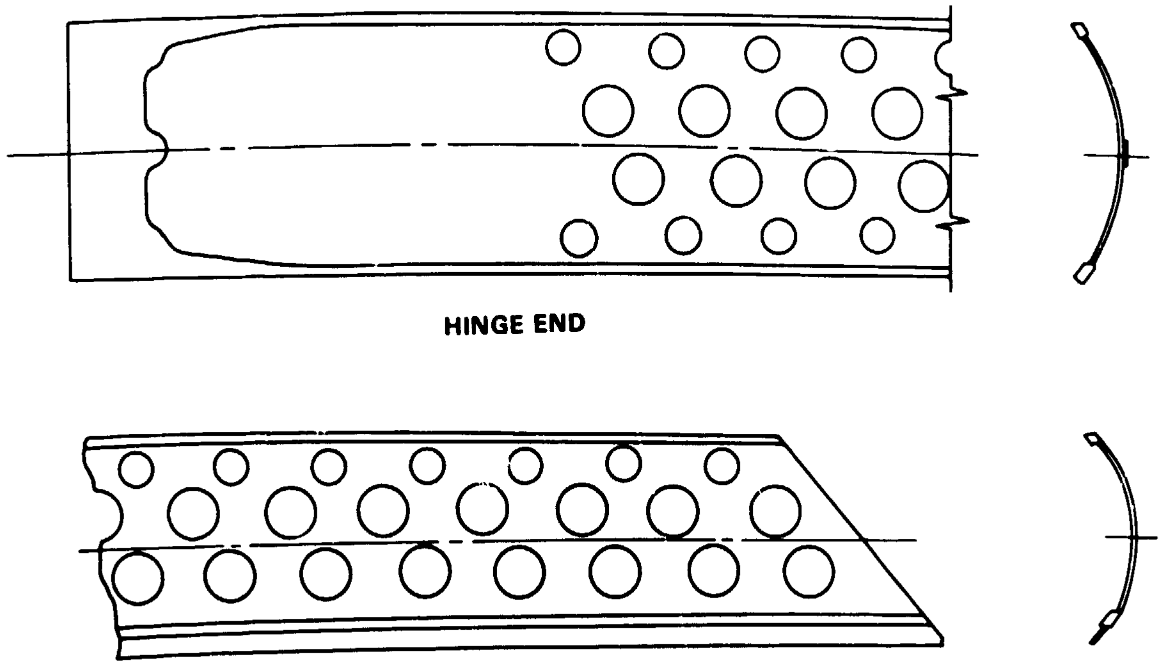

Figure 3. Reflector Rib

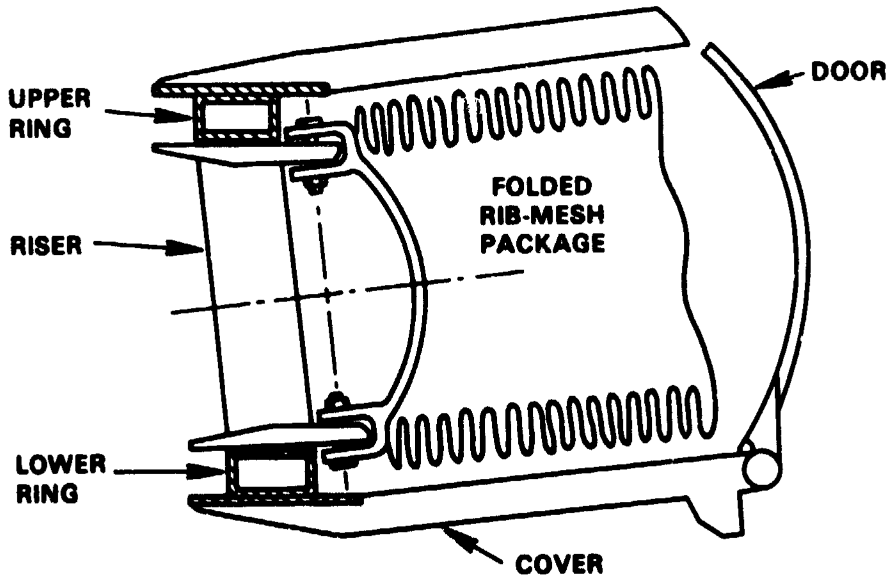

Figure 4. Hub Cross-Section and Rib Hinge

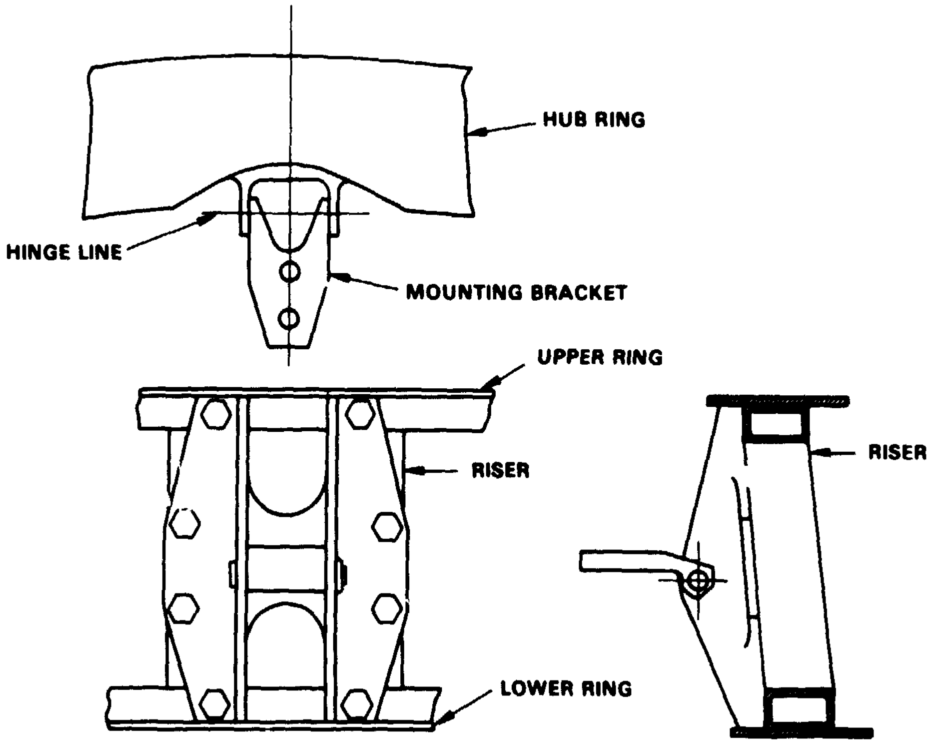

Figure 5. Reflector/Spacecraft Attachment

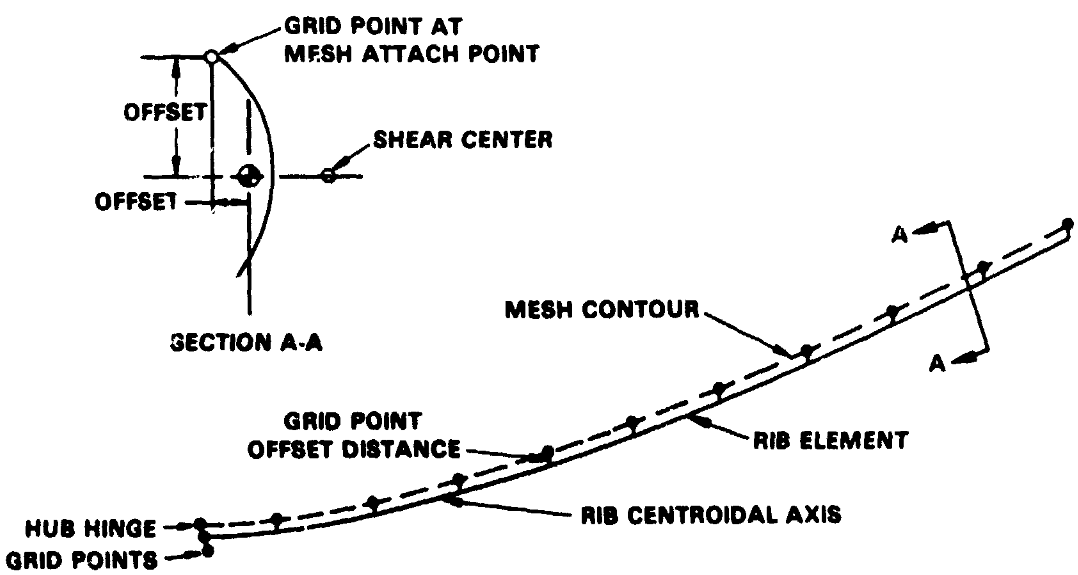

Figure 6. Rib Model

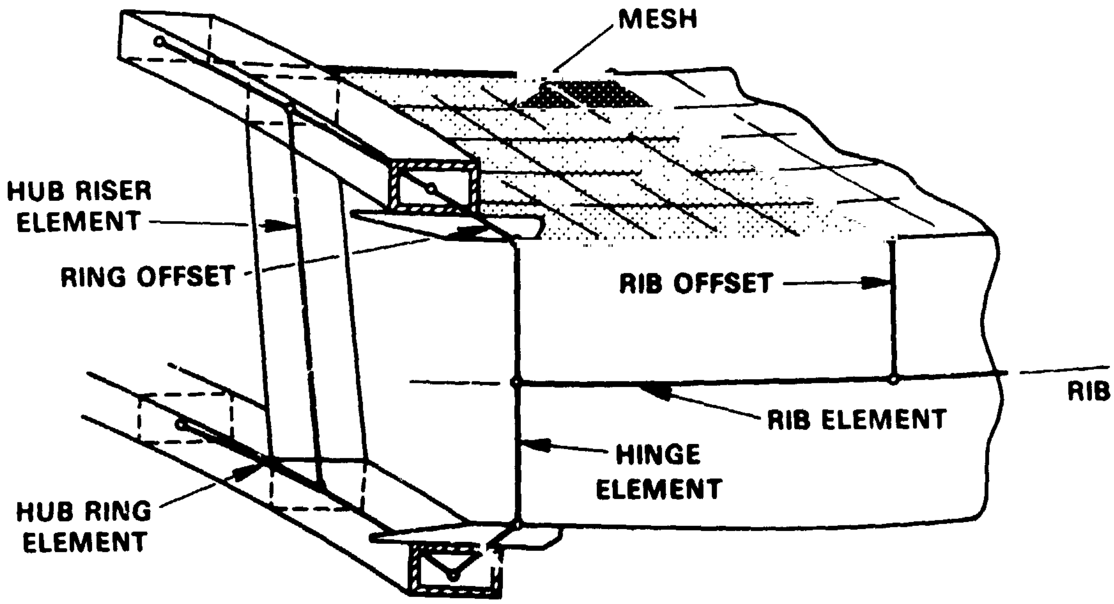

Figure 7. Hub Model

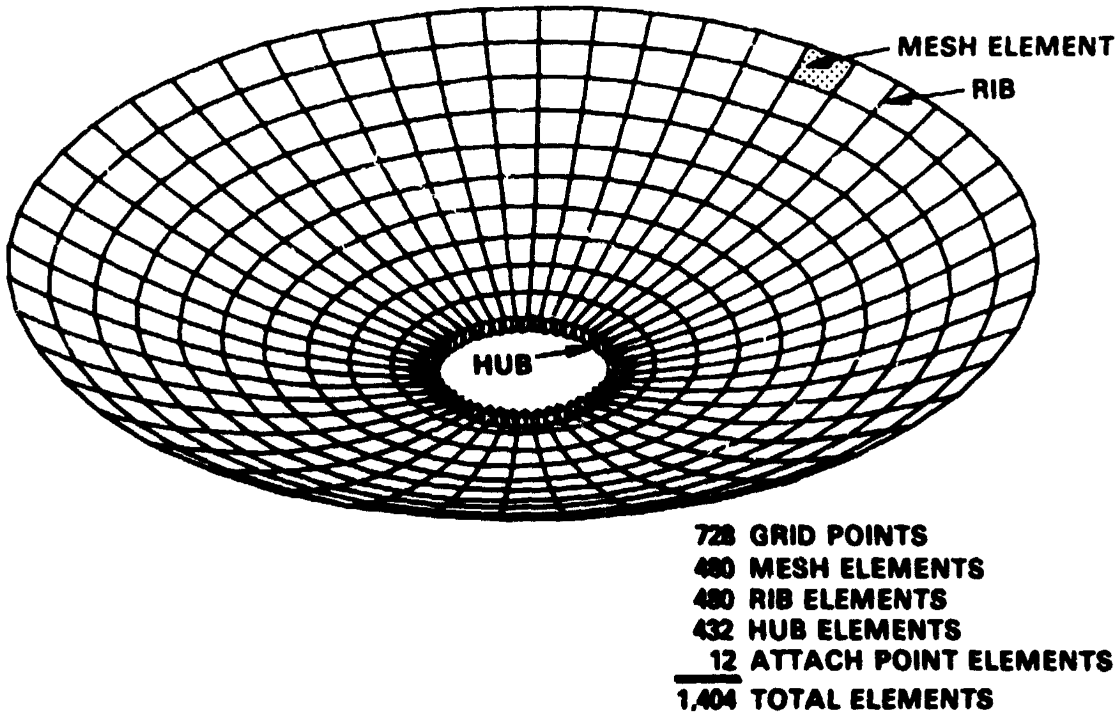

Figure 8. Complete Finite Element Model

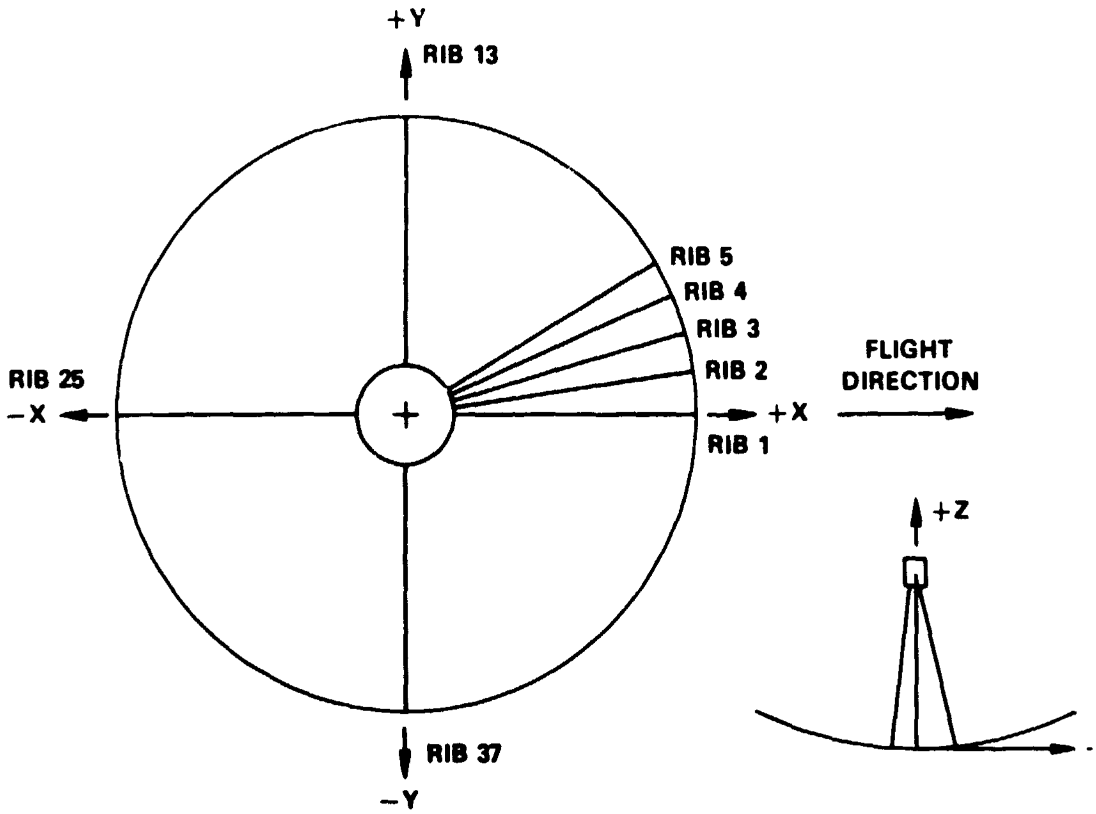

Figure 9. Reflector Rib Locations

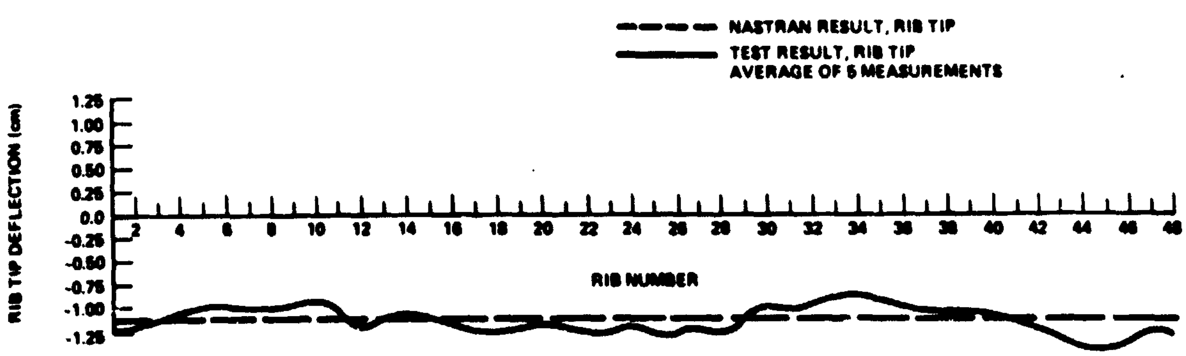

Figure 10. Rib Deflection 1g Analysis

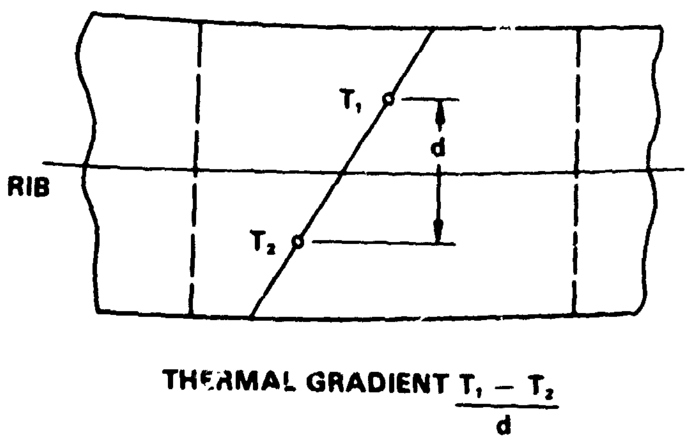

Figure 11. Rib Depthwise Thermal Gradient

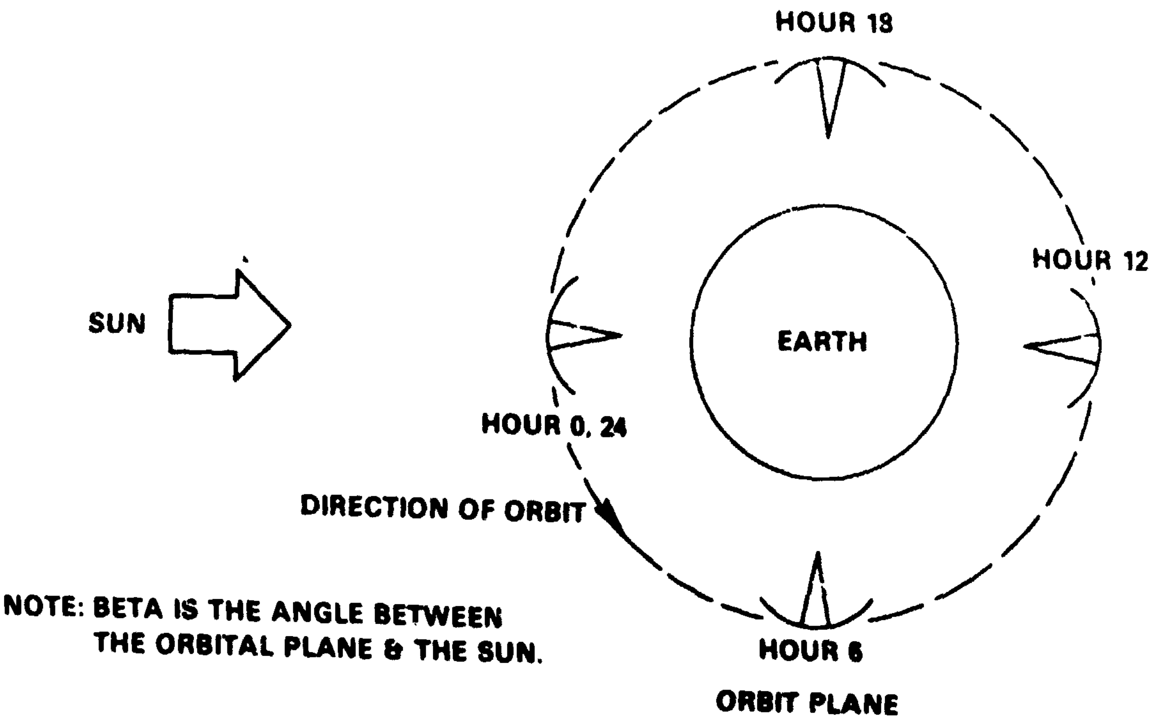

Figure 12. Sun-Earth-Spacecraft Orientations

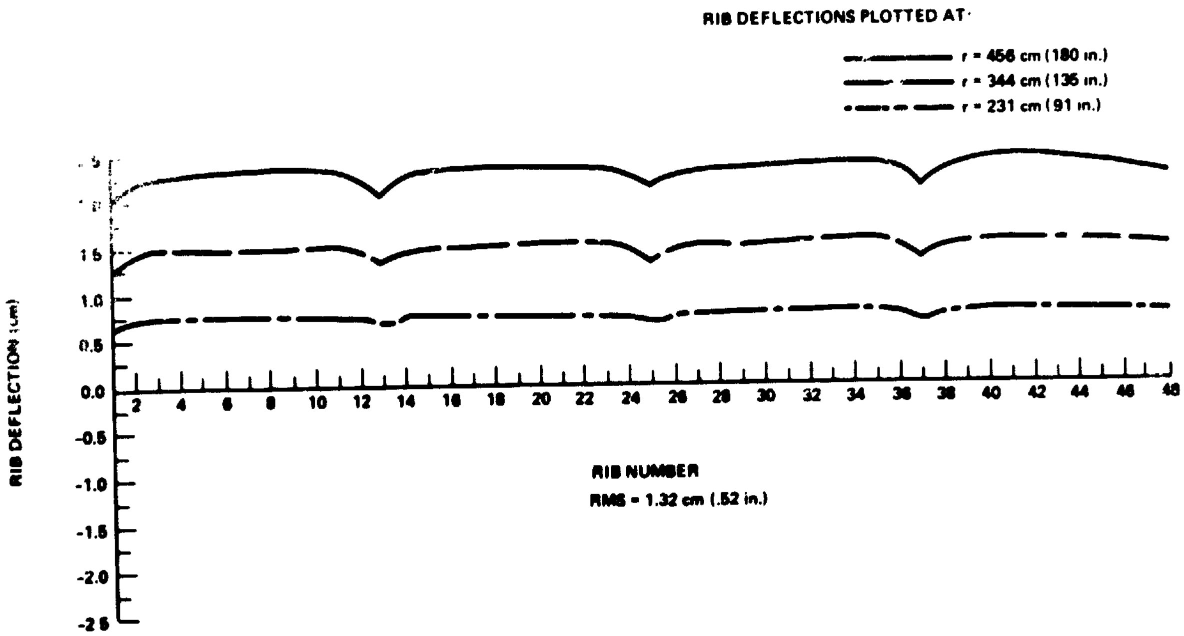

Figure 13. Rib Deflection Orbit Hour 12 Beta=0°

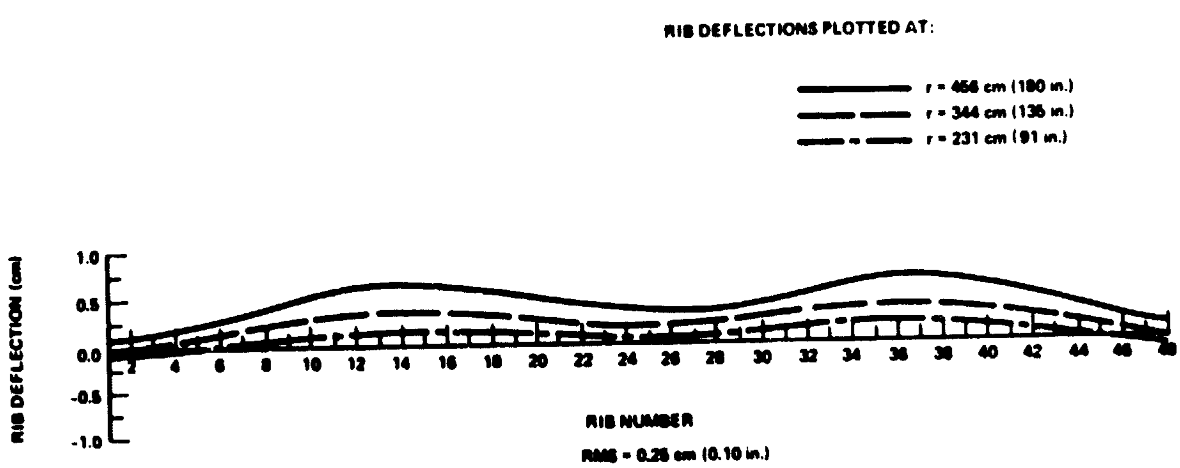

Figure 14. Rib Deflection Orbit Hour 24 Beta=0°

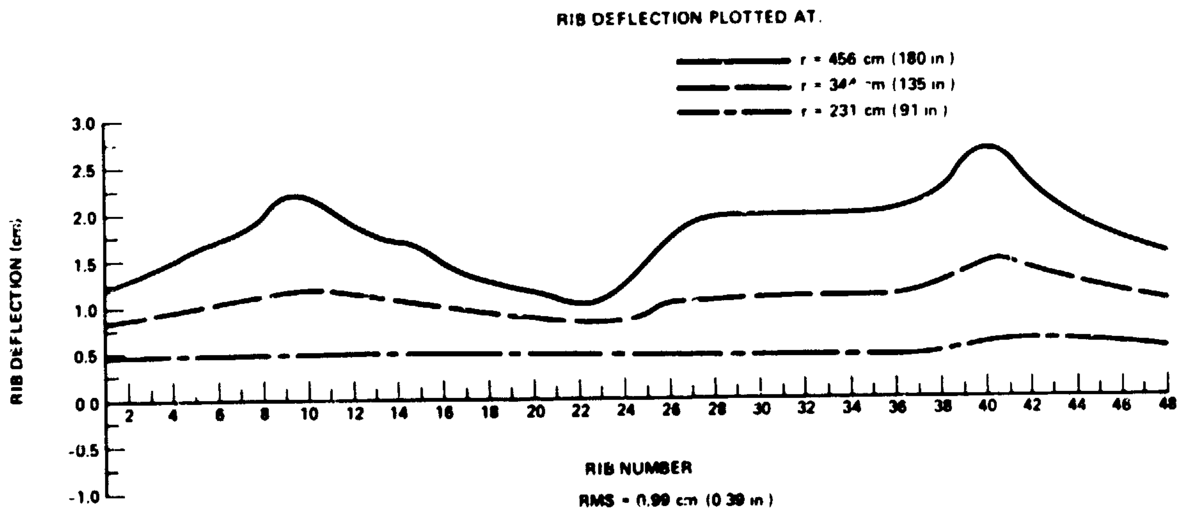

Figure 15. Rib Deflection Orbit Hour 5 Beta=0°

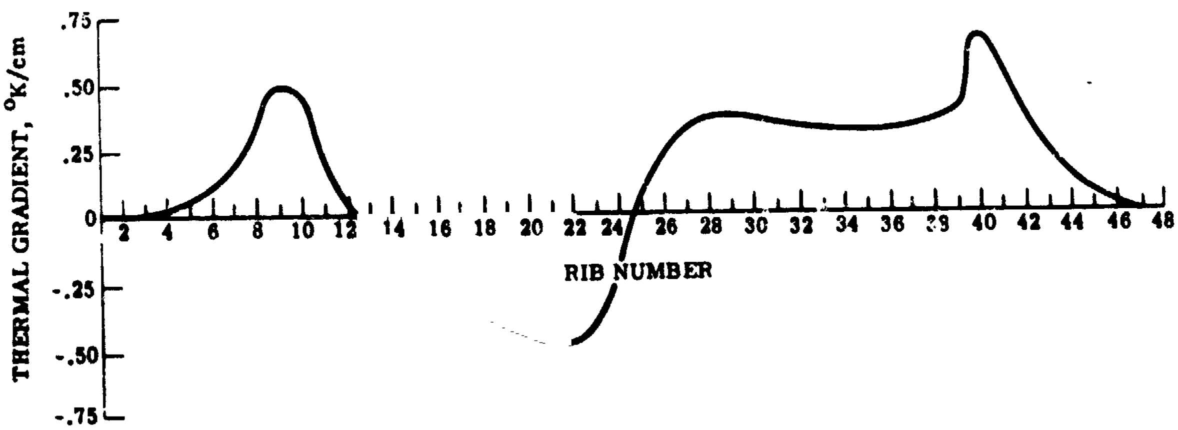

Figure 16. Average Depthwise Thermal Gradient
Orbit Hour 5 Beta=0°

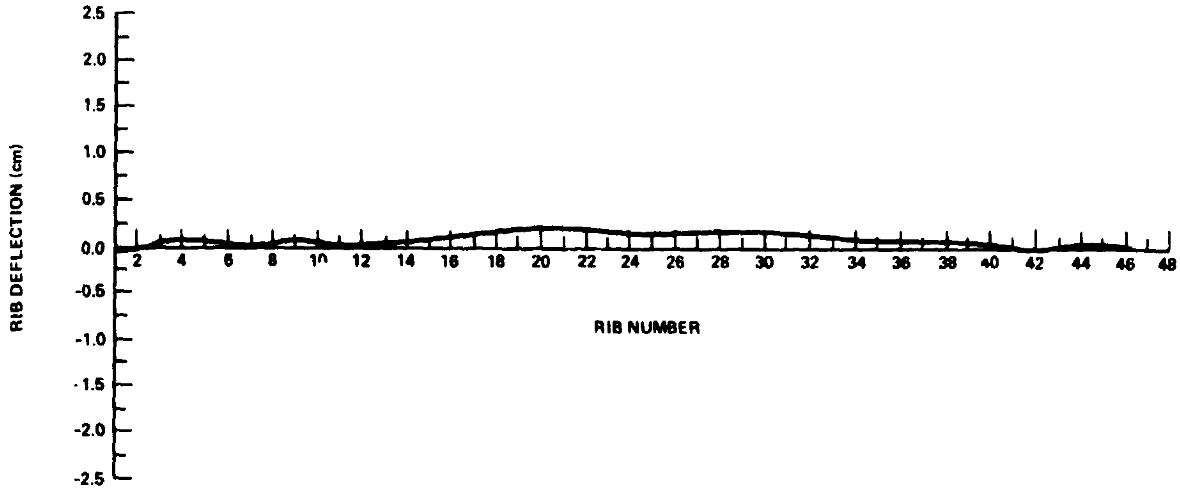

Figure 17. Case 1 — Effect of Rib Temperatures
Orbit Hour 5 Beta = 0°
No Mesh, No Depthwise Rib Gradient

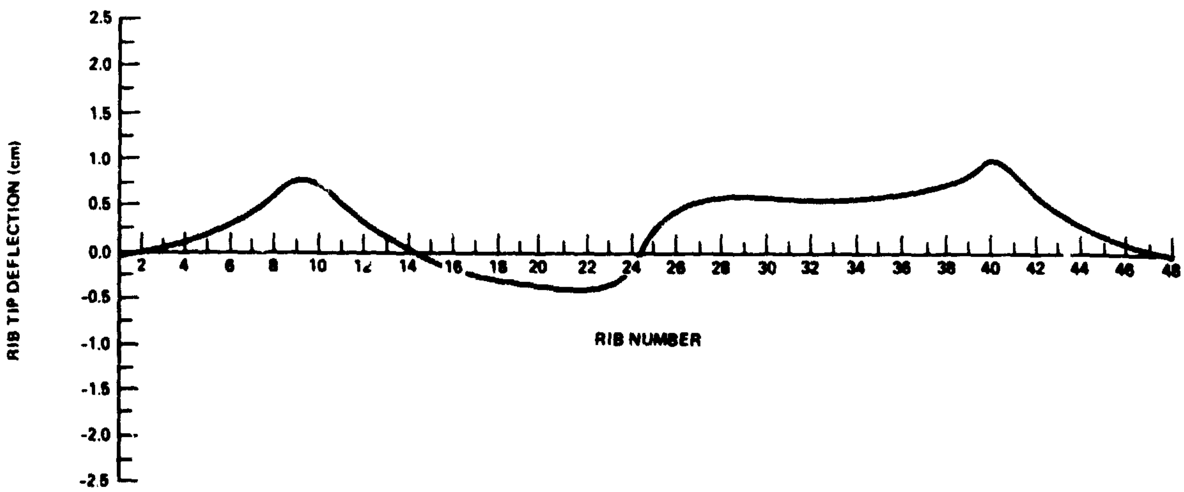

Figure 18. Case 2 — Effect of Depthwise Rib Gradients & Rib Temperatures
Orbit Hour 5 Beta = 0°
No Mesh

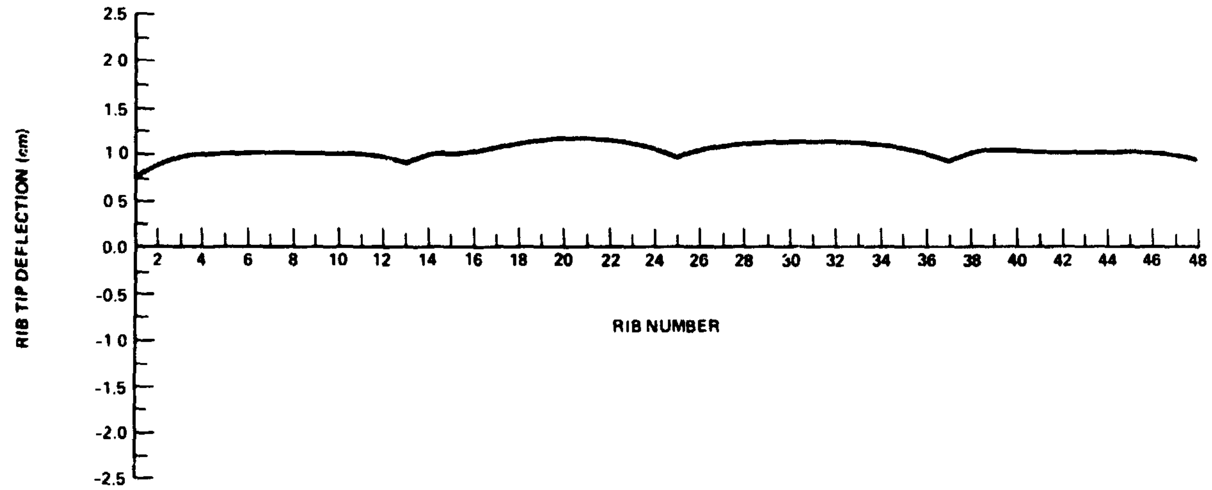

Figure 19. Case 3 — Effect of Circumferential Mesh
Orbit Hour 5 Beta=0°
No Radial Mesh, No Depthwise Rib Gradient

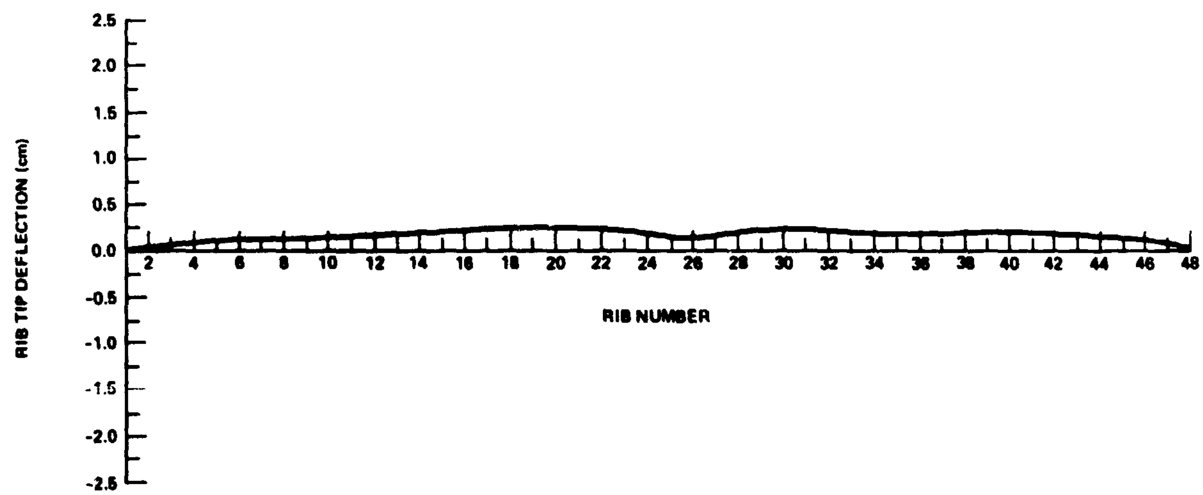

Figure 20. Case 4 — Effect of Radial Mesh
Orbit Hour 5 Beta=0°
No Circumferential Mesh, No Depthwise Rib Gradient

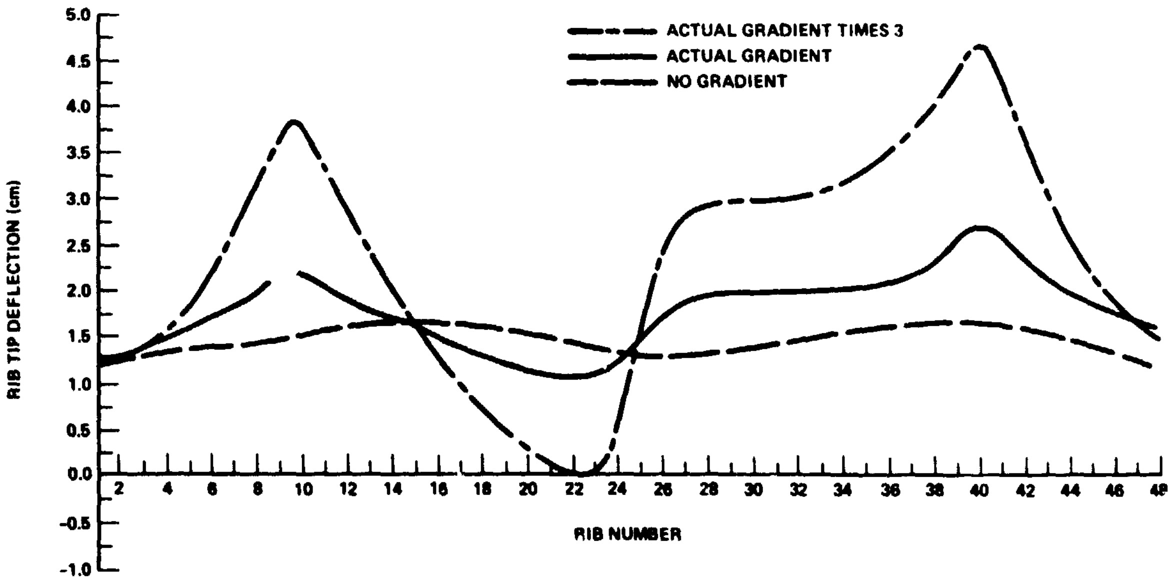

Figure 21. Case 5 — Effect of Varying Depthwise Rib Gradient
Orbit Hour 5 Beta=0°

N74-14594

STRUCTURAL ANALYSIS OF LIGHT AIRCRAFT USING NASTRAN

By Michael T. Wilkinson and Arthur C. Bruce

Louisiana Tech University

The finite-element method has been used extensively for the analysis of major aerospace structures. However, there seems to have been little application of the method to light aircraft generally designated in the homebuilt or sport category. There are two principal reasons for the lack of utilization of computer methods in this area. First, designers of homebuilt aircraft have limited awareness of the ability of the method. Second, the high cost generally associated with any computer analysis frightens potential users away. The purpose of the present study was to determine whether application of NASTRAN to the structural analysis of light aircraft can be economically justified.

For a particular application a NASTRAN model has been made of the "Baby Ace" D model, a homebuilt design whose plans are distributed by the Ace Aircraft Company, Asheville, North Carolina. The basic design consists of a fabric-covered tubular steel fuselage and tail section. The wing is a fabric-covered spruce frame utilizing a Clark-Y airfoil. The aircraft is single place and designed for engines ranging from 48 to 63 kW (65 to 85 hp).

The NASTRAN model of the craft is shown in figure 1. It consists of 193 grid points connected by 352 structural members. All members are either rod or beam elements, including bending of unsymmetrical cross sections and torsion of noncircular cross sections. The model also contains pretensioned members to account for the preloaded drag wires on the wing and tail sections.

In the determination of the mass of the craft, consideration was given to both structural and nonstructural mass. The nonstructural mass consisted of such items as engine, fuel, instruments, pilot, wheels, fabric, and paint. This nonstructural mass made up approximately 83.4 percent of the total mass and was included by using numerous concentrated masses. The portion of the mass due to fabric, paint, welds, nails, and control wires amounted to 9.3 percent of the total mass and was "smeared" across the entire craft.

The aerodynamic loads applied to the Baby Ace were in accordance with FAA regulations governing the utility category aircraft. Using the flight envelope specified in these regulations, several flight conditions were selected, including a 4.4g stall condition at the maximum angle of attack of 19° and a 4.4g nonstall pullup at a low angle of 1.8°. In each case the analysis included the inertia relief feature of NASTRAN. The lift, drag, and aerodynamic moment of the wing were calculated in a consistent manner from the performance curves of the Clark-Y airfoil. Furthermore, aerodynamic forces were also applied to the tail section, assuming zero pitching acceleration. All loads were entered as concentrated forces at the grid points, and these forces were distributed over the wing and tail in a statically equivalent manner.

A summary of the results is presently being made. Preliminary analysis indicates that approximately 71 percent of the members have a factor of safety in excess of 5. No structural inadequacies have been determined at this time. Thus, it appears that the aircraft is overdesigned. Should further study of the data confirm this conclusion, areas will be designated where the weight can be reduced to save money and improve flight performance.

In addition, this problem is being studied by means of the substructure feature available in Level 15.

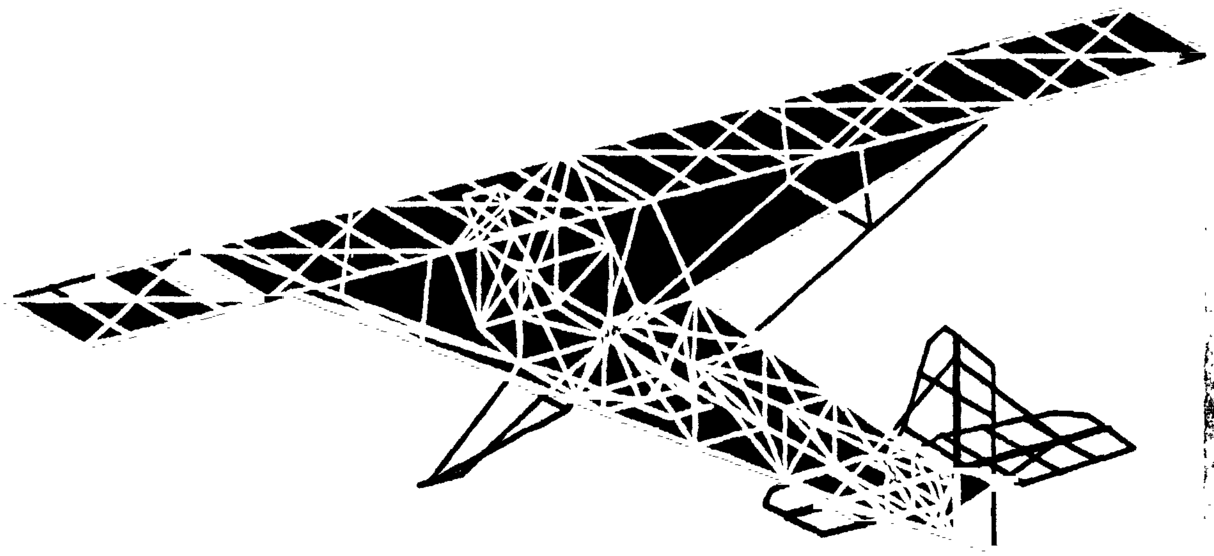

Figure 1.- Structural members of Baby Ace.

N74-14595

TRANSIENT ANALYSIS USING CONICAL SHELL ELEMENTS

By Jackson C. S. Yang, Jack E. Goeller,
and William T. Messick

Naval Ordnance Laboratory

SUMMARY

The use of the NASTRAN conical shell element in static, eigenvalue, and direct transient analyses is demonstrated. The results of a NASTRAN static solution of an externally pressurized ring-stiffened cylinder agree well with a theoretical discontinuity analysis. Good agreement is also obtained between the NASTRAN direct transient response of a uniform cylinder to a dynamic end load and one-dimensional solutions obtained using a method of characteristics stress wave code and a standing wave solution. Finally, a NASTRAN eigenvalue analysis is performed on a hydroballistic model idealized with conical shell elements.

INTRODUCTION

One of the principal areas of interest at the Naval Ordnance Laboratory is high-speed water entry of naval ordnance. In order to achieve stable water entry (no broaching) at low entry angles off the horizontal, the nose is frequently made blunt so that the impact force is nearly axial. The rise time of the impact force can be quite small, depending on the entry angle. Hence, a transient analysis of structural response is required. This paper deals with an analysis of a ring-stiffened hydroballistic model which is designed to impact the water at very high speeds. The NASTRAN conical shell element appeared to be useful since many of the models tested at NOL are axisymmetric, monocoque structures of contour shape which are exposed to external pressure and axial and transverse loads. However, there has been little reported use of this element. Reference 1 illustrates its use in a modal analysis of a ring-stiffened shell and demonstration problem 1.5 (reference 2) is a static loading of a uniform cylindrical shell. In order to gain confidence in the use of the conical shell element before modeling the hydroballistic model, simple structures were analyzed and the results compared to theoretical values. NASTRAN runs were made on the CDC 6400 computer at NOL using Level 15.1.1.

SYMBOLS

A	cross-sectional area of shell
E	modulus of elasticity
F_o	constant end load on cylindrical shell
h	thickness of cylindrical shell
L	length of cylindrical shell
m	mass per unit length of cylindrical shell
M_x	axial moment per unit length
R	radius of neutral axis of circular cylinder
t	time
τ	rise time of force pulse
u	axial displacement
x	axial distance
δ	displacement of circular shell at junction with ring stiffener
ν	Poisson's ratio
σ_ϕ	hoop stress
σ_x	axial stress
ω_r	r^{th} eigenvalue in circular frequency

EXTERNALLY PRESSURIZED RING-STIFFENED CYLINDER

The ring-stiffened shell section of a hydroballistic model was analyzed to determine the stresses when it is exposed to external pressure during launch in the gas gun. A midsection consisting of three typical bays was analyzed. The shell was assumed to be clamped at each end (no pressure applied at ends). Figure 1 depicts the finite elements used in synthesizing the NASTRAN model of the ring-stiffened cylindrical shell. The overall model had 96 rings (or grid circles) and 95 elements, yielding a total of 471 degrees of freedom for each harmonic.

The zeroth harmonic was used in the problem since the loading was axisymmetric. The material for the model is aluminum. Element forces, bending moments, stresses and ring point deflections were obtained for an externally applied pressure load of 6.894 (10^6) N/M^2. To gain further insight in using conical shell elements, multipoint constraints were applied to the ring at the junction between the ring stiffener and the cylindrical shell. This eliminates the overlapping of material from the stiffener and the cylindrical shell, see Figure 1. The number of elements was also varied to observe the effect of element size.

A discontinuity analysis was done on the ring-stiffened cylinder in order to assess the accuracy of the NASTRAN results. The rings were considered to have a thick-walled Lamé stress distribution caused by the discontinuity shear force at the ring-shell junction. The short shell between rings was considered a beam on an elastic foundation so that displacement and slope relations from reference 3 were used. By using compatibility of slopes and displacements at the junction, the discontinuity shear and bending moment were obtained. Axial and hoop stresses were calculated from

$$\sigma_x = \pm \frac{6M_x}{h^2}$$

$$\sigma_\phi = \frac{E\delta}{R} \pm \nu\frac{6M_x}{h^2}$$

The significant results from the NASTRAN static analysis (rigid format one) and the discontinuity analysis are presented in Figures 2 through 5. Figure 2 shows a comparison of the radial displacement along the center bay. Figure 3 shows the hoop stress at the inside and outside wall. The agreement is quite good. Figures 4 and 5 show the comparison of the axial bending moment and axial stress. The agreement is quite good in close proximity to the stiffener, but gradually deviates near the midspan of the bay. This might possibly be improved by using smaller elements. The ring size was very important around the stiffeners because of the rapid attenuation of the bending moment. Very few differences were observed when MPC was used at the junctions of the shell and the stiffeners. This indicates that the overlapping does not have too much effect on the results for the shell-to-ring thickness ratio used in this problem.

RESPONSE OF UNIFORM CYLINDER TO DYNAMIC AXIAL LOAD

In a typical water-entry body, the structure is exposed to transient loading and the body must be considered as free-free. Before proceeding to actual modeling of the complex structure involving stiffening rings, etc., several simplified structural models were investigated and comparisons made with known classical solutions. Rigid format nine, "direct transient analysis," was used in the NASTRAN program. Figure 6 depicts the finite elements used in synthesizing the NASTRAN model of the cylindrical shell. The overall model had 21 rings (or grid circles) and 20 elements, yielding a total of 42 degrees of freedom for each harmonic. The zeroth harmonic was used in the problem since the loading was axisymmetric.

The transient dynamic stresses, element forces, and deflections were obtained for selected elements and rings. Three cases of dynamic loads were applied to one end of the cylindrical shell. The dynamic loads consist of a constant force with two different rise times and a trapezoidal pulse. These dynamic loads are specified on TABLED1, TLOAD1, and DAREA cards. The structure was considered as having free-free boundary conditions. Comparisons of the NASTRAN results were made with one-dimensional stress wave code which uses the method of characteristics and also a one-dimensional closed form standing wave solution. These latter solutions do not include the effect of hoop stress as the NASTRAN element does.

The standing wave solution was obtained for a free-free bar loaded at the end $x = 0$, by a force which is a ramp to time t_o and a constant F_o after t_o. The displacement of the bar is given by (see reference 4)

$0 \leq t \leq t_o$

$$u(x,t) = \frac{F_o}{mLt_o}\frac{t^3}{6} + \frac{F_o}{EAL}\left(\frac{t}{t_o}\right)\left[\frac{(L-x)^2}{2} - \frac{1}{6}L^2\right]$$

$$- \frac{2F_o}{mLt_o}\sum_{r=1}^{r=\infty}\frac{\sin \omega_r t}{\omega_r^3}\cos\left(\frac{r\pi x}{L}\right)$$

$t_o \leq t$

$$u(x,t) = \frac{F_o}{mL}\left[\frac{t_o^2}{6} + \frac{t^2}{2} - \frac{t_o t}{2}\right] + \frac{F_o}{EAL}\left[\frac{(L-x)^2}{2} - \frac{1}{6}L^2\right]$$

$$- \frac{2F_o}{mLt_o} \sum_{r=1}^{\infty} \frac{\sin \omega_r t - \sin \omega_r (t-t_o)}{\omega_r^3} \cos \left(\frac{r\pi x}{L}\right)$$

$$\text{where } \omega_r = r\pi \sqrt{\frac{EA}{mL^2}}$$

The first term is the rigid body motion. The second term may be looked upon as the static deformation; the series represents the harmonic oscillation terms. The stress can be computed from

$$\sigma_x = E \frac{\partial u}{\partial x}$$

Figure 7 shows a comparison of displacement at the end (x = 0) where the force is applied and at the midspan (x = 152.4 cm). The NASTRAN solution follows the simplified theoretical solution reasonably well. Figure 8 shows a comparison of the axial stress at the neutral axis of the first element and the midspan element. This axial stress was used since the theoretical solution ignores bending stress. The comparisons are, in general, not bad. There appears to be some long-time effect, but this might be due to the rather large element size used in the NASTRAN solution. Figures 9 and 10 show similar comparisons, except a shorter rise time was used on the loading functions. Figure 11 shows a comparison of axial stress at the first element and midspan element for a trapezoidal loading pulse. Again, the comparison with the one-dimensional stress wave theory is reasonably good.

EIGENVALUE ANALYSIS OF HYDROBALLISTIC MODEL

The hydroballistic model and the finite element discretization are shown in Figure 12. The length of the model is 345.12 cm and the body diameter is 34.29 cm. It consists of a thick-walled titanium nose section and ring-stiffened aluminum mid and tail sections. The aluminum skin is .794 cm thick. Four equally spaced fins are attached to the midsection and four to the tail section.

The blunt nose of the model causes the load at water impact to be nearly axial. Therefore, the axial mode of vibration of the model was examined. Figure 12 shows the 74 rings and 74 conical shell elements used to represent the model. The neutral axis of some of the elements has been moved instead of retaining the original positions and using MPC's to connect the rings.

The reason is that in a static analysis of a clamp band which had MPC'd rings at discontinuities in section, an ill-conditioned stiffness matrix was obtained. The "epsilon sub E" check yielded values on the order of one. Since the changes in stiffness of the hydroballistic model sections were even more severe, it was thought that for a first solution, a slight loss in accuracy from modifying the model would be acceptable.

The eigenvalue analysis was performed for axial vibration by allowing radial and axial displacement and axial rotations at each ring. Thus, a 222-degree-of-freedom model was analyzed. The first ten modes of vibration are given in Table 1. The fundamental mode of 282 cycles per second seems reasonable. Shifting the neutral axes of some shell sections yielded a well-conditioned matrix with the "epsilon sub E" check having a value of 3×10^{-13}.

The transient response to an axial impulse will be obtained and the results compared to the data obtained from the instrumented hydroballistic model with a water-entry velocity of 305 meters per second.

CONCLUSIONS

The results obtained from using the NASTRAN conical shell element agree well with theory. Using a 90-degree orientation for the conical shell element and an MPC for representing a ring stiffener yields excellent results. However, using MPC's to connect discontinuities in neutral axis radii can lead to ill-conditioned matrices.

Using the conical shell element in static analyses is routine. However, in the process of applying rigid format nine (direct transient analysis) to conical elements, a number of non-standard procedures must be practiced in order to obtain the results. The P field in the DAREA bulk data card must be determined by the following formula:

$$P = \text{ring ID} + 10^6 * (\text{Harmonic} + 1)$$

In the case control deck, reference to "grid points" is by the same formula. In the executive control deck, an alter must be used to switch to Sort 1 output. This enables the output to be printed in an orderly fashion.

It is hoped that some of the bugs encountered in using the conical shell element will be eliminated so that more use can be made of it. For axisymmetric structures subjected to loads which may be accurately expressed with a small number of harmonics, it is less costly to use this element than to model with a large number of plates.

ACKNOWLEDGEMENTS

The authors would like to thank Dr. G. Everstine of the Naval Ship Research and Development Center and Mr. R. Edwards of the Naval Ordnance Laboratory for their helpful assistance and suggestions.

REFERENCES

1. Everstine, G., Ring-Stiffened Cylinder, Proceedings of the NSRDC-NASTRAN Colloqium, held at NSRDC, Washington, D. C., 12-13 Jan 1970, Paper 3.3

2. NASTRAN Demonstration Problem Manual (Level 15), NASA SP-224(01), Jun 1972

3. Hetényi, M., Beams on Elastic Foundation, The University of Michigan Press, Ann Arbor, Michigan, 1967

4. Meirovitch, Leonard, Analytical Methods in Vibrations, Macmillan Company, New York, New York, 1967

Table 1 - Eigenvalues for the Hydroballistic Model

Mode Number	Eigenvalue (cycles/second)
1	0.0
2	282
3	644
4	843
5	1365
6	1692
7	2300
8	2582
9	2975
10	3194

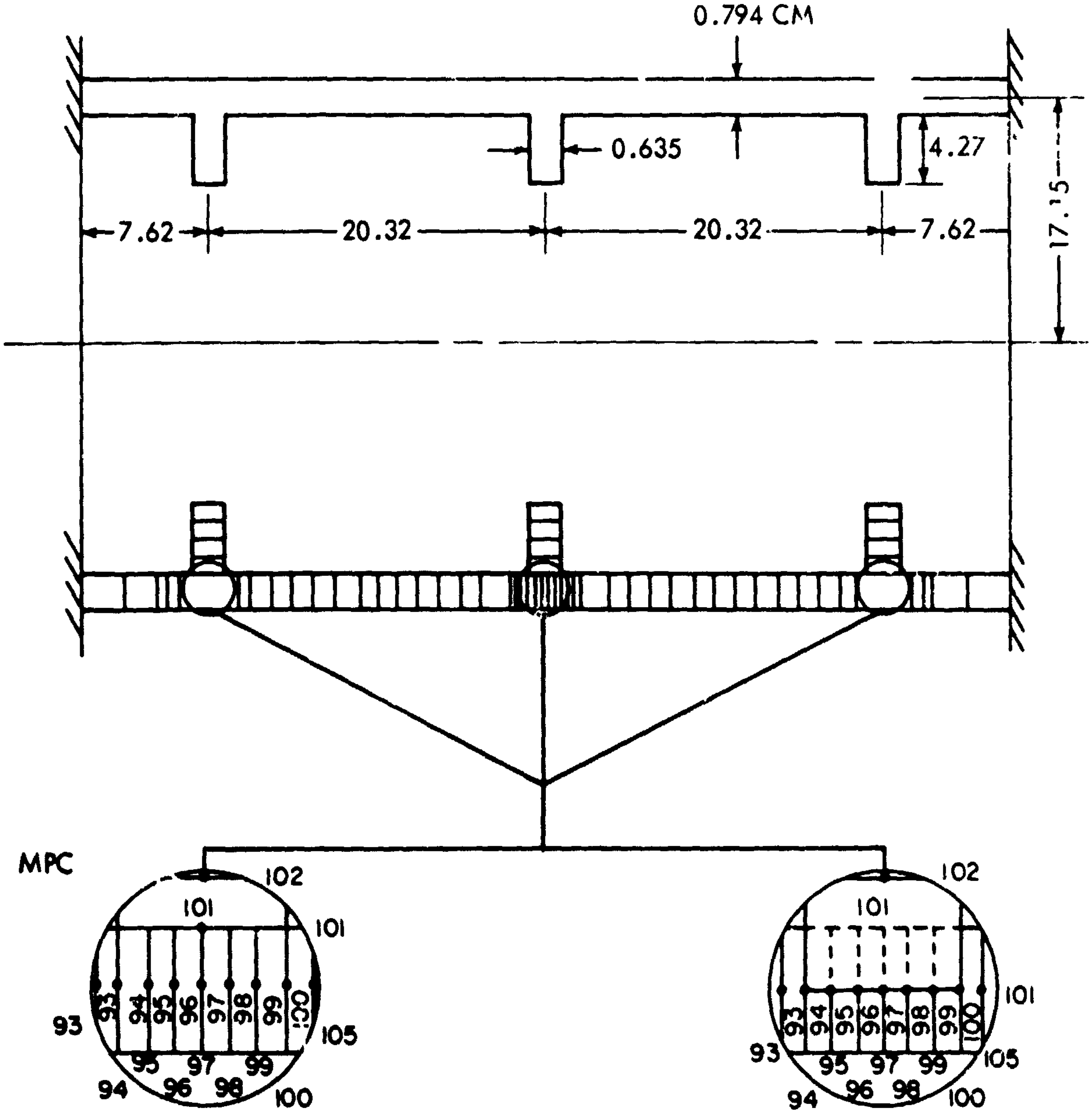

FIGURE 1 NASTRAN MODEL OF EXTERNALLY PRESSURIZED RING-STIFFENED SHELL

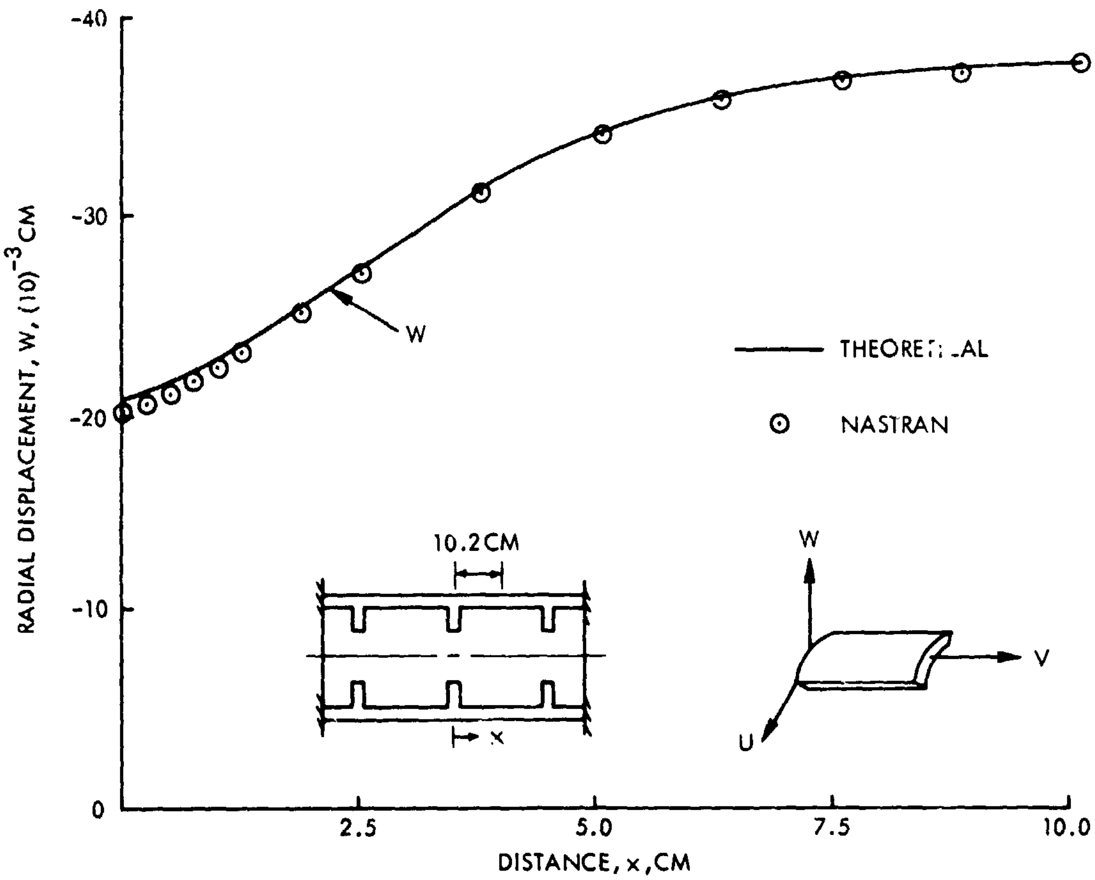

FIGURE 2 RADIAL DISPLACEMENT

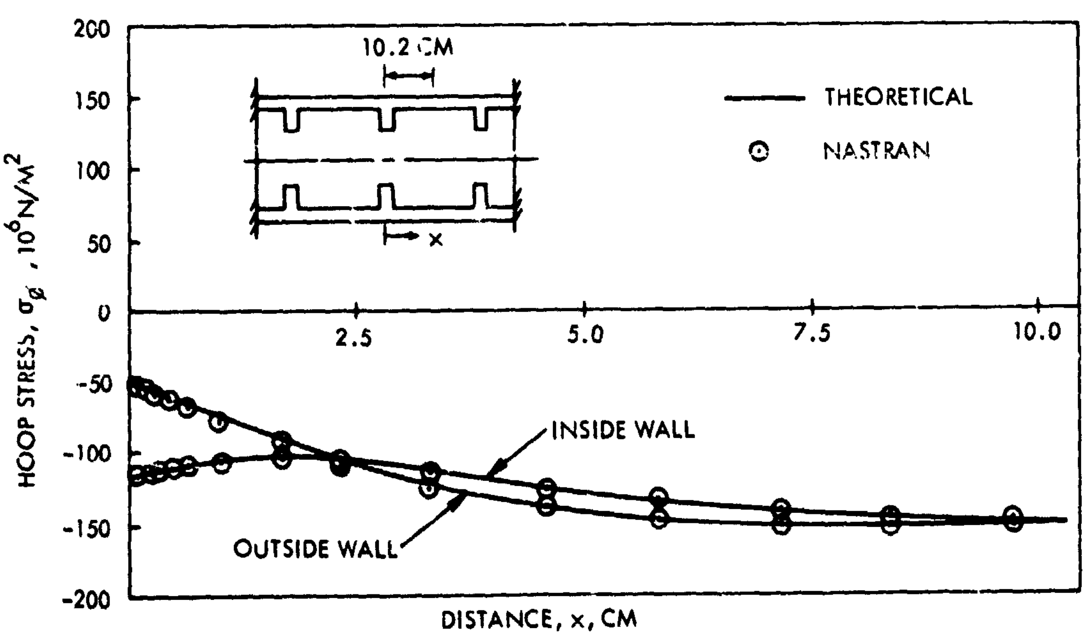

FIGURE 3 HOOP STRESS

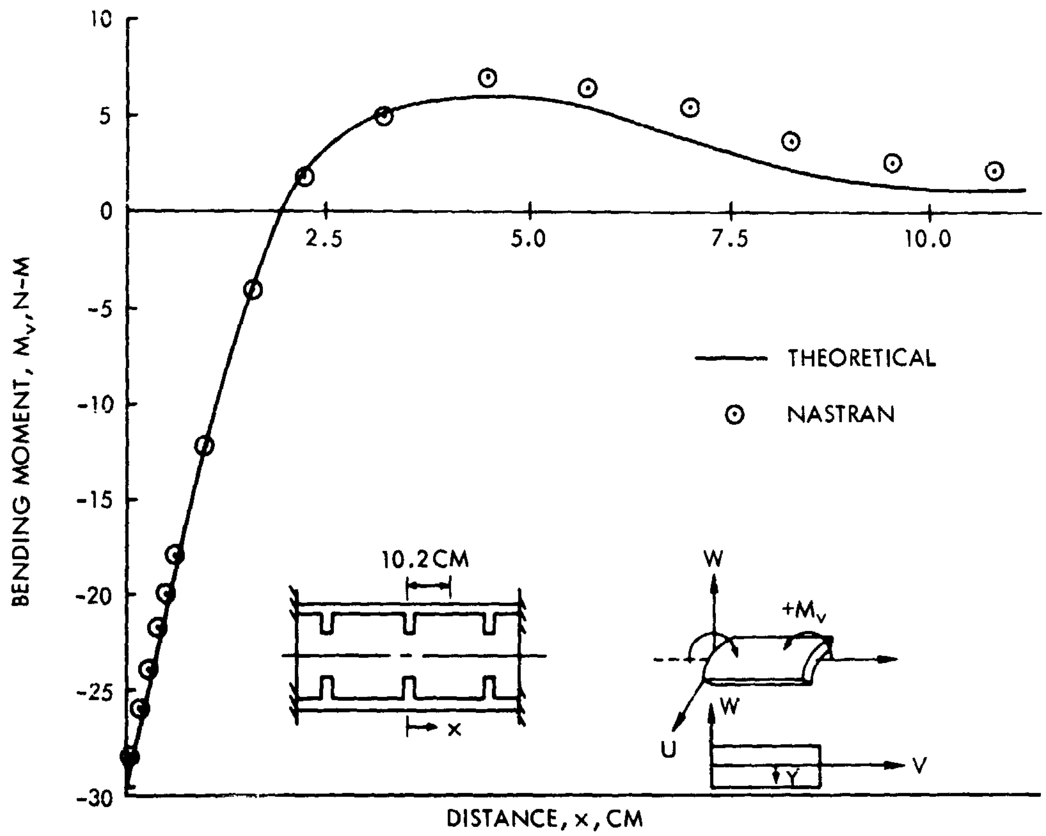

FIGURE 4 AXIAL BENDING MOMENT

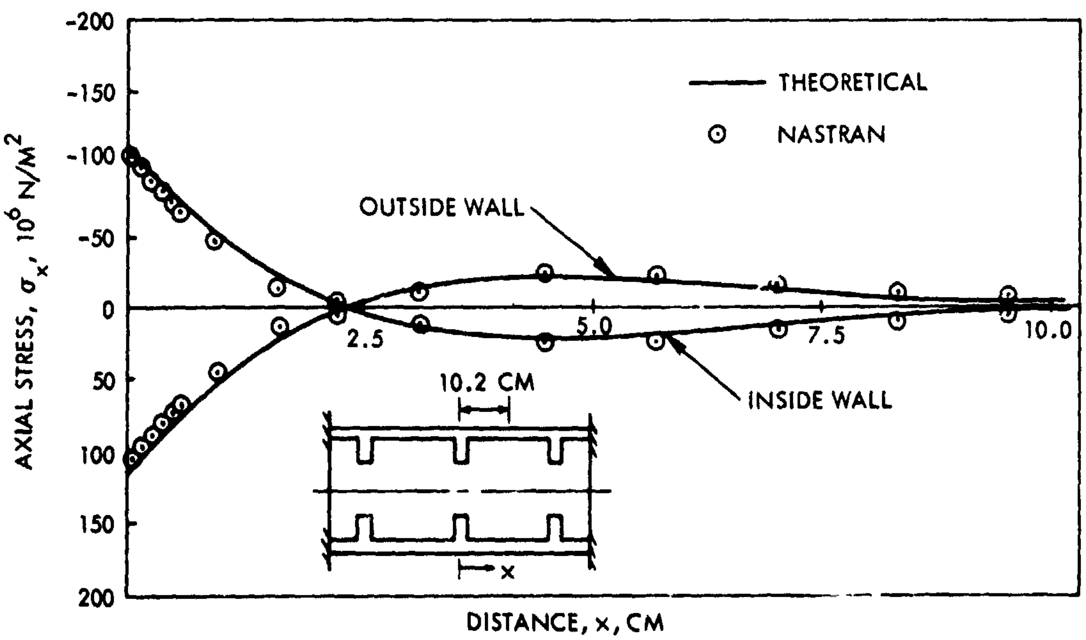

FIGURE 5 AXIAL STRESS

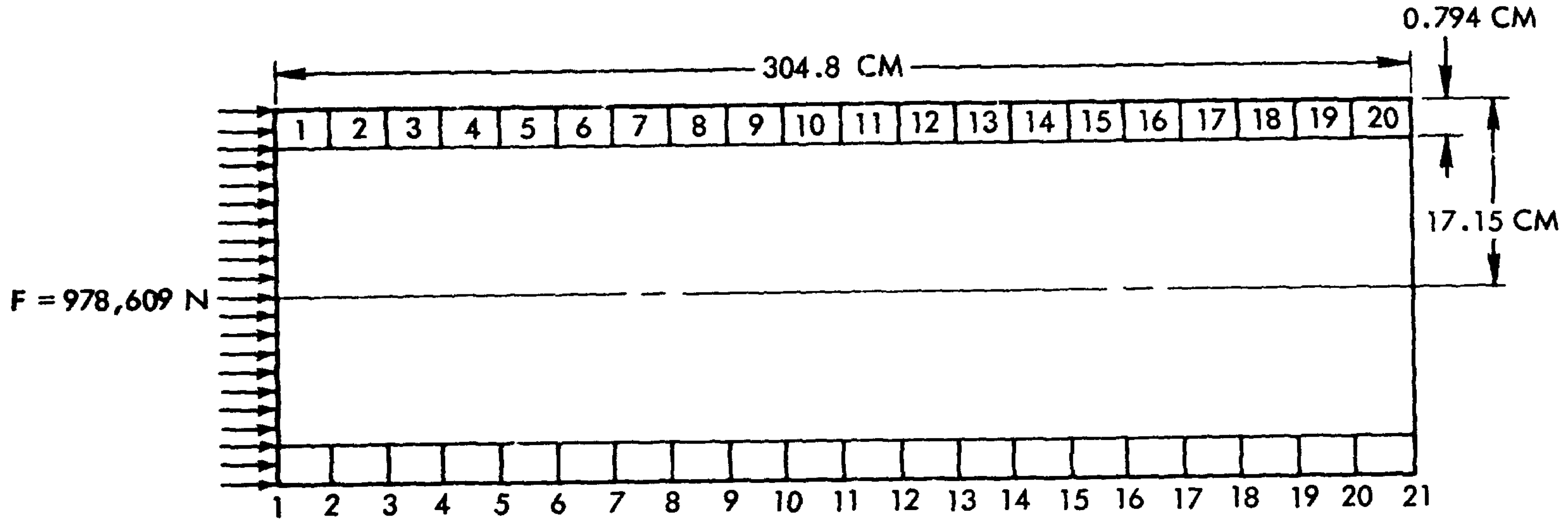

FIGURE 6 NASTRAN MODEL OF END-LOADED CYLINDER

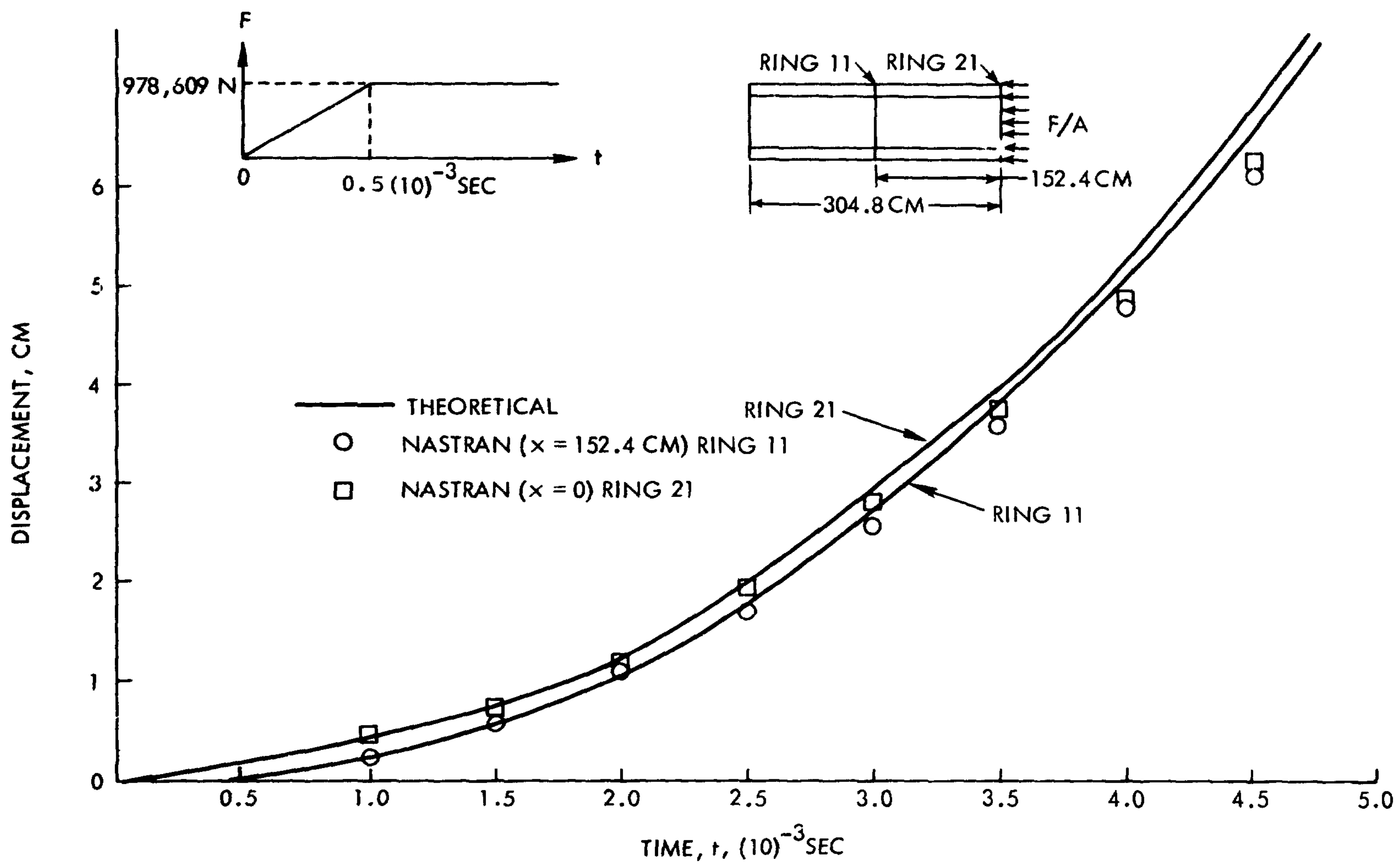

FIGURE 7 AXIAL DISPLACEMENT

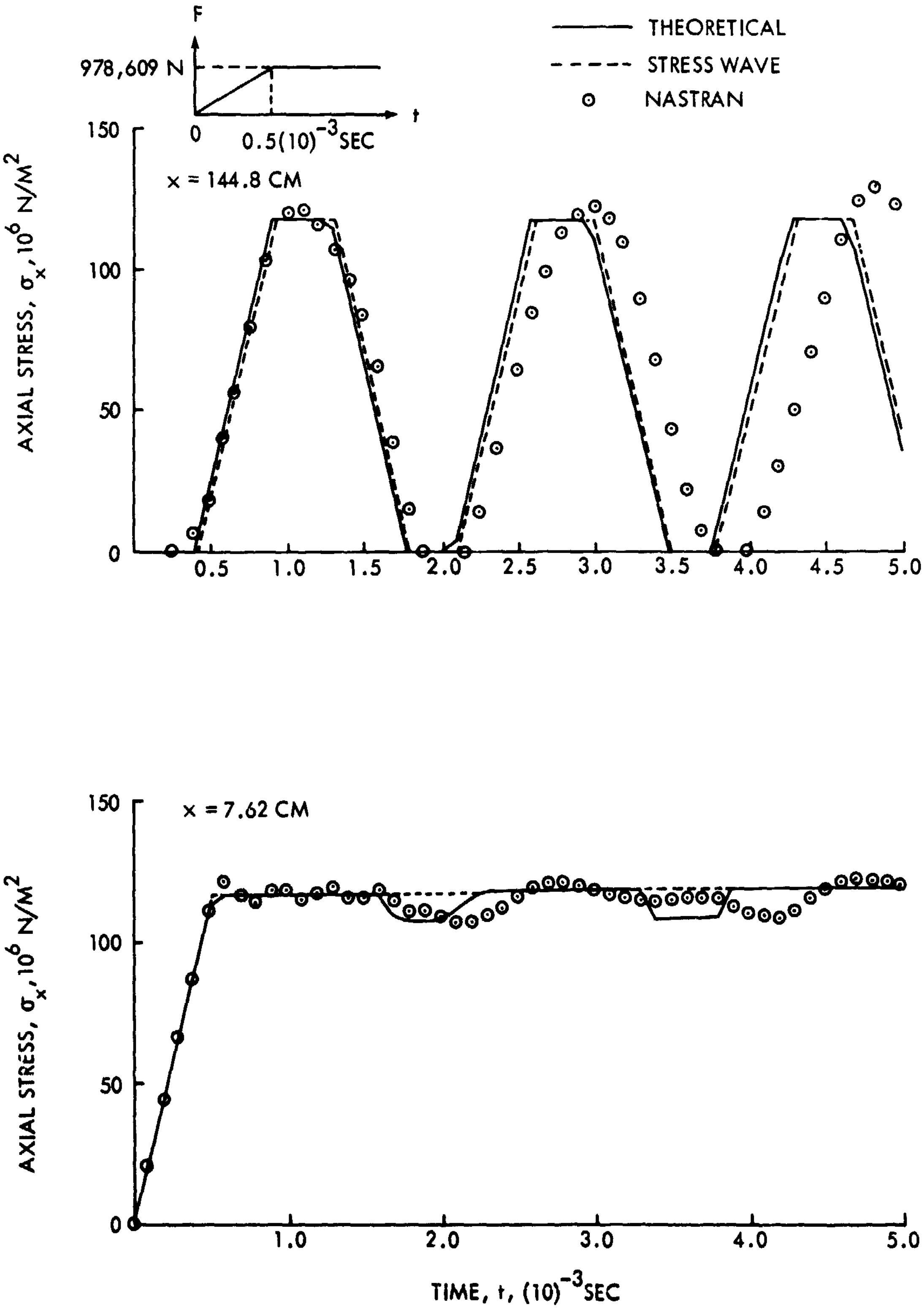

FIGURE 8 AXIAL STRESS

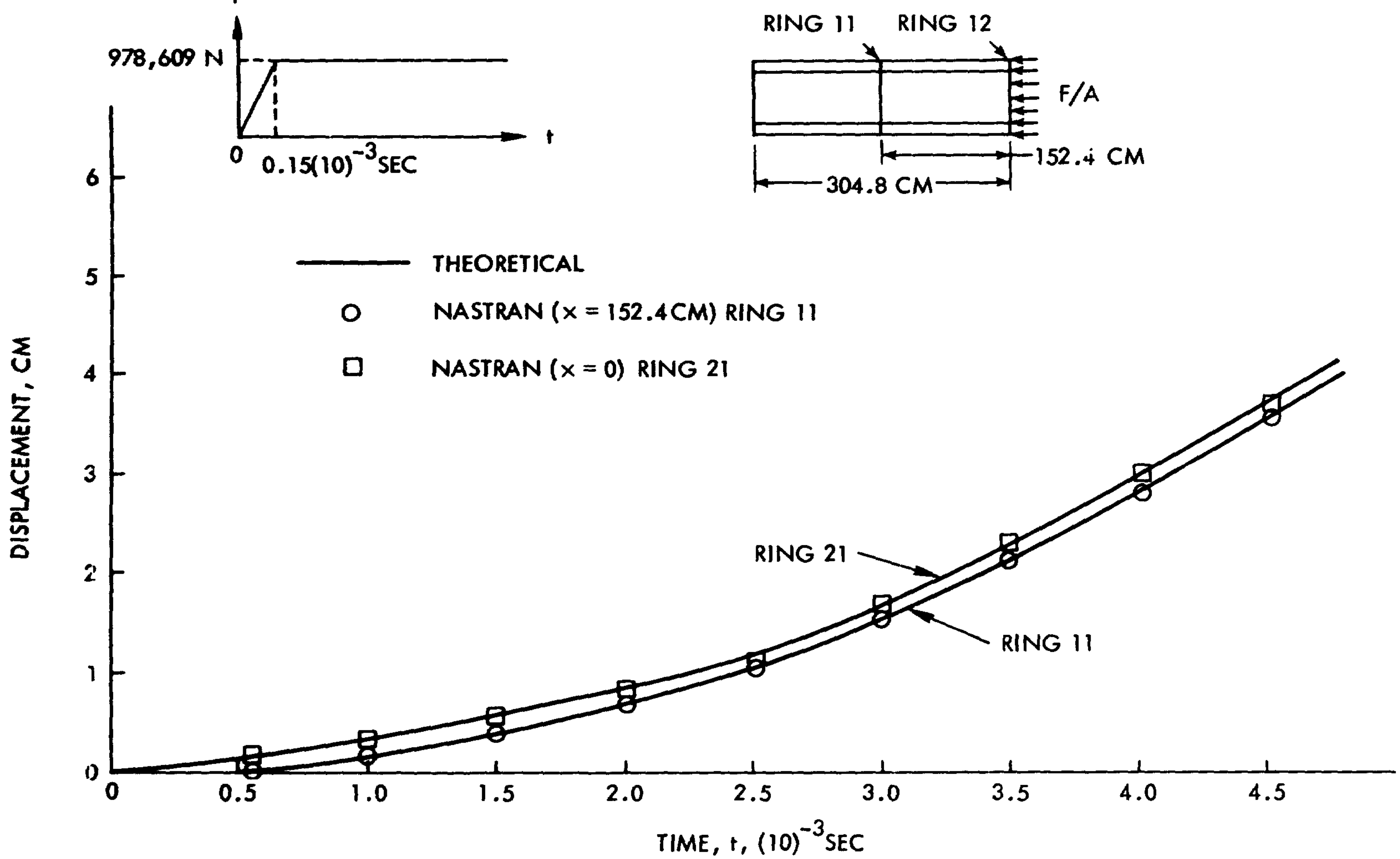

FIGURE 9 AXIAL DISPLACEMENT

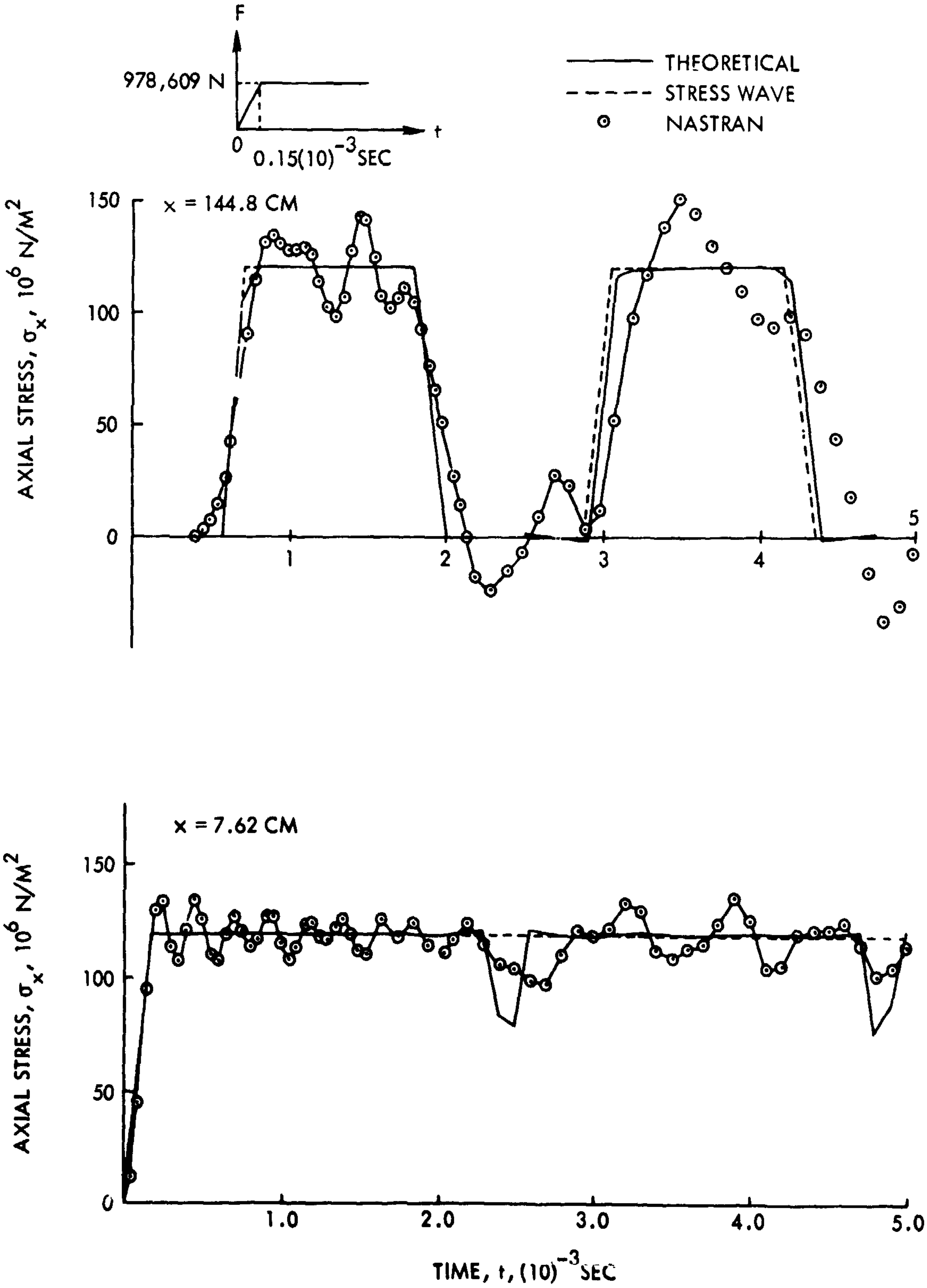

FIGURE 10 AXIAL STRESS

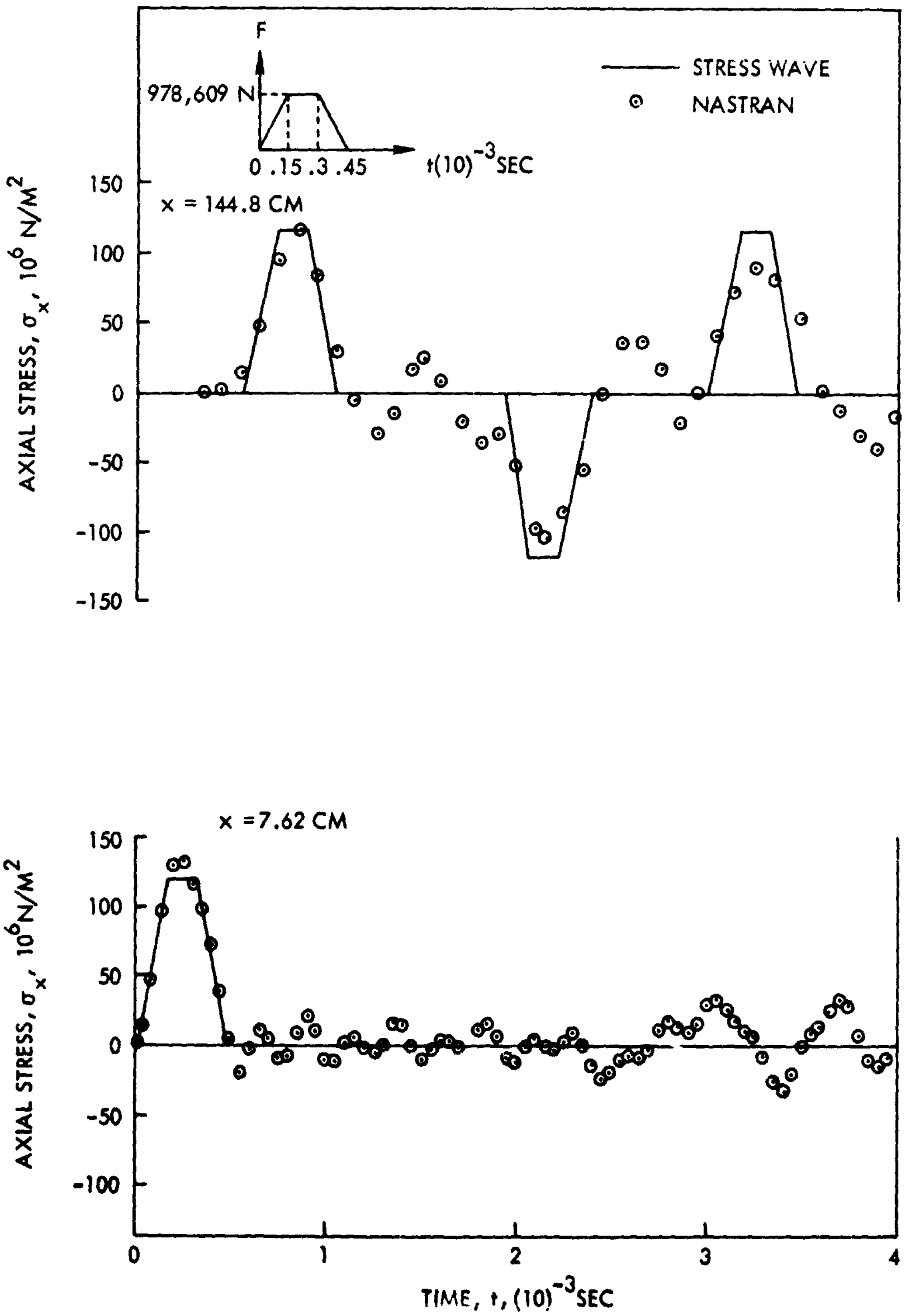

FIGURE 11 AXIAL STRESS

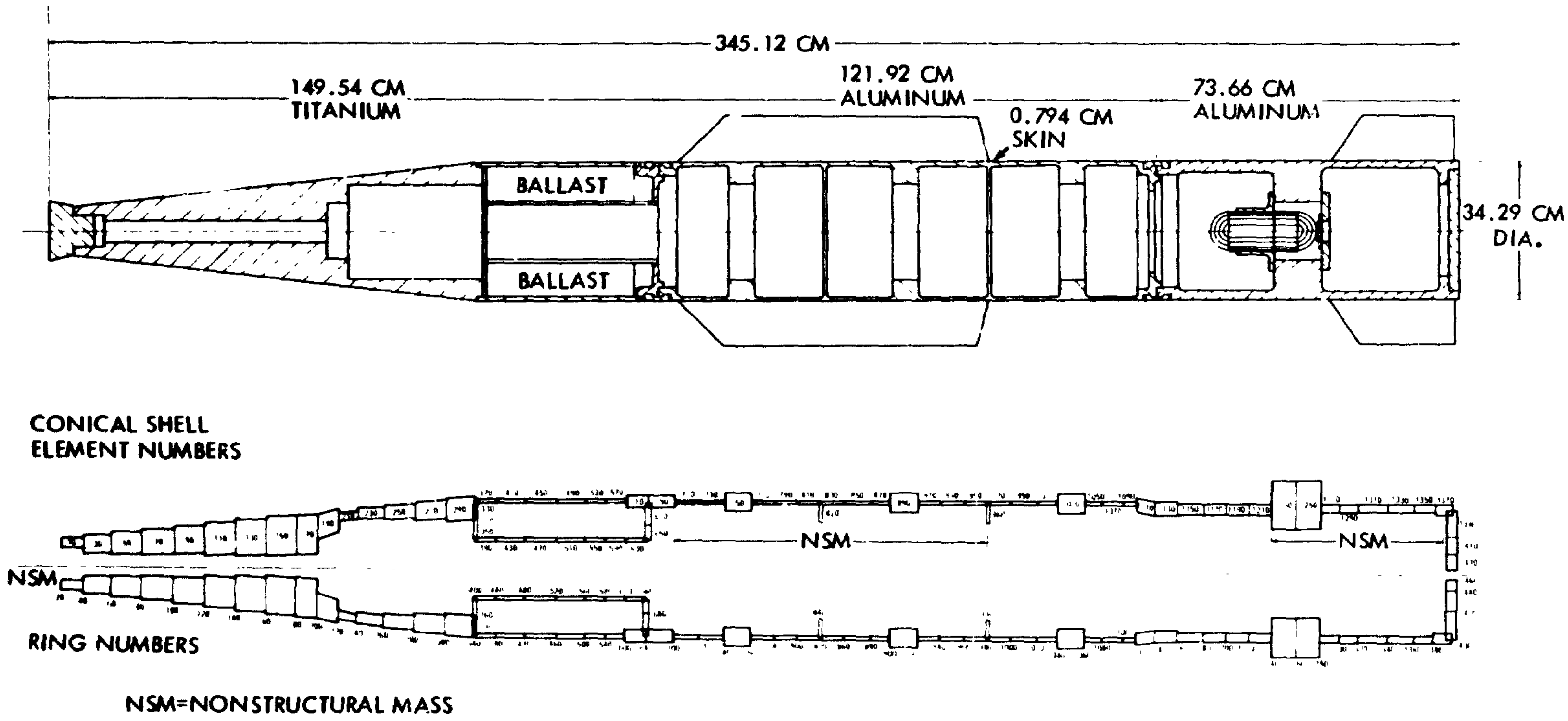

FIG. 12 HYDROBALLISTIC MODEL AND FINITE ELEMENT IDEALIZATION

N74-14594

DYNAMIC ANALYSIS OF A LONG SPAN, CABLE-STAYED FREEWAY BRIDGE USING NASTRAN

By W. L. Salus and R. E. Jones
Boeing Aerospace Company

M. W. Ice
Boeing Computer Services, Inc.

SUMMARY

The dynamic analysis for earthquake- and wind-induced response of a long span, cable-stayed freeway bridge by NASTRAN in conjunction with post-processors is described. Details of the structural modeling, the input data generation, and numerical results are given. The influence of the dynamic analysis on the bridge design is traced from the project initiation to the development of a successful earthquake and wind resistant configuration.

INTRODUCTION

During the summer of 1972, plans were formulated to design and build a new freeway bridge in Seattle, Washington, crossing the lower Duwamish waterway. This structure, called the West Seattle Freeway Bridge, is to provide a four lane highway and public transit connection between the city and the nearby residential and commercial area of West Seattle. The Duwamish waterway at this location is navigable by large vessels and the bridge is required to be both high and long, so as not to interfere with the water traffic. For these and esthetic reasons, a cable-stayed design was decided upon. Figure 1 illustrates the initial design concept(1). Planview and elevation view curvatures are required by the orientations of the connecting freeway approach structures. The main foundation, supporting the tower from which the cables are suspended, is located near the edge of the waterway channel, and all foundations are supported by piles driven into the deep, soft, saturated soil at the site. The initial design incorporated a deck structure consisting of a slab supported by girders and a rigid-frame type of tower structure, as shown in the figure.

Because of Seattle's location in an earthquake zone, and because bridges such as the West Seattle design are subject to wind-induced oscillations, it was decided by the Seattle City Engineering Department to conduct a thorough dynamic analysis. The Boeing Company was engaged to perform this analysis.

---

(1) Configuration and detail design data shown in this paper were provided by the firm of Knoerle, Bender, Stone, and Associates, Inc., Consulting Engineers, Seattle, Washington; retained by the City of Seattle to perform the engineering design for the West Seattle Freeway Bridge project.

The initial work plan included analyses of a number of different bridge preliminary designs, including both concrete and steel deck constructions, in support of the development of a final structural design concept. Finite element analysis was decided upon. The need for parameter studies of the configurations of the deck, pile foundations, and the tower and pier structures was forseen. Thus, a large number of analyses, with little setup time between them, was anticipated, and a simple computer model was desired. However, the nature of the deck design, particularly the combination of girders with a long span curved in both elevation and planform, suggested that a complex structural behavior might occur, requiring a correspondingly careful structural modeling. Therefore it was decided to perform two types of analyses, the first quick and simple, representing the deck structure as a single curved beam, and the second more detailed, representing the structural components of the deck by individual finite elements in the computer model. Figures 2 and 3 are computer plots which illustrate these two models. Though Figure 3 is quite crowded with element lines, the individual girder web and flange elements can be seen at the right end of the span. A verification of the validity of the data computed with the simple model was planned to be obtained by a comparison of its modes and frequencies with those of the complex mode. This, in addition to arranging the computer coding to facilitate convenience in parameter studies, constituted the overall work plan for the structural modeling.

The specific goals of the dynamic analysis were the calculation of earthquake-induced stresses in the structure and the calculation of the critical windspeeds at which aerodynamically induced unstable deck oscillations could occur. Predictions of these data were made on the sequence of bridge designs which were generated as the project developed. It was found that both earthquake- and wind-induced responses are critical design conditions, and that the initial types of design configurations were not capable of withstanding these responses (Reference 1). On the basis of these early evaluations, criteria were developed for achieving dynamically satisfactory designs. Principally, these criteria specified the frequencies of the structural vibration modes to avoid large earthquake response and specified the deck torsional stiffness and the shape of the deck cross-section to avoid wind-induced unstable oscillations.

The criteria led to a modification of the deck cross-section to the slant-sided, multicell closed section shown in Figure 4a and to a modification of the tower to the wall-type configuration shown in Figure 4b. Designs incorporating the features of Figure 4 are satisfactory for both wind- and earthquake-induced dynamic response. Currently, additional studies are underway to optimize this basic design for earthquake resistance by adjusting its vibration mode frequencies to avoid the known frequencies of principal earthquake excitation. This work has achieved a significant reduction in the required reinforcing steel. The detail design phase of the work will continue to be supported by dynamic analysis until the design is finalized, in the fall of 1973.

This paper discusses those aspects of the work which are associated with the finite element idealization and the modal analysis. This work has been done with the NASTRAN system, which has proved to be a highly effective tool in this application.

SELECTION OF NASTRAN

The NASTRAN system has several features which are advantageous for this problem, leading to its choice over other available structural analyzers. Several of these features are mentioned briefly in this section; others are discussed in more detail in later descriptions of the finite element idealizations. The use of combined cylindrical and cartesian coordinates was helpful in modeling the combined circular arc and straight line geometry of the bridge planform. The ability to specify nonstructural mass on the CBAR elements was useful since structural data were provided in the form of mass per running foot on major structural members. The multi-point constraint feature was particularly useful for representing the connectivity between different portions of the bridge structure. In particular, this was necessary to represent proper connections of the deck structure to the supporting cables, piers, and the tower, and to represent the footing connections to the piles. Multipoint constraints were also used in the more complex model (called the 3D model) to connect the individual girders to the deck slab. The NASTRAN plotting feature was used to obtain pictorial descriptions of the structural vibration modes. In the case of seismic analysis this is particularly important, because seismic response is strongly dependent on both the shape and the direction of principal modal motions. Hence, pictorial data permit a quick, qualitative assessment of the likely seismic importance of the structural modes. And finally, since the seismic and flutter analyses were done by additional processing of the results of the modal analysis, a convenient data access system such as the NASTRAN checkpoint/restart tape feature was required. Thus NASTRAN appeared to be particularly well suited to the technical requirements of the problem.

Additional motivation for using NASTRAN was provided by the availability of Boeing's input language, SAIL, which has been adapted for NASTRAN input. Most of the bulk data were generated automatically by the use of SAIL. Bridge geometric data were provided in equation form, which can be coded directly in SAIL's automatic grid point generation format. In addition, SAIL has the capability to generate data within special (parameter-controlled) subroutines, called external data generators. External data generators were used to generate NASTRAN multi-point constraint equations, the girder plus slab deck simulation of the 3D model, and the pile foundation simulations. These data generation routines are designed such that a set of input parameters controls the generation of data. By changing a few of these parameters, a complete new set of data can be produced, simulating a new design concept. Through such automatic input generation it was possible to obtain rapid turnaround of analyses to support the design development.

A separate computer program was written to perform the seismic analysis, using the response spectrum analysis method. This analysis requires the mode shapes, frequencies, generalized mass, and internal element forces produced in the modal analysis. The NASTRAN checkpoint/restart tape provided access to these data. Since NASTRAN normally does not checkpoint element forces, a simple Alter was used to checkpoint the element force file OEF1.

BEAM (STICK) FINITE ELEMENT MODEL

Purpose

To perform dynamic analysis in support of design trade studies, a simple model of the bridge structure, easily modified and with reasonably short run time, was set up. Called the "stick" model, it uses simple, beam type representations of all structural components. Because of the simplicity of this model, it was possible to make parametric studies of important parameters, such as the tower stiffness and the earth lateral resistance to pile motions, in order to assess the importance of these factors early in the program.

Description of the Model

There were two basic configurations from which the parameter studies were made: the steel bridge alternate and the concrete bridge alternate. The models of each of these configurations included the tower, piers (four piers in the steel model, three in the concrete model), the footings, piling, and earth springs to represent lateral earth resistance to pile motions, and the deck itself. The modeling of the piers, footings, piles and earth springs was of primary importance in seismic response. The deck modes and consequently the deck modeling were of primary interest in the flutter analysis. The finite element models included the main span portion of the overall bridge structure, which is defined by the locations at which the deck bending continuity with the approach spans is terminated. This arrangement resulted in analyzing the main span plus several shorter adjacent spans, as required for the particular configuration in question.

Figures 5 and 6 illustrate the steel and concrete finite element models. The outward appearances of the two models are alike except that the concrete model has one less pier and a slightly modified tower appearance. In reality, however, the deck properties obviously change as do the grid point locations and all mass and stiffness properties.

The deck geometry in the plan view is a straight line for somewhat less than half the span and a circular arc for the remaining part. The steel bridge initially analyzed is 1215 feet long and the concrete bridge is 1040 feet long. The deck describes a parabolic arc vertically with a peak elevation of 156 feet. The deck structure consists of the concrete slab of the roadbed and the integrally constructed concrete or steel supporting girders. The outermost girders are of fascia box construction. Figure 1C showe a typical cross section for the concrete alternate. The section properties change along the span as required by the design moments and the applicable design code loading conditions.

The tower supports the deck through pin supports. The four cable stays attach to the top of the tower and to the deck 175 feet on either side. The piers support the deck by roller type supports which permit relative longitudinal motions. The tower and pier footings are supported on pile groups which vary in size with 306 piles maximum for the tower and 66 piles minimum for one of the piers.

The piling simulation is shown by Figure 7. Both pile elements and elements representing earth lateral stiffness are employed. Four simulated piles can provide a correct representation of pile group behavior, and this number was chosen to keep to a minimum the number of elements in the model. Each of the four piles in a simulated pile group consists of two CBAR elements, and is fixed at the base (called the point of fixity) and provided with four springs (oriented parallel and perpendicular to the span) to resist motion relative to the surrounding earth. In the figure, for simplicity, earth springs are shown on only one pile. The point of fixity is determined from a detailed pile deflection analysis*, and is the uppermost point at which zero pile bending slope occurs together with a very small pile deflection.

The earth spring element properties are defined by effectively integrating the distributed earth lateral stiffness over a pile length which is considered tributory to a particular pile grid point. The application of earth lateral resistance at only two points on the pile is an approximation of a type customarily made in discrete element analysis, and would not normally be a cause for concern. In the present case, however, because lateral earth stiffness was found to be a very important parameter, it was desired to verify the adequacy of the discrete representation. This was accomplished by comparing pile deflections computed for the two grid point pile to those obtained for a many grid point - many earth spring representation. The two grid point pile was found to predict deflection within 10% at the top of the pile. This accuracy is suitable for the dynamic analysis, and further refinement within the framework of linear elastic analysis does not appear worthwhile.

The simulated pile and earth spring stiffnesses in the finite element model are determined to provide the actual combined stiffness of the entire pile group. Denoting by k_h the earth spring stiffness which would be computed for one actual pile within a pile group, the following is the spring stiffnesses required in the finite element simulation.

$$k_{h_{model}} = k_h \cdot N \cdot \frac{1}{4}$$

N is the number of piles in the group. The 1/4 factor distributes the total group earth lateral stiffness to the four simulated piles. In addition, the piles are located within the footing area (Figure 7) such that the moments of inertia of the simulated pile areas about the footing longitudinal and transverse axes match those of the actual pile group. This provides simulation of pile group bending stiffnesses. The use of N in the k_h formula would appear to presume that all piles in the group sustain equal lateral loads from the earth. Since this is known to be untrue, an adjustment was made in the k_h earth property to account for group pile action. The combination of group action and vibratory behavior in the earthquake was accounted for by taking k_h to be one-sixth the static, single pile value. This adjustment is based on reported research on group pile

* Point of fixity and earth lateral stiffness data were provided by the firm of Shannon and Wilson, Soil Mechanics and Foundation Engineers, Seattle, Washington.

action[1]. However, in application to a particular pile group, such a factor is necessarily arbitrary, and it was felt necessary to evaluate the sensitivity of the structural behavior to variations in k_h. To accomplish this, a number of computer runs were made with widely varying earth spring stiffnesses. It was found that modal and earthquake response data are very sensitive to changes in earth spring stiffness for the case of relatively soft springs, with structural internal loads generally increasing with increasing spring stiffness. The final recommended spring stiffnesses are quite high, however, and in this range of values the modal and response data are reasonably insensitive to earth stiffness modifications.

The use of beam elements to represent the deck structure is an accurate idealization for all deformations except torsion. In the case of deck torsion, because of the torsion-bending behavior of the girders, a beam representation is necessarily approximate. The nature of the torsion-bending action is such that the effective torsional stiffness of the deck depends on the torsional mode shape, or wave length, to which the deck is subjected. This situation makes it possible to determine the deck torsional stiffness with acceptable accuracy by calculating the stiffness to correspond to the deck torsional vibration mode of greatest interest. The deck torsional modes are important principally because of their possible involvement in unstable aerodynamic motions (flutter). Therefore, the deck torsional stiffness was chosen specifically to obtain accurate modal data for the lowest (most flutter-critical) deck torsional mode. The half wave length (one lobe) of this mode (see Figure 1) is about 200 feet. Using this length, and postulating reasonable girder bending deformations in participation with deck torsional deflections, the girder torsion-bending contributions to the deck effective torsional stiffness were determined. These contributions are summed with the true torsional stiffness contribution, i.e., those of the slab and the closed box stiffness of the fascia girders, to obtain the total approximate deck torsional stiffness.

This procedure necessarily leaves higher deck torsional modes with less accurate (too low) torsional stiffnesses, and in general leaves overall bridge modes somewhat in error. These errors are negligible since, in the former case, only the lowest deck torsion mode was found to be a possible flutter candidate, and in the latter case the overall bridge modes are dominated by tower and deck bending and gross deck translational influences. It should be noted again that the torsion approximations were necessitated by the need for a simple, rapidly computed model. To completely resolve the deck torsion problem, as was done in the 3D model, would have sacrificed the utility of the stick model in the rapid turnaround design support activity. This was an unsatisfactory alternative. Moreover, calculations of the stick and 3D model modes confirmed the accuracy of the approach used.

Coding Details

The SAIL (Structural Analyzer Input Language) input language (Reference 2) was used in conjunction with NASTRAN bulk data in setting up the structural idealization. Details of the coding are described briefly below.

(1) This adjustment was provided by the firm of Shannon and Wilson.

1. Geometry: In using SAIL, the bridge geometry was programmed in the same form as it was provided by the design engineers. The grid point coordinates were coded in terms of "nose stations", the independent coordinate employed to measure distances along the deck cen' .line. The input was greatly simplified through the use of NASTRAN's multiple coordinate systems. Cylindrical coordinates were used for the portion of the bridge to the left of the tower in Figures 5 and 6, which is a circular arc in planview. The remaining straight segment of the bridge was input in the rectangular cartesian coordinate system. In the vertical plane, the deck describes a parabolic arc of the form

$$Z = 155.7 - \frac{(\text{Nose Sta} - 17070.)^2}{36666.67}$$

which was coded directly into the SAIL input deck. An important advantage of the SAIL input lies in the fact that variable gridpoint locations and variable numbers of elements are handled in so simple fashion that generation of multiple idealizations is a minor task.

2. Multiple Point Constraints: MPC equations were found to be a convenient and powerful tool in representing the various connectivities encountered in the bridge structure. Structural idealizations using MPC equations are described briefly below.
   (a) The cables are rigidly attached to the deck at offset nodes.
   (b) The deck is attached to the tower structure in such a manner that all degrees of freedom except deck vertical bending rotation are required to be compatible. In addition, the deck elastic axis is offset (vertically above) its supporting cross member in the tower structure, because of the depths of the girders, the cross member, and the bearing fitting hardware.
   (c) Similar to the tower attachment described above, the vertically offset deck attachment to the piers was enforced by MPC equations. In this case the connectivity between the longitudinal motions of the deck and the piers was in some designs pinned and in some designs represented by a roller support.
   (d) All footings are connected to the upper ends of the piles by full fixity conditions enforced by MPC equations.
   (e) In the complex (3D) deck idealization discussed later, MPC equations provided the connectivity between the girder webs and the deck slab representation.

   The repetitive nature of MPC equations suggests their generation by a subroutine. This is discussed briefly under item 3., below.

3. External Data Generators (EDG):
   (a) The external data generator is a feature within SAIL which provides a subroutine type of input generation capability. It is most conveniently used for multiple generations of large groups of similar elements and/or grid points. In the present problem, this situation occurs for the pile foundations. The pile group, including the footing, is a set of 25 elements,

29 grid points, plus multipoint and single point constraint conditions. All of these input data are prepared by the EDG, in the manner of a subroutine, needing only one set of coding for any number of foundation designs to be generated. The use of the EDG permits simple and rapid parameter studies on items such as stiffnesses, dimensions, etc., of the pile foundations.

(b) The extensive use of multiple point constraints was simplified by creating EDG's specifically for the generation of MPC equations. This was done for both cylindrical and rectangular cartesian coordinate systems. The parameter set for the EDG consists of a list of the two or more nodes to be constrained. The EDG recovers the coordinates corresponding to these nodes and automatically calculates the constraint equations for a full six degree of freedom connectivity. This is particularly useful when cylindrical equations are employed and in parametric studies where grid point changes would otherwise require numerous, potentially erroneous, hand calculations. The EDG for the pile group generation, described above, calls the EDG for MPC equations as required to fix the piles to the footings.

Computation Details

The steel bridge idealization shown in Figure 5 was analyzed in 23 different configurations corresponding to various design changes and parameter studies. The basic model consisted of 199 grid points, 95 CBAR elements, and 80 CONROD elements. There were 166 MPC equations which in combination with boundary conditions and matrix reductions reduced the eigenproblem to 158th order. The runs averaged 6 minutes CPU time on the IBM 370 to extract the eigenvalues by Givens' Method and compute 70 modes. About one-third of the computer time was spent in applying the MPC equations. The basic concrete bridge idealization shown in Figure 6 was analyzed in 5 different configurations. The model consisted of 167 grid points, 84 CBAR elements, and 64 CONROD elements. There were 149 MPC equations which in combination with boundary conditions and matrix reductions reduced the eigenproblem to 143rd order. The runs averaged 5 minutes 48 seconds CPU time on the IBM 370 to extract the eigenvalues and compute 70 modes.

THREE-D MODEL

Purpose

Although the stick model was conceived to be acceptably accurate for both the seismic and flutter studies, a refined idealization, the 3D model, was set up for the concrete alternate to verify the stick model accuracy. The model was called 3D in reference to the idealization of the bridge deck by a slab element (represented as a beam) and individual girder web and flange elements. The beam type idealization of the tower, piers, footings, and piles is unchanged from the stick model. A computer plot of the structure is shown on Figure 3.

As discussed earlier, the weakness of the stick model lies in its simulation of deck torsional stiffness as that of a single member, while in reality the built-up deck resists torsion largely through girder bending. Therefore, the 3D model has as its purpose the accurate representation of girder bending participation in the overall deck deformations.

Description of the Deck Model

Figure 8 shows schematically three types of behavior of a slab-girder deck. The first two apply to a bridge curved in planform, and the last applies for either straight or curved decks. All indicate that deck bending, either vertical or horizontal, will couple with torsion. The three cases are explained in the text of the figure. Basically, the coupling results from two facts: (1) in curved decks, torsion results in lower flange motion toward or away from the center of curvature, with a consequent tendency toward hoop stresses; (2) in horizontal bending of slab-girder configurations, the elastic shear forces are aligned with the shear center of the section (above the deck) while the inertia forces are aligned with the mass center. The tendency toward coupling of bending and torsion which is described by the figure will affect vibration modes by tending to make the mode shapes three-dimensional in character and difficult to identify as pure bending or torsional motions.

In order to represent these coupling tendencies in the finite element mode, it is necessary to meet several requirements:

1. Individual girder flanges must be represented in at least axial and horizontal bending properties.
2. Diaphragms, cross-bracing, and girder web lateral bending stiffness, all of which control lateral motion and therefore hoop forces in the flanges, must be modeled.
3. Flanges must be properly "driven" by the webs; therefore webs must be attached to the slab in such a way that continuity of displacement and rotation components is provided.
4. Structural masses should be properly located.

All of these requirements were met except the fourth. In the location of the masses, to simplify the computational problem, the deck mass properties were concentrated at the centerline of the slab. For the designs studied, however, the resulting error in mass placement was very small.

Figure 9 shows the elements used in the 3D model. The deck slab is represented as a beam having axial, vertical and horizontal bending and shear, and torsional stiffnesses. The centerline of the slab is assigned the deformational freedoms of the deck structure, which are the six linear and rotational displacements. All deck motions are constrain to these six freedoms. The fascia box girders have a closed cell torsional stiffness. This stiffness was added to the torsional stiffness of the deck slab. Flanges are represented by beam elements which have axial and horizontal bending and shear stiffnesses. The handling of the webs presented difficult problems. It is known, and was further verified by calculations, that the NASTRAN plate elements with bending, shear and direct stress stiffnesses are of poor accuracy when used as web elements of girders, particularly for unsymmetrical cross sections. The erroneous behavior arises from the me brane stiffness of the plate. In order to avoid this difficulty, the girder webs were represented by combining shear-only plates with bending plates whose only stiffness is lateral bending. Because the latter plates cannot maintain the spacing between the flanges and the deck, posts are used at the ends of the elements. The axial-force stiffnesses (areas) of the girder webs are assigned to the deck slab and to the lower girder flanges such that: (1) the elastic axis of the composite deck in vertical bending is preserved; (2) the bending moment of inertia of the web of each girder about the composite deck elastic axis is preserved. These conditions provide accuracy in girder an deck bending and torsional behavior. Axial stretching stiffness of the total deck structure, an unimportant factor in the modal analysis, is approximated by these conditions.

Coding Details

As with the stick model, the 3D model made use of both external data generators and multiple point constraints. The geometry was complicated by the banking of the bridge deck (superelevation). Again due to the repetitive nature of the input, SAIL was uniquely suited for data preparation. The principal coding problem is the generation of gr point and constraint data for the nine girders.

The deck centerline geometry and the variable superelevation were computed within the SAIL coding, using the equations and data provided by the designers. Using the computed centerline and superelevation geometrical data in the input parameter set, along with component structural data, the deck structure EDG was called. The EDG set up the upper girder web (and flange) grid points, the lower girder web (and flange) grid points, the girder flange and web elements, the MPC equations which serve to couple the girder elements to the six freedoms of the deck centerline, and in addition defined the freedoms to be reduced in the eigensolution. The MPC equations rigidly connect the upper girder web grid point freedoms to the six freedoms of the grid points on the deck slab centerline. The EDG is called once for each nose station at which a deck grid point is located, thus significantly reducing the magnitude of the coding task. This idealization in effect imposes deck cross-sectional bracing (diaphragms) at each dec grid point. This is a correct requirement since the designed diaphragms are located at approximately the same nose station spacing as are the deck grid points.

Computational Details

The 3D concrete bridge model shown in Figure 3 was subjected to modal analysis. The finite element idealization consisted of 623 grid points, 242 CBAR elements, 280 CONROD elements, 207 CQUAD1 plates, and 207 CSHEAR webs. There were 1945 MPC equations which in combination with boundary conditions and matrix reductions reduced the eigenproblem to 149th order. A CPU run-time of 19 minutes and 20 seconds on the IBM 370 computer was required to extract the eigenvalues by Givens' Method and to compute 20 modes.

SEISMIC AND FLUTTER ANALYSES

The seismic analysis was performed by the response spectrum method. The full details of this method are outside the scope of this paper. Portions of the overall methodology are described in Reference 3. The earthquake input data used are in the form of response spectra, and are specifically derived for the West Seattle site conditions[1].

The bridge response was determined in terms of its normal vibration modes. The response spectrum method provides maximum individual modal responses to the earthquake excitation. Modal summation is required over very few modes, for most earthquake analyses, and is done either as an absolute value sum or a root-square-sum, based on judgement and recommendations from past experience (Ref. 3)

The response spectrum method uses for input the modal analysis data, consisting of vibration mode period, generalized mass, and mode shape. In particular, modal response depends on the degree of coupling between the mode and the uniform vector field which describes the motions of the earthquake. This aspect of the seismic analysis requires the accessing and processing of very large amounts of structural and modal data. A new computer program, used as a NASTRAN post processor, was written to perform the work. This program obtains all needed data from the NASTRAN checkpoint/restart tape. The set of data read from the tape consists of files EQEXIN, GPDT, MGG, LAMA, PHIG, and OEF1. The complete modal and seismic analysis can be done in a single computer run, or the NASTRAN and seismic runs can be done separately. The seismic post processing program was found to be very convenient and provided a rapid analysis tool. Overnight turnaround on combined modal and seismic analyses was routinely obtained.

Flutter analysis was done for two types of flutter mechanisms: (1) single degree of freedom stall flutter; and (2) classical bending-torsion flutter. The calculations were done by existing Boeing flutter analysis programs, based on theoretical methods which are beyond the present scope. Aerodynamic data were obtained from wind tunnel tests on models of the various bridge deck sections, and modal data were obtained from the NASTRAN analyses. A subroutine within the seismic program was used to read the normal modes from the NASTRAN checkpoint/restart tape and to punch out on cards the required rotation and vertical translation displacements of the deck.

1 Data provided by the firm of Shannon and Wilson

TYPICAL NUMERICAL RESULTS

Seismic Analysis

Each modal analysis computer run provided complete modal data, including element internal loads, and also SC4020 plots of the mode shapes. Figures 10 and 11 are computer plots of the modes which were predicted to be the most important seismic motions of the West Seattle bridge. The plots shown are for the concrete alternate, but all configurations show essentially the same principal types of motions. The first is a lateral swaying and the second a combined longitudinal - vertical motion which is strongly influenced by the cables. The latter is the bridge fundamental mode. These modes are important seismically for two reasons: (1) their modal frequencies lie in a range of strong seismic input; (2) their mode shapes involve essentially unidirectional motions of the major bridge masses, thus obtaining strong coupling with the uniform seismic excitation.

Figures 12 and 13 show tower moments and shears which were computed for the initial steel and concrete designs. The moments and shears shown are those resisting a lateral swaying motion, and are caused primarily by modes of the type of Figure 11. The stresses for the concrete alternate are larger than those for the steel due mainly to the greater deck mass of the concrete design and the close proximity of the concrete modal period to a period of strong seismic excitation. These results proved excessively severe for strength design purposes.

As described earlier, the dynamic analysis was continued in support of trade studies for the development of a design configuration which is satisfactory for earthquake conditions Figure 14 shows the results obtained for a set of seven designs which differ from one another primarily in tower configuration. All designs utilize a steel deck structure. From these results tower alternate A was chosen as the recommended configuration[1]. The figure lists the modes and modal periods which are critical for both longitudinal and transverse earthquake excitations, and gives the resulting maximum tower bending moments. The curve shown in the lower right corner of the figure is the earthquake response spectrum used in the calculations.

As discussed earlier, a matter of concern was the effect of the approximation of the deck torsional stiffness on the accuracy of the stick model modes. It was for this reason that the 3D model was used to compute a more accurate set of modal data. Figures 15 and 16 show 3D model modes corresponding to the stick model modes of Figures 10 and 11. The agreement in mode shape is excellent. Figure 17 shows the lowest 3D model mode in which deck torsion is important. This mode shape justifies the manner of computation (the choice of wave length) of the stick model deck torsional stiffness which was described earlier. Figure 18 shows a comparison of stick model and 3D model modal data for the first ten modes for the concrete alternate. The frequencies are tabulated together with a brief description of the modal motions. Note that in several cases corresponding modes have changed order slightly, due to small changes in closely spaced frequencies. A careful study of all modal data has shown that in the

1 The defining of these configurations and the choice of tower alternate A were done by the firm of Knoerle, Bender, Stone, and Associates, Inc.

et of the first ten modes only the ninth stick model mode fails to agree closely with a :orresponding 3D model mode. All other modes show good agreement in both mode hape and frequency.

'lutter Analysis

'he flutter wind speeds were determined for the initial concrete and steel designs and or the current configuration which has been optimized for dynamic response conditions. 'or the initial concrete and steel designs, respectively, single degree of freedom stall 'lutter was predicted at steady horizontal windspeeds of 77 miles/hour in the lowest orsion mode and 46 miles per hour in the fundamental vertical bending mode. For the ›ptimized design a torsion stall flutter speed of 244 miles per hour was predicted, with he improvement primarily a result of improved aerodynamic shape of the deck section ind increased torsional stiffness of the closed box girder design.

:ONCLUSION

'he results of the dynamic analyses showed that the initial bridge designs were deficient n their ability to withstand a major earthquake or a sustained high wind condition. Through the early dynamic analysis parameter studies, however, the directions required 'or fruitful design modification were defined. A continuing program is in progress to mplement these modifications into the design. This work has resulted in a bridge con-'iguration which is satisfactory in resistance to both seismic and wind-induced motions. Currently, further design trade studies in conjunction with dynamic analysis are under-way to optimize the design of the lower portion of the tower and the bridge foundation 'or improved earthquake resistance.

This use of the NASTRAN system in the field of civil engineering structures has demon-strated a potential for such applications. The benefits of such sophisticated analysis appear particularly great in consideration of the complex structural configurations and severe design conditions which are becoming increasingly common in the field of civil engineering structural design.

References

1. Jones, R.E., and Wagner, R.T.: Dynamic Analysis of the Proposed West Seattle Freeway Bridge. Boeing document D180-15357, 1973.

2. Ice, M.W.: NASTRAN User Interfaces - Automated Input Innovations. NASA TM X-2378 Colloquium, Langley Research Center, Hampton, Virginia. Sept. 1971.

3. Harris, C.M., and Crede, C.E.: "Shock and Vibration Handbook", Volume 3 McGraw-Hill, 1961, Chapter 50.

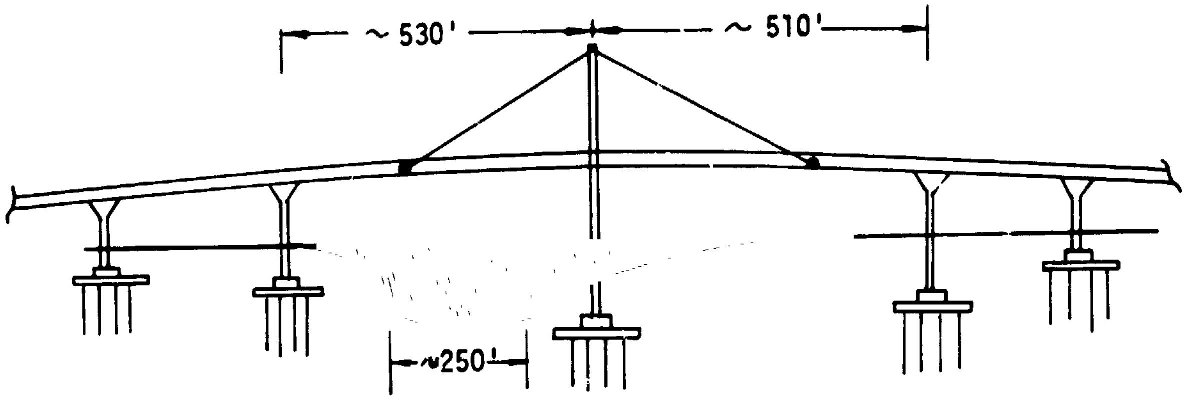

Figure 1a: ELEVATION VIEW

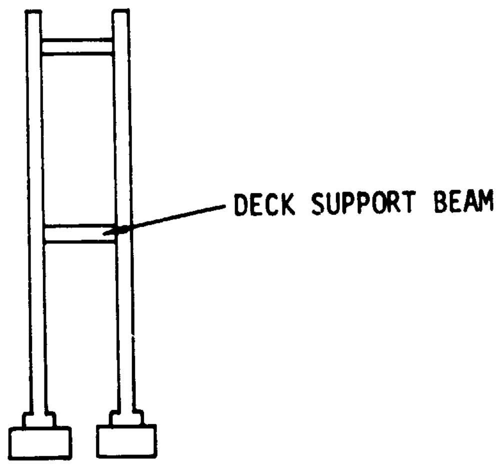

Figure 1b: TOWER CONFIGURATION- ELEVATION VIEW

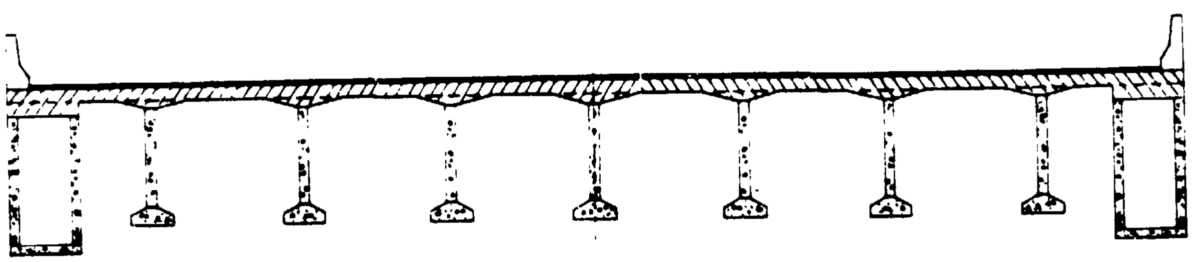

Figure 1c: TYPICAL DECK CROSS-SECTION

Figure 1: INITIAL BRIDGE DESIGN CONFIGUATION

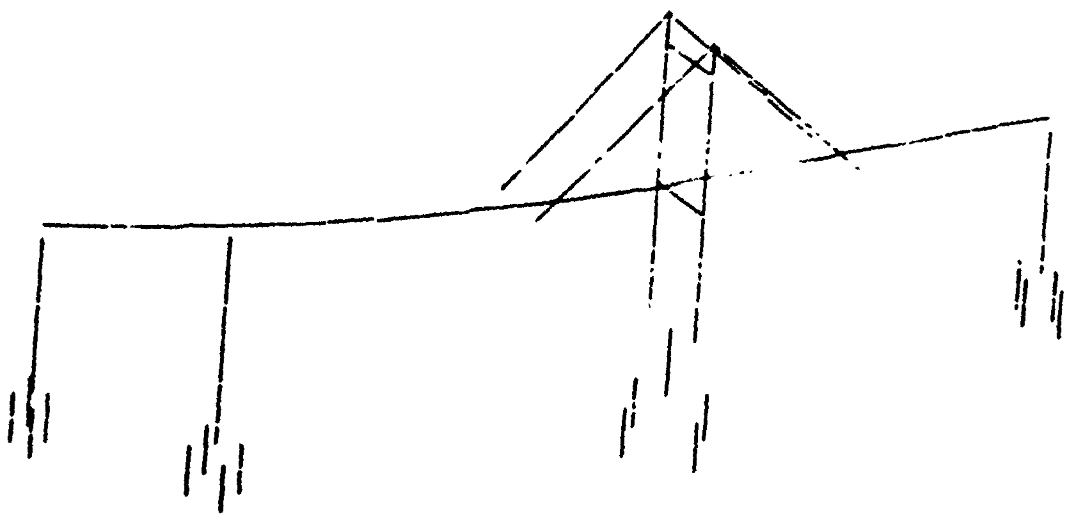

Figure 2: SIMPLE MODEL-CONCRETE ALTERNATE

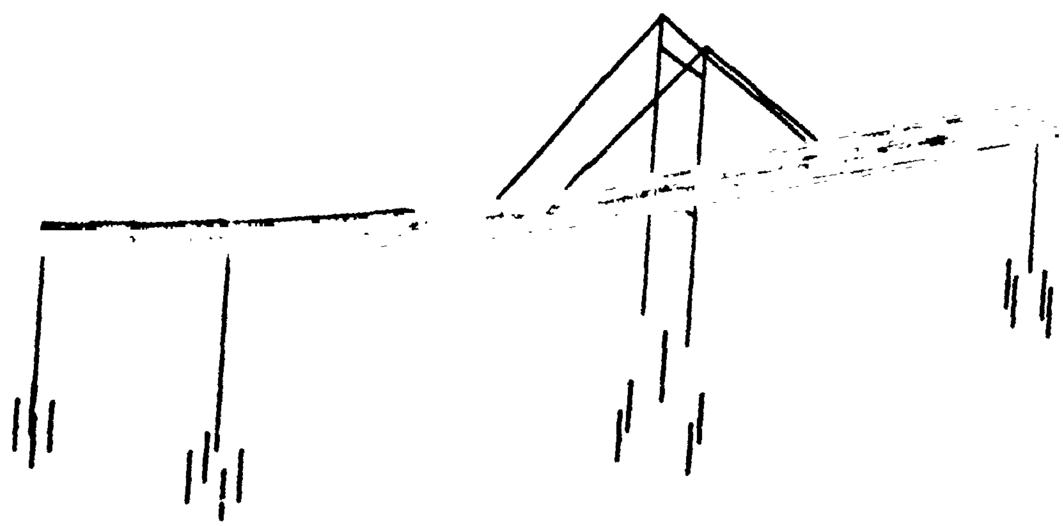

Figure 3 : THREE - D MODEL -- CONCRETE ALTERNATE

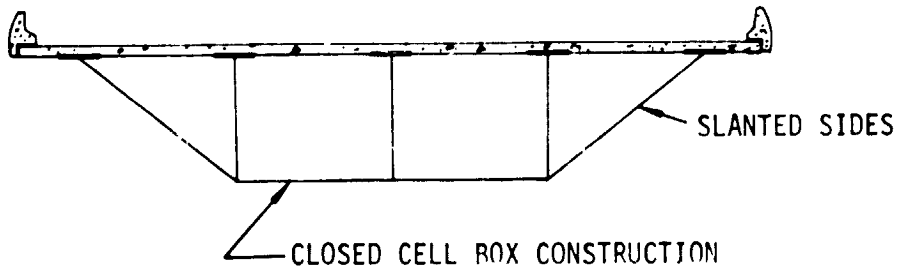

Figure 4a: DECK CROSS-SECTION

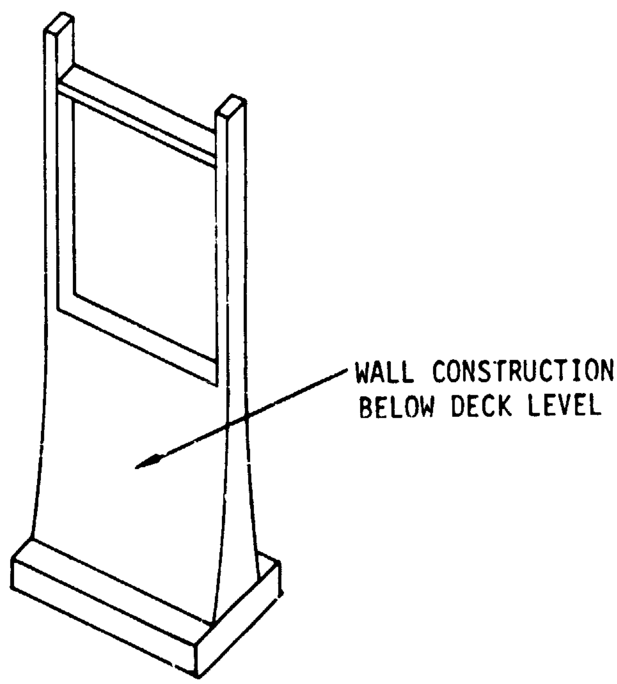

Figure 4b: TOWER CONFIGURATION

Figure 4: STRUCTURAL CONFIGURATIONS TO RESIST EARTHQUAKE AND HIGH WIND CONDITIONS

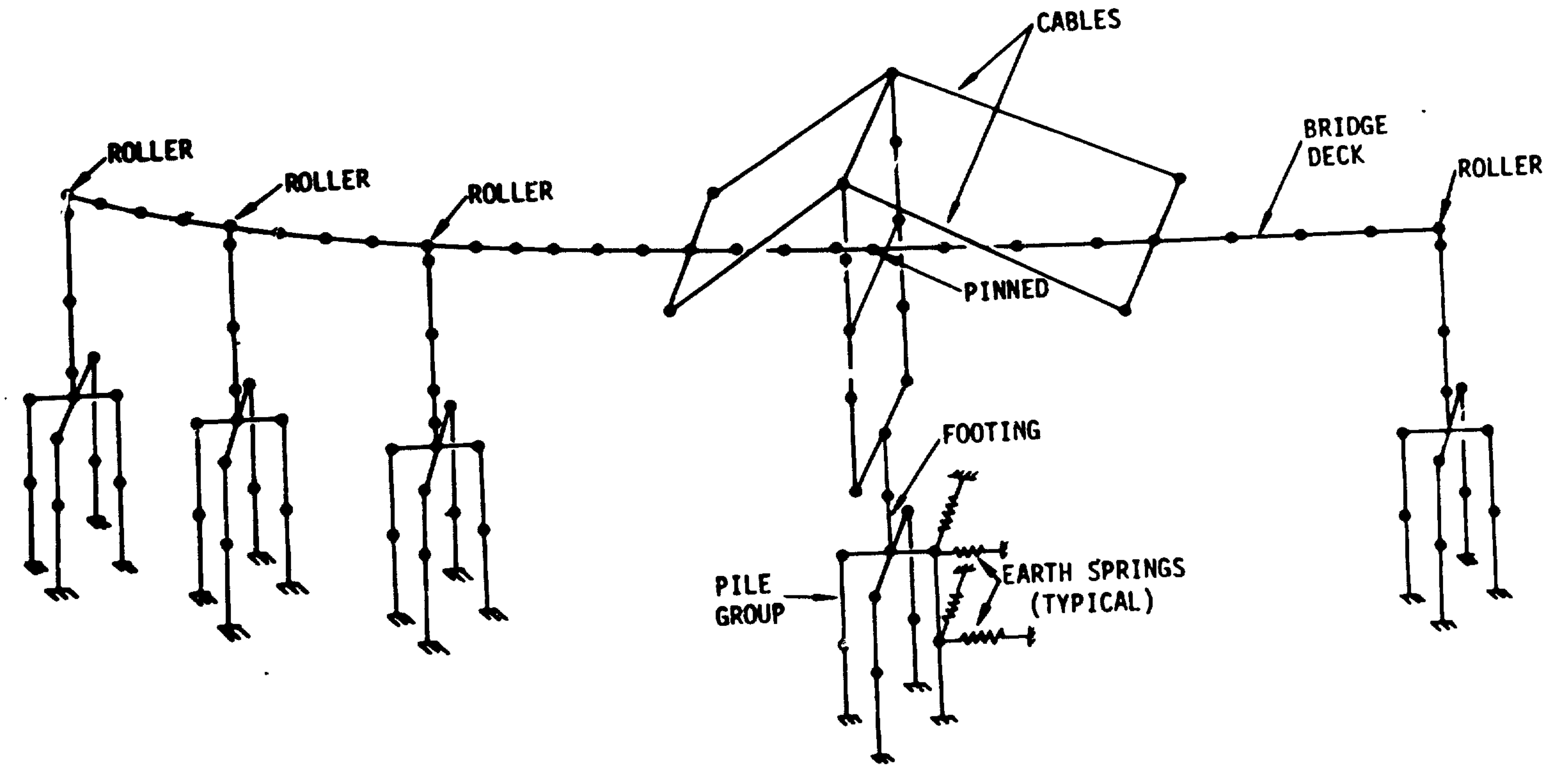

Figure 5 : STEEL FINITE ELEMENT (STICK) MODEL

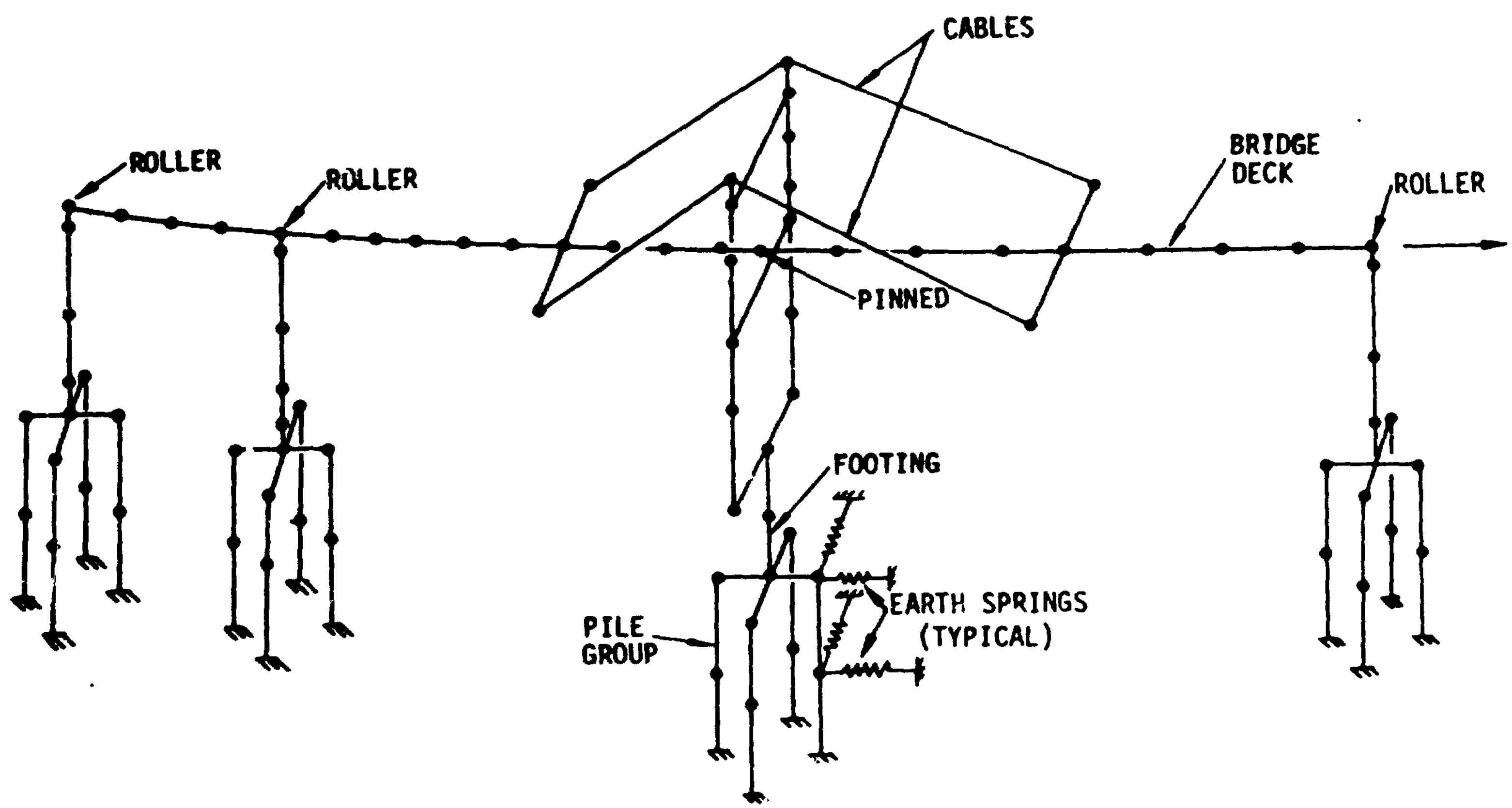

Figure 6 : CONCRETE FINITE ELEMENT (STICK) MODEL

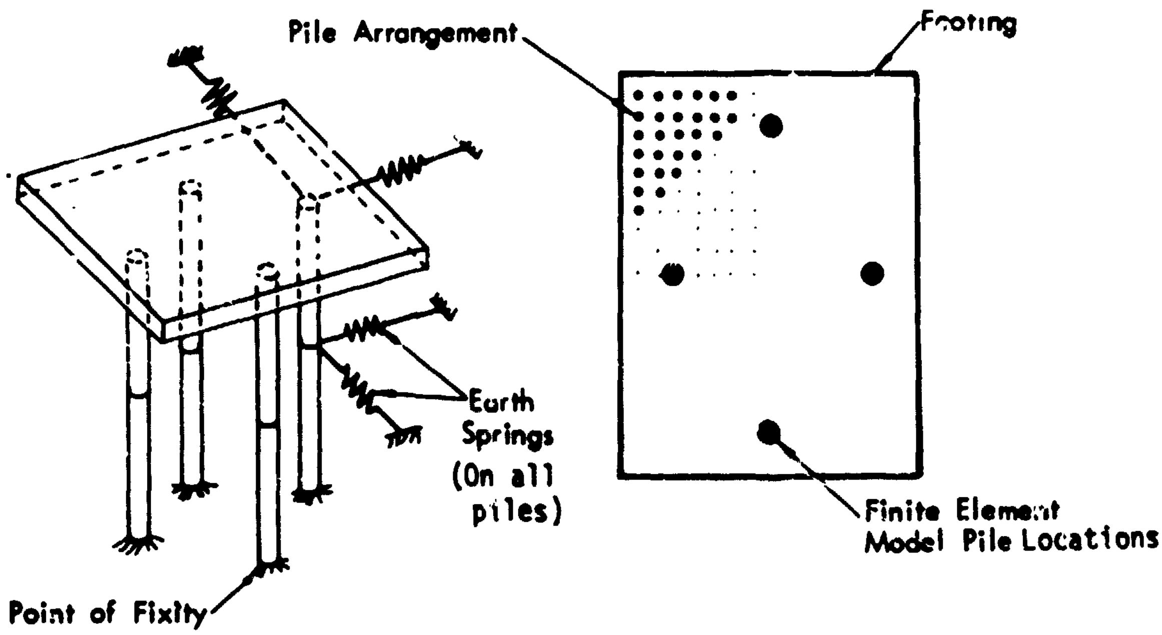

Figure 7 : FINITE ELEMENT PILE ARRANGEMENT

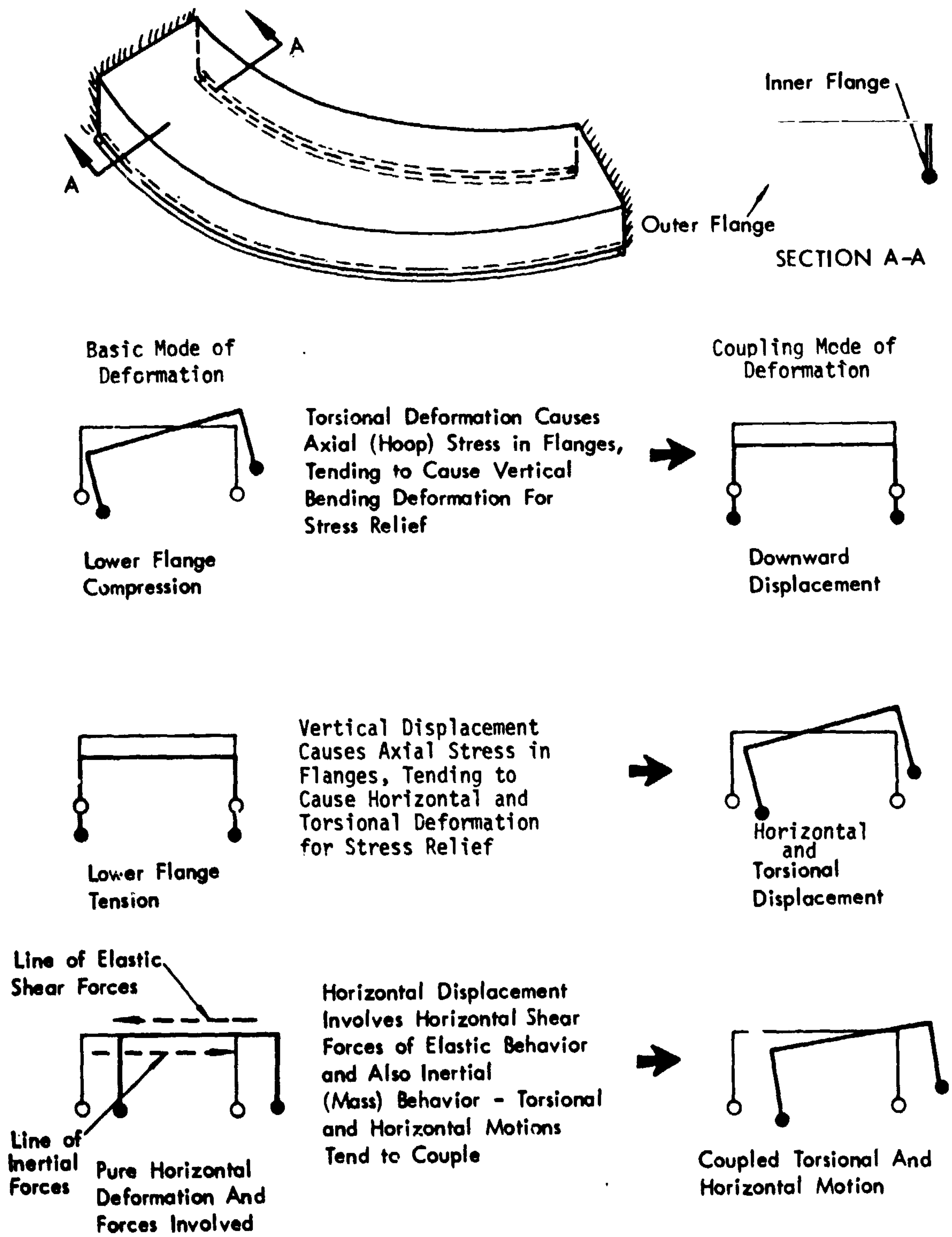

Figure 8 : BENDING-TORSION COUPLING OF SLAB - GIRDER DECK

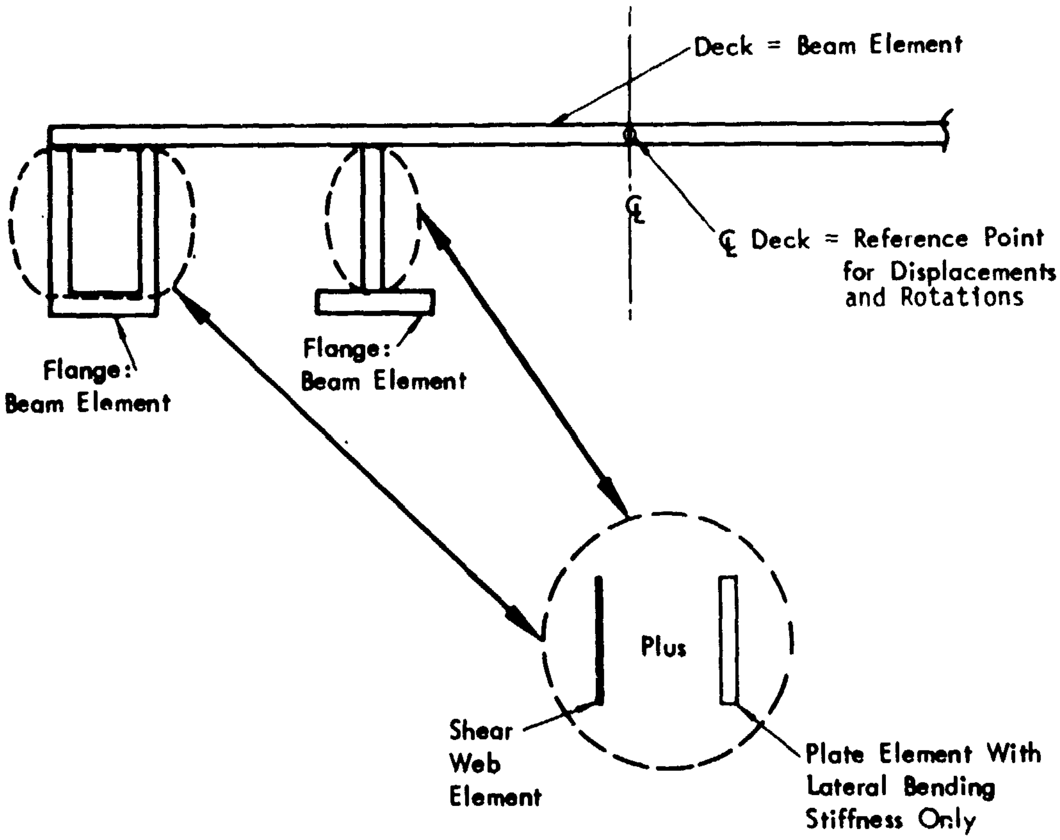

NOTES:
- Girder Web Axial Area Assigned to Deck and Flange.
- Box Torsional Stiffness of Fascia Girder Assigned to Deck.
- Deck - Flange Spacing Maintained by Posts at Ends of Elements.

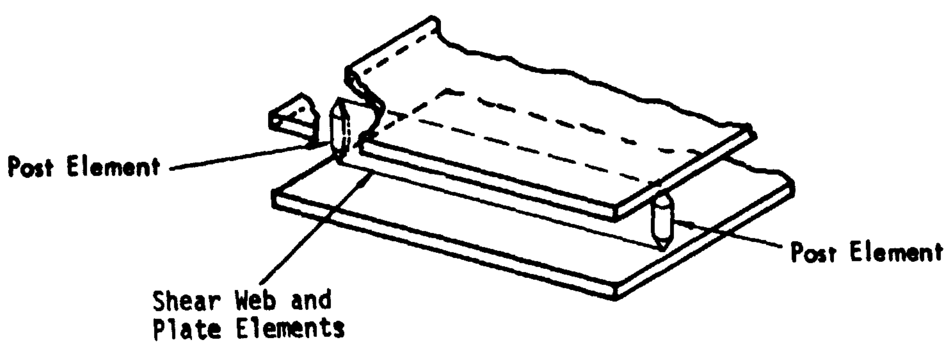

Figure 9 : ELEMENTS USED IN 3D MODEL

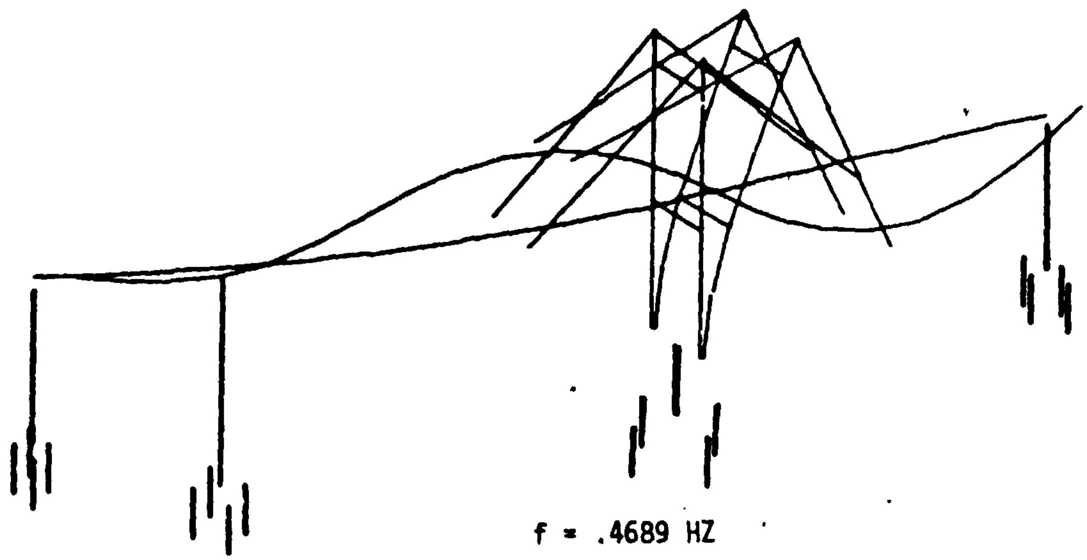

f = .4689 HZ

Figure 10: LONGITUDINAL AND VERTICAL MOTIONS
- CONCRETE ALTERNATE

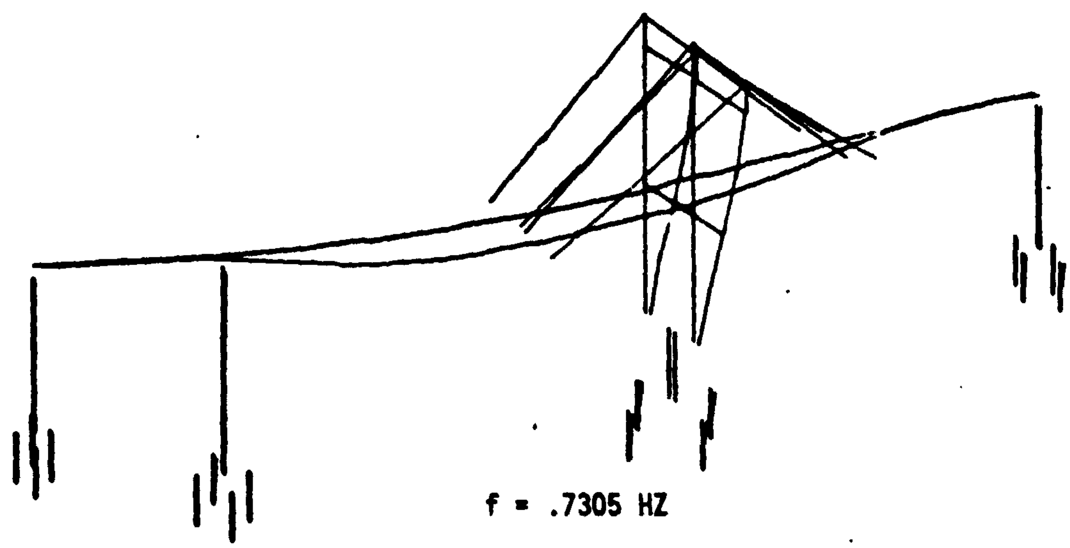

f = .7305 HZ

Figure 11: LATERAL MOTION- CONCRETE ALTERNATE

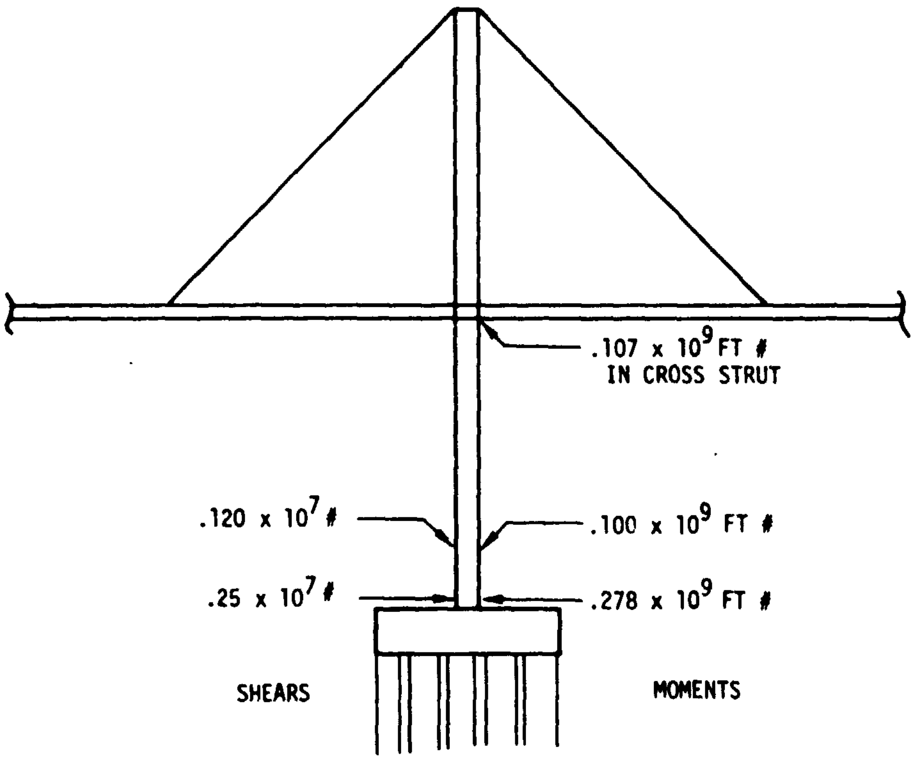

Figure 12 : SEISMIC MOMENTS AND SHEARS IN TOWER - STEEL ALTERNATE

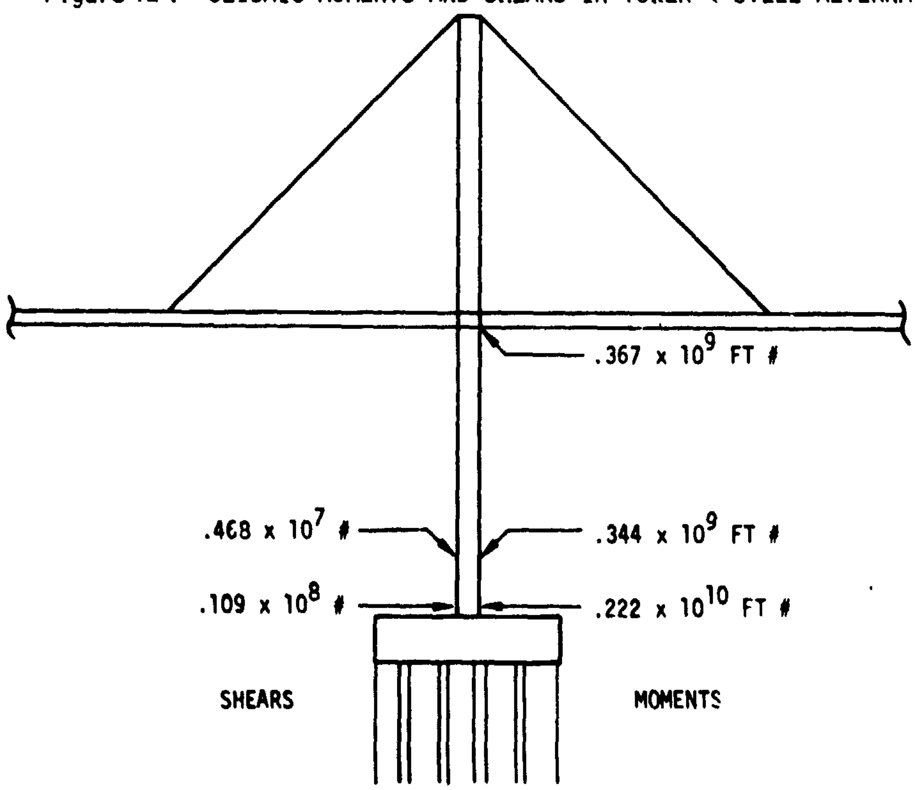

Figure 13 : SEISMIC MOMENTS AND SHEARS IN TOWER - CONCRETE ALTERNATE

TOWER ALTERNATE	TOWER SIZE C.S. DIMS	TOWER SIZE CONC AREA	SHAFT SIZE	FOOTING SIZE S	FOOTING SIZE H	FOOTING SIZE L	NO PILES	CRITICAL MODES LONGIT	CRITICAL MODES TRANSV	CRITICAL PERIODS LONGIT	CRITICAL PERIODS TRANSV	STRUT M_a	TOWER BASE LONGIT M_b	TOWER BASE TRANSV M_c	SHAFT M_d	FOOTING LONGIT M_e	FOOTING TRANSV M_f	TOWER REINFORC'G	WT ABOVE FOOTING	TOTAL WEIGHT	COMMENTS
E	8 × 40	196 ft²	H-Shape 90 × 20 + 12 × 12 Wings	108	96	23	288	1 4	2 8	2.08 1.12	1.97 .77	189,000	540,240	163,880	1,483,880	1,809,880	1,388,880	5.5 to 7.4 Steel req'd at base 750 #14	47,870	77,480	Excessive reinforcing in tower (Approx 4 rows of #14 at 6" in outside wall of base). Due to 8' width [illegible] recommended because of geometry and reinforcement required
F	8 × 28	161 ft²	90 × 32	102	88	21	272	1 3	2 8	2.46 .22	2.02 .79	168,380	434,430	138,430	1,253,600	1,384,800	1,070,840	Solid section req'd at base with 7 to 7.5% Steel 1075 #14	47,700	75,880	Same as for Alternate E except reinforcing at base required [illegible] 7 rows of #14 at 6" around periphery of solid section. Not recommended because of geometry and reinforcement required
G	10 × 24	180 ft²	94 × 30	108	96	21	288	1 3	2 8	2.85 1.47	1.74 .76	337,320	408,420	288,750	1,125,440	1,49[illegible],980	1,875,580	Solid section req'd at base with 6.5 to 7% Steel 1075 #14	47,370	77,190	Excessive reinforcing in tower. Approx 8 rows of #14 at 6" around periphery of solid section. Not recommended because of geometry and reinforcement required
H	12 × 30	213 ft²	98 × 38	120	102	21	340	1 3	2 4	2.35 .16	1.96 .81	463,880	513,770	430,300	1,475,760	1,865,220	2,947,980	Solid section req'd at base with 5 to 5.5% Steel 1260 #14	56,080	86,710	Excessive reinforcing in tower. Approx 8 rows of #14 at 6 around periphery of solid section. This alternate has the largest vertical load and the largest moment values. Not recommended because of excessive reinforcement, number of piles required and total weight
A	15 × 24	140 ft²	120 × 20	108	96	23	288	2 8	4 9	1.33 .89	.96 .62	—	217,730	146,280	1,183,170	1,475,400	2,207,430	4% Steel req'd at base 380 #14	45,080	74,870	Reinforcing heavy in tower. Approx 3 rows of #14 at 6" in outside wall of base but adequate to place. No clearance problems in fitting anchor plates and cable connections. Recommended

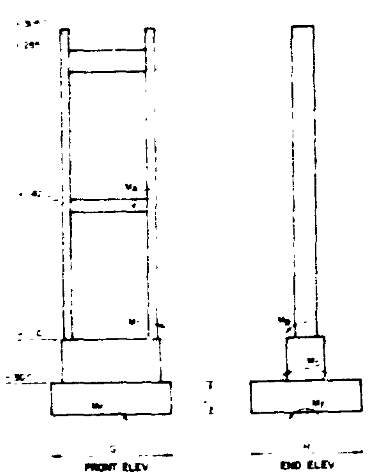

TOWER ALTERNATE E, F, G OR H

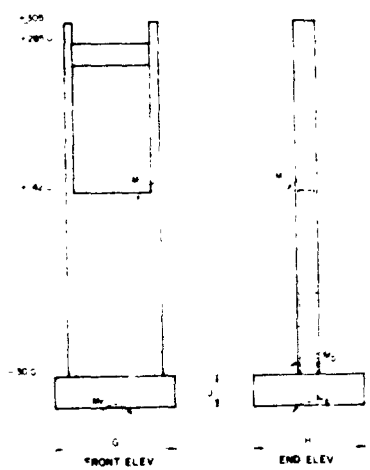

TOWER ALTERNATE A

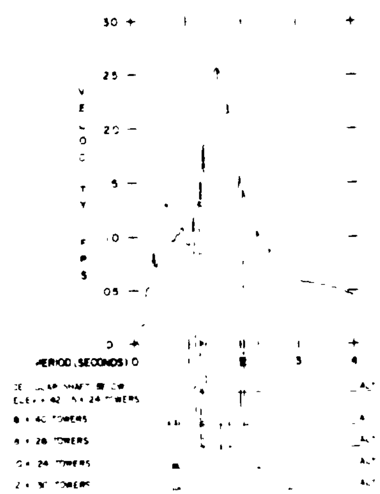

VELOCITY RESPONSE SPECTRA

EARTHQUAKE 28, 5% DAMPING, ELEVATION -56

NOTES

All dimensions are in feet, all moments are in kip feet and all weights are in kips.

All weights below elev -12 are buoyant.

Total weights include 10' thick seal.

Moments shown are from dynamic stick model computer runs and are the sum of the 2 largest model values.

Footing sizes based on Group VII loads using moment values = Dead Load Moment + 0.5 Dynamic Stick Model Moment.

A minimum tower length of 24' required for a feasible cable assembly and connection. A minimum 7' internal width required for anchorage and working area.

WEST SEATTLE FREEWAY

TOWER ALTERNATES AT UNIT 5

Figure 14: RESULTS OF EARTHQUAKE ANALYSIS TRADE STUDIES

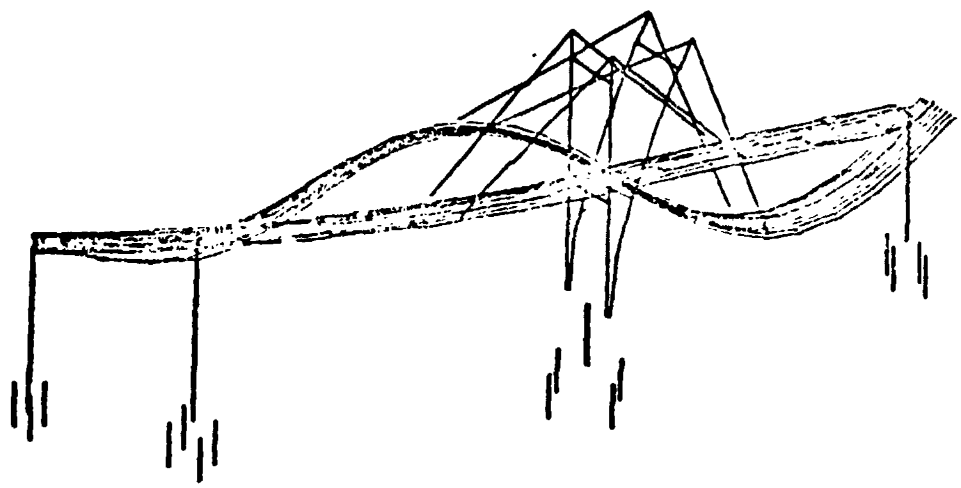

f = .44 HZ

Figure 15: LONGITUDINAL AND VERTICAL MOTIONS -CONCRETE ALTERNATE

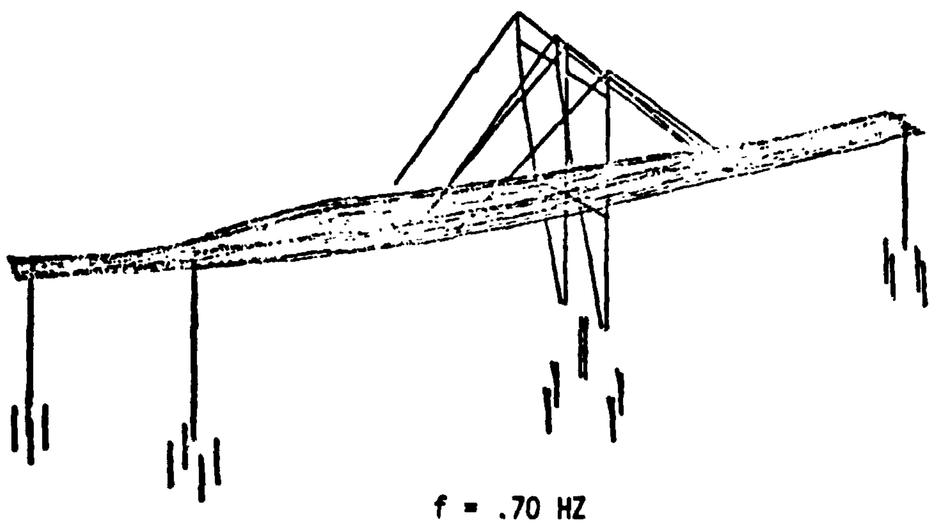

f = .70 HZ

Figure 16: LATERAL MOTION - CONCRETE ALTERNATE

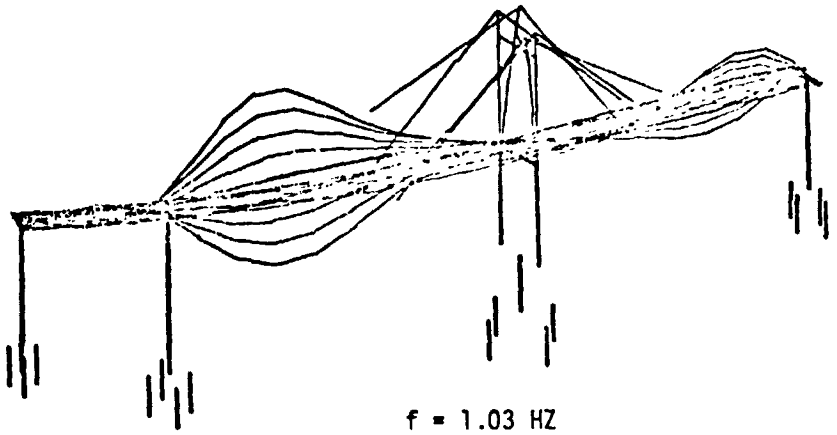

f = 1.03 HZ

Figure 17: LONGITUDINAL, VERTICAL AND TORSION MOTIONS - CONCRETE ALTERNATE

CONCRETE ALTERNATE - STICK MODEL		CONCRETE ALTERNATE - 3D MODEL	
FREQUENCY (HZ)	MODE TYPE	FREQUENCY (HZ)	MODE TYPE
.4689	Y, Z	.44	Y, Z
.7132	Y, (P)	.70	X
.7305	X	.71	Y, (P)
.8109	Y, (P)	.81	Y, (P)
.8537	Y, Z	.81	Y, Z
.9429	Y, Z	.87	Y, Z
.9513	Y, (P)	.95	Y, (P)
1.014	Y, Z, T	1.03	Y, Z, T
1.065	X, Z, T	1.15	X, Y, Z, T
1.244	X, T	1.19	X, T

X = LATERAL

Y = LONGITUDINAL

Z = VERTICAL

T = TORSION

(P) = PIER ONLY

Figure 18: COMPARISON OF 3D AND STICK MODEL MODAL DATA

N74-14597

NASTRAN ANALYSIS OF THE

1/8-SCALE SPACE SHUTTLE DYNAMIC MODEL

By Murray Bernstein, Philip W. Mason, Joseph Zalesak,
David J. Gregory, and Alvin Levy

Grumman Aerospace Corporation

INTRODUCTION

The Space Shuttle configuration has more complex structural dynamic characteristics than previous launch vehicles primarily because of the high modal density at low frequencies and the high degree of coupling between the lateral and longitudinal motions. An accurate analytical representation of these characteristics is a primary means for treating structural dynamics problems during the design phase of the Shuttle program. The 1/8-scale model program was developed to explore the adequacy of available analytical modeling technology and to provide the means for investigating problems which are more readily treated experimentally. The basic objectives of the 1/8-scale model program are

(1) To provide early verification of analytical modeling procedures on a Shuttle-like structure

(2) To demonstrate important vehicle dynamic characteristics of a typical Shuttle design

(3) To disclose any previously unanticipated structural dynamic characteristics

(4) To provide for development and demonstration of cost effective prototype testing procedures

This paper constitutes a progress report on the program to date.

The work described herein has been conducted primarily under contract for the NASA Langley Research Center.

DESCRIPTION OF STRUCTURAL MODEL

The model is designed to represent the important structural dynamics characteristics of a Shuttle-like vehicle while keeping the fabrication costs low.

The general arrangement of the model is shown in figure 1. The original basis for the design was a 21.35 MN (4.8×10^6 lb) GLOW, 55.474 m (182 ft) long parallel burn configuration (Grumman Design 619). Subsequently, under Rockwell International sponsorship, the forward solid rocket booster to external tank attachment design was modified to a single point connection representing the RIC prototype as of December 1972.

Figure 1 illustrates a mock-up of the 1/8-scale model which is approximately 7.315 m (24 ft) from the external tank nose cone to the solid rocket booster tie-down plane. The total model is composed of 4 major components: the Orbiter, external tank, and two solid rocket boosters. The Orbiter is shown in figure 2, without the cargo bay doors, and in figure 3 with the cargo bay doors and nonstructural plastic fairings that complete the contours of the vehicle.

Figure 4 shows the Orbiter fuselage under assembly and figure 5 is a NASTRAN plot of the finite-element model. The fuselage structural model is approximately 3.543 m (11.625 ft) long, contains 21 frame stations, and is constructed of 2024 aluminum. The bottom shell of the fuselage is 0.635 mm (0.025 in.) thick while the side walls and top shell are 0.508 mm (0.020 in.) thick. The cargo bay doors are made up of segments of 0.4064 mm (0.016 in.) aluminum sheet that are attached to the frames. The details of the attachment to the frames prevent the doors from resisting fuselage bending but allow them to act in resisting shear.

The fuselage frames in the region of the cargo bay are constructed of aluminum sheet that has been bent to form a channel section. The tapered side wall channel section and the lower portion are attached back to back to form a U-shaped frame. The major bulkheads are of stiffened sheet construction.

The delta wing shown in figure 6 consists of 6 spars and 4 ribs that are formed from 0.8128 mm (0.032 in.) 2024 aluminum sheet. The covers are 0.5080 mm (0.020 in.) thick. NASTRAN plots of the finite-element model are shown in figures 7 and 8.

The fin structure, which includes only the structure from the fuselage to the center of gravity of the physical fin model, contains 3 spars and a closure rib. The webs are 0.8128 mm (0.032 in.) thick while the covers are 0.5080 mm (0.020 in.) thick. NASTRAN plots of the finite-element model are shown in figures 9 and 10.

A NASTRAN plot of the cargo bay doors is shown in figure 11 and a schematic illustrating the connection of the door shell to the door frames is shown in figure 12.

The external tank contains four main components, the LOX tank, inter tank skirt, LH_2 tank, and the aft tank skirt. A NASTRAN plot of the entire structure is shown in figure 13. The total structure is approximately 6.858 m (270 in.) long and has a radius of 0.5029 m (19.8 in.). The orbiter interstage points are located totally within the LH_2 part of the external tank; the forward interstage at station 148.756 transmits vertical and side loads while the aft center-line interstage at station 245.7536 transmits thrust and side load. Inclined bars also at station 245.7536 connect with the orbiter at B.L. 13.75 and with the tank at B.L. 16.4631 to provide the necessary determinate supports. The solid rocket booster is connected to the tank at the forward end at the inter tank skirt. This pin connection transfers vertical, side, and all drag loads. The aft tank/SRB interstage is located at tank station 270.988 and consists of 3 bars capable of transmitting vertical and side load as well as roll moment.

The liquid oxygen tank, figure 14, is a shell of revolution composed of a conical shell, a cylindrical shell, and two quasi elliptical end domes which are each formed from two tangential spherical segments. The overall length is 1.98 m (78 in.). The tank is 2219 aluminum and all shell segments are welded at the joints. The primary gage is 0.508 mm (0.020 in.) with the lower dome being 0.406 mm (0.016 in.), and the total tank structure is connected to the inter tank skirt via a Y-ring located at the aft end of the cylindrical portion of the tank.

Figure 15 shows the liquid oxygen tank connected to the inter tank skirt and to the forward tank/SRB interstage. Figures 16, 17, and 18 show additional details of the external tank structure. The LOX tank is of monolithic construction whereas the remainder of the external tank is of ring stiffened sheet construction, the sheet being thickened where large drag loads exist. The LH_2 tank is 2024 aluminum and the overall length is 4.27 m (168 in.). The chem-milled tank skin thickness is primarily 0.406 mm (0.016 in.) and typically increases to 0.635 mm (0.025 in.) in load carrying areas such as the orbiter interstage connections.

The solid rocket booster consists of a cylinder, a forward tank/SRB interstage, shown in figure 15, and an SRB aft skirt as shown in figure 19. The cylinder is 2024 aluminum and is approximately 3.7338 m (147 in.) long, 5.080 mm (0.2 in.) thick, and has a radius of 0.2477 m (9.75 in.).

A more complete description of the model design is presented in Reference 1. The significant structural dynamic characteristics to be represented in a model for various problem areas which are the basis for a model design are described in Reference 2.

ANALYTICAL MODELING PROCEDURE

Basic Philosophy

The entire vehicle has been analyzed by using NASTRAN. In setting up the model and analysis procedures the following guide lines were established:

(1) The model should be of sufficient refinement to adequately predict overall dynamic behavior. No attempt would be made to try to predict local panel motions.

(2) The detail of modeling should be of sufficient refinement to allow us to predict internal load distributions that would be adequate for a preliminary design of the structure. Although we had no intention of computing internal loads we considered the analysis to be representative of an actual prototype design situation and we were interested in how NASTRAN would blend into a design environment.

(3) The total structure would be analyzed by employing sub-structuring techniques to see how well this aspect of NASTRAN would blend into a design environment. NASTRAN could, in principle, of course handle the entire structure as a single unit, but we did not feel that this represented a realistic situation.

(4) Separate analyses of the LOX and SRB were performed to investigate the hydroelastic and viscoelastic capabilities of NASTRAN.

(5) The NASTRAN weight analysis capability was used to calculate the individual component and total weights for the nonfluid portions of the model. A supplementary weight check was conducted and the NASTRAN results adjusted where necessary. Structural grid points were used as dynamic mass points using Guyan reduction as required. This procedure differs from Grumman's usual practice, which is to establish a weights model independent of the structural model. By this approach, unit loads on the weights model mass points are then beamed to appropriate structural node points. The dynamic model is then the same as the weights model or is a subset of it. This procedure inherently results in a small dynamic model and additional reduction schemes are not necessary. The equivalent

reduction takes place in the beaming of the unit loads from the weights model to the structural model. This method was not used because it would have required more extensive alters to the NASTRAN rigid formats, it would not use NASTRAN weight analysis capability, and it would have produced basic mode data at non physical points which might hinder test correlation.

Overall Analysis Flow

A schematic diagram of the analysis flow is shown in figure 20. As indicated the Orbiter was divided into five substructures: fuselage, cargo doors, fin, wing, and payload. The external tank was divided into two substructures: the LOX tank and the aft portion of the external tank that consisted of the inter tank skirt, LH_2 tank and aft tank skirt. The solid rocket booster was handled as a single unit consisting of the forward skirt, propellant cylinder and propellant, and the aft skirt.

In the analysis each of the five Orbiter substructures was analyzed to produce reduced stiffness and mass matrices for selected dynamic points and interface attachment points. Modes for these components were then obtained with the interfaces held, the exception to this being the fuselage which was analyzed in a free-free state. This was done to aid in checking and to help understand the behavior of the combined vehicle. The five substructure stiffness and mass matrices were then merged to form total Orbiter mass and stiffness matrices. These matrices were again reduced by "freeing up" the substructure interface points to yield final stiffness and mass matrices that were used in the modal analysis.

As mentioned earlier, seperate analyses were run on the LOX tank and the SRB to study the hydroelastic capability of NASTRAN and to investigate the effect of the viscoelastic properties of the propellant on the damping characteristics of the SRB. In the overall flow the SRB matrices were first reduced and then merged with the Orbiter and external tank matrices to form a total Shuttle system of equations. The LOX tank was not reduced in this process.

The aft portion of the external tank was reduced, analyzed seperately, and merged with the other components in forming the total Shuttle system of equations.

Substructuring Procedure

The basic substructuring procedure for combining elements as presented in the NASTRAN User's Manual has been followed with some minor changes in the assumptions used, and with more extensive DMAP alters. These alters are written for both Rigid Format 3 which permits the use of more efficient eigenvalue analysis procedures while assembling the orbiter model and also for Rigid Format 7. The latter is required because the hydroelastic model of the LO_2 tank results in nonsymmetric mass and stiffness matrices which cannot be treated in Rigid Format 3. The viscoelastic properties of the propellant also are accurately represented in Rigid Format 7.

The analytical model is assembled in two phases. The flow diagram for the analysis is shown in figure 21. In the first phase, each substructure is analyzed and checked separately. The output from this phase is assembled onto a copy tape for the symmetric and antisymmetric cases and then coupled in Phase 2.

The following changes to the basic substructuring assumptions have been made in formulating this procedure:

Any external supports present are included in the Analysis Set (a-set).

Any zero stiffness degrees of freedom and symmetric or antisymmetric boundary constraints at the model plane of symmetry, are included in the Single Point Constraint Set. No other degrees of freedom are included in this set.

Masses which are associated with zero stiffness degrees of freedom will be lost unless these degrees of freedom are "beamed" to adjacent points using Multipoint Constraints.

The interface degrees of freedom may be sequenced differently and in different coordinate systems in any two substructures to be coupled. Multipoint Constraints are used to relate the appropriate degrees of freedom irrespective of local coordinate systems or initial sequencing.

Although the general theory presented in the NASTRAN User's Manual for substructuring is correct, it does not provide analysis checks at various critical points in the procedure. Structural plots provide analysis checks in this substructuring procedure but are not considered sufficient for verifying more than structural topology.

The following checks have been incorporated in the analysis by means of extensive DMAP alters:

A rigid body check is made in Phase 1 after the generation of the reduced stiffness and mass matrices. Temporary rigid body supports are included in the deck as SUPORT cards for this purpose.

The structural transformation matrices Gm, Go and D are used to generate equilibrium matrices for the various constraint sets except single point constraints. These equilibrium matrices represent resultants about a chosen origin due to unit applied loads at the appropriate degrees of freedom.

Provision is made to compute either free-free modes or free modes with the substructure held at the interface. This is necessary if each substructure is to be checked independently in Phase 1.

A rigid body mass matrix relative to the basic origin is computed and compared with the general mass matrix calculated by the Grid Point Weight Generator. This check verifies that no mass has been lost in the reduction process.

The DMAP statements to perform these functions for Rigid Format 3 are presented in the Appendix.

Finite Element Model

The number of grid points and elements used in the five Orbiter substructures are shown in table 1. The fuselage shell structure was modeled using CQDMEM2 elements, a new element in NASTRAN but one that has been used widely at Grumman. It is essentially a quadrilateral that is composed of four triangles which have a common central node defined by the intersection of lines that connect the midpoints of the opposite sides of the quadrilateral. The four corner nodes need not lie in a plane. The fuselage U frames (see figures 4 and 5) and keel were idealized using CROD and CSHEAR elements. Here effective cap areas were calculated for the CROD elements to represent the appropriate bending behavior. CBAR elements with appropriate offsets were used to represent thin ring type frames such as the engine compartment closure frame (see figure 2).

The webs in the wing ribs and spars (see figures 6, 7, and 8) were idealized with CSHEAR elements. Again the effective rib and spar bending material was incorporated into CROD elements in the upper and lower covers. The covers themselves were represented by CQDMEM2 elements and some CTRMEM elements that occur at the leading edge. Intermediate node lines that lie between the spar and rib node lines were established to further refine the grid used in the covers. The geometry of these lines is essentially set by the location of fuselage frames.

The idealization of the fin follows closely the same scheme used in the wing (see figures 9 and 10).

The shell portion of the cargo bay door (figure 11) was idealized using CQDMEM2 elements with the exception of a few CQUAD2 elements that were required for local stability to provide an attachment point of the doors to the fuselage. The door frames were idealized as CSHEAR and CROD elements. Note that these frames contain two webs (figure 12), one common lower cap, and two upper caps that connected to the forward and aft shell segments. This allows the doors to "breath" in longitudinal direction.

Although provision was made for testing four payload configurations, the analysis included only one that represented the full up payload of 289 kN (65 000 lb). The stiffened box section payload was represented by a series of CBAR elements. The payload is shown mounted in the fuselage in figure 2.

The fluid in the LOX tank was represented by a network of four concentric fluid rings, 13 levels deep. The shell was idealized as CQUAD2 and CTRIA2 plates while the Y-ring was represented by CBAR elements. The shell was divided into $22\frac{1}{2}°$ segments in the circumferential direction and 17 stations in the meridional direction.

The aft portion of the external tank (figure 13) was modeled using CQUAD2 elements to represent the shell. Double frames exist at the forward and aft portions of the inter tank skirt and an additional longitudinal node line is picked up in this region to account for the SRB drag attachment and the stiffening that exists in the shell. Five heavy frames exist in the aft external tank; the first at STA 99.98 which is the forward tank/SRB interstage; the second at STA 148.756 which is the orbiter forward interstage; the third and fourth at stations 229.156 and 245.7536 which pick up the orbiter aft interstage fitting; and the fifth at station 270.988 which is the aft tank/SRB interstage.

These heavy frames have internal struts to provide additional stiffening to the interstage attachment points (figure 18). The remainder of the frames are light and are included to prevent shell buckling. In the prototype design, the real shell was stiffened in the longitudinal direction. In the model this stiffening plus the skin thickness was lumped to yield an effective thickness which was then scaled to the dimensions of the 1/8-scale model. This was done for the sake of economy in constructing the 1/8-scale model.

The solid rocket booster finite element idealization consists of CQUAD2 plate elements (containing membrane and bending properties) to represent the skin, straps, and plates; three-dimensional elements to represent the propellant; and offset bar elements to represent the frames and longerons. A NASTRAN generated plot of the outer shell is shown in figure 22 along with the frame stations. The thickness of the forward skirt varies from 1 to 6 mm (0.040 to 0.230 in.), the propellant cylinder thickness is 5 mm (0.1875 in.) and the aft skirt thickness is 2 mm (0.062 in.). The propellant is modeled by three layers (in the radial direction) of three-dimensional elements whose properties are $E^1 = 172.37\ MN/m^2$ (25×10^3 psi), $\nu = 0.49$, $\rho = 1716.15\ kg/m^3$ ($0.062\ lb/in^3$) and a structural damping factor $\beta = 0.52$ where $\beta = G''/G' = E''/E'$ ($E = E' + E^{11}$, $G = G' + G''$). The total weight of the structure and propellant is 11 kN (2520 lb).

ANALYTICAL RESULTS

Orbiter Component Analysis

The analysis of the separate components conducted as part of Phase 1 is used to establish confidence in the finite element models at that level. The NASTRAN generated weights were compared with those determined independently and discrepancies were rectified. The vibration eigenvalues and eigenvectors were calculated for the components restrained at their supports, or free, whichever seemed most applicable. These were examined and any departure from anticipated results was investigated. This check helped uncover problems in the way constraints were specified and some other data difficulties. The lowest frequency modes obtained during these component analyses were as follows:

Fuselage:			
Free, symmetric	62.2 Hz	129.9 Hz	
Free, antisymmetric	89.1 Hz	128.3 Hz	
Payload:			
Restrained, symmetric	81.2 Hz	268.5 Hz	627.7 Hz
Restrained, antisymmetric	68.6 Hz	175.4 Hz	462.8 Hz
Cargo doors:			
Free, symmetric	4.6 Hz	10.7 Hz	17.6 Hz
Restrained, antisymmetric	156.4 Hz	622.2 Hz	1054.6 Hz
Wing:			
Restrained	77.6 Hz	158.3 Hz	259.9 Hz
Fin:			
Restrained, symmetric	264.2 Hz	841.3 Hz	1263.3 Hz
Restrained, antisymmetric	107.8 Hz	407.2 Hz	1018.7 Hz

Total Orbiter Analysis

After the individual components were analyzed, the entire orbiter vehicle was coupled and a vibration analysis was performed in Rigid Format 3. PLOTEL elements were used to connect the grid points retained for plotting purposes. In order to examine the deformation more readily, both a side view and a bottom view were plotted for each mode. Only the latter includes the payload. The deformed shape was plotted together with the X, Y, and Z vectors from the underformed location. The first two elastic modes are shown in figures 23 to 26. The first mode at 53.0 Hz exhibits fuselage vertical bending, fin pitching, and wing motion. Wing motion appears to be due to flexibility in the root restraint and the deformed shape is almost a straight line. The maximum motion point is at the fin tip and results from pitching of the back part of the model. The second elastic mode at 62.6 Hz is principally wing bending with some payload and fuselage vertical bending.

Initial comparisons with test data indicate that there is more flexibility in the fin and wing attachment in the physical model than was allowed for in the analyses. The orbiter finite element model is readily adapted to exploring these effects and several runs were made varying the fin attachment. Results showed that the aft frame in the orbiter offers little stiffness to the aft fin spar in the vertical direction, but the forward frames are very significant. The first symmetric mode calculated with the forward frame vertical forces eliminated from the NASTRAN model is shown in figures 27 and 28. The frequency dropped from 53.0 to 48.0 and the relative deformation of the fin is easily noted.

LO_2 Tank Analysis

The full LO_2 tank model, with no omits, was analyzed for the zeroth and first harmonics only for the frequency range from 8 Hz to 135 Hz. This frequency range was selected to avoid calculating the slosh modes which were not considered significant in our analysis. The modes obtained can be most readily characterized by the variation in pressure.

SUMMARY OF HYDROELASTIC MODES

[1/8-scale LO_2 tank]

Frequency, Hz	Characteristic pressure pattern
Zeroth pressure harmonic (circumferential pressure = cos 0θ)	
22.9	No nodal surfaces
75.2	1 node at about midtank
91.5	2 nodes
115.2	3 nodes
First pressure harmonic (circumferential pressure = cos 1θ)	
19.2	No nodal surfaces
60.5	1 node
110	2 nodes
134.3	3 nodes

The corresponding grid point deformation for the original structural idealization indicated irregularities associated with the finite element model of the lower dome. Since the pressure gradations in the lower hydroelastic modes were relatively uniform, it appears suitable to investigate the effects of dome finite element size and geometry using static pressure loading to save computer time. The static loading produced deformations very similar to those in the fundamental hydroelastic modes. One modification attempted, the use of membrane elements in place of plate elements, gave no appreciable improvement. The original finite element grid was then refined by adding more elements, and the geometry was corrected. The resulting deformation pattern was considered acceptable. The current version of the tank dome finite element representation is shown in figure 29. Both the undeformed shape and the pattern under a uniform pressure of 6.9 kN/m^2 (1 psi) are shown.

External Tank Analysis

In assembling the external tank model, the LH_2 tank including the skirts at both ends was analyzed as an empty free shell. Vibration modes resulting from these computations indicated that above the first bending mode at 139.2 Hz, the modes of the central portion of the LH_2 tank in the areas of the light frames exhibited radial deformation typical of shell modes in cylinders.

An interesting comparison of the NASTRAN calculated weights and those determined independently by a weights engineer is as follows:

Tank weight as calculated from structural drawings, including fittings, fasteners, etc.	603.2 N	(135.6 lb)
Finite-element model weight (twice the half tank weight)	589.4 N	(132.5 lb)
c.g. position aft of forward dome as calculated by weights engineer	1.901 m	(75.14 in.)
c.g. position as calculated by NASTRAN for the finite element model	1.912 m	(75.29 in.)

The weight of the LH_2 is distributed as nonstructural mass in the CQUAD2 and CTRIA2 elements.

After the LH_2 tank model is checked, it is reduced and coupled with the LO_2 model. Analysis for this coupled structure has not yet been completed.

SRB Analysis

In order to obtain a guide for the finite element idealization of an empty tank, the SRB was modeled as a cylinder of radius 0.25 m (10 in.) and length 5.08 m (200 in.). The finite element idealization consisted of 21 bays along the length and 12 bays around the circumference. The following table represents a comparison of results between NASTRAN using the Givens method, Grumman's STARS-2V program, and NASA Langley's SRA program (refs. 3 and 4, respectively). The STARS-2V and SRA programs are based on thin-shell orthotropic theory. The accuracy of the NASTRAN results are relatively good for the lower modes and depend upon the relative complexity of the eigenvectors.

EMPTY CYLINDER VIBRATION ANALYSIS

Frequency, Hz			% Error
STARS-2V	SRA	NASTRAN (householder method)	
52.0 (n=2, 1st)	51.56 (n=2, 1st)	55.2	6
52.4 (n=2, 2nd)	51.66 (n=2, 2nd)	54.9	5
66.6 (n=2, 3rd)	66.04 (n=2, 3rd)	73.9	11
119.3 (n=1, 1st)	120.46 (n=1, 1st)	122.5	3
120.4 (n=2, 4th)	--	171.8	42
147.1 (n=3, 1st)	--	165.1	12

The undamped vibrational modes for the full cylinders are tabulated in the tables that follow. The modes of most interest are the 1st and 2nd bending modes and the longitudinal rod and thickness shear mode. Figures 30(a) and 30(b) show cross sectional views of the vibrational motion, and figures 31(a), 31(b), and 31(c) show orthographic views of the motion obtained from the NASTRAN analysis. The first table also includes the results for simple beam theory for the modes of interest (bending and longitudinal) based on the composite properties of the tank. Using a structural damping factor of 0.52 for the propellant elements, the complex eigenvalues for the lowest bending and longitudinal modes were obtained (Rigid Format 7) and compared with the undamped modes as tabulated in the second table. Simple beam theory (no shear) predicts a value of $1/Q = 0.028$, which agrees with the bending mode. The difference between this value and that for the longitudinal mode is due to the thickness shear effects. (See figure 30(b).) It was found that the damped vibrational analysis was run more efficiently by analyzing the undamped system first in order to narrow the search range. However, computer running times were still quite long.

VIBRATION ANALYSIS OF FULL PROPELLANT CYLINDER

Mode	Frequency, Hz	
	NASTRAN	Simple beam theory
n=1, m=1	56.4	58.4
n=0, torsion	171.4	
n=1, m=2	173.0	161.0
n=0, longitudinal	196.1	180.2

VIBRATION ANALYSIS USING DAMPED SOLID FINITE ELEMENTS

Mode	Frequency, Hz		Damping value, 1/Q (a)
	Undamped	Damped	
Bending - 1st	56.38	56.39	0.027
Longitudinal - 1st	196.0	197.1	.056

[a] $1/Q = \eta$ where η is the equivalent damping constant; c.f., Tong, Kin N.: Theory of Mechanical Vibrations. John Wiley & Sons, Inc., 1960, p. 15.

Total Vehicle Analysis

At the time of this writing, vibration analysis results for the completely coupled shuttle configuration were not available.

NASTRAN EXPERIENCES

Hydroelastic Analysis

Some difficulties were encountered in attempting to run the hydroelastic analysis. Before setting up the 1/8-scale model LO_2 tank, the program was run for a small problem containing 86 degrees of freedom in the analysis a-set. After this had been run successfully, the LO_2 tank which had 717 a-set degrees of freedom, was modeled and submitted for computation. A summary of the difficulties encountered [illegible] conducting the larger hydroelastic analysis are as follows:

(a) Hydroelastic problems will not run in Level 15-5 of NASTRAN. A system ØC1 error occurs while executing module GKAD. This error has been reported to NSMO and is listed as SPR [illegible].

(b) Often only a single Eigenvalue is extracted, using the Inverse Power Method, although more are present. This we now feel is a function of incorrect completion codes. This error is now listed as SPR 995.

(c) Fluid rings must be input in ascending order on RINGFL cards or program terminates with error No. 2001. This error has been reported to NSMO and is listed as SPR 1017.

(d) Fluid element identification numbers are limited in size to approximately 30 000 or less. Numbers greater than this cause a ØC5 system error in Module TA1. This error is now listed as SPR 1016.

(e) BAROR card causes fatal error in hydroelastic analysis. This error has been reported to NSMO.

(f) Data block M_{AA} is not pooled correctly in module SMP2 in Level 15.1. This causes fatal error 1105 if program is checkpointed. (Problem runs without checkpoint). This error has been reported to NSMO.

One continued difficulty was the large amount of computer running time required for the eigenvalue solutions in Rigid Format 7.

No information is available either in the literature or from NSMO regarding the reduction of the number of D.O.F. when using fluid elements in hydroelastic problem. And yet, if shuttle hydroelastic analyses are to be accomplished in moderate computer time then a major reduction seems advisable. In order to determine i[illegible]h a reduction is possible, a small hydroelastic problem was used. It was found that using the internally generated fluid point numbers on OMIT cards did not violate any NASTRAN rules and the program ran successfully to completion. These internal numbers may be calculated following the rules in the NASTRAN User's Manual or an unreduced problem may be run as far as GP4 with diagnostic 21 turned on.

A review of the frequencies shown in the following table indicates that the results are comparable for the lower frequency modes.

EFFECT OF REDUCING FLUID POINTS IN HYDROELASTIC ANALYSIS

[Simple 1/8-segment of hemispherical tank, total degrees of freedom = 154]

Mode	Frequency, hz	
	No omitted points analysis D.O.F. = 85	Omitted fluid points analysis D.O.F. = 77
1	283	292
2	421	436
3	536	544
4	606	698
5	697	797

SRB Analysis

For the empty propellant cylinder the inverse power method found erroneous roots and left out some roots. These roots were subsequently found using the Givens method and the erroneous roots did not appear. The Givens method generally did not work for large problems on level 15.5 but did work on level 15.1. The damped vibrational analysis, using Rigid Format 7, gave a fatal error message after finding the eigenvalues. The eigenvalue running times tended to be long (1000 CPU seconds on an IBM 370/165 for 176 reduced D.O.F. using the DFT method). These errors did not occur for very small prototype problems. Other difficulties that were encountered included erroneous fatal messages; for example, a U602 message was encountered for a singular matrix. These errors also seemed to be a function of the large size problems under consideration.

Orbiter Coupling Analysis

Once the DMAP alters were debugged, essentially no major problems were encountered as far as obtaining results for the orbiter. The incorporated checks and plots proved to be major aides in "debugging" the input data to Phase 1. Experience with the various alters is listed below:

(1) Incorporating the rigid body checks in phase 1 is essential in determining if there are any erroneous constraints in the substructures.

(2) If the rigid body check is not satisfactory and the erroneous constraint is limitted to a single constraint, then printing the reduced rigid body support stiffness $[X]$ and obtaining from it the resultants of the rigid body forces helps in locating the coordinates of the erroneous constraint.

(3) If the trouble is caused by MPC's then the resultants of the m-set loads helps in locating MPC errors.

(4) If MPC's and SPC's are in error, mode plots are helpful in locating erroneous SPC's and sometimes MPC's.

(5) If free-free modes are obtained, then printing the member forces and/or SPC forces for the rigid body modes may help in locating the erroneous constraint since the structure should be free of stress.

(6) Mode plots in phase 1 have helped in determining whether the appropriate nodes have been selected as dynamic degrees of freedom. In some cases "soft spots" were accidentally selected for the a-set and these caused local motions to show up in the mode plots.

In order to obtain plots in the coupling run (phase 2) it is suggested that grid points rather than scalar points be used in the coupling phase. PLOTEL elements were then used to connect the grid points creating a pseudostructure that is suitable for plotting. The grid points established in phase 2 were the grid points that are associated with the substructure a-set degrees of freedom. All non-strainable D.O.F. were removed by SPC's. It should be noted that each substructure had a unique grid point numbering system so that the grid cards in the a-set of each substructure could be duplicated and incorporated in phase 2. Common interface points were made common by MPC's.

If necessary the a-set of a given substructure was increased so that a more realistic plot could be obtained. This also necessitated having x, y, and z D.O.F. at all points to be plotted so that all significant motion is displayed.

To prevent loss of mass, it is recommended that mass should not be assigned to grid points having nonstrainable D.O.F., such as, intermediate grid points in a planar frame. If assigning mass to such nodes is necessary, then MPC's should be used instead of SPC's to remove the singularity from the stiffness matrix; this will conserve the total mass distribution.

System Experience

One of the fallouts of our analysis of the 1/8-scale model has been a further evaluation and demonstration of the program that is scheduled to eventually replace our own in-house system. Partly as a result of this work, we believe that NASTRAN is ready to handle the analysis of large aerospace vehicles such as the shuttle. We would like to point out, however, some additional features associated with NASTRAN which must be given consideration.

(1) The learning curve for NASTRAN is rather flat. If you want to be in a position of making extensive alters to the rigid formats, and any aerospace company faced with large complex problems must be in this position, then the investment in learning time is large. Future levels of NASTRAN should concentrate on building a system that is more easily altered. We feel that it is far more important to devote NASTRAN funds to developing a sound basic system than to adding capability for solving specialized problems.

(2) Our in-house developed postprocessor for converting selected NASTRAN element corner forces, for example, membrane elements and rod-shear panel assemblies, has been completed (available from level 15.5). Although not used on the 1/8-scale model analysis this program is a necessity if we are to obtain internal member loads in a form required by our designers.

(3) Experience in running large problems in NASTRAN should be established prior to actual run submissions. Adequate time should be provided for difficulties encountered the first few times a new problem is run. The availability of experienced computer systems analysts capable of assisting in such difficulties helps materially in expediting NASTRAN analyses.

ACKNOWLEDGEMENT

We would like to thank the members of the Vibration Section, Structures and Dynamics Division, Langley Research Center, for their guidance and assistance in the work described herein.

REFERENCES

1. Grumman Aerospace Corp.: Design of a Space Shuttle Structural Dynamics Model. NASA CR-112205, [1973].

2. Grumman Aerospace Corp.: Preliminary Shuttle Structural Dynamics Modelin Design Study. NASA CR-112196, Nov. 1972.

3. Svalbonas, V.: Numerical Analysis of Stiffened Shells of Revolution - Theory Manual for STARS-2S, -2B, -2V Programs. IOM 000-STMECH-038, Grumman Aerospace Corp., May 10, 1973.

4. Cohen, Gerald A.: User Document for Computer Programs for Ring-Stiffened Shells of Revolution. NASA CR-2086, 1973.

APPENDIX

NASTRAN SUBSTRUCTURING ANALYSIS FOR NORMAL MODES

ALTERED RIGID FORMAT 3 FOR PHASE 1 OR 2

Incorporated New Bulk Parameters

(1)	NOSUB	Number of substructures to be coupled in this run. Default = 1, which indicates a phase 1 run, where one substructure will be reduced.
(2)	TPCOPY≥0	Will put reduced stiffness and mass matrix (Kaa & Maa) on tape INPT. Default = -1
(3)	TPNAME	Label name of INPT. Use only when TPCOPY≥0
(4)	RMODE≥0	Causes restrained free modes to be obtained. The restraints are defined in an input column partition matrix {CPAJC}, which will partition the a-set into J & C sets. Default = -1. In this case free-free modes will be obtained if there is a SUPORT card in the BULK data, defining the rigid body supports. Although {CPAJC} is not used when RMODE = -1, it must be defined in the BULK data. It is sufficient to define it as a 1 × 1 matrix. Also, don't forget the EIGR card if modes are to be obtained.
(5)	TPNAME9	Label name of INP9, which contains the column partition vector, reduced stiffness, and mass for each reduced substructure. The column partition vectors are used to merge the reduced stiffness and mass of each reduced substructure into a common pseudostructure lineup. Use this parameter only when NOSUB>1.
(6)	TPCOPYN≥0	Will put the pseudostructure eigenvalues and eigenvectors in substructure lineups on tape (INP1, INP2, etc.) for further processing, in this case final substructure mode shapes. Default = -1.
(7)	TPNAMEN	Common label name of INP1, INP2, etc. Use only when TPCOPYN≥0.

Incorporated New Bulk Input Matrices

The following input matrices must be defined in the BULK data on DMI cards whether they are needed or not. If they are not needed, defining them as a 1 × 1 matrix will suffice.

(1) EQR Matrix

This matrix expresses the resultants about an origin, due to unit rigid body support loads. The rigid body degrees of freedom are defined on the standard NASTRAN SUPORT card. The EQR matrix is necessary if the checks, which are incorporated in the ALTERS, are to be performed. The origin chosen, should be the same origin defined on the standard GRDPNT parameter card.

(2) CPAJC Matrix

This matrix is used when restrained-free modes are to be obtained (RMODE=1). This matrix is a column partitioning vector which defines the restrained degrees of freedom from the analysis set (a-set) degrees of freedom.

IMPORTANT NOTE:

When doing a coupling run, where all substructures have been reduced and on tape, it was necessary to input in the BULK data at least one element, to prevent a fatal error in module TA1. A thin, string-like rod will suffice. The element must be counted as a substructure so that the new NOSUB parameter was increased by one.

Alters Incorporated (General Flow)

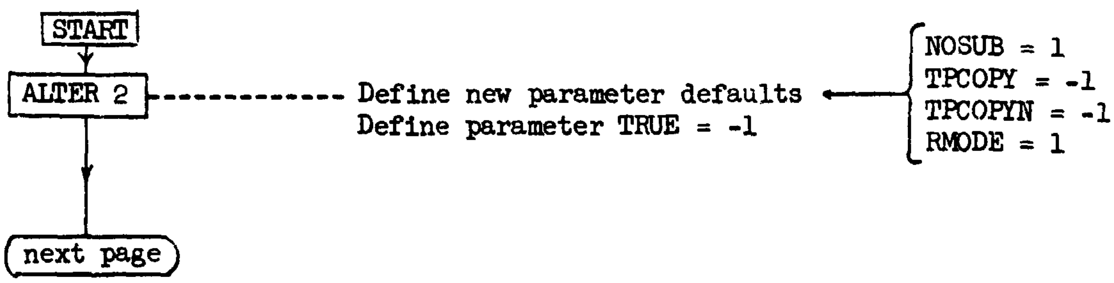

ALTER 23, 23 Page 193	Delete original error (possible not to have structural elements in BULK for coupling run). Also defines coupling parameter and other parameters and performs appropriate purges.
ALTER 24	Insert LABEL L24 (referenced in ALTER 23, 23)
ALTER 25	Insert COND L27, NOSIMP (Skips generation of stiffness Kggx if no structural elements)
ALTER 27	Insert LABEL L27 (referenced in ALTER 25)
ALTER 29	Insert { COND L29, COUPLE JUMP L30 LABEL L29 } Possible not to have mass in BULK for coupling run.
ALTER 30	Insert LABEL L30 (referenced in ALTER 30)
ALTER 37, 37 Page 195	If this is a coupling run (phase 2), this alter will read in reduced substructure matrices from tape and merge them into pseudostructure g-lineup. The combined stiffness and mass are then added to the unreduced substructure stiffness and mass (if any).
ALTER 40,40	Change input Kggx to Kggy in SMA3 module (Kggy includes reduced substructure stiffnesses, if any)
ALTER 48, 48	Change Mgg to Mggy in EQUIV statement. Mggy includes reduced substructure masses, if any. Also changes the mass matrix Mgg to a weight matrix and prints it out (Wgg = Mgg × 386.4)
ALTER 49	Insert { COND L49, COUPLE JUMP LBL4 LABEL L49 } Skips GPSP module if a coupling run
ALTER 58, 58	Change Mgg to Mggy in MCE2 Module (Mggy includes any reduced substructure mass if any.)

Next Page

ALTER 74 ------------ SEEMAT KAA, MAA (pictoral view to see if there are zeros on diagonal

ALTER 84
Page 197
---------- This package can be considered a quality control module. It generates checks to ensure that there are no errant constraints and no mass has been lost. See detailed flow. This alter also puts the reduced stiffness and mass on tape provided the parameter TPCOPY is not less than zero.

ALTER 89, 89
Page 201
-------- Obtains restrained free modes (fixed at interface) or directs flow to obtain free-free modes.

ALTER 91, 91 -------- Change MI to MM in original statement

ALTER 93 ---------- Insert LABEL L93 (referenced in ALTER 89, 89)

ALTER 112
Page 202
---------- If a coupling run (phase 3), this alter extracts out eigenvalues and eigenvectors for each reduced substructure and puts them on separate tapes. These tapes can then be used in a PHASE 3 run to obtain detailed substructure mode shapes.

END ALTER

ALTER 23,23 DETAILED FLOW

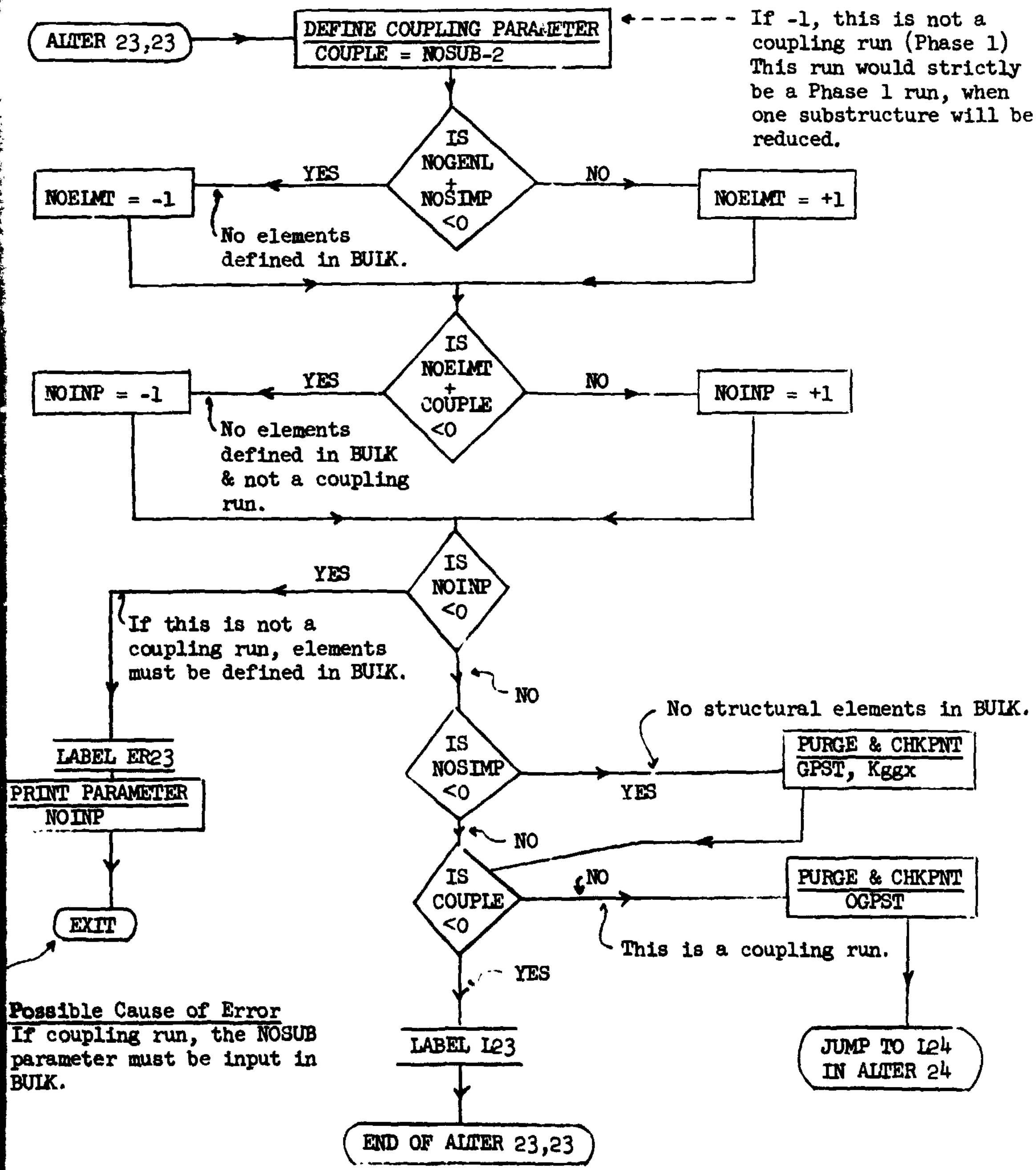

ALTER 37, 37 DETAILED FLOW

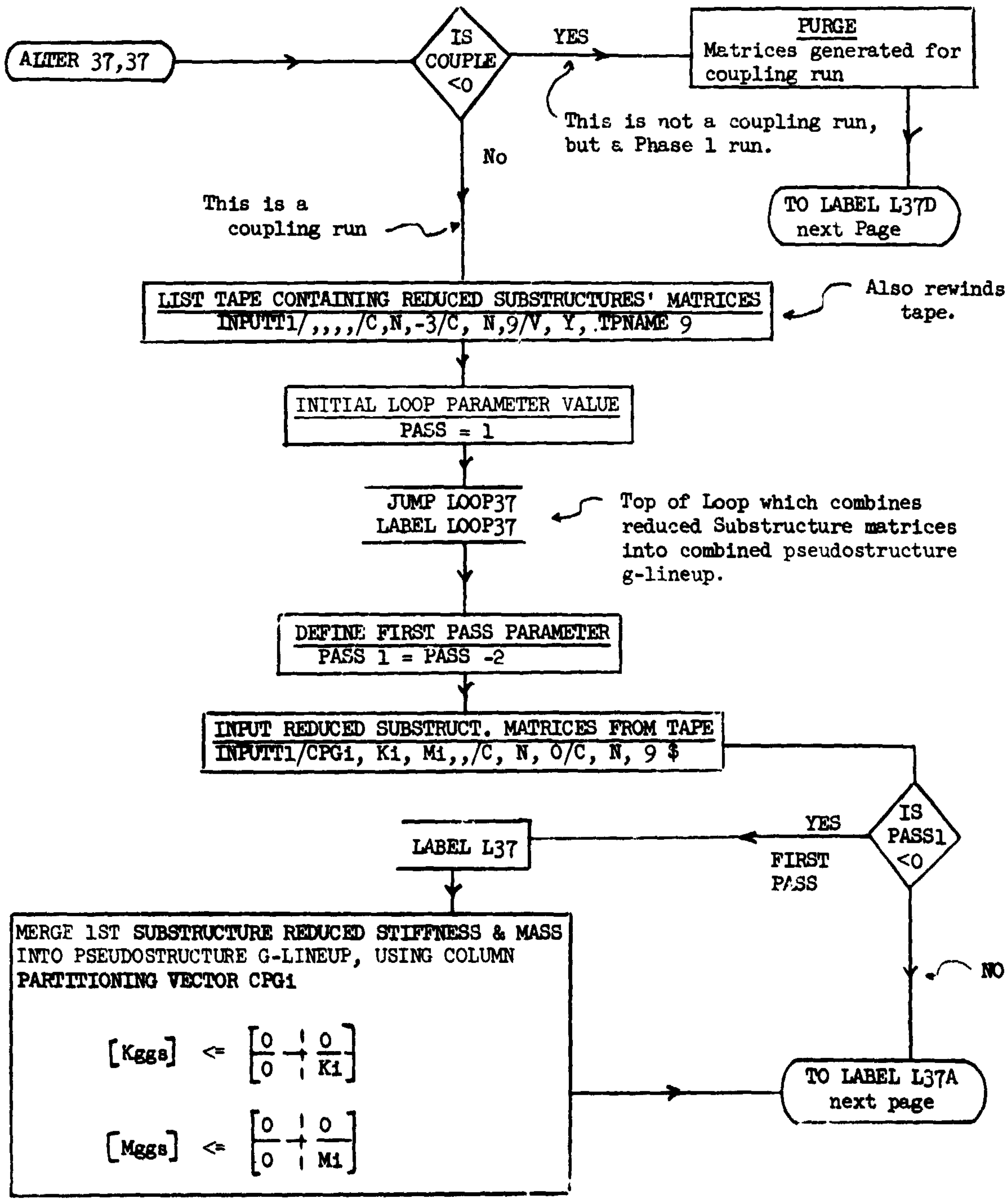

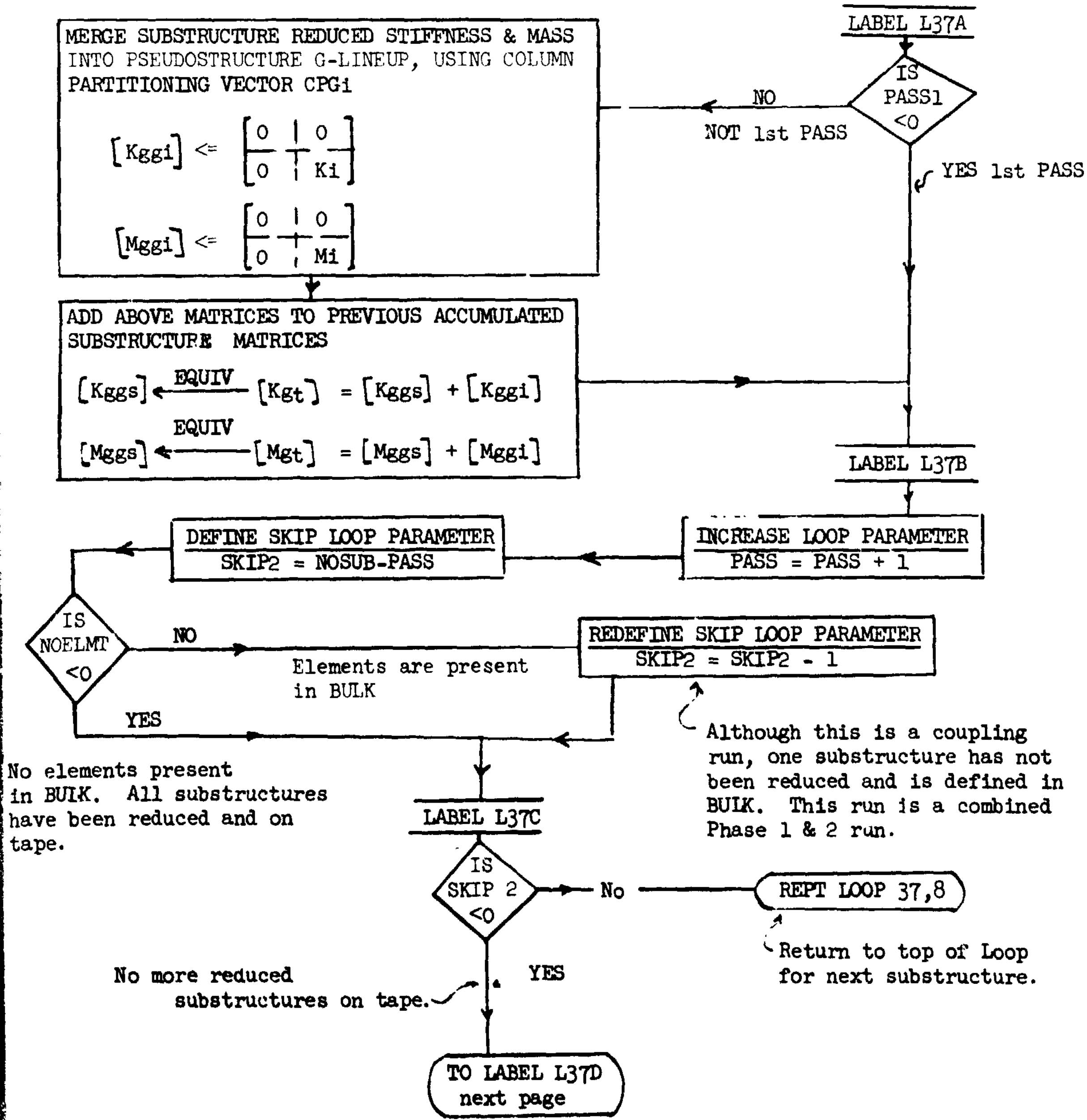
LABEL L37A
IS PASS1 <0
NO
NOT 1st PASS
YES 1st PASS
MERGE SUBSTRUCTURE REDUCED STIFFNESS & MASS INTO PSEUDOSTRUCTURE G-LINEUP, USING COLUMN PARTITIONING VECTOR CPGi
[Kggi] <= [0 | 0 / 0 | Ki]
[Mggi] <= [0 | 0 / 0 | Mi]
ADD ABOVE MATRICES TO PREVIOUS ACCUMULATED SUBSTRUCTURE MATRICES
[Kggs] ← EQUIV — [Kgt] = [Kggs] + [Kggi]
[Mggs] ← EQUIV — [Mgt] = [Mggs] + [Mggi]
LABEL L37B
INCREASE LOOP PARAMETER
PASS = PASS + 1
DEFINE SKIP LOOP PARAMETER
SKIP2 = NOSUB-PASS
IS NOELMT <0
NO
Elements are present in BULK
REDEFINE SKIP LOOP PARAMETER
SKIP2 = SKIP2 - 1
Although this is a coupling run, one substructure has not been reduced and is defined in BULK. This run is a combined Phase 1 & 2 run.
YES
No elements present in BULK. All substructures have been reduced and on tape.
LABEL L37C
IS SKIP 2 <0
No
REPT LOOP 37,8
Return to top of Loop for next substructure.
YES
No more reduced substructures on tape.
TO LABEL L37D next page

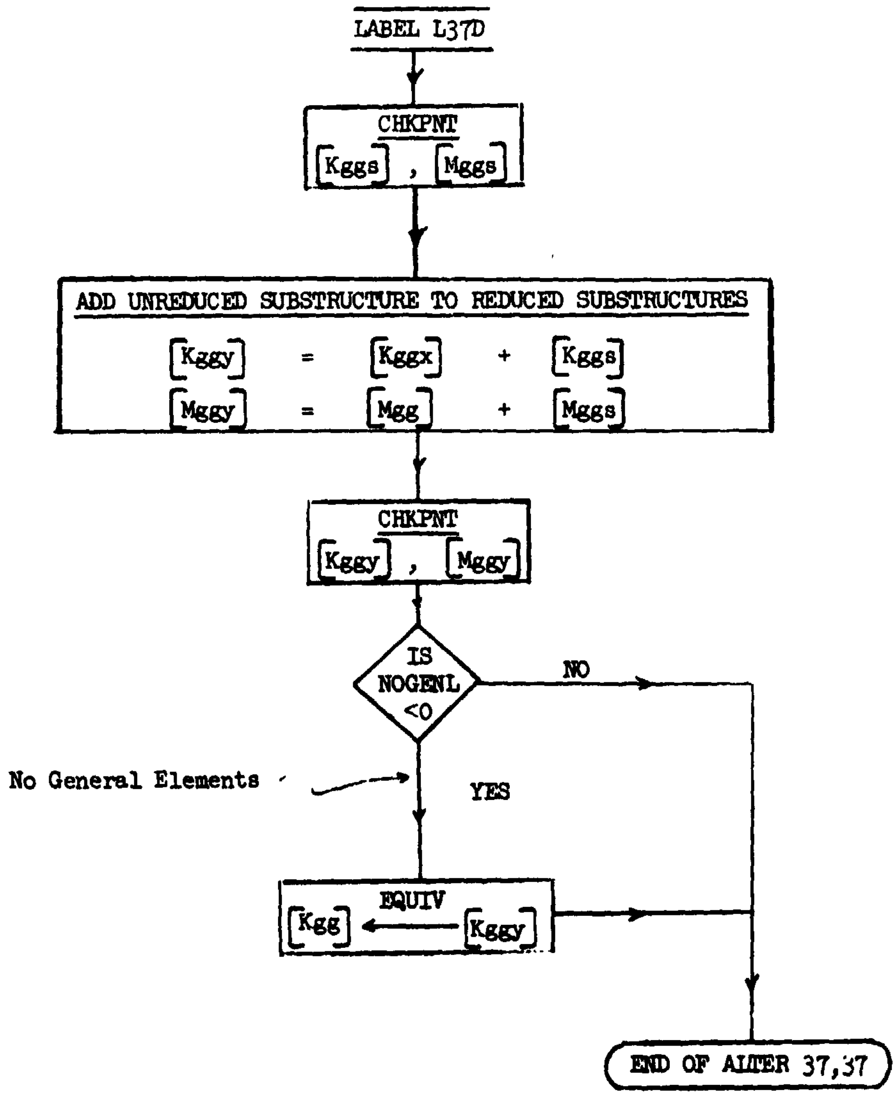

LABEL L37D
CHKPNT
[Kggs] , [Mggs]
ADD UNREDUCED SUBSTRUCTURE TO REDUCED SUBSTRUCTURES
[Kggy] = [Kggx] + [Kggs]
[Mggy] = [Mgg] + [Mggs]
CHKPNT
[Kggy] , [Mggy]
IS NOGENL <0
NO
No General Elements
YES
EQUIV
[Kgg] [Kggy]
END OF ALTER 37,37

ALTER 84 DETAILED FLOW

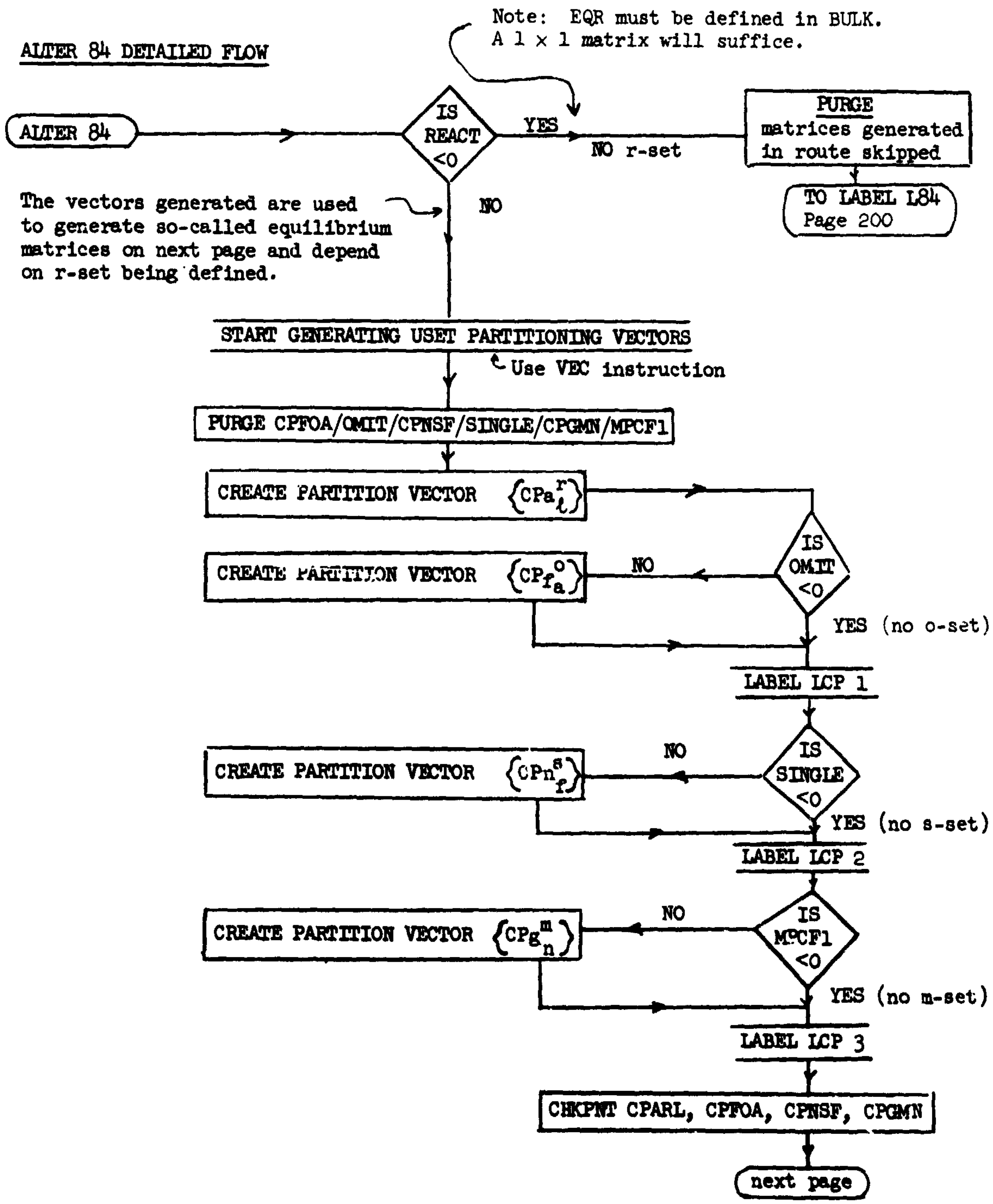

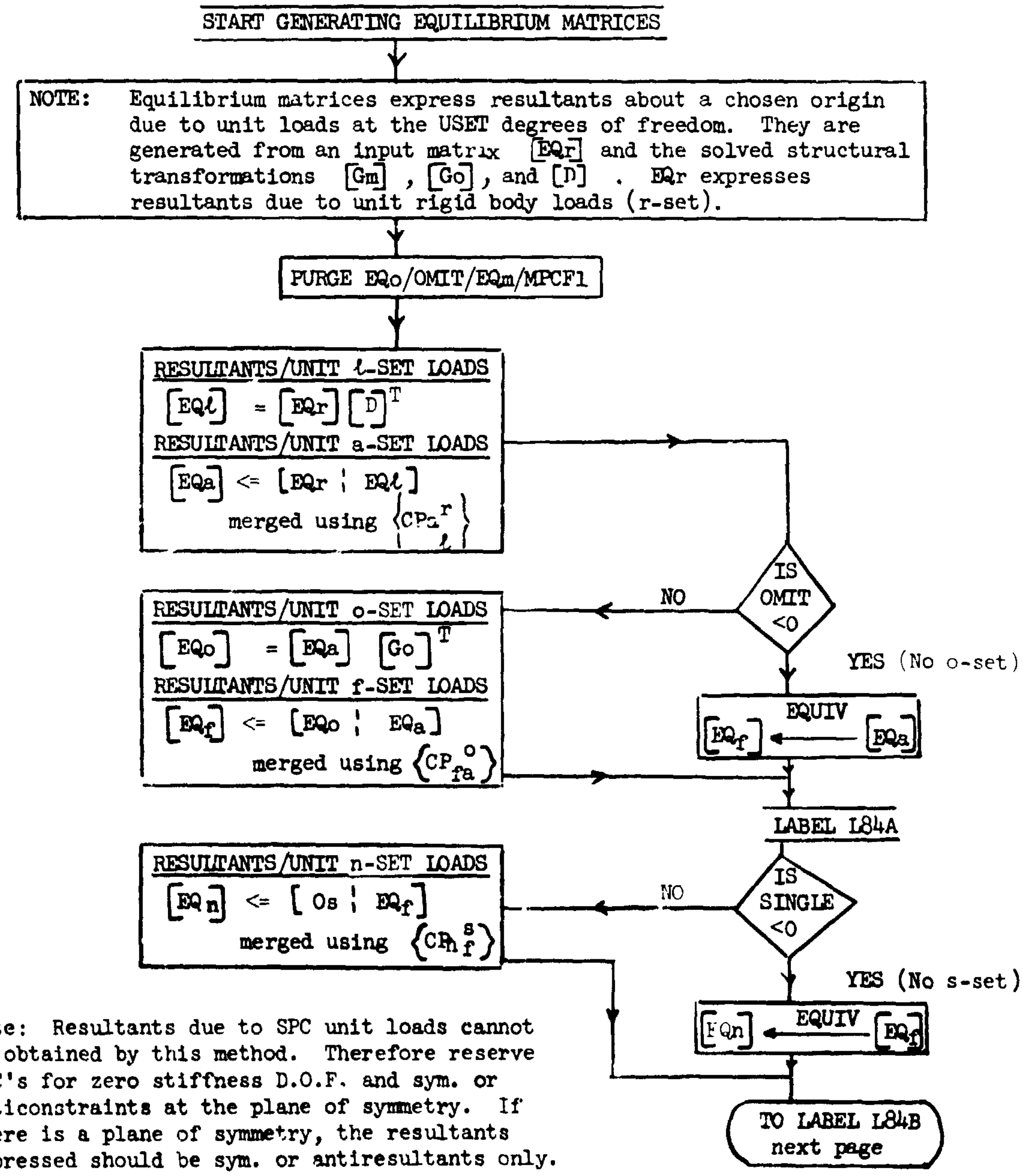

Note: Resultants due to SPC unit loads cannot be obtained by this method. Therefore reserve SPC's for zero stiffness D.O.F. and sym. or anticonstraints at the plane of symmetry. If there is a plane of symmetry, the resultants expressed should be sym. or antiresultants only.

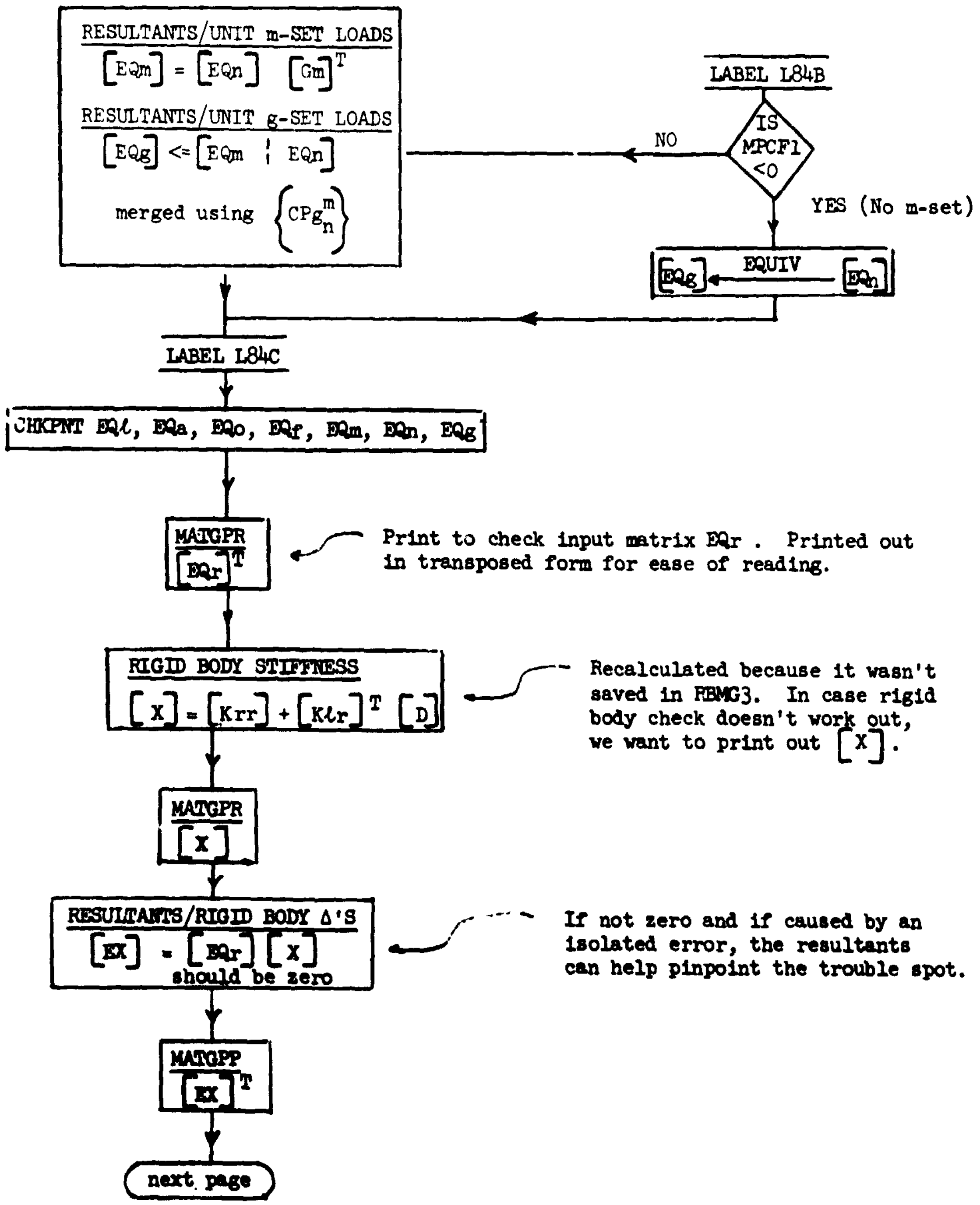
RESULTANTS/UNIT m-SET LOADS
[EQm] = [EQn] [Gm]T
RESULTANTS/UNIT g-SET LOADS
[EQg] <= [EQm ¦ EQn]
merged using {CPg m n}
LABEL L84B
IS MPCF1 <0
NO
YES (No m-set)
EQUIV
[EQg] [EQn]
LABEL L84C
CHKPNT EQℓ, EQa, EQo, EQf, EQm, EQn, EQg
MATGPR
[EQr]T
Print to check input matrix EQr . Printed out in transposed form for ease of reading.
RIGID BODY STIFFNESS
[X] = [Krr] + [Kℓr]T [D]
Recalculated because it wasn't saved in RBMG3. In case rigid body check doesn't work out, we want to print out [X].
MATGPR
[X]
RESULTANTS/RIGID BODY Δ'S
[EX] = [EQr] [X]
should be zero
If not zero and if caused by an isolated error, the resultants can help pinpoint the trouble spot.
MATGPR
[EX]T
next page

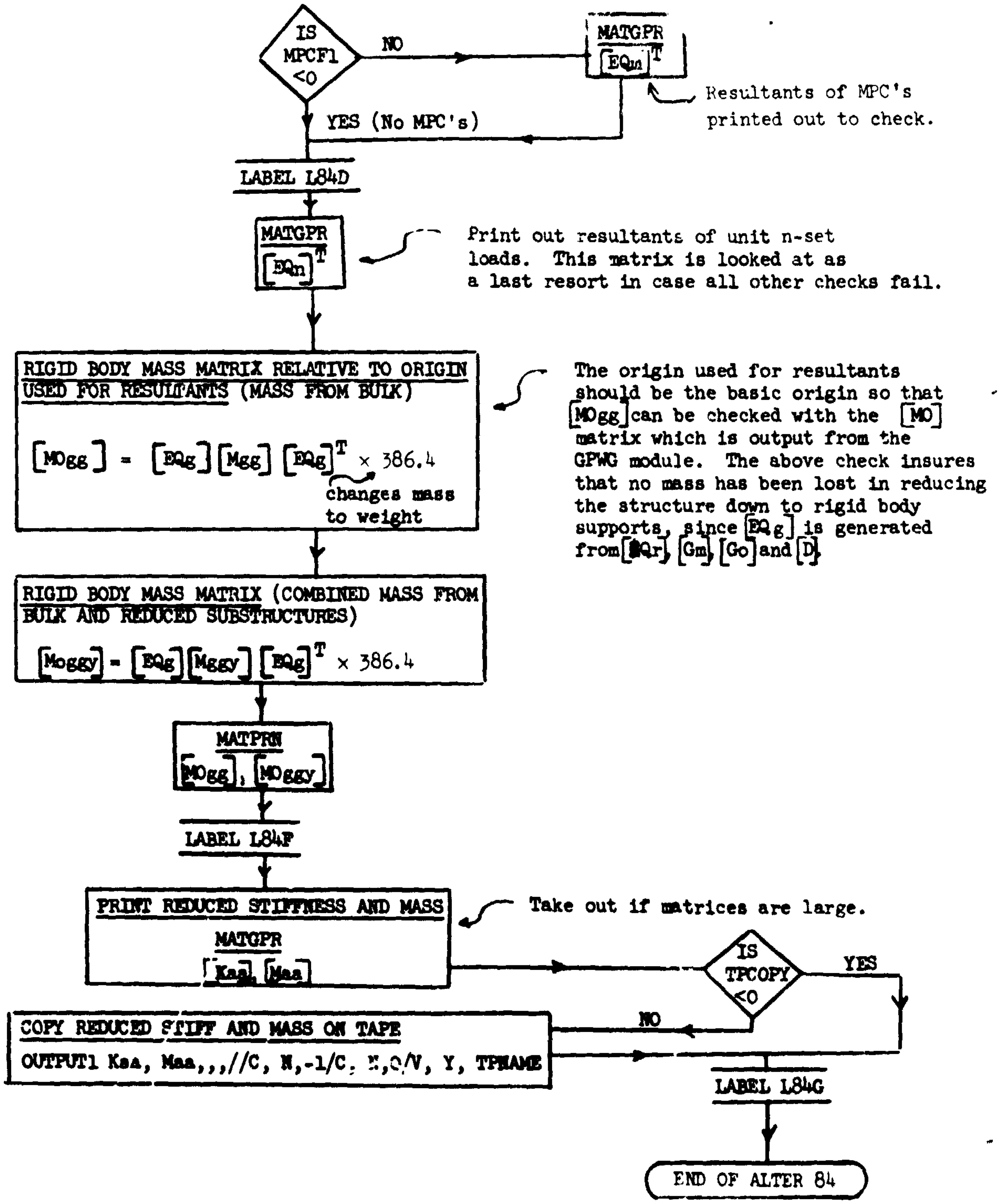
IS MPCF1 <0
NO
MATGPR
[EQm]^T
Resultants of MPC's printed out to check.
YES (No MPC's)
LABEL L84D
MATGPR
[EQn]^T
Print out resultants of unit n-set loads. This matrix is looked at as a last resort in case all other checks fail.
RIGID BODY MASS MATRIX RELATIVE TO ORIGIN USED FOR RESULTANTS (MASS FROM BULK)
[MOgg] = [EQg] [Mgg] [EQg]^T × 386.4
changes mass to weight
The origin used for resultants should be the basic origin so that [MOgg] can be checked with the [MO] matrix which is output from the GPWG module. The above check insures that no mass has been lost in reducing the structure down to rigid body supports, since [EQg] is generated from [EQr], [Gm], [Go] and [D].
RIGID BODY MASS MATRIX (COMBINED MASS FROM BULK AND REDUCED SUBSTRUCTURES)
[MOggy] = [EQg] [Mggy] [EQg]^T × 386.4
MATPRN
[MOgg], [MOggy]
LABEL L84F
PRINT REDUCED STIFFNESS AND MASS
MATGPR
[Kaa], [Maa]
Take out if matrices are large.
IS TPCOPY <0
YES
NO
COPY REDUCED STIFF AND MASS ON TAPE
OUTPUT1 Kaa, Maa,,,//C, N,-1/C, N,0/V, Y, TPNAME
LABEL L84G
END OF ALTER 84

ALTER 89,89 DETAILED FLOW

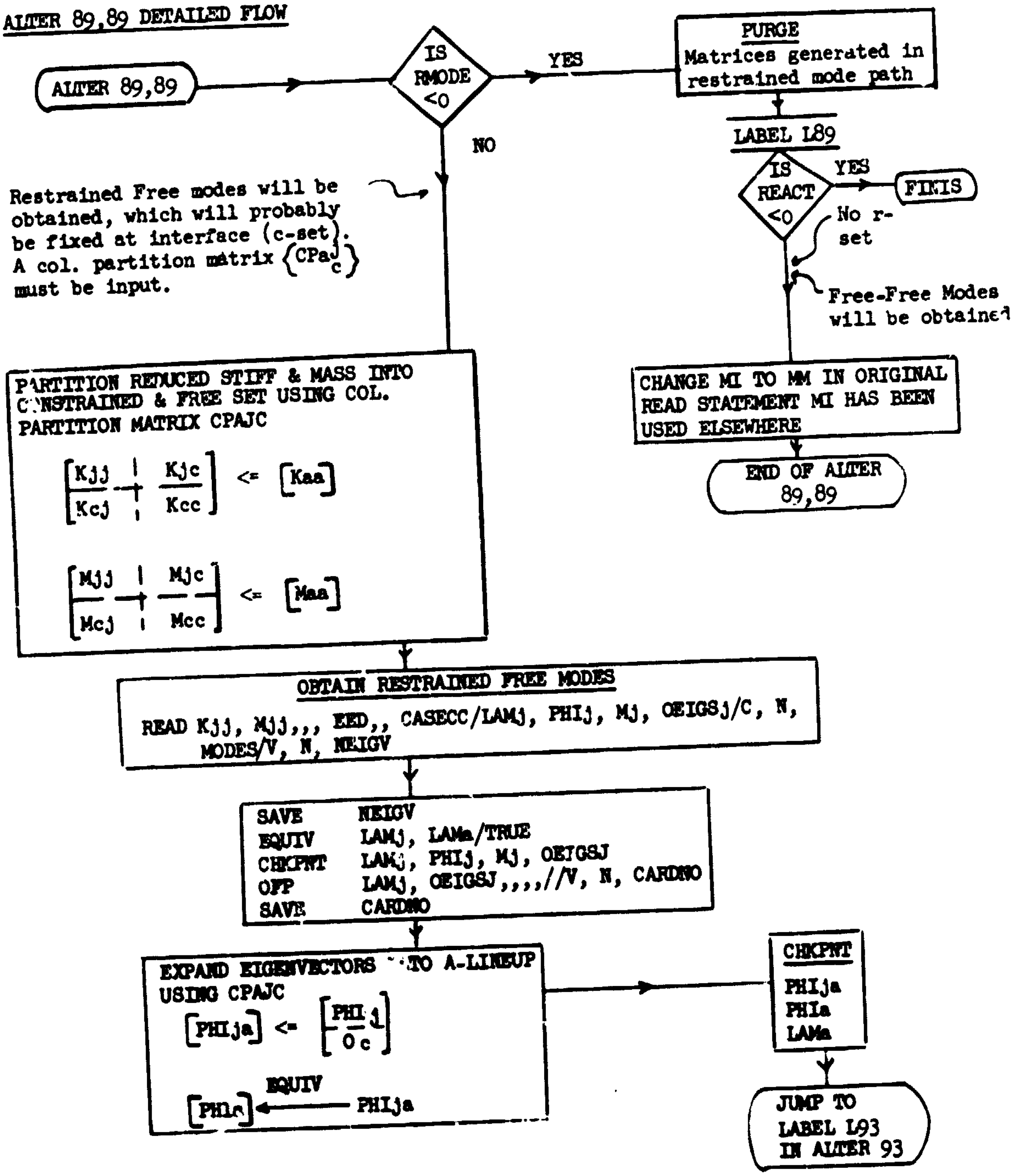

ALTER 112 DETAILED FLOW

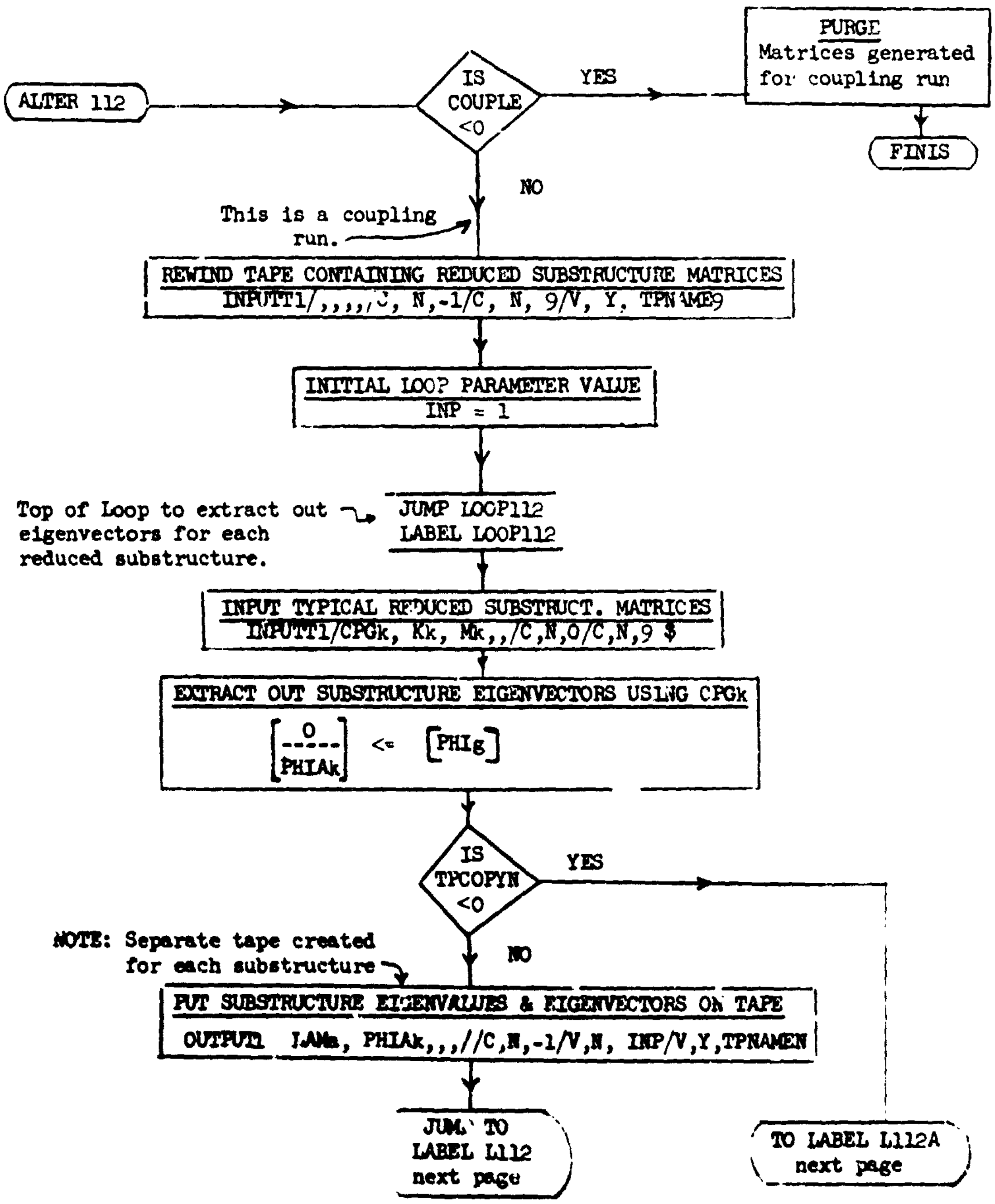

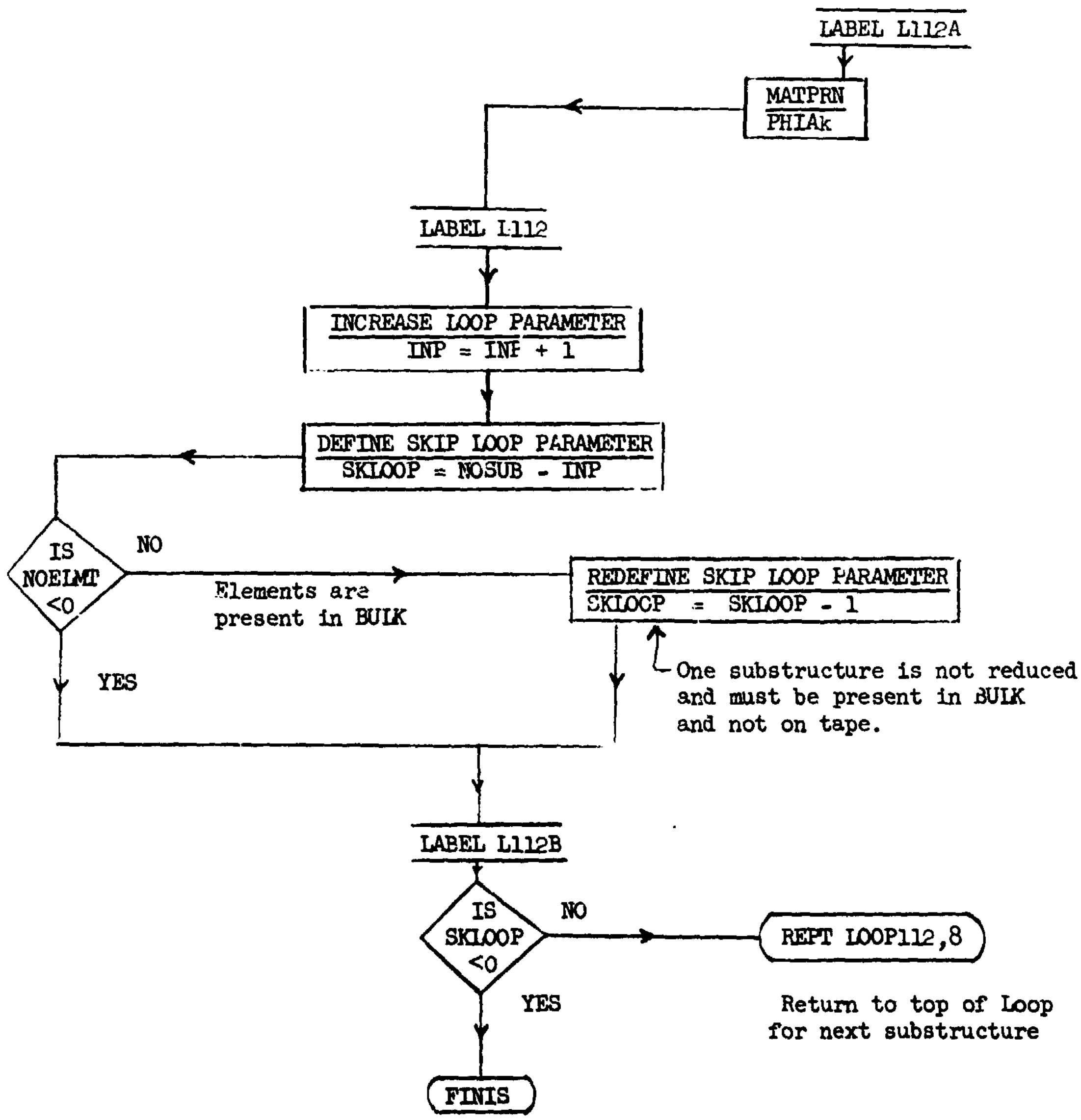
LABEL L112A
MATPRN
PHIAk
LABEL L112
INCREASE LOOP PARAMETER
INP = INP + 1
DEFINE SKIP LOOP PARAMETER
SKLOOP = NOSUB - INP
IS NOELMT <0
NO
Elements are present in BULK
REDEFINE SKIP LOOP PARAMETER
SKLOOP = SKLOOP - 1
One substructure is not reduced and must be present in BULK and not on tape.
YES
LABEL L112B
IS SKLOOP <0
NO
REPT LOOP112,8
Return to top of Loop for next substructure
YES
FINIS

N A S T R A N   E X E C U T I V E   C O N T R O L   D E C K   E C H O

```
ID PHASE2 DPBTSR1
APP        DISP
TIME       30
CHKPNT   YES
SOL        3,0
DIAG     7,8,13,14,19,21,22
ALTER  2    $ PARAMETER DEFAULTS
PARAM    //C,N,NOP/V,Y,NOSUB=1
PARAM    //C,N,NOP/V,Y,TPCOPY=-1
PARAM    //C,N,NOP/V,Y,TPCOPYN=-1
PARAM    //C,N,NOP/V,Y,PMODE=-1
PARAM    //C,N,NOP/V,N,TRUE=-1
$
ALTER 23,23 $ DETERMINES COUPLING PARAMETER & PERFORMS PURGES
PARAM    //C,N,SUB/V,N,COUPLE/V,Y,NOSUB/C,N,2 $
PARAM    //C,N,AND/V,N,NOELMT/V,N,NOGENL/V,N,NOSIMP $
PARAM    //C,N,AND/V,N,NOINP/V,N,NOELMT/V,N,COUPLE $
COND     ER23,NOINP $ WILL EXIT IF NOT A COUPLING RUN & NO ELEMENTS
PURGE    GPST,KGGX/NOSIMP
CHKPNT   GPST,KGGX
COND     L23,COUPLE
PURGE    OGPST/TRUE
JUMP     L24
LABEL    ER23
PRTPARM //C,N,0/C,N,NOINP $
EXIT
LABEL    L23
$
ALTER 24
LABEL    L24
ALTER 25
COND     L27,NOSIMP
ALTER 27
LABEL    L27
ALTER 29
COND     L29,COUPLE
JUMP     L30
LABEL    L29
ALTER 30
LABEL    L30
$
ALTER 37,37 $ IF COUPLING RUN,COMBINES SUBSTRUCTURES.
$             THE FOLLOWING MATRICES FOR EACH SUBSTRUCT. ASSUMED ON INP9
$             CPGI = COLUMN PARTITIONG VECTOR FOR MERGING KI & MI
$             KI & MI = REDUCED STIFFNESS & MASS
PURGE    CPGI,KI,MI,KGGI,MGGI,KGGS,MGGS,KGT,MGT/COUPLE
COND     L370,COUPLE  $ SKIP,NOT A COUPLING RUN
INPUTT1 /,,,,/C,N,-3/C,N,9/V,Y,TPNAME9 $ LIST TAPE & REWIND
PARAM    //C,N,NOP/V,N,PASS=1  $ INITIAL LOOP PASS PARAMETER
```

N A S T R A N   E X E C U T I V E   C O N T R O L   D E C K   E C H O

```
JUMP     LOOP37
LABEL    LOOP37  $ TOP OF LOOP
PARAM    //C,N,SUB/V,N,PASS1/V,N,PASS/C,N,2
INPUTT1  /CPGI,KI,MI,,/C,N,0/C,N,9 $
COND     L37,PASS1   $ SKIP TO L37 IF FIRST PASS
JUMP     L37A
LABEL    L37
MERGE,   ,,,KI,CPGI,/KGGS/C,N,-1/C,N,2/C,N,6
MERGE,   ,,,MI,CPGI,/MGGS/C,N,-1/C,N,2/C,N,6
LABEL    L37A
COND     L37B,PASS1   $ SKIP TO L37B IF FIRST PASS
MERGE,   ,,,KI,CPGI,/KGGI/C,N,-1/C,N,2/C,N,6
MERGE,   ,,,MI,CPGI,/MGGI/C,N,-1/C,N,2/C,N,6
ADD      KGGS,KGGI/KGT $
EQUIV    KGT,KGGS/TRUE
ADD      MGGS,MGGI/MGT $
EQUIV    MGT,MGGS/TRUE
LABEL    L37B
PARAM    //C,N,ADD/V,N,PASS/V,N,PASS/C,N,1
PARAM    //C,N,SUB/V,N,SKIP2/V,Y,NOSUB/V,N,PASS
COND     L37C,NOELMT
PARAM    //C,N,SUB/V,N,SKIP2/V,N,SKIP2/C,N,1
LABEL    L37C
COND     L37D,SKIP2
REPT     LOOP37,8
LABEL    L37D
CHKPNT   KGGS,MGGS
ADD      KGGX,KGGS/KGGY $
ADD      MGG,MGGS/MGGY $
CHKPNT   KGGY,MGGY
EQUIV    KGGY,KGG/NOGENL $
$
ALTER 40,40
SMA3     GEI,KGGY/KGG/V,N,LUSET/V,N,NOGENL/V,N,NOSIMP
ALTER 48,48
ADD      MGG,/MGG/C,Y,ALPHA=(386.4,0.0) $
MATGPR   GPL,USET,SIL,MGG//C,N,G
EQUIV    KGG,KNN/MPCF1/MGGY,MNN/MPCF1
ALTER 49
COND      L49,COUPLE
JUMP     LBL4
LABEL    L49
ALTER 58,58
MCE2     USET,GM,KGG,MGGY,,/KNN,MNN,, $
ALTER 74
SEEMAT KAA,MAA,,,//C,N,PRINT
$
ALTER   84
PURGE    CPARL,CPFDA,CPNSF,CPGMN,EQR,EQL,EQA,EQC,EQF,EGN,EQM,EQG/REACT
PURGE  EX,EXT,EIMT,FONT,EQGT,EQGTC,MOGG,MOGGY/REACT
```

```
COND     L84F,REACT   $ R-SET MUST BE DEFINED TO GENERATE EQG
PURGE    CPFOA/OMIT/CONSF/SINGLE/CPGMN/MPCF1
VEC      USET/CPARL/C,N,A/C,N,F/C,N,L $
COND     LCP1,OMIT
VEC      USET/CPFOA/C,N,F/C,N,O/C,N,A $
LABEL    LCP1
COND     LCP2,SINGLE
VEC      USET/CONSF/C,N,N/C,N,S/C,N,F $
LABEL    LCP2
COND     LCP3,MPCF1
VEC      USET/CPGMN/C,N,G/C,N,M/C,N,N $
LABEL    LCP3
CHKPNT   CPFOA,CONSF,CPGMN,CPARL
PURGE    EQO/OMIT/EQM/MPCF1
TRNSP    DM/DMT
MPYAD    EQR,DMT,/EQL/C,N,0/C,N,1/C,N,0
MERGE    EQR,,EQL,,CPARL,/EQA/C,N,1/C,N,2/C,N,2
EQUIV    EQA,EQF/OMIT
COND     L84A,OMIT
TRNSP    GO/GOT
MPYAD    EQA,GOT,/EQO/C,N,0/C,N,1/C,N,0
MERGE    EQO,,EQA,,CPFOA,/EQF/C,N,1/C,N,2/C,N,2
LABEL    L84A
EQUIV    EQF,EQN/SINGLE
COND     L84B,SINGLE
MERGE,   ,,EQF,,CONSF,/EQN/C,N,1/C,N,2/C,N,2
LABEL    L84B
EQUIV    EQN,EQG/MPCF1
COND     L84C,MPCF1
TRNSP    GM/GMT
MPYAD    EQN,GMT,/EQM/C,N,0/C,N,1/C,N,0
MERGE    EQM,,EQN,,CPGMN,/EQG/C,N,1/C,N,2/C,N,2
LABEL    L84C
CHKPNT   EQL,EQA,EQO,EQF,EQN,EQM,EQG
TRNSP    EQR/EQRT
MATGPR   GPL,USET,SIL,EQRT//C,N,R
MPYAD    KLR,DM,KRR/K/C,N,1 $
MATGPR   GPL,USET,SIL,X//C,N,R
MPYAD    EQR,X,/EX/C,N,0/C,N,1/C,N,0 $
TRNSP    EX/EXT
MATGPR   GPL,USET,SIL,EXT//C,N,R
COND     L84D,MPCF1
TRNSP    EQM/EQMT
MATGPR   GPL,USET,SIL,EQMT//C,N,M
LABEL    L84D
TRNSP    EQN/EQNT
MATGPR   GPL,USET,SIL,EQNT//C,N,N
TRNSP    EQG/EQGT
ADD      EQGT,/EQGTC/C,Y,ALPHA=(386.4,0.0) $
$  ASSUME CONVERSION OF MASS TO LBS = 386.4
```

```
SMPYAD    EIG,MGG,EIGTC,,,/MOGG/C,N,3/C,N,1/C,N,0 $
SMPYAD  EIG,MGGY,EIGTC,,,/MOGGY/C,N,3/C,N,1/C,N,0 $
MATPRN  MIGG,MOGGY,,,// $
LABEL   L84F
COND    L84G,TPCOPY
OUTPUT1 KAA,MAA,,,//C,N,-1/C,N,0/V,Y,TPNAME
LABEL   L84G
ALTER 89,99
PURGE   KJJ,KCJ,KJC,KCC,MJJ,MCJ,MJC,MCC,PHIJ,MJ,OEIGSJ,PHIJA/RMODE
COND    L91,RMODE   $ IF - FREE-FREE MODES WILL BE OBTAINED
$ IF RESTRAINED MODES ARE TO BE OBTAINED CPAJC MUST INPUT
PARTN   KAA,CPAJC,/KJJ,KCJ,KJC,KCC/C,N,-1/C,N,2/C,N,6/C,N,2/C,N,2/C,N,6
PARTN   MAA,CPAJC,/MJJ,MCJ,MJC,MCC/C,N,-1/C,N,2/C,N,6/C,N,2/C,N,2/C,N,6
READ    KJJ,MJJ,,,EED,,CASECC/LAMJ,PHIJ,MJ,OEIGSJ/C,N,MODES/V,N,NEIGV $
SAVE    NEIGV
EQUIV   LAMJ,LAMA/TRUE
CHKPNT  LAMJ,PHIJ,MJ,OEIGSJ
OFP     LAMJ,OEIGSJ,,,,//V,N,CARDNO
SAVE    CARDNO
MERGE   PHIJ,,,,,CPAJC/PHIJA/C,N,1/C,N,2/C,N,2
EQUIV   PHIJA,PHIA/TRUE
CHKPNT  PHIJA,PHIA,LAMA
JUMP    L93
LABEL   L91
COND    FINIS,REACT
READ    KAA,MAA,MR,DM,EED,USET,CASECC/LAMA,PHIA,MM,OEIGS/C,N,MODES/V,N,
        NEIGV $
ALTER 91,91
CHKPNT  LAMA,PHIA,MM,OEIGS $
ALTER 93
LABEL   L93
$
ALTER 112
PURGE   CPGK,KK,MK,PHIAK/COUPLE
COND    FINIS,COUPLE
INPUTT1 /,,,,/C,N,-1/C,N,9/V,Y,TPNAME9   $ REWIND INP9
PARAM   //C,N,NOP/V,N,INP=1 $
JUMP    LOOP112
LABEL   LOOP112
INPUTT1 /CPGK,KK,MK,,/C,N,0/C,N,9 $
PARTN   PHIG,,CPGK/,PHIAK,,/C,N,1 $
COND    L112A,TPCOPYN
OUTPUT1 LAMA,PHIAK,,, //C,N,-1/V,N,INP/V,Y,TPNAMEN
JUMP    L112
LABEL   L112A
MATPRN  PHIAK,,,,// $
LABEL   L112
PARAM   //C,N,ADD/V,N,INP/V,N,INP/C,N,1 $
PARAM   //C,N,SUB/V,N,SKLOOP/V,Y,NOSUB/V,N,INP
COND    L112B,NOELMT
```

N A S T R A N   E X E C U T I V E   C O N T R O L   D E C K   E C H O

```
PARAM    //C,N,SUB/V,N,SKLOOP/V,N,SKLOOP/C,N,1
LABEL    L1122
COND     FINIS,SKLOOP
REPT     LOOP112,8
ENDALTER
CEND
```

TABLE 1.- STATISTICAL DESCRIPTION OF 1/8-SCALE MODEL

COMPONENT	No. GRID POINTS	No. CBAR	No. CQDMEM2	No. CSHEAR	No. CROD	No. CTRMEM	No. CQUAD2	TOTAL No OF MEMBERS	SYMM. CASE		ANTI-SYMM. CASE	
									D.O.F. AFTER SPC & MPC	D.O.F. AFTER GUYAN	D.O.F. AFTER SPC & MPC	D.O.F. AFTER GUYAN
PAYLOAD	12	8	-	-	-	-	-	8	24	24	26	26
FIN	59	-	24	22	65	-	-	111	101	25	99	24
WING	192	-	149	81	187	8	-	425	531	183	531	183
DOORS	134	9	20	64	178	-	16	287	396	26	384	26
FUSELAGE	537	93	336	172	616	7	-	1224	1417	246	1368	222
TOTAL ½ ORBITER	934	110	529	339	1046	15	16	2055	2469	504	2408	481
ORBITER ANALYSIS	215	CONTAINS 125 PLOTEL ELEMENTS							400	339	378	324

COMPONENT	No. GRID POINTS	No. FLUID POINTS	No. CBAR	No. CROD	No. CQUAD2	No. CTRIA2	No. CHEXA1	No. CFLUID	TOTAL No. OF MEMBERS	SYMM. CASE		ANTI-SYMM. CASE	
										D.O.F. AFTER SPC & MPC	D.O.F. AFTER GUYAN	D.O.F. AFTER SPC & MPC	D.O.F. AFTER GUYAN
S R B	755	-	99	-	268	-	432	-	799	3114	212	3114	212
LH_2 TANK	215	-	135	26	172	16	-	-	349	1107	216	1111	194
LOX TANK	137	51	8	-	112	16	-	50	186	766			
TOTAL ½ BOOSTER	1107	51	242	26	552	32	432	50	1334	4987			

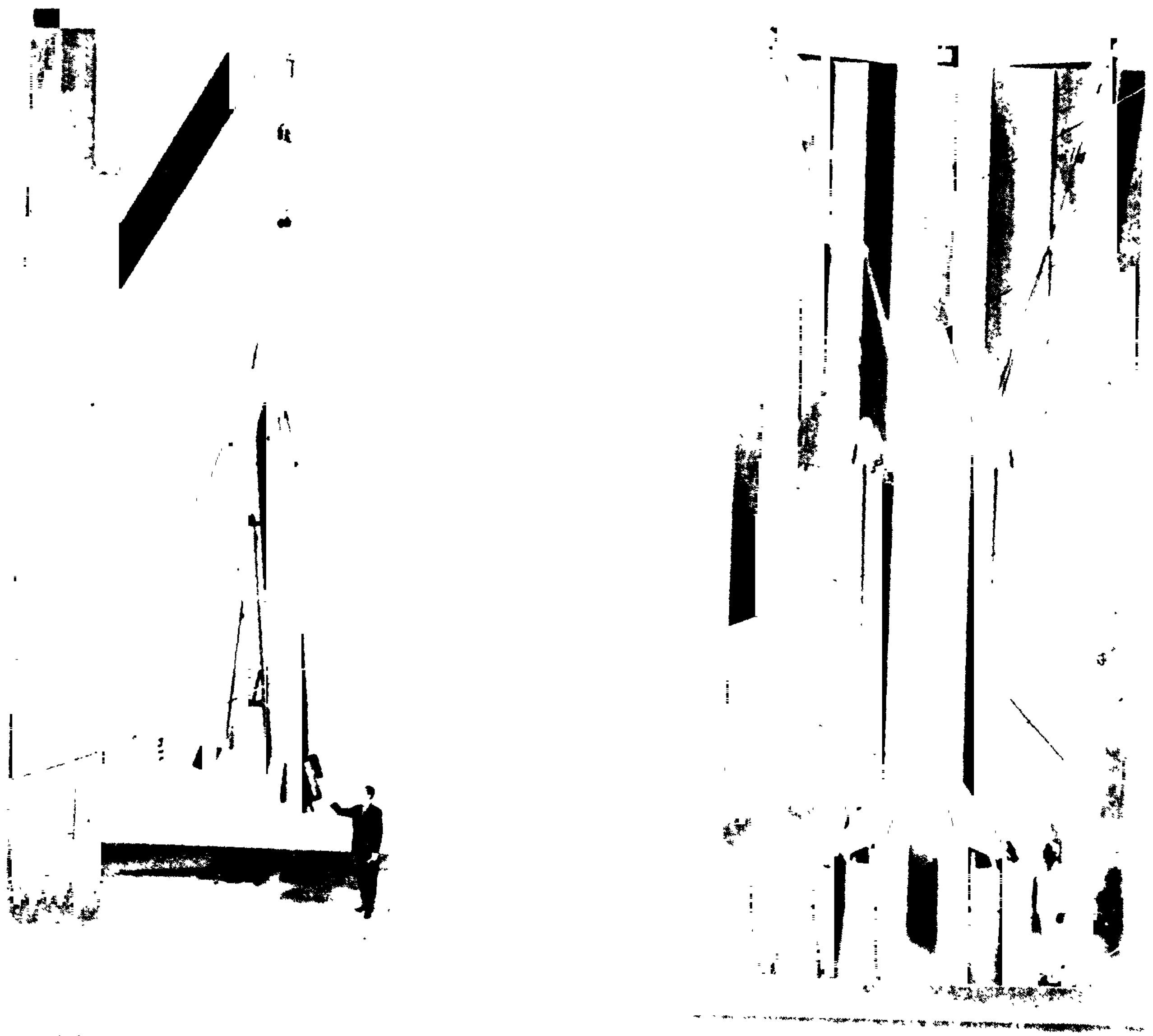

Figure 1.- Mock-up of 1/8-scale space shuttle structural dynamics model.

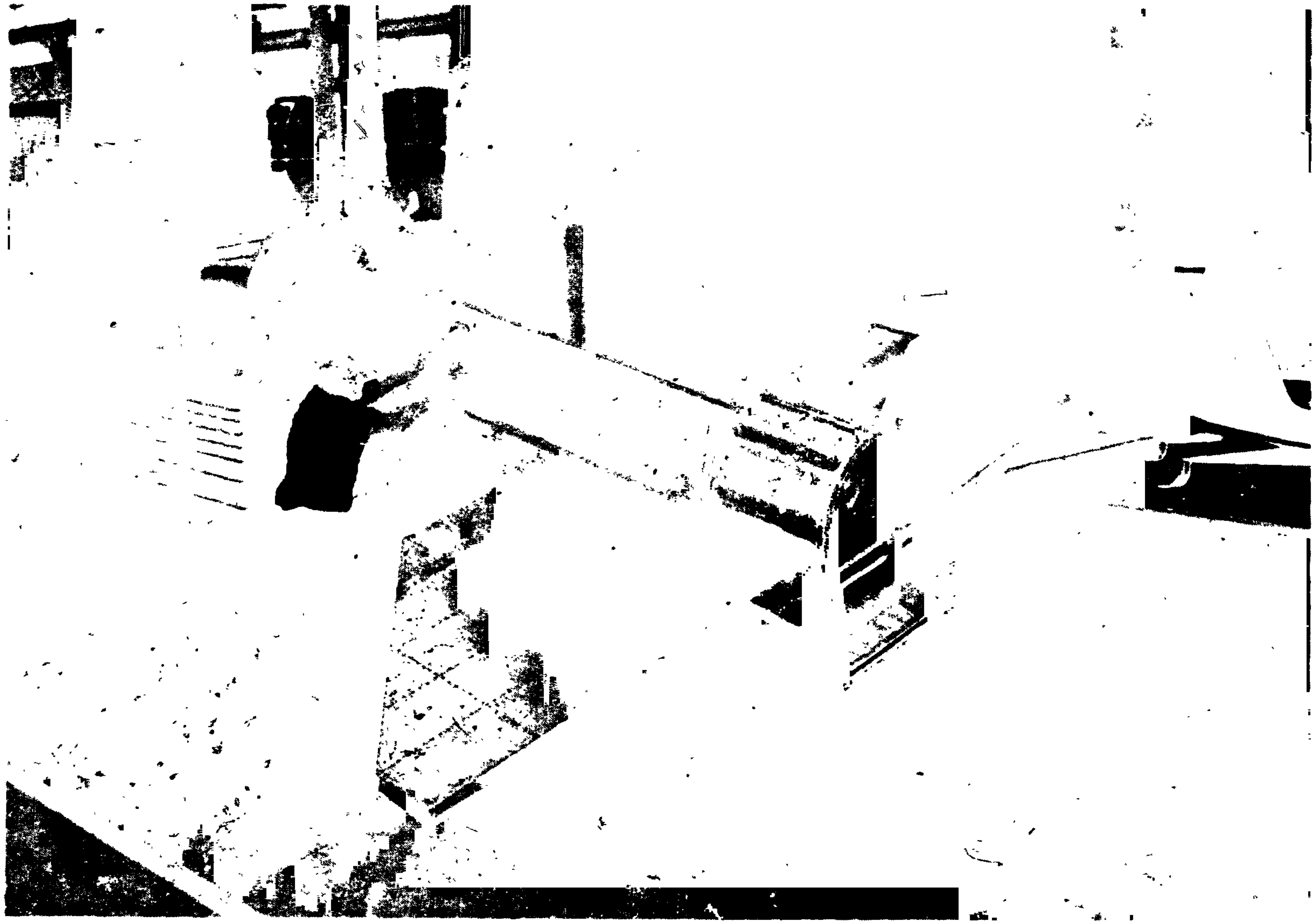

Figure 2.- The 1/8-scale orbiter model.

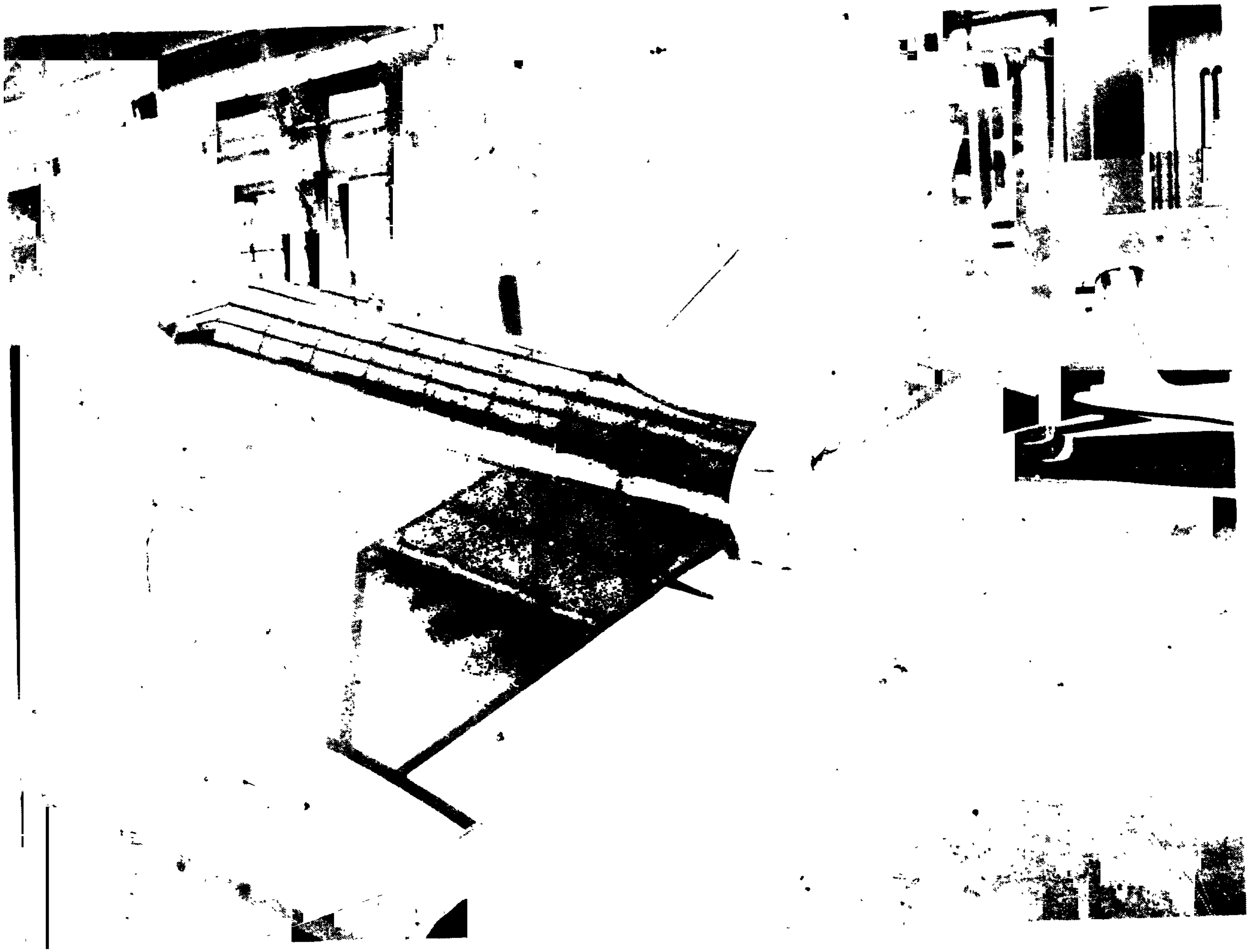

Figure 5.- Orbiter with plastic fairings.

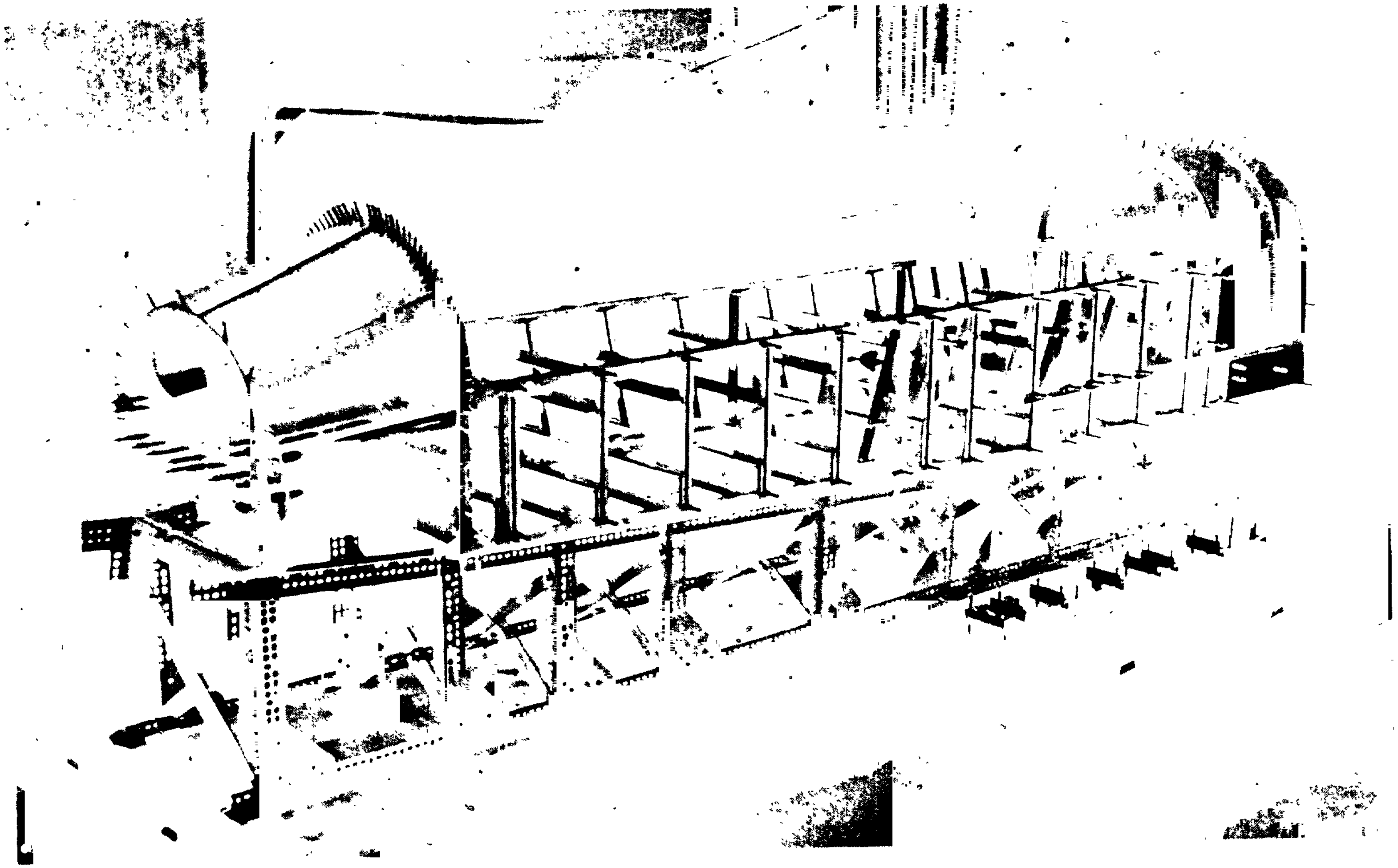

Figure 4.- Orbiter fuselage under assembly.

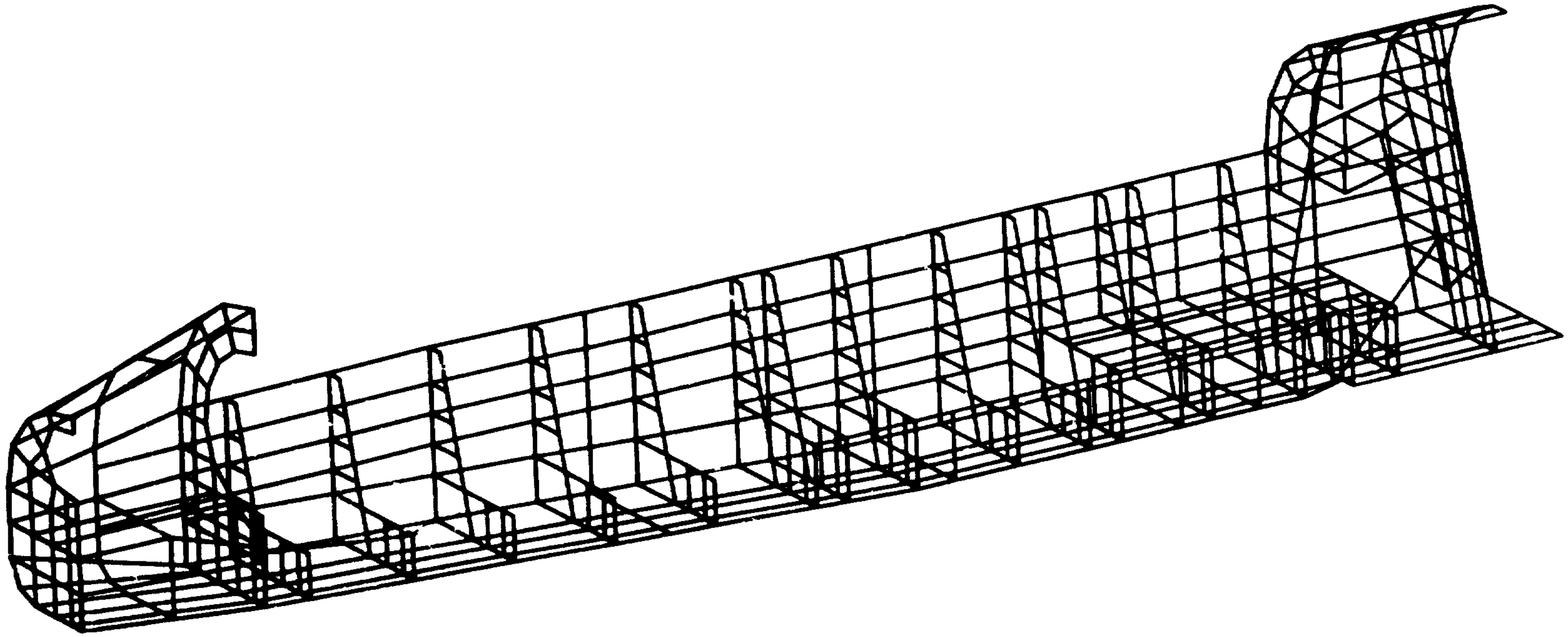

Figure 5.- NASTRAN plot of orbiter fuselage.

Figure 6.- Orbiter wing under assembly.

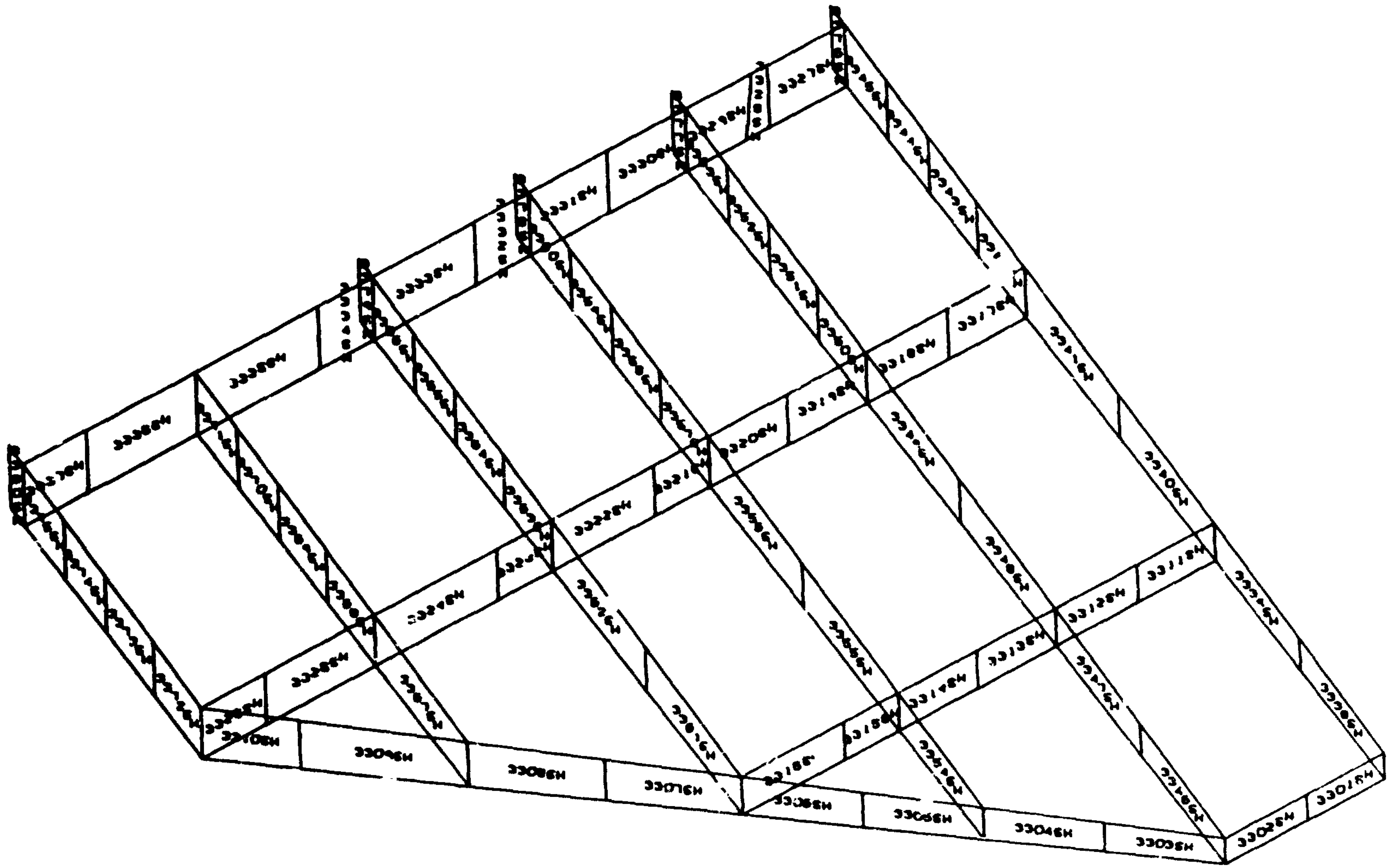

Figure 7.- NASTRAN plot of wing rib and spar shear webs.

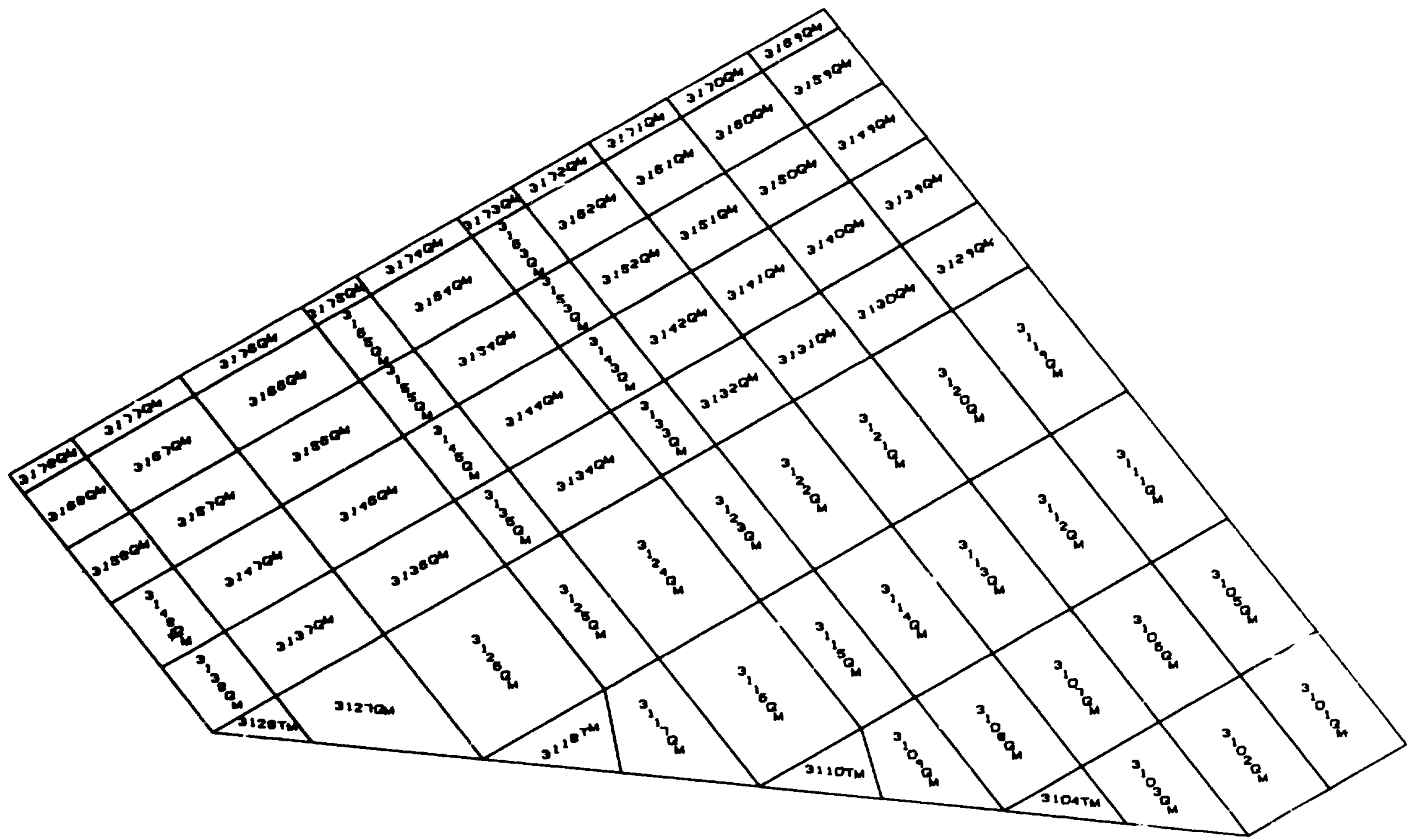

Figure 8.- NASTRAN plot of wing top cover.

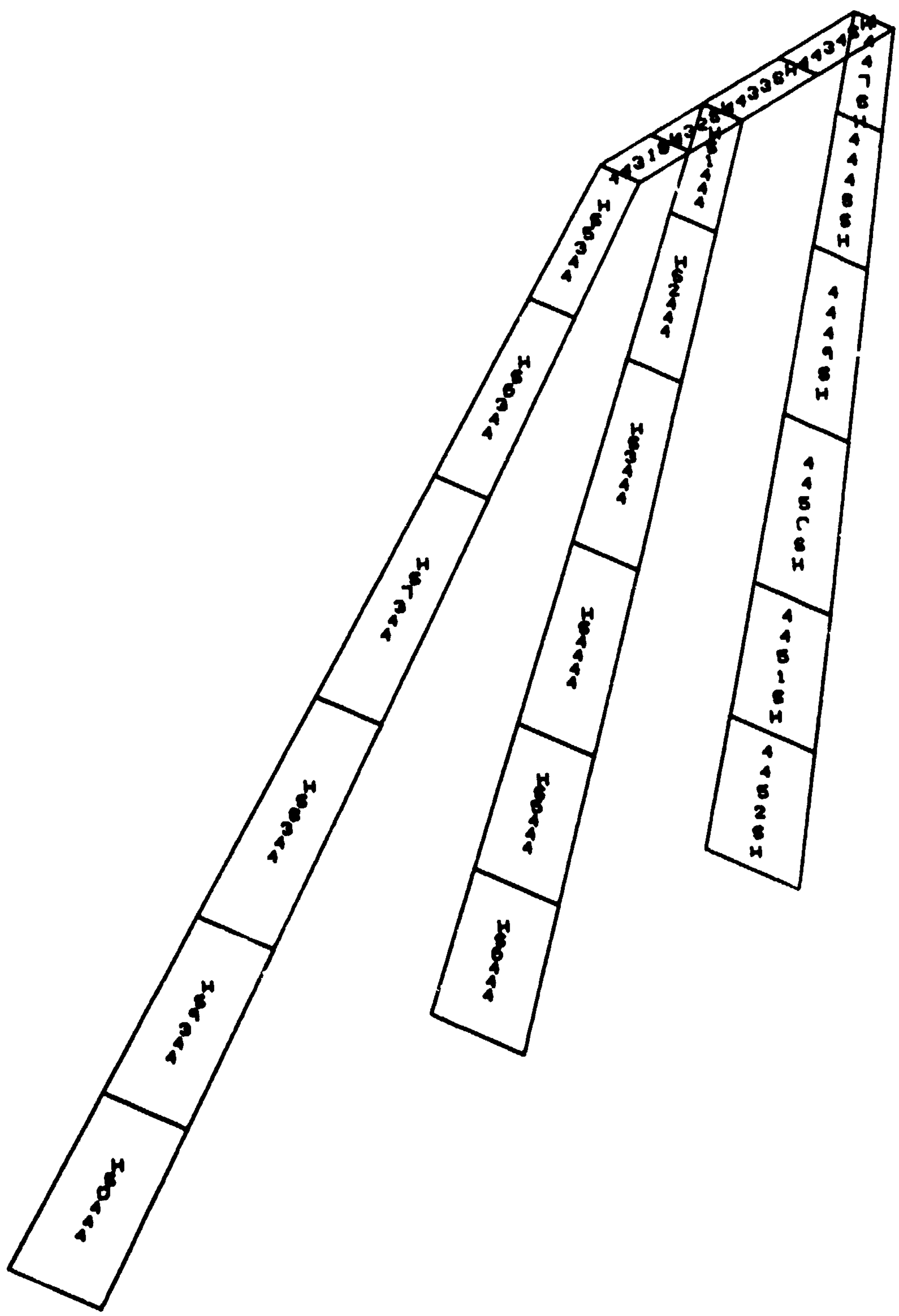

Figure 9.- NASTRAN plot of fin webs.

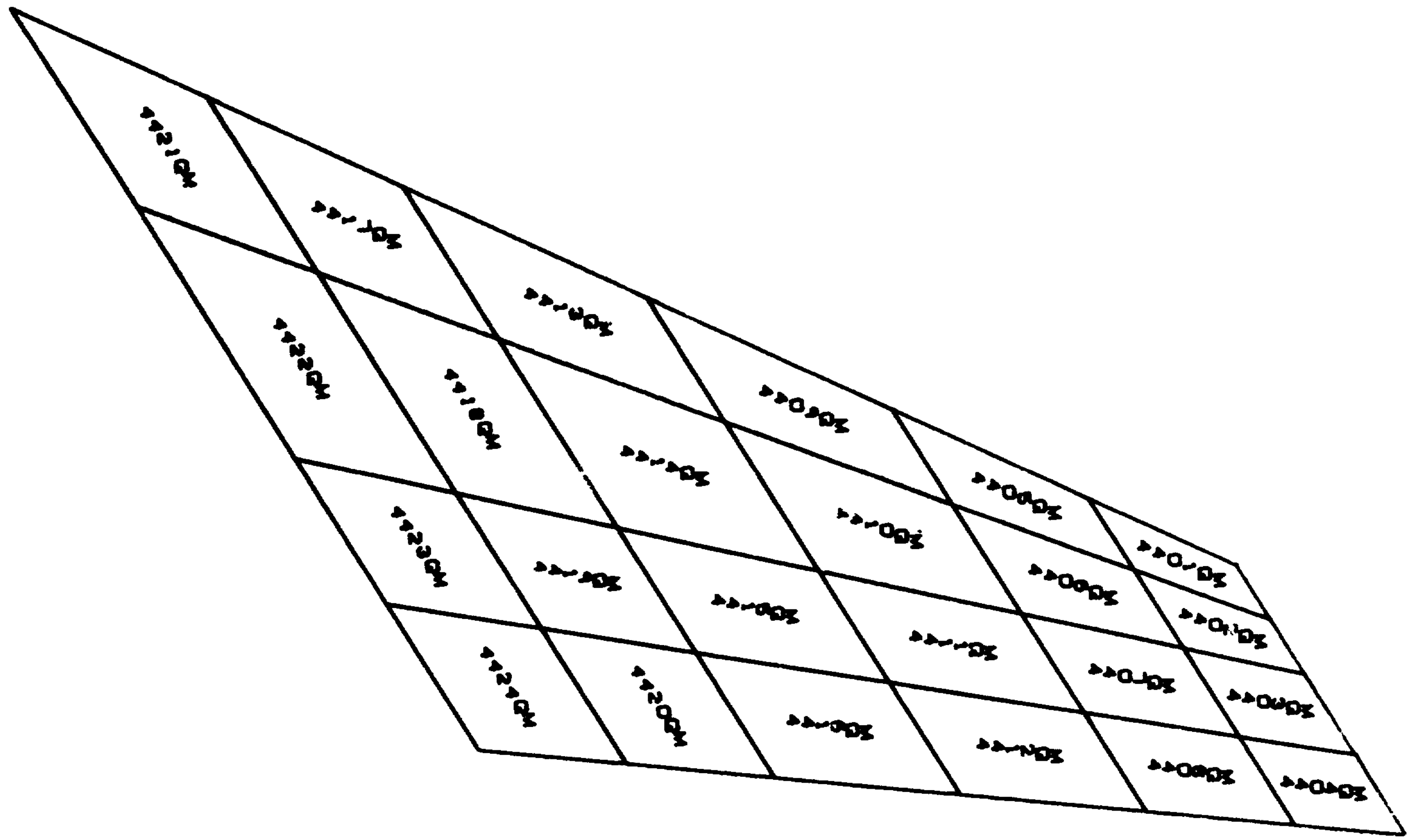

Figure 10.- NASTRAN plot of fin cover.

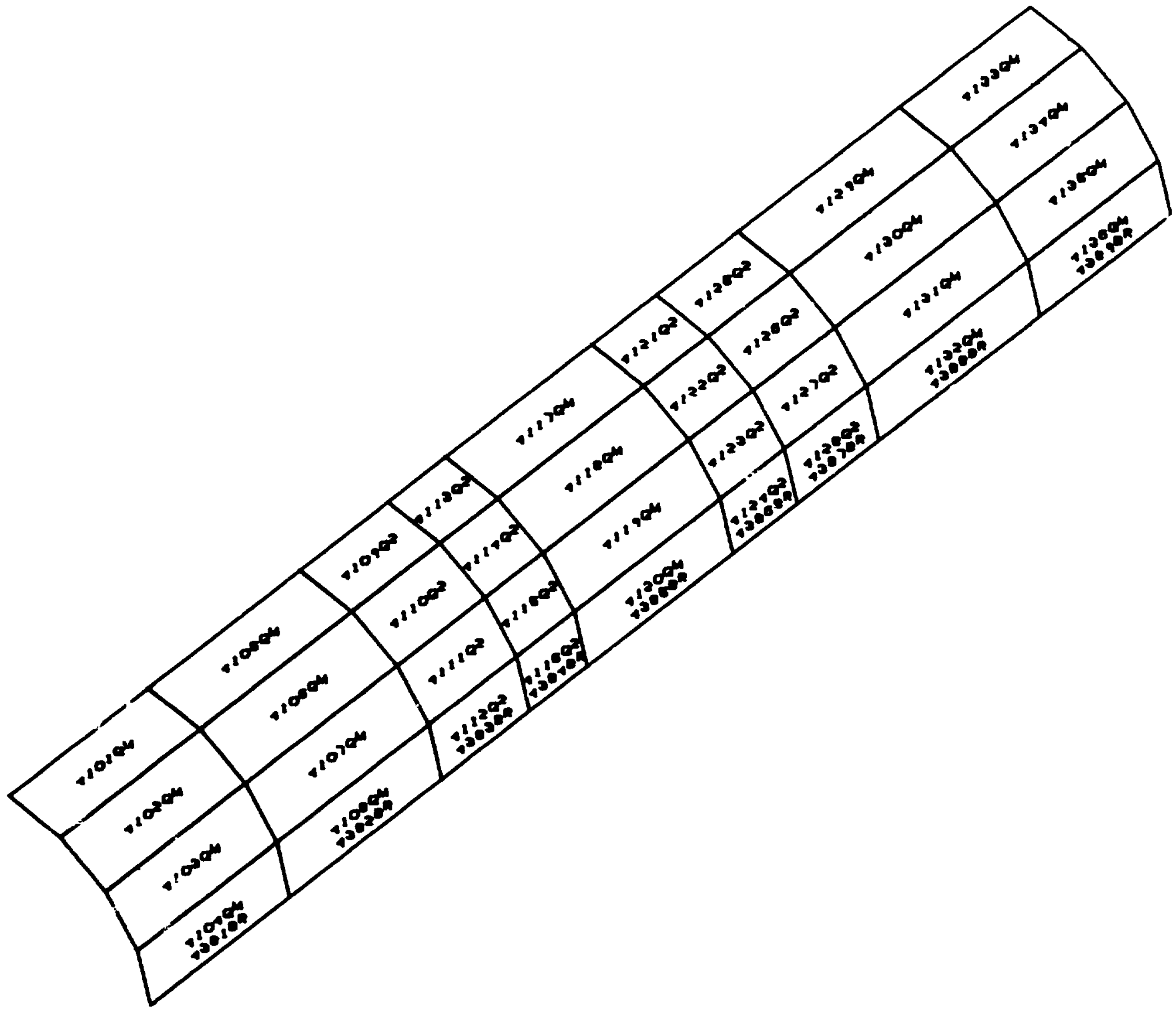

Figure 11.- NASTRAN plot of cargo bay door covers.

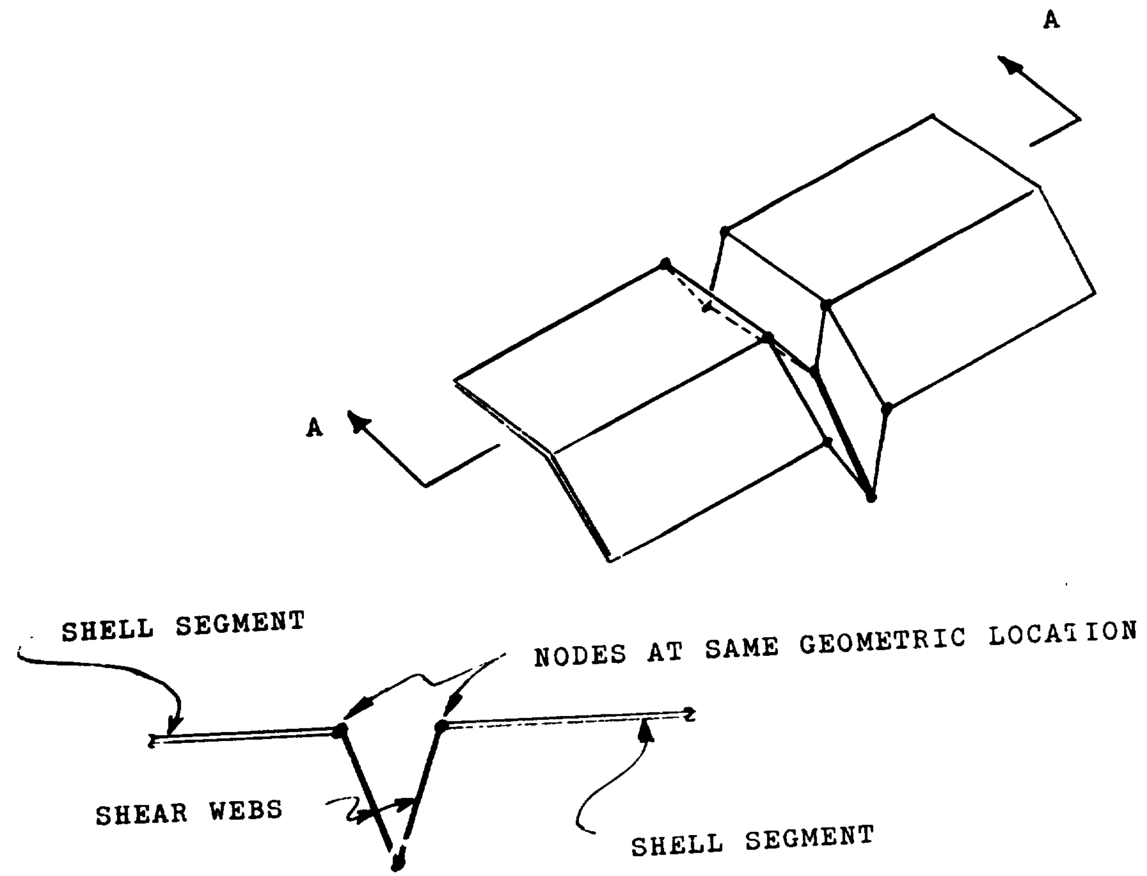

SECTION A-A

Figure 12.- Schematic of cargo door joints.

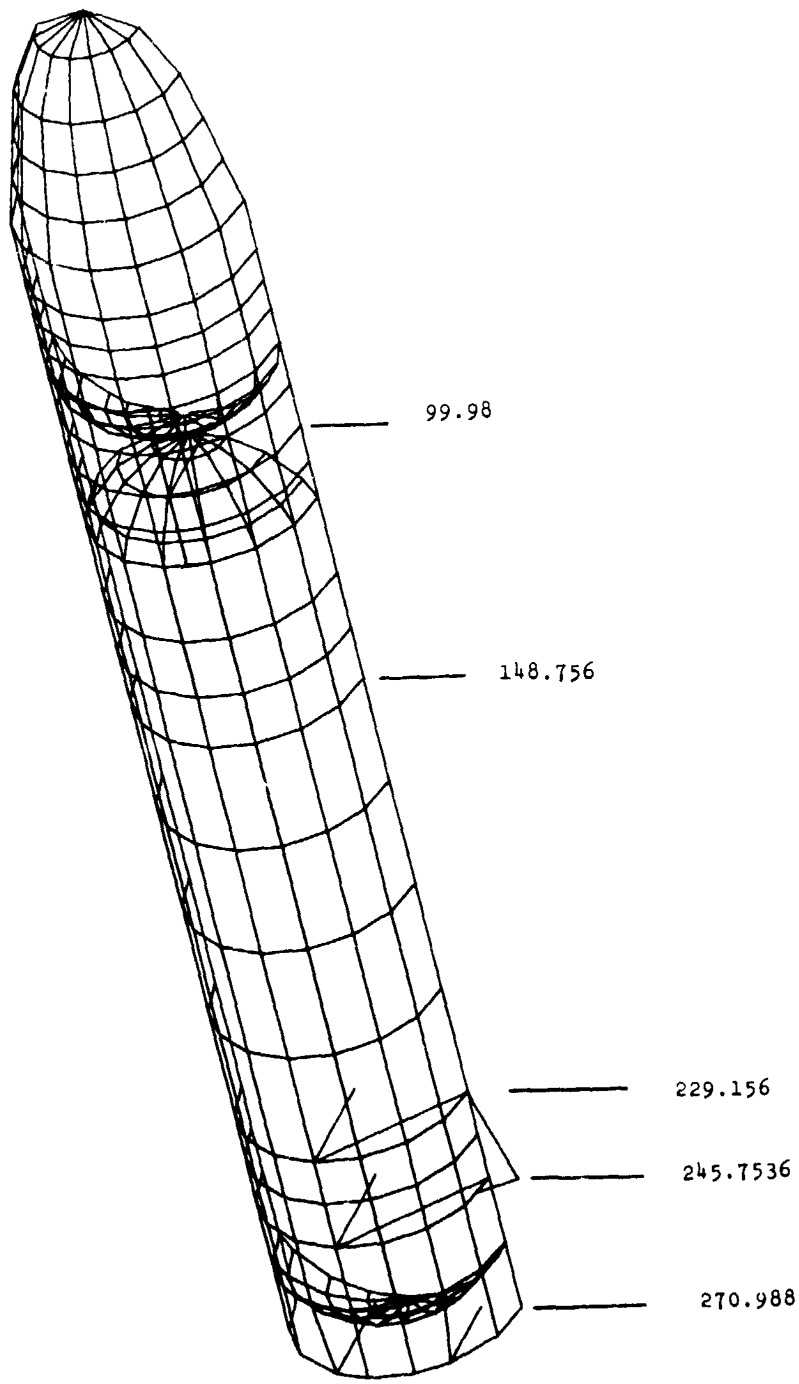

Figure 13.- NASTRAN plot of external tank.

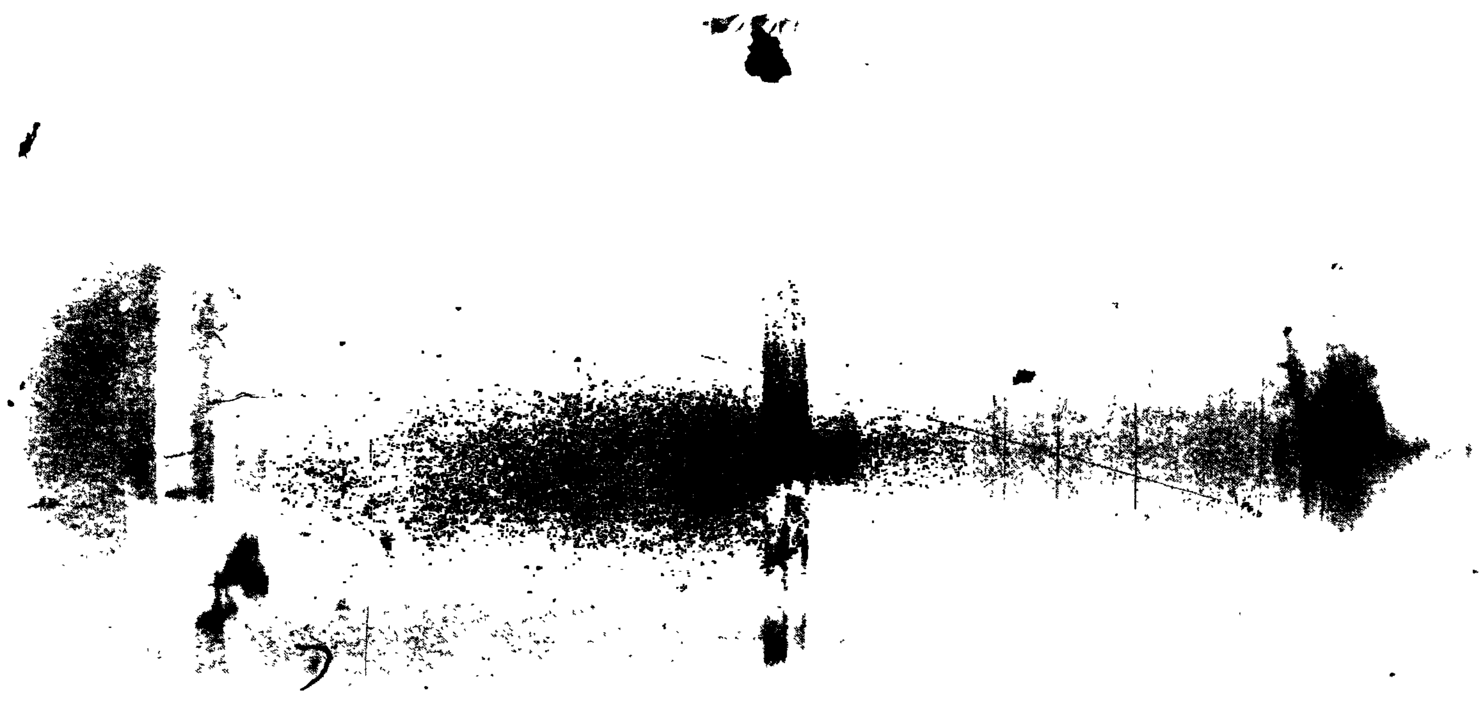

Figure 14.- Liquid oxygen tank.

Figure 15.- LOX tank connected to inter tank skirt and forward tank/SRB interstage.

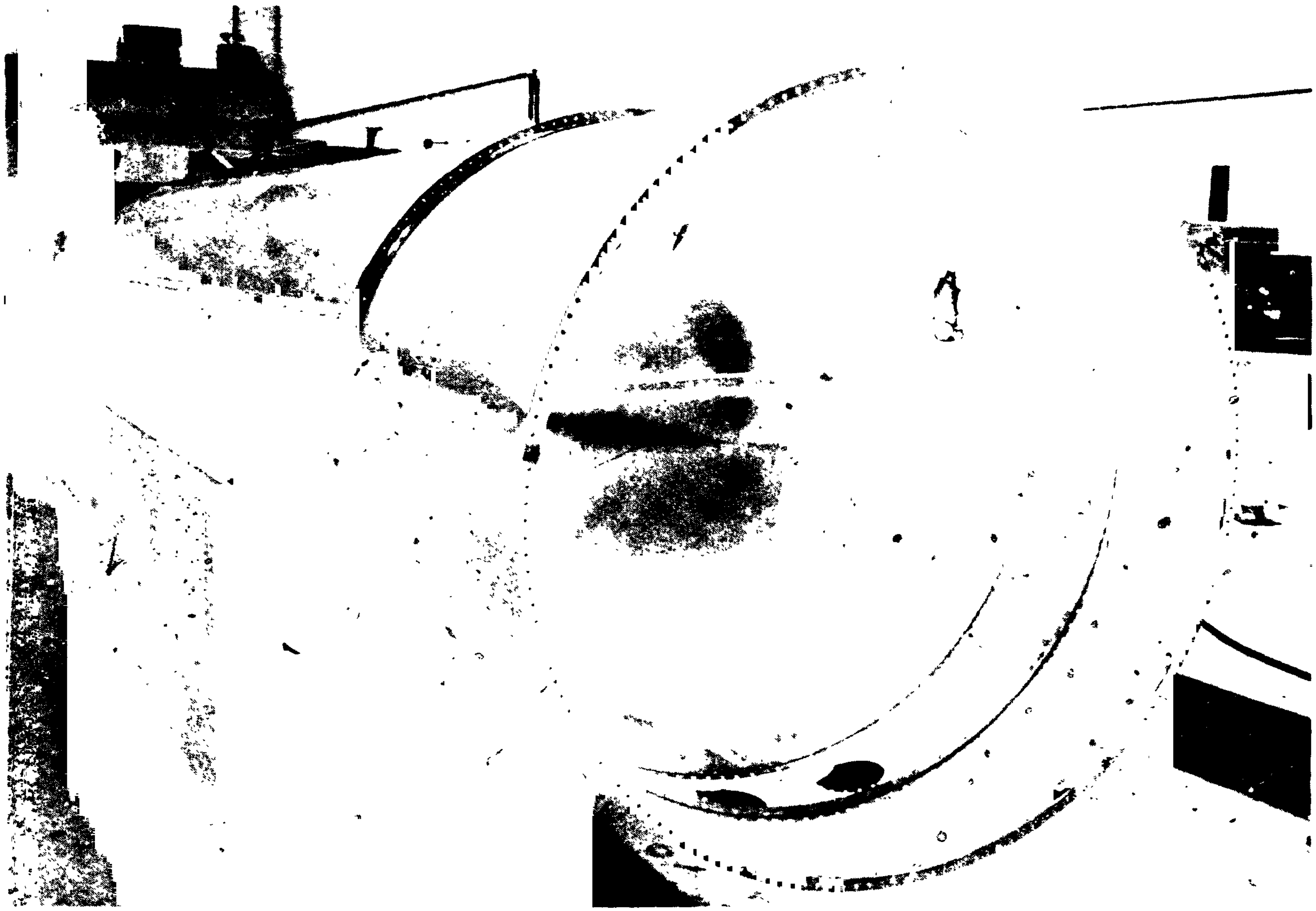

Figure 16.- LH_2 tank and inter tank skirt.

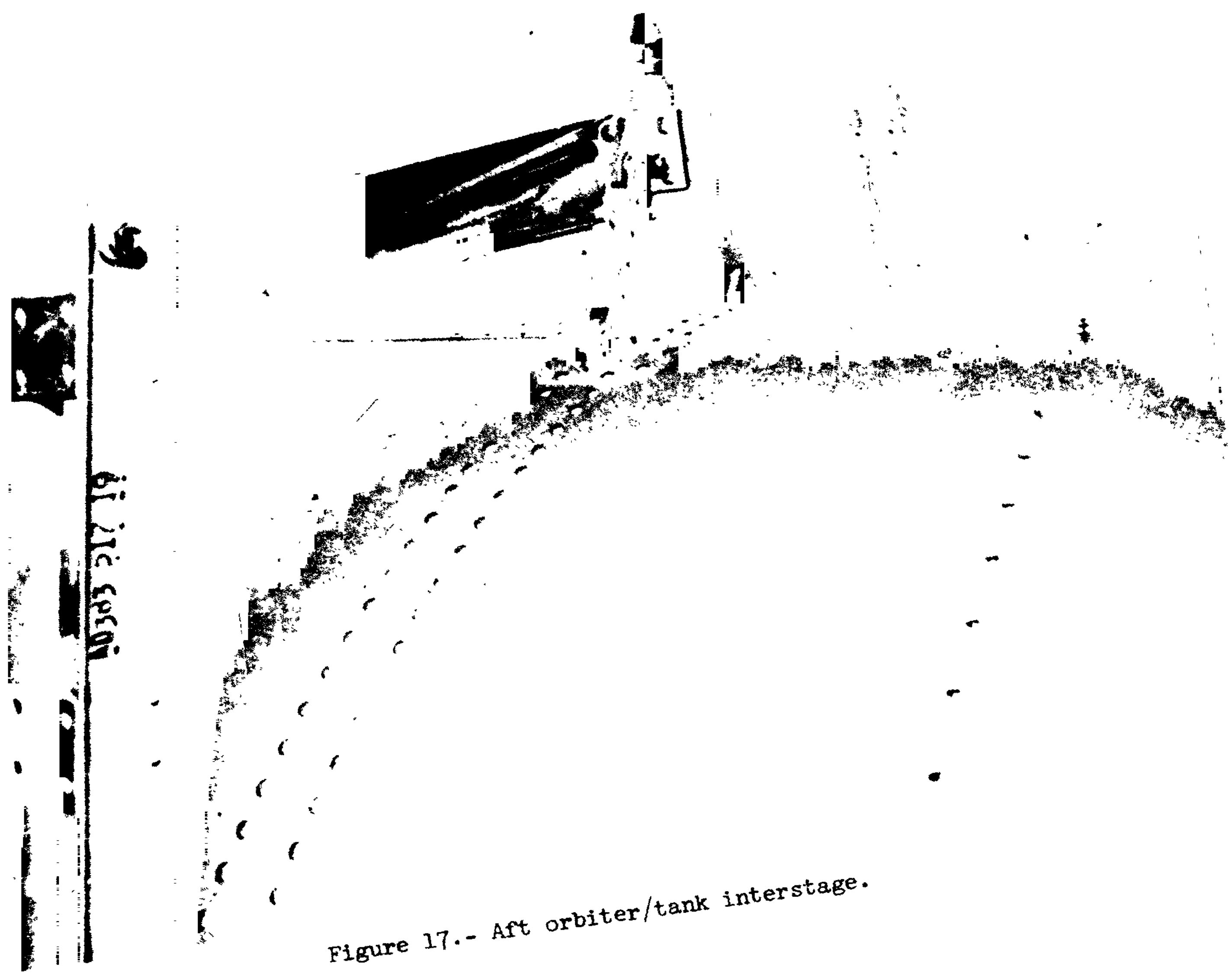

Figure 17.- Aft orbiter/tank interstage.

Figure 18.- LH_2 tank under assembly.

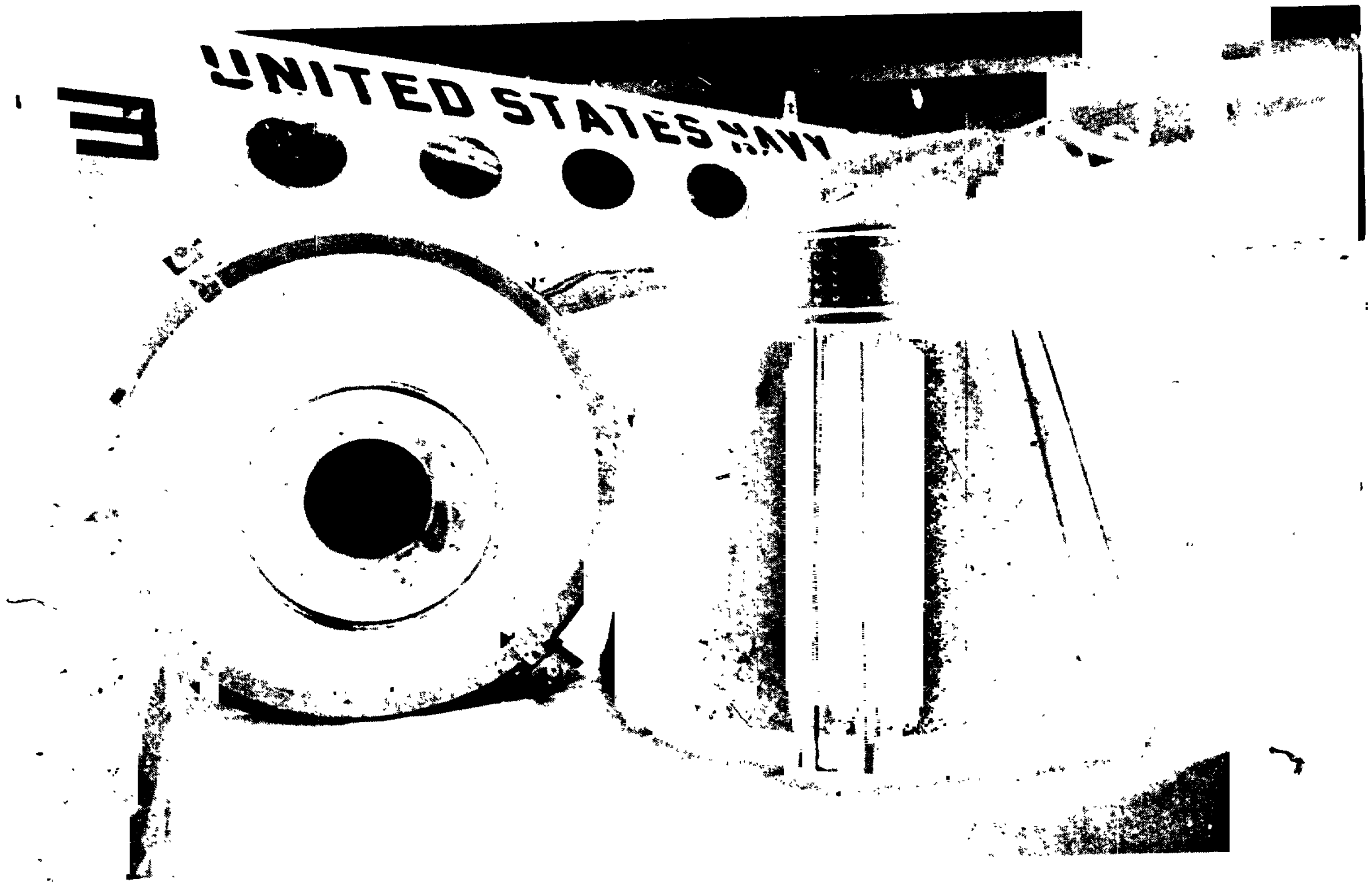

Figure 19.- Solid rocket booster aft skirt.

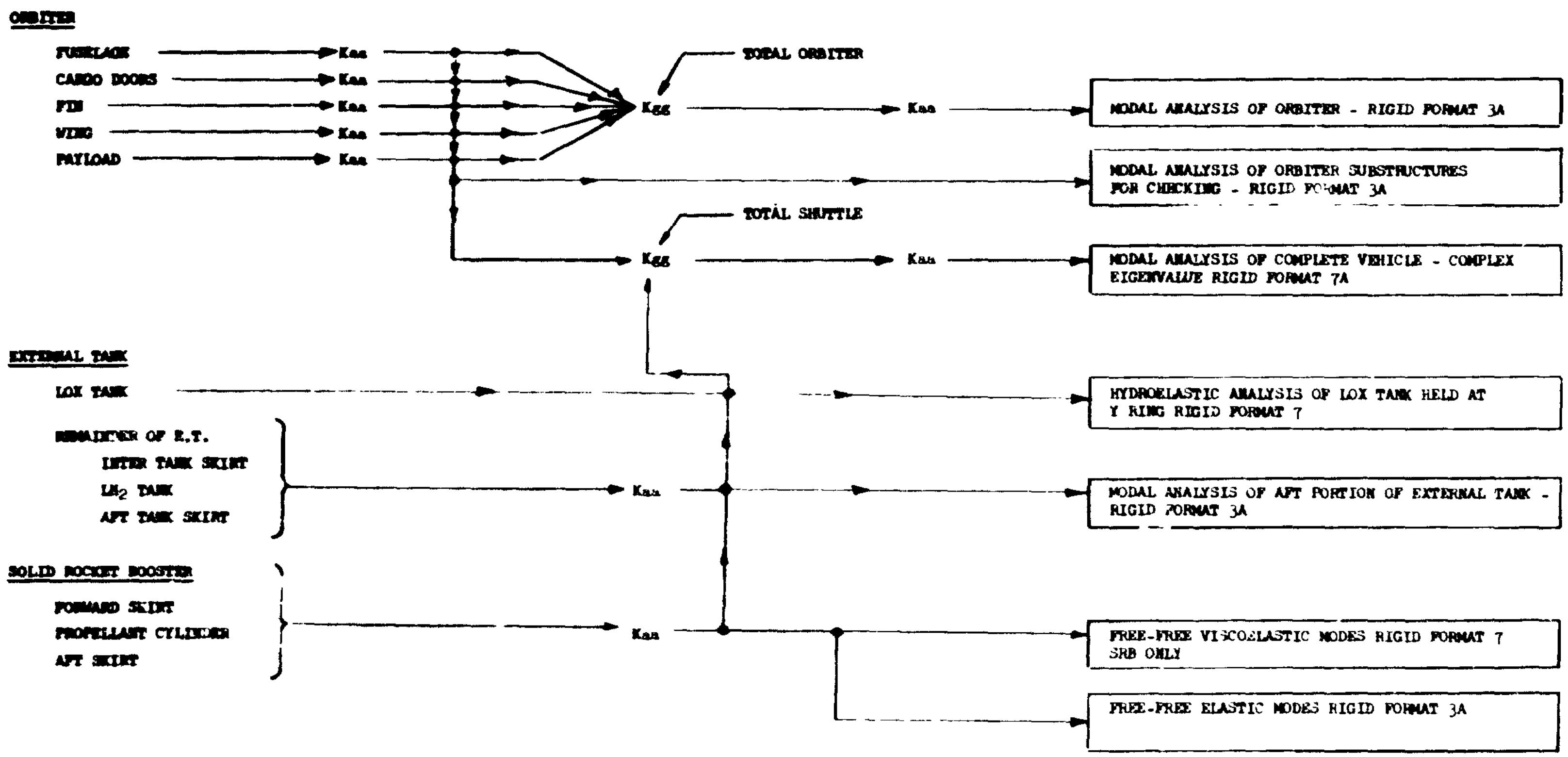

Figure 20.- Schematic diagram of analysis flow. The letter A affixed to the Rigid Format Number denotes DMAP Alteration of that format.

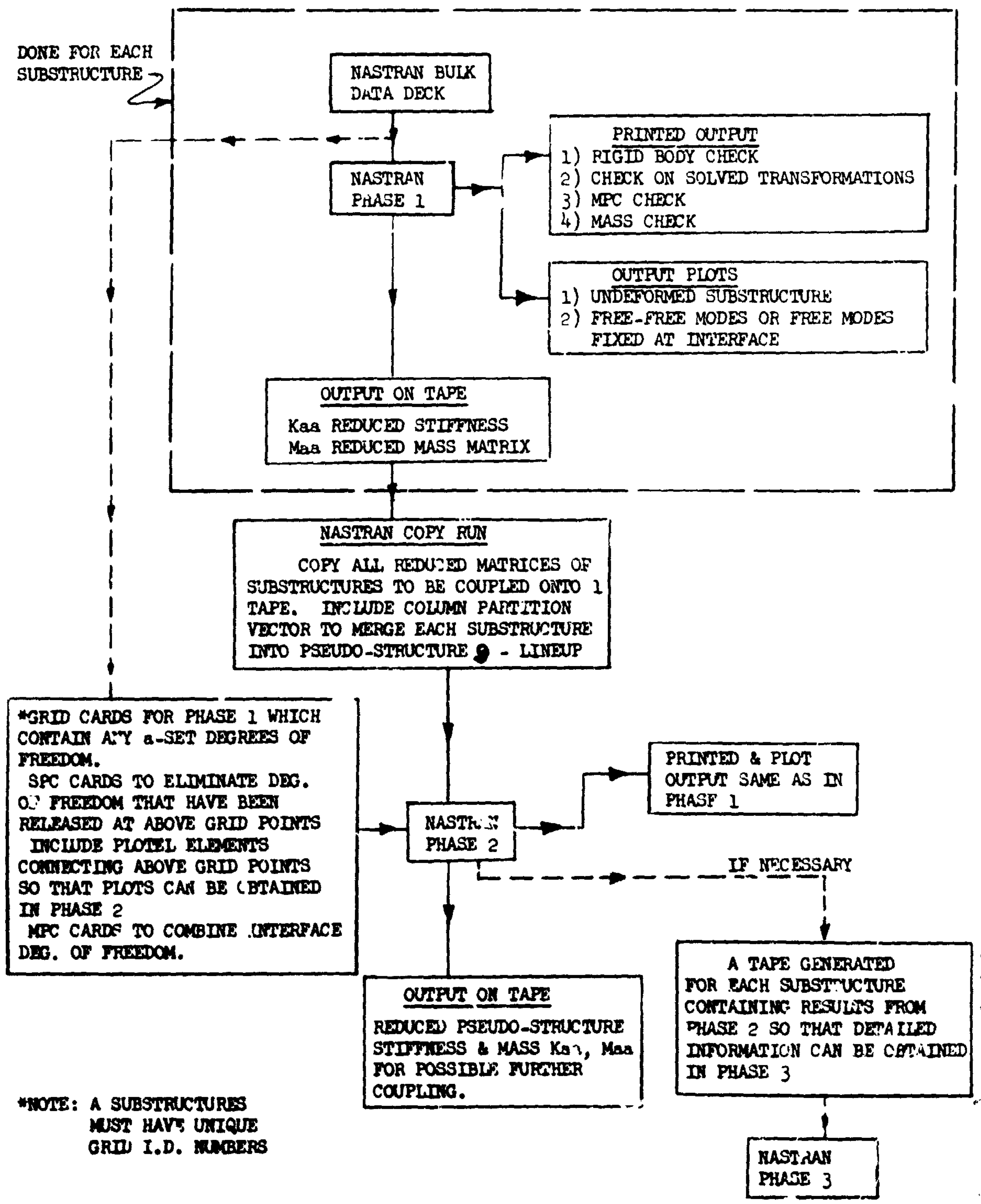

Figure 21.- Flow diagram for NASTRAN substructuring to obtain normal modes (Rigid Format 3).

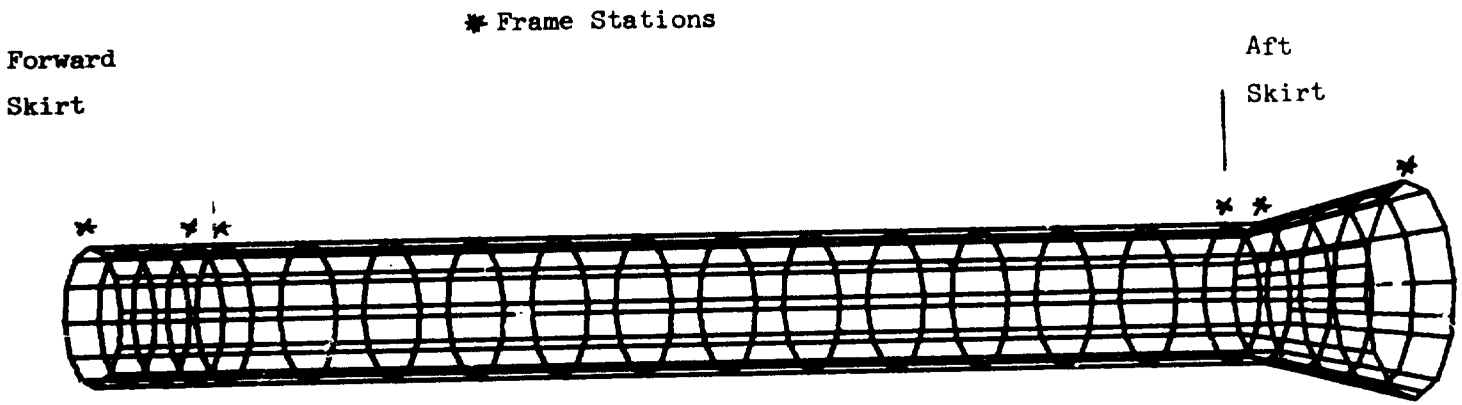

Figure 22.- Solid rocket booster idealization.

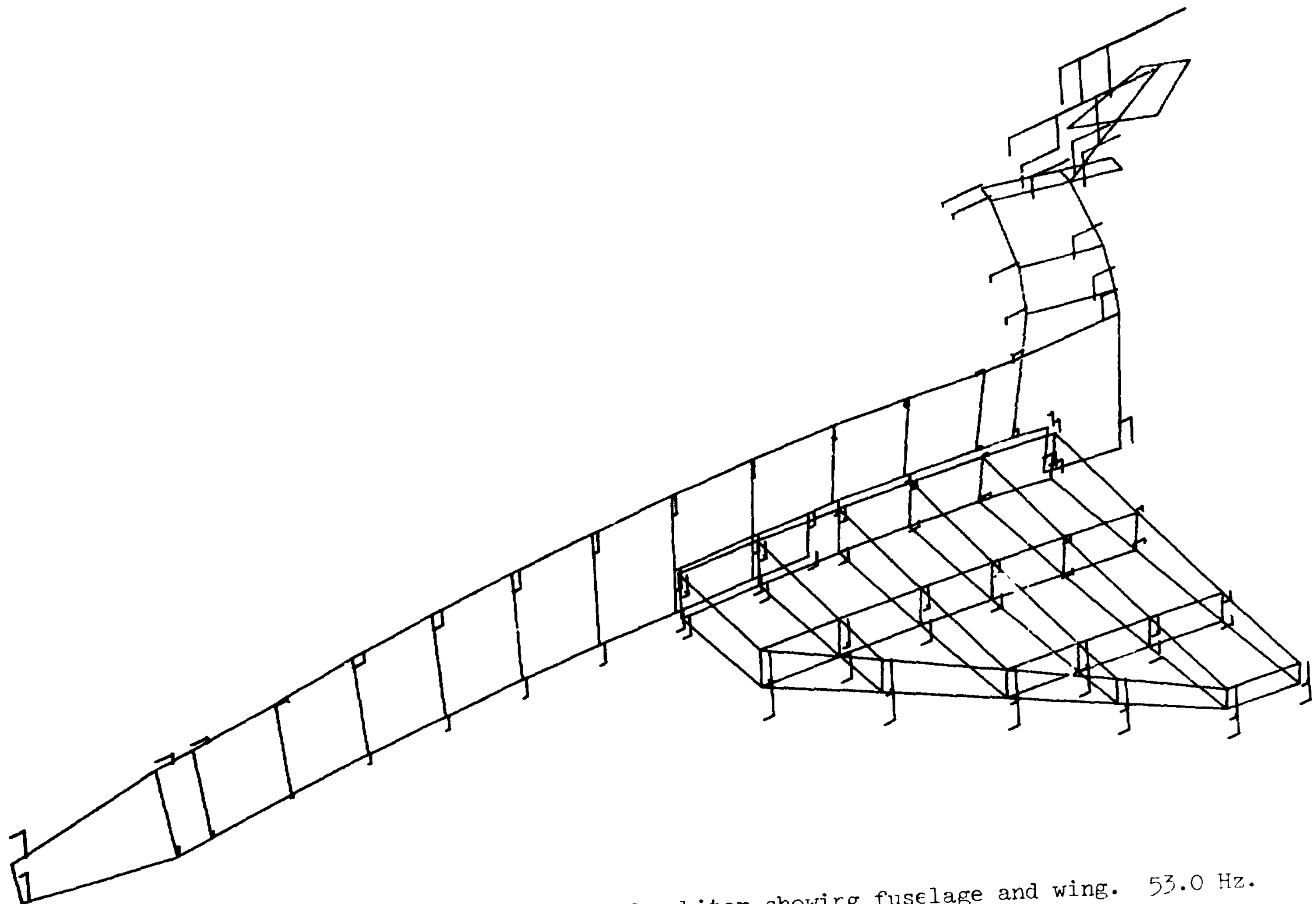

Figure 23.- First elastic symmetric mode of orbiter showing fuselage and wing. 53.0 Hz.

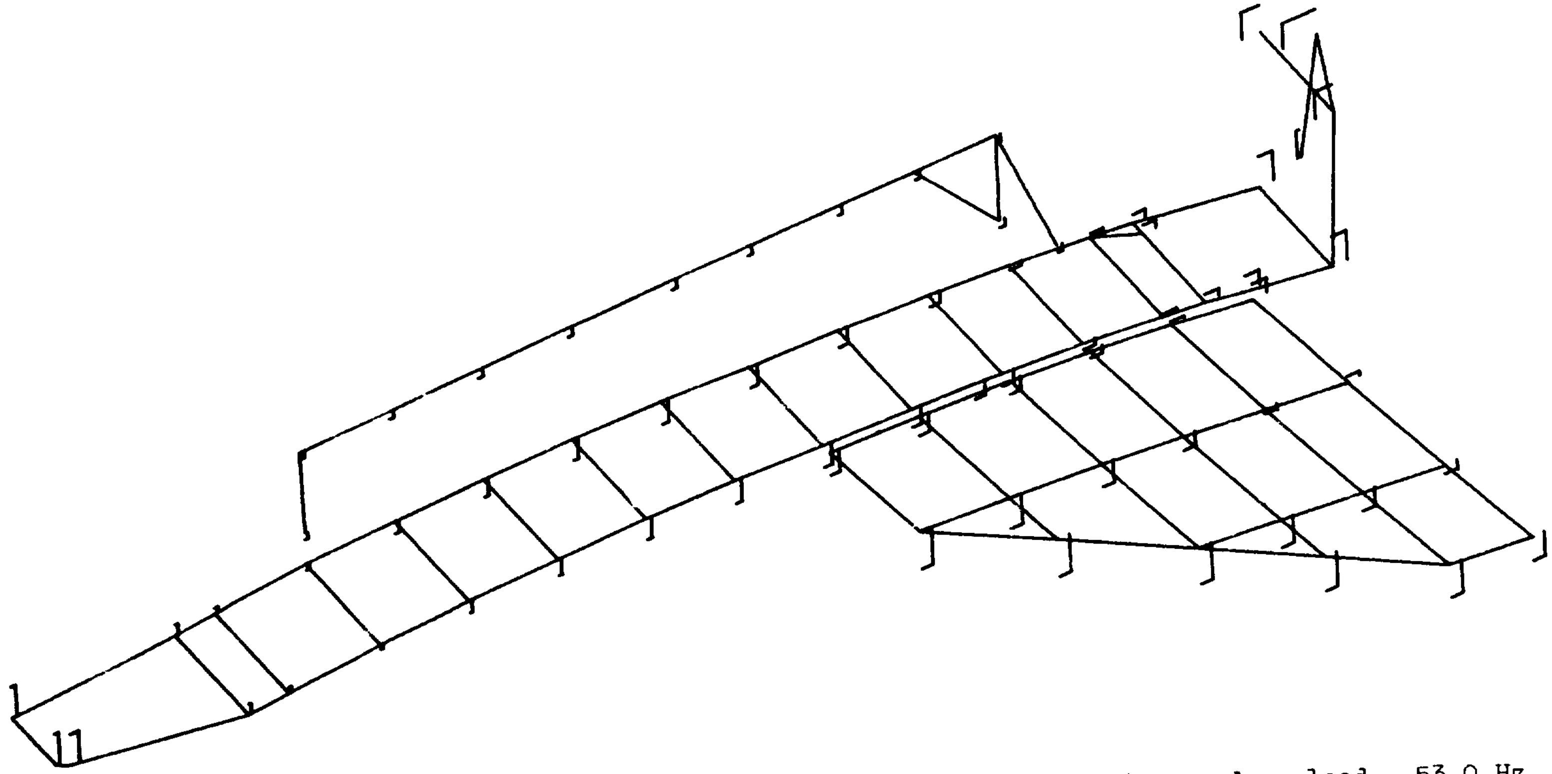

Figure 24.- First elastic symmetric mode of orbiter showing bottom surface and payload. 53.0 Hz.

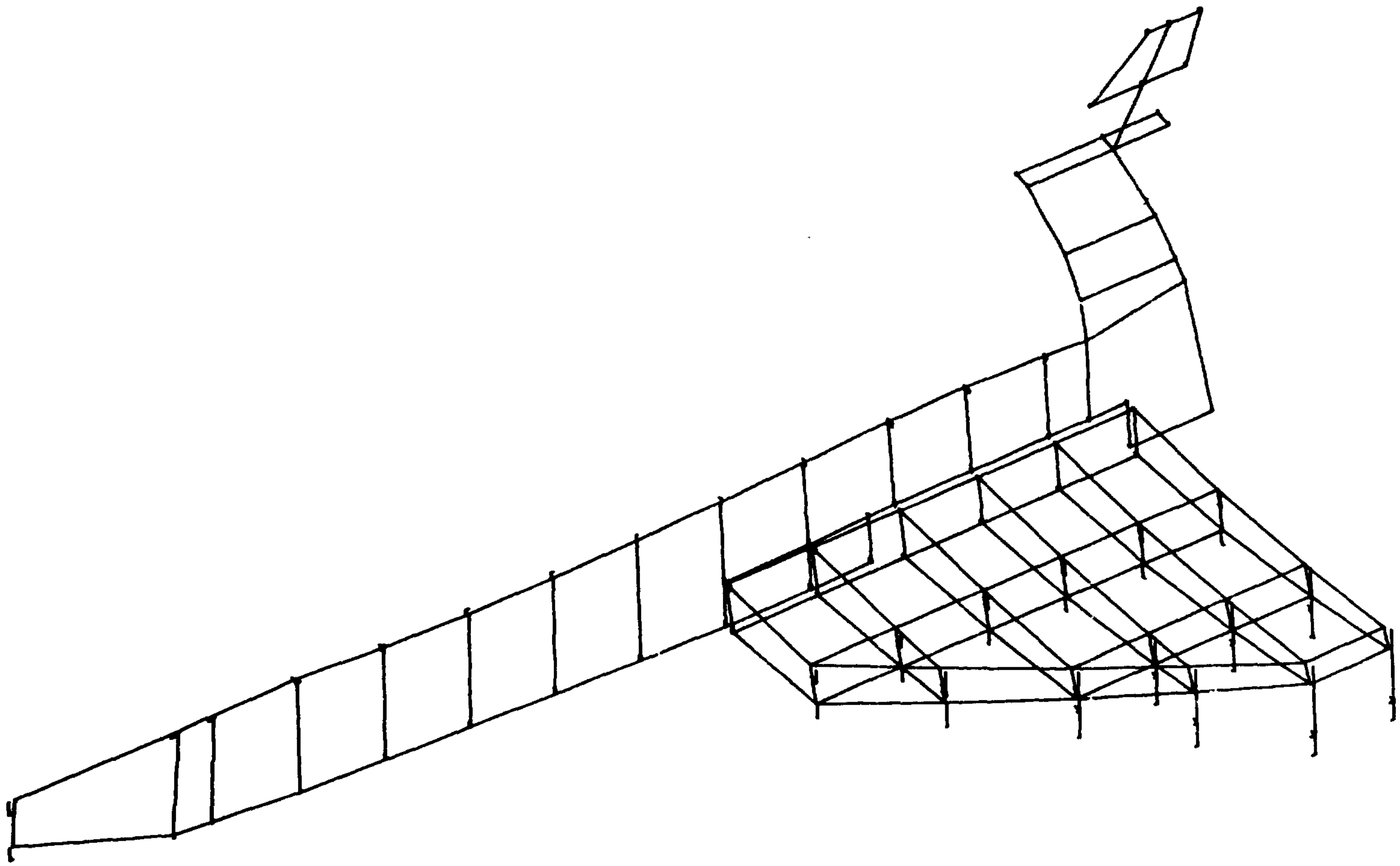

Figure 25.- Second elastic symmetric mode of orbiter showing fuselage and wing. 62.6 Hz.

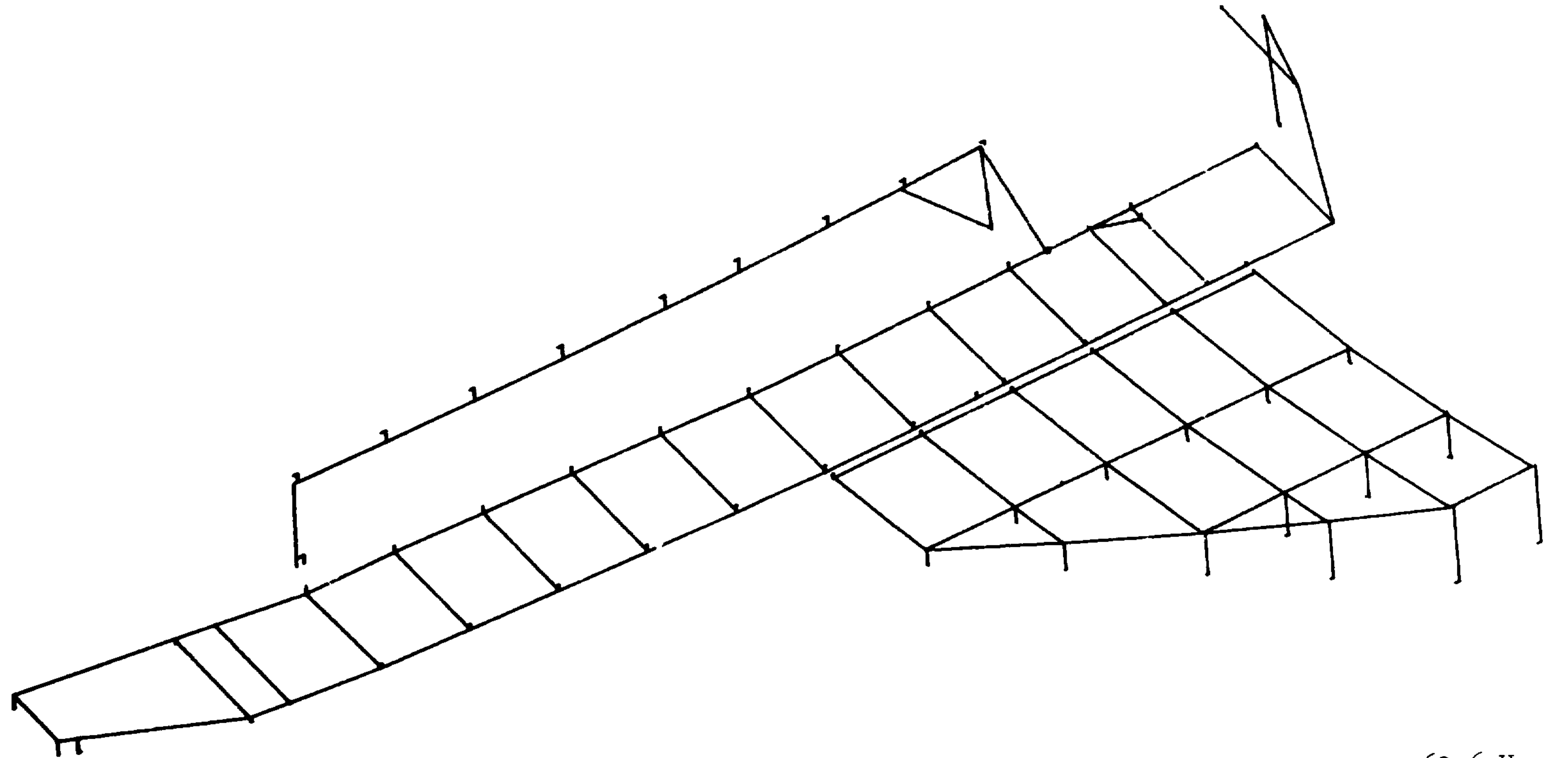

Figure 26.- Second elastic symmetric mode of orbiter showing bottom surface and payload. 62.6 Hz.

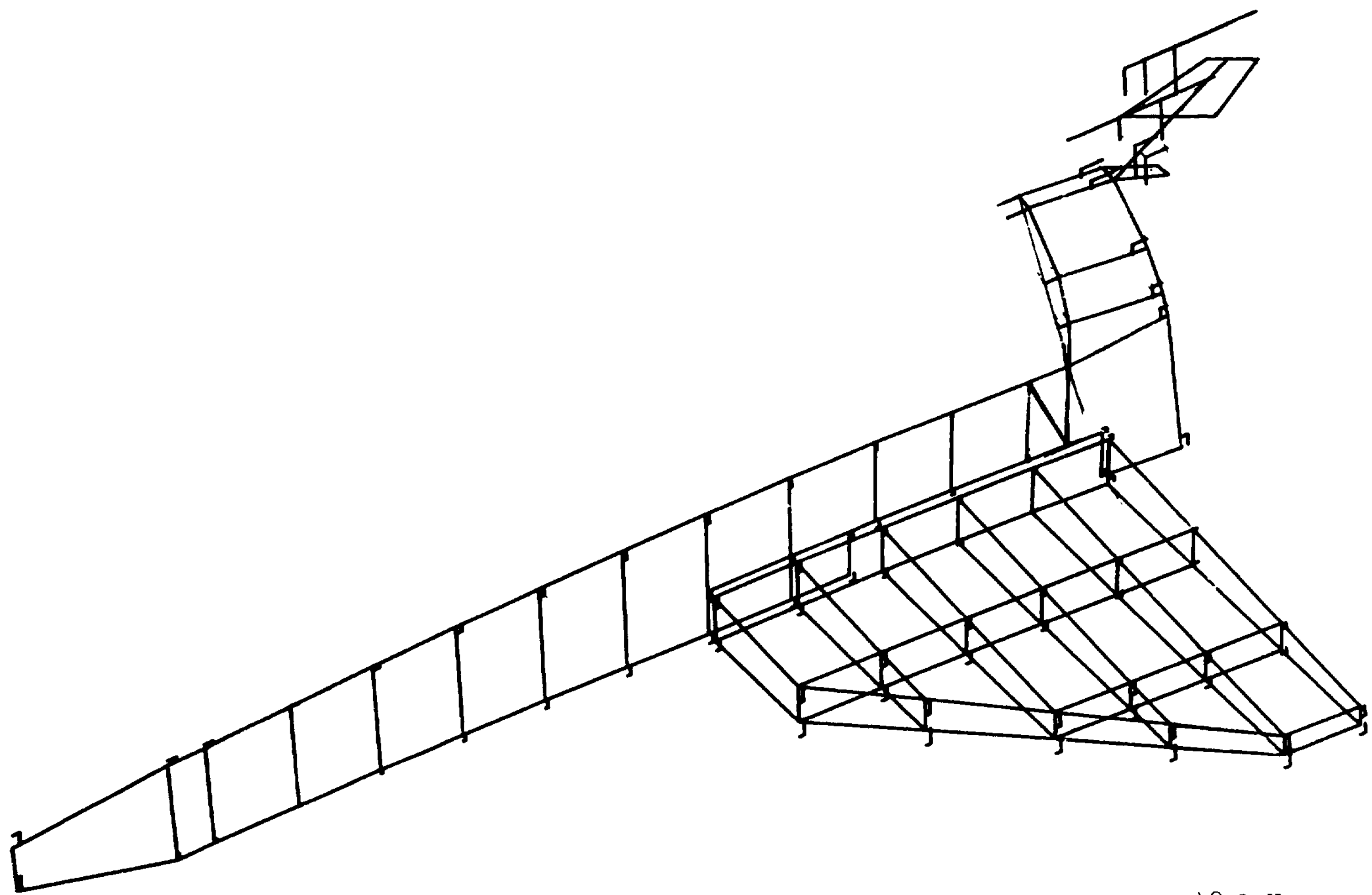

Figure 27.- First elastic symmetric mode of orbiter with forward fin spar cut. 48.1 Hz.

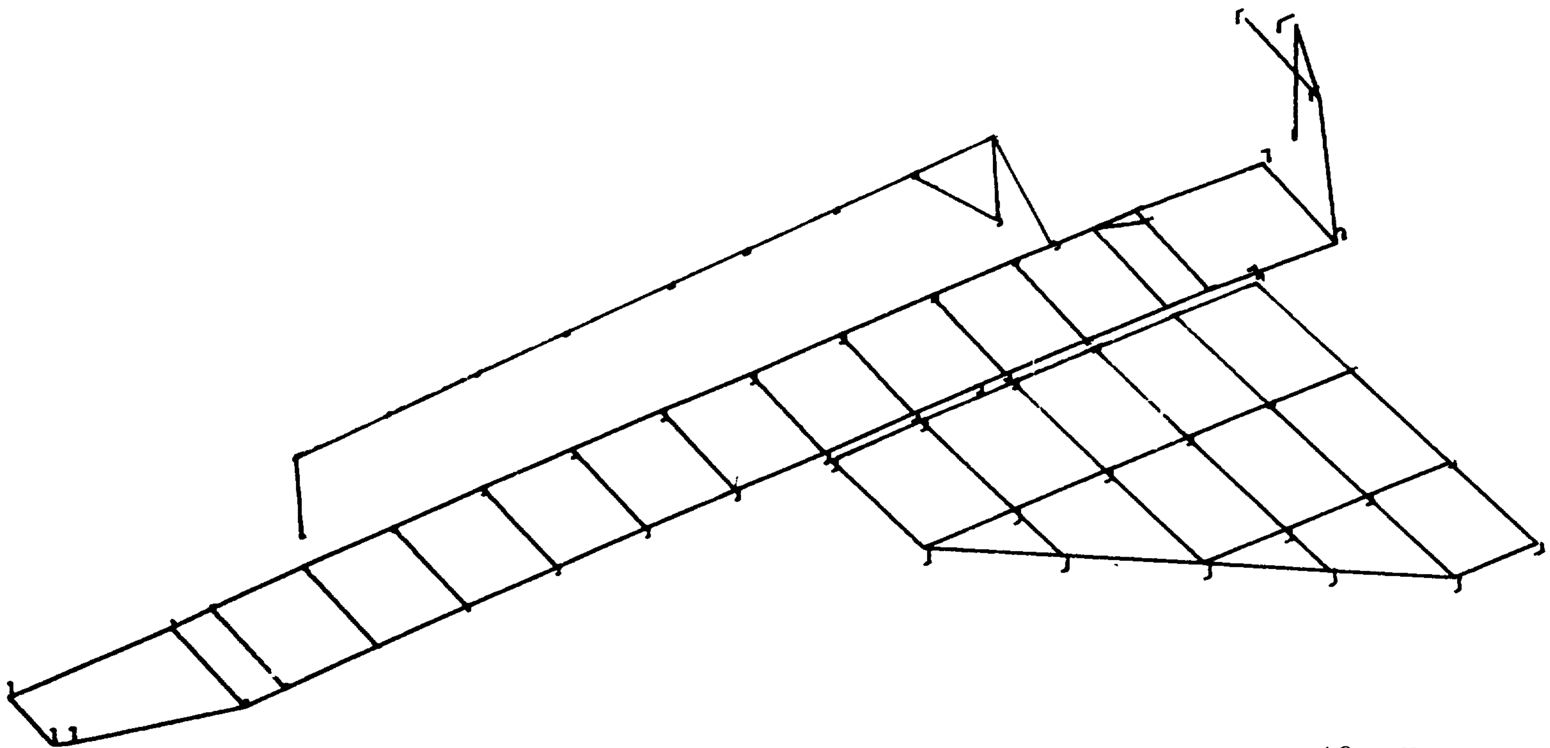

Figure 28.- First elastic symmetric mode of orbiter with forward fin spar cut. 48.1 Hz.

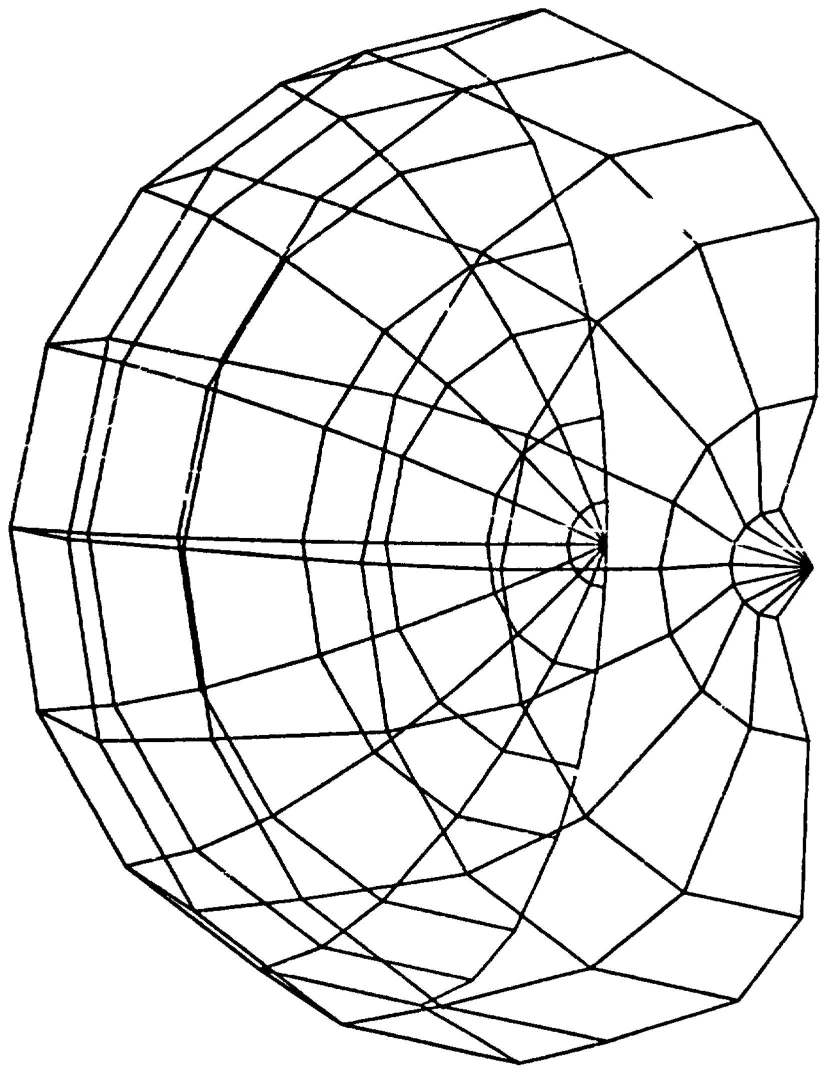

Figure 29.- Deformation of tank dome under 6.9 kN/m^2 (1 psi) showing original and deformed shapes.

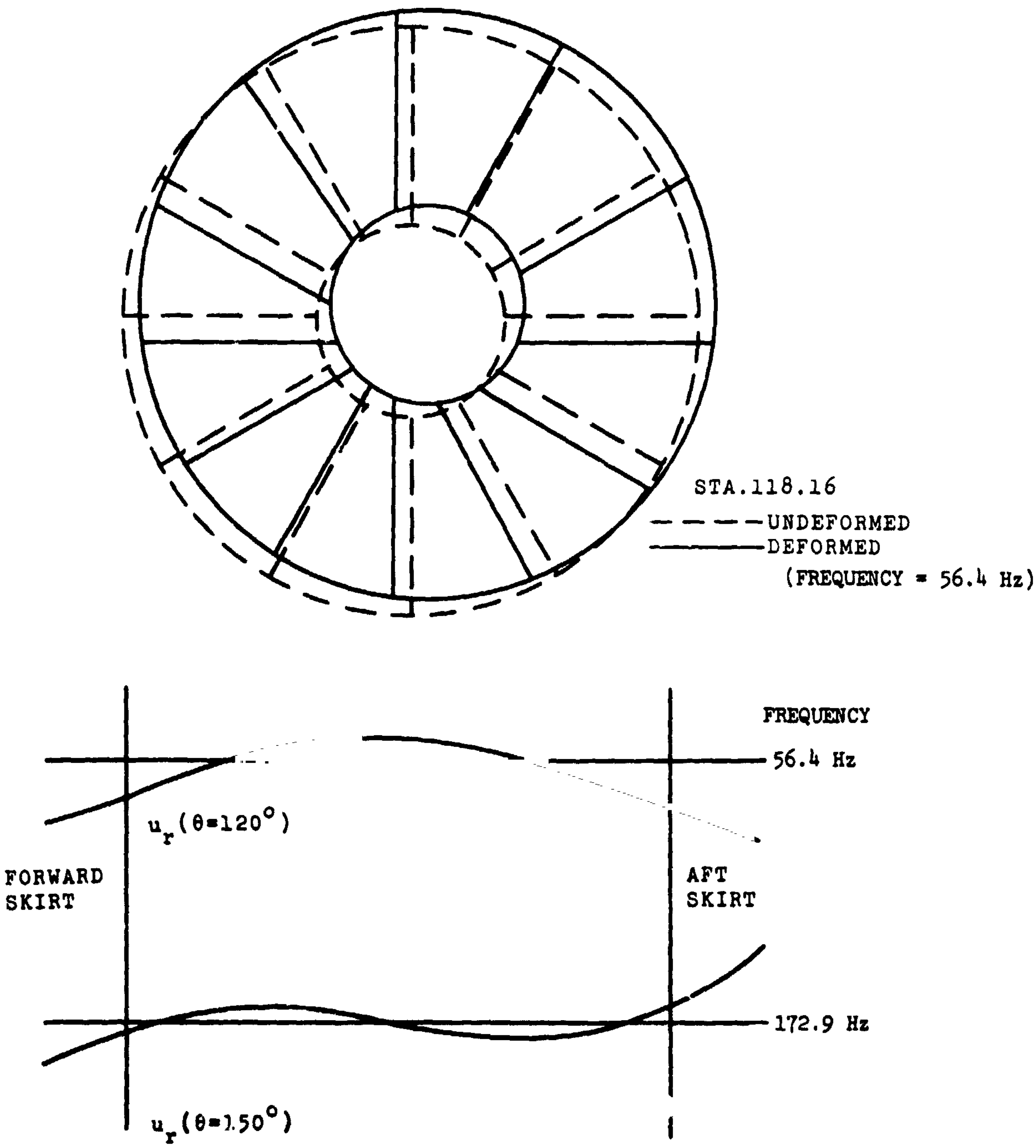

(a) First and second free bending modes.

Figure 30.- Shape for SRB modes.

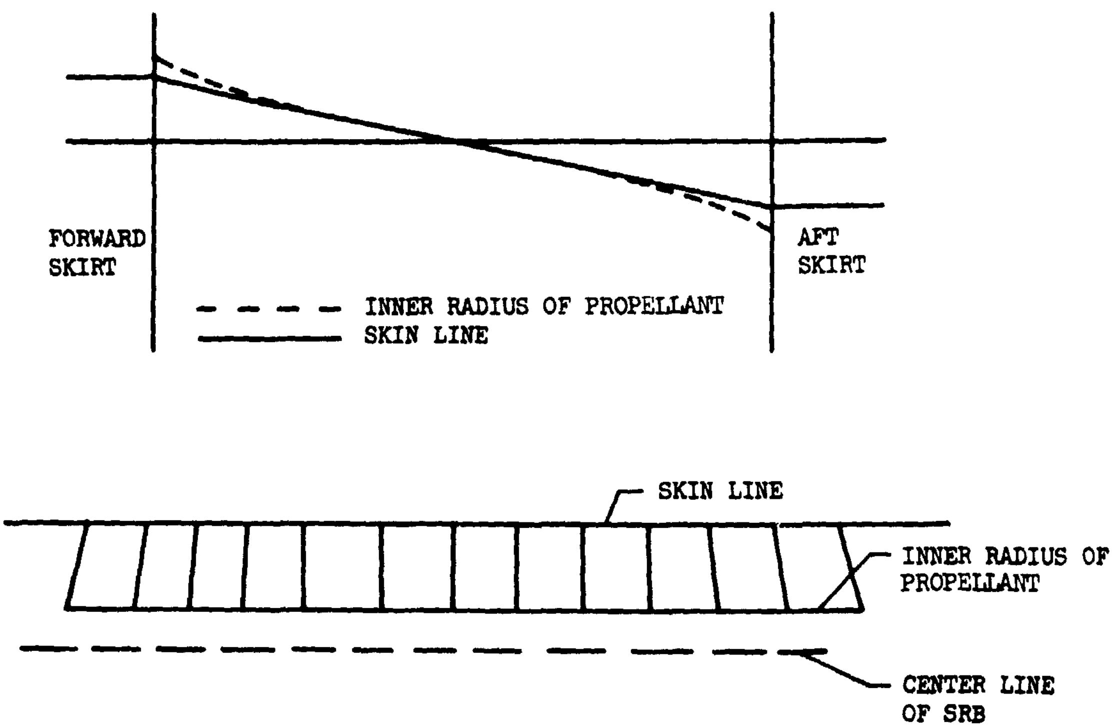

(b) Free longitudinal rod mode showing longitudinal thickness shear deflection. 196.0 Hz.

Figure 30.- Concluded.

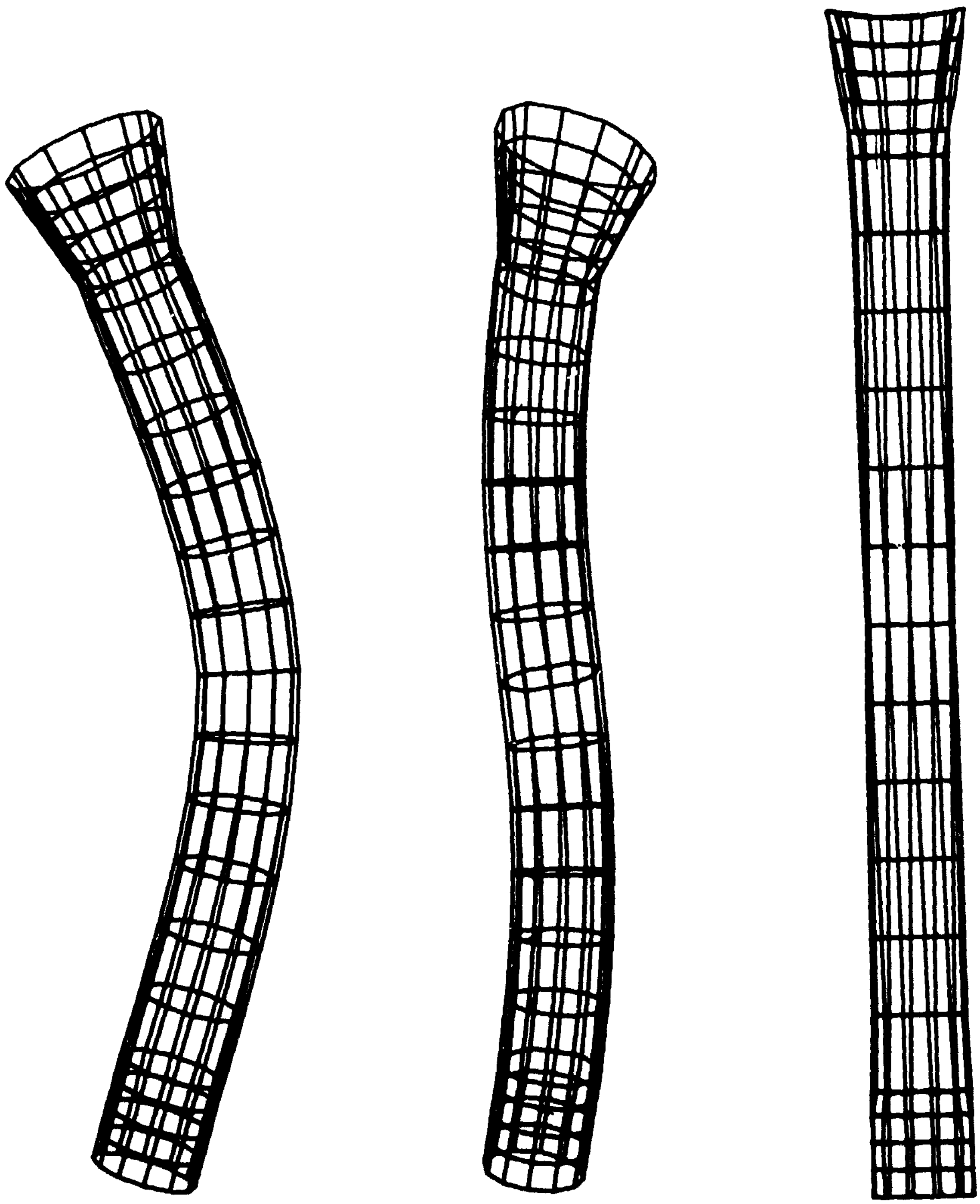

(a) First free bending mode. 56.4 Hz.

(b) Second free bending mode. 173.0 Hz.

(c) Longitudinal mode showing some torsion. 196.1 Hz.

Figure 31.- Shapes for SRB bending modes.

N74-14598

SEISMIC ANALYSIS OF NUCLEAR POWER PLANT STRUCTURES

by

James Chi-Dian Go
Computer Sciences Corporation

ABSTRACT

Primary structures for nuclear power plants are designed to resist expected earthquakes of the site. Two intensities are referred to as Operating Basis Earthquake and Design Basis Earthquake. These structures are required to accommodate these seismic loadings without loss of their functional integrity. Thus, no plastic yield is allowed.

This paper describes the application of NASTRAN in analyzing some of these seismic induced structural dynamic problems and shows that NASTRAN, with some modifications, can be used to analyze most structures that are subjected to seismic loads. A brief review of the formulation of seismic-induced structural dynamics is also presented.

Two typical structural problems were selected to illustrate the application of the various methods of seismic structural analysis by the NASTRAN system.

INTRODUCTION

This paper describes the basic formulation and the method of solution by NASTRAN for the structural responses due to seismic disturbances. Some illustration problems are also presented. The discussion is primarily aimed at nuclear power plant structures; however, it could be applied to other types of structures since the seismic requirements on nuclear power plants are more stringent than most other structures.

ANALYTICAL FORMULATION

The seismic loading is described by the ground acceleration, $A(t)$. Disregarding the soil-structure interaction effect, the structure is subjected to the ground acceleration at its foundation. Thus, the equation of motion for the structure can be expressed as

PRECEDING PAGE BLANK NOT FILMED

$$[M]\{\ddot{X}\} + [C]\{\dot{X}\} + [K]\{X\} = -[M]\{\alpha\}A(t) \tag{1}$$

where

$[M]$	mass matrix
$[C]$	damping matrix
$[K]$	stiffness matrix
$\{X\}$	displacement matrix
$\{\alpha\}$	directional cosines that relate $\{X\}$ to A (t)
A (t)	ground acceleration

Expressing equation (1) by normal mode coordinates, we reduced it to the following uncoupled equation:

$$M_i\ddot{Y}_i + 2\lambda_i M_i \omega_i \dot{Y}_i + K_i Y_i = -\Gamma_i M_i A(t) \tag{2}$$

where

$[\phi]$	characteristic matrix
$\{X\}$	$[\phi]\{Y\}$
$\{\dot{X}\}$	$[\phi]\{\dot{Y}\}$
$\{\ddot{X}\}$	$[\phi]\{\ddot{Y}\}$
M_i	$\{\phi_i\}^T[M]\{\phi_i\}$ = Generalized mass for the i^{th} mode
λ_i	$\dfrac{\{\phi_i\}^T[C]\{\phi_i\}}{2\omega_i\{\phi_i\}^T[M]\{\phi\}}$ = Damping ratio for the i^{th} mode
Γ_i	$\dfrac{\{\phi_i\}^T[M]\{\alpha\}}{\{\phi_i\}^T[M]\{\phi_i\}}$ = Participation factor for the i^{th} mode
ω_i	Undamped circular frequency of the i^{th} mode
$\{\phi_i\}$	Mode shape matrix of the i^{th} mode
$\{\phi_i\}^T$	Transpose of ϕ_i

ω_i and $\{\phi_i\}$ are calculated from:

$$\left|[K] - \omega^2[M]\right| = 0 \tag{3}$$

METHODS OF SOLUTION

The NASTRAN system offers the following methods of solution:

(1) Rigid Format 3; Mode Shape Analysis:

The frequencies of the structure are obtained by Rigid Format 3. From these frequencies an equivalent static load is estimated to facilitate the preliminary design and analysis. The Uniform Building Code accepts this approximate analysis without further analysis by spectrum method or transient method

(2) Rigid Format 9; Direct Transient

The degrees of freedom of the structure are condensed by Guyan reduction. The mass of the structure is distributed and input via CONM2 cards. The forcing function, $-A(t)M_i$ is input by TLOAD1 cards, where $A(t)$ is the ground acceleration history and M_i the concentrated mass specified by CONM2 cards. The time function, $A(t)$, is specified by TABLE1 cards, and the scale factors of DAREA cards are set equal to the numerical values of M_i.

(3) Rigid Format 8 or 11; Direct Frequency Responses or Model Frequency and Random Response

The mass of the structure is distributed at the active DOF and input via CONM2 cards. The loading is input by RLOAD1 cards. The loading is equal to $-SA(f) * M_i$ where $SA(f)$ is the seismic spectrum, M_i is the mass at DOF i, and f are the frequencies. SA(f) is input by TABLED1 and M_i by DAREA cards as scale factors. These analyses should be performed by restarting from Rigid Format 3 run.

ILLUSTRATION PROBLEMS

(1) Heat Exchanger (Test Model)

The heat exchanger structure as shown in Figure 1 is analyzed according to Uniform Building Code, UBC. The frequencies were obtained by Rigid Format 3. An equivalent static load was computed according to UBC and static analysis was made under the combined loadings of this equivalent seismic load, thermal loads and differential air pressure. Results of this combined loading was compared with other specified combined loadings. Under this seismic analysis, this heat exchanger is only qualified as a separate test unit and not as a part of any nuclear power plant.

(2) Shielding Structures

Figures 2 and 3 show the NASTRAN model of an interim fuel element decaying shielding system. This system consists of a cover plate, a neutron shield, and a thermal shield. The transport equipment which is movable and locked on the cover when in use is considered as nonstructural mass. The cover plate, the neutron, and the thermal shield are modeled by plate elements and connecting bars by bar elements. This model has about 1200 DOF and was condensed to about 250 DOF by Guyan reduction. The difference between the fundamental frequency of the original model and of the Guyan model is less than 1%.

CONCLUSION

From the experiences based on these analyses, it is obvious that NASTRAN can be used to analyze structural dynamics under seismic loads. The NASTRAN system has no limitation on the structural model size as imposed in most other general purpose structural analysis programs. Other advantages in using the NASTRAN system in dealing with seismic analysis are:

Restart and loading combinations

Flexible I/O format

Model applicable to all computers and analysis

Complete selection of analysis methods

We did not make any cost comparison with any other programs; however, we believe the overall cost (man-hours plus computer charges) are lower than other major programs.

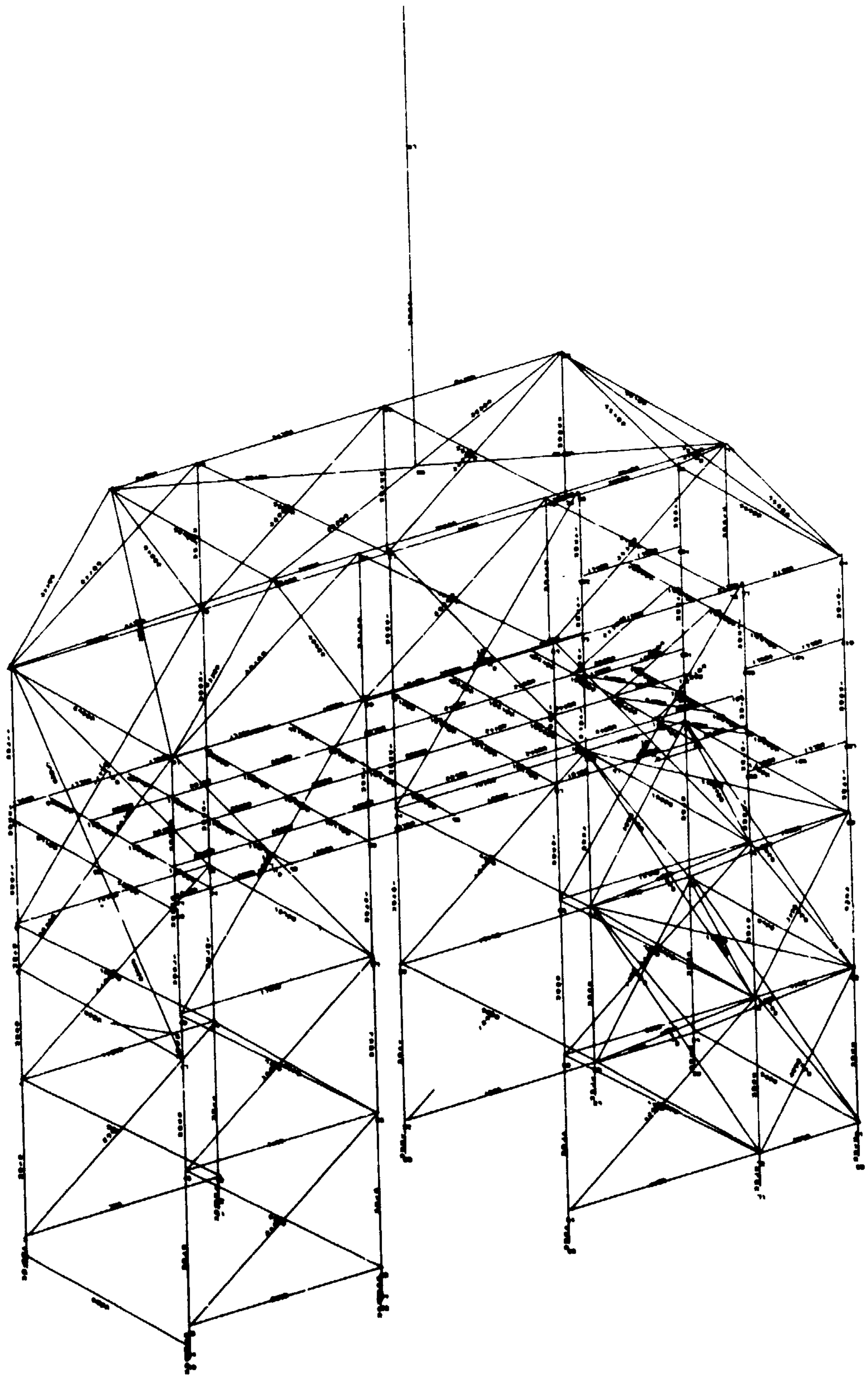

Figure 1.- Heat exchanger (test unit).

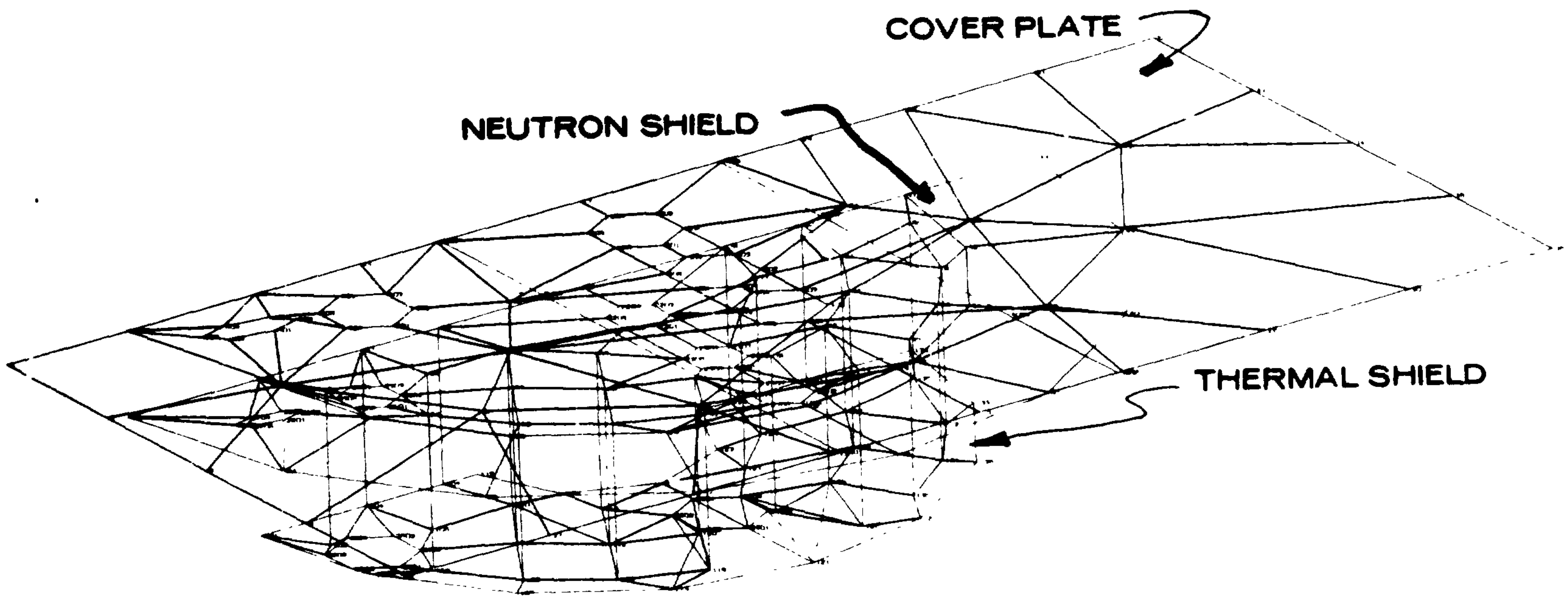

Figure 2.- Undeformed structural model.

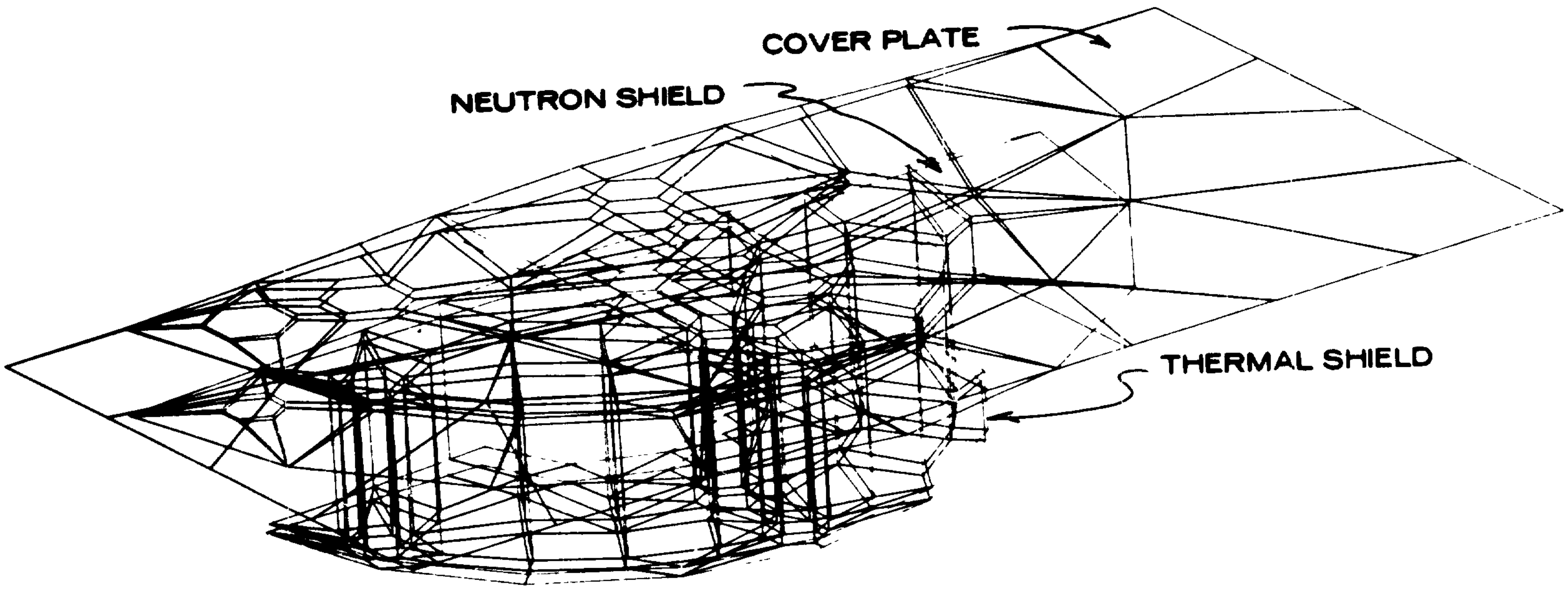

Figure 3.- Mode shape.

N74-14579

BLADE DYNAMICS ANALYSIS USING NASTRAN

By Peter S. Kuo

Avco Lycoming Division
Stratford, Connecticut

SUMMARY

The complexities of turbine engine blade vibration are compounded by blade geometry, temperature gradients, and rotational speeds. Experience indicates that dynamics analysis using the finite element approach provides an effective means for predicting vibration characteristics of compressor and turbine blades whose geometry may be irregular, have curved boundaries, and be subjected to high temperatures and speeds.

The NASTRAN program was chosen to help analyze the dynamics of normal modes, rotational stiffening and thermal effects on the normal modes, and forced responses. The program has produced reasonable success. This paper presents the analytical procedures and the NASTRAN results, in comparison with a conventional beam element program and laboratory data.

INTRODUCTION

Accurate prediction of blade vibration in axial-flow compressors and turbines is one of the most important design steps in the development of modern gas-turbine engines. This prediction includes the calculations of blade natural frequencies and modes, rotational stiffening and thermal effects on the normal modes, and the blade forced responses. Vibration analyses performed previously with the use of beam element theory and a lumped mass approach were found to be inadequate because of the structural complexity in advanced blade design. The NASTRAN (NASA STRUCTURAL ANALYSIS) finite element method, modeling by plate elements, has produced reasonable agreement with the measured data, and therefore a computerized blade geometry generator has been developed to reduce the structural idealization effort. This development is incorporated with other dynamic analyses using NASTRAN.

NASTRAN BLADE DYNAMICS ANALYSIS PROCEDURE

A complete dynamics analytical procedure primarily for determining blade frequencies and modes using NASTRAN (Level 12.0) has been developed at Avco Lycoming Division. An outline of the theoretical approaches is described as follows:

1) An automated blade geometry generator using streamline definition is provided as a NASTRAN preprocessor, which constructs a grid-point pattern following the blade streamline flows and/or curved boundaries. This generator produces an accurate NASTRAN model of an irregular blade configuration, and it minimizes the input data preparation.

2) After the geometry of a blade is generated, NASTRAN normal mode analysis (Rigid Format #3) is used to perform the static natural frequency and mode shape calculations (no rotational stiffening effect). The eigenvalue extraction method (Inverse Power) is selected to determine the roots within a frequency range of interest. The results of the calculation for natural frequencies and modes are examined for design use.

3) The effect of rotational (inertia) stiffening on the natural frequencies and mode shapes of a rotating blade must be considered in the analysis. This is achieved, within the NASTRAN program, by introducing the preload stiffening effects ("differential stiffness" terms) into the free-mode calculations (Reference 1).

PRECEDING PAGE BLANK NOT FILMED

4) Temperature variations in a blade will affect the structural stiffness and therefore the eigenvalue solutic Temperature distribution is reflected by material property changes, so the effect of temperature gradier can then be accounted for in the normal mode analysis with or without rotational stiffening effect.

5) The calculated eigenvectors from the previous analyses may be utilized as input data to the related mo of the NASTRAN program for a forced response analysis. An example of such an application is the NASTRAN transient analysis using the modal formulation method.

DESCRIPTION OF NASTRAN BLADE MODEL GENERATOR

A computer program to automate a blade structural model has been provided as the NASTRAN preproce: The model generator provides a punchout or a printout or both for all necessary definitions in a form suitable 1 NASTRAN bulk data input (Reference 2). This input includes the GRID space coordinates, CTRIA2 definition PTRIA2 properties, MPC constraint conditions, etc.

The program takes a blade geometry defined by a set of aerodynamic flow streamlines and the associated blade profiles (airfoils) to form a NASTRAN finite element model. The model grid-point pattern follows the streamline flows or the curved boundaries, or both, of the structure. The object of the model design is to ob an accurate blade model definition and to minimize the bandwidth of the gridwork for best computing efficien Finite elements with nearly equilateral triangles are formed by interconnecting the grid points. This interconne tion represents the middle surface of the curved blade, which has a rectangular XYZ-coordinate system referred the axial, tangential, and radial directions of the rotating machine. The calculation procedure for finite element presentation involves the following:

The program,

1) Determines the camber-line of a blade section given on a nonplanar surface.

2) Divides the camber-line and the blade length into segments according to an input percent value.

3) Calculates the cross-sectional thickness at each grid point location, starting at the leading edge and termin ing at the trailing edge.

4) Interconnects the grid points between the two adjacent blade sections to form finite elements with nearly equilateral triangles, starting from the tip and ending at the hub.

5) Transfers the initial vertical axis of a section to be coincident with the blade stacking line forming a rectangular XYZ-coordinate system referred to the axial, tangential, and radial direction of a rotor.

6) Deletes the rotational degree of freedom normal to the blade surface by defining multiple-point-constraint (MPC) conditions at each grid point. This constraint will eliminate the grid-point singularities.

As a demonstration related to the above calculation procedure, Figure 1 shows: a) a typical airfoil turbi blade section, b) the composite view of the airfoil profiles, and c) the two-dimensional blade model plotted by the generator.

Another example shown in Figure 2 is an undeformed compressor blade model with a streamline grid-point pattern. This figure was generated by the NASTRAN program in orthographic projection with the use of the NASTRAN preprocessor.

RESULTS

1) Normal Mode Analysis

NASTRAN normal mode analysis (Rigid Format #3) was performed to determine the natural frequencies and modes of both compressor and turbine blades of representative configurations. The blades analyzed are variable in geometry and are assumed cantilevered at their root fixity with complete boundary single-point constraints.

A) Compressor Blade Example

A compressor blade whose characteristics are a wide chord and thin section geometry (Figure 3) was chosen to demonstrate the NASTRAN calculations. This full-size blade has an approximate geometry as follows: aspect ratio = 1.75 (blade length/chord length at tip), twisting angle = 31 degrees (at the tip), and the maximum thickness taper ratio = 0.35 (tip/hub). Table 1 presents a summary of vibration data obtained from: 1) NASTRAN (using finite plate elements), 2) lumped mass vibration program analysis (using beam theory, Reference 3), and 3) shaker test of the actual blade.

Figures 3 and 4 show the resonant frequencies and nodal patterns (zero deflection lines) determined by the shaker test while using a stroboscope, hand-held vibration pickup, and oscilloscope.

The corresponding NASTRAN orthographic projections of the undeformed and deformed models are shown in Figures 5 and 6.

B) Turbine Blade Example

A shaker test was conducted with a power turbine blade, in a manner similar to the test with the compressor blade, to determine the resonant frequencies and vibration modes of a 10X size cast-aluminum model. The measured data were then used to confirm those from the NASTRAN analysis for the actual engine blade size by applying an equivalent scale factor.

The test model on its shaker mounting and the NASTRAN model generated by the preprocessor are shown in Figures 7 and 8, respectively.

Table 2 represents the results (natural frequencies and mode shapes) obtained from NASTRAN as well as by measurements.

2) Blade Rotational Stiffening Calculations

The present NASTRAN normal mode analysis is limited to nonrotating structures. However, the effect of rotational stiffening on the natural frequencies of a rotating blade can be included by using the program's DMAP (Direct Matrix Abstraction Program) feature. This objective is achieved by altering the original computational sequences so that the terms of the "differential stiffness" can be combined with the structural stiffness matrices (References 1 and 4).

The effect of rotational stiffening in the rotational field of a compressor blade (Figure 3) has been demonstrated. The frequency increase with respect to rotational speed are plotted on an excitation diagram (Figure 9). This data is compared with the corresponding data computed by an in-house vibration program, which employ the "transfer matrix" technique applied to a lumped parameter model of the beam.

3) Blade Modal Transient Response

The performance of the NASTRAN modal transient response (Rigid Format #12) was investigated with the use of the existing compressor blade model (Figure 5). The program's general functions were demonstrated by several computer runs with simplified dynamic loadings, so that the time-dependent forced responses of a blade may be studied in plots of displacement, velocity, and stress versus time. One of such plots, illustrating transient motion resulting from an arbitrary loading and damping, is shown in Figure 10 as an example.

4) Blade Thermal Variation Effect

The combined effect of high-temperature gradients associated with rotational speed fields on the dynamic characteristics of a turbine blade must be analyzed. The steady-state thermal variations within the structure will be reflected by material property changes from element to element. By superposing the thermal and centrifugal influences, the simulation of engine operating environments for a turbine blade can be accomplished. No numerical example is presented here.

DISCUSSION OF RESULTS

1) From the results summarized in Table 1, the NASTRAN finite element method has proved to be superior in accuracy to the vibration program employing beam theory. The use of a conventional beam element to idealize a blade structure will result in two inherent restrictions related to the beam theory: 1) neglecting warping displacements (i.e., plane sections remain plane), and 2) assuming no chordwise flexibility (i.e., each section retains its cross-sectional shape). The exclusion of warping constraints has significantly decreased the torsional rigidity, and therefore the torsional frequencies, of the beams. For the compressor blade analyzed, deviations of 29 and 30 percent compared with NASTRAN were found for the first and second torsional frequency respectively. However, a torsional frequency increase of more than 100 percent has been reported in thin-walled beams with open cross sections due to the inclusion of the warping effect (Reference 5).

The second restriction (above), assuming no cross-sectional deformation of the beam elements, introduces considerable errors in bending modes of higher order. The errors are particularly high for the blades with low aspect ratio and thin cross section, where the blade chordwise deformations must not be neglected.

2) The overall correlation between the laboratory measurements and NASTRAN normal mode analysis has been reasonably good, especially in the case of compressor blades, and for the frequencies of lower modes. Deviation of results attributed to mechanical tolerances, methods of measurement, and thickness approximation in model idealization may be expected. One of the significant differences is the turbine blade mode No. 4 (Table 2), which has not been identified by the NASTRAN in the search of eigenvalue solutions (Inverse Power Method). However, since test modes 4 and 5 show small distinction between their nodal patterns, it suggests that the additional laboratory confirmations are desirable before any conclusions may be made regarding the missing mode.

3) In the excitation diagram (Figure 9), the rotational stiffening effects obtained from the beam element model and the plate element model (NASTRAN) are compared. To simplify the comparisons, however, the bending frequency curves (dashed) generated by the beam program are assumed to be coincident with NASTRAN data at the zero speed so that the trend of frequency increases predicted by both programs can be compared directly. The NASTRAN-computed points at 12,000 and 20,000 rpm show a reasonable relation with the results from the beam program. Variation exists in the second blade bending mode; in this case NASTRAN indicates a smaller frequency gain. The difference could be attributed to the coupling effect between the NASTRAN second bending and first torsion modes because of their closeness in frequency. In addition, the centrifugal stiffening effect on torsional modes has also been predicted by NASTRAN (neglected in the beam program because of lack of elastic axis information), although the percentages of increase are relatively smaller.

The natural frequencies are observed to increase as the product (rotational speed)^2 (disk radius) increases since centrifugal force is a stiffening influence. However, the amplitude of frequency increase is also a function of blade aspect ratio and blade setting angle (Reference 6). The present study does not have sufficient data to evaluate these individual parameters, but it is felt that the plate finite element method will reflect the similar trend as experienced by the beam theory for these parameters.

4) In the forced response plot (Figure 10), the blade is acted on by an external harmonic force (arbitrary amplitude) having a frequency of 60 Hz which is 8.8 times as slow as the first mode of the blade (529 Hz). The cosine function periodic force is applied at a grid point on the leading edge in X-direction. The predicted transient response is constructed for a selected point on the tip. As shown in the plot, the total response at any instant between 0 and 0.022 seconds consists of the damped free vibration superposed on the forced motion. The displacement of the free vibration will, after a short time, disappear due to damping effect. Only the forced motion may continue. The higher frequency (529 Hz) appearing in the response corresponds to the first mode of the blade. Two lowest natural modes were introduced into the modal formulation transient response analysis.

CONCLUDING REMARKS

The automated blade geometry generator has significantly simplified the data preparation effort for the NASTRAN program. However, due to the generalized nature of this program (Level 12.0), the computing efficiency associated with eigenvalue extraction is low so that its use is costly.

NASTRAN finite element modeling using a plate element has provided an effective means for predicting blade vibrations. This conclusion is based on a comparison of results obtained from the NASTRAN program with experimental results and classical theory.

ACKNOWLEDGEMENT

The author expresses his gratitude to Dr. H. Klein and Mr. E. Beardsley for their many valuable suggestions in the preparation of this paper. Special recognition is given to Mr. F. Gybowski for his computer programming work related to the blade model generator.

REFERENCES

1) Anon.: NASTRAN Newsletter. March 13, 1972.

2) McCormick, Caleb W., Editor: The NASTRAN Users' Manual. September 1970.

3) Towgood, D.: Coupled Bending-Bending-Torsion Vibration of Rotating Twisted and Tapered Blading, Using The Transfer Matrix Approach. Avco Lycoming Division Technical Report No. AND 065-10, Project Contract No. 555-8100.

4) MacNeal, Richard H., Editor: The NASTRAN Theoretical Manual, September 1970.

5) Skattum, Knut S.: Modeling Techniques of Thin-Walled Beams With Open Cross Sections. NASA TM X-2637, NASTRAN Users' Experiences, September 1972.

6) Dokainish, M. A. and Rawtani, S.: Vibration Analysis of Rotating Cantilever Plates, International Journal for Numerical Methods in Engineering, vol 3, pp. 233-248, 1971.

Table 1. Summary of Compressor Blade Vibration Data

Natural Frequencies and Modes

Mode No.	Mode Name	Natural Frequencies, Hz		
		1. NASTRAN	2. Vibration Program (Beam Theory)	3. Shaker Test
1	1st Bending	529	540	486
2	2nd Bending	2026	2100	1856
3	1st Torsion	2125	1650	2130
4	3rd Bending	4483	4850	3410 3940 4200
5	2nd Torsion	4871	3740	4730 5300
6	4th Bending	6173	6400	–

Table 2. TURBINE BLADE VIBRATION DATA COMPARISONS NATURAL FREQUENCY AND MODES

MODE NO.	SHAKER TEST-TURBINE BLADE MODEL (10 x SIZE) MODE SHAPE	SHAKER TEST NATURAL FREQUENCY, Hz*	NASTRAN RESULTS ENGINE BLADE (1 × SIZE) NATURAL FREQUENCY, Hz*	NASTRAN MODE SHAPE	REMARKS
1	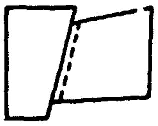	3.800	3.850	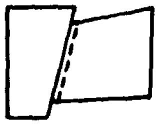	Test Frequency Was Adjusted to Compensate Model Root Radius Variation
2	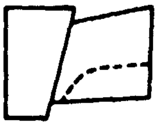	7.940	7 700	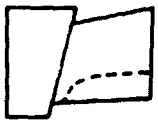	
3	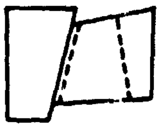	9.910	9.420		
4	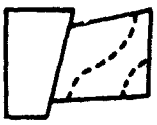	12 610	–		NASTRAN Does Not Yield this Mode
5	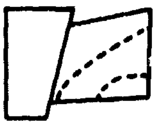	14.620	14,180		
6		16 320	16.760		
7	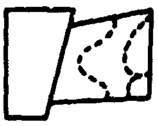	23.990	21.890		
8	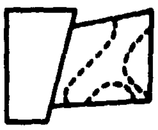	24 500	23.510		

*The Listed Model Blade (10 x Size) Frequencies Are in Terms of the Equivalent Actual Engine Blade at Room Temperature

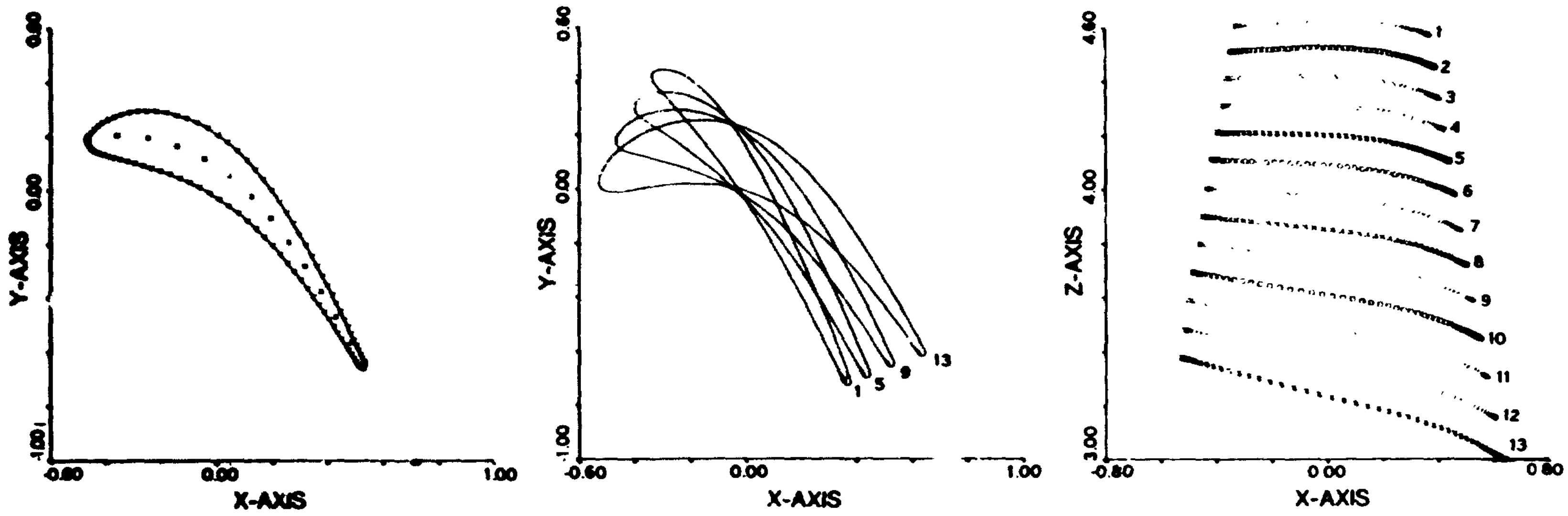

a) A Typical Turbine Blade Airfoil Section Showing the Calculated Camber Line

b) The Composite View of the Airfoil Pro...s

c) A Two-Dimensional Blade Model Generated by the Preprocessor

Figure 1.- Illustration of plots obtained from the blade model generator.

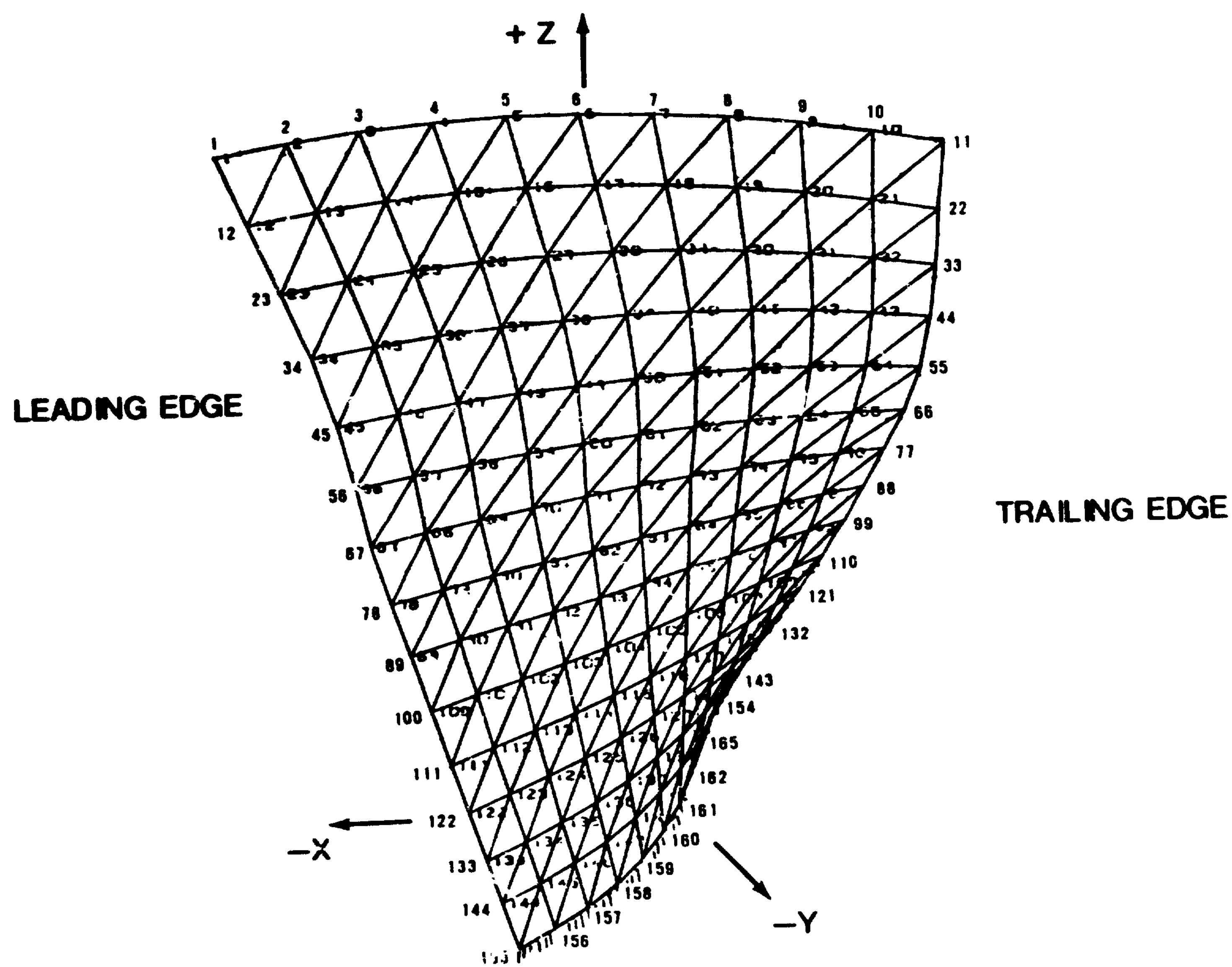

Figure 2.- Example of NASTRAN undeformed compressor blade model generated by using the blade model generator.

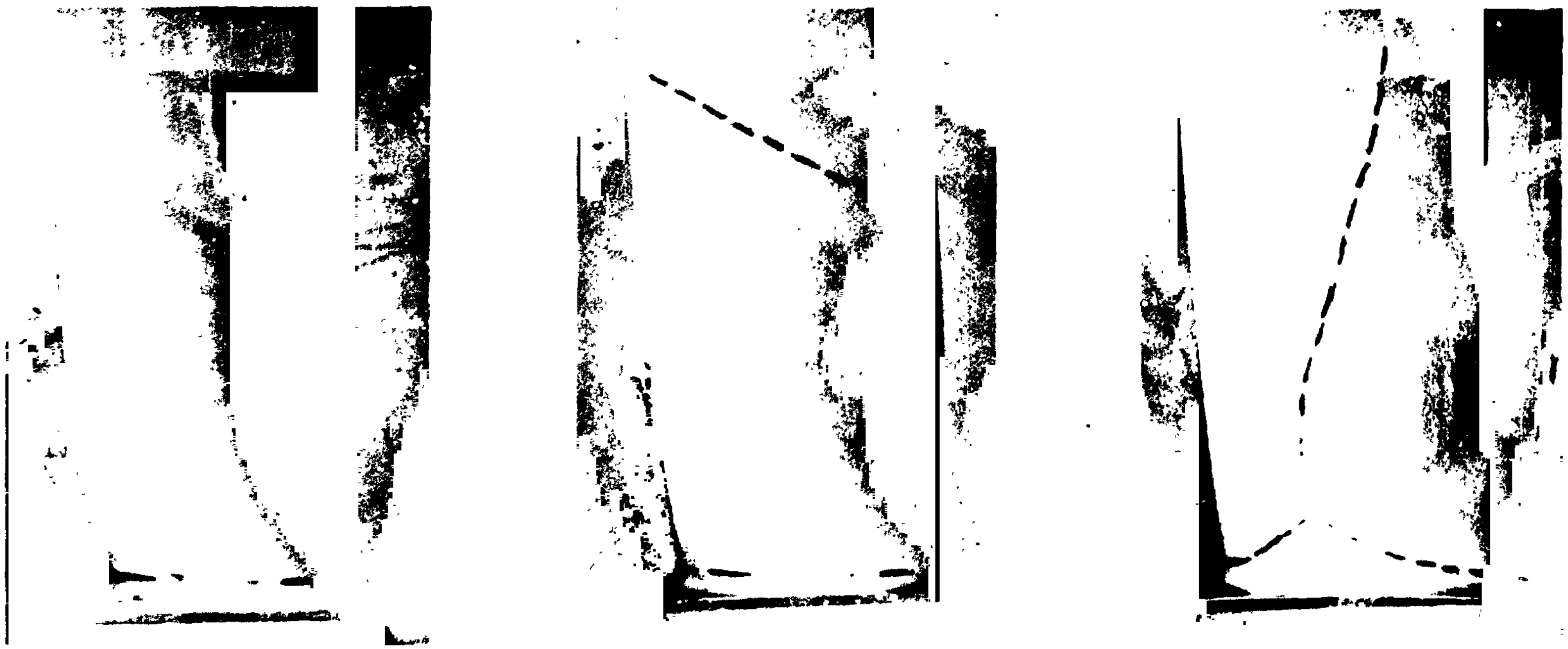

Figure 3.- Shaker-test – wide-chord compressor-blade-measured natural frequencies and nodal patterns (modes 1, 2, and 3).

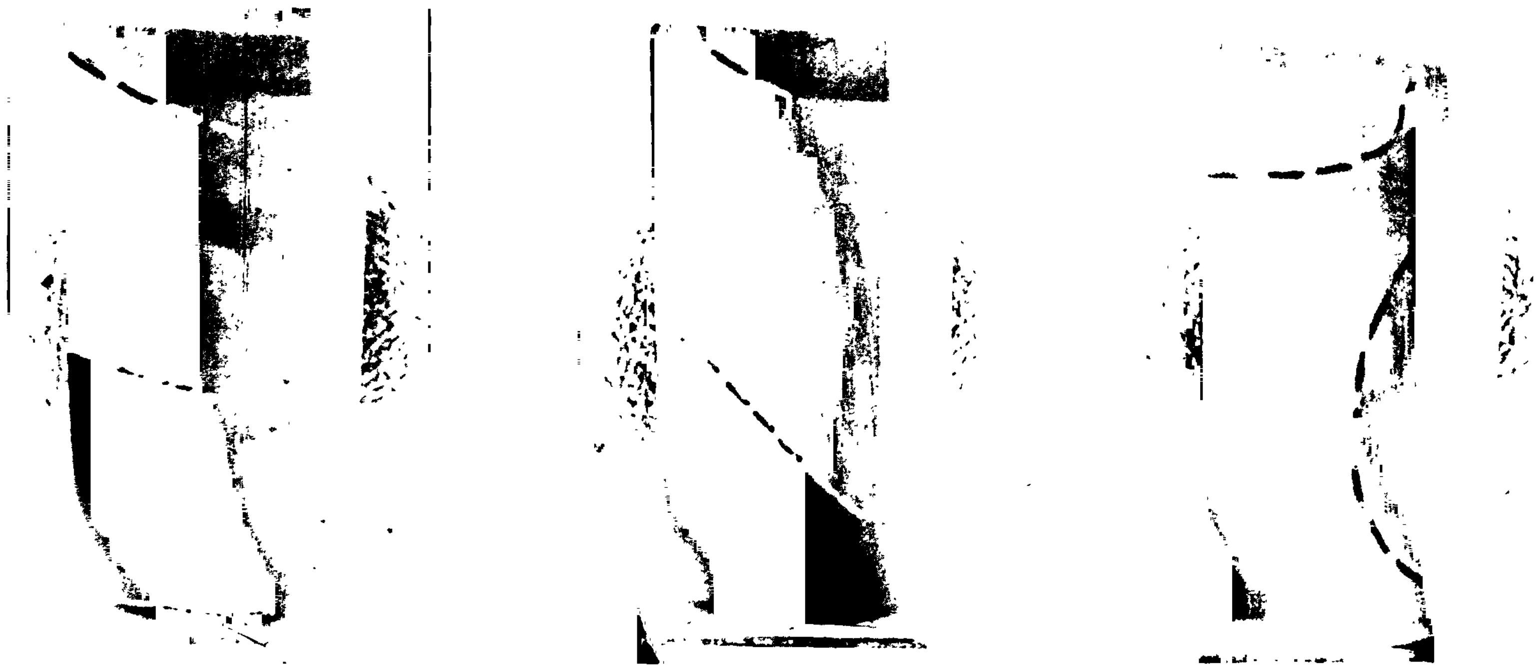

3410 Hz
THIRD BENDING

3940 & 4200 Hz
THIRD BENDING

5020 Hz
SECOND TORSION

Figure 4.- Shaker-test – wide-chord compressor-blade-measured natural frequencies and nodal patterns (modes 4, 5, and 6).

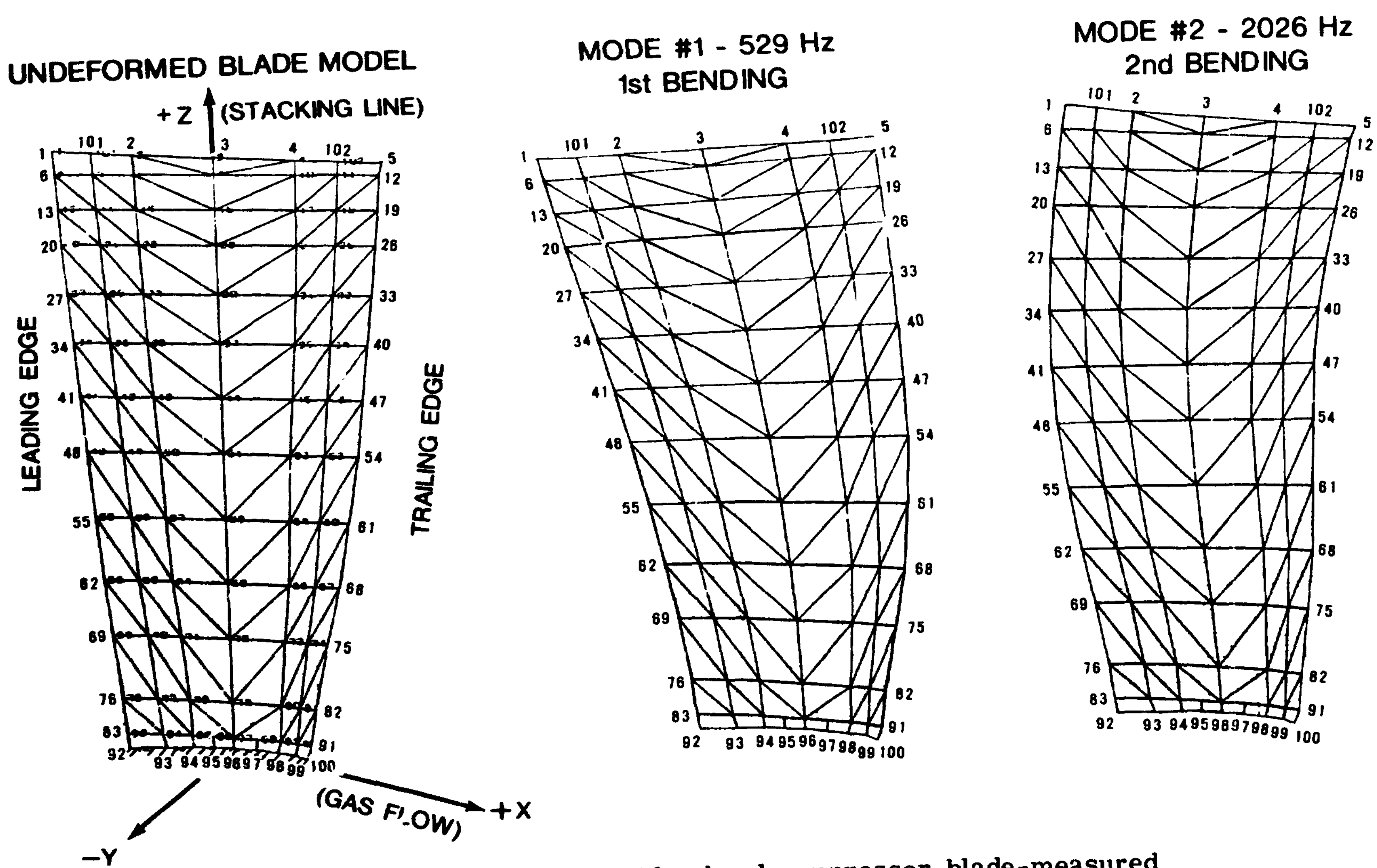

Figure 5.- NASTRAN model – wide-chord compressor-blade-measured natural frequencies and mode shapes (undeformed model, modes 1 and 2).

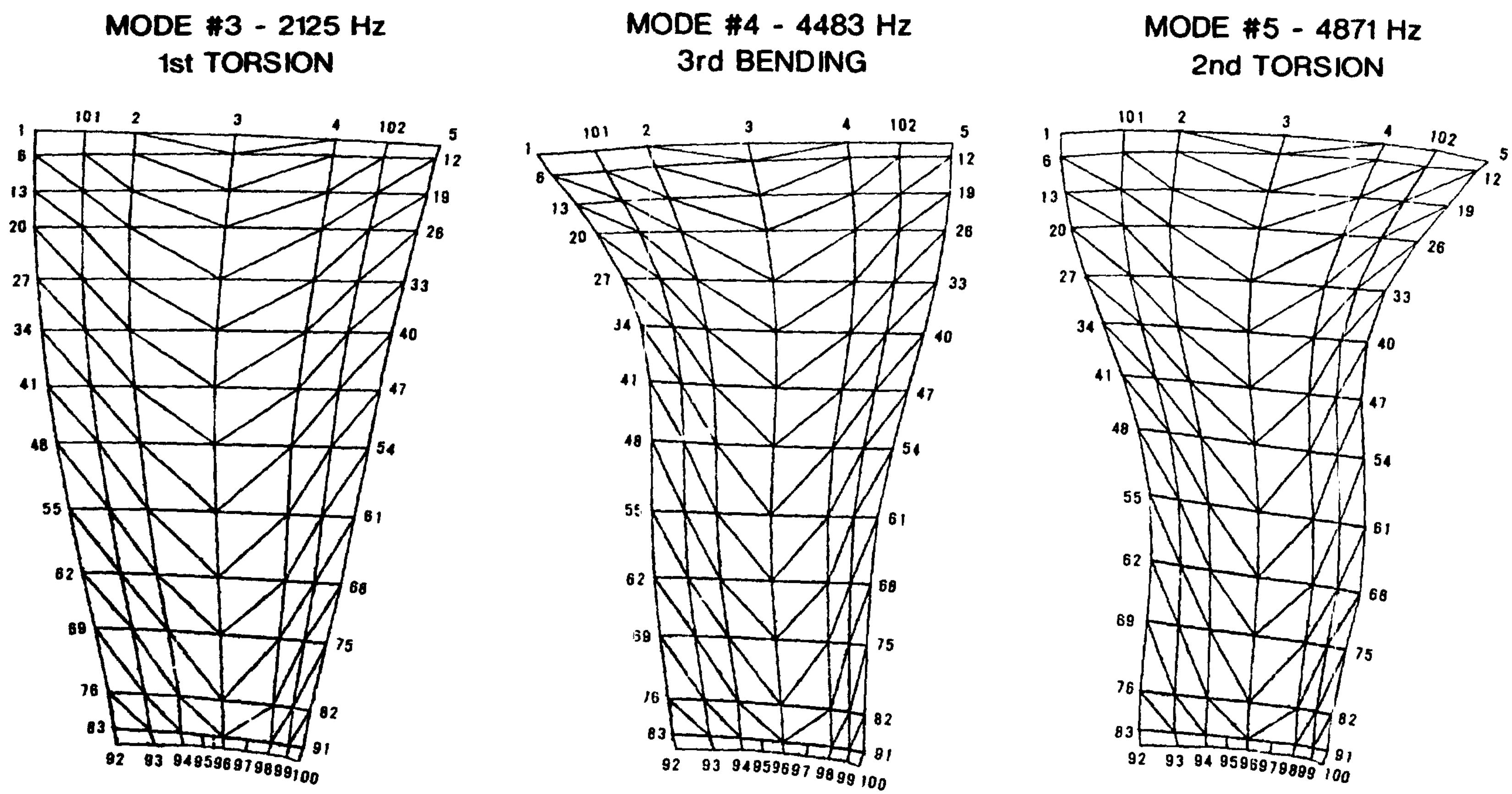

Figure 6.- NASTRAN model – wide-chord compressor-blade-measured natural frequencies and mode shapes (modes 3, 4, and 5).

Figure 7.- Vibration test setup. Power turbine blade (10 × size) aluminum model.

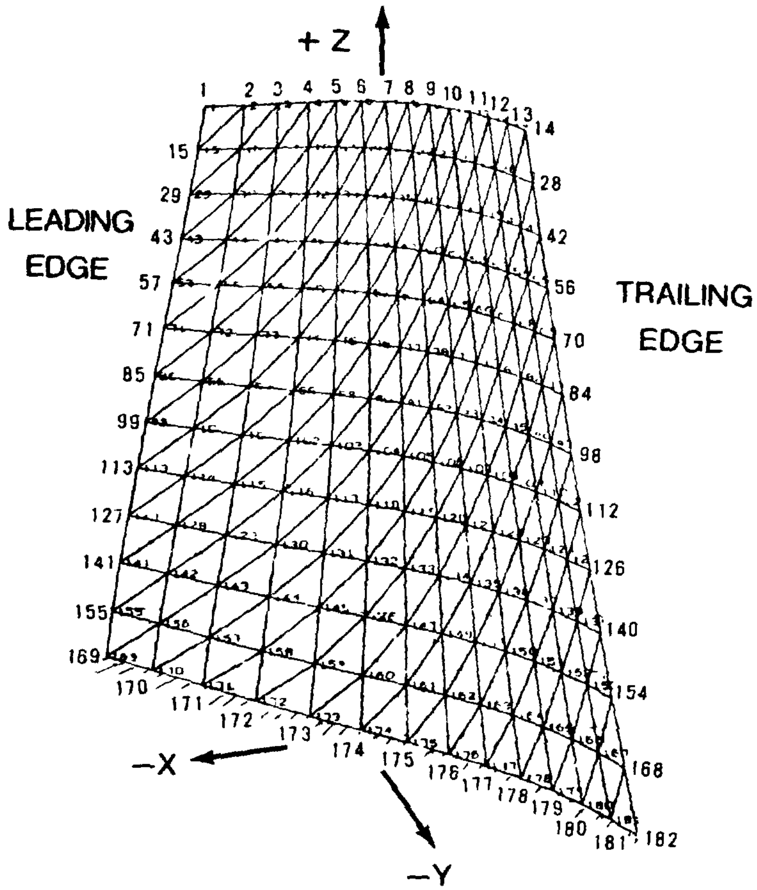

Figure 8.- NASTRAN undeformed turbine blade model.

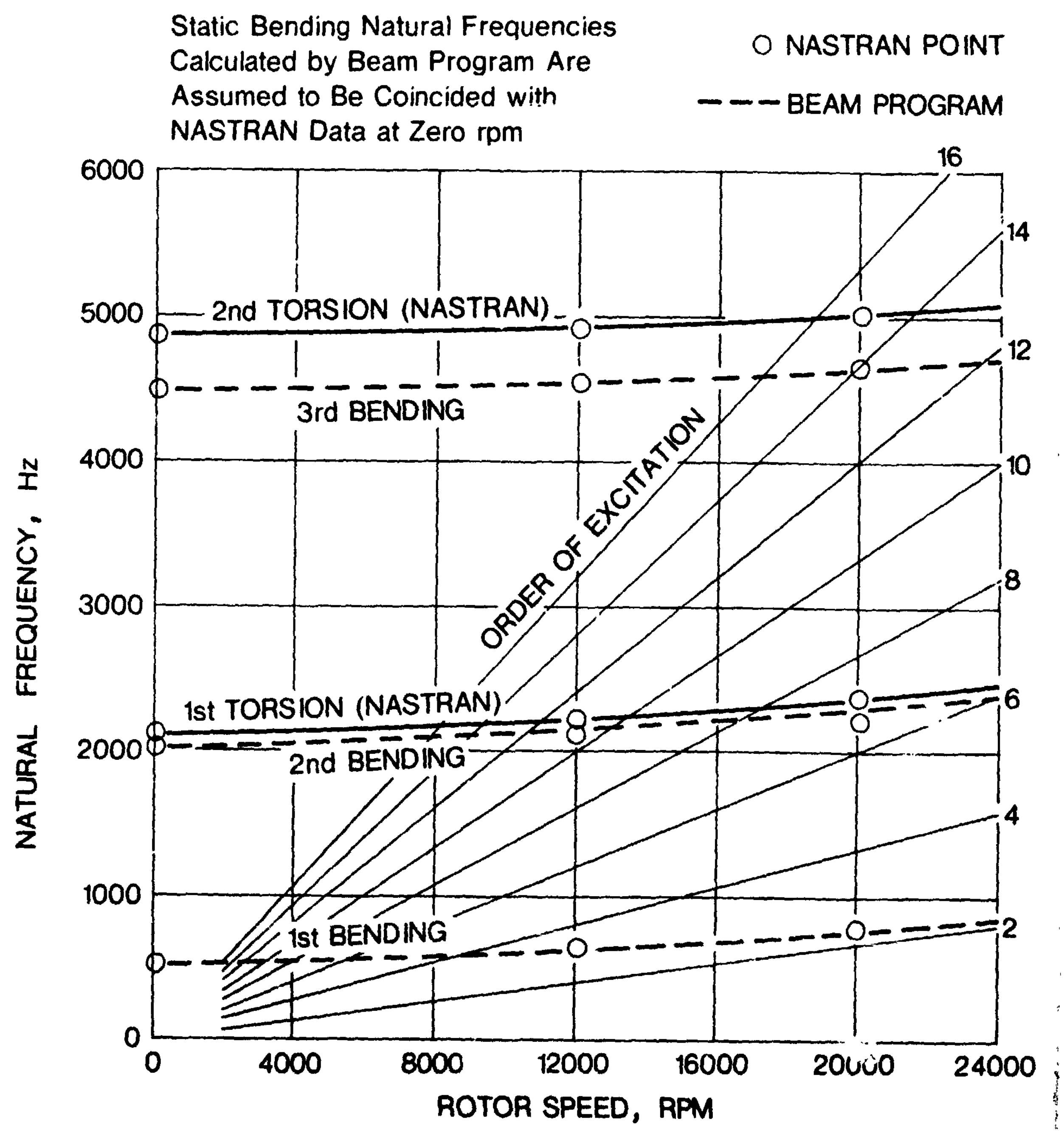

Figure 9.- Excitation diagram of the wide-chord compressor blade showing the rotational stiffening effects.

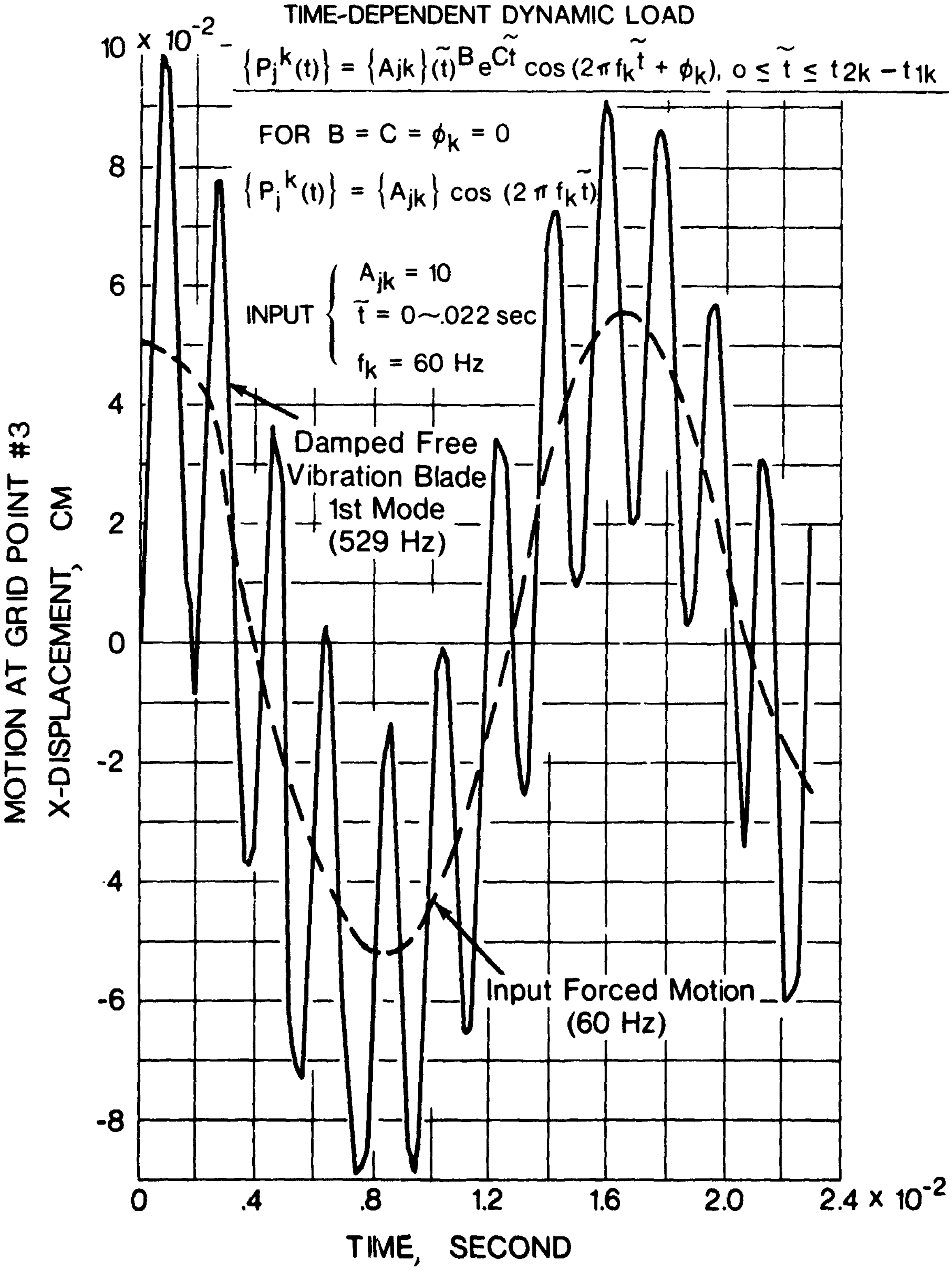

Figure 10.- Example of starting transient of the wide-chord compressor blade.

N74-14600

A NASTRAN DMAP ALTER FOR DETERMINING A LOCAL STIFFNESS MODIFICATION TO OBTAIN A SPECIFIED EIGENVALUE

By William R. Case, Jr.

NASA Goddard Space Flight Center

SUMMARY

This paper describes a technique, which has been programmed as a DMAP Alter to Rigid Format 3, for determining a stiffness matrix modification to obtain a specified eigenvalue for a structure. The stiffness matrix modifications allowable are those that can be described as the product of a single scalar variable and a matrix of constant coefficients input by the user. The program solves for the scalar variable multiplier which will yield a specified eigenvalue for the complete structure (provided it exists), makes the modification to the stiffness matrix, and proceeds in Rigid Format 3 to obtain the eigenvalues and eigenvectors of the modified structure.

INTRODUCTION

The motivation for devising a technique for determining a local stiffness modification to obtain a specified eigenvalue stemmed from several launch loads analyses performed at the Goddard Space Flight Center in which these analyses were updated using data from hardmount spacecraft vibration tests. Quite often, spacecraft are attached to their launch vehicle via a Marmon type clamp band. Generally, the clamp band attaches the spacecraft to an adapter section which in turn is bolted to the launch vehicle. However, the stiffness of the clamp band is often not known well enough to make an accurate analytical prediction of the fundamental mode of the spacecraft adapter structure when cantilevered from the base of the adapter, as it is in the spacecraft vibration tests. Thus, the original launch loads analyses are updated to reflect these discrepancies once the modes of the spacecraft-adapter structure have been measured in tests.

PRECEDING PAGE BLANK NOT FILMED

Updating any finite element model to agree with modal data obtained from tests usually requires a trial and error process in which some local stiffness is adjusted until the fundamental mode of the model agrees with the test data. However, if a value for the local stiffness exists which will give the finite element model the measured eigenvalue, then this stiffness can be found analytically.

The DMAP Alter presented computes the value of the stiffness (or stiffness change) and adds this to the original stiffness matrix for the finite element model. The program then proceeds in Rigid Format 3 to compute the remaining eigenvalues and eigenvectors for the finite element model.

THEORETICAL DESCRIPTION

In real eigenvalue analysis, NASTRAN solves for the eigenvalues and eigenvectors for the analysis (or U_a) degrees of freedom from

$$[K_{aa} - \lambda M_{aa}] \quad \{U_a\} = 0 \tag{1}$$

The stiffness matrix for the U_a degrees of freedom is obtained from the original U_g degrees of freedom through the application of constraints and Guyan reduction. The stiffness matrix K_{gg} for the U_g degrees of freedom can be considered to be the sum of two matrices

$$K_{gg} = K_{gg_o} + \Delta K_{gg} \tag{2}$$

where K_{gg_o} contains the stiffnesses for the finite element model which will not be modified and ΔK_{gg} contains all of those stiffnesses that will be modified. The modification technique described in this paper is one in which the stiffnesses to be modified are <u>all</u> proportional to some scalar variable, which will be denoted as β. Thus, ΔK_{gg} can be written as

$$\Delta K_{gg} = \beta K'_{gg} \tag{3}$$

where K'_{gg} are the values of the ΔK_{gg} coefficients per unit value of the scalar variable β. The K'_{gg} matrix could represent, for example, the portion of the finite element model represented by several beam elements of the same cross section whose moment of inertia we wanted to vary. In this case, β would be the moment of inertia of those beams and K'_{gg} would be the stiffness coefficients for these beams per unit moment of inertia.

In general, ΔK_{gg} can be any portion of the finite element model whose stiffness coefficients vary proportionally to some known variable. This variable could not, therefore, be the thickness of plate elements since the bending stiffness varies as the cube of the thickness while the transverse shear and membrane stiffnesses vary with the first power of the thickness. If, however, the plates were pure bending plates (no membrane or transverse shear), then all of the stiffness coefficients would vary with the cube of the thickness and we would be able to express the stiffness of those plate elements by an equation of the type in equation (3) where β could be taken as the cube of the thickness or the bending rigidity D.

Thus, considering only those applications in which the stiffness matrix for a portion of the structure can be represented as in equation (3) where β is a single scalar variable, the stiffness matrix for the complete structure (eq. (2)) becomes

$$K_{gg} = K_{gg_o} + \beta K'_{gg} \tag{4}$$

The stiffness matrix in equation (4) can be reduced to the analysis set of degrees of freedom U_a through the application of multi and single point constraints and through the Guyan reduction of the omitted points as mentioned above. The only restriction in the DMAP Alter presented herein is that the degrees of freedom that have stiffnesses that will be modified are not allowed to belong to the "O" set (omitted coordinates).

Following the normal procedures for reducing from the U_g to the U_a degrees of freedom (with the restrictions mentioned above), the eigenvalue problem as stated in equation (1) can be written as

$$[K_{aa_o} + \beta K'_{aa} - \lambda M_{aa}] \quad \{U_a\} = 0 \qquad (5)$$

The problem is to find a value of β that will result in one of the eigenvalues (usually the first nonzero eigenvalue) attaining a specified value, say λ_1. Setting λ equal to the specified value λ_1 in equation (5) results in the equation

$$[(K_{aa_o} - \lambda_1 M_{aa}) + \beta K'_{aa}] \quad \{U_a\} = 0 \qquad (6)$$

In order for there to be a nontrivial solution to equation (6), the determinant of the coefficient matrix must vanish. This will result in a polynomial in β equal to zero, that is,

$$p(\beta) = 0$$

Thus, the solution for the value of β that will provide a specified eigenvalue (provided such value of β exists) may be obtained by solving an eigenvalue problem, using equation (6), for β. This can be readily accomplished in NASTRAN using the module READ by inputting to READ the matrix $(K_{aa_o} - \lambda_1 M_{aa})$ as the "stiffness" matrix and the matrix K'_{aa} as the "mass" matrix. The resulting "eigenvalue" found by READ will be the value of β that will provide the stiffness modification necessary for the structure to have the real eigenvalue λ_1.

It should be pointed out that there is no guarantee that the process will always work. There may be no modification of the portion of the structure we are attempting to modify that will result in the specified eigenvalue λ_1. However, the analyst can often tell, by comparison of his original finite element modes with those obtained from tests, what portion of the model appears to be too stiff or too flexible. In these instances, the procedure outlined in this paper for determining the stiffness modification should relieve the analyst of the burden of making arbitrary changes in the stiffnesses and solving repeated eigenvalue problems until the model agrees with the test. Since the technique outlined is one in which a stiffness change is determined which will provide one eigenvalue equal to a specified value, it appears that it will be most useful when there is disagreement between the original model and test results in a fundamental mode. It should also be mentioned that the stiffness change, while providing a specified fundamental mode, will obviously yield higher modes different from those obtained from the original or unmodified finite element model. There is no guarantee that these new higher modes will agree any better with the test modes than those from the original model.

INPUT TO THE PROGRAM

The data deck required to make a run to modify part of the structure and obtain the resulting eigenvalues will be discussed in terms of changes to a normal deck for Rigid Format 3, real eigenvalue analysis.

Case Control Deck

Two subcases are required. In the first subcase, a METHØD card selects an EIGB bulk data card which will be used for the eigenvalue extraction for β.

The second subcase contains the normal case control cards that the user would have in any Rigid Format 3 run including a METHØD card which selects the EIGR bulk data card for the real eigenvalues λ. The result of this subcase will be the normal real eigenvalue analysis output with one of the modes equal to the specified eigenvalue (to be specified in the Bulk Data Deck).

Bulk Data Deck

1. Input of the normal finite element model of the structure which would be used in a real eigenvalue analysis. From this finite element model the stiffness matrix K_{gg_o} will be built by NASTRAN. This could be the identical cards used to

describe the structure if an original modal analysis had been performed and the user were now rerunning it to modify part of the structure. In this case, the value of β determined in the current run would be the change in stiffness of the modified part of the structure. Included in these cards, of course, is the EIGR card requested by subcase 2 which will find all desired modes subsequent to the modification.

2. DMIG input of K'_{gg}.

3. EIGB card requested by subcase 1 for finding the "eigenvalue" β. <u>The normalization for the eigenvector must be MASS</u>. If the scalar variable multiplier of K'_{gg} is, for example, the moment of inertia of some of the beam elements, then the search range should be the range over which the user expects the change in this variable to lie (change with respect to the value that is in the finite element model in item 1).

4. A PARAM bulk data card with parameter name = FREQ and value equal to the frequency (in Hz) of the mode the user wishes to specify.

DMAP ALTER DESCRIPTION

Appendix A lists the DMAP Alters to Rigid Format 3, Level 15.1.0, required to solve for the stiffness modification, to assemble the new stiffness matrix, and to proceed in Rigid Format 3 to obtain all of the desired eigenvalues and eigenvectors of the modified system. Several of the Alter statements are discussed in the appendix to clarify their function. In general, all the DMAP modules used but one are standard DMAP modules described in the NASTRAN User's or Programmer's Manuals. The module SCALAR, however, is a new module written and added to NASTRAN at the Goddard Space Flight Center and will be an available DMAP module in level 16 when it is released. Basically, this is a module that accepts matrices as input and will output one coefficient of the matrix as a NASTRAN complex, single or double precision parameter that can be used, for example, in the DMAP module ADD to multiply other matrices by. This was needed since the only way the scalar value of β could be obtained as data that could be used in subsequent DMAP statements was in the matrix

KHHK output from module GKAM following the eigenvalue extraction for β. The module SCALAR was used to extract β from KHHK. The matrix KHHK is the "modal stiffness" matrix found from the eigenvalue run to obtain β. If the normalization on the EIGB bulk data card requests normalization to unit modal mass, then the coefficient in KHHK will be β.

SAMPLE PROBLEMS

Using the DMAP Alter program, two sample problems have been run. Figure 1 shows a beam finite element model of the UK-5 spacecraft and adapter to be flown on the Scout vehicle. The spacecraft and adapter are attached via a Marmon clamp, which in this finite element model is modeled as a scalar spring. In the original analysis, the model contained no scalar spring element for the clamp band and the adapter and spacecraft were assumed rigidly connected. The fundamental bending mode obtained from this finite element model was 43 Hz. Subsequent tests of the system indicated that the first mode was at 33 Hz and that the Marmon clamp did not appear "infinitely" stiff. Thus, the model was modified by including a spring between the adapter and spacecraft. The second run, made to determine the value that the spring should have to obtain a 33 Hz first bending mode contained the following changes:

1. removal of the MPC rigid constraint at the adapter/spacecraft interface that was used in the original analysis to simulate zero bending flexibility at that joint

2. addition of DMIG matrix input of a scalar spring stiffness matrix per unit value of stiffness:

$$K'_{gg} = \begin{bmatrix} 0 & 0\ldots & 0 & 0\ldots & 0 \\ \vdots & \vdots & \vdots & \vdots & \vdots \\ 0 & 0\ldots & 1 & -1\ldots & 0 \\ 0 & 0\ldots & -1 & 1\ldots & 0 \\ \vdots & \vdots & \vdots & \vdots & \vdots \\ 0 & 0 & 0 & 0 & 0 \end{bmatrix}$$

where the nonzero values correspond to the rows and columns represented by the grid points and rotational degrees of freedom to which the scalar spring connects

3. EIGB bulk data card to find k_s (β is k_s in this problem) with eigenvector normalization to MASS

4. PARAM FREQ bulk data card with value 33 Hz (complex single precision)

The data deck for this run is listed in Appendix B. The output from subcase 1 gave the value of k_s needed to obtain a 33 Hz first bending mode, namely, 4.3×10^9 N/m (24.5×10^6 lb/in). Subcase 2 then was executed to obtain the eigenvalues and eigenvectors for the system with this spring in the model. The resulting eigenvalues were a 33 Hz first mode with the second mode changing, in this case, by only a few percent from that obtained from the original model.

Figure 2 shows another problem run using the DMAP Alter. In this case, the structure is a stiffened plate simply supported on all four sides. The plate is stiffened with an I-beam whose area and offset distance are specified but whose moment of inertia (about the beam centroidal axis) may be varied. The problem is to determine the moment of inertia of the beam that will give a 40 Hz first symmetric bending mode of the structure. The structure was modeled with a 5x5 mesh of grid points equally spaced in one quadrant of the plate. The DMIG matrix K'_{gg} in this problem consisted of the stiffness of the beams (due to the bending moment of inertia only) for all of the grid points to which the beams were attached. The Bulk Data input for the finite element model consisted of the normal input for such a structure but with zero bending inertia for the beams (the area and offset distance were input on the CBAR cards). The first subcase solved for the moment of inertia of the beams that would result in a 40 Hz first symmetric bending mode of the structure. This was determined as 855.8 cm^4 (20.56 in^4). Subcase 2 then proceeded to obtain the eigenvalues and eigenvectors of the modified system and it was determined that the first mode was at 40 Hz.

ACKNOWLEDGEMENT

The help of Mr. Reginald Mitchell of the Goddard Space Flight Center is greatly appreciated for his programming efforts in writing the module SCALAR needed in the DMAP Alter.

APPENDIX A

DMAP ALTER FOR DETERMINING LOCAL STIFFNESS CHANGE TO OBTAIN A SPECIFIED EIGENVALUE (RIGID FORMAT 3)

```
 1  ALTER 45

 2  MTRXIN     ,MATPOOL,EQEXIN,SIL,/DKGGP,,/V,N,LUSET/V,N,NODKP/
               C,N,0/C,N,0  $

 3  SAVE       NODKP  $

 4  MATGPR     GPL,USET,SIL,DKGGP//C,N,G/C,N,G  $

 5  ALTER 48

 6  EQUIV      DKGGP,DKNNP/MPCF1  $

 7  ALTER 58

 8  MCE2       USET,GM,DKGGP,,,/DKNNP,,,  $

 9  ALTER 61

10  EQUIV      DKNNP,DKFFP/SINGLE  $

11  ALTER 64

12  UPARTN     USET,DKNNP/DKFFP,,,/C,N,N/C,N,F/C,N,S  $

13  ALTER 67

14  EQUIV      DKFFP,DKAAP/OMIT  $

15  ALTER 70

16  UPARTN     USET,DKFFP/DKAAP,,,/C,N,F/C,N,A/C,N,O  $

17  ALTER 75,76

18  ADD        MAA,/MAA1/C,Y,FREQ  $

19  ADD        MAA1,/MAA2/C,Y,FREQ  $

20  ADD        MAA2,KAA/DAA/C,N,(39.47842,0.0)/C,N,(-1.0,0.0)  $

21  DPD        DYNAMICS,GPL,SIL,USET/GPLD,SILD,USETD,,,,,,,EED,
               EQDYN/V,N,LUSET/V,N,LUSETD/V,N,NOTFL/V,N,NODLT/
               V,N,NOPSDL/V,N,NOFRL/V,N,NONLFT/V,N,NOTRL/
               V,N,NOEED/C,N,123/V,N,NOUE  $
```

```
22  SAVE      NOEED  $

23  COND      ERROR2,NOEED  $

24  CHKPNT    EED  $

25  READ      DAA,DKAAP,,,EED,USET,CASECC/LAMAK,PHIAK,MIK,OEIGSK/
              C,N,BUCKLING/V,N,NEIGVK/C,N,1  $

26  SAVE      NEIGV  $

27  OFP       LAMAK,OEIGSK,,,,//V,N,CARDNOK  $

28  SAVE      CARDNOK  $

29  GKAM      ,PHIAK,MIK,LAMAK,,,,,CASECC/MHHK,,KHHK,PHIDHK/
              C,N,-1/C,N,1/C,Y,LFREQ=0.0/C,Y,HFREQ=0.0/C,N,-1/
              C,N,-1/C,N,-1/V,N,NOCUP/V,N,FMODE  $

30  SCALAR    KHHK//C,N,1/C,N,1/V,N,BETA  $

31  SAVE      BETA  $

32  ADD       DKAAP,KAA/KAAT/V,N,BETA  $

33  COND      LBL6,REACT  $

34  RBMG1     USET,KAAT,MAA/KLL,KLR,KRR,MLL,MLR,MRR  $

35  ALTER 85,90

36  READ      KAAT,MAA,MR,DM,EED,USET,CASECC/LAMA,PHIA,MI,OEIGS/
              C,N,MODES/V,N,NEIGV/C,N,2  $

37  SAVE      NEIGV  $

38  CASE      CASECC,/CASEX2/C,N,TRAN/V,N,REPEATT=2/V,N,NOLOOP  $

39  ALTER 105,105

40  SDR2      CASEX2,CSTM,MPT,DIT,EQEXIN,SIL,,,BGPDP,LAMA,QG,
              PHIG,EST,/,OQG1,OPHIG,OES1,OEF1,PPHIG/C,N,REIG  $

41  ALTER 109,109

42  PLOT      PLTPAR,GPSETS,ELSETS,CASEX2,BGPDT,EQEXIN,SIP,,PPHIG/
              PLOTX2/V,N,NSIL/V,N,LUSET/V,N,JUMPPLOT/V,N,PLTFLG/
              V,N,PFILE  $

43  ENDALTER
```

DESCRIPTION OF DMAP ALTER STATEMENTS

2. MTRXIN reads DMIG cards which contain the coefficients of the K'_{gg} matrix input by the user. These are the stiffness coefficients (for the portion of the structure which will be modified) per unit value of the parameter that they vary with. These can easily be determined by running Rigid Format 1, up through GP4, with the bulk data containing all grid points, coordinate systems, and elements for the portion of the model to be modified.

5-16. These Alters perform the reduction on the K'_{gg} matrix at the same location in Rigid Format 3 that the reductions are performed on the stiffness matrix for the remainder of the structure (K_{gg_o}).

18-20. Formulate the matrix $K_{aa_o} - \lambda_1 M_{aa}$ using the input parameter FREQ which is FREQ = $\frac{1}{2\pi}\sqrt{\lambda_1}$. That is, FREQ is the frequency in Hz of the mode we are specifying the eigenvalue for.

25. Solve an eigenvalue problem for β using the buckling option in READ. The resulting "modal stiffness" matrix, KHHK, which will be output from module GKAM, will contain β on the diagonal since the eigenvector normalization on the EIGB bulk data card is a normalization on unit modal mass.

29. GKAM outputs the matrix KHHK.

30. SCALAR (discussed above) extracts a value from KHHK and outputs it as a parameter (BETA).

32. ADD formulates the total stiffness $K_{aa_o} + \beta K'_{aa}$.

36. READ extracts the eigenvalues and eigenvector of the modified system, one of which will be the specified eigenvalue λ_1.

APPENDIX B

CASE CONTROL AND BULK DATA DECKS FOR UK-5 S/C - ADAPTER STIFFNESS MODIFICAT

```
TITLE = UK5 SPACECRAFT AND EH SECTION
SUBTITLE = CANTILEVERED MODE SHAPES (LATERAL)
LABEL = STIFFNESS CALCULATION FOR CLAMP BAND FOR 33 HZ FIRST BENDING
ECHO = UNSORT
MPC = 52
SUBCASE 1
  METHOD = 1
SUBCASE 2
  METHOD = 2
    OUTPUT
      VECTOR = ALL
      ELFORCE = ALL
      SPCF = ALL
BEGIN BULK
$
$ LATERAL MODES
$
GRDSET                                                  1345
BAROR                                   0.      1.      0.      1
EIGB    1       INV     5.+6    5.+7    1       1               1.-4    +EIG
+EIG1   MASS
EIGR    2       INV     25.     400.    3       3               1.-4    +EIG
+EIG2   MAX
PARAM   GRDPNT  0
PARAM   WTMASS  .002591
$
$ EH SECTION
$
GRID    501             47.77   0.      0.              123456
GRID    502             44.     0.      0.
GRID    503             40.     0.      0.
GRID    504             37.27   0.      0.
CBAR    5001    5001    502     501
CBAR    5002    5002    503     502
CBAR    5003    5003    504     503
PBAR    5001    5001     2.634    94.4    94.4    72.6    .989          +B50
PBAR    5002    5001     2.138    59.5    59.5    45.8    .989          +B50
PBAR    5003    5001     1.710    29.2    29.2    22.4    .989          +B50
+B5011                                                                  +B50
+B5021                                                                  +B50
+B5031                                                                  +B50
+B5012   .185    .185
+B5022   .185    .185
+B5032   .185    .185
MAT1    5001    1.+7    1.+7    .3
$
$ CONSTRAIN S/C - ADAPTER INTERFACE GRID POINTS TO BE THE
$ SAME EXCEPT IN ROTATIONAL DEGREE OF FREEDOM
$
MPC     51      504     1       1.0     601     1       -1.0
MPC     52      504     2       1.0     601     2       -1.0
```

```
$ ***************************************************
$ UK5 SPACECRAFT
$ ***************************************************
GRID    601             37.27   0.0     0.0
GRID    602             33.77   0.0
GRID    603             30.27   0.0
GRID    604             26.77   0.0
GRID    605             23.27   0.0
GRID    606             19.77   0.0
GRID    607             16.27   0.0
GRID    608             12.77   0.0
GRID    609             10.27   0.0
CBAR    6001    6001    602     601
CBAR    6002    6002    603     602
CBAR    6003    6003    604     603
CBAR    6004    6004    605     604
CBAR    6005    6005    606     605
CBAR    6006    6006    607     606
CBAR    6007    6007    608     607
CBAR    6008    6008    609     608
PBAR    6001    6001    3.062   37.05                   7.297           +B6011
PBAR    6002    6001    3.441   44.87                   4.072           +B6021
PBAR    6003    6001    3.525   64.                     8.861           +B6031
PBAR    6004    6001    3.225   89.1                    10.809          +B6041
PBAR    6005    6001    3.075   118.5                   13.492          +B6051
PBAR    6006    6001    3.165   156.5                   10.618          +B6061
PBAR    6007    6001    3.505   199.5                   7.328           +B6071
PBAR    6008    6001    3.965   238.6                   25.31           +B6081
+B6011                                                                  +B6012
+B6021                                                                  +B6022
+B6031                                                                  +B6032
+B6041                                                                  +B6042
+B6051                                                                  +B6052
+B6061                                                                  +B6062
+B6071                                                                  +B6072
+B6081                                                                  +B6082
+B6012  .1907
+B6022  .1697
+B6032  .1589
+B6042  .1591
+B6052  .1515
+B6062  .1349
+B6072  .1207
+B6082  .1067
MAT1    6001    1.+7    1.+7    .3
DMIG    DKGGP   0       6       1       2
DMIG    DKGGP   504     6               504     6        1.0            +DK1
DMIG    DKGGP   601     6               504     6       -1.0            +DK2
+DK1    601     6       -1.0
+DK2    601     6        1.0
PARAM   FREQ    33.     0.
ENDDATA
```

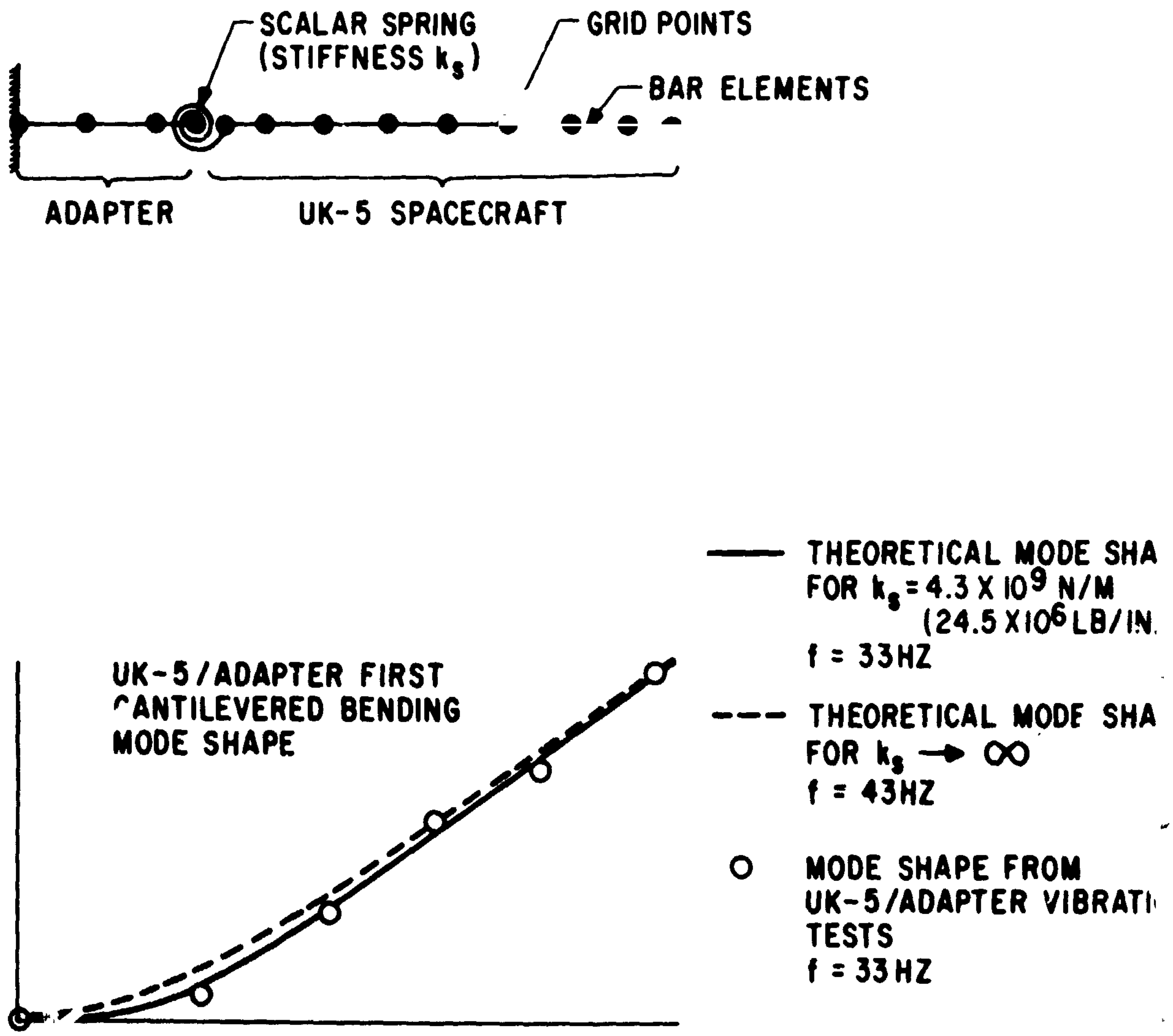

Figure 1.- Clamp-band stiffness modification to obtain 33 Hz first bending mode for the UK-5 spacecraft and adapter.

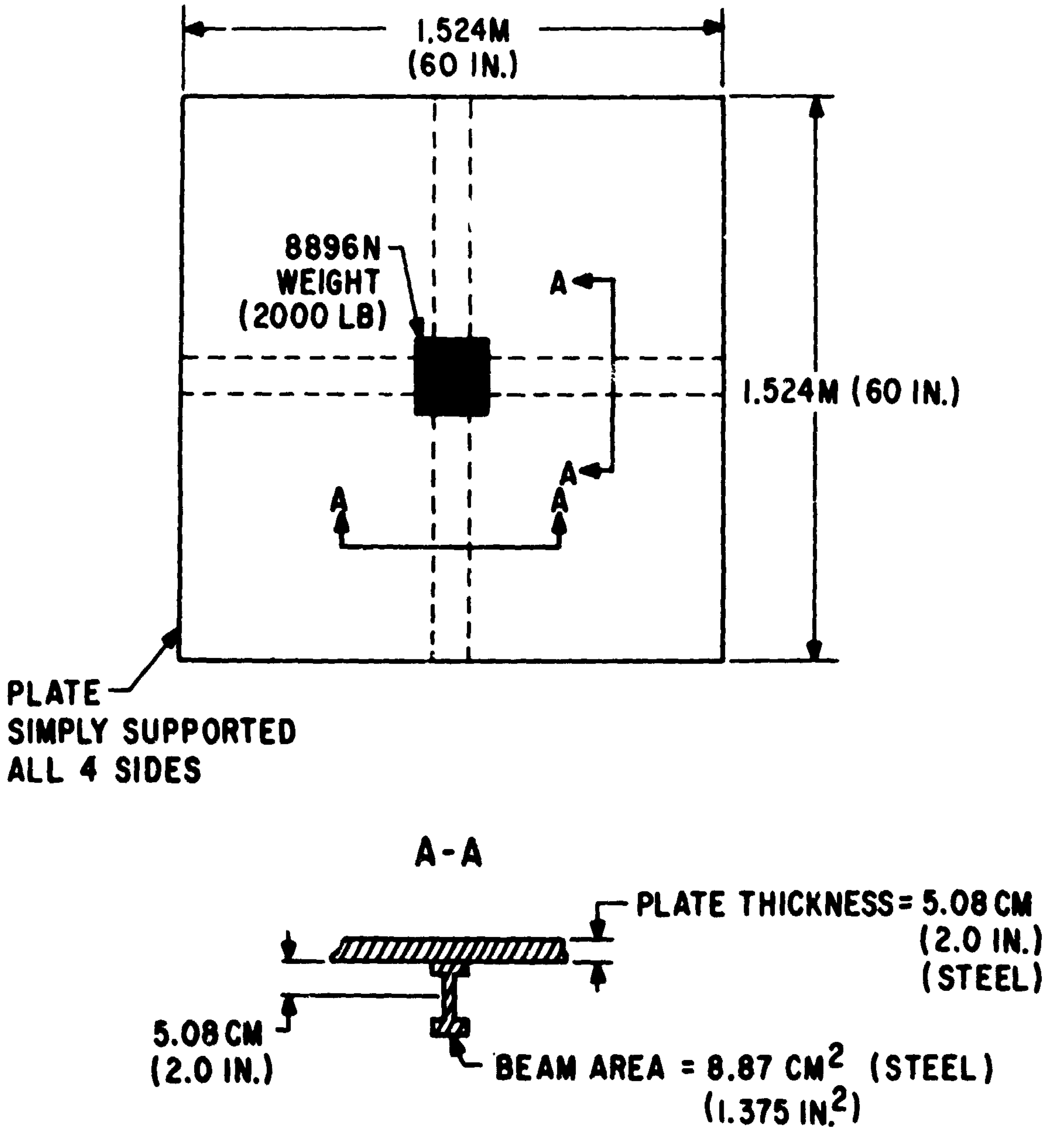

Figure 2.- Stiffener EI modification to obtain 40 Hz first mode for the simply supported stiffened plate.

N74-14601

NASTRAN MULTIPARTITIONING AND "ONE-SHOT" SUBSTRUCTURING

By Alvin Levy

Grumman Aerospace Corporation, Bethpage, New York

SUMMARY

For intermediate size problems where all the data is acces-
ıle, the present method of substructuring in three separate phases
ır static analysis) is unneccessarily cumbersome. The versa-
.ity of NASTRAN's DMAP and internal logic lends itself to find-
; a practical alternative to these procedures whereby self-
ıtained special-purpose ALTER packages can be written to be run
one pass. Two examples are presented here under the titles of
.tipartitioning and "one-shot" substructuring. The flow of
.tipartitioning resembles that of the present three-phase sub-
ructuring. The basic effect is to partition the structure
o substructures and operate on each substructure separately.
s can be used to reduce the bandwidth of a given problem as
l as to store information which will allow a change to be made
one of the substructures in a later run. This latter pro-
lure is carried out in a second program titled "one-shot" sub-
ructuring.

INTRODUCTION

At present, in order to use NASTRAN substructuring for a
atic analysis, the user must perform a three-phase analysis on
e structure as discussed in reference 1. In Phase I, the stiff-
ss and load matrices are computed and saved for each substruc-
re. This requires a separate computer run for each substruc-
re. Phase II merges the reduced matrices from Phase I and
mputes the substructure boundary (a-set) displacements. This
quires the input of one tape for each substructure, an ALTER
ckage to suit the given problem, and user-generated partition
ctors or multipoint constraints. In Phase III, each substruc-
re is restarted by using as input the a-set displacements computed
Phase II and Phase III gives as output the final solution. Once
ain, this procedure requires a separate run for each substructure.

PRECEDING PAGE BLANK NOT FILMED

One of the useful applications of substructuring is to allow the user to make changes to one or more of the substructures and regenerate solutions with a minimum of man and machine effort. This application requires the user to execute one Phase I run for each substructure change, one Phase II run, and as many Phase III runs as there are total substructures.

Some of the practical difficulties encountered at present are summarized as follows:

1) Each phase must be run consecutively and this increases the real-time requirements.

2) For Phases I and III each substructure must be run independently. This increases the cost.

3) The user must take care in handling the tapes and restart dictionaries used in the various phases.

4) For Phase II, the user must write a DMAP ALTER to suit the given problem. This requires taking into account the number of substructures involved. The user must also input a partition vector for each substructure.

5) If a substructure is changed and the problem rerun, the three phases must be run consecutively once again.

For many large-scale problems encountered, especially where information is gathered at different locations, this procedure will be practical, but for many cases of intermediate and large size problems where all the data is accessible and fits within the storage capacity of the computer, this procedure seems unnecessarily cumbersome.

A practical alternative to these procedures is to write special purpose programs through the use of DMAP ALTER packages, each suitable for a given need and each self contained in one program to be run in one pass. Examples of this are presented in the present paper and are titled multipartitioning and "one-shot" substructuring. These procedures contain the following features:

1) Only DMAP ALTER statements are involved so that no additional capabilities need be included in NASTRAN, although some are suggested in order to make the methods more effi ient and flexible.

2) The complete substructuring (multipartitioning) analysis can be carried out in one run.

3) If a change is made in one of the substructures the program only requires as input the changed substructure and again gives a complete analysis of the entire structure in one run.

4) The rules for setting up the program for a given problem do not require the user to make any changes in the DMAP ALTER package.

5) The need for partition vectors has been eliminated.

6) The instructions to be followed for generating the required Case Control and Bulk Data Decks are simple.

7) There is a minimum of tape handling and no restart dictionaries required.

At present the ALTER packages presented here for static analysis carry the limitation that when making changes to a given substructure for a follow-up substructure analysis, the elements adjacent to the boundary points (a-set) must be unchanged in stiffness because the contribution due to these elements cannot be distinguished in forming $[\bar{K}_{aa}]$. (See fig. 1.)

MULTIPARTITIONING AND ONE-SHOT SUBSTRUCTURING

The program flows for multipartitioning and one-shot substructuring are given in figure 1 and the specific DMAP ALTER packages are given in figures 2 and 3. In the multipartitioning package the entire data for a complete structure is given as input, along with the a-set points used to partition the structure and the grid points which are contained in each substructure. The program then partitions the stiffness matrix by isolating each partitioned substructure. The individual substructures are then operated on separately as if the boundary degrees of freedom (a-set degrees of freedom) are completely fixed. The interaction effects are then summed and the a-set points are solved for. This information is then passed back to each substructure and the solution for each substructure is carried out. It can be seen that this method follows the normal procedure of substructuring without having to form partition vectors for each substructure. The overall effect is to partition the stiffness matrix as would normally be done by using the partitioning (ASET or OMIT) feature, but the name multipartitioning comes from the similarity between the present method and the method of partitioning coupled with resequencing of nodes which results in a reduction of the bandwidth. A demonstration of this method is shown in figure 4. Figure 4(a) represents a finite-element idealization where the nodes are numbered to produce the minimum bandwidth. The idealization is partitioned into two sections as shown. Figure 4(b) represents the initial structure before partitioning and figure 4(c) after partitioning. The bandwidth has been reduced from 7 (assuming one degree of freedom per node) to 6. If we use the methods of multipartitioning the two subdivisions are treated separately; thus, the bandwidth is reduced to 4 as shown in figure 4(d). This reduction could also be accomplished by using the method of partitioning (fig. 4(c)) along with reordering the nodes as shown in figure 4(d).

We can now make a change in one of the substructures and repeat the analysis. Only the data for the changed substructure is required, along with the stored information (on tape) of the old complete structure. Required calculations for the new structure are carried out (see fig. 1) and the complete analysis of all the substructures proceeds as before.

USER PROCEDURES

The user procedures will be given by ionstration. Figure 5(a) represents a structure to be analyzed by the present methods. The structure is subdivided into three substructures and we are interested in two different loading conditions. The three substructures are shown in figure 5(b). (An intermediate solution for the three substructures fixed at the a-set points is included in the ALTER package.)

The Executive Control Deck contains the multipartitioning ALTER package (fig. 2). The Case Control Deck and Bulk Data Deck are shown in figure 6. The Bulk Data Deck will be discussed first. The elements, grid points, loads, and property cards are as usual. The ASET card defines the boundary points of the substructures. The boundary conditions (simply supported in this case) are placed on the grid point identifications (for simplicity). All the grid points not included in the a-set are placed on SPC cards as follows: those contained in substructure i are placed in SPC set number 100 + i (see SPC and SPC1 cards) and then added together so that SPC set j contains all points not in substructure j (see SPCADD cards). This method is used in the program to partition out each substructure. One auxiliary device must be mounted (INPT) for the multipartitioning program. If information is to be retained for subsequent use (e.g., to change one of the substructures) then three additional tapes must be mounted (INP3, INP4, and INP5), and a parameter TAPE=1 must be defined. (See PARAM card.) With a slight modification to the DMAP ALTER packages, this can be reduced to one additional tape. The Case Control Deck first defines sets corresponding to the nodes and elements contained within each substructure. If these sets are omitted, the output for a given substructure will contain null values for quantities corresponding to nodes and elements not contained in the given substructure but contained in the total substructure. The subcase definitions are as follows: the first digit refers to the substructure and the second digit corresponds to the load case (e.g., SUBCASE 31 corresponds to substructure 3 load case 1). The subcase sequence is as shown, i.e., each subcase is defined as many times as there are loading conditions, where the number of subcases must be the same for each substructure. The subcase numbering system is only suggested as a mnemonic to be used for ordering the subcases correctly.

Figure 5(c) represents a change in geometry of substructure 2. Any change can be made (geometry, material properties) so long as the elements adjacent to the a-set points remain unchanged in stiffness. The Executive Control Deck now contains the one-shot substructuring ALTER package (fig. 3). The Bulk Data Deck contains only the new substructure and load conditions along with the a-set points for the complete structure (fig. 7). The ASET card must contain the same number of degrees of freedom as in the original multipartitioning run and the a-set points contained in the changed substructure must occupy the same relative position as before. For this purpose fictitious grid points (or scalar points) must be defined and constrained on SPC cards. Two parameters are defined in the Bulk Data Deck. NUMSUB is set equal to the total number of substructures and SUBNUM is set equal to the number of the substructure to be changed. The Case Control Deck contains one subcase for each load condition and the number of load conditions must be the same as in the original multipartitioning run.

CONCLUDING REMARKS

It has been shown that using NASTRAN's DMAP capabilities one can write ALTER packages to handle special cases of substructuring to be run in a single pass, without the use of new modules. These programs result in a saving of computer cost and real time as well as lessening the chance of error due to data handling. However, greater versatility could be obtained if some additional capabilities were included in the NASTRAN program. These capabilities include set definitions for elements, grid points, and a-set (and o-set) degrees of freedom.

In connection with "partitioning" methods a recent publication (ref. 2) should be of interest.

REFERENCES

1. MacNeal, Richard H., ed.: The NASTRAN Theoretical Manual. NASA SP-221 (01), 1972.

2. Meyer, Christian: Solution of Linear Equations – State-of-the-Art. J. Struct. Div., ASCE, vol. 99, no. ST7, July 1973, pp. 1507-1526.

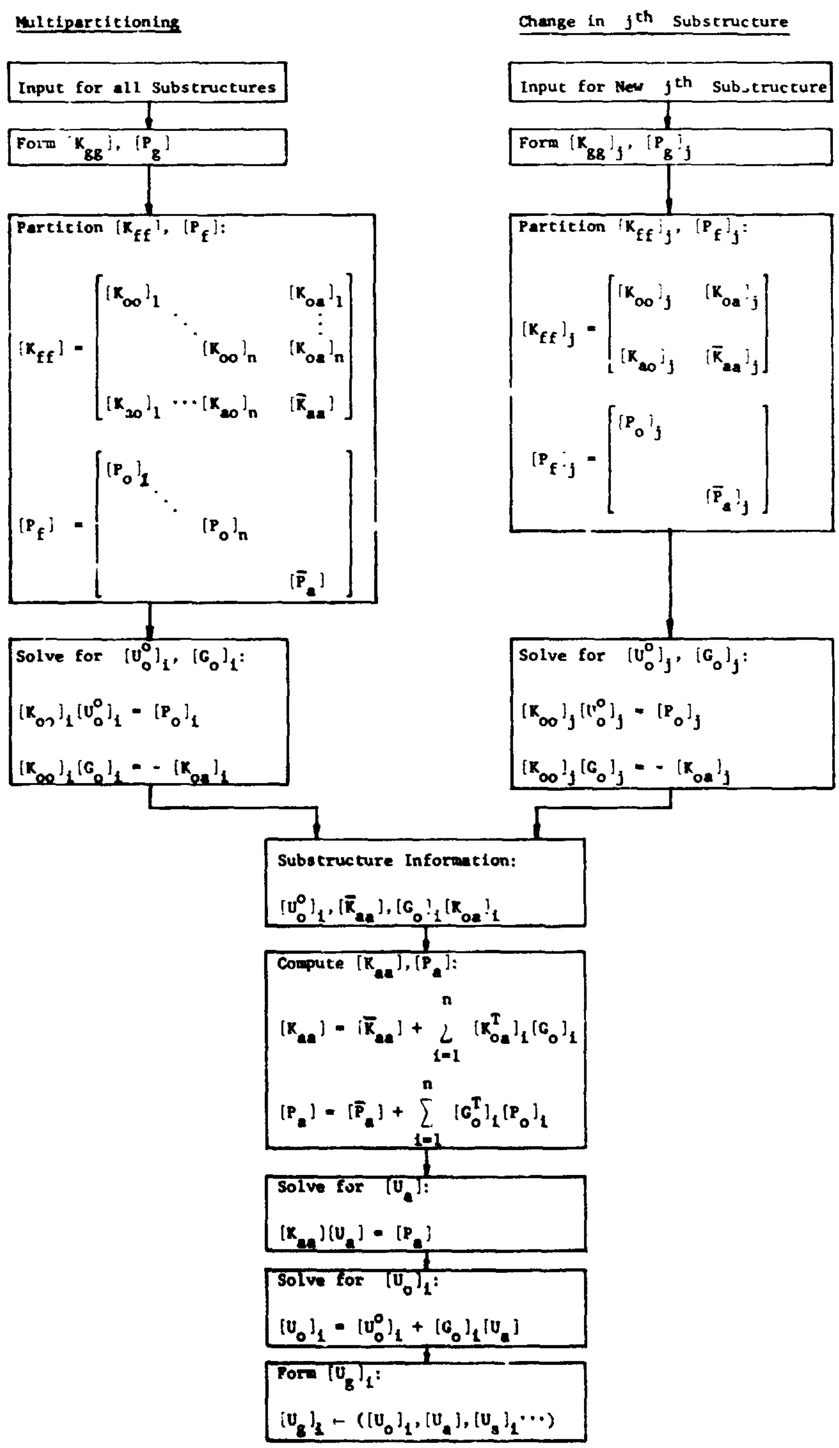

Figure 1.- Scheme for multipartitioning and one-shot substructuring.

```
ALTER 1,1
BEGIN NO.1 STATIC ANALYSIS-SERIES M1-MULTIPARTITIONING $
ALTER 50
PARAM //C,N,NOP/V,N,P1=-1
PARAM //C,N,NOP/V,N,TRUE=-1 $
PARAM //C,N,NOP/V,Y,TAPE=-1 $
$ INITIALIZE TAPE - WRITE LABEL AND REWIND
OUTPUT1, ,,,,//C,N,-1/C,N,0/C,N,TPO $
COND TPNO1,TAPE
$ INFORMATION TO BE SAVED FOR SUBSEQUENT RUNS- IF NOT DESIRED SET
$                     TAPE=-1 ON PARAM BULK DATA CARD
OUTPUT1, ,,,,//C,N,-1/C,N,3/C,N,TP3 $
OUTPUT1, ,,,,//C,N,-1/C,N,4/C,N,TP4 $
OUTPUT1, ,,,,//C,N,-1/C,N,5/C,N,TP5 $
LABEL TPNO1
ALTER 54
$  FORM PARTITION VECTOR G(L,COMP)
VEC USET/V/C,N,G/C,N,L/C,N,COMP $
CHKPNT V $
$  FORM PARTITION VECTOR F(L,COMP)
VEC USET/VFLC/C,N,F/C,N,L/C,N,COMP $
CHKPNT VFLC $
PRTPARM //C,N,0 $
ALTER 75
$  PARTITION OUT L-SET
$  L-SET IS SAME FOR ALL SUBSTRUCTURES
UPARTN USET,KFF/KLLB,,KAO,/C,N,F/C,N,A/C,N,O $
CHKPNT KLLB,KAO $
ALTER 84
JUMP LBL7 $
ALTER 94
PARAM //C,N,SUB/V,N,NULL/C,N,-1/V,N,P1 $
COND LBLN1,NULL
$  INITIALIZE KLLT TO NULL , FIRST PASS ONLY
ADD KLL,/KLLT/C,N,(0.0,0.0) $
CHKPNT KLLT $
COND TPNO2,TAPE
OUTPUT1 KLLB,,,,//C,N,0/C,N,3 $
LABEL TPNO2
LABEL LBLN1
COND TPNO3,TAPE
OUTPUT1 KAO,GO,,,// C,N,0/C,N,3 $
LABEL TPNO3
ADD KLL,KLLT/KLLX/ $
CHKPNT KLLX $
EQUIV KLLX,KLLT/TRUE $
CHKPNT KLLT $
COND LBL5A,P1 $
$  SUBTRACT KLLB FROM KLLT EACH PASS AFTER THE FIRST
$  FIRST PASS GIVES TOTAL CONTRIBUTION OF KLLB
$  SINCE L-SET IS SAME FOR ALL SUBSTRUCTURES
ADD KLLT,KLLB/KLLXX/C,N,(1.0,0.0)/C,N,(-1.0,0.0) $
CHKPNT KLLXX $
EQUIV KLLXX,KLLT/TRUE $
CHKPNT KLLT $
LABEL LBL5A
ALTER 96
$  PARTITION OUT L-SET
$  L-SET IS SAME FOR ALL SUBSTRUCTURES
PARTN PG,,V/PLB,,,/C,N,1/C,N,2/C,N,2 $
CHKPNT PLB $
ALTER 100,101
SSG2 USET,GM,YS,KFS,GO,,PG/,PO,PS,PL $
CHKPNT PO,PS,PL $
```

Figure 2.- DMAP ALTER package for multipartitioning.

```
ALTER 102
COND LBLN2,NULL
$  INITIALIZE PLT TO NULL, FIRST PASS ONLY
ADD PL,/PLT/C,N,(0.0,0.0) $
CHKPNT PLT $
COND TPNO4,TAPE
OUTPUT1 PLB,,,,//C,N,0/C,N,4 $
LABEL TPNO4
LABEL LBLN2
TRNSP GO/GOT $
COND TPNO5,TAPE
OUTPUT1 GOT,PO,,,//C,N,0/C,N,4 $
LABEL TPNO5
ADD PL,PLT/PLX/ $
CHKPNT PLX $
EQUIV PLX,PLT/TRUE $
CHKPNT PLT $
COND LBL10A,P1 $
$  SUBTRACT PLB FROM PLT EACH PASS AFTER THE FIRST
$  FIRST PASS GIVES TOTAL CONTRIBUTION OF PLB
$  SINCE L-SET IS SAME FOR ALL SUBSTRUCTURES
ADD PLT,PLB/PLXX/C,N,(1.0,0.0)/C,N,(-1.0,0.0) $
CHKPNT PLXX $
EQUIV PLXX,PLT/TRUE $
CHKPNT PLT $
LABEL LBL10A
FBS LOO,UOO,PO/UOOV $
CHKPNT UOOV $
MATPRN UOOV,PO,,,//$
MATGPR GPL,USET,SIL,UOOV//C,N,O $
MATGPR GPL,USET,SIL,PO//C,N,O $
ALTER 103,111
PARAM //C,N,ADD/V,N,P1/V,N,P1/C,N,1 $
OUTPUT1 USET,UOOV,GO,PG,//C,N,0/C,N,0 $
ALTER 118
SOLVE KLLT,PLT/ULLB/C,N,1 $
CHKPNT ULLB $
MATPRN ULLB,PLT,KLLT,, // $
PARAM //C,N,NOP/V,N,NSKIP1=1 $
INPUTT1 /,,,,/C,N,-3/C,N,0/C,N,SUB
LABEL LBL110
INPUTT1 /USET1,UOOV1,GO4,PC1,/C,N,0/C,N,0 $
SDR1 USET1,PG1,ULLB,UOOV1,,GO4,,,,,/UGV,PGG,/V,N,NSKIP1/C,N,STATICS $
CHKPNT UGV,PGG $
MATPRN UGV,PGG,,,// $
PARAM //C,N,ADD/V,N,NSKIP1/V,N,NSKIP1/C,N,1 $
PARAM //C,N,SUB/V,N,P1/V,N,P1/C,N,1 $
COND LBL80,P1 $
REPT LBL110,100 $
JUMP ERROR1 $
LABEL LBL80 $
PARAM //C,N,NOT/V,N,TEST1/V,N,P1 $
COND ERROR5,TEST1 $
SDR2 CASECC,CSTM,MPT,,EQEXIN,SIL,,EDT,BGPDT,PGG,,UGV,EST,/OPG1,,OUGV1,
          OES1,OEF1,/C,N,STATICS $
OFP OPG1,OUGV1,OES1,OEF1,,//V,N,CARDNO $
SAVE CARDNO $
PRTPARM //C,N,0 $
COND TPNO9,TAPE
OUTPUT1 CASECC,CSTM,MPT,EQEXIN,SIL//C,N,0/C,N,5 $
OUTPUT1 EDT,BGPDT,PGG,EST,//C,N,0/C,N,5 $
INPUTT1 /,,,,/C,N,-3/C,N,3/C,N,TP3 $
INPUTT1 /,,,,/C,N,-3/C,N,4/C,N,TP4 $
INPUTT1 /,,,,/C,N,-3/C,N,5/C,N,TP5 $
LABEL TPNO9
ALTER 119,126
ENDALTER
```

Figure 2.- Concluded.

```
ALTER 1,1
BEGIN NO.1 STATIC ANALYSIS-SERIES M1-ONE SHOT SUBSTRUCTURING $
ALTER 50
PARAM //C,N,NOP/V,N,P1=-1
PARAM //C,N,NOP/V,N,TRUE=-1 $
$ SUBNUM = NO.OF SUBSTRUCTURE TO BE CHANGED,DEFAULT=-1 CORR. TO NO CHANGE
$ NUMSUB = NO. OF SUBSTRUCTURES - ONLY USED IF SUBNUM POSITIVE
PARAM //C,N,NOP/V,Y,SUBNUM=-1 $
PARAM //C,N,NOP/V,Y,NUMSUB=1 $
PARAM //C,N,SUB/V,N,NUMS1/V,Y,NUMSUB/C,N,1 $
PARAM //C,N,SUB/V,N,SUB1/C,N,1/V,Y,SUBNUM $
PARAM //C,N,NOT/V,N,OUTP/V,Y,SUBNUM $
ALTER 54
$  FORM PARTITION VECTOR G(L,COMP)
VEC USET/V/C,N,G/C,N,L/C,N,COMP $
CHKPNT V $
$  FORM PARTITION VECTOR F(L,COMP)
VEC USET/VFLC/C,N,F/C,N,L/C,N,COMP $
CHKPNT VFLC $
PRTPARM //C,N,0 $
ALTER 75
$  PARTITION OUT L-SET
$  L-SET IS SAME FOR ALL SUBSTRUCTURES
UPARTN USET,KFF/KLLB,,KAO,/C,N,F/C,N,A/C,N,0 $
CHKPNT KLLB,KAO $
ALTER 84
JUMP LBL7 $
ALTER 96
$  PARTITION OUT L-SET
$  L-SET IS SAME FOR ALL SUBSTRUCTURES
PARTN PG,,V/PLB,,,/C,N,1/C,N,2/C,N,2 $
CHKPNT PLB $
ALTER 100,101
SSG2 USET,GM,YS,KFS,GO,,PG/,PO,PS,PL $
CHKPNT PO,PS,PL $
ALTER 102
FBS LOO,UOO,PO/UOOV $
CHKPNT UOOV $
MATPRN UOOV,PO,,,//$
MATGPR GPL,USET,SIL,UOOV//C,N,0 $
MATGPR GPL,USET,SIL,PO//C,N,0 $
ALTER 103,111
PARAM //C,N,ADD/V,N,P1/V,N,P1/C,N,1 $
ALTER 118
COND LBOUT,SUBNUM $
PARAM //C,N,SUB/V,N,P1/V,Y,NUMSUB /C,N,1 $
INPUTT1 /,,,,/C,N,-3/C,N,3 $
INPUTT1 /,,,,/C,N,-3/C,N,4 $
INPUTT1 /KLLB1,,,,/C,N,0/C,N,3 $
INPUTT1 /PLB1,,,,/C,N,0/C,N,4 $
ADD KLLB1,/KLLT/ $
ADD PLB1,/PLT/ $
LABEL FMKPL $
COND LBLSUB,SUB1 $
MPYAD KAO,GO,KLLT/KLLTX2/C,N,0 $
EQUIV KLLTX2,KLLT/TRUE $
MPYAD GO,PO,PLT/PLTX2/C,N,1 $
EQUIV PLTX2,PLT/TRUE $
PARAM //C,N,SUB/V,N,SUB1/V,N,SUB1/C,N,100 $
$ SKIP UNWANTED INFORMATION OF NON CHANGED SUBSTRUCTURES
INPUTT1 /DUM1,DUM2,,,/C,N,0/C,N,3 $
INPUTT1 /DUM3,DUM4,,,/C,N,0/C,N,4 $
JUMP LB111 $
LABEL LBLSUB $
INPUTT1 /KAO1,GO1,,,/C,N,0/C,N,3 $
INPUTT1 /GOT1,PO1,,,/C,N,0/C,N,4 $
```

Figure 3.- DMAP ALTER package for one-shot substructuring.

```
MPYAD KAO1,GO1,KLLT/KLLTX3/C,N,0 $
EQUIV KLLTX3,KLLT/TRUE $
MPYAD GOT1,PO1,PL,/PLTX3/C,N,0 $
EQUIV PLTX3,PLT/TRUE $
PARAM //C,N,ADD/V,N,SUB1/V,N,SUB1/C,N,1 $
LABEL LB111 $
PARAM //C,N,SUB/V,N,NUMS1/V,N,NUMS1/C,N,1 $
COND LBOUT,NUMS1 $
REPT FMKPL,100 $
LABEL LBOUT $
SOLVE KLLT,PLT/ULLB/C,N,1 $
CHKPNT ULLB $
MATPRN ULLB,PLT,KLLT,, // $
PARAM //C,N,NOP/V,N,NSKIP1=1 $
INPUTT1 /,,,,/C,N,-3/C,N,0/C,N,SUB $
PARAM //C,N,SUB/V,N,SUB1/C,N,1/V,Y,SUBNUM $
LABEL LBL110
INPUTT1 /USET1,UOOV1,GO4,PG1,/C,N,0/C,N,0 $
COND LBLNM,SUB1 $
JUMP LBLOO $
LABEL LBLNM $
EQUIV ULLB,ULX2/TRUE/UOOV1,UOX2/TRUE/PG1,PGX2/TRUE $
JUMP LBLNO $
LABEL LBLOO $
$ CREATE NULL MATRICES FOR NON CHANGED SUBSTRUCTURES
ADD ULLB,/ULX1/C,N,(-1.0,0.0) $
ADD ULLB,ULX1/ULX2  $
ADD UOOV1,/UOX1/C,N,(-1.0,0.0) $
ADD UOOV1,UOX1/UOX2 / $
ADD PG1,/PGX1/C,N,(-1.0,0.0) $
ADD PG1,PGX1/PGX2/ $
PARAM //C,N,ADD/V,N,NSKIP1/V,N,NSKIP1/C,N,1 $
PARAM //C,N,SUB/V,N,SUB1/V,N,SUB1/C,N,100 $
LABEL LBLNO $
SDR1 USET1,PGX2,ULX2,UOX2,,GO4,,,,,/UGV,PGG,/V,N,NSKIP1/C,N,STATICS $
CHKPNT UGV,PGG $
MATPRN UGV,PGG,,,// $
PARAM //C,N,ADD/V,N,NSKIP1/V,N,NSKIP1/C,N,1 $
PARAM //C,N,SUB/V,N,P1/V,N,P1/C,N,1 $
PARAM //C,N,ADD/V,N,SUB1/V,N,SUB1/C,N,1 $
COND LBL80,P1 $
REPT LBL110,100 $
JUMP ERROR1 $
LABEL LBL80 $
PARAM //C,N,NOT/V,N,TEST1/V,N,P1 $
COND ERROR5,TEST1 $
INPUTT1 /,,,,/C,N,-3/C,N,5 $
INPUTT1 /CASECC1,MPT1,EQEXIN1,SIL1,BGPDT1/C,N,0/C,N,5 $
INPUTT1 /PGG1,EST1,,,/C,N,0/C,N,5 $
SDR2 CASECC1,,MPT1,,EQEXIN1,SIL1,,,BGPDT1,PGG,,UGV,EST1,/OPG11,,
      OUGV11,OES11,OEF11,/C,N,STATICS $
OFP OPG11,OUGV11,OES11,OEF11,,//V,N,CARDNO $
SAVE CARDNO $
PARAM //C,N,NOP/V,N,NSKIP4=1 $
SDR1 USET,PG,ULLB,UOOV,,GO,,,,,/UGVN,PGN,/V,N,NSKIP4/C,N,STATICS $
SDR2 CASECC,CSTM,MPT,,EQEXIN,SIL,,EDT,BGPDT,PGN,,UGVN,EST,/OPG1,,
         OUGV1,OES1,OEF1,/C,N,STATICS $
OFP OPG1,OUGV1,OES1,OEF1,,//V,N,CARDNO $
SAVE CARDNO $
PRTPARM //C,N,0 $
INPUTT1 /,,,,/C,N,-3/C,N,3/C,N,TP3 $
INPUTT1 /,,,,/C,N,-3/C,N,4/C,N,TP4 $
INPUTT1 /,,,,/C,N,-3/C,N,5/C,N,TP5 $
ALTER 119,126
ENDALTER
```

Figure 3.- Concluded.

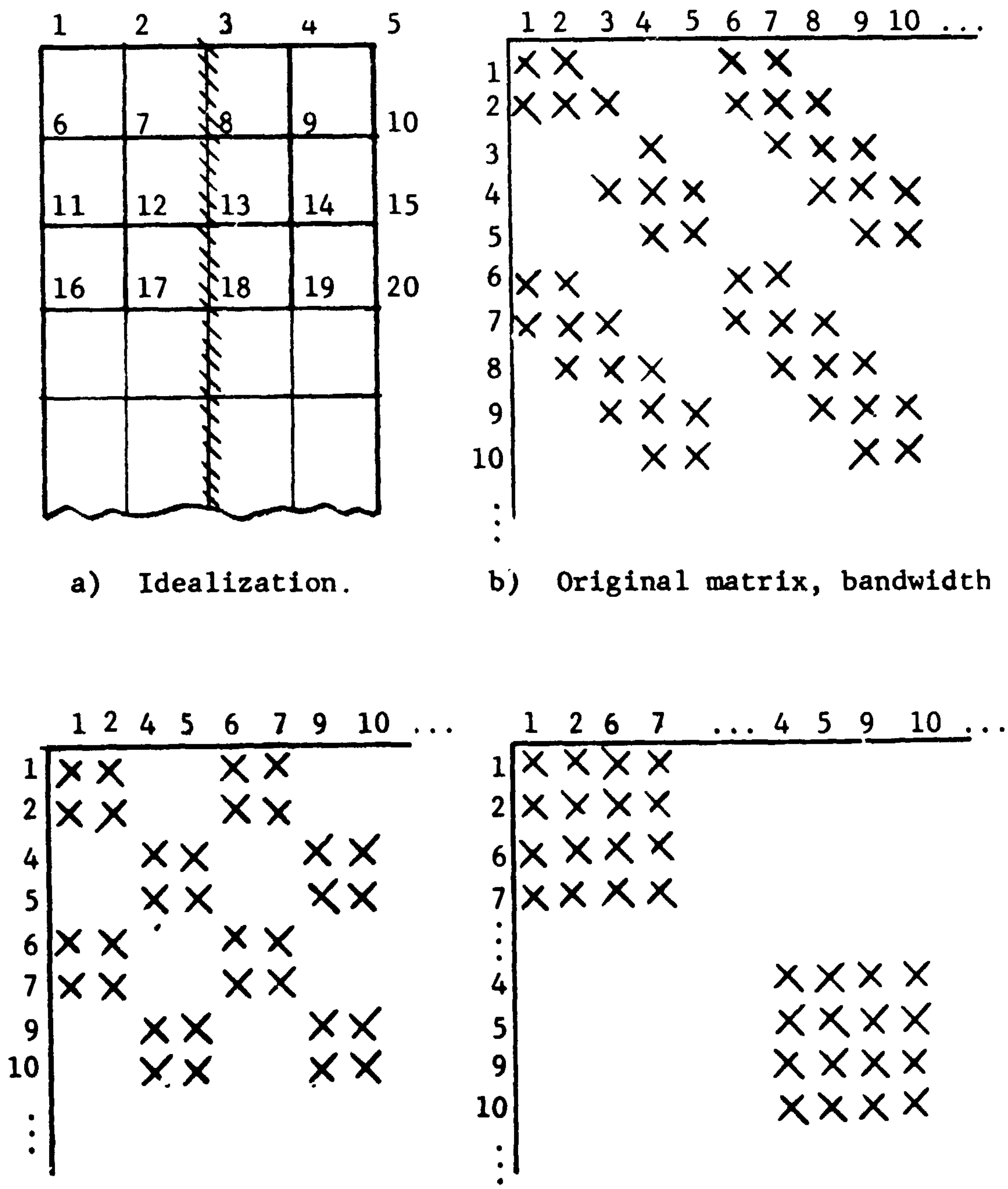

a) Idealization.

b) Original matrix, bandwidth = 7.

c) Partitioned matrix, bandwidth = 6.

d) Multipartitioned matrix, bandwidth = 4.

Figure 4.- Example of multipartitioning to reduce bandwidth.

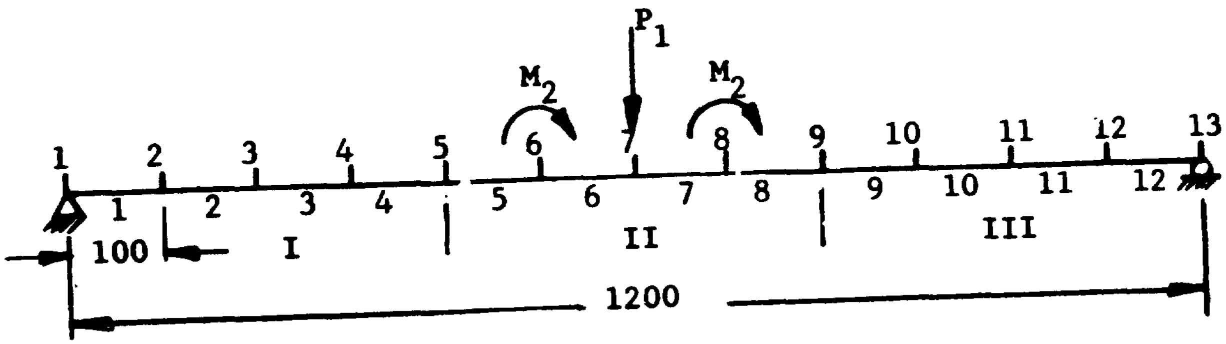

a) Simply supported beam divided into three substructures.

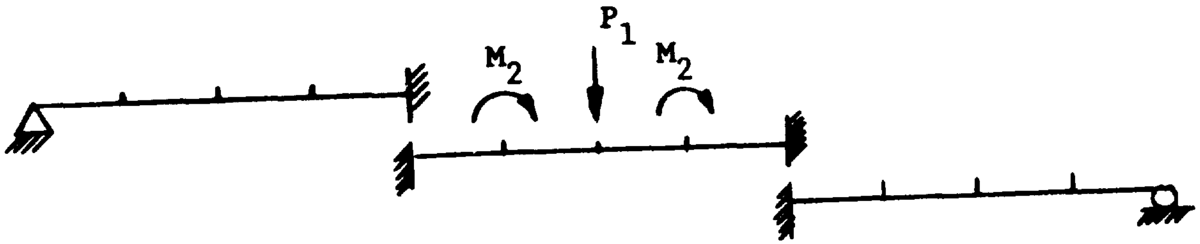

b) Intermediate solution.

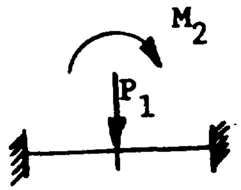

c) Change in geometry and load conditions on substructure II.

Figure 5.- Sample problem for multipartitioning and one-shot substructuring.

```
TITLE=MULTIPARTITIONING
SUBTITLE=BEAM DIVIDED INTO THREE SUBSTRUCTURES
SET 1=1 THRU 5
SET 2=5 THRU 9
SET 3=9 THRU 13
SET 4=1 THRU 4
SET 5=5 THRU 8
SET 6=9 THRU 12
DISP = ALL
STRESS = ALL
FORCE = ALL
OLOAD=ALL
SUBCASE 11
  LABEL = SUBSTRUCTURE ONE,LOAD ONE
    SPC = 1
DISP=1
OLOAD=1
STRESS=4
FORCE=4
SUBCASE 12
  LABEL = SUBSTRUCTURE ONE,LOAD TWO
    SPC = 1
DISP=1
OLOAD=1
STRESS=4
FORCE=4
SUBCASE 21
  LABEL = SUBSTRUCTURE TWO,LOAD ONE
    SPC = 2
      LOAD = 1
DISP=2
OLOAD=2
STRESS=5
FORCE=5
SUBCASE 22
  LABEL = SUBSTRUCTURE TWO,LOAD TWO
    SPC = 2
      LOAD = 2
DISP=2
OLOAD=2
STRESS=5
FORCE=5
SUBCASE 31
  LABEL = SUBSTRUCTURE THREE,LOAD ONE
    SPC = 3
DISP=3
OLOAD=3
STRESS=5
FORCE=6
SUBCASE 32
  LABEL = SUBSTRUCTURE THREE,LOAD TWO
    SPC = 3
DISP=3
OLOAD=3
STRESS=5
FORCE=6
```

Figure 6.- Example problem Case Control and Bulk Data Decks for multipartitioning.

```
BEGIN BULK
ASET    5       126     9       126
CBAR    1       100     1       2                       1.0             1
CBAR    2       100     2       3                       1.0             1
CBAR    3       100     3       4                       1.0             1
CBAR    4       100     4       5                       1.0             1
CBAR    5       100     5       6                       1.0             1
CBAR    6       100     6       7                       1.0             1
CBAR    7       100     7       8                       1.0             1
CBAR    8       100     8       9                       1.0             1
CBAR    9       100     9       10                      1.0             1
CBAR    10      100     10      11                      1.0             1
CBAR    11      100     11      12                      1.0             1
CBAR    12      100     12      13                      1.0             1
FORCE   1       7       0       1.0                     -1.0
GRDSET          0                                       0       345
GRID    1               0.0                                     12345
GRID    2               100.0
GRID    3               200.0
GRID    4               300.0
GRID    5               400.0
GRID    6               500.0
GRID    7               600.0
GRID    8               700.0
GRID    9               800.0
GRID    10              900.0
GRID    11              1000.0
GRID    12              1100.0
GRID    13              1200.0                                  2345
MAT1    100     1.0+8           0.0
MOMENT  2       6       0       1.0                             -1.0
MOMENT  2       8       0       1.0                             -1.0
PARAM   TAPE    1
PBAR    100     100     60.0    500.0
SPC     101     1       6
SPC     103     13      16
SPC1    101     123456  2       THRU    4
SPC1    102     123456  6       THRU    8
SPC1    103     123456  10      THRU    12
SPCADD  1       102     103
SPCADD  2       103     101
SPCADD  3       101     102
ENDDATA
```

Figure 6.- Concluded.

```
TITLE=ONE SHOT SUBSTRUCTURING
SUBTITLE=CHANGE IN SUBSTRUCTURE TWO
DISP=ALL
OLOAD=ALL
  FORCE=ALL
SUBCASE 21
 LABEL=SUBSTRUCTURE TWO,LOAD ONE
 LOAD=1
SUBCASE 22
 LABEL=SUBSTRUCTURE TWO,LOAD 2
 LOAD=2
BEGIN BULK
ASET    101     126     103     126
CBAR    101     200     101     102                     1.0
CBAR    102     200     102     103                     1.0
FORCE   1       102     0       1.0                     -1.0
GRDSET          0                                       0       345
GRID    101             0.0
GRID    102             100.0
GRID    103             200.0
MAT1    200     1.0+8           0.0
MOMENT  2       102     0       1.0     0.0     0.0     -1.0
PARAM   NUMSUB  3
PARAM   SUBNUM  2
PBAR    200     200     60.0     500.0
ENDDATA
```

Figure 7.- Example problem Case Control and Bulk Data Decks for one-shot substructuring.

N74-14602

NORMAL MODE ANALYSIS OF A ROTATING GROUP OF LASHED TURBINE BLADES Y SUBSTRUCTURES

By A. W. Filstrup

Westinghouse Research and Development Center

SUMMARY

A group of 5 lashed identical steam turbine blades is studied through the use of single level substructuring using NASTRAN Level 15.1. An altered version, similar to DMAP Program Number 3 of the NASTRAN Newsletter, of Rigid Format 13.0 was used. Steady-state displacements and stresses due to centrifugal loads are obtained both without and with consideration of differential stiffness. The normal mode calculations were performed for blades at rest and at operating speed. Substructuring lowered the computation costs of the analysis by a factor of four.

INTRODUCTION

Triangular plate elements have been used by Westinghouse and others (see Ref. 1) in NASTRAN to analyze rotating turbine blades.

There was a need to analyze a group of five lashed 0.79-m (31-inch) steam turbine blades for operation at 60 revolutions per second. Steady-state displacements and stresses were needed as well as the natural frequencies, mode shapes, and stress patterns.

Based on NASTRAN calculations on a single 0.79-m blade with associated lashing wires, it was decided that a finite element mesh of 700 CTRIA2 elements and 407 grid points would be used to represent each turbine blade. The root flexibility was approximated by 11 CELAS2 elements.

It was discovered that approximately two hundred degrees of freedom would be required in the a-set for each blade using Guyan reduction, if accurate stress results were to be found for the modes to be evaluated. Whether or not Guyan reduction was to be used and whether the inverse power or Givens method were used for the eigenvalue extraction, it was apparent that calculation costs would have been prohibitive if substructuring were not used.

This paper describes the successful substructuring analysis of the group of blades. The steady-state stresses were obtained for operation at 60 revolutions per second and the natural frequencies were obtained for the first nine modes at both 0 revolutions per second and at 60 revolutions per second.

METHOD OF ANALYSIS

The finite element mesh used to represent a turbine blade or substructure is shown in Fig. 1. The middle sections of the lashing wires and airfoil are sl Each lashing wire actually resembles a variable thickness plate more than a wire The auxiliary program which produces these plots views normal to the middle surface of the lashing wire. The airfoil is highly twisted, and near the base it is highly curved. No one viewing angle could provide a clear representation of element layout. Thus the auxiliary program which produces the element geometry and isostress plots opens up each cross section. Different scales are used for the lashing wires than for the airfoil in figure 1.

Each blade or substructure has 407 grid points. The 2442 degrees of freedom associated with these points are reduced through single point constraint and omits to an a-set of 301 degrees of freedom. One hundred twenty of these degrees of freedom are at the tips of the lashing wires and are required for connecting adjacent blades or substructures. Sixty degrees of freedom are common between adjacent blades.

The combined matrices for the group of five blades then has 1505 less four times sixty or 1265 degrees of freedom. Single point constraints to remove rotations about the normals to the surface of the exterior lashing wires reduce the system of equations to be solved to 1245. The half-bandwidth is 301 with no active columns. No secondary Guyan reduction was performed to reduce the number of degrees of freedom as the resulting bandwidth would have to be significantly larger than 301 for accurate results. The inverse power method with shifts was used to solve the eigenvalue problems.

The identical substructure concept as described in Sec. 1.10.5 of reference 2 was used. Five phases were required as shown in figure 2. In some cases it was deemed advisable to use more than the one user tape shown between phases. Even though the differential stiffness would be somewhat different for each of the five substructures, only one (the center blade) was generated in Phase III and used in Phase IV. This approach reduced the total calculation costs by about 20%. The inaccuracies of this approximation were felt to be about the same as those due to some of the other approximations made. Runs IV and V were split into several parts to enable shorter individual runs.

The mesh for the airfoil was generated by a preprocessor computer program. The meshes for the platform and the two lashing wires were generated by hand. The isostress lines for the centrifugal loading and for the scaled eigenvectors for the airfoil and lashing wires were plotted with a postprocessor computer program which reads images of punched element stress cards. A

STRESS(PRINT,PUNCH) = ALL

card was placed in the Case Control Deck. However, job control cards were used to store the card images on two disks and to prevent the punching of cards. Over two hundred thousand card images were produced in the Phase V runs. An intermediate program was written to enable the isostress plotting program to handle the stress information on the disk more efficiently.

Table 1 shows the calculation times for the substructuring analysis for each phase. The mesh was generated on a CDC 6600 computer and the other runs were made on an IBM 370-165 computer.

Table 2 shows the projected calculation times for the analysis of five blades without substructuring provided enough disk space were available which is extremely doubtful. In addition, checkpointing and restarting would be essential due to the extremely long total running times. However, Level 15.1 NASTRAN requires that this be done on a single physical tape which obviously would not hold enough information. The user would be required to use DMAP statements to transfer data from one run to another on user tapes rather than checkpoint tapes. Even then, some matrices might be too large to fit on a single tape.

When costs of the CALCOMP plotter are added to the computer costs shown, the total cost for a nonsubstructuring analysis, if possible, would have been about four times the total cost of the substructuring analysis performed in this study.

The arrangement of the NASTRAN decks including the Executive Control Decks are shown in the appendix.

RESULTS AND DISCUSSION

The natural frequencies, mode shapes, and stresses for the first nine modes of a group of five lashed rotating steam turbine blades were found. The natural frequencies, in general, agreed well with experimental values.

A Campbell Diagram was prepared to determine possible resonances during various operating conditions.

The pseudo steady-state deformations and stresses due to the centrifugal forces at operating speed were found. This enables the calculations of the fluid flow through the row of blades through the passages that actually occur in operation and not through the passages in the undeformed condition. Thus, NASTRAN provides the designer of flexible turbine blades with a tool to help obtain near optimal fluid flow characteristics between the airfoils.

A sample isostress plot for one of the surfaces for one of the blades for one of the modes is shown in figure .

RECOMMENDATIONS

1. NASTRAN Level 15 with its substructuring capability can and should be used for many structural problems.

2. When preparing data for large problems, a mesh generator computer program should be used as much as possible.

3. For very rigid rotating turbine blades or blade groups, Rigid Formats 1 and 3 will give accurate results and should be used. For more flexible blades, Rigid Formats 4 and 13, which include the differential stiffness matrix should be used. For even more flexible blades, it may be necessary to ALTER the centripetal acceleration matrix (see Ref. 3) into Rigid Formats 4 and 13.

4. In order to encourage more users to use the substructure capability of NASTRAN and in order to reduce the effort of the user in creating and checking DMAP packages and substructuring data, it is urged that substructuring be made more automatic (see Ref. 4).

5. Rigid Format 13 should be documented in the NASTRAN documentation.

ACKNOWLEDGEMENTS

The author would like to thank Mr. Yung Fan for making the computer runs and Mr. Carl Hennrich for his advice throughout the NASTRAN phase of the study.

CONCLUSIONS

1. The determination of the natural frequencies, mode shapes and states of stress for lashed rotating and non-rotating steam turbine blades is feasible using the general purpose computer program NASTRAN.

2. Substructuring can greatly reduce the computer costs of large problems. For the analysis performed here, the total computer expenses including mesh generation and stress plotting were one-fourth what they would have been without substructuring. The NASTRAN runs cost one-sixth as much using substructuring than they would have cost without substructuring.

3. Choice of the proper root flexibility is important to produce accurate frequencies and stresses for all modes.

4. Mode shapes and isostress lines for the fifth through ninth modes varied significantly between those found at 0 revolutions per second and those found at 60 revolutions per second. This variation is due both to the flexibility of the blade group and to the coupling between modes as the frequencies are close together. The mode shape of the fifth mode at zero revolutions per

second is similar to the mode shape of the sixth mode at 60 revolutions per second.

REFERENCES

1. Van Nimwegen, R. R., and Tepper, S.: High Pressure Turbine Blade Stress Analysis. NASTRAN: Users' Experiences. NASA TM X-2637, 1972, pp. 477-484.

2. McCormick, C. W., ed.: The NASTRAN User's Manual. NASA SP-222(01), 1972.

3. Patel, J. S., and Seltzer, S. M.: Complex Eigenvalue Analysis of Rotating Structures. NASTRAN: Users' Experiences. NASA TM X-2637, 1972, pp. 197-234.

4. Hennrich, C. W., and Konrath, E. J., Jr.: Substructure Analysis Techniques and Automation. NASTRAN: Users' Experiences. NASA TM X-2893, 1973, pp. 323-393. (Paper no. 17 of this compilation.)

APPENDIX

```
NASTRAN SUBSTRUCTURE ANALYSIS
DIFFERENTIAL STIFFNESS MODAL AND STATIC SOLUTION
IDENTICAL SUBSTRUCTURES
LISTING OF ---PHASE 1---
   (INITIAL SUBSTRUCTURE ANALYSIS)


ID DIFFMOD,PHASE1
DIAG 2,8,13,14
APP DISP
TIME 25
SOL 13,0
CHKPNT YES
ALTER 40,40
SMA3 GEI,KGGX/KGG/V,N,LUSET/V,N,NOGENL/V,N,NOSIMP$
ALTER 76
JUMP LBLX$
ALTER 78
LABEL LBLX$
ALTER 86
FBS LOO,UOO,PO/UOOV$
CHKPNT UOOV$
OUTPUT1 KAA,PL,PARVECT1,PARVECT2,PARVECT3//C,N,-1/C,N,0$
OUTPUT1 PARVECT4,PARVECT5,,,//C,N,0/C,N,0$
ALTER 87 145
ALTER 151 152
ENDALTER
CEND
   (CASE CONTROL DECK)
BEGIN BULK
   (INCLUDE ALL NECESSARY STR  TURAL DATA PLUS THE SUBSTRUCTURING
    MATRIX OPERATORS    )
ENDDATA
END* $ INCLUDE THIS CARD FOR IBM 360/370

  ---COMMENTS---
     DISP APPROACH.
     ALL ANALYSIS SET DEGREES OF FREEDOM SHOULD BE INCLUDED ON ASET CARDS.
     PARTITIONING VECTORS WHICH PROVIDE THE INFORMATION OF HOW THESE
     SUBSTRUCTURES ARE TIED TOGETHER, MUST BE INCLUDED IN BULK DATA CARDS.
  --------------
```

```
  NASTRAN SUBSTRUCTURE ANALYSIS
  DIFFERENTIAL STIFFNESS MODAL AND STATIC SOLUTION
  IDENTICAL SUBSTRUCTURES
  LISTING OF ---PHASE II---
     (STATIC SUBSTRUCTURE COUPLING ANALYSIS)

ID DIFDYNM,PHASE2
TIME 30
APP DMAP
DIAG 2,8,13,14
BEGIN$
PARAM //C,N,NOP/V,N,TRUE=-1$
INPUTT1 /KAA,PL,,,/C,N,-3/C,N,1$    INP1
FILE KAA=SAVE/PL=SAVE$
LABEL LOOP99$
INPUTT1 /E,,,,/C,N,0/C,N,1$
MERGE, ,,,KAA,E,/KGGT$
ADD KGG,KGGT/KT$
EQUIV KT,KGG/TRUE$
MERGE, ,PL,,,,E/PGT/C,N,+1$
ADD PG,PGT/PT$
EQUIV PT,PG/TRUE$
REPT LOOP99,4$
PARTN KGG,SPCV,/KRED,,,/C,N,-1$
PARTN PG,,SPCV/PRED,,,/C,N,1$
SOLVE KRED,PRED/ULVT/C,N,1$
MATPRN ULVT,,,,//$
MERGE, ULVT,,,,,SPCV/ULVTT/C,N,1$
MATPRN ULVTT,,,,//$
$   WRITE USER'S TAPE FOR PHASE 3 DATA RECOVERY.
INPUTT1 /,,,,/C,N,-3/C,N,1$    INP1
INPUTT1 /,,,,/C,N,2/C,N,1$      INP1
OUTPUT1, ,,,,//C,N,-1$
LABEL LOOP98$
INPUTT1 /Q,,,,/C,N,0/C,N,1$
MATPRN Q,,,,//$
PARTN ULVTT,,Q/,ULV,,/C,N,1$
MATPRN ULV,,,,//$
OUTPUT1 Q,ULV,,,//$INPT
REPT LOOP98,4$
OUTPUT1, ,,,,//C,N,-3$
END$
CEND
    (CASE CONTROL DECK)
BEGIN BULK
     INCLUDE MATRIX OPERATORS
ENDDATA
END* $ INCLUDE THIS CARD FOR IBM 360/370

  ---COMMENTS---
     DMAP APPROACH.
     REPEATING LOOPS.
     ADDITIONAL SINGLE POINT CONSTRAINTS ARE APPLIED VIA MATRIX PARTITION.
     PARTITIONING VECTOR SPCV MUST BE INCLUDED IN BULK DATA DECK.
     THE BULK DATA DECK MUST INCLUDE THE DMI CARDS FOR THE INITIALI-
     ZATION OF KGG AND PG.
  --------------
```

```
NASTRAN SUBSTRUCTURE ANALYSIS
DIFFERENTIAL STIFFNESS MODAL AND STATIC SOLUTION
IDENTICAL SUBSTRUCTURES
LISTING OF ---PHASE III---
   (STATIC DATA RECOVERY AND INITIAL DIFFERENTIAL STIFFNESS)


ID DIFFDYN,PHASE3
DIAG 2,8,13,14
APP DISP
SOL 13,0
CHKPNT YES
TIME 70
ALTER 3,7
ALTER 19,93
INPUTT1 /,,,,/C,N,-1$
OUTPUT1, ,,,,//C,N,-1/C,N,1$
PARAM //C,N,NOP/V,N,MARK=2$
SAVE MARK$
PARAM //C,N,NOP/V,N,BLADE=0 $
JUMP LOOP99$
LABEL LOOP99$
PARAM //C,N,ADD/V,N,BLADE/V,N,BLADE/C,N,1$
PRTPARM //C,N,0/C,N,BLADE $
INPUTT1 /E,UIV,,,/C,N,0$
ALTER    103
FILE KBLL=SAVE/MAA=SAVE/PBL=SAVE$
PARAM //C,N,SUB/V,N,MARK/V,N,MARK/C,N,1$
PRTPARM //C,N,0/C,N,MARK$
COND DIFF3,MARK$
JUMP SKIPDF$
LABEL    DIFF3$
PARAM //C,N,ADD/V,N,MARK/V,N,MARK/C,N,100$
ALTER      104
SAVE       DSCOSET$
ALTER 105,105
ALTER 106,107
EQUIV     KDGG,KDNN/MPCF2/MGG,MNN/MPCF2$
ALTER 108,108
ALTER       110,110
MCE2       USET,GM,KDGG,MGG,,/KDNN,MNN,,$
ALTER 114,114
ALTER       116,116
SCE1       USET,KDNN,MNN,,/KDFF,KDFS,KDSS,MFF,,$
ALTER 117,117
```

```
CHKPNT KDFS  $
ALTER 120,120
ALTER 124,124
ALTER       125
EQUIV       PL,PBL/DSCOSET/PS,PBS/DSCOSET/YS,YBS/DSCOSET/UOOV,UBOOV/
            DSCOSET$
CHKPNT       PBL,PBS,YBS,UBOOV$
PARAM //C,N,MPY/V,N,NDSKIP/C,N,0/C,N,0$
DSMG2 MPT,KAA,KDAA,KFS,KDFS,KSS,KDSS,PL,PS,YS,UOOV/KBLL,KBFS,KBSS,
      PBL,PBS,YBS,UBOOV/V,N,NDSKIP/V,N,REPEATD/V,N,DSCOSET$
SAVE  NDSKIP,REPEATD $
CHKPNT KBLL,KBFS,KBSS,PBL,PBS,YBS,UBOOV $
LABEL SKIPDF$
OUTPUT1 E,,,,//C,N,0/C,N,1$
REPT LOOP99,4  $
OUTPUT1 KBLL,MAA,PBL,,//C,N,0/C,N,1$
JUMP FINIS$
ENDALTER
$
$  CHECKPOINT DICTIONARY ENTER HERE
$
CEND
    (CASE CONTROL DECK)
BEGIN BULK
ENDDATA
END* $ INCLUDE THIS CARD FOR IBM 360/370

  ---COMMENTS---
     APPROACH DISP.
     RESTART.
     REPEATING LOOPS.
     THE DIFFERENTIAL STIFFNESS MATRICES MAY BE CONSIDERD AS IDENTICAL
     FOR ALL SUBSTRUCTURES PROVIDED THAT THE BOUNDARY EFFECTS ARE NOT LARGE.
     FOR SAVING COMPUTING TIME, THE CENTER BLADE DIFFERENTIAL STIFFNESS
     MATRIX IS CHOSEN TO REPRESENT ALL.
     FOR GENERATING THE A-SET DIFFERENTIAL STIFFNESS MATRIX, THE USER
     MAY EITHER CHOOSE TO USE MODULE SMP1 OR SMP2, THE LATER IS USED IN
     THIS ANALYSIS.
     SOME DATA SETS IN CHKPNT STATEMENTS ARE SELECTIVELY DELETED, FOR
     NASTRAN DOES NOT ALLOW MULTI-REEL CHECK-POINT TAPE, HENCE CANNOT
     ACCOMMODATE ALL THE LARGE SIZE DATA SETS.  PROGRAM INTERRUPTION
     WOULD OCCUR IF THE CHECK-POINT TAPE HAD REACHED TO AN END.
  -------------
```

```
NASTRAN SUBSTRUCTURE ANALYSIS
DIFFERENTIAL STIFFNESS MODAL AND STATIC SOLUTION
IDENTICAL SUBSTRUCTURES
LISTING OF ---PHASE IV---
   (DIFFERENTIAL STIFFNESS STATIC AND DYNAMIC COUPLING ANALYSIS)


ID DIFFDYN,PHASE4
DIAG 2,8,13,14,16
APP DISP
TIME 100
SOL 13,0
ALTER 1
PARAM //C,N,NOP/V,N,TRUE=-1 $
$ TRUE USED AS PARAMETER IN EQUIV STATEMENTS TO EQUIVALENCE DATA BLOCKS
$
$ DMAP ALTER.  SOL 13,0   PHASE IV.
$ REPEATING LOOP.
$ OMIT, SPC, MPC AND SUPPORT CARDS ARE PERMITTED HERE
$
$ USER MUST USE SPOINT CARD TO ENABLE USE OF SPC AND MPC CARDS
$ USER MUST CREATE NULL SQUARE KT AND MT MATRICES WITH DMI CARDS IN
$      THE BULK DATA DECK
$
ALTER 6,41
ALTER 48,50
ALTER 54,110 $ SKIP STATIC SOLUTION AND FORMULATION OF DIFFERENTIAL
$      STIFFNESS MATRIX
INPUTT1 /,,,,/C,N,-3$
INPUTT1 /KDBB,MBB,PBL,,/C,N,+5/C,N,0$   SKIP 5 BLOCKS AND READ INPT.
FILE KDBB=SAVE/MBB=SAVE/PBL=SAVE$
INPUTT1 /,,,,/C,N,-3$        REWIND INPT.
JUMP LOOP99 $
LABEL LOOP99$ READ AND COMBINE PARTITION, STIFFNESS AND MASS MATRICES
INPUTT1 /E,,,,/C,N,0$      READ PARTITIONING VECTORS FROM INPT.
MERGE, ,,,KDBB,E,/KDAAT1$
ADD KT,KDAAT1/KTT$
EQUIV KTT,KT/TRUE$
MERGE, ,,,MBB,E,/MAAT1$
ADD MT,MAAT1/MTT$
EQUIV MTT,MT/TRUE$
MERGE, ,PBL,,,,E/PBT/C,N,+1$
ADD PB,PBT/PT$
EQUIV PT,PB/TRUE$
REPT LOOP99,4$ TOTAL MATRICES NOW FORMED
EQUIV KT,KDNN/MPCF2 / MT,MNN/MPCF2 $
COND LBL2D,MPCF2 $
MCE1 USET,RG/GM$
MCE2 USET,GM,KT,MT,,/KDNN,MNN,,$
ALTER 116,116
SCE1 USET,KDNN,MNN,,/KDFF,KDFS,KDSS,MFF,,$
ALTER 122,122
SMP1 USET,KDFF,,,/GO,KDAA,NULL1,NULL2,NULL3,,,,,$
ALTER 125
RBMG2 KDAA/LLL,ULL $
CHKPNT LLL ULL $
EQUIV PB,PLB/NOSET $
CHKPNT PLB $
COND PHA4L1,NOSET $
SSG2 USET,GM,YS,KDFS,GO,,PB/,POB,PSB,PLB$
CHKPNT POB,PSB,PLB $
LABEL PHA4L1 $
SSG3 LLL,ULL,KDAA,PLB,NULL2,NULL3,NULL1,POB/UBLV,UBOOV,RBULV,RBUOV/V,N,
       OMIT/V,Y,IRES=-1/C,N,1/V,N,EPSI $
```

```
SAVE EPSI $
CHKPNT UBLV,UOOV,RULV,RUOV $
COND PHA4L2,IRES $
MATGPR GPL,USET,SIL,RBULV//C,N,L $
MATGPR  GPL,USET,SIL,RBUOV//C,N,O $
LABEL  PHA4L2 $
SDR1  USET,PB,UBLV,UBOOV,YS,GO,GM,PSB,KOFS,KOSS,/UBGV,PBGG,QBG/C,N,1/C,
      N,BKLO $
MATPRN UPGV,,,,//$
PURGE PBGG,QBG/TRUE $
PARAM //C,N,NOP/V,N,SUP=0 $
INPUTT1 /,,,,/C,N,-3 $
OUTPUT1, ,,,,//C,N,-1/C,N,2 $ INP2
JUMP LOOP97 $
LABEL LOOP97 $
PARAM //C,N,ADD/V,N,SUB/V,N,SUP/C,N,1 $
PRTPARM //C,N,0/C,N,SUP $
INPUTT1 /XX,,,,/C,N,0 $
PARTN UBGV,,XX/,UPV,,/C,N,1 $
MATPRN UBV,,,,//$
OUTPUT1 XX,UBV,,,//C,N,0/C,N,2 $ INP2
REPT LOOP97,4 $
OUTPUT1, ,,,,//C,N,-3/C,N,2 $     INP2
ALTER 138,145
MATPRN PHIG,,,,//$
OUTPUT1, ,,,,//C,N,-1/C,N,1$INP1
INPUTT1 /,,,,/C,N,-3$
OUTPUT1 LAMA,,,,//C,N,0/C,N,1$
PARAM //C,N,NOP/V,N,BLADE=0 $
JUMP LOOP98 $
LABEL LOOP98$ PREPARE AND PLACE PARTITIONED EIGENVECTORS ON TAPE
PARAM //C,N,ADD/V,N,BLADE/V,N,BLADE/C,N,1$
PRTPARM //C,N,0/C,N,BLADE $
INPUTT1 /Q,,,,/C,N,O $
MATPRN Q,,,,//$
PARTN PHIG,,Q/,PHI,,/C,N,1$
MATPRN PHI,,,,//$
OUTPUT1 PHI,,,,//C,N,0/C,N,1$
REPT LOOP98,4 $
OUTPUT1,,,,, //C,N,-3/C,N,1 $
ENDALTER
CEND
    (CASE CONTROL DECK)
BEGIN BULK
      INCLUDE MATRIX OPERATORS
      INCLUDE PSEUDOSTRUCTURE DATA
ENDDATA
END= $ INCLUDE THIS CARD FOR IBM 360/370

   ---COMMENTS---
      APPROACH DISP.
      REPEATING LOOPS.
      SIMILAR TO PHASE II, BUT USE ALTER OF RIGID FORMAT 13 IN ORDER TO
      EASE THE IMPLEMENTATION OF APPLYING SECOND ORDER OMIT AND CONSTRAINTS
      FOR EIGEN-VALUE EXTRACTION.
      NO SECOND ORDER OMIT IS APPLIED IN THE PRESENT ANALYSIS.
   --------------
```

```
NASTRAN SUBSTRUCTURE ANALYSIS
DIFFERENTIAL STIFFNESS MODAL AND STATIC SOLUTION
IDENTICAL SUBSTRUCTURES
LISTING OF ---PHASE V---
   (DATA RECOVERY)


ID PHASE,FIVE$    MODAL DIFFERENTIAL
TIME 25
APP DISP
DIAG 2,8,13,14
SOL 13,0
ALTER 30,135
PARAM    //C,N,NOP/V,N,TRUE=-1  $
INPUTT1 /,,,,/C,N,-3/C,N,1 $
JUMP LOOP98 $
LABEL LOOP98 $
ADD       INDICA,PLUS1000/TEMP   $
EQUIV  TEMP,INDICA/TRUE   $
MATPRN  INDICA,,,,//    $
OUTPUT3 INDICA,,,,//C,N,1/C,Y,N1=MAD $
INPUTT1 /UBV,,,,/C,N,1/C,N,1 $
FILE UBOOV=SAVE/YBS=SAVE/GO=SAVE/UM=SAVE/GM=SAVE/PBS=SAVE/KBFS=SAVE/
     KBSS=SAVE$
SDR1 USET,,UBV,UBOOV,YBS,GO,GM,PBS,KBFS,KBSS,/UBGV,,
     QBG/V,N,NOSKIP/C,N,DS1 $
CHKPNT UBGV,QBG $
SDR2 CASECC,CSTM,MPT,DIT,EQEXIN,SIL,GPTT,EDT,BGPDT,,
     QBG,UBGV,EST,/,OQBG1,OUBGV1,OESB1,OEFB1,PUBGV1/C,N,DS1 $
OFP OQBG1,OUBGV1,OESB1,OEFB1,,//V,N,CARDNO $
REPT LOOP98,4 $
INPUTT1 /LAMA,,,,/C,N,-3$
JUMP LOOP99$
LABEL LOOP99$
ADD       INDICA,PLUS1000/TEMP1    $
EQUIV     TEMP1,INDICA/TRUE     $
MATPRN  INDICA,,,,//    $
OUTPUT3  INDICA,,,,//C,N,1/C,Y,N1=MAD    $
INPUTT1 /PHIA,,,,/C,N,0$
ALTER 145
REPT LOOP99,4$
ENDALTER
$
$  CHECKPOINT DICTIONARY ENTER HERE
$
CEND
    (CASE CONTROL DECK)
BEGIN BULK
ENDDATA
END* $ INCLUDE THIS CARD FOR IBM 360/370

  ---COMMENTS---
     APPROACH DISP.
     REPEATING LOOPS.
     THIS RUN GENERATES A HUGE AMOUNT OF STRESS OUTPUT, A OUTPUT3 HAS
     TO BE USED TO MARK THE STRESS FILE, OTHERWISE IT WOULD NOT BE EASY
     TO PLOT IT ON A CALCOMP PLOTTER.
  --------------
```

```
  NASTRAN SUBSTRUCTURE ANALYSIS
  DYNAMIC SOLUTION WITHOUT DIFFERENTIAL STIFFNESS
  DMAP PROGRAM TO COMBINE TAPES
  INPUT TAPE INPT CONTAINS STIFFNESS, LOAD AND PARTITION MATRICES
       (PHASE I OUTPUT)
  INPUT TAPE INP1 CONTAINS MASS MATRIX
       (PHASE III OUTPUT)
  OUTPUT TAPE INP2
```

```
ID TAPES,TWOONE $
TIME 2
APP DMAP
DIAG 2,8,13,14
BEGIN $
INPUTT1 /KAA,PL,E1,E2,E3/C,N,-3$
INPUTT1 /E4,E5,,,/C,N,0$
INPUTT1 /,,,,/C,N,-3/C,N,1$
INPUTT1 /MAA,,,,/C,N,+6/C,N,1$
OUTPUT1, ,,,,//C,N,-1/C,N,2$
OUTPUT1 KAA,MAA,E1,E2,E3//C,N,0/C,N,2$
OUTPUT1 E4,E5,,,//C,N,0/C,N,2$
OUTPUT1, ,,,,//C,N,-3/C,N,2$
INPUTT1 /,,,,/C,N,-3$
END $
CEND
```

```
ID BSVIRB,PHASE2
TIME 95
APP DISP
DIAG 1,2,8,13,14,16
SOL 3,0
ALTER 1
$
$     DMAP ALTER,  SOL 3,0   PHASE II.
$     REPEATING LOOP.
$     OMIT, SPC, MPC AND SUPPORT CARDS ARE PERMITTED HERE.
$
PARAM //C,N,NOP/V,N,TRUE=-1$
$ TRUE USED AS PARAMETER IN EQUIV STATEMENTS TO EQUIVALENCE DATA BLOCKS
PARAM //C,N,NOP/V,Y,ISTFSEE=-1 $
$ ISTFSEE CONTROLS WHETHER PICTORIAL MATRIX PRINTER USED FOR STIFFNESS
$      TO SEE USE      PARAM   ISTFSEE 1      CARD IN BULK DATA DECK
$ MUST BE VARIABLE AS USED IN COND STATEMENT
PARAM //C,N,NOP/V,Y,MASSSEE=-1 $
$ MASSSEE CONTROLS WHETHER PICTORIAL MATRIX PRINTER USED FOR MASS
$      TO SEE USE      PARAM   MASSSEE 1      CARD IN BULK DATA DECK
$ MUST BE A VARIABLE AS USED IN COND STATEMENT
ALTER 6,41
INPUTT1 /KAA1,MAA1,,,/C,N,-3/C,N,1 $ INP1 -- TWO TAPES
$ INPUTT1 /Z,KAA1,MAA1,,/C,N,-3/C,N,1 $ INP1 -- SIX TAPES
FILE KAA1=SAVE/MAA1=SAVE$
COND SMSEE1,ISTFSEE $
SEEMAT KAA1,,,,// $ PRINTS LOCATION OF NON-ZERO TERMS OF KAA1 MATRIX
LABEL SMSEE1 $
```

```
COND MMSEE1,MASSSEE $
SEEMAT MAA1,,,,//$ PRINTS LOCATION OF NON-ZERO TERMS OF MAA1 MATRIX
LABEL MMSEE1 $
$ PARAM //C,N,NOP/V,N,IPT#0 $ SIX TAPES
LABEL LOOP99$
$ BEGIN LOOP 99
$ PARAM //C,N,ADD/V,N,IPT/V,N,IPT/C,N,1 $ SIX TAPES
$ PRTPARM //C,N,0/C,N,IPT $ SIX TAPES
$ INPUTT1 / E,,,,/C,N,-3/V,N,IPT $ SIX TAPES
INPUTT1 /E,,,,/C,N,0/C,N,1 $ INP1  --  TWO TAPES
MATPRN E,,,,//$
MERGE, ,,,KAA1,E,/KGGT$
ADD KGG,KGGT/KT$
$ KT AND MT ARE CONSIDERED AS SCRATCH DATA BLOCKS AND MUST NOT BE
$      REFERENCED OUTSIDE OF LOOP99
EQUIV KT,KGG/TRUE$
MERGE, ,,,MAA1,E,/MGGT$
ADD MGG,MGGT/MT$
EQUIV MT,MGG/TRUE$
COND SMSEE2,ISTFSEE $
SEEMAT KGG,,,,// $ PRINTS LOCATION OF NON-ZERO TERMS OF KGG MATRIX
LABEL SMSEE2 $
COND MMSEE2,MASSSEE $
SEEMAT MGG,,,,// $ PRINTS LOCATION OF NON-ZERO TERMS OF MGG MATRIX
LABEL MMSEE2 $
REPT LOOP99,4$
$ THE 4 IN REPT LOOP99,4$ INDICATES THAT LOOP99 IS GONE THROUGH 5 TIMES
$      TO CHANGE NUMBER OF IDENTICAL SUBSTRUCTURES ANALYZED FROM 5,
$      CHANGE THIS NUMBER TO ONE LESS THAN THE NUMBER OF IDENTICAL
$      SUBSTRUCTURES
$ END LOOP 99
ALTER 50,54
ALTER 105,106
OUTPUT1 LAMA,,,,//C,N,-1/C,N,0$
$ PARAM //C,N,NOP/V,N,IP1#0 $ SIX TAPES
INPUTT1 /Q1,Q2,,,/C,N,-3/C,N,1 $ INP1 -- TWO TAPES
LABEL LOOP98$
$ PARAM //C,N,ADD/V,N,IP1/V,N,IP1/C,N,1 $ SIX TAPES
$ PRTPARM //C,N,0/C,N,IP1 $ SIX TAPES
$ INPUTT1 /Q,,,,/C,N,-3,V,N,IP1 $ SIX TAPES
INPUTT1 /Q,,,,/C,N,0/C,N,1 $ INP1 -- TWO TAPES
$ Q CORRESPONDS TO E IN LOOP99
PARTN PHIG,,Q/,PHIZ,,/C,N,1$
OUTPUT1   PHIZ,,,,//C,N,0/C,N,0$
REPT LOOP98,4$
SDR2 CASECC,CSTM,MPT,DIT,EQEXIN,SIL,,,BGPDT,LAMA,QG,PHIG,,/,
     OQG1,OPHIG,,,/C,N,REIG$
OFP OPHIG,OQG1,,,,//V,N,CARDNO$
ALTER 108,112
ALTER 114,115
ENDALTER
CEND
```

TABLE 1

Calculation Times for Substructuring Analysis of 5 Lashed
80-cm (31-in.) Steam Turbine Blades

Phase	Description of Run	Computer Field Length	CPU Seconds or CP Seconds	CRU Hours or CS Seconds
0	Generation of Airfoil Mesh Using MESH6	6500 200000_8	427	462 CS
I	Generation of Matrices for Substructure	370 500K	872	0.940 CRU
II	Combination of Matrices and Solution of Reduced Static Elastic Problem	370 500K	502	0.704 CRU
III	Preparation of Output Displacements, Forces and Stresses for Static Elastic Problem and Generation of Substructure Differential Stiffness Matrix	370 500K	2457	3.042 CRU
IV	Static Differential Stiffness Reduced Solution	370 520K	683	0.923 CRU
	Determination of Eigenvalues and Reduced Eigenvectors for Modes 1, 2, 3, 4 and 8 at 3600 rpm	370 520K	3852	2.128 CRU

TABLE 1 (Continued)

Phase	Description of Run	Computer Field Length	CPU Seconds or CP Seconds	CRU Hours or CS Seconds
IV Contd.	**Determination of Eigenvalues and Reduced Eigenvectors for Modes 5, 6, 7, 8, and 9 at 3600 rpm**	370 520K	3592	4.472 CRU
	Determination of Eigenvalues and Re-duced Eigenvectors for Mode 4 at 3600 rpm	370 520K	1384	1.780 CRU
	Determination of Eigenvalues for Modes 1, 2, 3 and 4 at 0 rpm. No reduced Eigenvectors	370 520K	Computer	Error-No Charge
	Determination of Eigenvalues and Reduced Eigenvectors for Modes 5, 6, 7 and 8 at 0 rpm	370 520K	3487	4.177 CRU
	Determination of Eigenvalues and Reduced Eigenvectors for Modes 7, 8, 9 at 0 rpm	370 520K	2084	2.546 CRU
V	Stress Recovery for Static Differential Stiffness and Modes 1, 2, 3, 4 and 8 at 3600 rpm	370 500K	1179	1.866 CRU
	Stress Recovery for Modes 5, 6, 7, 8 and 9 at 3600 rpm	370 500K	860	1.400 CRU

TABLE 1 (Continued)

Phase	Description of Run	Computer Field Length	CPU Seconds or CP Seconds	CRU Hours or CS Seconds
V Cont.	Stress Recovery for Modes 5, 6, 7 and 8 at 0 rpm	370 500K	742	1.214 CRU
VI	Separate Data on the Two Discs Used to Enable Plotting in Smaller Runs. 2 Runs	370	100/run	.400 CRU/run
VII	Stress Plotting on both Surfaces of Airfoil of Either Maximum and Minimum Principal Stresses or X and Y Stresses Using NASPLT. 30 Runs.	370 350K	137/run	.150 CRU/run
	Stress Plotting on both Surfaces of Outer Lashing Wire of Maximum Principal, Minimum Principal, X and Y Stresses Using NASPLT. 15 Runs.	370 350K	75/run	.099 CRU/run
	Stress Plotting on Both Surfaces of Inner Lashing Wire of Maximum Principal, X and Y Stress Using NASPLT. 15 Runs.	370 350K	69/run	.094 CRU/run
TOTAL			28600	462 CS 33.4 CRU

TABLE 2

Estimated Calculation Times for Non-Substructuring Analysis of 5 Lashed 80-cm (31-in.) Steam Turbine Blades Using Level 15 NASTRAN on the IBM 370-165 Assuming Adequate Disk and Core Space Were Available

Phase	Description	Field Length	CPU Seconds	CRU Hours
0	Generation of Airfoil Meshes	-	-	-
I	Form Matrices	500K	1260	1.4
II	Solve Elastic Static Problem	500K	1170	1.5
III	Output Elastic Results and Create Differential Stiffness Matrix for Blade Set	500K	10500	7
IV	Differential Stiffness Static Solution	500K	1170	1.5
	Natural Frequencies and Eigen-vectors (13 Modes)	850K	8000/mode	11/mode
V	Stress Recovery	Same as with Substructuring		
VI	Separation of Data on Discs	Same as with Substructuring		
VII	Plotting Isostress Lines	Same as with Substructuring		
TOTAL			124000	162

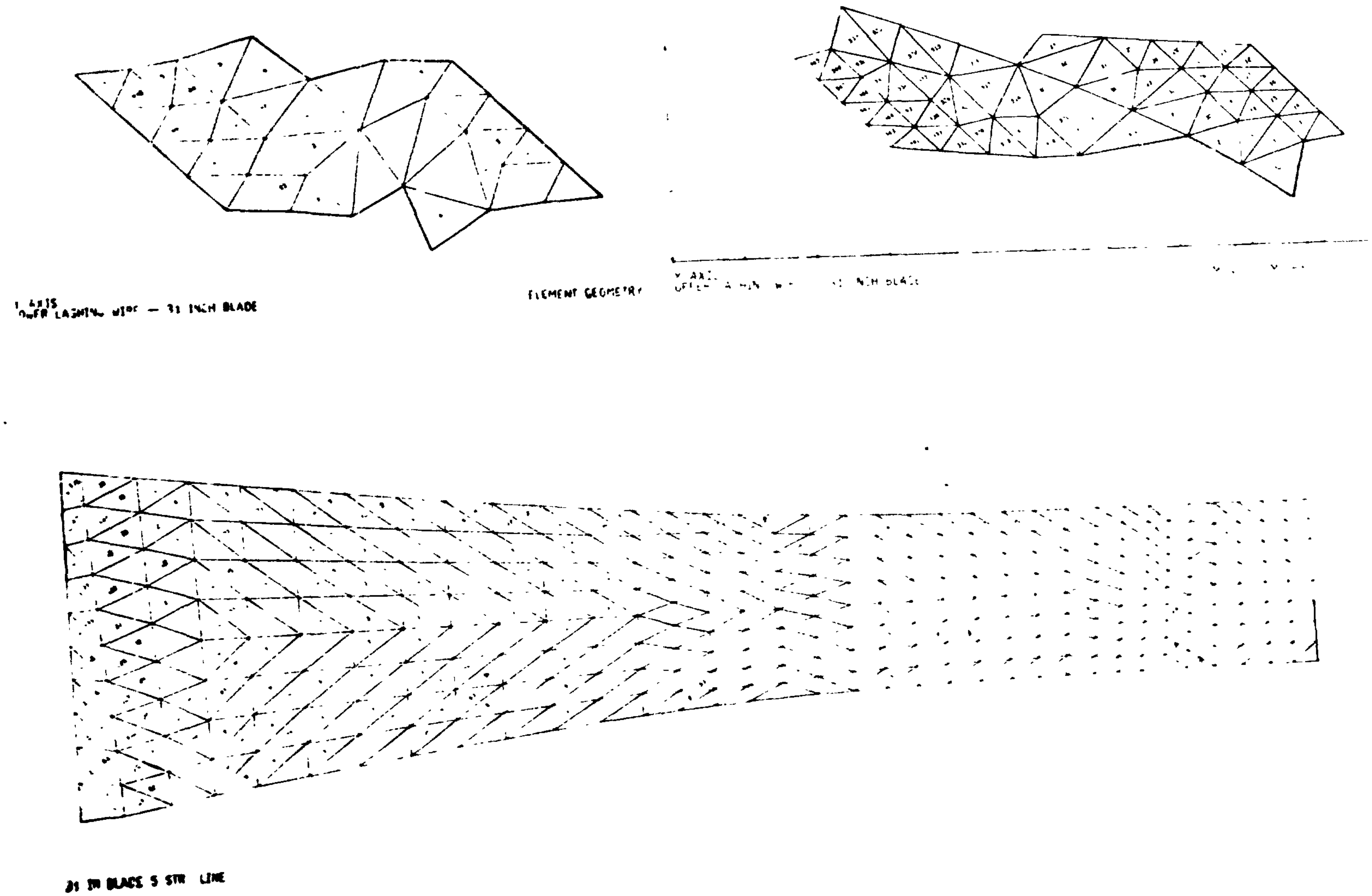

Figure 1 - Finite Element Mesh for Airfoil and Lashing Wires.

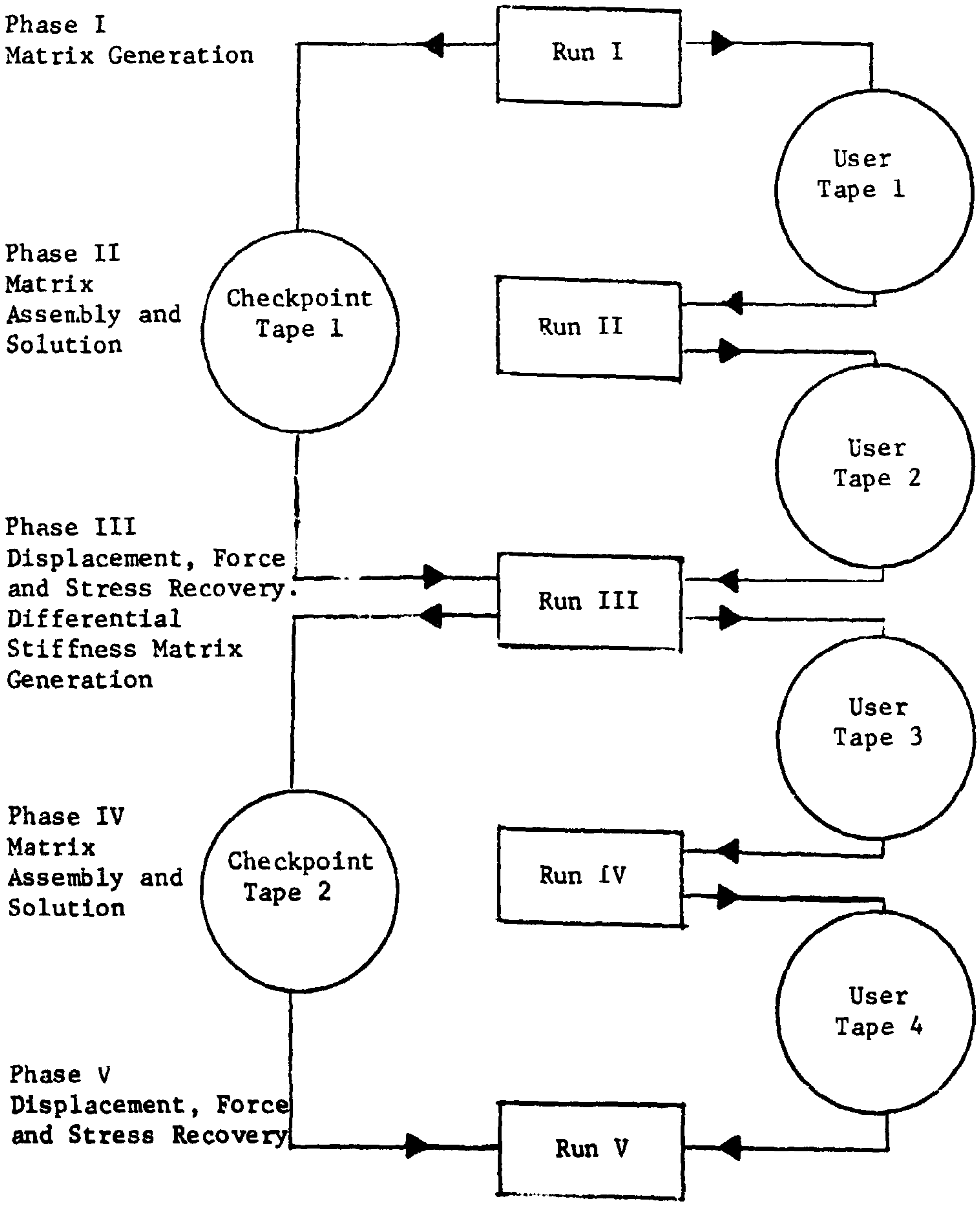

Figure 2 - Substructure Runs for Static or Dynamic (Natural Frequency) Analysis, with Differential Stiffness, of Identical Substructures.

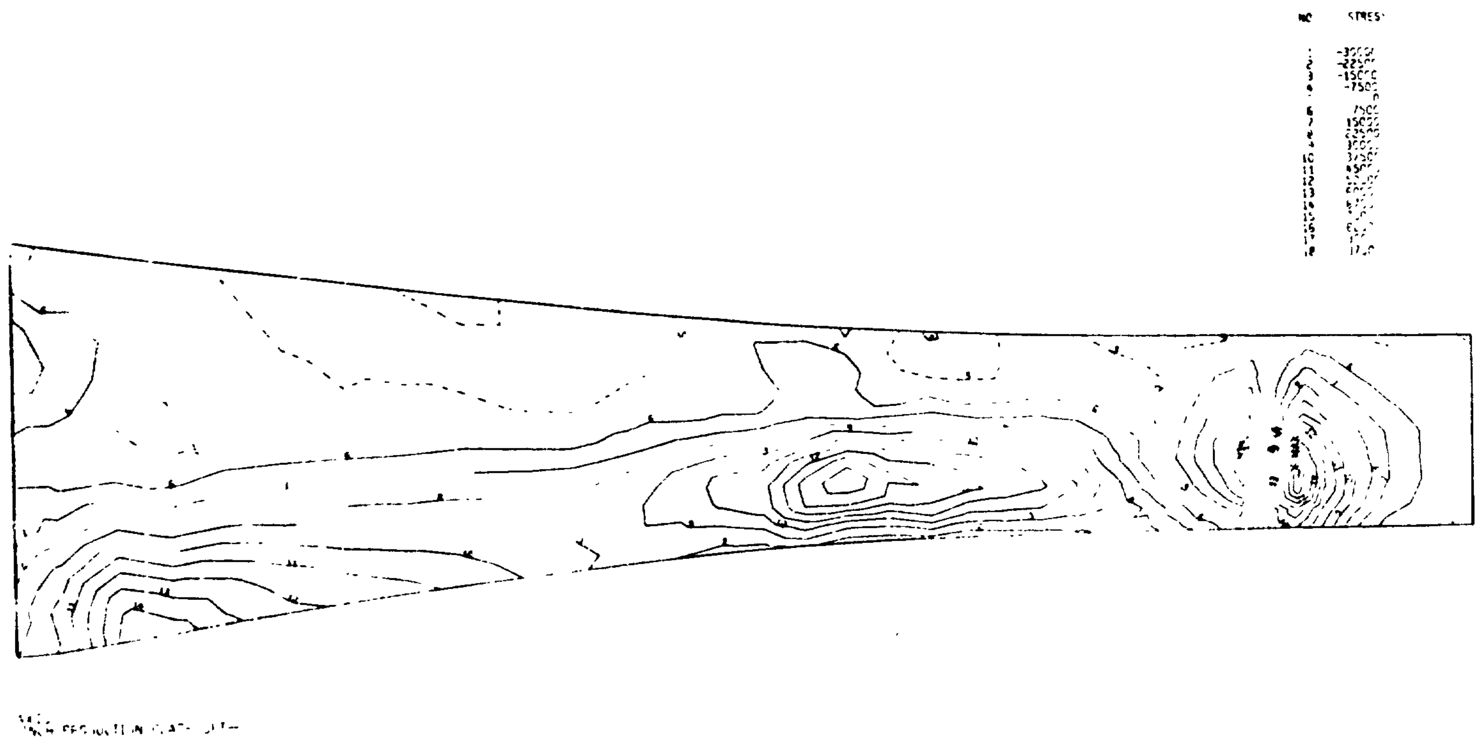

Figure 3 - Sample Isostress Pattern on Surface of Airfoil.

N74-14603

SUBSTRUCTURE ANALYSIS TECHNIQUES AND AUTOMATION

By Carl W. Hennrich and Edwin J. Konrath, Jr.

Software Sciences, Inc.
Hampton, Virginia

SUMMARY

A basic automated substructure analysis capability for NASTRAN is presented which eliminates most of the logistical data handling and generation chores that are currently associated with the method. Rigid formats are proposed which will accomplish this using three new modules, all of which can be added to Level 16 with a relatively small effort.

INTRODUCTION

Prior to Level 15, no real substructure analysis capability existed in any NASA released version of the NASTRAN program. With the pre-release of Levels 8 and 11, users began expressing the desirability and necessity for a substructure analysis capability. Several user organizations attempted, with limited success, to accomplish substructure analysis by using the checkpoint/restart capability of NASTRAN coupled with the direct matrix abstraction (DMAP) approach. Other organizations utilized user-developed utility modules and Rigid Format DMAP alter packages, thus taking advantage of the Rigid Formats whenever possible.

The latter method with an expansion of user options was adapted by NASA for inclusion in Level 15 and is fully described in Section 4.3 of the Theoretical Manual (reference 1) and Section 1.10 of the User's Manual (reference 2). The casual user may well be quite frustrated with this method since its generality requires the user to design a specific approach for the problem at hand. This involves externally generated partitioning vectors as well as DMAP alter packets which are often unfamiliar to the engineer user. In addition, little assistance is provided in the form of qualitative verification of the hand-generated coupling data or of the resulting coupled matrices. The probability of undetected user-generated errors in this process is therefore rather high. Furthermore, the user must develop customized DMAP packages for any problem that does not match the currently published substructure alter packages.

PRECEDING PAGE BLANK NOT FILMED

The currently available Level 15 technique was intended as a general but preliminary capability. The upgrading of this capability with user conveniences and qualitative data checks has been requested by many. As NASTRAN's substructure analysis capabilities are improved, serious users will explore many different approaches. Several techniques and utility module designs developed by necessity will be discussed for use with Levels 15 and 16. Along these lines, several aids are suggested herein. Some take advantage of existing code and capability while others indicate the need for additional user-developed utility modules as well as modifications to several existing modules. The techniques discussed are intended for the casual engineer user and are therefore used somewhat more rigidly than might normally be expected with utility modules. It is hoped, however, that the concepts described will stimulate other serious user teams to develop structurally-oriented and utility modules to ease the difficulties encountered in carrying out an effective substructure analysis.

All new and modified routines and modules are based on the Level 16 version of NASTRAN currently undergoing validation. Many of the techniques described are valid for Level 15, however, and can be installed in that level with slightly more difficulty since many Level 16 features will also have to be installed. It should be possible for a reasonably competent experienced team to install the capability described with a nominal effort.

SYMBOLS

K	Stiffness matrix
P	Load vector matrix
u	Displacement vector matrix
G	Transformation matrix
M	Mass matrix

Subscripts:

f	Free (unconstrained) set
a	Analysis (boundary) set
o	Omitted (interior) set
g	All degrees of freedom set

Superscripts:

T	Transpose operator
-1	Inverse operator
i	Substructure index
o	Related only to the omitted (interior) set

Other Symbols:

-	Pre-reduction portion of a matrix
[ ]	Matrix
{ }	Matrix of vectors
^	Related to pseudomodel.

Symbols appearing in the appendices are defined in the appropriate appendix as necessary.

OBJECTIVE AND SCOPE

A sample substructure analysis model is shown in figure 1. The grid points on the top surface of this model which are to be coupled are identified by letters. Substructure analysis implicitly assumes that each substructure is analyzed separately and subsequently combined with other previously analyzed substructures to form a pseudostructure as shown in figure 2. Once the pseudostructure is solved, the detailed solutions for each of the substructures may be obtained by a set of data recovery runs. The objective of the techniques and new capability to be presented herein is to define a basic substructure analysis capability which will require a minimum amount of user-generated data and logistics.

With this objective in mind, the scope will be limited to providing a basic capability; therefore, many desired features will be omitted in order to focus attention on the fundamentally important capabilities. In the discussion that follows, the limitations that result from this restricted scope will be identified. It should be kept in mind that most, if not all, of these limitations can be removed by additions to the basic capability once it is implemented.

DISCUSSION

The theory, utilization and programming aspects of NASTRAN's substructure analysis capabilities are discussed in references 1-3. Necessary and desirable features of any substructure analysis capability have been given by many, including papers presented at the first Users' Colloquium (references 4 and 5). For ease of reference, the basic theory is given in the following section as an aid to the interested reader.

The difficulty in carrying out a substructure analysis with NASTRAN lies in the logistical procedures rather than with any inherent deficiency with NASTRAN itself. This logistic problem is illustrated in figures 2 and 3 where the number of runs and retainable data files is seen to be large. The data requirements for substructure analysis in Levels 15 and 16 and for the capability described in this paper, which we shall designate Level 16.X, are tabulated in table 1.

The major disadvantages to the current (Level 15) substructure analysis capability of NASTRAN are:

1. The user must generate partitioning vectors

2. A DMAP alter packet appropriate to the problem being run must be created.

These disadvantages can be overcome relatively easily if a few modest restrictions are imposed. This will be illustrated for the two most commonly used rigid formats, Static Analysis and Normal Modes Analysis which, when upgraded as described herein, will not require the generation of an alter packet to run.

The restrictions that will be imposed are listed in table 2 and are summarized here.

1. Only one (1) level of substructure analysis is supported, consisting of a maximum of twenty (20) substructures.

2. The degrees of freedom at coupled boundary points must agree in number, meaning and direction.

3. The internal sequence of all points on the boundary between any two substructures must be the same.

4. All subcases must be defined in all runs.

5. Output may be obtained during Phase II for any degrees of freedom present as identified by the pseudostructure map printout (see fig. 4).

Advantage features provided are:

1. If the grid points of the substructures are numbered uniquely, the user may request automatic coupling to occur. If exceptions occur, they may be handled by means of bulk data.

2. The minimum required data are the DTI data cards defining the number of substructures present and other logistical control information.

3. If topologically equivalent substructures are present, only one needs to be input; coupling data cards will be required in this case since the grid points are no longer unique.

Level 16.X overcomes the most serious objections by providing an automated capability. This capability is implemented by the addition of new modules, rigid formats, and a user-oriented data table specification. These facets are discussed in the sections which follow the theoretical discussion. As far as the rigid format is concerned, the new modules appear as structural matrix assemblers similar to SMA3 with the substructures appearing internally as arbitrarily defined super elements.

THEORY

The basic theory used as a basis for the implementation of substructure analysis is presented here for the convenience of the reader. Full treatment is given in Section 4.3 of the Theoretical Manual (reference 1). The NASTRAN set notation will be employed.

For static analysis, the free (f) degrees of freedom of the substructure are allocated to the a-set, which contains all boundary degrees of freedom, (i.e., degrees of freedom which are to be coupled to similar degrees of freedom at some grid point in another substructure), and the o-set, which contains the non-boundary degrees of freedom. The equilibrium equations are written as

$$\left[\begin{array}{c|c} \bar{K}_{aa} & K_{ao} \\ \hline K_{oa} & K_{oo} \end{array}\right] \left\{\begin{array}{c} u_a \\ \hline u_o \end{array}\right\} = \left\{\begin{array}{c} \bar{P}_a \\ \hline P_o \end{array}\right\} \qquad (1)$$

from which

$$[K_{aa}]\{u_a\} = \{P_a\} \qquad (2)$$

where

$$[K_{aa}] = [\bar{K}_{aa}] + [G_o]^T[K_{oa}] \tag{3}$$

$$\{P_a\} = \{\bar{P}_a\} + [G_o]^T\{P_o\} \tag{4}$$

and

$$[G_o] = -[K_{oo}]^{-1}[K_{oa}] \quad . \tag{5}$$

Also, the displacements of the interior points are given by

$$\{u_o\} = \{u_o^o\} + [G_o]\{u_a\} \tag{6}$$

where

$$\{u_o^o\} = [K_{oo}]^{-1}\{P_o\} \quad . \tag{7}$$

Equations 3, 4, 5 and 7 can be carried out in Phase I. Equation 2 must be deferred to Phase II where the missing contributions to $[K_{aa}]$ from the other substructures are available. Equation 6 consists of two parts, one of which (equation 7) is evaluated in Phase I. The other part depends on the solution generated in Phase II. Equation 6 is therefore done in Phase III.

In Phase II, the substructure boundary matrices $[K_{aa}^i]$ and $\{P_a^i\}$, which are brought in from User Files generated by the Phase I runs, are expanded to pseudomodel g-size.

$$[K_{aa}^i] \rightarrow [\hat{K}_{gg}^i] \tag{8}$$

$$\{P_a^i\} \rightarrow \{\hat{P}_g^i\} \tag{9}$$

and added to form

$$[\hat{K}_{gg}] = \sum_i [\hat{K}_{gg}^i] \tag{10}$$

$$\{\hat{P}_g\} \quad \sum_i \{\hat{P}_g^i\} \tag{11}$$

from which a normal solution proceeds.

After the solution $\{\hat{u}_g\}$ is obtained, the boundary displacements are simply extracted by

$$\{u_a^i\} \leftarrow \{\hat{u}_g\} \quad . \tag{12}$$

The merge and partitioning operations defined by equations 8, 9 and 12 require information identifying degrees of freedom in each substructure with corresponding degrees of freedom of the pseudomodel.

For normal modes analysis, the mass matrix is arbitrarily reduced via the Guyan reduction

$$[M_{aa}] = [\bar{M}_{aa}] + [M_{oa}]^T[G_o] + [G_o]^T[M_{oa}] + [G_o]^T[M_{oo}][G_o] \tag{13}$$

described in reference 6 and carried into Phase II in the same way as $[K_{aa}]$.

In dynamics rigid formats, the viscous and structural damping matrices are similarly treated.

NEW MODULE DESCRIPTIONS

Three new modules are presented in this section which form the basis for the automation of the basic automatic substructure analysis technique. These modules can be either added to DMAP alter packets currently being utilized or to new rigid formats as will be shown in the following section.

The three new modules are:

SSMA	Substructure Matrix Assembler
SSVE	Substructure Vector Extractor
UDBR	User File Data Block Recovery

Descriptions of these modules are presented on the following pages using the format prescribed for Section 5 of the NASTRAN User's Manual.

I. NAME: SSMA (Substructure Matrix Assembler)

II. PURPOSE: Generates matrices from substructures -

1. Obtains substructure matrices and other data from designated User Files.

2. Assembles g-sized stiffness, mass, viscous damping, structural damping and/or load vector matrices for all substructures designated.

3. Outputs appropriate diagnostic and information messages and summary information.

III. DMAP CALLING SEQUENCE:

```
SSMA    GEØM4,UFTABLE / K,M,B,K4,P,PSD / C,Y,PØPT / C,Y,GENSAME /
        V,N,LUSET $
```

IV. INPUT DATA BLOCKS:

GEØM4 - Contains SAME data

UFTABLE - User File information

V. OUTPUT DATA BLOCKS:

K,M,B,K4,P - Stiffness, mass, viscous damping, structural damping and load vector matrices

PSD - Pseudostructure data table

VI. PARAMETERS:

PØPT - Integer-input, default=1.
=+1, print pseudostructure map
=-1, do not print map

GENSAME - Integer-input, default =-1.
=-1, coupling data is taken from GEØM4
=+1, automatic coupling based on grid point identification numbers will be employed (GEØM4 data is also used if present).

LUSET - Integer-output, default=0. Number of degrees of freedom in pseudostructure g-set.

VII. REMARKS:

1. SSMA will read User Files INPT, INP1, INP2, ---, INP9 as specified by the data on UFTABLE.

2. Any or all outputs may be purged.

3. GEØM4 may be purged if GENSAME=+1.

4. UFTABLE may not be purged.

I. NAME: SSVE (Substructure Vector Extractor)

II. PURPOSE: Generates a User File containing substructure boundary displacement vectors.

III. DMAP CALLING SEQUENCE:

```
SSVE     PSD,LA,UGV // $
```

IV. INPUT DATA BLOCKS:

PSD - Pseudostructure data table (generated by SSMA)

LA - Eigenvalue table

UGV - Displacement vector

V. OUTPUT DATA BLOCKS: None

VI. PARAMETERS: None

VII. REMARKS:

1. Companion module to SSMA, requires pseudostructure data table (PSD) output from SSMA as input.

2. SSVE will write a User File on INPT, INP1, INP2, ---, or INP9 as specified by the data block UFTABLE and passed to the module via PSD.

I. NAME: UDBR (User File Data Block Recovery)

II. PURPOSE: Recovers data blocks from a given User File according to information contained on a directory data block (the first data block on the file).

III. DMAP CALLING SEQUENCE:

```
UDBR     / DB1,DB2,DB3,DB4,DB5 / C,Y,SUBID / C,Y,UNIT / C,Y,USRTPID2 $
```

IV. INPUT DATA BLOCKS: None

V. OUTPUT DATA BLOCKS:

DBi - Data Blocks recovered by module.

VI. PARAMETERS:

SUBID - Integer-input,default=0. Substructure identification number.

UNIT - Integer-input,default=0. Permanent file code as follows:

0	INPT
1	INP1
2	INP2
.	.
.	.
.	.
9	INP9

USRTPID2 - BCD-input, default=XXXXXXXX. User File identification code.

VII. REMARKS:

1. The User File is assumed to have been generated by module S[illegible]VE.

2. The number and kind of data blocks recovered depends on the directory data block contents.

NEW RIGID FORMATS

In order to simultaneously use the new utility modules previously defined and to relieve the user of the burdensome chore of preparing DMAP alter packets, new rigid formats have been developed, one for each major analysis capability. Static Substructure Analysis, Rigid Format 16, is given in Appendices B, C and D where the solution subset numbers 1, 2 and 3 are indicative of Phase I, II and III, respectively. If subset 0 (see Appendix A) is used, an ordinary Static Analysis will result. Normal Modes Substructure Analysis, Rigid Format 17, is illustrated for Phase II by Appendix E. These new rigid formats are fully compatible with all existing displacement rigid formats, including restart capability, as defined by Rigid Format Series N which is scheduled for Level 16 of NASTRAN.

Many of the DMAP instruction sequences contained in these rigid formats can be used by current Level 15 users with appropriate caution.

USER DATA REQUIREMENTS

The Phase II coupling process requires that matrices and data tables generated in several Phase I runs be recovered from User Files. Many possible data input configurations are possible, depending on the sequence of Phase I runs and reruns which led up to the Phase II analysis. In order to allow the greatest amount of flexibility in the automated process, a table data block containing user file information will be used to control the Phase II assembly process. This can ultimately be generated from a Case Control packet. For the purposes of the current design, however, this table will be assumed to be input via DTI bulk data cards as illustrated in figure 8 and described in some detail in Appendix F. The UFTABLE data block that results will be required input to module SSMA previously discussed. Future expansion to include control of the load assembly process, as well as features not currently envisioned, is easily accomplished since the records of table data blocks are open-ended.

USAGE

The usage of the capability just presented is shown by the sample data decks in figures 5, 6, 7 and 8. It is to be emphasized that, within the limitations previously described, the burden on the user is minimal. The primary requirement is that the small UFTABLE data block be prepared on DTI cards for input to Phase II. Job control language is still necessary, of course, and will not be discussed here since the subject is not only machine-dependent but usually highly installation-dependent as well.

The user accomplishes substructure matrix generation (Phase I) as presently described in the Level 15 User's Manual without the alter packet. The new modules SSMA and SSVE are used to automate the matrix coupling (Phase II) and thereby eliminate the chore of generating complicated DMAP alter packets. No longer must the user supply the input, merge, add, and equivalence statements for the coupling of each matrix of every substructure. Now one module (SSMA) replaces all of the above-mentioned DMAP statements. The user supplies only substructure names and identification values via bulk data cards to inform SSMA how many substructures are being coupled and to relate the substructures to user-supplied coupling data. The substructure's parameter value is used to indicate the presence of identical substructures. The user may also include user file labels from Phase I, names of matrices to be read from each user file, and, when tapes are used, the installation's tape code when requesting multiple-reel tapes. All tape changes and mount requests are handled similarly to the current NASTRAN user tape modules with the exception that the user is uninvolved once the installation's job control language requirements are met. NASTRAN with one module (SSMA) now requests user tapes, verifies the correct mounting and builds all the coupled matrices, taking full advantage of any identical substructures that exist. Module SSVE is similarly used to request an output tape and uncouple the substructure solution vectors.

As a final indication of the usefulness of the techniques developed, the sample problem used in reference 2 is presented in Appendix G. It is seen that truly little effort is required on the part of the user to prepare data for a substructure analysis using Level 16.X features.

FUTURE IMPROVEMENTS

Once the basic capability becomes implemented, an environment will exist with respect to which improvements can be made. Several of these potentially useful improvements are described in the paragraphs which follow.

One early addition should be to provide data checking capability for points being coupled between substructures. These checks will require that additional geometric information about boundary grid points be carried forward from Phase I. This information can then be automatically recovered in Phase II via SSMA and either used inside that module or passed out of the module in the form of data blocks to be used by other new modules.

Another improvement which can be added relatively easily to the basic capability is the ability to introduce and symbolically manipulate and generate geometrically related loading conditions in Phase II. This also requires the availability of additional geometric information in Phase II. At this point, it will be possible to introduce direct matrix input as a representation of loading conditions. This capability will complement the existing capability for users who may desire to input loading matrices generated by programs external to NASTRAN.

The ability to relate degrees of freedom of the pseudostructure to externally designated degree of freedom descriptions in Phase II requires only that the correspondence be known. Since this information is contained in the ASET data blocks input from the Phase I runs, it is easy to conceive of a translator module which will accept data referencing external degrees of freedom (e.g., SPC, ØMIT, FØRCE cards) and generate equivalent data blocks containing internal pseudostructure degree of freedom descriptions. With this capability, analyses of pseudostructure models can be carried out as if they were simple structures.

Non-conforming boundaries can be handled with an extra transformation step. If [Q] is chosen so that the transformed displacement vector

$$\{u\}^* = [Q]^T\{u\} \tag{14}$$

has the desired sequence but the same values, then

$$[Q]^{-1} = [Q]^T \tag{15}$$

and the conformable matrices and vectors are easily computed as

$$[K]^* = [Q]^T[K][Q] \tag{16}$$

and

$$\{P\}^* = [Q]^T\{P\} \quad . \tag{17}$$

After solution, the reverse transformation is merely

$$\{u\} = [Q]\{u\}^* \tag{18}$$

Since [Q] has an extremely low density, NASTRAN's sparce matrix multiply routines will carry out the indicated computations most efficiently. The essential task is the generation of the [Q] data. With suitable arbitrary conventions, this can be accomplished within the module SSMA and included in the PSD data block for transfer to other modules such as SSVE where the reverse transformation can be made.

Multi-level substructure analysis, while not covered explicitly by the scope of this effort, can be obtained with a small modification to the existing capability herein defined. In this case, the ASET data block output from Phase II will contain both the pseudostructure degrees of freedom and the equivalent Phase I external degree of freedom designations. Since several Phase I external degree of freedom designations may exist for each Phase II degree of freedom, the data block becomes somewhat more complex but no essential new difficulty is encountered. Once the correspondence recognition feature is accomplished, multi-level substructure analysis capability essentially becomes open-ended with no real limit to the possible number of levels. Since the degree of freedom correspondence is automatically carried forward at each level, it will be possible to return directly to the original substructures in any data recovery phase. In addition, the substructure formed at any level can be analyzed by itself. Figure 9 illustrates this process.

A user convenience improvement would be to replace the DTI form of the input of the table UFTABLE described earlier with a Case Control Deck packet similar to the structure plotter request packet. This will require new code in the Input File Processor (IFP) portion of the preface which will read the data cards, analyze them for correctness and form the UFTABLE data block. When implemented, the present requirement for a dummy UFTABLE input for subset 0 will be eliminated. The language specifications can be made as user-oriented as desired since IFP will interpret the statements and form the UFTABLE data block. At such time as the data block UFTABLE is added to the FIAT as a recognized output from the preface, an EQUIV DMAP instruction will be needed in the rigid formats if DTI input is also to be available.

Another enhancement will be to allow the coupling of individual degrees of freedom at a grid point rather than all unconstrained degrees of freedom as will be done in Level 16. This task is not dependent on anything presented in this paper but can be done at any time since it merely involves the definition of a new data card similar to the present SAME card (see figure 10) and the addition of minor processing logic in the Level 16 module PVEC.

Several other improvements which will either remove restrictions or extend the capability can be envisioned. The important point is that any or all of these improvements can be relatively easily made once the basic capability is operational.

CONCLUSION AND RECOMMENDATIONS

An approach has been presented by which basic automatic substructure analysis can be added to NASTRAN. It is suggested that this technique can be implemented in Level 16 with a relatively small level of effort. While the resulting capability will not completely satisfy all potential users, it is felt that most substructure analyses will be encompassed. Furthermore, reasonable extensions of the techniques presented can be made which will result in any degree of further sophistication, convenience and automation that can be supported by resources that are made available for this purpose.

APPENDIX A

RIGID FORMAT DMAP LISTING FOR SØL 16, (0)

STATIC SUBSTRUCTURE ANALYSIS (ALL PHASES)

Subset 0 of Rigid Format 16 contains all DMAP instructions for Static Substructure Analysis. If run without subsets 1, 2, or 3, a complete static analysis will result which is equivalent to Rigid Format 1. Selection of one of the subsets 1, 2 or 3, however, reduces Rigid Format 16 to a DMAP sequence which will automatically solve Phase I, II or III of Static Substructure Analysis. These subsets are displayed in Appendices B, C and D. The DMAP compilation listing of SØL 16,0 constitutes the remainder of this Appendix, including an explanatory description of the DMAP similar to that found in Section 3 of the NASTRAN User's Manual.

APPENDIX A

```
RIGID FORMAT DMAP LISTING
SERIES N *** BASIC STATIC SUBSTRUCTURE ANALYSIS ***

RIGID FORMAT 16 - SUBSET ZERO

   N A S T R A N   S O U R C E   P R O G R A M   C O M P I L A T I O N
DMAP-DMAP INSTRUCTION
 NO.

  1  BEGIN     NO.16 BASIC STATIC SUBSTRUCTURE ANALYSIS - SERIES N $

  2  FILE      LLL=TAPE $

  3  FILE      UG=APPEND/PGG=APPEND/UGV=APPEND/UM=SAVE/KNN=SAVE $

  4  JUMP      PH2BK1 $

  5  PARAM     //C,N,ADD/V,N,PHASE2/C,N,0/C,N,-1 $

  6  SSMA      GEOM4,UFTABLE/KGGPS,,,,PGPS,PSDATA/C,Y,PRTOPT/C,Y,GENSAME/ V,N,
               LUSET $

  7  SAVE      LUSET $

  8  CHKPNT    KGGPS,PGPS,PSDATA $

  9  LABEL     PH2BK1 $

 10  GP1       GEOM1,GEOM2,/GPL,EQEXIN,GPDT,CSTM,BGPDT,SIL/V,N,LUSET/   V,N,
               NOGPDT $

 11  SAVE      LUSET $

 12  CHKPNT    GPL,EQEXIN,GPDT,CSTM,BGPDT,SIL $

 13  GP2       GEOM2,EQEXIN/ECT $

 14  CHKPNT    ECT $

 15  PARAML    PCDB//C,N,PRES/C,N,/C,N,/C,N,/V,N,NOPCDB $

 16  PURGE     PLTSETX,PLTPAR,GPSETS,ELSETS/NOPCDB $

 17  COND      P1,NOPCDB $

 18  PLTSET    PCDB,EQEXIN,ECT/PLTSETX,PLTPAR,GPSETS,ELSETS/V,N,NSIL/    V,N,
               JUMPPLOT=-1 $

 19  SAVE      NSIL,JUMPPLOT $

 20  PRTMSG    PLTSETX// $

 21  PARAM     //C,N,MPY/V,N,PLTFLG/C,N,1/C,N,1 $

 22  PARAM     //C,N,MPY/V,N,PFILE/C,N,0/C,N,0 $

 23  COND      P1,JUMPPLOT $

 24  PLOT      PLTPAR,GPSETS,ELSETS,CASECC,BGPDT,EQEXIN,SIL,,,,/PLOTX1/    V,N,
```

APPENDIX A

```
RIGID FORMAT DMAP LISTING
SERIES N *** BASIC STATIC SUBSTRUCTURE ANALYSIS ***

RIGID FORMAT 16 - SUBSET ZERO

   N A S T R A N   S O U R C E   P R O G R A M   C O M P I L A T I O N
DMAP-DMAP INSTRUCTION
 NO.
               NSIL/V,N,LUSET/V,N,JUMPPLOT/V,N,PLTFLG/V,N,PFILE $

 25  SAVE      JUMPPLOT,PLTFLG,PFILE $

 26  PRTMSG    PLOTX1// $

 27  LABEL     P1 $

 28  CHKPNT    PLTPAR,GPSETS,ELSETS $

 29  GP3       GEOM3,EQEXIN,GEOM2/SLT,GPTT/V,N,NOGRAV $

 30  SAVE      NOGRAV $

 31  PARAM     //C,N,AND/V,N,NOMGG/V,N,NOGRAV/V,Y,GRDPNT=-1 $

 32  PURGE     MGG,MELM,MDICT/NOMGG $

 33  CHKPNT    SLT,GPTT $

 34  TA1       ECT,EPT,BGPDT,SIL,GPTT,CSTM/EST,GEI,GPECT,/V,N,LUSET/   V,N,
               NOSIMP/C,N,1/V,N,NOGENL/V,N,GENEL $

 35  SAVE      NOSIMP,NOGENL,GENEL $

 36  PARAM     //C,N,AND/V,N,NOELMT/V,N,NOGENL/V,N,NOSIMP $

 37  COND      ERROR4,NOELMT $

 38  PURGE     KGGX,GPST/NOSIMP/OGPST/GENEL $

 39  CHKPNT    EST,GPECT,GEI,GPST,OGPST $

 40  OPTPR1    MPT,EPT,ECT,DIT,EST/OPTP1/V,N,PRINT/V,N,TSTART/V,N,COUNT $

 41  SAVE      PRINT,TSTART,COUNT $

 42  CHKPNT    OPTP1 $

 43  JUMP      LOOPTOP $

 44  LABEL     LOOPTOP $

 45  COND      LBL1,NOSIMP $

 46  PARAM     //C,N,ADD/V,N,NOKGGX/C,N,1/C,N,0 $

 47  EMG       EST,CSTM,MPT,DIT,GEOM2,/KELM,KDICT,MELM,MDICT,,/V,N,NOKGGX/ V,
               N,NOMGG/C,N,/C,N,/C,N,/C,Y,COUPMASS/C,Y,CPBAR/C,Y,CPROD/C,Y,
               CPQUAD1/C,Y,CPQUAD2/C,Y,CPTRIA1/C,Y,CPTRIA2/  C,Y,CPTUBE/C,Y,
               CPQDPLT/C,Y,CPTRPLT/C,Y,CPTRBSC $
```

APPENDIX A

RIGID FORMAT DMAP LISTING
SERIES N *** BASIC STATIC SUBSTRUCTURE ANALYSIS ***

RIGID FORMAT 16 - SUBSET ZERO

N A S T R A N   S O U R C E   P R O G R A M   C O M P I L A T I O N

```
DMAP-DMAP INSTRUCTION
 NO.

 48  SAVE     NOKGGX,NOMGG $
 49  CHKPNT   KELM,KDICT,MELM,MDICT $
 50  COND     JMPKGG,NOKGGX $
 51  EMA      GPECT,KDICT,KELM/KGGX,GPST $
 52  CHKPNT   KGGX,GPST $
 53  LABEL    JMPKGG $
 54  COND     JMPMGG,NOMGG $
 55  EMA      GPECT,MDICT,MELM/MGG,/C,N,-1/C,Y,WTMASS=1.0 $
 56  CHKPNT   MGG $
 57  LABEL    JMPMGG $
 58  COND     LBL1,GRDPNT $
 59  COND     ERROR2,NOMGG $
 60  GPWG     BGPDT,CSTM,EQEXIN,MGG/OGPWG/V,Y,GRDPNT/C,Y,WTMASS $
 61  OFP      OGPWG,,,,,//V,N,CARDNO $
 62  LABEL    LBL1 $
 63  EQUIV    KGGX,KGG/NOGENL $
 64  CHKPNT   KGG $
 65  COND     LBL11A,NOGENL $
 66  SMA3     GEI,KGGX/KGG/V,N,LUSET/V,N,NOGENL/V,N,NOSIMP $
 67  CHKPNT   KGG $
 68  LABEL    LBL11A $
 69  JUMP     PH2BK2 $
 70  ADD      KGG,KGGPS/KGGT $
 71  EQUIV    KGGT,KGG/PHASE2 $
 72  CHKPNT   KGG $
 73  LABEL    PH2BK2 $
```

RIGID FORMAT DMAP LISTING
SERIES N *** BASIC STATIC SUBSTRUCTURE ANALYSIS ***

RIGID FORMAT 16 - SUBSET ZERO

N A S T R A N   S O U R C E   P R O G R A M   C O M P I L A T I O N

DMAP-NO.	DMAP INSTRUCTION	
74	PARAM	//C,N,MPY/V,N,NSKIP/C,N,0/C,N,0 $
75	JUMP	LBL11 $
76	LABEL	LBL11 $
77	GP4	CASECC,GEOM4,EQEXIN,SIL,GPDT/RG,YS,USET,ASET/V,N,LUSET/ V,N, MPCF1/V,N,MPCF2/V,N,SINGLE/V,N,OMIT/V,N,REACT/V,N,NSKIP/V,N, REPEAT/V,N,NOSET/V,N,NOL/V,N,NOA/C,Y,SUBID $
78	SAVE	MPCF1,MPCF2,SINGLE,OMIT,REACT,NSKIP,REPEAT,NOSET,NOL,NOA $
79	COND	ERROR3,NOL $
80	PARAM	//C,N,AND/V,N,NOSR/V,N,SINGLE/V,N,REACT $
81	PURGE	KRR,KLR,QR,DM/REACT/GM/MPCF1/GO,KOO,LOO,PO,UOOV,RUOV/OMIT/PS, KFS,KSS/SINGLE/QG/NOSR $
82	CHKPNT	KRR,KLR,QR,DM,GM,GO,KOO,LOO,PO,UOOV,RUOV,PS,KFS,KSS,QG,USET,RG, YS,ASET $
83	COND	LBL4,GENEL $
84	GPSP	GPL,GPST,USET,SIL/OGPST/V,N,NOGPST $
85	SAVE	NOGPST $
86	COND	LBL4,NOGPST $
87	OFP	OGPST,,,,,//V,N,CARDNO $
88	LABEL	LBL4 $
89	EQUIV	KGG,KNN/MPCF1 $
90	CHKPNT	KNN $
91	COND	LBL2,MPCF2 $
92	MCE1	USET,RG/GM $
93	CHKPNT	GM $
94	MCE2	USET,GM,KGG,,,/KNN,,, $
95	CHKPNT	KNN $
96	LABEL	LBL2 $
97	EQUIV	KNN,KFF/SINGLE $

APPENDIX A

```
RIGID FORMAT DMAP LISTING
SERIES N *** BASIC STATIC SUBSTRUCTURE ANALYSIS ***

RIGID FORMAT 16 - SUBSET ZERO

   N A S T R A N   S O U R C E   P R O G R A M   C O M P I L A T I O N
DMAP-DMAP INSTRUCTION
 NO.

 98  CHKPNT    KFF $

 99  COND      LBL3,SINGLE $

100  SCE1      USET,KNN,,,/KFF,KFS,KSS,,, $

101  CHKPNT    KFS,KSS,KFF $

102  LABEL     LBL3 $

103  EQUIV     KFF,KAA/OMIT $

104  CHKPNT    KAA $

105  COND      LBL5,OMIT $

106  SMP1      USET,KFF,,,/GO,KAA,KOO,LOO,,,,, $

107  CHKPNT    GO,KAA,KOO,LOO $

108  LABEL     LBL5 $

109  EQUIV     KAA,KLL/REACT $

110  CHKPNT    KLL $

111  PARAM     //C,N,SUB/V,N,PHASE1/C,N,0/C,Y,SUBID=0 $

112  COND      LBL7,PHASE1 $

113  COND      LBL6,REACT $

114  RBMG1     USET,KAA,/KLL,KLR,KRR,,, $

115  CHKPNT    KLL,KLR,KRR $

116  LABEL     LBL6 $

117  RBMG2     KLL/LLL $

118  CHKPNT    LLL $

119  COND      LBL7,REACT $

120  RBMG3     LLL,KLR,KRR/DM $

121  CHKPNT    DM $

122  LABEL     LBL7 $

123  SSG1      SLT,BGPDT,CSTM,SIL,EST,MPT,GPTT,EDT,MGG,CASECC,DIT/PG/V,N,
               LUSET/V,N,NSKIP $
```

APPENDIX A

```
RIGID FORMAT DMAP LISTING
SERIES N *** BASIC STATIC SUBSTRUCTURE ANALYSIS ***

RIGID FORMAT 16 - SUBSET ZERO

   N A S T R A N   S O U R C E   P R O G R A M   C O M P I L A T I O N
DMAP-DMAP INSTRUCTION
 NO.

124  JUMP      PH2BK3 $

125  ADD       PG,PGPS/PGT $

126  EQUIV     PGT,PG/PHASE2 $

127  LABEL     PH2BK3 $

128  CHKPNT    PG $

129  EQUIV     PG,PL/NOSET $

130  CHKPNT    PL $

131  COND      LBL10,NOSET $

132  SSG2      USET,GM,YS,KFS,GO,DM,PG/QR,PO,PS,PL $

133  CHKPNT    QR,PO,PS,PL $

134  LABEL     LBL10 $

135  COND      PH1BK1,PHASE1 $

136  SSG3      LLL,KLL,PL,LOO,KOO,PO/ULV,UOOV,RULV,RUOV/V,N,OMIT/V,Y,IRES=-1/
               V,N,NSKIP/V,N,EPSI $

137  SAVE      EPSI $

138  CHKPNT    ULV,UOOV,RULV,RUOV $

139  COND      LBL9,IRES $

140  MATGPR    GPL,USET,SIL,RULV//C,N,L $

141  MATGPR    GPL,USET,SIL,RUOV//C,N,O $

142  LABEL     LBL9 $

143  JUMP      PH3BK1 $

144  LABEL     PH1BK1 $

145  COND      SKIP,OMIT $

146  FBS       LOO,,PO/UOOVX $

147  EQUIV     UOOVX,UOOV/PHASE1 $

148  CHKPNT    UOOV $

149  LABEL     SKIP $
```

APPENDIX A

```
RIGID FORMAT DMAP LISTING
SERIES N *** BASIC STATIC SUBSTRUCTURE ANALYSIS ***

RIGID FORMAT 1 - SUBSET ZERO

   N A S T R A N   S O U R C E   P R O G R A M   C O M P I L A T I O N
DMAP-DMAP INSTRUCTION
 NO.

150  OUTPUT1  ASET,KLL,PL,,//C,N,-1/C,N,0/C,Y,USRTP1D1 $

151  PARAM    //C,N,ADD/V,N,PHASE3/C,N,0/C,N,-1 $

152  UDBR     /ULVX,,,,/C,Y,SUBID/C,Y,UNIT/C,Y,USRTP1D2 $

153  EQUIV    ULVX,ULV/PHASE3 $

154  CHKPNT   ULV $

155  LABEL    PH3BK1 $

156  SDR1     USET,PG,ULV,UOOV,YS,GO,GM,PS,KFS,KSS,QR/UGV,PGG,QG/V,N,NSKIP/
              C,N,STATICS $

157  CHKPNT   UGV,PGG $

158  COND     LBL8,REPEAT $

159  REPT     LBL11,100 $

160  JUMP     ERROR1 $

161  PARAM    //C,N,NOT/V,N,TEST/V,N,REPEAT $

162  COND     ERROR5,TEST $

163  LABEL    LBL8 $

164  CHKPNT   QG $

165  JUMP     PH2BK4 $

166  SSVE     PSDATA,,UGV// $

167  LABEL    PH2BK4 $

168  SDR2     CASECC,CSTM,MPT,DIT,EQEXIN,SIL,GPTT,EDT,BGPDT,,QG,UGV,EST,,PGG/
              OPG1,OQG1,OUGV1,OES1,OEF1,PUGV1/C,N,STATICS $

169  COND     LBLOFP,COUNT $

170  OPTPR2   OPTP1,OES1,EST/OPTP2,EST1/V,N,PRINT/V,N,TSTART/V,N,COUNT $

171  EQUIV    EST1,EST/COUNT/OPTP2,OPTP1/COUNT $

172  COND     LOOPEND,PRINT $

173  LABEL    LBLOFP $

174  PARAM    //C,N,MPY/V,N,CARDNO/C,N,0/C,N,0 $
```

APPENDIX A

RIGID FORMAT DMAP LISTING
SERIES N *** BASIC STATIC SUBSTRUCTURE ANALYSIS ***

RIGID FORMAT 16 - SUBSET ZERO

```
    N A S T R A N   S O U R C E   P R O G R A M   C O M P I L A T I O N
DMAP-DMAP INSTRUCTION
 NO.

175  OFP       OUGV1,OPG1,OQG1,OEF1,OES1,//V,N,CARDNO $

176  SAVE      CARDNO $

177  COND      P2,JUMPPLOT $

178  PLOT      PLTPAR,GPSETS,ELSETS,CASECC,BGPDT,EQEXIN,SIL,PUGV1,,GPECT,OES1/
               PLOTX2/V,N,NSIL/V,N,LUSET/V,N,JUMPPLOT/V,N,PLTFLG/V,N,PFILE $

179  SAVE      PFILE $

180  PRTMSG    PLOTX2// $

181  LABEL     P2 $

182  LABEL     LOOPEND $

183  COND      FINIS,COUNT $

184  REPT      LOOPTOP,100 $

185  JUMP      FINIS $

186  LABEL     ERROR1 $

187  PRTPARM   //C,N,-1/C,N,STATICS $

188  LABEL     ERROR2 $

189  PRTPARM   //C,N,-2/C,N,STATICS $

190  LABEL     ERROR3 $

191  PRTPARM   //C,N,-3/C,N,STATICS $

192  LABEL     ERROR4 $

193  PRTPARM   //C,N,-4/C,N,STATICS $

194  LABEL     ERROR5 $

195  PRTPARM   //C,N,-5/C,N,STATICS $

196  LABEL     FINIS $

197  END       $

     **NO ERRORS FOUND - EXECUTE NASTRAN PROGRAM**
```

APPENDIX A

Description of DMAP Operations for Basic Static Substructure Analysis

6. SSMA analyzes and/or generates coupling data and forms coupled substructure matrices $[K_{gg}^{ps}]$ and $\{P_g^{ps}\}$.

10. GP1 generates coordinate system transformation matrices, tables of grid point locations, and tables for relating internal and external grid point numbers.

13. GP2 generates Element Connection Table with internal indices.

17. Go to DMAP No. 27 if no plot package is present.

18. PLTSET transforms user input into a form used to drive structure plotter.

20. PRTMSG prints error messages associated with structure plotter.

23. Go to DMAP No. 27 if no undeformed structure plot request.

24. PLØT generates all requested undeformed structure plots.

26. PRTMSG prints plotter data and engineering data for each undeformed plot generated.

29. GP3 generates Static Loads Table and Grid Point Temperature Table.

34. TA1 generates element tables for use in matrix assembly and stress recovery.

37. Go to DMAP No. 192 and print error message if no elements have been defined.

40. ØPTPR1 property optimization module for Level 16.

45. Go to DMAP No. 62 if there are no structural elements.

47. EMG generates structural element matrix tables and dictionaries for later assembly.

50. Go to DMAP No. 53 if no stiffness matrix is to be assembled.

51. EMA assembles stiffness matrix $[K_{gg}^{x}]$ and Grid Point Singularity Table.

54. Go to DMAP No. 57 if no mass matrix is to be assembled.

55. EMA assembles mass matrix $[M_{gg}]$.

58. Go to DMAP No. 62 if no weight and balance request.

59. Go to DMAP No. 188 and print error message if no mass matrix exists.

60. GPWG generates weight and balance information.

61. ØFP formats weight and balance information and places it on the system output file for printing.

63. Equivalence $[K_{gg}^{x}]$ to $[K_{gg}]$ if no general elements.

65. Go to DMAP No. 68 if no general elements.

66. SMA3 adds general elements to $[K_{gg}^{x}]$ to obtain stiffness matrix $[K_{gg}]$.

70. Add $[K_{gg}]$ and $[K_{gg}^{ps}]$ to form $[K_{gg}^{total}]$.

APPENDIX A

71. Equivalence $[K_{gg}^{total}]$ to $[K_{gg}]$ if coupling phase.

75. Go to next DMAP instruction if cold start or modified restart. LBL11 will be altered by the Executive System to the proper location inside the loop for unmodified restarts within the loop.

76. Beginning of Loop for additional constraint sets.

77. GP4 generates flags defining members of various displacement sets (USET), forms multipoint constraint equations $[R_g]\{u_g\} = 0$ and forms enforced displacement vector $\{Y_s\}$.

79. Go to DMAP No. 190 and print error message if no independent degrees of freedom are defined.

83. Go to DMAP No. 88 if general elements present.

84. GPSP determines if possible grid point singularities remain.

86. Go to DMAP No. 88 if no Grid Point Singularity Table.

87. ØFP formats the table of possible grid point singularities and places it on the system output file for printing.

89. Equivalence $[K_{gg}]$ to $[K_{nn}]$ if no multipoint constraints.

91. Go to DMAP No. 96 if MCE1 and MCE2 have already been executed for current set of multipoint constraints.

92. MCE1 partitions multipoint constraint equations $[R_g] = [R_m \,\vdots\, R_n]$ and solves for multipoint constraint transformation matrix $[G_m] = -[R_m]^{-1}[R_n]$.

94. MCE2 partitions stiffness matrix

$$[K_{gg}] = \left[\begin{array}{c:c} \bar{K}_{nn} & K_{nm} \\ \hdashline K_{mn} & K_{mm} \end{array}\right]$$

and performs matrix reduction

$$[K_{nn}] = [\bar{K}_{nn}] + [G_m^T][K_{mn}] + [K_{mn}^T][G_m] + [G_m^T][K_{mm}][G_m] \ .$$

97. Equivalence $[K_{nn}]$ to $[K_{ff}]$ if no single-point constraints.

99. Go to DMAP No. 102 if no single-point constraints.

100. SCE1 partitions out single-point constraints

$$[K_{nn}] = \left[\begin{array}{c:c} K_{ff} & K_{fs} \\ \hdashline K_{sf} & K_{ss} \end{array}\right] .$$

103. Equivalence $[K_{ff}]$ to $[K_{aa}]$ if no omitted coordinates.

105. Go to DMAP No. 108 if no omitted coordinates.

106. SMP1 partitions constrained stiffness matrix

$$[K_{ff}] = \left[\begin{array}{c|c} \bar{K}_{aa} & K_{ao} \\ \hline K_{oa} & K_{oo} \end{array}\right] ,$$

solves for transformation matrix $[G_o] = -[K_{oo}]^{-1}[K_{oa}]$

and performs matrix reduction $[K_{aa}] = [\bar{K}_{aa}] + [K_{oa}^T][G_o]$.

109. Equivalence $[K_{aa}]$ to $[K_{\ell\ell}]$ if no free-body supports.

112. Go to DMAP No. 122 if initial substructure data reduction (Phase I).

113. Go to DMAP No. 116 if no free-body supports.

114. RBMG1 partitions out-free body supports

$$[K_{aa}] = \left[\begin{array}{c|c} K_{\ell\ell} & K_{\ell r} \\ \hline K_{r\ell} & K_{rr} \end{array}\right] .$$

117. RBMG2 decomposes constrained stiffness matrix $[K_{\ell\ell}] = [L_{\ell\ell}][U_{\ell\ell}]$.

119. Go to DMAP No. 122 if no free-body supports.

120. RBMG3 forms rigid body transformation matrix

$$[D] = -[K_{\ell\ell}]^{-1}[K_{\ell r}] ,$$

calculates rigid body check matrix

$$[X] = [K_{rr}] + [K_{\ell r}^T][D] ,$$

and calculates rigid body error ratio

$$\epsilon = \frac{||X||}{||K_{rr}||} .$$

123. SSG1 generates static load vectors $\{P_g\}$.

125. Add $\{P_g\}$ and $\{P_g^{ps}\}$ to form $\{P_g^{total}\}$.

126. Equivalence $\{P_g^{total}\}$ to $\{P_g\}$ if coupling phase.

129. Equivalence $\{P_g\}$ to $\{P_\ell\}$ if no constraints applied.

132. SSG2 applies constraints to static load vectors

$$\{P_g\} = \begin{Bmatrix} \bar{P}_n \\ \hline P_m \end{Bmatrix} , \qquad \{P_n\} = \{\bar{P}_n\} + [G_m^T]\{P_m\} ,$$

$$\{P_n\} = \begin{Bmatrix} \bar{P}_f \\ \hline P_s \end{Bmatrix} , \qquad \{P_f\} = \{\bar{P}_f\} - [K_{fs}]\{Y_s\} ,$$

$$\{P_f\} = \begin{Bmatrix} \bar{P}_a \\ \hline P_o \end{Bmatrix} , \qquad \{P_a\} = \{\bar{P}_a\} + [G_o^T]\{P_o\} ,$$

$$\{P_a\} = \begin{Bmatrix} P_\ell \\ \hline P_r \end{Bmatrix}$$

and calculates determinate forces of reaction $\{q_r\} = -\{P_r\} - [D^T]\{P_\ell\}$.

135. Go to DMAP No. 144 if intial substructure data reduction (Phase I).

136. SSG3 solves for displacements of independent coordinates

$$\{u_\ell\} = [K_{\ell\ell}]^{-1}\{P_\ell\} ,$$

solves for displacements of omitted coordinates

$$\{u_o^o\} = [K_{oo}]^{-1}\{P_o\} ,$$

calculates residual vector (RULV) and residual vector error ratio for independent coordinates

$$\{\delta P_\ell\} = \{P_\ell\} - [K_{\ell\ell}]\{u_\ell\} ,$$

$$\varepsilon_\ell = \frac{\{u_\ell^T\}\{\delta P_\ell\}}{\{P_\ell^T\}\{u_\ell\}}$$

[illegible] vector (RUOV) and residual vector error ratio for omitted coordinates

$$\{\delta P_o\} = \{P_o\} - [K_{oo}]\{u_o^o\} ,$$

APPENDIX A

$$\varepsilon_o = \frac{\{u_o^T\}\{\delta P_o\}}{\{P_o^T\}\{u_o^o\}}$$

139. Go to DMAP No. 142 if residual vectors are not to be printed.

140. MATGPR prints the residual vector for independent coordinates (RULV).

141. MATGPR prints the residual vector for omitted coordinates (RUØV).

145. Go to DMAP No. 149 if no omits.

146. FBS solve for displacements of the omitted coordinates

$$\{u_o^{ox}\} = [K_{oo}]^{-1}\{P_o\}$$

147. Equivalence $\{u_o^{ox}\}$ to $\{u_o^o\}$ if initial substructure data reduction (Phase I).

150. ØUTPUT1 write a user file on INPT containing analysis set information, $[K_{\ell\ell}]$ and $\{P_\ell\}$

152. UDBR recover $\{u_\ell^x\}$ from coupling phase user file for substructure SUBID (Phase III)

153. Equivalence $\{u_\ell^x\}$ to $\{u_\ell\}$ for substructure data recovery.

156. SDR1 recovers dependent displacements

$$\begin{Bmatrix} u_\ell \\ \hline u_r \end{Bmatrix} = \{u_a\} \;, \qquad \{u_o\} = [G_o]\{u_a\} + \{u_o^o\} \;,$$

$$\begin{Bmatrix} u_a \\ \hline u_o \end{Bmatrix} = \{u_f\} \;, \qquad \begin{Bmatrix} u_f \\ \hline Y_s \end{Bmatrix} = \{u_n\} \;,$$

$$\{u_m\} = [G_m]\{u_n\} \;, \qquad \begin{Bmatrix} u_n \\ \hline u_m \end{Bmatrix} = \{u_g\} \;,$$

and recovers single-point forces of contraint

$$\{q_s\} = -\{P_s\} + [K_{fs}^T]\{u_f\} + [K_{ss}]\{Y_s\} \;.$$

158. Go to DMAP No. 163 if all constraint sets have been processed.

159. Go to DMAP No. 76 if additional sets of constraint need to be processed.

160. Go to DMAP No. 186 and print error message if number of loops exceeds 100.

APPENDIX A

162. Go to DMAP No. 194 and print error message if multiple boundary conditions are attempted with improper subset.

166. SSVE partitions $\{u_g\}$ into substructure solution vectors and forms user file.

168. SDR2 calculates element forces and stresses (ØES1, ØES1) and prepares load vectors, displacement vectors and single-point forces of constraint for output (ØPG1, ØUGV1, PUGV1, ØQG1).

170. ØPTPR2 property optimization module for Level 16.

172. Go to DMAP No. 182 if no property optimization print control.

175. ØFP formats tables prepared by SDR2 and places them on the system output file for printing.

177. Go to DMAP No. 181 if no deformed structure plots are requested.

178. PLØT generates all requested deformed structure plots.

180. PRTMSG prints plotter data and engineering data for each deformed plot generated.

183. Go to DMAP No. 197 if property optimization looping is finished.

184. Go to DMAP No. 44 if property optimization looping is not finished.

185. Go to DMAP No. 197 and make normal exit.

187. STATIC ANALYSIS ERRØR MESSAGE NØ. 1 - ATTEMPT TØ EXECUTE MØRE THAN 100 LØØPS.

189. STATIC ANALYSIS ERRØR MESSAGE NØ. 2 - MASS MATRIX REQUIRED FØR WEIGHT AND BALANCE CALCULATIØNS.

191. STATIC ANALYSIS ERRØR MESSAGE NØ. 3 - NØ INDEPENDENT DEGREES ØF FREEDØM HAVE BEEN DEFINED.

193. STATIC ANALYSIS ERRØR MESSAGE NØ. 4 - NØ ELEMENTS HAVE BEEN DEFINED.

195. STATIC ANALYSIS ERRØR MESSAGE NØ. 5 - A LØØPING PRØBLEM RUN ØN NØN-LØØPING SUBSET.

APPENDIX B

RIGID FORMAT DMAP LISTING FOR SØL 16, (1,7,8,9)

STATIC SUBSTRUCTURE ANALYSIS PHASE I

Subset 1 of Rigid Format 16 reduces the rigid format to a DMAP sequence which solves Phase I of static substructure analysis. No new modules of interest are included. ØUTPUT1, DMAP No. 150, is used to transfer the reduced boundary matrices onto User Files from which they are recovered in Phase II. The compilation listing of this DMAP sequence constitutes the remainder of this Appendix. Subsets 7, 8 and 9 remove non-essential capabilities for the purposes of this presentation. These capabilities, which may be utilized if desired, are:

Subset	Capability
7	Structure plotter
8	Grid Point Weight Generator
9	Property optimization

Appendix A contains a full listing of Rigid Format 16.

APPENDIX B

RIGID FORMAT DMAP LISTING
SERIES N *** BASIC STATIC SUBSTRUCTURE ANALYSIS ***

RIGID FORMAT 16 - SUBSET ONE, SEVEN, EIGHT, NINE

```
   N A S T R A N   S O U R C E   P R O G R A M   C O M P I L A T I O N
DMAP-DMAP INSTRUCTION
 NO.

  1  BEGIN    NO.16 BASIC STATIC SUBSTRUCTURE ANALYSIS - SERIES N $

  2  FILE     LLL=TAPE $

 10  GP1      GEOM1,GEOM2,/GPL,EQEXIN,GPDT,CSTM,BGPDT,SIL/V,N,LUSET/  V,N,
              NOGPDT $

 11  SAVE     LUSET $

 12  CHKPNT   GPL,EQEXIN,GPDT,CSTM,BGPDT,SIL $

 13  GP2      GEOM2,EQEXIN/ECT $

 14  CHKPNT   ECT $

 29  GP3      GEOM3,EQEXIN,GEOM2/SLT,GPTT/V,N,NOGRAV $

 30  SAVE     NOGRAV $

 31  PARAM    //C,N,AND/V,N,NOMGG/V,N,NOGRAV/V,Y,GRDPNT=-1 $

 32  PURGE    MGG,MELM,MDICT/NOMGG $

 33  CHKPNT   SLT,GPTT $

 34  TA1      ECT,EPT,BGPDT,SIL,GPTT,CSTM/EST,GEI,GPECT,/V,N,LUSET/   V,N,
              NOSIMP/C,N,1/V,N,NOGENL/V,N,GENEL $

 35  SAVE     NOSIMP,NOGENL,GENEL $

 36  PARAM    //C,N,AND/V,N,NOELMT/V,N,NOGENL/V,N,NOSIMP $

 37  COND     ERROR4,NOELMT $

 38  PURGE    KGGX,GPST/NOSIMP/OGPST/GENEL $

 39  CHKPNT   EST,GPECT,GEI,GPST,OGPST $

 45  COND     LBL1,NOSIMP $

 46  PARAM    //C,N,ADD/V,N,NOKGGX/C,N,1/C,N,0 $

 47  EMG      EST,CSTM,MPT,DIT,GEOM2,/KELM,KDICT,MELM,MDICT,,/V,N,NOKGGX/ V,
              N,NOMGG/C,N,/C,N,/C,N,/C,Y,COUPMASS/C,Y,CPBAR/C,Y,CPROD/C,Y,
              CPQUAD1/C,Y,CPQUAD2/C,Y,CPTRIA1/C,Y,CPTRIA2/  C,Y,CPTUBE/C,Y,
              CPQDPLT/C,Y,CPTRPLT/C,Y,CPTRBSC $

 48  SAVE     NOKGGX,NOMGG $

 49  CHKPNT   KELM,KDICT,MELM,MDICT $
```

APPENDIX B

```
RIGID FORMAT DMAP LISTING
SERIES N *** BASIC STATIC SUBSTRUCTURE ANALYSIS ***

RIGID FORMAT 16 - SUBSET ONE, SEVEN, EIGHT, NINE

   N A S T R A N   S O U R C E   P R O G R A M   C O M P I L A T I O N
DMAP-DMAP INSTRUCTION
NO.

 50  COND      JMPKGG,NOKGGX $

 51  EMA       GPECT,KDICT,KELM/KGGX,GPST $

 52  CHKPNT    KGGX,GPST $

 53  LABEL     JMPKGG $

 54  COND      JMPMGG,NOMGG $

 55  EMA       GPECT,MDICT,MELM/MGG,/C,N,-1/C,Y,WTMASS=1.0 $

 56  CHKPNT    MGG $

 57  LABEL     JMPMGG $

 62  LABEL     LBL1 $

 63  EQUIV     KGGX,KGG/NOGENL $

 64  CHKPNT    KGG $

 65  COND      LBL11A,NOGENL $

 66  SMA3      GEI,KGGX/KGG/V,N,LUSET/V,N,NOGENL/V,N,NOSIMP $

 67  CHKPNT    KGG $

 68  LABEL     LBL11A $

 74  PARAM     //C,N,MPY/V,N,NSKIP/C,N,0/C,N,0 $

 77  GP4       CASECC,GEOM4,EQEXIN,SIL,GPDT/RG,YS,USET,ASET/V,N,LUSET/ V,N,
               MPCF1/V,N,MPCF2/V,N,SINGLE/V,N,OMIT/V,N,REACT/V,N,NSKIP/V,N,
               REPEAT/V,N,NOSET/V,N,NOL/V,N,NOA/C,Y,SUBID $

 78  SAVE      MPCF1,MPCF2,SINGLE,OMIT,REACT,NSKIP,REPEAT,NOSET,NOL,NOA $

 79  COND      ERROR3,NOL $

 80  PARAM     //C,N,AND/V,N,NOSR/V,N,SINGLE/V,N,REACT $

 81  PURGE     KRR,KLR,QR,DM/REACT/GM/MPCF1/GO,KOO,LOO,PO,UOOV,RUOV/OMIT/PS,
               KFS,KSS/SINGLE/QG/NOSR $

 82  CHKPNT    KRR,KLR,QR,DM,GM,GO,KOO,LOO,PO,UOOV,RUOV,PS,KFS,KSS,QG,USET,RG,
               YS,ASET $

 83  COND      LBL4,GENEL $

 84  GPSP      GPL,GPST,USET,SIL/OGPST/V,N,NOGPST $
```

APPENDIX B

```
RIGID FORMAT DMAP LISTING
SERIES N *** BASIC STATIC SUBSTRUCTURE ANALYSIS ***

RIGID FORMAT 16 - SUBSET ONE, SEVEN, EIGHT, NINE

   N A S T R A N   S O U R C E   P R O G R A M   C O M P I L A T I O N
DMAP-DMAP INSTRUCTION
 NO.

 85  SAVE     NOGPST $
 86  COND     LBL4,NOGPST $
 87  OFP      UGPST,,,,,//V,N,CARDNO $
 88  LABEL    LBL4 $
 89  EQUIV    KGG,KNN/MPCF1 $
 90  CHKPNT   KNN $
 91  COND     LBL2,MPCF2 $
 92  MCE1     USET,RG/GM $
 93  CHKPNT   GM $
 94  MCE2     USET,GM,KGG,,,/KNN,,, $
 95  CHKPNT   KNN $
 96  LABEL    LBL2 $
 97  EQUIV    KNN,KFF/SINGLE $
 98  CHKPNT   KFF $
 99  COND     LBL3,SINGLE $
100  SCE1     USET,KNN,,,/KFF,KFS,KSS,,, $
101  CHKPNT   KFS,KSS,KFF $
102  LABEL    LBL3 $
103  EQUIV    KFF,KAA/OMIT $
104  CHKPNT   KAA $
105  COND     LBL5,OMIT $
106  SMP1     USET,KFF,,,/GO,KAA,KOO,LOO,,,,, $
107  CHKPNT   GO,KAA,KOO,LOO $
108  LABEL    LBL5 $
109  EQUIV    KAA,KLL/REACT $
110  CHKPNT   KLL $
```

APPENDIX B

```
RIGID FORMAT DMAP LISTING
SERIES N *** BASIC STATIC SUBSTRUCTURE ANALYSIS ***

RIGID FORMAT 16 - SUBSET ONE, SEVEN, EIGHT, NINE

   N A S T R A N   S O U R C E   P R O G R A M   C O M P I L A T I O N
DMAP-DMAP INSTRUCTION
 NO.

111  PARAM    //C,N,SUB/V,N,PHASE1/C,N,0/C,Y,SUBID=0 $
112  COND     LBL7,PHASE1 $
113  COND     LBL6,REACT $
114  RBMG1    USET,KAA,/KLL,KLR,KRR,,, $
115  CHKPNT   KLL,KLR,KRR $
116  LABEL    LBL6 $
117  RBMG2    KLL/LLL $
118  CHKPNT   LLL $
119  COND     LBL7,REACT $
120  RBMG3    LLL,KLR,KRR/DM $
121  CHKPNT   DM $
122  LABEL    LBL7 $
123  SSG1     SLT,BGPDT,CSTM,SIL,EST,MPT,GPTT,EDT,MGG,CASECC,DIT/PG/V,N,
              LUSET/V,N,NSKIP $
128  CHKPNT   PG $
129  EQUIV    PG,PL/NOSET $
130  CHKPNT   PL $
131  COND     LBL10,NOSET $
132  SSG2     USET,GM,YS,KFS,GO,DM,PG/QR,PO,PS,PL $
133  CHKPNT   QR,PO,PS,PL $
134  LABEL    LBL10 $
145  COND     SKIP,OMIT $
146  FBS      LOO,,PO/UOOVX $
147  EQUIV    UOOVX,UOOV/PHASE1 $
148  CHKPNT   UOOV $
149  LABEL    SKIP $
150  OUTPUT1  ASET,KLL,PL,,//C,N,-1/C,N,0/C,Y,USKTPID1 $
```

APPENDIX B

```
 RIGID FORMAT DMAP LISTING
 SERIES N *** BASIC STATIC SUBSTRUCTURE ANALYSIS ***

 RIGID FORMAT 1[illegible] - SUBSET ONE, SEVEN, EIGHT, NINE

    N A S T R A N   S O U R C E   P R O G R A M   C O M P I L A T I O N
DMAP-DMAP INSTRUCTION
 NO.

185  JUMP      FINIS $

188  LABEL     ERROR2 $

189  PRTPARM   //C,N,-2/C,N,STATICS $

190  LABEL     ERROR3 $

191  PRTPARM   //C,N,-3/C,N,STATICS $

192  LABEL     ERROR4 $

193  PRTPARM   //C,N,-4/C,N,STATICS $

196  LABEL     FINIS $

197  END       $

      **NO ERRORS FOUND - EXECUTE NASTRAN PROGRAM**
```

APPENDIX C

RIGID FORMAT DMAP LISTING FOR SØL 16, (2,6,7,8,9)

STATIC SUBSTRUCTURE ANALYSIS PHASE II

Subset 2 of Rigid Format 16 reduces the rigid format to a DMAP sequence which solves Phase II of static substructure analysis. The new modules of interest are SSMA, the Substructure Matrix Assembler, DMAP No. 6, and SSVE, the Substructure Vector Extractor, DMAP No. 166. The compilation listing of this DMAP sequence constitutes the remainder of this Appendix. Subsets 6, 7, 8 and 9 remove non-essential capabilities for the purposes of this presentation. These capabilities, which may be utilized if desired, are:

Subset	Capability
6	Checkpoint
7	Structure Plotter
8	Grid Point Weight Generator
9	Property optimization

Appendix A contains a full listing of Rigid Format 16.

APPENDIX C

```
RIGID FORMAT DMAP LISTING
SERIES N *** BASIC STATIC SUBSTRUCTURE ANALYSIS ***

RIGID FORMAT 16 - SUBSET TWO, SIX, SEVEN, EIGHT, NINE

   N A S T R A N   S O U R C E   P R O G R A M   C O M P I L A T I O N
DMAP-DMAP INSTRUCTION
 NO.

  1  BEGIN     NO.16 BASIC STATIC SUBSTRUCTURE ANALYSIS - SERIES N $

  2  FILE      LLL=TAPE $

  3  FILE      UG=APPEND/PGG=APPEND/UGV=APPEND/GM=SAVE/KNN=SAVE $

  5  PARAM     //C,N,ADD/V,N,PHASE2/C,N,0/C,N,-1 $

  6  SSMA      GEOM4,UFTABLE/KGGPS,,,,PGPS,PSDATA/C,Y,PRTOPT/C,Y,GENSAME/ V,N,
               LUSET $

  7  SAVE      LUSET $

 10  GP1       GEOM1,GEOM2,/GPL,EQEXIN,GPDT,CSTM,BGPDT,,,/V,N,LUSET/  V,N,
               NOGPDT $

 11  SAVE      LUSET $

 12  CHKPNT    GPL,EQEXIN,GPDT,CSTM,BGPDT,SIL $

 13  GP2       GEOM2,EQEXIN/ECT $

 29  GP3       GEOM3,EQEXIN,GEOM2/SLT,GPTT/V,N,NOGRAV $

 30  SAVE      NOGRAV $

 31  PARAM     //C,N,AND/V,N,NOMGG/V,N,NOGRAV/V,Y,GRDPNT=-1 $

 32  PURGE     MGG,MELM,MDICT/NOMGG $

 34  TA1       ECT,EPT,BGPDT,SIL,GPTT,CSTM/EST,GEI,GPECT,/V,N,LUSET/   V,N,
               NOSIMP/C,N,1/V,N,NOGENL/V,N,GENEL $

 35  SAVE      NOSIMP,NOGENL,GENEL $

 36  PARAM     //C,N,AND/V,N,NOELMT/V,N,NOGENL/V,N,NOSIMP $

 38  PURGE     KGGX,GPST/NOSIMP/OGPST/GENEL $

 45  COND      LBL1,NOSIMP $

 46  PARAM     //C,N,ADD/V,N,NOKGGX/C,N,1/C,N,0 $

 47  EMG       EST,CSTM,MPT,DIT,GEOM2,/KELM,KDICT,MELM,MDICT,,/V,N,NOKGGX/ V,
               N,NOMGG/C,N,/C,N,/C,N,/C,Y,COUPMASS/C,Y,CPBAR/C,Y,CPROD/C,Y,
               CPQUAD1/C,Y,CPQUAD2/C,Y,CPTRIA1/C,Y,CPTRIA2/  C,Y,CPTUBE/C,Y,
               CPQDPLT/C,Y,CPTRPLT/C,Y,CPTRBSC $

 48  SAVE      NOKGGX,NOMGG $
```

APPENDIX C

```
RIGID FORMAT DMAP LISTING
SERIES N *** BASIC STATIC SUBSTRUCTURE ANALYSIS ***

RIGID FORMAT 16 - SUBSET TWO, SIX, SEVEN, EIGHT, NINE

   N A S T R A N   S O U R C E   P R O G R A M   C O M P I L A T I O N
DMAP-DMAP INSTRUCTION
NO.

 50  COND      JMPKGG,NOKGGX $

 51  EMA       GPECT,KDICT,KELM/KGGX,GPST $

 53  LABEL     JMPKGG $

 54  COND      JMPMGG,NOMGG $

 55  EMA       GPECT,MDICT,MELM/MGG,/C,N,-1/C,Y,WTMASS=1.0 $

 57  LABEL     JMPMGG $

 62  LABEL     LBL1 $

 63  EQUIV     KGGX,KGG/NOGENL $

 65  COND      LBL11A,NOGENL $

 66  SMA3      GEI,KGGX/KGG/V,N,LUSET/V,N,NOGENL/V,N,NOSIMP $

 68  LABEL     LBL11A $

 70  ADD       KGG,KGGPS/KGGT $

 71  EQUIV     KGGT,KGG/PHASE2 $

 74  PARAM     //C,N,MPY/V,N,NSKIP/C,N,0/C,N,0 $

 75  JUMP      LBL11 $

 76  LABEL     LBL11 $

 77  GP4       CASECC,GEOM4,EQEXIN,SIL,GPDT/RG,YS,USET,ASET/V,N,LUSET/ V,N,
               MPCF1/V,N,MPCF2/V,N,SINGLE/V,N,OMIT/V,N,REACT/V,N,NSKIP/V,N,
               REPEAT/V,N,NOSET/V,N,NOL/V,N,NOA/C,Y,SUBID $

 78  SAVE      MPCF1,MPCF2,SINGLE,OMIT,REACT,NSKIP,REPEAT,NOSET,NOL,NOA $

 79  COND      ERROR3,NOL $

 80  PARAM     //C,N,AND/V,N,NOSR/V,N,SINGLE/V,N,REACT $

 81  PURGE     KRR,KLR,QR,DM/REACT/GM/MPCF1/GO,KOO,LOO,PO,UOOV,RUOV/OMIT/PS,
               KFS,KSS/SINGLE/QG/NOSR $

 89  EQUIV     KGG,KNN/MPCF1 $

 91  COND      LBL2,MPCF2 $

 92  MCE1      USET,RG/GM $

 94  MCE2      USET,GM,KGG,,,/KNN,,, $
```

APPENDIX C

```
RIGID FORMAT DMAP LISTING
SERIES N *** BASIC STATIC SUBSTRUCTURE ANALYSIS ***

RIGID FORMAT 16 - SUBSET TWO, SIX, SEVEN, EIGHT, NINE

   N A S T R A N   S O U R C E   P R O G R A M   C O M P I L A T I O N
DMAP-DMAP INSTRUCTION
 NO.

 96  LABEL     LBL2 $

 97  EQUIV     KNN,KFF/SINGLE $

 99  COND      LBL3,SINGLE $

100  SCE1      USET,KNN,,,/KFF,KFS,KSS,,, $

102  LABEL     LBL3 $

103  EQUIV     KFF,KAA/OMIT $

105  COND      LBL5,OMIT $

106  SMP1      USET,KFF,,,/GO,KAA,KOO,LOO,,,,, $

108  LABEL     LBL5 $

109  EQUIV     KAA,KLL/REACT $

113  COND      LBL6,REACT $

114  RBMG1     USET,KAA,/KLL,KLR,KRR,,, $

116  LABEL     LBL6 $

117  RBMG2     KLL/LLL $

119  COND      LBL7,REACT $

120  RBMG3     LLL,KLR,KRR/DM $

122  LABEL     LBL7 $

123  SSG1      SLT,BGPDT,CSTM,SIL,EST,MPT,GPTT,EDT,MGG,CASECC,DIT/PG/V,N,
               LUSET/V,N,NSKIP $

125  ADD       PG,PGPS/PGT $

126  EQUIV     PGT,PG/PHASE2 $

129  EQUIV     PG,PL/NOSET $

131  COND      LBL10,NOSET $

132  SSG2      USET,GM,YS,KFS,GO,DM,PG/QR,PO,PS,PL $

134  LABEL     LBL10 $

136  SSG3      LLL,KLL,PL,LOO,KOO,PO/ULV,UOOV,RULV,RUOV/V,N,OMIT/V,Y,IRES=-1/
               V,N,NSKIP/V,N,EPSI $
```

APPENDIX C

```
RIGID FORMAT DMAP LISTING
SERIES N *** BASIC STATIC SUBSTRUCTURE ANALYSIS ***

RIGID FORMAT 16 - SUBSET TWO, SIX, SEVEN, EIGHT, NINE

   N A S T R A N   S O U R C E   P R O G R A M   C O M P I L A T I O N
DMAP-DMAP INSTRUCTION
 NO.

137  SAVE     EPSI $

139  COND     LBL9,IRES $

140  MATGPR   GPL,USET,SIL,RULV//C,N,L $

141  MATGPR   GPL,USET,SIL,RUOV//C,N,O $

142  LABEL    LBL9 $

156  SDR1     USET,PG,ULV,UOOV,YS,GO,GM,PS,KFS,KSS,QR/UGV,PGG,QG/V,N,NSKIP/
              C,N,STATICS $

158  COND     LBL8,REPEAT $

159  REPT     LBL11,100 $

160  JUMP     ERROR1 $

161  PARAM    //C,N,NOT/V,N,TEST/V,N,REPEAT $

162  COND     ERROR5,TEST $

163  LABEL    LBL8 $

166  SSVE     PSDATA,,UGV// $

168  SDR2     CASECC,CSTM,MPT,DIT,EQEXIN,SIL,GPTT,EDT,BGPDT,,QG,UGV,EST,,PGG/
              OPG1,OQG1,OUGV1,OES1,OEF1,PUGV1/C,N,STATICS $

174  PARAM    //C,N,MPY/V,N,CARDNO/C,N,0/C,N,0 $

175  OFP      OUGV1,OPG1,OQG1,OEF1,OES1,//V,N,CARDNO $

176  SAVE     CARDNO $

185  JUMP     FINIS $

186  LABEL    ERROR1 $

187  PRTPARM  //C,N,-1/C,N,STATICS $

188  LABEL    ERROR2 $

189  PRTPARM  //C,N,-2/C,N,STATICS $

190  LABEL    ERROR3 $

191  PRTPARM  //C,N,-3/C,N,STATICS $

194  LABEL    ERROR5 $
```

APPENDIX C

```
RIGID FORMAT DMAP LISTING
SERIES N *** BASIC STATIC SUBSTRUCTURE ANALYSIS ***

RIGID FORMAT 16 - SUBSET TWO, SIX, SEVEN, EIGHT, NINE

   N A S T R A N   S O U R C E   P R O G R A M   C O M P I L A T I O N
DMAP-DMAP INSTRUCTION
 NO.

195  PRTPARM  //C,N,-5/C,N,STATICS $

196  LABEL    FINIS $

197  END      $

      **NO ERRORS FOUND - EXECUTE NASTRAN PROGRAM**
```

APPENDIX D

RIGID FORMAT DMAP LISTING FOR SØL 16,(3,6,7,8,9)

STATIC SUBSTRUCTURE ANALYSIS PHASE III

Subset 3 of Rigid Format 16 reduces the rigid format to a DMAP sequence which solves Phase III of static substructure analysis. The new module of interest is UDBR, the User File Data Block Recovery, DMAP No. 152. The compilation listing of this DMAP sequence constitutes the remainder of this Appendix. Subsets 6,7,8 and 9 remove non-essential capabilities for the purposes of this presentation. These capabilities, which may be utilized if desired, are:

Subset	Capability
6	Checkpoint
7	Structure Plotter
8	Grid Point Weight Generator
9	Property optimization

Appendix A contains a full listing of Rigid Format 16.

APPENDIX D

```
RIGID FORMAT DMAP LISTING
SERIES N *** BASIC STATIC SUBSTRUCTURE ANALYSIS ***

RIGID FORMAT 16 - SUBSET THREE, SIX, SEVEN, EIGHT, NINE

   N A S T R A N   S O U R C E   P R O G R A M   C O M P I L A T I O N
DMAP-DMAP INSTRUCTION
 NO.

  1  BEGIN     NO.16 BASIC STATIC SUBSTRUCTURE ANALYSIS - SERIES N $

  2  FILE      LLL=TAPE $

 10  GP1       GEOM1,GEOM2,/GPL,EQEXIN,GPDT,CSTM,BGPDT,SIL/V,N,LUSET/   V,N,
               NOGPDT $

 11  SAVE      LUSET $

 12  CHKPNT    GPL,EQEXIN,GPDT,CSTM,BGPDT,SIL $

 13  GP2       GEOM2,EQEXIN/ECT $

 29  GP3       GEOM3,EQEXIN,GEOM2/SLT,GPTT/V,N,NOGRAV $

 30  SAVE      NOGRAV $

 31  PARAM     //C,N,AND/V,N,NOMGG/V,N,NOGRAV/V,Y,GRDPNT=-1 $

 32  PURGE     MGG,MELM,MDICT/NOMGG $

 34  TA1       ECT,EPT,BGPDT,SIL,GPTT,CSTM/EST,GEI,GPECT,/V,N,LUSET/    V,N,
               NOSIMP/C,N,1/V,N,NOGENL/V,N,GENEL $

 35  SAVE      NOSIMP,NOGENL,GENEL $

 36  PARAM     //C,N,AND/V,N,NOELMT/V,N,NOGENL/V,N,NOSIMP $

 37  COND      ERROR4,NOELMT $

 38  PURGE     KGGX,GPST/NOSIMP/OGPST/GENEL $

 45  COND      LBL1,NOSIMP $

 46  PARAM     //C,N,ADD/V,N,NOKGGX/C,N,1/C,N,0 $

 47  EMG       EST,CSTM,MPT,DIT,GEOM2,/KELM,KDICT,MELM,MDICT,,/V,N,NOKGGX/ V,
               N,NOMGG/C,N,/C,N,/C,N,/C,Y,COUPMASS/C,Y,CPBAR/C,Y,CPROD/C,Y,
               CPQUAD1/C,Y,CPQUAD2/C,Y,CPTRIA1/C,Y,CPTRIA2/  C,Y,CPTUBE/C,Y,
               CPQDPLT/C,Y,CPTRPLT/C,Y,CPTRBSC $

 48  SAVE      NOKGGX,NOMGG $

 50  COND      JMPKGG,NOKGGX $

 51  EMA       GPECT,KDICT,KELM/KGGX,GPST $

 53  LABEL     JMPKGG $

 54  COND      JMPMGG,NOMGG $
```

```
RIGID FORMAT DMAP LISTING
SERIES N *** BASIC STATIC SUBSTRUCTURE ANALYSIS ***

RIGID FORMAT 1o - SUBSET THREE, SIX, SEVEN, EIGHT, NINE

   N A S T R A N   S O U R C E   P R O G R A M   C O M P I L A T I O N
DMAP-DMAP INSTRUCTION
 NO.

 55  EMA      GPECT,MDICT,MELM/MGG,/C,N,-1/C,Y,WTMASS=1.0 $

 57  LABEL    JMPMGG $

 62  LABEL    LBL1 $

 63  EQUIV    KGGX,KGG/NOGENL $

 65  COND     LBL11A,NOGENL $

 66  SMA3     GEI,KGGX/KGG/V,N,LUSET/V,N,NOGENL/V,N,NOSIMP $

 68  LABEL    LBL11A $

 74  PARAM    //C,N,MPY/V,N,NSKIP/C,N,0/C,N,0 $

 77  GP4      CASECC,GEOM4,EQEXIN,SIL,GPDT/RG,YS,USET,ASET/V,N,LUSET/ V,N,
              MPCF1/V,N,MPCF2/V,N,SINGLE/V,N,OMIT/V,N,REACT/V,N,NSKIP/V,N,
              REPEAT/V,N,NOSET/V,N,NOL/V,N,NOA/C,Y,SUBID $

 78  SAVE     MPCF1,MPCF2,SINGLE,OMIT,REACT,NSKIP,REPEAT,NOSET,NOL,NOA $

 79  COND     ERROR3,NOL $

 80  PARAM    //C,N,AND/V,N,NOSR/V,N,SINGLE/V,N,REACT $

 81  PURGE    KRR,KLR,QR,DM/REACT/GM/MPCF1/GO,KOO,LOO,PO,UOOV,RUOV/OMIT/PS,
              KFS,KSS/SINGLE/QG/NOSR $

 83  COND     LBL4,GENEL $

 84  GPSP     GPL,GPST,USET,SIL/OGPST/V,N,NOGPST $

 85  SAVE     NOGPST $

 86  COND     LBL4,NOGPST $

 87  OFP      OGPST,,,,,//V,N,CARDNC $

 88  LABEL    LBL4 $

 89  EQUIV    KGG,KNN/MPCF1 $

 91  COND     LBL2,MPCF2 $

 92  MCE1     USET,RG/GM $

 94  MCE2     USET,GM,KGG,,,/KNN,,, $

 96  LABEL    LBL2 $

 97  EQUIV    KNN,KFF/SINGLE $
```

RIGID FORMAT DMAP LISTING
SERIES N *** BASIC STATIC SUBSTRUCTURE ANALYSIS ***

RIGID FORMAT 16 - SUBSET THREE, SIX, SEVEN, EIGHT, NINE

```
   N A S T R A N   S O U R C E   P R O G R A M   C O M P I L A T I O N
DMAP-DMAP INSTRUCTION
 NO.

 99  COND      LBL3,SINGLE $

100  SCE1      USET,KNN,,,/KFF,KFS,KSS,,, $

102  LABEL     LBL3 $

103  EQUIV     KFF,KAA/OMIT $

105  COND      LBL5,OMIT $

106  SMP1      USET,KFF,,,/GO,KAA,KOO,LOO,,,,, $

108  LABEL     LBL5 $

109  EQUIV     KAA,KLL/REACT $

113  COND      LBL6,REACT $

114  RBMG1     USET,KAA,/KLL,KLR,KRR,,, $

116  LABEL     LBL6 $

117  RBMG2     KLL/LLL $

119  COND      LBL7,REACT $

120  RBMG3     LLL,KLR,KRR/DM $

122  LABEL     LBL7 $

123  SSG1      SLT,BGPDT,CSTM,SIL,EST,MPT,GPTT,EDT,MGG,CASECC,DIT/PG/V,N,
               LUSET/V,N,NSKIP $

129  EQUIV     PG,PL/NOSET $

131  COND      LBL10,NOSET $

132  SSG2      USET,GM,YS,KFS,GO,DM,PG/QR,PO,PS,PL $

134  LABEL     LBL10 $

136  SSG3      LLL,KLL,PL,LOO,KOO,PO/ULV,UOOV,RULV,RUOV/V,N,OMIT/V,Y,IRES=-1/
               V,N,NSKIP/V,N,EPSI $

137  SAVE      EPSI $

139  COND      LBL9,IRES $

140  MATGPR    GPL,USET,SIL,RULV//C,N,L $

141  MATGPR    GPL,USET,SIL,RUOV//C,N,O $
```

APPENDIX D

```
RIGID FORMAT DMAP LISTING
SERIES N *** BASIC STATIC SUBSTRUCTURE ANALYSIS ***

RIGID FORMAT 16 - SUBSET THREE, SIX, SEVEN, EIGHT, NINE

   N A S T R A N   S O U R C E   P R O G R A M   C O M P I L A T I O N
DMAP-DMAP INSTRUCTION
 NO.

142  LABEL     LBL9 $

151  PARAM     //C,N,ADD/V,N,PHASE3/C,N,0/C,N,-1 $

152  ULBR      /ULVX,,,,/C,Y,SUBID/C,Y,UNIT/C,Y,USRTPID2 $

153  EQUIV     ULVX,ULV/PHASE3 $

156  SUR1      USET,PG,ULV,UOOV,YS,GC,GM,PS,KFS,KSS,QR/UGV,PGG,QG/V,N,NSKIP/
               C,N,STATICS $

161  PARAM     //C,N,NOT/V,N,TEST/V,N,REPEAT $

162  COND      ERROR5,TEST $

168  SUR2      CASECC,CSTM,MPT,DIT,EQEXIN,SIL,GPTT,EDT,BGPDT,,QG,UGV,EST,,PGG/
               OPG1,OQG1,OUGV1,OES1,OEF1,PUGV1/C,N,STATICS $

174  PARAM     //C,N,MPY/V,N,CARDNO/C,N,0/C,N,0 $

175  OFP       OUGV1,OPG1,OQG1,OEF1,OES1,//V,N,CARDNO $

176  SAVE      CARDNO $

185  JUMP      FINIS $

188  LABEL     ERROR2 $

189  PRTPARM   //C,N,-2/C,N,STATICS $

190  LABEL     ERROR3 $

191  PRTPARM   //C,N,-3/C,N,STATICS $

192  LABEL     ERROR4 $

193  PRTPARM   //C,N,-4/C,N,STATICS $

194  LABEL     ERROR5 $

195  PRTPARM   //C,N,-5/C,N,STATICS $

196  LABEL     FINIS $

197  END       $

       **NO ERRORS FOUND - EXECUTE NASTRAN PROGRAM**
```

APPENDIX E

RIGID FORMAT DMAP LISTING FOR SØL 17,(2,6,7,8)

NORMAL MODES SUBSTRUCTURE ANALYSIS PHASE II

Subset 2 of Rigid Format 17 reduces the rigid format to a DMAP sequence which solves Phase II of normal modes substructure analysis. The new modules of interest are SSMA, the Substructure Matrix Assembler, DMAP No. 5, and SSVE, the Substructure Vector Extractor, DMAP No. 127. The compilation listing of this DMAP sequence constitutes the remainder of this Appendix. Subsets 6, 7 and 8 remove non-essential capabilities for the purposes of this presentation. These capabilities, which may be utilized if desired, are:

Subset	Capability
6	Checkpoint
7	Structure Plotter
8	Grid Point Weight Cenerator

APPENDIX E

```
RIGID FORMAT DMAP LISTING
SERIES N *** BASIC NORMAL MODES SUBSTRUCTURE ANALYSIS ***

RIGID FORMAT 17 - SUBSET TWO, SIX, SEVEN, EIGHT

   N A S T R A N   S O U R C E   P R O G R A M   C O M P I L A T I O N
DMAP-DMAP INSTRUCTION
 NO.

  1  BEGIN    NO.17 BASIC NORMAL MODES SUBSTRUCTURE ANALYSIS - SERIES N $

  2  FILE     LLL=TAPE $

  4  PARAM    //C,N,ADD/V,N,PHASE2/C,N,0/C,N,-1 $

  5  SSMA     GEOM4,UFTABLE/KGGPS,MGGPS,,,,PSDATA/C,Y,PRTOPT/C,Y,GENSAME/V,N,
              LUSET $

  6  SAVE     LUSET $

  7  CHKPNT   KGGPS,MGGPS,PSDATA $

  9  GP1      GEOM1,GEOM2,/GPL,EQEXIN,GPDT,CSTM,BGPDT,SIL/V,N,LUSET/  V,N,
              NOGPDT $

 10  SAVE     LUSET $

 12  GP2      GEOM2,EQEXIN/ECT $

 28  GP3      GEOM3,EQEXIN,GEOM2/,GPTT/V,N,NOGRAV $

 30  TA1      ECT,EPT,BGPDT,SIL,GPTT,CSTM/EST,GEI,GPECT,/V,N,LUSET/   V,N,
              NOSIMP/C,N,1/V,N,NOGENL/V,N,GENEL $

 31  SAVE     NOGENL,NOSIMP,GENEL $

 32  PARAM    //C,N,ADD/V,N,NOELTS/V,N,PHASE2/V,N,NOSIMP $

 33  COND     ERROR1,NOELTS $

 34  PURGE    KGGX,GPST,MGG/NOSIMP/OGPST/GENEL $

 36  COND     LBL1,NOSIMP $

 37  PARAM    //C,N,ADD/V,N,NOKGGX/C,N,1/C,N,0 $

 38  PARAM    //C,N,ADD/V,N,NOMGG/C,N,1/C,N,0 $

 39  EMG      EST,CSTM,MPT,DIT,GEOM2,/KELM,KDICT,MELM,MDICT,,/V,N,NOKGGX/ V,
              N,NOMGG/C,N,/C,N,/C,N,/C,Y,COUPMASS/C,Y,CPBAR/C,Y,CPROD/C,Y,
              CPQUAD1/C,Y,CPQUAD2/C,Y,CPTRIA1/C,Y,CPTRIA2/  C,Y,CPTUBE/C,Y,
              CPQDPLT/C,Y,CPTRPLT/C,Y,CPTRBSC $

 40  SAVE     NOKGGX,NOMGG $

 42  COND     JMPKGG,NOKGGX $

 43  EMA      GPECT,KDICT,KELM/KGGX,GPST $
```

```
RIGID FORMAT DMAP LISTING
SERIES N *** BASIC NORMAL MODES SUBSTRUCTURE ANALYSIS ***

RIGID FORMAT 17 - SUBSET TWO, SIX, SEVEN, EIGHT

   N A S T R A N   S O U R C E   P R O G R A M   C O M P I L A T I O N
DMAP-DMAP INSTRUCTION
 NO.

 45  LABEL    JMPKGG $

 46  COND     ERROR1,NOMGG $

 47  EMA      GPECT,MDICT,MELM/MGG,/C,N,-1/C,Y,WTMASS=1.0 $

 52  LABEL    LBL1 $

 53  EQUIV    KGGX,KGG/NOGENL $

 54  CHKPNT   KGG $

 55  COND     LBL11,NOGENL $

 56  SMA3     GEI,KGGX/KGG/V,N,LUSET/V,N,NOGENL/V,N,NOSIMP $

 58  LABEL    LBL11 $

 60  ADD      KGG,KGGPS/KGGT $

 61  EQUIV    KGGT,KGG/PHASE2 $

 63  ADD      MGG,MGGPS/MGGT $

 64  EQUIV    MGGT,MGG/PHASE2 $

 65  CHKPNT   MGG $

 67  PARAM    //C,N,MPY/V,N,NSKIP/C,N,0/C,N,0 $

 68  GP4      CASECC,GEOM4,EQEXIN,SIL,GPDT/RG,,USET,ASET/V,N,LUSET/   V,N,
              MPCF1/V,N,MPCF2/V,N,SINGLE/V,N,OMIT/V,N,REACT/V,N,NSKIP/V,N,
              REPEAT/V,N,NOSET/V,N,NOL/V,N,NOA/C,Y,SUBID $

 69  SAVE     MPCF1,MPCF2,SINGLE,OMIT,REACT,NSKIP,REPEAT,NOSET,NOL,NOA $

 70  COND     ERROR3,NOL $

 71  PURGE    KRR,KLR,DM,MLR,MR/REACT/GM/MPCF1/GO/OMIT/KFS/SINGLE/UG/NOSET $

 79  EQUIV    KGG,KNN/MPCF1/MGG,MNN/MPCF1 $

 81  COND     LBL2,MPCF2 $

 82  MCE1     USET,RG/GM $

 84  MCE2     USET,GM,KGG,MGG,,/KNN,MNN,, $

 86  LABEL    LBL2 $

 87  EQUIV    KNN,KFF/SINGLE/MNN,MFF/SINGLE $
```

APPENDIX E

```
RIGID FORMAT DMAP LISTING
SERIES N *** BASIC NORMAL MODES SUBSTRUCTURE ANALYSIS ***

RIGID FORMAT 17 - SUBSET TWO, SIX, SEVEN, EIGHT

   N A S T R A N   S O U R C E   P R O G R A M   C O M P I L A T I O N
DMAP-DMAP INSTRUCTION
 NO.

 89  COND     LBL3,SINGLE $

 90  SCE1     USET,KNN,MNN,,/KFF,KFS,,MFF,, $

 92  LABEL    LBL3 $

 93  EQUIV    KFF,KAA/OMIT $

 94  EQUIV    MFF,MAA/OMIT $

 96  COND     LBL5,OMIT $

 97  SMP1     USET,KFF,,,/GO,KAA,KOO,LOO,,,,, $

 99  SMP2     USET,GO,MFF/MAA $

101  LABEL    LBL5 $

106  COND     LBL6,REACT $

107  RBMG1    USET,KAA,MAA/KLL,KLR,KRR,MLL,MLR,MRR $

109  RBMG2    KLL/LLL $

111  RBMG3    LLL,KLR,KRR/DM $

113  RBMG4    DM,MLL,MLR,MRR/MR $

115  LABEL    LBL6 $

116  DPD      DYNAMICS,GPL,SIL,USET/GPLD,SILD,USETD,,,,,,EED,EQDYN/V,N,
              LUSET/V,N,LUSETD/V,N,NOTFL/V,N,NODLT/V,N,NOPSDL/V,N,NOFRL/   V,
              N,NONLFT/V,N,NOTRL/V,N,NOEED/C,N,/V,N,NOUE $

117  SAVE     NOEED $

118  COND     ERROR2,NOEED $

120  READ     KAA,MAA,MR,DM,EED,USET,CASECC/LAMA,PHIA,MI,OEIGS/C,N,MODES/V,N,
              NEIGV $

121  SAVE     NEIGV $

123  PARAM    //C,N,MPY/V,N,CARDNO/C,N,0/C,N,0 $

124  OFP      LAMA,OEIGS,,,,//V,N,CARDNO $

125  SAVE     CARDNO $

127  SSVE     PSDATA,LAMA,PHIA// $

133  COND     FINIS,NEIGV $
```

APPENDIX E

```
RIGID FORMAT DMAP LISTING
SERIES N *** BASIC NORMAL MODES SUBSTRUCTURE ANALYSIS ***

RIGID FORMAT 17 - SUBSET TWO, SIX, SEVEN, EIGHT

   N A S T R A N   S O U R C E   P R O G R A M   C O M P I L A T I O N
DMAP-DMAP INSTRUCTION
 NO.

134  SDR1      USET,,PHIA,,,GO,GM,,KFS,,/PHIG,,QG/C,N,1/C,N,REIG $

136  PARAM     //C,N,SUB/V,N,SCALAR/V,N,SIL/V,N,LUSET $

137  EQUIV     SIL,SIP/SCALAR/BGPDT,BGPDP/SCALAR $

139  COND      LBL7,SCALAR $

140  PLTTRAN   BGPDT,SIL/BGPDP,SIP/V,N,LUSET/V,N,LUSEP $

141  SAVE      LUSEP $

143  LABEL     LBL7 $

148  SDR2      CASECC,CSTM,MPT,DIT,EQEXIN,SIL,,,BGPDP,LAMA,QG,PHIG,EST,,/ ,
               OQG1,OPHIG,OES1,OEF1,PPHIG/C,N,REIG $

149  OFP       OPHIG,OQG1,OEF1,OES1,,//V,N,CARDNO $

150  SAVE      CARDNO $

156  JUMP      FINIS $

157  LABEL     ERROR1 $

158  PRTPARM   //C,N,-1/C,N,MODES $

159  LABEL     ERROR2 $

160  PRTPARM   //C,N,-2/C,N,MODES $

161  LABEL     ERROR3 $

162  PRTPARM   //C,N,-3/C,N,MODES $

163  LABEL     FINIS $

164  END       $

      **NO ERRORS FOUND - EXECUTE NASTRAN PROGRAM**
```

APPENDIX F

UFTABLE USAGE WITH RIGID FORMATS 16 AND 17

Subset 0 requires a dummy form of the direct input table UFTABLE as shown:

DTI	UFTABLE	0							
DTI	UFTABLE	1	DUMMY	DATA	FØR	SUBSET	ZERØ	ENDREC	

Subsets 1 and 3 do not need or use UFTABLE.

Subset 2 requires UFTABLE for information about the Phase I user files, identification of identical substructures, and, if desired, a user defined label for the coupling phase output user file. The content of the table will vary depending on where the Phase I materials were generated (e.g., Rigid Format 16 subset 1 or Rigid Format 1 with alters). The minimum data requirements are illustrated in example a. below with example b. showing the form for identifying items generated by rigid formats other than the coupling phase rigid format.

EXAMPLE a. (four substructures, N=4)

Card	1	2	3	4	5	6	7	8	9	10
1	DTI	UFTABLE	0	4	16					
2	DTI	UFTABLE	1	2		INP1	WIDGET02		ENDREC	
3	DTI	UFTABLE	2	4		INP2	WIDGET04		ENDREC	
4	DTI	UFTABLE	3	6		INP3	WIDGET06		ENDREC	
5	DTI	UFTABLE	4	9		INP4	WIDGET09		ENDREC	
6	DTI	UFTABLE	5	0		INPT	WDGTPH2		ENDREC	

EXAMPLE b. (five substructures, N=5)

Card	1	2	3	4	5	6	7	8	9	10
1	DTI	UFTABLE	0	5	17					+A00
2	DTI	UFTABLE	1	10		INP1	GRØUP4		ENDREC	+A01
3a	DTI	UFTABLE	2	13		INP4	PLT4	104823	NAMES	+A02
3b	+A02	A	AS138	K	KLL13	M	M134F		ENDREC	+A03
4	DTI	UFTABLE	3	23	1[illegible]				ENDREC	+A04
5	DTI	UFTABLE	4	16	10				ENDREC	+A05
6a	DTI	UFTABLE	5	237		INP3				+A06
6b	+A06	A	3	K	1	M	2		ENDREC	+A07

Remarks:

1. Card 1 defines the trailer for UFTABLE. Field 4 specifies that the table has N substructures. SSMA will use the information in field 5 to recognize that the tables were prepared for use with Rigid Format 16 and 17 for examples a and b respectively.

2. Cards starting with card 2 define records 1 thru N of UFTABLE, where N is the number of substructures. Field 4 gives the substructure identification number for use with the Phase II SAME bulk data cards and the Phase III data recovery module UDBR. Field 6 gives the GINØ file name for the User File containing the data for each substructure. Field 7 contains the User File Label for SSMA verification. Field 8 contains an optional tape reel identification number.

3. Optional data (shown in example b on card 3) is input whenever the data blocks required are not in the expected order on the User File as defined by the convention established for the Rigid Format being utilized. In the example, the ASET data block has the name AS13B, the stiffness matrix has the name KLL13 and the mass matrix has the name M134F.

4. In example a, card 6 defines the User File Label and GINØ file name to be used by SSVE when writing the Phase II output onto a User File. In example b, since five substructures are present and no card 7 is input, default values will be automatically implied.

APPENDIX G

SAMPLE PROBLEM DATA DECK LISTING

As an illustration of the automation that is introduced as a result of this new capability, the example used in the NASTRAN User's Manual (reference 2, p. 1.10-2 (6/1/72)) will be presented here. The sketch below shows the model for the problem being solved.

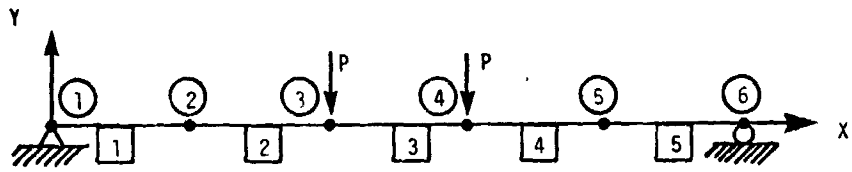

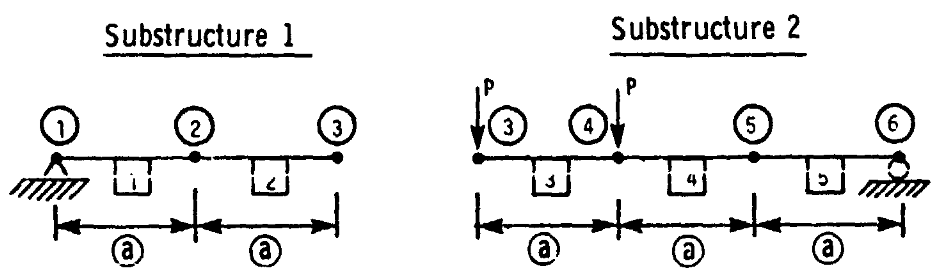

② Grid point numbers

$\boxed{3}$ Element numbers

ⓐ = 6.096 m (240 in)

E = 207 GPa $(30 \times 10^6$ psi)

I = 2.08×10^{-4} m^4 (500 in^4)

P = 4.448 kN (1000 lb)

APPENDIX G

The following data deck is used for Phase I of substructure 1:

```
ID        PHASE ØNE $
TIME      2
CHKPNT    YES
APP       DISP
SØL       16,1
CEND
TITLE = PHASE ØNE - SUBSTRUCTURE 1 - RIGID FØRMAT 16
SPC  =    101
BEGIN BULK
ASET      3         126
CBAR      1          10       1      2          1.0              1
CBAR      2          10       2      3          1.0              1
GRID      1                                            345
GRID      2                 240.                       345
GRID      3                 480.                       345
MAT1     11        30.+6
PARAM    SUBID       10
PARAM    USRTPID1  BEAMS1
PBAR     10          11      60.   500.
SPC      101          1      12
ENDDATA
```

APPENDIX G

The following data deck is used for Phase I of substructure 2:

```
ID        PHASE ØNE $
TIME      2
CHKPNT    YES
APP       DISP
SØL       16,1
CEND
TITLE = PHASE ØNE - SUBSTRUCTURE 2 - RIGID FØRMAT 16
SPC = 201
LØAD = 202
BEGIN BULK
ASET        3       126
CBAR        3        10        3       4             1.0               1
CBAR        4        10        4       5             1.0               1
CBAR        5        10        5       6             1.0               1
FØRCE     202         3             1000.           -1.0
FØRCE     202         4             1000.           -1.0
GRID        3                480.                             345
GRID        4                720.                             345
GRID        5                960.                             345
GRID        6               1200.                             345
MAT1       11       30.+6
PARAM     SUBID      20
PARAM     USRTPID1 BEAMS2
PBAR       10        11       60.    500.
SPC       201         6        2
ENDDATA
```

APPENDIX G

The following data deck is used for Phase II.

```
ID       PHASE TWØ
TIME     2
APP      DISP
SØL      16,2
CEND
TITLE = PHASE TWØ - RIGID FØRMAT 16
BEGIN BULK
DTI      UFTABLE 0       2       16
DTI      UFTABLE 1      10               INP3    BEAMS1          ENDREC
DTI      UFTABLE 2      20               INP7    BEAMS2          ENDREC
DTI      UFTABLE 3       0               INPT    BEAMPH2         ENDREC
PARAM    GENSAME 1
ENDDATA
```

The NASTRAN Data Deck for the Phase III analysis of substructure 1 is given as follows:

```
ID       PHASE THREE $
TIME     2
APP      DISP
SØL      16,3
READ CARDS FRØM 3 $ RESTART DICTIØNARY FRØM UNIT 3
CEND
TITLE = PHASE THREE - SUBSTRUCTURE 1 - RIGID FØRMAT 16
DISP = ALL
ELFØRCE = ALL
ØLØAD = ALL
SPCFØRCE = ALL
BEGIN BULK
PARAM    USRTPID2 BEAMPH2
ENDDATA
```

APPENDIX G

The NASTRAN Data Deck for the Phase III analysis of substructure 2 is given below:

```
ID        PHASE THREE $
TIME      2
APP       DISP
SØL       16,3
READ CARDS FRØM 92 $ RESTART DICTIØNARY FRØM UNIT 92
CEND
TITLE = PHASE THREE - SUBSTRUCTURE 2 - RIGID FØRMAT 16
DISP = ALL
ELFØRCE = ALL
ØLØAD = ALL
SPCFØRCE = ALL
BEGIN BULK
PARAM     USRTPID2 BEAMPH2
ENDDATA
```

REFERENCES

1. MacNeal, R. H. (Editor): The NASTRAN Theoretical Manual (Level 15). NASA SP-221(01), April 1972.

2. McCormick, C. W. (Editor): The NASTRAN User's Manual (Level 15). NASA SP-222(01), June 1972.

3. Anon.: The NASTRAN Programmer's Manual (Level 15). NASA SP-223(01), September 1972.

4. Grooms, H. R. and Yahata, S.: Space Shuttle - The Need for Substructuring. NASTRAN: Users' Experiences. NASA TM X-2378, September 1971, pp. 769-778.

5. Hansen, S. D. and Hansteen, H. B.: Data Management Requirements for Large Problems. NASTRAN: Users' Experiences. NASA TM X-2378, September 1971, pp. 533-550.

6. Guyan, R. J.: "Reduction of Stiffness and Mass Matrices". AIAA Journal, Vol. 3, No. 2, February 1965.

TABLE 1

DATA REQUIREMENTS

	ITEM	LEVEL 15	LEVEL 16	LEVEL 16.X
Phase I	• DMAP Alter Packet	Required	Required	None
	• CHKPNT File	Tape	Tape (or Disk)	Disk (or Tape)
	• Output User File	Tape for Module ØUTPUT1	Tape (or Disk) for Module ØUTPUT1	Disk (or Tape) for Module ØUTPUT1
Phase II	• DMAP (or Alter Packet)	Required	Required	None
	• Input User Files	Tape(s) for Module INPUTT1	Tape (or Disk) for Module INPUTT1	Disk (or Tape) Automatically Processed by Module SSMA
	• Treatment of Identical Subroutines	Possible by DMAP	Handled by Module PVEC Parameters and DMAP Alters	Automatic via Simple User Data
	• Coupling Information	USER CREATED (GOOD LUCK!)	Generated by Modules PVEC/VEC	Automatically Generated
	• Pseudomodel Description	User Supplied	Can be Obtained from PVEC on Extra Run	Automatic
	• Output User File	Tape for Module ØUTPUT1	Tape (or Disk) for Module ØUTPUT1	Disk (or Tape) Automatically Processed by Module SSVE
Phase III	• DMAP Alter Packet	Required	Required	None
	• Restart File	Tape	Tape (or Disk)	Disk (or Tape)
	• Restart Dictionary	Cards Required from Phase I	Cards Required from Phase I	Can be Requested from Ext. File
	• Input User File	Tape for Module INPUTT1	Tape (or Disk) for Module INPUTT1	Disk (or Tape) for Module UDBR

TABLE 2

ASSUMPTIONS AND RESTRICTIONS

- Only one (1) level of substructures is allowed.
- The Number of substructures may not exceed twenty (20).
- Coordinate systems of points to be coupled are parallel. This is not verified by program.
- Degrees of freedom at two points to be coupled are the same. Exceptions can be handled via multipoint constraints in Phase II.
- The sequence (internal) of points along the boundary between any two substructures is the same.
- All subcases must be defined in the Case Control Decks for all runs.
- Static loads applied geometrically must be defined in Phase I. Loads may be applied to the pseudostructure degrees of freedom in Phase II in the usual way.
- Output obtained in Phase II must be requested using pseudostructure degree of freedom identifiers.
- Only a single boundary condition is considered; geometrically specified boundary conditions must be defined in Phase I.

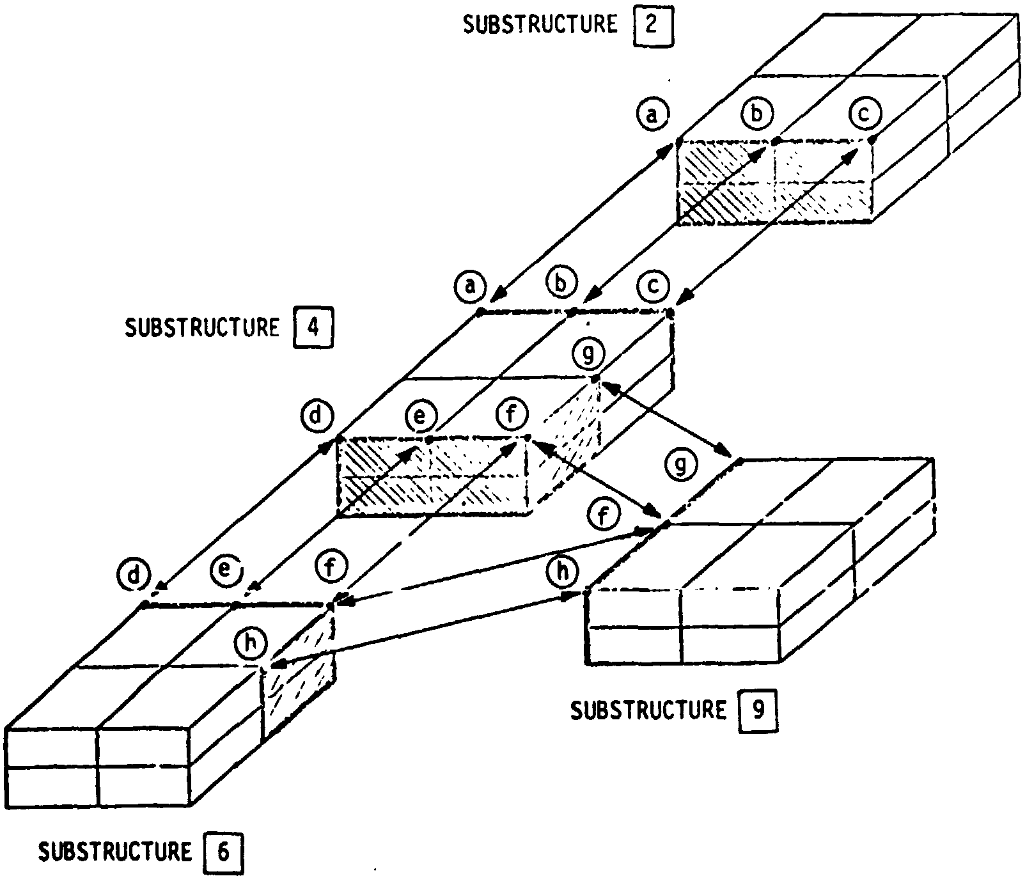

(For clarity, only connected points on the top surface are shown.)

FIGURE 1. SAMPLE STATIC SUBSTRUCTURE ANALYSIS PROBLEM MODEL

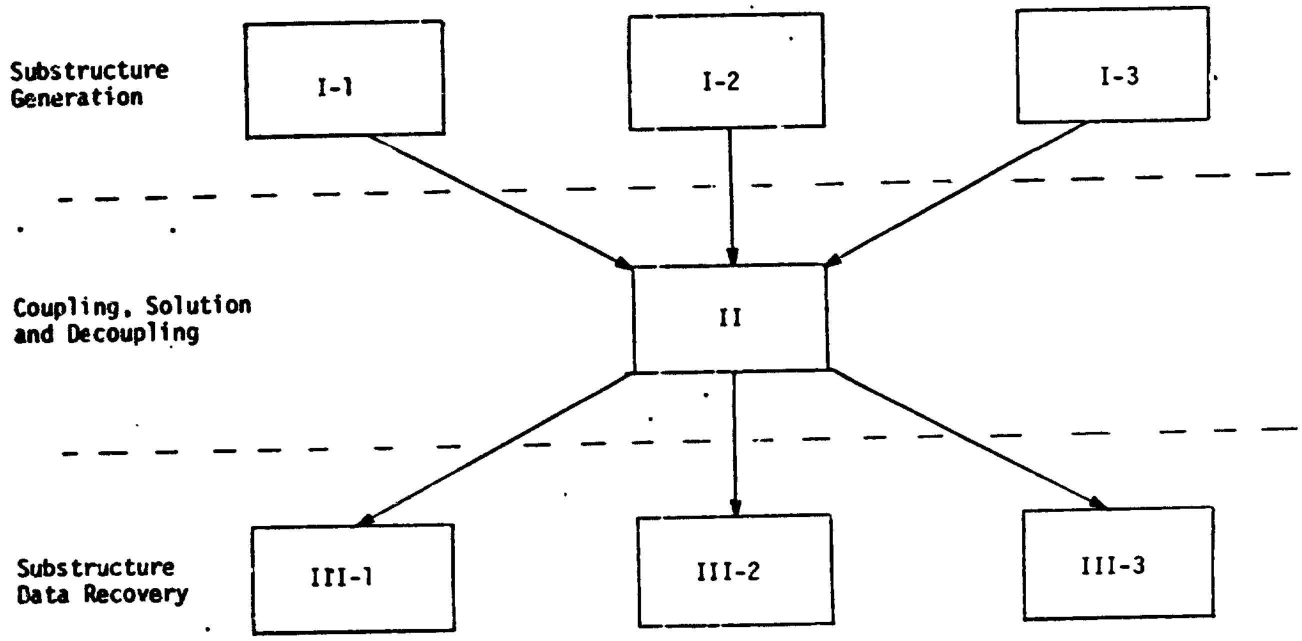

FIGURE 2. SUBSTRUCTURE ANALYSIS RUN FLOW

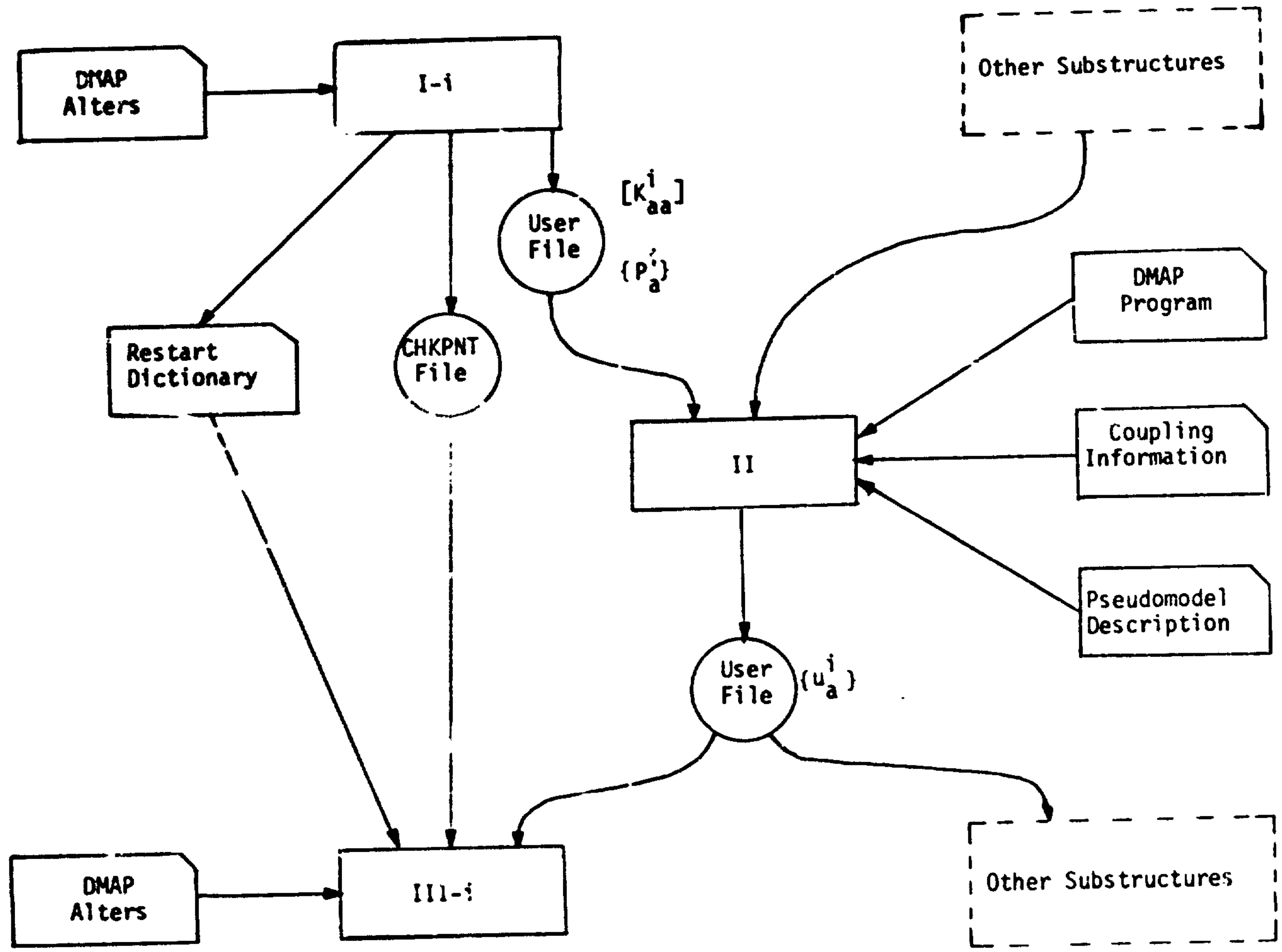

FIGURE 3. SUBSTRUCTURE ANALYSIS DATA LOGISTICS (STATICS)

The pseudomodel map shown below was generated by module PVEC for the structure shown in figure 1.

Internal DØF	Substructure Identification Number 2	4	6	9
3			6013-3	9001-3
6			6016-3	9004-3
9			6019-3	9007-3
12		4001-3	6021-3	
15		4002-3	6022-3	
18		4004-3	6024-3	
21		4005-3	6025-3	
24		4006-3	6026-3	9014-3
27		4007-3	6027-3	
30		4008-3	6028-3	
33		4009-3	6029-3	9017-3
36		4013-3		9021-3
39		4016-3		9024-3
42		4019-3		9027-3
45	2002-3	4022-3		
48	2003-3	4023-3		
51	2004-3	4024-3		
54	2005-3	4025-3		
57	2006-3	4026-3		
60	2007-3	4027-3		
63	2008-3	4028-3		
66	2009-3	4029-3		

Notes:

1. For clarity, only the "3" degree of freedom is shown.

2. Single-point constraints have been applied to point 1 in substructure 2 and point 3 in substructure 4.

FIGURE 4. PSEUDOMODEL MAP

```
       ID PHASE ØNE
       TIME     10
       CHKPNT   YES,DISK
       APP      DISP
(1)    SØL      16,1 $ BASIC STATIC SUBSTRUCTURE ANALYSIS
       CEND
          {Case Control Deck}
       BEGIN BULK
          {Structural Data for Substructure}
(2)    PARAM   SUBID    10
(3)    PARAM   USRTPID1 ABC
       ENDDATA
```

Notes:

1. Solution subset 1 is used for Phase I runs.
2. User-specified substructure identification number.
3. User-specified User File identification code.

FIGURE 5

LEVEL 16.X PHASE I DATA DECK

```
        ID PHASE TWØ
        TIME     10
        APP      DISP
(1)     SØL      16,2 $ BASIC STATIC SUBSTRUCTURE ANALYSIS
        CEND

          {Case Control Deck}

        BEGIN BULK

(2)       {DTI definition of User File Data}

(3a)    PARAM   GENSAME  -1
(4)     PARAM   PRTØPT    1

(3b)      {Coupling Data (can be optional)}

        ENDDATA
```

Notes:

1. Solution subset 2 is used for Phase II runs.

2. User-specified data providing

    a. Number of substructures
    b. Identification numbers for both real and identical substructures
    c. User File Data Location Information and Identification Codes

3a and b. Coupling Information

(a) GENSAME=+1 means coupling data automatically generated
GENSAME=-1 means coupling data supplied by user via SAME cards (fig. 10).

(b) See figure 8.

4. Pseudostructure map print option.

FIGURE 6

LEVEL 16.X PHASE II DATA DECK

```
      ID PHASE THREE
      TIME    10
      APP     DISP
(1)   SØL     16,3 $ BASIC STATIC SUBSTRUCTURE ANALYSIS
(2)   READCARDS FRØM 3 $ RESTART DICTIØNARY FRØM UNIT 3
      CEND

        {Case Control Deck}

      BEGIN BULK
(3)   PARAM   USRTPID2  XYZ
      ENDDATA
```

<u>Notes</u>:

1. Solution subset 3 is used for Phase III runs.
2. The Problem Tape Dictionary is recovered from Unit 3.
3. User-specified User File Identification Code from Phase II.

FIGURE 7

<u>LEVEL 16.X PHASE III DATA DECK</u>

	1	2	3	4	5	6	7	8	9	10
	DTI	TPTABLE	0[a]	4[b]	16[c]					+DTI-000
	+DTI-000	ENDREC								
1st substructure	DTI	TPTABLE	1	10[d]		INP1[e]	SUB1[f]		ENDREC	+DTI-001
2nd substructure	DTI	TPTABLE	2	20		INP4	TRY2SUB2	104823[g]		+DTI-002
	+DTI-002	A[h]	3[i]	K	1	P	2		ENDREC	+DTI-003
3rd substructure	DTI	TPTABLE	3	-21[j]	20[j]				ENDREC	+DTI-004
4th substructure	DTI	TPTABLE	4	40		INP4	PLT4SUB4		NAMES[k]	+DTI-005
	+DTI-005	A	A04[ℓ]	K	K1048				ENDREC	+DTI-006
Combined structure (optional)	DTI	TPTABLE	5	1010		CØUPLE4			ENDREC	+DTI-007

(a) DTI Record Number
(b) Number of Substructures
(c) Rigid Format
(d) Substructure Identification Number
(e) User File GINØ Name
(f) User File Label (optional)

(g) Tape Reel Number (optional)
(h) Data Block Code } (optional)
(i) Data Block Position }
(j) Identical Substructure Reference
(k) Option Code } (optional)
(ℓ) Data Block Name }

FIGURE 8. USER FILE COUPLING DATA

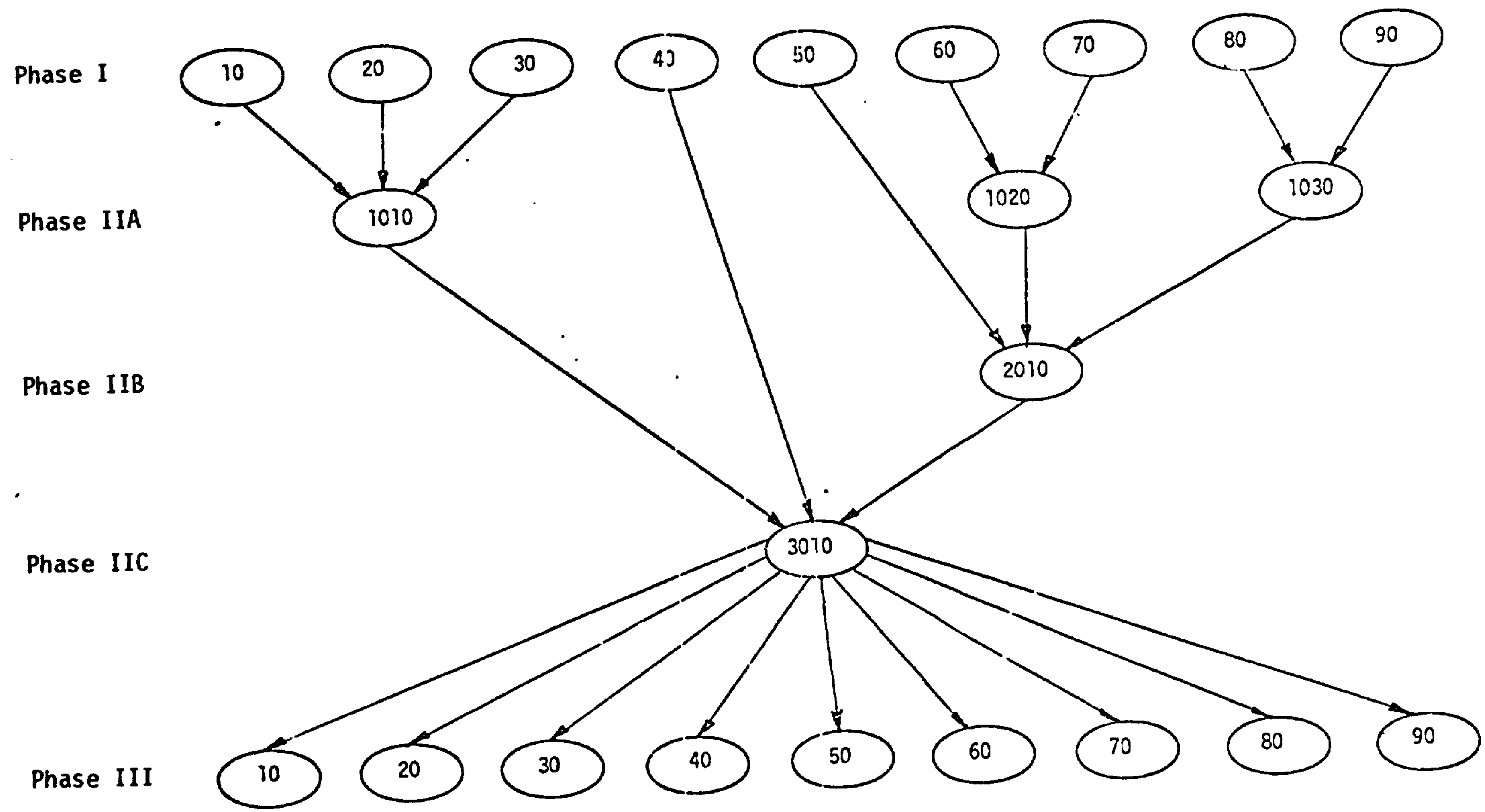

FIGURE 9. MULTI-LEVEL SUBSTRUCTURE ANALYSIS

Input Data Card SAME Joining Data

Description: Defines grid or scalar points which are to be coupled in a substructure analysis.

Format and Example:

1	2	3	4	5	6	7	8	9	10
SAME	S	G	S	G	S	G	S	G	abc
SAME	3	79	4	216	6	93			ABC

+bc	S	G	S	G	etc.				
+BC	7	42							

etc.

Alternate Form

SAME	S	G1	"THRU"	G2	S	G1	"THRU"	G2	+abc
SAME	10	1	THRU	60	20	101	THRU	160	ABC

+abc	S	G1	"THRU"	G2	etc.				
+BC	30	526	THRU	585					

etc.

Field	Contents
S	Substructure identification number (Integer > 0)
G, G1, G2	Grid or Scalar point identification number (Integer > 0; G1 < G2)

Remarks:

1. Up to four grid or scalar points (in four different substructures) may be coupled by a single card. As many continuation cards as required may be used.
2. No degrees of freedom of coupled points may be members of the o-set.
3. The substructure identification numbers should be written in ascending order.
4. If two SAME cards are to be joined, the highest numbered substructure entry on the first one should be repeated on the second one.
5. If the alternate form is used, all of the grid and scalar points G1 thru G2 are assumed. Each G1 THRU G2 sequence must define the same number of points.

FIGURE 10. SAME CARD DESCRIPTION

N74-14604

NASTRAN CYCLIC SYMMETRY CAPABILITY

By R. H. MacNeal and R. L. Harder

The MacNeal-Schwendler Corp., Los Angeles

and J. B. Mason

NASA Goddard Space Flight Center

SUMMARY

The paper describes a recent development for NASTRAN which facilitates the analysis of structures made up of identical segments symmetrically arranged with respect to an axis. The key operation in the method is the transformation of the degrees of freedom for the structure into uncoupled *symmetrical components*, thereby greatly reducing the number of equations which are solved simultaneously. A further reduction occurs if each segment has a plane of reflective symmetry. The only required assumption is that the problem be linear. The capability, as developed, will be available in Level 16 of NASTRAN for static stress analysis, steady state heat transfer analysis, and vibration analysis.

The paper includes a discussion of the theory, a brief description of the data supplied by the user, and the results obtained for two example problems. The first problem concerns the acoustic modes of a long prismatic cavity imbedded in the propellant grain of a solid rocket motor. The second problem involves the deformations of a large space antenna. The latter example is the first application of the NASTRAN Cyclic Symmetry capability to a really large problem.

INTRODUCTION

Many structures, including pressure vessels, rotating machines, and antennas for space communications, are made up of virtually identical segments that are symmetrically arranged with respect to an axis. There are two types of cyclic symmetry as shown in Figures 1 and 2: *simple rotational symmetry*, in which the segments do not have planes of reflective symmetry and the boundaries between segments may be general doubly-curved surfaces, and *dihedral symmetry*, in which each segment has a plane of reflective symmetry and the boundaries between segments are planar. In both cases, it is most important for reasons of economy to be able to calculate the thermal and structural response by analyzing a subregion containing as few segments as possible.

Principles of reflective symmetry (which are not, in general, satisfied by cyclically symmetric bodies) can reduce the analysis region to one-fourth of the whole. Principles of cyclic symmetry, on the other hand, can reduce the analysis region to a single segment in the case of dihedral symmetry and to a pair of segments in the case of simple rotational symmetry. Neither accuracy nor generality need be lost in the process, except that the treatment is limited to linear relationships between degrees of freedom.

Special procedures for the treatment of Cyclic Symmetry have recently been added to NASTRAN under the sponsorship of the Goddard Space Flight Center. The procedures will be available in Level 16 of NASTRAN. This paper includes a discussion of the theory, a description of the special input data, and the solutions of example problems. More complete information, including detailed descriptions of new functional modules and DMAP ALTERS for Rigid Formats 1 and 3, is contained in Ref. 1.

The use of cyclic symmetry will allow the analyst to model (i.e., make a NASTRAN Bulk Data Deck for) only one of the identical substructures. There will also be a large saving of computer time for most problems.

THEORY

Two types of cyclic symmetry are shown in Figures 1 and 2, where they are called *rotational* symmetry and *dihedral* symmetry. The latter term is borrowed from Herman Weyl who used it in his mathematical treatment of symmetry, Ref. 2. Note that dihedral symmetry is a special case of rotational symmetry. In both cases, the body is composed of identical segments, each of which obeys the same physical laws. The distortions (deflections or temperature changes) of the segments are not independent, but must satisfy compatibility at the boundaries between segments. Cyclic transforms will be defined, which are linear combinations of the distortions of the segments. The transformed equations of compatibility are such that the "transformed segments" are coupled singly or in pairs which can be solved *independently*. This feature results in a significant reduction of computational effort *beyond* the normal possibilities of substructure analysis.

In the theory given below, the form of the transformation is not derived, but just stated. The validity of the method is then demonstrated. A step-by-step inductive derivation of the transformation will be found in Ref. 3. The theory will be presented first for the more general but simpler case of rotational symmetry, after which the additional special features for dihedral symmetry will be introduced.

Theory for Rotational Symmetry

The total body consists of N identical segments, which are numbered consecutively from 1 to N. The user supplies a NASTRAN model for one segment. All other segments and their coordinate systems are rotated to equally-spaced positions about the polar axis. The boundaries must be *conformable*; i.e., when the segments are put together, the grid points and the displacement coordinate systems of adjacent segments must coincide. This is easiest to insure if a cylindrical or spherical coordinate system is used, but such is not required. The user will also supply a paired list of grid points on the two boundaries of the segment where connections will be made. For static analysis the user may also supply a set of loads and/or enforced displacements for each of the N segments.

The two boundaries will be called sides 1 and 2. Side 2 of segment n is connected to side 1 of segment n+1, see Figure 1. Thus, the components of displacement satisfy

$$u_1^{n+1} = u_2^n \qquad n = 1, 2, \ldots, N \tag{1}$$

where the superscript refers to the segment index and the subscript refers to the side index. This applies to all degrees of freedom which are joined together. We also define $u^{n+1} = u^1$, so that Equation 1 will refer to all boundaries. Equation 1 is the equation of constraint between the physical segments.

The rotational transformation is given by

$$u^n = \bar{u}^o + \sum_{k=1}^{k_L} [\bar{u}^{kc} \cos(n-1)ka + \bar{u}^{ks} \sin(n-1)ka] + (-1)^{n-1} \bar{u}^{N/2} \tag{2}$$

$$a = 2\pi/N, \quad n = 1, 2, \ldots, N$$

where u^n *can be any component* of a displacement, force, stress, temperature, etc., in the n^{th} segment. The last term exists only when N is even. The summation limit k_L = (n-1)/2 if N is odd and (N-2)/2 if N is even. $\bar{u}^o$, $\bar{u}^{kc}$, $\bar{u}^{ks}$, and $\bar{u}^{N/2}$ are the transformed quantities which will be referred to as *symmetrical components*. They are given this designation by virtue of their similarity to the symmetrical components used by electrical engineers in their analysis of polyphase networks, Ref. 4. Note also the similarity of Equation 2 to a Fourier series decomposition, except that the number of terms is finite. On this account, Equation 2 could be called a finite Fourier transformation, Ref. 5.

Equation 2 can be displayed in the matrix form

$$\lfloor u \rfloor = \lfloor \bar{u} \rfloor [T] \tag{3}$$

where

$$\lfloor u \rfloor = \lfloor u^1, u^2, u^3, \ldots, u^N \rfloor$$

and

$$\lfloor \bar{u} \rfloor = \lfloor \bar{u}^o, \bar{u}^{1c}, \bar{u}^{1s}, \bar{u}^{2c}, \bar{u}^{2s}, \ldots, \bar{u}^{N/2} \rfloor$$

Each element in the first row vector can represent all of the unknowns in one segment.

The expanded form of the transformation matrix is

$$[T] = \left[\begin{array}{cccccc}
1 & 1 & 1 & \cdot\ \cdot\ \cdot & 1 \\
\hline
1 & \cos a & \cos 2a & \cdot\ \cdot\ \cdot & \cos (N-1)a \\
0 & \sin a & \sin 2a & \cdot\ \cdot\ \cdot & \sin (N-1)a \\
\hline
1 & \cos 2a & \cos 4a & & \cos (N-1)2a \\
\cdot & \cdot & \cdot & & \cdot \\
\cdot & \cdot & \cdot & & \cdot \\
\cdot & \cdot & \cdot & & \cdot \\
0 & \sin k_L a & \sin 2k_L a & \cdot\ \cdot\ \cdot & \sin (N-1)k_L a \\
\hline
1 & -1 & 1 & \cdot\ \cdot\ \cdot & -1
\end{array}\right] \tag{4}$$

The last row exists only for even N. The transformation matrix, [T], has the property

$$[T]\ [T]^T = [D] = \begin{bmatrix}
N & & & & & & & \\
& N/2 & & & & & & \\
& & N/2 & & & & & \\
& & & N/2 & & & & \\
& & & & \cdot & & & \\
& & & & & \cdot & & \\
& & & & & & \cdot & \\
& & & & & & & N
\end{bmatrix} \tag{5}$$

i.e., the rows of [T] are orthogonal.

Since D is nonsingular,

$$[T][T]^T[D]^{-1} = [I] \tag{6}$$

Thus, $[T]^{-1} = [T]^T[D]^{-1}$ and

$$\lfloor\bar{u}\rfloor = \lfloor u\rfloor[T]^{-1} = \lfloor u\rfloor[T^T D^{-1}] \tag{7}$$

In summation form, Equation 7 becomes

$$\bar{u}^o = (1/N)\sum_{n=1}^{N} u^n \tag{8a}$$

$$\bar{u}^{kc} = (2/N)\sum_{n=1}^{N} u^n \cos(n-1)ka \tag{8b}$$

$$\bar{u}^{ks} = (2/N)\sum_{n=1}^{N} u^n \sin(n-1)ka \tag{8c}$$

$$\bar{u}^{N/2} = (1/N)\sum_{n=1}^{N} (-1)^{n-1} u^n \text{ (N even only)} \tag{8d}$$

It should be noted that Equations 8 apply to applied loads and to internal forces as well as displacement components. The validity of the symmetrical components $\lfloor\bar{u}\rfloor$ to represent the motions of the system follows from the existence of $[T]^{-1}$. It remains only to show that they are useful. The equations of motion at points interior to the segments are linear (homogenous of degree 1) in displacements, forces, and temperatures; they are identical for all segments; and they are not coupled between segments.

Thus, the equations of motion (for example $[K]\{u\}^n = \{P\}^n$ in static analysis) can be additively combined using one of the sets of coefficients in Equation 8, thereby obtaining the equations of motion for one of the transformed variables which will have identically the same form (e.g., $[K]\{\bar{u}\}^{kc} = \{\bar{P}\}^{kc}$) as the equations of motion for one of the physical segments.

The equations of motion at points on the boundaries between segments are treated by employing the notion of a rigid constraint connecting adjacent points. To transform the compatibility equation of constraint (1), notice that

$$u_1^{n+1} = \bar{u}_1^o + \sum_{k=1}^{k_L} [\bar{u}_1^{kc} \cos nka + \bar{u}_1^{ks} \sin nka] + (-1)^n \bar{u}_1^{N/2} \tag{9}$$

Using the identities cos nka = cos(n-1)ka·cos ka - sin(n-1)ka·sin ka and sin nka = sin(n-1)ka·cos ka + cos(n-1)ka·sin ka, Equation 9 may be written

$$u_1^{n+1} = \bar{u}_1^o + \sum_{k=1}^{k_L} \begin{bmatrix} (\bar{u}_1^{kc} \cos ka + \bar{u}_1^{ks} \sin ka) \cos(n-1)ka \\ +(-\bar{u}_1^{kc} \sin ka + \bar{u}_1^{ks} \cos ka) \sin(n-1)ka \end{bmatrix} - (-1)^{n-1} \bar{u}_1^{N/2} \tag{10}$$

Comparing Equation 10 with Equation 2 evaluated at side 2 as required by Equation 1, and equating the coefficients of terms with the same dependence on n, we obtain

$$\bar{u}_1^o = \bar{u}_2^o \tag{11a}$$

$$\left.\begin{aligned} \bar{u}_1^{kc} \cos ka + \bar{u}_1^{ks} \sin ka &= \bar{u}_2^{kc} \qquad (11b) \\ -\bar{u}_1^{kc} \sin ka + \bar{u}_1^{ks} \cos ka &= \bar{u}_2^{ks} \qquad (11c) \end{aligned}\right\} \; k = 1, \cdots, k_L$$

$$-\bar{u}_1^{N/2} = \bar{u}_2^{N/2} \tag{11d}$$

Equations 11 are the equations of constraint for the symmetrical components. The only symmetrical components coupled by the compatibility constraints are 1c and 1s, 2c and 2s, etc. Thus, there are several *uncoupled* models; the K=0 model contains the $\bar{u}^o$ degrees of freedom; the K = 1 model, the $\bar{u}^{1c}$ and $\bar{u}^{1s}$ degrees of freedom, etc.

There is a somewhat arbitrary choice regarding where to transform the variables in the NASTRAN analysis. NASTRAN structural analysis can start with a structure defined with single and multipoint constraints, applied loads, thermal fields, etc., and reduce the problem to the "analysis set," $\{u_a\}$, where

$$[K_{aa}]\{u_a\} = \{P_a\} \tag{12}$$

The vector $\{u_a\}$ contains only independent degrees of freedom. The decision was made in developing the cyclic symmetry capability to first reduce each segment individually to the "analysis" degrees of freedom and then to transform the remaining freedoms to symmetrical components. This approach has several advantages, including elimination of the requirement to transform temperature vectors and single-point enforced displacements, because these quantities are first converted into equivalent loads. More importantly, if the "ØMIT" feature is used to remove internal degrees of freedom, it need only be applied to one segment. The ØMIT feature greatly reduces the number of degrees of freedom which must be transformed. The user specifies all constraints internal to the segments with standard NASTRAN data cards. If constraints (MPC, SPC, and/or ØMIT) are applied to degrees of freedom on the boundaries, they will take precedence over the intersegment compatibility constraints; i.e., an intersegment compatibility constraint will *not* be applied to any degree of freedom which is constrained in some other way. SUPPØRT data cards are forbidden because they are intended to apply to overall rigid body motions and will not, therefore, be applied to each segment. In the case of static analysis, the analysis equations for the segments are

$$[K]\{u\}^n = \{P\}^n \qquad n = 1, 2, \ldots, N \tag{13}$$

The analysis equations for the symmetrical components, prior to applying the intersegment constraints, are

$$[K]\{\bar{u}\}^x = \{\bar{P}\}^x \qquad x = 0, 1c, 1s, 2c, \ldots, N/2 \tag{14}$$

where $\{\bar{P}\}^x$ is calculated using Equations 8. The matrix $[K]$ is the same for Equations 13 and 14 and is the KAA stiffness matrix of NASTRAN for one segment.

We come now to the matter of applying the intersegment compatibility constraints. It is recognized that not all of the degrees of freedom in any transformed model can be independent, but it is easy to choose an independent set. We include in the independent set, $\{\bar{u}\}^K$, all points in the interior and on boundary 1 (for both $\bar{u}^{kc}$ and $\bar{u}^{ks}$, if they exist). The values of displacement components at points on boundary 2 can then be determined from Equations 11. The transformation to the new set of *independent* degrees of freedom is indicated by

$$\{\bar{u}\}^{kc} = [G_{ck}]\{\bar{u}\}^K \tag{15a}$$

$$\{\bar{u}\}^{ks} = [G_{sk}]\{\bar{u}\}^K \tag{15b}$$

where each row of $[G_{ck}]$ or $[G_{sk}]$ contains only a single nonzero term if it is an interior or side 1 degree of freedom and either one or two nonzero terms if it is a degree of freedom on side 2. In arranging the order of terms in $\{\bar{u}\}^K$, the user can specify either that they be sequenced with all $\{\bar{u}\}^{kc}$ terms preceding all $\{\bar{u}\}^{ks}$ terms, or that they be sequenced with $\{\bar{u}\}^{kc}$ and $\{\bar{u}\}^{ks}$ grid points alternating. It should be emphasized that the kind of vectors used in transformation of Equations 3 and 15 are quite different. In Equation 3, there is one component (or column) for each segment; in Equation 15, there is one component (or row) for each degree of freedom in a segment.

Equation 15 is used to transform Equation 14 to the following set of equations which satisfy the intersegment compatibility conditions:

$$[\bar{K}]^K\{\bar{u}\}^K = \{\bar{P}\}^K \tag{16}$$

where
$$[\bar{K}]^K = [G^T_{ck}\ KG_{ck} + G^T_{sk}\ KG_{sk}] \tag{17}$$

and
$$\{\bar{P}\}^K = [G^T_{ck}]\{\bar{P}\}^{kc} + [G^T_{sk}]\{\bar{P}\}^{ks} \tag{18}$$

Because NASTRAN has sparse matrix routines of near optimum efficiency, the time for the calculations indicated in Equations 17 and 18 will not be appreciable. After solving Equation 16 by decomposition and substitution, the symmetrical component variables, $\{\bar{u}\}^{kc}$ and $\{\bar{u}\}^{ks}$, are found from Equations 15. The physical segment variables, $\{u\}^n$, are found from Equation 2. The $\{u\}^n$ are NASTRAN vectors of the analysis set. They may be expanded to $\{u_g\}$ size by recovering dependent quantities. Stresses in the physical segments are then obtained via the normal stress reduction procedures.

The user may take an alternate route if he knows the transformed values, $\{\bar{P}^{kc}\}$ and $\{\bar{P}^{ks}\}$, for the forcing functions (loads, enforced displacements, and temperatures). This will, for example, be the case in a stress analysis which follows a temperature analysis of the same structural model. These data may be input directly to NASTRAN, which will convert them to the transformed load vectors, $\{\bar{P}\}^K$. Data reduction may also be performed on the transformed quantities to obtain the symmetrical components of stresses, etc.

A shortened approximate method for static analysis is available merely by setting

$$\{\bar{u}\}^K = 0 \tag{19}$$

for all K > KMAX. This is similar to truncating a Fourier series. The stiffness associated with larger K's (short azimuthal wave lengths) tends to be large, so that these components of displacement tend to be small.

The cyclic symmetry method has also been coded for vibration analysis. The equation of motion in terms of independent degrees of freedom is

$$[\bar{K}^K - \omega^2\bar{M}^K]\{\bar{u}\}^K = 0 \tag{20}$$

where $[\bar{M}]^K$ is derived by replacing [M] for [K] in Equation 17. The symmetrical components are recovered with Equation 15. No provision has been made to recover physical segment data in vibration analysis, because the physical interpretation of Equation 4 is straightforward. (Each row of [T] is a vector of the factors for each segment.) The available output data does, however, include the symmetrical components of dependent displacements, internal forces, and stresses.

Theory for Dihedral Symmetry

Dihedral symmetry refers to the case when each individual segment has a plane of reflective symmetry, see Figure 2. The segments are divided about their midplanes to obtain 2N substructures. The midplane of a segment is designated as side 2. The other boundary, which must also be planar, is called side 1. The two halves of the segment are called the right "R" and left "L" halves. The user prepares model information for one R half segment. He must also supply a list of points on side 1 and another list of points on side 2.

For the case of dihedral symmetry, the cyclic transformation described earlier is used in conjunction with reflective symmetry of the segments. The two transformations are commutable, so they may be done in either order. The reflective transform for a segment is

$$u^{n,R} = u^{n,S} + u^{n,A} \tag{21a}$$

$$u^{n,L} = u^{n,S} - u^{n,A} \tag{21b}$$

Here, the superscript n refers to the n^{th} segment, and R, L the right and left halves. S and A refer to the symmetric and antisymmetric reflective components.

In the R half segment, displacement components are referred to a right hand coordinate system and in the L half segment, displacement components are referred to a left hand coordinate system. The inverse reflective transform is

$$u^{n,S} = \tfrac{1}{2}(u^{n,R} + u^{n,L}) \tag{22a}$$

$$u^{n,A} = \tfrac{1}{2}(u^{n,R} - u^{n,L}) \tag{22b}$$

Reflective symmetry is seen to be very simple. The equations of motion at interior points of the S and A half-segment models are identical in form provided that unsymmetrical effects, such as Coriolis forces, are excluded.

The $u^{n,S}$ and $u^{n,A}$ components may be transformed as follows using rotational principles.

$$u^{n,x} = \bar{u}^{o,x} + \sum_{k=1}^{k_L} [\bar{u}^{kc,x} \cos(n-1)ka + \bar{u}^{ks,x} \sin(n-1)ka] + (-1)^{n-1} \bar{u}^{N/2,x} \tag{23}$$

where x may be either S (symmetric) or A(antisymmetric). The inverse transformation can be found by Equations 8 for both the symmetric and antisymmetric parts.

The constraints between the half segments are summarized in Table 1. The constraints shown apply between points joined together at the boundary planes. "Even components" include displacements parallel to the radial planes between segment halves, rotations about the axes normal to the planes, and temperatures in a thermal analysis. "Scalar points" in a structural analysis have arbitrarily been categorized as even components. "Odd components" include displacements normal to the radial planes and rotations about axes parallel to the planes. In Table 1 the constraint equations for the S and A half-segment model are obtained by substituting Equations 21 into the equations for the L and R half-segment model. The constraint equations for the dihedral transform model are obtained by substituting for $u^{n,x}$ and $u^{n+1,x}$ from Equation 23 and comparing terms with the same dependence on n. It can be seen in the table that the k = 0 and k = N/2 models are completely uncoupled. There is coupling between the kc,S and ks,A models and also between kc,A and ks,S models. These two sets of constraint equations are related and one can be found from the other by substituting $\bar{u}^{kc,S}$ for $\bar{u}^{ks,S}$ and $\bar{u}^{ks,A}$ for $-\bar{u}^{kc,A}$ in the constraint equations. With these substitutions, and noting that the equations of motion are identical at interior points, it is seen that we only need to analyze one coupled pair of symmetric and antisymmetric half segments with different load sets for the $(\bar{u}^{kc,S}, \bar{u}^{ks,A})$ case and the $(\bar{u}^{ks,S}, -\bar{u}^{kc,A})$ case.

As in the case of general rotational symmetry, a combined set of independent degrees of freedom is formed from the half models. The independent set $\{\bar{u}\}^k$ includes all interior points, the points on side 2 of each half segment which are not constrained to zero, and new degrees of freedom, $\{\bar{u}_1\}^K$, on side 1 such that, for *even* components in the $(\bar{u}^{kc,S}, \bar{u}^{ks,A})$ case:

$$\bar{u}_1^{kc,S} = \cos\frac{k\pi}{N}\,\bar{u}_1^K \tag{24a}$$

$$\bar{u}_1^{ks,A} = \sin\frac{k\pi}{N}\,\bar{u}_1^K \tag{24b}$$

while for *odd* components:

$$\bar{u}_1^{kc,S} = -\sin\frac{k\pi}{N}\,\bar{u}_1^K \tag{25a}$$

$$\bar{u}_1^{ks,A} = \cos\frac{k\pi}{N}\,\bar{u}_1^K \tag{25b}$$

Equations 24 and 25 are equivalent to the constraints in the third column of Table 1. The transformation to the new set of independent freedoms may be expressed as

$$\{\bar{u}\}^{kc,S} = [G_{SK}]\{\bar{u}\}^K \tag{26a}$$

$$\{\bar{u}\}^{ks,A} = [G_{AK}]\{\bar{u}\}^K \tag{26b}$$

where each row of $[G_{SK}]$ or $[G_{AK}]$ contains at most a single nonzero term. The transformation matrices for the $(\bar{u}^{ks,S}, -\bar{u}^{kc,A})$ case are identical.

The final equation which is solved in static analysis is

$$[\bar{K}]^K\{\bar{u}\}^K = \{\bar{P}\}^K \tag{27}$$

where the stiffness matrix

$$[\bar{K}]^K = [G_{SK}^T\ K\ G_{SK} + G_{AK}^T\ K\ G_{AK}] \tag{28}$$

and the load vector is obtained by successive application of the inverse reflective symmetry transform, Equations 22, the inverse cyclic symmetry transform, Equations 8, and the final reduction to independent freedoms.

The form of the latter is, for the $(\bar{u}^{kc,S}, \bar{u}^{ks,A})$ case,

$$\{\bar{P}\}^K = [G_{SK}]^T\{\bar{P}\}^{kc,S} + [G_{AK}]^T\{\bar{P}\}^{ks,A} \tag{29}$$

and for the $(\bar{u}^{ks,S}, -u^{kc,A})$ case,

$$\{\bar{P}\}^K = [G_{SK}]^T\{\bar{P}\}^{ks,A} - [G_{AK}]^T\{\bar{P}\}^{kc,A} \tag{30}$$

The data reduction which follows the solution of Equation 27 in static analysis includes the application of the symmetry transformation to obtain $u^{n,R}$ and $u^{n,L}$, followed by the expansion to $\{u_g\}$ size for each half segment and the calculation of internal loads and stresses. Similar to the case of rotational symmetry, the data reduction for vibration analysis is limited to the recovery of eigenvectors, internal forces, and stresses for symmetrical component sets $\bar{u}^{kc,S}$ and $\bar{u}^{ks,A}$.

SUMMARY OF USER-SUPPLIED INFORMATION

The cyclic symmetry modification to NASTRAN allows the solution of structures with rotational or dihedral symmetry by modeling only one of the identical segments. Special Bulk Data cards and parameters are introduced to specify the method of joining the segments. Solutions are obtained by special DMAP ALTERS to Rigid Formats 1 and 3. In static analysis, input and output data for each individual segment are designated as separate subcases. The output includes, of course, the simultaneous effects of the loads on all segments. The constrained degrees of freedom and material properties must be the same for all segments. For static analysis, the loads, the values of enforced displacements, and the temperatures may vary from segment to segment. Separate loading conditions are also treated as subcases so that the total number of subcases equals the number of segments (or half segments) times the number of loading conditions.

The SPCD Bulk Data card (Figure 3) is useful for applying enforced boundary displacements (or temperatures). These values are requested by a load set; thus, if different displacements are specified on different segments (i.e., in different subcases), the requested SPC constraint set will not change. This must be done, since looping on constraint sets is not supported in cyclic symmetry analysis.

A Bulk Data card, CYJØIN (see Figure 4), is used to specify how the segments are to be connected. Existing MPC, SPC, and ØMIT constraints may be used within the segments. The SUPØRT card for free bodies is forbidden when cyclic symmetry is used, since *segment* free body modes do not necessarily imply *overall* free body modes. Constraints between segments are applied automatically to the degrees of freedom at grid points specified on CYJØIN Bulk Data cards which are not otherwise constrained. Grid points are not allowed to be placed on the axis of symmetry.

The user must also define the following parameters by means of PARAM Bulk Data cards:

Parameter	Description
CYTYPE	Type of problem: RØT for rotational symmetry, DRL for dihedral symmetry using right and left halves, DSA for dihedral using symmetric and antisymmetric components.
N	Integer - The number of segments.
K	Integer - The value of the harmonic index, used only for eigenvalue analysis.
KMAX	Integer - The maximum value of K, used for static analysis. (Default is ALL)
CYCIØ	Integer - +1 for physical segment representation, -1 for cyclic transform representation for input and output of data. Static analysis, default = 1.
CYCSEQ	Integer - Used for method of sequencing the equations in the solution set. +1 for all cosine then all sine terms, -1 for alternating. Default = -1.
NLØAD	The number of loading conditions in static analysis. Default = 1.

MODIFICATIONS OF THE NASTRAN CODE

The NASTRAN modifications for cyclic symmetry include DMAP ALTERS to the Executive Control Deck and three new functional modules. The ALTERS and the details of the new functional modules are described in Reference 1. Briefly, the functions of the three modules are as follows:

The first module, called CPCYC, is a geometry processor acting on the CYJØIN data. It identifies and classifies the degrees of freedom involved in the boundary constraints.

The second module, called CYCT1, is used only in static analysis. It transforms excitation quantities (loads) from physical segment components to symmetrical components and it also transforms output displacements from symmetrical components to physical segment components. It is used for both types of symmetry (rotational and dihedral). All input and output quantities are "analysis-size" $\{u_a\}$ vectors.

The third module, called CYCT2, is used to transform load vectors and mass and stiffness matrices from symmetrical components to the solution set (see Equations 16, 17, 18, 28, 29, 30) and also to transform the results back to the symmetrical component sets.

ADVANTAGES

The NASTRAN cyclic symmetry capability will result in a large saving of user effort and computer time for most applications. The savings result from the following effects:

1. Grid point geometry and element data are prepared for only one segment in the case of rotational symmetry or one half segment in the case of dihedral symmetry.

2. The transformed equations are uncoupled, except within a given harmonic index, K, which reduces the order of the equations which must be solved simultaneously to 1/N or 2/N (where N is the number of segments or symmetrical half segments) times the order of the original system.

3. Solutions may be restricted to a partial range of the harmonic index, K, (e.g., to the lower harmonic orders) which results in a proportionate reduction in solution time. Some accuracy is thereby lost in the case of static analysis but not in vibration analysis.

4. In the case of static analysis, the ØMIT feature may be used to remove all degrees of freedom at internal grid points without any loss of accuracy. Since this reduction is applied to a single segment *prior* to the symmetry transformations, it can greatly reduce the amount of subsequent calculation.

It is instructive to compare the advantages of the NASTRAN cyclic symmetry capability with those offered by reflective symmetry and by conventional substructuring techniques. The savings offered by cyclic symmetry will always equal or exceed those provided by reflective symmetry except for possible differences due to time spent in transforming variables. For example, when an object has two planes of symmetry and two symmetrical segments (the minimum possible number in this case), the minimum region sizes are both equal to one half segment for the two methods. They are also equal when the object has four symmetrical segments. The advantages of cyclic symmetry for these cases are restricted to those offered by the ØMIT feature in static analysis and by a higher degree of input and output data organization. Any larger number of symmetrical segments increases the advantage of cyclic symmetry because the size of the fundamental region is smaller.

A method of conventional substructuring which recognizes identical substructures can also restrict the amount of grid point geometry and element data preparation to a single substructure and can use the ØMIT feature in the same way as cyclic symmetry. The advantage which cyclic symmetry retains over conventional substructuring lies in its decomposition of degrees of freedom into uncoupled harmonic sets. This is an important advantage for eigenvalue extraction, but the advantage for static analysis is relatively small and depends in a complex manner on the number of segments and on the method of matrix decomposition.

In addition to the analysis of structures made up of a finite number of identical substructures, cyclic symmetry can also be used for purely axisymmetric structures. In this case the circumferential size of the analysis region is arbitrarily selected to be some small angle, for example, one degree. Grid points are then placed on the boundary surfaces but not in the interior of the region, and the region is filled with ordinary three-dimensional elements. The principal advantage of this procedure is that ordinary three-dimensional elements are used in place of *specialized* axisymmetric elements. In NASTRAN the number of available types and features for ordinary three-dimensional elements far exceeds those available for axisymmetric elements, so that cyclic symmetry immediately enlarges the analysis possibilities for axisymmetric structures. In particular, the rotational symmetry option can accommodate axisymmetric structures with nonorthotropic material properties, which the available axisymmetric procedures cannot. It is possible, in the long run, that cyclic symmetry will completely replace the relatively expensive NASTRAN axisymmetric capability. New input data cards modeled on existing axisymmetric data cards are needed to facilitate the use of cyclic symmetry for this purpose.

EXAMPLE PROBLEMS

Acoustic Vibrations of the Central Cavity in a Solid Rocket Motor

NASTRAN includes the ability to solve the acoustic wave equation which may be written in vector notation as

$$\nabla \cdot \frac{1}{\rho} \nabla P = \omega^2 \frac{1}{B} P \tag{31}$$

where P is the pressure, ρ is the density, B is the bulk modulus, and ω is the frequency in radians per unit time. The theoretical development of finite fluid elements for solving problems with axisymmetric geometry is described in Section 16.3 of the NASTRAN Theoretical Manual, Reference 6. One of the products of that development, namely the family of CSLØT elements, can be used to solve the planar wave equation for a fluid disk of either constant or variable thickness, provided that there is no variation of pressure normal to the plane of the disk.

The CSLØT elements were used, in the present application, to model the prismatic central cavity of a typical solid rocket motor whose cross section is shown in Figure 5. The cross-section has dihedral symmetry with seven segments (fourteen half segments). The axial length of the cavity is long compared to its diameter, and the problem of interest was the calculation of the lowest lateral vibration mode, i.e., the lowest mode exhibiting a pressure gradient across the diameter of the cavity. From the derivations described earlier in the paper, it is clear that the vibration modes of the cavity have distinct harmonic indices K; it is also clear, from physical reasoning, that K = 1 produces the lowest lateral mode. Thus, calculations were restricted to K = 1.

The finite element model for a single half segment is shown in Figure 6. It contains 71 grid points (with one degree of freedom per grid point), 39 triangular CSLØT3 elements and 29 quadrilateral CSLØT4 elements. A model based on reflective symmetry would have seven times as many finite elements. The mesh spacing is finer in the region where large pressure gradients are expected. Details of the modeling process for this problem are described in Reference 7. The frequency of the lowest lateral mode was calculated to be 17410 hertz. The distribution of radial velocities at lobe throats is indicated in Figure 5. The mode shape results produced by the computer are the symmetrical components, $\bar{u}^{1c,S}$ and $\bar{u}^{1s,A}$, for the pressures at grid points, and for the velocity components within elements. The formulas used to get physical components, obtained by combining Equations 21 and 23, are

Right Half Segments:

$$u^{n,R} = \bar{u}^{1c,S} \cos(n-1)a + \bar{u}^{1s,A} \sin(n-1)a \tag{32a}$$

Left Half Segments:

$$u^{n,L} = \bar{u}^{1c,S} \cos(n-1)a - \bar{u}^{1s,A} \sin(n-1)a \tag{32b}$$

Parabolic Reflector for the ATS-F Spacecraft

An artist's rendering of the deployed Lockheed 30-ft parabolic reflector on the ATS-F spacecraft is shown in Figure 7. The antenna is composed of 48 flexible aluminum ribs cantilevered symmetrically about a central hub at 7.5 degree increments. The reflective surface consists of a thin mesh woven from copper coated dacron yarn. When deployed, the mesh is under tension so as to remain taut during orbit.

The parabolic ribs have an "open-C" (i.e., semi-lenticular) cross section which tapers in both width and depth from the rib attachment at the central hub to the outer tip. This construction permits the ribs to be wrapped tightly around the hub in the stored configuration. As shown in Figure 8, integral stiffeners and varying diameter holes to accommodate deformations during storage are characteristic of the design. The nonisotropic mesh is formed by double strand radial and single strand circumferential yarn. Tests have shown that

Poisson's ratio is essentially zero for this material so that circumferential and radial yarns can be assumed to act independently.

It is clear from the shape of the ribs that the structure does not possess dihedral symmetry. It does, however, possess rotational symmetry and it was modeled by describing only one 7.5 degree segment. For the analysis the chosen segment had the rib centrally located with the mesh extending 3.75 degrees on either side. The rib was modeled using 745 grid points, i.e., 5 grid points through each section at 149 sections along the rib. 592 CQUAD2 elements, 60 CONRØD elements, and 300 CBAR elements were employed. The thicknesses of the quadrilaterals were adjusted to account for the holes, and the bars and rods were used to represent the integral stiffeners. 50 additional grid points were used to model the mesh, i.e., one mesh point on either side of the rib at each of 25 stations along the rib. The effects of the radial mesh strands were neglected in the analysis and only the circumferential strands were included. To represent the elastic stiffness of the mesh, 50 CRØD elements were attached circumferentially at the same 25 stations along the rib. 100 CELAS2 elements were employed at these stations to represent the radial and axial "string-stiffness" arising from the pre-tension in the mesh.

The ØMIT feature was utilized to reduce the original problem of nearly 4600 degrees of freedom to an analysis set containing 234 freedoms. This was accomplished by eliminating all freedoms on the rib except those at 14 points distributed along the edge next to the reflector. The 234 members of the analysis set consisted of 3 x 50 = 150 translational degrees of freedom at the boundary mesh points and 6 x 14 = 84 translational and rotational degrees of freedom along the rib. Model generation, Guyan reduction, and extraction of three eigenvalues using the inverse power method took about 30.0 minutes of CPU time on the Goddard Space Flight Center IBM 360/95 computer.

The computed frequencies for the three lowest axisymmetric (K = 0) modes and the lowest lateral (K = 1) mode are as follows:

K value	Freq.(hertz)
0	1.19 (test 1.17)
0	6.11
0	6.46
1	4.73

In the lowest K = 0 mode the tips of the ribs move collectively in the azimuthal direction. Its computed frequency compares well with the experimentally measured frequency.

REFERENCES

1. "NASTRAN Cyclic Symmetry User's Guide," The MacNeal-Schwendler Corporation Report EC-180, July 1972.

2. H. Weyl, "Symmetry," Lectures given at the Institute for Advanced Study, reprinted in The World of Mathematics, Simon and Schuster, New York, Vol. 1, pp 671-724, 1956.

3. R. H. MacNeal, "Principles of Rotor Dynamics," The MacNeal-Schwendler Corp. Report MSR-36, May 1973, Chapter 3.

4. C. E. Fortescue, "Method of Symmetrical Coordinates Applied to the Solution of Polyphase Networks," AIEE Transactions, Vol. 37, Part II, pp 1027-1140, 1918.

5. R. W. Hamming, Numerical Methods for Scientists and Engineers, McGraw-Hill Book Company, pp 67-78, 1962.

6. R. H. MacNeal (ed.), "The NASTRAN Theoretical Manual (Level 15)," NASA SP-221(01), April 1972.

7. "Analysis of a Solid Rocket Motor Cavity," The MacNeal-Schwendler Corporation Report MS-220, November 22, 1972.

	L and R Half-Segment Model	S and A Half-Segment Model	Dihedral Transform Model
Side 1 Even Comp	$u^{n+1,R} = u^{n,L}$	$u^{n+1,S} + u^{n+1,A} = u^{n,S} - u^{n,A}$	$u^{o,A} = -su^{kc,S} + cu^{ks,A} =$ $-su^{ks,S} - cu^{kc,A} = u^{N/2,S} = 0$
Side 1 Odd Comp	$u^{n+1,R} = -u^{n,L}$	$u^{n+1,S} + u^{n+1,A} = -u^{n,S} + u^{n,A}$	$u^{o,S} = cu^{kc,S} + su^{ks,A} =$ $cu^{ks,S} - su^{kc,A} = u^{N/2,A} = 0$
Side 2 Even Comp	$u^{n,L} = u^{n,R}$	$u^{n,A} = 0$	$\bar{u}^{o,A} = \bar{u}^{kc,A} = \bar{u}^{ks,A} = \bar{u}^{N/2,A} = 0$
Side 2 Odd Comp	$u^{n,L} = -u^{n,R}$	$u^{n,S} = 0$	$\bar{u}^{o,S} = \bar{u}^{kc,S} = \bar{u}^{ks,S} = \bar{u}^{N/2,S} = 0$

where $c = \cos k\pi/N$, $s = \sin k\pi/N$

Table 1. Boundary Compatibility Constraints for the Case of Dihedral Symmetry

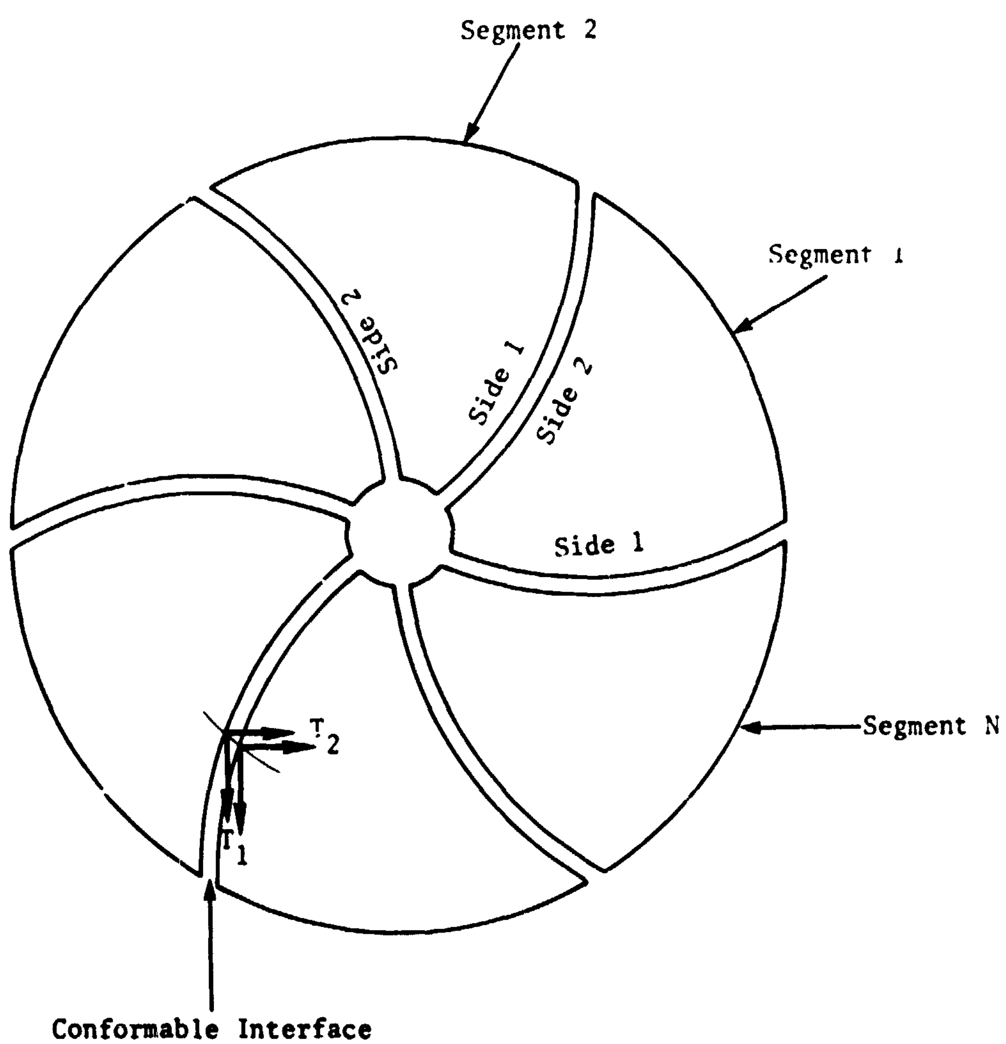

1. The user models one segment.
2. Each segment has its own coordinate system which rotates with the segment.
3. Segment boundaries may be curved surfaces. The local displacement coordinate systems must conform at the joining points. The user gives a paired list of points on Side 1 and Side 2 which are to be joined.

Figure 1. Rotational Symmetry

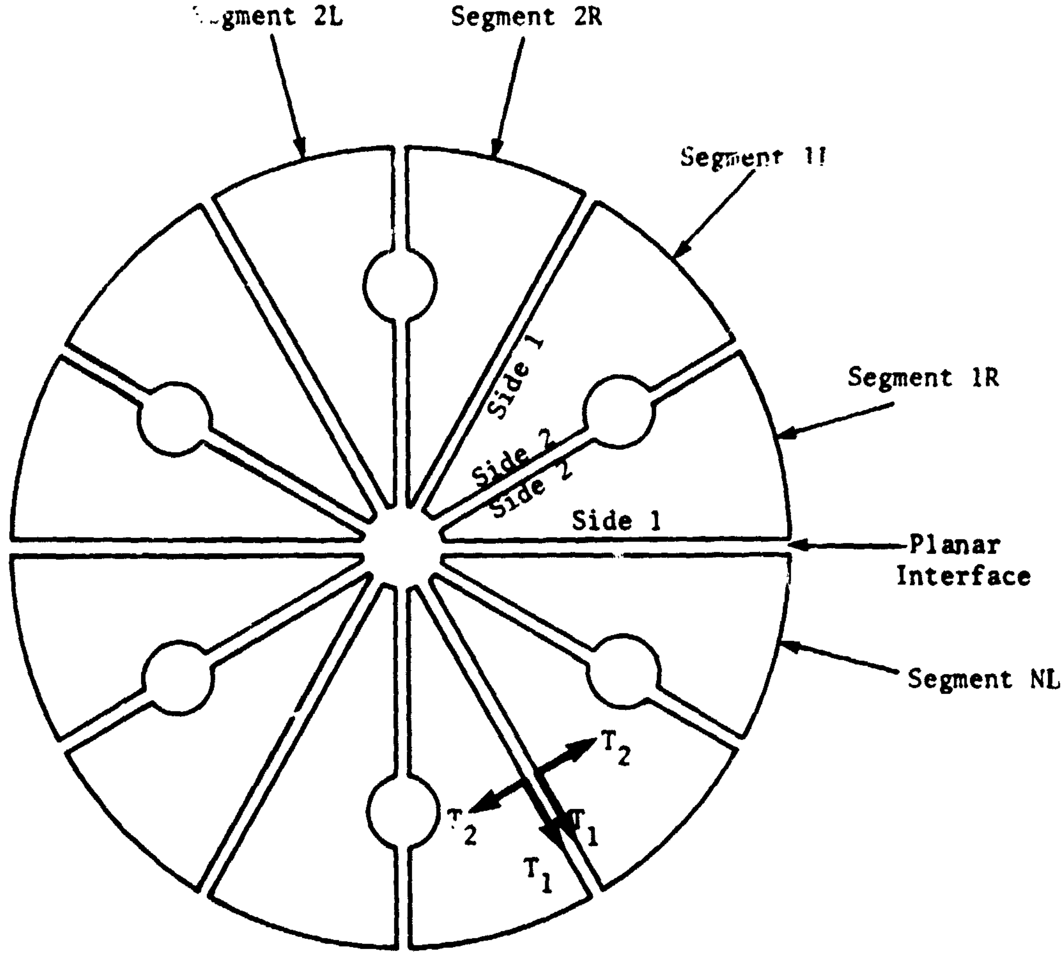

1. The user models one-half segment (an R segment). The L half segments are mirror images of the R half segments.
2. Each half segment has its own coordinate system which rotates with the segment. The L half segments use left hand coordinate systems.
3. Segment boundaries must be planar. Local displacement systems axes, associated with intersegment boundaries, must be in the plane or normal to the plane. The user lists the points on Side 1 and Side 2 which are to be joined.

Figure 2. Dihedral Symmetry

Input Data Card SPCD

Description: Defines an enforced displacement value for static analysis, which is requested as a LØAD.

Format and Example:

1	2	3	4	5	6	7	8	9	10
SPCD	SID	G	C	D	G	C	D		
SPCD	100	32	436	-2.6	5		+2.9		

Field	Contents
SID	Identification number of a static load set. (Integer > 0)
G	Grid or scalar point identification number (Integer > 0)
C	Component number (6 ≥ Integer ≥ 0 ; up to six unique such digits may be placed in the field with no imbedded blanks)
D	Value of enforced displacement for all coordinates designated by G and C (Real)

Remarks:

1. A coordinate referenced on this card must be referenced by an SPC or SPC1 data card.
2. Values of D will override to values specified on an SPC Bulk Data card, if the LØAD set is requested.
3. The Bulk Data LØAD combination card will *not* request an SPCD.
4. At least one Bulk Data load card (FØRCE, SLØAD, etc.) is required in the load set selected in case control.

Figure 3. SPCD Bulk Data Card Format

Input Data Card CYJØIN

Description: Defines boundary points of segments in cyclic symmetry problems.

Format and Example:

1	2	3	4	5	6	7	8	9	10
CYJØIN	SIDE	C	G1	G2	G3	G4	G5	G6	abc
CYJØIN	1		7	9	16	25	33	64	ABC

+bc	G7	G8	G9	-etc.-					
+BC	72								

Alternate Form

CYJØIN	SIDE	C	GID1	"THRU"	GID2				
CYJØIN	2	5	6	THRU	32				

Field	Contents
SIDE	Side Identification (Integer 1 or 2)
C	Coordinate System (BCD R,C or S or blank)
Gi,GIDi	Grid or scalar point identification numbers (Integer > 0)

Remarks:

1. CYJØIN Bulk Data cards are only used for cyclic symmetry problems. A parameter (CTYPE) must specify rotational or dihedral symmetry.

2. For rotational problems there must be one logical card for SIDE=1 and one for SIDE=2. The two lists specify grid points to be connected, hence both lists must have the same length.

3. For dihedral problems, side 1 refers to the boundary between segments and side 2 refers to the middle of a segment. A coordinate system must be referenced in field 3, where R = rectangular, C = cylindrical, and S = spherical. If a rectangular system is chosen, the 1 and 3 axes must lie in the boundary plane.

4. All components of displacement at boundary points are connected to adjacent segments, except those constrained by SPC, MPC, or ØMIT.

Figure 4. CYJØIN Bulk Data Card Format

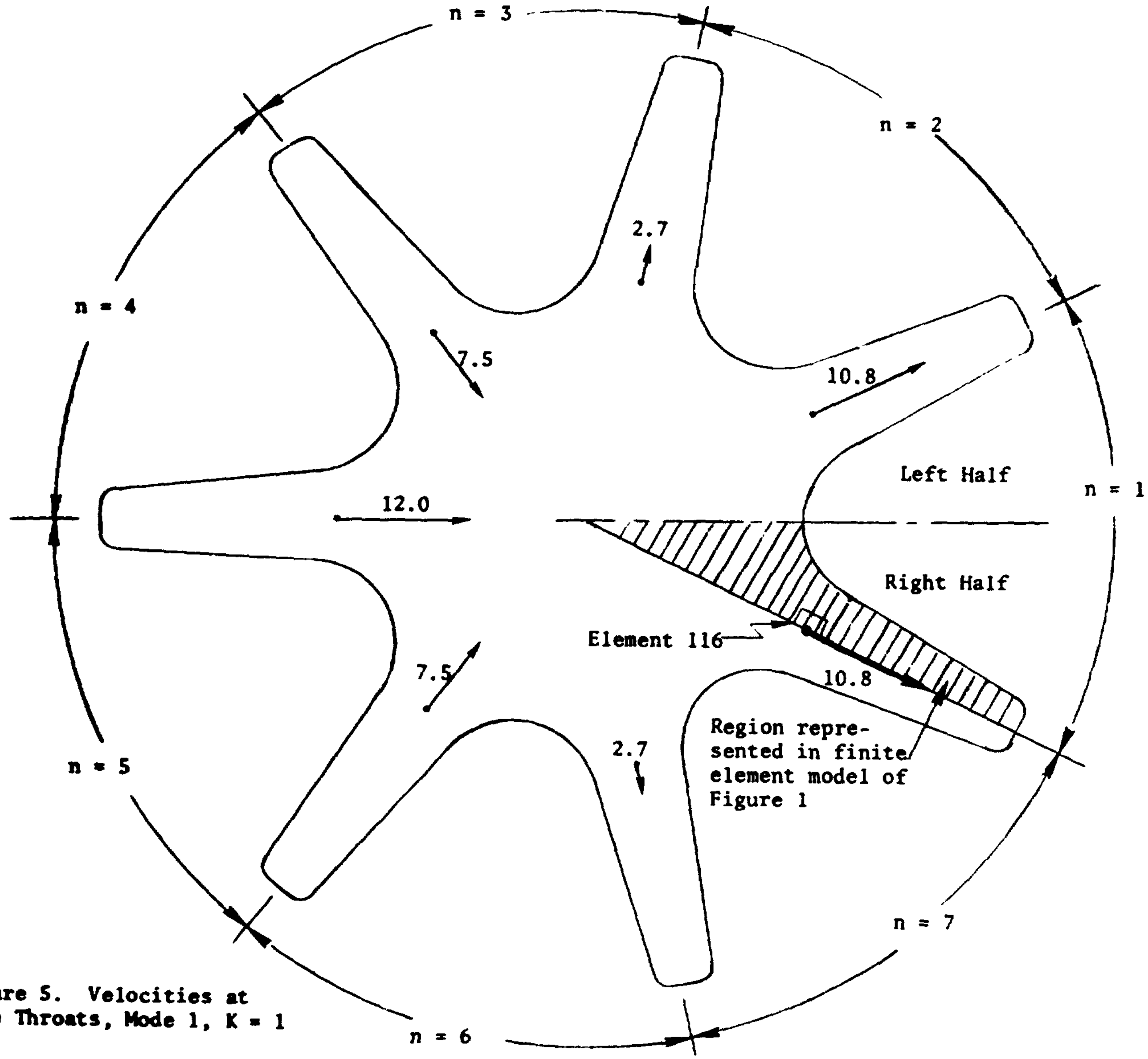

Figure 5. Velocities at Lobe Throats, Mode 1, K = 1

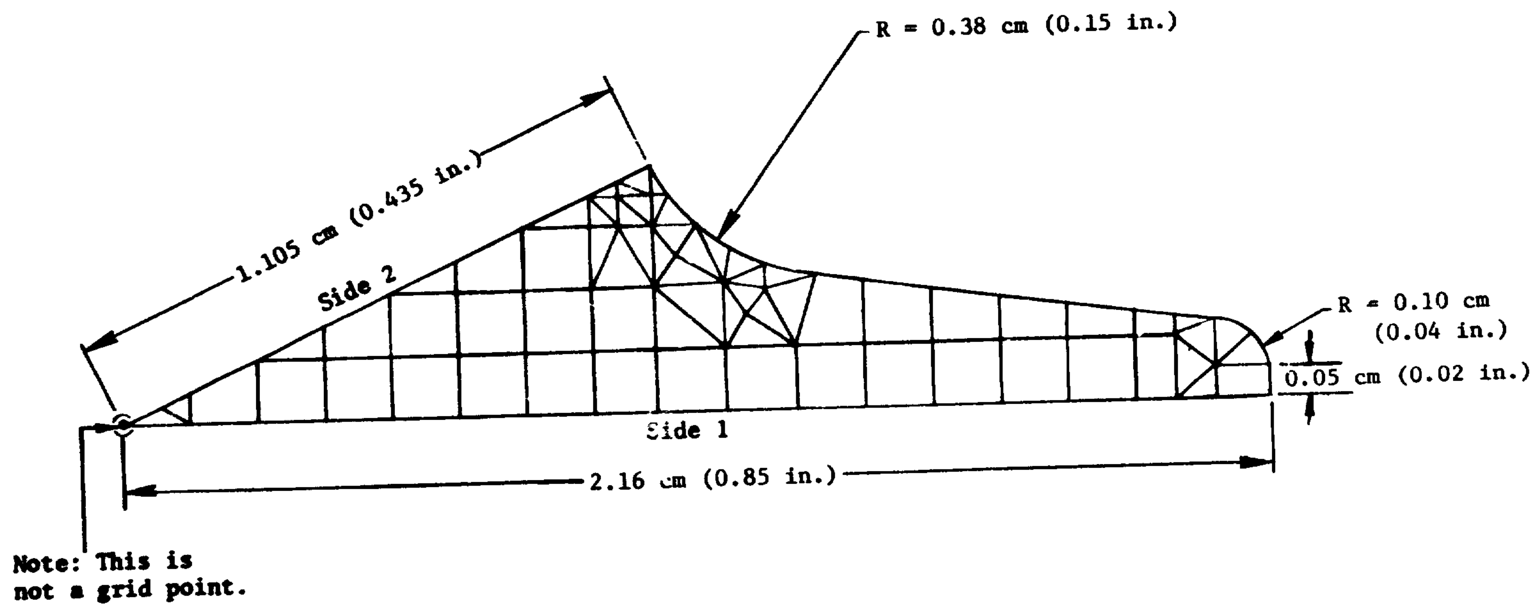

Figure 6. Finite Element Model
1/14 Sector of Cross Section

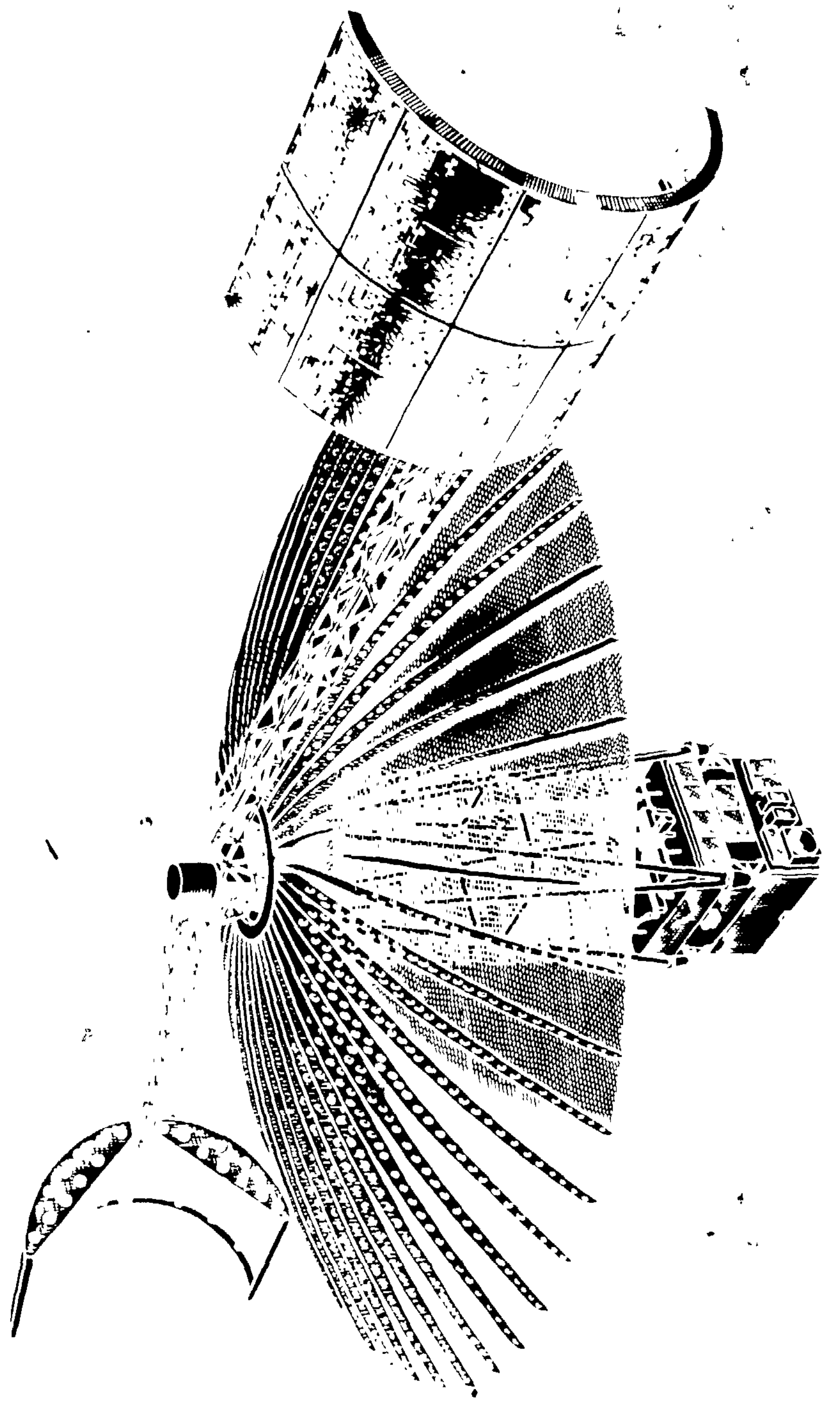

Figure 7. ATS-F Spacecraft with 30-ft Parabolic Reflector

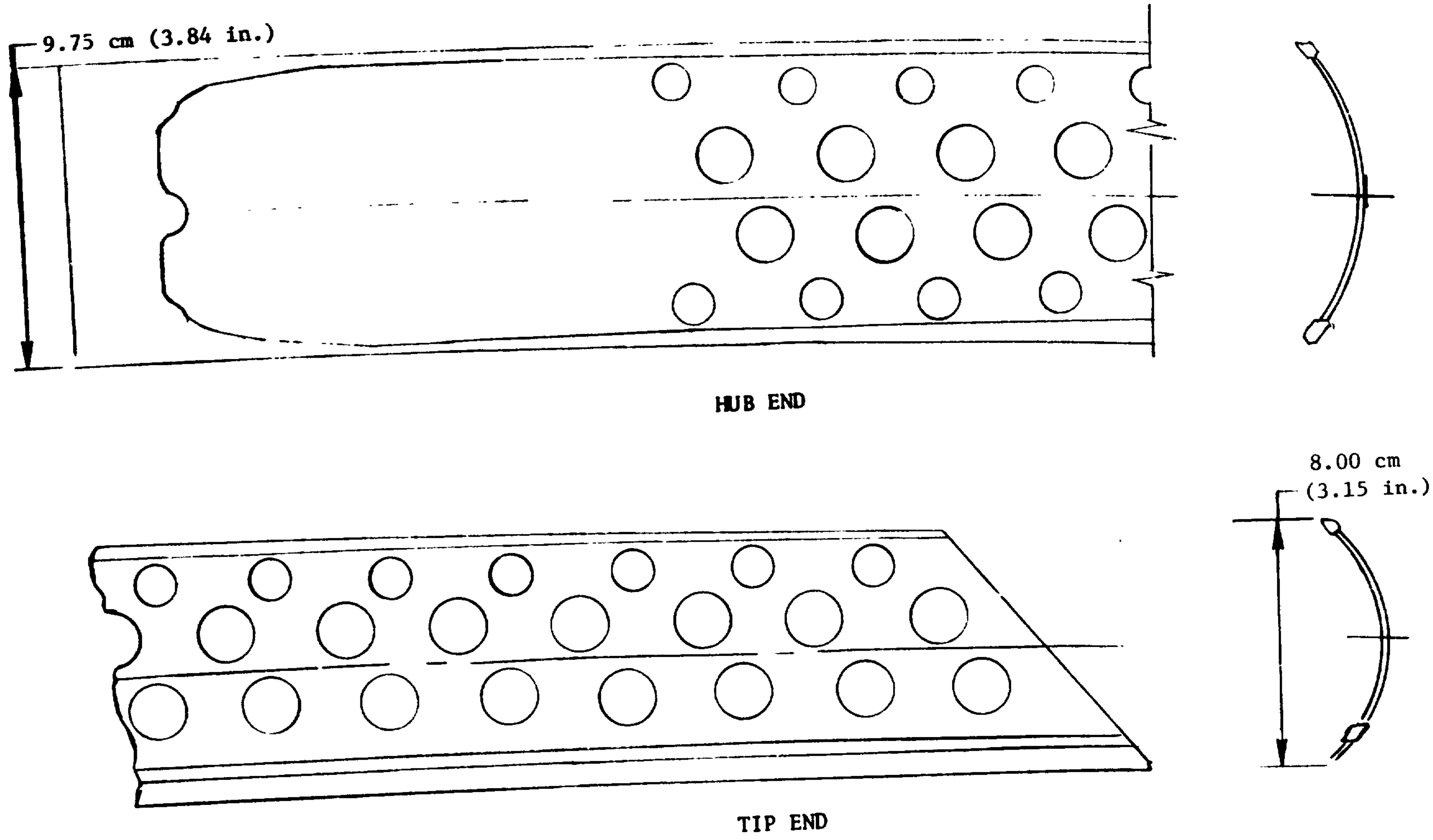

Figure 8. ATS-F Antenna Rib (Typ.)

N74-14665

THREE ISOPARAMETRIC SOLID ELEMENTS FOR NASTRAN

By Stephen E. Johnson and Eric I. Field

Universal Analytics, Inc.
Los Angeles, California

SUMMARY

Linear, quadratic, and cubic isoparametric hexahedral solid elements have been added to the element library of NASTRAN. These elements are available for static, dynamic, buckling, and heat-transfer analyses. Because the isoparametric element matrices are generated by direct numerical integration over the volume of the element, variations in material properties, temperatures, and stresses within the elements are represented in the computations. In order to compare the accuracy of the new elements, three similar models of a slender cantilever were developed, one for each element. All elements performed well. As expected, however, the linear element model yielded excellent results only when shear behavior predominated. In contrast, the results obtained from the quadratic and cubic element models were excellent in both shear and bending.

INTRODUCTION

New aerospace vehicle concepts, such as the Space Shuttle, have added impetus for the continued updating of NASTRAN with the best state-of-the-art finite element technology. In response to this need, the three-dimensional family of linear, quadratic, and cubic isoparametric hexahedral solid elements were developed for and installed in NASTRAN. These three new elements significantly improve NASTRAN's capability to solve any three-dimensional solid problem requiring static, dynamic, buckling, and/or heat-transfer analysis.

THEORETICAL BACKGROUND

Hexahedron solid isoparametric elements may be used to analyze any three-dimensional continuum composed of isotropic or anisotropic materials. Examples include thick inserts in rocket engine nozzles, thermal protection system insulations, soil structure interaction problems, and geometrically complex thick-walled mechanical components such as pumps, valves, etc. These solid elements have only three degrees of freedom at each grid point (the three displacement components), and they may be combined with all other nonaxisymmetric NASTRAN elements.

The isoparametric solid elements were first presented by Irons, Ergatoudis and Zienkiewicz [Refs. 1 to 4]. Isoparametric solid elements employing either eight, twenty or thirty-two grid points have been found to be suitable to solve most problems (Figure 1). These elements correspond to assuming a linear, quadratic, and cubic variation of displacement, respectively. Clough [Ref. 5] conducted an evaluation of three-dimensional solid elements and showed that the isoparametric elements were superior to other solid elements. He further

PRECEDING PAGE BLANK NOT FILMED

pointed out that the choice of which isoparametric element is best to use depends on the type of problem being solved. For problems involving shear and bending type deformations, the higher order elements are preferred over the linear elements which should be used for problems in which shear stresses predominate. It is for this reason that all three isoparametric elements have been incorporated into NASTRAN.

The governing equations for isoparametric elements are based on minimum energy principles. The derivation of these equations assumes a displacement function over the element which depends on grid point displacements only. The governing equations are obtained by minimizing the Potential Energy which is evaluated in terms of these displacement functions.

Displacement Functions

The name isoparametric is derived from the fact that the interpolating or shape functions used to represent the deformation of the element are also used to represent the geometry of the element. This choice insures that the element displacement functions satisfy the criteria necessary for convergence of the finite element analysis [Ref. 4]. Referring to the curvilinear coordinates (ξ,η,ζ) shown in Figure 1, the rectangular basic x,y,z coordinates at any point in the element are obtained from the NASTRAN basic coordinates at each of the n grid points by:

$$\begin{Bmatrix} x \\ y \\ z \end{Bmatrix} = \sum_{i=1}^{n} N_i \ (\xi,\eta,\zeta) \begin{Bmatrix} x \\ y \\ z \end{Bmatrix}_i \tag{1}$$

where the $N_i(\xi,\eta,\zeta)$ are shape functions which depend on the number of grid points used to define the element geometry. The N_i functions are either linear quadratic, or cubic, and correspond to employing two, three, or four grid points respectively, along each edge of the element. This choice insures that there are no geometric gaps between grid points. Expressions for the shape functions may be found in Reference 6.

The deformation of the element is represented with the identical interpolating functions used to define the geometry; that is:

$$\begin{Bmatrix} u \\ v \\ w \end{Bmatrix} = \sum_{i=1}^{n} N_i \ (\xi,\eta,\zeta) \begin{Bmatrix} u \\ v \\ w \end{Bmatrix}_i \tag{2}$$

where u, v and w are displacements along the x, y and z basic coordinate axes. The displacement functions $N_i(\xi,\eta,\zeta)$ satisfy the required convergence criterion of adequately representing a constant strain state, and insure interelement compatibility along the complete element boundary [Ref. 4].

Strain-Displacement Relations

Equation (2) may be used in the well-known strain-displacement relations for a three-dimensional continuum [Ref. 7] to define the strain vector $\{\varepsilon\}$ in terms of the grid point displacements:

$$\{\varepsilon\} = \left[C_1 \;\vdots\; C_2 \;\vdots\; \cdots \;\vdots\; C_n \right] \begin{Bmatrix} u_1 \\ v_1 \\ w_1 \\ \hdashline \vdots \\ \hdashline u_n \\ v_n \\ w_n \end{Bmatrix} = [C]\,\{u_e\} \tag{3}$$

where

$$[C_i] = \begin{bmatrix} \frac{\partial N_i}{\partial x} & 0 & 0 \\ 0 & \frac{\partial N_i}{\partial y} & 0 \\ 0 & 0 & \frac{\partial N_i}{\partial z} \\ \frac{\partial N_i}{\partial y} & \frac{\partial N_i}{\partial x} & 0 \\ 0 & \frac{\partial N_i}{\partial z} & \frac{\partial N_i}{\partial y} \\ \frac{\partial N_i}{\partial z} & 0 & \frac{\partial N_i}{\partial x} \end{bmatrix} \tag{4}$$

In order to evaluate the strain matrix [C], the derivatives of the shape functions N_i with respect to x, y, and z must be calculated. Since N_i is defined in terms of ξ, η and ζ, it is necessary to use the relation that

$$\begin{Bmatrix} \frac{\partial N_i}{\partial x} \\ \frac{\partial N_i}{\partial y} \\ \frac{\partial N_i}{\partial z} \end{Bmatrix} = [J]^{-1} \begin{Bmatrix} \frac{\partial N_i}{\partial \xi} \\ \frac{\partial N_i}{\partial \eta} \\ \frac{\partial N_i}{\partial \zeta} \end{Bmatrix} \tag{5}$$

where [J] is the Jacobian matrix. It is easily evaluated by noting that

$$[J] = \begin{bmatrix} \frac{\partial x}{\partial \xi} & \frac{\partial y}{\partial \xi} & \frac{\partial z}{\partial \xi} \\ \frac{\partial x}{\partial \eta} & \frac{\partial y}{\partial \eta} & \frac{\partial z}{\partial \eta} \\ \frac{\partial x}{\partial \zeta} & \frac{\partial y}{\partial \zeta} & \frac{\partial z}{\partial \zeta} \end{bmatrix} = \begin{bmatrix} \frac{\partial N_1}{\partial \xi}, & \frac{\partial N_2}{\partial \xi}, & \cdots & \frac{\partial N_n}{\partial \xi} \\ \frac{\partial N_1}{\partial \eta}, & \frac{\partial N_2}{\partial \eta}, & \cdots & \frac{\partial N_n}{\partial \eta} \\ \frac{\partial N_1}{\partial \zeta}, & \frac{\partial N_2}{\partial \zeta}, & \cdots & \frac{\partial N_n}{\partial \zeta} \end{bmatrix} \begin{bmatrix} x_1 & y_1 & z_1 \\ x_2 & y_2 & z_2 \\ \vdots & \vdots & \vdots \\ x_n & y_n & z_n \end{bmatrix} \qquad (6)$$

where the subscripts 1, 2, ... n denote the n grid points of an element.

Stress-Strain Relations

The stress-strain relations for a general elastic material are

$$\{\sigma\} = [G_e] \{\varepsilon - \varepsilon_t\} \qquad (7)$$

where $\{\sigma\}$ is the 6x1 stress vector in the basic coordinate system, $[G_e]$ is a 6x6 symmetric elastic material matrix, and $\{\varepsilon_t\}$ is the 6x1 thermal strain vector. This thermal strain vector is defined as

$$\{\varepsilon_t\} = \{\alpha_e\} \cdot \sum_{i=1}^{n} N_i \ (\xi,\eta,\zeta) \ T_i \qquad (8)$$

where $\{\alpha_e\}$ is a vector of 6 thermal expansion coefficients, and T_i is the temperature at the i^{th} element grid point.

Stiffness, Mass, and Load Matrices

The stiffness, mass, and load matrices for the isoparametric element are derived by application of the Principle of Virtual Work. These element matrices, relative to the basic coordinate system, are given by

$$[K_{ee}] = \int_{-1}^{+1} \int_{-1}^{+1} \int_{-1}^{+1} [C]^T \ [G_e] \ [C] \ |J| \ d\xi \ d\eta \ d\zeta \qquad (9)$$

$$[M_{ee}] = \int_{-1}^{+1} \int_{-1}^{+1} \int_{-1}^{+1} \rho [N]^T \ [N] \ |J| \ d\xi \ d\eta \ d\zeta \qquad (10)$$

$$\{P_e^t\} = \int_{-1}^{+1}\int_{-1}^{+1}\int_{-1}^{+1} [C]^T\ [G_e]\ \{\alpha_e\}\ |J| \left(\sum_{i=1}^{n} N_i\ T_i\right) d\xi\ d\eta\ d\zeta \qquad (11)$$

$$\{P_e^P\} = -\int_{-1}^{+1}\int_{-1}^{+1} P_{-\zeta}\ [N(\xi,\eta,-1)]^T\ |J|\ \{J_\zeta^{-1}\}\ d\xi\ d\eta$$

$$-\int_{-1}^{+1}\int_{-1}^{+1} P_{-\eta}\ [N(\xi,-1,\zeta)]^T\ |J|\ \{J_\eta^{-1}\}\ d\xi\ d\zeta$$

$$\vdots$$

$$+\int_{-1}^{+1}\int_{-1}^{+1} P_{+\zeta}\ [N(\xi,\eta,+1)]^T\ |J|\ \{J_\zeta^{-1}\}\ d\xi\ d\eta \qquad (12)$$

where $[K_{ee}]$ is the element stiffness matrix in the basic coordinate system, $[M_{ee}]$ is the mass matrix, $\{P_e^t\}$ is the thermal load vector, and $\{P_e^P\}$ is the pressure load vector derived from surface pressures on each of the six faces of the solid element. $|J|$ is the determinant of the Jacobian matrix, and $[N]$ is a matrix of the isoparametric shape function defined by

$$[N] = \left[\begin{array}{ccc|ccc|c|ccc} N_1 & 0 & 0 & N_2 & 0 & 0 & & N_n & 0 & 0 \\ 0 & N_1 & 0 & 0 & N_2 & 0 & \cdots & 0 & N_n & 0 \\ 0 & 0 & N_1 & 0 & 0 & N_2 & & 0 & 0 & N_n \end{array}\right] \qquad (13)$$

$P_{-\zeta}$ is the uniform normal pressure (positive outward) applied to the face of the element where $\zeta = -1$; $P_{-\eta}$ is the pressure applied to the face where $\eta = -1$, etc.; and $\{J_\xi^{-1}\}$, $\{J_\eta^{-1}\}$, and $\{J_\zeta^{-1}\}$ are the first, second, and third columns, respectively, of the inverse of the Jacobian matrix. Products like $|J|\ \{J_\xi^{-1}\}$ in the expression for pressure load are equivalent to a vector of direction cosines multiplied by a surface area scaling factor relating the curvilinear coordinates to the basic coordinate system.

The integrals in equations (9) to (12) are evaluated numerically by using the method of Gaussian Quadrature [Ref. 8]. In the above equations, therefore, $[C]$, $|J|$, and $[N]$ must be evaluated at each interior point used for numerical integration. $[G_e]$, $\{\alpha_e\}$, and ρ can also be evaluated at each integration point. Thus, variations in these quantities are allowed because of, say, temperature-dependent material.

The computations for the isoparametric elements are carried out in the basic coordinate system. If the global coordinate system at any grid point is different from the basic system, the final matrices and vectors are transformed into that global system.

Stress Recovery

The equation for calculating element stresses at any interior point of an isoparametric element may be obtained by combining equations (3), (7), and (8) as follows:

$$\{\sigma\} = [G_e]\left([C]\{u_e\} - \{\alpha_e\}\cdot\left(\sum_{i=1}^{n} N_i\ T_i\right)\right) \tag{14}$$

$[C]$ and N_i are functions of the element curvilinear coordinates ξ,η,ζ evaluated at the point at which stresses are desired.

Differential Stiffness Matrix

The differential stiffness matrix for the isoparametric solid element is derived by adding the energy of an initial stress state to the potential energy function. This additional energy is derived in Reference 9 and is given by

$$W_p = \frac{1}{2}\int_V \Big[\omega_x^2(\sigma_y + \sigma_z) + \omega_y^2(\sigma_x + \sigma_z) + \omega_z^2(\sigma_x + \sigma_y) - 2\,\omega_x\,\omega_y\,\tau_{xy} - 2\,\omega_y\,\omega_z\,\tau_{yz} - 2\,\omega_z\,\omega_x\,\tau_{zx}\Big]dV \tag{15}$$

where the rotations are given by the relations

$$\left.\begin{aligned} \omega_x &= \frac{1}{2}\left(\frac{\partial w}{\partial y} - \frac{\partial v}{\partial z}\right) \\ \omega_y &= \frac{1}{2}\left(\frac{\partial u}{\partial z} - \frac{\partial w}{\partial x}\right) \\ \omega_z &= \frac{1}{2}\left(\frac{\partial v}{\partial x} - \frac{\partial u}{\partial y}\right) \end{aligned}\right\} \tag{16}$$

These rotations may be expressed in terms of the grid point displacements by using equation (1):

$$\begin{Bmatrix} \omega_x \\ \omega_y \\ \omega_z \end{Bmatrix} = \left[\bar{C}_1 \;\vdots\; \bar{C}_2 \;\vdots\; \cdots\cdots \;\vdots\; \bar{C}_n\right]\{u_e\} = [\bar{C}]\{u_e\} \tag{17}$$

where

$$[\bar{C}_i] = \frac{1}{2}\begin{bmatrix} 0 & -\frac{\partial N_i}{\partial z} & \frac{\partial N_i}{\partial y} \\ \frac{\partial N_i}{\partial z} & 0 & -\frac{\partial N_i}{\partial x} \\ -\frac{\partial N_i}{\partial y} & \frac{\partial N_i}{\partial x} & 0 \end{bmatrix} \quad (18)$$

Substituting equation (17) into equation (15) and adding this function to the potential energy expression yields the differential stiffness matrix:

$$[K^d_{ee}] = \int_{-1}^{+1}\int_{-1}^{+1}\int_{-1}^{+1} [\bar{C}]^T \begin{bmatrix} \sigma_y + \sigma_z & -\tau_{xy} & -\tau_{zx} \\ -\tau_{xy} & \sigma_x + \sigma_z & -\tau_{zy} \\ -\tau_{zx} & -\tau_{zy} & \sigma_x + \sigma_y \end{bmatrix} [\bar{C}]\ |J|\ d\xi\ d\eta\ d\zeta \quad (19)$$

As with the structural stiffness matrix, this integral is evaluated using the method of Gaussian Quadrature. The differential stiffness is computed in the basic coordinate system and then transformed, as required, to the NASTRAN global system.

IMPLEMENTATION

Many existing NASTRAN functional modules and subroutines were modified to implement the isoparametric solid elements. Several new subroutines were also added. These modules and brief descriptions of the changes to each are listed in Table 1. The detailed description of these changes presented in Reference 10 can be used to augment the NASTRAN Programmer's Manual instructions, Section 6.8, to assist in the installation of other new elements of similar complexity. Many of the changes are those normally required when implementing new elements. However, in this case, changes were also required in the PLØT module (to plot three-dimensional elements), the GP3 module (to process a new external pressure load). and in various other modules to accommodate the large space requirements of the 32-grid-point cubic element.

It should be noted that the isoparametric elements were installed in functional modules SMA1, SMA2, and DSMG1 on an interim basis only. The element matrix subroutines were designed specifically for the new Element Matrix Generator module and will be made available with Level 16 of NASTRAN.

EVALUATION

A slender cantilever beam model was chosen to evaluate the performance of the three new isoparametric solid elements in NASTRAN. This model was chosen for two reasons: (1) theoretical solutions are well known, and (2) solid finite elements characteristically do not perform well when used to model structures which exhibit predominant bending behavior.

Three models were prepared as shown in Figures 2, 3, and 4, one with each of the three elements: IHEX1, IHEX2, and IHEX3, the linear, quadratic, and cubic elements, respectively. All three beam models had a length (L) of 3.66m (144 in.) and a uniform rectangular cross section with depth (D) of 0.61m (24 in.) and width (W) of 0.30m (12 in.). The same uniform material properties shown in Table 2 were used for all three models. Static, normal modes, and buckling analyses were performed for each of the beam models.

Statics

For the static analyses, all degrees of freedom at the base of the beam (z = 0) were completely fixed. All three models were subjected to the same four loading conditions:

1. Linear thermal gradient (Y-direction)
   $T = 322.04$ K at $Y = 0$ (120° F at $Y = 0$)
   $T = 188.71$ K at $Y = 0.61$m (-120° F at $Y = 24$ in.)
2. Uniform temperature rise
   $\Delta T = 55.56$ K (100° F)
3. Compressive axial pressure (Z-direction)
   $P_Z = -2.954 \times 10^8$ N/m^2 at $Z = 3.66$m (-42837 psi at $Z = 144$ in.)
4. Transverse pressure (Y-direction)
   $P_Y = 6.895 \times 10^5$ N/m^2 at $Y = 0$ (100 psi at $Y = 0$)

The results for the tip displacements are summarized in Table 3, where the computed solutions are compared with the theoretical solutions. The maximum error for the linear IHEX1 element was 10.3% for the transverse pressure load. For the quadratic and cubic elements, IHEX2 and IHEX3, the maximum errors of 4.5% and 3.5%, respectively, occurred in the solutions for the thermal gradient load. For the transverse pressure load, the errors were 1.6% for the IHEX2 element model, and 1.1% for IHEX3. Thus, the higher order isoparametric solid elements perform very well when used to model the bending behavior of this beam.

Normal Modes

In the normal mode analyses, the same single point constraints were applied to all three models in the following manner: All Z components of displacement in the plane Z = 0 and all Y components along the line Z = 0, Y = 0.30m (12 in.), were fixed. For the IHEX1 and IHEX3 models only, all X components along the line Z = 0, X = 0, were fixed. For the IHEX2 model only, the X components along the line Z = 0, X = -0.15m (6 in.), were fixed. This system of constraints was chosen to allow dilatation at the base of the beam. The particular set of constraints used for the IHEX2 model has the additional advantage of symmetry.

The inverse power method was used to extract the first three normal modes of each model. The results for the natural frequencies are summarized in Table 4. The computed natural frequencies for the IHEX2 and IHEX3 models are within 3.0 per cent of the theoretical solution. The natural frequency for the IHEX1 model is 2.7% off for bending in the Y-direction, but it is off by 18.3% and 15.8% for the two bending modes about the X-direction. These errors are probably caused by an insufficient number of elements through the width of the beam in the X-direction. Using a smaller mesh size with more IHEX1 elements would improve these results at the expense of increased computer costs. This problem, therefore, serves to demonstrate even more clearly the superiority of the IHEX2 and IHEX3 elements over the IHEX1 element for modeling the bending behavior of structures.

All the computed mode shapes for all three models showed excellent correlation with the theoretical solution [Ref. 11]. Comparative plots of the mode shapes are not included in this paper because there would be no visible distinction between computed and theoretical solutions.

Buckling

Each of the three beam models was used to compute the critical buckling load for axial pressure. The same system of constraints used to compute normal modes was used to compute the axial pressure buckling load. The applied pressure on the end of the beam was -2.954×10^8 N/m^2 (42,837 psi). This amounts to a total applied force of -5.406×10^7 N (-1.234×10^7 lb), which is equal to the theoretical critical load for buckling in the X-direction. Therefore, the fundamental eigenvalue for buckling should have been unity.

Again, the inverse power method was used to extract the three lowest buckling modes. The results for the buckling eigenvalues λ are presented in Table 5. The IHEX2 and IHEX3 element results are excellent. They are within 0.7% of the theoretical solution. The eigenvalue for the IHEX1 element model is in error by less than 10% for buckling in the Y-direction. However, it is off by more than 40% for both buckling modes in the X-direction. This situation is similar to that of the normal mode problem for the IHEX1 element model. Again, it is probably due to the lack of an adequate number of elements through the width of the beam in the X-direction.

As was the case for the normal modes problem, the mode shapes computed by NASTRAN for buckling were very close to the theoretical shapes. Thus, no plots comparing computed shapes with theoretical shapes are included in this paper.

CONCLUDING REMARKS

All three isoparametric solid elements produced good results for static, normal mode, and buckling analyses. As expected, the linear element results showed that it is best used when shear behavior predominates. The superiority of the quadratic and cubic elements was confirmed by the excellent results obtained in both the bending and the shear behavior of a cantilever beam model. Therefore, the implementation of these three isoparametric solid elements, which provide for variations in both material properties and stresses throughout the element, does greatly enhance the total modeling capability of NASTRAN.

REFERENCES

1. B. M. Irons, "Engineering Application of Numerical Integration in Stiffness Methods," AIAA J. 4, pp. 2035-2037, November 1966.

2. B. M. Irons and O. C. Zienkiewicz, "The Iso-Parametric Element System - A New Concept in Finite Element Analysis," Conf. Recent Advances in Stress Analysis, J.B.C.S.A., Royal Aero. Soc., London, 1968.

3. I. Ergatoudis, "Quadrilateral Elements in Plane Analysis and Introduction to Solid Analysis," M.Sc. Thesis, University of Wales, Swansen, 1966.

4. I. Ergatoudis, B. M. Irons, and O. C. Zienkiewicz, "Curved, Isoparametric, 'Quadrilateral' Elements for Finite Element Analysis," Int. J. Solids Struct., Vol. 4, pp. 31-42, 1968.

5. R. W. Clough, "Comparison of Three Dimensional Finite Elements," Symp. Appl. Finite Element Method in Civil Engr., Vanderbilt Univ., Nashville, Tenn., Nov. 1969.

6. O. C. Zienkiewicz, The Finite Element Method in Engineering Science, McGraw-Hill, London, p. 121, 1971.

7. S. Timoshenko and J. N. Goodier, Theory of Elasticity, 2nd Ed., McGraw-Hill, New York, p. 223, 1951.

8. Z. Kopal, Numerical Analysis, 2nd Edition, Chapman and Hill, 1961.

9. R. H. MacNeal, ed., The NASTRAN Theoretical Manual, NASA SP-221(01), April 1972.

10. E. I. Field and S. E. Johnson, Addition of Three-Dimensional Isoparametric Elements to NASA Structural Analysis Program (NASTRAN), NASA CR-112269, Jan. 24, 1973.

11. W. C. Hurty and M. F. Rubinstein, Dynamics of Structures, Prentice-Hall, Inc., Englewood Cliffs, N.J., 1964.

12. S. P. Timoshenko and J. M. Gere, Theory of Elastic Stability, McGraw-Hill, New York, 1961.

TABLE 1. FUNCTIONAL MODULE MODIFICATIONS TO IMPLEMENT ISOPARAMETRIC SOLID ELEMENTS

IFP	-	New Bulk Data cards were added
GP2	-	Array sizes were increased to accommodate elements with 32 grid points
PLTSET	-	Array sizes were increased to accommodate elements with 32 grid points
PLØT	-	Capability for plotting solid elements was implemented
GP3	-	Processing of the isoparametric element pressure card was implemented
TA1	-	Capability to append grid point temperatures to EST/ECPT entries was implemented
SMA1	-	Stiffness and conductance matrix generation for the new elements was implemented
SMA2	-	Mass and capacitance matrix generation for the new elements was implemented
SSG1	-	Load vector generation for thermal and pressure loads on the new elements was implemented
DSMG1	-	Differential stiffness matrix generation for the new elements was implemented
SDR2	-	Stress calculations for individual grid points of the new elements was implemented
ØFP	-	Stress printout formats for the new elements were implemented

TABLE 2. MATERIAL PROPERTIES OF THE CANTILEVER BEAM MODELS

Symbol	Description	Value (SI)	Value (English)
E	Young's modulus	2.068×10^{11} N/m^2	30×10^6 lb/in^2
ν	Poisson's ratio	0.3	0.3
α	Coef. of thermal expansion	$2.570 \times 10^{-5} \frac{m}{m - {}^\circ K}$	$1.428 \times 10^{-5} \frac{in}{in - {}^\circ F}$
ρ	Mass density	20.86 kg/m^3	7.535×10^{-4} lb/in^3

TABLE 3. COMPARISON OF TIP DEFLECTIONS FOR NASTRAN AND THEORETICAL SOLUTIONS FOR FOUR STATIC LOADING CONDITIONS

Load Case	Description	NASTRAN Solutions						Theoretical Solution*
		IHEX1 Model		IHEX2 Model		IHEX3 Model		
		Defl., cm	Error, %	Defl., cm	Error, %	Defl., cm	Error, %	Tip Defl., cm
1	Thermal Gradient	3.668	2.5	3.932	4.5	3.894	3.5	3.762
2	Uniform Temperature	.5367	2.8	.5344	2.3	.5304	1.6	.5222
3	Axial Compression	-.5179	0.8	-.5187	0.7	-.5199	0.4	-.5222
4	Transverse Pressure	.3612	10.3	.3965	1.6	.3985	1.1	.4028

***Theoretical Solutions**

Load Case 1

$$\delta_Y = \frac{\alpha \Delta T L^2}{2D}$$

$\delta_Y = 3.762$ cm

Load Case 2

$$\delta_Z = \alpha \Delta T L$$

$\delta_Y = .5222$ cm

Load Case 3

$$\delta_Z = \frac{P_Z L}{E}$$

$\delta_Y = -.5222$ cm

Load Case 4

$$\delta_Y = \frac{3P_Y L^4}{2ED^3}\left[1 + \frac{4D^2}{5L^2}\right]$$

$\delta_Y = .4028$ cm

TABLE 4. COMPARISON OF NATURAL FREQUENCIES FOR NASTRAN AND THEORETICAL SOLUTIONS

Mode	Description	NASTRAN Solutions						Theoretical Solution, cps [Ref. 11]
		IHEX1 Model		IHEX2 Model		IHEX3 Model		
		Freq., cps	Error, %	Freq., cps	Error, %	Freq., cps	Error, %	
1	First Bending Mode in the X-Direction	22.0	18.3	18.6	0	18.6	0	18.6
2	First Bending Mode in the Y-Direction	38.3	2.7	36.5	2.1	36.5	2.1	37.3
3	Second Bending Mode in the X-Direction	135.3	15.8	114.3	2.1	113.3	3.0	116.8

TABLE 5. COMPARISON OF BUCKLING EIGENVALUES FOR NASTRAN AND THEORETICAL SOLUTIONS

Mode	Description	NASTRAN Solutions						Theoretical Solution λ [Ref. 12]
		IHEX1 Model		IHEX2 Model		IHEX3 Model		
		λ	Error, %	λ	Error, %	λ	Error, %	
1	X-Direction	1.406	40.6	1.002	.2	1.001	.1	1.0
2	Y-Direction	4.391	9.8	3.981	.5	3.979	.5	4.0
3	X-Direction	12.809	42.3	9.037	.4	8.934	.7	9.0

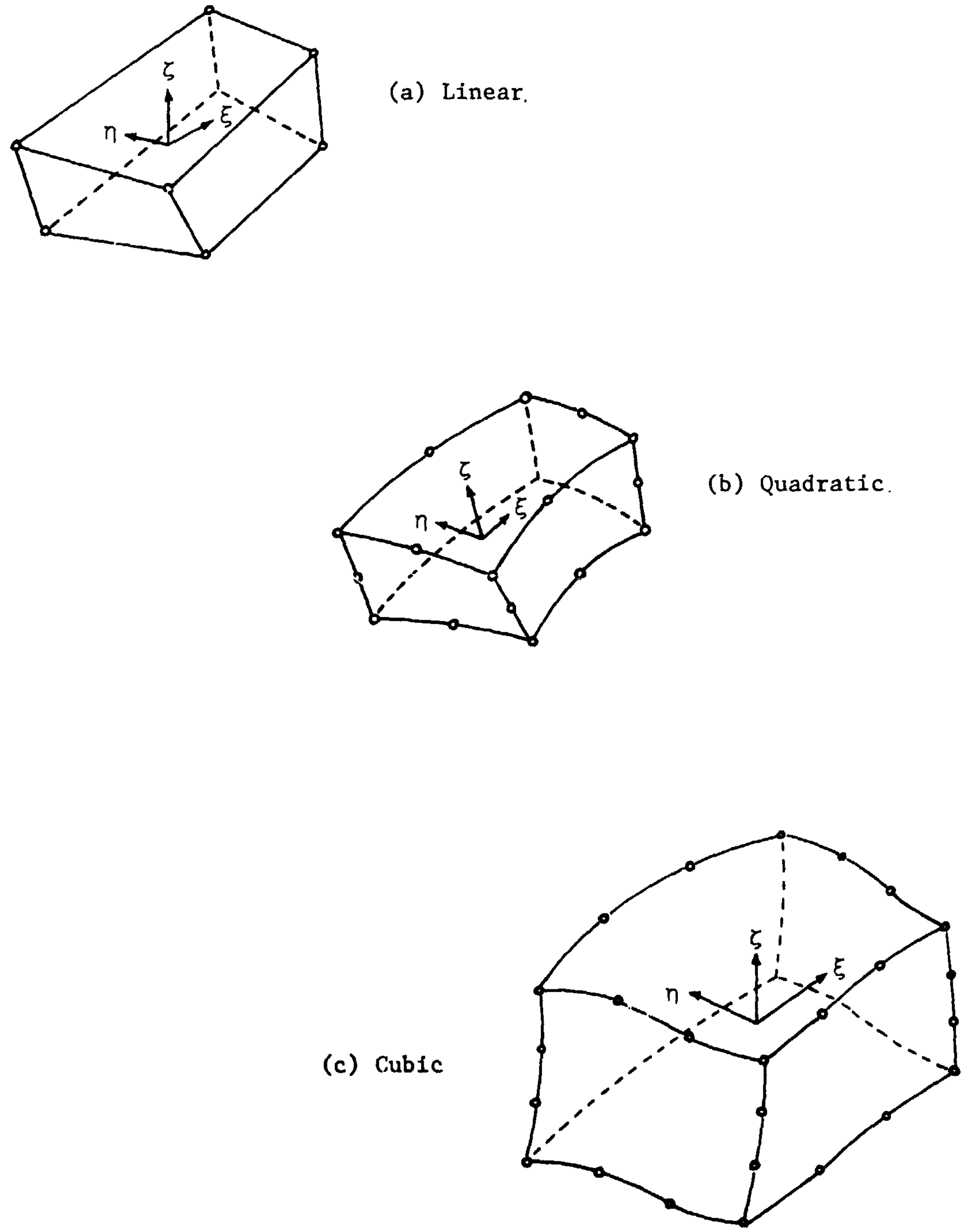

FIGURE 1. THREE ISOPARAMETRIC ELEMENTS

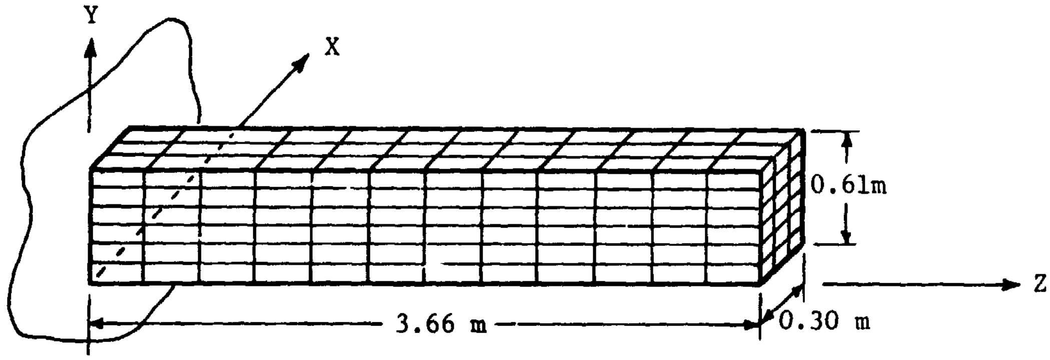

FIGURE 2. IHEX1 MODEL -- 216 ELEMENTS AND 364 GRID POINTS
MATRIX ORDER (g-SET) = 1092, SEMI-BANDWIDTH = 102.

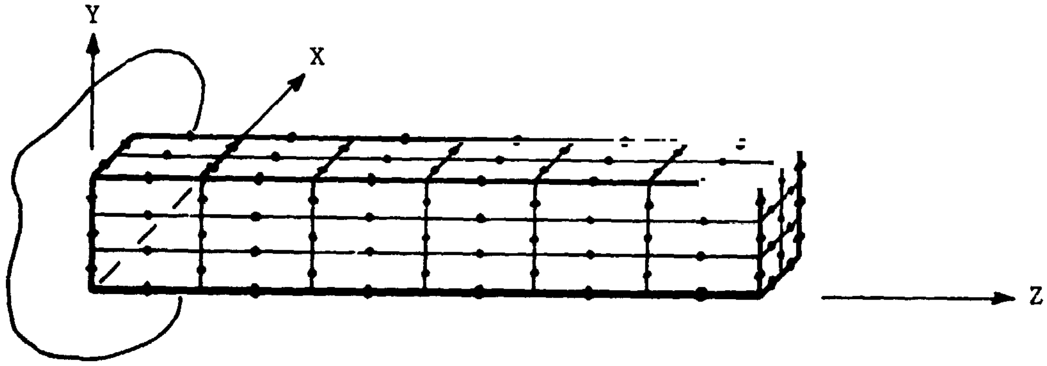

FIGURE 3. IHEX2 MODEL -- 36 ELEMENTS AND 275 GRID POINTS
MATRIX ORDER (g-SET) = 825, SEMI-BANDWIDTH = 156.

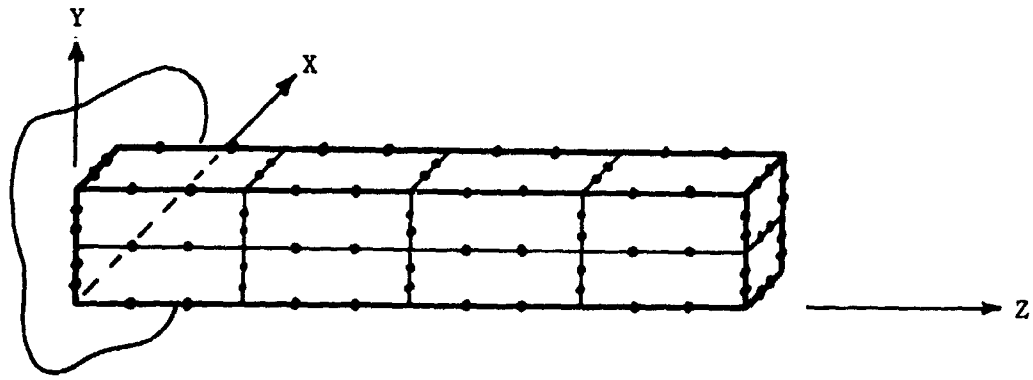

FIGURE 4. IHEX3 MODEL -- 8 ELEMENTS AND 148 GRID POINTS
MATRIX ORDER (g-SET) = 444, SEMI-BANDWIDTH = 132.

PLACING THREE-DIMENSIONAL ISOPARAMETRIC ELEMENTS INTO NASTRAN

By M. B. Newman and A. W. Filstrup

Westinghouse Research and Development Center

SUMMARY

Linear (8 node), parabolic (20 node), cubic (32 node) and mixed (some edges linear, some parabolic and some cubic) have been inserted into NASTRAN, Level 15.1. First the dummy element feature was used to check out the stiffness matrix generation routines for the linear element in NASTRAN. Then, the necessary modules of NASTRAN were modified to include the new family of elements. The matrix assembly was changed so that the stiffness matrix of each isoparametric element is only generated once as the time to generate these higher order elements tends to be much longer than the other elements in NASTRAN. This paper presents some of the experiences and difficulties of inserting a new element or family of elements into NASTRAN.

INTRODUCTION

In solving many structural problems at Westinghouse, it has become apparent that in order to obtain the accuracy required, three-dimensional finite elements would be required. It also became apparent that three-dimensional finite elements based on constant strain tetrahedra like the CTETRA, CWEDGE, CHEXA1 and CHEXA2 elements in NASTRAN are too stiff to give accurate results at a reasonable cost for many problems.

Because of this, a Westinghouse proprietary program, WISEC, was developed for heat conduction and static linear elastic analysis using three dimensional isoparametric elements. Because of the large general purpose capability of NASTRAN, both for types of problems solved and for types of elements used, it was decided to place these elements into NASTRAN.

Even though three-dimensional isoparametric elements were then to be and now have been placed into NASTRAN by Dr. E. I. Field and Mr. S. E. Johnson of Universal Analytics (see Ref. 1), and are to be included in Level 16 NASTRAN now scheduled to be released in 1974, it was decided to place three-dimensional isoparametric elements into Level 15.1 NASTRAN. First we would have use of this element in NASTRAN at an earlier date than we would if we waited until Level 16 was released. Second, we would gain experience and familiarity with NASTRAN which would enable us to more easily make any future modifications which we would desire. A third benefit, which we didn't realize at the time, is the fact that the family of elements we added can have different number of grid or nodal points on the various edges as shown in figure 1. As we understand, Level 16 NASTRAN will have elements which are either linear (2 points on each edge), parabolic (3 points on each edge) or cubic (4 points on each edge). Mixed elements, like that shown in figure 1, can be used to reduce the number of degrees of freedom in portions of the structure not requiring the higher order elements without introducing incompatibilities between adjacent elements. The order of an element is taken to be that of its highest ordered edge.

As the theory of three-dimensional isoparametric elements is explained elsewhere, for instance in Refs. 1 to 4, it will not be repeated here.

At the present time, the stiffness and mass matrices have been successfully inserted and tested. The differential stiffness matrix is due to be added shortly.

The work described in this report was performed with Level 15.1 NASTRAN on an IBM 370-165. It is planned to insert the changes into Level 15.5 NASTRAN on a CDC 6600.

RECOMMENDATIONS

1. For anyone making changes in NASTRAN, an up-to-date Programmer's Manual is of great aid. Unfortunately, the latest available Programmer's Manual is not always for the latest available level of NASTRAN.

2. Many of the tables present in Level 15.1 NASTRAN are too short to permit elements with as many degrees of freedom as the isoparametric elements. These tables should be increased in length to permit easier insertion of new elements.

METHOD AND EXPERIENCES

NASTRAN is an extremely large system comprised of fifteen super links with approximately 850 subprograms whose source statements are on over 200,000 card images. NASTRAN is indeed a very large and complex program and, at first glance, a dense forest that seems too difficult to enter. As one starts to review the large NASTRAN Programmer's Manual (approximately 15 centimeters thick) and examine the materials the authors of NASTRAN have distributed, the forest does not seem as dense. This section of the paper describes our experiences in adding new elements to the NASTRAN system.

The three-dimensional isoparametric elements added presented many problems that the usual NASTRAN elements did not encounter. The tables were much larger, for example. The number of nodes that described our cubic isoparametric element varies from ten to thirty-two nodes. This number forced us to expand the Element Connection and Properties Tables and other array sizes that dealt with nodes. The concept of a variable number of nodes per element was also a departur from the usual NASTRAN practice of a constant number of nodes per element type.

For these higher order elements, the computer time necessary to create the element matrices was quite large; hence, a procedure to create the element matrices once and to save them had to be incorporated into the element level subprograms.

The release we used to incorporate the new elements was level 15.1. The computer used was an IBM 370-165 operating under the ASP system. The Programmer's Manual we had was for Level 12 which caused some difficulty but not too much. We will outline the procedure we used in adding the new elements.

First one should review the materials distributed with the Level 15 system. Figure 2 is a VTOC (Volume Table of Contents) of the distributed system. Pages 5.3-13 and 5.3-14 of the Programmer's Manual (ref. 5) describes each of the data sets of the distributed system. The data sets which are most useful to us are SOU1, the partitioned data set containing the FORTRAN source programs, SUBSYS, also a partitioned data set containing the linkage editor control cards for the fifteen super links of NASTRAN; the partitioned data set OBJ, which contains all the load modules of each individual subroutine of the system; the partitioned data set NSTNLMOD, which contain the fifteen link-edited super links which constitute the NASTRAN executable set.

The next step of the procedure should be to set up a development disk with at least two data sets which we named NEWOBJ and NADEV. NEWOBJ corresponds to OBJ, and NADEV corresponds to NSTNLMOD. It would be advisable to set up a data set corresponding to SOU1 but we elected to keep all of our new source programs in card-deck form. The IBM 370 utility program IEHMOVE or IEBCOPY can be used to move the fifteen link edited links from NSTNLMOD to the development pack. NADEV's initial allocation should be as large as possible as this data set will be modified frequently. An alternate approach, which we did not use but one that could have saved us some grief would be to set up fifteen different data sets rather than one partitioned data set with fifteen members. Then each time we needed to link-edit, we would scratch the particular data set and recreate the new link edited data set (instead of member). This procedure would keep us from using up all the extents of a partitioned data set and not having to compress the partitioned set which we had to do approximately every twenty to twenty-five re-link edits. Figure 3 is the VTOC of our development disk. The other utility that we made quite frequent use of was IEBPTPCH. With the use of this utility we can either list or punch a member of SOU1 or any of the other partitioned data sets. The JCL for PUNCHIT is given in Figure 4 and for PRINIT in Figure 5. With these two decks we can list or punch subroutines from SOU1. The punched routine could then be modified for our new element. Another utility which could have been used for modifying source decks is IEBUPDATE which we did not use. The next step in the process is to compile either a modified subprogram of the NASTRAN system or to compile one of our new subprograms. The compiled program is placed into our partitioned data set NEWOBJ. The JCL for this procedure is shown in Figure 6. When all the decks for one of the links has been compiled, the next step is to link edit this link.

The link editor allows one to specify a group of libraries of programs via the LKED.XXX DD cards. In our case, we described two libraries, OBJ which contained all the original unmodified or distributed load modules and NEWOBJ, the modified and new load modules. Each library is given a DD name, for the partitioned set OBJ the name LKED.LIB is used and for NEWOBJ we chose to use the name LKED.LIP. The overlay control cards can be punched and listed from the data set SUBSYS for this link. The control card deck is then modified to reflect the modifications made to the link. See Figure 7 for the JCL and modified control deck for the Link Edit step. The SYSLMOD DD card defines the output load module for the linkage editor and places the load module in the data set NADEV.

The next step is to run a NASTRAN problem to test the procedure implemented. Alters can be made to the DMAP program to extract contents of tables or of generated matrices. In addition, print statements can be made within the modified programs to print out calculated results. If these print statements are used, they should be activated by a specific DIAG that is not in use by the NASTRAN system. See pages 3.3-15 and 3.3-15a of the NASTRAN Programmer's Manual for DIAGS not in use by the system. Figure 8 gives an example of the use of alter statements and demonstrates the use of DIAG setting for controlling debug printing. In debugging a modified link, a dump is quite helpful on the occurrence of a system fatal error. The most important part of the dump is the save area trace which lists the routines last used when the error occurred. Usually this is sufficient and a full dump is not necessary. NASTRAN has built into the system a use of the SNAP macro which dumps only the save areas. Use of DIAG 1 will produce a full dump.

The link edit procedure for NASTRAN links is rather costly on the IBM 370-165 because of the extremely large number of segments in each of the links. Hence, whenever possible, we did as much checking of a modified module with a nonoverlayed FORTRAN run. For example, in checking out the stiffness matrix routines for the isoparametric elements we ran a simple model in NASTRAN, and with the Alter statements we printed the contents of the ECPT (Element Connection and Properties Tables). A main program which simulates SMA1 was written to supply the proper ECPT to the element stiffness matrix routines and the element matrices were generated and printed out. When we were satisfied that the routines operated properly we modified our link-edit control deck and link edited the new element stiffness matrix routines into our data set NADEV. A run of the same model would then produce the element stiffness matrices, displacements, and stresses. Figure 7 is our JCL and control deck for the insertion of stiffness matrix routines into link 3.

The procedure for the variable number of grid points for mixed elements (one that is not full) was implemented in the following manner. The connection cards for the element were left blank at positions where grid points were missing from the full element. A modification of TA1A and TA1B was made to enter a zero as the grid point number for the missing grid points. For the grid points present, the degree of freedom for that grid point (a nonzero value) was entered as the grid point number. All tables such as ECPT, EST (Element Summary Table) have nonzero values for grid points present in the element and zeros for missing grid points. The length of the grid point table is fixed for each element type, for example, twenty for CSOLID2, the quadratic isoparametric. This table is then used as a guide to all processing of the mixed element. The modifications to TA1A and TA1B were suppled to us by Carl Hennrich of MacNeal-Schwendler Company.

The procedure used for saving the element matrices and not recreating them each time they are needed was as follows: A scratch tape was assigned to be used in the element matrix subroutine. This tape had to be assigned a GINO buffer at a level where all buffers are assigned for this module. Also an array had to be assigned for record keeping of saved elements. Initilization of counters had to be done at the level where the buffer was assigned. At the element level the routine would first ask if this element had previously been encountered. This is done by a search through the table of all elements that have been saved. If found, the tape record number is extracted from the table and the tape is positioned by GINO commands to the proper record. The record is read into core and the sub matrices needed for this call are assembled from the total element matrix and given to the subroutine which is assembling the total mass or stiffness matrix. If this element has not been encountered, the element matrix is calculated, and the tape is positioned to the end of last element written, and the new element matrix is written on the scratch tape. The element number and record number is entered into the table. This procedure was suggested in the Programmers Manual, Page 4.87-1, last two sentences of paragraph 3. GINO proved very useful here in that the records saved were of variable length because of the three types of elements and because of the use of mixed elements within a type. The variable length could be stored in the record and using GINO's capability of reading and writing segmented or partial records we could read the number of words for the variable length record. To add scratch tapes to an existing module the MPL (Module Property List) had to be modified by recompiling the block data program XMPLBD, see pages 2.4-21 and 2.4-22 of the Programmers Manual.

DISCUSSION

The new Programmer's Manual for version 15.1 has an excellent chapter on adding a structural element. This was an update of a NASA Fourteenth Quarterly Report for NASTRAN, January 1970. This chapter gives a step-by-step procedure of all routines and tables that have to be modified to accommodate a new element. The Fourteenth Quarterly Report aided us greatly in getting through most of the input problems of NASTRAN.

From this step-by-step procedure, one can see that adding a new element to NASTRAN is not that difficult because of the excellent documentation and supplies that have been distributed.

ACKNOWLEDGMENTS

The authors would like to thank S-Y Lien and W. VanBuren for providing the isoparametric routines and C. W. Hennrich, R. Gillian, and M. M. Hurwitz for NASTRAN consultation.

REFERENCES

1. Field, E. I., and Johnson, S. E.: Addition of Three-Dimensional Isoparam Elements to NASA Structural Analysis Program (NASTRAN). NASA CR-112269 1973.

2. Zienkiewicz, O. C.: The Finite Element Method in Fngineering Science. McGraw-Hill Book Co., Inc., 1971, pp. 129-153.

3. Zienkiewicz, O. C., Irons, B. M., Ergatoudis, J., Ahmad, S. and Scott, F. Iso-Parametric and Associated Element Families for Two- and Three-Dimensional Analysis. Chapter 13 of Finite Elements in Stress Analysis I. Holand and K. Bell, eds., Tapir Forlag (Trondheim, Norway) 1969.

4. MacNeal, R. H., ed.: The NASTRAN Theoretical Manual. NASA SP-221(01), 1!

5. Anon.: The NASTRAN Programmer's Manual. NASA SP-223(01), 1972.

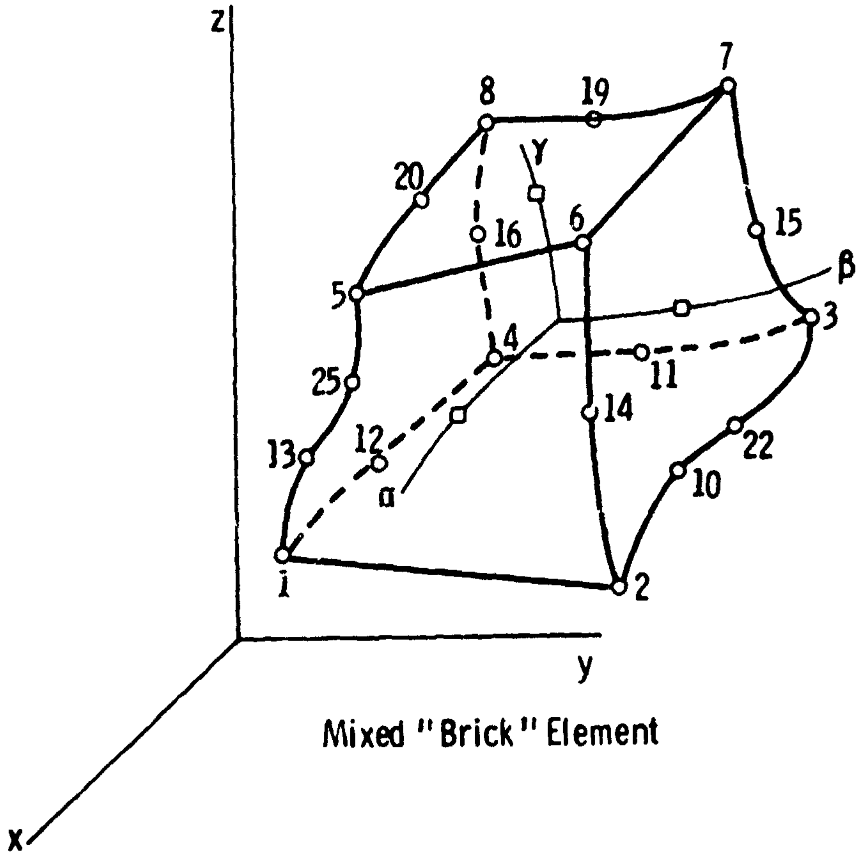

Mixed "Brick" Element

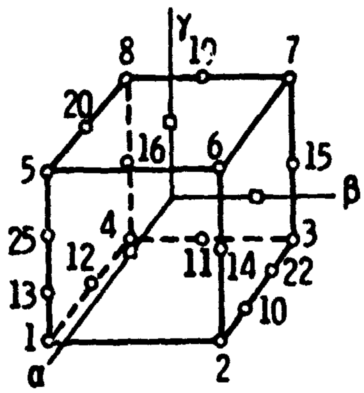

Local Coordinate System

Figure 1.- Mixed 3-D isoparametric element. Variable number of grid points.

```
VOLUME              FORMAT 4 DSCB AT     0/  2/ 1  (CC/HH/R)                          14/31/09.98    73.165

EXTENT OF VTOC    - FROM    0/  2 TO   0/  4      SEQUENCE NUMBER =  0     CODE = 01        3 TRACKS ALLOCATED
DEVICE CHARACTERISTICS             NUMBER OF LOGICAL CYLINDERS = 203
                                   NUMBER OF TRACKS PER LOGICAL CYLINDER =  20
                                   NUMBER OF BYTES PER TRACK =  7294
                                   NUMBER OF FULL DSCBS PER TRACK =  25
                                   NUMBER OF PDS DIRECTORY BLOCKS PER TRACK =  17

FORMAT 5 DSCB AT   0/  2/ 2  (CC/HH/R)              EXTENTS OF AVAILABLE SPACE

        STARTING AT RELATIVE TRACK     1 (  0/  1)  THERE ARE   0 CYLINDERS AND AN ADDITIONAL  1 TRACKS AVAILABLE
        STARTING AT RELATIVE TRACK 3368 (168/  8)  THERE ARE   1 CYLINDERS AND AN ADDITIONAL 12 TRACKS AVAILABLE
        A TOTAL OF    33 TRACKS AVAILABLE

ASTMLMCP                                  FORMAT 1 DSCB AT      0/  2/ 3  (CC/HH/R)

        NUMBER OF EXTENTS =  1            DATA SET ORGANIZATION IS  PARTITIONED               RECORD FORMAT IS  U
        BLOCKSIZE = 7294           LOGICAL RECORD LENGTH =    0
        SECONDARY ALLOCATION  -  CODE = 80            QUANTITY =   20
        THE LAST BLOCK WAS WRITTEN ON RELATIVE TRACK1027  AS RECORD NUMBER   6
        THERE ARE  5794 BYTES REMAINING ON THAT TRACK FOLLOWING THE BLOCK
        EXTENT  1           FROM   0/  5  TO   51/ 14       SEQUENCE NUMBER =  0      CODE = 01      1030 TRACKS ALLOCAT

OBJ                                       FORMAT 1 DSCB AT      0/  2/ 4  (CC/HH/R)

        NUMBER OF EXTENTS =  2            DATA SET ORGANIZATION IS  PARTITIONED               RECORD FORMAT IS  U
        BLOCKSIZE = 7294           LOGICAL RECORD LENGTH = 7294
        SECONDARY ALLOCATION  -  CODE = 80            QUANTITY =    2
        THE LAST BLOCK WAS WRITTEN ON RELATIVE TRACK 566  AS RECORD NUMBER    9
        THERE ARE  3197 BYTES REMAINING ON THAT TRACK FOLLOWING THE BLOCK
        EXTENT  1           FROM  51/ 15  TO   80/  0       SEQUENCE NUMBER =  0      CODE = 01       566 TRACKS
        EXTENT  2           FROM  80/  1  TO   80/  2       SEQUENCE NUMBER =  1      CODE = 01         2 TRACKS
                                                                                  A TOTAL OF  568 TRACKS  ALLOCA

SOU1                                      FORMAT 1 DSCB AT      0/  2/ 5  (CC/HH/R)

        NUMBER OF EXTENTS =  1            DATA SET ORGANIZATION IS  PARTITIONED               RECORD FORMAT IS  FB
        BLOCKSIZE = 7280           LOGICAL RECORD LENGTH      80
        SECONDARY ALLOCATION  -  CODE = 40            QUANTITY =    2
        THE LAST BLOCK WAS WRITTEN ON RELATIVE TRACK2014  AS RECORD NUMBER   2
        THERE ARE  4622 BYTES REMAINING ON THAT TRACK FOLLOWING THE BLOCK
        EXTENT  1           FROM  80/  3  TO  180/ 19       SEQUENCE NUMBER =  0      CODE = 01      2017 TRACKS ALLOCAT

SOU2                                      FORMAT 1 DSCB AT      0/  2/ 6  (CC/HH/R)

        NUMBER OF EXTENTS =  1            DATA SET ORGANIZATION IS  PARTITIONED               RECORD FORMAT IS  FB
        BLOCKSIZE = 7280           LOGICAL RECORD LENGTH =   80
        SECONDARY ALLOCATION  -  CODE = 80            QUANTITY =    1
        THE LAST BLOCK WAS WRITTEN ON RELATIVE TRACK    6  AS RECORD NUMBER   2
        THERE ARE  5000 BYTES REMAINING ON THAT TRACK FOLLOWING THE BLOCK
```

Figure 2.- VTOC distributed system V15.

```
                                              FORMAT 1 DSCB AT      0/  2/ 7  (CC/HH/R)
SOU3                                                                                            RECORD FORMAT IS  FB
          NUMBER OF EXTENTS =  1          DATA SET ORGANIZATION IS  PARTITIONED
          BLOCKSIZE = 7280          LOGICAL RECORD LENGTH =    80
          SECONDARY ALLOCATION  -  CODE = 80          QUANTITY =        2
          THE LAST BLOCK WAS WRITTEN ON RELATIVE TRACK 109  AS RECORD NUMBER    4
          THERE ARE  2468 BYTES REMAINING ON THAT TRACK FOLLOWING THE BLOCK
          EXTENT  1          FROM 181/ 10  TO  187/  0          SEQUENCE NUMBER =  0       CODE = 01       111 TRACKS ALLOCAT

                                              FORMAT 1 DSCB AT      0/  2/ 8  (CC/HH/R)
SUBSYS                                                                                          RECORD FORMAT IS  FB
          NUMBER OF EXTENTS =  1          DATA SET ORGANIZATION IS  PARTITIONED
          BLOCKSIZE = 3200          LOGICAL RECORD LENGTH =    80
          SECONDARY ALLOCATION  -  CODE = 80          QUANTITY =        1
          THE LAST BLOCK WAS WRITTEN ON RELATIVE TRACK  25  AS RECORD NUMBER    2
          THERE ARE  6591 BYTES REMAINING ON THAT TRACK FOLLOWING THE BLOCK
          EXTENT  1          FROM 187/  1  TO  188/  6          SEQUENCE NUMBER =  0       CODE = 01        26 TRACKS ALLOCAT

                                              FORMAT 1 DSCB AT      0/  2/ 9  (CC/HH/R)
UMFINDTA                                                                                        RECORD FORMAT IS  FB
          NUMBER OF EXTENTS =  1          DATA SET ORGANIZATION IS  SEQUENTIAL
          BLOCKSIZE = 7280          LOGICAL RECORD LENGTH =    80
          SECONDARY ALLOCATION  -  CODE = 80          QUANTITY =        1
          THE LAST BLOCK WAS WRITTEN ON RELATIVE TRACK 140  AS RECORD NUMBER    1
          THERE ARE   769 BYTES REMAINING ON THAT TRACK FOLLOWING THE BLOCK
          EXTENT  1          FROM 188/  7  TO  195/  7          SEQUENCE NUMBER =  0       CODE = 01       141 TRACKS ALLOCAT

                                              FORMAT 1 DSCB AT      0/  2/10  (CC/HH/R)
CENGDATA                                                                                        RECORD FORMAT IS  FB
          NUMBER OF EXTENTS =  1          DATA SET ORGANIZATION IS  PARTITIONED
          BLOCKSIZE = 7280          LOGICAL RECORD LENGTH =    80
          SECONDARY ALLOCATION  -  CODE = 80          QUANTITY =        1
          THE LAST BLOCK WAS WRITTEN ON RELATIVE TRACK  43  AS RECORD NUMBER    2
          THERE ARE  4673 BYTES REMAINING ON THAT TRACK FOLLOWING THE BLOCK
          EXTENT  1          FROM 195/  8  TO  197/ 11          SEQUENCE NUMBER =  0       CODE = 01        44 TRACKS ALLOCAT

                                              FORMAT 1 DSCB AT      0/  2/11  (CC/HH/R)
UTILMODS                                                                                        RECORD FORMAT IS
          NUMBER OF EXTENTS =  4          DATA SET ORGANIZATION IS  PARTITIONED
          BLOCKSIZE = 7294          LOGICAL RECORD LENGTH = 7294
          SECONDARY ALLOCATION  -  CODE = 20          QUANTITY =        2
          THE LAST BLOCK WAS WRITTEN ON RELATIVE TRACK  15  AS RECORD NUMBER    3
          THERE ARE  4414 BYTES REMAINING ON THAT TRACK FOLLOWING THE BLOCK
          EXTENT  1          FROM 197/ 12  TO  198/  1          SEQUENCE NUMBER =  0       CODE = 01        10 TRACKS
          EXTENT  2          FROM 198/  2  TO  198/  3          SEQUENCE NUMBER =  1       CODE = 01         2 TRACKS
          EXTENT  3          FROM 198/  4  TO  198/  5          SEQUENCE NUMBER =  2       CODE = 01         2 TRACKS
                                                                                     A TOTAL OF     14 TRACKS  ALLOCA
          THIS DSCB IS CHAINED TO A FORMAT 3 DSCB AT     0/  2/12  (CC/HH/R)

FORMAT 3 DSCB AT    0/  2/12  CC/HH/R)            EXTENTS CONTINUED FROM A FORMAT 1 DSCB
```

Figure 2.- Concluded.

```
VOLUME              FORMAT 4 DSCB AT     0/  1/ 1  (CC/HH/R)                    14/31/13.13    73.165

EXTENT OF VTOC   - FROM   0/  1 TO   0/  4      SEQUENCE NUMBER =  0      CODE = 01         4 TRACKS ALLOCATED
DEVICE CHARACTERISTICS              NUMBER OF LOGICAL CYLINDERS = 203
                                    NUMBER OF TRACKS PER LOGICAL CYLINDER =  20
                                    NUMBER OF BYTES PER TRACK =  7294
                                    NUMBER OF FULL DSCBS PER TRACK =  25
                                    NUMBER OF PDS DIRECTORY BLOCKS PER TRACK =  17


FORMAT 5 DSCB AT    0/  1/ 2  (CC/HH/R)              EXTENTS OF AVAILABLE SPACE

         STARTING AT RELATIVE TRACK     5 (  0/  5)  THERE ARE   0 CYLINDERS AND AN ADDITIONAL 15 TRACKS AVAILABLE
         STARTING AT RELATIVE TRACK 3840 (192/  0)  THERE ARE   8 CYLINDERS AND AN ADDITIONAL  0 TRACKS AVAILABLE
         A TOTAL OF  175 TRACKS AVAILABLE


NEWOBJ                                          FORMAT 1 DSCB AT      0/  1/ 3  (CC/HH/R)

         NUMBER OF EXTENTS =  1           DATA SET ORGANIZATION IS  PARTITIONED              RECORD FORMAT IS  FB
         BLOCKSIZE = 3120          LOGICAL RECORD LENGTH =   80
         SECONDARY ALLOCATION  -  CODE = C0           QUANTITY =     0
         THE LAST BLOCK WAS WRITTEN ON RELATIVE TRACK 269  AS RECORD NUMBER    3
         THERE ARE  2485 BYTES REMAINING ON THAT TRACK FOLLOWING THE BLOCK
         EXTENT  1            FROM   1/  0  TO   15/ 19      SEQUENCE NUMBER =  0      CODE = 81       300 TRACKS ALLOCAT


NADEV2                                          FORMAT 1 DSCB AT      0/  1/ 4  (CC/HH/R)

         NUMBER OF EXTENTS = 11           DATA SET ORGANIZATION IS  PARTITIONED              RECORD FORMAT IS  U
         BLOCKSIZE = 7294          LOGICAL RECORD LENGTH =     0
         SECONDARY ALLOCATION  -  CODE = C0           QUANTITY =    20
         THE LAST BLOCK WAS WRITTEN ON RELATIVE TRACK2081  AS RECORD NUMBER  15
         THERE ARE    887 BYTES REMAINING ON THAT TRACK FOLLOWING THE BLOCK
         EXTENT  1            FROM  32/  0  TO  100/ 19      SEQUENCE NUMBER =  0      CODE = 81       1380 TRACKS
         EXTENT  2            FROM 101/  0  TO  120/ 19      SEQUENCE NUMBER =  1      CODE = 81        400 TRACKS
         EXTENT  3            FROM  16/  0  TO   23/ 19      SEQUENCE NUMBER =  2      CODE = 81        160 TRACKS
                                                                                    A TOTAL OF 1940 TRACKS  ALLOC
         THIS DSCB IS CHAINED TO A FORMAT 3 DSCB AT    0/  1/ 5  (CC/HH/R)


FORMAT 3 DSCB AT    0/  1/ 5  CC/HH/R)              EXTENTS CONTINUED FROM A FORMAT 1 DSCB

         EXTENT  4            FROM  24/  0  TO   31/ 19      SEQUENCE NUMBER =  3      CODE = 81        160 TRACKS
         EXTENT  5            FROM 121/  0  TO  143/ 19      SEQUENCE NUMBER =  4      CODE = 81        460 TRACKS
         EXTENT  6            FROM 144/  0  TO  151/ 19      SEQUENCE NUMBER =  5      CODE = 81        160 TRACKS
         EXTENT  7            FROM 152/  0  TO  159/ 19      SEQUENCE NUMBER =  6      CODE = 81        160 TRACKS
         EXTENT  8            FROM 160/  0  TO  167/ 19      SEQUENCE NUMBER =  7      CODE = 81        160 TRACKS
         EXTENT  9            FROM 168/  0  TO  175/ 19      SEQUENCE NUMBER =  8      CODE = 81        160 TRACKS
         EXTENT 10            FROM 176/  0  TO  183/ 19      SEQUENCE NUMBER =  9      CODE = 81        160 TRACKS
         EXTENT 11            FROM 184/  0  TO  191/ 19      SEQUENCE NUMBER = 10      CODE = 81        160 TRACKS
                                                                                    A TOTAL OF 1580 TRACKS  ALLOCA
```

Figure 3.- VTOC of development system.

```
//PUNCHIT JOB (R0XXXXX,R0R0),'MBNEWMAN',REGION=100K,TIME=(,39)          JOB CARD
/*VOLREQ ID=(NASTRAN15)                                    DISTRIBUTED SYSTEM V.15
//   EXEC PGM=IEBPTPCH
//SYSPRINT DD SYSOUT=A
//SYSUT1   DD DSNAME=SOU1,UNIT=SYSDA,DISP=OLD,VOL=SER=VOLNUM,
//         DCB=(RECFM=FB,LRECL=80,BLKSIZE=7280)
//SYSUT2  DD SYSOUT=3
//SYSIN  DD  *
  PUNCH TYPORG=PO,MAXNAME=60,MAXFLDS=60
  MEMBER NAME=DS1
    RECORD FIELD=(80)
  MEMBER NAME=DS1A
    RECORD FIELD=(80)
  MEMBER NAME=DS1ABD
    RECORD FIELD=(80)
/*

     NOTE  SOU1 IS DATA SET NAME.  VOLNUM IS DISK VOLUME SERIAL NUMBER
```

Figure 4.- Punch source from SOU1.

```
//PRINIT JOB (R0XXXXX,R0R0T,'MBNEWMAN',REGION=100K,TIME=(,39)           JOB CARD
/*VOLREQ ID=(NASTRAN15)                                    DISTRIBUTED SYSTEM V.15
/*FORMAT PR,DDNAME=SYSUT2,TRAIN=HN
//    EXEC PGM=IEBPTPCH
//SYSPRINT DD SYSOUT=A
//SYSUT1 DD UNIT=SYSDA,VOLUME=SER=VOLNUM,DISP=OLD,
//     DCB=(RECFM=FB,LRECL=80,BLKSIZE=7280),DSN=SOU1
//SYSUT2  DD SYSOUT=A
//SYSIN  DD  *
      PRINT  TYPORG=PO,MAXFLDS=80,MAXNAME=80,MAXLINE=45
      MEMBER NAME=READ1
    RECORD FIELD=(80)
      MEMBER NAME=READ2
    RECORD FIELD=(80)
/*
```

Figure 5.- Prints source from SOU1.

```
//COMPILE JOB (RDXXXXX,RDRD),'MBNEWMAN',REGION=200K,TIME=(,39)          JOB CARD
/*VOLREW ID=(NASTRANDEV)                                            DEVELOPMENT DISK
//      EXEC    FORTGC,PARM.FORT='NODECK'
//FORT.SYSLIN  DD  UNIT=2314,DISP=SHR,VOL=SER=VOLDEV,
//           DSN=NEWOBJ(IFX1BD)
//FORT.SYSIN  DD  *
      BLOCK DATA
CIFX1BD
      COMMON /IFPX1/ N,I1(100),I2(100),I3(100),I4(100),I5(100),I6(120),
     *           I7(64)
      DATA N/310/
      DATA I1/4HGRID,4H    ,4HGRDS,4HET  ,4HADUM,4H1   ,4HSEQG,4HP
     5        ,4HCORD,4H1R  ,4HCORD,4H1C  ,4HCORD,4H1S  ,4HCORD,4H2R
     9        ,4HCORD,4H2C  ,4HCORD,4H2S  ,4HPLOT,4HEL  ,4HSPC1,4H
     3        ,4HSPCA,4HDD  ,4HSUPO,4HRT  ,4HOMIT,4H    ,4HSPC ,4H
     7        ,4HMPC ,4H    ,4HFORC,4HE   ,4HMOME,4HNT  ,4HFORC,4HE1
     1        ,4HMOME,4HNT1 ,4HFORC,4HE2  ,4HMOME,4HNT2 ,4HPLOA,4HD
     5        ,4HSLOA,4HD   ,4HGRAV,4H    ,4HTEMP,4H    ,4HGENE,4HL
     9        ,4HPROD,4H    ,4HPTUB,4HE   ,4HPVIS,4HC   ,4HADUM,4H2
      DATA I5/4HTEMP,4HP1  ,4HTEMP,4HP2  ,4HTEMP,4HP3  ,4HTEMP,4HRB
     5        ,4HGRID,4HB   ,4HFSLI,4HST  ,4HRING,4HFL  ,4HPRES,4HPT
     9        ,4HCFLU,4HID2 ,4HCFLU,4HID3 ,4HCFLU,4HID4 ,4HAXIF,4H
C    3        ,4HBDYL,4HIST ,4HFREE,4HPT  ,4HSELE,4HCT  ,4HSELE,4HCT1
     3        ,4HBDYL,4HIST ,4HFREE,4HPT  ,4HASET,4H    ,4HASET,4H1
     7        ,4HCTET,4HRA  ,4HCWED,4HGE  ,4HCHEX,4HA1  ,4HCHEX,4HA2
     1        ,4HDMIA,4HX   ,4HFLSY,4HM   ,4HAXSL,4HOT  ,4HCAX1,4HF2
     5        ,4HCAX1,4HF3  ,4HCAX1,4HF4  ,4HCSLO,4HT3  ,4HCSLO,4HT4
     9        ,4HGRID,4HF   ,4HGRID,4HS   ,4HSLBD,4HY   ,4HCHBD,4HY
     3        ,4HWHBD,4HY   ,4HMAT4,4H    ,4HMAT5,4H    ,4HSAME,4H
C    ADD CSOLID1,CSOLID2,CSOLID3 NAMES TO DIRECTORY OF CONNECTION CARD NAMES MAN
     7        ,4HSAME,4H1   ,4HINPU,4HT    ,4HOUTP,4HUT  ,4HCSOL,4HID1
     1        ,4HCSOL,4HID2 ,4HCSOL,4HID3  ,4H****,4H****,4H****,4H****
     5        ,4H****,4H****,4H****,4H****,4H****,4H****,4H****,4H****
     9        ,4H****,4H****,4H****,4H**** /
      DATA I6/4H****,4H****,4H****,4H****,4H****,4H****,4H****,4H****
     5        ,4H****,4H****,4H****,4H****,4H****,4H****,4H****,4H****
     9        ,4H****,4H****,4H****,4H****,4H****,4H****,4H****,4H****
     3        ,4H****,4H****,4H****,4H****,4H****,4H****,4H****,4H****
     7        ,4H****,4H****,4H****,4H****,4H****,4H****,4H****,4H****
     1        ,4H****,4H****,4H****,4H****,4H****,4H****,4H****,4H****
     5        ,4H****,4H****,4H****,4H****,4H****,4H****,4H****,4H****
     9        ,4H****,4H****,4H****,4H****,4H****,4H****,4H****,4H****
     3        ,4H****,4H****,4H****,4H****,4H****,4H****,4H****,4H****
     7        ,4H****,4H****,4H****,4H****,4HDECO,4HMUPT,4HCPBA,4HR
     1        ,4HCPRD,4HD   ,4HCPTU,4HBE  ,4HCPWU,4HAD1 ,4HCPWU,4HAD2
     5        ,4HCPTR,4HIA1 ,4HCPTR,4HIA2 ,4HCPWD,4HPLT ,4HCPTR,4HPLT
     9        ,4HCPTR,4HBSC ,4HCOUP,4HMASS,4HGRDP,4HNT  ,4HWTMA,4HSS
     3        ,4HIRES,4H    ,4HLFRE,4HQ   ,4HMFRE,4HQ   ,4HLMOD,4HES
     7        ,4HG   ,4H    ,4HW3  ,4H    ,4HW4  ,4H    ,4HMODA,4HCC   /
      DATA I7/4HMPCS,4H    ,4HSPCS,4H    ,4HLOAD,4HS   ,4HMETH,4HODS ,
     5         4HDEFO,4HRMS ,4HTEMP,4HLDS ,4HTEMP,4HMTS ,4HICS ,4H     ,
     9         4HAOUT,4HS   ,4HLOOP,4HS   ,4HLOOP,4H1S  ,4HDLOA,4HDS   ,
     3         4HFREQ,4HS   ,4HTFS ,4H    ,4HPLOT,4HS   ,4HTSTE,4HPS   ,
     7         4HPOUT,4HS   ,4HTEMP,4HMXS ,4HDSCO,4HS   ,4HK2PP,4HS    ,
     1         4HM2PP,4HS   ,4HB2PP,4HS   ,4HCMET,4HHODS,4HSDAM,4HPS   ,
     5         4HPLCO,4HS   ,4HNLFO,4HRCES,4HXYOU,4HTS  ,4HDELE,4HTES  ,
     9         4HRAND,4HOMS ,4HAXYO,4HUTS ,4HNOLO,4HOPS ,4H****,4H****/
      END
/*
```

Figure 6.- Compiles and puts object intc de· elopment data set NEWOBJ.

```
//LNKEDT JOB (RDXXXXX,RDRD),'MBNEWMAN',REGION=275K,TIME=2                  JOB CARD
/*VOLREQ ID=(NASTRAN15)                                      DISTRIBUTED SYSTEM V.15
/*VOLREQ ID=(NASTRANDEV)                                           DEVELOPMENT DISK
//  EXEC FORTHL,PARM.LKED='MAP,LIST,OVLY,DC,LET,SIZE=(262K,72K)'
//LKED.SYSLIB DD DISP=SHR,DSN=SYS1.ERRPK
//             DD DISP=SHR,DSN=SYS1.FORTLIB
//LKED.SYSLMOD DD UNIT=SYSDA,DISP=SHR,VOL=SER=VOLDEV,DSN=NADEV2,
//         SPACE=(CYL,(68,8,5))
//LKED.LIP DD UNIT=SYSDA,DISP=SHR,VOL=SER=VOLDEV,DSN=NEWOBJ
//LKED.LIB DD UNIT=SYSDA,DISP=SHR,VOL=SER=VOLNUM,DSN=OBJ
//LKED.SYSIN DD *
    INCLUDE LIP(LIEN,KISOPR)                                                 00
   CHANGE EXIT(PXIT36)                                                 00000010
    INCLUDE LIB(PEXIT)                                                 00000020
    INCLUDE LIB(PXIT36)                                                00000030
    INCLUDE LIB(LINKNSU3,XSEM3)                                        00000040
    INCLUDE LIB(CORSZ)                                                 00000050
    INCLUDE LIB(SEMDBD,RETURN,XEOT,MAPFNS,TMTOGO,CONMSG)               00000060
    INCLUDE LIB(MESAGE,SSWTCH,GOPEN,FREAD,CLSTAB,OPNCOR,FNAME)         00000070
    INCLUDE LIB(PRELOC,WRTIRL)                                         00000080
  OVERLAY A                                                            00000090
    INCLUDE  LIB(PAGE)                                                 00000100
  OVERLAY A1                                                           00000110
    INCLUDE LIB(MSGWRT,USRMSG)                                         00000120
  OVERLAY A1                                                           00000130
    INCLUDE LIB(BTSTRP)                                                00000140
   CHANGE NTRAN(PEXIT),LINK(PEXIT)                                     00000150
    INCLUDE LIB(ENDSYS)                                                00000160
  OVERLAY  ENDSSS                                                      00000170
     INSERT  ENDSSS                                                    00000180
  OVERLAY A1                                                           00000190
    INCLUDE LIB(QPARAM)                                                00000200
  OVERLAY A1                                                           00000210
    INCLUDE LIB(XSAVE)                                                 00000220
  OVERLAY A1                                                           00000230
    INCLUDE LIB(XCEI)                                                  00000240
  OVERLAY A1                                                           00000250
    INCLUDE LIB(XCHK)                                                  00000260
  OVERLAY A1                                                           00000270
    INCLUDE LIB(GNFIST,RPDABD,XSFA,XSOSGN,ACLEAN,XPUNP,XDPH)           00000280
    INCLUDE LIB(XPOLCK,XPURGE)                                         00000290
     INSERT XSFA1                                                      00000300
  OVERLAY ESFA                                                         00000310
     INSERT ESFA,OSCENT                                                00000320
  OVERLAY A1                                                           00000330
    INCLUDE LIB(TABPT,TABPRT,MATDUM,MATPRN)                            00000340
  OVERLAY TABPRX                                                       00000350
     INSERT TABPRX                                                     00000360
  OVERLAY A1                                                           00000370
    INCLUDE LIB(PRTPRM)                                                00000380
  OVERLAY A                                                            00000390
    INCLUDE LIP(GPTABD)                                                00000400

    INCLUDE LIB(DELSET)                                                00000401
    INCLUDE LIB(HMAT,BISRCH)                                           00000410
    INCLUDE LIB(GMMATD,PRETRD,INVERD,GMMATS,PREMAT)                    00000420
    INCLUDE LIB(SAXB,DAXB,SADOTB,DADOTB)                               00000430
     INSERT GPTA1                                                      00000440
     INSERT HMTOUT                                                     00000450
     INSERT HMATDD                                                     00000460
     INSERT  MATIN,MATOUT                                              00000470
```

Figure 7.- Link edit and puts execution module into NADEV development set.

FIGURE 7 CONTINUED

```
 OVERLAY SMA1
   INCLUDE LIP(SMA1BD)
    INSERT  SMA1CL,SMA1IO,SMA1BK,SMA1ET,SMA1DP
    INSERT SMA1HT
  CHANGE KBEAM(PEXIT)
     INCLUDE LIP(SMA1A)
   INSERT SMA1SC,APLE
   INCLUDE LIB(SMA1B,DETCK)
   INCLUDE LIP(SMA1)
  CHANGE KBEAM(PEXIT)
   INCLUDE LIB(PLA1)
 OVERLAY SMAEL
   INCLUDE LIB(KROD,KBAR,KTUBE,KPANEL,KELAS)
   INCLUDE LIB(KTRMEM,KQDMEM,KTRBSC,KTRPLT,KQDPLT,KTRIQD,HHBDY,HRING)
 OVERLAY SMAEL
   INCLUDE LIB(KCONE,KCONEX)
 OVERLAY SMAEL
   INCLUDE LIB(KTRIRG,KTRAPR,DKI,DKINT,DKK,DKM,DKJ,DKEF,DK89,DK100)
   INCLUDE LIB(DK211,DK219,DKJAB,KFAC)
 OVERLAY SMAEL
   INCLUDE LIB(KTORDR,DMATRX,ROMBDK,D4K,D5K,D6K)
 OVERLAY SMAEL
   INCLUDE LIB(KFLUD2,KFLUD3,KFLUD4,KSLOT,KTETRA,KSOLID,KPLIST)
 OVERLAY SMAEL
   INCLUDE LIB(KDUM1,KDUM2,KDUM3,KDUM4,KDUM5,KDUM6,KDUM7,KDUM8,KDUM9)
  OVERLAY SMAEL
   INSERT KISOPR
   INSERT DTOT,FORMTD,INV3X3,JTPTN,MATERL,MBC1A,MMAT,MULTPN,MXYZ,NSELEC
   INSERT PARTL,PARXYZ,SETCON
   INSERT SMA1PD,ELDATA,NMAT,FRONT3,PARTIL
 OVERLAY SMA1
  CHANGE MBEAM(PEXIT)
  INCLUDE LIP(SMA2A)
  INCLUDE LIB(SMA2B)
  INCLUDE LIP(SMA2BD,SMA2)
   INSERT SMA2SC,MAPLE
     INSERT  SMA2CL,SMA2IO,SMA2BK,SMA2ET,SMA2DP
 OVERLAY  SMAEL2
   INCLUDE LIB(MROD,MBAR,MTUBE,MASSD,BVISC,MCONMX,MCONE)
   INCLUDE LIB(MSOLID,MFLUD2,MFLUD3,MFLUD4,MFREE,MSLOT)
   INCLUDE  LIB(MASSTQ)
   INCLUDE LIB(MCBAR,MCROD,MTRBSC,MQDPLT,MTRPLT,MTRIQD)
 OVERLAY  SMAEL2
   INCLUDE LIB(MTRIRG,MTRAPR,DMI,DMINT,DMK,DMM, 4J,DMEF,DM89,DM100)
   INCLUDE LIB(MFAC,DMJAB,DM219,DM211,MTORDR)
 OVERLAY SMAEL2
   INCLUDE LIB(MDUM1,MDUM2,MDUM3,MDUM4,MDUM5,MDUM6,MDUM7,MDUM8,MDUM9)
  OVERLAY SMAEL2
   INCLUDE LIP(MISOPR,MLIEN)
  INSERT SMA2PD,ELDAT2,NMAT2,FRONT2,PARTI2
 OVERLAY OEND(REGION)
    INSERT SMA1X

    INSERT SMA2X
 OVERLAY EJDUM2
   INCLUDE LIB(EJDUM2)
    INSERT EJDUM2
  ENTRY LINKNS03
 NAME LINKNS03(R)
/*
```

Figure 7.- Concluded.

```
//ALTEX JOB (RDXXXXX,RDRD),'MBNEWMAN',REGION=300K,TIME=(,59)              JOB CARD
/*VOLREQ ID=(NASTRANDEV)                                                  DEVELOPMENT DISK
/*FORMAT PR,DDNAME=FT04F001,TRAIN=HN
/*FORMAT PR,DDNAME=FT06F001,TRAIN=HN
/*FORMAT PR,DDNAME=SNAPSHOT,TRAIN=HN
//S2  EXEC  F56THG
//PROG.NAME DD DSNAME=SYS1.LINKLIB(VTOCPRT),VOLUME=REF=SYSLIB1,          A
//            DISP=OLD
//GO.DD2 DD UNIT=SYSDA,DISP=OLD,VOLUME=(PRIVATE,RETAIN,SER=(VOLDEV))
//GO.SYSIN  DD  *
VOLDEV
EOJ
//   EXEC NSTMBN
//NASTRAN.STEPLIB  DD  UNIT=2314,VOL=SER=VOLDEV,DISP=SHR,DSN=NADEV2
//NASTRAN.SNAPSHOT DD UNIT=(CTC,,DEFER),DCB=BLKSIZE=882
//SYSIN DD *
NASTRAN BUFFSIZE=1800,SYSTEM(31)=4096,SYSTEM(9)=35,CONFIG=10
ID   MARV,NEWMAN
APP  DISP
SOL 1,0
TIME 5
DIAG 15
DIAG 2,8,13,14
DIAG 19,21,22
DIAG 25                                                                  MBNDEBUG
ALTER 21
TABPT GPTT,,,, //$
ALTER 26
TABPT GPCT,,,, // $
TABPT ECPT,GPTT,EST,, // $
TABPT EQEXIN,GEOM2,,, // $
ALTER 111
MATPRN UG',PGG,UG,, //  $
ENDALTER
CEND
OLOAD=ALL
SPC=111
SPCF=ALL
STRESS=ALL
ELFORCE=ALL
DISP=ALL
LOAD=100
TITLE=TEST OF BODY FORCE --- 1 CSOLID2 ELEMENT
ECHO=BOTH
BEGIN BULK
GRDSET                                              456
GRID     1              1.     -1.     0.
GRID     2              1.      1.     0.
GRID     3             -1.      1.     0.
GRID     4             -1.     -1.     0.
GRID     5              1.     -1.     3.
GRID     6              1.      1.     3.
```

Figure 8.- VTOC example and use of ALTER for table and matrix printouts.

```
GRID    7               -1.     1.      3.
GRID    8               -1.     -1.     3.
GRID    9               1.      0.      0.
GRID    10              0.      1.0     0.0
GRID    11              -1.0    0.0     0.0
GRID    12              0.0     -1.0    0.0
GRID    13              1.0     -1.0    1.5
GRID    14              1.0     1.0     1.5
GRID    15              -1.0    1.0     1.5
GRID    16              -1.0    -1.0    1.5
GRID    17              1.0     0.0     3.0
GRID    18              0.0     1.0     3.0
GRID    19              -1.0    0.0     3.0
GRID    20              0.0     -1.0    3.0
CSOLID2 1       10                                                      GE1
GE1     1       2       3       4       5       6       7       8       GE2
GE2     9       10      11      12      13      14      15      16      GE3
GE3     17      18      19      20
SPC     111     5       1       -.9E-05 8       12      .9E-05
SPC     111     5       2       .9E-05  8       3       .3E-05
SPC     111     5       3       .3E-05  17      1       -.9E-05
SPC     111     6       12      -.9E-05 17      2       0.0
SPC     111     6       3       .3E-05  17      3       .15E-05
SPC     111     7       1       .9E-05  18      1       0.0
SPC     111     7       2       -.9E-05 18      2       -.9E-05
SPC     111     7       3       .30E-05
SPC     111     18      3       .15E-05
SPC     111     19      1       .9E-05
SPC     111     19      2       0.0
SPC     111     19      3       .15E-05
SPC     111     20      1       0.0
SPC     111     20      2       .9E-05
SPC     111     20      3       .15E-05
MAT1    10      1.E07           .3      4.0
GRAV    100             25.     -1.0    0.0     00.0
ENDDATA
/*
```

Figure 8.- Concluded.

N74-14607

NEW PLATE AND SHELL ELEMENTS FOR NASTRAN

By R. Narayanaswami*
NASA Langley Research Center

SUMMARY

A new higher order triangular plate-bending finite element is presented in this paper which possesses high accuracy for practical mesh subdivisions and which uses only translations and rotations as grid point degrees of freedom. The element has 18 degrees of freedom (d.o.f.), viz., the transverse displacement and two rotations at the vertices and mid-side grid points of the triangle. The transverse displacement within the element is approximated by a quintic polynomial; the bending strains thus vary cubically within the element. Transverse shear flexibility is taken into account in the stiffness formulation. Two examples of static and dynamic analysis are included to show the behavior of the element. Excellent accuracy is achieved in all cases.

This element, designated as TR-18, is demonstrated to be an ideal candidate for generation of a family of plate and shell elements for inclusion into NASTRAN. The following elements are specifically mentioned in this context, viz., (i) triangular plate element, (ii) quadrilateral plate element, (iii) curved triangular shell element, (iv) curved quadrilateral shell element and (v) plates with membrane-bending coupling and multilayered plates. The present paper describes the detailed theoretical derivations for the aforementioned elements. In addition, the behavior of the TR-18 element and associated quadrilateral plate element is illustrated by two sample problems. Comparisons with existing elements in the literature and the present NASTRAN quadrilateral elements are shown.

INTRODUCTION

NASTRAN presently (Level 15.5) has, in all, a total of nine different forms of plate elements in two different shapes (triangular and quadrilateral). The present NASTRAN basic bending element, TRBSC, the basic unit from which the bending properties of the other plate elements are formed, uses a cubic displacement field (with the x^2y term omitted). This constrains the normal slope (on the exterior edges of the TRPLT bending element) to vary linearly, which in turn makes the element overly stiff. A need thus exists for a more accurate plate bending element for NASTRAN.

A brief review of some of the more important plate bending elements is now made. Formulations of triangular plate bending finite elements were given as long ago as 1966 by Clough and Tocher (ref. 1) and by Bazeley et al. (ref. 2). The conforming elements presented therein allow only a linear variation of slope normal to an edge and have since been found to be overly

*NRC-NASA Resident Research Associate.

stiff, whereas the nonconforming element given in ref. 2 uses a cubic polynomial for transverse displacement and is not of very high accuracy. Improvements to these elements have been made by using higher degree polynomials for transverse displacements; indeed elements of very high accuracy have been reported by Argyris (ref. 3), Bell (ref. 4) and Cowper et al. (ref. 5) using quintic polynomials for the displacements field. But these elements have strains, curvatures and/or higher order derivatives of displacements as grid point degrees of freedom (d.o.f.) which lead to an inconsistency when abrupt thickness or material property variation occurs. That is to say that the continuity of strains and curvatures implied by their use as degrees of freedom at grid points is violated wherever concentrated loads, changes in slope, changes in thickness, or connections to other structures occur. In short, the proper use of elements that assume continuity of strains and curvatures is restricted to regions where discontinuities do not occur. Further, the existence of higher order derivatives makes it difficult to impose boundary conditions on these and indeed the simple interpretation of energy derivatives as "nodal forces" disappears (ref. 6). Bell has also developed another element in ref. 4, designated T-15 by him, which has only displacements and rotations as degrees of freedom. But it has a major drawback in that not all grid points of the element have the same d.o.f.; consequently, it becomes difficult, if not impossible, to consider connections of this element with other finite elements. Thus the practical use of the T-15 element in general purpose programs is severely limited.

A need still exists to develop a new accurate plate bending finite element that has the advantages of the accuracy associated with a high order displacement polynomial but does not have the disadvantages discussed above and is therefore suitable for inclusion in general purpose computer programs like NASTRAN.

In this paper, a triangular element and an associated quadrilateral element are developed that use only displacements and rotations as grid point degrees of freedom and use a quintic polynomial for lateral displacement. The quadrilateral element is formed by four triangular elements. The stiffness, consistent mass and load matrices of the separate triangles are evaluated and added by the direct stiffness technique to form the respective matrices for the quadrilateral. The terms associated with the internal grid points are then eliminated by static condensation. None of the elements discussed in references 1 to 5 possess the property of transverse shear flexibility. This has been taken into account in the present paper by a procedure based on that used in NASTRAN (ref. 7).* The components of transvers shear strain are quadratic functions of position. Convergence to the limiting case of zero transverse shear strain is uniform.

In addition, three elements, viz., (i) a curved triangular shell element, (ii) a curved quadrilateral shell element, and (iii) a multilayered plate element can be derived from the TR-18 element. Together with the quadrilateral plate element, these elements constitute the TR-18 family of elements.

*A similar procedure for incorporation of transverse shear flexibility into a quartic element was communicated to the author by Dr. R. H. MacNeal of MacNeal-Schwendler Corporation.

LIST OF SYMBOLS

$\{a\}$	Column vector of coefficients
a,b,c	Dimensions of triangular element in local co-ordinates (fig. 1)
a_1, a_2, a_3	Coefficients of quintic polynomial
$[B_1],[B_2],[B_3]$	Matrices relating strains and generalized displacements
$[C]$	Row vector relating transverse displacement to generalized displacement
$[D]$	Matrix relating bending stresses and bending strains
D	Plate flexural rigidity, $Et^3/12(1 - \nu^2)$
E	Elastic modulus
$[G_o]$	Matrix relating interior grid point displacement to exterior grid point displacements of quad-element
$[J]$	Matrix relating transverse shear forces and strains
$[K]$	Stiffness matrix
L	Length of side of plate
$[M]$	Consistent mass matrix
$\{M\}$	Vector of bending and twisting moments per unit length
N	Number of elements per side of plate
$[Q]$	Matrix relating grid-point displacement vector and vector of polynomial coefficients
$[R]$	Augmented matrix of Q and constraint relations
$[S]$	Matrix relating vector of polynomial coefficients and grid point displacement vector
T	Kinetic energy
$[T_1],[T_2]$	Transformation matrices
t	Thickness of plate
$[U]$	Matrix of transformation of strain components
U	Strain energy
$\{V\}$	Vector of transverse shears per unit length
w	Lateral displacement
w_c	Central deflection
x,y,z	Co-ordinate axes in the local system
X,Y,Z	Co-ordinate axes in the global system
α	Rotation of xz plane at each grid point
β	Rotation of yz plane at each grid point
γ_{xz}, γ_{yz}	Transverse shear strains
$\{\gamma\}$	Vector of transverse shear strains
$\{\delta\},\{\Delta\}$	Column vectors of grid point displacement in local or global system
ϕ	Inclination of material orientation axis to x-axis
$\{\phi\}$	Displacement vector of quadrilateral element
ν	Poisson's ratio
ρ	Mass density of plate material
λ	Non-dimensional parameter of eigenvalues, $\rho t\omega^2 L^4/D$
$[\lambda]$	Direction cosine matrix of quadrilateral median plane
ω	Circular frequency of plate vibration
$\{\chi\}$	Bending strains

$\chi_x, \chi_y, \chi_{xy}$ Bending strains

TRIANGULAR PLATE ELEMENT TR-18

In this section of the paper, the derivation of the stiffness matrix, consistent load vector and consistent mass matrix of the triangular plate element is given. The procedure for the derivation is described in detail in reference 8, and hence only essential details are presented here.

The element has 18 d.o.f., the transverse displacement and 2 rotations at each vertex and at the mid-point of each side. Three additional conditions are introduced, viz., the slope normal to each edge (hereinafter called normal slope) varies cubically along each edge. This establishes 3 constraint equation between the coefficients of the polynomial for displacements, which, together wi the 18 d.o.f., uniquely determine the 21 coefficients in the quintic polynomial. The variation of deflection along any edge is a quintic polynomial in the edgewise co-ordinate; the six coefficients of this polynomial are uniquely determined by deflection and edgewise slope at the 3 grid points of the edge. Displacements are thus continuous between two elements that have a common edge. The normal slope along each edge is constrained to vary cubically; however, since the normal slopes are defined only at 3 points along an edge, there is no normal slope continuity between 2 elements that have a common edge. The element thus belongs to the class of non-conforming elements. The development of this element follows closely that of Cowper et al. (ref. 5).

Element Geometry

Rectangular cartesian co-ordinates are used in the formulation. An arbitrary triangular element is shown in figure 1, where X, Y, and Z are a system of global co-ordinates and x, y, z are the system of local co-ordinates for the triangular element. The grid points of the element are numbered in counterclockwise direction as shown. The following relationship between the dimensions of the triangular element a, b, c, the inclination θ between the X and x axes and the co-ordinates of the vertices of the element can be easily derived (see fig. 1):

$$\cos\theta = (X_3 - X_1)/r \qquad \sin\theta = (Y_3 - Y_1)/r \tag{1}$$

where

$$r = [(X_3 - X_1)^2 + (Y_3 - Y_1)^2]^{1/2} \tag{2}$$

$$a = (X_3 - X_5)\cos\theta - (Y_5 - Y_3)\sin\theta$$

$$= \{(X_3 - X_5)(X_3 - X_1) + (Y_3 - Y_5)(Y_3 - Y_1)\}/r \tag{3}$$

and similarly,

$$b = \{(X_5 - X_1)(X_3 - X_1) + (Y_5 - Y_1)(Y_3 - Y_1)\}/r \tag{4}$$

$$c = \{(X_3 - X_1)(Y_5 - Y_1) - (Y_3 - Y_1)(X_5 - X_1)\}/r \tag{5}$$

Displacement Function

The deflection $w(x, y)$ within the triangular element is assumed to vary as a quintic polynomial in the local co-ordinates, i.e.,

$$\begin{aligned} w(x,y) = {} & a_1 + a_2x + a_3y + a_4x^2 + a_5xy + a_6y^2 + a_7x^3 + \\ & a_8x^2y + a_9xy^2 + a_{10}y^3 + a_{11}x^4 + a_{12}x^3y + a_{13}x^2y^2 + \\ & a_{14}xy^3 + a_{15}y^4 + a_{16}x^5 + a_{17}x^4y + a_{18}x^3y^2 + a_{19}x^2y^3 + \\ & a_{20}xy^4 + a_{21}y^5 \end{aligned} \tag{6}$$

There are 21 constants, a_1 to a_{21}. These are evaluated as follows:

The element has 18 d.o.f. At each grid point there are 3 displacement components as d.o.f., viz., w, displacement in z-direction, α, rotation about the x-axis and β, rotation about y-axis. The rotations α and β are obtained from the definitions of transverse shear strains γ_{xz} and γ_{yz}, i.e.,

$$\left.\begin{aligned} \gamma_{xz} &= \frac{\partial w}{\partial x} + \beta \\ \gamma_{yz} &= \frac{\partial w}{\partial y} - \alpha \end{aligned}\right\} \tag{7}$$

It can be shown (ref. 8) that γ_{xz} and γ_{yz}, and hence α and β, at any grid point can be expresred in terms of the constants a_1 to a_{21}. Thus 18 relations between grid point displacement values and the constants are obtained. Three constraints among the coefficients in the above polynomial (eq. (6)) are now introduced so that the normal slope varies cubically along each edge. It is clear that the three constraint equations will involve only the coefficients of the fifth degree terms in equation (6), since the lower degree terms satisfy the condition of cubic normal slope automatically. Moreover the conditions depend only on the direction of an edge and not on its position. Along the edge defined by grid points 1 and 3, where $y = 0$, the condition of cubic normal slope requires that

$$a_{17} = 0 \tag{8}$$

It can be shown (ref. 8) that the condition for cubic variation of normal slope along edge 1-5 is

$$5b^4c\, a_{16} + (4b^3c^2 - b^5)a_{17} + (3b^2c^3 - 2b^4c)a_{18} + (2bc^4 - 3b^3c^2)a_{19} +$$

$$(c^5 - 4b^2c^3)a_{20} - 5bc^4\, a_{21} = 0 \tag{9}$$

and the condition for cubic variation of the normal slope along the edge 3-5 (see fig. 1) is

$$5a^4c\, a_{16} + (-4a^3c^2 + a^5)a_{17} + (3a^2c^3 - 2a^4c)a_{18} + (-2\, ac^4 + 3a^3c^2)a_{19} +$$

$$(c^5 - 4a^2c^3)\, a_{20} + 5ac^4a_{21} = 0 \tag{10}$$

The 18 relations between grid point displacements (w, α and β at each of the six grid points) and the coefficients of the polynomial, together with the three constraint equations (8), (9), and (10), uniquely determine the coefficients a_1 to a_{21}. The following equations can therefore be written:

$$\{\delta\} = [Q]\,\{a\} \tag{11}$$

and

$$\{a\} = [S]\,\{\delta\} \tag{12}$$

where [Q] is the 18 x 21 matrix involving the co-ordinates of grid points substituted into the function w (eq. (6)) and the appropriate expressions of α and β; $\{a\}$ is the column vector of coefficients a_1 to a_{21}, and [S] is a 21 x 18 matrix and consists of the first 18 columns of the inverse of an augmented matrix of [Q] and the three constraint equations (8), (9), and (10).

Stiffness Matrix

The following relationships are obtained from the theory of deformation for plates (ref. 9). In the present notation, the curvatures are defined by

$$\begin{Bmatrix} \chi_x \\ \chi_y \\ \chi_{xy} \end{Bmatrix} = \begin{Bmatrix} -\dfrac{\partial\beta}{\partial x} \\ \dfrac{\partial\alpha}{\partial y} \\ \dfrac{\partial\alpha}{\partial x} - \dfrac{\partial\beta}{\partial y} \end{Bmatrix} \tag{13}$$

Bending and twisting moments are related to curvatures by

$$\begin{Bmatrix} M_x \\ M_y \\ M_{xy} \end{Bmatrix} = [D] \begin{Bmatrix} \chi_x \\ \chi_y \\ \chi_{xy} \end{Bmatrix} \tag{14}$$

where [D] is, in general, a full symmetric matrix of elastic coefficients.

Shear forces (and hence shear strains) are proportional to the third derivatives of the displacements. Since the displacement within the element is assumed to vary as a quintic polynomial, shear strains are expressed by a quadratic polynomial as follows:

$$\left.\begin{aligned} \gamma_x &= b_1 + b_2x + b_3y + b_4x^2 + b_5xy + b_6y^2 \\ \gamma_y &= c_1 + c_2x + c_3y + c_4x^2 + c_5xy + c_6y^2 \end{aligned}\right\} \tag{15}$$

The shear forces V_x, V_y are related to γ_x, γ_y by

$$\begin{Bmatrix} V_x \\ V_y \end{Bmatrix} = t^* \, [G] \begin{Bmatrix} \gamma_x \\ \gamma_y \end{Bmatrix} \tag{16}$$

where G is in general a full 2 x 2 symmetric matrix and t^* is an effective thickness of the element.

It can be shown that b_1 to b_6 and c_1 to c_6 can be expressed in terms of the coefficients a_1 to a_{21} (ref. 8) and hence $\begin{Bmatrix} \gamma_{xz} \\ \gamma_{yz} \end{Bmatrix}$ can be expressed as

$$\{\gamma\} = [B_1]\ \{a\} \tag{17}$$

where $[B_1]$ is as given in reference 8. The curvature $\{\chi\}$ is now split into 2 parts, i.e.,

$$\{\chi\} = \{\chi_1\} + \{\chi_2\} \tag{18}$$

where

$$\{\chi_1\} = \left\{ \begin{array}{c} \dfrac{\partial^2 w}{\partial x^2} \\ \dfrac{\partial^2 w}{\partial y^2} \\ 2\,\dfrac{\partial^2 w}{\partial x \partial y} \end{array} \right\} \qquad \{\chi_2\} = \left\{ \begin{array}{c} -\dfrac{\partial \gamma_{xz}}{\partial x} \\ -\dfrac{\partial \gamma_{yz}}{\partial y} \\ -\dfrac{\partial \gamma_{xz}}{\partial y} - \dfrac{\partial \gamma_{yz}}{\partial x} \end{array} \right\} \tag{19}$$

It follows that $\{\chi_1\}$ is the vector of curvatures in the absence of transverse shear and $\{\chi_2\}$ is the contribution of transverse shear to the vector of curvatures. Now $\{\chi_1\}$ and $\{\chi_2\}$ are expressed in terms of generalized co-ordinates $\{a\}$ as

$$\{\chi_1\} = [B_2]\ \{a\} \tag{20}$$

and

$$\{\chi_2\} = [B_3]\ \{a\} \tag{21}$$

where $[B_2]$ and $[B_3]$ are given in reference 8. Thus,

$$\{\chi\} = \{\chi_1\} + \{\chi_2\} = \left([B_2] + [B_3]\right)\ \{a\} \tag{22}$$

The generalized stiffness matrix can be obtained as (ref. 8):

$$[K]_{gen} = \iint \left\{ \left([B_2] + [B_3]\right)^T [D] \left([B_2] + [B_3]\right) + [B_1]^T\ [C][B_1] \right\} dx\ dy \tag{23}$$

The element stiffness matrix in the local co-ordinate system, $[K]_e$, is, by virtue of equation (12),

$$[K]_e = [S]^T [K]_{gen} [S] \tag{24}$$

The element stiffness matrix in the global co-ordinate system, $[K]_g$, is

$$[K]_g = [T_2]^T [K]_e [T_2] \tag{25}$$

where $[T_2]$ is the transformation matrix of displacement vectors from global to local co-ordinates of element.

The evaluation of the elements of the generalized stiffness matrix, $[K]_{gen}$ of equation (23), in closed form is, though straightforward, very tedious. This is due to the lengthy expressions involved in the triple matrix products. The integration involved in equation (23) is now split into 5 integrals as follows:

$$\begin{aligned} [K]_{gen} = & \iint [B_2]^T [D] [B_2] \, dx \, dy \\ & + \iint [B_2]^T [D] [B_3] \, dx \, dy + \iint [B_3]^T [D] [B_2] \, dx \, dy \\ & + \iint [B_3]^T [D] [B_3] \, dx \, dy + \iint [B_1]^T [G] [B_1] \, dx \, dy \end{aligned} \tag{26}$$

The first term $\iint [B_2]^T [D][B_2] \, dx \, dy$ is evaluated in closed form; the other four terms are evaluated using numerical integration. The numerical integration formulas used are listed in ref. 8. If the plate is assumed to be rigid in transverse shear, the matrices $[B_1]$ and $[B_3]$ are null and the last four terms of equation (26) vanish.

Consistent Mass Matrix

It can be shown that the generalized consistent mass matrix is (ref. 8)

$$[M]_{gen} = \rho t \iint [C]^T [C] \, dx \, dy \tag{27}$$

where $[C] = [1 \; x \; y \; x^2 \; xy \; y^2 \; ..... \; y^5]$.

The mass matrix can be transformed to element co-ordinates and global co-ordinates by the same transformations as those used for stiffness matrix. Thus,

$$[M]_e = [S]^T \, [M]_{gen} \, [S] \tag{28}$$

and

$$[M]_g = [T_2]^T \, [M]_e \, [T_2] \tag{29}$$

where the subscripts e and g on $[M]$ stand for element and global system, respectively.

Consistent Load Vector

It can be shown that the generalized consistent load vector is, (ref. 8)

$$[P]_{gen} = \iint \, [C]^T \, q \, dx \, dy \tag{30}$$

where q is the distributed loading.

The consistent load vector can now be transformed to element and global co-ordinates by

$$[P]_e = [S]^T \, [P]_{gen} \tag{31}$$

$$[P]_g = [T_2]^T \, [P]_e \tag{32}$$

THE QUADRILATERAL PLATE ELEMENT

The quadrilateral element is formed from four of the triangular elements just described. Two arrangements of the quadrilateral element are shown in Figures 3(a) and 3(b).

The quadrilateral element has eight grid points on its edges. In the arrangement of the quadrilateral element shown in Figure 3(a), which will be designated as QUAD1, the quadrilateral is divided, first into 2 triangles by one diagonal and then again into 2 more triangles by the other diagonal. In each case one additional grid point, at the mid-point of the diagonal, is introduced; the stiffness, mass and load matrices of the triangles are evaluated and added and the terms associated with the internal grid point are eliminated by static condensation. The stiffness, mass and load matrices of the quadrilateral element are obtained by adding one-half the contribution of each case. In the arrangement of the quadrilateral element shown in Fig. 3(b), designated as QUAD5, five additional grid points are introduced internally so that the quadrilateral is divided into four triangular elements. The eight grid points on the edges are numbered 1 to 8. Grid point 9 is located at the intersection of lines joining mid-points of opposite edges. Grid points 10 to 13 are located at the middle of the lines joining grid point 9 to each of the corners of the quadrilateral. The stiffness, mass and load matrices of the triangular elements are evaluated, as described previously, and added by the direct stiffness technique to form the respective matrices for the quadrilateral. The internal grid points are then eliminated by static condensation.

In a preliminary operation, the grid points of the quadrilateral are adjusted to lie in a median plane. The median plane is selected to be parallel to, and midway between, the diagonals of the quadrilateral. The adjusted quadrilateral is the normal projection of the given quadrilateral on the median plane. The short line segments joining the corners of the original and projected quadrilateral elements are assumed to be rigid in bending and extension. The quadrilateral element and its projection onto the median plane is shown in Fig. 3(c).

FORMULATION AND SOLUTION OF EQUATIONS

The global stiffness matrices, load vectors, and mass matrices for the complete structure modeled by these elements are assembled from the corresponding matrices of the individual elements by standard methods (ref. 6) to form the matrix equation

$$[K]\ \{U\} = \{P\} \tag{33}$$

Because the d.o.f. at grid points consist of displacements and rotations, it presents no difficulty to specify the appropriate geometric boundary conditions at any irregular and/or complex boundary. After the boundary conditions are applied, the matrix equation (33) is solved by Gaussian elimination to obtain the global displacement vector $\{U\}$.

DISCUSSION OF RESULTS

The triangular and quadrilateral elements are used to solve two problems in statics and dynamics of thin isotropic plates. Only the results for the simply supported plate are presented here; the interested reader may consult ref. 8 for details. The problem analyzed is that of the statics and dynamics of a square plate with edges simply supported. All calculations were carried out on the CDC 6400/6600 series of computers with SCOPE operating system of the Langley Research Center. Single precision arithmetic was used throughout. A value of Poisson's ratio of 0.0 is used in all problems. It is mentioned in this context that other finite-element analyses in the literature use 0.3 as the value of Poisson's ratio.

Static Analysis of a Square Plate

The arrangement of the finite elements in a quarter of the square plate is shown in Fig. 4. The number of subdivisions of the edge of the square is denoted by N. Due to symmetry, only one-quarter of the plate is analyzed. The calculated values of the deflection at the center of the simply supported plate are given in Table 1 and compared with the exact solution given by Timoshenko (ref. 9). These values together with other known finite element analyses available in the literature (refs. 3, 4, 5 and 10) are also compared in Figures 5 and 6 in plots of deflection versus mesh size using a linear scale for N^{-1}.

As seen from table 1, the "Q" arrangement is found to give better results than the "P" arrangement for the uniformly distributed loading; however, the "P" arrangement is found to be better, in general, for concentrated loads. For the clamped plate, the "P" arrangements are found to be slightly better than the "Q" arrangements, as noted from ref. 8. For the quadrilateral element, QUAD1 is found to be superior to QUAD5.

The high accuracy achieved with the present elements (triangular and quadrilateral), even for the coarsest mesh, is evident from Table 1 and Figures 5 and 6 for the simply supported plate. In the case of the clamped plate, the results for the coarsest grid are not as accurate as in the case of the simply supported plate (ref. 8); however, as the element size is decreased the values of deflection obtained with the present elements approach very rapidly the exact results.

Free Vibration of a Square Plate

The natural frequencies of a simply supported square plate were determined using the triangular and quadrilateral elements. The non-dimensional eigen-values are

$$\lambda = \rho t \omega^2 L^4 / D \qquad (34)$$

ρ = mass density

t = thickness of plate

ω = circular frequency

L = length of side of square plate

D = $Et^3/12(1 - \nu^2)$, the flexural rigidity of the plate.

The exact eigenvalues for the simply supported plate are given by

$$\lambda = (r^2 + s^2)^2 \pi^4 \tag{35}$$

where r and s refer to the number of half-waves parallel to the edge directions.

The lowest 6 values obtained using the present elements and the exact results are shown in Table 2. The eigenvalue problems were solved using a Jacobi routine that produced the complete set of eigenvalues and eigenvectors. Consistent mass matrix was used for treatment of inertia. It is seen that the lowest eigenvalue is calculated to within 1% of exact result. Good agreement is noticed for higher eigenvalues as well.

THE TR-18 FAMILY OF ELEMENTS

A number of finite element formulations for doubly curved shells are presently available, the notable among them being the works of Ahmad, Irons and Zienkiewicz (Ref. 11), Bonnes, Dhatt, Giroux, and Robichand (Ref. 12), Strickland and Loden (Ref. 13), Key and Beisinger (Ref. 14), Dhatt (Ref. 15), and Olson and Lindberg (Ref. 16). Some of these have neglected transverse shear deformations whereas some others use sub-triangles and/or second and higher order derivatives of the displacements of the element as degrees of freedom, thus complicating the formulation. A need still exists for an accurate shell element that has only translations and rotations as d.o.f.

Such shell elements can be derived using the TR-18 plate element; the formulation presented here is simple and includes transverse shear deformations; it is based on the linear shear deformation theory of thin shells as given by Washizu (Ref. 17).

Using shallow shell theory, flat plate elements can be easily converted to curved shell elements. The linear strain triangular membrane element, known as TRIM6 in the literature, can be combined with the TR-18 plate element to develop a doubly curved shallow shell triangular element. The surface of the shell will be approximated by a quadratic polynomial of the position coordinates of the base triangle. By a procedure analogous to that discussed for the quadrilateral plate element, a quadrilateral shallow shell element can be developed. Multilayered plates, and plates with coupled membrane and bending deformations, can be designed using TR-18 plate elements.

Fig. 7 shows a differential element dA on the middle surface of the doubly curved shell with orthogonal curvilinear surface co-ordinates ξ_1, ξ_2, ξ_3. A right handed cartesian co-or te system X, Y, Z is also shown. In Fig. 8 and Fig. 9 the curved triangular shell element is shown in basic and local coordinate systems. The differential surface element is expressed as

$$dA = \alpha_1 \ \alpha_2 \ d\xi_1 \ d\xi_2 \tag{36}$$

where α_1 and α_2 are the Lamé parameters.

If the surface $z(x,y)$ of an element is shallow, the following relations are valid

$$\left(z_{,x}\right)^2 \ll 1 \qquad \left(z_{,y}\right)^2 \ll 1 \qquad \left|z_{,x}\, z_{,y}\right| \ll 1 \tag{37}$$

where

$$z_{,x} = \frac{\partial z}{\partial x} \qquad z_{,y} = \frac{\partial z}{\partial y}$$

The set of orthogonal curvilinear co-ordinates (ξ_1, ξ_2, ξ_3) over the surface of the shallow element dA can be replaced by a set of shallow cartesian co-ordinates (x,y,z) where

$$\xi_1 = x \qquad \xi_2 = y \tag{38}$$

and Lamé parameters $\alpha_1 = \alpha_2 \approx 1$ (39)

From eq. (36), (38) and (39), $dA = dx\ dy$ (40)

The curvatures of the shallow element can then be approximated by

$$\frac{1}{R_{11}} = -z_{,xx} \tag{41}$$

$$\frac{1}{R_{22}} = -z_{,yy} \tag{42}$$

[illegible] (43)

The curved triangular element, shown in Fig. [illegible], is defined by grid points 1 to 6, the points being numbered in a counter-clockwise direction. The points 2, 4, and 6 are at the middle of the sides of the element. The basic co-ordinates of the nodes are X_1, Y_1, Z_1 through X_6, Y_6, Z_6. The x-y plane of the local co-ordinate system is parallel to the plane of the three corners of the triangle (points 1, 3 and 5 of the element). The x-axis is parallel to the side 1-3 of the triangular element. Each point on the surface of the triangular element determines, and is determined by, its projection in the x-y plane.

The transformation matrix between local and basic co-ordinates is given by

$$\begin{Bmatrix} X \\ Y \\ Z \end{Bmatrix} = \begin{bmatrix} \lambda_{11} & \lambda_{12} & \lambda_{13} \\ \lambda_{21} & \lambda_{22} & \lambda_{23} \\ \lambda_{31} & \lambda_{32} & \lambda_{33} \end{bmatrix} \begin{Bmatrix} x \\ y \\ z \end{Bmatrix} + \begin{Bmatrix} X_0 \\ Y_0 \\ Z_0 \end{Bmatrix} \tag{44}$$

where $\begin{Bmatrix} X_0 \\ Y_0 \\ Z_0 \end{Bmatrix}$ is the vector from the origin of the basic co-ordinate system to the origin of the local co-ordinate system. The distances X_0, Y_0, Z_0 are not involved in the calculation of the stiffness matrix of the element since only the differences of co-ordinates are used; hence they are discarded. The inversion of equation (44) yields

$$\begin{Bmatrix} x \\ y \\ z \end{Bmatrix} = \begin{bmatrix} \lambda_{11} & \lambda_{21} & \lambda_{31} \\ \lambda_{12} & \lambda_{22} & \lambda_{32} \\ \lambda_{13} & \lambda_{23} & \lambda_{33} \end{bmatrix} \begin{Bmatrix} X \\ Y \\ Z \end{Bmatrix} \tag{45}$$

It may be seen that λ_{11}, λ_{21} and λ_{31} are components in X, Y and Z directions of a unit vector along the x direction; and so on for λ_{12}, λ_{13}, etc.

An analytical description of the surface of the element suitable for application of shallow shell theory is obtained by assuming that the elevation of the shell middle surface may be expressed as a quadratic polynomial in the local co-ordinates of the element, i.e.,

$$z(x,y) = f_1 + f_2 x + f_3 y + f_4 x^2 + f_5 xy + f_6 y^2 \tag{46}$$

This implies that the shell element has constant curvatures and is consistent with the approximations of shallow shell theory. Knowing the co-ordinates x, y, z of the six points of the triangular element, the constants f_1 to f_6 can be evaluated.

Symbolically

$$\{z\} = [Q_1]\ \{f\} \tag{47}$$

or

$$\{f\} = [Q_1]^{-1}\ \{z\} \tag{48}$$

where $[Q_1]$ is a 6 x 6 matrix of the co-ordinates of the six points of the element substituted into equation (46).

Degrees of freedom and assumed displacement function.- The element has 30 degrees of freedom (d.o.f.), with 5 d.o.f. per grid point. These are the three translations u, v, w in the x, y, and z directions and the rotations of the xz and yz planes, α and β. The displacements u, v, w are positive in the positive co-ordinate directions; the slopes are positive when they cause compression at the top of the surface. The u and v d.o.f. are assumed to vary over the element by a full quadratic polynomial of local co-ordinates, as follows:

$$u = a_1 + a_2x + a_3y + a_4x^2 + a_5xy + a_6y^2 \tag{49}$$

$$v = a_7 + a_8x + a_9y + a_{10}x^2 + a_{11}xy + a_{12}y^2 \tag{50}$$

The deflection w will be defined by a quintic polynomial as in equation (6). The coefficients a_1 to a_{21} of equation (6) will be renumbered a_{13} to a_{33} respectively. The 33 coefficients a_1 to a_{33} can be uniquely determined from the 30 d.o.f. of the shell element (5 d.o.f. each at six grid points) together with the 3 constraint equations (8), (9), and (10).

Strain-displacement relations.- The expressions for transverse shear strains and bending strains for the curved shell element are the same as those for the TR-18 element (eqs. (7) and (13)). The membrane strains are

$$
\left.\begin{aligned}
e_x &= \frac{\partial u}{\partial x} - w\,\frac{\partial^2 z}{\partial x^2} \\
e_y &= \frac{\partial v}{\partial y} - w\,\frac{\partial^2 z}{\partial y^2} \\
e_{xy} &= \frac{\partial u}{\partial y} + \frac{\partial v}{\partial x} - 2w\,\frac{\partial^2 z}{\partial x \partial y}
\end{aligned}\right\} \tag{51}
$$

Stiffness matrix.- The stiffness matrix can be evaluated by the standard procedures (ref. 6). The element can then be tested against other elements (refs. 11 to 16) for suitability as well as accuracy. At the time of writing of this paper, the calculations for the element have not been completed.

Curved Quadrilateral Shell Element

A curved quadrilateral shell element can be constructed from the curved triangular shell elements by a procedure analogous to that of the construction of the quadrilateral plate element from the TR-18 element.

Plates With Membrane-Bending Coupling

Plates with coupled membrane and bending deformations and multilayered plates (fig. 10) can be analyzed by means of the elements presented earlier herein. Multilayered plates will produce coupling between membrane and bending deformations when the plate is not symmetrical with respect to its middle surface. A general form of the coupled stress-strain relationship can be expressed as

$$
\begin{Bmatrix} \{F\} \\ \{M\} \\ \{V\} \end{Bmatrix} = \begin{bmatrix} [A] & [B] & 0 \\ [B]^T & [D] & 0 \\ 0 & 0 & t^*[G] \end{bmatrix} \begin{Bmatrix} \{\varepsilon_m\} \\ \{\chi\} \\ \{\gamma\} \end{Bmatrix} \tag{52}
$$

where

$\{F\}$ is a vector of membrane force components F_x, F_y, F_{xy}

$\{M\}$ is a vector of bending and twisting moments M_x, M_y, M_{xy}

$\{V\}$ is a vector of transverse shear components V_x, V_y

$\{\varepsilon_m\}$ is a vector of membrane strain components ε_x, ε_y, ε_{xy}

$\{\chi\}$ is a vector of curvatures χ_x, χ_y, χ_{xy}

$\{\gamma\}$ is a vector of average transverse shear strain γ_x, γ_y

[A] is a 3 x 3 matrix, $\sum_{k=1}^{N} [G_e](t_k - t_{k-1})$

[B] is a 3 x 3 matrix, $\sum_{k=1}^{N} [G_e] \dfrac{t_k^2 - t_{k-1}^2}{2}$

[D] is a 3 x 3 matrix, $\sum_{k=1}^{N} [G_e] \dfrac{t_k^3 - t_{k-1}^3}{3}$

[G] is a 2 x 2 transverse shear matrix

$[G_e]$ is a 3 x 3 matrix of elastic coefficients

t_k is the distance to the outer edge of plate (or layer in a multilayer plate) from reference surface

t_{k-1} is the distance to the inner edge of plate (or layer in a multilayered plate) from reference surface

t^* is an effective thickness for the element

The inplane strain vector at any point is

$$\{\varepsilon\} = \{\varepsilon_m\} - z\,\{\chi\} \tag{53}$$

where z is the distance from the reference surface. The strain energy of the plate element is

$$U = \frac{1}{2} \int [\{F\}^T\{\varepsilon_m\} + \{M\}^T\{\chi\} + \{V\}^T\{\gamma\}]dA \tag{54}$$

where the integration is carried out over the surface of the element. The stiffness matrix for the triangular and quadrilateral elements can be evaluated by the usual procedures (refs. 6 and 8).

CONCLUDING REMARKS

New triangular elements and associated quadrileteral elements for plate and shell analysis having only displacement and rotations as grid point degrees of freedom are described in this paper. The examples presented for plate elements demonstrate that high accuracy is achievable using these elements for practical subdivisions.

The effect of transverse shear deformations is included in the element formulation. Transverse shear strains vary quadratically within the element; convergence to the limiting case of zero transverse shear strain is uniform. The present elements are expected to give better approximations than most displacement model plate bending elements for solving problems where transverse shear effects are significant.

Finally, it is remarked that these elements are ideally suited for inclusion into general purpose computer programs due to (i) simplicity of formulation, (ii) use of only displacements and rotations as grid point degrees of freedom, (iii) high accuracy for practical mesh subdivisions and (iv) inclusion of transverse shear flexibility in the element properties.

REFERENCES

1. Clough, R. W.; and Tocher, J. L.: Finite Element Stiffness Matrices for Analysis of Plate Bending. Matrix Methods in Structural Mechanics, AFFDL-TR-66-80, U.S. Air Force, Nov. 1966, pp. 515-545. (Available from DDC as AD 646 300.)

2. Bazeley, G. P., et al.: Triangular Elements in Plate Bending - Conforming and Non-Conforming Solutions. Matrix Methods in Structural Mechanics, AFFDL-TR-66-80, U.S. Air Force, Nov. 1966, pp. 547-576. (Available from DDC as AD 646 300.)

3. Argyris, J. H., et al.: Some New Elements for the Matrix Displacement Method. Proceedings of Second Conference on Matrix Methods in Structural Mechanics, AFFDL-TR-68-150, U.S. Air Force, Oct. 1968.

4. Bell, K.: Triangular Bending Elements. Chapter 7 in Finite Element Methods in Stress Analysis, I. Holland and K. Bell, eds., Techn. Univ. of Norway, Trondheim, 1969.

5. Cowper, G. R., et al.: A High Precision Triangular Plate Bending Element. Aeronautical Report LR-514, National Research Council of Canada, Ottawa, Canada, Dec. 1968.

6. Zienkiewicz, O. C.: Finite Element Method in Engineering Science, McGraw-Hill, London, 1971.

7. MacNeal, R. H., ed.: The NASTRAN Theoretical Manual (Level 15). NASA SP-221(01), 1972.

8. Narayanaswami, R.: New Triangular and Quadrilateral Plate-Bending Finite Elements. NASA TN D-7407, 1973.

9. Timoshenko, S.; and Woinowsky-Krieger, S.: Theory of Plates and Shells, 2nd ed., McGraw-Hill, New York, 1959.

10. Bell, K.: New Triangular Plate-Bending Finite Element. International Journal for Numerical Methods in Engineering, Vol. 1, 1969.

11. Ahmad, S.; Irons, B. M.; and Zienkiewicz, O. C.: Curved Thick Shell and Membrane Elements With Particular Reference to Axisymmetric Problems. Proceedings of Second Conference on Matrix Methods in Structural Mechanics AFFDL-TR-68-150, U.S. Air Force, Oct. 1968.

12. Bonnes, G.; Dhatt, G.; Giroux, Y. M.; and Robichaud, L. P. A.: Curved Triangular Elements for the Analysis of Shells. Proceedings of Second Conference on Matrix Methods in Structural Mechanics, AFFDL-TR-68-150, U.S. Air Force, Oct. 1968.

13. Strickland, G. E.; and Loden, W. A.: A Doubly Curved Triangular Shell Element. Proceedings of Second Conference on Matrix Methods in Structural Mechanics, AFFDL-TR-68-150, U.S. Air Force, Oct. 1968.

14. Key, S. W.; and Beisinger, Z. E.: The Analysis of Thin Shells With Transverse Shear Strains by the Finite Element Method. Proceedings of Second Conference on Matrix Methods in Structural Mechanics, AFFDL-TR-68-150, U.S. Air Force, Oct. 1968.

15. Dhatt, G. S.: Numerical Analysis of Thin Shells by Curved Triangular Elements Based on Discrete-Kirchoff Hypothesis. Proceedings of Symposium on Application of FEM in Civil Engineering, Nashville, Tennessee, Nov. 1969.

16. Olson, M. D.; and Lindberg, G. M.: Dynamic Analysis of Shallow Shells With a Doubly Curved Triangular Finite Element. J. Sound & Vib. 19(3), 1971, pp. 299-318.

17. Washizu, K.: Variational Methods in Elasticity and Plasticity. Pergamon Press, Toronto, Canada, 1968.

TABLE 1

Coefficients for Central Deflection of Simply Supported Square Plate of Side L

$\left[E = 1.0 \times 10^8; \quad \nu = 0.0\right]$

Number of elements per side, N	Coefficient $1000\, w_c D / PL^2$ due to central concentrated load P				Coefficient $1000\, w_c D / q_o L^4$ due to uniformly distributed load q_o			
	Triangular element		**Quadrilateral element**		Triangular element		Quadrilateral element	
	Q arrangement	P arrangement	QUAD 1	QUAD 5	Q arrangement	P arrangement	QUAD 1	QUAD 5
2	11.827079	12.064944	11.886797	12.294189	4.080739	4.173045	4.115169	4.177057
4	11.766154	11.705526	11.704203	11.760712	4.066626	4.074954	4.068629	4.078833
6	11.690134	11.647158	11.653533	11.673154	4.064244	4.066794	4.064797	4.068828
8	11.656354	11.627134	11.632881	11.642431	4.063427	4.064620	4.063666	4.065832
12	11.628511	11.612820	11.616516	11.620020	4.062843	4.063288	4.062927	4.063869
Exact (ref. 9)	11.600				4.062			

TABLE 2

Nondimensional Eigenvalue Numbers of Simply Supported Square Plate

Mode, (r,s)	Number of elements per side, N								Exact solution
	2				4				
	Triangular element		Quadrilateral element		Triangular element		Quadrilateral element		
	Q arrangement	P arrangement	QUAD 1	QUAD 5	Q arrangement	P arrangement	QUAD 1	QUAD 5	
(1,1)	386.14	384.97	388.10	387.20	388.93	388.74	389.08	388.53	389.64
(1,2)	2477.59	2477.59	2558.41	2628.19	2415.26	2415.26	2420.91	2427.66	2435.23
(2,2)	6541.93	6541.94	7997.35	8910.19	6179.56	6179.56	6209.53	6195.16	6234.18
(1,3)	7149.37	10008.09	10116.30	10413.34	9482.08	9331.84	9620.47	9769.04	9740.91
	9922.22	10458.52	10201.76	11160.88	9704.72	9548.69	9620.47	9769.04	
(2,3)					16144.46	16144.65	16358.12	16436.21	16462.14
(3,3)					30843.18	30676.12	31361.90	31498.11	31560.55

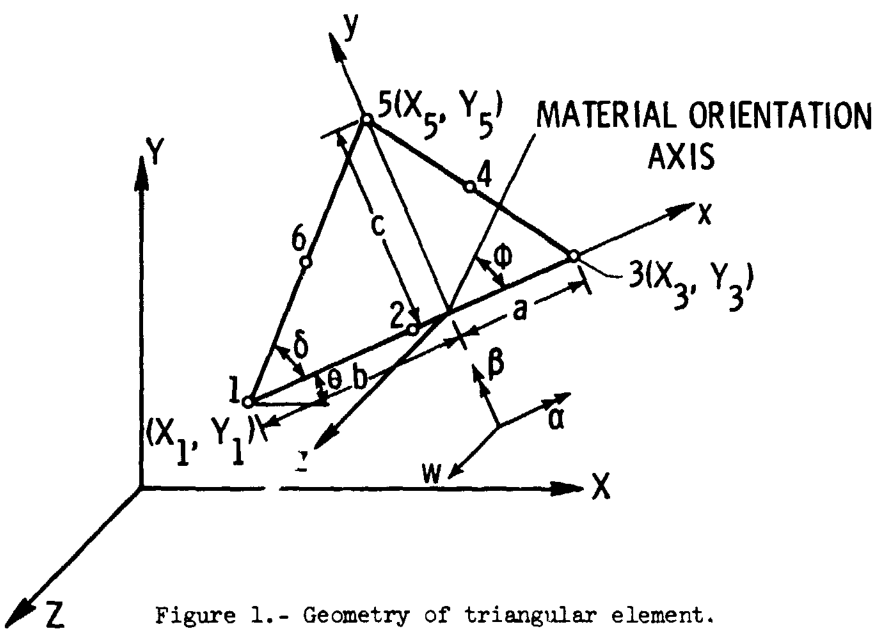

Figure 1.- Geometry of triangular element.

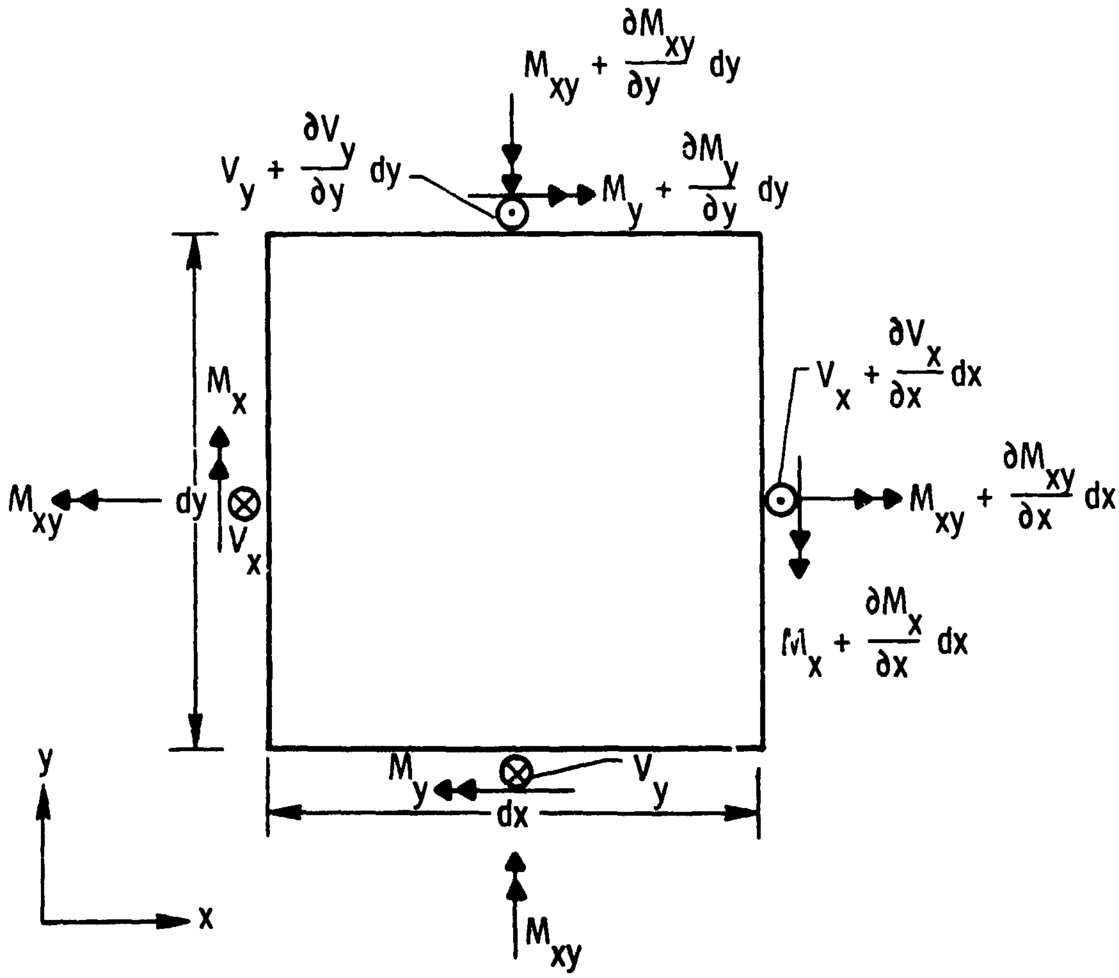

Figure 2.- Sign convention for moments and shears.

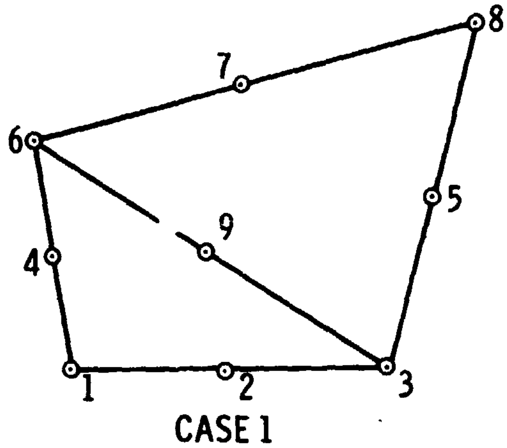

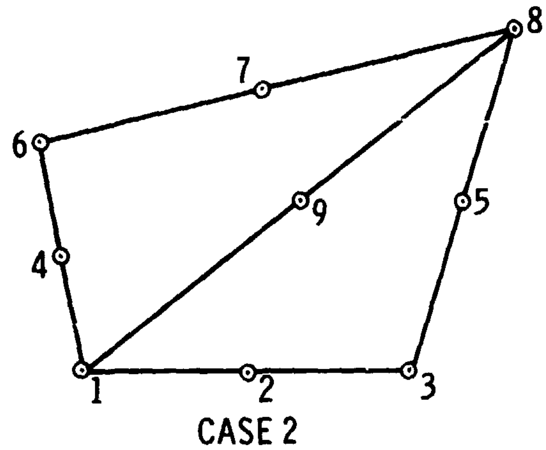

Figure 3(a).- Quadrilateral element (QUAD1) geometry.

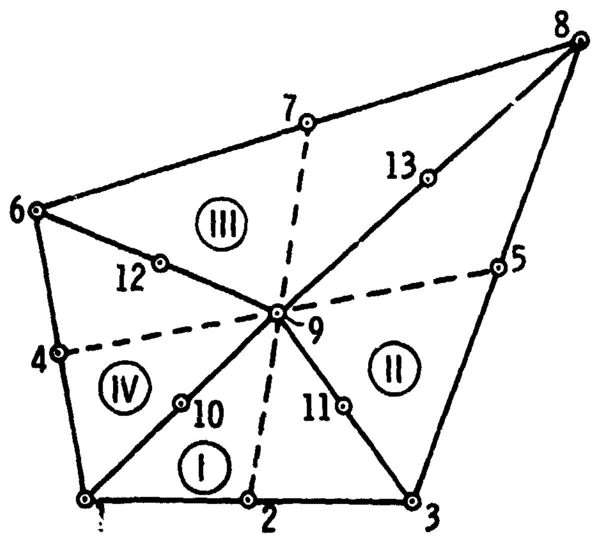

Figure 3(b).- Quadrilateral element (QUAD5) geometry.

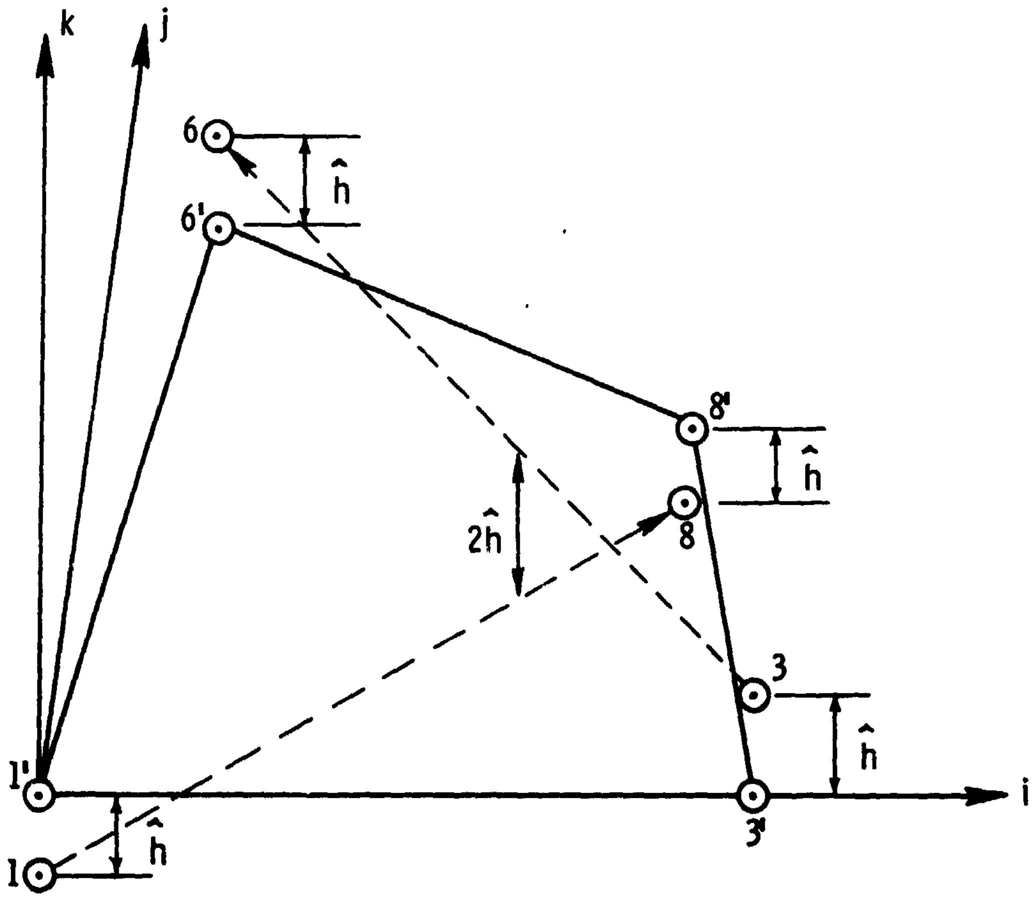

Figure 3(c).- Median plane for quadrilateral element.

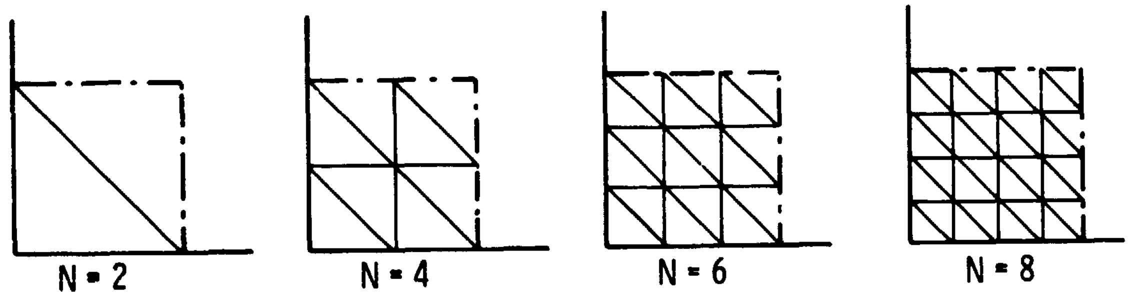

P arrangements of triangular element mesh idealization

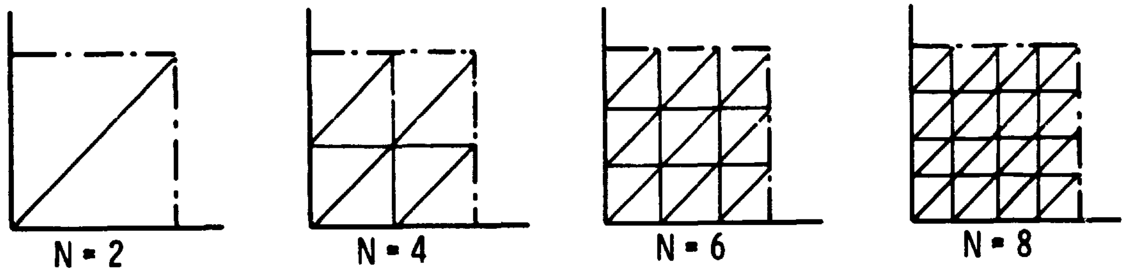

Q arrangements of triangular element mesh idealization

Figure 4.- Finite element idealization of square plate.

Notation	Element Shape	Reference
N	T (Q-mesh)	Present paper
P	T (P-mesh)	Present paper
Q1	Q	Present paper
Q5	Q	Present paper
ACM	R	1
HCT	T	1
Z	T	2
TUBA-6	T	3
B-2	T (T-18)	4,10
B-3	T (T-21)	4,10
C-N	T (Q-mesh)	5
C-P	T (P-mesh)	5
NQ	Q	7
CFQ	Q	9

T - Triangular; Q - Quadrilateral; R - Rectangular

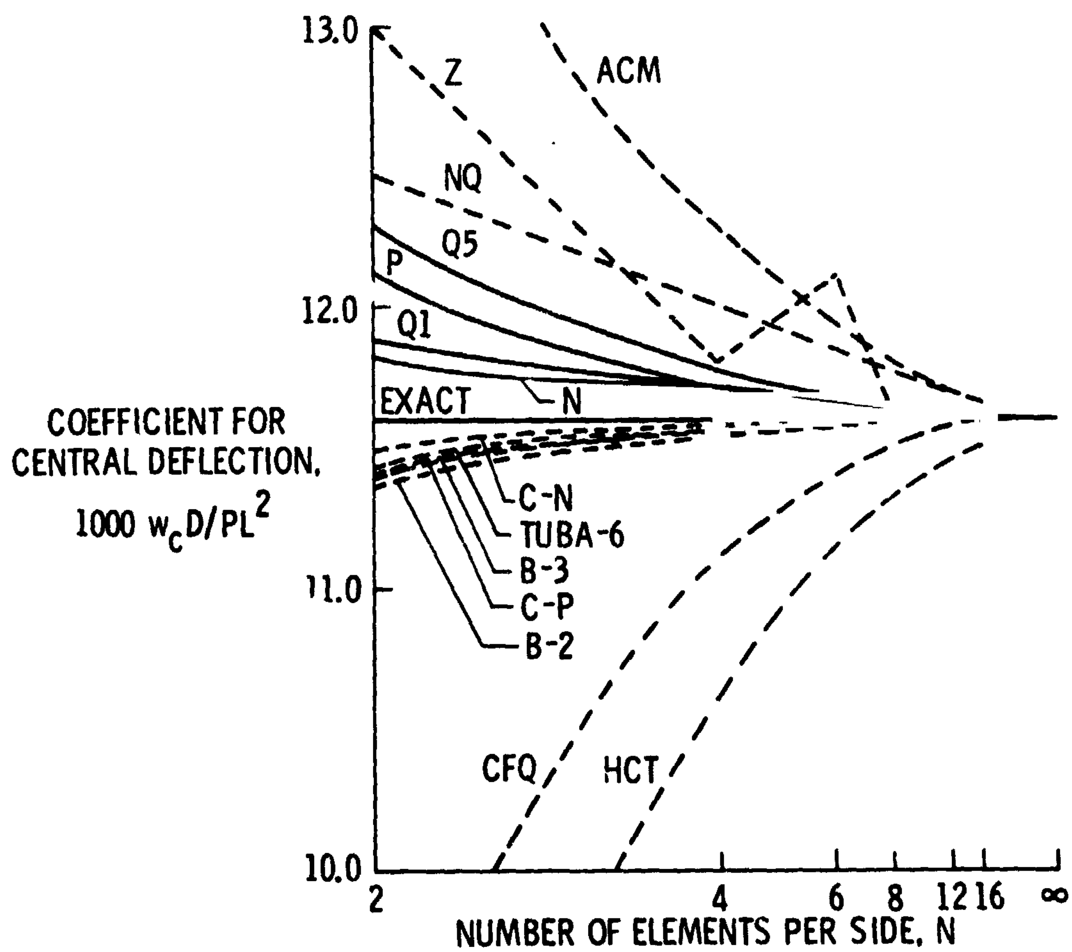

Figure 5.- Simply supported square plate: central deflection w_c under central point load P.

Notation	Element Shape	Reference
N	T (Q-mesh)	Present paper
P	T (P-mesh)	Present paper
Q1	Q	Present paper
Q5	Q	Present paper
ACM	R	1
HCT	T	1
Z	T	2
TUBA-6	T	3
B-1	T (T-15)	4
B-2	T (T-18)	4,10
B-3	T (T-21)	4,10
C-N	T (Q-mesh)	5
C-P	T (P-mesh)	5
NQ	Q	7
CFQ	Q	9

T - Triangular; Q - Quadrilateral; R - Rectangular

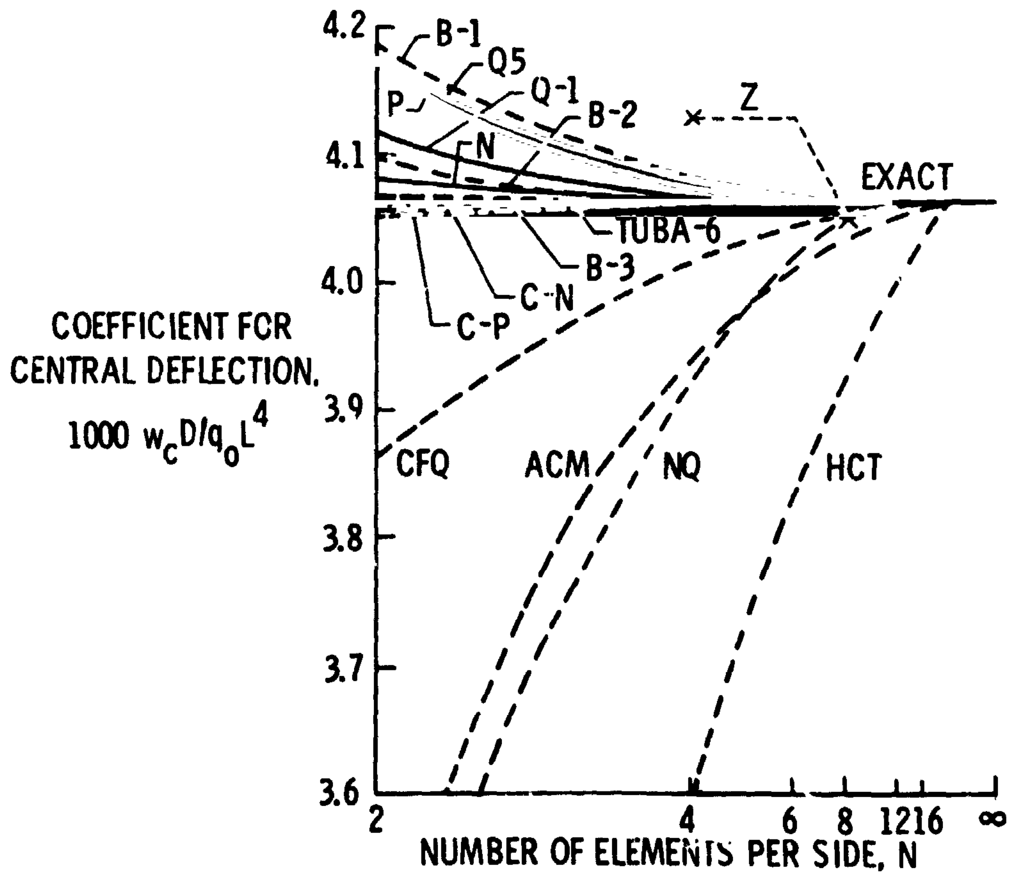

Figure 6.- Simply supported square plate: central deflection w_c under uniformly distributed load q_o.

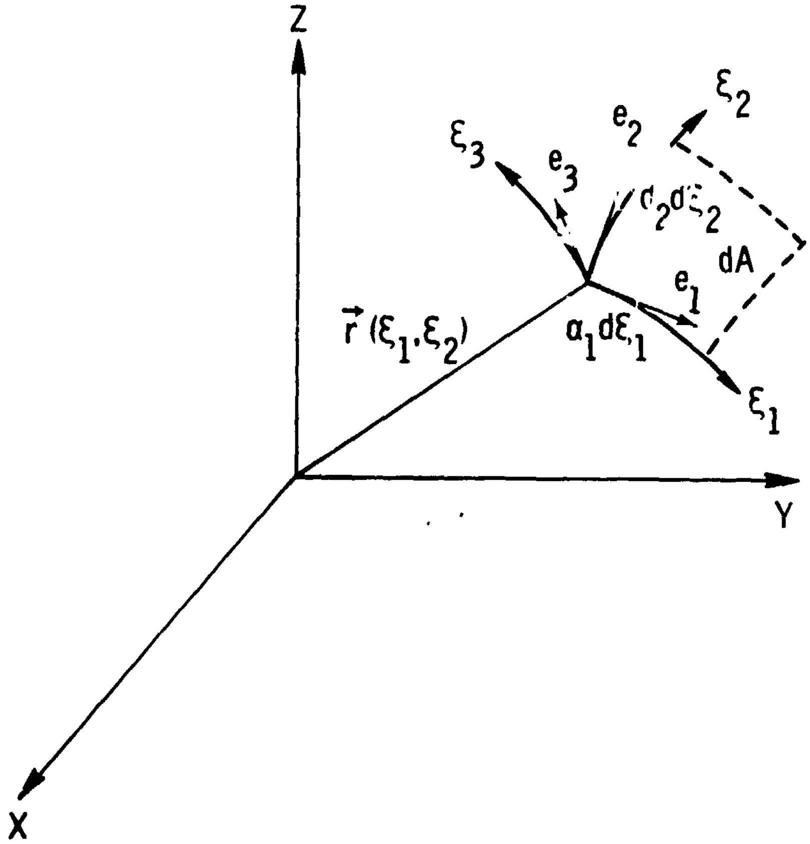

Figure 7.- Differential element.

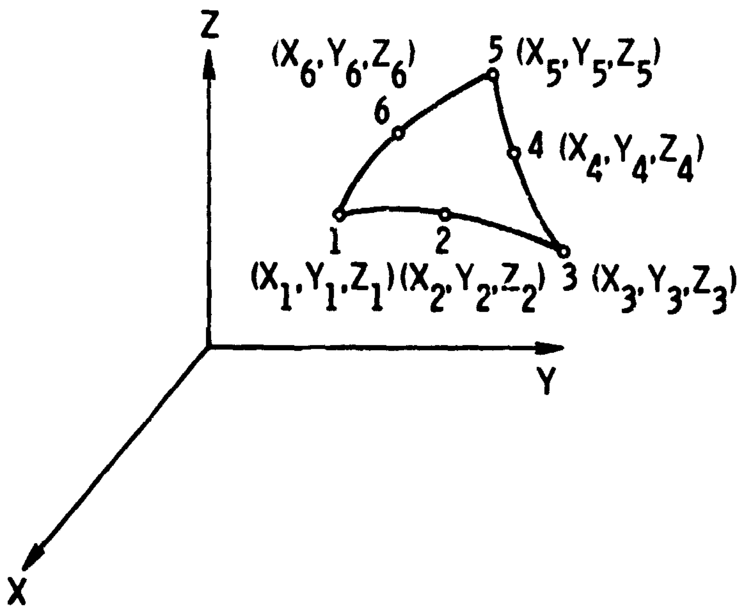

Figure 8.- Curved triangular shell element in basic co-ordinate system.

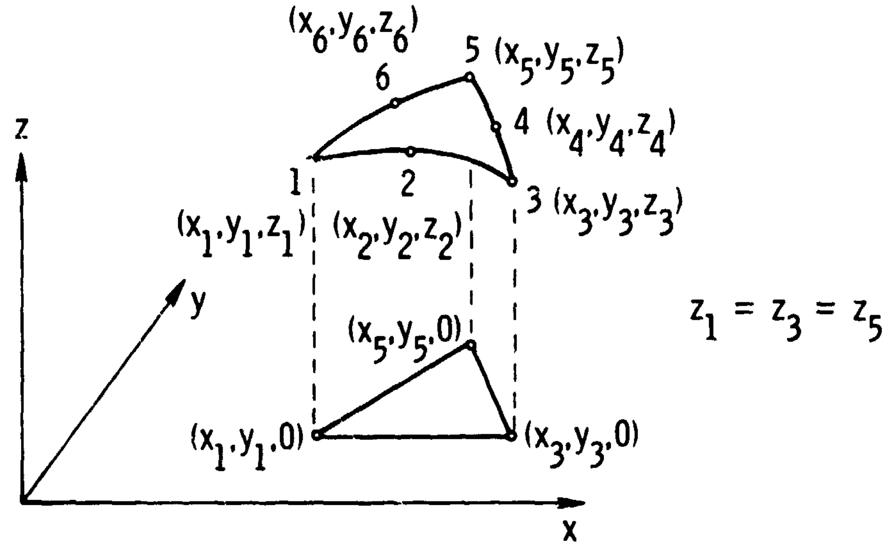

Figure 9.- Curved triangular shell element in local co-ordinate system.

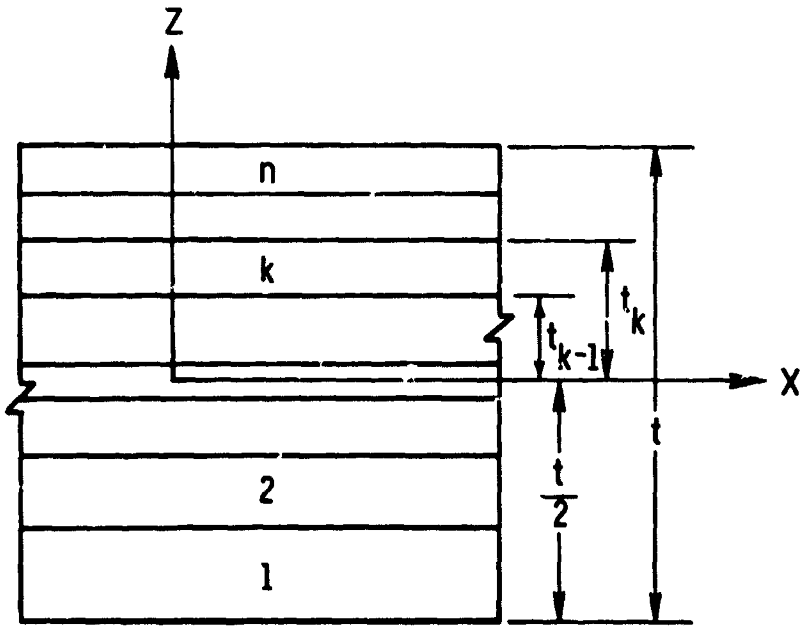

Figure 10.- Multilayered plate geometry.

N74-14608

FAST MODAL EXTRACTION IN NASTRAN VIA THE FEER COMPUTER PROGRAM

By Malcolm Newman and Aaron Pipano

Israel Aircraft Industries, Ltd.
Lod Airport, Israel

SUMMARY

A new eigensolution routine, FEER (Fast Eigensolution Extraction Routine), used in conjunction with NASTRAN at Israel Aircraft Industries is described. The FEER program is based on an automatic matrix reduction scheme whereby the lower modes of structures with many degrees of freedom can be accurately extracted from a tridiagonal eigenvalue problem whose size is of the same order of magnitude as the number of required modes. The process is effected without arbitrary lumping of masses at selected node points or selection of nodes to be retained in the analysis set.

The results of computational efficiency studies are presented, showing major arithmetic operation counts and actual computer run times of FEER as compared to other methods of eigenvalue extraction, including those available in the NASTRAN READ module. It is concluded that the tridiagonal reduction method used in FEER would serve as a valuable addition to NASTRAN for highly increased efficiency in obtaining structural vibration modes.

INTRODUCTION

One of the most burdensome computational tasks in discretized structural systems centers around the extraction of mode shapes and frequencies when the orders of the matrices are large. The difficulties are compounded as the number of required eigensolutions increases and multiple or near-multiple eigenvalues are encountered.

Currently, NASTRAN provides three methods for modal extraction (refs. 1 and 2): the Tridiagonal or Givens method, the Inverse Power Method with Shifts, and the Determinant method. In each method the problem size encountered is equal to the number of degrees-of-freedom in the analysis set which, given typical, present-day problem applications, may run into the thousands. One means of reducing the size of the analysis set is via the Guyan reduction (ref. 3), which has been incorporated into NASTRAN. This technique, which is similar in concept to the Kaufman - Hall reduction (ref. 4), requires a "judicious" elimination of selected mass degrees-of-freedom and an attempt is made to account for the influence of the eliminated nodes through equivalent energy criteria. As demonstrated by Levy (ref. 5), such an intuitive approach involves a great deal of guesswork and can lead to grossly inaccurate results, particularly in systems with relatively non-uniform mass distributions.

What is required to circumvent these difficulties is a more automated eigenreduction scheme which yields accurate lower modes of the structural system. In essence, the problem may be posed as follows:

Given the nth order eigenvalue problem

$$[K]\{\phi\} = \omega^2[M]\{\phi\} \tag{1}$$

where [K] and [M] are symmetric and non-negative definite, we wish to approximate the modal vectors by

$$\{\phi\} \approx [T]\{\delta\} \tag{2}$$

where [T] is a suitably constructed transformation matrix of size nxm (m<<n) and $\{\delta\}$ is an m-component vector of generalized coordinates. Using a Rayleigh-Ritz procedure the resulting reduced, mth order eigenproblem is of the form

$$[\bar{K}]\{\delta\} = \bar{\omega}^2[\bar{M}]\{\delta\} \tag{3}$$

where

$$[\bar{K}] = [T]^T [K] [T] \tag{4a}$$

$$[\bar{M}] = [T]^T [M] [T] \tag{4b}$$

and $\bar{\omega}$ is an approximate modal frequency. If a specified number of lower modes are to be accurately obtained, then the individual nth order vectors comprising the transformation matrix must be sufficiently rich in the corresponding modal vectors. Thus, the practical value of the reduction scheme hinges on its ability to generate such a transformation matrix with a minimum of computational effort.

A number of closely related methods involving eigenreduction concepts have been proposed previously. In the work of Hestenes and Karush (ref. 6), eigensolutions were obtained via a block power method (iterating with several vectors simultaneously as opposed to a single vector) and a reduced eigenvalue problem was employed to orthogonalize and improve successive blocks of vectors between iteration steps. More recently, Jennings and Orr (ref. 7), Dong, Wolf and Peterson (ref. 8), and Bathe and Wilson (ref. 9) proposed similar techniques using the Inverse Power Method in conjunction with simultaneous sets of vectors (alternately called Simultaneous Iteration, Subspace Iteration and Block-Stodola methods). In each of these approaches, however, the functional role of the reduced eigenproblem is to improve a subspace of approximate modal vectors with central emphasis being placed on a block-type Inverse Power method.

In this report, a new eigenreduction routine, FEER (Fast Eigensolution Extraction Routine) is described, wherein a single reduced eigenproblem is generated for the accurate extraction of any specified number of lower modes. Further, the transformation matrix is generated vector-by-vector in such a way that the reduced eigenproblem is tridiagonal in form. The FEER program is now being used in conjunction with NASTRAN at Israel Aircraft Industries to obtain much more economical eigensolutions than currently possible with the NASTRAN READ module.

The tridiagonal reduction method employed in FEER was first suggested by Crandall (ref. 10) as a truncated version of the Lanczos algorithm (ref. 11). However, it was soon discovered that the original scheme possessed numerical instabilities (refs. 12 and 13). The necessary improvements to correct these weaknesses were made by Ojalvo and Newman (ref. 14), who were the first to develop a successful tridiagonal reduction program for large scale structural dynamics problems. The FEER computer program contains further refinements later introduced by Newman and Pipano (ref. 15), including:

1. Highly efficient numerical computation schemes, using packing techniques which take advantage of matrix sparsity.

2. Calculation of accurate upper and lower bounds on the extracted eigenvalues.

3. Accommodation of singular mass matrices and stiffness matrix singularities associated with rigid body modes.

TRIDIAGONAL REDUCTION METHOD

Preliminary Operations

Employing the NASTRAN notation, the structural eigenvalue problem is of the form

$$[K_{aa}]\{\phi_a\} = \omega^2 [M_{aa}]\{\phi_a\} \tag{5}$$

Both $[K_{aa}]$ and $[M_{aa}]$ are nth order symmetric, non-negative and semi-definite matrices corresponding to the analysis set. Hence, they may both be singular, but all the eigenvalues are zero or positive.

In order to obtain a decomposable matrix, a small, positive shift parameter, α , is chosen such that

$$\omega^2 = \omega_o^2 - \alpha \tag{6}$$

Then

$$[K_{aa} + \alpha M_{aa}]\{\phi_a\} = \omega_o^2 [M_{aa}]\{\phi_a\}. \tag{7}$$

It can be easily shown that the shifted stiffness matrix is non-singular and positive-definite provided that the system masses generate kinetic energy due to any kinematically admissible rigid body motions of the structure. This requirement is always satisfied by the mass matrix in a physically well-posed problem.

In order to maintain the elements of the subsequent trial vectors on the order of unity, a positive mass-scaling parameter, S, is also employed, such that

$$[M_{aa}] = \frac{1}{S} [\bar{M}] \tag{8}$$

If a Cholesky symmetric decomposition of the shifted stiffness matrix is performed:

$$[K_{aa} + \alpha M_{aa}] = [L]\,[L]^T \tag{9}$$

it follows that the eigenvalue problem equation (7). ... be converted to the form

$$[B]\{x\} = \lambda\{x\} \tag{10}$$

where

$$[B] = [L]^{-1}[\bar{M}]\,[L^{-1}]^T \tag{11a}$$

$$\{x\} = [L]^T\,\{\phi_a\} \tag{11b}$$

and

$$\lambda = \frac{S}{\omega^2+\alpha} \tag{11c}$$

The above triangular matrix inverses are treated as purely operational symbols, since in actual numerical operations forward and backward passes on vectors are employed.

Generation of the Reduced Eigenproblem

A reduction of the nth order eigenvalue problem, equation (10), is effected through the transformation

$$\underset{n\times 1}{\{\bar{x}\}} = \underset{n\times m}{[V]}\,\underset{m\times 1}{\{y\}} \tag{12}$$

where $\{\bar{x}\}$ is an approximation of $\{x\}$ and $m < n$. The transformation matrix is taken to be unitary, so that

$$[V]^T[V] = [I]. \tag{13}$$

The reduced mth order eigenproblem is then

$$[A]\{y\} = \bar{\lambda}\{y\} \tag{14}$$

where

$$[A] = [V]^T[B][V] \tag{15}$$

and $\bar{\lambda}$ is an approximation of the eigenvalue λ.

The essence of the reduction scheme lies in the choice of the transformation matrix [V]. In the tridiagonal reduction method, the Lanczos algorithm (refs. 11 and 13) is used to build the [V] matrix, vector by vector, i.e.,

$$[V] = [\{v_1\}\ \{v_2\} \text{-------}\ \{v_m\}] \tag{16}$$

such that the reduced mxm matrix [A], is tridiagonal and its eigenvalues approximate the higher end of the eigenspectrum of [B] (or, equivalently, the lower natural frequencies of the structure).

The algorithm yields

$$[A] = \begin{bmatrix} a_{11} & d_2 & & & \\ d_2 & a_{22} & d_3 & & \\ & d_3 & a_{33} & \ddots & \\ & & \ddots & \ddots & d_m \\ & & & d_m & a_{mm} \end{bmatrix} \tag{17}$$

where the matrix coefficients are <u>theoretically</u> given by the recurrence formulas

$$\begin{aligned} a_{ii} &= \{v_i\}^T[B]\{v_i\} \\ d_i &= \{v_{i-1}\}^T[B]\{v_i\} \qquad ; \quad i = 1,m \\ \{\bar{v}_{i+1}\} &= [B]\{v_i\}-a_{ii}\{v_i\}-d_i\{v_{i-1}\} \\ \{v_{i+1}\} &= \{\bar{v}_{i+1}\}/[\{\bar{v}_{i+1}\}^T\{\bar{v}_{i+1}\}]^{1/2} \end{aligned} \tag{18}$$

The process is initialized by choosing an initial trial vector, $\{v_1\}$ and setting $\{v_{-1}\} = \{0\}$; $d_1 = 0$.

The initial trial vector should contain all components of the system eigenvectors and must be constrained to eliminate spurious eigensolutions ($\omega^2 \to \infty$) due to mass matrix singularities. These requirements are satisfied by setting

$$\{v_1\} = [B]\{w\}/[(Bw)^T(Bw)]^{1/2}, \tag{19}$$

where {w} is an n-element vector obtained from a random number generator routine.

Reorthogonalization of the Trial Vectors

Although the trial vectors $\{v_i\}$ generated in equations (18) form a theoretically orthogonal set, it has been shown (ref. 16) that they rapidly degrade as the computations proceed, such that the later vectors are far removed from orthogonality to the earlier ones. This is caused by unavoidable computational round-off, which, because of repeated multiplications by the unreduced eigenmatrix, [B], tends to amplify the contributions of the lower frequency eigenvector components. To correct this problem, Gregory (ref. 12) experimented with the use of higher precision arithmetic, but found only marginal improvements in the final results. Later, Lanczos suggested a single reorthogonalization of the trial vectors. While this improves matters substantially, it still does not eliminate the precision problem adequately. However, Ojalvo and Newman (ref. 14) found that the introduction of an iterative reorthogonalization loop can make the trial vectors as orthogonal as necessary for extremely large systems. The procedure is as follows:

Denote each new vector obtained from equations (18) as $\{v^o_{i+1}\}$ and iterate,

$$\begin{aligned} \{v^1_{i+1}\} &= \{v^o_{i+1}\} - \sum_{j=1}^{i}[\{v_j\}^T\{v^o_{i+1}\}]\{v_j\} \\ \{v^2_{i+1}\} &= \{v^1_{i+1}\} - \sum_{j=1}^{i}[\{v_j\}^T\{v^1_{i+1}\}]\{v_j\} \end{aligned} \tag{19}$$

until an acceptable vector

$$\{v^{s+1}_{i+1}\} = \{v^s_{i+1}\} - \sum_{j=1}^{i}[\{v_j\}^T\{v^s_{i+1}\}]\{v_j\}$$

is found which satisfies the orthogonality criterion

$$\max_{1\le j\le i}\left|\{v_j\}^T\{v^s_{i+1}\}\right| \le 10^{2-t} \tag{20}$$

where t is the total number of decimal digits carried by the computer.

A normalized form of the reorthogonalized trial vector is finally obtained through

$$\{v_{i+1}\} = \{v_{i+1}^{s+1}\}/[\{v_{i+1}^{s+1}\}^T\{v_{i+1}^{s+1}\}]^{1/2} \tag{21}$$

Experiences gained through application of the FEER program to a large variety of problem types and sizes have indicated that an average of only two reorthogonalizations are required per trial vector generation.

Size Criteria for the Reduced Eigenproblem

As a result of numerical experiments and applications (refs. 14, 15, 17-19), it has been found that in cases where $m \ll r$ (where r is the total number of structural modes, including rigid body modes, and m is the size of the reduced eigenvalue problem), a first grouping of more than m/2 lower frequencies of the reduced system are in accurate agreement with the corresponding number of exact frequencies, provided that $m \geq 7$, i.e., when at least seven trial vectors are chosen. The remaining reduced system frequencies are spread across the remaining exact spectrum, with the last one representing a lower bound on the highest exact frequency of the unreduced problem.

Thus, if the user requests q lower frequencies of the structure, the order of the reduced eigenvalue problem is

$$m = \left\{ \begin{array}{ll} \min\,[2q+1, r]; & q > 3 \\ \min\,[7, r]\;; & q \leq 3 \end{array} \right\} \tag{22}$$

It should be noted that in all cases $m \leq r$, and whenever m is set equal to r, <u>all</u> the structural modes of the unreduced problem are generated.

Error Bounds on the Computed Eigenvalues

One of the inherently striking features of the tridiagonal reduction method is that the solution of the reduced, tridiagonal eigenproblem

$$[A]\{y\} = \bar{\lambda}\{y\} \tag{23}$$

and the off-diagonal elements of [A] automatically provide accurate error-bound parameters for the extracted eigenvalues. In particular, it can be shown (ref.20) that absolute error bounds for each approximate root, $\bar{\omega}_i^2$, are found from the inequality

$$\left| \frac{\bar{\omega}_i^2 + \alpha}{\omega_i^2 + \alpha} - 1 \right| \leq \frac{\left| d_{m+1} \cdot (y_f)_i \right|}{\bar{\lambda}_i} \tag{24}$$

where ω_i^2 is an exact system root, d_{m+1} is the (m+1)th off-diagonal element of an [A] matrix of order m+1, and y_{fi} is the last element of the eigenvector corresponding to $\bar{\lambda}_i$.

Program FEER Flow Diagrams and Sample Output

The overall flow diagram for implementation of the tridiagonal reduction method in FEER is shown in figure 1. The reduced system eigenvalue problem is solved in block 7 by means of a Q-R algorithm which takes advantage of the symmetrical, tridiagonal form of the eigenmatrix and the physical modal vectors and frequencies are finally computed in block 9. The details of block 6, "Execute Tridiagonal Reduction Algorithm", are given in figure2. Block 6.4 and the associated peripheral test conditions are used to generate re-start vectors whenever premature vanishing of a trial vector occurs. This is usually due to the existence of multiple or near-multiple eigenvalues, as described in reference 13. Figure 3 shows a representative eigenvalue table produced by FEER. In this example, the order of the stiffness matrix was 3,072, while the size of the reduced problem was 41. As shown by the error bound listing, FEER generated 21 lower frequencies to within an accuracy of .01%, using only 362 seconds of CPU time on a CDC-6600 computer.

COMPUTATIONAL EFFICIENCY STUDIES

A count of the major arithmetic operations expended in FEER is summarized in Table 1, where n denotes the size of the stiffness matrix in the analysis set, b and $\bar{b}$ are average semi-band widths of the stiffness and mass matrices, respectively, and q is the number of accurate modes requested by the user. Each operation is assumed to consist of a multiplication followed by an addition.

It should be noted that the average bandwidth parameters are used primarily to provide a measure of the number of non-zero matrix elements. In actuality, FEER employs efficient packing routines which do not require a uniform band structure for efficient computational operations. It can be seen that the major computational effort involves decomposition of the modified stiffness matrix (step 3) and provides the leading term of $1/2\ nb^2$ in the total operation count. One of the positive features of the tridiagonal reduction method is that only one such decomposition is performed regardless of the number of roots required.

Operation count and storage requirements for several alternate eigensolution methods are compared with FEER in Table 2. The purpose of this comparison is to provide an indication of the potential efficiency of each method, assuming that an equally adept and knowledgable programmer has had a chance to employ the same time-saving tricks in each case. For this reason, several excellent solution techniques which achieve high efficiency through special data handling and storage methods (see for example, refs. 21 and 22), but nevertheless show a high minimum operation count, have not been included in the comparison. As in Table 1, the counts are presented in terms of average bandwidths which are again to be interpreted as a measure of non-zero matrix entries rather than in terms of a specific band structure.

It can be seen that in the Givens method the operation count $(\frac{2}{3}n^3)$ and the storage requirements as well $\left(0(n^2) \right)$ become prohibitively large when the size of analysis set grows beyond more than a few hundred degrees-of-freedom.

The leading term in the Inverse Power Method (NASTRAN) is $qnb^2/2$ as compared to $nb^2/2$ for FEER, since at least one shift per extracted root and a subsequent triangular decomposition is typically required in the former method. Based on this assumption and the additional supposition that an average of seven iterations per eigenvector are required in the Inverse Power method, theoretical operation-count ratios (Inverse Power Method/FEER) are presented as a function of semi-band width and the number of required roots in figures 4 and 5 for the cases of diagonal and consistent mass matrices. These curves provide only an approximate estimate of the relative time savings actually accrued for several reasons. First, the structure of the stiffness matrix influences the decomposition strategy employed in NASTRAN via the active column approach. In addition, there is no a-priori knowledge of the actual number of shifts and iterations which will be required in the Inverse Power method for any given problem application. In general, both the number of shifts and iterations tend to increase with the number of roots extracted, so that the curves indicating improved efficiency of the Inverse Power method for a very large number of extracted roots and small bandwidths are unrealistic.

Table 2 also shows approximate operation counts and storage requirements for Gupta's Sturm Sequence method (ref. 23) and a current version of the subspace or Block-Stodola method (ref. 9). The storage requirements for each of these methods, as well as the Inverse Power and FEER methods, are all on the same order of magnitude. In Gupta's method the count of $25nb^2q$ is based on his assumption that approximately $2nb^2$ operations are involved in examining the Sturm sequence for one trial root value, and that about twelve such values must be examined for each accurately predicted root (ref. 9). With regard to the Subspace Iteration method, the leading term in the count, nb^2, is twice as large as in FEER and all other terms involving the same functional forms of the parameters n, b, $\bar{b}$, q are also much larger. In addition, the reduced eigenproblem which is solved for improvement of the subspace is not tridiagonal so that the count for this operation is on the order of q^3 as compared to q^2 for the tridiagonal reduction method. Finally, the assumption of eight subspace iterations may not be very reliable, since this depends on the choice of the starting subspace, which is somewhat arbitrary.

Table 3 presents a set of actual computer runs comparing the CPU execution times of FEER vs. the Inverse Power and Givens methods in the NASTRAN READ module. The results indicate that the more efficient decomposition operations and shift strategy incorporated into Level 15 have yielded significant improvements in the Inverse Power method as compared to the Level 12 version (see also ref.24).

However, the run times for comparable or identical problems are generally 5 to 20 times faster with FEER than with the Level 15 Inverse Power method when between 5 and 20 accurate modes are requested. This result is in rough agreement with the operation count ratios shown in figures 4 and 5. In problem No.2, which is relatively small and could therefore be treated with the Givens method, the execution time via FEER was approximately 3 times as fast, since only 35 modes were requested, while in the Givens method the user has no choice and must pay the penalty of having all the eigenvalues calculated (in this particular case, 105).

CONCLUDING REMARKS

Significant computational efficiencies are achieved in the FEER program primarily due to the tridiagonal reduction method of modal extraction. Basically, the subspace of trial vectors generated via this method are sufficiently rich in the lower modes to provide a single, reduced, tridiagonal eigenproblem whose solution provides these modes with a high degree of accuracy. This feature distinguishes it from the usual subspace or block iteration methods, where the trial vector subspace is established somewhat arbitrarily and subsequently improved through repeated solutions of reduced eigenproblems. The tridiagonal reduction method employs only a single, intitial shift of eigenvalues and hence requires only one matrix decomposition. It is consequently much more efficient than the Inverse Power Method with shifts when more than one or two lower modes are required. FEER is also extremely efficient for out-of-core operations and requires only (15,000 + 7.n) central memory words, where n is the order of the analysis set. Another feature of the method is that the reduced problem is generated automatically, starting with a random trial vector, and this avoids one of the basic weaknesses of techniques requiring either a judicious selection of starting vectors or retained nodes.

It is concluded that the tridiagonal reduction method used in FEER would serve as a valuable addition to NASTRAN for increased efficiency in obtaining structural vibration modes.

REFERENCES

1. MacNeal, R.H., et al: The NASTRAN Theoretical Manual (Level 15). NASA SP-221(01), April, 1972.

2. McCormick, C.W., et al: The NASTRAN User's Manual (Level 15). NASA SP-222(01), June, 1972.

3. Guyan, R.J. : Reduction of Stiffness and Mass Matrices. AIAA J., vol. 3, no. 2, 1965, p. 380.

4. Kaufman, S., and Hall, D.B. : Reduction of Mass and Loading Matrices. AIAA J., vol. 6, no. 3, 1968, pp. 550-551.

5. Levy, R. : Guyan Reduction Solutions Recycled for Improved Accuracy. NASA TM X-2378, vol. 1, Sept., 1971, pp.201-220.

6. Hestenes, M.R., and Karush, W. : J. Res. Nat. Bur. Stand., vol. 47, 1951, p. 45.

7. Jennings, A., and Orr, D.R.L. : Application of the Simultaneous Iteration Method to Undamped Vibration Problems. Int. J. Numer. Meth. Eng., vol. 3, no. 1 1971, pp.13-24.

8. Dong, S.B., Wolf, J.A., Jr., and Peterson, F.E.: On a Direct-Iterative Eigensolution Technique. Int. J. Numer, Meth. Eng., vol. 4, no.2, 1972, pp. 155-161.

9. Bathe, K-J., and Wilson, E.L.: Solution Methods for Eigenvalue Problems in Structural Mechanics. Int. J. Numer. Meth. Eng., vol. 6, no. 2, 1973, pp. 213-226.

10. Crandall, S.H. : Engineering Analysis. McGraw-Hill, N.Y., 1956, pp. 106-109

11. Lanczos, C. : An Iteration Method for the Solution of the Eigenvalue Problem of Linear Differential and Integral Operators. J. Res. Nat. Bur. Stand., vol. 45, 1950, pp.225-282.

12. Gregory, R.T. : Results Using Lanczos' Method for Finding Eigenvalues of Arbitrary Matrices. J. Soc. Ind. & Appl. Math., vol. 6, 1958, pp. 182-188.

13. Wilkinson, J.H. : The Algebraic Eigenvalue Problem. Clarendon Press, Oxford, 1965.

14. Ojalvo, I.U., and Newman, M. : Vibration Modes of Large Structures by an Automatic Matrix-Reduction Method. AIAA J., vol. 8, no. 7, 1970, pp.1234-1239.

15. Newman, M., and Pipano, A.: Vibration Modes via Program NEWLAS, Chapter C-Program FEER (Fast Eigenvalue Extraction Routine). IAI TR 4842/6277, June, 1971, pp.7-16.

16. Causey, R.L., and Gregory, R.T. : On Lanczos' Algorithm for Tridiagonalizing Matrices. Soc. Ind. and Appl. Math. Rev., vol. 3, 1961, pp. 322-328.

17. Potts, J.S., Newman, M., and Wang, S.L. : HABEAS - A Structural Dynamics Analysis System. Proc. 24th Nat. Conf. Assoc. Comp. Mach., ACM Publ. P-69, 1969, pp. 647-664.

18. Meissner, C., Ojalvo, I., and Berson, M: Dynamic Analysis of the USS Atlanta Blast-Hardened Deckhouse. H. Belock Assoc. Rept. 154-3, Apr., 1968.

19 Ojalvo, I., Landsman, D., and Peterson, J. : Structural Dynamic Simulation of Gun Blast Effects Upon the Basic Point Defense Director. H. Belock Assoc. Rept. 97-3, Aug. 1967.

20. Newman, M. : Proposed Additions to the NASTRAN Theoretical Manual (Level 15) for the Tridiagonal Reduction Method of Eigenvalue Extraction. IAI TR 4842/6278, Feb., 1973.

21. Whetstone, W.D., and Jones, C.E. : Vibrational Characteristics of Linear Space Frames. Proc. ASCE: J. Struct. Div., vol. 95, no. ST 10, 1969, pp. 2077-2091.

22. Whetstone, W.D. : Computer Analysis of Large Linear Frames. Proc. ASCE: J. Struct. Div., vol. 95, no. ST 11, 1969, pp.2401-2417.

23. Gupta, K.K. : Vibration of Frames and Other Structures with Banded Stiffness Matrix. Int. J. Numer. Meth. Eng., vol. 2, no. 2, 1970, pp. 221-228.

24. Raney, J.P., and Weidman, D.J. : NASTRAN: A Progress Report. NASA TM X-2637, Sept., 1972, pp. 1-11.

25. Thornton, E.A. : A NASTRAN Correlation Study for Vibrations of a Cross-Stiffened Ship's Deck. NASA TM X-2637, Sept. 1972, pp. 145-159.

TABLE 1

SUMMARY OF MAJOR OPERATIONS AND STORAGE REQUIREMENTS

- TRIDIAGONAL REDUCTION METHOD (PROGRAM FEER)

Operation	Major Calculations	Approximate Operation Count	Approximate Storage Requirements*
1. Stiffness matrix shift	$[\bar{K}] = [K_{aa} + \lambda M_{aa}]$	$n\bar{b}$	
2. Mass matrix scaling	$[\bar{M}] = S[M_{aa}]$	$n\bar{b}$	
3. Cholesky decomposition of $[\bar{K}]$	$[\bar{K}] = [L][L]^T$	$\frac{1}{2}nb^2$	
4. Tridiagonal Reduction Algorithm and reorthogonalization of trial vectors; i = 1,2, ...2q	$[B] = [L]^{-1}[\bar{M}][L^{-1}]^T$ $a_{i,i} = \{v_i\}^T[B]\{v_i\}$ $d_i = \{v_{i-1}\}^T[B]\{v_i\}$ $\{\bar{v}_{i+1}\} = [B]\{v_i\} - a_{ii}\{v_i\} - d_i\{v_{i-1}\}$ $\bar{d}_{i+1} = [\bar{v}^T_{i+1}\,\bar{v}_{i+1}]^{\frac{1}{2}}$ $\{v^1_{i+1}\} = \{\bar{v}_{i+1}\}/\bar{d}_{i+1}$ $\{v^{s+1}_{i+1}\} = \{v^s_{i+1}\} - \sum_{j=1}^{i}[v_j^T\, v^s_{i+1}]\{v_j\}$; $s=1,2,\ldots,t$ $d^t_{i+1} = [\{v^t_{i+1}\}^T\{v^t_{i+1}\}]^{\frac{1}{2}}$ $\{v_{i+1}\} = \{v^t_{i+1}\}/d^t_{i+1}$	$4qn(b+\bar{b}+2q+1)$	$n(b+2q)$
5. Q-R iterations to obtain 2q modes of the tridiagonal [A]matrix; i=1,2, ...,2q	$[T_1] = [A]$ $[T_{k+1}] = [Q_k]^T[T_k][Q_k]$; $k = 1,2,\ldots,m$ $[\bar{\lambda}_i] = [T_m]$ $([A] - \bar{\lambda}_i[I])\{y_i^{k+1}\} = \{y_i\}^k$; $k = 1,2,\ldots,t$ $\{y_i\} = \{y_i^t\}$	$80q^2$	
6. Recovery of physical eigenvalues and eigenvectors; i=1,2,...2q	$\omega_i^2 = \frac{1}{\bar{\lambda}_i} - \lambda$ $\{\phi_i\} = [L^{-1}]^T[V]\{y_i\}$	$2nq^2$	
Total operations for q lowest eigenvalues and associated eigenvectors, assuming two reorthogonalizations per trial vector and two Q-R iterations of the reduced, tridiagonal matrix		$n[\frac{1}{2}b^2 + 4q(b+\bar{b}+1) + 10q^2+2\bar{b}] + 80q^2$	

*Minimum core storage = (15,000 + 7n) central memory words

TABLE 2

OPERATION COUNT AND STORAGE COMPARISONS FOR ALTERNATE EIGENSOLUTION METHODS

Method	Approximate Operation Count (Significant Terms)	Approximate Storage Requirements
Givens' Method - NASTRAN, plus Q-R iterations (all eigenvalues and q eigenvectors obtained)	$\frac{2}{3}n^3 + n^2(q + 10) + n(q(9 + \bar{b}) + \frac{1}{2}\bar{b}^2) + 4b\bar{b}$	$O(n^2)$
Inverse Power Method - NASTRAN (assuming one shift per root and seven iterations per eigenvector)	$nq(\frac{1}{2}b^2 + 15(b + \bar{b}) + 7q - 5)$	$O(nb)$
Gupta's Sturm Sequence method (assuming twelve iterations per root)	$25nb^2q$	
Subspace Iteration Method (assuming eight iterations and one Q-R eigensolution per iteration)	$n(b^2 + 32q(b + \bar{b}) + 64q^2 + 5b + \bar{b}) + 40q^2(q + 16)$	
Tridiagonal Reduction Method - Program FEER (assuming two reorthogonalizations per trial vector and two Q-R iterations of the reduced, tridiagonal matrix)	$n(\frac{1}{2}b^2 + 4q(b + \bar{b}) + 10q^2 + 2\bar{b}) + 80q^2$	

TABLE 3

EXECUTION TIME (CPU SECONDS): FEER vs. NASTRAN READ MODULE

Problem No.	Description	Unrestrained Degrees of Fredom	Average Semi-Band Width	No. of Accurate Modes Obtained	CPU Execution Time, Sec.*					
					CDC 6500 - 145 K_8			CDC 6600 - 145 K_8		
					FEER	NASTRAN Level 12.1	NASTRAN Level 15.1	FEER	NASTRAN Level 12.1	NASTRAN Level 15.1
1	Simply Supported Plate	105	30	16	11	790/INV				
2	Simply Supported Plate	105	30	35	17	58/GIV				
3	Free-Free Plate	130	30	10	12			7		93/INV
4	Engine Mount	195	20	7	12		95/INV			
5	Wing/Fuselage	195	25	4			63/INV			
6	Clamped Plate	225	51	10	26					
7	Control Surface	332	37	12	34		250/INV**			
8	Commodore Jet-Total Aircraft	456	30	14	42	1,044/INV				
9	Delta Wing	485	90	30	213					
10	Wing/Fuselage	594	55	1			455/INV			
11***	Ships Deck	1,028		25					4,752/ GUYAN+GIV	
12		1,056	102	10	235					
13	Clamped Plate	1,056	102	30	616					
14		3,072	102	20				362		
15		4,128	102	7				244		

* INV - Inverse Power Method with Shifts
GIV - Givens' Method
GUYAN + GIV - Guyan Reduction followed by Givens' Method.

** Only one mode extracted by NASTRAN at this time limit.

*** Reference 25.

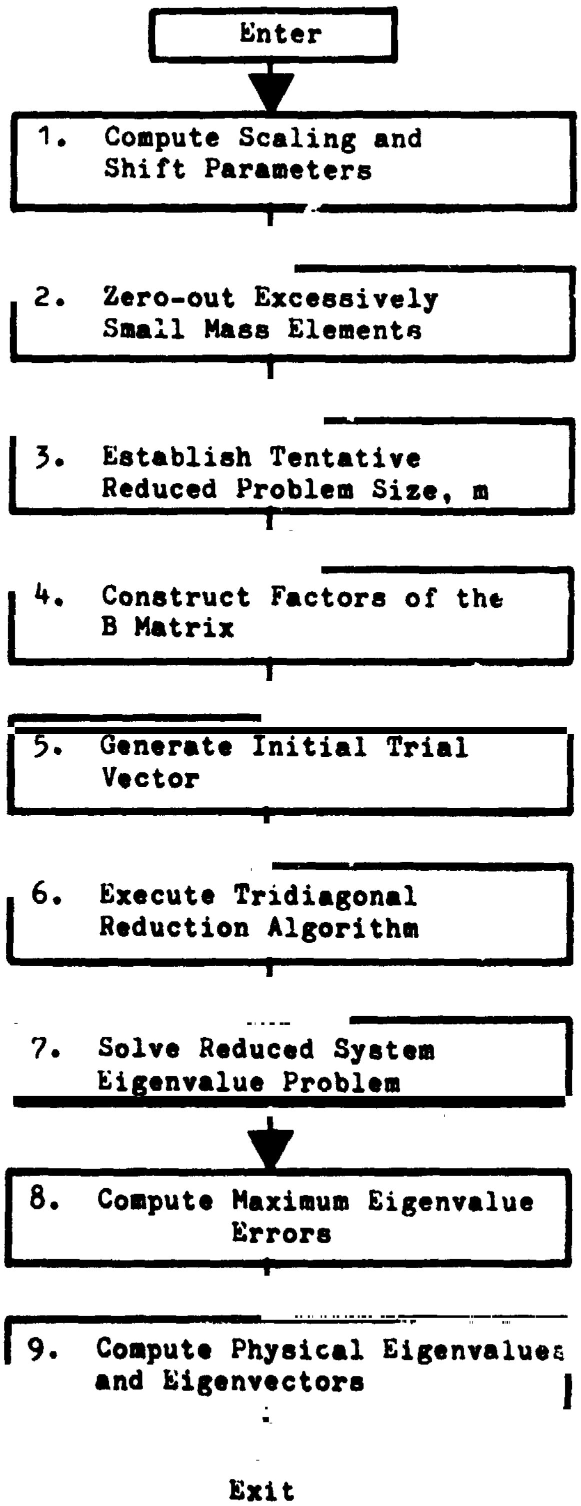

Figure 1. - Overall flow diagram for tridiagonal reduction method

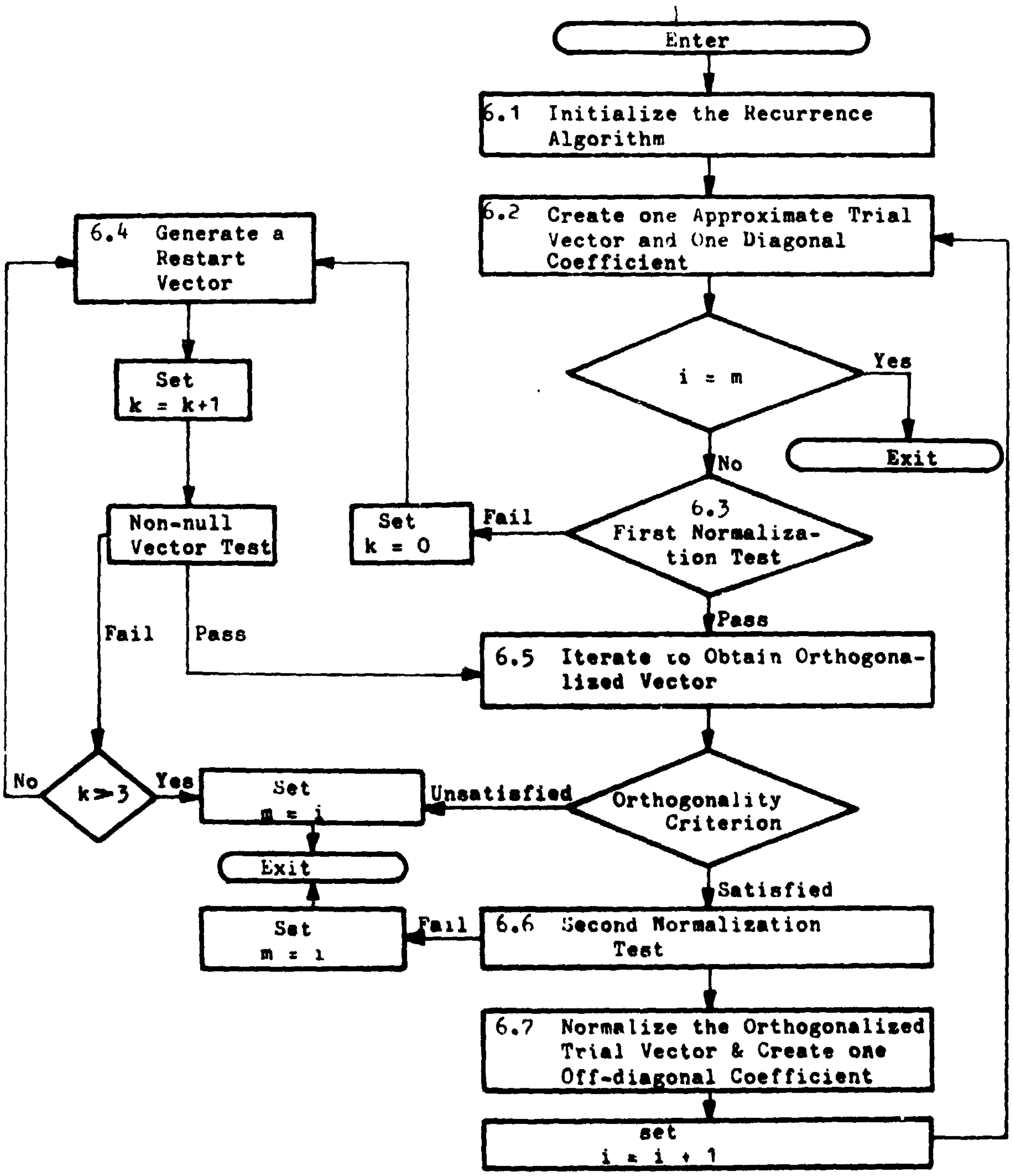

Figure 2. - Flow diagram for block 6, execute tridiagonal reduction

IN THE FOLLOWING TABLE 21 LOWEST EIGENVALUES ARE ACCURATE TO WITHIN A MAXIMUM ERROR OF .01000 PERCENT

MODE NO.	EIGENVALUE	RADIANS	CYCLES	GENERALIZED MASS	GENERALIZED STIFFNESS	PERCENT ERROR IN EIGENVALUE
1	.1516298E+07	.1231381E+04	.1959863E+03	.5957395E-03	.9033186E+03	.3605223E-26
2	.6303399E+07	.2510657E+04	.3995835E+03	.6269459E-03	.3951890E+04	.8112854E-25
3	.6303399E+07	.2510657E+04	.3995835E+03	0.	0.	.5102502E-28
4	.1365802E+08	.3695675E+04	.5881858E+03	0.	0.	.9802869E-25
5	.2025778E+08	.4500864E+04	.7163348E+03	0.	0.	.1685580E-26
6	.2045452E+08	.4522668E+04	.7198349E+03	0.	0.	.5055913E-24
7	.3169857E+08	.5630148E+04	.8960659E+03	0.	0.	.4462429E-20
8	.3169857E+08	.5630148E+04	.8960659E+03	0.	0.	.1171522E-20
9	.5186382E+08	.7201654E+04	.1146179E+04	0.	0.	.4522379E-11
10	.5186382E+08	.7201654E+04	.1146179E+04	0.	0.	.1861807E-11
11	.5613377E+08	.7492047E+04	.1192396E+04	0.	0.	.6991707E-20
12	.6821361E+08	.8259153E+04	.1314485E+04	0.	0.	.1963082E-15
13	.6879770E+08	.8294438E+04	.1320101E+04	0.	0.	.4804483E-16
14	.1015335E+09	.1007638E+05	.1603706E+04	0.	0.	.3552703E-08
15	.1015556E+09	.1007748E+05	.1603881E+04	0.	0.	.1346240E+01
16	.1116596E+09	.1056691E+05	.1681776E+04	0.	0.	.6173331E-07
17	.1118589E+09	.1057629E+05	.1683269E[illegible]	0.	0.	.1709451E-07
18	.1349183E+09	.1161543E+05	.184865[illegible]	0.	0.	.1786617E-07
19	.1586191E+09	.1259441E+05	.2004462E+04	0.	0.	.1326203E-05
20	.1780326E+09	.1334289E+05	.2123586E+04	0.	0.	.5758552E-03
21	.1791420E+09	.1338439E+05	.2130192E+04	0.	0.	.8491525E-02
22	.2137861E+09	.1461869E+05	.2326637E+04	0.	0.	.1601388E-02
23	.2444191E+09	.1563398E+05	.2488209E+04	0.	0.	.8689251E+00
24	.2476670E+09	.1573744E+05	.2504691E+04	0.	0.	.8118341E+01
25	.2502427E+09	.1581906E+05	.2517692E+04	0.	0.	.1519093E+01
26	.3006779E+09	.1734007E+05	.2759757E+04	0.	0.	.1230935E+00
27	.3637937E+09	.1907338E+05	.3035622E+04	0.	0.	.3486279E+01
28	.3812355E+09	.1952525E+05	.3107540E+04	0.	0.	.4125696E+01
29	.4131330E+09	.2032580E+05	.3234951E+04	0.	0.	.1852755E+01
30	.5212692E+09	.2283132E+05	.3633718E+04	0.	0.	.1102166E+02
31	.6037743E+09	.2457139E+05	.3910500E+04	0.	0.	.7405199E+01
32	.7102992E+09	.2665144E+05	.4241708E+04	0.	0.	.1292237E+02
33	.8542359E+09	.2922680E+05	.4651590E+04	0.	0.	.2118042E+02
34	.1046307E+10	.3234666E+05	.5148131E+04	0.	0.	.2159101E+02
35	.1373508E+10	.3706221E+05	.5898634E+04	0.	0.	.3031538E+02
36	.1813366E+10	.4258363E+05	.6777395E+04	0.	0.	.4064077E+02
37	.2567842E+10	.5067368E+05	.8064999E+04	0.	0.	.4085212E+02
38	.4030054E+10	.6348271E+05	.1010359E+05	0.	0.	.4964692E+02
39	.7178549E+10	.8472632E+05	.1348461E+05	0.	0.	.6007299E+02
40	.1564334E+11	.1250733E+06	.1990644E+05	0.	0.	.9484936E+02
41	.5015635E+11	.2239561E+06	.3564373E+05	0.	0.	.1162810E+03

Figure 3. - Extraction of 21 accurate roots via Program FEER; CDC - 6600 Computer

Order of stiffness matrix = 3,072
Average semi-band width = 102
No. of vectors generated = 2
CPU time = 362 sec.

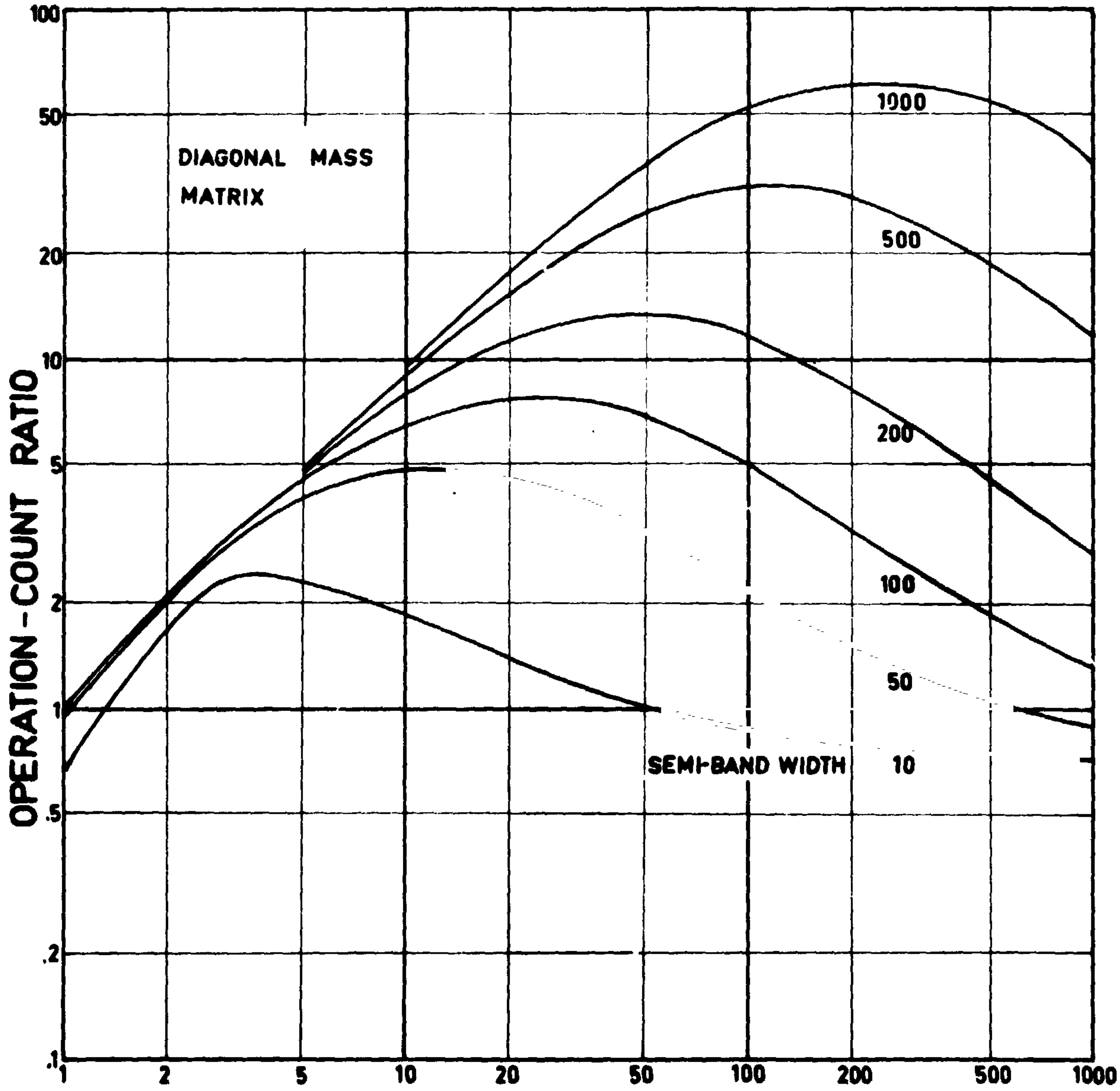

FIGURE 4.-THEORETICAL OPERATION-COUNT RATIO (INVERSE POWER METHOD/FEER)-DIAGONAL MASS MATRIX; INDEPENDENT OF PROBLEM SIZE FOR N≥200

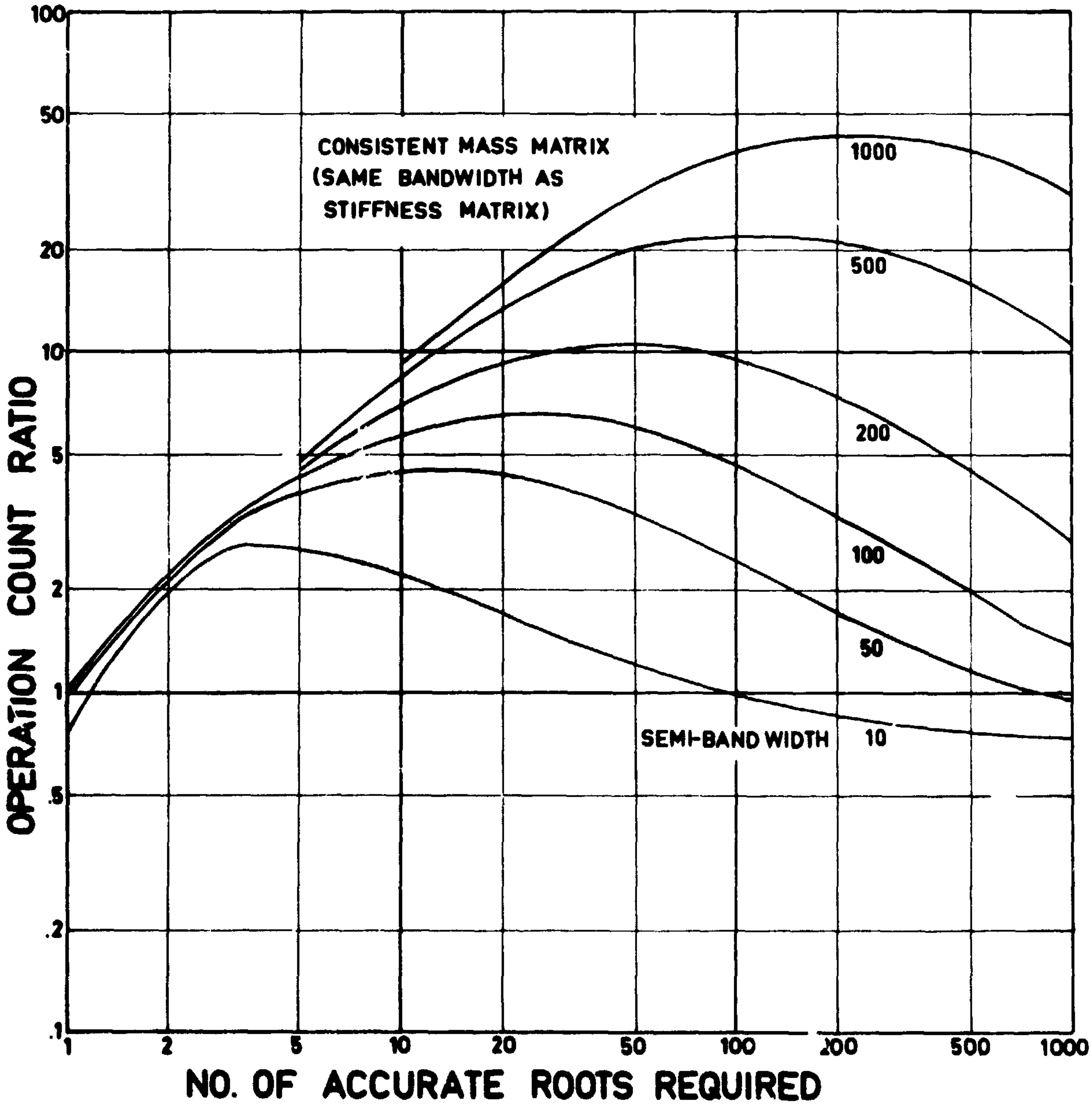

FIGURE 5 - THEORETICAL OPERATION-COUNT RATIO (INVERSE POWER METHOD/ FEER)-CONSISTENT MASS MATRIX; INDEPENDENT OF PROBLEM SIZE FOR N≥200

N74-14609

SUBSONIC FLUTTER ANALYSIS ADDITION TO NASTRAN

Robert V. Doggett, Jr.
NASA Langley Research Center
Hampton, Virginia

and

Robert L. Harder
The MacNeal-Schwendler Corporation
Los Angeles, California

SUMMARY AND ABSTRACT

A subsonic flutter analysis capability has been developed for NASTRAN, and a developmental version of the program has been installed on the CDC 6000 series digital computers at the Langley Research Center. The flutter analysis is of the modal type, uses doublet lattice unsteady aerodynamic forces, and solves the flutter equations by using the k-method. Surface and one-dimensional spline functions are used to transform from the aerodynamic degrees of freedom to the structural degrees of freedom. Some prelininary applications of the method to a beamlike wing, a platelike wing, and a platelike wing with a folded tip are compared with existing experimental and analytical results.

INTRODUCTION

The available standard level of the NASA structural analysis computer program (NASTRAN) can be used to solve flutter problems by using the "direct input matrix" feature of the program to add the required unsteady aerodynamic force matrices to the appropriate structural matrices and solve the resulting eigenvalue problem. This procedure is inefficient and is not routinely used by aeroelasticians. However, since its first public release in 1970, NASTRAN has proven to be a very useful tool to many persons interested in flutter, but this use has been limited to using the program to calculate the structural modes and frequencies that are required as input to separate special-purpose flutter analysis computer programs. This use of NASTRAN by aeroelasticians has created some interest in incorporating a flutter analysis capability in NASTRAN. At the first NASTRAN Users' Experiences Colloquium (ref. 1) a paper (ref. 2) was presented that described the results of a design study for a complete NASTRAN aeroelastic analysis capability. By using this design study as a guideline, the NASA has sponsored the development of a subsonic flutter analysis addition to NASTRAN.

The purpose of this paper is to describe this new flutter analysis capability and present some results from preliminary applications of the program.

The technique developed is of the modal type, uses doublet lattice unsteady aerodynamic forces, uses one-dimensional and surface spline functions to transform from aerodynamic degrees of freedom to structural degrees of freedom, and solves the flutter equations by using the k-method. The program is in what might be termed a developmental form, has only been installed on the CDC 6000 series digital computers at the Langley Research Center, and is not available for general release to the public. Results from preliminary applications of the program to a beamlike wing, a platelike wing, and a platelike wing with a folded tip are compared with existing analytical and experimental results.

OBJECTIVES AND GUIDELINES

The basic steps required in a flutter analysis are shown in the block diagram presented in figure 1. A characterization of each step is shown on the right in the figure. The overall objective of the NASTRAN subsonic flutter analysis was to provide a fully automated means for proceeding through these steps in an efficient manner to determine the flutter characteristics of complex structural and aerodynamic configurations. The development was constrained to the use of existing, proven state-of-the-art techniques. Therefore, the major effort was to assemble the selected procedures into the NASTRAN environment. One of the most significant guidelines was that there would be no constraints imposed on the structural idealization by aerodynamic considerations, and that the aerodynamic idealization would be made totally independent of structural modeling considerations. That is, the structure can be represented by an optimum selection and arrangement of structural elements and degrees of freedom, and the aerodynamic characteristics can be determined by an optimum selection of aerodynamic degrees of freedom. This guideline dictated providing a very general capability for the structural-aerodynamic interface which is required to transform the aerodynamic degrees of freedom to the structural degrees of freedom. Additional guidelines were that the technique should be easy to use and that the input data requirements associated with the unsteady aerodynamics and flutter solution and the format of the output results be in a form not totally unfamiliar to aeroelasticians. Another guideline that should be mentioned is that, where practical, the new procedures required for flutter analysis would be made as general as possible so that the basic capability can be easily expanded, if so desired at a later date, to accommodate additional aerodynamic theories, flutter solution procedures, and so forth. Naturally, it was required that the flutter analysis be compatible with the existing NASTRAN general structural capability and contain such existing features as the restart capability. Further, it was required that the flutter analysis be incorporated into a standard level version (level 15.1 was chosen) so that the NASTRAN program which contains the flutter analysis will also have all the other basic capabilities.

METHOD IMPLEMENTED

A modal flutter analysis method has been implemented in NASTRAN. The set of linear equations of motion that must be solved to determine the flutter condition may be expressed in matrix notation in the following form:

$$\left[\left[\frac{k^2}{b^2}[M] + \frac{\rho}{2}[Q(M_o,k)]\right]\lambda^2 + [K]\right]\{u_h\} = 0 \qquad (1)$$

here

- M = generalized structural mass
- K = generalized structural stiffness
- Q = generalized unsteady aerodynamic force (function of M_o and k)
- b = reference length
- M_o = Mach number
- k = reduced frequency, $b\omega/V$
- V = velocity
- u_h = generalized modal coordinate
- ρ = fluid density
- λ = complex eigenvalue

NASTRAN already contains the capability of generating the generalized ass and stiffness matrices required by equation (1) but does not contain any nternal aerodynamic force capability. So one of the major tasks was to add he required unsteady aerodynamics. Since an important objective was to be ble to analyze the most general aerodynamic configurations possible, the oublet lattice unsteady aerodynamics method was selected for inclusion since his method is applicable to a broad range of configurations. The flutter olution method implemented was the k-method which is the one most commonly sed in flutter analysis. A modal formulation was chosen for two reasons. The irst reason is that this is standard practice; the second reason is that the rder of the final matrix equations that must be solved is relatively small. he aerodynamic-structural interface is accomplished by the use of one-imensional and surface spline functions.

The k-Method of Solution

The k-method of flutter solution requires the repeated solution of equa-ion (1). The aerodynamic forces are functions of the three parameters, ensity, Mach number, and reduced frequency. To solve equation (1) values of wo of the parameters, usually density and Mach number, are held constant, and he eigenvalue equation is solved repeatedly for different values of reduced requency. The way equation (1) is developed, the damping, velocity, and requency of the system can be determined from the eigenvalues by using the elationships

$$g = 2\,\lambda_{REAL}/\lambda_{IMAG}$$

$$f = k\,\lambda_{IMAG}/2\pi b$$

$$V = \lambda_{IMAG}$$

Since the flutter point is on the boundary between stable (damped) and unstable (divergent) sinusoidal oscillations, the flutter condition occurs for the particular combination of parameters that causes the damping to equal zero ($g = 0$). The flutter velocity is usually determined by graphically plotting the damping versus velocity (g - V plots) obtained for each solution of the eigenvalue problem. A number of loci, equal to the order of the problem, will be obtained. The curve which crosses the $g = 0$ axis at the lowest value of velocity determines the critical flutter condition. The k-method implemented in NASTRAN includes the generation of both damping and frequency versus velocity plots (f - V plots). Also, the capability is provided for selecting any one of the three aerodynamic parameters as the one to be varied.

Unsteady Aerodynamic Theory

The unsteady aerodynamic theory implemented in the NASTRAN flutter analysis is the subsonic doublet lattice method (ref. 3). Of the available proven theories, this technique is probably the most general in that it can be applied to multiple nonplanar mutually interfering lifting surfaces and can be used to calculate body-lifting surface interference effects. The doublet lattice method adapted for NASTRAN use is similar to that described in references 4 and 5. The program described in these references includes slender-body aerodynamics to calculate body, or fuselage, forces but this feature has not been included in NASTRAN although the work required to implement body forces has been determined.

The doublet lattice method requires that the aerodynamic surfaces be subdivided into a grid of trapezoidal boxes. An example box arrangement is illustrated in figure 2. The analyst is required to specify the box arrangement subject to certain geometric constraints. For example, two of these constraints are that the boxes must be arranged in streamwise columns parallel to the free stream and that surface discontinuities such as fold lines must lie on box boundaries. The geometric constraints on the box arrangement are not severe and provide sufficient latitude to model adequately very general configurations. For the unsteady flow case, a spanwise line of acceleration potential doublets is placed at the one-quarter-chord station of each box. The doublets are related to pressure and hence to the force on each box. An aerodynamic influence coefficient matrix is generated which relates the force on the boxes to the downwash on the boxes. The force acts at the one-quarter-chord point and the downwash point is the three-quarter-chord point. Both of these points are at the box midspan station. Typical force and downwash points are shown in figure 2. The downwash is a function of the streamwise slope and the vertical displacement normal to the boxes. Each box may be thought of in the context of being a finite element with the degrees of freedom (deflection at one-quarter-chord point, and deflection and slope at three-quarter-chord point) defined at two different points within each box. In the NASTRAN flutter development, it was decided that it would be desirable to have only one aerodynamic grid point for each box. The point selected was the center of each box. A transformation is used to convert the force and downwash at the one-quarter and three-quarter-chord points of each box to corresponding forces and downwashes at the centers of each box. Therefore, there is one aerodynamic grid point for each box.

Structural-Aerodynamic Interface (Geometry Interpolation)

One of the most significant features of the NASTRAN flutter analysis is the geometry interpolation capability that provides for the interconnection of the aerodynamic and structural models of the system. Since a very general capability is provided for the structural-aerodynamic interface, the structural model can be that best suited from structural considerations alone, and the choice of aerodynamic model is dictated by aerodynamic considerations alone. The geometry interpolation provides a transformation from the aerodynamic degrees of freedom to the structural degrees of freedom. This transformation is accomplished by the use of one-dimensional and surface spline functions. (See refs. 6 and 7.) The traditional one-dimensional spline has been generalized to include torsional rotations in addition to bending deformations. Since these functions are based on the small deflection equations of infinite beams and plates, respectively, they are very good for the interpolation of the deformations of general structural systems. If the structure is expected to behave like a beam as would be the case for a high-aspect-ratio jet transport wing, the one-dimensional spline would be used; if the structure is expected to behave like a plate, say a low-aspect-ratio wing, the surface spline would be the appropriate choice. The use of combinations of the two splines is permissible and would be applied, for example, to a complete aircraft where the fuselage had the character of a beam and the wing was expected to exhibit platelike behavior.

Aerodynamic Force Interpolation

The k-method type flutter solution requires the solution of the flutter eigenvalue problem many times so that a relatively closely spaced sequence of points can be determined to make the $g - V$ plots since the behavior of the loci of roots on the plot can often be quite complex and lead to misinterpretation of the results. Since one of the most expensive parts of a flutter analysis is the determination of the unsteady aerodynamic forces, it is desirable to actually calculate the aerodynamic forces for a minimum number of values of the independent aerodynamic parameter, Mach number, or reduced frequency. Fortunately, experience has shown that although the behavior of the solutions of the flutter equations as displayed on a $g - V$ diagram may be complex, the variation of the aerodynamic forces with reduced frequency or Mach number is generally smooth and well behaved. Consequently, it has become more or less standard practice in aeroelasticity to evaluate the aerodynamic forces at a relatively small number of values of the independent variable and interpolate to determine the forces at additional values of the independent parameter. This interpolation is relatively inexpensive when compared to the cost of actually calculating the aerodynamic forces and results in the loss of very little accuracy. Aerodynamic force interpolation has been included in the NASTRAN flutter analysis. Both one-dimensional and surface splines are used. If the flutter calculations are limited to a constant Mach number, the linear spline is used to interpolate over a range of reduced frequencies. If a set of aerodynamic forces have been determined at two or more Mach numbers, the surface spline is used to interpolate to intervening Mach numbers. Experience with the one-dimensional spline has shown that it is very good for aerodynamic interpolation. However, there are some indications that the accuracy of the surface spline technique, although it is satisfactory, is not as good as the linear spline. This is probably caused by the fact that the character of the three-dimensional behavior of the aerodynamic forces is not platelike.

FLUTTER ANALYSIS RIGID FORMAT

The assembly of the components of the flutter analysis into a NASTRAN rigid format (labeled Rigid Format 45) required the use of many existing functional modules, the modification to a few existing modules, and the development of six completely new modules. An annotated block diagram of the new rigid format is presented in figure 3. The structural analysis section is essentially identical to existing Rigid Format 10 (Modal Complex Eigenvalue Analysis) down to the point of complex eigenvalue analysis. The existing module PLOT was modified to accommodate plotting of the aerodynamic geometry. Both undeformed and deformed plots are available. Changes were made to the XYTRAN and XYPLOT modules for the purpose of making g - V and f - V plots. An upper Hessenberg method of complex eigenvalue extraction was added to module CEAD since this procedure is better suited to the requirements of flutter analysis than the two methods already available.

The completely new modules are the Aerodynamic Pool Distributor (APD), Geometry Interpolation (GI), Aerodynamic Matrix Generator (AMG), Aerodynamic Matrix Processor (AMP), Flutter Analysis Phase 1 (FA1), and Flutter Analysis Phase 2 (FA2). Module APD forms tables of aerodynamic data, defines the boundaries of the aerodynamic elements, and locates and orients displacement components at aerodynamic grid, or control, points. Module AMG evaluates the aerodynamic influence coefficient matrix at specified values of Mach number and reduced frequency, and determines the transformations needed to convert these matrices from the points required by the doublet lattice theory (one-quarter and three-quarter box chord stations) to the center of the aerodynamic boxes. Module GI generates the transformations required to give the structural displacements at the center of the aerodynamic boxes in terms of the deformations at the structural grid points. The AMP module calculates the generalized aerodynamic force matrices by using the mode shapes determined in the structural part of the rigid format (READ module), the aerodynamic matrices determined in AMG, and the transformation information calculated in GI. The module FA1 prepares the modal matrices for complex eigenvalue extraction by module CEAD. Also, the interpolation of the aerodynamic forces is carried out in this module, if a solution is required for a combination of parameters for which the generalized aerodynamic matrices were not determined previously. The module FA2 gathers data for reduction and presentation. For example, the velocity and frequency are determined from the eigenvalues calculated by CEAD, and a line of printer output is prepared for each loop through the flutter solution. The three modules FA1, CEAD, and FA2 are in a loop within the rigid format. This loop is repeated until solutions have been obtained for all the reduced frequencies, Mach numbers, and densities requested.

PRELIMINARY APPLICATIONS

The NASTRAN flutter analysis has been applied to some simple geometric configurations. The results of three of these applications, a beamlike wing, a platelike wing, and a platelike wing with a folded tip, are presented in this section. The NASTRAN results are compared with other available analytical results and experimental data. Some discussion of the features of the NASTRAN analysis is included with the discussion of the applications.

The first application is the 15° swept wing shown in figure 4. Additional information concerning this wing may be found in references 8 and 9. This model was essentially a swept beam, and the NASTRAN structural model used consisted of 10 BAR elements as shown in the figure. The aerodynamic model consisted of 24 boxes arranged in six spanwise divisions of four chordwise boxes each. Unlike the requirements of the structural part of NASTRAN where the coordinates of each structural grid point are required input, a large number of aerodynamic boxes (and aerodynamic grid points which are located at the center of each box) are generated from a minimum amount of information. The aerodynamic boxes are assembled into panels, or groups, where each panel contains several boxes. For the beam example, all of the boxes belonged to a single panel. Only a single bulk data card (actually a parent card plus one continuation card) was required to define the aerodynamic boxes for this example. For each group, the only information required is the coordinates of the inboard and outboard leading-edge corners of the panel (points marked "a" and "b" in the fig.), the inboard and outboard chords (indicated by C_1 and C_2 in the fig.), the number of chordwise boxes, and the number of spanwise boxes if the boxes are to be equally spaced. If the boxes are not to be equally spaced, then the desired spacing is provided in terms of fraction chord and span divisions. The boxes for this example are equally spaced. Also, note that different coordinate systems were used to define the structural and aerodynamic models. A one-dimensional spline function was used for interpolation in this example. Presented in figure 5 are the results of the NASTRAN calculations for this wing at a Mach number of 0.45 and a density of 1.185 kg/m^3. Three modes were used in the analysis. The results are presented in the form of a g - V plot where only the critical root is shown. The circle symbols indicate the calculated points. The calculated flutter speed is determined by the point at which the line faired through the symbols crosses the $g = 0$ axis. Indicated on the figure, in addition to the NASTRAN result, are the experimental flutter result from reference 8 and the calculated flutter result from reference 9 which were obtained using linearized lifting-surface theory. The NASTRAN calculated velocity is in good agreement with the experimental value. The calculated flutter speed from reference 9 is about 5 percent lower than the NASTRAN calculated value. The agreement with respect to flutter frequency is not so good.

The wing geometry, structural model, and aerodynamic model for the platelike wing are presented in figure 6. Copies of NASTRAN computer-generated plots of the structural and aerodynamic models are presented in figure 7. The structural model consisted of 36 quadrilateral plate elements (QUAD2); the aerodynamic model consisted of 50 boxes, 10 spanwise divisions of unequal spacing, and five equally spaced chordwise boxes. As was done for the beam model, the entire wi... made up a single aerodynamic panel. The surface spline was used to perform the required structural-aerodynamic interface for this example. The calculated g - V curve is presented in figure 8, and only the critical locus of points is shown. These results are for a Mach number of 0.80 and a density of .700 kg/cu m. Four modes were used in the analysis. The solid symbols indicate calculated values for which the generalized aerodynamic forces were calculated. The open symbols indicate results obtained by using interpolated generalized aerodynamic forces. The calculated and interpolated results appear to lie on the same curve and could not be distinguished from one another had not different symbols been used. Tabulated on the figure are the NASTRAN calculated flutter speed and frequency, and some unpublished analytical results. Also included in the table are some NASTRAN calculated results for an aerodynamic model that had eight equally spaced chordwise boxes and the same spanwise arrangement shown in figure 6 for the 50-box case. The unpublished analytical results were obtained by using a doublet lattice computer program similar, but not identical, to the one modified for NASTRAN use. The surface spline was also used for the structural-aerodynamic interface in obtaining the unpublished result. The experimentally determined model natural frequencies were used to determine the generalized stiffnesses used in the unpublished results. Since the measured frequencies did not agree precisely with the calculated frequencies, some of the 7-percent difference between the two results may be attributed to this frequency difference. However, the results are still in good agreement. The two NASTRAN calculations gave essentially the same results.

The final application to be discussed is a platelike wing with a folded tip. A photograph of this model is presented in figure 9, and the geometry, structural model, and aerodynamic model are presented in figure 10. The tip fin is inclined with respect to the wing by 60°. Copies of NASTRAN generated computer plots of the structural and aerodynamic elements are presented in figure 11. The wing portion of this model was the same as the platelike wing previously discussed, and this portion was modeled in the same fashion as the plate wing (36 QUAD2 structural elements and 50 aerodynamic boxes comprising one aerodynamic panel). An additional 60 QUAD2 structural elements were used to model the folded tip. The folded tip was a separate aerodynamic panel and was composed of a total of 50 boxes that were arranged into five equal chordwise divisions and 10 unequal spanwise divisions as indicated in the figure. One provision provided by the program is that there may or may not be aerodynamic interference, or coupling, between boxes located in different panels, or groups, depending on the user to make the selection. This feature allows for the omission of coupling when it is known to be unimportant and thereby reduces the time required to compute the aerodynamic matrices, or allows for the independent investigation of aerodynamic interference effects. In the present example, aerodynamic coupling between the wing panel and the tip panel was included. The surface spline option was used to perform the required aerodynamic-structural interface. Four different spline functions were used, two for each aerodynamic panel. The interpolation for the 25 inboard wing aerodynamic boxes used one spline function, and the 25 outboard boxes used another spline function. The same type of arrangement was used for the tip fin. Since the analyst specifies the structural grid points that are to be used for interpolating for each aerodynamic box, it is not necessary that a single spline function be used for each aerodynamic panel.

The results of NASTRAN calculations for a Mach number of 0.90 and a density of 0.861 kg/m^3 are presented in figure 12 in the form of the g - V plot for the critical eigenvalue. Four modes were used in this analysis. The data obtained by using calculated generalized aerodynamic forces are indicated by the solid symbols in the figure, and the results using interpolated generalized aerodynamic forces are indicated by the open symbols. The comparison of the results using calculated generalized aerodynamic forces with those obtained using interpolated forces indicates that they all lie on the same g - V curve. Also tabulated on the figure are an unpublished calculated result and an unpublished wind-tunnel experimental result. The unpublished calculated result was obtained in a fashion similar to that previously described for the platelike wing example. The two calculated results are in good agreement with respect to both flutter velocity and frequency. The experimental flutter velocity is about 9 percent lower than the NASTRAN calculated value. Both calculated flutter frequencies are somewhat higher than the experimental frequency.

In discussing these three applications, some mention has been made of the simplicity of the input data requirements associated with the aerodynamics portion of the NASTRAN program. This point is somewhat dramatically indicated by the fact that for the wing with tip fin case, of a total of 401 bulk data cards used, only 28 were directly associated with the aerodynamics or flutter solution.

Since the NASTRAN flutter analysis is relatively new, its efficiency has not been fully evaluated nor have all of its potential options been exercised. However, it is of interest to examine some of the central processing unit (CPU) computer times required by some of the individual functional modules for a program execution. Presented in figure 13 is a listing of CPU times for the CDC 6600 computer obtained for the wing with the folded tip fin. In this case, five modes were calculated by the real eigenvalue module, and the four lowest modes were used in the flutter analysis. The generalized aerodynamic forces were determined at three values of reduced frequency and interpolated to two additional values so the flutter eigenvalue problem was solved five times. Additional information describing this example is shown on the figure. Also included on the figure are the total CPU time, the peripheral processor time (CPU), and calls to the operating system (O/S calls).

CONCLUDING REMARKS

A subsonic flutter analysis capability has been developed for NASTRAN. This flutter analysis is of the modal type, uses doublet lattice unsteady aerodynamic forces, and solves the flutter equations by using the k-method. One-dimensional and surface spline functions are used to transform from aerodynamic degrees of freedom to structural degrees of freedom. This capability has been incorporated into a version of NASTRAN, and this version has been installed on the CDC 6000 series computers at the Langley Research Center. This version is in a developmental stage and is not now available for general release. In this paper, a general description of the new flutter analysis rigid format has been presented. Results of some preliminary applications of the NASTRAN flutter analysis to a beamlike wing, a platelike wing, and a platelike wing with a folded tip have been presented, and these results compared with existing experimental and analytical results.

REFERENCES

1. Anon.: NASTRAN: Users' Experiences. NASA TM X-2378, 1971.

2. Harder, Robert L., MacNeal, Richard H., and Doggett, Robert V., Jr.: A Design Study for the Incorporation of Aeroelastic Capability Into NASTRAN. NASTRAN: Users' Experiences, NASA TM X-2378, Sept. 1971, pp. 779-795.

3. Albano, Edward, and Rodden, William P.: A Doublet Lattice Method for Calculating Lift Distributions on Oscillating Surfaces in Subsonic Flows. AIAA Journal, Vol. 7, No. 2, Feb. 1969, pp. 279-285.

4. Giesing, J. P., Kalman, T. P., and Rodden, W. P.: Subsonic Unsteady Aerodynamics for General Configurations: Part II, Volume I, Application of the Doublet-Lattice Method and the Method of Images to Lifting-Surface/Body Interference. AFFDL-TR-71-5, Part II, Vol. I, Aug. 1971, Air Force Flight Dynamics Laboratory, Wright-Patterson Air Force Base, Ohio.

5. Giesing, J. P., Kalman, T. P., and Rodden, W. P.: Subsonic Unsteady Aerodynamics for General Configurations: Part II, Volume II, Computer Program N5KA. AFFDL-TR-71-5, Part II, Vol. II, April 1972, Air Force Flight Dynamics Laboratory, Wright-Patterson Air Force Base, Ohio.

6. Greville, T. N. E., ed.: Theory and Application of Spline Functions. Academic Press, 1969.

7. Harder, Robert L., and Desmarais, Robert N.: Interpolation Using Surface Splines. AIAA Journal of Aircraft, Vol. 9, No. 2, Feb. 1972, pp. 189-191.

8. Tuovila, W. J., and McCarty, John Locke: Experimental Flutter Results for Cantilever-Wing Models at Mach Numbers up to 3.0. NACA RM L55E11, 1955.

9. Yates, E. Carson, Jr., and Bennett, Robert M.: Use of Aerodynamic Parameters From Nonlinear Theory in Modified-Strip-Analysis Flutter Calculations for Finite-Span Wings at Supersonic Speeds. NASA TN D-1824, 1963.

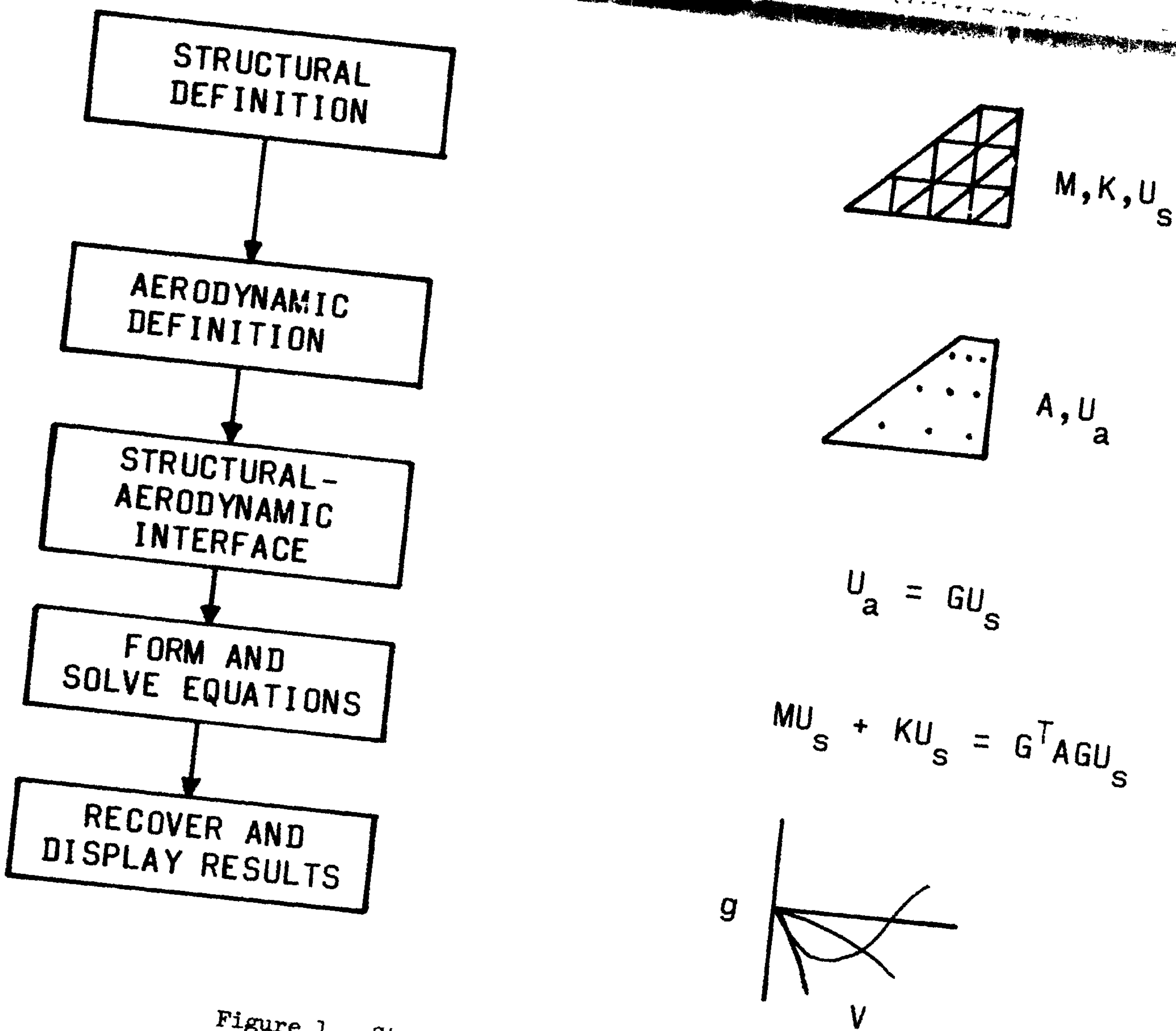

Figure 1.– Steps required in flutter analysis.

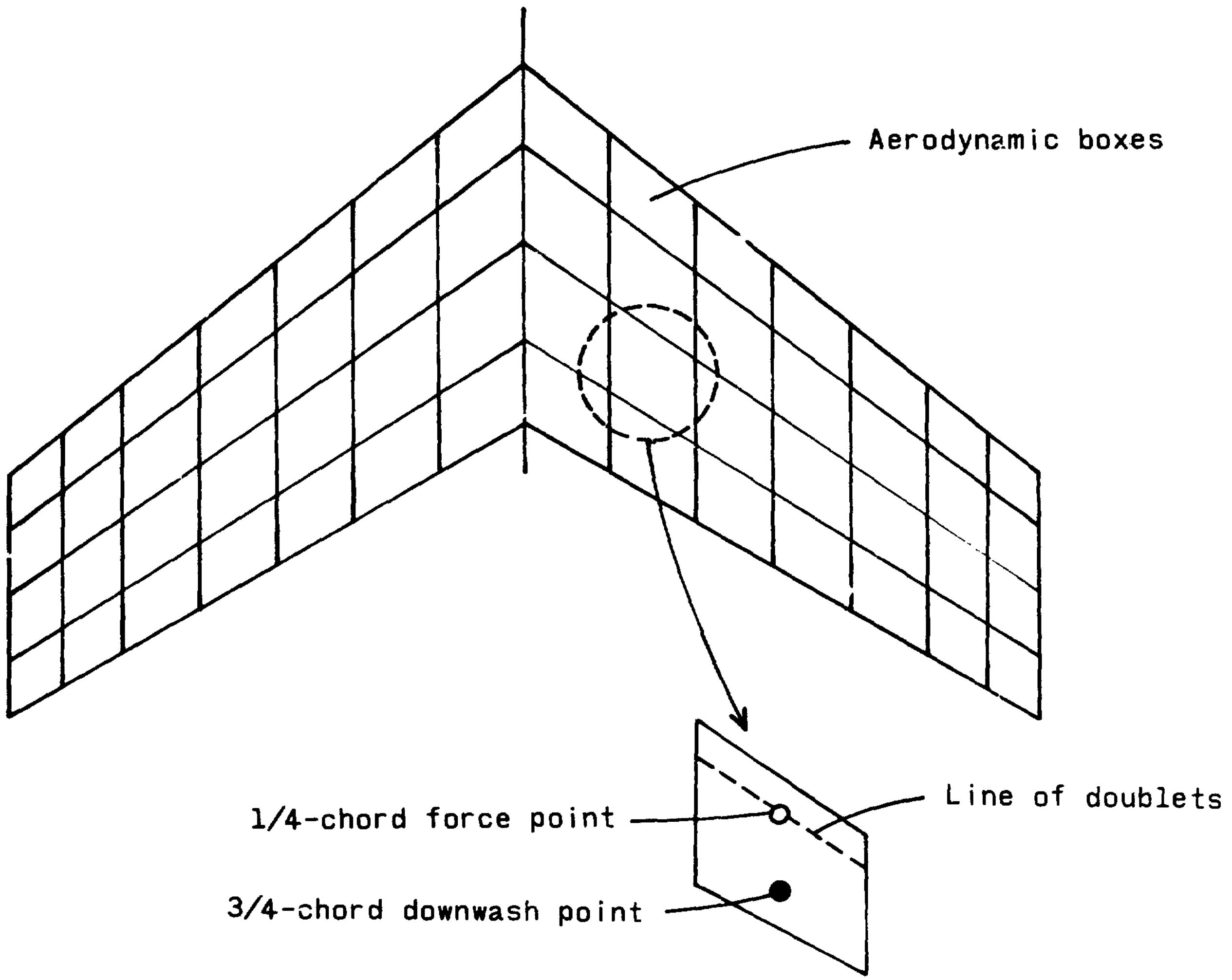

Figure 2.— Sample arrangement of doublet lattice aerodynamic boxes.

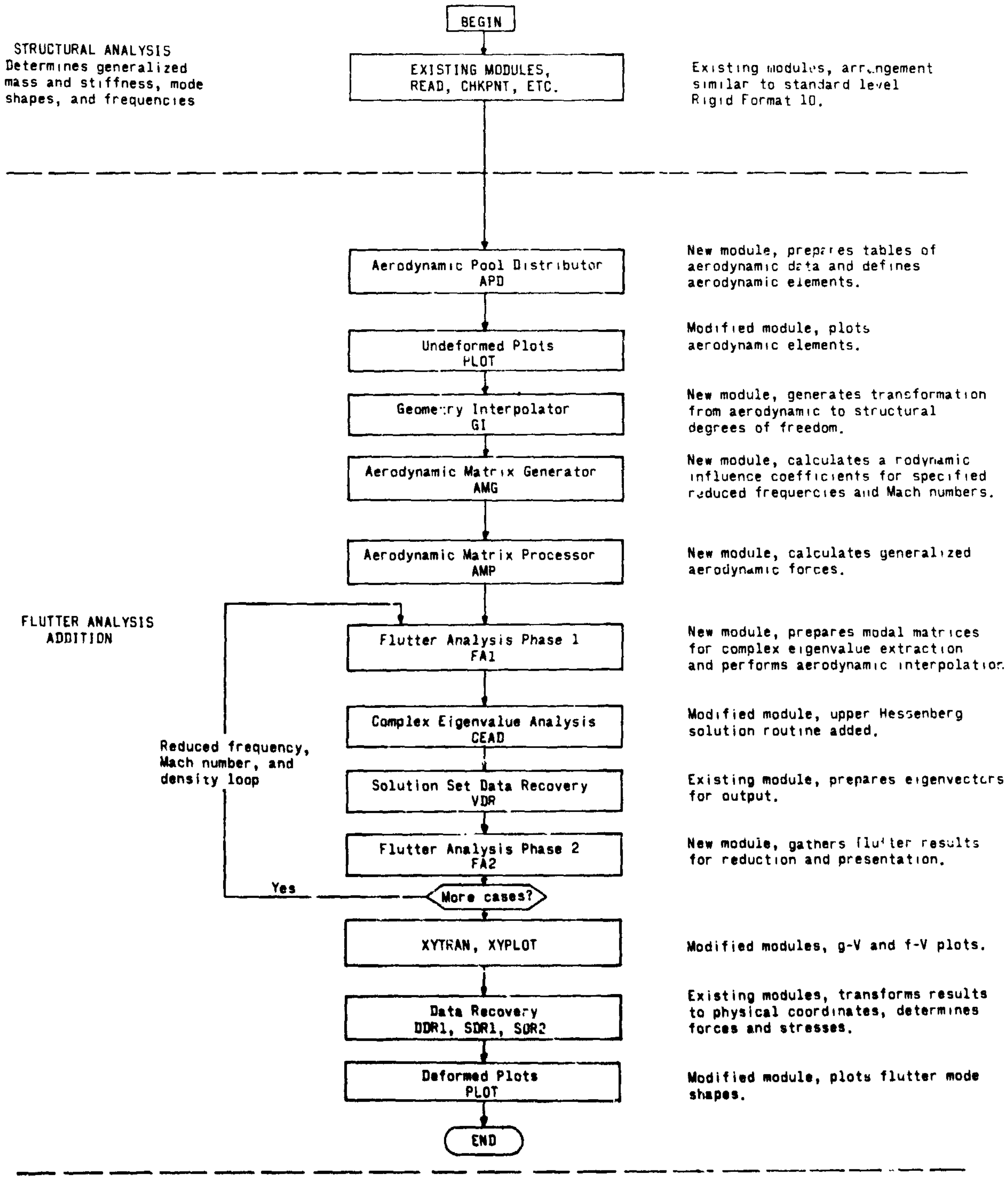

Figure 3.– Block diagram of flutter analysis rigid format.

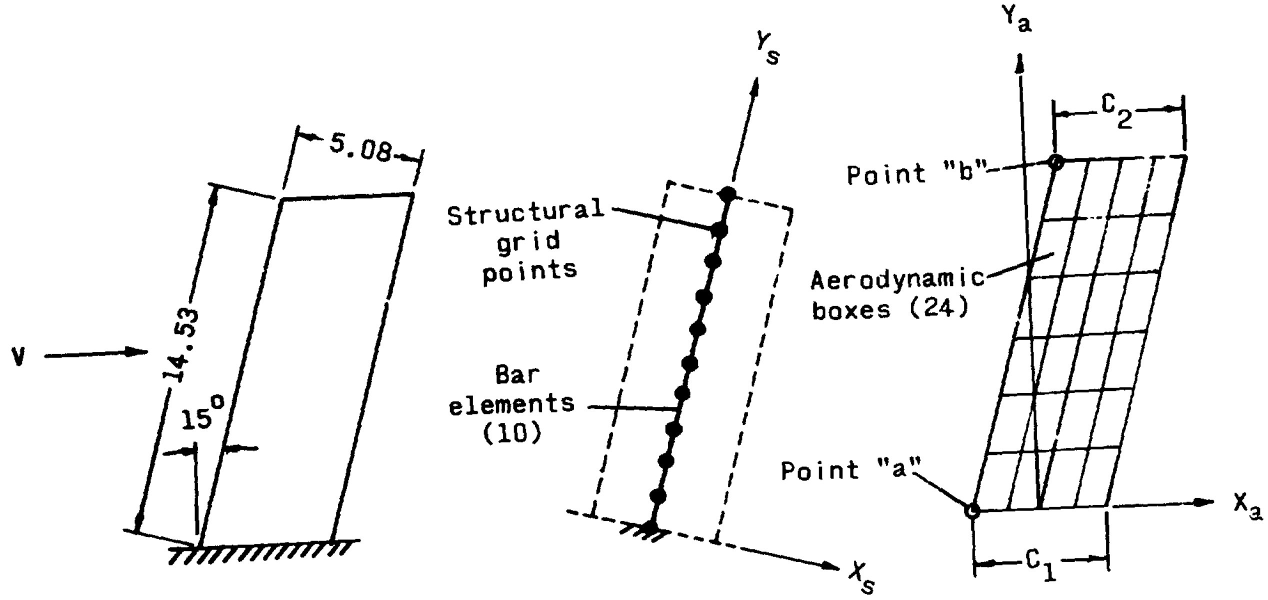

Figure 4.– Geometry, structural modeling, and aerodynamic modeling of beamlike wing. (All linear dimensions are in centimeters.)

METHOD	V_f, m/sec	f_f, Hz
—○— NASTRAN	152.9	140
□ Calc., Ref. 9	145.3	178
△ Exp., Ref 8	150.9	120

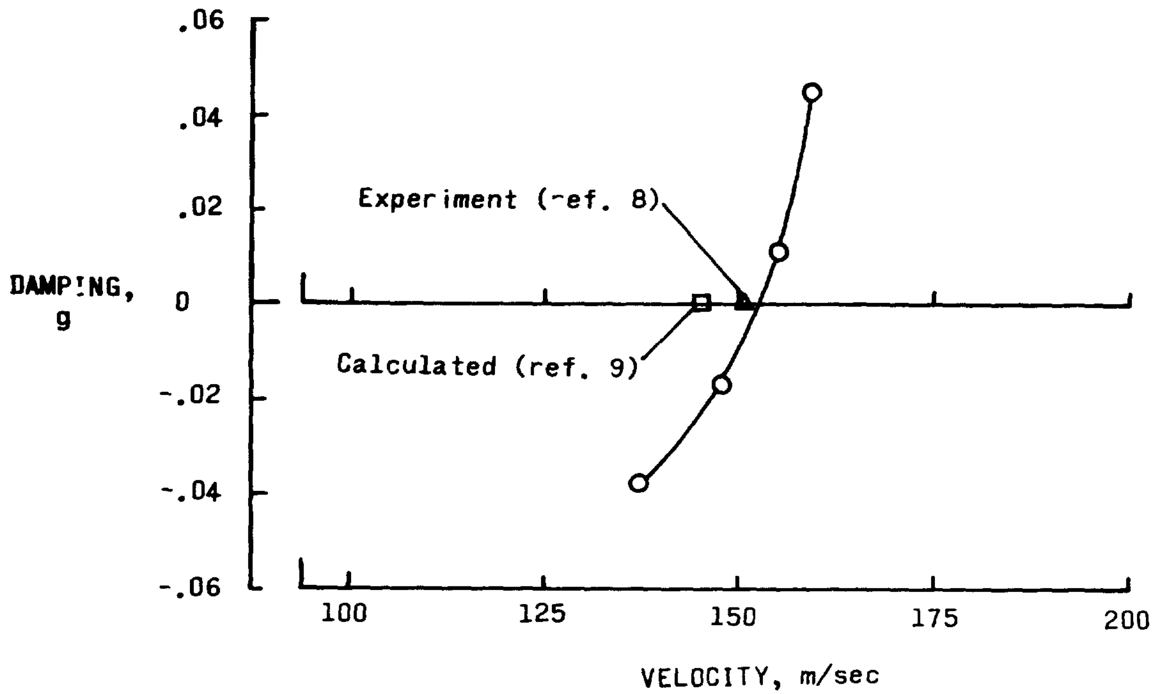

Figure 5.– Beamlike wing flutter results for a Mach number of 0.45 and a density of 1.185 kg/m^3.

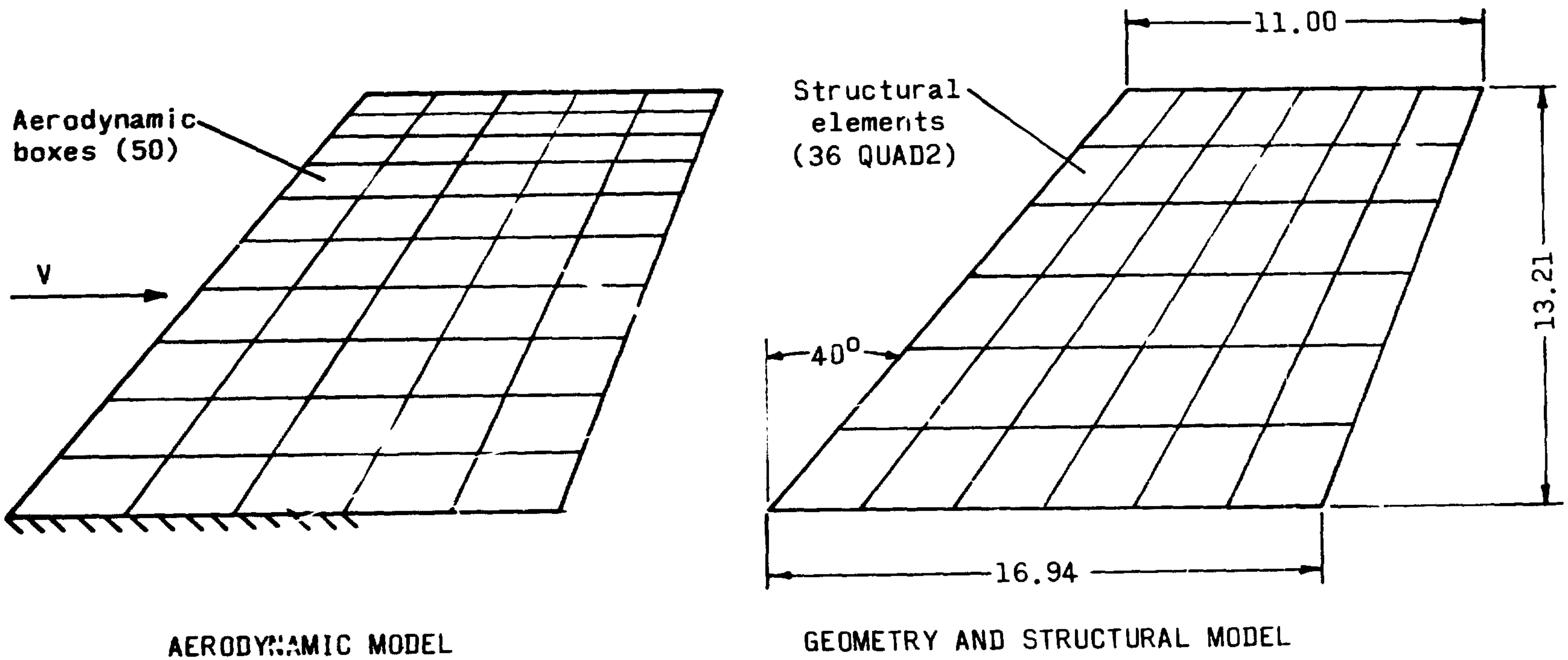

Figure 6.– Geometry, structural modeling, and aerodynamic modeling of platelike wing. (All linear dimensions are in centimeters.)

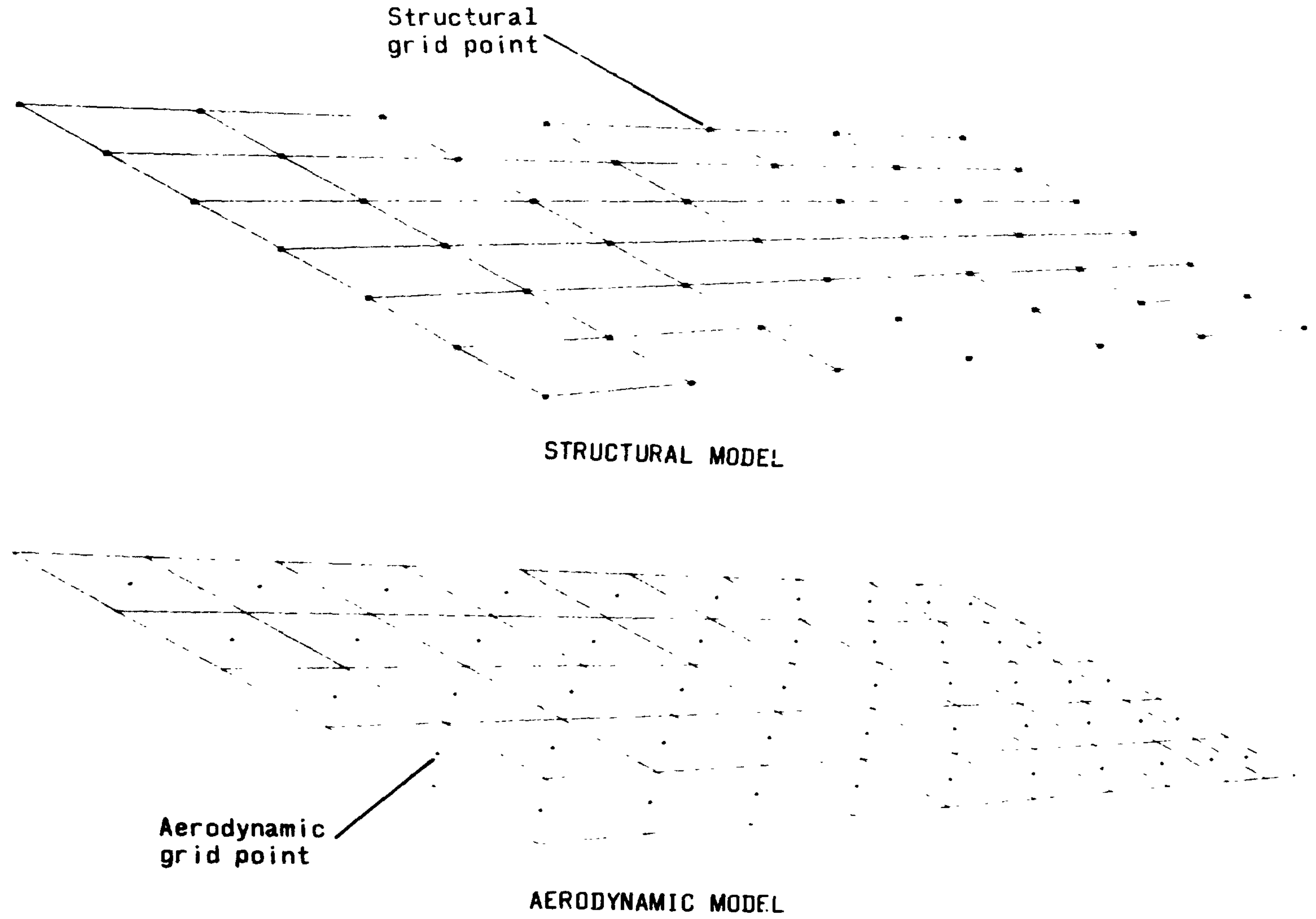

Figure 7.– Computer-generated plots of structural and aerodynamic models for platelike wing.

METHOD	V_f, m/sec	f_f, Hz
—o— NASTRAN (50 boxes)	382.3	160.7
NASTRAN (80 boxes)	382.3	163.4
□ Calc., Unpub.	411.5	167.9

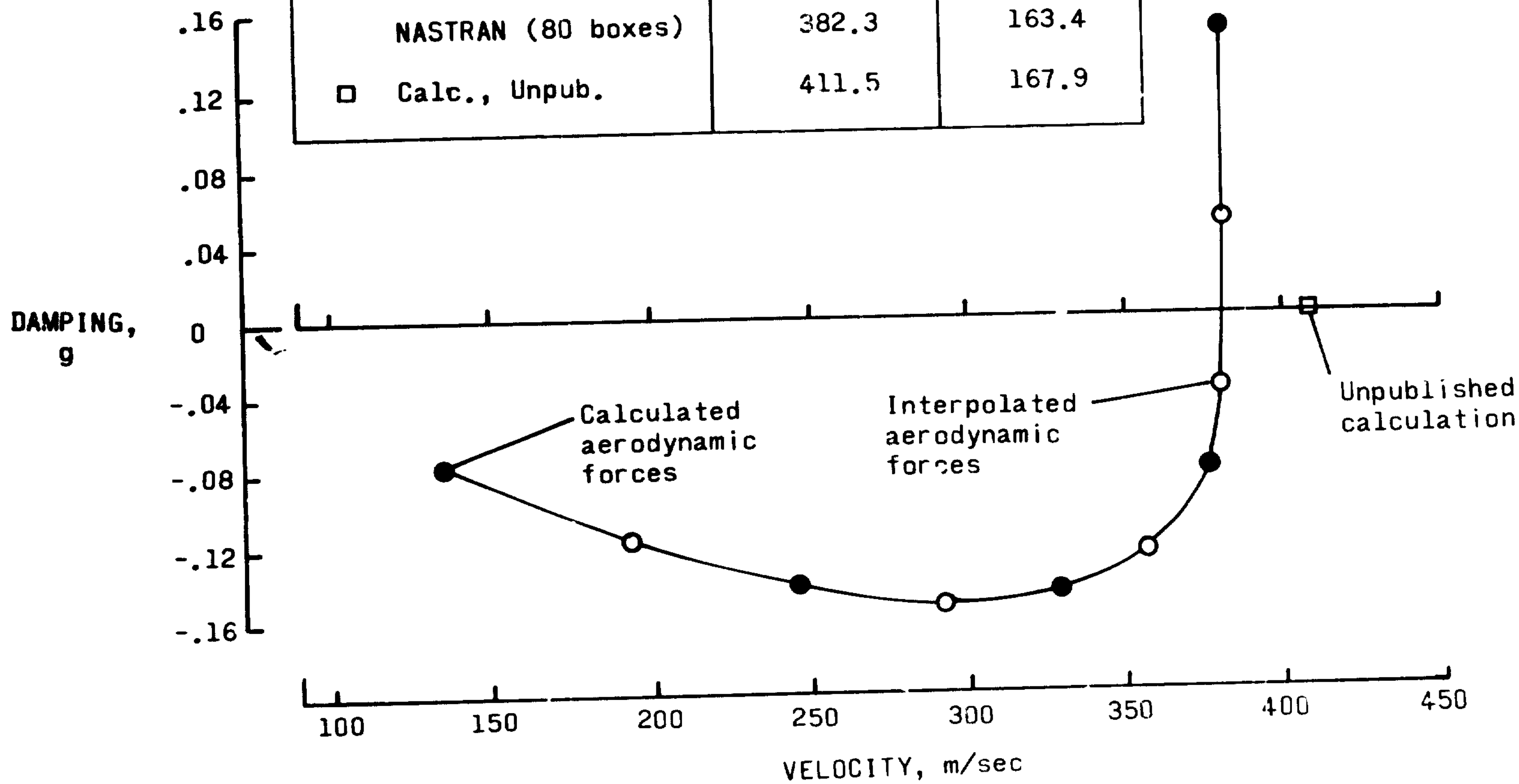

Figure 8.– Platelike wing flutter results for a Mach number of 0.80 and a density of 2.700 kg/m^3.

Figure 9.- Photograph of platelike wing with folded tip fin.

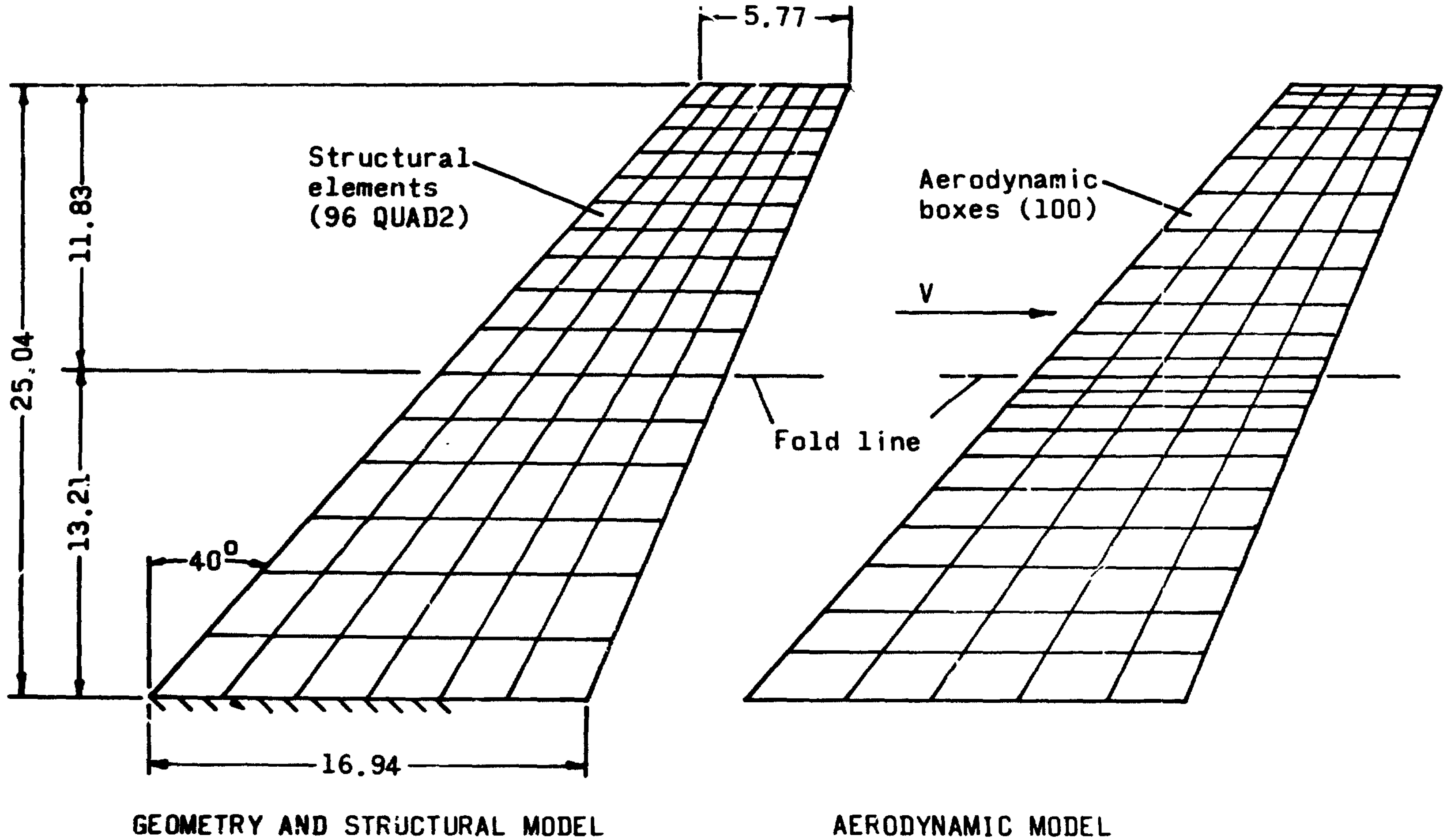

Figure 10.– Geometry, structural model, and aerodynamic model of platelike wing with folded tip fin. (All linear dimensions are in centimeters.)

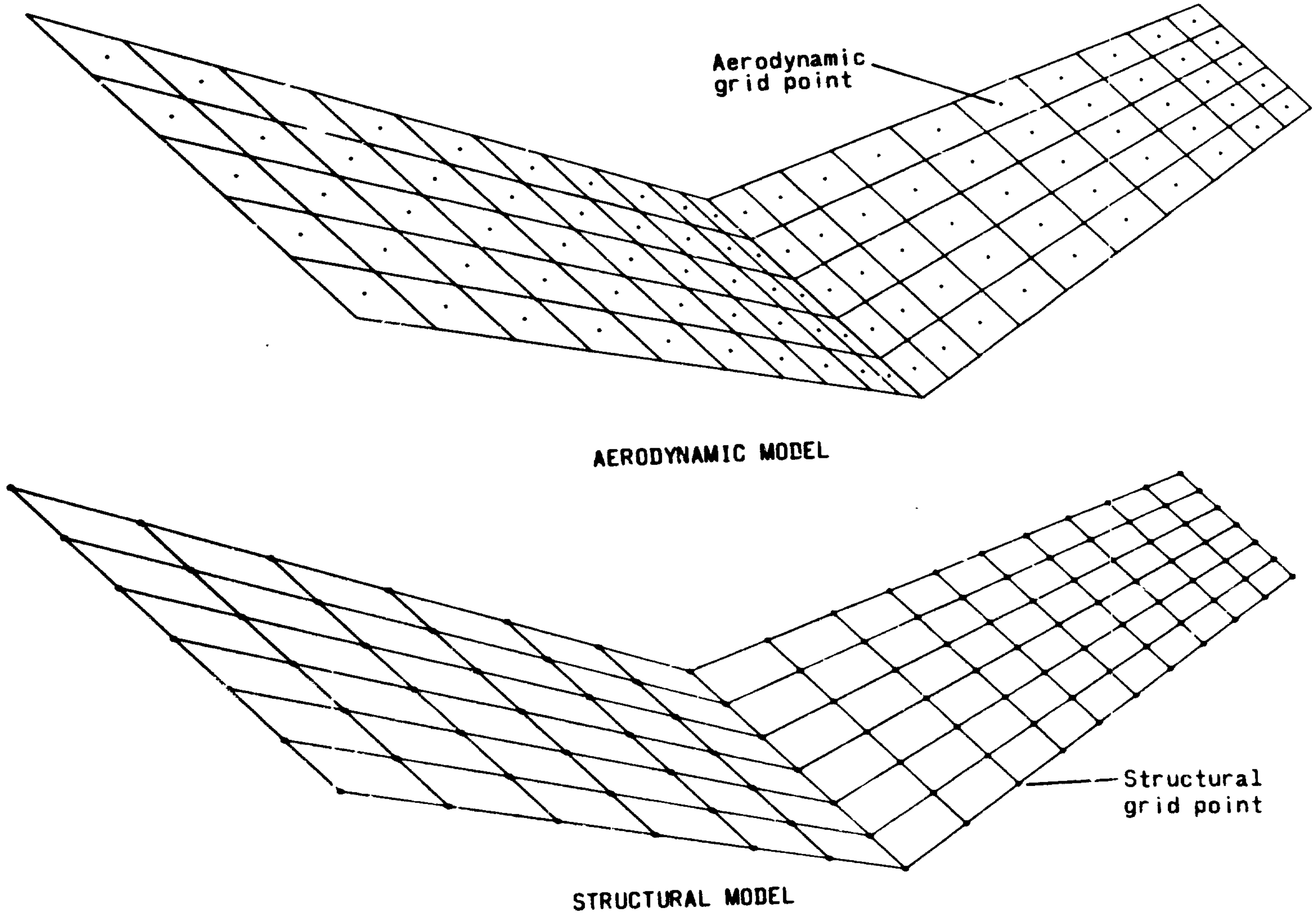

Figure 11.– Computer-generated plots of structural and aerodynamic models for wing with folded tip fin.

METHOD	V_f, m/sec	f_f, Hz
—○— NASTRAN	306.3	56.7
□ Calc., Unpub.	304.8	56.1
△ Exp., Unpub.	278.9	40.0

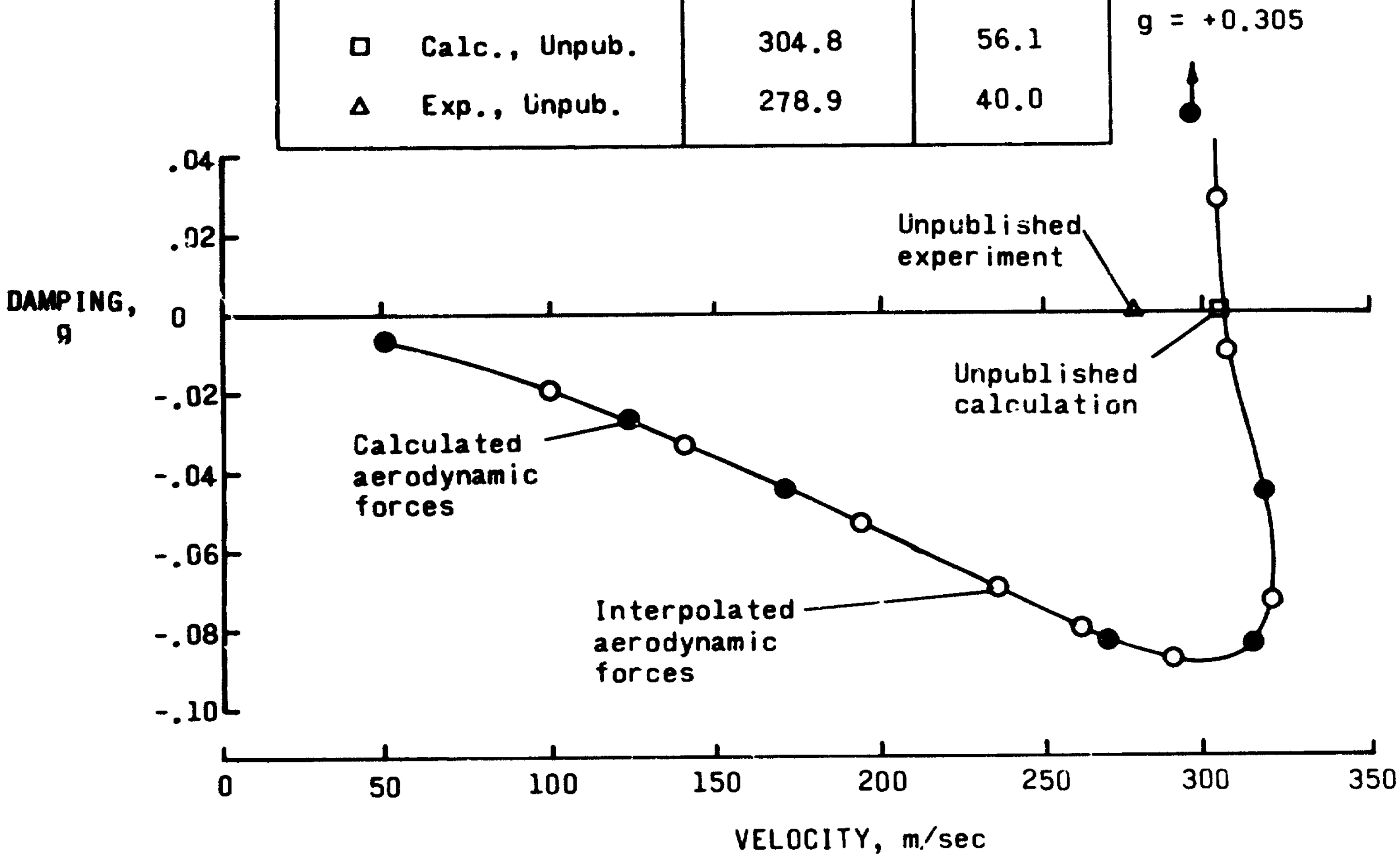

Figure 12.— Platelike wing with folded tip fin flutter results for a Mach number of 0.90 and a density of 0.861 kg/m^3.

NASTRAN MODULE	CPU TIME, sec	FUNCTION
IFP	2.958	Sort input data, set up restart tables, etc.
GP1 to READ	191.208	Form structural matrices (96 QUAD2 elements)
READ thru GKAM	396.798	Real eigenvalue analysis (5 modes)
APD	.962	Generate aerodynamic elements (100 boxes)
GI	25.196	Geometry interpolation (4 surface splines)
AMG	195.404	Generate aerodynamic influence coefficient matrices (3 values of reduced frequency)
AMP	126.566	Generate generalized aerodynamic matrices (4 modes)
FA1-CEAD-FA2	8.648	Flutter solution for 5 reduced frequencies, aerodynamic interpolation for 2 reduced frequencies
XYTRAN, XYPLOT	.510	g-V plot and f-V plot

Total CPU time = 966.3 sec
Total PPU time = 2822.7 sec
O/S calls = 36401

Figure 13.– Sample flutter solution computer times.

N74-14610

CRACKED FINITE ELEMENTS PROPOSED FOR NASTRAN

By J. A. Aberson, The Lockheed-Georgia Company
and J. M. Anderson, Georgia Institute of Technology

SUMMARY

The recent introduction of special crack-tip singularity elements, usually referred to as cracked elements, has brought the power and flexibility of the finite-element method to bear much more effectively on fracture mechanics problems. This paper recalls the development of two cracked elements and presents the results of some applications proving their accuracy and economy. Judging from the available literature on numerical methods in fracture mechanics, it seems clear that the elements described have been used more extensively than any others in practical fracture mechanics applications.

INTRODUCTION

The study of crack growth behavior by classical continuum linear fracture mechanics has been limited primarily to simple structural configurations and loadings. Because of the ease with which the finite-element method handles discontinuous loads and boundary conditions, attempts have been made to use this method to study fracture in complex structures. The capability of conventional elements and conventional modeling procedures to predict crack-tip parameters accurately has been found to be limited and uneconomical. The most significant and accurate results obtained through use of standard methods are those which follow the work reported by Chan et. al. (ref. 1) and Kobayashi et. al. (ref. 2). The method followed by Kobayashi, for example, is to use the crack-opening displacements to solve a sequence of two simultaneous equations relating displacements to the two stress-intensity factors, K_I and K_{II}, for the opening and sliding fracture modes, respectively. These results are then interpreted or extrapolated to predict values at the crack tip. The difficulty in applying this approach lies in trying to accurately depict the extreme stress gradient existing in the near vicinity of a crack tip. The detail required for a model to reasonably characterize this gradient makes the procedure expensive and cumbersome. For example, Oglesby and Lomacky (ref. 3) indicate that the maximum permissible element size necessary to insure acceptable accuracy in the computed stress-intensity factors is of the order of 1/300th of the crack half-length. To achieve detail of this order, substructure analyses have usually been used. That is, a coarse model is first analyzed to obtain boundary conditions which are then imposed on a more refined local model of the crack region. In some instances results from the second model have been used to analyze a third and even more finely modeled localized region of the crack tip. Obviously, considerable modeling and computer efforts are necessary to carry out such analyses.

Another approach, which is similar to that used by Chan and Kobayashi, is a combination of finite-element and boundary-collocation analyses. In this method, displacements and stresses from a conventional finite element model - which may or may not contain some representation of a crack - are used as boundary points in a boundary collocation solution for the crack. This is the procedure followed by Freese and Kaldjian (ref. 4), for example. The disadvantage of this combined approach is that it is not easily applicable since considerable experience in fracture analysis and complex variables is required to obtain consistently accurate results.

In an attempt to circumvent the economic problem of the conventional approach and the applicability problem of the combined approach, research and development efforts have been turned toward formulating elements which are capable of characterizing the crack-tip stress singularity internally. These singularity elements - cracked finite elements - provide a new means for computing stress-intensity factors and thereby predicting crack growth. Two such elements have been developed and implemented at the Lockheed-Georgia Company. These elements have received extensive usage in project and contract work and have provided considerable substantiation of the accuracy of the approach used in their formulation. A description of the formulation and implementation of these elements follows.

TECHNICAL DEVELOPMENT

The Williams' series of stress functions (refs. 5 and 6)* is the basis for all boundary collocation and cracked finite-element schemes to estimate stress-intensity factors. This series gives the following familiar expressions for the in-plane stresses for the plane crack problem illustrated in figure 1.

$$\sigma_r(r,\theta) = \sum_{n=1}^{\infty} \frac{n}{4} \cdot r^{\frac{n}{2}-1} \left\{ s_n \left[-(n+2) \cos\left(\frac{n}{2}+1\right)\theta + f(n)(n-6) \cos\left(\frac{n}{2}-1\right)\theta \right] \right.$$

$$\left. + a_n \left[g(n)(n+2) \sin\left(\frac{n}{2}+1\right)\theta - (n-6) \sin\left(\frac{n}{2}-1\right)\theta \right] \right\}$$

$$\sigma_\theta(r,\theta) = \sum_{n=1}^{\infty} \frac{n}{4} (n+2) \, r^{\frac{n}{2}-1} \left\{ s_n \left[\cos\left(\frac{n}{2}+1\right)\theta - f(n) \cos\left(\frac{n}{2}-1\right)\theta \right] \right.$$

$$\left. + a_n \left[-g(n) \sin\left(\frac{n}{2}+1\right)\theta + \sin\left(\frac{n}{2}-1\right)\theta \right] \right\} \qquad (1)$$

* An error in reference 5 was subsequently corrected by Williams in reference 6.

and

$$\tau_{r\theta}(r,\theta) = \sum_{n=1}^{\infty} \frac{n}{4} r^{\frac{n}{2}-1} \left\{ s_n \left[(n+2) \sin\left(\frac{n}{2}+1\right)\theta - f(n)(n-2) \sin\left(\frac{n}{2}-1\right)\theta \right] \right.$$

$$\left. + a_n \left[g(n)(n+2) \cos\left(\frac{n}{2}+1\right)\theta - (n-2) \cos\left(\frac{n}{2}-1\right)\theta \right] \right\}$$

in which

$$f(n) = \frac{\frac{n}{2}+1}{\frac{n}{2}+(-1)^n}$$

and (2)

$$g(n) = \frac{\frac{n}{2}-(-1)^n}{\frac{n}{2}+1}$$

The independent constants associated with the symmetric (even in θ) and antisymmetric (odd in θ) parts of the Williams' series have been denoted in equation (1) by s_n and a_n, respectively. Even though an expression for the second antisymmetric term has been formally written, it should be noted before proceeding that it never contributes to any of the stresses. Thus in the usual finite-element description, a_2 is not a legitimate generalized coordinate.

The leading terms in equation (1) are singular like $r^{-1/2}$; all subsequent terms are nonsingular. The coefficients s_1 and a_1 are related to the opening and sliding mode stress-intensity factors K_I and K_{II} by the following formulas:

$$\left.\begin{aligned} K_I &= \lim_{r\to 0} \sqrt{2\pi r}\, \sigma_\theta(r,0) = 3\sqrt{2\pi}\, s_1 \\ K_{II} &= \lim_{r\to 0} \sqrt{2\pi r}\, \tau_{r\theta}(r,0) = \sqrt{2\pi}\, a_1 \end{aligned}\right\} \qquad (3)$$

The strains corresponding to the stresses in equation (1) are obtained through Hooke's law. The strain-displacement equations in plane polar coordinates can then be integrated for the radial and tangential displacement components $u_r(r,\theta)$ and $u_\theta(r,\theta)$, respectively. See, for example, reference 7 and the subsequent correction. The resulting displacement components are

$$u_r(r,\theta) = K \cos\theta + H \sin\theta$$

$$+ \sum_{n=1}^{\infty} \frac{1}{4G} r^{\frac{n}{2}} \left\{ s_n \left[-(n+2) \cos\left(\frac{n}{2}+1\right)\theta - f(n)(6-8\sigma-n) \cos\left(\frac{n}{2}-1\right)\theta \right] \right.$$

$$\left. + a_n \left[(n+2)\, g(n) \sin\left(\frac{n}{2}+1\right)\theta + (6-8\sigma-n) \sin\left(\frac{n}{2}-1\right)\theta \right] \right\} \qquad (4)$$

and

$$u_\theta(r,\theta) = Fr + H \cos\theta - K \sin\theta$$

$$+ \sum_{n=1}^{\infty} \frac{1}{4G} r^{\frac{n}{2}} \left\{ s_n \left[(n+2) \sin\left(\frac{n}{2}+1\right)\theta - f(n)(6-8\sigma+n) \sin\left(\frac{n}{2}-1\right)\theta \right] \right.$$

$$\left. + a_n \left[(n+2)\, g(n) \cos\left(\frac{n}{2}+1\right)\theta - (6-8\sigma+n) \cos\left(\frac{n}{2}-1\right)\theta \right] \right\}$$

in which F, H, and K are rigid-body displacement parameters and G is the shear modulus. The dimensionless elastic constant σ is given by

$$\sigma = \begin{cases} \nu & \text{(for plane strain)} \\ \dfrac{\nu}{1+\nu} & \text{(for plane stress)} \end{cases}$$

where ν is Poisson's ratio.

Most cracked finite elements developed to date (c.f. refs. 8-11) incorporate only the leading symmetric terms in equations (1) and (4). Creager, at the Lockheed-California Company in 1970, attempted to include subsequent terms in the Williams' series but was unsuccessful due to inadequate element geometry. This was successfully accomplished by Wilson (ref. 12) with a symmetric element, which makes use of the first four terms. Wilson's element, however, has the disadvantage of being semicircular and, hence, is awkward to use in conjunction with conventional elements which almost always have straight boundaries. Moreover, the Wilson element (as well as some others previously referenced) has fewer degrees of freedom than are needed for independence of the nodal displacements. At best this requires that the stiffness matrix of the cracked element receive special attention in forming the stiffness matrix of the assembly.

At Lockheed-Georgia, the decision was made at the outset to develop a cracked finite element that is a high-order element in that it

(i) incorporates many of the terms in the Williams' series;
(ii) has a perfect balance between actual degrees of freedom and number of nodal displacements; and
(iii) has a convenient shape for interfacing with conventional elements.

The first feature permits accurate estimates of stress-intensity factors with relatively coarse finite-element grids, while the second and third features allow the numerical analyst to add the cracked element to an assembly in the same way that he adds a conventional element.

Because many fracture mechanics problems are symmetric about the plane of the crack, two elements were developed at Lockheed-Georgia. One takes only the symmetric terms in the Williams' series and, hence, is applicable only to symmetric problems ($K_{II} = 0$); the other makes use of both symmetric and anti-symmetric terms and is applicable to unsymmetric or mixed mode (K_I and K_{II}) problems.

Plane-Deformation Symmetric Element

Figure 2 shows the eight-node-symmetric element. The elemental coordinate system has its origin at the crack tip. The element is rectangular with a three-to-one aspect ratio. Placement of the nodes relative to the rectangle is pre-determined with a node at each corner plus nodes at the one-third points of each of the long sides. The choice of the symmetric element's shape - three equal squares - was considered convenient since the use of regular mesh spacings is common in finite-element models. This geometry has also proven to be effective when used with constant-strain triangles. The lower side (nodes 6, 7, 8, and 1) is coincident with the crack direction and presumed axis of symmetry. Nodes 6 and 7 are on the free crack face. Nodes 8 and 1 are on the prolongation of the crack. They are constrained rigidly as to vertical displacement and are free of shear forces - conditions consistent with symmetry.

The element has sixteen displacement degrees of freedom - two per node corresponding to the in-plane displacement components. Thus, in keeping with feature (ii) mentioned previously, it incorporates the first thirteen symmetric terms of the Williams' series plus the three displacement degrees of freedom associated with rigid-body displacement in the plane. In the following, the thirteen Williams' coefficients and the three rigid-body parameters are referred to as the sixteen generalized coordinates of the element. The stresses and displacements corresponding to these sixteen generalized coordinates are evaluated on the boundary of the element. Products of stress and displacement contributing to boundary work are formed and integrated. The result is a homogeneous quadratic form in the generalized coordinates, and the coefficient of each term is an element of the cracked element's stiffness matrix with respect to the generalized coordinates.

Once the stiffness matrix relative to generalized coordinates is determined, the stiffness matrix relative to nodal displacements is formed using equation (4).

To date this element has not failed to substantiate any reliable stress-intensity factor to within 2% difference. And more often than not, this was accomplished with a relatively coarse finite-element grid. Results obtained with the symmetric element will be discussed later in the section "Applications."

Plane-Deformation Unsymmetric Element

The ten-node unsymmetric element is shown in figure 3. The element is square with equally spaced nodes around its boundary. As before, the shape (4 equal squares) and relative location of the nodes are fixed, and were chosen to provide modeling convenience. Again, the actual size of the element and its elastic constants dictated by the particular application are input parameters. The generalized coordinates correspond to the first nine symmetric terms and first eight antisymmetric terms of the Williams' series plus the three rigid-body displacement parameters. The stiffness matrix was again generated by integration around the boundary.

Results obtained with this element are presented in the following section. Although sufficient, the accuracy obtained with this unsymmetric element is not as impressive as that obtained with the symmetric element previously discussed. This is understandable in light of the fact that the unsymmetric element has fewer degrees of freedom that it can bring to bear on each mode. Of course, it can be used in a much wider class of crack problems and is more practical for industrial applications. In the following section some examples are given which show the accuracy and applicabilities of both the symmetric and unsymmetric elements.

APPLICATIONS

To illustrate the capabilities of the two elements, four examples of their usage follow. These examples were chosen to demonstrate first, the accuracy and economy of the elements and second, the capacities of the elements to perform analyses for structural configurations of practical importance. The four cases are drawn from a wide range of work involving use of the cracked elements and represent typical rather than most favorable results.

The cracked elements are implemented in a standard single-precision finite-element displacement-method program which employs a banded Cholesky decomposition solution procedure. This program, which operates on a Univac 1106 computer, was used for all four examples.

Case 1: Symmetric-Element Test Case

This example, shown on figure 4, was one of the first analyzed with the symmetric element. However, it exhibits the degree of accuracy which has been consistently achieved in numerous subsequent problems. The finite-element model has 31 nodes, 35 constant-strain triangles, and 1 eight-node cracked element. The three configurations of single-edge crack, double-edge crack and center crack were all individually analyzed with this one model for an a/w ratio of 1/3. The model grid, which is quite coarse, results in the single-edge crack model having 57 displacement degrees of freedom (DOF) while the double-edge and center models have 51 DOF each. Comparisons of the stress-intensity factors computed using these configurations with ASTM values are shown on figure 4. The accuracy of the finite-element predictions are impressive ($\leq$ 1.5% error) for all three cases. Computer time to perform each analysis was 3 to 4 seconds.

Subsequent work with this finite-element model and others like it showed comparable results, with refinements in the grid bringing steady convergence toward ASTM values.

Case 2: Symmetric Cracked Hole

The symmetric problem depicted in figure 5 was analyzed in order to assess the accuracy of the formula

$$K_I = \beta_{Bowie}\, \beta_{Isida}\, \sigma \sqrt{\pi a} \tag{5}$$

which is routinely used to estimate stress-intensity factors for this geometry. In equation (5) β_{Bowie} and β_{Isida} are the correction factors, respectively, associated with Bowie's (ref. 13) analysis for the presence of the hole and Isida's (ref. 14) analysis for the finite-width effect. The finite-element grid as shown in figure 5 was established (i) to permit the location of the cracked element to be easily changed to simulate growth of the symmetric crack, and (ii) to permit the width of the plate to be readily changed by removing columns of constant-strain triangular elements from the right edge. The stress-intensity factors computed in this parametric study are listed in table 1. An important conclusion to be drawn from these results is that the value predicted by equation (5) seems adequate for short cracks, but becomes quite inaccurate and nonconservative as the crack grows long.

Such parametric analyses are of practical value, however, only if they can be quickly and economically accomplished. The use of the symmetric cracked element made it possible for a relatively coarse model (figure 5) to give accurate answers. The analysis of this coarse model required 28 000 words of computer storage and approximately 20 seconds of computer time. The total study, which includes model conception, data input, and 21 separate analyses, required less than 1 man-day of engineering effort and 7 minutes of computer time. Subsequent studies of other parameters, e.g. fastener loads or fastener interference, could now be accomplished with even less effort since the model can be saved and reused.

In general, the computer times and storage cited above are economical, and, in addition, are well within the operational limits of most remote access or time-sharing computer facilities. This economy and ready availability in a remote access mode (Univac DEMAND) have resulted in widespread application of cracked elements at the Lockheed-Georgia Company in studies such as the one described above.

Case 3: Pin-Loaded Lug

The structural member shown on figure 6 is a lug and occurs frequently in aerospace structures. The lug's lack of geometric symmetry greatly hampers the use of approximate methods to adequately estimate its stress-intensity factors K_I and K_{II} when a crack appears. Such cracked geometry is easily handled, however, with the unsymmetric cracked element. The lug and the pin loading it are modeled with constant-strain triangles and a cracked element as shown on figure 7. The unsymmetric cracked element is shown in its initial position. As in the previous example, the model grid was constructed to permit the position of the cracked element to be easily changed to simulate the growth of the crack. Results of the analyses are given in Table 2. The small value of K_{II} relative to K_I for the initial position indicates that the behavior of the crack is primarily mode I or opening mode from the beginning. Figure 8 depicts the mode I behavior as the crack progresses from the hole to the outer edge.

This analysis, which is considered to be in error by less than 3 percent, was accomplished at the cost of 1 man-day and 4 minutes of computer time in 35 000 words of computer storage.

Case 4: 45-Degree Slanted Crack Test Specimen

This last example demonstrates the use of cracked elements to calibrate test configurations for accurate reduction of test data. The specimen shown by figure 9 contained an initial 45° center crack, and was subjected to a constant-amplitude tension-tension load. The maximum tension to minimum tension ratio was 0.1. The specimen was modeled with constant-strain triangles and an unsymmetric cracked element as shown by figure 10. The path taken by the crack during the cyclic test was simply traced on the finite-element model. The center section of the model was reconstructed seven times to accomodate the cracked elements for dimensionless projected crack lengths $\lambda = a/w$ of 0.3, 0.35, 0.4, 0.5, 0.6, 0.7, and 0.8. The steel loading pins for the test were modeled by spring elements spread over the approximate bearing surfaces as shown.

The results from the analyses of this model are shown on figure 11. The curves on figure 11 are considered accurate within 2 percent. These results show an interesting and potentially significant feature not found in similar work reported by Iida and Kobayashi (ref. 15). For $0.5 \leq \lambda \leq 0.75$ the mode I stress-intensity factor K_I is greater than K_I for a straight crack of the same projected length. This increase in K_I (the "hump" in figure 11) occurs when K_{II} goes to zero and could easily account for the increased crack-growth rates observed for this type of specimen. However, the significant point to this analysis is that an accurate knowledge of K_I and K_{II} for test articles permits a concise reduction of crack-growth-rate data for later design usage.

The analysis of this case required approximately 80 seconds of computer time for each configuration. The total for all seven configurations, including data input and modifications, was 9.4 minutes.

CONCLUSIONS

The incorporation into NASTRAN and other finite element codes of cracked elements appears to be both a timely and practical effort, for there is a growing concern among those involved in aerospace design with being able to perform reliable fracture analyses of damaged or flawed structures. This concern arises partly from anticipation of difficulties of meeting certain design "fracture criteria" imposed by procuring agencies for new aerospace vehicles and partly from recent experiences with existing airplanes. For whatever reasons, the fact is that fracture mechanics and fracture analyses have become significant and necessary steps in the design and modifications of aerospace structures. Thus, there is a pressing need for accurate production analysis tools to enable designers to apply new fracture criteria. Cracked finite elements, such as those discussed in this paper, are such tools. Their ease of application makes it possible for analysts and designers not extensively trained in fracture mechanics but familiar with finite element methods to compute accurate stress-intensity factors.

REFERENCES

1. Chan, S. K., Tuba, I. S., and Wilson, W. K.: On the Finite Element Method in Linear Fracture Mechanics. Engineering Fracture Mechanics, 2, 1970, pp. 1-17.

2. Kobayashi, A. S., Maiden, D. E., Simon, B. J., and Iida, S: Application of the Method of Finite Element Analysis to Two-Dimensional Problems in Fracture Mechanics. University of Washington, Department of Mechanical Engineering, ONR Contract Nonr-477(39), NR 064 478, TR No. 5, Oct. 1968.

3. Oglesby, J. J., and Lomacky, O.: An Evaluation of Finite Element Methods for the Computation of Elastic Stress Intensity Factors. Navy Ship Research and Development Center, NAVSHIPS Project SF 35.422.210, Task 15055, Report Number 3751, December 1971.

4. Freese, C. E., and Kaldjian, M. J.: Collocation and Finite Elements for Crack Analysis. Proceedings of the 13th Annual Symposium: Fracture and Flaws, University of New Mexico College of Engineering, March 1973.

5. Williams, M. L.: On the Stress Distribution at the Base of a Stationary Crack. Journal of Applied Mechanics, Vol. 24, No. 1, March 1957, pp. 109-114.

6. Williams, M. L.: Stress Singularities Resulting from Various Boundary Conditions in Angular Corners of Plates in Extension. Journal of Applied Mechanics, Vol. 74, December 1952, pp. 526-528.

7. Gross, B., Roberts, E., and Srawley, J. E.: Elastic Displacements for Various Edge-Cracked Plate Specimens. Internat. J. Fracture Mechanics, vol. 4, no. 3, Sept. 1968. Also errata, Internat. J. Fracture Mechanics, vol. 6, 1970.

8. Byskov, E.: The Calculation of Stress Intensity Factors Using the Finite Element Method with Cracked Elements. International Journal of Fracture Mechanics, Vol. 6, No. 2, June 1970, pp. 159-167.

9. Tracey, D. M.: Finite Elements for Determination of Crack Tip Elastic Stress Intensity Factors. Engineering Fracture Mechanics, Vol. 3, 1971, pp. 255-265.

10. Walsh, P. F.: The Computation of Stress Intensity Factors by a Special Finite Element Technique. International Journal of Solids and Structures, Vol. 7, 1971, pp. 1333-1342.

11. Pian, T. H. H., Tong, P., and Luk, C. H.: Elastic Crack Analysis by a Finite Element Hybrid Method. AFOSR-TR-72-0752, U.S. Air Force, Dec. 1971. (Available from DDC as AD 739 988.)

12. Wilson, W. K.: Crack Tip Finite Elements for Plane Elasticity. Westinghouse Research Laboratories Scientific Paper 71-1E7, FMPWR-P2, June 1971.

13. Bowie, O. L.: Analysis of an Infinite Plate Containing Radial Cracks Originating from the Boundary of an Internal Circular Hole. Journal of Mathematics and Physics, Vol. 35, 1956.

14. Isida, M.: On the Tension of a Strip with a Central Elliptical Hole. Transactions, Japanese Society of Mechanical Engineers, Vol. 22, 1956.

15. Iida, S., and Kobayashi, A. S.: Crack Propagation Rate in 7075-T6 Plates Under Cyclic Tensile and Transverse Shear Loadings. Journal of Basic Engineering, Transactions ASME, Series D, Vol. 91, No. 4, Dec. 1969, pp. 764-769.

Table 1. A Study of Finite-Width Panel with Two Symmetric Cracks Coming From a Hole

$\frac{W}{r}$	$\frac{a}{r}$	β(ISIDA)	β(BOWIE)	$\frac{K_I[\text{FROM EQ. (5)}]}{\sigma\sqrt{\pi a}}$	$\frac{K_I[\text{ELEMENT}]}{\sigma\sqrt{\pi a}}$	% DIFFERENCE
	0.3	1.02	2.15	2.19	2.18	-0.46
	1.9	1.08	1.23	1.33	1.42	6.33
8.0	3.5	1.25	1.12	1.40	1.52	7.89
	5.1	1.61	1.07	1.72	1.90	9.47
	6.7	3.14	1.05	3.29	4.08	19.36
	0.3	1.02	2.15	2.19	2.19	0.0
	1.5	1.10	1.29	1.42	1.47	3.40
6.4	2.7	1.27	1.16	1.48	1.53	3.27
	3.9	1.61	1.11	1.78	1.87	4.81
	5.1	3.01	1.07	3.21	3.96	18.94
	0.3	1.04	2.15	2.23	2.23	0.0
	1.1	1.13	1.42	1.61	1.62	0.62
4.8	1.9	1.31	1.23	1.62	1.64	1.22
	2.7	1.63	1.16	1.89	1.99	5.03
	3.5	2.89	1.12	3.24	3.57	9.24
	0.3	1.11	2.15	2.39	2.42	1.24
	0.7	1.21	1.64	1.99	2.01	1.00
3.2	1.1	1.39	1.42	1.97	2.02	2.48
	1.5	1.65	1.29	2.13	2.29	6.99
	1.9	2.40	1.23	2.95	3.25	9.23
1.6	0.3	1.873	2.15	4.01	4.46	10.09

Table 2. Results from Analysis of the Lug Model

$\frac{a}{r}$	$\frac{K_I}{\sigma_B \sqrt{\pi a}}$	$\frac{K_{II}}{\sigma_B \sqrt{\pi a}}$
0.1112	2.770	0.123
0.3335	1.796	-0.002
0.5559	1.586	0.004
0.7782	1.775	0.004

crack length = a

hole radius = r

mean bearing stress = σ_B

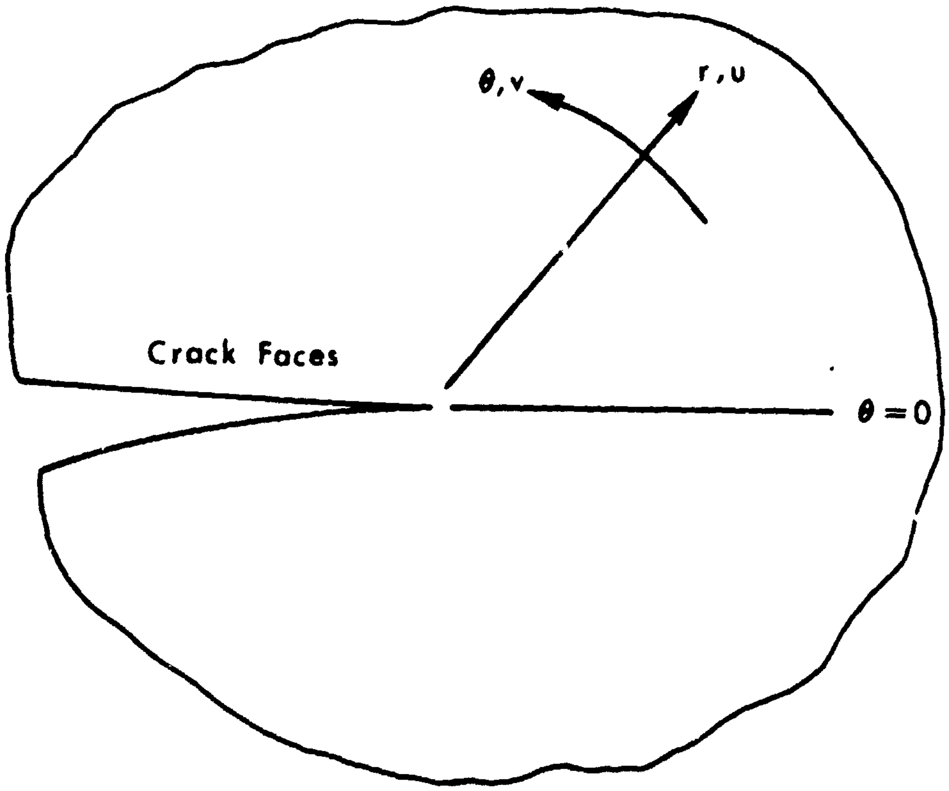

Figure 1.- Neighborhood around a crack tip.

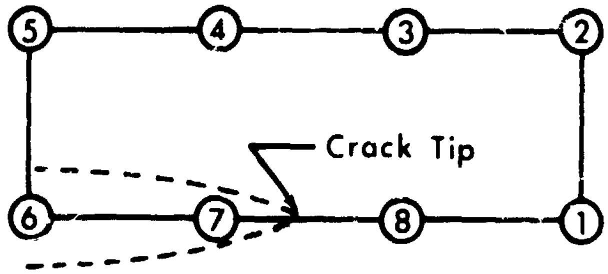

Figure 2.- Eight-node element for symmetric problems.

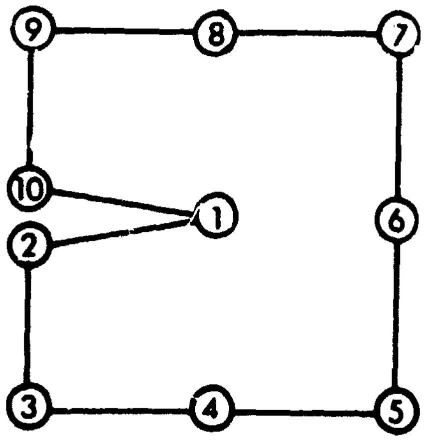

Figure 3.- Ten-node element for unsymmetric problems.

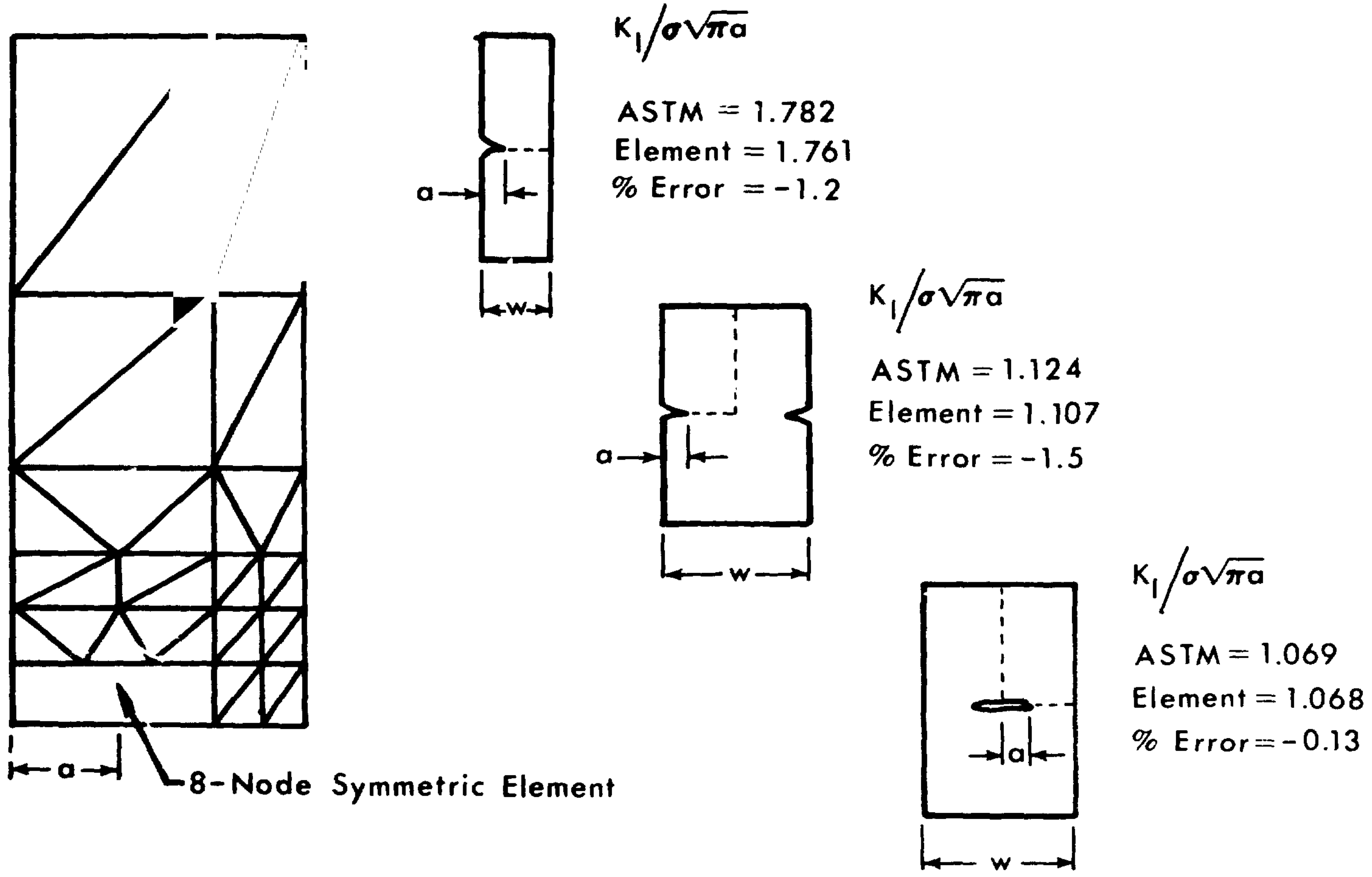

Figure 4.- Results for single-edge, double-edge, and center cracked tension panels with a/w = 1/3.

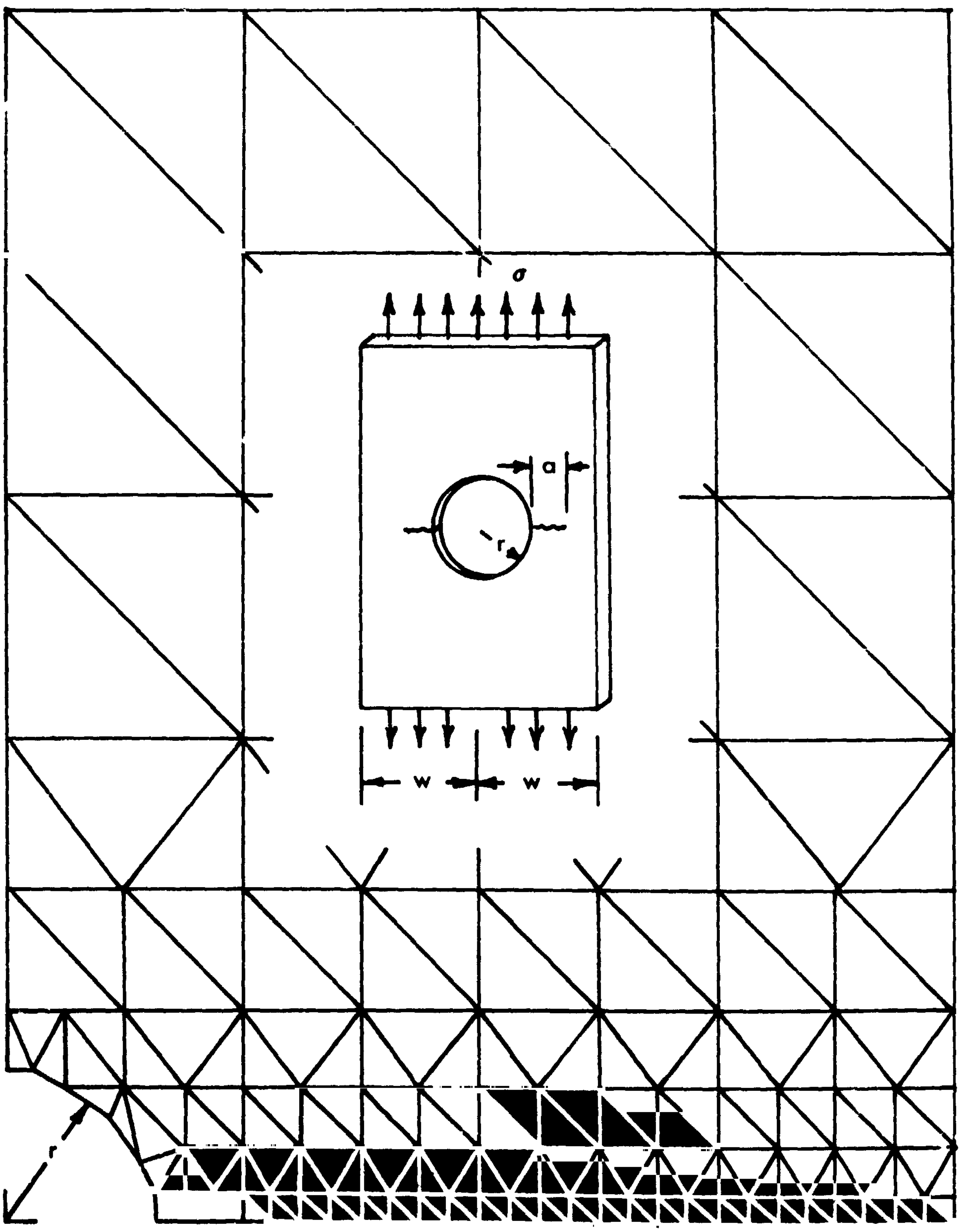

Figure 5.- Symmetric cracks growing from a hole in a finite-width panel.

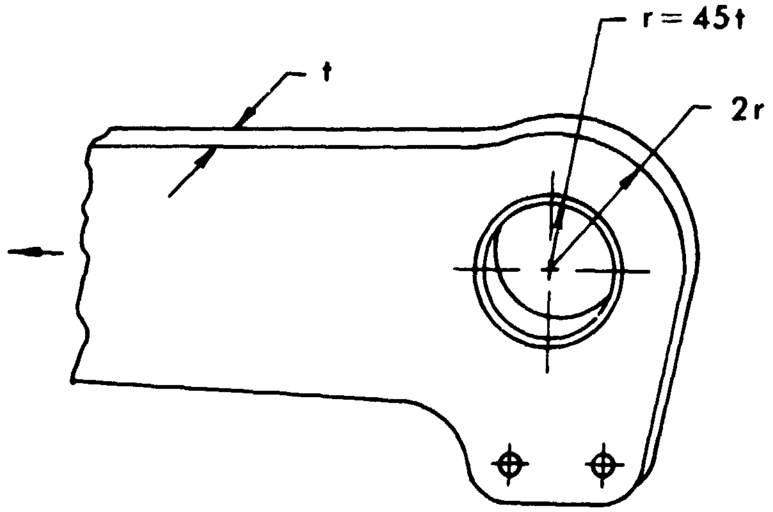

Figure 6.- Lug geometry.

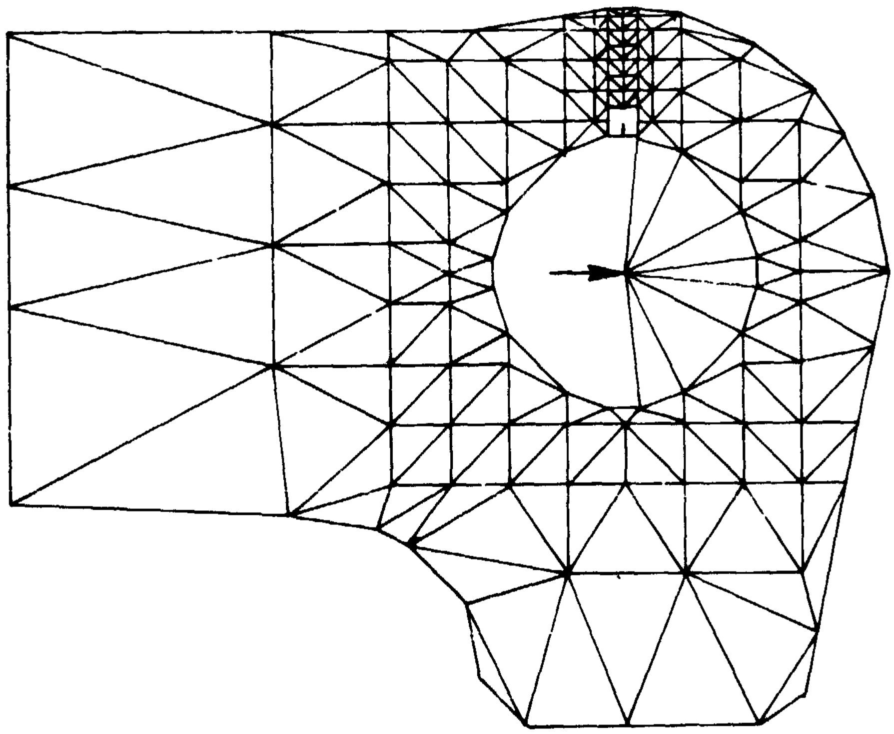

Figure 7.- Finite-element idealization of the lug.

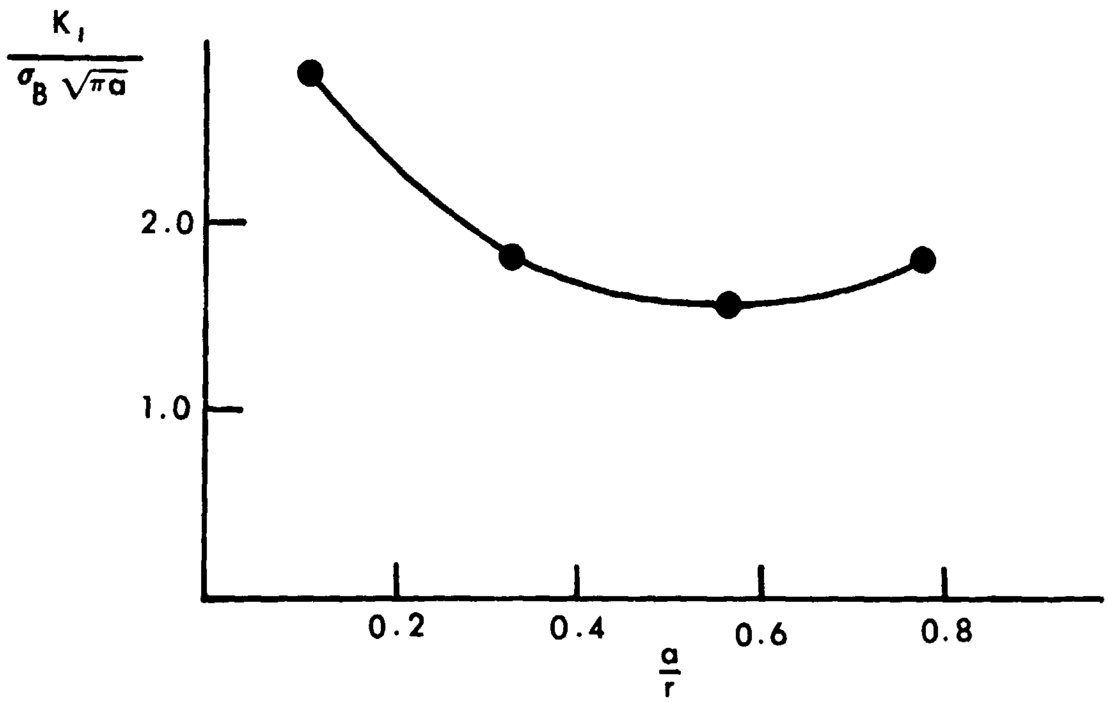

Figure 8.- Stress-intensity factor versus crack length for the lug model.

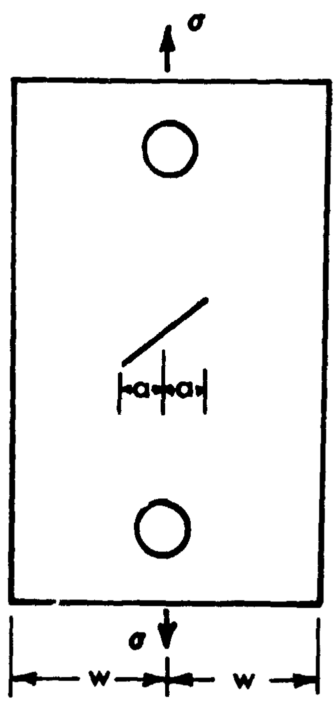

Figure 9.- Tension specimen with a 45° center crack.

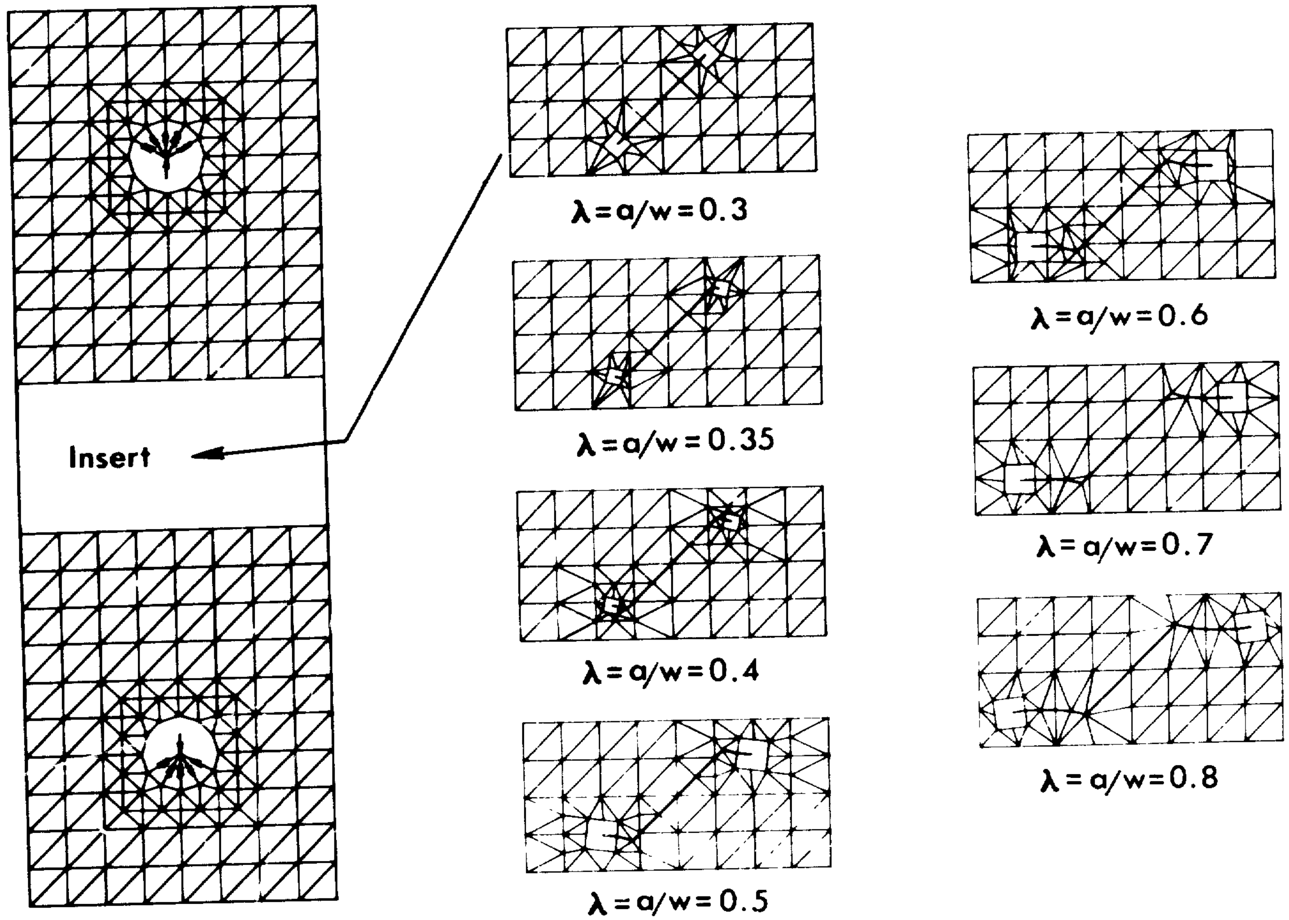

Figure 10.- Finite-element models of tension specimen where initial 45^{o} crack grew experimentally as modeled.

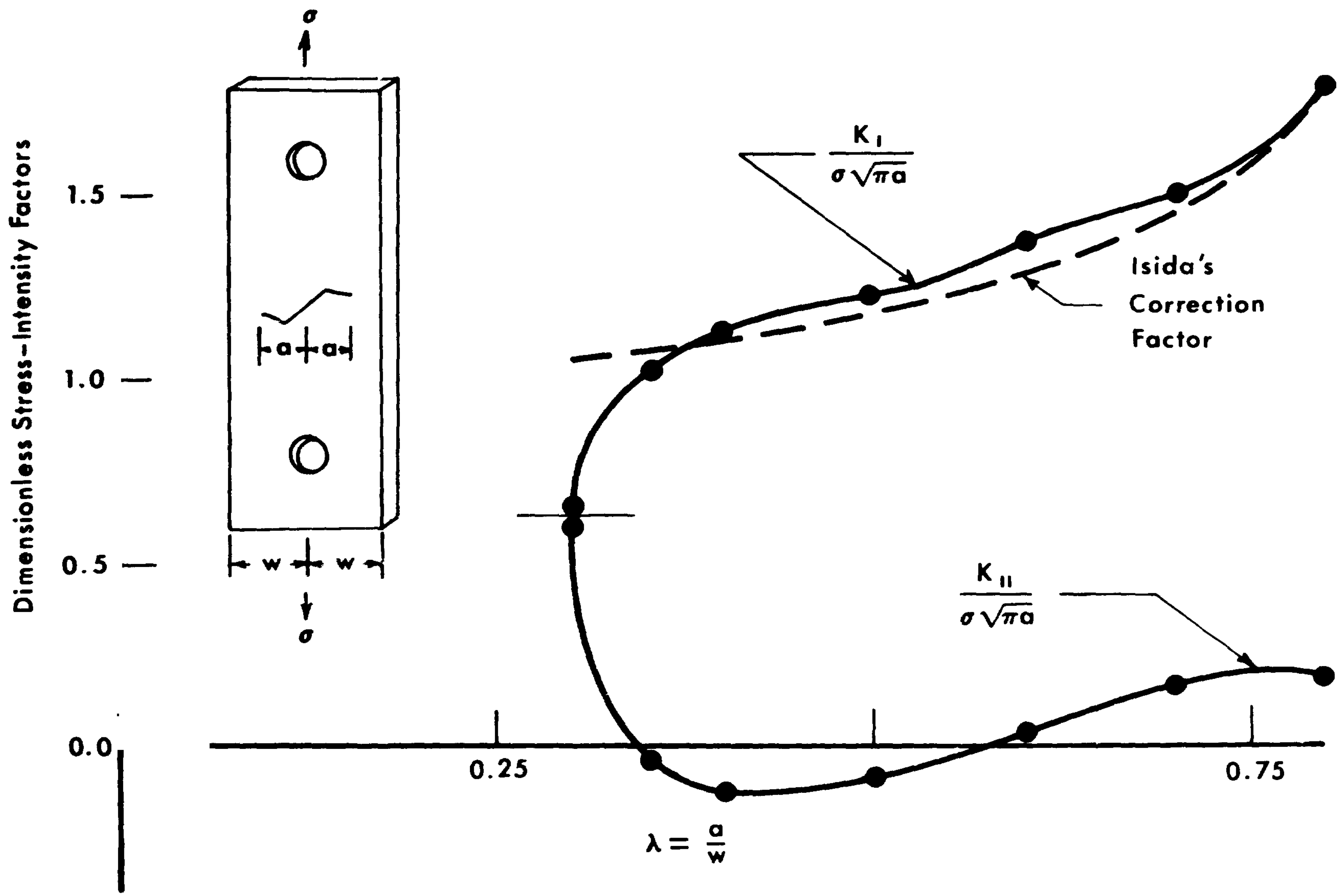

Figure 11.- Stress-intensity factors from the finite-element model shown in figure 10.

N74-14611

THE CONSTRAINT METHOD - A NEW FINITE ELEMENT TECHNIQUE

By Chung-Ta Tsai

McDonnell Douglas Astronautics Company - East, St. Louis

and

Barna A. Szabo

Washington University, St. Louis

SUMMARY

A new approach to the finite element method which utilizes families of conforming finite elements based on complete polynomials is presented here. Finite element approximations based on this method converge with respect to progressively reduced element sizes as well as with respect to progressively increasing orders of approximation. Numerical results of static and dynamic applications of plates are presented to demonstrate the efficiency of the method. Comparisons are made with plate elements in NASTRAN and the high-precision plate element developed by Cowper and his co-workers. Some considerations are given to implementation of the constraint method into general purpose computer programs such as NASTRAN.

INTRODUCTION

With the availability of general purpose computer programs, such as NASTRAN, at reasonable cost, utilization of the finite element approximations is common practice. In the conventional finite element method, a continuous structure is idealized by discrete structural elements which are joined together at nodes. Structural characteristics are expressed in terms of nodal variables. Improvement of accuracy is generally made with respect to progressively reduced element sizes. If certain conditions are met, then the finite element approximation will converge to the true solution when the element sizes are reduced (Ref. 1).

Unfortunately, reliable and practical error estimation techniques are not yet available. In important analytical computations it is usually necessary to complete two or more calculations of the same problem in order to establish the validity of the finite element model itself. The calculations usually employ progressively refined finite element nets, although upper and lower bound estimates have been proposed also (Ref. 2). This is a tedious and costly process involving a considerable amount of duplicated effort.

Much interest has been shown in the development of high-precision finite elements so that better accuracy could be obtained with fewer elements. Incorporation of such elements into the NASTRAN program was reported to be under development (Refs. 3 and 4).

Computational experiments as well as theoretical considerations have shown that, in terms of the number of variables needed to carry an analysis to a specified level of precision, the high-order or high-precision finite elements are more efficient than the low-order ones. This is particularly true in vibration and buckling analyses where eigenvalue problems must be solved in terms of the problem variables. An additional fact in favor of using fewer high-precision finite elements is that the number of necessary man-computer interface operations and the volume of data processing services are roughly proportional to the number of finite elements employed.

In view of these findings it is logical to explore potential benefits to be gained from the convergence process based on progressively increasing orders of polynomial approximation. In this convergence process, the finite element net is held constant and the order of polynomial approximating functions is varied. Existing error bounds such as that proposed by Fried (Ref. 5) indicate that the convergence rate will be exponential in this case, whereas the convergence rate is geometrical when the finite element sizes are reduced. It is noted that this error bound is valid only when the exact solution is sufficiently smooth and free from singularities.

While there are many competing formats for stating finite element approximation problems, it was found that it is convenient to state the general problem as a quadratic programming problem. In this formulation, which will be referred to as the constraint method in the following discussions, the functional to be approximated (usually the potential energy expression) is written as a quadratic expression of the unknown coefficients of the polynomial approximating functions. The interelement continuity conditions and principal boundary conditions are stated as linear equality constraints. An advantage of this formulation is that all matrices that are necessary to define the numerical problem can be generated automatically for arbitrary orders of approximation. The finite elements so constructed will exhibit convergence with respect to reduced element sizes as well as with respect to increasing orders of polynomial approximation. Because of the latter type of convergence, it is unnecessary to reconstruct the finite element model when higher accuracy is sought. Additional advantages of this formulation are: (a) Since the unknowns are the scalar coefficients of the approximating polynomial sequences, it is not necessary to transform the variables and stiffness matrices from one coordinate system to another. (b) All finite elements can be made mutually compatible by specifying the appropriate connectivity through the constraint equations. This is a very important feature of the new method because it permits consideration of structural stiffeners with greater ease than the standard finite element methods. (c) The new method will yield the exact solution when the exact solution is a polynomial with a degree less than or equal to the degree of the approximating polynomials, regardless of the number or orientation of the finite element employed. (d) The accuracy of solution and the computational efficiency are not sensitive to input numbering schemes (therefore, the method provides flexibility to the users in generating the structural models). (e) The number of elements depends solely on the geometrical configuration of the structure to be analyzed, not on the desired degree of precision as in conventional analysis. Thus only the minimum number of elements sufficient for idealizing the structure needed to be defined. Other factors, such as existence of point loads and/or discrete supports, do not preclude the use of large elements.

In the following, a solution technique utilizing the essential features of this formulation is discussed and applications of the constraint method are illustrated with numerical examples for static and dynamic analysis of plates. Comparison is made with results obtained by plate elements in the NASTRAN program and the 18 degrees-of-freedom plate element presented by Cowper et al. (Ref. 6).

THE CONSTRAINT METHOD

In the constraint method, the finite element approximation is treated as a direct energy minimization problem in which the minimum potential energy is sought subject to certain linear constraints. As in the conventional finite element method, the structure is idealized by discrete elements whose displacement characteristics are approximated by the polynomial functions defined over the element domains. Usually, the unknown variables are the coefficients in the assumed polynomials, although other variable definitions may be used also. The total potential energy is minimized with respect to these unknown coefficients subject to constraints which ensure satisfaction of both inter-element continuity and kinematic boundary conditions.

Detailed formulation of the constraint method has been presented elsewhere (Refs. 7 to 10). It will be outlined here as follows:

The total potential energy π is obtained by assembling the element potential energies π_K, expressed in terms of the coefficients of the approximating polynomials as

$$\pi = \sum_K \pi_K = 1/2 \lfloor a \rfloor [S] \{a\} - \lfloor Z \rfloor \{a\} \tag{1}$$

In equation (1), $\lfloor a \rfloor$ is a row vector, containing the polynomial coefficients and $\{a\}$ is transpose of $\lfloor a \rfloor$; $[S]$ is a symmetric, positive matrix containing a set of submatrices along its diagonal; $\lfloor Z \rfloor$ is a row vector associated with applied loading. This equation is treated as a quadratic objective function which is to be minimized subject to the following linear constraints:

$$[P] \{a\} = \{R\} \tag{2}$$

where $[P]$ and $\{R\}$ define the interelement continuity and the external boundary conditions. For homogeneous boundary conditions $\{R\}$ is null.

Several different algorithms can be used for solving the problem represented by equations (1) and (2). Most of these require separation of the independent variables from the dependent ones in the constraint equations. Then the problem can be reduced to solving a system of simultaneous linear algebraic equations as explained in Appendix A.

For structures subject to dynamic loading, inertia properties must be introduced in addition to the structural stiffnesses. In the case of free vibration, the equation of motion for the Kth element is expressed as

$$[S]_K \{a\}_K + [M]_K \{\ddot{a}\}_K = 0 \tag{3}$$

where $[M]_K$ is the consistent mass matrix and $\{\ddot{a}\}_K$ is the second derivative of $\{a\}_K$ with respect to time. The unconstrained equations of motion for the entire system are obtained by summation and can be written as

$$[S] \{a\} + [M] \{\ddot{a}\} = 0 \tag{4}$$

After separating the independent and the dependent variables in the constraint set (see Appendix A), the unknown variables $\{a\}$ can be expressed in terms of the free variables $\{a_c\}$, and the constrained equations of motion become

$$[H^T] [S] [H] \{a_c\} + [H^T] [M] [H] \{\ddot{a}_c\} = - [H^T] [S] \{h\} \tag{5}$$

The matrix $[H]$ and the vectors $\{a_c\}$ and $\{h\}$ are defined in Appendix A.

For homogeneous boundary conditions, $\{h\}$ vanishes and equation (5) becomes

$$[\bar{S}] \{a_c\} + [\bar{M}] \{\ddot{a}_c\} = 0 \tag{6}$$

where $[\bar{S}]$ and $[\bar{M}]$ are the constrained stiffness and mass matrices, respectively:

$$[\bar{S}] = [H^T] \; [S] \; [H] \tag{7}$$

$$[\bar{M}] = [H^T] \; [M] \; [H] \tag{8}$$

It is noted that the eigenvalue problem associated with equation (6) is relatively small since all dependent variables were eliminated.

An important feature of this formulation is that all finite element approximation problems can be fully defined by the matrices [S], $\{Z\}$, [P], $\{R\}$, and [M] (for dynamic application) for arbitrary orders of approximation. These matrices can be generated automatically for any given problem.

NUMERICAL EXAMPLES

The efficiency of the constraint method is illustrated with examples for static and dynamic analyses of structural plates. A comparison is made with results obtained using plate elements in the NASTRAN program and the high-precision plate element presented by Cowper et al. (Ref. 6). Emphasis is on the accuracy and convergence of the constraint method with respect to increasing orders of approximation and using a minimum number of elements. Additional numerical results for static analysis of plates and shells can be found in references 7 to 10.

Static Analysis

The first example problem for static application is the simply-supported equilateral triangular plate (Fig. 1(a)) under uniform pressure q. The exact solution of this problem is a 5th order polynomial (Ref. 11).

The constraint method gave the exact solution when the 5th order polynomial was employed, and only one finite element was necessary. The results obtained by the 18 degrees-of-freedom high-precision element (also based on the 5th order polynomial) for various finite element layouts were presented in reference 6 for displacements and bending moments at the centroid of the plate. Figure 1(b) shows the layout given in reference 6 for N=1 and N=36, where N is the total number of elements. Finite element layouts (N=25 and 100) used in the NASTRAN model are shown in figure 1(c). Due to symmetry, only one-half of the plate was considered. Results at the centroid of the plate are given in table 1. It is seen that 36 high-precision elements with 108 degrees-of-freedom (DOF) were needed to obtain precision to five significant digits whereas only 6 DOF were needed in the constraint method to achieve similar precision. The NASTRAN results were obtained by interpolation. Employing 100 CTRPLT elements with 166 DOF, 10 percent error was observed. Additional comparisons between NASTRAN plate elements and the constraint method are presented in figures 2 and 3 for the displacement and bending moment M_x along the centerline of the plate, respectively. The NASTRAN

100-element model gave satisfactory answers for the displacements but only marginal accuracy for moment. Similar accuracy was observed for the bending moment M_y along the same line.

The second example is a rectangular plate with two opposite edges simply supported, the third edge free, and the fourth edge fixed under uniform pressure q (Fig. 4(a)). This is an interesting problem because it comprises all common boundary conditions. Due to symmetry, only one-half of the plate was considered. Finite element layouts are shown in figures 4(b) and 4(c) for the constraint method and the NASTRAN model, respectively. The quadrilateral bending element CQDPLT was used in the NASTRAN model with 300 DOF. Results obtained by the constraint method were also reported elsewhere (Ref. 7). Rapid convergence was observed with respect to increasing orders of approximation. It was found that very good results were obtained for the 6th order approximation with 21 DOF (free variables). These are compared with the NASTRAN results in figures 5 and 6 for bending moments along a line in the middle of the rectangular plate. It is seen that correlation of the NASTRAN results for M_y with the exact solution is not as good as for M_x. In this case the NASTRAN model overestimates the maximum M_y by about 50%. It should be noted, however, that NASTRAN gave satisfactory results along the centerline of the plate.

Dynamic Analysis

The first example for dynamic application is a cantilevered triangular plate. Natural frequency of the plate was solved by the constraint method for various combinations of finite element layouts and orders of approximation. Results are given in table 2 together with the results obtained by the high-precision 18 degrees-of-freedom plate element and the experimental data (Ref. 12). The results show that in the constraint method monotonic convergence can be achieved by increasing the orders of approximation as well as by reducing element sizes. It is noted that the DOF represent the total number of equations in the associated eigenvalue problems. Comparable results were obtained by the constraint method with fewer DOF.

The next dynamic problem is the free vibration of a simply-supported square plate shown in figure 7(a). Two elements were used for one-half of the plate in the constraint method (Fig. 7(b)), and 200 elements in the NASTRAN model (Fig. 7(c)). Natural frequencies of the first three modes are presented in table 3. Monotonic convergence was obtained by increasing the orders of approximation in the constraint method. The NASTRAN results, presented in reference 13, are also given for comparison. It is significant that the resulting number of DOF for the eigenvalue problem is much smaller in the constraint method.

IMPLEMENTATION

Implementation of the constraint method in conjunction with the solution algorithm given in Appendix A may be divided into the following steps:

1. Define structural model

   a. Joint coordinates
   b. Element incidence (including order of approximation that can be provided by default value)
   c. Element compatibility (this data can be generated automatically from Element Incidence or by user's input)
   d. Element and material properties
   e. Applied loads (referred to individual element ID and define point of application by its coordinates or joint ID if the joint exists; only element ID is required for distributed load)
   f. External boundary condition (referred to individual element ID and define locations for point supports; define element boundary number for line support)

2. Generate and assemble matrix

   a. Unconstrained stiffness matrix $[S]_K$, $[S]$ (one functional routine for each element type of any order of approximation)
   b. Unconstrained mass matrix $[M]_K$, $[M]$ (one functional routine for each element type of any order of approximation)
   c. Unconstrained load vector $\{Z\}_K$, $\{Z\}$ (point load, uniform or nonuniform distributed load for any other order of approximation)
   d. Constraint matrix $[P]$ (two parts: interelement compatibility and external boundary conditions)
   e. Enforced displacement vector $\{R\}$ (null or constant value)

3. Determine the rank of $[P]$ and separate independent and dependent columns in $[P]$ into matrices $[B]$ and $[C]$. This can be accomplished by using the product form of inverse to obtain $[B^{-1}]$ directly.

4. Constrained matrix generation

   a. Compute transformation matrices $[H]$ (equation (A7)) and $\{h\}$ (equation (A8))
   b. Constrained stiffness matrix $[\overline{S}]$ (equation (7))
   c. Constrained mass matrix $[\overline{M}]$ (equation (8))
   d. Constrained load vector $\{\overline{Z}\} = [H^T]\{Z\}$
   e. Constrained enforced displacement vector $\{\overline{R}\} = [H^T]\,[S]\,\{h\}$

5. Equation solver

   a. For static problem, solve $[\bar{S}]\{a_c\} = \{\bar{Z}\} - \{\bar{R}\}$ for $\{a_c\}$ Compute $\{a_b\}$ (equation (A5)) and then $\{a\}$ (equation (A4)). Separate $\{a\}$ into $\{a_k\}$. K=1, 2, . . . N, for each individual element.
   b. For dynamic problem, solve $[\bar{S}]\ \{a_c\}\ +\ [\bar{M}]\ \{\ddot{a}_c\}\ =\ 0$

6. Output data processing

   a. Compute results for each element directly from the approximating polynomials whose coefficiencs are determined in step 5.
   b. Users define the element ID and desired locations of output recovery; some default values may be provided.

NASTRAN Implementation

In executing these operations, step 1 requires some modification of NASTRAN procedures. In particular, the element compatibility data needed in constructing the constraint matrix [P] in step 2, and the options for specifying uniform line support conditions must be revised. Steps 2 through 4 are new except that the current multiple-point constraints and enforced displacement in NASTRAN can be included in steps 2d and 2e. The current equation solvers in NASTRAN may be used in step 5. New NASTRAN functional modules are also required for output data recovery in step 6, since the results are obtained directly from the approximating polynomials.

It should be noted that finite elements generated by the constraint method can be combined with existing elements in NASTRAN if it is so desired. In this case, the unknown variables consist of both coefficients in the assumed polynomials and nodal variable components. The elements can be connected together by the constraint equations.

CONCLUDING REMARKS

The constraint method is an efficient and cost effective approach to finite element approximations. It reduces modeling time significantly because fewer elements are needed. The structural model thus may be generated faster and with fewer errors. The accuracy and computational efficiency are not sensitive to input numbering schemes, and remodeling is not required for greater accuracy. Results presented herein and those obtained in other test cases (Refs. 7 to 10) indicate that highly accurate results can be obtained by the constraint method at reduced computer costs. It is desirable, however, to solve some larger problems to provide better comparisons between this approach and the current approaches to finite element structural analysis.

Efficiency of this approach may be further improved by the development of efficient algorithms for obtaining $[B^{-1}]$. Such an effort is currently underway at Washington University in St. Louis.

Implementation of the constraint method into the existing general purpose computer program such as NASTRAN is considered feasible and worthy of further investigation.

APPENDIX A

A SOLUTION ALGORITHM FOR THE CONSTRAINT METHOD

The problem is to minimize the total potential energy (equation (A1)) subject to a set of constraints (equation (A2)):

$$\text{Min.} \quad \pi = \frac{1}{2} \lfloor a \rfloor [S] \{a\} - \lfloor Z \rfloor \{a\} \tag{A1}$$

$$\text{Subject to:} \qquad [P] \{a\} = \{R\} \tag{A2}$$

We begin by selecting m linearly independent columns from [P] and renaming them [B]. Then equation (A2) can be written as

$$[B] \{a_b\} + [C] \{a_c\} = \{R\} \tag{A3}$$

where vector $\{a_b\}$ contains the variables associated with the linearly independent columns in [B], and $\{a_c\}$ contains the remaining variables in $\{a\}$. Vector $\{a\}$ is related to $\{a_b\}$ and $\{a_c\}$ by the following equation

$$\{a\} = [T] \begin{Bmatrix} a_b \\ a_c \end{Bmatrix} \tag{A4}$$

in which [T] is the appropriate permutation matrix.

From equation (A3), we can write

$$\{a_b\} = [B^{-1}] \{R\} - [B^{-1}] [C] \{a_c\} \tag{A5}$$

Substituting equation (A5) into equation (A4), vector $\{a\}$ can be expressed in terms of $\{a_c\}$ as

$$\{a\} = [H] \{a_c\} + \{h\} \tag{A6}$$

where

$$[H] = [T] \begin{bmatrix} -[B^{-1}] [C] \\ [I] \end{bmatrix} \tag{A7}$$

$$\{h\} = [T] \begin{Bmatrix} [B^{-1}] \{R\} \\ \{0\} \end{Bmatrix} \tag{A8}$$

Substituting equation (A6) into equation (A1), the total potential energy π can be written as

$$\pi = \frac{1}{2} \lfloor a_c \rfloor [H^T] [S] [H] \{a_c\} +$$

$$\lfloor a_c \rfloor [H^T] [S] \{h\} + \frac{1}{2} \lfloor h \rfloor [S] \{h\}$$

$$- \lfloor a_c \rfloor [H^T] \{Z\} - \lfloor h \rfloor \{Z\} \qquad \text{(A9)}$$

Minimizing π with respect to the elements of $\{a_c\}$, we have

$$[H^T] [S] [H] \{a_c\} + [H^T] \Big([S] \{h\} - \{Z\} \Big) = 0 \qquad \text{(A10)}$$

Equation (A10) represents a set of simultaneous algebraic equations. It is noted that the original n variables in $\{a\}$ were reduced to n-m, where m is the rank of the constraint matrix [P]. When the boundary displacements vanish, $\{R\}$ is null. Equation (A10) then becomes

$$[H^T] [S] [H] \{a_c\} - [H^T] \{Z\} = 0 \qquad \text{(A11)}$$

Once $\{a_c\}$ is solved, $\{a_b\}$ can be obtained from equation (A5).

REFERENCES

1. Tong, P.; and Pian, T. H. H.: The Convergence of Finite Element Method in Solving Linear Elastic Problems. International Journal of Solids and Structures, Vol. 3, 1967, pp. 865-879.

2. Fraeijs de Veubeke, B.; Sander, G.; and Bechers, P.: Dual Analysis by Finite Elements: Linear and Nonlinear Applications. USAF Report AFFDL-7R-72-93, December 1972.

3. Raney, J. P.; Weidman, D. J.; and Adelman, H. M.: NASTRAN: Status, Maintenance, and Future Development of New Capability. NASA TM X-2378, Sept. 1971.

4. Raney, J. P.; and Weidman, D. J.: NASTRAN: A Progress Report. NASA TM X-2637, Sept. 1972.

5. Fried, Isaac: Discretization and Round-off Error in the Finite Element Analysis of Elliptic Boundary Value Problems. Doctoral Dissertation, Department of Aeronautics and Astronautics, MIT, June 1971.

6. Cowper, G. R.; Kosko, E.; Lindberg, G. M.; and Olson, M. D.: Static and Dynamic Applications of a High-Precision Triangular Plate Bending Element. AIAA Journal, Vol. 7, No. 10, Oct. 1969.

7. Tsai, Chung-Ta: Analysis of Plate Bending by the Quadratic Programming Approach. D. Sc. Dissertation, Washington University, St. Louis, Dec. 1971.

8. Szabo, B. A.; and Tsai, Chung-Ta: The Quadratic Programming Approach to the Finite Element Method. International Journal for Numerical Methods in Engineering, Vol. 5, No. 3, Jan.-Feb. 1973, pp. 375-381.

9. Chen, K. C.: High Precision Finite Elements for Plane Elastic Problems. D. Sc. Dissertation, Washington University, St. Louis, May 1972.

10. Gould, P. L.; Szabo, B. A.; and Suryoutomo, H. B.: Curved Rotational Shell Elements by the Constraint Method. Proceeding of the International Conference on Variational Methods in Engineering, Southampton University, England, Sept. 1972.

11. Timoshenko, S.; and Woinowsky-Krieger, S.: Theory of Plates and Shells. 2nd Edition, McGraw-Hill, 1959.

12. Gustafson, P. N.; Stokey, W. F.; and Zorowski, C. F.: An Experimental Study of Natural Vibrations of Cantilevered Triangular Plates. Journal of the Aeronautical Sciences, Vol. 20, 1953, pp. 331-337.

13. NASTRAN Demonstration Problem Manual. NASA SP-224, Oct. 1969.

TABLE 1   SOLUTION FOR S.S. EQUILATERAL TRIANGULAR PLATE

METHOD	NO. OF ELEMENTS	DEGREES OF FREEDOM	DISPLACEMENT AT CENTROID	BENDING MOMENT AT CENTROID
CONSTRAINT METHOD (EXACT)	1	6	1.02880	2.40740
COWPER	1	3	.617284	1.08333
	36	108	1.02881	2.40792
NASTRAN	25	46	.92	1.78
	100	166	.99	2.19

TABLE 2   NATURAL FREQUENCY OF CANTILEVERED TRIANGULAR PLATE (STEEL, T = .061")

	CONSTRAINT METHOD						COWPER (REF. 6)		
FINITE ELEMENT LAYOUTS	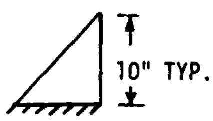			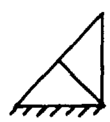			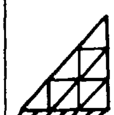	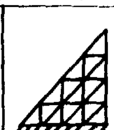	EXPERIMENT (REF. 12)
ORDER OF APPROX.	4TH	5TH	6TH	4TH	5TH	6TH	5TH		
D O F	6	10	15	12	20	30	36	60	
MODE NO.									
1	36.8757	36.6528	36.6024	36.5538	36.5331	36.5158	36.6419	36.6201	34.5
2	156.983	144.025	139.187	141.0743	139.3590	138.9769	139.3265	139.2633	136
3	219.501	197.770	194.499	203.3356	194.0896	193.5854	194.1408	194.0186	190

TABLE 3 NATURAL FREQUENCY OF THE SIMPLY-SUPPORTED SQUARE PLATE

	CONSTRAINT METHOD			NASTRAN	EXACT
ORDER OF APPROXIMATION	4TH	5TH	6TH	3RD	
D O F	6	12	20	590	
MODE NO.					
1	.9298	.9081	.9069	.9056	.9069
2	2.6972	2.3962	2.2782	2.2634	2.2672
3	5.1170	4.6325	4.5474	4.5329	4.5345

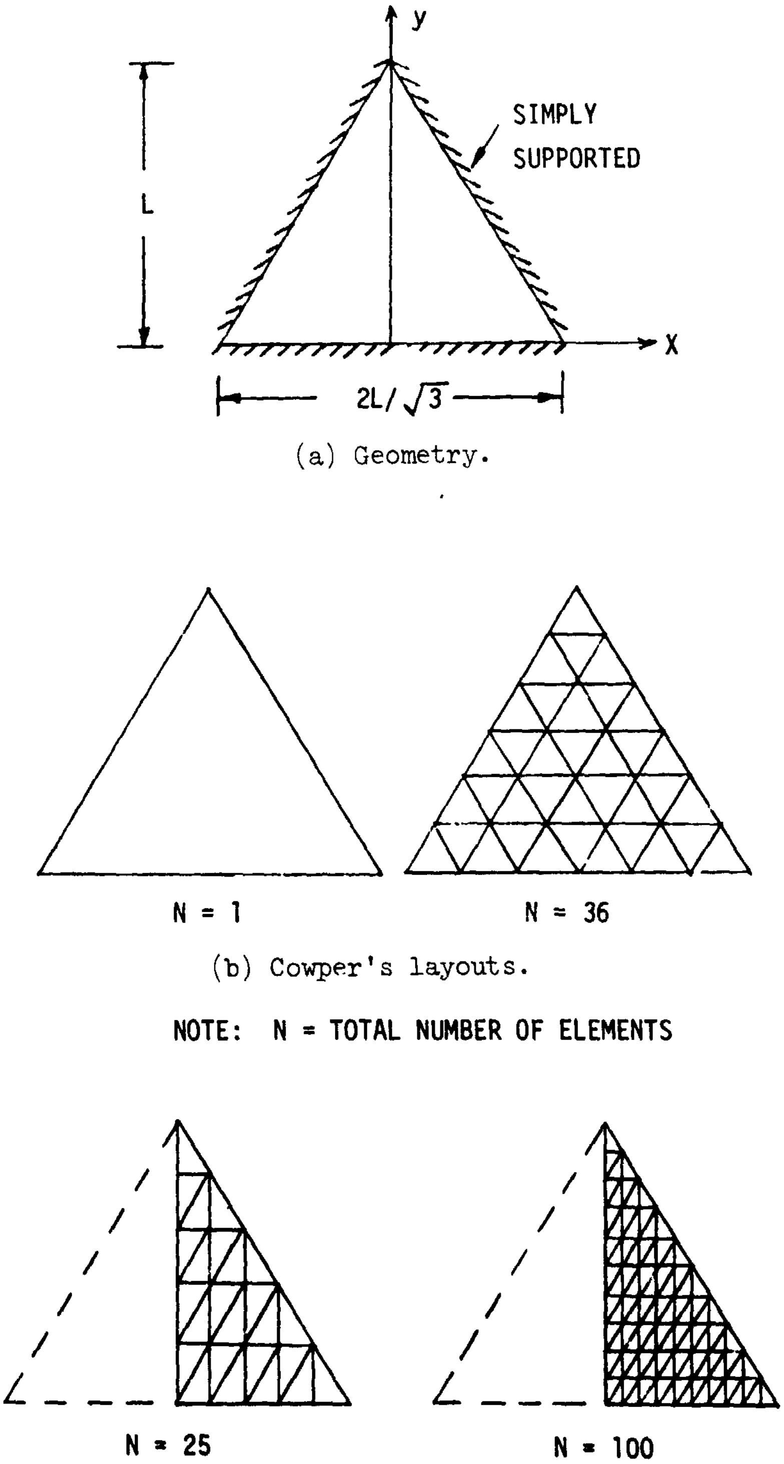

(a) Geometry.

(b) Cowper's layouts.

(c) NASTRAN layouts (1/2 plate).

Figure 1.- Simply-supported equilateral triangular plate.

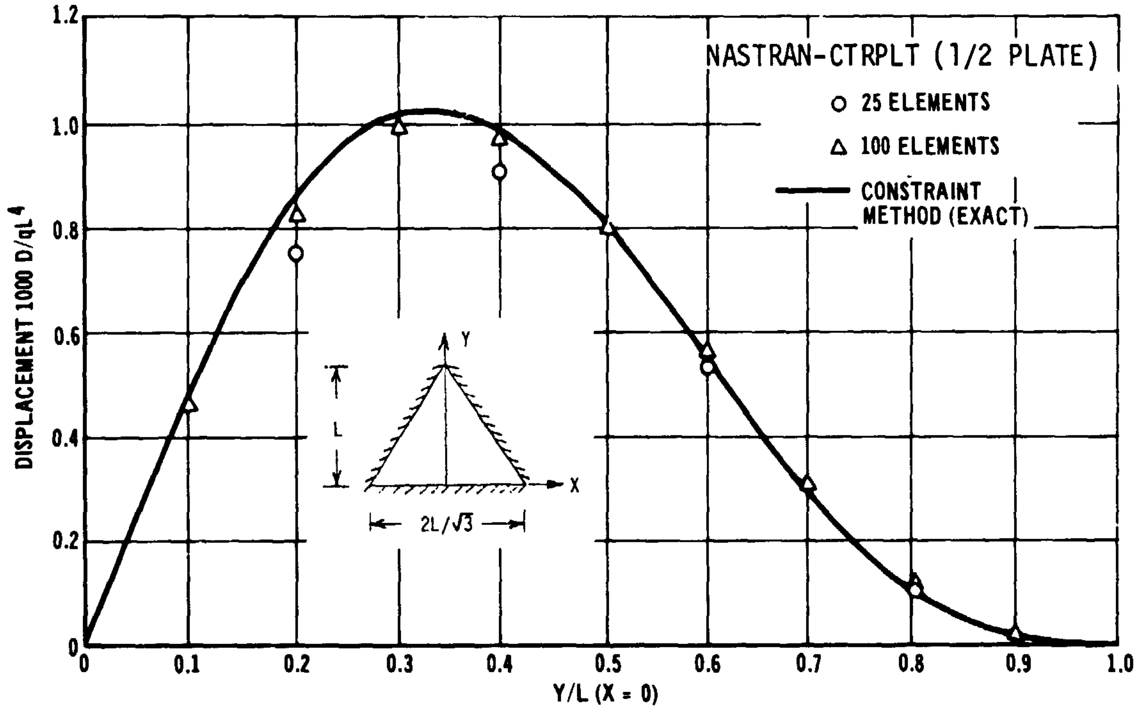

Figure ?.- Displacement along centerline of the equilateral triangular plate.

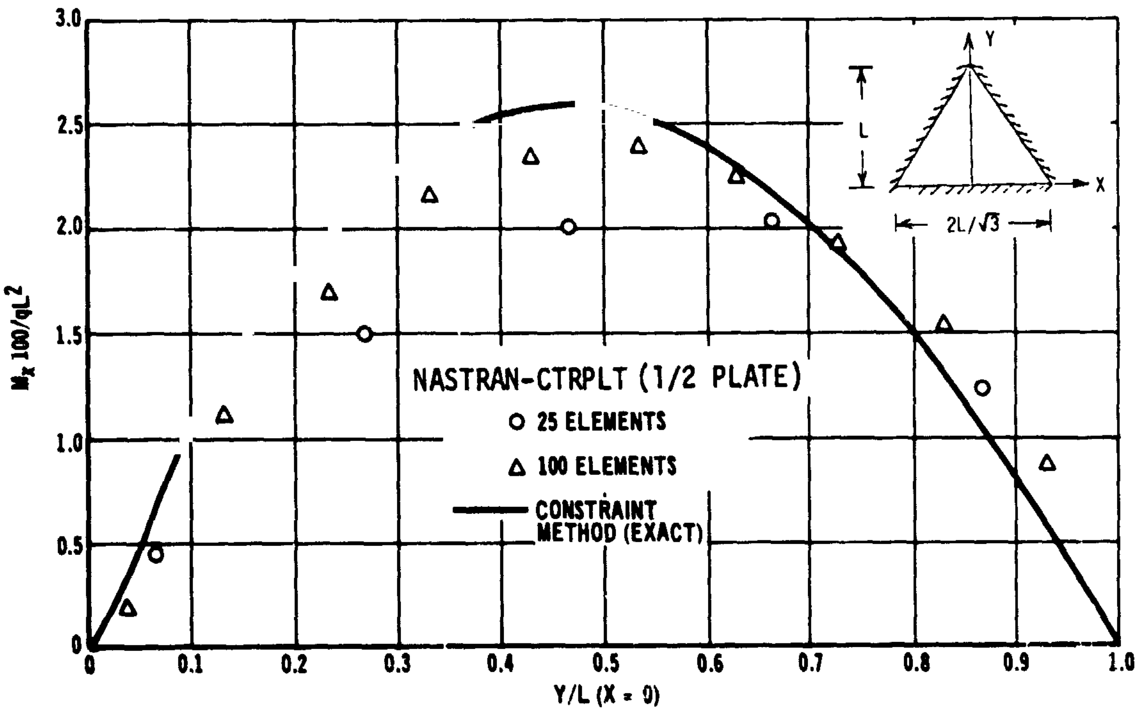

Figure 3.- Moment along centerline of the equilateral triangular plate.

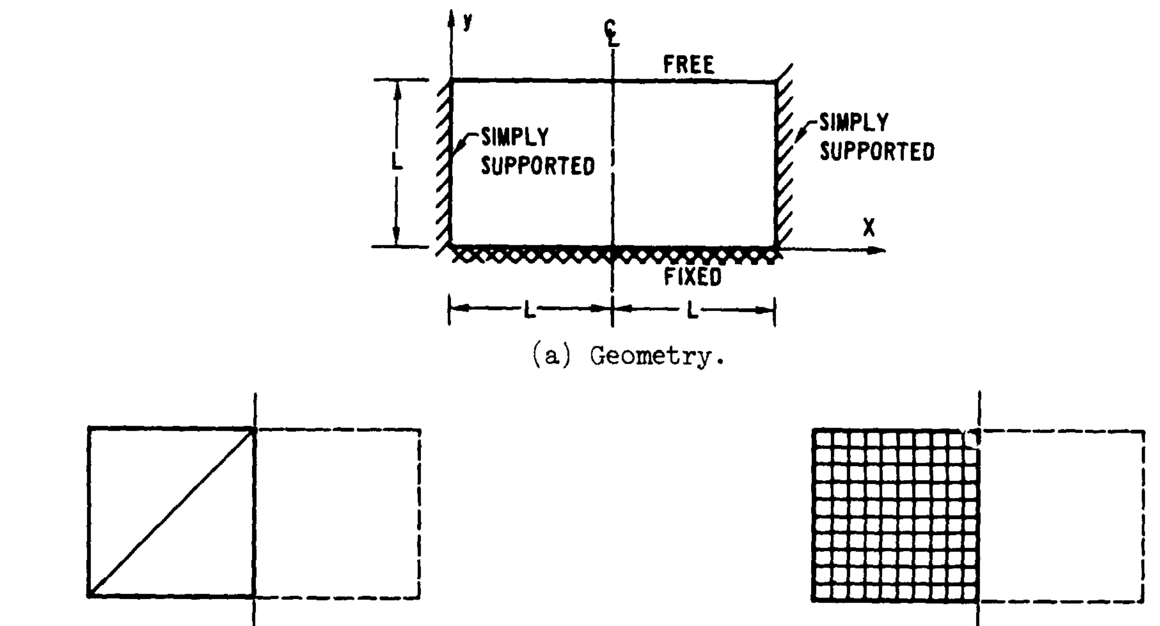

(a) Geometry.

(b) Finite element layout for the constraint method.

(c) Finite element layout for NASTRAN.

Figure 4.- The rectangular plate problem.

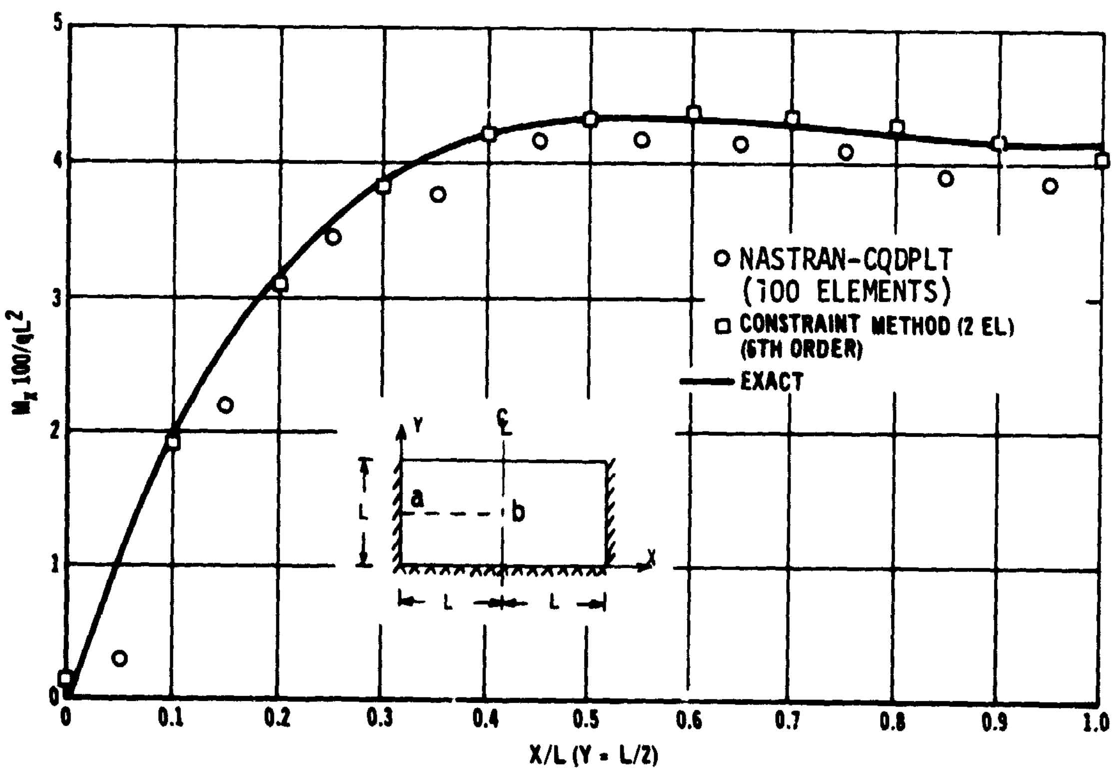

Figure 5.- M_X along line ab of the rectangular plate.

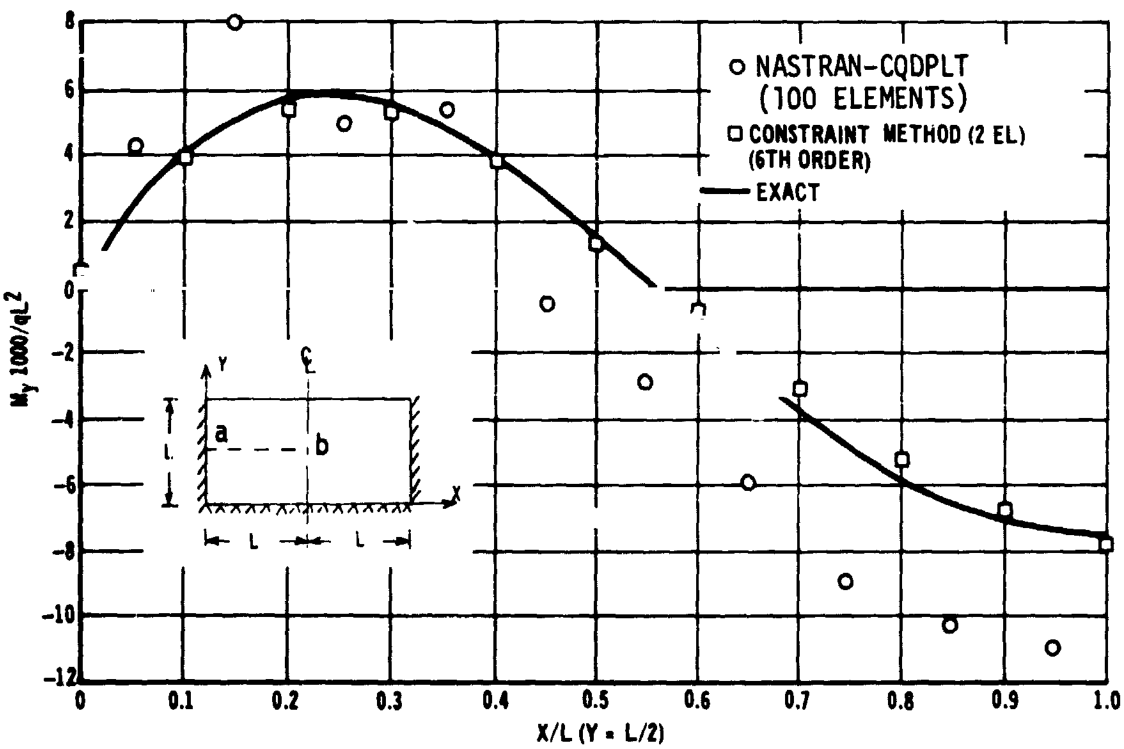

Figure 6.- M_y along line ab of the rectangular plate.

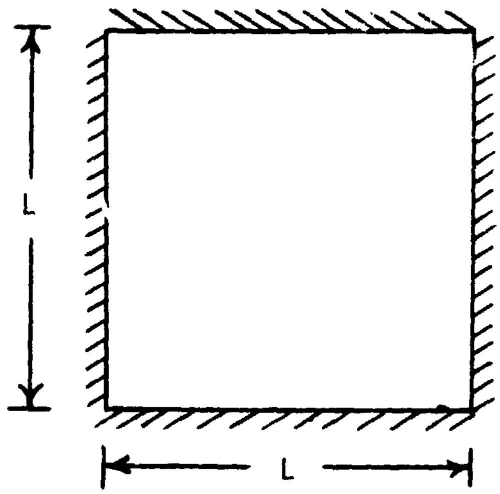

(a) Simply-supported square plate.

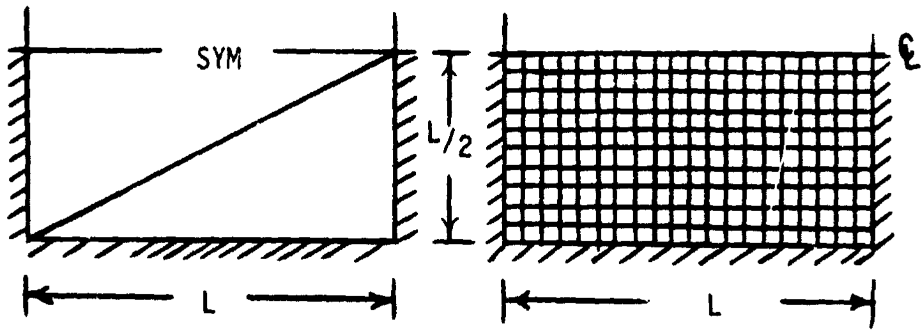

(b) Constraint method (2 elements). (c) NASTRAN (200 elements).

Figure 7.- Simply-supported square plate problem.

N74-14612

NASTRAN DISTRIBUTION THROUGH COSMIC

By Margaret K. Park

COSMIC, University of Georgia

The NASTRAN program package is one of the most important in terms of size and use in the COSMIC inventory at the University of Georgia. In this presentation, a brief history of the COSMIC facility as it relates to the NASTRAN program package will be presented, followed by a discussion of the NASTRAN disseminations.

COSMIC, which is the acronym for the COmputer Software Management and Information Center, is operated by the University of Georgia's Computer Center under contract to NASA. It was established in 1966 out of the Marshall Space Flight Center's Technology Utilization Office and operated under their sponsorship until the contract was moved to the Headquarters Office in July 1968. The purpose of COSMIC is to make available to the public the computer software and documentation developed as part of the NASA program. It is, perhaps, best described as a clearinghouse for the NASA-sponsored computer software, although the functions specified under the contract go much further than simply duplicating the programs and documentation for distribution. A sizeable portion of the workscope involves screening the programs to insure that they are free of syntax errors, that all necessary subroutines are present, and that the documentation includes sufficiently detailed instructions to allow purchasers "skilled in the art" to install and operate the program or system. Computer software is contributed from 14 major NASA facilities and their contractors, and COSMIC is currently handling an inventory of approximately 1200 computer programs and corresponding documentation for some 30 different computers.

NASTRAN is one of the largest, if not the largest, software systems distributed by COSMIC, and it is almost certainly the most widely used system. Three major releases — levels 8, 12, and 15.1 — have been distributed, and, as is apparent from Table 1, the number of distributed copies of levels 12 and 15.1 has significantly increased over the number of level 8 disseminations. The documentation counts represent the number of individual manuals and are estimates for levels 8 and 12. Various options were available for these two releases, with manuals included in some of the package options, and individual counts for manuals were not maintained. The Special Problem Reports (SPR's) are also distributed by COSMIC as they are made available from the NASTRAN office. During the past year, there were 5 SPR's distributed for a total of 106 copies (not included in Table 1).

TABLE 1. DISTRIBUTION OF NASTRAN RELEASES

	Programs	Documents
Level 8	21	500
Level 12	78	4900
Level 15.1	79	4400

As you are no doubt aware, levels 12 and 15.1 were available in four options, one each for the UNIVAC 1108 and CDC 6000 series equipment and two versions for the IBM 360/370 series equipment. The distribution of program copies by version is shown in Table 2.

TABLE 2. DISTRIBUTION OF PROGRAM COPIES BY VERSION

	Level 12	Level 15.1
UNIVAC 1108	17	16
CDC 6000 series	13	20
IBM 360/370 series	48	43

A cursory survey of NASTRAN purchasers reveals that COSMIC has distributed to practically every major type of industry in the country; to private business; to government agencies and defense bases; and to educational institutions. As a clearinghouse or distribution facility, the COSMIC files contain little more than the name of the purchasing officer at these organizations. The Computer Sciences Corporation study, which was completed in 1972 and was based primarily on the data for levels 8 and 12, does provide some information on the uses which are being ma e of NASTRAN and the advantages which have been realized. The results of this study have been published in references 1 and 2.

There is little question but that NASTRAN has provided an excellent showcase for NASA's Technology Utilization program, and the COSMIC staff is pleased to have had a small part in making it available as part of NASA's mission to transfer space technology to the public.

REFERENCES

1. Anon.: NASTRAN Benefits Analysis. Vol. I - Executive Summary. Contract No. NAS5-11724, Computer Sciences Corp., Feb. 15, 1972. (Available as NASA CR-125882.)

2. Anon.: NASTRAN Benefits Analysis. Vol. II - Final Technical Report. Contract No. NAS5-11724, Computer Sciences Corp., Feb. 15, 1972. (Available as NASA CR-125883.)

N74-14613

THE APPLICATION OF NASTRAN AT SPERRY UNIVAC HOLLAND

By G. Koopmans
Sperry UNIVAC Application/Research Department

SUMMARY

Very divergent problems arising with different calculations indicate that NASTRAN is not always accessible for common use. Problems with engineering, modelling, and use of the program system are analysed and a way of solution is outlined. Related to this, some supplementary modifications are made at Sperry UNIVAC Holland to facilitate the program for the less skilled user. The implementation of a new element also gives an insight into the use of NASTRAN at Sperry UNIVAC Holland.

INTRODUCTION

As the users of UNIVAC computers are from very different kinds of industries like shipbuilders, petrochemical industries, and building industries, the variety of problems coming from these users is very large. This variety results in experience not with one special kind of calculation nor one special kind of construction, but with a wide area of problems arising in the use of NASTRAN. These problems can roughly be divided into three different groups:

(1) Recognition of what is to be calculated and how

(2) Construction of a model

(3) Handling the NASTRAN program

These are the basic problems for every less skilled user of NASTRAN and the Application/Research Department of Sperry UNIVAC has to give reasonable answers to these questions. The correctness and accuracy of NASTRAN is hardly a question. Except for very complicated structures and calculations, the prospective user accepts NASTRAN as the best available tool, in spite of the monopoly of ASKA at the Dutch universities and the almost historical preference for ICES. The description of the following calculations illustrates the procedure of tackling different types of problems. As the details and numerical results of the calculations give no essential information, they are not shown.

RECOGNITION OF WHAT IS TO BE CALCULATED AND HOW

One of our customers had problems with a propulsion system for ships. A simplified schematic diagram is shown in figure 1. There was serious damage on the roller

PRECEDING PAGE BLANK NOT FILMED

bearings of the hollow shaft for reasons other than torsional frequencies. Obviously, something was wrong with the design of the system. Together with the customer a summary was made of all possible sources of damage. After that, a selection from among parts of the system was made to determine the loading conditions that had to be calculated. The conclusion was to make a static analysis to determine whether the connection between the hollow shaft and the gear wheel was strong enough and also to make an analysis of the natural frequencies of the shaft and gear wheel with NASTRAN. A model was made from triangular and quadrilateral ring elements and rigid formats 1 and 12 were used.

The result of these analyses was that the connection seemed barely strong enough and that the gear frequency was almost the same as the natural frequency of the shaft and wheel with four other natural frequencies in the same region. Combined, these could be the source of damage. Obviously, modelling and calculating with NASTRAN was no problem. The only way to solve the problem was to make an extensive overview of possible sources. If that were available, the rest would be no problem because almost everything could be calculated with a program like NASTRAN. So this is essentially a problem that only can be solved with engineering practice. Only a methodical approach to a problem like this can give a satisfactory result, and simple rules cannot be given for solving these problems.

CONSTRUCTION OF A MODEL

Two entirely different examples will show problems arising with modelling. For building blocks of flats, one of our customers, a building contractor, wants to know the loads on the piles, the stresses in the structure, and the possible overload the structure may absorb for a certain wall thickness. When the problem is stated this way, it seems to be a stability problem, hardly solvable because of the properties of the material, reinforced concrete. Nevertheless, the biggest problem for the building contractor is how to make a model because he has no idea about the effect of the element and element size on his results. As all his problems are topologically almost the same – only walls and floors – like figure 2, the best thing to do is to make a preprocessor for NASTRAN with a simple mesh generator resulting in a model like figure 3. This procedure was entirely sufficient for this model.

A totally different modelling problem was the stress calculation of a reactor containment vessel of a nuclear power plant. This is a kind of pressure vessel with a radius of about 90 feet and about 140 feet high (see fig. 4). One of the greatest problems was a crane girder at the top of the vessel. Because of the rotational symmetry of the vessel, the conical shell element could be used, but the bulkheads of the girder disturbed the symmetry and prevented the use of this model. Modelling with plate elements would increase computer time enormously. The solution was the use of multipoint constraints. With several hundred multipoint constraints, the bulkheads had a zero inplane stiffness. This condition gave the model a reasonable stiffness. Of course, this is not a completely new way of using these multipoint constraints, but it shows again that intelligent modelling can give accurate results, shorter computing times, and simpler models.

So if modelling is a serious problem, either a skilled user of the finite-element method, or, for simple models, some piece of software must make the model. The fact that a simple model description is important pleads for a general mesh generator, so that only a description of the contours and the element kind will produce an optimal mesh.

HANDLING THE NASTRAN PROGRAM

An underestimation of this problem is dangerous because a program will be used if it is easy to use. For a common user, a large program like NASTRAN is never easy to use. Therefore, it must be made as easy as possible; that is: little input, only a few control cards, surveyable output, and so on. This statement results in some remarkable conclusions. The way of substructuring in NASTRAN seems to be too complicated for a common user. Usually, he wants to use more core for calculating the whole model at once if possible, instead of calculating substructures and saving computer time. For this reason, enlarging the available core is desirable. This enlargement could be done by some alterations in the subroutine MAPFNS.

With the updating program (see fig. 5) the available core on the UNIVAC 1108 is increased to 117K words. Another way to make NASTRAN as easy to handle as possible is to reduce the number of control cards. This can be done by a subroutine called LINKO. (See fig. 6.) This FORTRAN program tests the run condition word and after that starts the sequence of link steps. For this purpose file 12 is available if no BCD plot file is used. The executive control language of all link steps is written on this file 12 and LINKO takes the control. Already with these few alterations NASTRAN seems to be more accessible.

If there is a problem in handling the NASTRAN system, often it can be solved by making simplifications in different fields. Of course, the simplification is only valid for relatively simple calculations using only rigid formats without DMAP sequence alterations. But most of the calculations are as simple as that.

NEW ELEMENT

The data processing division of Rijkswaterstaat, Ministry of Transport Water Control and Public Works, an engineering firm of Netherlands government, has developed three plate elements – a triangular, a rectangular, and a quadrilateral element. They have implemented them in ICES. UNIVAC has obtained these elements for implementing in NASTRAN. The stiffness matrix of these elements is derived by the method of assumed stress distribution as outlined by Pian (ref. 1). In this method the expression for the strain energy in the element requires both displacement compatibility and stress equilibrium conditions. These elements have now been tested. The results will be available for all interested people as soon as all advantages and disadvantages of these elements are known.

CONCLUDING REMARKS

Although the emphasis in using NASTRAN is mostly for complicated constructions and calculations, most of the computing time used by NASTRAN is for relatively simple problems. To simplify the use of NASTRAN, many alterations can be introduced, mainly in the field of reducing input data. Related to that, a more automatic input generation should be desirable.

REFERENCE

1. Pian, T. H. H.: Derivation of Element Stiffness Matrixes by Assumed Stress Distributions. AIAA J., vol. 2, no. 7, July 1964, pp. 1333-1336.

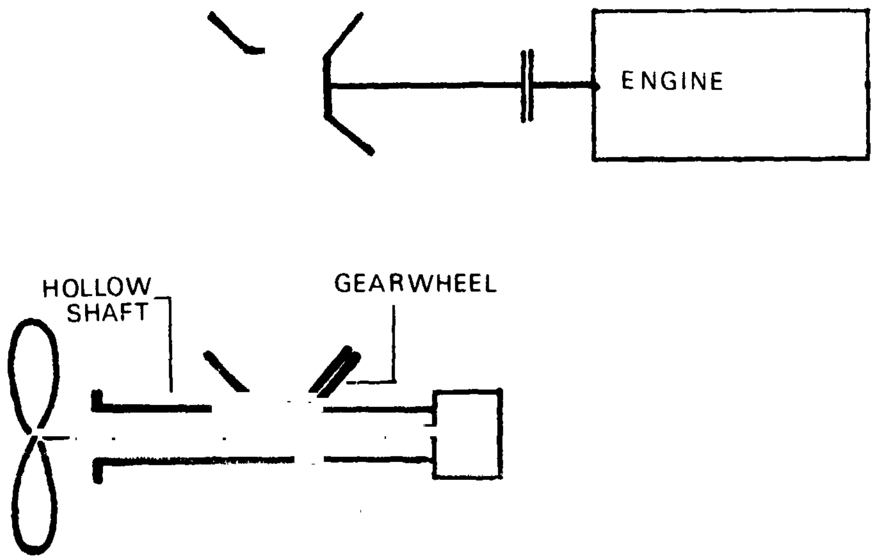

Figure 1.- Propulsion system.

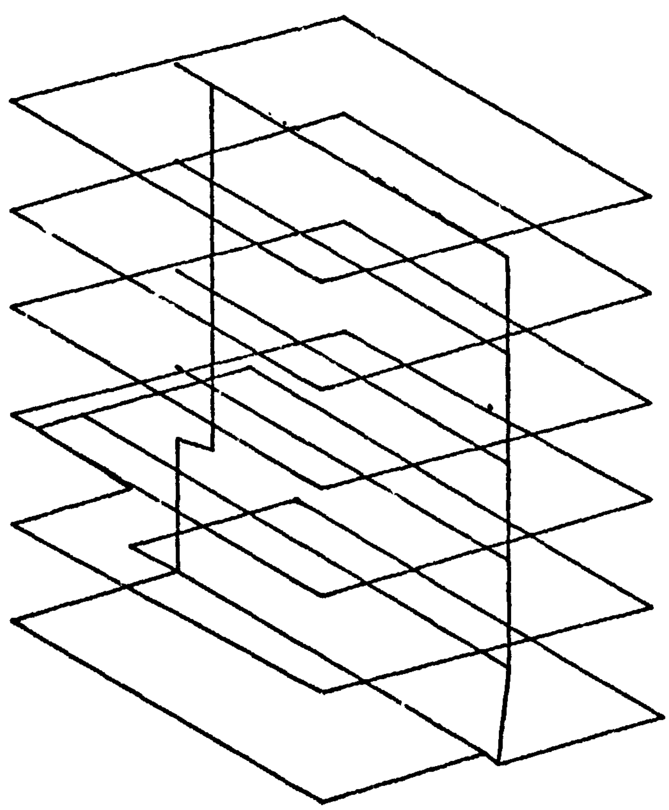

Figure 2.- Contour plot of a block of flats.

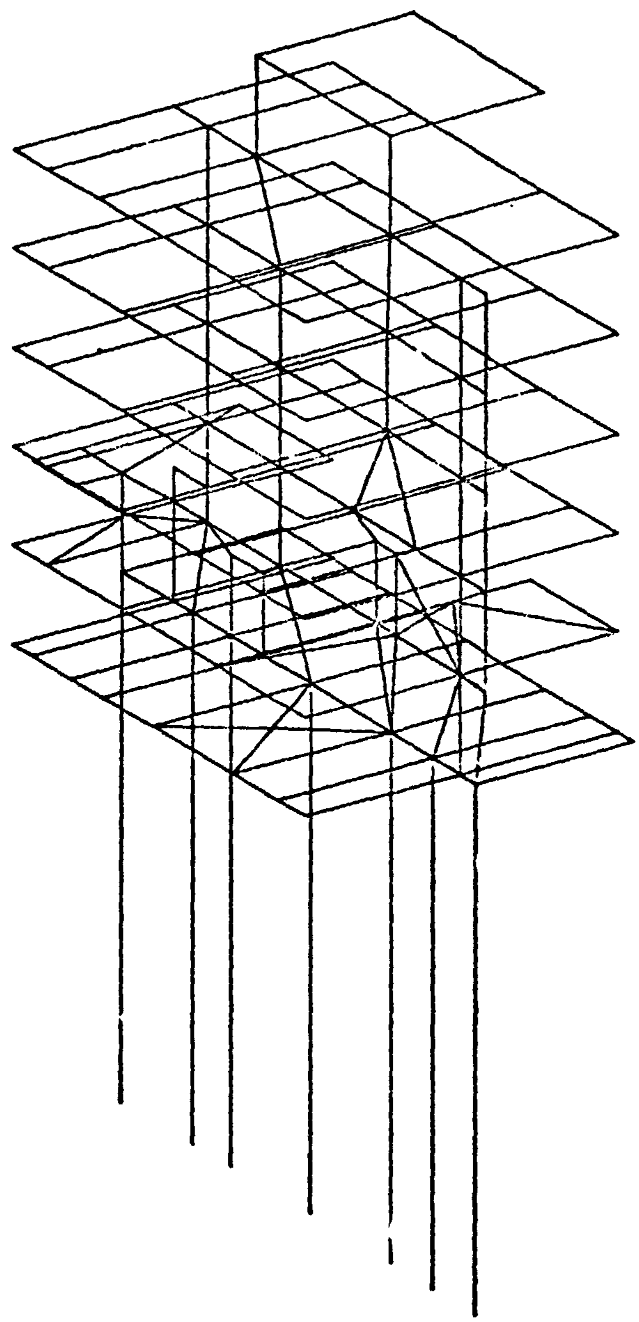

Figure 3.- Element plot.

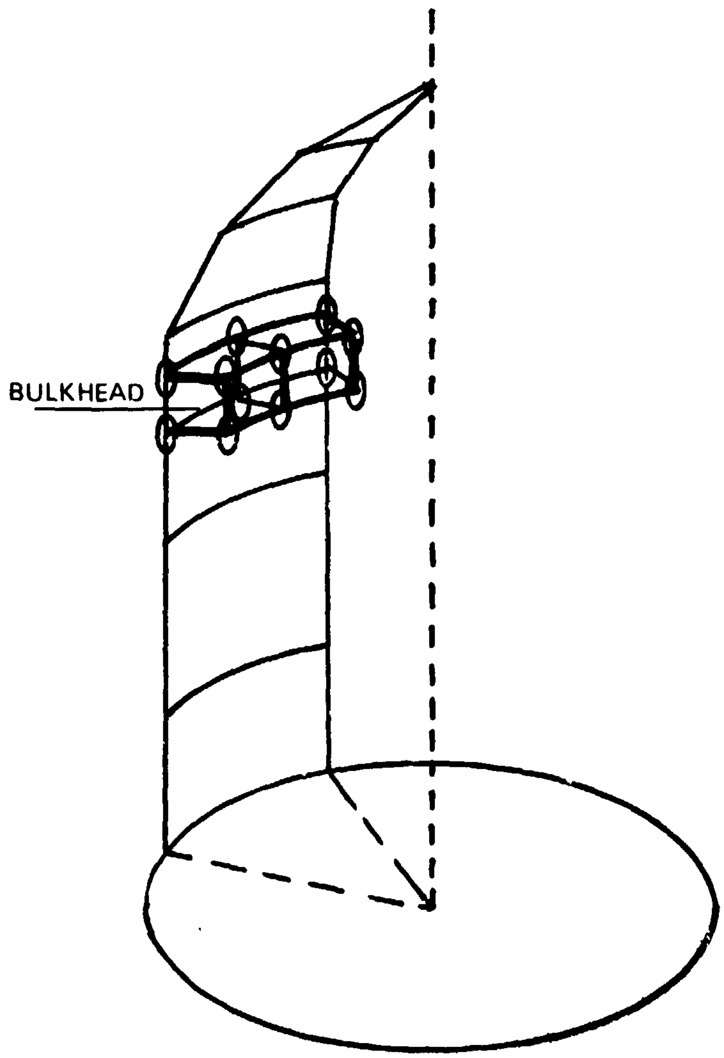

Figure 4.- Reactor containment.

```
@RUN,/TP NASTRA,NASTRAN01,UNIVAC,3,600
@ASG,T  SYM.,F2/1000//2000
@ASG,T  OBJ.,F2/500//1000
@ASG,A  NASTRAN15-S.
@ASG,A  NAS15-S.
@COPIN    NAS15-S.,SYM.
@COPIN,S  NAS15-S.,SYM.
@COPY,G  NASTRAN15-S.,OBJ.
@FREE   NASTRAN15-S.
@COPY,S  OBJ.,SYM.
@FREE   NAS15-S.
@ASG,A  NAS15-RC.
@MSG  NAS15-RC MET RING
@FOR,SU  SYM.WPLT10,OBJ.WPLT10
-46,46
      N=  IABS(N-M*TEN(I))
@ASM,SU  SYM.MAPFNS,OBJ.MAPFNS
-16,17
AND*    L        A0,0,X11
        L        A0,0,A0
        L        A1,1,X11
        L        A1,0,A1
        AND      A0,A1
-23,24
ORF*    L        A0,0,X11
        L        A0,0,A0
        L        A1,1,X11
        L        A1,0,A1
        OR       A0,A1
-30,32
XOR*    L        A0,0,X11
        L        A0,0,A0
        L        A1,1,X11
        L        A1,0,A1
        XOR        A0,A1
        S        A1,A0
-37,37
COMPL*  L        A0,0,X11
        LN       A0,0,A0
-41,44
LSHIFT* L        A0,1,X11
         L       A1,0,A0
        S,J1     A1,$+4
        L        A0,0,X11
```

Figure 5.- Updating program.

```
          L         A0,0,A0
          JZ        A1,3,X11
-49,52
RSHIFT*   L         A0,1,X11
          L         A1,0,A0
          S,J1      A1,S+4
          L         A0,0,X11
          L         A0,0,A0
          JZ        A1,3,X11
-99,99
          L,016     A1,0337770
-105,105
          L         A2,1,X11
          SN        A1,0,A2
-110,110
SETC*     L         A0,0,X11
          L         A0,0,A0
-125,125
          L         A1,0,X11
          S         A0,0,A1
-134,134
          L         A0,0,X11
          S         A1,0,A0
-138,138
FACIL*    L         A1,0,X11
          L         A1,0,A1
-148,148
OUT       L         A0,1,X11      . STORE FLAG IN IO
          S         A1,0,A0
-155,155
TSWAP*    L         A1,0,X11
          L         A1,0,A1
-164,164
          L         A1,1,X11
          L         A1,0,A1
-176,176
          L         A2,1,X11
          L         A2,0,A2
*COPOUT   SYM.,NAS15-RC.
*COPOUT   OBJ.,NAS15-RC.
```

Figure 5.- Concluded.

```
@FOR,SI   LINKO,LINKO
      DIMENSION  B(3)
      DIMENSION  C(14,4)
      DATA  (( C(I,J),I=1,14),J=1,4)
     1  42HK      LMNO   LMNP   KOO    LMNOP  KP     KPQ    ,
     2  42HKOP    KOP    KO     LMN    KOP    LMN    KOP    ,
     3  42HKLMN   KLMN   KLMN   KLMN   KLMN   KLMN   KLMN   ,
     4  42HKLMN   KLMN   KLMN   KLMN   KLMN   KLMN   KLMN   ,
     5  42HJN     JN     JN     JN     JN     JN     JN     ,
     6  42HJN     JN     JN     JN     JN     JN     JN     ,
     7  42HJMN    JMN    JMN    JMN    JMN    JMN    JMN    ,
     8  42HJMN    JMN    JMN    JMN    JMN    JMN    JMN    ,
      REWIND 12
      B(1)=6H@ADD,E
      B(2)=6H  12.
      B(3)=6H  .
      CALL EROPT(I)
      J=4
      IF(I.EQ.6HM      ) J=3
      IF(I.EQ.6HL      ) J=2
      IF(I.EQ.6HU      ) J=1
      IF(J.EQ.4) I=6HM
      CALL ERTRAN(8,M)
      M=FLD(30,6,M)
      READ(5,30,END=100,ERR=100) A
   30 FORMAT(F8.0)
  100 CONTINUE
      IF(M.LT.10) WRITE(12,10)C(M,J),M,I
      IF(M.GT.9.AND.M.LT.15) WRITE(12,20) C(M,J),M,I
      IF(M.EQ.15) STOP
      CALL ERTRAN(6,B)
      STOP
   10 FORMAT(
     2  5H@XQT,,A6,13H NASTRAN.LINK,I1,4H .   ,/,
     3  5H@XQT,,A6,25H NASCON.LINKO/NASTRAN .   )
   20 FORMAT(
     2  5H@XQT,,A6,13H NASTRAN.LINK,I2,4H .   ,/,
     3  5H@XQT,,A6,25H NASCON.LINKO/NASTRAN .   )
      END
@ASM,SI   EROPT,EROPT
          AXR$.
$(1).
EROPT*.
          SX        X11,(*REOX11*)
```

Figure 6.- LINKO subroutine.

```
          SA        A0,('REDA0 ')
          SA        A1,('REDA1 ')
          SA        A2,('REDA2 ')
          SR        R1,('REDR1 ')
          ER        OPT$
          SA        A0,('OPTIES')
          LX        X11,0,X11
          LXI,U     X11,1
          L,U       A2,037
          SZ        ('LETTER')
LUS.
          L         A1,('      ')
          L,U       R1,5
LUS1.
          AN,U      A2,1
          S,S1      A2,('LETTER')
          TNE,U     A2,4
          J         EINDLUS
NEXT.
          JNB       A0,EINDLUS1
          DSL       A0,1
          SSL       A1,5
          A         A1,('LETTER')
          JGD       R1,LUS1
          J         EINDLUS
EINDLUS1.
          SSL       A0,1
          J         LUS1
EINDLUS.
          S         A1,0,*X11
          TZ        A0
          J         LUS
          LA        A0,('REDA0 ')
          LA        A1,('REDA1 ')
          LA        A2,('REDA2 ')
          LR        R1,('REDP1 ')
          LX        X11,('REDX11')
```

Figure 6.- Concluded.

N74-14614

SOME STUDIES ON THE USE OF NASTRAN FOR NUCLEAR POWER PLANT STRUCTURAL ANALYSIS AND DESIGN

By Achyut V. Setlur and Munirathnam Valathur

Pioneer Service & Engineering Co.
Chicago, Illinois

SUMMARY

This paper presents some of the studies made on the use of NASTRAN for nuclear power plant analysis and design. These studies indicate that NASTRAN could be effectively used for static, dynamic and special purpose problems encountered in the design of such plants. Normal mode capability of NASTRAN is extended through a post-processor program to handle seismic analysis. Static and dynamic substructuring is discussed. Extension of NASTRAN to include the needs in the civil engineering industry is discussed.

INTRODUCTION

With the ever increasing size of nuclear power plants now under construction and those comtemplated in the future coupled with growing concern of the owner, engineer, regulatory bodies and the public on the quality and safety of such plants, a greater emphasis is continuously being laid on the specification of more reliable loads and material properties together with more sophisticated tools and procedures for analysis and design. Anticipating this trend, Pioneer Service & Engineering Co. initiated a study of the currently available computer programs in the area of statics, dynamics and stability of structures including capabilities for handling physical and geometric nonlinearities. It was quickly realized that no single computer program would be uniformly effective for such a broad spectrum of requirements. However, it was also found that NASTRAN was the best candidate to handle a major portion of the requirements. It is not the intent of this paper to enumerate the capabilities of NASTRAN. Only those features which were found particularly useful are mentioned in the sequel.

A typical pressurized water nuclear power plant structure consists of several buildings which may be connected to one another at the foundation level and/or at several higher elevations. The reactor shield building is typically a reinforced or pre-stressed concrete cylindrical shell with a spherical or elliptical cap. The adjoining buildings and the internals of the reactor building have shear walls as their lateral load carrying elements. Thus, the entire structural system consists of a complex of shear

PRECEDING PAGE BLANK NOT FILMED

walls, slabs, pre-stressed shells, and steel or concrete columns and roof structure as seen in Figures 1 and 2. This system has to be analysed for several load conditions and their pre-assigned combinations. These load conditions are static (e.g. dead and live loads) or dynamic (e.g. base excitation due to earthquake ground motion) in nature. Hence, a program which uses the data base and matrices generated for the static problem to perform a dynamic analysis would be most suited for such combinations. This capability is found in NASTRAN and is an important advantage over other programs.

Features in NASTRAN, Level 15.1, which would be required for the efficient processing of static and dynamic problems were checked out using simple models. Some of the experiences are discussed below. Since NASTRAN does not support modal spectral analysis for base excitation and does not combine static and dynamic results, post-processors were developed for these specific tasks and are briefly presented. Finally, some suggestions for incorporating new features in NASTRAN which would be effective in civil engineering structural analysis are noted.

SUBSTRUCTURING

Anticipating that the structural model of the entire power plant for static and dynamic analyses would result in a large number of degrees of freedom, and also noting that the structures within the total system have well defined boundaries, it was found that the substructuring technique would be a logical and effective approach. To make efficient use of the features available in NASTRAN, the intermediate results obtained from static substructuring should be used for the dynamic analysis or vice versa. The schematic diagram shown in Figure 3 uses the above feature. Post-processing phases are also shown in the figure. All interfacing between the post-processors and NASTRAN is accomplished through NASTRAN generated data blocks placed on tape or disks using OUTPUT2 module.

The scheme shown in Figure 3 was tested using the simple plate problem given in the Demonstration Manual (Reference 1). The 5 x 10 element half-plate model is shown in Figure 4. Symmetric boundary conditions were assumed along the line of symmetry. Inplane deflections and normal rotations are constrained. The half-plate model is arbitrarily separated into two substructures, referred to as SUB 1 and SUB 2. Two load cases for the static problem and the simply supported boundary conditions were specified in Phase I. The static problem was run first with the symmetric boundary conditions specified in Phase II. This was done so that, if results for antisymmetric conditions were necessary at a later stage, they could have been obtained without going through Phase I again. Slight changes to the ALTER package for substructuring as given in the User's Manual (Reference 2) were made so that the OUTPUT1 data blocks of the two substructures could be placed on the same tape. The results of the static analysis were printed and placed on tape using the OUTPUT2 module. The dynamic analysis was carried out utilizing the stiffness matrix generated in Phase I of the static analysis. The mass matrix was not generated in the static part since no GRAV loads were applied, hence, Phase I of the dynamic analysis using the stiffness matrix KAA of the static part and using a restart with a rigid format switch was executed. In this phase only the mass matrix was computed. If a GRAV load was introduced in the static analysis, the MAA matrix would have been generated and stored. Then, it would not have been necessary to run the Phase I of the dynamic analysis. Modes and frequencies of vibration of the example problem agreed very well with those given in the Demonstration Manual.

Phase III of the dynamic analysis was successfully completed using check pointed tape of Phase I static analysis and with a switch in rigid format. However, it was found that attempting Phase III of the dynamic analysis using the check pointed tape of Phase I of the dynamic analysis, which, in turn, was generated from the check pointed tape of Phase I of the static problem, resulted in a fatal error. In other words, multiple restarts were unsuccessful.

SEISMIC ANALYSIS

The seismic analysis of a structure can be approached in two different ways, (a) by the modal analysis using the ground response spectra and combining the individual modal responses in a predetermined procedure (e.g. square-root-of-sum-of-the-squares); and (b) by modal or direct integration of the equations of motion using a given time-history of ground acceleration. These approaches and their pros and cons are discussed in any standard book on earthquake engineering (e.g. Reference 3) and hence, will not be detailed here. In practice, the first approach is more commonly used because of its simplicity and the ease of defining the inputs. Hence, this approach will be discussed in what follows.

The dynamic models of the total structural system used by other investigators (References 4 and 5) are shown in Figure 5. The first of these two models involves the assumption that the individual buildings and their internals can be lumped to form a set of cantilever "flagpoles". The complex arrangement of the buildings together with their low profile makes this assumption a gross one. The second model assumes that the shear walls can be represented as horizontal springs and the floor as a rigid diaphragm. This would have been a valid assumption for a tall building but is not entirely applicable for nuclear plant structures.

Our approach is to model the vertical shear wall elements and the horizontal slabs using membrane and plate elements of NASTRAN. This would result in a structural model with a large number of degrees of freedom. It is, however, not essential nor economical to retain all of these degrees of freedom in the dynamic analysis. Hence, substructuring and Guyan reduction are necessary. The pertinent equations for seismic analysis of the structure using the modal approach are given below.

$$I_H \ddot{U}_H + B_{HH} \dot{U}_H + K_{HH} U_H = -\phi_A^T M_{AA} \; J \; a_g \tag{1}$$

where M, B, K, and I are the mass, damping, stiffness, and identity matrices, subscripts H and A refer to the modal displacement and analysis sets respectively in Phase II of the substructuring procedure, ϕ is the mass normalized eigenmatrix, J is an A x 3 matrix of ones and zeroes which selects the masses which excite the motion in the given directions, and a_g is a component vector of the ground acceleration time-history. It is noted that the matrices on the left hand side are all assumed to be of the diagonal form representing uncoupled modal equations.

The matrix product

$$\phi_A^T M_{AA} J$$

represents the participation factors, PF, of each mode for each of the three components of ground motion. These quantities are computed in NASTRAN through the following ALTER package for Rigid Format 3.

```
ALTER  93
MPYAD MAA, PHIA, /X/C, N, O/C,N, 1/C, N, O/C, N, 1 $
MPYAD J, X, /PF/C, N, 1/C, N, 1/C, N, O/ C, N, 1 $
MATPRN PF , , , ,  / / $
ENDALTER
```

The matrix J is supplied to NASTRAN through DMI bulk data cards. Since the J matrix depends on the a-set of Phase II, care should be exercised to keep track of the degrees of freedom which are present and the order of their occurrence in the a-set.

In Phase III of the substructuring procedure, the results of the modal analysis for each substructure are printed out as well as made available on tape or disk through the OUTPUT2 feature. The DMAP alter package for Rigid format 3 is given below

```
ALTER   107
OUTPUT2   OPHIG, OQG1, OEF1, OES1, //C, N, -1/C, N, 11 $
OUTPUT2   , , , , / / C, N, -9/C, N, 11 $
ENDALTER
```

The modal results of each substructure are post-processed using the above output values, the acceleration response spectra and the participation factors to obtain the individual modal contributions of the processed quantity. For the i-th mode, the modal contribution for the displacement at a point j for the component of ground motion along X- direction is given by

$$d_j^i\ (X) = \frac{S_a^i}{\omega_i^2}\ PF^i\ (X)\ .\ \phi_j^i \qquad (2)$$

where S_a^i is the spectral response acceleration for i-th frequency. The response acceleration spectra are derived from the acceleration time-history, a_g.

The total displacement at the point j for X- direction ground motion is approximated as

$$d_j\ (X) = [\Sigma_{i=1}^N\ (d_j^i\ (X)\ )^2\ ]^{\frac{1}{2}} \qquad (3)$$

Finally, the total displacement at the point j for the three component earthquake motion is obtained as

$$d_j = [\ (d_j\ (X)\ )^2 + (d_j\ (Y)\ )^2 + (d_j\ (Z)\ )^2\ ]^{\frac{1}{2}} \qquad (4)$$

Similar expressions are used for combining forces, stresses etc. The final results are again placed on a tape or disk in a format similar to that of NASTRAN. This makes it convenient to combine the results of static and dynamic analyses.

SUGGESTED ADDITIONS TO NASTRAN FOR CIVIL ENGINEERING NEEDS

a. The single most useful addition to NASTRAN would be the ability to specify loads within the span of BAR elements and the cabability of obtaining output at intermediate cross sections within the BAR element.

b. Capability of specifying different acceleration magnitudes at different mass point for the same load case in the static rigid format rather than a single acceleration value presently available. This feature would, then, be useful in approximating the seismic analysis as a quasi-static analysis for structures where such approximation is permissible.

c. Capability of specifying non-linear relationship between stress resultants and corresponding deformations (e.g. moment-curvature relation) for use in conjunction with the BAR elements. This would allow elasto-plastic analysis of three-dimensional frames.

d. For CQUAD2 and CTRIA2 elements, at present, only bending stress resultants (forces) are printed. The output should also include membrane forces.

CONCLUDING REMARKS

Some studies have been conducted on the use of NASTRAN for nuclear power plant analysis and design. These studies indicate that NASTRAN could be effectively used for such problems. DMAP alter packages and post-processors have been written to extend NASTRAN's capability to seismic base excitation problems. Static and dynamic analysis using substructures have been attempted with switch in rigid format restarts. Post-processors for combining static and dynamic (seismic) solution have been written for use in design sub-routines. Finally, some additions to NASTRAN are suggested which when implemented would make the program more effective in solving civil engineering structural analysis problems.

REFERENCES

1. The NASTRAN Demonstration Manual, NASA SP 224, September 1970.

2. McCormick, C. W., ed.: The NASTRAN User's Manual (Level 15), NASA SP 222 (01), June 1972.

3. Weigel, Robert L., ed. : Earthquake Engineering. Prentice-Hall, Inc. 1970.

4. Blume, John A., Sharpe, Roland L., and Kost, Garrison: Earthquake Engineering for Nuclear Reactor Facilities. Report No. JAB-101, John A. Blume & Associates, January 1971.

5. Bergstrom, Richard N., Chu, Shih-Lung, and Small, Robert J.: Seismic Analysis of Nuclear Power Plant Structures. Journal of the Power Division, A. S. C. E., Vol. 97. No. PO2, March, 1971.

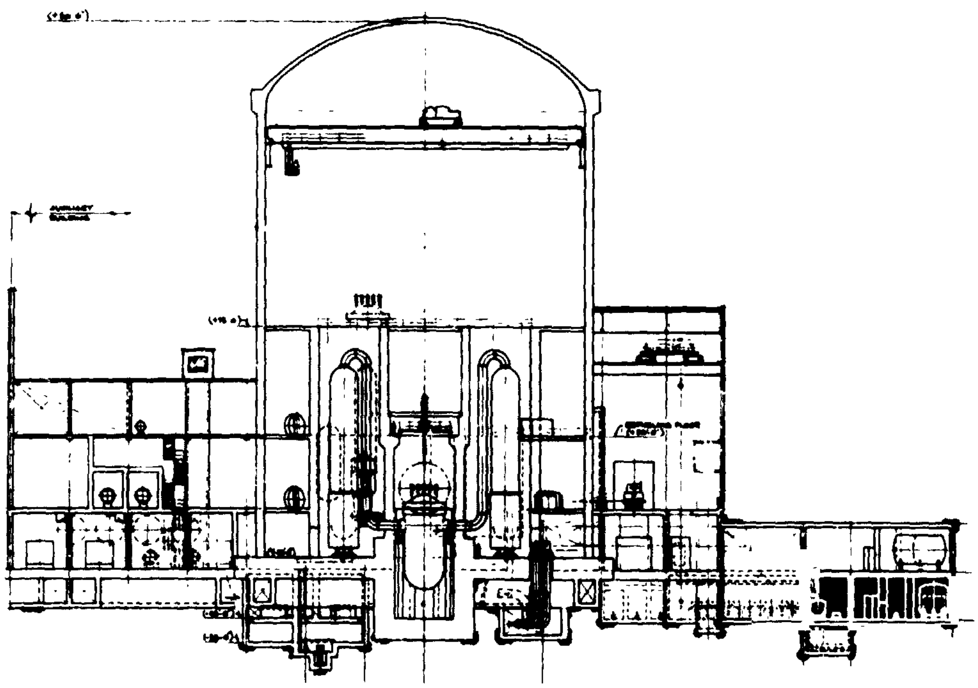

Figure 1.- Section of typical pressurized water nuclear power plant structure.

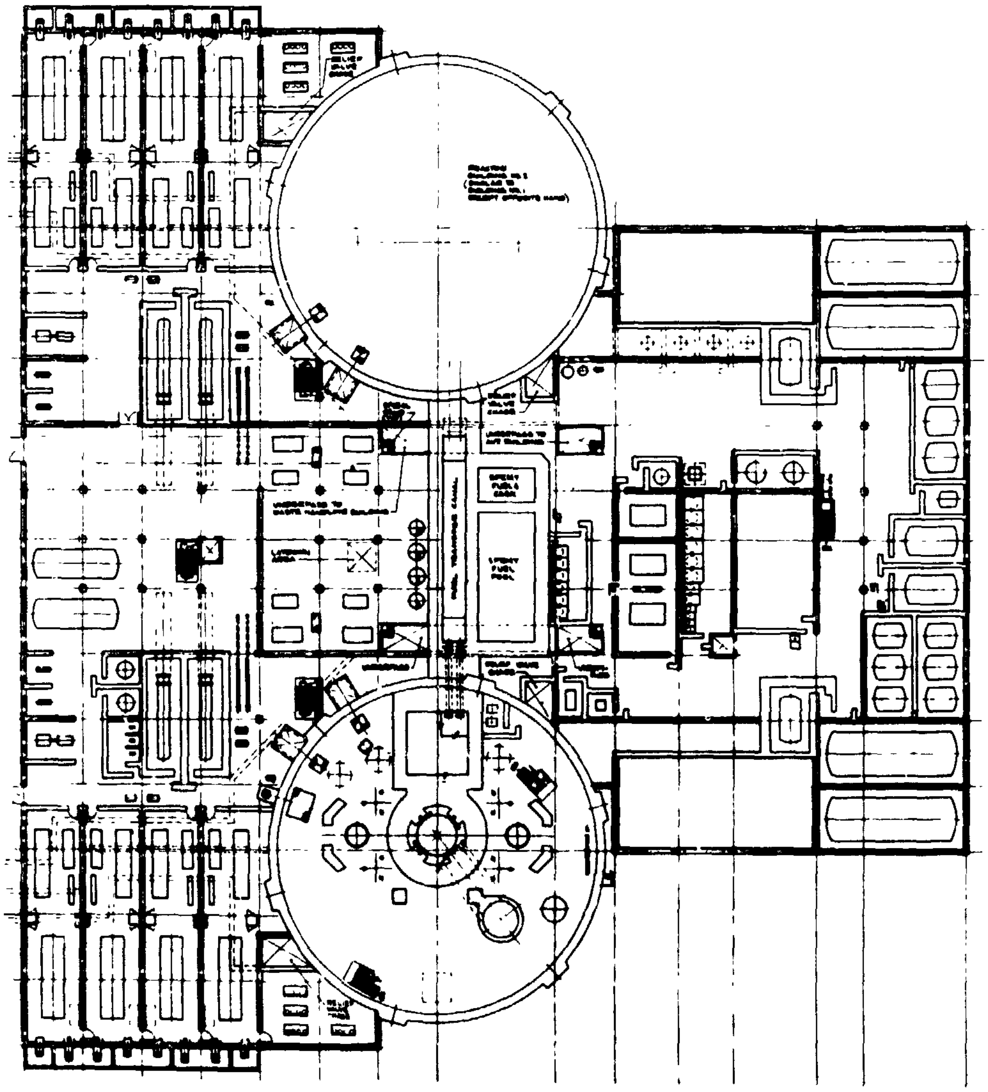

Figure 2.- Plan of typical pressurized water nuclear power plant structure.

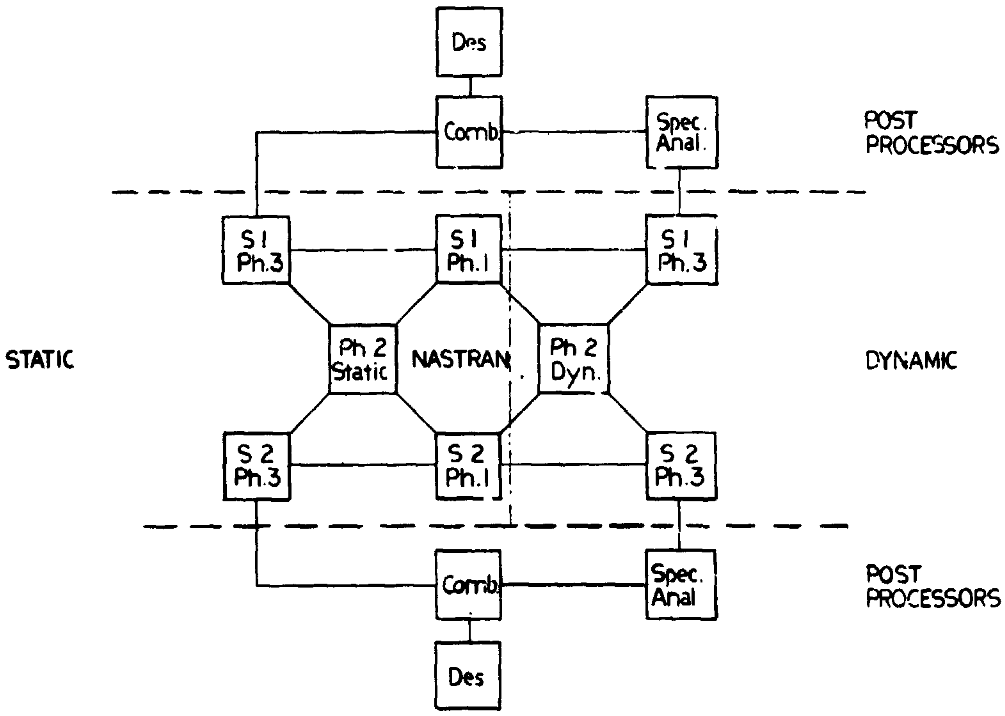

Figure 3.- Block diagram for two substructures.

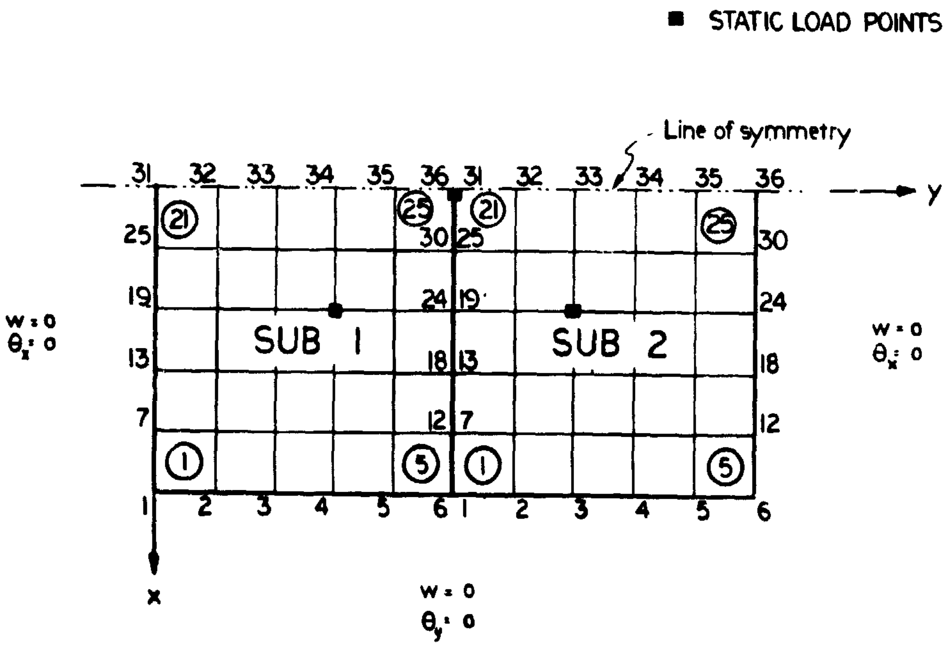

Figure 4.- Example for static and dynamic substructuring.

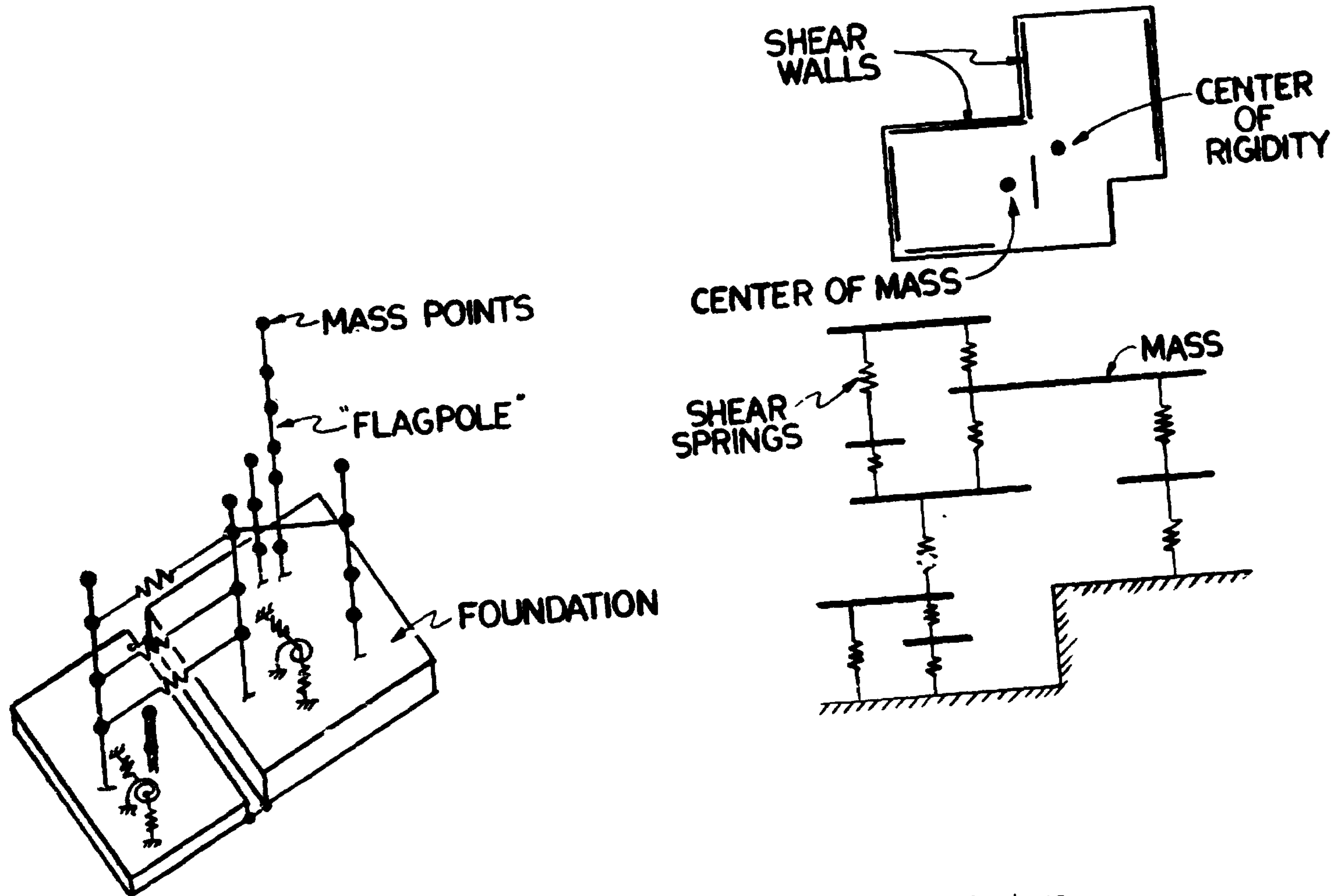

Figure 5.- Dynamic models used by other investigators.

N74-14415

NASTRAN USERS' EXPERIENCE OF AVCO AEROSTRUCTURES DIVISION

By Charles L. Blackburn and Carl A. Wilhelm

Avco Aerostructures Division, Nashville, Tennessee

SUMMARY

This paper discusses the NASTRAN experiences of a major structural design and fabrication subcontractor that has less engineering personnel and computer facilities than those available to large prime contractors. Efforts to obtain sufficient computer capacity and the development and implementation of auxiliary programs to reduce manpower requirements are described. Applications of the NASTRAN program for training users, checking out auxiliary programs, performing in-house research and development, and structurally analyzing an Avco designed and manufactured missile case are presented.

INTRODUCTION

The Avco Aerostructures Division has long been actively engaged in the research and development areas of structural analyses. Since 1966, particular emphasis has been placed on finite element techniques utilizing the displacement method. Such efforts yielded a static analysis program for both the IBM 360/Model 40 and IBM 1130 computers. Although the program was somewhat limited in the types of finite elements, the objective for solving structural problems containing a large number of degrees of freedom was achieved. This objective, however, was not obtained without the sacrifice of computer efficiency due to a requirement for large amounts of peripheral processing time. For example, the IBM 1130 could accommodate a structural model with nearly 1000 degrees of freedom, but approximately 10 hours were necessary for a solution. Run times of 3 and 4 hours were not uncommon for IBM 360/40 analyses. Only bar, triangular membrane plate, and rectangular membrane plate elements were available in the IBM 1130 program, but the IBM 360/40 program also included the triangular bending plate element. (Plate elements assumed constant stress conditions.) It became immediately apparent that the complete capability for performing structural analyses (i.e., static, vibration, buckling, etc.) by finite element techniques was not within the practical upper limits of Avco A/D's computer facilities.

In the latter part of 1970, Avco A/D became aware of the Industry Research Associate Program initiated by the NASA-Langley Research Center. The value of the program for providing a mutual interchange of technology was immediately recognized and Avco became an active participant in January 1971. The initial participation consisted of two engineering personnel being assigned to the Structures Division of the Structure Directorate. It was in this time period that the NASTRAN Systems Management Office (NSMO) was established in the Structures Division at NASA-Langley (October 4, 1970) and the first public release of NASTRAN through COSMIC occurred (November 1970). Since NASTRAN was being heavily used at NASA-Langley and other government centers for testing and evaluation, NASA-assigned Avco personnel could evaluate the program and become qualified users while performing their assigned tasks. This NASTRAN experience is one excellent example of the spin-off benefits from the NASA/Industry Research Associate Program.

It was obvious from the initial confrontation of the Avco associates with the NASTRAN program that it would enable us to attain our research and development goals. However, the in-house computer capacity at Avco A/D was still not adequate to accommodate the program. A survey of the local (Nashville) computing facilities was undertaken to determine if any computers, suitable for NASTRAN operations, were available. In-house terminals, as supplied by computer leasing services, were disregarded since the NASTRAN usage was unpredictable; operating costs could be excessive on a per run basis. A computer service, NLT Computer Services Corporation, which primarily serves the local banking and insurance interests, was found to have computers compatible with the NASTRAN program; namely, an IBM 360, Model 65 and an IBM 370, Model 155 computer. Arrangements were made with NLT for implementation of the level 12 NASTRAN on each of their computers. Further, it was decided that, whenever possible, auxiliary NASTRAN programs capable of generating and checking input data and manipulating output data (i.e., resizing routines) would be incorporated on the in-house IBM 360/40. The inconvenience of the data management problem presented by this approach was considered less undesirable than the economic problem of using the NLT computer services for all cases. Avco A/D acquired the NASTRAN program in October 1971 and had it operational on the NLT computers approximately one month later. The implementation of the program by NLT personnel will be discussed in this report. Further, this unique arrangement between the financial and technical community will be described with particular emphasis on the problems encountered due to different terminologies and concepts.

A description of Avco's auxiliary computer routines to be used with the NASTRAN analysis program is included in the paper. For example, the data generation programs described in references 1 and 2 have been converted from a CDC 6000 series computer to the IBM 360/40 computer with some modifications. Also, a program which checks the NASTRAN input data for format and syntax errors and incomplete and/or duplicate data and generates a tape for plotting undeformed structure has been developed. This check-out program is similar to the special NASTRAN program described in reference 3.

In addition, results obtained from various NASTRAN investigations of widely varying types of structure are presented. For each of the investigations, the results describe operational problems, run times, and core requirements (including comparisons of the IBM 360/65 and IBM 370/155 computers whenever possible) plus comparisons of the NASTRAN results with theoretical or experimental data.

The paper also discusses the importance of a NASTRAN type program to Avco Aerostructures Division as a major subcontractor to the prime aerospace contractors.

AVCO/NLT NASTRAN IMPLEMENTATION AND OPERATION

An interfacing of the capabilities and facilities of the Avco Aerostructures Division and the NLT Computer Services Corporation was required to accommodate the NASTRAN program. The acquisition (and updating) and execution of NASTRAN was the responsibility of Avco. The implementation and maintenance of NASTRAN was the responsibility of NLT. Obviously, NASTRAN bridges the gap that exists between the capabilities of the technical and financial communities; namely, scientific programmers.

Before NASTRAN, NLT had provided a data processing service only and was completely inexperienced with respect to scientific computer programs. However, the program was implemented in approximately one week and operational in less than one month on the IBM 370, Model 155 and the IBM 360, Model 65 computers. The primary difficulty encountered in the implementation of the program was NLT personnel's lack of familarity with the OS operating system. (NLT uses the DOS operating system for their data processing services.) Minor problems occurred due to a reluctance to believe the disk space requirements of NASTRAN. Some check-out problems were encountered in the execution of the demonstration problems because of core size requirements. Further, the punched output for the restart deck of demonstration problem 1-1 was completely unexpected. Cpu times for the execution of certain demonstration problems on the IBM 370/155 computer are presented in table 1 along with compatible cpu times obtained from various computers as given in reference 4. Although more specific and concise documentation pertaining to the implementation would be desired, the ease in making NASTRAN operational has been substantiated. In all cases, COSMIC was very prompt in identifying user problems and giving a solution.

Some operational problems have been encountered due to the conflict of NASTRAN with the previous experience of NLT personnel. A limit of 900 cpu seconds was a standard NLT computer exit. This limit was based on previous experience which normally indicated the presence of a programming error (i.e., a 'hard DO loop'). Execution of NASTRAN has made them accustomed to exceeding the 900 cpu seconds restriction which is now deleted from all NASTRAN problems. The computer operator confused the OPTP (old problem tape) and NPTP (new problem tape) with the output and input tapes, respectively. Whether or not this contributed to an apparent problem of tape management was never identified.

It is believed that this arrangement permits smaller engineering departments to attain a structural analysis capability that may otherwise be impractical and uneconomical.

AUXILIARY PROGRAMS

Since the different physical locations of the Avco engineers and the NLT computers presented a data handling problem, it was decided that NASTRAN auxiliary programs would be installed on Avco A/D's in-house IBM 360, Model 40 computer. Further, those routines which would check hand generated input data or automatically generate the input data offer an economic advantage in the decrease of aborted analyses (computer cost) due to input errors and the reduction of manpower for data preparation.

A special NASTRAN program which checks the input data for mispunched data cards and incorrectly transcribed data and generates a tape for undeformed structure plots has been developed for the IBM 360/40 computer. This program is functionally equivalent to the check-out program for the CDC 6000 series computer described in reference 3. The program operates under the OS 360/PCP operating system and requires 210K bytes of a 256K byte core and a disk drive for peripheral storage. Only subroutine BTSTRP required a revision due to the necessary reduction in the length of a GINO buffer from 1803 to 250. This change caused a corresponding reduction in the default parameters of the block sizes contained on the PROC job control card to SP2=1, BLK1=1028, and BLK2=1032.

The automated input data generation routines, as described in references 1 and 2, have been converted from the CDC 6000 series computer to the IBM 360/40 computer. These routines offer a substantial reduction in the man-hours required for model generation since they require a minimum of input data which can be obtained from engineering drawings. This manpower reduction is particularly attractive to smaller engineering departments such as Avco A/D because a complex structural analysis can be performed by a minimum number of engineering personnel. In conducting some recent NASTRAN analyses, finite element models of a delta wing and a segment of a missile case were generated by these automated routines in less than 4 man-hours each. The generality of the routines was demonstrated in reference 2 and their versatility has permitted the modeling of a railroad passenger car by Avco A/D. Another routine which automatically generates a triangular or quadrilateral mesh about a circular cutout in a flat panel, as investigated in reference 5, was modified to yield punched NASTRAN input data. Presently, programs are being developed which will calculate the stiffness coefficients for specialized structural elements (i.e., reinforced concrete or integrally stiffened plate elements) and punch the data on cards with an input format consistent with NASTRAN.

The contour plotting routines that are described and demonstrated in reference 1 have been converted from the CDC 6000 series computers to the IBM 360/40 computer. Since Avco A/D lacks an in-house plotting capability, the plotting routine has been modified to yield a printed output of the planar coordinates of each contour line to permit manual plotting. A plotting service, similar to the Avco/NLT computer arrangement, could be obtained since plotters that are compatible with the routine and NASTRAN are available in the Nashville area.

Currently, a fully stressed design technique is being developed which is almost identical to the routine incorporated in the [illegible] program (ref. 6) and the SAVES program (ref. 2). The input and output formats for this routine are compatible with the NASTRAN output and input formats, respectively. A simplified design criterion for the sizing of rod and bar elements has been incorporated into the program.

APPLICATIONS

Since the acquisition of NASTRAN by Avco A/D in October 1971, it has been used for performing in-house research and development programs, check-out and verification of auxiliary routines, and analysis of existing structural designs. The following discussion is directed to three investigations of widely varying types of structure.

Reinforced Concrete Slab - The purpose of this study was to evaluate a method of modeling reinforced concrete with finite elements that are sufficiently accurate and economically feasible. Quadrilateral membrane and bending plate elements were used to represent the concrete slab and rod elements were used to model the reinforcing rods. The representation of each reinforcing rod would yield a finite element model with a maximum mesh size dictated by the reinforcement spacing. Since this spacing is relatively small, it is conventional to represent several reinforcement rods by a single rod element which is positioned between two nodes along the edge of a larger plate element. This method is commonly called the lumping technique and results in large rod elements at the neutral axis of the plate's cross sectional area. However, the reinforcement rods are usually displaced to the tension side of the neutral axis and thus cannot be included by the conventional lumping technique. For this study, continuity of the reinforcing rods and concrete (no slipping) was assumed. The elongations of the rods are considered equal to their normal displacements on the edgewise face of the plate element at the intersecting rods. A linear variation of the translational and rotational displacements is assumed between two nodes of a particular edge for computing the normal displacements. This computation of the normal displacement at the reinforcement rod position was accomplished by use of the multipoint constraint equations contained in NASTRAN.

The subject of the investigation was a square, simply supported, reinforced concrete slab with reinforcing rods spaced at 25.4 cm. intervals along each 609.6 cm. edge. The slab was 20.32 cm. thick and subjected to a dead weight loading. The reinforcement rods (diameter = 1.90 cm.) were at a depth of 3.49 cm. from the tension side of the concrete. The non-linear properties of the concrete due to its inability to withstand tensile stresses were neglected. Model mesh sizes of 4 x 4 and 6 x 6 (corresponding to element sizes of 152.4 x 152.4 cm. and 101.6 x 101.6 cm., respectively) were investigated. Figure 1 presents a comparison of the rod stresses for each NASTRAN analysis with the theoretical results determined from closed form equations on page 3?6 of reference 7. Figures 2 and 3 show a comparison of the maximum compression stresses in the concrete and lateral displacement of the slab, respectively. Whenever necessary, NASTRAN results are extrapolated to the desired locations.

The coarse mesh model (4 x 4) required 218 cpu seconds for a solution on the IBM 370/155 computer and 260 cpu seconds were required for an IBM 360/65 computer solution of the fine mesh model (6 x 6) using Level 12 NASTRAN. Due to the difference in problem size, it was not possible to evaluate the computing speed of the different computers. However, the prohibitive time required for processing and manipulating multipoint constraint relationships was indicated by this investigation. Approximately 20% of the total cpu time was used on the multipoint constraints for each model. It is because of this time penalty that the previously mentioned auxiliary program for generating NASTRAN punched input of stiffness coefficients for specialized structural elements is being developed. The NASTRAN run time will be further reduced by the time required to calculate the stiffness. Obviously, the NASTRAN output would have to be used in an additional auxiliary program to determine the actual internal loads and stresses (i.e., axial stress in reinforcement rods).

These preliminary NASTRAN results show good agreement with theoretical results. Further validation of the computational efficiency and accuracy is required when the auxiliary routines become operational. This method is also applicable to integrally stiffened or semi-monocoque panels and other structures wherein an assemblage of finite elements is represented by a discrete structural element.

Structural Effects of Wing Camber Variations - This study was primarily initiated to check out the lifting surface data generation routine. To provide additional NASTRAN experience, it was decided to conduct a simple design study to evaluate the change in stiffness and strength due to camber variations of a wing. The wing has a delta planform and a modified diamond airfoil section with a 3% maximum thickness. A uniform pressure loading was applied to the structural model. For a maximum camber of 1.50% chord, the finite element model is identical to the lumped finite element model of the baseline wing structure used in the study described in reference 2. The normalized tip deflection and stress distribution in the lower surface skins near the wing-fuselage intersection for varying amounts of camber are shown in figure 4.

The finite element model of each wing configuration is identical except for the 'out of plane' geometry changes caused by camber variations. If everything remains the same except for wing configuration, the cpu time should be constant. Although there was some unexplained but minor variations in the cpu times, approximately 490 and 580 seconds were required for NASTRAN Level 12 solutions on the IBM 360/65 and IBM 370/155 computers, respectively. These times are contradictory and have not been explained by NLT systems personnel except to speculate that it could be due to the operating system. In all cases, the OS/MVT/HASP operating system was used.

Honeycomb Shell - This study was initiated to determine a possible cause for observable damage on Avco designed and manufactured missile case sections due to operational transportation conditions. The objective of the investigation was to determine the cause of the damage and study possible design changes in the transporter to prevent the re-occurrence of structural damage. The sections of concern are lightweight honeycomb shells with ring frames at the ends of each section. The damage occurred at one of the transporter's support saddles which was located such that the honeycomb shell would rest on it. The missile case sections were modeled by CQUAD2 elements for the shells and CBAR elements for the frames. The loads applied to the models were in accordance with loading conditions used for testing. Clamped boundary conditions were assumed at the intersection of the honeycomb structure and the relatively thick-walled back-up structure. Those grid points in contact with the saddle were not allowed to translate in the lateral direction. Results from a corresponding analysis and the test condition are shown in figure 5 in which the variation of the outer face sheet longitudinal (membrane) stress about the circumference of the shell is presented. The variation of the test data (+ θ and - θ) is due to the lack of symmetry of the structure caused by cutouts for doors and access ports. Although a good correlation of NASTRAN and test data was obtained, some variations should be expected since the cutouts were ignored in the finite element model. However, a NASTRAN analysis did predict a core shear failure at the exact location where observable damage did occur as indicated in figure 6.

RECOMMENDATIONS AND CONCLUSIONS

Based on the NASTRAN experience obtained to date at Avco A/D, the following changes or improvements would be desired.

1. The development of a mathematical technique for estimating the time and core requirements for finite element models of various sizes and degrees of complexity would reduce turn around time. This technique could be in the form of empirical relationships amenable to programming on an office size computer.

2. Since the static analysis portion of NASTRAN receives the greater usage, a mini NASTRAN which only contains the rigid format 1 and reduced buffer sizes to allow for execution on smaller computers (i.e., IBM 360/40) would probably prove economical.

3. The margin of safety pertaining to compression members is not conventional since a positive margin of safety is understrength and vice versa for a NASTRAN analysis. This may be corrected by using a negative number to designate the allowable compressive stress on the materials property card.

In conclusion, the development and continuing maintenance and improvement of the NASTRAN program has made it possible for companies with limited engineering manpower and computer facilities to attain a proficiency in structural analysis. Prior to NASTRAN, a large amount of the independent research and development funds was expended on the development of structural analysis methods based on finite element techniques. This effort can now be directed to structural research utilizing NASTRAN as the analysis tool. Further, the implementation of NASTRAN by systems personnel who are completely inexperienced with scientific programs and comprehension of the program by new users attests to its usability.

REFERENCES

1. Giles, G. L., and C. L. Blackburn, "Procedure for Efficiently Generating, Checking, and Displaying NASTRAN Input and Output Data for Analysis of Aerospace Vehicle Structures," TM X-2378 NASTRAN: Users' Experience, Vol. II, NASA, Sept. 1971, pp. 679-696.

2. Giles, G. L., C. L. Blackburn, and S. C. Dixon, "Automated Procedures for Sizing Aerospace Vehicle Structures (SAVES)," Journal of Aircraft, Vol. 9, No. 12, Dec. 1972, pp. 812-819.

3. Smith, W. W., "A Special NASTRAN Program for Input Checking and Undeformed Structure Plotting," TM X-2378 NASTRAN: Users' Experience, Vol. II, NASA, Sept. 1971, pp. 559-568.

4. Raney, J. P., and D. J. Weidman, "NASTRAN: A Progress Report," TM X-2637 NASTRAN: Users' Experiences, NASA, Sept. 1972, pp. 1-12.

5. Blackburn, C. L., and R. M. Hackett, "Photoelastic Verification of Direct Stiffness Method Applied to Flat Plates with Reinforced Holes," presented at the Society for Experimental Stress Analysis National Spring Meeting, Huntsville, Alabama, May 19-22, 1970 (Paper No. 1633).

6. Giles, Gary L., "Procedure for Automating Aircraft Wing Structural Design," Journal of the Structural Division, ASCE, Jan. 1971, pp. 99-113.

7. Timoshenko, S., and S. Woinowsky-Krieger, Theory of Plates and Shells, McGraw-Hill, New York, 1959.

8. MacNeal, R. H. (Editor), "The NASTRAN Theoretical Manual," NASA SP-221, Sept. 1970.

9. McCormick, C. W. (Editor), "The NASTRAN User's Manual," NASA SP-222, Sept. 1970.

10. Douglas, F. J. (Editor), "The NASTRAN Programmer's Manual," NASA SP-223, Sept. 1970.

TABLE 1. COMPARISON OF LEVEL 12 EXECUTION TIMES (CPU SECONDS)

FOR NASTRAN DEMONSTRATION PROBLEMS

Problem No.	Form & Version	Computer Configuration/Series/Model IBM 370/155	IBM 360/95	IBM 360/67	CDC 6600	UNIVAC 1108
1-1	U	116	60	108	31	72
1-1A	R	72	30	102	24	24
1-2	U	166	84	264	72	60
1-3	U	242	114	336	120	96
1-4	U-1	1022	020	1464	666	1020
1-4	U-2	2665	380	--	--	--
1-5	U	1505	660	1800	--	1080
1-6	U	68	48	132	30	24
1-7	U	251	60	270	120	90
2-1	U	88	72	168	30	24
3-1	U-1	1567	720	3900	828	660
3-1	U-2	3088	610	--	--	--
4-1	U	328	168	486	144	90
5-1	U	863	408	1134	486	318

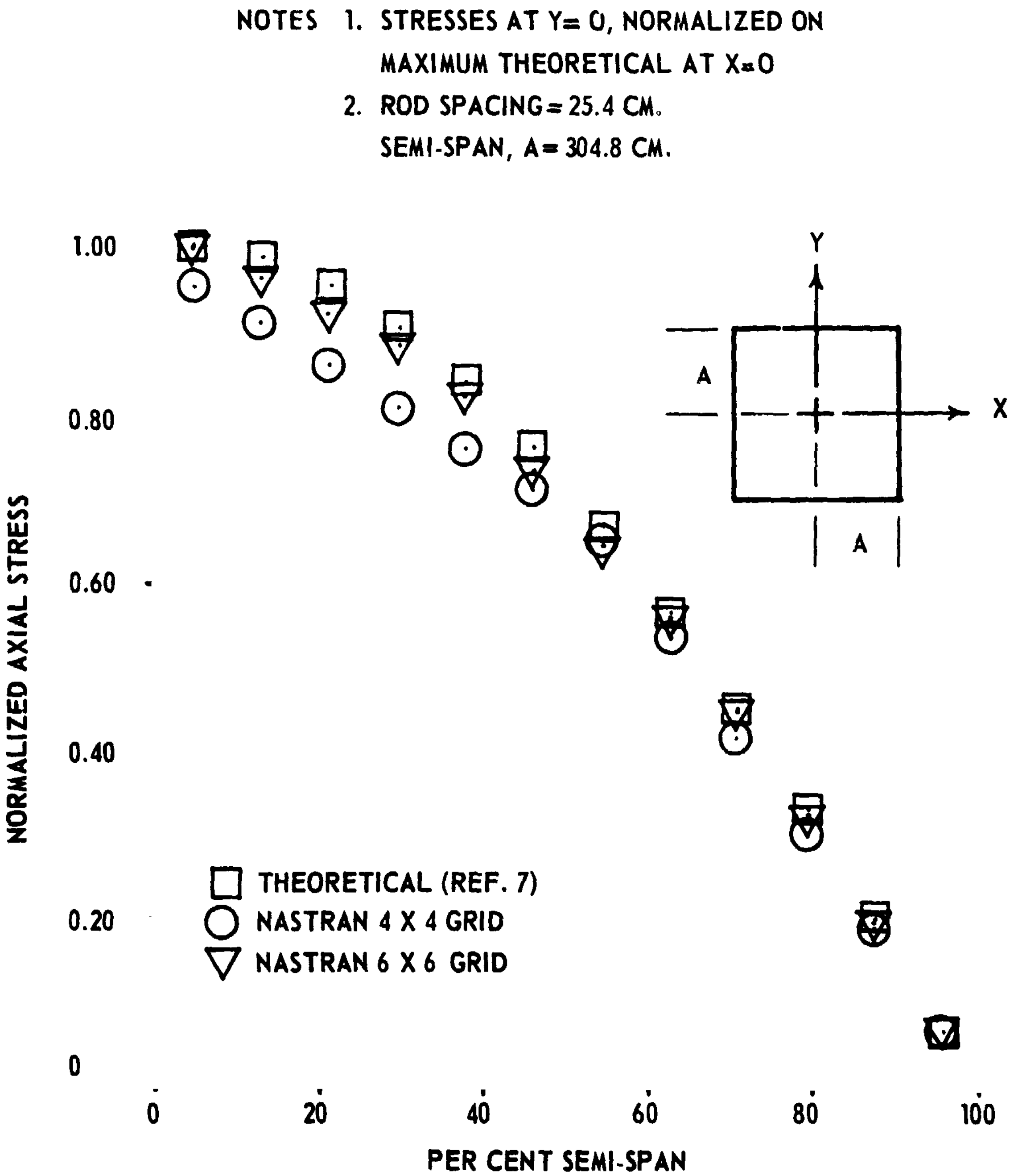

Figure 1. · Variation of rod axial stresses in a square, simply supported, reinforced concrete slab subjected to a dead weight loading.

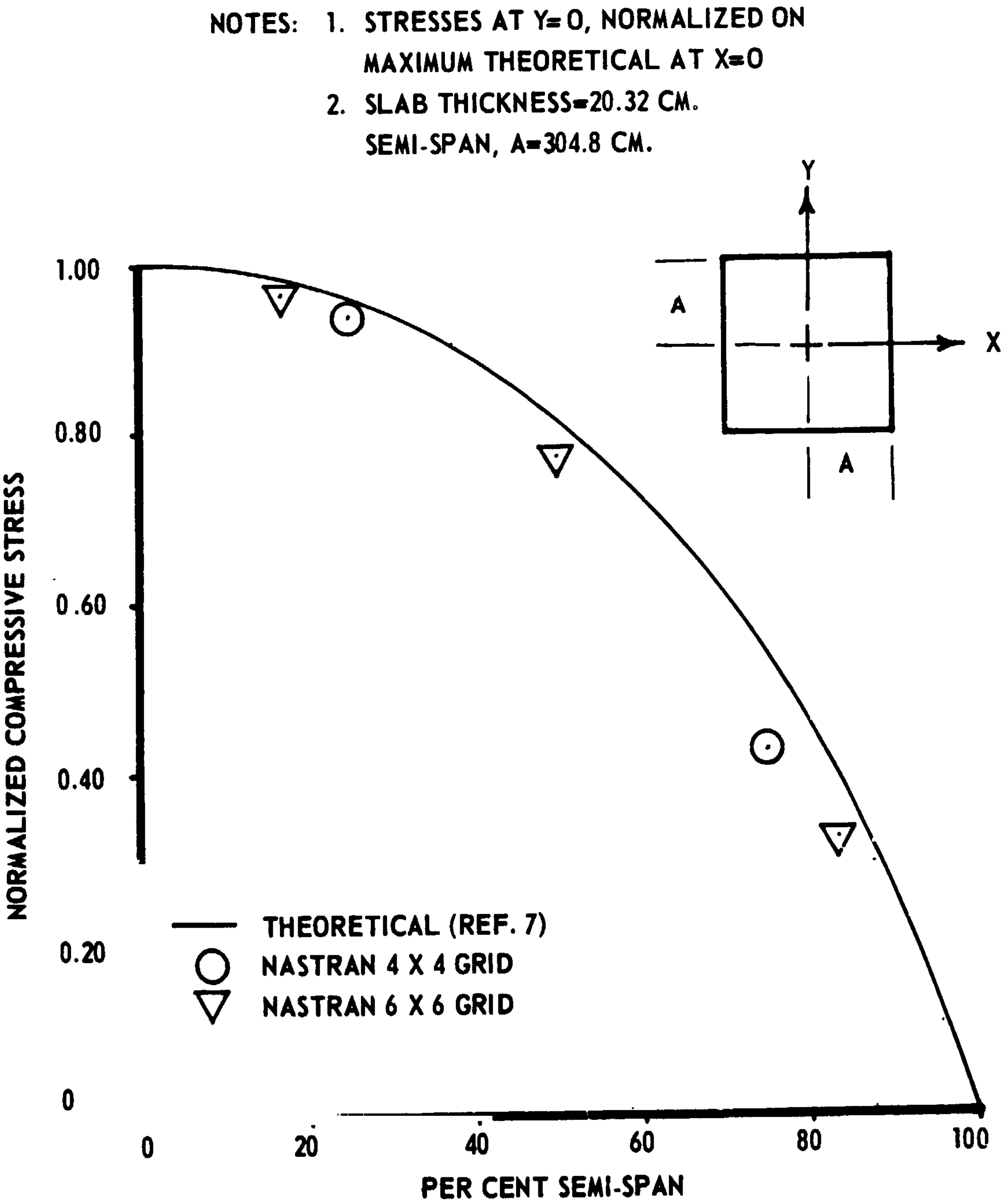

Figure 2. - Variation of concrete compressive stresses in a square, simply supported, reinforced concrete slab subjected to a dead weight loading.

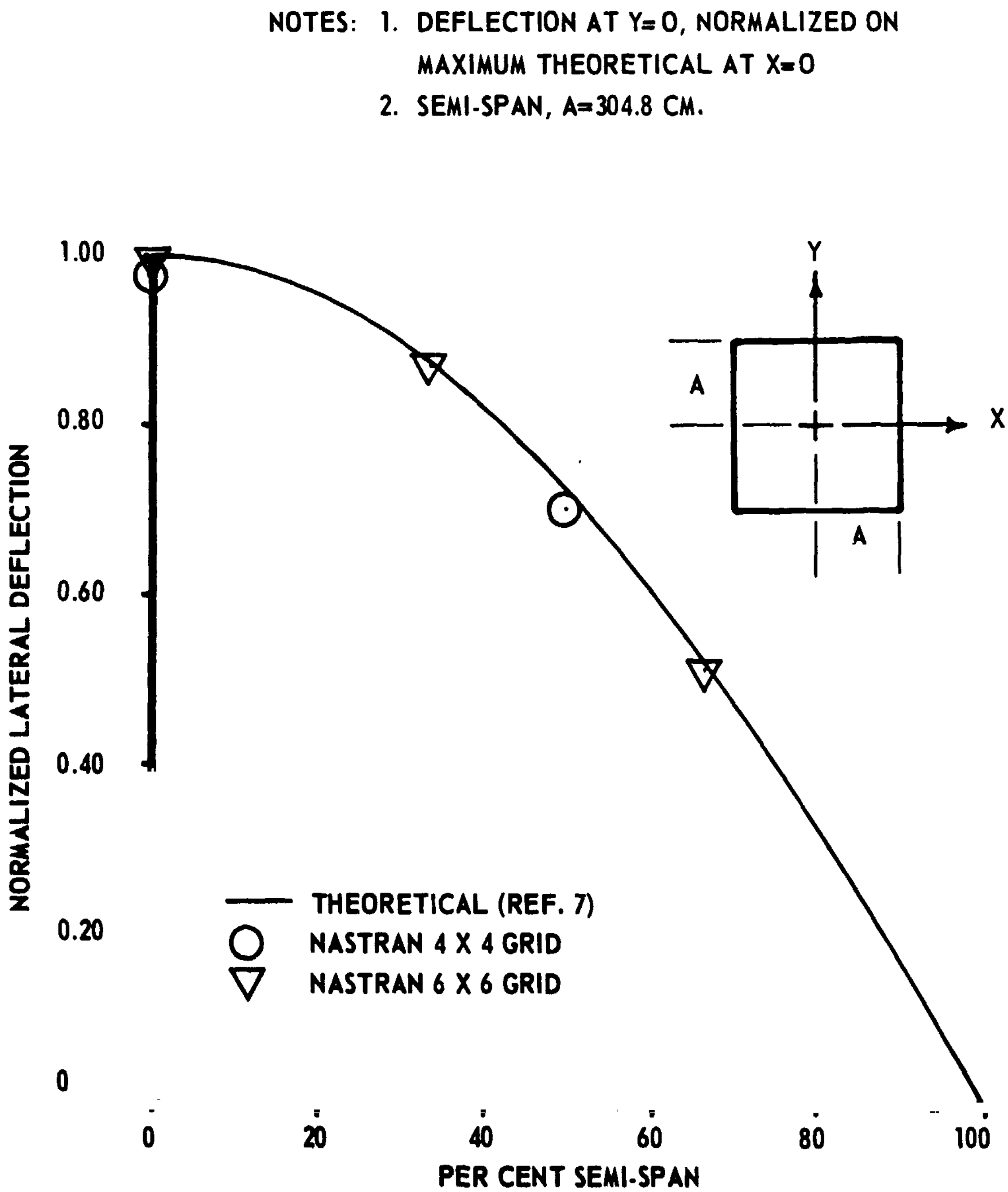

Figure 3. - Variation in lateral deflection of a square, simply supported, reinforced concrete slab subjected to a dead weight loading.

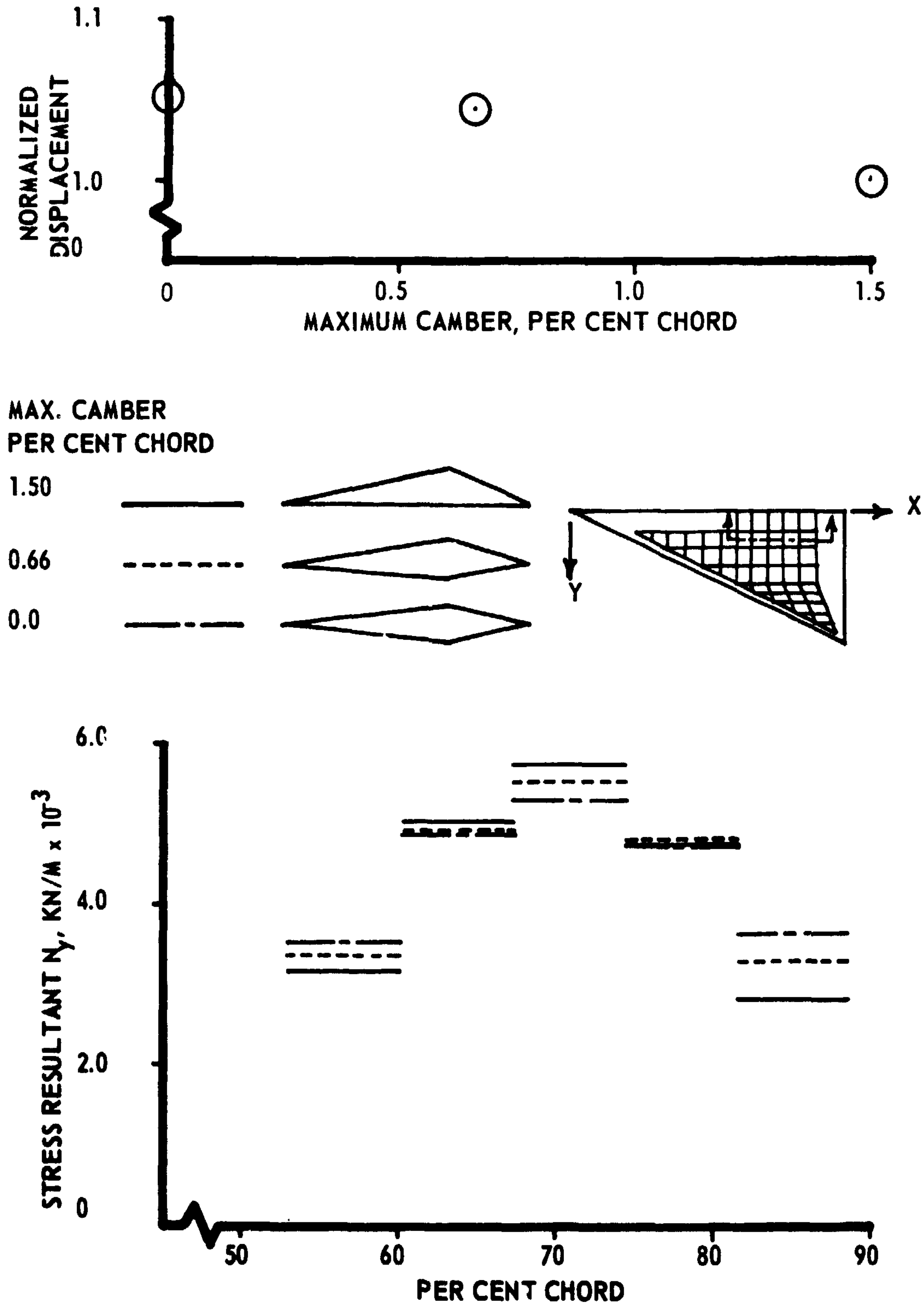

Figure 4. - Stress distribution near wing-fuselage intersection and normalized tip deflection for varying degrees of camber.

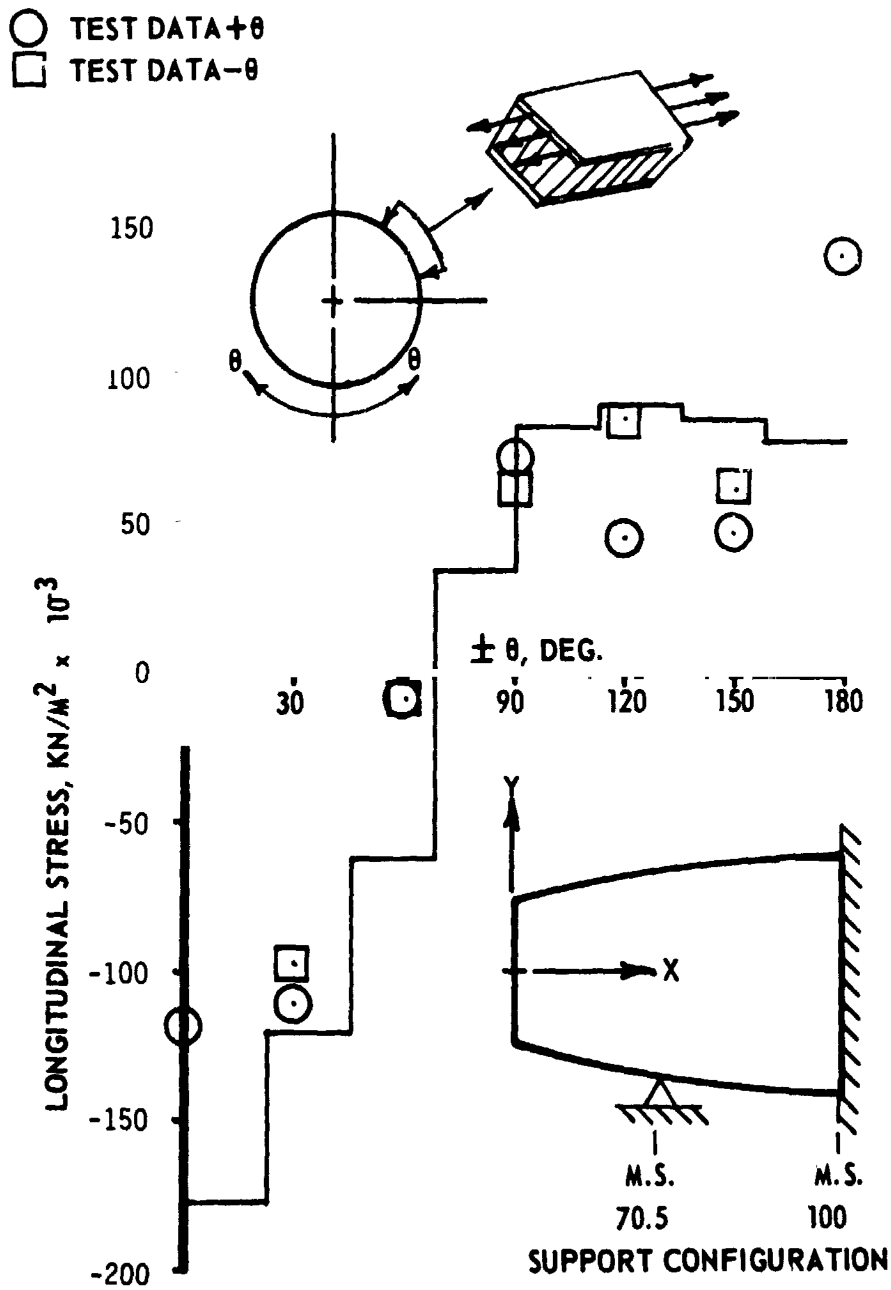

Figure 5. - Variation of outer face sheet longitudinal stress at M.S. 70.5 for symmetric vertical loading.

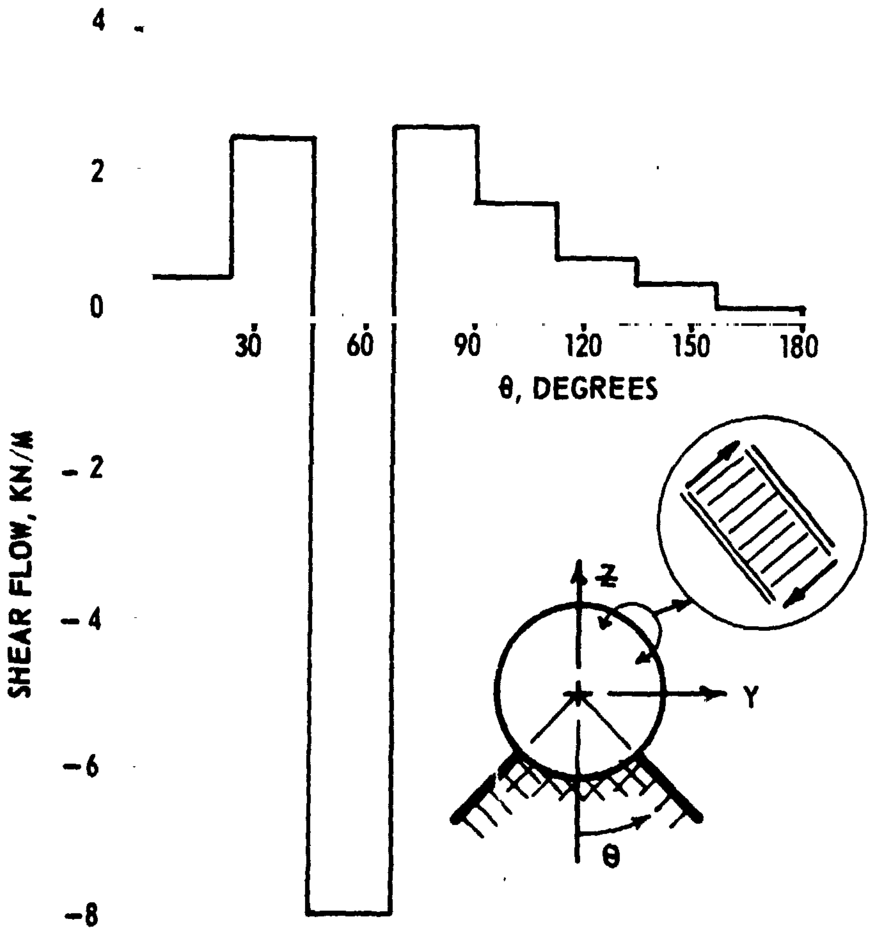

Figure 6. - Circumferential transverse shear flow (core) for cradle support enclosed angle = 90°

N74-14614

STATIC AND DYNAMIC HELICOPTER AIRFRAME

ANALYSIS WITH NASTRAN

By H. E. Wilson and J. D. Cronkhite

Bell Helicopter Company

SUMMARY

The use of NASTRAN at Bell Helicopter Company for structural static and dynamic analysis of a helicopter airframe is described. Analysis of airframe internal loads, main rotor isolation systems, and airframe vibration is discussed. The use of each rigid format for these types of analysis is summarized. Suggested improvements to NASTRAN to increase its effectiveness in performing helicopter airframe analysis are given.

INTRODUCTION

Before the availability of large finite element programs, internal loads were calculated from two-dimensional shear and moment diagrams and the dynamic behavior was approximated with a Myklestad-type beam analysis. After the development of NASTRAN, and other similar programs, more exact analyses could be performed. However, before NASTRAN can be executed, the helicopter airframe must be represented as a three-dimensional finite element model which involves generation of a large amount of input data to define the structure. A typical airframe structural model is shown in figure 1. In addition to developing a structural model, the problem of distributing structural and nonstructural weight to the appropriate areas of the finite element model proved to be a time consuming and tedious task requiring many judgmental decisions. An automated procedure for distribution of weight items to the structural model was devised so that NASTRAN could be used efficiently for both static and dynamic structural analysis.

AIRFRAME STATIC ANALYSIS

A static analysis of a helicopter airframe involves the determination of internal loads and stresses using NASTRAN[1]. To facilitate the use of NASTRAN various preprocessor and postprocessor computer programs were written. The preprocessor programs include automatic data generation of finite element models of certain types of structure such as the tail boom, elevator, and vertical tail as shown in figure 2. The representation of the inertia loads is provided with an interface program to NASTRAN.

The interface program calculates six load vectors which represent the inertia reactions for independently applied unit translation and angular accelerations at the helicopter center of gravity. By scaling the inertia reactions to balance the applied loads and applying a set of determinant constraints, a NASTRAN static analysis can be done.

Postprocessors are used to calculate shear flows and adjusted rod loads for rod-shear panel type structure, to scan the output from several subcases and determine the critical loading condition for each element, and to present the output data in a report format.

Alternate output from the inertia distribution program is concentrated weights punched on data cards in NASTRAN format. These weights may be used directly in a static analysis with inertia relief, natural frequency analysis, or dynamic response analysis.

AIRFRAME DYNAMIC ANALYSIS

Main Rotor Isolation

Dynamic analysis of the helicopter involves evaluating different methods of isolating the excitation of the main rotor from the airframe. These methods include a focused pylon[2] for isolation of horizontal main rotor excitation and nodal beam[3] for isolation of vertical excitation. A sketch and brief explanation of these systems is shown in figure 3. NASTRAN models of these systems are developed using bars, linkages (rods), scalar springs, multipoint constraints, and concentrated masses.

Vibration response characteristics of the isolation system can be evaluated by attaching it to a rigid body fuselage. Natural frequencies, mode shapes, and frequency response characteristics of the main rotor isolation system can then be determined without having to consider the added complexity of elastic and dynamic effects of the fuselage. After having developed and tuned this type of model, the isolation system is incorporated into a structural dynamic airframe model to do a vibration analysis of the entire coupled system.

Airframe Vibration

The airframe dynamic response analysis is performed by combining the main rotor pylon and isolation system with the elastic airframe model. The airframe model will be either an elastic axis representation made up of bar elements with fuselage section properties or a built-up three-dimensional representation using bars, rods, shear panels, and membrane elements to model the structure. The elastic axis models have from 300 to 400 degrees of freedom and the three-dimensional models usually have 1200 to 1400 degrees of freedom maximum.

A modal approach is most often used for a vibration analysis of the airframe where the system degrees of freedom are reduced below 200 and the natural frequencies and mode shapes are computed using the GIVENS eigenvalue extraction method. This method is used primarily because of the number of modes required for low frequency (0 to 50 hertz) vibration response analysis, usually at least 30 modes.

The principal types of dynamic analysis done with the airframe model are the following:

(1) Tuning the airframe natural frequencies with respect to main rotor excitation harmonics by making structural and weight changes.

(2) Determining the steady state frequency response characteristics of the airframe where forces and moments are applied separately at degrees of freedom having excitation sources and the forcing frequency is swept over the range of interest (usually 0 to 50 hertz).

(3) Determining the steady state response to in-flight rotor harmonic excitation.

(4) Determining the transient response of the airframe to weapon firing using NASTRAN and a hybrid computer. The NASTRAN normal mode data for the airframe model is input to a hybrid computer program which computes the airframe response. A simplified flow diagram of the hybrid analysis is shown in figure 4.

SUMMARY OF THE USE OF NASTRAN RIGID FORMATS FOR AIRFRAME ANALYSIS

Rigid Format 1 - Static Analysis

Rigid format 1 is used to calculate the internal loads of the helicopter for the different design loading conditions. The static structural model typically contains 2500 to 3000 degrees of freedom and is modeled primarily with rods, bar, and shear panels. The initial run, when the stiffness matrix is decomposed, takes about 60 cpu minutes on an IBM 360-65 computer. Each succeeding loading condition takes approximately 20 cpu minutes.

Rigid Format 2 - Static Analysis With Inertial Relief

The weight distribution of the helicopter is checked with this rigid format. It performs a static analysis of a free helicopter in flight with steady loads applied. The results from rigid format 2 can be compared with those obtained using format 1 to ensure a correct inertial representation is achieved.

Rigid Format 3 - Normal Mode Analysis

This rigid format is used for tuning of the airframe natural frequencies with respect to predominant excitation frequencies. The natural frequencies and normal mode data output from NASTRAN are also used in other programs such as the hybrid computer program previously discussed or combined with main rotor analysis programs to determine the response of the coupled rotor and airframe.

The flexibility matrix ($[K]^{-1}$) and mass matrix are output and used in a flutter program. The natural frequencies and mode shapes for the zero velocity case are compared to the NASTRAN results as a check on the flutter program.

Rigid Format 4 - Static Analysis With Differential Stiffness

Rigid format 4 has been used for designing the static stops for the main rotor pylon support system. The use of differential stiffness reduced the loads caused by crash conditions, thus saving weight in the design. The inclusion of second order differential stiffness effects would allow NASTRAN to be used to solve several other structural problems such as tension stresses developed in membrane plates due to transverse pressures.

Rigid Format 5 - Buckling

The stability analysis in NASTRAN is used on a limited basis. Many degrees of freedom are required to obtain an accurate solution to a built-up three-dimensional model. A buckling analysis was performed on a helicopter tail boom. For a model containing 1800 degrees of freedom, NASTRAN predicted an eigenvalue of 6 when using the limit design loads. The analysis took over 4 cpu hours. It was felt this eigenvalue was too high, but to remodel finer and probably reduce the eigenvalue would take excessive cpu time.

Rigid Format 6 - Piecewise Linear

The piecewise linear solution in NASTRAN has never been used successfully. It could be a very helpful analytical tool if it functioned properly.

Rigid Format 7 - Direct Complex Eigenvalue Analysis

This rigid format is time consuming. An improved complex eigenvalue routine is desired, a preferred method would be a QR algorithm such as the available ALLMAT routine[4].

Rigid Format 8 - Direct Frequency Response Analysis

Internal oscillatory loads and stresses for the response to rotor harmonic excitation are calculated with rigid format 8. This rigid format would seldom be used if the mode acceleration technique in rigid format 11 worked on the level 15.1 version of NASTRAN.

Rigid Format 9 - Direct Transient Response

Rigid format 9 is used to calculate transient internal loads and stresses for such problems as panel response to blast overpressures, airframe response to gun recoil, and landing loads. As with rigid format 8, this rigid format would seldom be used if the mode acceleration technique worked in rigid format 12.

Rigid Format 10 - Modal Complex Eigenvalue Analysis

As in rigid format 7, run times have been excessive. An improved complex eigenvalue method is needed to make use of this rigid format practical.

Rigid Format 11 - Modal Frequency Response Analysis

Rigid format 11 is used to analyze steady state response of the airframe to harmonic excitation with varying frequencies to simulate shake test results. It is also used to analyze steady state response to in-flight rotor harmonic excitation. Mode acceleration is required to obtain internal loads. In our current level, 15.1, it does not work. Therefore, to get the internal loads, rigid format 8 must be executed.

Rigid Format 12 - Modal Transient Response Analysis

This rigid format is used to analyze transient response problems as described in rigid format 9.

DMAP Approach

DMAP programming has been found difficult to use. However, some DMAP alters are made. DMAP alters are used to obtain special output to be used in other analyses. Mode printout and normal mode plotting are altered into rigid format 11. DMAP is used to add differential stiffness to real eigenvalue analysis to determine centrifugal stiffening effects on rotor blades.

CONCLUSIONS

NASTRAN has been found to be very useful in performing aircraft structural analysis. When coupled with preprocessor and postprocessor programs, it has been used very efficiently and effectively in the design environment. It is felt, though, that NASTRAN's effectiveness can be greatly enhanced for our use with the following incorporations:

(1) Fix the mode acceleration technique in rigid formats 11 and 12.

(2) An improved complex eigenvalue solution is needed in rigid formats 7 and 10.

(3) Add rotating beam dynamic effects such as the addition of Coriolis acceleration terms.

(4) Add rotary transformation from rotor blade rotating system to the fixed airframe system.

(5) Rotor blade aerodynamics should be included along with (3) and (4) for analysis of the coupled rotor and airframe.

(6) Second order differential stiffness terms need to be added in rigid format 4.

(7) Piecewise linear analysis should be improved.

REFERENCES

1. Gallian, D. A., and Wilson, H. E.: The Integration of NASTRAN Into Helicopter Airframe Design/Analysis. 29th Annual National Forum of the American Helicopter Society, Washington, D.C., May 1973.

2. Balke, R. W.: Development of the Kinematic Focal Isolation System for Helicopter Rotors. 38th Shock and Vibration Symposium, St. Louis, May 1968.

3. Shipman, D. P., White, J. A., and Cronkhite, J. D.: Fuselage Nodalization. 28th Annual National Forum of the American Helicopter Society, Washington, D.C., May 1972.

4. Wilkinson, J. H.: The Algebraic Eigenvalue Problem. Oxford University Press, 1965.

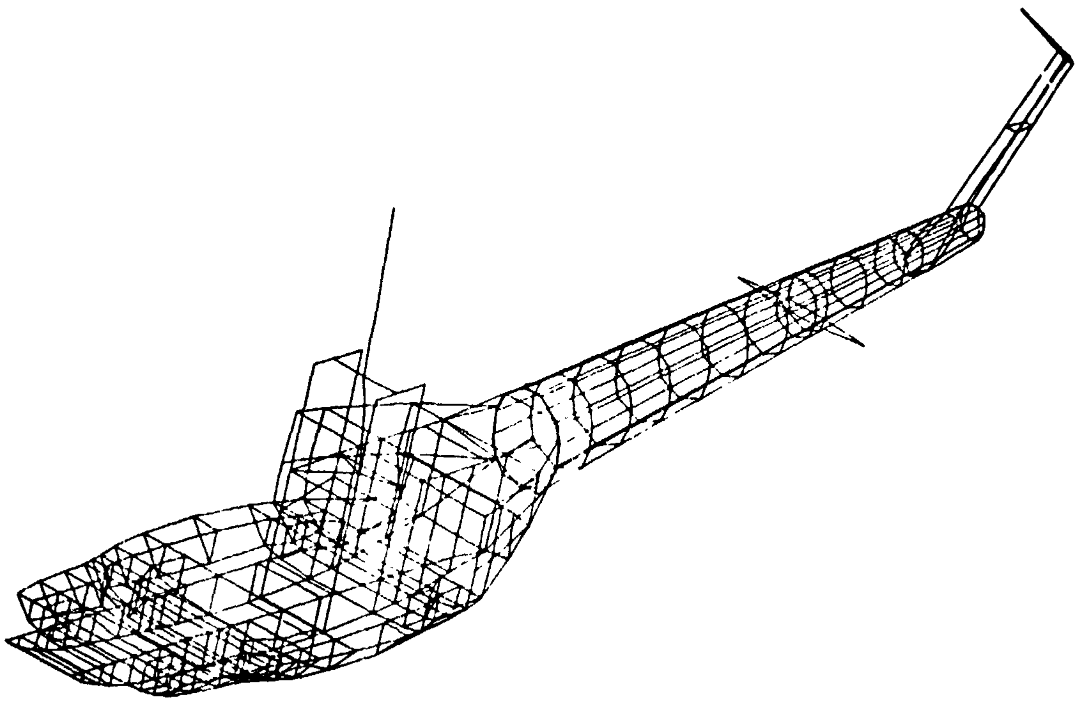

Figure 1.- Finite Element Model of Helicopter Airframe

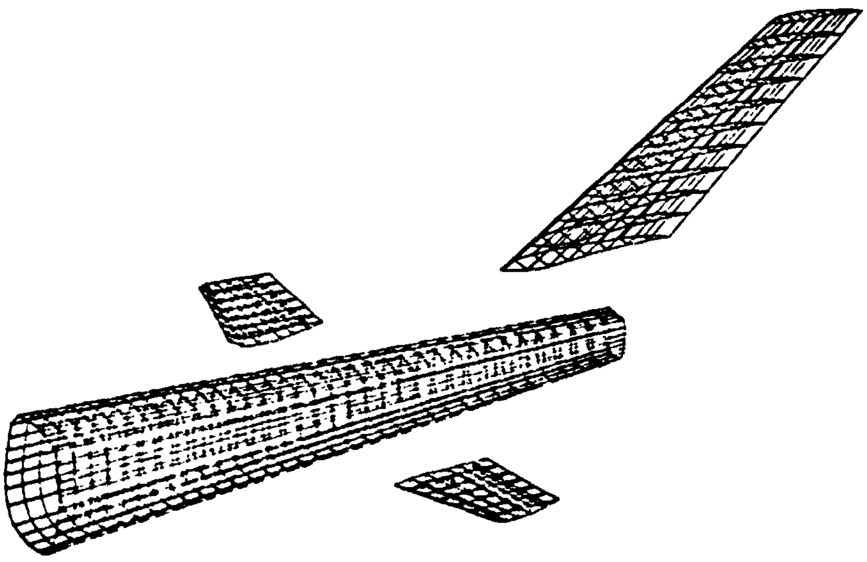

Figure 2.- Computer Generated Model

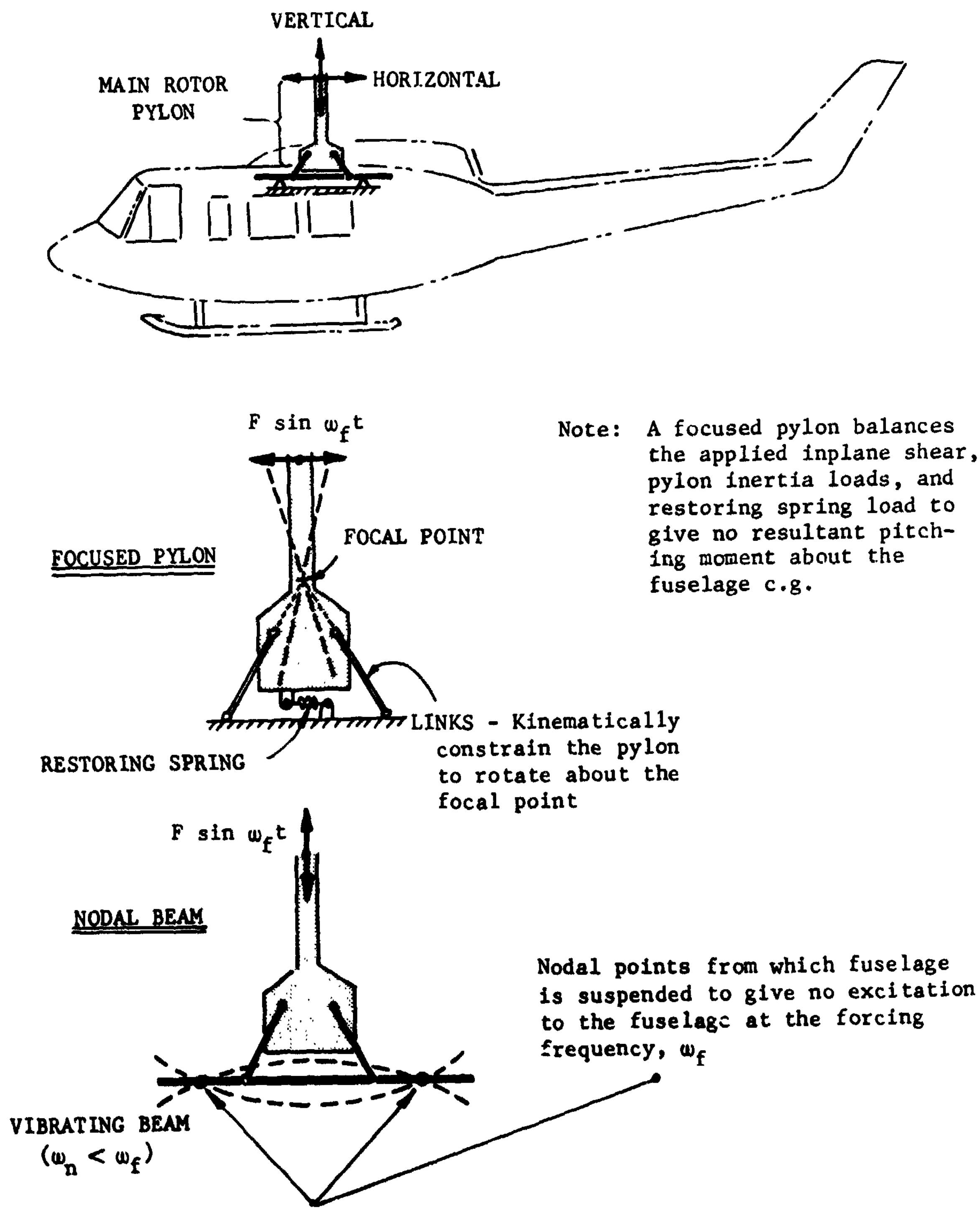

Figure 3.- Focused Pylon and Nodal Beam - Used for Isolation of the Airframe From Main Rotor Excitation

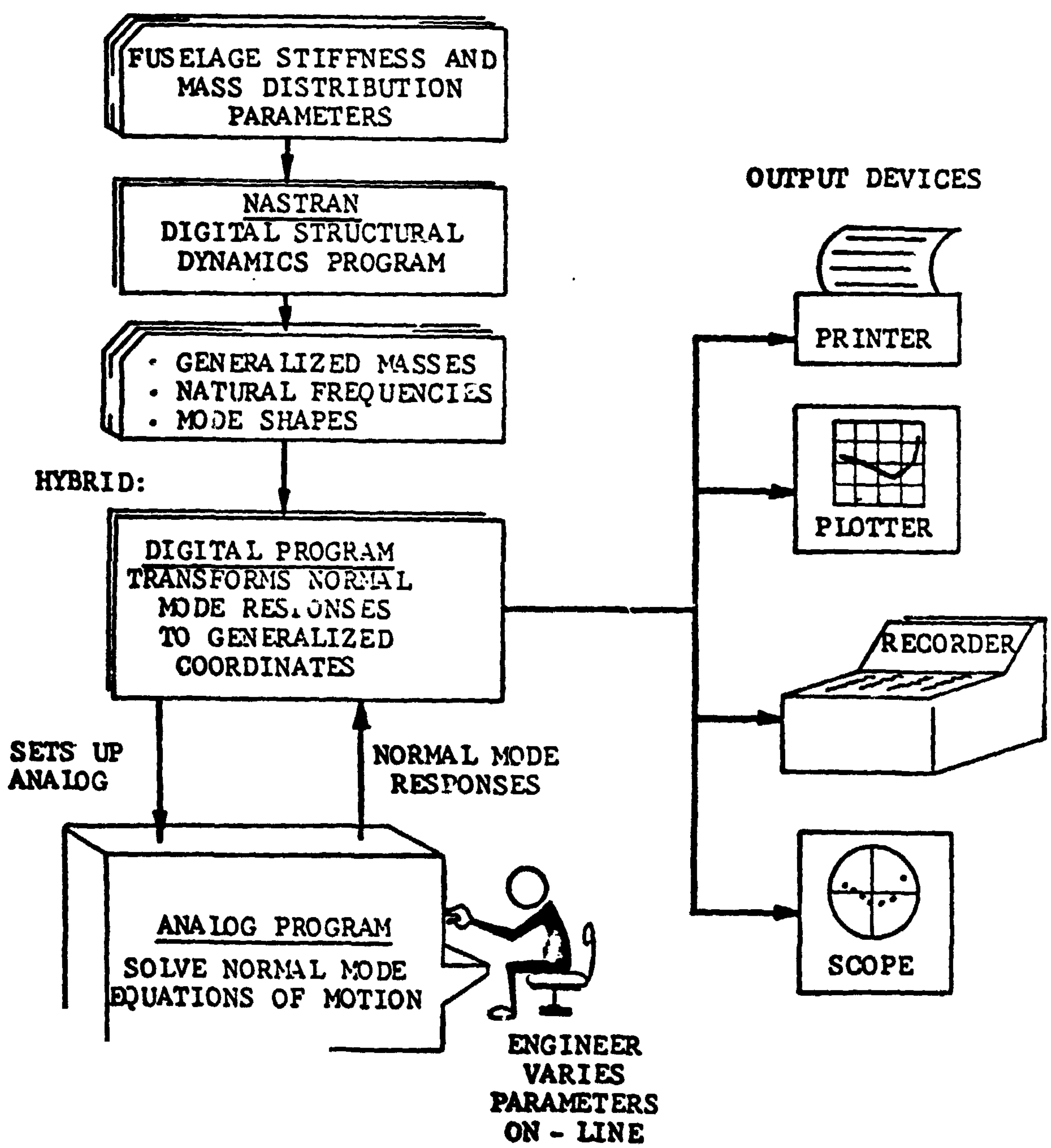

Figure 4.- Flow Diagram of the Dynamic Analysis on the Hybrid Computer

N74-14617

RESPONSE ANALYSIS OF AN AUTOMOBILE SHIPPING CONTAINER

By Lo-Ching Hua
Analytical Engineering Services, Inc.

and Sang H. Lee and Bradford Johnstone
Pullman-Standard

INTRODUCTION

Rail shipment of automobiles on open rack cars has been plagued with heavy damage claims. To alleviate this problem, systems are needed to enclose the automobile more fully during transit and to mechanize the loading and unloading operations. The Stac-Pac system was developed to meet this need by Southern Pacific Transportation Company.

The system consists of flatcars, Stac-Pac containers, and special loading and unloading equipment. Each 27.2-m (89 1/3 ft) piggyback-type flatcar carries four containers. Three full-size automobiles are carried in each container. The containers are loaded close together on the flatcar so that the automobiles are fully protected during shipment from manufacturer to distribution terminal.

Pullman-Standard developed a container design for the Stac-Pac system and conducted vibration tests to verify the system structural integrity. A dynamic analysis was also made, using NASTRAN, and the results of the test and analysis are compared in this paper.

AUTOMOBILE SHIPPING CONTAINER

The Stac-Pac container built by Pullman-Standard is made of hot-rolled steel (fig. 1). The enclosure of the container is made of thin steel sheet. It serves the dual purpose of protecting the automobile and functioning as shear panels for the structure. The side posts, deck system, and automobile restraining mechanism are made of steel sheets and formed structural shapes. All the substructures are welded assemblies. The container structure is then assembled from these substructures with friction-type bolts. This production method has made the container structure to be effective against dynamic loads.

The outside dimensions of the container are approximately 2.4 m (8 ft) in width, 4.6 m (15 ft) in height, and 6.1 m (20 ft) in length. This size will fit the flatcar construction and satisfy the rail transport regulations. Within this allowable space, the container has to be designed to carry three full-size sedans. It is interesting to note that the tight spatial requirement has made the designing task very challenging.

Recent shipments of automobiles in this type of container has reduced the damage rate to a negligible level. Eventually, the fleet of flatcars and containers will probably extend the automaker's production line to the dealer's show room. In view of the large production potential and the length of service life, it is very desirable to optimize the container to minimize the cost of construction and maintenance. Pullman-Standard has carried out extensive designing and testing programs and has chosen NASTRAN as the analytical tool to achieve this optimization. The analytical and experimental results and the correlation are reported herein.

VIBRATIONAL TEST

The vibrational test was carried out for the purposes of determining the response of the structure under simulated rail transport environment and evaluating the fatigue life.

A 27.2-m-long (89 1/3 ft) flatcar normally used for carrying Stac-Pac containers was the test bed. The container was mounted at one end of the flatcar. The end position containers are usually subjected to maximum road excitation. A variable-speed shaker consisting of two eccentrically mounted rotating disks was located approximately 0.6 m (2 ft) from the open end of the container with the axes of rotation parallel to the long axis of the flatcar. In this particular test, the initial position and phase lag of the disks were arranged so that the maximum vertical and horizontal excitation would occur in phase.

For the purpose of monitoring test data, a number of strain gages and accelerometers were mounted on the container at key locations. During the test, the time histories of these strains and accelerations were directly recorded on photosensitive paper.

Vibration amplitudes and test frequencies were based on road test data. In this test, two frequencies of 5.0 and 6.25 Hz were used (1 Hz = 1 cps). The maximum acceleration at the base of the front post of the container is approximately 0.4g and 0.7g for the 5.0-Hz and 6.25-Hz excitation, respectively. The fatigue test was performed with 50 hours of continuous excitation at 6.25 Hz. During this period of 50 hours, the structure of the container would encounter about 1 million cycles of stress reversal at the amplitude level indicated by the aforementioned 0.7g acceleration. There was no failure of structural members or connections at the end of the test. The accelerations and strains recorded show good correlation with the theoretical results computed by NASTRAN. Representative sets of data are presented in figure 2.

THEORETICAL ANALYSIS

NASTRAN Rigid Format 8, Direct Frequency Response, was used for theoretical analysis. The first part of the analysis was done on the container structure alone with a 32 grid point model. This small model served as a pilot analysis for the purposes of studying the general dynamic behavior of the container and verifying the proper running of NASTRAN on a CDC 6400 computer under Operating System Scope 3.4.

The final response analysis was performed with a model which included the shaker, container, and flatcar. The model had 145 grid points and 300 CBAR and

67 CSHEAR elements. Two major assumptions were made in the process of formulating the model. First, the formed structural shapes were assumed to be capable of resisting all the moment and force components. Second, the thin steel sheets were assumed to be functioning as shear panels only. The correlation between the theoretical and experimental accelerations shown in figure 2 indicates that the assumptions were correct.

The theoretical model is supported by two hinges at the center plates of the flatcar. Therefore, free-free rotational vibration is allowed about the axis passing through these two hinges. The COUPMASS feature in NASTRAN was used to obtain an even mass distribution of the model. The centrifugal forces generated by the rotation of the disks of the shaker were used as the input excitation. The responses of the container were computed by NASTRAN in terms of grid point displacements and accelerations as well as forces and stresses in the structural elements. The output of the program gives the response quantities in the form of magnitude and phase angle. Both the print and punch options were requested in the output. The card images of punch file are stored on magnetic tapes. These data will be reprocessed by an in-house program to compute the responses of the container at 36 time intervals in the excitation cycle. The instantaneous structural deformations at each interval will be plotted to serve as visual aids. Both the 5.0-Hz and 6.25-Hz responses were computed. The calculated accelerations are shown in figure 2.

CONCLUDING REMARKS

The analytical results from NASTRAN have correlated well with the experimental data. NASTRAN has proved to be a powerful tool in this application of analyzing railroad transportation equipment. In particular, NASTRAN can be used to optimize many design parameters with a reasonable amount of time and expenditure and to minimize repetitious testing procedures and prototype improvement in further refinement of the container design.

In the railroad industry, a trial-and-error approach using static analysis and testing has been the general practice. Dynamic analysis has not been applied in designing railroad equipment except in a few cases. The dynamic analysis reported herein indicates that a substantial saving in cost and time can be realized in new product development compared with the conventional approach.

The COUPMASS feature in NASTRAN helps to distribute the masses of the container more evenly with a relatively small number of grid points available in the theoretical model. It is a very useful option.

The direct solution technique that computes the total response solutions in one single run is far simpler than the modal analysis. Direct solution frees the analyst from the time consuming effort of computing and identifying the many vibrational modes to obtain the total response solution. Although the computing cost of direct solution is higher, the added cost is compensated by the saving in time and effort.

ACKNOWLEDGEMENTS

The Engineering personnel of the Southern Pacific are commended for their perserverance in pioneering this container concept. The authors also thank G. S. McNally for his support of the NASTRAN analysis. The data reduction efforts of T. Rowe and D. Green of Pullman-Standard Research & Development are much appreciated.

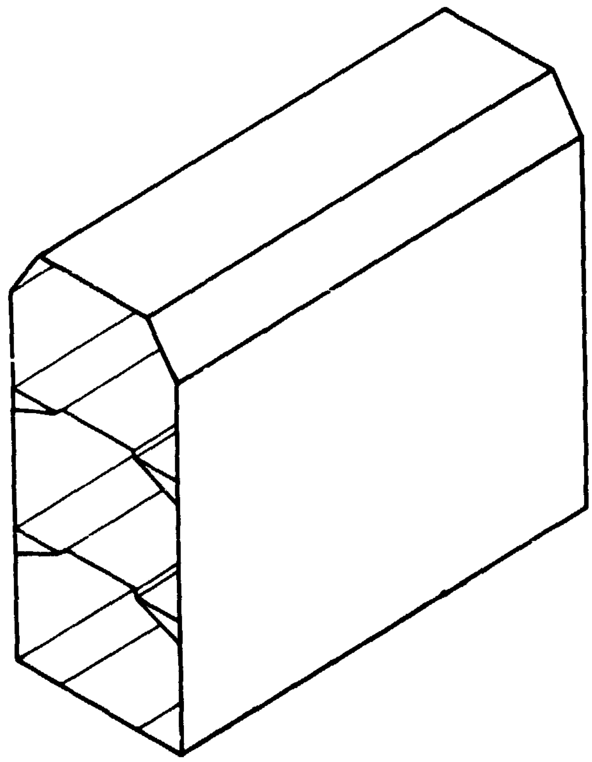

Figure 1.- Stac-Pac container.

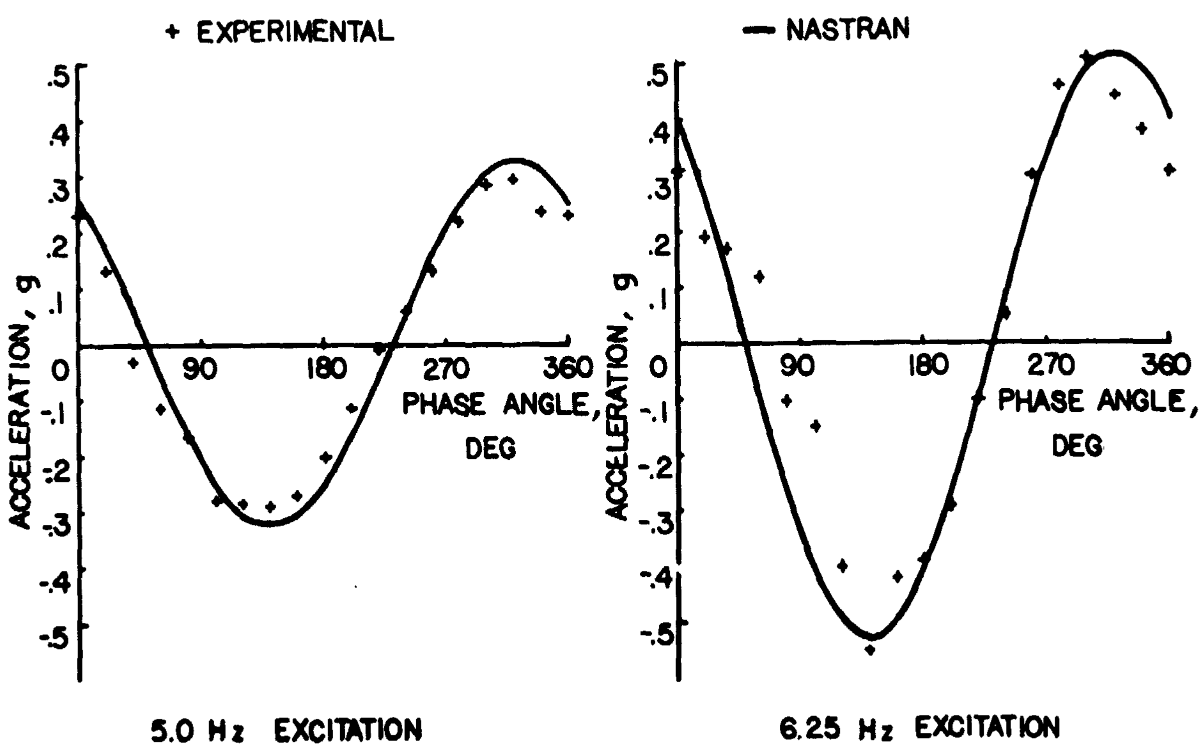

Figure 2.- Lateral acceleration of the container at 2nd deck.

N74-14418

IMPLEMENTATION EXPERIENCES OF NASTRAN ON CDC CYBER 74 SCOPE 3.4 OPERATING SYSTEM

By

James Chi-Dian Go
Computer Sciences Corp.

and

Ronald G. Hill
Westinghouse Hanford Company

SUMMARY

This paper describes the experiences of the implementation of the NASTRAN system on the CDC CYBER 74 SCOPE 3.4 Operating System. This Operating System is relatively new; however, due to the great flexibility of the NASTRAN system, no major problems were encountered.

INTRODUCTION

The implementation was fairly straightforward. Only minor changes were made. Various sizes of benchmark and test problems, ranging from two hours to less than one minute CP time, were run on CDC CYBER SCOPE 3.3, UNIVAC EXEC-8 and CDC CYBER SCOPE 3.4. No numerical discrepancy was found on the outputs of these test problems.

PROGRAM IMPLEMENTATION

The NASTRAN system was installed from the Level 15.1.1 executable, TAPE 1. This is accomplished by first making a library from the third file of the COSMIC supplied TAPE 3. This is needed by the NASTRAN boot program to satisfy externals (also to guarantee that SCOPE 3.4 routines would not come in and interfere). Second, a small COMPASS program called APACTGR is placed as the second record in the BOOT overlay.* The SCOPE utility routine COPYN is used, and the resulting file-name must be TAPE 1. This edited file may now be used to execute NASTRAN. The deck is listed below.

---

*This was suggested by Dr. James Rogers, Langley Research Center, NASA.

At present NASTRAN cannot be updated under SCOPE 3.4. The LRC compiler will not execute on our system and NASTRAN FORTRAN is not compatible with either RUN or FTN. Also, the NASTRAN COMPASS routines have to be modified to interface properly with 6RM. This updating problem can be fixed by acquiring LRC compiler source and LRC library and correcting the SCOPE 3.4 interface problem.

NASTRAN INSTALLATION DECK

```
NASTRAN,MT2,T6000.                                      JIM GO
ACCOUNT(PW=JGO123,UN=JIMCGO)
REQUEST,TP1,HY,VSN=TAPE1.  NASTRAN TAPE1
REQUEST,TP3,HY,VSN=TAPE3.  NASTRAN TAPE3
RFL(300000)
COMPASS.              ASSEMBLY APACTGR
REWIND(LGO)
COPYN(,TAPE1,TP1,LGO)            EDIT IN APACTGR
SKIPF(TP3,2,17,B)          SKIP TO NASTRAN LIBRARY
COPYBF(TP3,LIB)            COPY TO DISK
UNLOAD(TP1)
UNLOAD(TP3)
REQUEST,NASTLIB,*PF.
EDITLIB.               MAKE USERS LIBRARY
CATALOG(NASTLIB,NASTRANLIBRARY,ID=JIMCGO)
LIBRARY(NASTLIB)       DECLARE USERS LIBRARY
REQUEST,NASTRAN,*PF.
TAPE1. CATLOG(NASTRAN)
EXIT.    HAVE
CATALOG(NASTRAN,NASTRAN15,ID=JIMCGO,XR=JIMCGO)
NASTRAN. ATTACH
789
        IDENT       APACTGR
        ENTRY       APACTGR
APACTGR   DATA        0
        EQ          APACTGR
        END
789
1,1,TP1
1,1,LGO
1,*,TP1
"
LIBRARY(NASTLIB,NEW)
ADD(*,LIB)
```

```
FINISH.
ENDRUN.
789
ID BAR, OFFSET
SOL 1,0
APP DISPLACEMENT
TIME 5
CEND
TITLE = BAR OFF SET TEST RUN WITH UNIFORM LOAD
LOAD = 1
MAXLINES = 10000
LINE = 38
SPCFORCE = ALL
STRESS = ALL
DISP = ALL
BEGIN BULK
GRID    1                                       123456
GRID    2               2.5     -4.0
GRID    3               5.0                     123456
GRID    4                       5.0             123456
CBAR    1       1       1       2       4               2       +B1
+B1                     -5.     -4.
CBAR    2       1       2       3       4               2       +B2
+B2                                     5.      -4.
PBAR    1       1       1.0     2.0     2.0     1.0     1000.           +PB1
+PB1    2.0     1.0     -2.0    -1.0    2.0     -1.0    -2.0    1.0     +PB2
+PB2    1.0     1.0
MAT1    1       3 +7    1.2+7           0.0     6.5-6   70.     0.02    +M1
+M1     2.0+4   20.+3   1.8+4
GRAV    1               1.0             -1.0
ENDDATA
789
6789
```

PROGRAM CHECK RUNS

The benchmark and test problems employed range from more than two hours to less than one minute CP time. Most of these are actual reactor hardware problems that we are analyzing. These problems were run on CDC SCOPE 3.3, UNIVAC EXEC-8 and CDC SCOPE 3.4 The numerical outputs are almost identical between UNIVAC EXEC-8 and CDC and identical between CDC SCOPE 3.3 and 3.4.

Some typical run times and charge times, together with the brief description of the test problems, are shown as follows:

Test problem 1 has 994 GRID points and about 2500 DOF. The model consists only of plate elements. The run time shown was for static analysis.

Test problem II has 216 GRID points and about 500 dynamic DOF. The model consists of plate and bar elements. The run time shown was for normal mode analysis.

		Run Time Sec.	
Problem No.		CDC CYBER SCOPE 3.3	CDC CYBER SCOPE 3.4
I	CP	3316	3504
	IO	10949	411
	Charge Time	9972	7369
II	CP	1557	1708
	IO	3223	291
	Charge Time	4046	3683

WORK IN PROGRESS

We are currently implementing some special features into the NASTRAN system for our particular needs. Among these are: (a) incorporating some non-linear material capabilities which are in the formulation stage; (b) creating a seismic analysis Rigid Format which will be based on Rigid Format 3; and (c) replacing the NASTRAN plotting package with CALCOMP'S.

CONCLUSIONS

The implementation of NASTRAN on CDC SCOPE 3.4 encountered only a few minor problems which were readily corrected. This CYBER 74 SCOPE 3.4 Level 15.1.1 NASTRAN is now functioning as well as the other versions.

With similar hardware configuration, the CP time is about the same between SCOPE 3.3 and 3.4; however, the IO time of SCOPE 3.4 showed a significant improvement over SCOPE 3.3. The results obtained on CDC CYBER and UNIVAC 1108 are fairly close to those obtained by NASA. Many of the structural models had to be reduced in size in order to run them on UNIVAC 1108; with CYBER 7.4 SCOPE 3.4 we are now able to run all our structural problems without extensive model condensation. This makes the application of the NASTRAN system to large structural problems more straightforward and reduces extensive reliance on users' engineering judgment in structural modeling. We also believe this version will enable us to extend the capability of NASTRAN to non-linear material and geometry structural problems in the near future.

N74-14619

A METHOD FOR TRANSFERRING NASTRAN DATA BETWEEN DISSIMILAR COMPUTERS

By James L. Rogers, Jr.

NASA Langley Research Center

INTRODUCTION

The NASTRAN computer program is capable of executing on three different types of computers: namely, the CDC 6000 series, the IBM 360-370 series, and the UNIVAC 1100 series. A typical activity requiring transfer of data between dissimilar computers is the analysis of a large structure such as the Space Shuttle by substructuring. Models of portions of the vehicle which have been analyzed by subcontractors using their computers must be integrated into a model of the complete structure by the prime contractor on his computer. Presently the transfer of NASTRAN matrices or tables between two different types of computers is accomplished by punched cards or a magnetic tape containing card images. These methods of data transfer do not satisfy the requirements for intercomputer data transfer associated with a substructuring activity because (1) accuaracy will be lost due to the precision limitations (10 significant digits) of the NASTRAN Direct Matrix Input (DMI) punched card, and (2) large order matrices make card handling too cumbersome.

To provide a more satisfactory transfer of data, two new programs, RDUSER and WRTUSER, were created (ref. 1). These two programs, used in conjunction with the NASTRAN modules OUTPUT2 and INPUTT2 available in Level 15 and later versions of NASTRAN, allow data to be transferred between computers without loss of accuracy and without handling large decks of punched cards. The purpose of this paper is to describe both the method used for data transfer and the special features of the utility programs RDUSER and WRTUSER. Although data may come from any computer program using the NASTRAN user tape format, examples in this paper will be confined to NASTRAN data since RDUSER and WRTUSER were written with the NASTRAN user in mind.

OVERVIEW OF PROGRAMS

Beginning with Level 15, NASTRAN provided the capability of using FORTRAN WRITE statements to write intermediate data blocks (matrices or tables) on a magnetic tape. This was made possible by the NASTRAN module OUTPUT2 which has the following calling sequence:

```
OUTPUT2   DB1, DB2, DB3, DB4, DB5//V, N, P1/V, N, P2/V, N, P3   $
```


PRECEDING PAGE BLANK NOT FILMED

where the DBi are the data blocks to be written in tape, P1 is a parameter for positioning the tape, P2 is the FORTRAN unit number assigned to the tape, and P3 is the FORTRAN User Tape Label (default = XXXXXXXX).

The tape created by OUTPUT2 is a binary tape. Tapes created by programs other than NASTRAN are acceptable as long as the data are output in the OUTPUT2 format. In order to write the header information on the tape, the P1 parameter must be -1 (rewind before writing) the first time OUTPUT2 is called in NASTRAN; otherwise P1 is 0. This binary tape must be converted to a BCD tape before it can be used on a computer of a different type. The conversion is performed by the utility program RDUSER which accepts tables and single-precision or double-precision real or complex matrices. No precision is lost in generating the BCD tape, and the problem of handling large numbers of punched cards is alleviated.

The tape containing the BCD data is transferred to another installation. Before these data can be used as input for NASTRAN at this installation, two tasks must be performed. The first task is to convert the source of the BCD tape written by RDUSER to another source form readable by the computer on which the data will be used. The second task is to convert the BCD tape into an acceptable binary form for the NASTRAN module INPUTT2. The program WRTUSER accomplishes both of these tasks. The calling sequence for the INPUTT2 module has the form

INPUTT2/DB1, DB2, DB3, DB4, DB5/V, N, P1/V, N, P2/V, N, P3 $

where the DBi are the data blocks to be recovered from the binary tape, P1 is a parameter for positioning the tape (P1 must be -1 for the first call to INPUTT2 and 0 for all succeeding calls), P2 is the FORTRAN unit number assigned to the binary tape, and P3 is the FORTRAN User Tape Label (default = XXXXXXXX). A flow chart of the complete tape interface method is shown in figure 1.

SPECIAL FEATURES

The RDUSER program has three special features that will be covered in this section. The first group of cards input to RDUSER is a set of comments written by the user to describe the matrices and tables. These cards are read with a free-field format allowing the user to write any description he desires. These comments are also written on the tape to be transferred to the other installation. WRTUSER reads and prints these comments; this allows the user receiving the tape to have some knowledge of the data written on the tape. The next group of cards input to RDUSER gives the data block name, a code for determining whether the data block is a matrix or a table, and a print option. This group of cards allows the user to omit any data block that is not needed. He does this by simply omitting the card on which the data block name appears. The print option allows the user to print (table 1) or not to print (table 2) elements of a matrix or table. Each of these features proves beneficial when transferring data between dissimilar computers.

VERIFICATION OF PROGRAMS

RDUSER and WRTUSER were executed for four* of the nine possibilities shown in figure 2 and found to possess the desired qualities lacking in DMI punched cards. Card handling for the input to NASTRAN was cut to the minimum. Square, rectangular, and symmetric matrices containing single-precision real, single-precision complex, double-precision real, and double-precision complex elements were used in the test runs. In each case the answers listed on one computer agreed with the answers listed on dissimilar and similar computers: this indicated that no precision was lost in the transfer.

REFERENCES

1. Rogers, James L., Jr.: Intercomputer Transfer in Full Precision of Arbitrary Data on Magnetic Tape Employing the NASTRAN User Tape Format. NASA TM X-2901, 1973.

---

*UNIVAC paths were not tested due to errors in the INPUTT2 and OUTPUT2 NASTRAN modules.

TABLE 1.- MATRIX ELEMENTS LISTED

```
THE TRAILER FOR THE MATRIX X        IS     103      4      4      1      4     16  10000

MATRIX X        IS A COMPLEX    4 COLUMN X    4 ROW  SQUARE  MATRIX

COLUMN        1
 4.641280517078492096061 4D-01 -3.606805862524229411 2923D-01I  1.895414024789845441887 3D-01  5.234410102764064376401 6D-02I

 3.293246813840795539363 2D-01  6.502883705380408974393 9D-03I  3.122779396003039220630 6D-02 -1.013480564129243255422 4D-02I

COLUMN        2
 2.095260449953171288939 3D-01 -2.769428374815721127788 5D-01I  5.078898775495388484557 7D-02  1.517066612931428082333 7D-01I

 1.552401806298719932897 3D-01 -3.955750570825884437908 8D-01I -1.998464251633280674980 1D-02  3.292869385092132006320 8D-01I

COLUMN        3
 1.055162900898288569351 3D+00  2.466289509979642247117 2D-01I  5.235032828655512560089 8D-01 -1.101167393338876365760 4D+00I

 6.879333888610013048037 2D-01  5.547193119546030004585 2D-01I  1.287648142250047422763 3D-02 -1.013831340825070981281 9D+00I

COLUMN        4
 1.481475413733646107061 8D-01 -3.723247673339535879222 2D-01I  3.430122184911166272058 8D-02  4.479191581102277552872 7D-01I

 1.181121325621723450183 3D-01 -1.293530090035766022538 2D-01I  1.788362291043565921455 6D-02 -4.993508265143248303630 2D-03I

THE NUMBER OF NON-ZERO WORDS IN THE LONGEST RECORD       16

THE DENSITY OF THIS MATRIX IS    100.00 PERCENT

THIS MATRIX IS DOUBLE PRECISION
```

TABLE 2.- MATRIX ELEMENTS OMITTED

```
THE TRAILER FOR THE MATRIX B        IS     102     4     4     1     1     3   5625

MATRIX B        IS A REAL      4 COLUMN X    4 ROW   SQUARE  MATRIX

THE NUMBER OF NON-ZERO WORDS IN THE LONGEST RECORD         3

THE DENSITY OF THIS MATRIX IS     56.25 PERCENT

THIS MATRIX IS SINGLE PRECISION
```

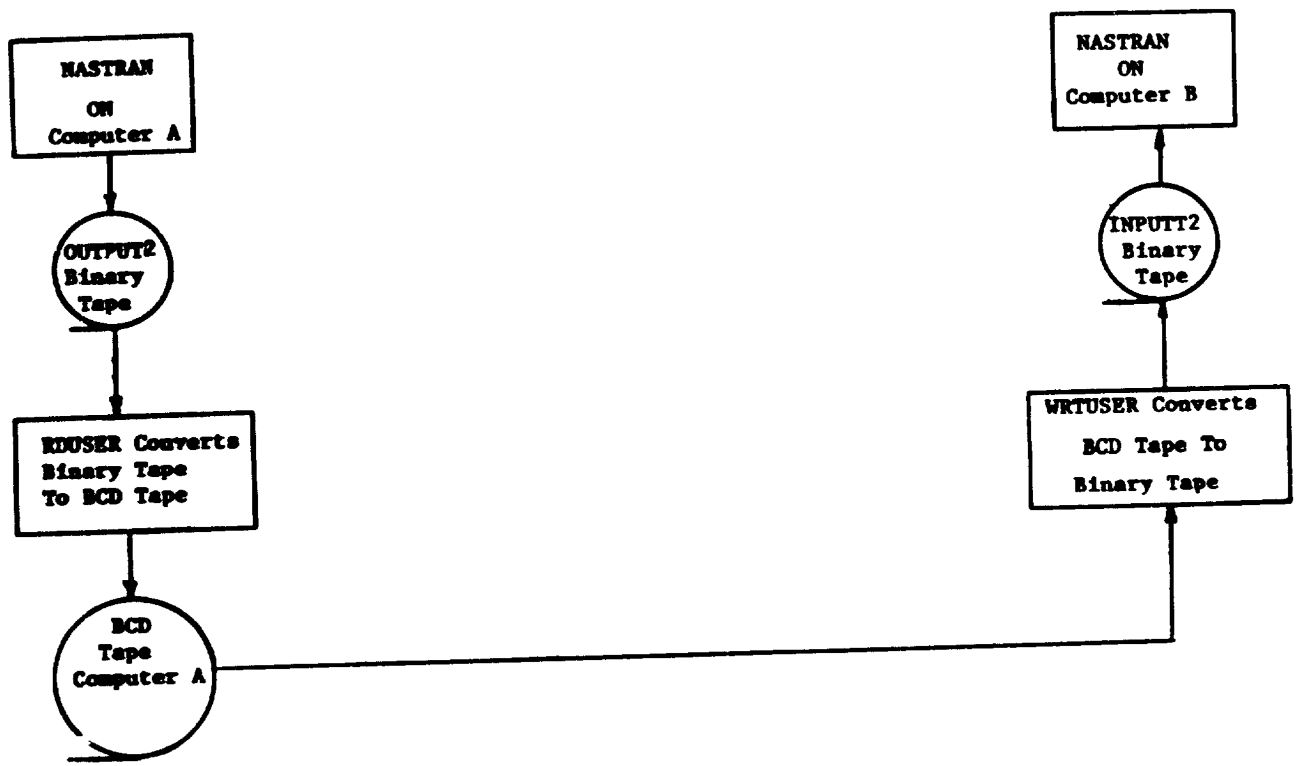

Figure 1. - Flow chart of NASTRAN tape interface method.

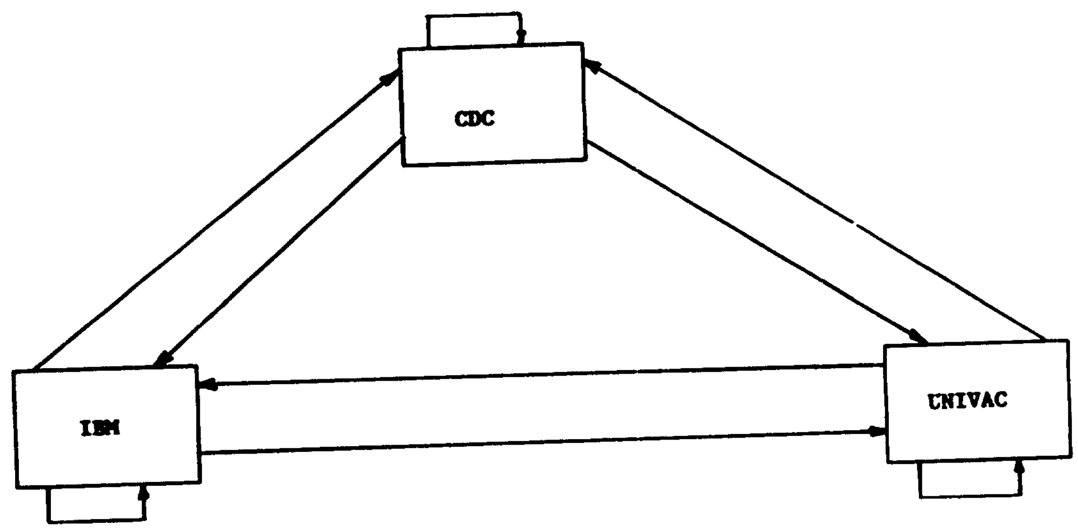

Figure 2. - Paths of data between computers.

N74-11620

AN INTERACTIVE NASTRAN PREPROCESSOR

By Willianna W. Smith
NASA Langley Research Center

SUMMARY

This paper describes a Langley Research Center version of NASTRAN Level 15.1.0 designed to provide the analyst with an added tool for debugging massive NASTRAN input data. The program checks all NASTRAN input data cards and displays on a CRT scope the graphic representation of the undeformed structure. In addition, the program permits the display and alteration of input data and allows reexecution without physically resubmitting the job. Core requirements on the CDC 6000 computer are approximately 77 000 octal words of central memory.

INTRODUCTION

As most NASTRAN users have discovered, there are input data errors made in defining a structure which are not illegal to the system but which will produce a rather oddly shaped graphic representation and erroneous analysis. It is imperative, therefore, that the structural plotter output be viewed before the user can be assured that his input data do not displace grid points or omit members. For a complex structure, it may be necessary to observe the picture from several orientations.

Motivated by the need for a complete checkout of structure-defining input data in the most rapid and efficient manner, development of an interactive type preprocessor was undertaken. Since the computer program described in reference 1 was already in existence, the decision was made to adapt it to the interacting CDC 250 CRT system. The Interactive NASTRAN Preprocessor Level 12.1.0 resulted from this adaptation. The NASTRAN portion has since been updated to Level 15.1.0.

The NASTRAN program and interactive graphic software used in the Interactive NASTRAN Preprocessor are designed to operate on the CDC 6600 computer at LRC, but the ideas are applicable to other NASTRAN computers.

PROGRAM DESCRIPTION

The following changes were made in the existing computer program (ref. 1):

1. NASTRAN routines[1] altered:

[1]Description of routines may be found in reference 2.

PRECEDING PAGE BLANK NOT FILMED

NAME	MODIFICATION
NASTRAN	Tape 4 declared
XSEM1	Added capability of displaying message on screen
IFP1D	Error "Plot Tape Not A Physical Tape" made nonfatal
SGINOFF	Plot file written on Tape 4
XSEM2	Added capability of displaying messages on screen
	Added labeled COMMON block with plot loop flag
	Added call to CRTPLOT subroutine
	Added statement to change a DMAP instruction parameter if plot loop flag set
PLOT	Test for physical tape ignored
PROCES	Added labeled COMMON block to hold view angles for display and alteration
	Add statements to save and restore view angles
LD50	Additions made to allow looping through PLTSET and PLOT instructions if angles altered and reexecution requested (appendix A)

2. Subroutine CRTPLOT (appendix B) was coded to read the NASTRAN General Purpose Plotter output file and translate it for display on the CDC 250 CRT terminal (fig. 1).

3. Interactive graphic routines[2] added to program:

SEMSAGE (same as MESAGE)	RSHFT
CDC250	ADVERSE

[2]See Langley Research Center Computer Programing Manual, Vol. II, Sections 3.2 and 3.11.

NEXT	SPACK (same as PACK)
PLT250	SLOCATE (same as LOCATE)
LODTBL	UNPK
DECOD3	CNTRLN
DECOD4	CREATEF
HOGWASH	DECOD1
WARTHOG	DECOD2
SCREEN	DROUTE
PLT000	EXOR
KEYBORD	I03
CRT250	NOTATE
SPCMAT	PLOTSW
KGLER	PLT9999
LOADADR	TRUNCL
CALPLT	SAVPLOT
WHERE	XMIT
ENCOD2	SCAN
STRCALL	

4. Modifications were made in the graphic routines where data statements were used to enter values for variables in labeled COMMON. Restrictions in the CDC Linkage Editor necessitated replacing the data statements with a Block Data subprogram.

5. Overlay structure (appendix C) was adjusted to incorporate graphic routines and subroutine CRTPLOT, which were added.

CAPABILITIES OF THE INTERACTIVE NASTRAN PREPROCESSOR

The Interactive NASTRAN Preprocessor has the following capabilities:

1. Analyzes all input data.

2. Displays the graphic representation of the undeformed structure on the CDC 250 CRT Scope.

3. The alphanumeric keyboard[3] on the CRT console provides a means for displaying the input and altering the input data.

4. Loops through the PLTSET and PLOT modules when only the view angle is altered are accomplished within the DMAP sequence of instructions. The program EDIT[4] initiates restarts when other input data are changed.

5. The CRT function keyboard has such options as (a) positive and negative magnification of the total display or a part of the display; (b) recording the plot vector file for postprocessing permanent hard copies; and (c) producing nonpermanent hard copies on a connected hard copy unit.

6. Executable in approximately 77 000 octal words of central memory.

LIMITATIONS OF THE INTERACTIVE NASTRAN PREPROCESSOR

The Interactive NASTRAN Preprocessor has the following limitations:

1. Operational on CDC 6000 Computer complex at LRC; however ideas are applicable to other NASTRAN computers.

2. Displacement approach must be used.

3. Does not contain NASTRAN checkpoint or restart capabilities.

4. No punch output available.

5. Alterations to input data are made internal to the computer only; therefore, the user should make note of modifications so that he may make appropriate changes in the physical deck.

OPERATIONAL INSTRUCTIONS

The interactive NASTRAN program is housed on a data cell and requires no physical tapes unless the user wishes to save the plot vector file for permanent hard copies. The EDIT program is also housed on a data cell.

[3] Langley Research Center Computer Programing Manual, Vol. II, Section 3.6.

[4] Langley Research Center Simulation Manual, Section 2221.1.

1. Deck Setup

```
                                                   Col. 68              Col. 78
JOB, ..........................                                            X
USER,..........................                                            X
FETCH(C1103, XXXX, BINARY, EDIT)     XXXX = data cell                      X
LOAD (EDIT)                                                                X
EXECUTE (BLOCKCC)                                                          X
COMMENT.                                X
COMMENT. END CONTROL BLOCK                                                 X
REQUEST, CRTTPE, CD. PLEASE ASSIGN XX  XX = CRT No.
FETCH (D3790, XXXX, BINARY, PREF1)   XXXX = data cell
NORFL.
LINECNT (10000)
PREF1. CATLOG (PREF)
COMMENT. END SETUP BLOCK
PREF.
REWIND (SAVPLT)
COPYBF (SAVPLT, TEMP)  Required if hard copy plots desired
BKS (TEMP, 1)
LOAD (EDIT)
COMMENT. END EXECUTE BLOCK
FETCH (P0077, XXXX, BINARY, DDIPRO) DDI, 80 Postprocessor   Required for
                                                            hard copy for
REWIND (TEMP)                                               plots
REWIND (SAVPLT)
DDIPRO (INITIALS, BLDG. NO., Division initials, zero)
COMMENT. END STOP BLOCK
EXIT.
```

1. Deck Setup (continued) | Col. 68 | Col. 78

LOAD (EXIT)

EXECUTE (RESTART)

COMMENT. END RESTART BLOCK

End of record card

NASTRAN data deck

End of file card

2. Input

Input data are the same as for a regular NASTRAN run with the exception that the user must request NASTPLT output on the PLOTTER case control card.

3. Output

The Program produces the normal NASTRAN printed output from the Preface area of the program and from the structural plot module. The graphic representation of the undeformed structure is displayed on the CRT as it is being generated. Plots may be recorded for obtaining hard copies on one of the available plotters by depressing the appropriate function key on the CRT console. The proper postprocessor control cards must have been included in the card deck.

Since changes are made internal to the computer only, the user should make note of any such modifications so that he can make the appropriate changes in the physical deck.

APPENDIX A

NASTRAN ROUTINE LD50

FOR INTERACTIVE NASTRAN PREPROCESSOR

FORTRAN Code for Subroutine LD50

```
      SUBROUTINE LD50(SUBSET)
      INTEGER RD(161)
      INTEGER RD1(61), RD2(100)
      EQUIVALENCE (RD(1),RD1), (RD(62),RD2)
      DATA NPTP/4HNPTP/
      INTEGER IS1(20)
      DATA IS1/1,1,1,1,1,1,1,1,1,1,1,1,1,1,1,1,1,1,1,1/
      DATA RD1/
     A4HBEGI, 4HN PR, 4HEFAC, 4HE - , 4HCHEC, 4HKS I, 4HNPUT, 4H AND,
     B4H PLO, 4HTS U, 4HNDEF, 4HORME, 4HD ST, 4HRUCT, 4HURE , 4HS    ,
     C4HGP1 , 4HGEOM, 4H1,GE, 4HOM2,, 4H/GPL, 4H,EQE, 4HXIN,, 4HGPDT,
     D4H,CST, 4HM,BG, 4HPDT,, 4HSIL/, 4HV,N,, 4HLUSE, 4HT/C,, 4HN,12,
     E4H3/V,, 4HN,NO, 4HGPDT, 4H S   , 4HSAVE, 4H LUS, 4HET S, 4HGP2 ,
     F4HGEOM, 4H2,EQ, 4HEXIN, 4H/ECT, 4H S   ,
     14HLABE, 4HL W1, 4H S   ,
     24HPLTS, 4HET P, 4HCDB,,
     G4HEQEX, 4HIN,E, 4HCT/P, 4HLTSE, 4HTX,P, 4HLTPA, 4HR,GP, 4HSETS,
     Z4H,ELS, 4HETS /
      DATA RD2/
     H4H/V,N, 4H,NS1, 4HL/V,, 4HN,JU, 4HMPPL, 4HOT S, 4HSAVE, 4H NS1,
     I4HL,JU, 4HMPPL, 4HOT S, 4HPRTM, [illegible]SG P, 4HLTSE, 4HTX//, 4H S   ,
     J4HSETV, 4HAL /, 4H/V,N, 4H,PLT, 4HFLG/, 4HC,N,, 4H1[illegible], 4HN,PF,
     K4HILE/, 4HC,N,  4HO S , 4HSAVE, 4H PLT, 4HFLG,, 4HPFIL, 4HE S ,
     L4HCOND, 4H P1,, 4HJUMP, 4HPLOT, 4H S   , [illegible]HPLOT, 4H PLT, 4HPAR,,
     M4HGPSE, 4HTS,E, 4HLSET, 4HS,CA, 4HSECC, 4H,BGP, 4HDT,E, 4HQEX1,
     N4HN,S1, 4HL,,/, 4HPLOT, 4HX1/V, 4H,N,N, 4HSIL/, 4HV,N,, 4HLUSE,
     O4HT/V,, 4HN,JU, 4HMPPL, 4HOT/V, 4H,N,P, 4HLTPL, 4HG/V,, 4HN,PF,
     P4HILE , 4HS    , 4HSAVE, 4H JUM, 4HPPLO, 4HT,PL, 4HTFLG, 4H,PF1,
     Q4HLE S, 4HPRTM, 4HSG P, 4HLOTX, 4H1//S,
     14HCOND, 4H W2,, 4HPFIL, 4[illegible]E S , 4HJUMP,4H P1 , 4HS    , 4HLABE,
     24HL W2, 4HS    , 4HREPT, 4H W1,, 4H100 ,4HS    ,
     34HLABF, 4HL P1, 4HS    ,
     R4HEND , 4HS    , 4H    , 4H    , 4H    , 4H    /
      CALL WRITE (NPTP,RD,160,1)
      CALL WRITE (NPTP,20,1,0)
      CALL WRITE (NPTP,1,1,0)
      CALL WRITE(NPTP,IS1,20,0)
      CALL WRITE(NPTP,0,1,0)
      RETURN
      END
```

```
DMAP-DMAP INSTRUCTION
  NO.
 1 BEGIN     PREFACE - CHECKS INPUT AND PLOTS UNDEFORMED STRUCTURE $

 2 GP1       GEOM1,GEOM2,/GPL,EQEXIN,GPDT,CSTM,BGPDT,SIL/V,N,LUSET/C,N,123/
             V,N,NOGPDT $

 3 SAVE      LUSET $

 4 GP2       GEOM2,EQEXIN/ECT $

 5 LABEL     W, $

 6 PLTSET    PCDB,EQEXIN,ECT/PLTSETX,PLTPAR,GPSETS,ELSETS /V,N,NSIL/V,N,
             JUMPPLOT $

 7 SAVE      NSIL,JUMPPLOT $

 8 PRTMSG    PLTSETX// $

 9 SETVAL    //V,N,PLTFLG/C,N,1/V,N,PFILE/C,N,0 $

10 SAVE      PLTFLG,PFILE $

11 COND      P1,JUMPPLOT $

12 PLOT      PLTPAR,GPSETS,ELSETS,CASECC,BGPDT,EQEXIN,SIL,,/PLOTX1/V,N,NSIL/
             V,N,LUSET/V,N,JUMPPLOT/V,N,PLTFLG/V,N,PFILE $

13 SAVE      JUMPPLOT,PLTFLG,PFILE $

14 PRTMSG    PLOTX1//$

15 COND      W2,PFILE $

16 JUMP      P1 $

17 LABEL     W2$

18 REPT      W1,100 $

19 LABEL     P1$

20 END       $
```

APPENDIX B

FORTRAN CODED SUBROUTINE CRTPLOT

```
      SUBROUTINE CRTPLOT
      COMMON/SPEC/NVIEW,CALPHA,CBETA,CGAMMA
      COMMON/CRT/NCRT
      DIMENSION A(30),ID(2)
      DIMENSION IANS(30)
      DIMENSION STRING(60)
      INTEGER PC,CI,TEN
      DATA ID/3HWWS,8HBIN 2058/
      DATA STRING/
     1  1H0,1H1,1H2,1H3,1H4,1H5,1H6,1H7,1H8,1H9,1HA,1HB,1HC,1HD,1HE,1HF
     2, 1HG,1HH,1HI,1HJ,1HK,1HL,1HM,1HN,1HO,1HP,1HQ,1HR,1HS,1HT,1HU,1HV
     3, 1HW,1HX,1HY,1HZ,1H(,1H),1H+,1H-,1H*,1H/,1H=,1H.,1H,,1H$,1H-,1H
     4, 12*0/
      EQUIVALENCE (IANS(1),IS2), (IANS(2),IS3), (IANS(3),IS4), (IANS(4),
     1IR0), (IANS(5),IR1), (IANS(6),IR2), (IANS(7),IR3), (IANS(8),IR4),
     2(IANS(9),CI), (IANS(10),PC), (IANS(11),IU2), (IANS(12),IU3),
     3(IANS(13),IU4), (IANS(14),IT0), (IANS(15),IT1), (IANS(16),IT2),
     4(IANS(17),IT3), (IANS(18),IT4), (IANS(19),IS0), (IANS(20),IS1),
     5(IANS(29),IU0), (IANS(30),IU1)
      NVIEW = 0
      NCRT=0
      NFIRST = 0
      REWIND 4
      WRITE(6,1001)
 1001 FORMAT(1H1)
      TEN = 10
      MASK = 77B
      CALL CDC 250
      CALL CALPLT(0,0,3)
      CALL SMESAGE(1,35HBEGIN EXECUTION OF CRT PLOT PROGRAM,35)
      CALL PARAMS
      CALL PARAMS(5LALPHA,CALPHA,4LBETA,CBETA,5LGAMMA,CGAMMA)
  800 READ(4) A
      IF(EOF,4) 99,10
   10 CONTINUE
      DO 1 I=1,30,3
      L = I+2
      K = 0
      DO 15 N=I,L
      DO 15 J=1,10
      K= K+1
      IF(J.EQ.1) GO TO 17
      CALL RSHFT(A(N),6)
   17 IANS(K) = (A(N).AND.MASK)
   15 CONTINUE
      IF(PC.GT.6) PC=PC-10
      IF(PC.EQ.0.OR.PC.EQ.2.OR.PC.EQ.3) GO TO 300
      R = TEN*(TEN*(TEN*(TEN*IR4 +IR3)+IR2)+IR1)+IR0
      S = TEN*(TEN*(TEN*(TEN*IS4 +IS3)+IS2)+IS1)+IS0
      T = TEN*(TEN*(TEN*(TEN*IT4 +IT3)+IT2)+IT1)+IT0
      U = TEN*(TEN*(TEN*(TEN*IU4 +IU3)+IU2)+IU1)+IU0
  300 NC = PC+1
      GO TO (401,402,403,404,405,406,406), NC
C*
C* PLOT COMMAND IS NO OPERATION
C*
  401 GO TO 1
C*
C* PLOT COMMAND IS START NEW PLOT
```

```
C*
  402 PLOTID = R
      XMIN = 0.0
      YMIN = 0.0
      XMAX = S
      YMAX = T
      XSCALE = 10.0/XMAX
      YSCALE = 10.0/YMAX
      GO TO 1
C*
C* PLOT COMMAND IS SELECT CAMERA
C*
  403 GO TO 1
C*
C* PLOT COMMAND IS SKIP TO A NEW FRAME
C*
  404 CONTINUE
      IF(NFIRST.EQ.0) GO TO 4041
      CALL CALPLT(0.0,-3)
      CALL SMESAGE(1,32HTO RECORD PLOT, DEPRESS FN KEY 6,32)
      CALL SMESAGE(1,34HTO CLEAR PICTURE, DEPRESS FN KEY 2,34)
      CALL SMESAGE(1,37HTO GO TO NEXT FRAME, DEPRESS FN KEY 3,37)
      CALL CALPLT(12.0,0.,-3)
      CALL SMESAGE(1,30HHIT KEY 45 TO END PLOT PROGRAM,30)
      CALL SMESAGE(1,39HHIT KEY 47 TO RE-DISPLAY PREVIOUS PLOTS,39)
      CALL SMESAGE(1,38HHIT ANY OTHER KEY TO CONTINUE PLOTTING,38)
      CALL NEXT(N)
      IF(N.EQ.45) GO TO 99
      IF(N.EQ.47) GO TO 199
      GO TO 1
 4041 CONTINUE
      NFIRST = 1
      GO TO 1
C*
C* PLOT COMMAND IS TYPE A CHARACTER
C*
  405 X = R*XSCALE
      Y = S*YSCALE
      CALL NOTATE(X,Y,.1,STRING(CI),0.0,1)
      GO TO 1
C*
C* PLOT COMMAND IS DRAW A LINE OR AN AXIS.
C*
  406 CONTINUE
      X1 = R*XSCALE
      Y1 = S*YSCALE
      X2 = T*XSCALE
      Y2 = U*YSCALE
      CALL CALPLT(X1,Y1,3)
      CALL CALPLT(X2,Y2,2)
 4062 GO TO 1
    1 CONTINUE
      GO TO 800
C*
C* RE-DISPLAY PREVIOUS PLOTS
C*
  199 REWIND 4
      GO TO 800
C*
C* END OF PLOT TAPE
```

```
C*                                                                      CRT0121
   99 CONTINUE                                                          CRT0122
      CALL CALPLT(0.0,999)                                              CRT0123
      CALL SMESAGE(1,20HEND OF FILE ON TAPE4,20)                        CRT0124
      REWIND 4                                                          CRT0125
C**********                                                             CRT0126
C                 BREAK POINT IN PROGRAM TO ALLOW OPERATOR TO DISPLAY   CRT0127
C                 AND/OR CHANGE THE CURRENTLY ESTABLISHED VIEW ANGLE.   CRT0128
C$$$$$$$$$$                                                             CRT0129
      CALL SMESAGE(1,50HTO DISPLAY AND/OR CHANGE THE CURRENTLY ESTABLISH CRT0130
     1ED,50)                                                            CRT0131
      CALL SMESAGE(1,34HVIEW ANGLE**ALPHA,BETA AND GAMMA**,34)          CRT0132
      CALL SMESAGE(1,43HALTER THE APPROPIATE ANGLE AND PRESS KEY 49,43) CRT0133
      CALL NEXT(NK)                                                     CRT0134
      IF(NK.NE.49) GO TO 499                                            CRT0135
      NVIEW = 1                                                         CRT0136
      NCRT = 2                                                          CRT0137
  499 WRITE(6,4999) NVIEW,NCRT,NK,CALPHA ,CBETA,CGAMMA                  CRT0138
 4999 FORMAT(12H0*****NVIEW=I4,7H  NCRT=I4,5H  NK=I4/                   CRT0139
     A10H0**CALPHA=E20.8,8H  CBETA=E20.8,9H  CGAMMA=E20.8)              CRT0140
      RETURN                                                            CRT0141
      END                                                               CRT0142
```

APPENDIX C

LINKAGE EDITOR CONTROL CARDS FOR

INTERACTIVE NASTRAN PREPROCESSOR

```
LINKEDIT LET,OUTFILE=NAST(T),PARAM(4)=20,PARAM(5)=50,PARAM(6)=6000,
 PARAM(2)=1200
LIBRARY NASTOBJ/WWS/BNFILE/XCAL
LINK  0
RENAME APACTGR = ABSENT.
RENAME LABRT = ABSENT.
RENAME GATOR = ABSENT.
RENAME   RECOVRY = RETURN  $$  RCV NOT AVAILABLE AT CDC DATA CENTER
RENAME   XWRITE(I06600) = WRITEX    $---BLAST I/O FEATURE---$
RENAME   XREAD (I06600) = READX     $---BLAST I/O FEATURE---$
RENAME  SYSTEM = SYSTEM.
RENAME   PEXIT = LINK20.
RENAME  MSGWRT = LINK20.
RENAME  RWUNLD = RETURN
INCLUDE NASTOBJ(GINO,         XCORSZ)
INCLUDE WWS(NASTRAN)
INCLUDE WWS(BLKDATA(TIME))
INCLUDE NASTOBJ(NASTRAN,BLKDATA(TIME),BLKDATA(GINO66),CONMSG)
INCLUDE NASTOBJ(I06600,DUMP,RETURN)
INCLUDE NASTOBJ(XEOT,TMTOGO,WRTTRL,RDTRL)
INCLUDE NASTOBJ(WRTTRLZ,MESAGE,FNAME)
INCLUDE NASTOBJ(OPNCOR,WRTCOR,RDCOR,OPNCORZ,PRELOC,LOCATE,PRELOCZ)
INCLUDE NASTOBJ(GOPEN,FREAD,CLSTAB,SSWTCH)
INCLUDE NASTOBJ(DSIGN) $ FIX FOR 0 ARGUMENTS
INCLUDE WWS(BLKDATA(SPEC))
INCLUDE WWS(BLKDATA(CRT))
INSERT CRT
INSERT  SYSTEM,GINOX,TIME,GINO66
INSERT  ZBLPKX,ZNTPKX,PACKX,UNPAKX
ENTRY  NASTRAN
END


LINK  1
RENAME CORSZ = XCORSZ
RENAME NTRAN=DUMP $ 1108 DECK ONLY
RENAME SEARCH=DUMP $ NOT USED ON THE 6400/6600
RENAME   SYSTEM = SYSTEM. $ RENAME THE CDC SYSTEM ROUTINE CALLS
RENAME   PEXIT = LINK20.
RENAME SEMTRN = RETURN
RENAME  XOR     = XORF
RENAME  LD01 = LD50
RENAME  LD02 = LD50
RENAME  LD03 = LD50
RENAME  LD04 = LD50
RENAME  LD05 = LD50
RENAME  LD06 = LD50
RENAME  LD07 = LD50
RENAME  LD08 = LD50
RENAME  LD09 = LD50
RENAME  LD10 = LD50
RENAME  LD11 = LD50
RENAME  LD12 = LD50
RENAME  LD13 = LD50
RENAME  LD45    = LINK20.
RENAME  LD46    = LINK20.
```

```
RENAME   LD47    = LINK20.                                                   LKED0056
RENAME   LD48    = LINK20.                                                   LKED0057
RENAME   LD49    = LINK20.                                                   LKED0058
RENAME   LD51    = LINK20.                                                   LKED0059
RENAME BUG = RETURN                                                          LKED0060
RENAME   TTLPGE = RETURN                                                     LKED0061
INCLUDE WWS(XSEM1)                                                           LKED0062
INCLUDE NASTOBJ(XSEM1,TAPBIT,PAGE,PAGE1,PAGE2,PAGEZZZ)                       LKED0063
INCLUDE NASTOBJ(BLKDATA(XSRTBD))                                             LKED0064
INSERT   XSRTBD,ZZZPAGE,BLANK,,                                              LKED0065
OVERLAY A1                                                                   LKED0066
INCLUDE NASTOBJ(MSGWRT,USRMSG)                                               LKED0067
OVERLAY A1                                                                   LKED0068
INCLUDE WWS(SMESAGE)                                                         LKED0069
INCLUDE WWS(CDC250,NEXT,PLT250)                                              LKED0070
INCLUDE WWS(LODTBL)                                                          LKED0071
INCLUDE BNFILE(CDC250,DECOD3,DECOD4,HOGWASH,LODTBL,NEXT,PLT250)              LKED0072
INCLUDE BNFILE(WARTHOG,SCREEN)                                               LKED0073
INCLUDE WWS(PLT000,KEYBORD,CRT250)                                           LKED0074
INCLUDE WWS(SPCMAT)                                                          LKED0075
INCLUDE WWS(KG1FR)                                                           LKED0076
INCLUDE XCAL(CALPLT)                                                         LKED0077
INCLUDE WWS(ENCOD2,RSHFT,ADVERSE,SPACK,SLOCATE,CALPLT,UNPK,CNTRLN)           LKED0078
INCLUDE WWS(CREATEF,DECOD1,DECOD2,DROUTE,EXOR,IO3,NOTATE,PLOTSW)             LKED0079
INCLUDE WWS(PLT9999,SAVPLOT,SCAN,STRCALL,TRUNCL,WHERE,XMIT,LOADADR)          LKED0080
INCLUDE WWS(BLKDATA(GRAPHNO))                                                LKED0081
INSERT GRAPHNO,LANGLEY,TRIAL,VPARMS                                          LKED0082
OVERLAY A1                                                                   LKED0083
INCLUDE WWS(BTSTRP)                                                          LKED0084
INCLUDE NASTOBJ(BTSTRP,ENDSYSZ,ENDSYS,BGNSYS)                                LKED0085
INSERT   ZENDSYS                                                             LKED0086
OVERLAY ENDSSS                                                               LKED0087
INSERT   ENDSSS                                                              LKED0088
OVERLAY A1                                                                   LKED0089
INCLUDE NASTOBJ(XPOLCK,XFILPS,XPLEQK,XPOLCKZ)                                LKED0090
OVERLAY X1X                                                                  LKED0091
INCLUDE NASTOBJ(XCEI,XPURGE)                                                 LKED0092
OVERLAY X1X                                                                  LKED0093
INCLUDE NASTOBJ(BLKDATA(XSFA1),XSFA,XSOSGN,XCLEAN,XPUNP,XDPH)                LKED0094
INSERT   XSFA1,ZXPOLCK                                                       LKED0095
OVERLAY ESFA                                                                 LKED0096
INSERT   ESFA                                                                LKED0097
OVERLAY A1                                                                   LKED0098
INCLUDE NASTOBJ(BLKDATA(IFPX0),BLKDATA(IFPX1),BLKDATA(UMFZZZ),SEMINT)        LKED0099
INSERT   IFPX0,XOLDPT,IFPX1,UMFZZZ                                           LKED0100
OVERLAY DD                                                                   LKED0101
INCLUDE NASTOBJ(XRCARD)                                                      LKED0102
OVERLAY D                                                                    LKED0103
INCLUDE NASTOBJ(GNFIAT,        XCSA,XRGDFM,XSBSET)                           LKED0104
INCLUDE NASTOBJ(WALTIM)                                                      LKED0105
OVERLAY E1                                                                   LKED0106
INSERT   XCSABF                                                              LKED0107
OVERLAY E1                                                                   LKED0108
INCLUDE WWS(LD50)                                                            LKED0109
OVERLAY D                                                                    LKED0110
INCLUDE NASTOBJ(SORT)                                                        LKED0111
OVERLAY DE                                                                   LKED0112
```

```
INCLUDE NASTOBJ(BLKDATA(IFP1A),FNDPLT)                                    LKED0113
INCLUDE WWS(IFP1D)                                                        LKED0114
INCLUDE NASTOBJ(IFP1,IFP1C,IFP1D,IFP1E,IFP1F,IFP1G,SWSRT)                 LKED0115
INSERT  SETUP,IFP1A                                                       LKED0116
OVERLAY IFP1X                                                             LKED0117
INSERT  IFP1X                                                             LKED0118
OVERLAY DE                                                                LKED0119
INCLUDE NASTOBJ(IFP4B,IFP4C,IFP4E,IFP4F,IFP4G,BISRCH)                     LKED0120
OVERLAY IFP45                                                             LKED0121
INCLUDE NASTOBJ(IFP4,IFP4A)                                               LKED0122
OVERLAY IFP4ZZ                                                            LKED0123
INSERT  IFP4ZZ                                                            LKED0124
OVERLAY IFP45                                                             LKED0125
INCLUDE NASTOBJ(IFP5,IFP5A)                                               LKED0126
OVERLAY IFP5ZZ                                                            LKED0127
INSERT  IFP5ZZ                                                            LKED0128
OVERLAY D                                                                 LKED0129
INCLUDE NASTOBJ(XFADJ1,XRECPS,XFADJ,CRDFLG,RPAGE,XBCDBI,EXTINT,INITCO)    LKED0130
INCLUDE NASTOBJ(XPRETY,INTEXT,XRECPSZ,ISFT)                               LKED0131
INSERT  ZXRECPS                                                           LKED0132
OVERLAY UMF                                                               LKED0133
INCLUDE NASTOBJ(XSORT)                                                    LKED0134
OVERLAY ESORT                                                             LKED0135
INSERT  ESORT                                                             LKED0136
OVERLAY UMF                                                               LKED0137
INCLUDE NASTOBJ(UMFEDT)                                                   LKED0138
OVERLAY UMFXXX                                                            LKED0139
INSERT  UMFXXX                                                            LKED0140
OVERLAY D                                                                 LKED0141
INCLUDE NASTOBJ(BLKDATA(XGPI2),BLKDATA(XGPIC),XGPI,XGPIDG,XGPIMW)         LKED0142
INCLUDE NASTOBJ(XGPIDGZ)                                                  LKED0143
INSERT  XGPIC,XGPID,XGPI2,XGPI3,XGPI4,XGPI5,XGPI6,XGPI7,XGPI8,XGPI2X      LKED0144
INSERT  ZXGPIDG                                                           LKED0145
OVERLAY E                                                                 LKED0146
INCLUDE NASTOBJ(BLKDATA(XLKSPC),XGPIBS,MPLPRT)                            LKED0147
INSERT  XLKSPC                                                            LKED0148
OVERLAY XGPI1 $ THIS MUST BE UNDER LONGEST SEGMENT UNDER OVERLAY E        LKED0149
INSERT  XGPI1                                                             LKED0150
OVERLAY E                                                                 LKED0151
INCLUDE NASTOBJ(XFLORD,XFLDEF)                                            LKED0152
OVERLAY E                                                                 LKED0153
INCLUDE NASTOBJ(OSCDMP)                                                   LKED0154
OVERLAY E                                                                 LKED0155
INCLUDE NASTOBJ(XOSGEN,XLNKHD,XIPFL,XPARAM,XSCNDM)                        LKED0156
OVERLAY DD                                                                LKED0157
INCLUDE NASTOBJ(IFPDCO)                                                   LKED0158
INCLUDE NASTOBJ(BLKDATA(IFPDTA))                                          LKED0159
INSERT  IFPDTA                                                            LKED0160
OVERLAY DDD                                                               LKED0161
INCLUDE NASTOBJ(RCARD,IFP)                                                LKED0162
INCLUDE NASTOBJ(BLKDATA(IFPX2),BLKDATA(IFPX3),BLKDATA(IFPX4))             LKED0163
INCLUDE NASTOBJ(BLKDATA(IFPX5),BLKDATA(IFPX6),BLKDATA(IFPX7))             LKED0164
INSERT  IFPX2,IFPX3,IFPX4,IFPX5,IFPX6,IFPX7                               LKED0165
OVERLAY DD1                                                               LKED0166
INCLUDE NASTOBJ(IFS1P)                                                    LKED0167
```

```
OVERLAY DD1
INCLUDE NASTOBJ(IFS2P)
OVERLAY IFPXX
INSERT  IFPXX
OVERLAY DD1
INCLUDE NASTOBJ(IFS3P)
OVERLAY DD1
INCLUDE NASTOBJ(IFS4P)
OVERLAY DD1
INCLUDE NASTOBJ(IFS5P)
OVERLAY DDD
INCLUDE NASTOBJ(BLKDATA(IFP3BD),IFP3,IFP3B)
INSERT  IFP3BD,IFP3LV
OVERLAY IFP3ZZ
INSERT  IFP3ZZ
ENTRY   XSEM1
END

LINK  2
RENAME CORSZ = XCORSZ
RENAME NTRAN=DUMP $ 1108 DECK ONLY
RENAME SEARCH=DUMP $ NOT USED ON THE 6400/6600
RENAME    PEXIT = LINK20.
RENAME   BTSTRP = RETURN
RENAME    SYSTEM = SYSTEM.
RENAME   SETC = RETURN
RENAME   TA1D    = RETURN
RENAME   TA1E    = RETURN
RENAME TAPSW1 = ABSENT.
RENAME OPMESG = ABSENT.
INCLUDE WWS(XSEM2)
INCLUDE NASTOBJ(XSEM2,TAPBIT,INTLST)
INCLUDE NASTOBJ(RDMODE,RDMODX,RDMODXZ)
INCLUDE NASTOBJ(RDMODY,RDWORD)
INSERT  ZRDMODX,BLANK,.
OVERLAY ONE
INCLUDE NASTOBJ(PAGE,PAGE1,PAGE2,PAGEZZZ)
INSERT  ZZZPAGE
OVERLAY A
INCLUDE NASTOBJ(MSGWRT,USRMSG)
OVERLAY A
INCLUDE WWS(SMESAGE)
INCLUDE WWS(LODTBL)
INCLUDE WWS(CDC250,NEXT,PLT250)
INCLUDE BNFILE(CDC250,DECOD3,DECOD4,HOGWASH,LODTBL,NEXT,PLT250)
INCLUDE BNFILE(WARTHOG,SCREEN)
INCLUDE WWS(PLT000,KEYBORD,CRT250)
INCLUDE WWS(SPCMAT)
INCLUDE WWS(KG1FR)
INCLUDE XCAL(CALPLT)
INCLUDE WWS(ENCOD2,RSHFT,ADVERSE,SPACK,SLOCATE,CALPLT,UNPK,CNTRLN)
INCLUDE WWS(CREATEF,DECOD1,DECOD2,DROUTE,EXOR,IO3,NOTATE,PLOTSW)
INCLUDE WWS(PLT9999,SAVPLOT,SCAN,STRCALL,TRUNCL,WHERE,XMIT,LOADADR)
INCLUDE WWS(PARAMS)
```

```
INCLUDE WWS(CRTPLOT)                                                       LKED0221
INCLUDE WWS(BLKDATA(GRAPHNO))                                              LKED0222
INSERT GRAPHNO,LANGLEY,TRIAL,VPARMS                                        LKED0223
OVERLAY A                                                                  LKED0224
INCLUDE NASTOBJ(ENDSYSZ,ENDSYS,BGNSYS)                                     LKED0225
INSERT  ZENDSYS                                                            LKED0226
OVERLAY ENDSSS                                                             LKED0227
INSERT  ENDSSS                                                             LKED0228
OVERLAY A                                                                  LKED0229
INCLUDE NASTOBJ(QPARAM)                                                    LKED0230
OVERLAY A                                                                  LKED0231
INCLUDE NASTOBJ(XSAVE)                                                     LKED0232
OVERLAY A                                                                  LKED0233
INCLUDE NASTOBJ(XCEI)                                                      LKED0234
OVERLAY A                                                                  LKED0235
INCLUDE NASTOBJ(XCHK)                                                      LKED0236
OVERLAY A                                                                  LKED0237
INCLUDE NASTOBJ(BLKDATA(XSFA1),XPURGE,XPUNP,XDPH)                          LKED0238
INCLUDE NASTOBJ(XPOLCK,XFILPS,XPLEQK,XPOLCKZ,XSFA,XCLEAN,XSOSGN,GNFIST)    LKED0239
INSERT  ZXPOLCK,XSFA1                                                      LKED0240
OVERLAY ESFA                                                               LKED0241
INSERT  ESFA                                                               LKED0242
OVERLAY A                                                                  LKED0243
INCLUDE NASTOBJ(TABPT,TABPRT)                                              LKED0244
OVERLAY TABPRX                                                             LKED0246
INSERT  TABPRX                                                             LKED0247
OVERLAY A                                                                  LKED0248
INCLUDE NASTOBJ(PRTPRM)                                                    LKED0249
OVERLAY A                                                                  LKED0250
INCLUDE NASTOBJ(BLKDATA(INPUTA,IUNION,INPUT)                               LKED0251
INSERT  INPUTA                                                             LKED0252
OVERLAY INPUTX                                                             LKED0253
INSERT  INPUTX                                                             LKED0254
OVERLAY A                                                                  LKED0255
INCLUDE NASTOBJ(EJECT,WRTMSG,PRTMSG)                                       LKED0256
OVERLAY XXPMSG                                                             LKED0257
INSERT  XXPMSG                                                             LKED0258
OVERLAY A                                                                  LKED0259
INCLUDE NASTOBJ(INPTT1)                                                    LKED0260
INCLUDE NASTOBJ(TPSWIT,FORFIL)                                             LKED0261
OVERLAY INP1XX                                                             LKED0262
INSERT  INP1XX                                                             LKED0263
OVERLAY A                                                                  LKED0264
INCLUDE NASTOBJ(INPTT2)                                                    LKED0265
OVERLAY INP2XX                                                             LKED0266
INSERT  INP2XX                                                             LKED0267
OVERLAY A                                                                  LKED0268
INCLUDE NASTOBJ(BLKDATA(CHAR94),AXIS,DRWCHR,IDPLOT,LINE,PLTSET,PRINT)      LKED0269
INCLUDE WWS(SGINOZZ)                                                       LKED0270
INCLUDE NASTOBJ(SCLOSE,SELCAM,SEOF,SGINOZZ,SKPFRM,SOPEN,STPLOT,SWRITE)     LKED0271
INCLUDE NASTOBJ(SYMBOL,TIPE,TYPINT,FNDPLT)                                 LKED0272
INSERT  CHAR94,CHRDRW,XXPARM,PLTDAT,SYMBLS,ZZSGINO                         LKED0273
OVERLAY DRAW                                                               LKED0274
INCLUDE NASTOBJ(LINE10,TYPE10,WPLT10)                                      LKED0275
OVERLAY LONGST                                                             LKED0276
INCLUDE NASTOBJ(DPLOT,DRAW        )                                        LKED0277
INCLUDE NASTOBJ(ELELBL,FIND,FNDSET,        GPTLBL,GPTSYM,HEAD,INTVEC)      LKED0278
INCLUDE WWS(PLOT)                                                          LKED0279
INCLUDE WWS(PROCES)                                                        LKED0280
INCLUDE NASTOBJ(MINMAX,PARAM,PERPEC,PLOT,PLTOPR,PROCES,SHAPE,WRTPRT)       LKED0281
INSERT  DRWDAT,RSTXXX                                                      LKED0282
OVERLAY XXPLOT                                                             LKED0283
```

```
INSERT   XXPLOT                                                        LKED0284
OVERLAY DRAW                                                           LKED0285
INCLUDE NASTOBJ(LINE9.TYPE9.WPLT9)                                     LKED0286
OVERLAY ONE                                                            LKED0287
INCLUDE NASTOBJ(SETVAL)                                                LKED0288
OVERLAY ONE                                                            LKED0289
INCLUDE NASTOBJ(BLKDATA(GPTA1).DELSET)                                 LKED0290
INSERT   GPTA1                                                         LKED0291
OVERLAY TA1GP1                                                         LKED0292
INCLUDE NASTOBJ(SORT)                                                  LKED0293
INSERT   SETUP                                                         LKED0294
OVERLAY GPX1                                                           LKED0295
INCLUDE NASTOBJ(GP1)                                                   LKED0296
OVERLAY GPA1                                                           LKED0297
INSERT   GPA1                                                          LKED0298
OVERLAY GPX1                                                           LKED0299
INCLUDE NASTOBJ(GP2)                                                   LKED0300
OVERLAY GPA2                                                           LKED0301
INSERT   GPA2                                                          LKED0302
OVERLAY TA1GP1                                                         LKED0303
INCLUDE NASTOBJ(COMECT.CNSTRC.DPLTST.SETINP)                           LKED0304
OVERLAY XXPSET                                                         LKED0305
INSERT   XXPSET                                                        LKED0306
OVERLAY ONE                                                            LKED0307
INCLUDE NASTOBJ(INPTT3)                                                LKED0308
OVERLAY ONE                                                            LKED0309
INCLUDE NASTOBJ(INPTT4)                                                LKED0310
ENTRY    XSEM2                                                         LKED0311
END                                                                    LKED0312

LINK 20                                                                LKED0314
RENAME CORSZ = XCORSZ                                                  LKED0315
RENAME APACTGR = ABSENT.      $ REMOVE THIS CARD WHEN RUNNING AT CYBERNETLKED0316
RENAME    SYSTEM = SYSTEM.                                             LKED0317
RENAME    EXIT(PEXIT, = PEXIT66                                        LKED0318
INCLUDE NASTOBJ(PEXIT.MSGWRT.USRMSG.PAGE.PAGE1.PAGE2.PAGEZZZ.PEXIT66)  LKED0319
ENTRY     PEXIT                                                        LKED0320
END                                                                    LKED0321
ENDLINKS                                                               LKED0313
```

REFERENCES

1. Smith, Willianna W.: A Special NASTRAN Program for Input Checking and Undeformed Structure Plotting. NASTRAN: Users' Experiences, NASA TM X-2378, 1971, pp. 559-568.

2. Douglas, Frank J., ed.: The NASTRAN Programmer's Manual. NASA SP-233, 1970.

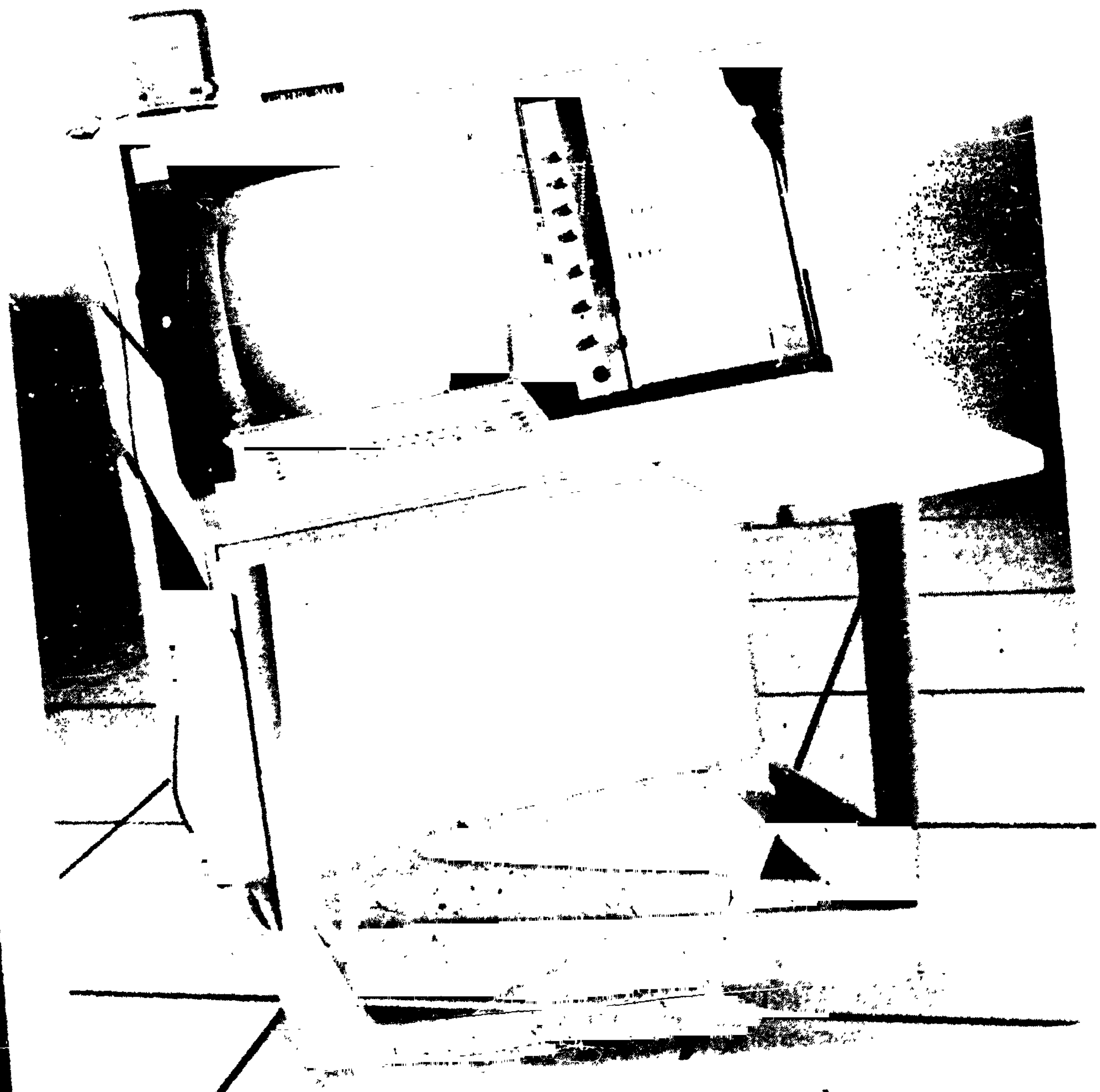

Figure 1. – CDC 250 CRT terminal.

N74-14622

NASTRAN DATA GENERATION OF HELICOPTER FUSELAGES USING INTERACTIVE GRAPHICS

By J. B. Sainsbury-Carter
and John H. Conaway

Sikorsky Aircraft
Division of United Aircraft Corporation
Stratford, Connecticut

SUMMARY

The development and implementation of a preprocessor system for the finite element analysis of helicopter fuselages is described. The system utilizes interactive graphics for the generation, display, and editing of NASTRAN data for fuselage models. It is operated from an IBM 2250 cathode ray tube (CRT) console driven by an IBM 370/145 computer. Real time interaction plus automatic data generation reduces the nominal 6 to 10 week time for manual generation and checking of data to a few days.

The interactive graphics system consists of a series of satellite programs operated from a central NASTRAN Systems Monitor. Fuselage structural models including the outer shell and internal structure may be rapidly generated. All numbering systems are automatically assigned. Hard copy plots of the model labeled with GRID or elements ID's are also available. General purpose programs for displaying and editing NASTRAN data are included in the system.

Utilization of the NASTRAN interactive graphics system has made possible the multiple finite element analysis of complex helicopter fuselage structures within design schedules.

INTRODUCTION

The problem of manual data generation for large finite element idealizations is well known. Helicopter fuselage models for static stress analysis with NASTRAN contain typically 2,000 to 10,000 input data cards. Manual generation and checking of data decks for these problems requires 6 to 10 weeks of tedious coding and corrections. With such large turnaround times, it is usually not possible to perform analysis of redesigned configurations within allotted design schedules.

The use of interactive graphics to display and check large structural models has been demonstrated (Reference 1). The automatic generation of data describing fuselage structures has been accomplished via batch type computer programs (References 2 and 3). This paper describes a system of programs for the automatic data generation, editing, and display of fuselage models which is fully interactive. Additional flexibility is acquired by including automatic data generation features in an interactive mode. This permits the rapid development

PRECEDING PAGE BLANK NOT FILMED

of large data decks for complex structures which do not lend themselves totally to simple mesh generation techniques.

INTERACTIVE GRAPHICS MONITORING SYSTEM FOR NASTRAN

The preprocessors used for helicopter fuselage data generation are part of a system of interactive graphics programs shown in Figure 1. The system is activated and controlled from the IBM 2250 CRT console. Each module is accessed from the central System Monitor program by selecting the program name from a main menu. The modular construction of the system provides flexible usage. Some of the modules are more general purpose in nature (i.e., the Geometry, Display, and Edit programs) and thus may be used in a variety of NASTRAN problems. At any time during operation of the system, control may be transferred to any module via the System Monitor.

The graphics system creates card input for NASTRAN which is independently executed in a batch mode. Hard copy plotting of CRT input displays and NASTRAN output for fuselage models is currently under development.

FUSELAGE INPUT DATA GENERATION

A large percentage of the required NASTRAN input for the stress analysis of a helicopter fuselage may be created in an interactive mode using the Fuselage Data Generator module. This program interacts with other Geometry and Files modules via the NASTRAN System Monitor, creating card images for the following types of Bulk Data:

Element connectivity

Grid point coordinates

Element geometric properties

Multipoint constraints

The design philosophy for this preprocessor placed considerable emphasis on user convenience and operational speed. Wherever possible, default options are built into the program to ensure rapid data generation with the minimum of commands. Within this philosophy, all GRID and element ID's are internally defined by the program.

The data generation is separated into two phases. The first phase comprises the generation of the fuselage outer shell consisting of frames, stringers, and shear panels. The second phase involves the generation of all the internal details such as bulkheads, floors, longitudinal walls, etc. This distinction between phases is made for the following reasons:

1.) The outer shell, in addition to exhibiting a larger amount of topological repeatability, is necessary to define the boundaries of the internal structure.

2.) The internal details are generally more variable in geometry and connectivity than the outside shell, as illustrated in Figure 2, and thus different algorithms are required for efficient data generation.

The order in which subprograms are used in the generation of fuselage data is arbitrary. The user selects the next module to be called via light pen from a CRT display. This arrangement provides flexibility of operation not available in a batch data generation mode. The user may generate, display, and store data at any stage in the model development, reentering previously executed modules for corrections whenever necessary.

In the normal sequence of phase 1 operation, the user first defines all unique frame contours using the two-dimensional Geometry module. This subprogram provides a wide variety of options for construction of general two-dimensional contours. The frame contour is developed by interpolating between input points with straight lines, conic sections, or cubic splines. Intermediate points are located by intersecting the contour with lines, and/or by specifying equal arc increments between previously defined points. To reduce the amount of input required from the user, symmetric repetitions of geometry are obtained by the reflection of the previously defined contour about an axis of symmetry.

When all points on the desired frame contours have been defined, the coordinate information is stored in the 2-D Files module for future reference. The points describing two or more frames are then transferred to the 3-D Geometry module (FMILL) where they are used as bounding contours to develop a shell surface. If only two frames are transferred, as shown in Figure 3a, straight line interpolation between corresponding points is used to define the shell. If more than two frames are transferred, a piecewise cubic surface is constructed between them.

All additional frame contours and their corresponding points are automatically generated in the 3-D Geometry module by intersecting the 3-D surfaces with planes as illustrated in Figure 3b.

The output of the 3-D Geometry module is the positions and ordering of a set of points describing a "regularized" fuselage shell (Figure 3b). A permanent file within the module may be used to store this information for future reference.

The shell established in the 3-D Geometry module is transferred to the Fuselage Data Generator via the NASTRAN System Monitor where perturbations on the regularized topology are performed to produce the actual fuselage geometry and connectivity. To increase clarity of display, a limited portion of the shell may be transferred at any one time to the Fuselage Data Generator. A perspective view of the fuselage shell looking down the longitudinal axis of the aircraft (spider diagram) is used in this module as illustrated in Figure 4a. The spider diagram allows the maximum amount of display without the confusion of overlayed lines. Cutouts (e.g.,doors, windows, landing ramps, etc.) or partial frames are introduced by deleting lines via the light pen (Figure 4b). Points may be added by keying in coordinates from the console and connectivity modified by adding lines between points detected by the light pen. Such modification enables the line connectivity to depart from the initial regularized topology, permitting duplication of any required structural model.

When the geometry and line connectivity of the shell has been established, element types are defined individually by light penning associated points or, in zones, by light penning points at zonal extremities. A default option defines frames as BAR elements, stringers as RODS, and quadrilateral panels by SHEAR elements. A modified connectivity display illustrated in Figure 4c indicates the position and type of the elements defining the skin. When the element definition is completed, section properties may be keyed in from the console and assigned to individual elements or zones.

Following completion of the fuselage shell mesh definition, the user may transfer the information associated with the spider diagram(s) to a permanent NASTRAN File. At this time, the previously defined geometry, connectivity, and property information is converted into NASTRAN Bulk Data, and all elements are compiled into a SET for future display or hard copy plot generation. These plots may be labeled with GRID ID's or element ID's.

The user may define internal details to be added to the model by returning to the Geometry modules. By intersecting the 3-D shell surface with the plane of a detail (e.g., bulkhead), boundary points of this structural unit are defined, compatible with the previously generated fuselage shell. These points are transferred to the 2-D Geometry module where point and line algorithms are used to construct a connectivity breakup. This information is then transferred to the Data Generator module where the elements are defined, section properties assigned, and the resulting Bulk Data merged with the file for the previously generated fuselage shell.

The Fuselage Data Generator module may also be used to create multipoint constraint data for NASTRAN. Large sets of MPC data are required to enforce rigid body assumptions on some internal details of the fuselage. This feature eliminates the need for modeling stiff structural units such as full bulkheads. MPC's are also used to distribute concentrated applied loads to individual grid points around the fuselage shell.

DISPLAY AND EDIT PROGRAMS

Transfer of control to the Display and Edit preprocessors may be accomplished via the NASTRAN System Monitor at any time. These general purpose programs permit a much greater flexibility for displaying and editing NASTRAN input data than the Fuselage Data Generator.

The Display program enables arbitrary selections of data to be shown on the CRT screen with greater user convenience and speed. The user may display structural segments previously defined in the Fuselage Data Generator as SETS.

This significantly reduces the time necessary to define elements for display. To add flexibility to the system, however, new groups of elements comprising structural segments not specified by the SET option may be generated by selecting the required element types and element identification numbers. Table 1 lists geometry types and their corresponding element types recognized by the display program.

Following satisfactory element selection, a display of the structural model appears with a menu of options. Two of these options enable rotation of the display about three orthogonal axes, scaling and selective zooming to be implemented, thus permitting the user to obtain an optimum orientation for visual inspection. The axis system for structural rotations is fixed relative to the screen and is always displayed, enabling the user to remain oriented regarding rotational commands. To increase the number of elements that can be displayed and simultaneously reduce image flicker, the geometry is internally scanned for multiply defined lines and the redundant lines are eliminated.

At any time during execution of the Display program, two additional features open to the user are "selective data retrieval and editing" and "free boundary analysis". The first feature permits extraction and identification of any element or grid point. By light penning a displayed line image, all associated element ID's are displayed. By light penning any two intersecting line images, the associated GRID ID is displayed. The corresponding Bulk Data card images of the extracted element or grid point are simultaneously shown below the structural display, permitting temporary editing and automatic incorporation of the change into the structural display.

The free boundary analysis produces a display of singly defined lines in the structural model, permitting the location of missing elements. If a single quadrilateral element had been inadvertently omitted from manual input of a shell structure, for example, only that quadrilateral would be displayed in addition to any natural structural free boundaries. All other element line images would be absent because of their multiple line definitions.

Much greater flexibility for data editing may be obtained by transfer of control to the Edit program via the NASTRAN System Monitor. The Edit permits modification or deletion of current data and the insertion of new data in the Executive Control, Case Control, or Bulk Data decks. Since the IBM 2250 CRT is capable of displaying only 72 characters across the screen as compared to 80 columns in the NASTRAN data card format, each card is broken into two lines. A menu comprising nine options accompanies the Edit program. Included within these options is the ability to page forward or backward through the data or to locate any card type and ID. Editing of any data may be accomplished by keying in new values from the console.

Concluding the Display and Edit phase, the permanent storage files may be updated with corrected data by transfer of control to the FILES program via the NASTRAN System Monitor.

ILLUSTRATIVE EXAMPLE

The complete structural model used during the analysis and design of the UTTAS helicopter fuselage is shown in Figure 2 . To illustrate the versatility of the described interactive graphics preprocessors, the input data are generated and checked for the circled substructure known as the transition region.

The transition region was chosen for this example due to its variety of characteristics pertinent to most fuselage structures. It contains nine frames, three cutouts, two bulkheads, a floor, and a vertical shear web. Of the nine frames, four are independent in shape. The other five frames are generated by linear interpolation. Five of the nine frames are partial (i.e., they do not span the entire circumference of the fuselage).

The outside shell and the floor are used to illustrate operation of the Fuselage Data Generator. One of the bulkheads is manually generated and used to demonstrate features of the Display and Edit programs.

Figure 5a shows the CRT display listing the various subprograms available within the NASTRAN interactive graphics system. Light penning "2D GEOM" enables the shapes of the four independent frames to be generated (Figure 5b). Due to the generality of frame shapes, each grid point is introduced by keying in the appropriate coordinates in the YZ plane. Dummy points are introduced, at three of the four frames, to maintain an equal number of points (46) at all frames. Partial frames are also temporarily generated as full frames. The four frames are stored in the 2D FILES subprogram, and transferred to FMILL, the 3-D Geometry module, where the node points are connected by lines (Figure 5c). The frames are not closed due to the limitation of the FMILL subprogram which generates only open surfaces. The remaining five frames are generated by intersecting the surface with planes at the appropriate frame station coordinates (Figure 5d).

The final details of the fuselage generation concentrate on the forward seven frames between Stations 398 and 443 as shown in Figure 5d . Transfer of these frames to the "GENERATE" module yields a connectivity display shown in Figure 6a . Partial frames and cutouts are created at this stage by deleting unwanted lines, Figure 6b . Dummy points are also removed and the line element connectivity completed, Figure 6c .

The introduction of new lines and definition of panel element is now performed, resulting in the display shown in Figure 6d , quadrilaterals being indicated by the symbol X, and triangles by the symbol Y, etc.

A series of hard copy plots of this SET of structural elements may be generated, denoting the element and node point ID's for future reference. Figure 6e shows such a plot for the shear panels corresponding to Figure 6d . The same elements are also assigned a SET number, aiding in their recall for further modification in the Display and Edit programs. Figure 6f is the true view of the structure corresponding to that displayed in Figures 6a to 6e .

At this time, properties are defined and associated with appropriate elements by either the light penning of individual elements or the definition of property zones.

A structural SET is generated in a similar manner for the aft two bays between frame stations 443 to 485. For illustrative purposes, these two SETS have been called up together by the Display program. In other structures, however, it may be expedient to use the Display and Edit programs to perform final adjustments in the structural configuration rather than develop the exact structure in the Fuselage Generator program.

Figures 7a and 7b represent two views of the SHEAR and TRMEM element connectivity of the generated outside shell described above. Figure 7c illustrates the stringers or ROD element connectivity and Figure 7d the frames.

Display of a manually generated ulkhead for frame station 443, Figure 8a , clearly indicates an error. Light penning the upper two erroneous lines reveals the associated element numbers to be 2986 and 2985 and the corresponding erroneous node point to be 1893. The data card image for this GRID point is shown below the display. Editing this card image enables immediate regeneration of the correlated display, Figure 8b . The associated data card image in permanent storage (GRID 1893) is shown in Figure 8c by transfer to the Edit subprogram. Visually the display in Figure 8b appears to be correct. Initiating the free boundary analysis feature, however, reveals a missing SHEAR element, Figure 8d . This element can be introduced in the Edit subprogram by keying in the missing Bulk Data card.

The generation of internal structure, such as a floor, requires returning to the spider diagram (Figure 6d) of the Fuselage Generator program. Light penning the grid points common to the floor, the outside shell, and any other previously defined internal structure, generates a 2-D display of the boundary of the required floor, Figure 9a .

Generation of the interna 'ement connectivity is rapidly performed as shown in Figure 9b . Figure shows the floor and vertical web viewed from the Display program.

Structural data generation by the interactive graphics system is managed by manipulating the many features built into the programs. The order in which the subprograms are used is completely general and problem dependent. Optimum utilization of the system is only achieved with practice.

CONCLUDING REMARKS

Dramatic time reductions (by an order of magnitude) for the generation of NASTRAN input data for fuselage structures has been achieved by the development and utilization of the subject interactive graphics preprocessor.

The modular design of the NASTRAN interactive graphics system permits subprograms to be called in an arbitrary order, allowing rapid data generation for complex fuselage models. The generality of the geometry definition, display, editing, and storage features also provides versatility needed for generation of models for many other structures.

ACKNOWLEDGEMENTS

The work presented in this paper was conducted at Sikorsky Aircraft, Stratford, Connecticut, under company sponsored research and development funds. The authors wish to express appreciation to R. Robbins and A. Williams for their valuable assistance and computer programming performed during the development of the interactive graphics system.

REFERENCES

1.) Cronk, Michael: An Interactive Computer Graphics Program for NASTRAN. NASTRAN: Users' Experiences, NASA TM X-2378, 1971, pp. 659-667.

2.) Galligan, D. A., and Wilson, H. E.: The Integration of NASTRAN into Helicopter Airframe Design/Analysis, presented at American Helicopter Society, May 1973.

3.) Giles, Gary L., and Blackburn, Charles L.: Procedure for Efficiently Generating, Checking, and Displaying NASTRAN Input and Output Data for Analysis of Aerospace Vehicle Structures. NASTRAN: Users' Experiences, NASA TM X-2378, 1971, pp. 679-696.

GEOMETRY TYPE	ELEMENT TYPE	MAX NUMBER
LINE	CROD, CBAR, CONROD, CTUBE, CVISC	1000
TRIANGLE	CTRMEM, CTRIA1, CTRIA2, CTRMPLT, CTRBSC	1000
QUADRILATERAL	CQDMEM, CSHEAR, CQUAD1, CQUAD2	1000
TRIANGULAR RING	CTRIARG	500
QUADRILATERAL RING	CTRAPRG	500
CONCENTRATED MASS POINTS	CONM1, CONM2	500

Table 1. Element Menu for Display and Edit Preprocessors

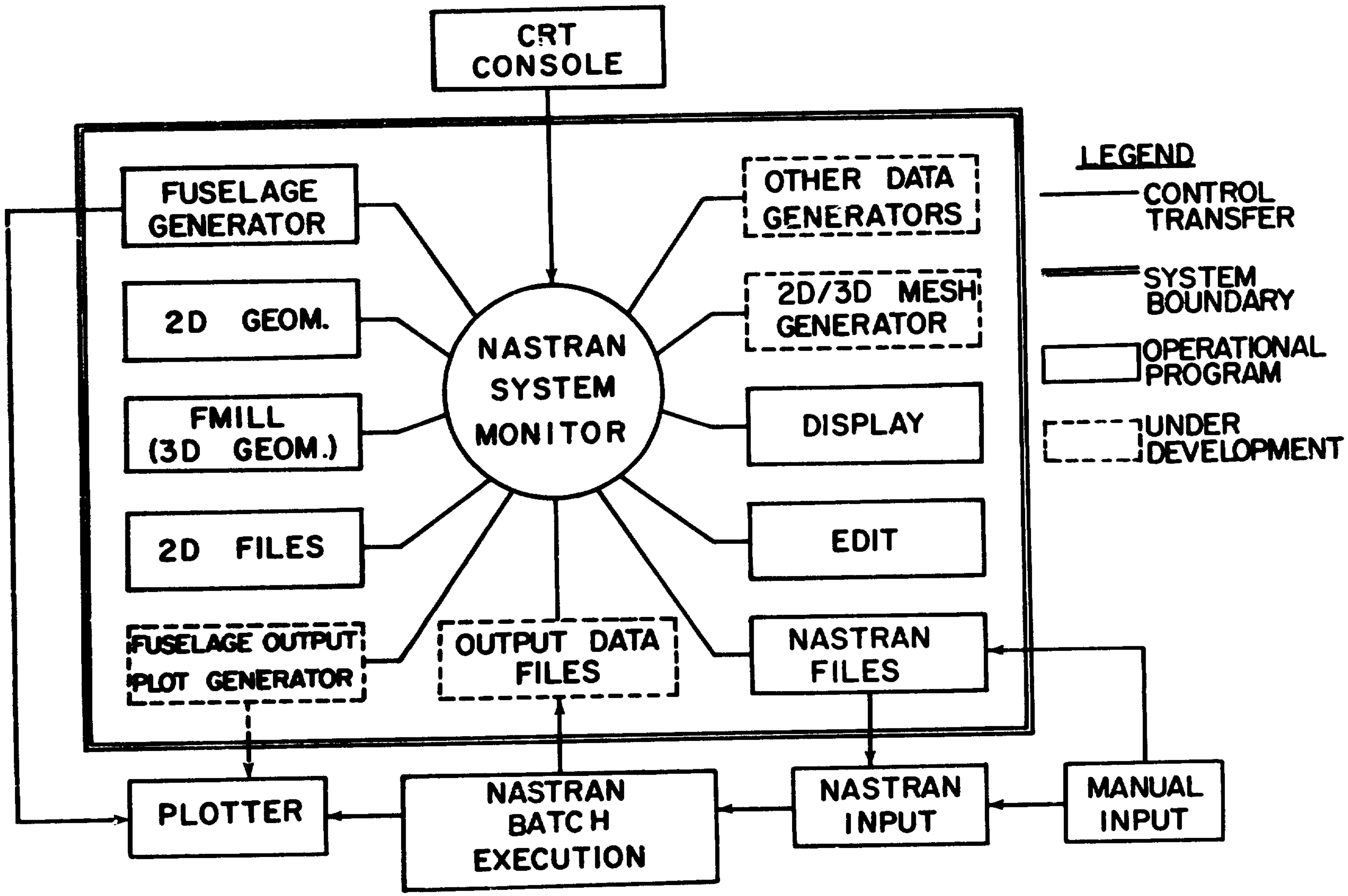

Figure 1. NASTRAN Interactive Graphics System

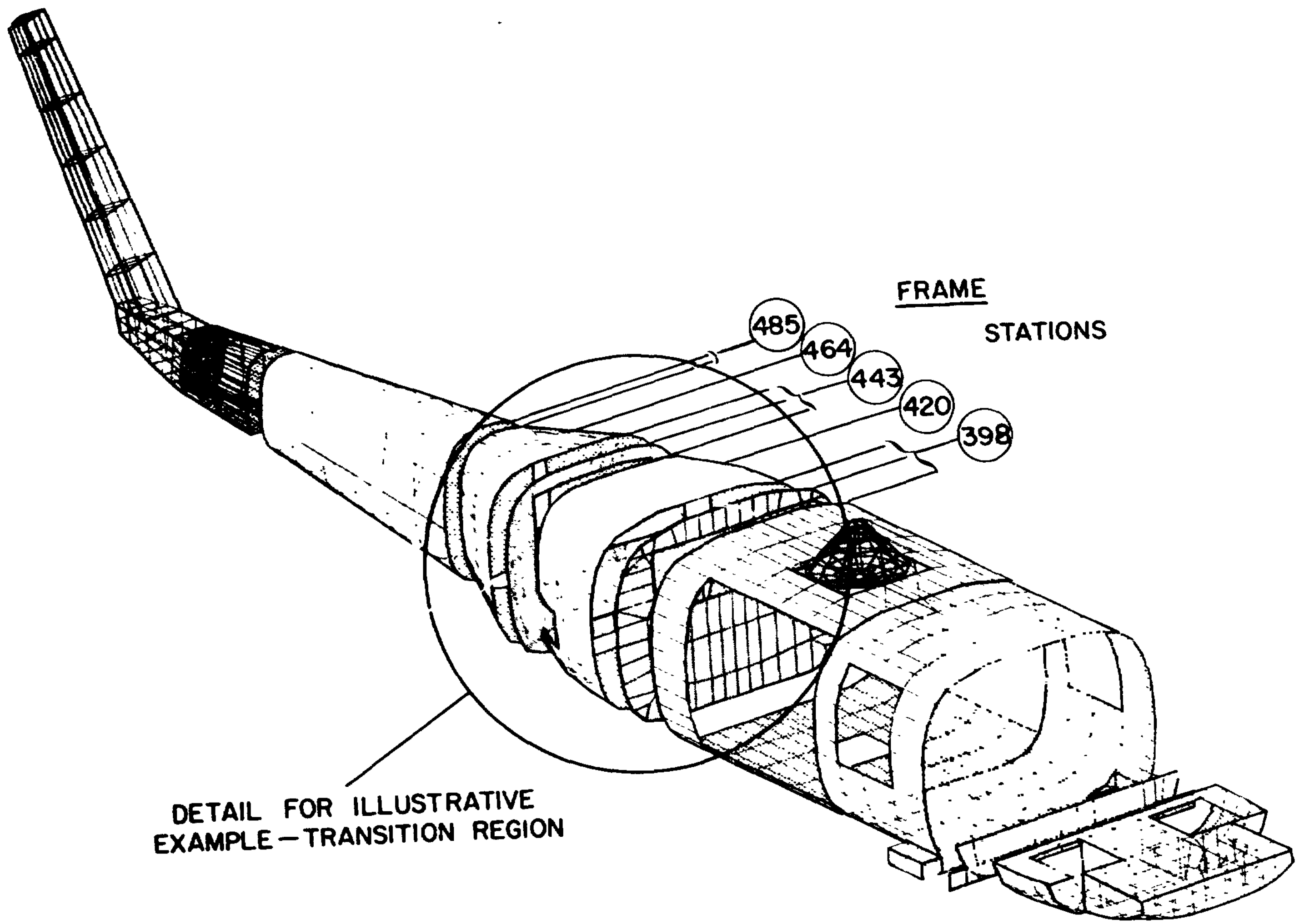

Figure 2. NASTRAN Structural Model for UTTAS Helicopter

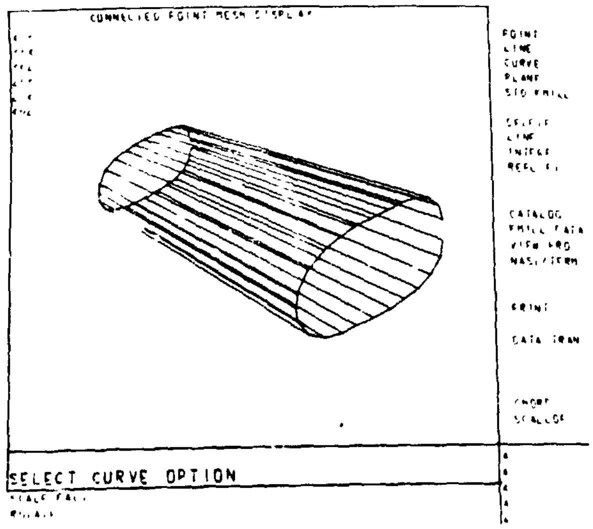

(a) Surface Definition

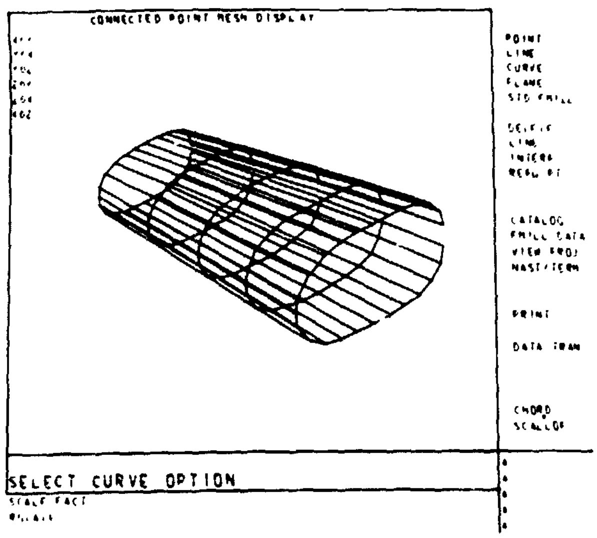

(b) Definition of Intermediate Frame Contours

Figure 3. 3-D Geometry Definition

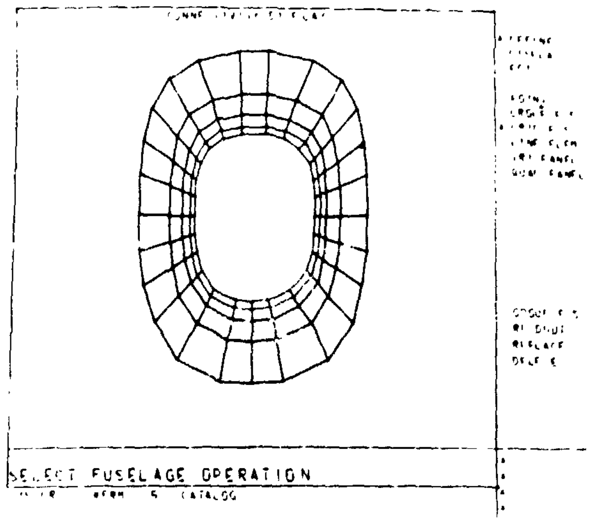

(a) Spider Diagram

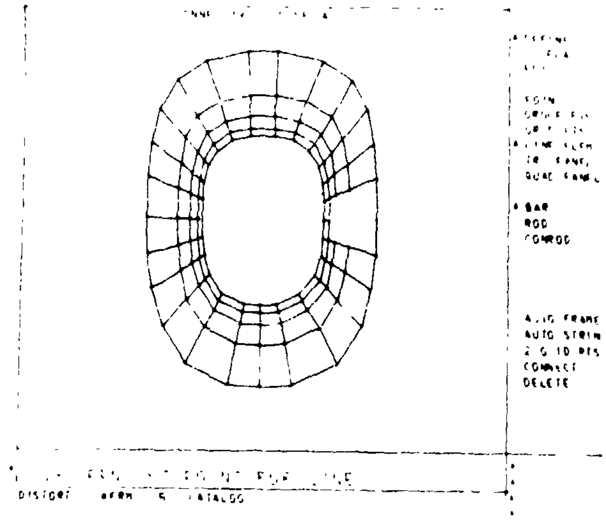

(b) Cutout Definition

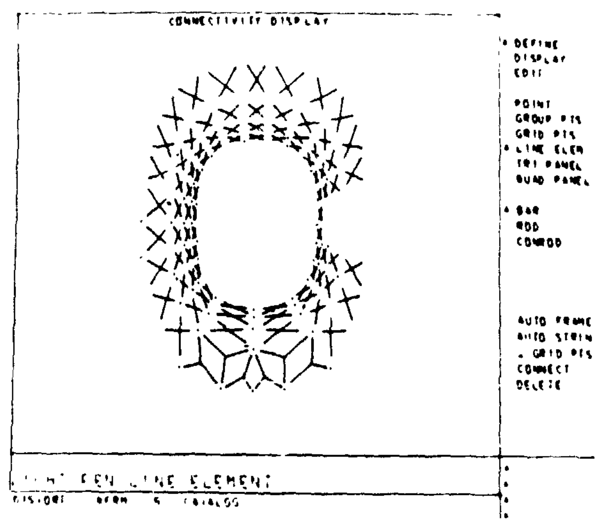

(c) Element Connectivity

Figure 4. Fuselage Generator Display

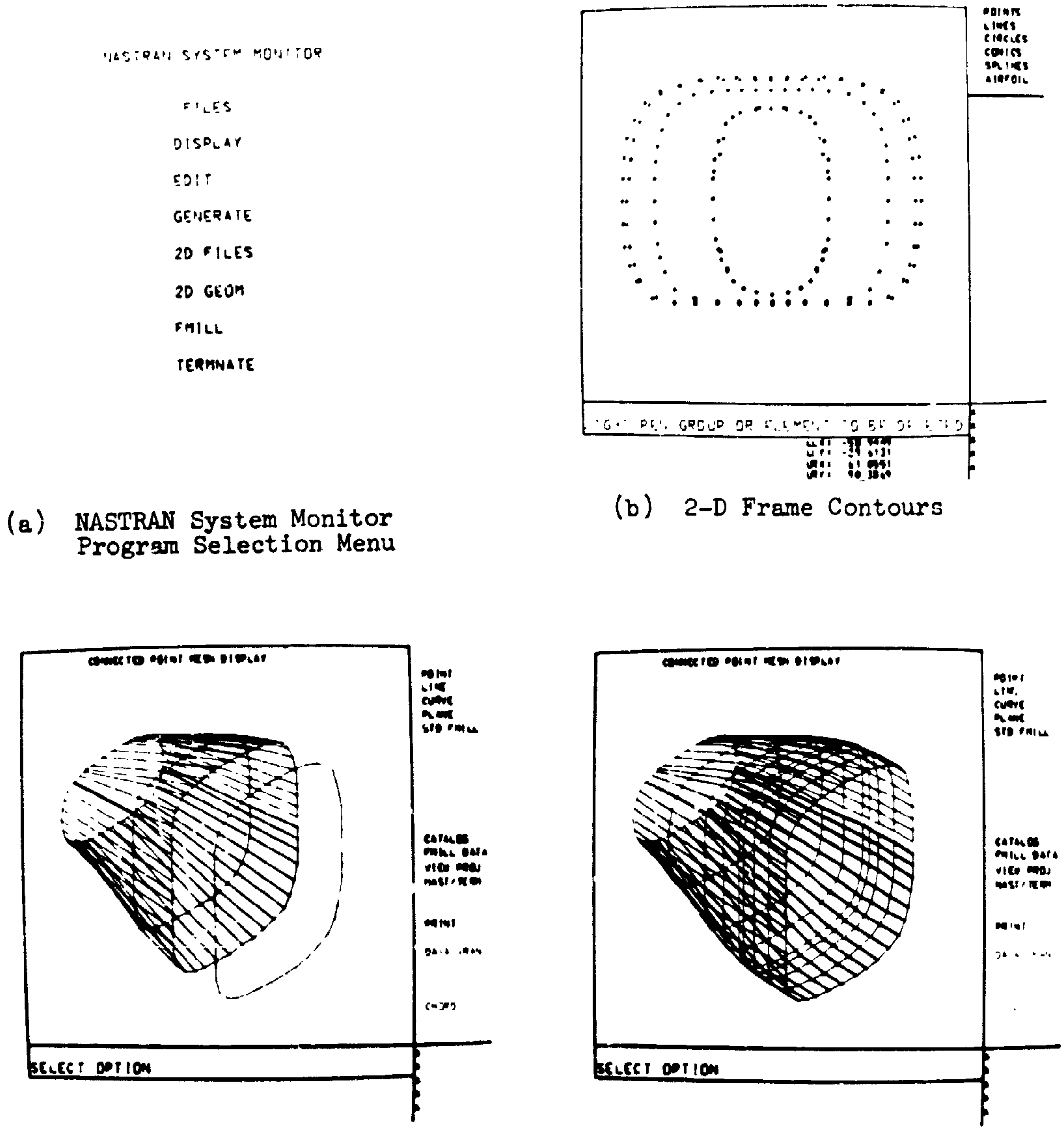

(a) NASTRAN System Monitor Program Selection Menu

(b) 2-D Frame Contours

(c) 3-D Line Connectivity

(d) Intermediate Frame Definition

Figure 5. UTTAS Transition Region - Geometry Definition

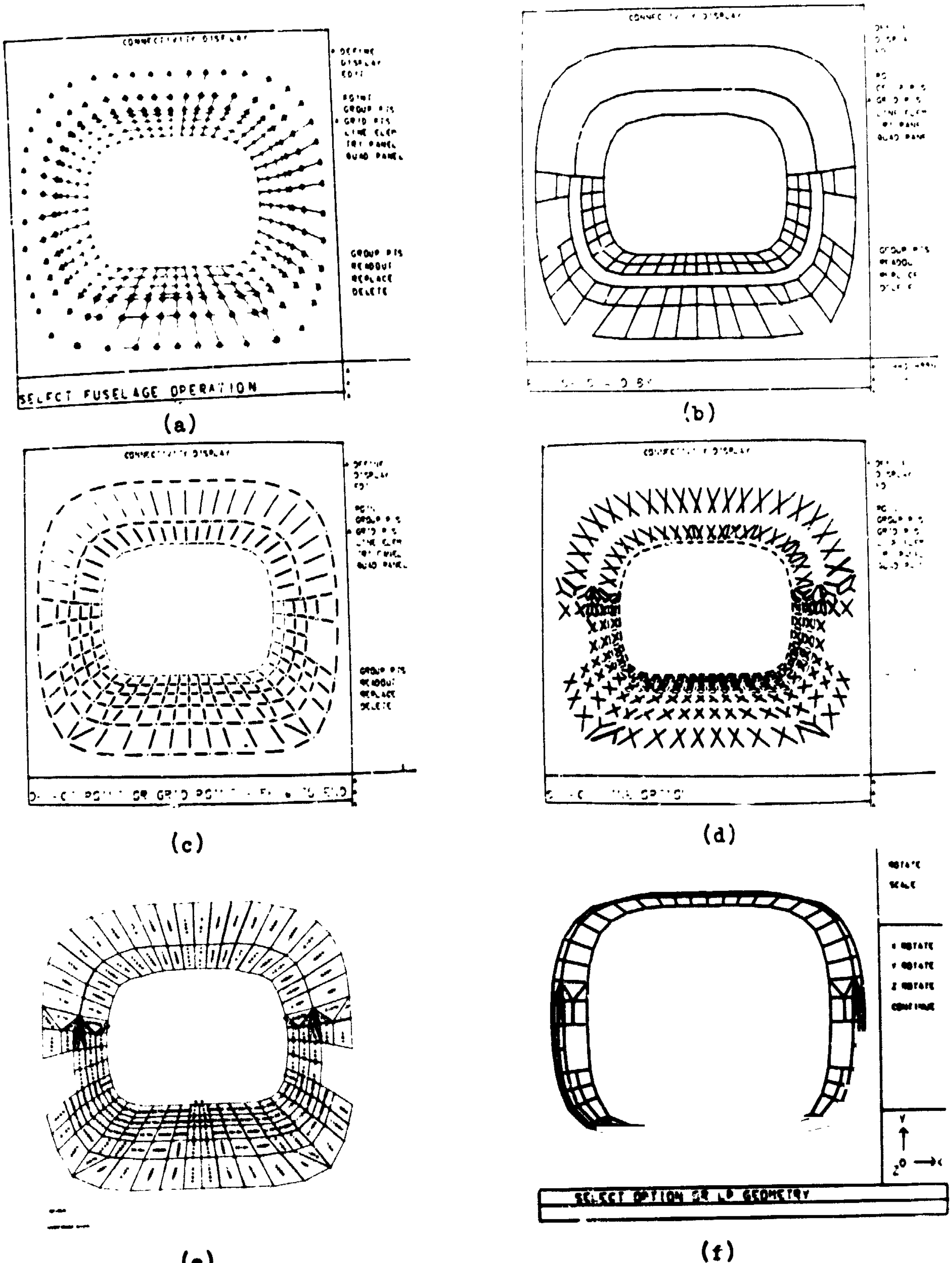

Figure 6. UTTAS Transition Region - Connectivity and Element Definition

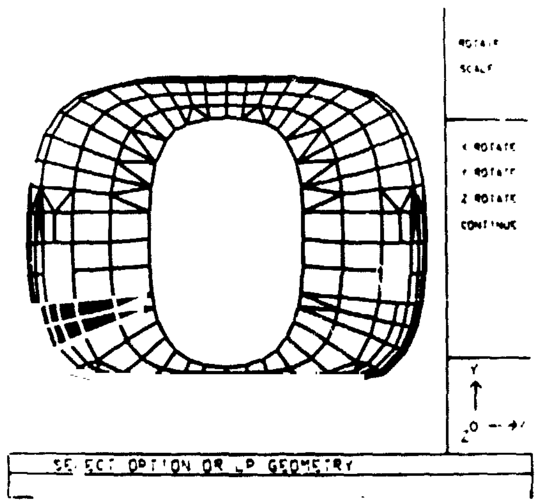

(a) Panel Display

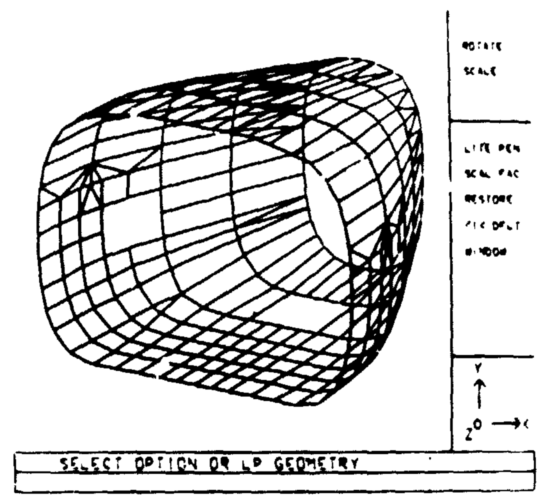

(b) Panel Display

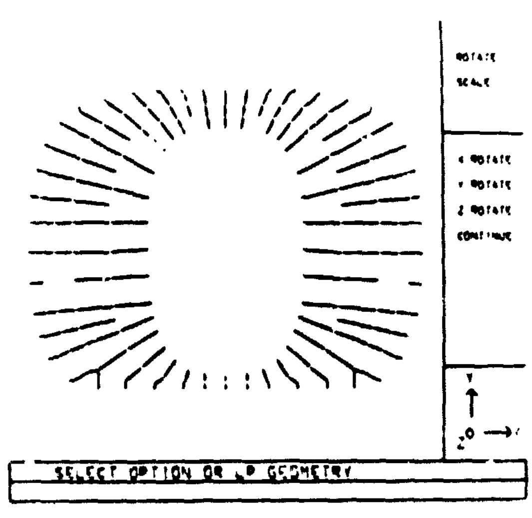

(c) Stringer Display

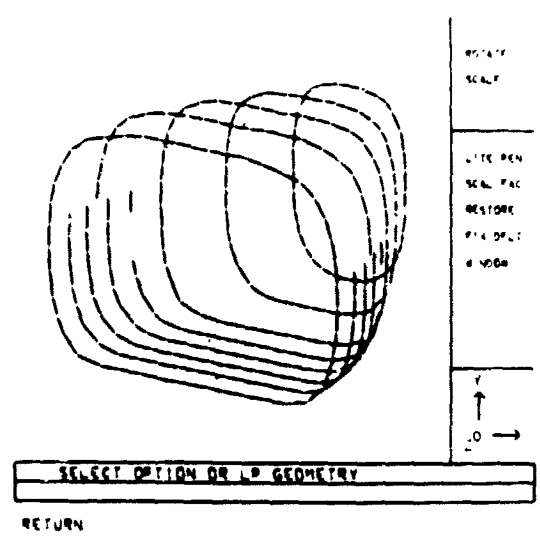

(d) Frame Display

Figure 7. UTTAS Transition Region - Display and Edit

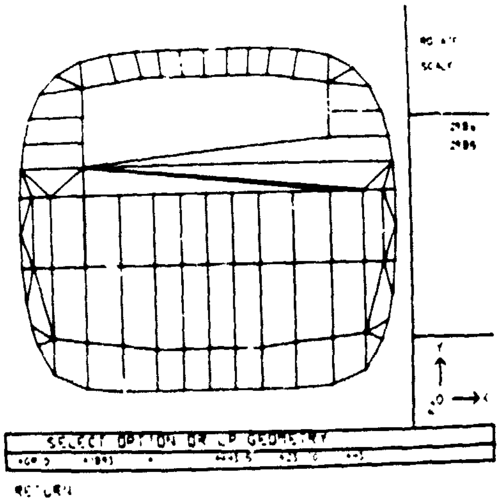

(a) Data Error Display

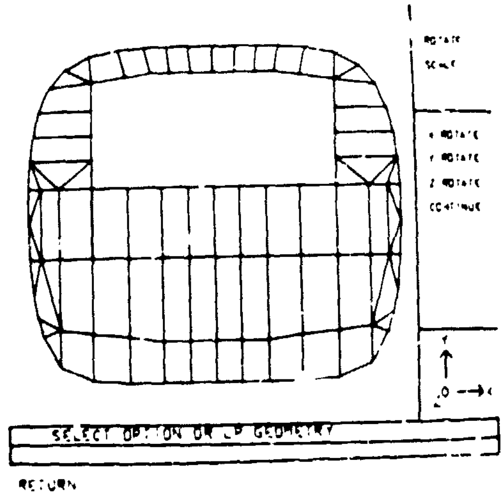

(b) Error Correction Display

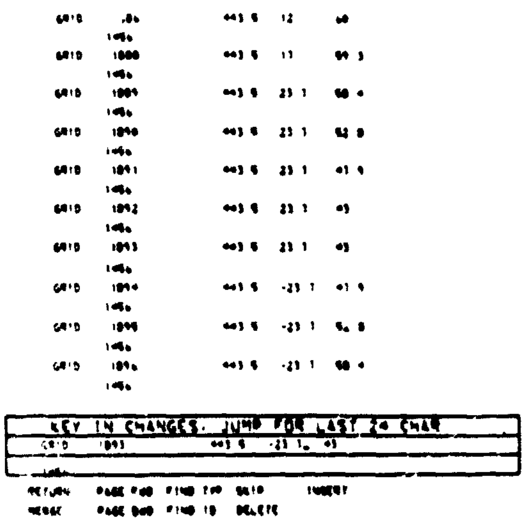

(c) Data Editing

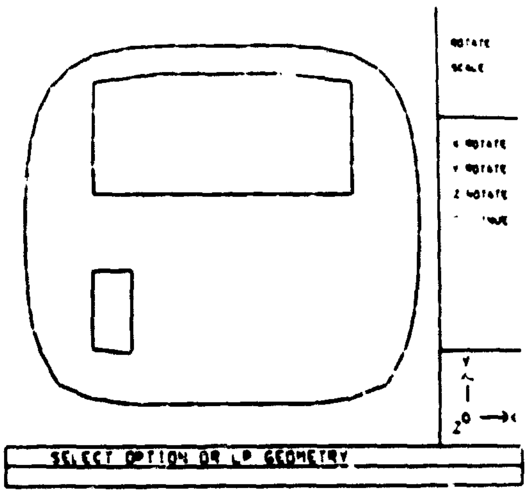

(d) Free Boundary Analysis

Figure 8. UTTAS Transition Region - Display and Editing of Manually Generated Bulkhead

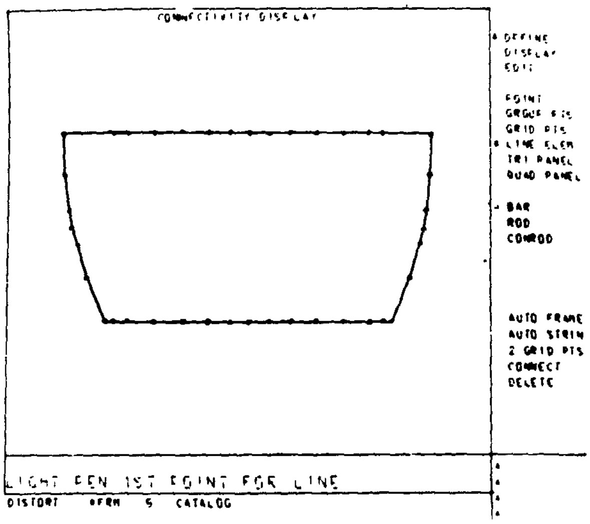

(a) Floor Boundary

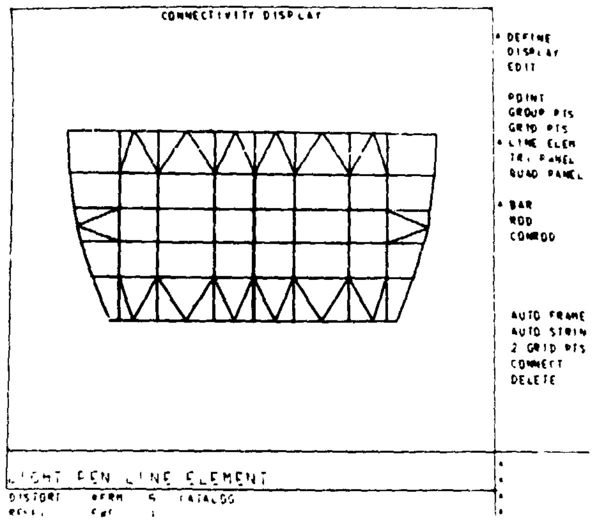

(b) Floor Connectivity

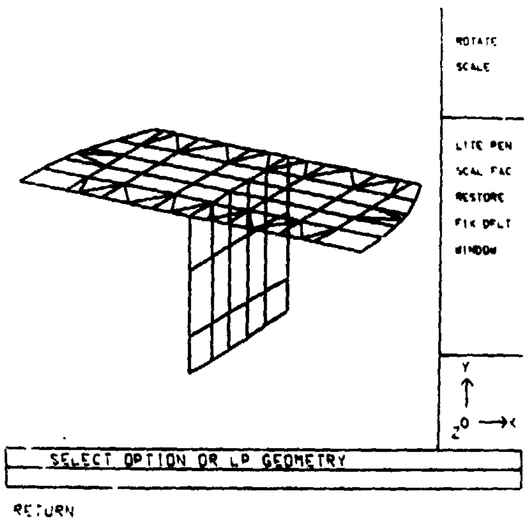

(c) Floor and Shear Web Display

Figure 9. UTTAS Transition Region - Generation of Floor and Shear Web

N74-14423

AN INTERACTIVE GRAPHICS SYSTEM TO FACILITATE FINITE ELEMENT STRUCTURAL ANALYSIS

BY ROBERT C. BURK AND FRED H. HELD
MCDONNELL DOUGLAS ASTRONAUTICS COMPANY - EAST

SUMMARY

Industry's growing use of finite element structural analysis requires that an increasing portion of the engineer's time be spent in building, checking, executing, and interpreting results of finite element models. The following discussion explains the use of a rapid, inexpensive, graphically oriented system for performing this job. With much of the bookkeeping drudgery removed and the visibility of results enhanced, the inspiration/perspiration ratio of the engineer is significantly improved.

INTRODUCTION

The effectiveness of a finite element analysis depends on the accuracy with which the model represents the actual structure and on the time and money spent to build, solve, and interpret the analysis results. Usually, finite element analysis involves the generation and manipulation of large quantities of data by hand using up valuable engineering time and introducing many opportunities for human errors. A typical analysis would normally require the following steps:

1. Idealize the actual structure into discrete elements.

2. Make sketches of the idealized model and label with node and element numbers for use in referencing element properties, applied loads, reactions, output results, etc.

3. Fill out data sheets.

4. Have data sheets keypunched.

5. Obtain listing of deck and check for any errors (keypunch or coding).

6. Make appropriate corrections.

7. Obtain batch plot of structure to check for incorrect element connectivity or node location.

8. Submit for batch solution.

9. Evaluate results for any errors. Often, several computer runs (with their corresponding costs and turnaround delays) are required before error-free output is obtained.

10. Obtain batch plots of deformed shape.

11. Make freebody sketches of components showing reactions and internal loads. These are used for detailed stress analysis and formal reports of the analysis.

Each of these steps takes time and allows considerable chance for error.

In order to minimize the time spent on each of the steps, to reduce the chance for error, and to enhance the understanding by the engineer, interactive graphics is being harnessed. Reference 1 presents an excellent review of the uses of interactive computer graphics. In the area of structural analysis computer graphic applications, a system developed for two-dimensional modeling and display of results is discussed. This has been implemented on both the UNIVAC 418 - DEC 340 and the IBM 360/50-IBM 2250. Reference 2 presents a system developed by the Jet Propulsion Laboratory using interactive graphics for three-dimensional model checking.

This paper presents a rapid, low cost system which uses interactive graphics in both the preprocessing and postprocessing of finite element data. It can be used with the NASTRAN, ICES STRUDL, and CASD (Computer Aided Structural Design -- an in-house developed and used program) finite element analysis programs to minimize modeling errors, reduce the time required for the design/analysis cycle, and maximize the visibility of results.

A PROMISING SOLUTION

The system being effectively used by the McDonnell Douglas Astronautics Company, Eastern Division, places the engineer at an interactive graphics terminal. He can build, check, edit, solve, and interpret the results of a finite element model static analysis without leaving his chair. Many useful alternatives are controlled by the user at his remote terminal.

The basic hardware employed is an inexpensive, semiportable, Computek interactive graphics terminal with attached hard copier and digitizing tablet (see Figure 1). The terminal is a teletype compatible device with a cathode ray tube (CRT) that can transmit and display both alphanumerics and graphics. A hand held stylus is used to identify point coordinates on the digitizing tablet. These coordinates along with the status of three push buttons and two switches are transmitted to the computer for processing. The stylus position on the tablet is tracked on the CRT, allowing the user to coordinate his input with the displayed image. The hard copier makes 8 1/2 by 11 inch copies of the current image on the screen (in approximately 10 seconds for about 6 cents each) for documentation. The terminal communicates with our XDS Sigma 7 conversational, direct access computer via a standard telephone. Thus, the user may locate his terminal anywhere electrical outlets and a telephone exist.

A finite element model analysis can be broken into three phases: preprocessing (model generation), problem solution, and postprocessing (interpretation of results). The use of our system will be explained in each of these phases and demonstrated with an example problem. The problem involves determination of internal loads and deflections for a swept, multi-cell wing structure subjected to a simplified landing condition.

PREPROCESSING

Preprocessing includes building, checking, and editing a finite element model to prepare it for solution. The preprocessing phase is schematically represented in Figure 2. There are several methods we use to build a finite element model. The most common method is to model in the interactive graphics mode using the finite element modeling (FEM) program. Alternately, the data can be entered in card format directly into an on-line file using a conversational terminal and the computer's editor system. The model data may also be entered onto data sheets, keypunched, then loaded into an on-line file on the computer. In many cases, a small special purpose computer program is used to generate sections of the desired model where extreme accuracy is required or where structural geometry is very repetitious. For all methods, the FEM program is used to display the model for checking and to make any additions or necessary corrections.

When using the FEM program, node geometry is normally digitized directly to the computer utilizing actual scale drawings or layouts of structural cross sections as shown in Figure 3. Optionally, points can be keyed in (to obtain a more accurate location) or specified as vertical or horizontal from previously defined nodes. Bar elements may be indicated between these nodes while in this two-dimensional mode. The wing problem was entered using the parallel rib stations as the entry planes. A typical CRT display of one of these sections, as copied by the attached hard copier, is shown in Figure 4. The type of operation performed is controlled by the menu items on the CRT and the position of the buttons and switches on the digitizing tablet. For example, after the first of the two similar root sections was idealized, the menu item "DUP ALL", along with the appropriate Y station value of the second station, was indicated. This is done by moving the hand-held stylus across the tablet until the cursor on the screen is in the target "O". The stylus is then depressed on the tablet which sends the tablet coordinates of this point to the computer. The computer decodes this into a selection of the appropriate menu item. For the "DUP ALL" item, the computer responds with a prompt on the screen to enter the new plane station. After these data are typed in from the keyboard, all elements in the current plane are duplicated at the newly defined plane. The other rib stations are entered by using the "NEW CUT" option on the menu and are digitized as was the first rib.

After building all cross sections, a three dimensional display is obtained by indicating the "EXIT" item of the "2-D Node Building Mode" menu. Control is then transferred to the "3-D Element Building Mode". The first activity in this mode is the display of the three-dimensional projection of the current model in the last defined orientation with a new menu along the right hand edge of the screen. This display is shown in Figure 5 for the example problem. All remaining connection elements are now added. This is accomplished by indicating the appropriate element type from the menu, and then indicating the corresponding nodes on the model. Representations of the elements (bars, bending bars, shear panels, triangular plates, and quadrilateral plates) are shown immediately on the CRT as they are generated, thus providing graphic assurance of model correctness. Many options are available in this mode and are displayed as a menu along the right hand side of the screen. One such option, "WINDOW", allows magnification of the specified portion of the display for ease in viewing or inputing data in complex areas. This display is obtained by indicating the menu item, then the lower left and upper right corner of the desired view. The screen is erased, the indicated portion of the model is rescaled to fill the screen, and the display redrawn. A companion menu item, "PAN", allows the operator to move the center of the window to a new point on the structure (at the same scale factor) as indicated by the location of the cursor. Thus, he can effectively pan across the structure in discrete steps at a magnified scale. Additional menu items allow the input of reaction and applied load vectors, load magnitudes (for up to six conditions), and symmetry plane (if any). The example problem, with reaction and force vectors at this stage of completion, is shown in Figure 6.

The problem is then stored in a data file in the appropriate format for one of the following three computer codes: NASTRAN, ICES STRUDL, or CASD. A set of standard program control "cards" and default value element properties are automatically inserted into the data file by the program.

On some models, we have saved 80 percent of the time over the old method of submitting tabulated data for keypunching. The example problem took 46 minutes of "clock on the wall time" and expended approximately 7 dollars of computer costs to bring it to this stage of completion.

At this point in the idealization, a listing of the data file is typically obtained on either a time-share alphanumeric terminal or a high-speed batch printer (See Figure 2) and appropriate solution commands and element properties edited from the default values, these same data can be edited for dynamic analysis (e.g., add inertia matrix) and solved for mode shapes and frequencies using the computer code consistent with the data format. Additional preprocessing programs can be run for such functions as adding the appropriate job control language header cards and performing additional data checks. For large, complex models, the geometry can be plotted on a remote plotter to obtain larger copies of the structural idealization. At the end of these operations, the completed model is ready for solution. Portions of the NASTRAN card image data file generated for the example problem are shown in Figure 7.

Having formulated the input data using preprocessing programs, such errors as "key punch errors", data in wrong card columns, incorrect node number reference, etc., are largely eliminated and the probability of a successful solution on the first try is greatly increased.

PROBLEM SOLUTION

Solution can be initiated by a command from the user's remote terminal, as shown in Figure 8. Small problems (less than 650 degrees of freedom), such as the example problem, are usually solved using an abbreviated version of CASD which can be executed in real time on the XDS Sigma 7 computer. Larger problems, and all NASTRAN and ICES STRUDL analyses, require a batch solution on our IBM 360/195-195 computer. In either case, results are normally routed back to an on-line disk file for subsequent batch listing and evaluation using postprocessing programs.

POSTPROCESSING

Postprocessing includes all processes that operate on the solution results. The postprocessing phase of our system is schematically represented in Figure 9. For example, the first postprocessing operation normally executed is the editing of the solution file to find any error statements. This can be performed at any terminal connected to the direct access computer.

The primary postprocessing tool is a program called VUOUT. This program allows results to be graphically displayed at the user's terminal. It permits isometric viewing for static loads of the undeflected shape with, optionally, the deflected shape (with any magnification), buckle shape (NASTRAN only), internal loads for axial bars and shear panels, applied joint loads, and reactions for static problems. These may be displayed with superimposed bar or node numbers, and may be of the entire model, or of only a specified small section. In addition, load sheet (free body) displays of a single bar or panel element with its applied loads may be requested. In this case, appropriate element properties (length, area, thickness, modulus of elasticity, etc.) can be displayed with the loads.

The program first processes the solution results line by line and writes the data into a compacted on-line file for ready access by the display subroutines. This file is only generated during the first viewing of the results. Subsequent reviewing of the data bypasses this step. The display technique requires only a minimal amount of data in core at any one time and hence allows the results of an essentially unlimited size model to be displayed. The type of display is controlled by the menu selections shown in Figure 10. Actual hard copies of the results of the example problem are shown in Figures 11 through 16. Hard copies provide a permanent record for futher study, stress analysis, and use in reports. The graphical displays highlight any errors and enhance the engineer's understanding of the problem, allowing a more creative use of the finite element technique.

CONCLUSION

The application of interactive graphics to finite element structural analysis is one of the most exciting developments since the introduction of high speed computers. Significant engineering time can be saved and the usability of results enhanced. It allows the engineer to concentrate on the creative aspects of his job, freeing him from tedious mechanical tasks of input coding and output data reduction. It is no substitute for good engineering, but rather provides another tool for unlocking the complexities of intricate structures. Interactive graphic displays of the problem and its solution enhance understanding of structural interactions.

The coupling of our preprocessing and postprocessing programs to work with analysis programs, such as NASTRAN, has given us an inexpensive tool to quickly analyze complex structures. This system has played an important part in our static and dynamic structural analyses of several projects including our NASA Space Shuttle effort, the Navy Harpoon missile, and the NASA Skylab, as well as several advanced design efforts. It has proven to be an effective tool to eliminate many errors associated with finite element model generation and interpretation of the analysis results.

ACKNOWLEDGEMENTS

The authors wish to acknowledge the many contributors to the structural analysis system presented herein. The basic system requirements were defined by the Strength and Structural Dynamics Departments of McDonnell Douglas Astronautics Company - East (MDAC-E). Actual software development was performed primarily by the authors, Dr. D.C. Tsai, and P. A. Giarritano. The CASD analysis program was developed by the Advanced Procedures Group within Structural Engineering at the Douglas Aircraft Company and incorporated into our XDS Sigma 7 computer by MDAC-E.

REFERENCES

1. Prince, M. David, Lockheed-Georgia Company, "Interactive Graphics for Computer-Aided Design," Addison-Wesley Publishing Co., 1971.

2. Katow, M. Smoot, Cooper, Barry M., "NASTRAN Data Generation and Management Using Interactive Graphics," paper contained in "NASTRAN User's Experiences," NASA TMX-2637, 1972.

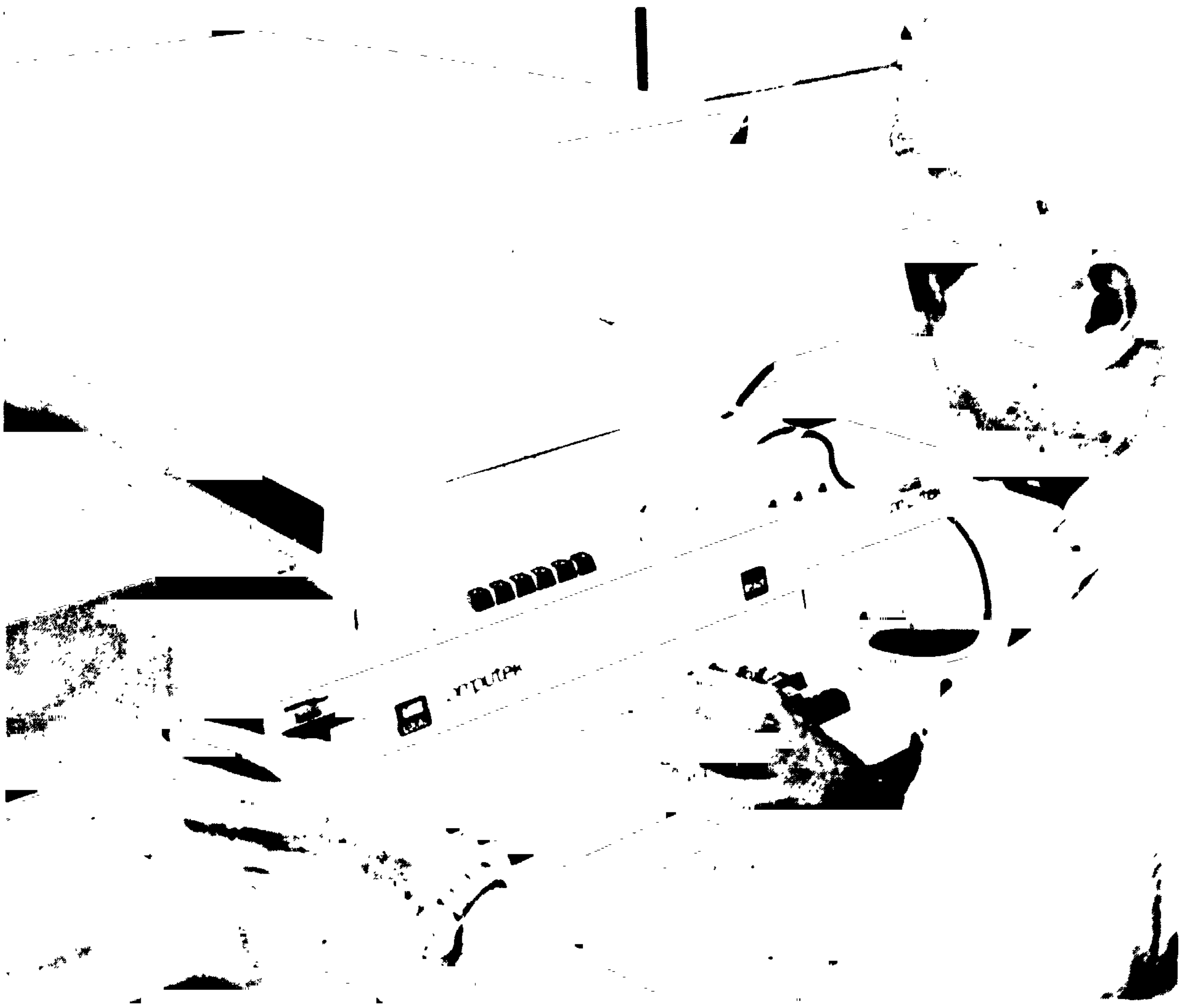

FIGURE 1.-
COMPUTEK INTERACTIVE GRAPHICS TERMINAL.

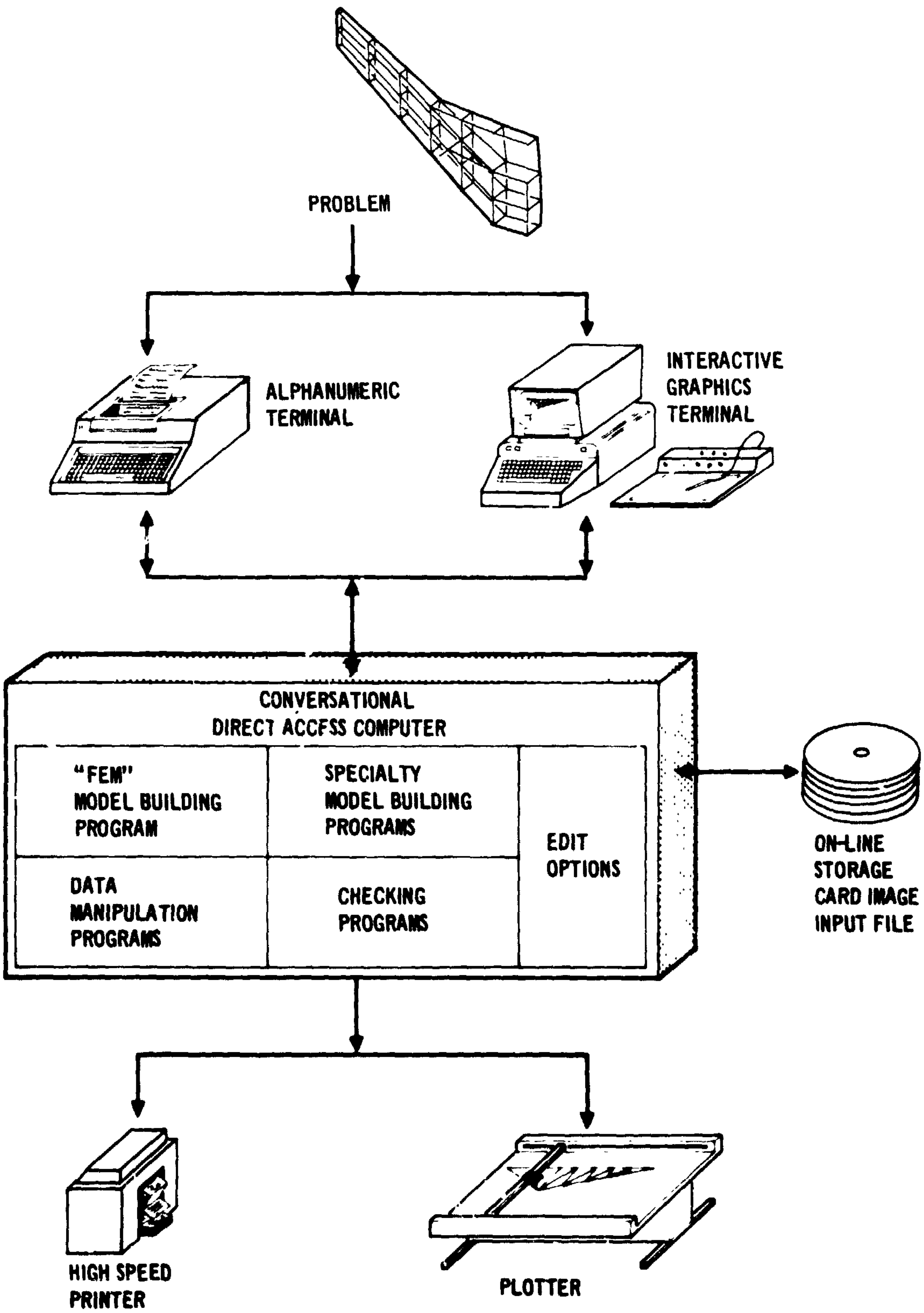

FIGURE 2. PREPROCESSING – BUILDING AND CHECKING THE FINITE ELEMENT MODEL.

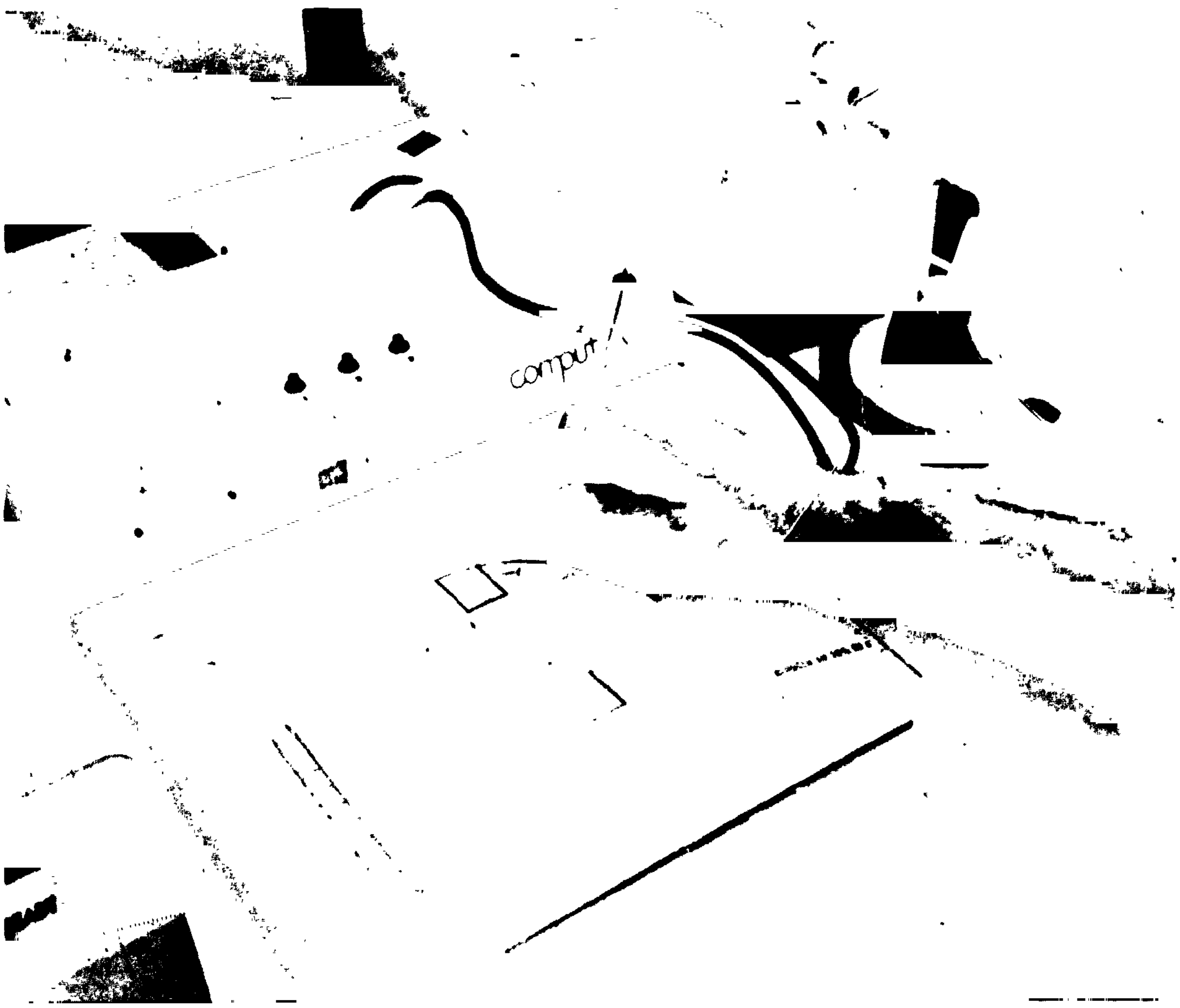

FIGURE 3.– NODE GEOMETRY IS ENTERED USING SCALE DRAWINGS.

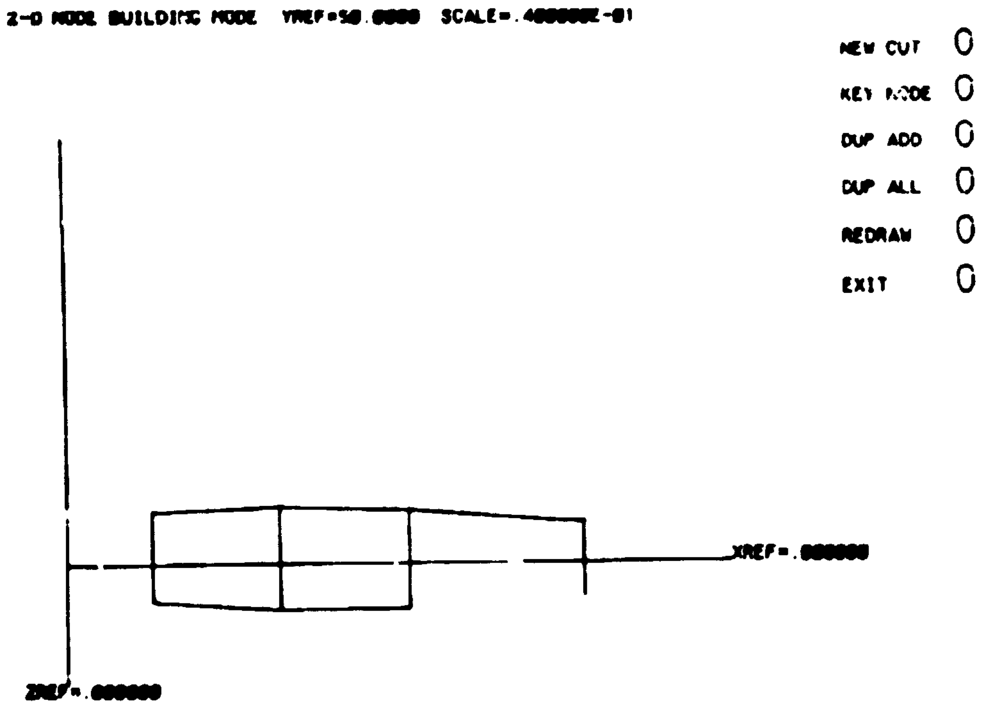

FIGURE 4.– "FEM" DISPLAY OF WING ROOT COMPLETED CROSS SECTION.

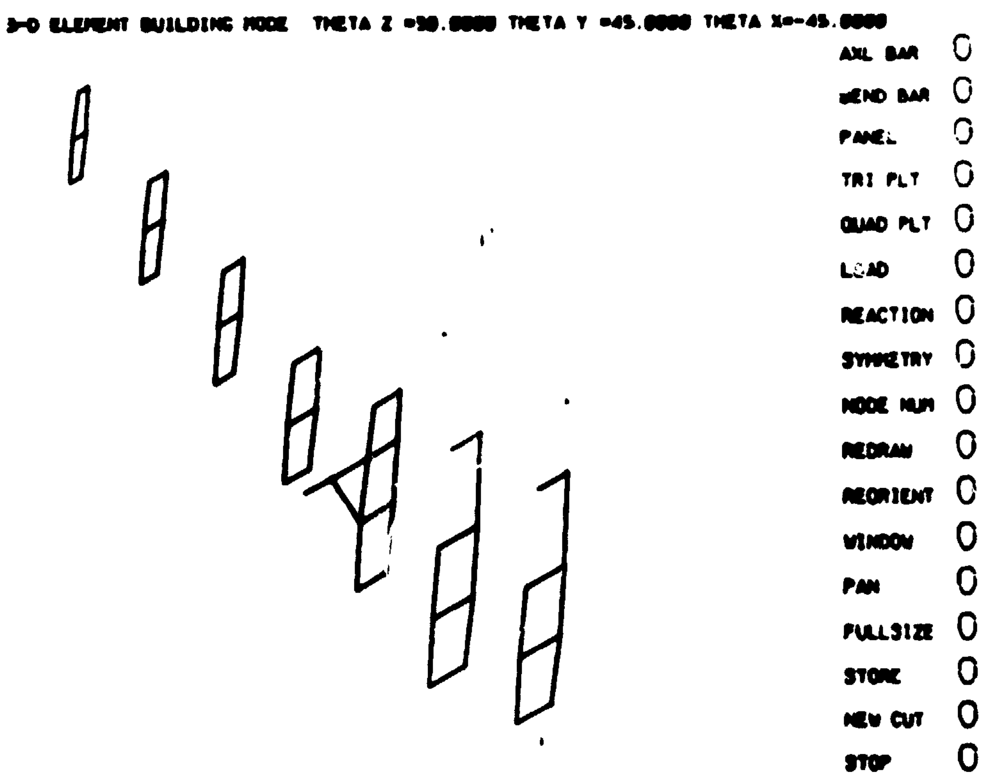

FIGURE 5.– "FEM" ISOMETRIC DISPLAY OF COMPLETED CROSS SECTIONS.

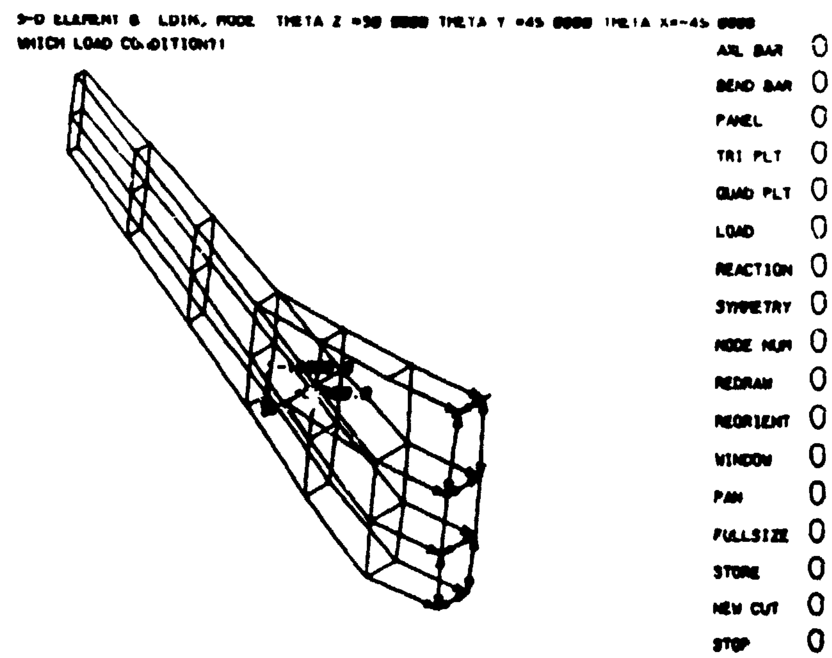

FIGURE 6.– "FEM" DISPLAY OF COMPLETED MODEL WITH FORCE VECTORS.

```
ID   FEM NASTRAN
APP   DISPLACEMENT
SOL 1,0
TIME   2
CEND
 TITLE = FEM,NASTRAN
 LOAD = 600
 SPC = 700
 DISPLACEMENT = ALL
 ELFORCE = ALL
 STRESS = ALL
 SPCFORCES = ALL
BEGIN BULK
CROD          1     430       1       2
CROD          2     430       2       3
CROD          3     430       3       4

CROD         98     430      21      31
CROD         99     430      27      14
CBAR        100     440      27      22      21                       2
CBAR        101     440      27      26      21                       2
CBAR        102     440      22      13      21                       2
CSHEAR      103     420       4      12      11       3
CSHEAR      104     420      12      20      19      11
CSHEAR      105     420       3      11      10       2

CSHEAR      163     420       1       8       7       2
CSHEAR      164     420       2       7       6       3
FORCE       600      26          -15000.  .00000  .00000-1.00000
FORCE       600      26           27300.-1.00000  .00000  .00000
GRID          1           14.84   50.00   24.83
GRID          2           16.42   50.00   61.98
GRID          3           15.24   50.00   92.37

GRID         52           27.30  350.00  173.52
GRID         53          -50.57  150.00  155.27
MAT1        300   1.0+7            0.3
PBAR        440     300      .1      2.      3.      4.
PQUAD2      410     300     0.1
PROD        430     300     0.1     1.0
PSHEAR      420     300     .02
PTRIA2      400     300     0.1
SPC         700       4       2      .0
SPC         700       5       2      .0

SPC         700       1       1      .0
SPC         700       1       3      .0
ENDDATA
```

FIGURE 7.– CARD IMAGE DATA FOR EXAMPLE PROBLEM.

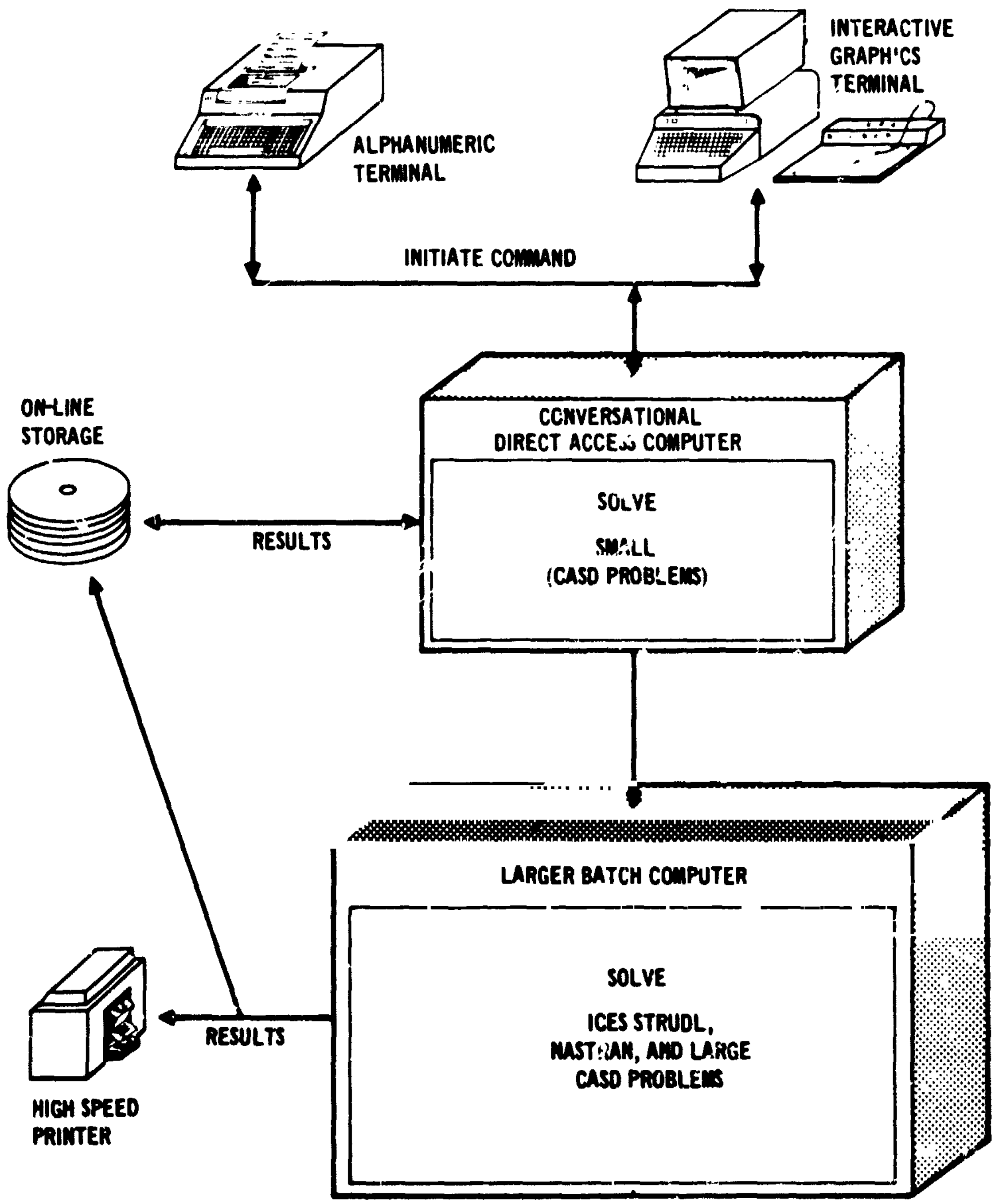

FIGURE 8. SOLUTION: SMALL PROBLEMS IN REAL TIME, LARGE PROBLEMS IN BATCH

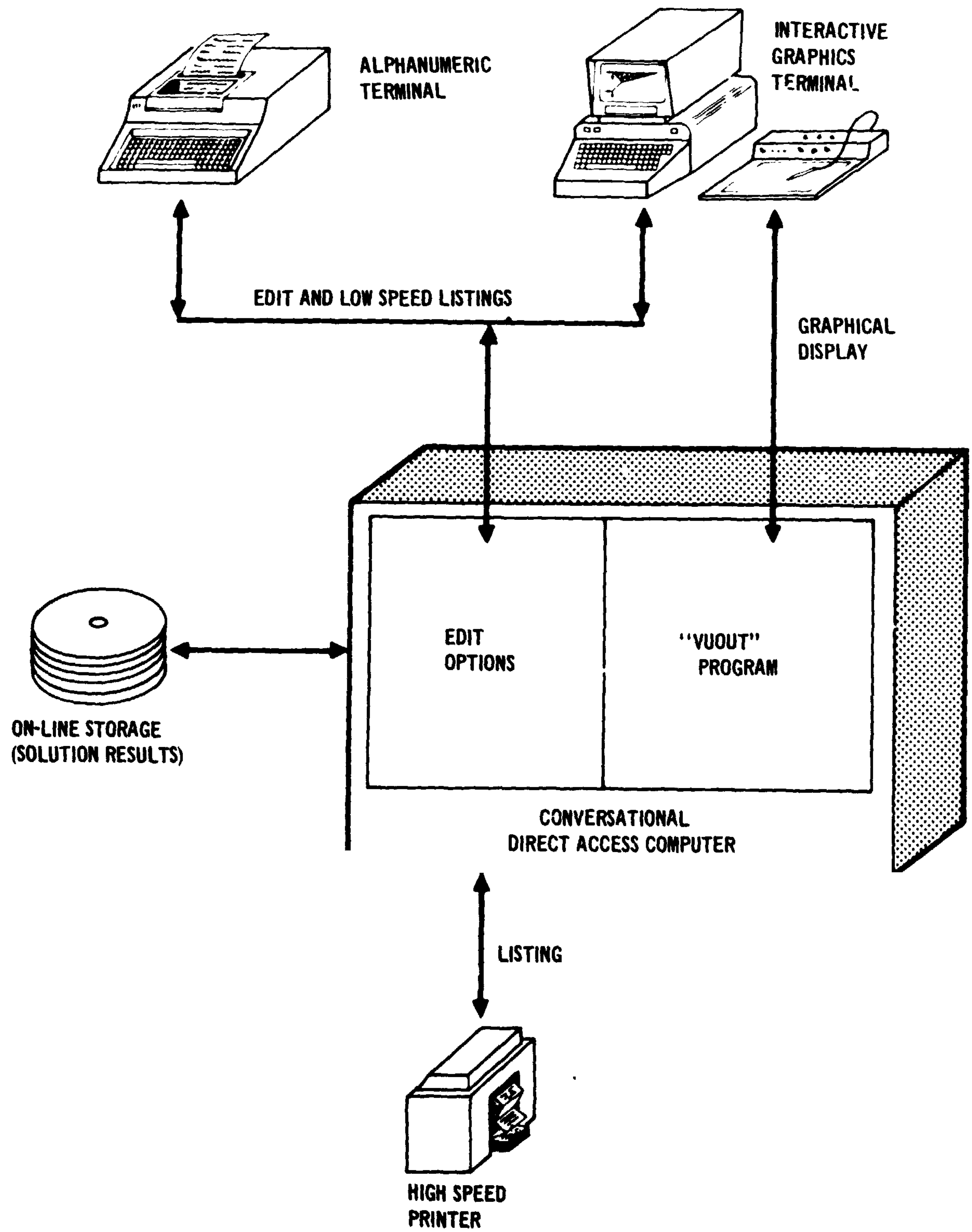

FIGURE 9. POSTPROCESSING—INTERPRETATION OF SOLUTION RESULTS.

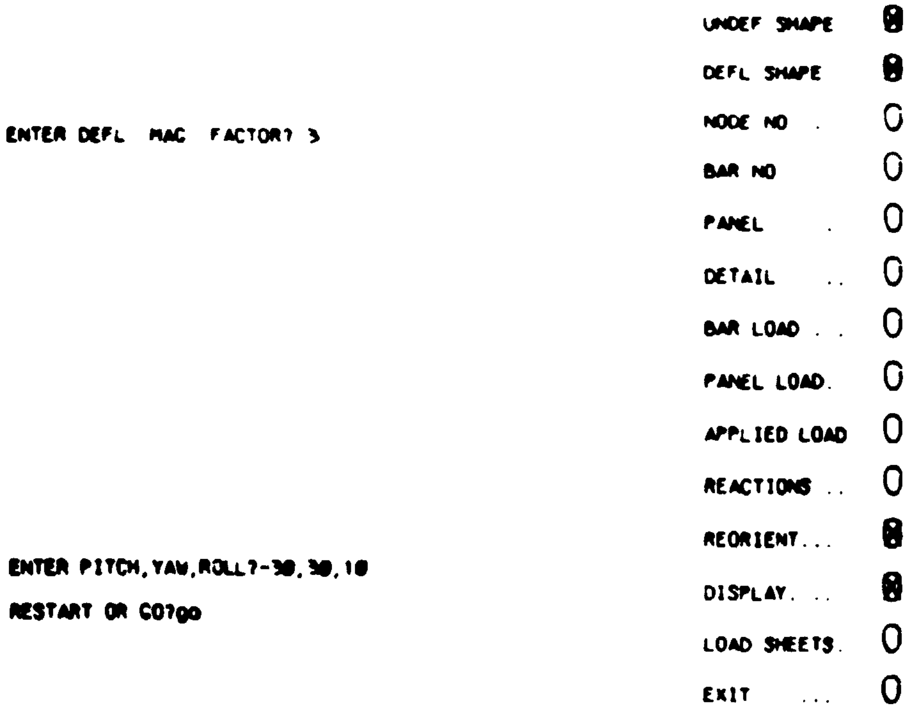

FIGURE 10.– "VUOUT" MENU OPTIONS FOR POSTPROCESSING DISPLAY.

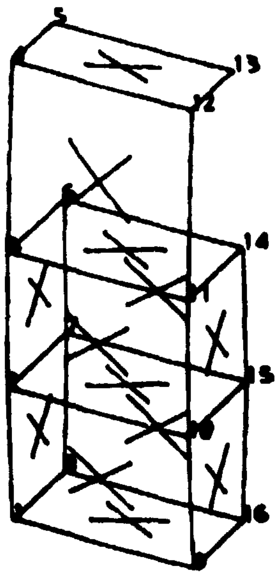

FIGURE 11.– "VUOUT" DISPLAY OF DETAIL SECTION WITH NODE NUMBERS AND PANELS INDICATED.

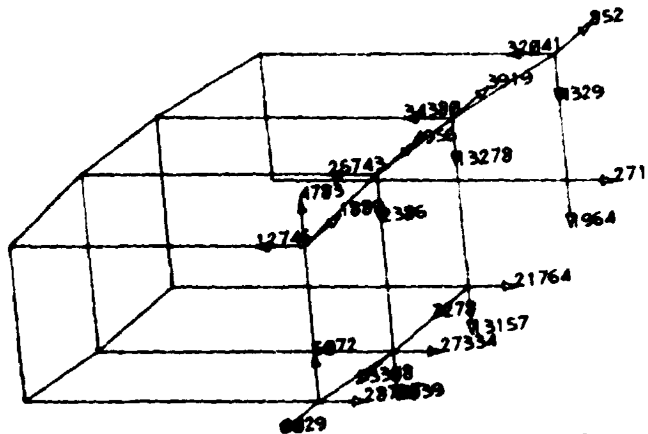

FIGURE 12.. "VUOUT" DISPLAY OF WING ROOT DETAIL WITH REACTIONS.

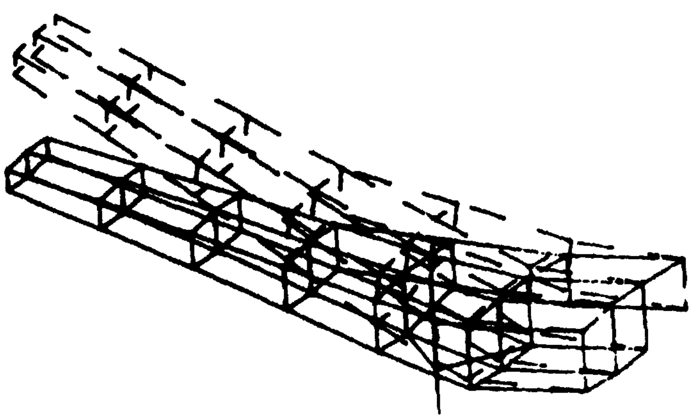

FIGURE 13.. "VUOUT" DISPLAY OF DEFLECTED/UNDEFLECTED SHAPE.

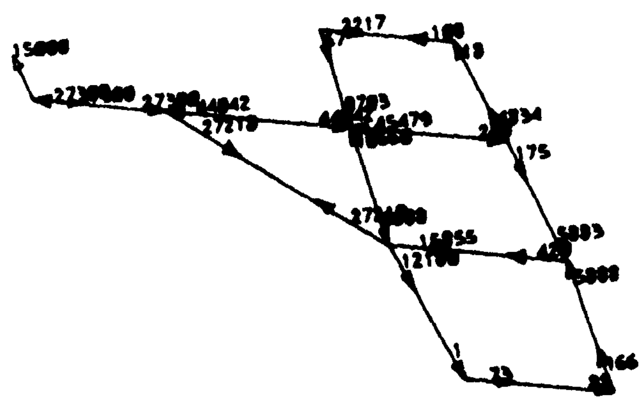

FIGURE 14.. "VUOUT" DISPLAY OF BAR LOADS ON DETAIL SECTION.

BAR NO. 102

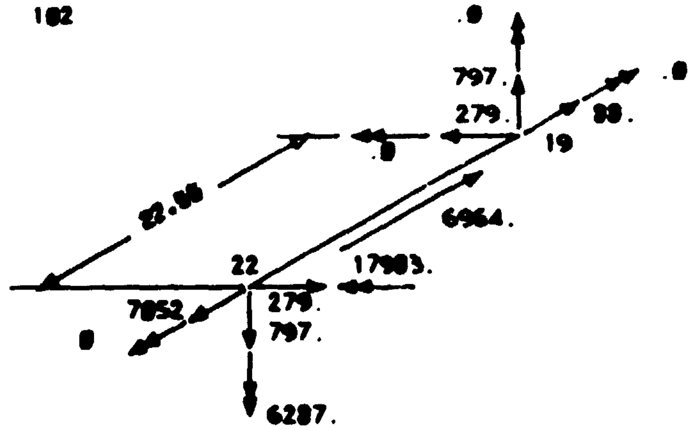

DESIGN LOAD CONDITION NO. 1

MEMBER PROPERTIES
A1= .1000 A2= .1000
IN= 2.000 IT= 2.000
J= .0000
E= 10.0 E 6

FIGURE 15.. TYPICAL "VUOUT" DISPLAY OF BAR LOAD SHEET.

SHEAR PANEL NO. 3

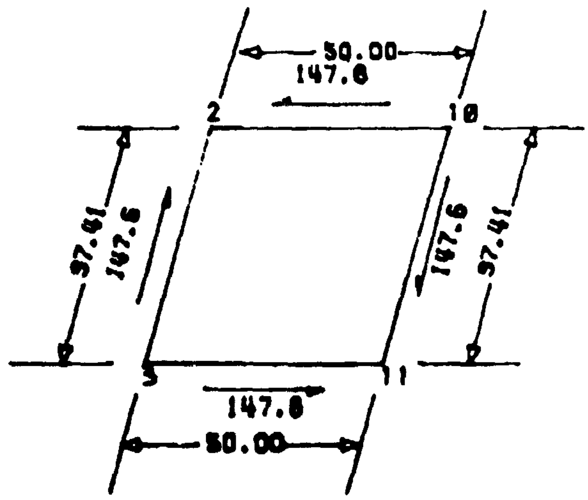

DESIGN LOAD CONDITION NO. 1

MEMBER PROPERTIES
T1= .020
T2= .020
G= 3.5 E 6

FIGURE 16.. TYPICAL "VUOUT" DISPLAY OF SHEAR PANEL LOAD SHEET.

N74-14624

PRECEDING PAGE BLANK NOT FILMED

A SIMPLIFIED MODAL PLOTTING TECHNIQUE FOR THE REPRESENTATION OF COMPLEX STRUCTURAL MODELS

By Stuart L. Hanlein

NASA Goddard Space Flight Center

SUMMARY

A plotting method has been developed that has proven to be useful in rapidly defining the mode shapes of a complex spacecraft. The reduction of the complex model to a simple "stick" plot is accomplished by augmenting the existing NASTRAN plot package with constrained plot elements. Both the existing NASTRAN modal plot package and the "stick" plots of a representative mode are presented for comparison.

INTRODUCTION

The NASTRAN plot package provides the capability of generating modal deformations (mode shapes) resulting from real eigenvalue analysis. These modal deformations of the structural model may be displayed in the deformed shape either alone or superimposed on the undeformed shape. Another available method of displaying the modal deformations is by means of displacement vectors at the grid points.

NASTRAN MODEL OF THE SPACECRAFT

When a complex structural model, such as the Applications Technology Satellite (ATS), is being analysed, problems arise in rapidly identifying characteristic mode shapes with the existing plot package. Figure 1 shows the NASTRAN plot of the undeformed structure in the launch configuration. This model consists of 311 grid points, 519 beam elements, 137 plate elements with 1696 degrees of freedom. The model was reduced to 217 dynamic degrees of freedom by the ASET option for the eigenvalue analysis, rigid format no. 3.

Figure 2, showing the deformed shape of the ATS structure superimposed on the undeformed shape, illustrates the difficulty in interpreting the mode shape from this type of plot. Orthographic projections of the modal deformations such as the side view shown in Figure 3 and the top view shown in Figure 4 are helpful but these are confusing also because of all the lines crossing over each other. Plots of subassemblies or selected structural elements may also be generated but then all of the components must be put together to get the total composite mode shape.

THIS PAGE BLANK NOT FILMED

This approach would require a considerable number of separate plots and views to obtain one mode shape. For the example of the ATS model, there are at least six (6) separate structural subassemblies that would have to be plotted and compared.

The use of displacement vector plots causes even more lines to be generated on the already crowded plot picture which only tends to confuse the modal representation of this complex structure.

SIMPLIFIED PLOTS

TRW Corporation of Redondo Beach, California has written a simplified modal plot routine for interpreting mode shapes. This routine is used to generate modal plots of structures undergoing modal vibration tests in their Computer Oriented Modal Control and Appraisal System (COMCAS). This routine consists of plotting the relative displacement of selected points on the structure being tested (in this case, the ATS spacecraft). These points are instrumented (directly or indirectly) on the structure for obtaining modal displacement response data. Orthographic "stick" type plots of these modal displacements in the three principle displacement axes versus the spacecraft longitudinal or vertical axis are generated. Figure 5 is typical of the TRW stick plots comparable to a NASTRAN projection of a mode shape shown in Figure 3.

CONVERSION OF NASTRAN MODAL PLOT TO STICK PLOTS

In order to compare the NASTRAN mode shapes with the TRW plotted mode shapes, the ATS structural model was "modified" to provide TRW type stick plots. The basic idea was that the TRW stick plot grid points are "tied" to the NASTRAN model by the use of SPC and MPC cards and the plotting program was instructed to plot only the stick points. A "Z"-axis for the structural model was generated with PLOTEL cards. This generated Z-axis was coincident with the Z-axis of the basic coordinate system. Spacecraft stations along this axis were indicated with appropriate numeric labels. Points representing structural components of the ATS were selected on this Z-axis to correspond with the TRW points. These points were then fully constrained to the original structural model by SPC and MPC cards to yield the desired displacements. For example, to obtain a plot of Y-axis modal displacement vs. Z-axis location, all degrees of freedom of the plot points except the Y-axis components are constrained. The purpose of this is to locate the position of the undeformed zero deflection upon the newly created Z-axis. (Incidentally this creates a raft of user warning messages about unconnected internal grid points). Then these points were appropriately connected by PLOTEL cards to give a continuous stick type plot of the spacecraft. The NASTRAN produced stick plot shown in Figure 6 is the equivalent of the TRW plot of Figure 5. By comparison of these two figures it is quite evident that the modal representations are the same. Obviously a separate set of MPC and SPC cards is required to represent each displacement direction. Thus each plot point on the spacecraft will have to be designated by a new grid point identification for each specific modal displacement plot desired. The displacements may be enlarged by scaling factors to emphasize the modal deflections (or to get closer agreement in this case). An ordinate axis could be created for the NASTRAN generated stick plot by introducing more PLOTEL's and labeling them accordingly. This would have to be done in combination with a printout of the modal displacements from the NASTRAN solution. By selecting different plotting symbols it is possible to follow the modal displacement of the prime structural components of the spacecraft.

CONCLUDING REMARKS

A quick glance at the simplified plots of the three (3) principal displacement axes will make the identification of the mode shape much easier than with the standard plot package. Bending modes and torsional modes become quite obvious with these plots as seen in Figures 7 and 8. For the ATS spacecraft, six (6) plots were generated for each mode. In addition to the three (3) plots of the X, Y and Z displacements, three (3) separate plots of the solar array portion of the spacecraft were generated to provide complete modal data. This was necessary in order to give a better representation of the breathing modes of this very flexible portion of the spacecraft. The organization of the stick plot package should be carefully planned in advance to give the maximum amount of modal data with the minimum number of plots. It is felt that this type of simplified stick plot will be helpful for investigating the mode shapes of complex structural models.

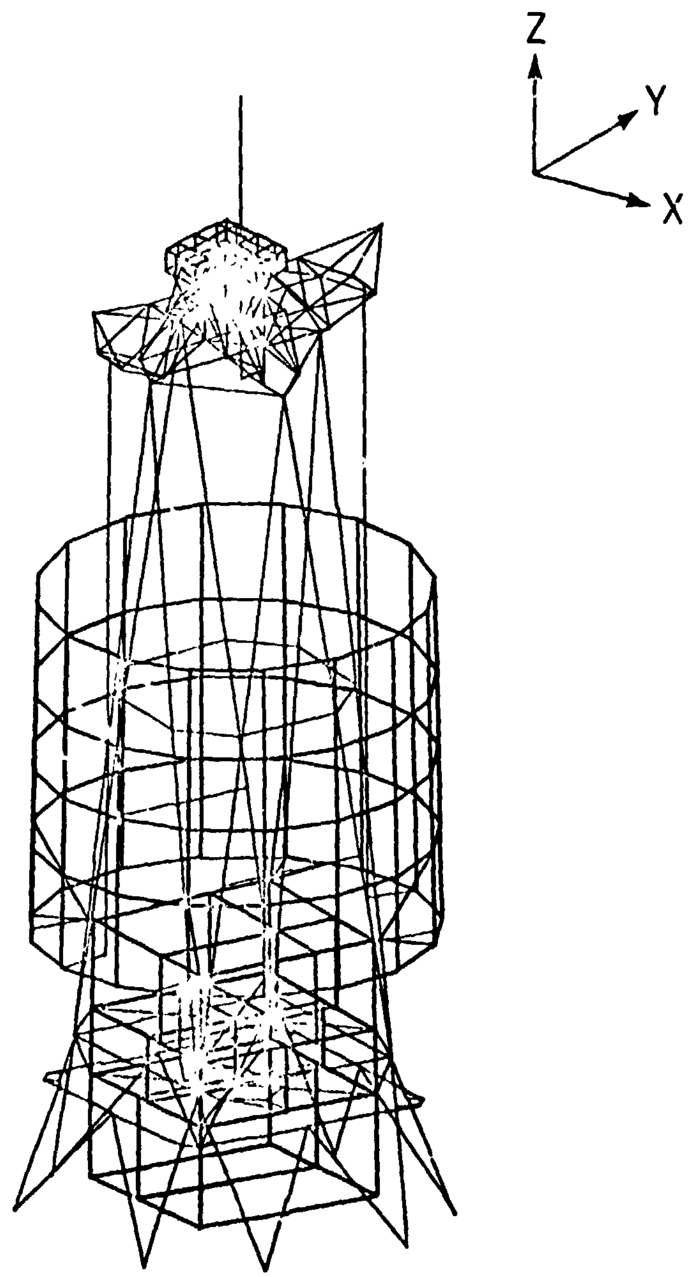

Figure 1.- NASTRAN Plot of the Undeformed Structural Model of the Applications Technology Satellite (ATS) in the Launch Configuration. (This figure is the best quality reproduction that could be made from the original computer-generated plot obtained by the author.)

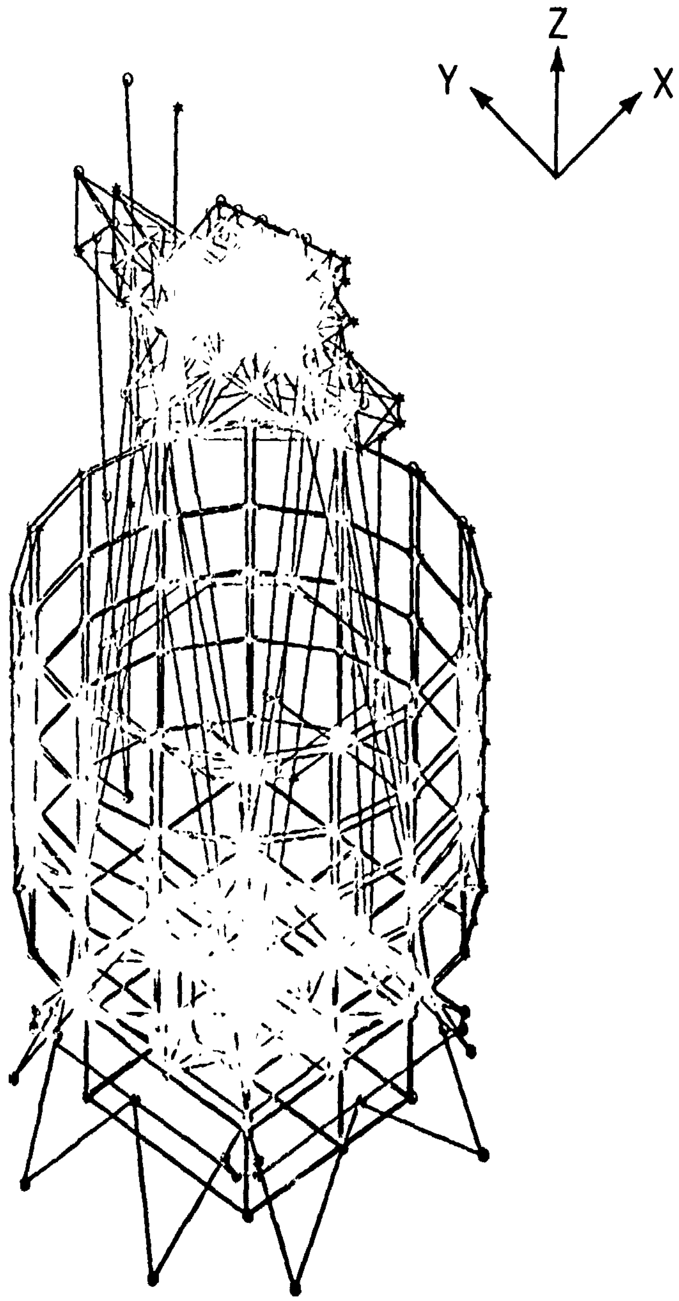

Figure 2.- NASTRAN Plot of Modal Deformation Superimposed on the Undeformed Shape (mode shape 1). (This figure is the best quality reproduction that could be made from the original computer-generated plot obtained by the author.)

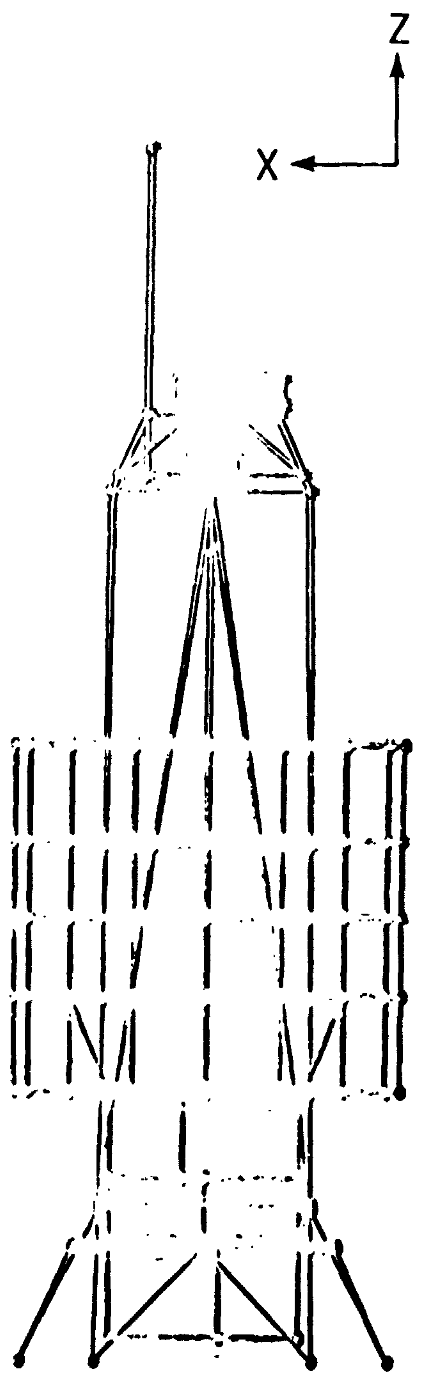

Figure 3.- NASTRAN Plot (Z-X plane, side view) of Modal Deformation Superimposed on Undeformed Shape (mode shape 1). (This figure is the best quality reproduction that could be made from the original computer-generated plot obtained by the author.)

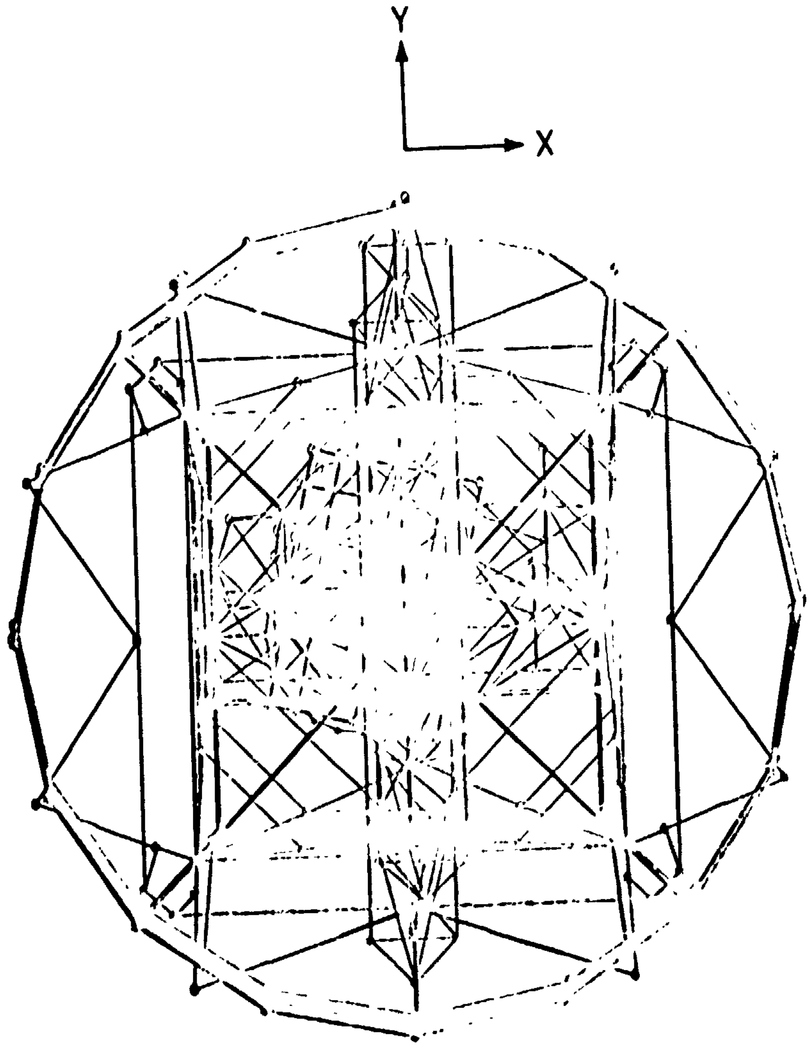

Figure 4.- NASTRAN Plot (X-Y plane, top view) of Modal Deformation Superimposed on the Undeformed Shape (mode 1). (This figure is the best quality reproduction that could be made from the original computer-generated plot obtained by the author.)

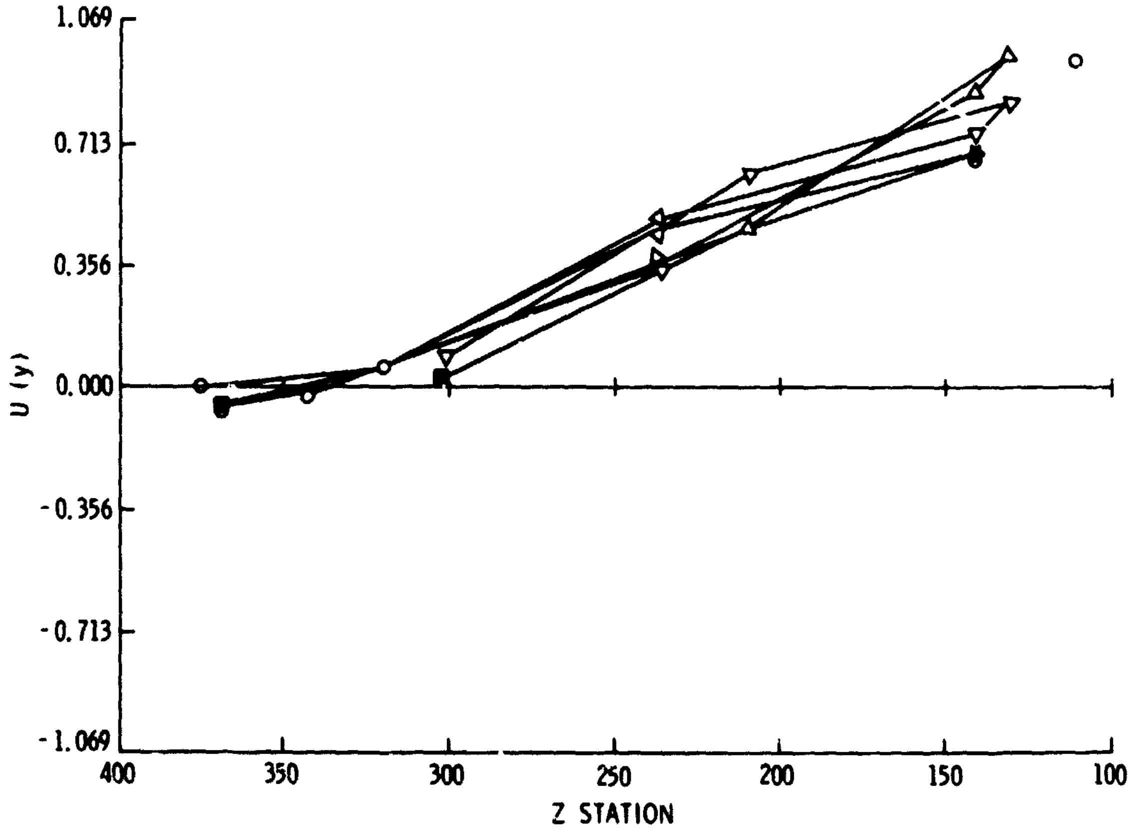

Figure 5.- TRW Stick Plot of Y-Displacement Along X-Axis from Vibration Test (experimentally determined plot).

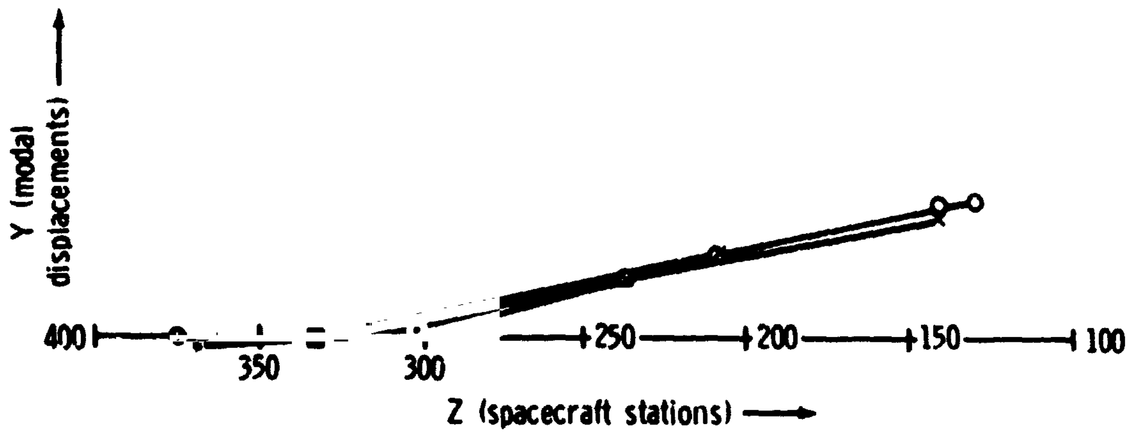

Figure 6.- NASTRAN Stick Plot of Y-Displacement Along the Z-Axis (analytically determined plot).

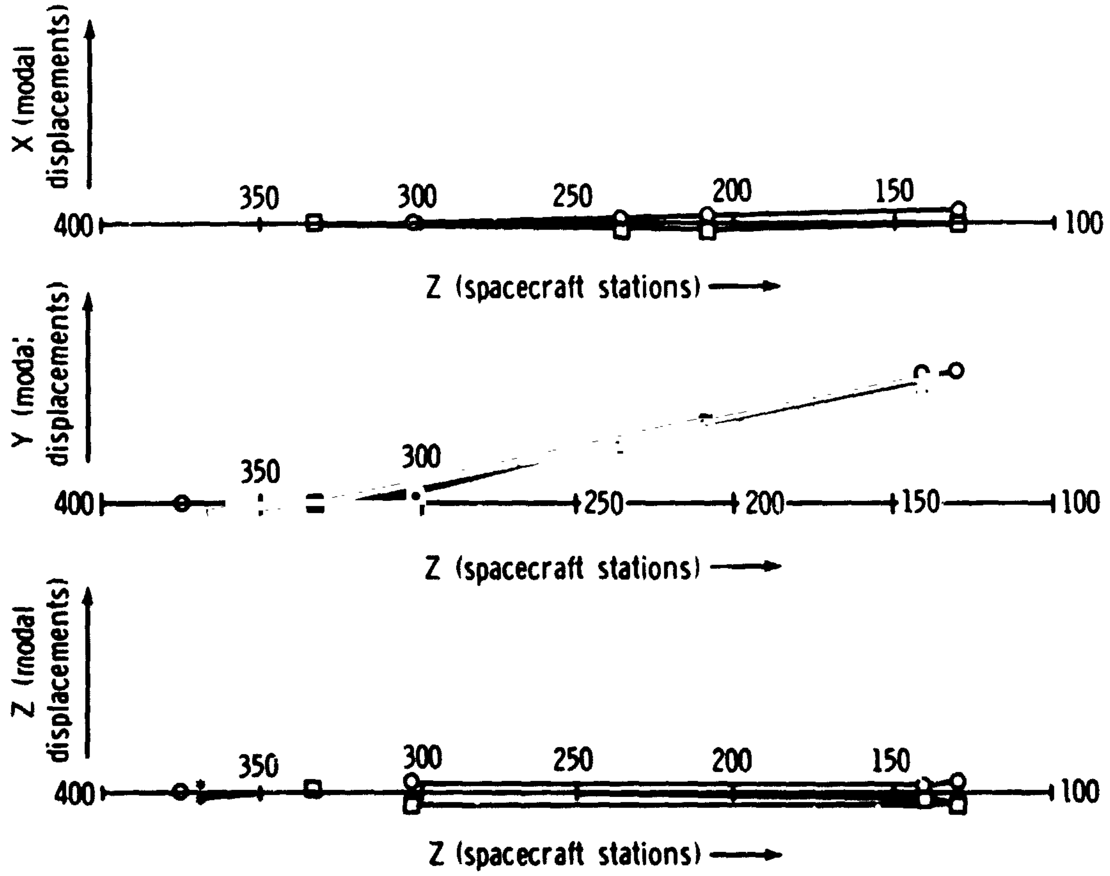

Figure 7.- NASTRAN Stick Plots of ATS Spacecraft Y-Axis Bending Mode.

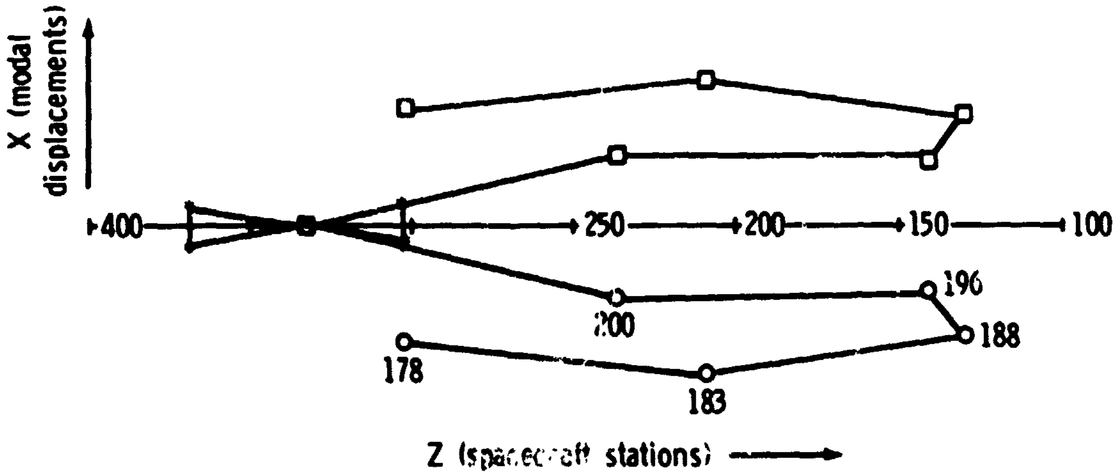

Figure 8.- ATS Spacecraft Torsional Mode Shape in Stick Plot Format.

NASTRAN POSTPROCESSOR PROGRAM FOR

TRANSIENT RESPONSE TO INPUT ACCELERATIONS

By Robert T. Wingate, Thomas C. Jones, and
Maria V. Stephens

NASA Langley Research Center

SUMMARY

The description of a transient analysis program for computing structural responses to input base accelerations is presented. A "hybrid" modal formulation is used and a procedure is demonstrated for generating and writing all modal input data on user tapes via NASTRAN. Use of several new Level 15 modules is illustrated along with a problem associated with reading the postprocessor program input from a user tape. An example application of the program is presented for the analysis of a spacecraft subjected to accelerations initiated by thrust transients. Experience with the program has indicated it to be very efficient and economical because of its simplicity and small central memory storage requirements.

INTRODUCTION

Design loads in aerospace subassemblies or components are often specified in terms of induced acceleration at the mounting interface. This concept has been traditionally used to qualify aerospace hardware by subjecting it to prescribed input accelerations on a vibration exciter. Transient analyses of subassemblies for prescribed acceleration inputs at the interface are, therefore, valuable for designing and augmenting vibration tests, and for computing design loads where vibration tests are not practical.

The transient analysis in the current level of NASTRAN (Level 15.1) does not directly provide for input acceleration forcing functions. By using the artifice of placing a large mass (with respect to the total system mass) at the desired acceleration input point, an input force equal to the total mass times the prescribed acceleration will approximate an acceleration input. Theoretically, as the fictitious added mass becomes infinite, the answer becomes exact. But as the mass becomes large, the mass matrix tends to become ill conditioned. Experience has indicated the "fictitious mass" approach is not desirable.

In addition, the current NASTRAN transient analysis allows for initial conditions only in the direct formulation. The modal formulation, which is generally faster and more economical to run, assumes zero initial conditions. In transient analyses of prestrained structures (such as a missile just prior to a burnout transient), the initial conditions become very important in predicting the magnitude of the structural loading.

PRECEDING PAGE BLANK NOT FILMED

The purpose of this paper is to describe a transient analysis program which has been developed to circumvent the abovementioned NASTRAN limitations. This program employs a modal formulation and allows for nonzero initial conditions. It is assumed that the modal input data have been generated and written on user tapes by NASTRAN. Hence, the program is termed a postprocessor program.

A complete derivation of the program theory is presented along with a detailed discussion on the generation and reading of NASTRAN user tapes. This exercise demonstrates the versatility of several of the new modules added to Level 15.1 as well as some of the limitations of user tapes. Finally, an example application of the program to the transient analysis of a spacecraft is presented.

SYMBOLS

[D]	rigid body transformation matrix for ℓ set
{F}	internal members load vector
[I]	identity matrix
[K]	stiffness matrix
[M]	mass matrix
$[\overline{M}_{ii}]$	generalized mass matrix (equation B10)
$[\overline{M}_{ir}]$	coupled flexible body, rigid body mass matrix (equation 5)
[P]	matrix of modal element force vectors
[RB]	expansion of rigid body transformation matrix to g set
{u}	vector of displacement components
{v}	time derivation of modal coordinate vector (equation 10)
$\lceil \beta_i \rfloor$	critical viscous modal damping coefficient matrix
$\lceil \omega_i^2 \rfloor$	eigenvalue matrix
$[\phi]$	matrix of modal eigenvectors
$\{\xi\}$	vector of modal coordinates

Subscripts: (See Appendix A)

α	subset of total members in structure
γ	subset of g set

Notation:

[ ]	square or rectangular matrix
$[\ ]^T$	transpose of matrix
$\lceil\ \rfloor$	diagonal matrix
{ }	column matrix

PROGRAM THEORY

In this section, the theoretical basis for a program to compute the transient response of a structure to acceleration forcing functions is given. The equations of motion are developed in terms of a "hybrid" modal formulation and reduced to a form which makes maximum use of NASTRAN generated eigenvalue data. Numerical solutions to the resulting equations are discussed along with treatment of the initial conditions. Finally, equations are presented for converting the modal response data into transient member loads and grid point accelerations.

In the derivations an attempt has been made to generally utilize the notation presented in the NASTRAN Manuals (references 1, 2, and 3) for ease of reading and implementation of the resulting equations. In particular, the set notation of Appendix A, which is taken from Section 1.7.3 of reference 3, is used throughout; although, the r set has a somewhat different meaning herein. This difference will become apparent in the course of the derivation.

Equations of Motion

Assuming no external loads are acting on the grid points of a structural system, the undamped equations of motion for displacement set $\{u_a\}$ become

$$\left[M_{aa}\right]\left\{\ddot{u}_a\right\} + \left[K_{aa}\right]\left\{u_a\right\} = 0 \tag{1}$$

where $\left[M_{aa}\right]$ and $\left[K_{aa}\right]$ are the reduced mass and stiffness matrices, respectively (see Section 3.5 of reference 2). It is assumed that the system described by equation (1) is not completely constrained against rigid body motions (i.e., it can have from 1 to 6 rigid body degrees of freedom). Equation (1) may be partitioned as follows:

$$\left[\begin{array}{c|c} M_{\ell\ell} & M_{\ell r} \\ \hline M_{\ell r}^T & M_{rr} \end{array}\right]\left\{\begin{array}{c} \ddot{u}_\ell \\ \hline \ddot{u}_r \end{array}\right\} + \left[\begin{array}{c|c} K_{\ell\ell} & K_{\ell r} \\ \hline K_{\ell r}^T & K_{rr} \end{array}\right]\left\{\begin{array}{c} u_\ell \\ \hline u_r \end{array}\right\} = 0 \tag{2}$$

where by definition, the subset $\{u_r\}$ of the displacement vector $\{u_a\}$, if constrained, would be just sufficient to eliminate rigid body motion without introducing redundant constraints. Selection of the subset $\{u_r\}$ is arbitrary and for the present analysis it is chosen to correspond to the input acceleration degrees of freedom (a.d.o.f.), and it is specified on a NASTRAN "SUPORT" Bulk Data Card. It should be noted that by using the r set for input accelerations, the a.d.o.f. are restricted to a maximum of six. This restriction is not a major limitation since the base of many components can be assumed to be rigidly constrained to a plane. The redundant points in the base can thus be assumed to be rigidly attached to a single acceleration input point.

The mathematical problem at hand is to determine the transient response of the $\{u_\ell\}$ subset to prescribed $\{\ddot{u}_r\}$ inputs. A solution using a modal formulation is presented in the following. This approach allows a significant reduction in size of the problem with little loss in accuracy by truncating the number of modes included in the solution.

Modal Coordinate Transformation

The following "hybrid" transformation between modal coordinates (ξ) and physical coordinates (u) is introduced:

$$\begin{Bmatrix} u_\ell \\ \hline u_r \end{Bmatrix} = \left[\begin{array}{c|c} \phi_{\ell i} & D_{\ell r} \\ \hline 0 & I \end{array}\right] \begin{Bmatrix} \xi_i \\ \hline u_r \end{Bmatrix} \tag{3}$$

where $\left[D_{\ell r}\right]$ is the rigid body mode matrix associated with the rigid body motion of the structure in response to displacements of the $\{u_r\}$ coordinates; $\left[\phi_{\ell i}\right]$ is the matrix of eigenvectors of the structure with the $\{u_r\}$ coordinates constrained to zero (see Appendix B); $\left[I\right]$ is the identity matrix; and $\{\xi_i\}$ is the vector of flexible body modal coordinates.

Modal Equations of Motion

Substituting equation (3) into equation (2); premultiplying by the transpose of the transformation matrix, and using equations (B5), (B6), (B10), and (B11) of Appendix B leads to the following

$$\left[\begin{array}{c|c} \overline{M}_{ii} & \overline{M}_{ir} \\ \hline \overline{M}_{ri} & \overline{M}_{rr} \end{array}\right] \begin{Bmatrix} \ddot{\xi}_i \\ \hline \ddot{u}_r \end{Bmatrix} + \left[\begin{array}{c|c} \overline{M}_{ii}\omega_i^2 & 0 \\ \hline 0 & 0 \end{array}\right] \begin{Bmatrix} \xi_i \\ \hline u_r \end{Bmatrix} = 0 \tag{4}$$

where

$$\left[\overline{M}_{ir}\right] = \left[\overline{M}_{ri}\right]^T = \left[\phi_{\ell i}^T\right]\left[M_{\ell\ell}D_{\ell r} + M_{\ell r}\right] \tag{5}$$

and
$$\left[\bar{M}_{rr}\right] = \left[D^T_{\ell r}M_{\ell\ell}D_{\ell r} + M^T_{\ell r}D_{\ell r} + D^T_{\ell r}M_{\ell r} + M_{rr}\right] \tag{6}$$

The upper partition matrix of equation (4) yields

$$\{\ddot{\xi}_i\} + \left[\omega_i^2\right]\{\xi_i\} = -\left[\bar{M}_{ii}\right]^{-1}\left[\bar{M}_{ir}\right]\{\ddot{u}_r\} \tag{7}$$

Adding viscous modal damping to equation (7) yields the desired equation of motion of the system as

$$\{\ddot{\xi}_i\} + \left[2\beta_i\omega_i\right]\{\dot{\xi}_i\} + \left[\omega_i^2\right]\{\xi_i\} = -\left[\bar{M}_{ii}\right]^{-1}\left[\bar{M}_{ir}\right]\{\ddot{u}_r\} \tag{8}$$

where β_i is the critical viscous damping ratio for the ith mode.

With the exception of the β_i values all of the other coefficient values are easily obtained as output quantities from a NASTRAN normal mode analysis (Rigid Format 3).

Method of Solution

The method of solution used in the program to solve the equations is a standard fourth order Runge-Kutta numerical integration routine with variable step size error control. Use of this subroutine required reduction of equation (8) to first order and generation of the initial conditions in terms of modal coordinates. These procedures are discussed in the following sections.

Reduction to first order equations. - Integration via the Runge-Kutta Subroutine requires the system equations to be a set of first order differential equations of the form

$$\{\dot{y}_j\} = \{f_j(y_1, y_2, \ldots y_n)\} \quad j = 1, 2, \ldots n \tag{9}$$

Equation (8) can be transformed to the form of (9) by introducing the auxiliary variable $\{v_i\}$ where

$$\{\dot{\xi}_i\} = \{v_i\} \tag{10}$$

Using equation (10), equation (8) then leads to

$$\{\dot{v}_i\} = -\left[2\beta_i\omega_i\right]\{v_i\} - \left[\omega_i^2\right]\{\xi_i\} - \left[1/\overline{M}_{ii}\right]\left[\overline{M}_{ir}\right]\{\ddot{u}_r\} \tag{11}$$

Equations (10) and (11) are now a set of equations in the form of equation (9) (as required) and are integrated simultaneously.

Initial conditions. - If the initial conditions are known for each of the $\{u_a\}$ coordinates, then the modal initial conditions can be determined by pre-multiplying equation (3) by the matrix

$$\left[\begin{array}{c|c} \phi_{\ell i}^T & 0 \\ \hline D_{\ell r}^T & I \end{array}\right]\left[\begin{array}{c|c} K_{\ell\ell} & K_{\ell r} \\ \hline K_{r\ell} & K_{rr} \end{array}\right]$$

using equations (B5), (B6), and (B11); and solving for $\{\xi_i\}$ to obtain

$$\{\xi_i\} = \left[\overline{M}_{ii}\omega_i^2\right]^{-1}\left[\phi_{\ell i}\right]^T\left[\begin{array}{c|c} K_{\ell\ell} & K_{\ell r} \end{array}\right]\left\{\begin{array}{c} u_\ell \\ \hline u_r \end{array}\right\} \tag{12}$$

By taking the time derivative of both sides of equation (12), the initial conditions for $\{\dot{\xi}_i\}$ can also be determined in terms of $\{\dot{u}_\ell\}$ and $\{\dot{u}_r\}$ values.

Since the initial conditions are not generally known in terms of the $\{u_a\}$ coordinates, a different approach was taken for the present program. This program assumes

$$\{\dot{v}_i(0)\} = 0 \tag{13}$$

and

$$\{v_i(0)\} = 0 \tag{14}$$

that is, the structure is assumed to be initially in a steady state deformed position. The initial conditions are then computed from equation (11) as

$$\{\xi_i(0)\} = -\left[1/\overline{M}_{ii}\omega_i^2\right]\left[M_{ir}\right]\{\ddot{u}_r(0)\} \tag{15}$$

Equations (14) and (15) thus yield the necessary, initial conditions for numerical integration of equations (10) and (11).

Computed Response Data

Having obtained the transient response of the modal coordinates, it is desirable to transform these variables into transient member loads and accelerations in terms of the physical $\{u_a\}$ coordinates.

The member loads are given by superposition as

$$\{F_\alpha\} = \left[P_{\alpha i}\right]\{\xi_i\} \tag{16}$$

where $\left[P_{\alpha i}\right]$ is a matrix of modal element force vectors for an arbitrary subset α of the total members in the system and $\{F_\alpha\}$ is the total load vector corresponding to the subset α. The modal member load vectors are obtainable as standard output from a NASTRAN Normal Mode Analysis.

Using equation (10), the grid point accelerations are computed from the second time derivative of the upper partition of equation (3) to be

$$\{\ddot{u}_\gamma\} = \left[\phi_{\gamma i}\right]\{\dot{v}_i\} + \left[RB_{\gamma r}\right]\{\ddot{u}_r\} \tag{17}$$

where γ is an arbitrary subset of the g set and $\left[RB_{gr}\right]$ is a merger of the rigid body transformation matrix $\left[D_{\ell r}\right]$ with the o , s , and m sets. The matrices $\left[\phi_{gi}\right]$ and $\left[RB_{gr}\right]$ are generated by NASTRAN and the subject postprocessor program selects the subset γ to be picked up for use in equation (17). The quantity $\{\dot{v}_i\}$ is given by equation (11) and $\{\ddot{u}_r\}$ is a given input vector.

If the quantities $\{u_\gamma\}$ and $\{\dot{u}_\gamma\}$ are also desired, equation (17) can be reduced to a set of first order equations to be integrated simultaneously with equations (10) and (11). For the present program, however, this was not done.

NASTRAN GENERATED INPUT DATA

The rigid body and flexible body modal data necessary for solution of the foregoing equations are easily generated by a NASTRAN Normal Mode Analysis and written out on user tapes. Hence, the present postprocessor program is designed to read the majority of its input directly from the NASTRAN user tapes.

A DMAP alter package is required to generate part of the NASTRAN data and to write the user tapes. Also, interrogation of the user tapes to read the data requires special considerations. Both of these aspects are discussed in the following sections.

DMAP Alter Package for Normal Mode Analysis

A listing of the DMAP alter package is given in Appendix C. A brief discussion and explanation of the most significant statement is given in the following tabulation. Note the use of the new Level 15 modules VEC, UMERGE, and OUTPUT2. (See sections 3,4, 5.2, and 5.3 of ref. 1 and section 3.5 of ref. 2)

DMAP Alter Statement No.	Function
2 and 3	Merge an r x r null matrix with the $D_{\ell r}$ matrix to create a pseudo a x r size rigid body modal matrix $\begin{bmatrix} D_{\ell r} \\ \hline 0 \end{bmatrix} \rightarrow \begin{bmatrix} RB_{ar} \end{bmatrix}$
4 through 20	Merge the omitted coordinates, single point constraint coordinates, and the multipoint constraint coordinates, if present, with $\begin{bmatrix} RB_{ar} \end{bmatrix}$ to obtain $\begin{bmatrix} RB_{gr} \end{bmatrix}$
6	Recovery of omitted coordinates $\begin{bmatrix} RB_{or} \end{bmatrix} = \begin{bmatrix} G_{oa} \end{bmatrix}\begin{bmatrix} RB_{ar} \end{bmatrix}$
7 and 8	Merging of omitted coordinates $\begin{bmatrix} RB_{ar} \\ \hline RB_{or} \end{bmatrix} \rightarrow \begin{bmatrix} RB_{fr} \end{bmatrix}$
12 and 13	Merging of SPC constraints assuming they are zero $\begin{bmatrix} RB_{fr} \\ \hline 0 \end{bmatrix} \rightarrow \begin{bmatrix} RB_{nr} \end{bmatrix}$
17	Recovery of dependent MPC coordinates $\begin{bmatrix} RB_{mr} \end{bmatrix} = \begin{bmatrix} G_{mn} \end{bmatrix}\begin{bmatrix} RB_{nr} \end{bmatrix}$
18 and 19	Merging of dependent MPC coordinates $\begin{bmatrix} RB_{nr} \\ \hline RB_{mr} \end{bmatrix} \rightarrow \begin{bmatrix} RB_{gr} \end{bmatrix}$
21	Prints $\begin{bmatrix} RB_{gr} \end{bmatrix}$

DMAP Alter Statement No.	Function
22 and 23	Write $\begin{bmatrix} RB_{gr} \end{bmatrix}$ on a user tape
24 and 25	Change the eigenvalue problem from "a" size to "ℓ" size in agreement with equation (B9)
26 and 27	Change the checkpointed modal matrix from "a" size to "ℓ" size
29	Merging of the "r" coordinates constrained to zero with the "ℓ" size modal matrix $\begin{bmatrix} \phi_{\ell i} \\ \hline 0 \end{bmatrix} \rightarrow \begin{bmatrix} \phi_{ai} \end{bmatrix}$
30 and 31	$\begin{bmatrix} \overline{M}_{ir} \end{bmatrix} = \begin{bmatrix} \phi_{\ell i} \end{bmatrix}^T \begin{bmatrix} M_{\ell\ell} D_{\ell r} + M_{\ell r} \end{bmatrix}$
32	Prints $\begin{bmatrix} \overline{M}_{ir} \end{bmatrix}$
33	Writes $\begin{bmatrix} \overline{M}_{ir} \end{bmatrix}$ on a user tape
35 and 36	Write the modal deflections (OPHIG), the modal SPC forces (OQG1), and the modal element forces (OEF1) on a user tape

Interrogation of User Tapes

When using NASTRAN user tapes for input to postprocessor programs, the analyst must read the tape and selectively extract the required input from the totality of data present. This task requires either a prior knowledge of the format used in writing the tape or interrogation of the tape to see how it is written.

Unfortunately, the user tapes generated by NASTRAN are written in unformated binary (i.e. with a mixture of integer, floating point, and alphanumeric formats). In addition, some of the data is packed (i.e., zeros omitted). This randomness eliminates a prior knowledge of the format.

Interrogation of the tapes using standard tape dump routines is also somewhat futile since these programs read and print all data in a single format. To illustrate this problem, 19 records of a typical user tape, written to an E format, are listed in figure 1. Obviously, much of the data given is meaningless.

This interrogation problem was circumvented for the present program by writing a special tape dump program for the Langley Research Center CDC 6000 series computer to read and print the mixed format. The program logic was patterned after the NASTRAN module TABPRT and a listing is given in Appendix D. Using the Appendix D program, the same tape used to generate figure 1 was again read and the results are given in figure 2. From this improved interrogation the analyst can easily find where desired data are located and adjust the read statements in the postprocessor program accordingly.

From the foregoing discussion, it is apparent that a postprocessor program must be dynamic. That is, the input read statements must be continually changed to fit each new problem after interrogation of the user tape.

EXAMPLE APPLICATION

The subject transient analysis program was developed in support of the Viking Project, which has a mission to soft-land a scientific payload on the surface of Mars in 1976. In particular, this program was intended to provide transient loads and accelerations in the Viking Dynamic Simulator (VDS) shown in figure 3 for input acceleration transients at the base of the Centaur truss adaptor. The VDS is a dummy spacecraft, which is dynamically similar to the actual Viking spacecraft, and will be flown on a proof (or test) flight of a new Titan D-1T Centaur launch vehicle configuration in 1974. This launch vehicle will be used for the Viking mission and is shown in figure 4 along with the Viking spacecraft.

Several discrete transient events induce high loads into the VDS with the more prominent of these being Titan Stage 0 Ignition, Titan Stage 1 Shutdown, and the Centaur Main Engine Cutoffs. All of these events were analyzed in detail using the subject program and some of the results from the Titan Stage 0 Ignition were selected as a typical illustration of input and output data.

Six degree-of-freedom acceleration inputs into the base of the VDS were determined analytically from a transient loads analysis of the actual Viking configuration as depicted in figure 5. Input to the transient analysis of the actual Viking configuration was based on measured force transients from previous Titan launches. The base of the VDS was constrained to a plane and the six components of acceleration were input at a single grid point in the center of the base.

A typical set of input translational components of acceleration are shown in figure 6. The longitudinal (or Z) component is seen to be the most significant and it starts at 1g (9.81 m/sec^2) to represent the initial gravity load on the vehicle resting on the launch pad. This gravity loading causes an initial condition on the modal coordinates $\{\xi_i(0)\}$ as indicated in equation (16). The near sinusoidal oscillation of the Z component after 0.5 second is attributed to excitation of a longitudinal mode of the vehicle by the initial thrust transient.

Using the input acceleration (see figure 6) and the modal data (for 18 modes) from the NASTRAN analysis, selected loads for VDS members and accelerations were computed using a viscous damping model which is a function of the modal frequencies. A typical load-versus-time response is shown for a member of the Viking Spacecraft Adaptor in figure 7. Similarly, the translational terms of the acceleration computed for the top of the VDS, are shown in figure 8.

A typical computer run for the example problem on the Langley Research Center CDC 6600 Computer required a storage of $53\ 000_8$ and 200 CPU seconds for execution (including time for generation of 31 output plots). A comparable NASTRAN transient analysis would require at least 120% increase in storage, and considerable increase in CPU time and calls to the operating system. Postprocessor programs thus are seen to offer potential economic savings in addition to special purpose capability.

CONCLUDING REMARKS

The transient analysis program described herein yields a simple, convenient, and economical approach for treating input accelerations and modal initial conditions. Other than the limitation of six on the maximum number of input acceleration components, the program is applicable to a broad spectrum of structural applications.

The fact that such a postprocessor program could be simply written to interface with NASTRAN demonstrates the expanded utility of NASTRAN via the new Level 15 utility modules and user tape option. Tailor-made programs such as the present one can be designed to be very efficient in comparison to NASTRAN. Thus, the authors would encourage further additions and refinement of postprocessor convenience modules rather than expanded capability and complexity of NASTRAN. In particular the formats for writing user tapes, so that they may be easily read by postprocessor programs, should be given prime consideration.

APPENDIX A

THE NESTED VECTOR SET CONCEPT USED TO REPRESENT COMPONENTS OF DISPLACEMENT

In constructing the matrices used in the Displacement Approach, each row and/or column of a matrix is associated closely with a grid point, a scalar point, or an extra point. Every grid point has 6 degrees of freedom associated with it, and hence 6 rows and/or columns of the matrix. Scalar and extra points only have one degree of freedom. At each point (grid, scalar, extra) these degrees of freedom can be further classified into subsets, depending on the constraints or handling required for particular degrees of freedom. (For example, in a two-dimensional problem all z degrees of freedom are constrained and hence belong to the s (single-point constraint) set.) Each degree of freedom can be considered as a "point," and the entire model is the collection of these one-dimensional points.

Nearly all of the matrix operations in displacement analysis are concerned with partitioning, merging, and transforming matrix arrays from one subset of displacement components to another. All the components of displacement of a given type (such as all points constrained by single-point constraints) form a vector set that is distinguished by a subscript from other sets. A given component of displacement can belong to several vector sets. The mutually exclusive vector sets, the sum of whose members are the set of all physical components of displacements, are as follows:

u_m points eliminated by <u>multipoint</u> constraints

u_s points eliminated by <u>single</u>-point constraints

u_o points <u>omitted</u> by structural matrix partitioning

u_r points to which determinate <u>reactions</u> are applied in static analysis,

u_ℓ the remaining structural points used in static analysis (points <u>left</u> over)

u_e <u>extra</u> degrees of freedom introduced in dynamic analysis to describe control systems

The vector sets obtained by combining two or more of the above sets are (+ sign indicates the union of two sets)

$u_a = u_r + u_\ell$, the set used in real eigenvalue <u>analysis</u>

$u_d = u_a + u_e$, the set used in dynamic analysis by the <u>direct</u> method

$u_f = u_a + u_o$, unconstrained (free) structural points

$u_n = u_f + u_s$, all structural points not constrained by multipoint constraints

$u_g = u_n + u_m$, all structural (grid) points including scalar points

$u_p = u_g + u_e$, all physical points

In dynamic analysis, additional vector sets are obtained by a modal transformation derived from real eigenvalue analysis of the set u_a. These are

ξ_o rigid body (zero frequency) modal coordinates

ξ_f finite frequency modal coordinates

$\xi_i = \xi_o + \xi_f$, the set of all modal coordinates

One vector set is defined that combines physical and modal coordinates. The set is $u_h = \xi_i + u_e$, the set used in dynamic analysis by the modal method.

The nesting of vector sets is depicted by the following diagram:

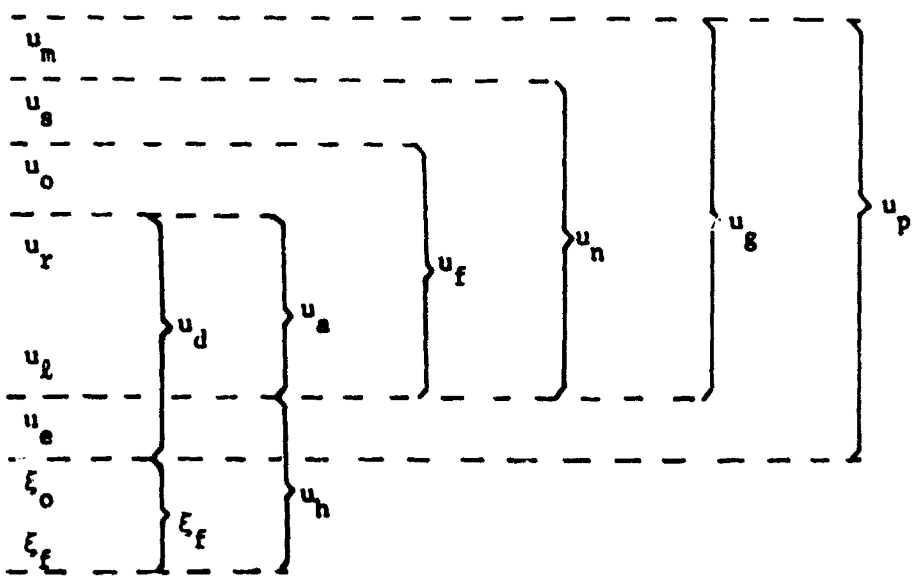

The data block USET (USETD in dynamics) is central to this set classification. Each word of USET corresponds to a degree of freedom in the problem. Each set is assigned a bit in the word. If a degree of freedom belongs to a given set, the corresponding bit is on. Every degree of freedom can then be classified by analysis of USET. The common block /BITPØS/ relates the sets to bit numbers.

APPENDIX B

MODAL PROPERTIES

In this section, several identities relating to both the rigid body modes and the flexible body modes are presented. Although these identities are perhaps familiar, they are included herein for completeness and continuity of notation.

Rigid Body Modal Properties

For periodic motion of frequency ω, equation (2) reduces to the eigenvalue equation

$$\left[\begin{bmatrix} K_{\ell\ell} & K_{\ell r} \\ K^T_{\ell r} & K_{rr} \end{bmatrix} - \omega^2 \begin{bmatrix} M_{\ell\ell} & M_{\ell r} \\ M^T_{\ell r} & M_{rr} \end{bmatrix}\right] \begin{Bmatrix} u_\ell \\ u_r \end{Bmatrix} = 0 \tag{B1}$$

The solution of equation (B1) yields the natural frequencies and the corresponding natural modes of the system. For the rigid body modes corresponding to $\omega = 0$, equation (B1) reduces to

$$\begin{bmatrix} K_{\ell\ell} & K_{\ell r} \\ K^T_{\ell r} & K_{rr} \end{bmatrix} \begin{Bmatrix} u_\ell \\ u_r \end{Bmatrix}_{rig.} = 0 \tag{B2}$$

Since the rigid body mode matrix $\left[D_{\ell r}\right]$ relates the rigid body motions $\{u_\ell\}_{rig.}$ in terms of $\{u_r\}_{rig.}$, the following transformation may be written:

$$\begin{Bmatrix} u_\ell \\ u_r \end{Bmatrix}_{rig.} = \begin{bmatrix} D_{\ell r} \\ I \end{bmatrix} \{u_r\}_{rig.} \tag{B3}$$

where $\left[I\right]$ is the identity matrix. Using equation (B3), equation (B2) gives

$$\begin{bmatrix} K_{\ell\ell} & K_{\ell r} \\ K^T_{\ell r} & K_{rr} \end{bmatrix} \begin{bmatrix} D_{\ell r} \\ I \end{bmatrix} \{u_r\}_{rig.} = 0 \tag{B4}$$

For arbitrary $\{u_r\}_{rig.}$ displacements, it follows from the partitions of (B4) that

$$\left[K_{\ell\ell}\right]\left[D_{\ell r}\right] + \left[K_{\ell r}\right] = 0 \tag{B5}$$

and

$$\left[K_{\ell r}^T\right]\left[D_{\ell r}\right] + \left[K_{rr}\right] = 0 \tag{B6}$$

Equations (B5) and (B6) thus yield two important identities relating the rigid body modes and the partitions of the stiffness matrix.

It should also be noted that solving equation (B5) for the rigid body mode matrix yields

$$\left[D_{\ell r}\right] = -\left[K_{\ell\ell}\right]^{-1}\left[K_{\ell r}\right] \tag{B7}$$

which is consistent with equation (41) in Section 3.5 of reference 2 and is the equation used in NASTRAN Rigid Format 3 to compute the rigid body mode matrix.

Flexible Body Modal Properties

By definition of the $\{u_r\}$ degrees-of-freedom, introduction of the constraint

$$\{u_r\} = 0 \tag{B8}$$

eliminates rigid body motion leaving only flexible body motion. Using equation (B8), the upper partition of equation (B1) yields the following eigenvalue equation for the flexible body modes:

$$\left[K_{\ell\ell} - \omega^2 M_{\ell\ell}\right]\{u_\ell\} = 0 \tag{B9}$$

The modal matrix $\left[\phi_{\ell i}\right]$ of the i eigenvectors of equation (B9) is shown in reference 4 to satisfy the following orthogonality relationships:

$$\left[\phi_{\ell i}\right]^T\left[M_{\ell\ell}\right]\left[\phi_{\ell i}\right] = \left[\bar{M}_{ii}\right] \tag{B10}$$

$$\left[\phi_{\ell i}\right]\left[K_{\ell\ell}\right]\left[\phi_{\ell i}\right] = \left[\bar{M}_{ii}\omega_i^2\right] \tag{B11}$$

The above equations provide the foundation for modal formulation.

APPENDIX C

DMAP ALTER PACKAGE

```
ALTER    81
VEC      USET/VA/C,N,A/C,N,L/C,N,R $
MERGE    DM,,,,,VA/RBA/C,N,0/C,N,2/C,N,2 $
EQUIV    RBA,RBF/OMIT $
COND     LBOM,OMIT $
MPYAD    GO,RBA,/RBO/C,N,0/C,N,1/C,N,0/C,N,1 $
VEC      USET/VF/C,N,F/C,N,A/C,N,O $
MERGE    RBA,RBO,,,,VF/RBF/C,N,0/C,N,2/C,N,2 $
LABEL    LBOM $
EQUIV    RBF,RBN/SINGLE $
COND     LBSS,SINGLE $
VEC      USET/VN/C,N,N/C,N,F/C,N,S $
MERGE    RBF,,,,,VN/RBN/C,N,0/C,N,2/C,N,2 $
LABEL    LBSS $
EQUIV    RBN,RBG/MPCF2 $
COND     LBMM,MPCF2 $
MPYAD    GM,RBN,/RBM/C,N,0/C,N,1/C,N,0/C,N,1 $
VEC      USET/VG/C,N,G/C,N,N/C,N,M $
MERGE    RBN,RBM,,,,VG/RBG/C,N,0/C,N,2/C,N,2 $
LABEL    LBMM $
MATGPR   GPL,USET,SIL,RBG//C,N,R/C,N,G $
OUTPUT2, ,,,,//C,N,-1/C,N,11 $
OUTPUT2, RBG,,,,//C,N,0/C,N,11 $
ALTER    89,89
READ     KLL,MLL,,,EED,,CASECC/LAMA,PHIL,MI,OEIGS/
ALTER    91,91
CHKPNT   LAMA,PHIL,MI,OEIGS $
ALTER    93
UMERGE   USET,PHIL,/PHIA/V,N,MAJOR=A/V,N,SUBO=L/V,N,SUB1=R $
MPYAD    MLL,DM,MLR/TMP/C,N,0/C,N,1/C,N,1/C,N,1 $
MPYAD    PHIL,TMP,/MIR/C,N,1/C,N,1/C,N,0/C,N,1 $
MATPRN   MIR,,,,// $
OUTPUT2, MIR,,,,//C,N,0/C,N,11 $
ALTER    105
OUTPUT2, OPHIG,OQG1,OEF1,,//C,N,0/C,N,11 $
OUTPUT2, ,,,,//C,N,-9/C,N,11 $
ENDALTER
```

APPENDIX D

MULTI-FORMAT TAPE DUMP PROGRAM

```
      PROGRAM A3930 (INPUT,OUTPUT,TAPE5=INPUT,TAPE6=OUTPUT,TAPE1)
C*********************************************************************C
C                                                                     C
C     THIS PROGRAM READS A N Y  TAPE WITH VARIABLE LENGTH BINARY RECORDS  C
C     REQUEST TAPE MUST BE LABELED AS TAPE1                           C
C     THE PROGRAM DETERMINES THE MODE (REAL,INTEGER OR ALPHA) OF EACH WORD  C
C     ON THE TAPE.                                                    C
C     THE PROGRAM  THEN PRINTS EACH RECORD IN THE CORRECT FORMAT.    C
C                                                                     C
C*********************************************************************C
      DIMENSION NN(513),FM(3),FMT(10)
      DATA FM /7H,A10,5X , 6H,E15.7 , 7H,I10,5X /
      DATA FMT(1),FMT(10),CPAREN /4H(11X , 1H) , 1H) /
      REWIND 1
      WRITE(6,1)
    1 FORMAT(1H1)
      NREC=0
    2 ICNT=IVAR(1,NN,0,513)
      IF(ICNT.EQ.0) STOP
      IF(ICNT.LT.0) GO TO 7
      NREC=NREC+1
      WRITE(6,3) NREC
    3 FORMAT(1H ,*RECORD*I4)
      DO 6 I=1,ICNT,8
      DO 4 J=1,8
      J2=I+J-1
      CALL WHAT(NN(J2),NTYPE)
      FMT(1+J)=FM(NTYPE)
      IF(J2.EQ.ICNT) GO TO 5
    4 CONTINUE
      GO TO 6
    5 FMT(2+J)=CPAREN
    6 WRITE(6,FMT) (NN(J),J=I,J2)
      GO TO 2
    7 WRITE(6,8)
    8 FORMAT(1H ,30H****P A R I T Y  E R R O R****)
      STOP
      END
```

```
      SUBROUTINE WHAT(N,NTYPE)
C     THIS SUBROUTINE DETERMINES THE MODE OF  N
C        NTYPE=1  IF N IS ALPHA
C        NTYPE=2  IF N IS REAL
C        NTYPE=3  IF N IS INTEGER
      INTEGER BB
      DATA BB/4H0000/
      CALL RSHFT(BB,-24)
      CALL RSHFT(BB, 24)
      IF(IABS(  N  ).LE.9999999999) GO TO 140
      M=N
      CALL RSHFT( M ,-24)
      CALL RSHFT( M , 24)
      IF( M .NE.BB) GO TO 100
      M=N
      CALL RSHFT( M ,54)
      IF( M .LT.1.OR. M .GT.47) GO TO 100
      M=N
      CALL RSHFT( M ,-6)
      CALL RSHFT( M ,54)
      IF( M .LT.1.OR. M .GT.47) GO TO 100
C     ALPHA        1
      NTYPE=1
      GO TO 4
C     REAL         2
  100 NTYPE=2
      GO TO 4
C     INTEGER      3
  140 NTYPE=3
    4 RETURN
      END
```

REFERENCES

1. McCormick, Caleb W., ed.: The NASTRAN User's Manual (Level 15). NASA SP-222(01), June, 1972.
2. MacNeal, Richard H., ed.: The NASTRAN Theoretical Manual (Level 15). NASA SP-221(01), April, 1972.
3. Anon.: The NASTRAN Programmer's Manual. NASA SP-223(01), September, 1972.
4. Hurty, Walter C. and Rubinstein, Moshe F.: Dynamics of Structures. Prentice-Hall, Inc., Englewood Cliffs, New Jersey, 1964, pp. 121-123.

```
$INPUT
NRCRDS  =  19.
NFILES  =  1.
MODE    =  0.
IPRTBIN =  1.
IPRTBCD =  0.
NUMPRTS =  0.
ISTRPRT =  1.
$END
*** FILE      1  RECORD     1 IS BINARY AND CONTAINS      1 WORDS. ***
BINARY REC
      0.
*** FILE      1  RECORD     2 IS BINARY AND CONTAINS      3 WORDS. ***
BINARY REC
      0.               0.               0.
*** FILE      1  RECORD     3 IS BINARY AND CONTAINS      1 WORDS. ***
BINARY REC
      0.
*** FILE      1  RECORD     4 IS BINARY AND CONTAINS      7 WORDS. ***
BINARY REC
      9.99009844-25    4.40421431E+52   1.15759000-174   -8.25896360E+65   3.33660815-185   -8.41192959E+70
      1.42361948-184
*** FILE      1  RECORD     5 IS BINARY AND CONTAINS      1 WORDS. ***
BINARY REC
      0.
*** FILE      1  RECORD     6 IS BINARY AND CONTAINS      2 WORDS. ***
BINARY REC
      2.41257557+175   2.41257557+175
*** FILE      1  RECORD     7 IS BINARY AND CONTAINS      1 WORDS. ***
BINARY REC
     -0.
*** FILE      1  RECORD     8 IS BINARY AND CONTAINS      1 WORDS. ***
BINARY REC
      0.
*** FILE      1  RECORD     9 IS BINARY AND CONTAINS      1 WORDS. ***
BINARY REC
      0.
*** FILE      1  RECORD    10 IS BINARY AND CONTAINS      2 WORDS. ***
BINARY REC
      2.54743304E-01   5.72023741-146
*** FILE      1  RECORD    11 IS BINARY AND CONTAINS      1 WORDS. ***
BINARY REC
     -0.
*** FILE      1  RECORD    12 IS BINARY AND CONTAINS      1 WORDS. ***
BINARY REC
      0.
*** FILE      1  RECORD    13 IS BINARY AND CONTAINS      7 WORDS. ***
```

Figure 1. - User Tape Interrogation Using Standard Tape Dump Program and Writing to an E Format

```
BINARY REC
     0.             0.             0.             0.             0.             0.
     0.
*** FILE     1  RECORD    14 IS BINARY AND CONTAINS     1 WORDS. ***
BINARY REC
    -0.
*** FILE     1  RECORD    15 IS BINARY AND CONTAINS     1 WORDS. ***
BINARY REC
     0.
*** FILE     1  RECORD    16 IS BINARY AND CONTAINS     7 WO     ***
BINARY REC
  2.54743304E-01 5.72023741-146 0.             0.             0.             0.
     0.
*** FILL     1  RECORD    17 IS BINARY AND CONTAINS     1 WORDS. ***
BINARY REC
    -0.
*** FILE     1  RECORD    18 IS BINARY AND CONTAINS     1 WORDS. ***
BINARY REC
     0.
*** FILE     1  RECORD    19 IS BINARY AND CONTAINS   146 WORDS. ***
BINARY REC
     0.             0.             0.             0.             0.             8.08468733E+02
     0.             0.             0.             0.             0.             0.
     0.             0.             0.             0.             0.             0.
     0.             0.             0.             0.             0.             0.
     0.             0.             0.             0.             0.             0.
     0.             0.             0.             0.             0.             0.
     0.             0.             0.             0.             0.             0.
     0.             0.             0.             0.             0.             0.
     0.             0.             9.29446985+131 1.49136233E-22 2.16410409+190 4.38648832-120
  2.10160831-117 1.44733759-269 -7.17396054E+57 -2.79367800E+77 -7.44354977E+57 6.41157294E-25
  7.89205938E+92 1.17649175E-50 6.79931385E-25 7.36131288-231 -7.17383055E+57 -7.17383055E+57
 -7.17383055E+57 -7.17383055E+57 -7.17383055E+57 -7.17383055E+57 -7.17383055E+57 -7.17383055E+57
 -7.17383055E+57 -7.17383055E+57 -7.17383055E+57 -7.17383055E+57 -7.17383055E+57 -7.17383055E+57
 -7.17383055E+57 -7.17383055E+57 -7.17383055E+57 -7.17383055E+57 -1.54824113E+68 -4.69837902+204
 -1.42785140+200 -8.24407186E+67 1.95028376-194 -2.37872618+197 2.05589076+278 -7.17383055E+57
 -7.17383055E+57 -7.17383055E+57 -7.17383055E+57 -7.17383055E+57 -7.17383055E+57 -7.17383055E+57
 -7.17383055E+57 -7.17383055E+57 -7.17383055E+57 -7.17383055E+57 -7.17383055E+57 -7.17383055E+57
 -7.17383055E+57 -7.17383055E+57 -7.17383055E+57 -7.17383055E+57 -7.17383055E+57 -7.17383055E+57
 -7.17383055E+57 -7.17383055E+57 -7.17383055E+57 -7.17383055E+57 -7.17383055E+57 -7.17383055E+57
 -1.71147519E+70 -5.63721099E+19 -2.29734750E+63 -2.56722218E+66 4.14837723+104 5.91089639E+93
  9.31443422E+13 7.58432902-197 3.78610085E+71 6.97155753-272 2.16655311E+17 -7.17383055E+57
 -7.17383055E+57 -7.17383055E+57 -7.17383055E+57 -7.17383055E+57 -7.17383055E+57 -7.17383055E+57
 -7.17383055E+57 -7.17383055E+57 -7.17383055E+57 -7.17383055E+57 -7.17383055E+57 -7.17383055E+57
 -7.17383055E+57 -7.17383055E+57 -7.17383055E+57 -7.17383055E+57 -7.17383055E+57 -7.17383055E+57
 -7.17383055E+57 -7.17383055E+57
```

Figure 1. - Concluded

```
RECORD  1
                3
RECORD  2
               10          18          72
RECORD  3
                7
RECORD  4
       NAST          RAN         FORT        TAP         E ID        COD         E -
RECORD  5
                2
RECORD  6
       XXXX          XXXX
RECORD  7
               -1
RECORD  8
                0
RECORD  9
                2
RECORD 10
       OPHI          6
RECORD 11
               -1
RECORD 12
                7
RECORD 13
              101           0       10656           0           0           0           0
RECORD 14
               -2
RECORD 15
                7
RECORD 16
       OPHI          6                 10          18          72           1           1
RECORD 17
               -3
RECORD 18
              146
RECORD 19
               21           7           0           1           1   8.0846873E+02   2           0
                1           0           0           0           0           0       0           0
                0           0           0           0           0           0       0           0
                0           0           0           0           0           0       0           0
                0           0           0           0           0           0       0           0
                0           0           0           0           0           0       0           0
                0           0
       =            ====        VIKI        NG D        YNAM        IC S        IMUL        ATOR
                                   A        NALY        TICA        L DY        NAMI        CS

       2                        LKC         -GDC        -VDS        MOD         EL 8        -3-7

       PDAT         ED V        EXT         . OF        IST         ROn         T WI        TH U
                                SCA         AND         PLLA
```

Figure 2. - User Tape Interrogation Using Tape Dump Program of Appendix D

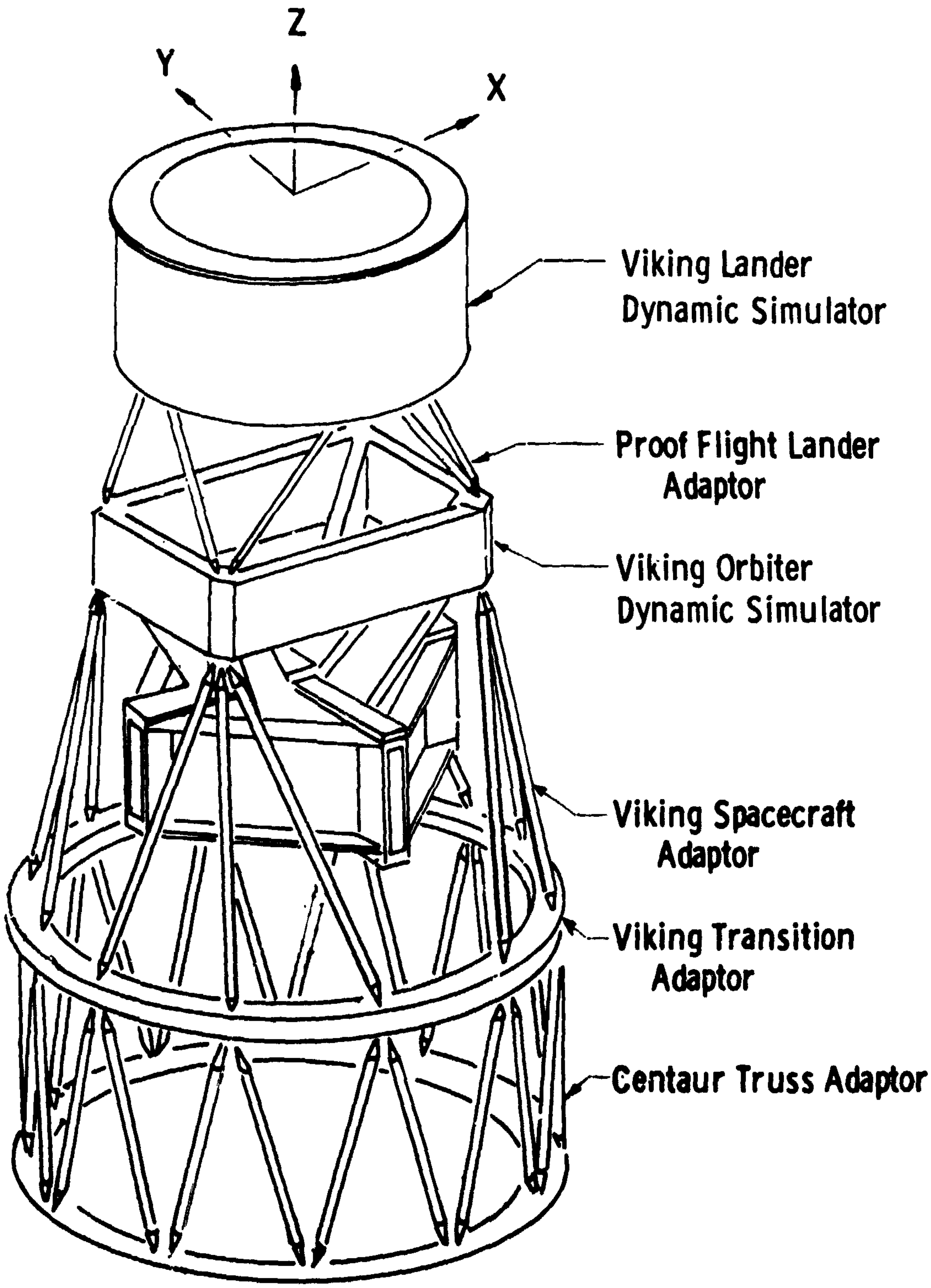

Figure 3. - Viking Dynamic Simulator

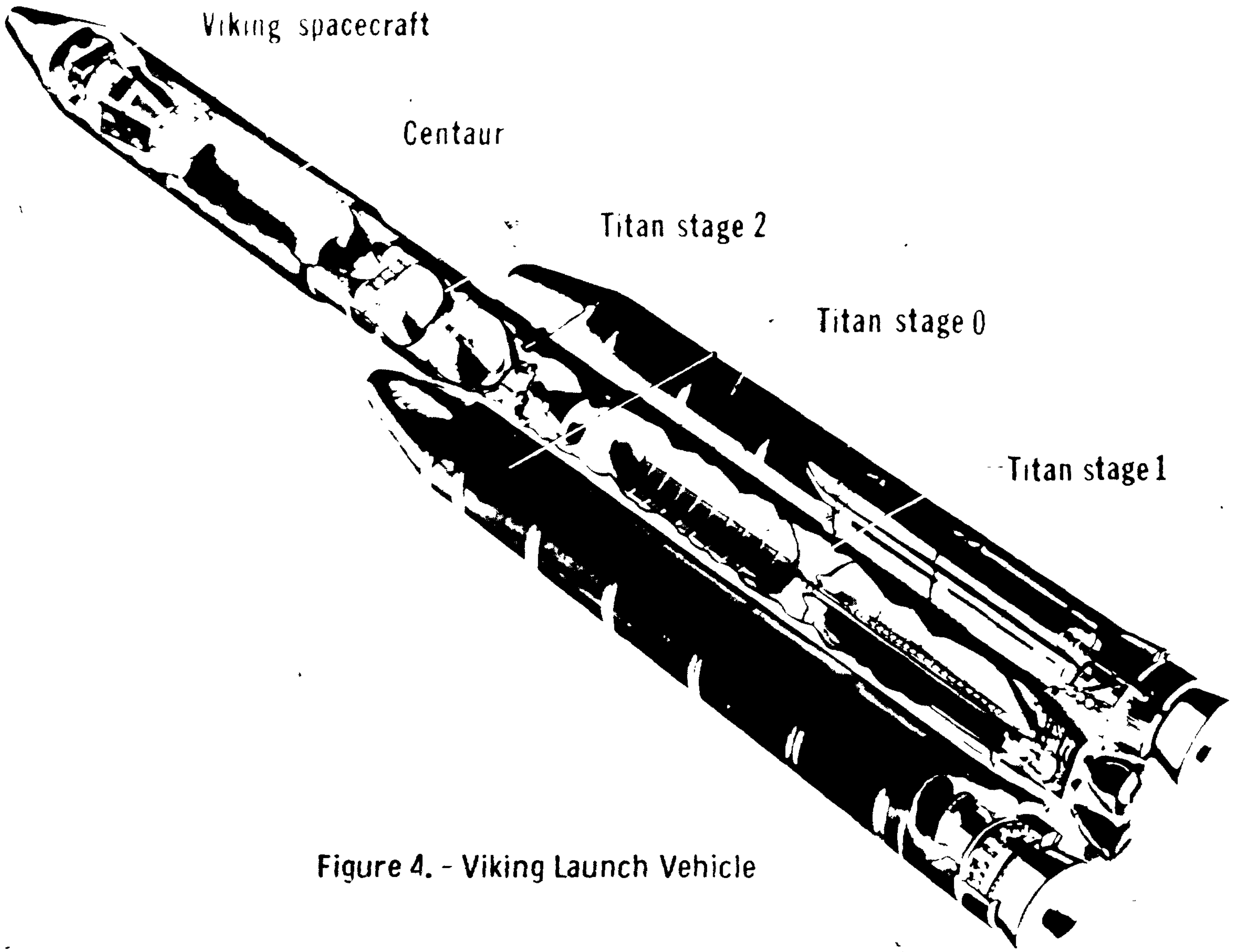

Figure 4. - Viking Launch Vehicle

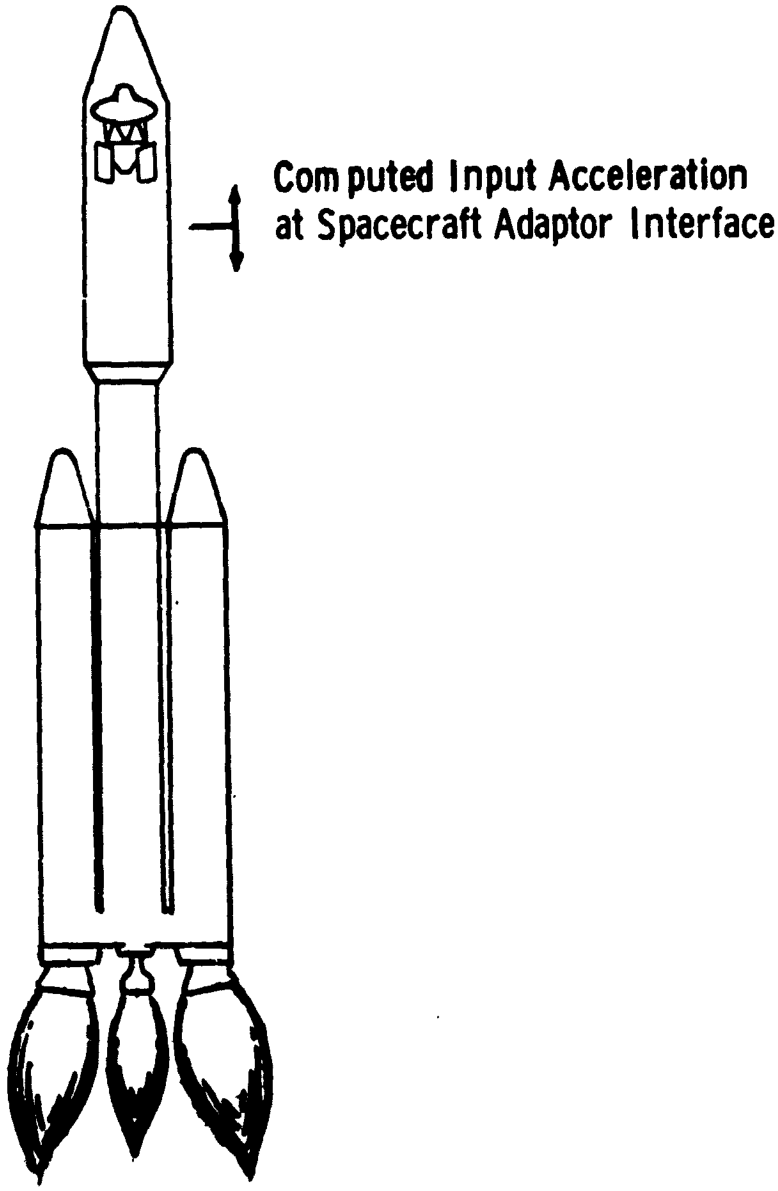

Figure 5. - Viking Configuration Used to Determine Input Acceleration-Time Histories

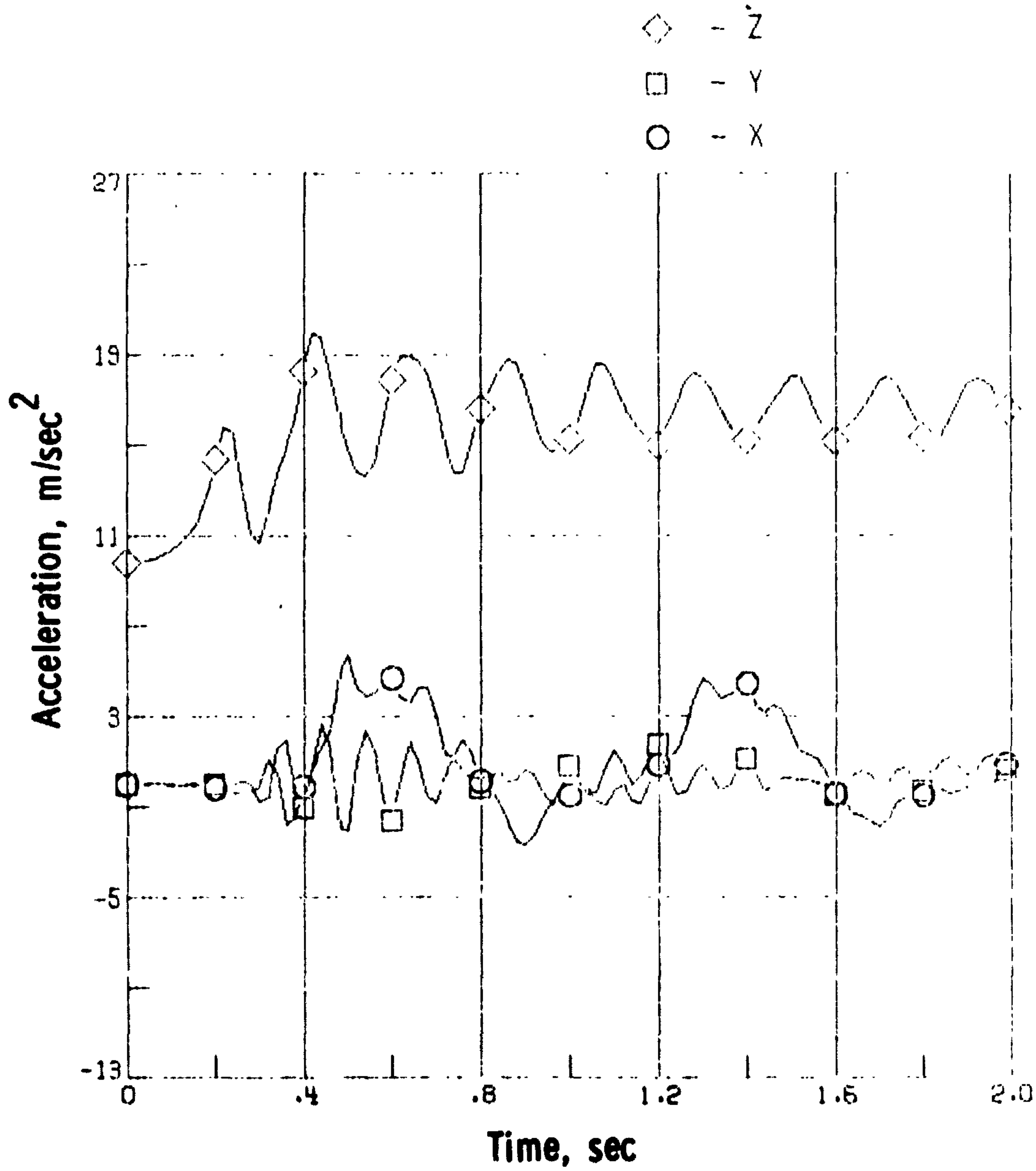

Figure 6. - Translational Accelerations Used As Input

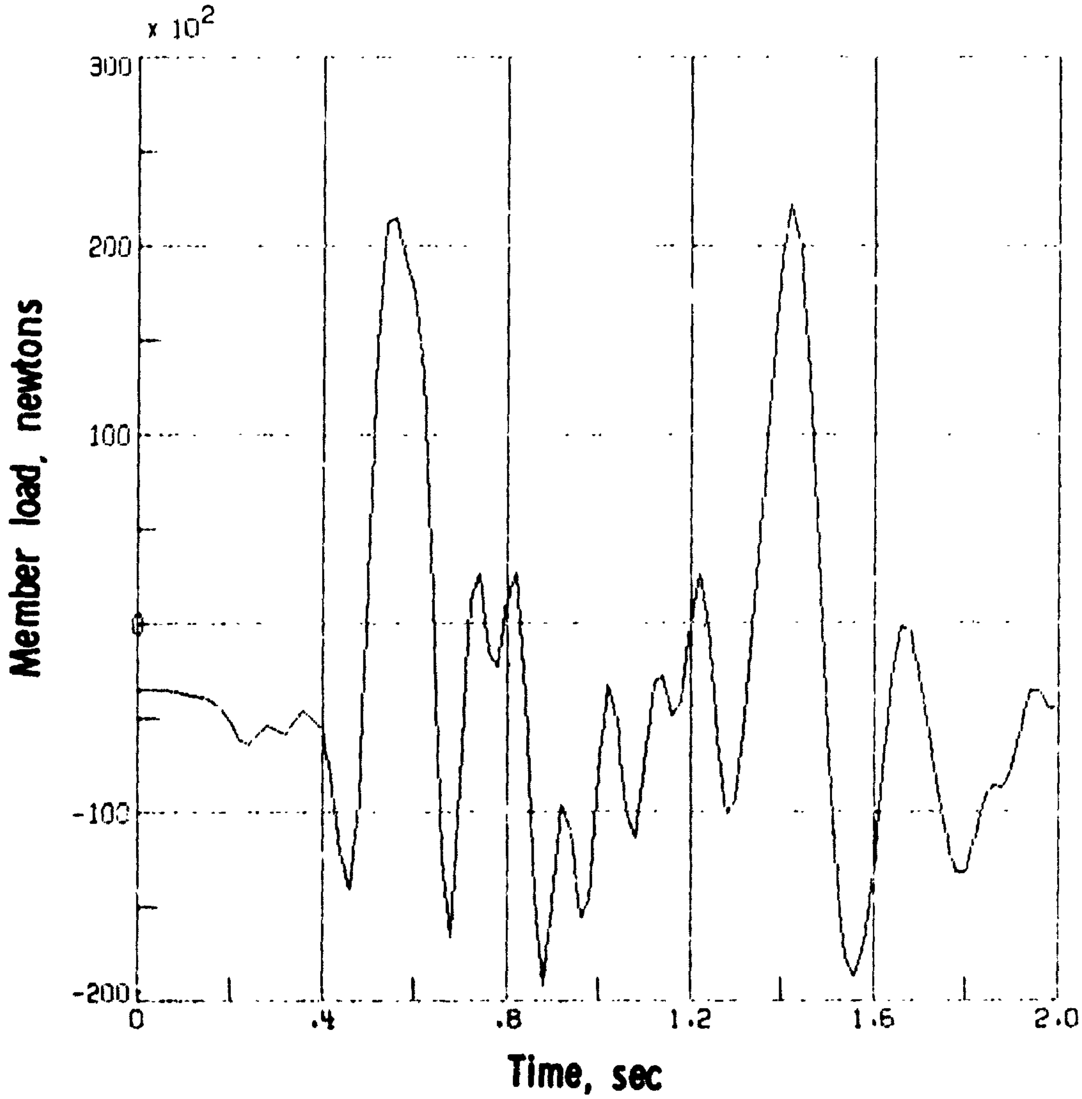

Figure 7. - Typical Load Versus Time for a Member of the Viking Spacecraft Adaptor Truss

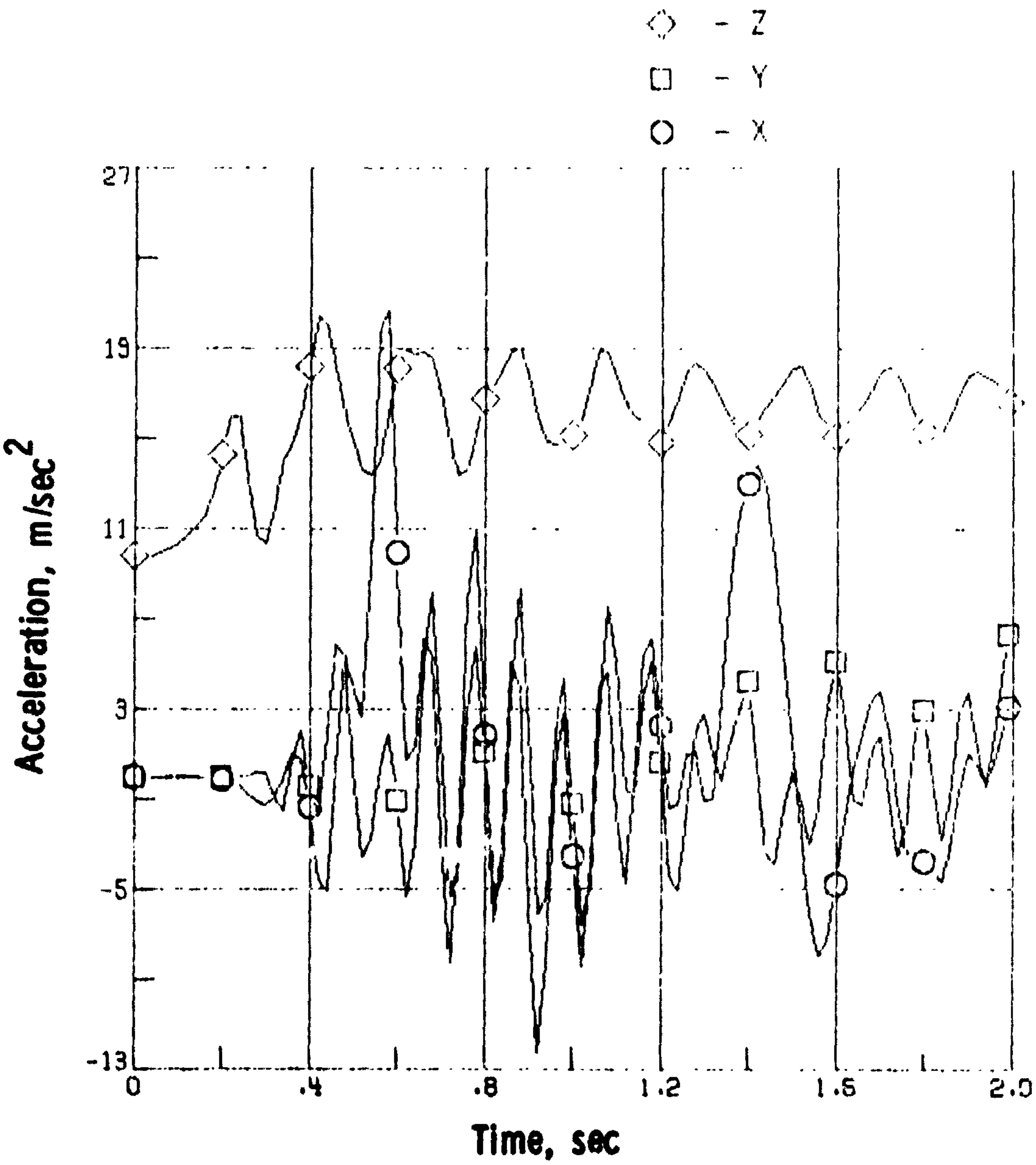

Figure 8. - Output Acceleration at the Top of the Viking Spacecraft

NASA-Langley, 1973 —— 32 L-9220